ANNUAL ISSUE 2007

PROGRESS IN PHYSICS

"All scientists shall have the right to present their scientific research results, in whole or in part, at relevant scientific conferences, and to publish the same in printed scientific journals, electronic archives, and any other media." — Declaration of Academic Freedom, Article 8

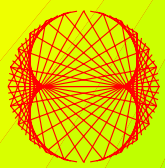

ISSN 1555-5534

The Journal on Advanced Studies in Theoretical and Experimental Physics, including Related Themes from Mathematics

PROGRESS IN PHYSICS

A quarterly issue scientific journal, registered with the Library of Congress (DC, USA). This journal is peer reviewed and included in the abstracting and indexing coverage of: Mathematical Reviews and MathSciNet (AMS, USA), DOAJ of Lund University (Sweden), Zentralblatt MATH (Germany), Referativnyi Zhurnal VINITI (Russia), etc.

Electronic version of this journal:
http://www.ptep-online.com
http://www.geocities.com/ptep_online

To order printed issues of this journal, contact the Editor-in-Chief.

Department of Mathematics, University of New Mexico, 200 College Road, Gallup, NM 87301, USA

ISSN: 1555-5534 (print)
ISSN: 1555-5615 (online)

Standard Address Number: 297-5092
Printed in the United States of America

JANUARY 2007 **VOLUME 1**

CONTENTS

Information for Authors and Subscribers

Progress in Physics has been created for publications on advanced studies in theoretical and experimental physics, including related themes from mathematics. All submitted papers should be professional, in good English, containing a brief review of a problem and obtained results.

All submissions should be designed in LaTeX format using *Progress in Physics* template. This template can be downloaded from *Progress in Physics* home page http://www.ptep-online.com. Abstract and the necessary information about author(s) should be included into the papers. To submit a paper, mail the file(s) to Chief Editor.

All submitted papers should be as brief as possible. Commencing 1st January 2006 we accept brief papers, no larger than 8 typeset journal pages. Short articles are preferable. Papers larger than 8 pages can be considered in exceptional cases (such as discoveries, etc.) to the section *Special Reports* intended for such publications in the journal.

All that has been accepted for the online issue of *Progress in Physics* is printed in the paper version of the journal. To order printed issues, contact Chief Editor.

This journal is non-commercial, academic edition. It is printed from private donations.

SPECIAL REPORT

WMAP: A Radiological Analysis

Pierre-Marie Robitaille

Dept. of Radiology, The Ohio State University, 130 Means Hall, 1654 Upham Drive, Columbus, Ohio 43210, USA

E-mail: robitaille.1@osu.edu

In this work, results obtained by the WMAP satellite are analyzed by invoking established practices for signal acquisition and processing in nuclear magnetic resonance (NMR) and magnetic resonance imaging (MRI). Dynamic range, image reconstruction, signal to noise, resolution, contrast, and reproducibility are specifically discussed. WMAP images do not meet accepted standards in medical imaging research. WMAP images are obtained by attempting to remove a galactic foreground contamination which is 1,000 times more intense than the desired signal. Unlike water suppression in biological NMR, this is accomplished without the ability to affect the signal at the source and without *a priori* knowledge. Resulting WMAP images have an exceedingly low signal to noise (maximum 1–2) and are heavily governed by data processing. Final WMAP internal linear combination (ILC) images are made from 12 section images. Each of these, in turn, is processed using a separate linear combination of data. The WMAP team extracts cosmological implications from their data, while ignoring that the ILC coefficients do not remain constant from year to year. In contrast to standard practices in medicine, difference images utilized to test reproducibility are presented at substantially reduced resolution. ILC images are not presented for year two and three. Rather, year-1 data is signal averaged in a combined 3-year data set. Proper tests of reproducibility require viewing separate yearly ILC images. Fluctuations in the WMAP images arise from the inability to remove the galactic foreground, and in the significant yearly variations in the foreground itself. Variations in the map outside the galactic plane are significant, preventing any cosmological analysis due to yearly changes. This occurs despite the masking of more than 300 image locations. It will be advanced that any "signal" observed by WMAP is the result of foreground effects, not only from our galaxy, but indeed yearly variations from every galaxy in the Universe. Contrary to published analysis, the argument suggests there are only questionable findings in the anisotropy images, other than those related to image processing, yearly galactic variability, and point sources. Concerns are also raised relative to the validity of assigning brightness temperatures in this setting.

1 Introduction

The WMAP satellite [1] was launched with the intent of measuring the microwave signals present in space. It is widely held that these signals are anisotropic and relay information relative to the creation and formation of the early Universe [1–27]. WMAP has been hailed as providing some of the most important findings in science [2]. Reports by Spergel et. al. [15] and Bennett et. al. [7] are highly cited [28]. The ensemble of WMAP publications [3–26] appears to constitute a phenomenal assortment of data. WMAP is being praised both for its precision and the insight it provides into the earliest stages of the formation of the Universe [1, 2]. NASA and the WMAP team of scientists, representing the premier academic institutions [1], have made numerous claims, most notably stating that their data enables them to visualize what happened in the first trillionth of a second after the Big Bang [27]. From data with a signal to noise just beyond 1, a number of constants is provided relative to the age of the Universe (13.7 ± 0.2 Gyr), the amount of dark energy ($\sim$73%), dark matter ($\sim$22%), and baryons density or "real" matter ($\sim$4%) [7, 25]. It is surmised that "decoupling" occurred just after the Big Bang (379 ± 8 kyr) at a redshift of 1089 ± 1. The thickness of the decoupling surface is given as 195 ± 2, and the total mass-energy in the Universe (1.02 ± 0.02) is also amongst the constants [7, 25].

WMAP does not measure the absolute intensity of any given microwave signal. Rather, it is equipped with antennae whose difference is constantly recorded. Thus, all WMAP data represent difference data. The satellite is positioned at the second Lagrange point of the Sun-Earth system, L2, approximately 1.5 million km from Earth. At this position, the Earth continually shields WMAP from the Sun, as they each complete their orbits. The first year of data collection extended from 10 August 2001 — 9 August 2002, with data release in March 2003. A complete 3-year average data set, spanning 10 August 2001 — 9 August 2004, was released in March 2006.

The WMAP satellite acquires signals at five observational frequencies: 23, 33, 41, 61, and 94 GHz. These are also

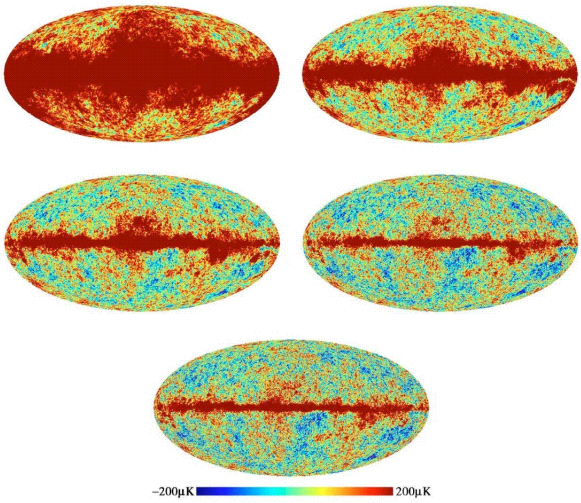

Fig. 1: The five frequency bands observed by the WMAP satellite. Images correspond to 23 GHz (K band, upper left), 33 GHz (Ka band, upper right), 41 GHz (Q band, middle left), 61 GHz (V band, middle right), and 94 GHz (W band, bottom). Reprinted portion of Figure 2 with permission from Tegmark M., de Oliveira-Costa A., Hamilton A.J.S. A high resolution foreground cleaned CMB map from WMAP. *Phys. Rev. D*, 2003, v. 68(12), 123523; http://link.aps.org/abstract/PRD/v68/e123523. Copyright (2003) by the American Physical Society.

known as the K, Ka, Q, V, and W bands. Images generated at these bands are displayed in Figure 1. Final anisotropy maps are prepared by combining the signals represented in Figure 1 with particular weighting at 61 GHz. Maps for each year are prepared individually and then combined "for a number of reasons" [23]. Extensive image processing is applied prior to generating the final anisotropy map (see Figure 2). The noise level in the data sets depends on the number of observations at each point. The major hurdle for WMAP is the presence of the strong foreground signal from our galaxy. In a sense, the WMAP team is trying to "look through" the galaxy, as it peers into the Universe.

In recent years, WMAP results have been widely disseminated both in the scientific literature and the popular press. Nonetheless, there are sufficient questions relative to the manner in which the WMAP data is processed and analyzed, to call for careful scrutiny by members of the imaging community. The implications of WMAP are not only financial and scientific but, indeed, have the potential to impact the course of science and human reason for many generations. As a result, images which are the basis of such specific scientific claims must adhere to standard practices in imaging science. Consequently, and given the precision of the constants provided by WMAP, it is appropriate to review the underlying images and subject them to the standards applied in radiological image analysis. These include most notably signal to noise, resolution, reproducibility, and contrast. These four characteristics represent universally accepted

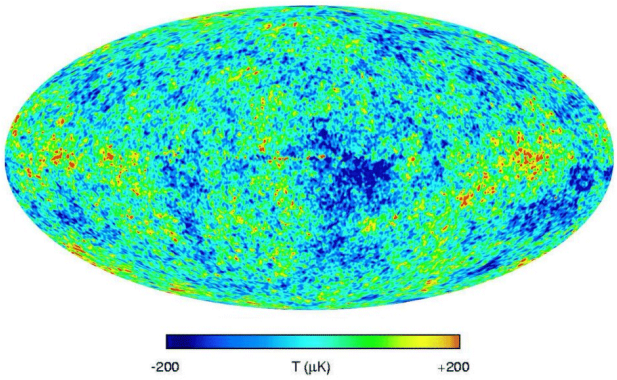

Fig. 2: Cleaned internal linear combination (ILC) map produced by the WMAP team [7]. This image corresponds to Figure 11 in Bennett et. al. [7]. Reproduced with permission of the AAS. Image provided courtesy of the NASA/WMAP team.

measures of image quality. However, before embarking on this exercise, it is important to address dynamic range and the removal of the galactic foreground. In addition, it is useful to review the procedure which the WMAP team employs in image reconstruction.

2 Image analysis

2.1 Dynamic range and the removal of the Galactic foreground

The WMAP satellite acquires its data in five frequency bands. Five images obtained at these bands (K, Ka, Q, V, and W) are displayed in Figure 1 [29]. The galactic foreground dominates this entire series of images. The foreground is seen as a bright red signal across the central portion of each frequency map. Indeed, the center of the galactic foreground, observed by WMAP, exceeds the desired anisotropic signal in brightness by a factor of $\sim$1,000 [11]. Therefore, the WMAP team is attempting to visualize extremely weak anisotropy in the presence of a much more powerful contaminating signal. This becomes a dynamic range issue analogous to water suppression in biological proton nuclear magnetic resonance (NMR).

Water suppression is an important technique in proton NMR, since most compounds of biochemical interest are typically found dissolved in the aqueous cytosol of the cell. This includes a wide array of proteins, signal messengers, precursors, and metabolic intermediates. Water is roughly 110 molar in protons, whereas the signal of interest to the biochemist might be 1–100 millimolar. In the best case scenario, biological proton NMR, like WMAP, presents a $\sim$1,000 fold problem in signal removal. In the worst case, factors of 100,000 or more must be achieved. Extensive experience in biological NMR obtained throughout the world has revealed that it is impossible to remove a contaminating signal on these orders of magnitude without either (1) ability

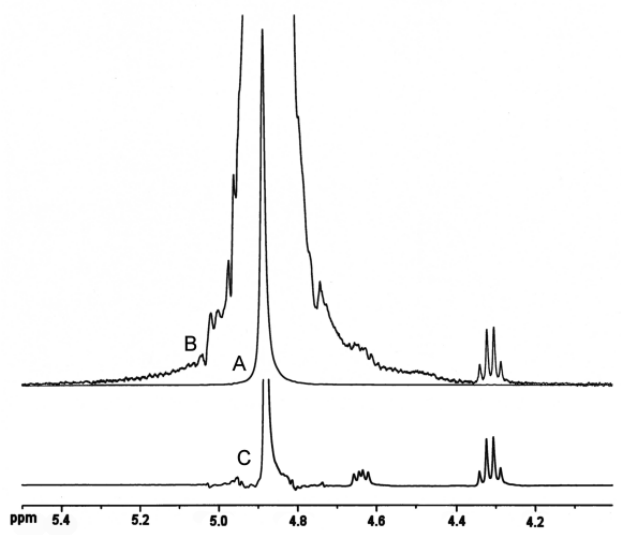

Fig. 3: Proton nuclear magnetic resonance (NMR) spectra acquired from a 0.1 M solution of 0.1 M N-benzoyl-L-arginine ethyl ester hydrochloride in water (A, B). The spectrum is shown in full scale (A). In (B) the vertical axis has been expanded by a factor of 100, such that the resonance lines from the N-benzoyl-L-arginine ethyl ester can be visualized. A ^{1}H-NMR spectrum acquired from 0.1 M N-benzoyl-L-arginine ethyl ester hydrochloride in deuterium oxide (D_2O) is also displayed (C). Spectra display only the central region of interest (4.0–5.5 ppm). Acquisition parameters are as follows: frequency of observation 400.1324008 MHz, sweep width 32,768 Hz, receiver gain 20, and repetition time 5 seconds. The sample dissolved in D_2O (C) was acquired first using a single acquisition and a 90 degree nutation. A field lock was obtained on the solvent. This was used in adjusting the field homogeneity for both samples. For (A) and (B), 20 acquisitions were utilized to enable phase cycling of the transmitter and receiver. In this case, the nutation angle had to be much less than 90 degrees in order not to destroy the preamplifier. A field lock could not be achieved since D_2O was not present in the sample. These slight differences in acquisition parameters and experimental conditions make no difference to the discussion in the text relative to problems of dynamic range.

to affect the signal at the source, and/or (2) *a priori* knowledge. Unfortunately for WMAP, neither of these conditions can be met in astrophysics.

In NMR, ability to effect signal at the source requires direct manipulation of the sample, either biochemically through substitution, or physically, through specialized spin excitation. Biochemical substitution involves the removal of the protons associated with water, using deuterium oxide (D_2O) as an alternative solvent [30]. Often, the sample is lyophilized [31]. That is, it is frozen and placed under vacuum so that all of the water can be removed through sublimation. The solvent is then replaced by the addition of D_2O. This process can be repeated several times to remove most of the exchangeable protons contained in the sample. The protons are hence replaced by deuterium, which is no longer detectable at the frequency utilized to acquire the desired proton NMR spectrum. Thus, in order to achieve a factor of 1,000 in suppression, the biochemist, in the laboratory, often invokes a rather dramatic modification of the sample at the source.

In Figure 3, a series of ^{1}H-NMR spectra is presented. Figure 3A corresponds to a mixture of 0.1 M N-benzoyl-L-arginine ethyl ester hydrochloride in water. Since water is 110 M in protons, this solution constitutes roughly a 1,000 fold excess of water protons versus sample protons. Interestingly, the only signal which can be detected in Figure 3A is that of water at 4.88 ppm. The multiple resonances from the N-benzoyl-L-arginine ethyl ester hydrochloride have about the same intensity as found in the line width. In Figure 3B, the same spectrum is reproduced but, this time, the vertical scale has been expanded 100 times. Now, the resonances from the sample are readily observed. The ratio of the water resonance in Figure 3A or B to the quartet at 4.3 ppm is 670. Note, however, that a doublet pair, located at $\sim$4.63 ppm (Figure 3B) is being distorted by the intense resonance line from water. This is easy to assess by examining Figure 3C, wherein a solution of 0.1 M N-benzoyl-L-arginine ethyl ester hydrochloride was reconstituted in 99.8% D_2O. In the D_2O spectrum (C), the ratio of the water resonance to the quartet at 4.3 ppm is 21. In this case, the water line is greatly attenuated, since most of the water protons have been replaced with deuterium. Indeed, substitution of D_2O for water (C) results in a 30 fold drop in the intensity of the water line. With this sample, all of the resonances from the N-benzoyl-L-arginine ethyl ester hydrochloride in the vicinity of the water resonance can be visualized, including the doublet pair, at 4.63 ppm. From this information, the ratio of the water to the doublet pair at 4.63 ppm is $\sim$1,500.

Through Figure 3, it is easy to envision the tremendous challenge involved in removing a contaminating signal which dominates the species of interest by $\sim$1,000 fold. In Figure 3B, it is readily apparent that the doublet pair at 4.63 ppm is being distorted by the water line. Consequently, the presence of the intense water resonance affects spins which are adjacent, not only co-resonant. The situation is actually much worse for WMAP as the satellite is attempting to visualize signals contained at the same frequency of observation as the galactic foreground signals. In a sense, the WMAP team is trying to see signals directly beneath the water line, not adjacent to it. To further aggravate the situation, the WMAP team is dealing with extremely weak signals, on the same order of magnitude as the noise floor (see below). Note that the obscured resonances at $\sim$4.63 ppm in the water spectrum would still have a signal to noise of $\sim$5:1, if the water line had not contaminated this region. This can be gathered by comparing Figures 3B and 3C. For WMAP, the signal to noise is less than 2:1, and the signal of interest is located at the same frequency of the contamination.

Relative to dynamic range and removal of a contaminating water signal in NMR however, an alternative to replacing

water with deuterium oxide exists. In fact, it is possible to utilize specialized spin excitation techniques which either exploit the position of the water line in the spectrum [32–36] or invoke gradient and/or multiple quantum selection [37–39]. Indeed, the approaches to water suppression and dynamic range problems in NMR are so numerous that only a few methods need be discussed to adequately provide experimental insight relative to WMAP.

If the experimentalist is not concerned with signals lying at the same frequency of the water resonance, it is sometimes possible to excite the spins in such a manner that the protons co-resonating with water are nulled and other regions of the spectrum are detected [32–36]. This approach is adopted by methods such as presaturation [32], jump-return [33], and other binomial sequences for spin excitation [34–36]. In each case, the spectral region near the water resonance is sacrificed in order to permit the detection of adjacent frequencies. Despite the best efforts, these methods depend on the existence of very narrow water line widths. Water suppression with these methods tends to be limited to factors of $\sim$100. The situation in-vivo might be slightly worse given the wider line widths typically observed in this setting. Despite this apparent success, these methods fail to preserve the signal lying "beneath" the water resonance. Such information is lost.

In certain instances, it is also possible to excite the spectrum by applying specialized gradient-based methods and quantum selection for spin excitation. In so doing, advantage is made of the unique quantum environment of the spins. These methods have the advantage that spins, which co-resonate with water, are not lost. As such, water suppression can be achieved while losing little or no chemical information. The most powerful of these methods often have recourse to gradient fields, in addition to RF fields, during spin excitation [37–39]. These approaches have been particularly important in the study of proteins in solution [39]. Using quantum selection, it is not unreasonable to expect spin excitation with factors of 1,000–10,000 or more in water suppression.

Methods which rely on coherence pathway selection, or hetero-nuclear multiple quantum selection, constitute important advances to NMR spectroscopy in general, and protein NMR in particular [39]. In the absence of these methods, modern aqueous proton NMR would be impossible. In fact, over the course of the last 50 years, it has been amply demonstrated that it is simply not possible to acquire any information of interest, near the water resonance in biological NMR, by data processing a spectrum obtained from an aqueous sample without *a priori* water suppression. Yet, the WMAP map team attempts the analogous data processing feat, in trying to remove the foreground galactic signal.

Unlike the situation in astrophysics, it is possible to address dynamic range issues in NMR, since the spectroscopist literally holds the sample in his hands. The required signals can be selected by directly controlling spin excitation and, therefore, the received signal. Water suppression is addressed prior to signal acquisition, by carefully avoiding the excitation of spins associated with water. The analogous scenario is not possible in astrophysics.

To a smaller extent, water suppression in biological NMR could perhaps be achieved with *a priori* knowledge (i.e. a perfect knowledge of line shapes, intensity, and position). However, such an approach has not yet been successfully implemented in the laboratory. As a result, *a priori* knowledge in NMR is theoretically interesting, but practically unfeasible. This is an even greater limitation in astrophysics where very limited knowledge of the sample exists. The vast experience of NMR scientists demonstrates that the removal of a strong contaminating signal, for the detection of a much weaker underlying signal, is impossible without affecting the signals at the source. Biological NMR has been in existence for over half a century. During most of this time, achieving a factor of 1,000 in signal removal was considered a dramatic achievement, even when combining spin excitation methods with lyophylization. Only in the past 15 years have methods improved, and this solely as a result of gradient-based or multiple-quantum techniques, which provide even more powerful spin selection during excitation [39]. Signal suppression, by a factor of 100, or more, while still viewing the underlying signal, depends on the ability to control the source. This has been verified in numerous laboratories where the sample is known and where the correct answer can be readily ascertained. As such, it is impossible for the WMAP team to remove the galactic foreground given the dynamic range situation between the contaminant and the signal of interest. Attempts to the contrary are futile, as indicated by the need to segment the final images into 12 sections, and alter, from section to section, the linear combination of data, as will be discussed below.

The galactic problem alone is sufficient to bring into question any conclusion relative to anisotropy from both WMAP and COBE. Nonetheless, additional insight can be gained by examining image reconstruction.

2.2 ILC image reconstruction

2.2.1 Combining section images

Despite this discussion relative to NMR, the WMAP team claims that removal of the galactic foreground is possible and therefore proceeds to ILC image generation. As mentioned above, the WMAP satellite obtains its data in five frequency bands (23, 33, 41, 61, and 94 GHz). In order to achieve galactic foreground removal, the WMAP team utilizes a linear combination of data in these bands, essentially adding and subtracting data until a null point is reached. In doing so, the WMAP team is invoking *a priori* knowledge which cannot be confirmed experimentally. Thus, the WMAP team makes the assumption that foreground contamination

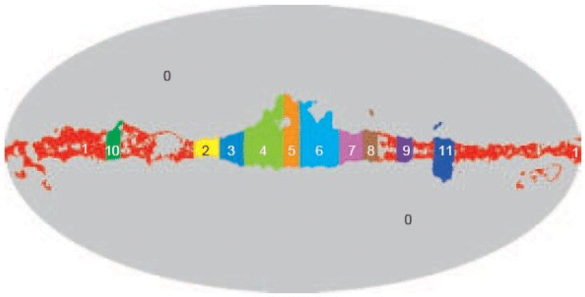

Fig. 4: Illustration of the 12 regions used to generate the ILC maps for year 3 average data. This image corresponds to the upper portion of Figure 8 in Hinshaw et. al. [23]. Reproduced with permission of the AAS. Image provided courtesy of the NASA/WMAP team.

is frequency dependent, while the anisotropy is independent of frequency. This approach, however, is completely unsupported by the experimental data, as will be discussed further below.

Furthermore, galactic foreground removal cannot be achieved with a single linear combination of data. Rather, WMAP achieves its final maps by first generating separately processed section images. Eleven of these regions lie directly in the galactic plane, as shown in Figure 4. Each section is processed individually. The twelve processed section images are then combined and smoothed to generate the final ILC maps.

The WMAP team invokes completely different linear combinations of data to process adjacent regions of the galactic plane. In medical imaging, there is seldom, if ever, the need to process final images in sections. Given this fact, note the processing applied to generate regions 4 and 5 in the 3-year average data (see Figure 4). The coefficients, for section 4, correspond to -0.0781, 0.0816, -0.3991, 0.9667, and 0.4289 for the K, Ka, Q, V, and W bands, respectively [23]. In sharp contrast, the coefficients for section 5 correspond to 0.1839, -0.7466, -0.3923, 2.4184, and -0.4635, for these same bands [23]. The WMAP team alters the ILC weights by regions, used in galactic signal removal, by more than a factor of 100% for the fourth coefficient, despite the adjacent locations of these sections. The same problem exists for several other adjacent sections in the galactic plane [23]. The sole driving force for altering the weight of these coefficients lies in the need to zero the foreground. The selection of individual coefficients is without scientific basis, with the only apparent goal being the attainment of a null point. The full list of ILC coefficients adopted by the WMAP team are reproduced in Table I (reprint of Table 5 in reference [23]). Analysis of this table reveals the tremendous coefficient variability used, from section to section, for zeroing the galactic foreground.

In generating the ILC maps, the WMAP team chose to primarily weigh the V-band. As a result, the coefficients selected tend to reflect this emphasis. However, there is no

Region	K-band	Ka-band	Q-band	V-band	W-band
0	0.1559	−0.8880	0.0297	2.0446	−0.3423
1	−0.0862	−0.4737	0.7809	0.7631	0.0159
2	0.0358	−0.4543	−0.1173	1.7245	−0.1887
3	−0.0807	0.0230	−0.3483	1.3943	0.0118
4	−0.0781	0.0816	−0.3991	0.9667	0.4289
5	0.1839	−0.7466	−0.3923	2.4184	−0.4635
6	−0.0910	0.1644	−0.4983	0.9821	0.4428
7	0.0718	−0.4792	−0.2503	1.9406	−0.2829
8	0.1829	−0.5618	−0.8002	2.8464	−0.6674
9	−0.0250	−0.3195	−0.0728	1.4570	−0.0397
10	0.1740	−0.9532	0.0073	2.7037	−0.9318
11	0.2412	−1.0328	−0.2142	2.5579	−0.5521

Table 1: ILC weights by regions. ILC coefficients used in the analysis of 3-year data by the WMAP team. This table corresponds to Table 5 in Hinshaw et. al. [23]. Utilized courtesy of the NASA/WMAP team.

a priori reason why the weighting could not have emphasized the Q band, for instance. This is especially true since anisotropy is advanced as being frequency independent. Indeed, it is interesting that the Q and W bands have coefficients on the order of -0.4, while lying in proximity to the V band which is given a weight of 2.4 for region 5.

Nonetheless, the scientifically interesting region in the ILC map corresponds to section 0 (see Figure 4). Thus, problems in removing the galactic foreground could be tolerated, given that the WMAP team has no other alternative. It is the processing utilized for section 0 which is most important. This brings yet another complication. Completely different ILC maps of the Universe would be obtained, if the WMAP team had decided to emphasize a frequency other than the V band. In that case, an altered set of cosmological constants is very likely to be generated, simply as a result of data processing.

In removing the galactic foreground, the WMAP team has assumed that the anisotropy is frequency independent. In reality, it is already clear that an ILC map generated with weighting on the Q-band, for instance, will be dramatically different. The requirement that the signals of interest are frequency independent cannot be met, and has certainly never been proven.

In the first data release, the only real requirement for generating the ILC maps was that the coefficients sum to 1. As such, an infinite number of maps can be generated. There is no single map of the anisotropy, since all maps are equally valid, provided coefficients sum to 1. In this regard, alternative anisotropic maps have been presented [29]. Tegmark et. al. [29] generate a new anisotropy map by permitting

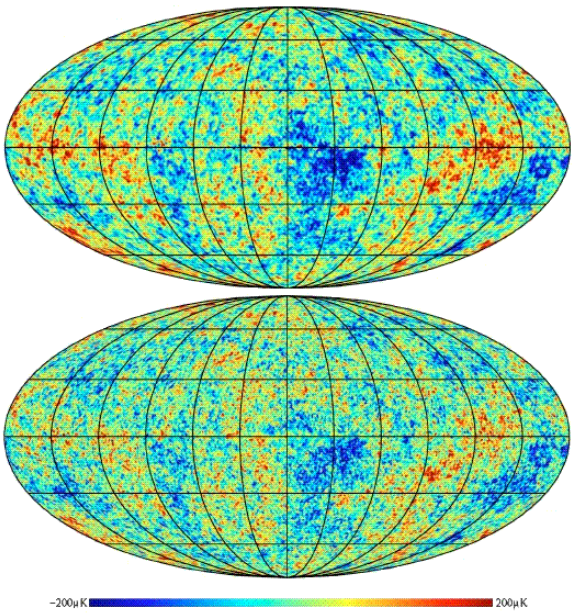

Fig. 5: Cleaned internal linear combination (ILC) anisotropy map produced by the WMAP team (top) and Wiener filtered anisotropy map (bottom) produced by Tegmark et. al. [29]. Reprinted portion of Figure 1 with permission from Tegmark M., de Oliveira-Costa A., Hamilton A.J.S. A high resolution foreground cleaned CMB Map from WMAP. *Phys. Rev. D*, 2003, v. 68(12), 123523; http://link.aps.org/abstract/PRD/v68/e123523. Copyright (2003) by the American Physical Society.

the coefficient weighting to depend both on angular scale and on distance to the galactic plane. This approach was substantially different from that implemented by the WMAP team and it reinforces the finding that no single anisotropy map exists. In Figure 5, it is apparent that the map generated by the WMAP team (top) does not agree with the map generated by Tegmark et. al. (bottom) [29].

An infinite number of maps can be generated from the 5 basis sets. There is no unique solution and therefore each map is indistinguishable from noise. There are no findings relative to anisotropy, since there are no features in the maps which could guide astrophysics relative to the true solution.

With the release of the 3-year data set however, the WMAP team claims that they can use mathematical methods to find the maximum likelihood sky map [23]. Unfortunately, there are no means to test the validity of the solution. In this regard, astrophysics is at a significant disadvantage relative to clinical MRI. Thus, the radiological scientist is guided by known anatomy, and by the results of all other imaging modalities focused on the same sample. This is not the case in astrophysics, since no single spectroscopic frequency holds an advantage over any other. There is no "known" signature to guide the choice of coefficients. A map might appear to be favored, however, devoid of secondary experimental verification, its legitimacy can never be established. Alternative methods could produce alternative maximum likelihood maps. Another level of testing is being added. Nonetheless, the conclusion remains that an infinite number of maps can be generated since, given sufficient resources, one can generate a number of maximal likelihood approaches with no clear way of excising the "true" solution. Therefore, any discussion relative to the cosmological significance of these results is premature.

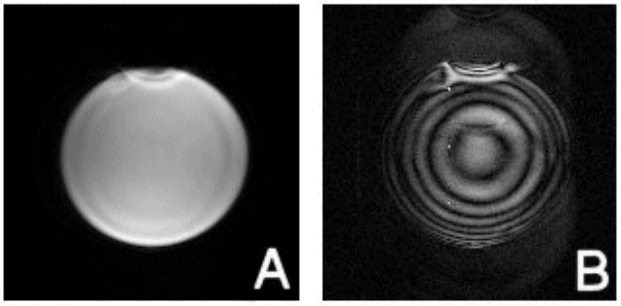

Fig. 6: Ultra High Field 8 Tesla MRI image of an 18 cm ball of mineral oil acquired using a 3-dimentional acquisition. A) Axial slice representing a region contained within the physical space occupied by the 18 cm mineral oil ball. (B) Axial slice through a region located outside the physical space occupied by the ball. Note that the image displayed in (B) should be entirely devoid of signal. The severe image processing artifacts contained in (B) are a manifestation that the processing of powerful signals can result in the generation of weak spurious ghost signals.

2.2.2 Generation of spurious signals

Attempts to remove, by signal processing, a powerful galactic signal will invariably generate unwanted features in the maps, indistinguishable from real findings. The process of removing an intense signal can result in the unexpected creation of many spurious weak ghost signals, at any point in the image plane. Therefore, it is crucial that the signal to noise, in the final image or spectrum of interest, be significant.

In biological NMR, the post-water suppression spectrum typically has good signal to noise. It would not be unusual to achieve 1,000 fold suppression of the water signal and obtain a spectrum with a signal to noise well in excess of 10, or even 100, for the species of interest. This signal to noise is high enough to differentiate it from spurious ghost signals, generated either directly by suppression or through data processing.

In MRI, it is well established that the processing of large signals can lead to spurious signal ghosts throughout an image or a set of images. This is displayed in Figure 6. Figure 6A shows an MRI image of an 18 cm phantom sample containing mineral oil. This image is part of a much larger group of images obtained during a 3D test study. In Figure 6B, a series of signal rings are observed. These rings are spurious ghosts. They were produced by obtaining a 3-dimensional data set on an 18 cm ball containing mineral oil, using an 8 Tesla MRI scanner [40–42]. The signal is acquired

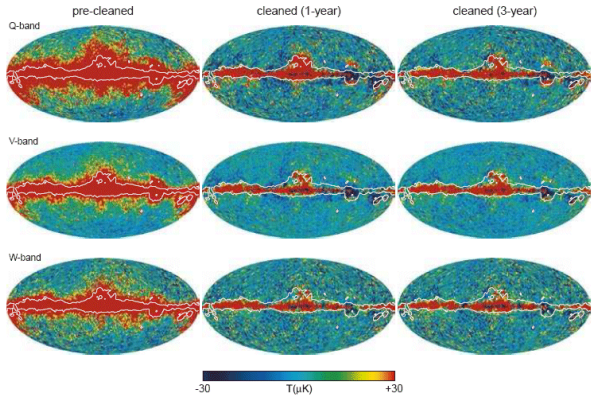

Fig. 7: Illustration of galactic foreground removal for year-1 and for the 3-year average. "Cleaning" is illustrated for the Q, V, and W bands. Similar data are not presented for the K and Ka bands [23]. This image corresponds to Figure 10 in Hinshaw et. al. [7]. Reproduced with permission of the AAS. Image provided courtesy of the NASA/WMAP team.

from the entire ball in the time domain and then Fourier transformed to achieve a set of images in the frequency domain [43]. *The image displayed in Figure 6B corresponds to an imaging slice which lies outside the actual physical space occupied by the ball.* Ideally, this image should be completely black. The spurious signal is a manifestation of a truncation artifact in Fourier transformation during data processing. There should be no signal in this image. However, for the sake of this discussion, it provides an excellent illustration of what can happen when powerful signals must be mathematically manipulated to generate final images.

While the WMAP team is not using simple Fourier transformation to process their images, this lesson nonetheless applies. When mathematically manipulating large signals, weak spurious signals can be created. This phenomenon is common to all image processing, and hence the importance of relatively strong signals of interest once the contaminating signal is removed. This is not the case for WMAP. The contaminating foreground is $\sim$1,000 times the "signal" of interest. Yet, the final signal to noise is poor.

The WMAP team invokes the "cleaning" of its raw images acquired at the K, Ka, Q, V, and W bands prior to presenting the images for these bands [7]. The affect of "cleaning" is demonstrated in Figure 7. Note how the process of "cleaning" the images appears to remove the galactic foreground for the Q, V, and W bands. Interestingly, similar images are not being presented for cleaning the K and Ka bands. This is precisely because the galactic signal contamination is so significant for these two bands. Indeed, the WMAP team needs to present the data for the K and Ka bands in this same figure, in order to place the galactic signal contamination and the associated "cleaning" in proper perspective.

While the galactic center appears to affect only a central region of the Q, V, and W bands in the cleaned image, the situation is more complex. In fact, it is impossible to discern if a given signal is truly independent of the galaxy at any location on the image. This is because the process of "cleaning" images, to remove powerful contaminating signals, is never clean. Mathematical manipulation of powerful signals, whose attributes are not fully characterized or understood, will invariably lead to the generation of image ghosts. Through "cleaning", the WMAP team is taking the risk that it is generating image ghosts. The removal of powerful signals, at certain image locations, can easily be associated with the generation of weak signals at the same (or other) image locations, just as a result of processing. The lesson from Figure 6 applies.

Consequently, the WMAP team is unable to distinguish whether the "features" found in its images are truly of cosmological importance, or whether these features are simply the result of processing (and/or acquiring) a much larger contaminating signal from the galaxy. It is clear, for instance, that K band reveals galactic signal at virtually every point in the sky map (see Figure 1). The same contaminations must be expected in all other bands. That the human eye fails to visualize contamination does not mean that contamination is absent. Because any real signal will be weak, and the contaminating signal is so strong, the WMAP team is unable to distinguish spurious ghosts related to either processing or acquisition from the actual signal of interest. This is true at every image location.

Data processing artifacts tend to be extremely consistent on images. Since similar mathematical methods must be utilized to clean the raw images and zero the galactic foreground, it is highly likely that a significant portion of the maps contains such spurious ghosts. This is especially true given that the WMAP team has chosen to invoke complex mathematical methods for "cleaning" their raw images. That a given image location cannot be positively ascertained to be free of contamination implies that none of the image locations can be validated as free of galactic ghosts on any map. Therein lies the overwhelming complication of dealing with powerful contaminating signals while trying to examine weak ones. Apparent anisotropy must not be generated by processing.

2.2.3 Signal to noise, contrast, and resolution

There is perhaps no more important determinant of image quality than signal to noise. In medicine, signal to noise can directly impact diagnosis. As such, radiological methods which are rich in signal to noise are always sought. If signal to noise is high ($>$100:1), then image quality will almost certainly be outstanding. Methods which have high signal to noise can "burn signal" to generate either contrast, resolution, or shortened exam times. Consequently, signal to noise is paramount. Without it, resolution will remain poor and

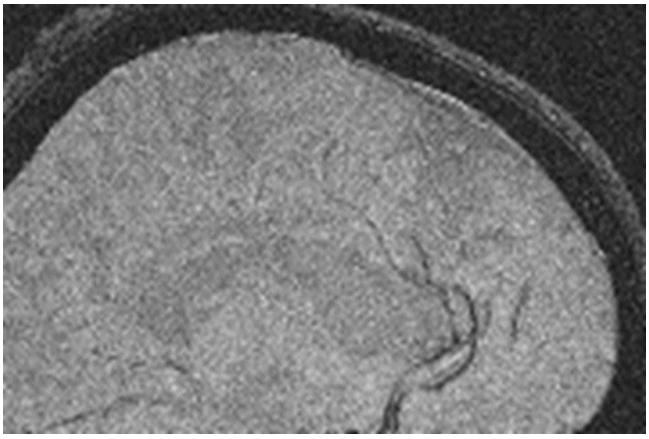

Fig. 8: Section (490 × 327) of a high resolution sagittal image of the human head acquired at 1.5 Tesla. Acquisition parameters are as follows: acquisition sequence = gradient recalled echo, matrix size = 512 × 512, slice thickness = 2 mm, field of view 20 cm × 20 cm, repetition time = 750 msec, echo time = 17 msec, and nutation angle = 45 degrees.

contrast will rapidly deteriorate. In fact, enhancements in signal to noise were the primary driving force for the introduction of Ultra High Field MRI [40–42].

In order to gain some insight into the importance of signal to noise, one can examine the images displayed in Figures 8 and 9. Figure 8 corresponds to a sagittal section of a human brain, acquired using a 1.5 Tesla MRI scanner. There are more than 15,000 such scanners in existence. In this image, the 1.5 Tesla instrument was brought to the very limits of its performance [43]. The resolution is high (matrix size = 512 × 512) and the slice thickness is thin (2 mm). At the same time, the nutation angle, echo times, and repetition times are all suboptimal. As a result, this image is of extremely poor clinical quality. The contrast between grey and white matter has disappeared and the signal to noise is ~ 5.

Figure 9 was acquired with the first UHFMRI scanner [40–42]. This scanner operates at a field strength of 8 Tesla. Note the phenomenal contrast, the delineation of grey and white matter and the appearance of vasculature. Interestingly, this image was acquired with a much larger image resolution (matrix size = 2,000 × 2,000) while maintaining nearly the

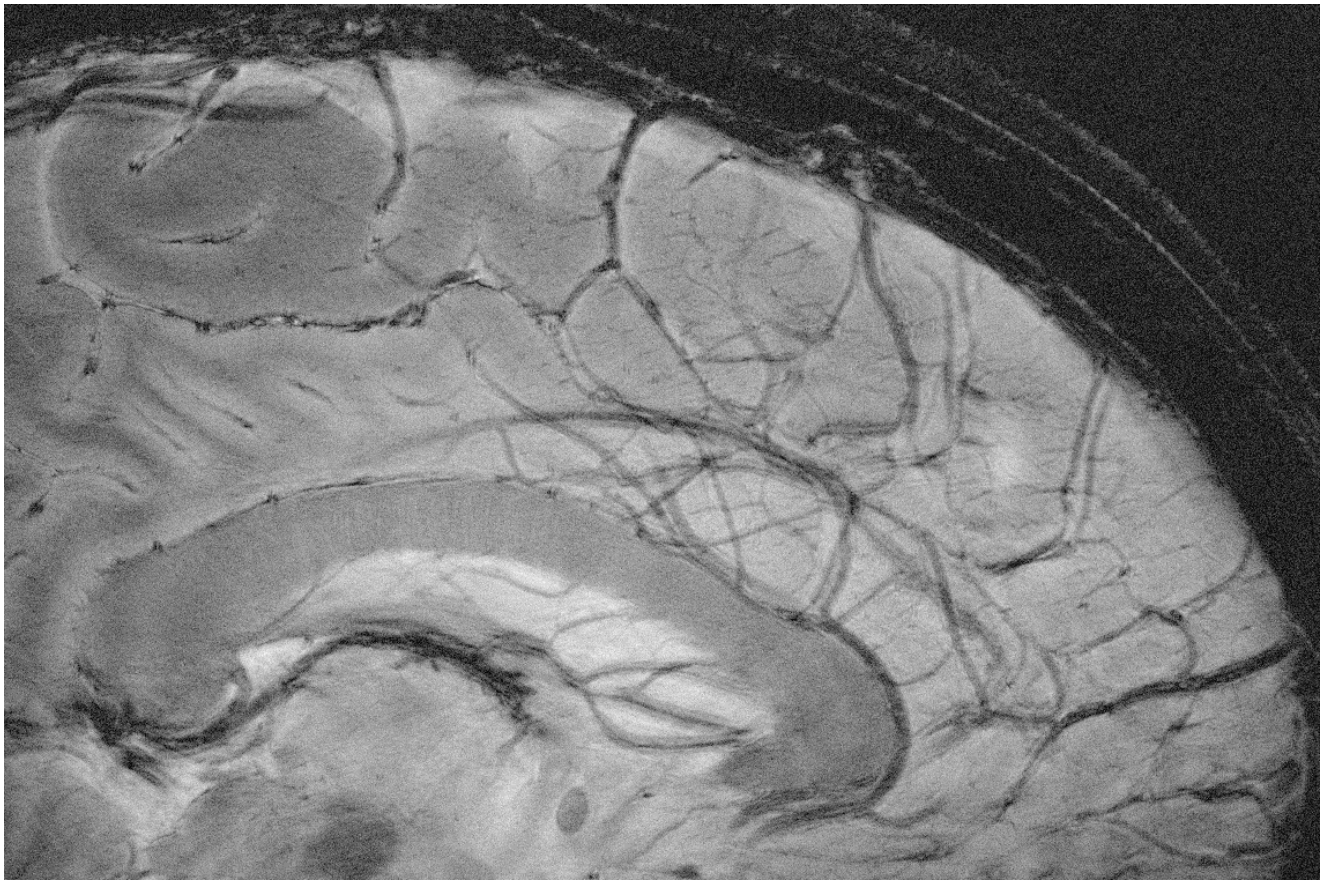

Fig. 9: Section (1139 × 758) of a high resolution sagittal image of the human head acquired at 8 Tesla. Acquisition parameters are as follows: acquisition sequence = gradient recalled echo, matrix size = 2,000 × 2,000, slice thickness = 2 mm, field of view 20 cm × 20 cm, repetition time = 750 msec, echo time = 17 msec, and nutation angle = 17 degrees. This image corresponds to Figure 3A in Robitaille P.M.L., Abduljalil A.M., Kangarlu A. Ultra high resolution imaging of the human head at 8 Tesla: 2K×2K for Y2K. *J Comp. Assist. Tomogr.*, 2000, v. 24, 2–7. Reprinted with permission.

same parameters as found for Figure 8. Despite higher resolution, the image has a signal to noise of ∼20. It did take longer to acquire, due to increased phase encoding steps, but the time per pixel remains less than that for Figure 8. Clearly, signal to noise can purchase both contrast and resolution.

Images with high signal to noise also tend to be "reliable". Namely, their gross features are rarely affected by minor fluctuations, in either the instrument or the sample. High signal to noise images tend to have the quality of stability and reproducibility, attributes which are often lost in low signal to noise images. In fact, the only measure of reliability for a low signal to noise image is reproducibility. It is important to establish that a low signal to noise image does not change from one acquisition to the next.

Figure 10A-C displays three low signal to noise images. In these images, a computer has added random noise, such that the final signal to noise is ∼2.5:1 in each case. Figure 10A corresponds to an axial image of the human head. Its identity is revealed by the presence of signal arising both from the brain and the scalp. The image is relatively uniform in signal, making the assignment simple. Figure 10B corresponds to a photograph of the Moon. The subject can be distinguished from other spherical objects (a baseball, the Sun, etc.) through the gentle change in contrast, produced by craters on the lunar surface. The object is difficult to identify since the shape provides few clues. Figure 10C corresponds to an MRI image of the author's wrist. In this image, it is increasingly difficult to ascertain the source. The maximal signal to noise remains ∼2.5:1. However, the signal distribution is no longer uniform. Faint features can be seen on the image, but no detail. Inhomogeneous signal distributions often make images more challenging to interpret, particularly when the origin of the sample is not known.

In Figure 11A-C, the images of Figure 10A-C are reproduced, but this time the signal to noise is at least 5:1. A nearly 10-fold increase in signal to noise for the head image (A) is now associated with increased contrast. The same holds true for the wrist image displayed (C) with a signal to noise of ∼40:1. Thus, the first rule of image contrast is that it is non-existent on low signal to noise images. It takes signal to make contrast. If the images in Figure 11 look so much more appealing, it is because they have higher signal to noise and contrast. It is also interesting that a mere doubling of signal to noise has such a dramatic effect for the Moon image. This highlights that there is also an enormous difference between an image with a 1.5:1 signal to noise and an image with a 2.5:1 signal to noise.

Unfortunately, in the WMAP images, the maximum signal to noise is just in excess of 1. This can be ascertained in Figures 12 and 13. Figure 12 displays a map of instrument noise released by NASA for WMAP. The largest signals on this map have a noise power of approximately 70 uK. Figure 12 displays a corresponding map, created by combining the Q and V bands. The galactic plane dominates the figure with

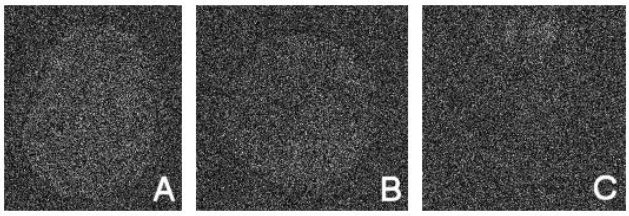

Fig. 10: A set of images generated by adding random noise to the images displayed in Figure 11. A maximum signal to noise of ∼2.5:1 is now illustrated. (A) MRI image of the human head at 1.5 Tesla, (B) photographic image of the Moon, and (C) MRI image of the author's wrist acquired at 8 Tesla.

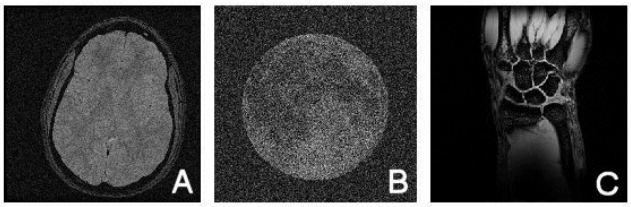

Fig. 11: Images displaying varying signal to noise. (A) MRI image of the human head at 1.5 Tesla with signal to noise ∼20:1, (B) photographic image of the Moon with the signal to noise adjusted to ∼5:1, and (C) MRI image of the human wrist acquired at 8 Tesla with the signal to noise ∼40:1. Note the dramatic effect on image quality for the moon image (B) in simply doubling the signal to noise (see Figure 10B).

signal truncated at the 100 uK level. Outside the galactic plane, few signals, if any, exist at the 100 uK level. As such, by combining the information in Figure 13 with the image in Figure 12, it is clear that the WMAP signal to noise is below 2:1 and probably below 1.5. In fact, since these images are obtained by difference methods, the signal to noise at many locations is much less than 1. It is clear that some of the data points on these images have signal values of 0. Therefore, the real signal to noise on the anisotropy maps is somewhere between 0 and 1.5 at all locations. Note, in contrast, that the example images in Figures 10A, B, and C had a maximum signal to noise of ∼2.5:1, well in excess of WMAP and without the presence of a contaminating foreground.

Relative to signal to noise, the WMAP team is unable to confirm that the anisotropic "signal" observed at any given point is not noise. The act of attributing signal characteristics to noise does not in itself create signal. Reproducibility remains the key, especially when signal to noise values are low.

2.2.4 Reproducibility

The presence of low signal to noise on an image is not unusual in science, and many a great discovery has been made through the careful analysis of the faintest signals. In medicine, the tremendous advancements in functional MRI mapping of the brain [44–46] stand perhaps without rival,

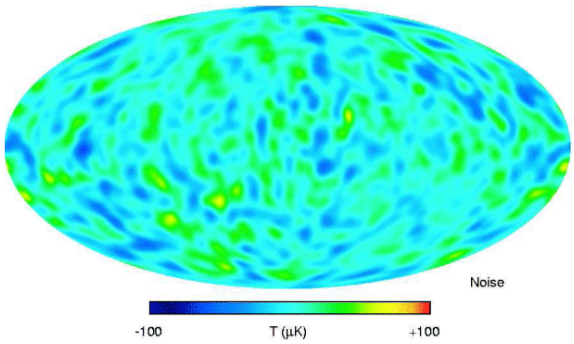

Fig. 12: Map of the instrument noise for WMAP. This image corresponds to the lower portion of Figure 9 in Bennett et. al. [7]. Reproduced with permission of the AAS. Image provided courtesy of the NASA/WMAP team.

relative to lack of signal to noise and the profoundness of the implications. Whenever the signal to noise is low, care must be exercised such that noise is not mistaken for signal. The key to this problem is reproducibility.

In medicine, when an image has poor signal to noise, it is vital that its central features be reproducible.

In fact, the only measure of reliability for a low signal to noise image is reproducibility. The information contained within the image must not change from one acquisition to the next. Correlation between an event and the change in an image are also powerful indicators that the change is real. This principle has been applied extensively in human functional MRI [44–46]. In this case, cognitive tasks, such as visual activation or finger tapping, can be directly correlated to very small changes on the MRI images of the human brain [44–46]. Often, changes on a pixel by pixel basis, with a signal to noise change on the order of 5:1 or even less, can be trusted simply based on correlation. In medicine, whenever a known physiological change (blood flow, blood oxygenation level, and myocardial contraction) can be correlated to radiological changes, even low signal to noise images can yield powerful diagnostic conclusions. Three components in this case act in unison to produce the diagnosis: instrument stability, image reproducibility, and the presence of correlation.

Note, most importantly, that in medicine, when low signal to noise images are used for diagnosis, it is never in the presence of strong overlapping contaminating signal. Moreover, in human functional imaging, a set of control images are acquired to help ensure that all perceived changes are real.

Unfortunately for WMAP, not only are the images obscured by galactic contamination, but they do not appear to be reproducible. In this regard, it is concerning that the WMAP team chooses to alter the ILC coefficients for generating section 0 from year to year. In fact, the coefficients used in year-1 (0.109, −0.684, −0.096, 1.921, and −0.250) are substantially different from those used in presenting a 3-year average (0.1559, −0.8880, 0.0297, 2.0446, and

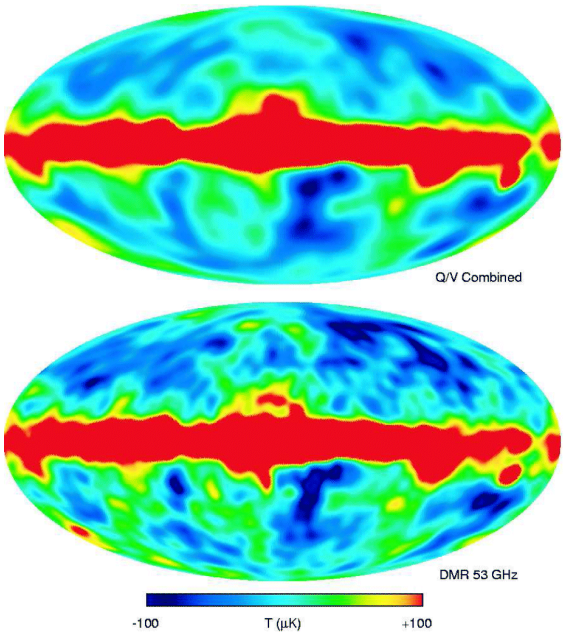

Fig. 13: The 53 GHz map from COBE (bottom) and the combined Q/V map generated by the WMAP team. This Figure corresponds to Figure 8 in Bennett et. al. [7]. Reproduced with permission of the AAS. Image provided courtesy of the NASA/WMAP team.

−0.3423). The coefficient for K band has changed by nearly 50%, while the coefficient for Q band not only changes sign, but decreases in magnitude by a factor of 3. Such changes cannot be simply explained by variations in instrument gain over time. The WMAP team does describe an attempt to find the maximum likelihood map in the 3-year data presentation. This new approach may account for some of the variability. Nonetheless, the WMAP team should have reprocessed the data from all years using this new approach, so that a direct comparison could be made between images processed with identical parameters.

It is also concerning that the WMAP team does not present separate ILC images for years 1, 2, and 3. Rather, after presenting the year-1 ILC image in 2003, they then compare it only to the 3-year average in 2006. However, the 3-year average contains data from the first year. The proper test for reproducibility involves the comparison of each yearly ILC image with one another, without invoking the 3-year average. Ideally, difference ILC images should be taken from year-1 and year-2, year-2 and year-3, and finally from year-1 and year-3. The WMAP team neglects to present these vital comparisons.

Despite these objections, the first year image simply does not agree with the 3-year average. It is true that the images generally agree, but this does not occur on a pixel by pixel, or even a regional basis. This can be readily visualized in the difference images displayed in Figures 14 and 15. In fact, the situation is actually worse than can be easily gathered, since the coefficients used in generating the first year ILC maps

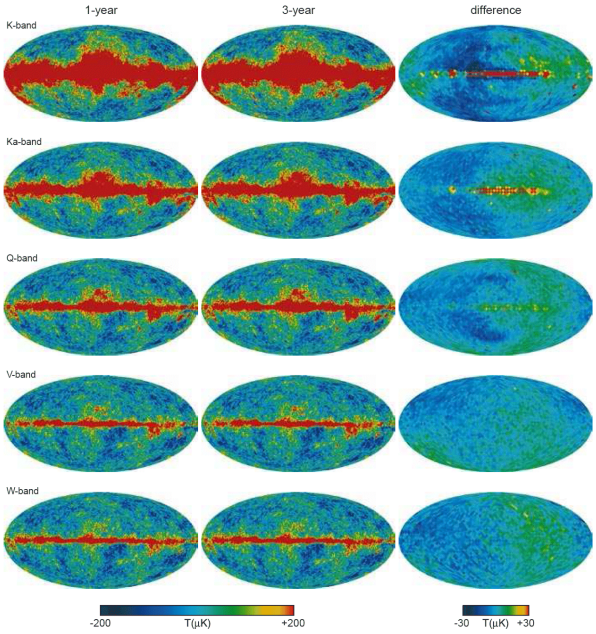

Fig. 14: Comparison of 3-year average data with year-1 data through difference for the K, Ka, Q, V, and W bands of the WMAP satellite. Note that the difference images are shown with reduced resolution contrary to established practices in imaging science. This figure corresponds to Figure 3 in Hinshaw et. al. [23]. Reproduced with permission of the AAS. Image provided courtesy of the NASA/WMAP team.

do not agree with those used for the 3-year average map. The comparison made by the WMAP team in Figure 15 is not valid, since the images were generated using different coefficients.

Perhaps most troubling, the WMAP team chooses to reduce the resolution on its difference images. This approach is known to minimize apparent differences. In imaging, the only resolution which can be claimed is that which can be trusted on difference. As such, if the difference images must be degraded to a pixel resolution of 4 degrees, then the WMAP team cannot claim to have imaged the sky at a 1 degree resolution.

Tremendous variability can be observed in the WMAP data sets. This is apparent by examining the variability found in the galactic foreground. It has been well established in astrophysics that galaxies can contain Active Galactic Nuclei. These have been studied extensively outside the microwave region [47]. These nuclei can vary by an order of magnitude in certain frequency bands [47]. Even in the microwave, it is clear that our own galaxy is highly variable from year to year. This is evidenced by the need to change, from year to year, the coefficients required to null the galactic contribution. The galaxy is highly variable in the microwave relative to the magnitude of any real anisotropy. This is an observation which could be made by examining old data from COBE [48]. Given this state, it is also clear that every galaxy in the

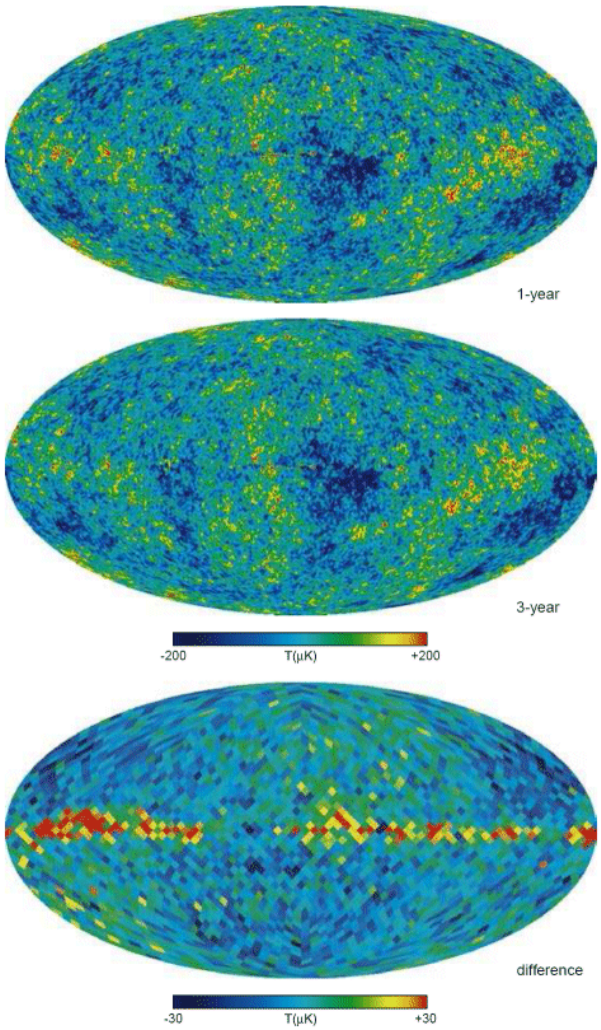

Fig. 15: Comparison of the 3-year average ILC map with the year-1 ILC map. Note that the difference images are shown at reduced resolution contrary to established practices in imaging science. This figure corresponds to Figure 9 in Hinshaw et. al. [23]. Reproduced with permission of the AAS. Image provided courtesy of the NASA/WMAP team.

Universe will also share in this variability in a manner which is completely dissociated from any cosmological implication. Indeed, herein lies another great problem for the cosmologist. It is impossible to visualize, in our lifetime, the true simple galactic variability not only from our galaxy, but from every other galaxy. Even a signal which appears stable over the course of humanity's existence may well be variable.

Consider the case where only 4 pixels vary substantially over the course of the WMAP experiment from year-1 to year-4. From this situation, it can be expected that as many as 1,000 pixels might vary over the course of 1,000 years. Yet, 1,000 years is barely on the cosmological timescale. Over the course of 1,000,000 years, a total of 1,000,000 pixels could be potentially affected. Even 1,000,000 years is just starting to be meaningful relative to cosmology. As a

result, the situation relative to WMAP and COBE is extremely difficult. In reality, in order to have true cosmological meaning, the maps must be temporally stable well beyond what has been determined to date. The situation is much worse than the hypothetical case described above, as significantly more than 4 pixels will vary between year-4 and year-1. The requirements for image stability in cosmology is well beyond the reach of both COBE and WMAP.

2.3 The flat model of the Universe

Bennett et. al. [7] claim that the WMAP results are consistent with a 2-dimensional flat model of the Universe. Clearly, by their intrinsic nature, these images are incapable of supporting any higher order model. WMAP cannot establish the origin of the photons which it detects other than in a directional sense. The satellite is completely unable to differentiate data based on distance to the source. In this respect, WMAP images resemble classic X-rays in medicine. Such images are 2-dimensional and unable to reveal the 3-dimensional nature of the human being. WMAP and X-rays stand in sharp contrast to the CT and MRI systems of today, which are able to provide a true 3-dimensional visualization of the human body. That the flat model of the Universe can be fitted is completely appropriate, given that this data cannot be utilized to model a 3-dimensional Universe.

2.4 The assignment of brightness temperature

Perhaps the most serious concern relative to the Penzias and Wilson, COBE, and WMAP findings involves the assignment of brightness temperatures [49]. The Universe is not in thermal equilibrium with a perfectly absorbing enclosure [49, 50, 51, 52]. As a result, the assignment of these temperatures constitutes a violation of Kirchhoff's Law [50, 52]. It is improper to assign a temperature merely because a spectrum has a thermal appearance. That a spectrum appears thermal does not imply that it was generated by a blackbody [52, 53]. Indeed, the proper application of the laws of Planck [54], Stefan [55], and Wien [56] requires that the emitting sample corresponds to a solid, best approximated on Earth by graphite or soot [50]. It has been advanced [49, 57–59], and it is herein restated, that the monopole signal first detected by Penzias and Wilson, and later confirmed by COBE, will eventually be reassigned to the oceans of the Earth. The brightness temperature does not appear to make any sense precisely because the oceans fail to meet the requirements set forth by Kirchhoff in assigning a temperature [50, 52, 53].

In this regard, the basis of universality in blackbody radiation has come under serious question [52, 53]. Blackbody radiation is not universal. Rather, it is strictly limited to an experimental setting which, on Earth, is best approximated by graphite and soot [52]. That Kirchhoff interchangeably used either an adiabatic enclosure or an isothermal one was a natural extension of his belief in universality. Nonetheless, it appears that the adiabatic case is not valid [52]. Kirchhoff's experiments far from supporting universality, actually constrains blackbody radiation to the perfect absorber [52]. Conditions for assigning a blackbody temperature are even more stringent [52] than previously believed [58]. As such, an adiabatic enclosure is not sufficient [52, 58]. Rather, in order to obtain a proper temperature, the enclosure can only be perfectly absorbing and isothermal. The assignment of these temperatures by the WMAP team constitutes an overextension of the fundamental laws which govern thermal emission, given the lack of universality [52, 53].

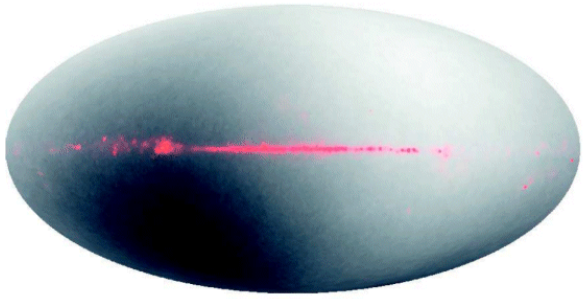

Fig. 16: The microwave dipole observed by the WMAP satellite. This image corresponds to the upper portion of Figure 10 in Bennett et. al. [7]. Reproduced with permission of the AAS. Image provided courtesy of the NASA/WMAP team.

2.5 The Dipole Temperature

Despite this discussion, it is nonetheless clear that the WMAP satellite has detected a CMB dipole signal presumably associated with motion of the local group [7, 23]. The dipole signal is shown in Figure 16. The presence of a dipole is thought, by many, as further proof for the presence of the monopole signal at the position of WMAP. The detection of this dipole by WMAP constitutes a finding of importance as it confirms earlier findings, both by the COBE team [60] and by the Soviet Relikt-1 mission [61]. Indeed, the discussion of the dipole is sufficiently important to be treated separately [62].

3 Conclusion

Analysis of data from WMAP exposes several problems which would not be proper in medical imaging. Experience from NMR spectroscopy relative to biological samples reveals that removal of a contaminating signal, which exceeds the signal of interest by up to a factor of 1,000, requires ability to control the sample at the source. This requirement can never be met by the WMAP team. It is impossible to remove this contamination and thereby "see beyond the galaxy". It is also dangerous to mathematically manipulate large signals during image reconstruction, especially when the final images have low signal to noise ratios. The

galactic signal is not stable from year to year, making signal removal a daunting task as seen by the yearly changes in ILC coefficients for regions 1–11. In actuality, the WMAP team must overcome virtually every hurdle known to imaging: foreground contamination and powerful dynamic range issues, low signal to noise, poor contrast, limited sample knowledge, lack of reproducibility, and associated resolution issues. It is clear that the generation of a given anisotropy map depends strictly on the arbitrary weighting of component images. The WMAP team attempts to establish a "most likely" anisotropy map using mathematical tools, but they have no means of verifying the validity of the solution. Another team could easily produce its own map and, though it may be entirely different, it would be equally valid. Figure 5 points to this fact. It remains surprising that separate ILC maps are not presented for years 1, 2, and 3. In addition, the WMAP team does not use the proper tests for reproducibility. Difference images between all three yearly ILC maps should be presented, without lowering the final resolution, and without changing the ILC coefficient from year to year. It is improper to compare images for reproducibility if they are not processed using identical methods. Reproducibility remains a critical issue for the WMAP team. This issue will not be easily overcome given human technology. In order to make cosmological interpretations, the WMAP images must be perfectly stable from year to year. Even fluctuation at the level of a few pixels has dramatic consequences, since the data must be stable on a cosmological timescale. This timescale extends over hundreds, perhaps thousands, or even millions of years. Finally, there are fundamental issues at stake, relative to the application of the laws of Kirchhoff [50], Planck [54], Stefan [55], and Wien [56]. It has not been established that the WMAP team is theoretically justified in assigning these temperatures.

The only significant observations relative to this satellite are related to the existence of a dipole signal [7, 23]. This confirms findings of both the NASA COBE [60], and the Soviet Relitk, satellites [61]. The WMAP satellite also highlights that significant variability exists in the point sources and in the galactic foreground. Relative to the Universe, the findings imply isotropy over large scales, not anisotropy. All of the cosmological constants which are presented by the WMAP team are devoid of true meaning, precisely because the images are so unreliable. Given the tremendous dynamic range problems, the inability to remove the galactic foreground, the possibility of generating galactic ghosts through "cleaning", the lack of signal to noise, the lack of reproducibility, the use of coefficients which fluctuate on a yearly basis, and the problem of monitoring results on a cosmological timescale, attempts to determine cosmological constants from such data fall well outside the bounds of proper image interpretation.

In closing, it may well be appropriate to reflect once again on the words of Max Planck [63]:

> "The world is teeming with problems. Wherever man looks, some new problems crops up to meet his eye — in his home life as well as in his business or professional activity, in the realm of economics as well as in the field of technology, in the arts as well as in science. And some problems are very stubborn; they just refuse to let us in peace. Our agonizing thinking of them may sometimes reach such a pitch that our thoughts haunt us throughout the day, and even rob us of sleep at night. And if by lucky chance we succeed in solving a problem, we experience a sense of deliverance, and rejoice over the enrichment of our knowledge. But it is an entirely different story, and an experience annoying as can be, to find after a long time spent in toil and effort, that the problem which has been preying on one's mind is totally incapable of any solution at all."

Acknowledgements

The author would like to thank The Ohio State University for ongoing support. Luc Robitaille was responsible for the retrieval and preparation of all figures for the manuscript. The assistance of Professor Robert W. Curley is acknowledged for sample preparation and NMR acquisition required in Figure 3. The members of the Center for Advanced Biomedical Imaging associated with the design and construction of the 8 Tesla UHFMRI system [40–41] are acknowledged for enabling the acquisition and processing of the images displayed in Figures 6, 8, 9, 10, and 11.

First published online on November 01, 2006
Corrections posted online on December 30, 2006

References

1. WMAP website, http://map.gsfc.nasa.gov/.
2. Seife C. Breakthrough of the year: illuminating the dark Universe. *Science*, 2003, v. 302, 2038–2039.
3. Bennett C.L., Bay M., Halpern M., Hinshaw G., Jackson C., Jarosik N., Kogut A., Limon M., Meyer S.S., Page L., Spergel D.N., Tucker G.S., Wilkinson D.T., Wollack E., Wright E.L. The Microwave Anisotropy Probe mission. *Astrophys. J.*, 2003, v. 583(1), 1–23.
4. Jarosik N., Bennett C.L., Halpern M., Hinshaw G., Kogut A., Limon M., Meyer S.S., Page L., Pospieszalski M., Spergel D.N., Tucker G.S., Wilkinson D.T., Wollack E., Wright E.L., Zhang Z. Design, implementation and testing of the MAP radiometers. *Astrophys. J. Suppl. Ser.*, 2003, v. 145(2), 413–436.
5. Page L., Jackson C., Barnes C., Bennett C.L., Halpern M., Hinshaw G., Jarosik N., Kogut A., Limon M., Meyer S.S., Spergel D.N., Tucker G.S., Wilkinson D.T., Wollack E., Wright E.L. The optical design and characterization of the

Wilkinson Microwave Anisotropy Probe. *Astrophys. J.*, 2003, v. 585(1), 566–586.

6. Barnes C., Limon M., Page L., Bennett C.L., Bradley S., Halpern M., Hinshaw G., Jarosik N., Jones W., Kogut A., Meyer S., Motrunich O., Tucker G., Wilkinson D., Wollack E. The MAP satellite feed horns. *Astrophys. J. Suppl. Ser.*, 2002, v. 143(2), 567–576.
7. Bennett C.L., Halpern M., Hinshaw G., Jarosik N., Kogut A., Limon M., Meyer S.S., Page L., Spergel D.N., Tucker G.S., Wollack E., Wright E.L., Barnes C., Greason M.R., Hill R.S., Komatsu E, Nolta M.R., Odegard N., Peiris H.V., Verde L, Weiland J.L. First-year Wilkinson Microwave Anisotropy Probe (WMAP) observations: preliminary maps and basic results. *Astrophys. J. Suppl. Ser.*, 2003, v. 148(1), 1–27.
8. Hinshaw G., Barnes C., Bennett C.L., Greason M.R., Halpern M., Hill R.S., Jarosik N., Kogut A., Limon M., Meyer S.S., Odegard N., Page L., Spergel D.N., Tucker G.S., Weiland J.L., Wollack E., Wright E.L. First year Wilkinson Microwave Anisotropy Probe (WMAP) observations: data processing methods and systematic error limits. *Astrophys. J. Suppl. Ser.*, 2003, v. 148(1), 63–95.
9. Jarosik N., Barnes C., Bennett C.L, Halpern M., Hinshaw G., Kogut A., Limon M., Meyer S.S., Page L., Spergel D.N., Tucker G.S., Weiland J.L., Wollack E., Wright E.L. First year Wilkinson Microwave Anisotropy Probe (WMAP) observations: on-orbit radiometer characterization. *Astrophys. J. Suppl. Ser.*, 2003, v. 148(1), 29–37.
10. Page L., Barnes C., Hinshaw G., Spergel D.N., Weiland J.L., Wollack E., Bennett C.L., Halpern M., Jarosik N., Kogut A., Limon M., Meyer S.S., Tucker G.S., Wright E.L. First year Wilkinson Microwave Anisotropy Probe (WMAP) observations: beam profiles and window functions. *Astrophys. J. Suppl. Ser.*, 2003, v. 148(1), 39–50.
11. Barnes C., Hill R.S., Hinshaw G., Page L., Bennett C.L., Halpern M., Jarosik N., Kogut A., Limon M., Meyer S.S., Tucker G.S., Wollack E., Wright E.L. First year Wilkinson Microwave Anisotropy Probe (WMAP) observations: galactic signal contamination from sidelobe pickup. *Astrophys. J. Suppl. Ser.*, 2003, v. 148(1), 51–62.
12. Bennett C.L., Hill R.S., Hinshaw G., Nolta M.R., Odegard N., Page L., Spergel D.N., Weiland J.L., Wright E.L., Halpern M., Jarosik N., Kogut A., Limon M., Meyer S.S., Tucker G.S., Wollack E. First year Wilkinson Microwave Anisotropy Probe (WMAP) observations: foreground emission. *Astrophys. J. Suppl. Ser.*, 2003, v. 148(1), 97–117.
13. Hinshaw G., Spergel D.N, Verde L., Hill R.S, Meyer S.S, Barnes C., Bennett C.L., Halpern M., Jarosik N., Kogut A., Komatsu E., Limon M., Page L., Tucker G.S., Weiland J.L., Wollack E., Wright E.L. First year Wilkinson Microwave Anisotropy Probe (WMAP) observations: the angular power spectrum. *Astrophys. J. Suppl. Ser.*, 2003, v. 148(1), 135–159.
14. Kogut A., Spergel D.N., Barnes C., Bennett C.L., Halpern M., Hinshaw G., Jarosik N., Limon M., Meyer S.S., Page L., Tucker G.S., Wollack E., Wright E.L. First year Wilkinson Microwave Anisotropy Probe (WMAP) observations: temperature-polarization correlation. *Astrophys. J. Suppl. Ser.*, 2003, v. 148(1), 161–173.
15. Spergel D.N., Verde L., Peiris H.V., Komatsu E., Nolta M.R., Bennett C.L., Halpern M., Hinshaw G., Jarosik N., Kogut A., Limon M., Meyer S.S., Page L., Tucker G.S., Weiland J.L., Wollack E., Wright E.L. First year Wilkinson Microwave Anisotropy Probe (WMAP) observations: determination of cosmological parameters. *Astrophys. J. Suppl. Ser.*, 2003, v. 148, 175–194.
16. Verde L., Peiris H.V., Spergel D.N., Nolta M.R., Bennett C.L., Halpern M., Hinshaw G., Jarosik N., Kogut A., Limon M., Meyer S.S., Page L., Tucker G.S., Wollack E., Wright E.L. First year Wilkinson Microwave Anisotropy Probe (WMAP) observations: parameter estimation methodology. *Astrophys. J. Suppl. Ser.*, 2003, v. 148(1), 195–211.
17. Peiris H.V., Komatsu E., Verde L., Spergel D.N., Bennett C.L., Halpern M., Hinshaw G., Jarosik N., Kogut A., Limon M., Meyer S.S., Page L., Tucker G.S., Wollack E., Wright E.L. First year Wilkinson Microwave Anisotropy Probe (WMAP) observations: implications for inflation. *Astrophys. J. Suppl. Ser.*, 2003, v. 148(1), 213–231.
18. Page L., Nolta M.R., Barnes C., Bennett C.L., Halpern M., Hinshaw G., Jarosik N., Kogut A., Limon M., Meyer S.S., Peiris H.V., Spergel D.N., Tucker G.S., Wollack E., Wright E.L. First year Wilkinson Microwave Anisotropy Probe (WMAP) observations: interpretation of the TT and TE angular power spectrum peaks. *Astrophys. J. Suppl. Ser.*, 2003, v. 148(1), 233–241.
19. Komatsu E., Kogut A., Nolta M.R., Bennett C.L., Halpern M., Hinshaw G., Jarosik N., Limon M., Meyer S.S., Page L., Spergel D.N., Tucker G.S., Verde L., Wollack E., Wright E.L. First year Wilkinson Microwave Anisotropy Probe (WMAP) observations: tests of Gaussianity. *Astrophys. J. Suppl. Ser.*, 2003, v. 148(1), 119–134.
20. Barnes C., Bennett C.L., Greason M.R., Halpern M., Hill R.S., Hinshaw G., Jarosik N., Kogut A., Komatsu E., Landsman D., Limon M., Meyer S.S., Nolta M.R., Odegard N., Page L., Peiris H.V., Spergel D.N., Tucker G.S., Verde L., Weiland J.L., Wollack E., Wright E.L. First year Wilkinson Microwave Anisotropy Probe (WMAP) observations: explanatory supplement. http://lambda.gsfc.nasa.gov/product/map/pub_papers/firstyear/supplement/WMAP_supplement.pdf
21. Nolta M.R., Wright E.L., Page L., Bennett C.L., Halpern M., Hinshaw G., Jarosik N., Kogut A., Limon M., Meyer S.S., Spergel D.N., Tucker G.S., Wollack E. First year Wilkinson Microwave Anisotropy Probe observations: dark energy induced correlation with radio sources. *Astrophys. J.*, 2004, v. 608(1), 10–15.
22. Jarosik N., Barnes C., Greason M.R., Hill R.S., Nolta M.R, Odegard N., Weiland J.L., Bean R., Bennett C.L., Dore O., Halpern M., Hinshaw G., Kogut A., Komatsu E., Limon M., Meyer S.S., Page L., Spergel D.N., Tucker G.S., Wollack E., Wright E.L. Three-year Wilkinson Microwave Anisotropy Probe (WMAP) observations: beam profiles, data processing, radiometer characterization and systematic error limits. *Astrophys. J.*, 2006, *submitted*.
23. Hinshaw G., Nolta M.R., Bennett C.L., Bean R., Dore O., Greason M.R., Halpern M., Hill R.S., Jarosik N., Kogut A., Komatsu E., Limon M., Odegard N., Meyer S.S., Page L.,

Peiris H.V., Spergel D.N., Tucker G.S., Verde L., Weiland J.L., Wollack E., Wright E.L. Three-year Wilkinson Microwave Anisotropy Probe (WMAP) observations: temperature analysis. *Astrophys. J.*, 2006, *submitted*.

24. Page L., Hinshaw G., Komatsu E., Nolta M.R., Spergel D.N., Bennett C.L., Barnes C., Bean R., Dore O., Halpern M., Hill R.S., Jarosik N., Kogut A., Limon M., Meyer S.S., Odegard N., Peiris H.V., Tucker G.S., Verde L., Weiland J.L., Wollack E., Wright E.L. Three-year Wilkinson Microwave Anisotropy Probe (WMAP) observations: polarization analysis. *Astrophys. J.*, 2006, *submitted*.
25. Spergel D.N., Bean R., Dore O., Nolta M.R., Bennett C.L., Hinshaw G., Jarosik N., Komatsu E., Page L., Peiris H.V., Verde L., Barnes C., Halpern M., Hill R.S., Kogut A., Limon M., Meyer S.S., Odegard N., Tucker G.S., Weiland J.L., Wollack E., Wright E.L. Three-year Wilkinson Microwave Anisotropy Probe (WMAP) observations: implications for cosmology. *Astrophys. J.*, 2006, *submitted*.
26. Barnes C., Bean R., Bennett C.L., Dore O., Greason M.R., Halpern M., Hill R.S., Hinshaw G., Jarosik N., Kogut A., Komatsu E., Landsman D., Limon M., Meyer S.S., Nolta M.R., Odegard N., Page L., Peiris H.V., Spergel D.N., Tucker G.S., Verde L., Weiland J.L., Wollack E., Wright E.L. Three-year Wilkinson Microwave Anisotropy Probe (WMAP) observations: three year explanatory supplement. http://map.gsfc.nasa.gov/m_mm/pub_papers/supplement/wmap_3yr_supplement.pdf
27. NASA, new satellite data on Universe's first trillionth second. WMAP Press Release. http://map.gsfc.nasa.gov/m_or/PressRelease_03_06.html.
28. In-cites. "Super hot" papers in science published since 2003. http://www.in-cites.com/hotpapers/shp/1-50.html.
29. Tegmark M., de Oliveira-Costa A., Hamilton A.J.S. A high resolution foreground cleaned CMB map from WMAP. *Phys. Rev. D*, 2003, v. 68(12), 123523.
30. Robitaille P.M.L., Scott R.D., Wang J., Metzler D.E. Schiff bases and geminal diamines derived from pyridoxal 5'-phosphate and diamines. *J. Am. Chem. Soc.*, 1989, v. 111, 3034–3040.
31. Robyt J.F., White B.J. Biochemical techniques: theory and practice. Brooks/Cole Publishing Company, Monterey, CA, 1987, p. 261–262.
32. Schaefer J. Selective saturation of Carbon-13 lines in Carbon-13 Fourier transform NMR experiments. *J. Magn. Reson.*, 1972, v. 6, 670–671.
33. Plateau P., Guerron M. Exchangeable proton NMR without baseline distortion, using new strong pulse sequences. *J. Am. Chem. Soc.*, 1982, v. 104, 7310–7311.
34. Redfield A.G, Kunz S.D., Ralph E.K. Dynamic range in Fourier transform proton magnetic resonance. *J. Magn. Reson.*, 1975, v. 19, 114–117.
35. Sklenar V., Starcuk Z. 1-2-1 pulse train: a new effective method of selective excitation for proton NMR in water. *J. Magn. Reson.*, 1983, v. 54, 146–148.
36. Turner D.L. Binomial solvent suppression. *J. Magn. Reson.*, 1983, v. 54, 146–148.
37. Hurd R.E. Gradient enhanced spectroscopy. *J. Magn. Reson.*, 1990, v. 87(2), 422–428.
38. Moonen C.T.W., van Zijl P.C.M. Highly effective water suppression for in-vivo proton NMR-spectroscopy (DRYSTEAM). *J. Magn. Reson.*, 1990, v. 88(1), 28–41.
39. Cavanagh J., Fairbrother J.W., Palmer III A.G., Skelton N.J. Protein NMR spectroscopy: principles and practice. Academic Press, New York, 1995.
40. Robitaille P.M.L., Abduljalil A.M., Kangarlu A., Zhang X., Yu Y., Burgess R., Bair S., Noa P., Yang L., Zhu H., Palmer B., Jiang Z., Chakeres D.M., Spigos D. Human magnetic resonance imaging at eight Tesla. *NMR Biomed.*, 1998, v. 11, 263–265.
41. Robitaille P.M.L., Abduljalil A.M., Kangarlu A. Ultra high resolution imaging of the human head at 8 Tesla: 2K × 2K for Y2K. *J Comp. Assist. Tomogr.*, 2000, v. 24, 2–7.
42. Robitaille P.M.L., Berliner L.J. (eds). Biological magnetic resonance: ultra high field magnetic resonance imaging. Springer, New York, 2006.
43. Liang Z.P., Lauterbur P.C. Principles of magnetic resonance imaging: a signal processing perspective. IEEE Press, New York, 2000.
44. Belliveau J.W., Kennedy Jr. D.N., McKinstry R.C., Buchbinder B.R., Weisskoff R.M., Cohen M.S., Vevea J.M., Brady T.J., Rosen B.R. Functional mapping of the human visual cortex by magnetic resonance imaging. *Science*, 1991, v. 254(5032), 716–9.
45. Ogawa S., Tank D.W., Menon R., Ellermann J.M., Kim S.G., Merkle H., Ugurbil K. Intrinsic signal changes accompanying sensory stimulation: functional brain mapping with magnetic resonance imaging. *Proc. Natl. Acad. Sci. USA*, 1992, v. 89(13), 5951–5.
46. Bandettini P.A., Jesmanowicz A., Wong E.C., Hyde J.S. Processing strategies for time-course data sets in functional MRI of the human brain. *Magn. Reson. Med.*, 1993, v. 30(2), 161–73.
47. Gaskell C.M., Klimek E.S. Variability of active galactic nuclei from the optical to X-Ray regions. *Astronom. Astrophysic. Trans.*, 2003, v. 22(4–5), 661–679.
48. COBE web site, http://lambda.gsfc.nasa.gov/product/cobe/.
49. Robitaille P.M.L. NMR and the age of the Universe. *American Physical Society Centenial Meeting*, BC19.14, March 21, 1999.
50. Kirchhoff G. Ueber das Verhaltnis zwischen dem Emissionsvermogen und dem absorptionsvermogen der Körper für Waeme und Litcht. *Annalen der Physik*, 1860, v. 109, 275–301.
51. Planck M. The theory of heat radiation. Philadelphia, PA., P. Blakiston's Son, 1914.
52. Robitaille P.M.L. On the validity of Kirchhoff's law of thermal emission. *IEEE Trans. Plasma Sci.*, 2003, v. 31(6), 1263–1267.
53. Robitaille P.M.L. An analysis of universality in blackbody radiation. *Progr. in Phys.*, 2006, v. 2, 22–23.
54. Planck M. Ueber das Gesetz der energieverteilung in Normalspectrum. *Annalen der Physik*, 1901, v. 4, 553–563.

55. Stefan J. Ueber die Beziehung zwischen der Wärmestrahlung und der Temperature. *Sitzungsberichte der mathematischnaturwissenschaftlichen Classe der kaiserlichen Akademie der Wissenschaften*, Wien 1879, v. 79, 391–428.

56. Wien W. Ueber die Energieverteilung in Emissionspektrum eines schwarzen Körpers. *Ann. Phys.*, 1896, v. 58, 662–669.

57. Robitaille P.M.L. The MAP satellite: a powerful lesson in thermal physics. *Spring Meeting of the American Physical Society Northwest Section*, F4.004, May 26, 2001.

58. Robitaille P.M.L. The collapse of the Big Bang and the gaseous Sun. *New York Times*, March 17, 2002.

59. Robitaille P.M.L. WMAP: an alternative explanation for the dipole. *Fall Meeting of the American Physical Society Ohio Section*, E2.0001, 2006.

60. Fixsen D.L., Gheng E.S., Gales J.M., Mather J.C., Shafer R.A., Wright E.L. The Cosmic Microwave Background spectrum from the full COBE FIRAS data set. *Astrophys. J.*, 1996, v. 473, 576–587.

61. Klypin A.A, Strukov I.A., Skulachev D.P. The Relikt missions: results and prospects for detection of the Microwave Background Anisotropy. *Mon. Not. Astr. Soc.*, 1992, v. 258, 71–81.

62. Robitaille P.M.L. On the origins of the CMB: insight from the COBE, WMAP and Relikt-1 satellites. *Progr. in Phys.*, 2007, v. 1, 19–23.

63. Planck M. Scientific autobiography. Philosophical Library, New York, 1949.

On the Origins of the CMB: Insight from the COBE, WMAP, and Relikt-1 Satellites

Pierre-Marie Robitaille

Dept. of Radiology, The Ohio State University, 130 Means Hall, 1654 Upham Drive, Columbus, Ohio 43210, USA

E-mail: robitaille.1@osu.edu

The powerful "Cosmic Microwave Background (CMB)" signal currently associated with the origins of the Universe is examined from a historical perspective and relative to the experimental context in which it was measured. Results from the COBE satellite are reviewed, with particular emphasis on the systematic error observed in determining the CMB temperature. The nature of the microwave signal emanating from the oceans is also discussed. From this analysis, it is demonstrated that it is improper for the COBE team to model the Earth as a 285 K blackbody source. The assignment of temperatures to objects that fail to meet the requirements set forth in Kirchhoff's law constitutes a serious overextension of the laws of thermal emission. Using this evidence, and the general rule that powerful signals are associated with proximal sources, the CMB monopole signal is reassigned to the oceans. In turn, through the analysis of COBE, WMAP, and Relikt-1 data, the dipole signal is attributed to motion through a much weaker microwave field present both at the position of the Earth and at the second Lagrange point.

1 Introduction

More than 40 years have elapsed since Penzias and Wilson first reported the existence of a thermal signal in the microwave region of the electromagnetic spectrum [1]. This measurement of the "Cosmic Microwave Background (CMB)" has been viewed as one of the most important in the history of science. Cosmology is now inextricably linked to its validity. Given this realization, it remains interesting that the logical steps first made by Penzias and Wilson [1] have not come under more considered review.

Penzias and Wilson [1] made the assumption that their signal was thermal in origin and inferred that the source could be treated as an ideal blackbody [2]. Without acknowledging the strict requirements involved in setting a blackbody temperature [2–4], they made recourse to the laws of thermal radiation, obtaining a temperature of 3.5 ± 1.0 K [1]. Although the cosmos can never meet the requirements for enclosure set forth by Kirchhoff [2], Dicke et. al. [5] would ultimately assign the signal to the average temperature of the Universe. Penzias and Wilson were thought to have discovered the "CMB", a powerful signal bathing everything.

The COBE satellite [6–12] provided the most important confirmation of the thermal nature of the "CMB" [1]. This satellite is positioned at an elevation of $\sim$900 km above sea level. COBE also reaffirmed the presence of a dipole signal presumably associated with motion of the local group. The dipole signature had been clearly observed by the Soviet Relikt-1 satellite [13], nearly 10 years earlier. Eventually, the WMAP satellite would affirm the existence of the dipole signal [14–16].

2 COBE and the assignment of temperatures

2.1 The "CMB" monopole

In acquiring the "CMB" signal [1], COBE produced a nearly perfect spectrum [11]. The signal to noise from the FIRAS instrument is exceedingly high. The error bars constitute a small fraction of the linewidth and must be expanded, by a factor of 400, to be visualized [11]. The validity of the absolute temperature was not questioned. The source responsible was thought to be at $\sim$3 K. Soon, the "CMB" became the central experimental proof for the Big Bang [17].

It has always been understood, in communications, that powerful signals imply proximal sources. This practical knowledge was neglected [1, 5]. Yet, concerns should have lingered over the amount of power found in the "CMB" [1, 11]. In addition, the experimental justification, for setting blackbody temperatures, was overlooked. The belief, that blackbody radiation was universal [4], enabled the dismissal of all laboratory experiments relative to its nature [3].

The experimental [3] and theoretical [4] basis of universality has now been brought into question. Blackbody radiation is not universal in nature [4], but, rather, is strictly limited to a physical setting best approached by graphite and soot on Earth [3]. A spectrum, like the "CMB" signal [11], may well appear to be thermal, but the temperature will not be valid unless the requirements set forth in Kirchhoff's experiment are strictly followed [3].

The Planckian equation [18] remains detached from the physical world. Thermal emission is explained mathematically [4], without regard to the physical setting. Blackbody radiation is the only process in physics wherein the setting,

transition species, and energy levels are devoid of physical meaning [3, 4]. In large part, this is a result of the erroneous belief in universality [3, 4]. Given universality, temperatures were set without the inconvenience of laboratory constraints.

2.2 The "CMB" dipole

In addition to the "CMB" monopole, the COBE satellite reports a dipole signature associated with motion [7], confirming Relikt-1 findings [13]. The WMAP satellite has also detected this dipole signal [19]. The dipole is thought to reflect a doppler phenomenon associated with motion of the local group. Based on COBE measurements, the dipole has an amplitude of 3.353 ± 0.024 mK in a direction $(l, b) = (264.26^\circ \pm 0.33^\circ, 48.22^\circ \pm 0.13^\circ)$, where l is the Galactic longitude and b, the latitude [15]. A nearly identical value, of 3.346 ± 0.017 mK in a direction $(l, b) = (263.85^\circ \pm 0.1^\circ, 48.25^\circ \pm 0.04^\circ)$, has been reported by the WMAP team [15]. Interestingly, the COBE satellite was able to determine a dipole value both from the DMR and the FIRAS instruments [6, 7]. The WMAP satellite is equipped solely with differential radiometers, and measures the dipole in a manner similar to the DMR on COBE [6, 14].

3 An alternative assignment for the "CMB" signals

3.1 Assignment of the monopole

During flight, the COBE satellite experienced an anomaly. "Most of the occurrences were in the High Frequency Region known as the South Atlantic Anomaly" [8]. Since the anomaly was produced over the Atlantic, it is interesting that the "CMB" results are devoid of interfering oceanic signals. The COBE team describes thermal instabilities when the limb of the Earth appears above the shield of the satellite. Data acquired during such events are discarded, but the COBE shield is not adequate to guard the instrumentation from the effects of being immersed in a scattered oceanic signal.

From the days of Penzias and Wilson [1], the Earth has not been considered as a powerful contaminating source for the "CMB". The COBE team believes that the Earth can be modeled as a circular source of emission, with a radius of $\sim 61^\circ$ and a mean temperature of 285 K [9]. All scattering of microwave signals, by the atmosphere, is neglected. Whether the Penzias and Wilson signal [1] is measured from the ground, using balloons, or from COBE, the monopole signature is noticeably clean. However, based on the extent of the oceanic surface, and the known behavior of the oceans in the microwave, it is inappropriate to model the Earth as a 285 K source [21].

Water is a good absorber of microwave power. This forms the basis of practical microwave applications. In addition, submarine communications, at microwave frequencies, are not possible while submerged, indicating powerful absorption. The oceans may be good absorbers of microwave power, but they are certainly not equal emitters. This is because liquids can never be in compliance with Kirchhoff's law [3, 20]. Liquids attempt to reach thermal equilibrium through conduction, thermal radiation, and convection. In fact, Planck has warned that objects, which sustain convection currents, can never be treated as blackbodies [20]. Nonetheless, it is unreasonable to believe that the oceans will be microwave silent on emission [21].

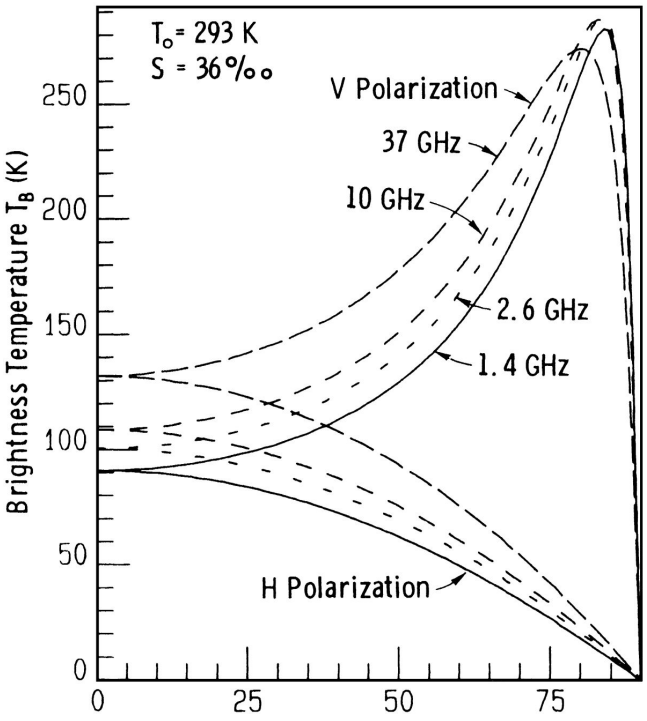

Fig. 1: Brightness temperature of a specular sea surface at 1.4, 2.6, 10, and 37 GHz. Note that when the angle of incidence approaches 90°, the brightness temperature of both the horizontal and vertical components falls to 0 K. As a result, the limb of the Earth appears as a source at nearly 0 K relative to COBE. The assumption that the Earth can be treated as a 285 K source is not valid. Reproduced by permission Figure 11.45 from F. T. Ulaby, R. K. Moore, A. K. Funk. Microwave remote sensing active and passive. — Volume 2: Radar remote sensing and surface scattering emission theory. Norwood (MA), Artech House, Inc., 1982. Copyright by Artech House, Inc., 1982.

The behavior of oceanic emissions in the microwave is not simple (see Figure 1), depending significantly on the angle of observation [21]. The oceans cannot be treated as a blackbody source simply based on this fact [3]. Note that the brightness temperature of the oceans is dependent on the angle of incidence. Brightness temperatures with a 0° angle of incidence are less than 130 K over the frequency range spanning 1.4–37 GHz. For the vertical polarization, the brightness temperature increases to ~ 270 K, as the angle of incidence is raised from 0° to $\sim 75^\circ$. The brightness tempe-

rature of the vertical polarization then precipitously drops to 0 K. For the horizontal polarization, the brightness temperature falls gradually from 100 to 0 K, as the incidence angle is increased from 0° to 90°. The situation relative to oceanic emission in the microwave is much more complex than currently assumed by the COBE team [21].

When these facts are combined with atmospheric scattering, concerns linger that the measured "CMB" signal is devoid of Earthly interference. It would have been reassuring if the "CMB" experiments were being contaminated by an oceanic signal whose contributions could not be easily suppressed. Yet, the Penzias and Wilson signal [1, 11] was devoid of external interference. Conversely, oceanographic studies reveal that the seas can produce signals with a brightness temperature near 0 K, as demonstrated in Figure 1. Given the power observed in the monopole [1, 11], it is reasonable that the oceans cannot produce interference in the measurements since, in reality, *they constitute the source of the "CMB"* [22–25].

3.2 Assignment of the dipole

It is currently believed that the dipole signal is being produced by motion of the Relikt-1, COBE, or WMAP satellites through a powerful "CMB" monopole field ascribed to the Universe. However, a second situation exists. The satellites could be flowing through a field much weaker than that detected on Earth. In this scenario, the strong monopole field detected on Earth does not exist at the position of WMAP [59]. Using the data available, it should be possible to distinguish between these two alternatives.

3.3 Absolute measurements and error bars in the COBE satellite

The source of Penzias and Wilson signal [1] and its assignment to the "CMB" may be resolvable from Earth. In the first scenario, discussed is section 3.2, the contribution to the dipole arises strictly from the "CMB" monopole, thought to be of cosmic origin. In the second scenario, the "CMB" temperature would reflect two effects: (1) the motion of the Earth through the weak microwave field also present at the position of WMAP, and (2) the additional effect from the monopole generated by the Earth. In this case, when viewed from COBE, the "CMB" temperature measured by FIRAS, and direct calibration, would not necessarily agree with that determined through visualization of the dipole.

Using the FIRAS instrument, COBE initially reports the "CMB" monopole temperature as 2.730 ± 0.001 K [11]. This temperature should have been extremely reliable, since the FIRAS data have tremendous signal to noise [11]. Moreover, FIRAS was equipped with an external calibrator [8]. In Fixsen et al. [11] the "CMB" temperature obtained from the dipole is first reported as 2.717 ± 0.003 K. These uncertainties are at the 1σ level. "By choosing the monopole temperature as the point to evaluate $dB\nu/dT$", the COBE team "has forced the dipole temperature to be that of the monopole" [7]. Despite this fact, the value of the "CMB" temperature, from the dipole measurement, is significantly lower than the value obtained from the monopole. The difference between these two numbers remains highly significant, even at the 99% confidence level. Considering the signal to noise using FIRAS, and the magnitude of the associated dipole, it is interesting that any systematic error exists. Such a dramatic divergence should not have been dismissed, especially since these two numbers might be expected to differ in the second scenario.

The COBE team also presents another method of assigning the "CMB" temperature, based on frequency calibration, using the CO and C^+ lines [11]. This third method yields a temperature of 2.7255 ± 0.0009 K [11]. This value rests on factors outside the "CMB" and the dipole. While appearing to be even more precise, this value may be more prone to error and less accurate. The key determinations remain those from FIRAS, with external calibration, and from the dipole.

In Fixsen et. al [11], the COBE team recognizes that the "CMB" temperatures derived, from the monopole and from the dipole, are irreconcilable. They attribute the difference to systematic errors. In order to address this issue, the error bars on the dipole measure are arbitrarily raised to 0.007 [11]. All statistical significance is removed to account for systematic error arising from the galactic cut [11]. The inequality in these two numbers was later reexamined. In Mather et al. [12], the absolute value of the "CMB" temperature assigned using FIRAS, and the external calibrator, is shifted to $2.725 \pm$ ± 0.002 K (2σ; 95% confidence interval). The change is attributed to systematic errors in the calibrator [12]. Yet, in Fixsen et al. [11], the FIRAS measure was thought to be accurate to within 1 mK, based on pre-flight calibration. The new value for the "CMB" temperature, provided by FIRAS, of 2.725 ± 0.002 K (2σ; 95% confidence interval), is now statistically different from the original value, of 2.730 ± 0.001 K (1σ), reported by the same instrument [11, 12].

The COBE FIRAS data has excellent signal to noise. Thus, it is troubling that a significant recalibration must be completed, nearly 10 years after launch. In the end, the prudent approach is to consider that the "CMB" temperatures, obtained from the monopole (2.730 ± 0.001 K at 1σ) and the dipole (2.717 ± 0.003 K at 1σ), are indeed significantly different, as initially reported. It is inappropriate to make so many adjustments for "systematic errors", and thereby remove a highly significant difference between two numbers, long after completion of an experiment, especially given that COBE remains in orbit.

If the "CMB" signal truly originates for the Universe, the "CMB" temperatures evaluated, from the dipole and from FIRAS, with external calibration, must be identical. However, the values might be expected to be different in the second scenario, wherein the "CMB" arises from the Earth

and a much weaker field is present in the Universe. As a result, it appears that the COBE satellite provides the first evidence that the "CMB" monopole does indeed arise from the Earth. The systematic error, first detected by COBE in the dipole evaluation of the "CMB" temperature [11], may be, in actuality, the critical proof.

The European Space Agency is now in the final stages of preparation for launching the PLANCK satellite [26]. This satellite is also equipped to scan the sky in the microwave band. Unlike WMAP, the PLANCK instruments are not differential. Consequently, this satellite should be able to finally establish that the Penzias and Wilson signal [1] does indeed arise from the Earth. Once positioned at L2, PLANCK will fail to detect the monopole signal [1]. Instead, its instrument will report only the galactic signal, the variable sources, and the weak noisy background currently attributed to anisotropy.

4 Conclusions

When Penzias and Wilson used thermodynamic principles to set a temperature of 3.5 K, they did not consider the phases of matter [1]. The signal did not change with the seasons [1], and the Earth was not at ∼3 K, so Dicke et. al. [5] surmised that it originated from the Universe. A powerful spectrum was present, but the concept that the receiver must be close to the source was not considered. They believed, much like Planck [20], that the laws of thermal emission [18, 27, 28] were universally applicable. Yet, Kirchhoff's law states that, for a blackbody, the temperature must be determined in the presence of thermal equilibrium, within an enclosure [2–4]. The Universe can never meet this requirement.

The oceans of the Earth cannot be treated as blackbodies, as demonstrated in Figure 1. The possibility should be considered that they are emitting at an apparent temperature, T_{app}, such that $T_{app} = T/\alpha$, where T corresponds to the real temperature and α is ∼100. Alpha may have a slight temperature or salinity dependence, since the Penzias and Wilson signal [1, 11] reflects a single spectrum. It is advanced that the apparent temperature, T_{app}, discussed above, corresponds to the ∼3 K signature previously assigned to the Cosmos. Through this simple introduction of α and T_{app}, the laws of Planck [18], Wien [27], and Stefan [28] can be reformulated for our oceans. This is the case, even if the oceans can produce additional emissions, in the infrared band, or elsewhere. The inclusion of an apparent temperature solves a problem, but the temperature is no longer real. Condensed matter physics may benefit in dissecting the lattice behavior responsible for oceanic emissions. In doing so, they may discover the importance in thinking, like Planck [18], of physical oscillators [25].

In regard to the interaction of the oceanic monopole signal, produced by the Earth, and the dipole signal, produced by motion through a weak microwave field of external origin, further insight may require the application of General Relativity [29].

It remains true that the temperature of the Universe can never be measured. That is a limitation given to us by Kirchhoff's law [2–4]. The enclosure required by Kirchhoff, during the experimental characterization of blackbody radiation, cannot be removed. At the same time, Kirchhoff's belief in universality is incorrect [3]. Indeed, this simple error will ultimately be viewed as the central oversight relative to the assignment of the Penzias and Wilson signal [1]. Kirchhoff erred 140 years ago relative to universality [3], and science failed to realize the profound implications [30]. There continues to be a lack of understanding relative to the fundamental experiments, which resulted in the laws of thermal radiation in general [18, 27, 28], and the complicating nature of liquids in particular.

Dedication

This work is dedicated to the memory of Charles-Auguste Robitaille.

First published online on November 01, 2006

References

1. Penzias A.A., Wilson R.W. A measurement of excess antenna temperature at 4080 Mc/s. *Astrophys. J.* 1965, v. 1, 419–421.
2. Kirchhoff G. Ueber das Verhaltnis zwischen dem Emissionsvermogen und dem absorptionsvermogen der Körper für Waeme und Litcht. *Annalen der Physik*, 1860, v. 109, 275–301.
3. Robitaille P.M.L. On the validity of Kirchhoff's law of thermal emission. *IEEE Trans. Plasma Sci.*, 2003, v. 31(6), 1263–1267.
4. Robitaille P.M.L. An analysis of universality in blackbody radiation. *Progr. in Phys.*, 2006, v. 2, 22–23.
5. Dicke R.H., Peebles P.J.E., Roll P.G., and Wilkinson D.T. Cosmic black-body radiation. *Astrophys. J.* 1965, v. 1, 414–419.
6. COBE web site, http://lambda.gsfc.nasa.gov/product/cobe/.
7. Fixsen D.J., Cheng E.S., Cottingham D.A., Eplee R.E., Isaacman R.B., Mather J.C., Meyer S.S., Noerdlinger P.D., Shafer R.A., Weiss R., Wright E.L., Bennett C.L., Boggess N.W., Kelsall T., Moseley S.H., Silverberg R.F., Smoot G.F., Wilkinson D.T. Cosmic Microwave Dipole spectrum measured by the COBE FIRAS Instrument. *Astroph. J.*, 1994, v. 420, 445–449.
8. Fixsen D.J., Cheng E.S., Cottingham D.A., Eplee R.E., Hewagama T., Isaacman R.B., Jensen K.A., Mather J.C., Massa D.L., Meyer S.S., Noerdlinger P.D., Read S.M., Rosen L.P., Shafer R.A., Trenholme A.R., Weiss R., Bennett C.L., Boggess N.W., Wilkinson D.T., Wright E.L. Calibration of the COBE FIRAS instrument. *Astrophys. J.*, 1994, v. 420, 457–473.
9. Bennett C.L., Kogut A., Hinshaw G., Banday A.J., Wright E.L., Gorski K.M., Wilkinson D.T., Weiss R., Smoot G.F., Meyer S.S., Mather J.C., Lubin P., Loewenstein K., Lineweaver C., Keegstra P., Kaita E., Jackson P.D., Cheng E.S.

Cosmic temperature fluctuations from two years of COBE differential microwave radiometers observations. *Astrophys. J.*, 1994, v. 436, 423–442.

10. Kogut A., Smoot G.F., Bennett C.L., Wright E.L., Aymon J., de Amici G., Hinshaw G., Jackson P.D., Kaita E., Keegstra P., Lineweaver C., Loewenstein K., Rokke L., Tenorio L., Boggess N.W., Cheng E.S., Gulkis S., Hauser M.G., Janssen M.A., Kelsall T., Mather J.C., Meyer S., Moseley S.H., Murdock T.L., Shafer R.A., Silverberg R.F., Weiss R., Wilkinson D.T. COBE differential microwave radiometers — preliminary systematic error analysis. *Astrophys. J.*, 1992, v. 401, 1–18.
11. Fixsen D.L., Gheng E.S., Gales J.M., Mather J.C., Shafer R.A., Wright E.L. The Cosmic Microwave Background spectrum from the full COBE FIRAS data set. *Astrophys. J.*, 1996, v. 473, 576–587.
12. Mather J.C., Fixsen D.J., Shafer R.A., Mosier C., Wilkinson D.T. Calibrator design for the COBE Far-Infrared Absolute Spectrophotometer (FIRAS). *Astrophys. J.*, 1999, v. 512, 511–520.
13. Klypin A.A, Strukov I.A., Skulachev D.P. The Relikt missions: results and prospects for detection of the Microwave Background Anisotropy. *Mon. Not. Astr. Soc.*, 1992, v. 258, 71–81.
14. WMAP website, http://map.gsfc.nasa.gov/.
15. Bennett C.L., Halpern M., Hinshaw G., Jarosik N., Kogut A., Limon M., Meyer S.S., Page L., Spergel D.N., Tucker G.S., Wollack E., Wright E.L., Barnes C., Greason M.R., Hill R.S., Komatsu E, Nolta M.R., Odegard N., Peiris H.V., Verde L, Weiland J.L. First-year Wilkinson Microwave Anisotropy Probe (WMAP) observations: preliminary maps and basic results. *Astrophys. J. Suppl.*, 2003, v. 148(1), 1–27.
16. Hinshaw G., Nolta M.R., Bennett C.L., Bean R., Dore O., Greason M.R., Halpern M., Hill R.S., Jarosik N., Kogut A., Komatsu E., Limon M., Odegard N., Meyer S.S., Page L., Peiris H.V., Spergel D.N., Tucker G.S., Verde L., Weiland J.L., Wollack E., Wright E.L. Three-year Wilkinson Microwave Anisotropy Probe (WMAP) observations: temperature analysis. *Astrophys. J.*, 2006, *submitted*.
17. Berger A. An introduction to the International Symposium George Lemaître. In: *The Big Bang and George Lemaître*, D. Reidel Publishing Company, Dordrecht, 1984, p. vii–xiv.
18. Planck M. Ueber das Gesetz der energieverteilung in Normalspectrum. *Annalen der Physik*, 1901, v. 4, 553–563.
19. Robitaille P.M.L. WMAP: a radiological analysis. *Progr. in Phys.*, 2007, v. 1, 3–18.
20. Planck M. The theory of heat radiation. Philadelphia, PA., P. Blakiston's Son, 1914.
21. Ulaby F.T., Moore R.K., Fung A.K. Microwave remote sensing active and passive — Volume 2: Radar remote sensing and surface scattering and emission theory. London, Addison–Wesley Publishing Company, 1982, p. 880–884.
22. Robitaille P.M.L. NMR and the Age of the Universe. *American Physical Society Centenial Meeting*, BC19.14, March 21, 1999.
23. Robitaille P.M.L. The MAP satellite: a powerful lesson in thermal physics. *Spring Meeting of the American Physical Society Northwest Section*, F4.004, May 26, 2001.
24. Robitaille P.M.L. The collapse of the Big Bang and the gaseous Sun. *New York Times*, March 17, 2002.
25. Robitaille P.M.L. WMAP: an alternative explanation for the dipole. *Fall Meeting of the American Physical Society Ohio Section*, E2.0001, 2006.
26. PLANCK website, http://www.rssd.esa.int/index.php?project=PLANCK&page=index.
27. Wien W. Ueber die Energieverteilung in Emissionspektrum eines schwarzen Körpers. *Ann. Phys.*, 1896, v. 58, 662–669.
28. Stefan J. Ueber die Beziehung zwischen der Wärmestrahlung und der Temperature. *Sitzungsberichte der mathematischnaturwissenschaftlichen Classe der kaiserlichen Akademie der Wissenschaften*, Wien 1879, v. 79, 391–428.
29. Rabounski D. The relativistic effect of the deviation between the CMB temperatures obtained by the COBE satellite *Progr. in Phys.*, 2007, v. 1, 24–26.
30. Robitaille P.M.L. The Solar photosphere: evidence for condensed matter. *Prog. in Phys.*, 2006, v. 2, 17–21.

The Relativistic Effect of the Deviation between the CMB Temperatures Obtained by the COBE Satellite

Dmitri Rabounski
E-mail: rabounski@yahoo.com

The Far-Infrared Absolute Spectrophotometer (FIRAS) on the COBE satellite, gives different temperatures of the Cosmic Microwave Background. This deviation has a theoretical explanation in the Doppler effect on the dipole (weak) component of the radiation, the true microwave background of the Universe that moves at 365 km/sec, if the monopole (strong) component of the radiation is due to the Earth. Owing to the Doppler effect, the dipole radiation temperature (determined by the 1st derivative of the monopole) is lower than the monopole radiation temperature, with a value equal to the observed deviation. By this theory, the WMAP and PLANCK satellites, targeting the L2 point in the Sun-Earth-Moon system, should be insensitive to the monopole radiation. In contrast to the launched WMAP satellite, the PLANCK satellite will have on board absolute instruments which will not be able to detect the measured temperature of the Cosmic Microwave Background. That the monopole (strong) component of the observed Cosmic Microwave Background is generated by the Earth is given a complete theoretical proof herein.

The COBE satellite, launched in 1989, has on board two instruments targeting the temperature of the Cosmic Microwave Background (CMB), namely the Far-Infrared Absolute Spectrophotometer (FIRAS) and the Differential Microwave Radiometer (DMR). FIRAS, having just a single channel for a signal, is sensitive to both the strong (monopole) and weak (dipole) components of the Background Radiation, and measures the general temperature in the Background without distinction between the monopole and dipole components of the field. The DMR has another construction: having a few channels for a signal, the DMR recognizes only the difference between the signals in the channels, and so gives just a difference between the temperature of the Background in the different directions. In other words, the DMR is sensitive to only the weak (dipole) component of the field that provides a possibility of direct search for its anisotropy [1].

The WMAP satellite launched in 2001 has on board only differential instruments working similarly to the DMR on COBE, so its data accounts only for the weak (dipole) component of the Background [2].

The anisotropy in the Background measured by the differential instruments is actually the same: DMR at COBE registered the anisotropy 3.353 ± 0.024 mK, while WMAP gave 3.346 ± 0.017 mK. The main direction of the anisotropy, by COBE, is $l = 264.26^\circ\pm0.33^\circ$, $b = 48.22^\circ\pm0.13^\circ$ (l is the Galactic longitude, b is the Galactic latitude). WMAP gives $l = 263.85^\circ\pm0.1^\circ$, $b = 48.25^\circ\pm0.04^\circ$ [3].

The absolute temperature of the Background initially obtained from the direct measurement by FIRAS

$$T_{FIRAS} = T_0 = 2.730 \pm 0.001\,\mathrm{K},$$

is the undifferentiated temperature of the monopole and dipole components of the field. However, the COBE team also extracted the absolute temperature from the 1st derivative of the monopole, which was interpreted as the actual temperature of the dipole component of the field. They obtained another numerical value [4]

$$T = 2.717 \pm 0.003\,\mathrm{K},$$

so the average deviation $\Delta T = 0.013$ K between these two results is a dozen times bigger than the measurement precision. So we have a minimal relative deviation between the CMB temperature by FIRAS from the monopole and from the 1st derivative of the monopole

$$\Delta T/T_0 = 0.33\% \text{ at } 1\sigma,$$

$$\Delta T/T_0 = 0.18\% \text{ at } 2\sigma,$$

which is small number, but is significantly not zero. So the CMB temperature measured by FIRAS from the monopole and its 1st derivative aren't the same. This is a systematic deviation with many years of the COBE observations. The COBE team attempted to explain the deviation as systematic errors in the calibration of the instruments. However, as pointed out by Robitaille [5], so large an increase of σ supposed by the COBE team is unlikely for the FIRAS instrument, which has excellent signal to noise ratio. The systematic deviation shouldn't be removed from the consideration.

As pointed out by Robitaille [5], this systematic deviation has no chance of being explained by anything other than the fact that the monopole and dipole components of the Background have *different origins*. He has elucidated the similarity of the Cosmic Microwave Background Radiation with radiation of Earth origin. He supposed that the monopole field has a different origin to that of the dipole, and is due to the Earth, not the whole Universe. According to

Robitaille [5, 6], the monopole (strong) field, is nothing but that generated by Earth objects (mostly oceans) and moves, in common with the Earth, with respect to the dipole (weak) field which is the real microwave background of the Universe.

Robitaille's claim, obtained from purely experimental analysis, can be easily checked by the relativistic effects which should appear in the COBE measurements, if the monopole field moves, in common with the Earth, with respect to the dipole field related to the whole Universe.

It follows from the measurement that the COBE satellite, in unison with the Earth, moves relative to the Cosmic Microwave Background with a velocity of 365 ± 18 km/sec [7]. DMR is sensitive to only the dipole field, so we are sure of the velocity with respect to the dipole field.

If the monopole field is due to the Earth, the COBE satellite is at rest with respect to the monopole field, but moves, in common with the Earth, at 365 ± 18 km/sec relative to the dipole field which is the true microwave background of the Universe. In such a case, two kinds of relativistic effects should appear for COBE: (1) the effects caused by the relative motion with respect to the dipole field (the Doppler effect and the effect of Special Relativity); (2) the effects caused by the physical properties of the local space of the COBE-bound observer, such as the presence of the Earth's gravitational field, and also the space rotation due to the daily rotation of the Earth (the effects of General Relativity).

By the Doppler effect, the temperature T of a radiation, the source of which moves with a velocity v at an angle θ relative to the direction from the observer to the source, differs from the same radiation's temperature T_0 measured when its source is at rest: $T=\frac{T_0}{1+\frac{\mathrm{v}}{c}\cos\theta}$. Assuming that the source of the dipole radiation moves with $\mathrm{v}=365\pm18$ km/sec away from the observer and the Earth (the monopole radiation source), we obtain

$$\frac{\Delta T}{T_0}=\frac{T_0-T}{T_0}=\frac{\mathrm{v}}{c}=0.12\%\pm0.006\%$$

i.e., due to the Doppler effect, the dipole radiation temperature T (measured by the 1st derivative of the monopole) should be 0.12% smaller than the monopole radiation temperature T_0 (measured by FIRAS).

This theoretical result is very close to the 0.18% registered at 2σ. In the real situation, this coincidence can be accounted for if one takes into account that fact that the COBE team provided different data for the dipole-measured temperature [5]. So the relativistic lowering of the Cosmic Microwave Background temperature due to the Doppler effect on its dipole component, the source of which moves away from the Earth (the source of the monopole), is in good agreement with that observed by COBE.

Now consider the effect of Special Relativity. It is well known [8], that the temperature T of radiation, the source of which moves relative to the observer with a velocity v, is: $T=T_0\sqrt{1-\frac{\mathrm{v}^2}{c^2}}$. With $\mathrm{v}=365$ km/sec we obtain the relativistic lowering of the observed temperature of the dipole radiation due to the Special Relativity effect

$$\frac{\Delta T}{T_0}=\frac{T_0-T}{T_0}=7.4\times10^{-7}=0.000074\%\,,$$

that is inconsequentially small for $\frac{\Delta T}{T_0}=0.12\%$ produced by the Doppler effect, and really registered by COBE. So there is no essential rôle played by Special Relativity in the relativistic lowering of the dipole radiation temperature.

The effects of General Relativity can also be examined. By General Relativity, if the monopole radiation is due to the Earth, it is affected by the gravitation and rotation of the Earth's space so that the temperature of the monopole radiation is as well higher than the dipole radiation far away from the Earth. It has been obtained that the temperature deviation between the monopole and dipole radiations expects to be $\sim10^{-8}\,\%$.

The effects caused by the COBE satellite itself (its own mass and spin), were a few orders smaller than the above effects caused by the Earth. The values are also inconsequentially small for 0.12% produced by the Doppler effect, and observed by COBE. So General Relativity's rôle in the relativistic lowering of the dipole radiation temperature is infinitesimal.

The General Relativity effects are bulky for deduction and calculation. For this reason the calculations for these effects are no presented in this paper.

We therefore conclude that:

> The different temperature of the Cosmic Microwave Background measured by the FIRAS instrument of COBE has a theoretical explanation in the Doppler effect on the dipole (weak) component of the radiation, the true microwave background of the Universe that moves away at 365 km/sec from the monopole (strong) component of the radiation due to the Earth. Owing to the Doppler effect, the CMB radiation temperature, measured by the 1st derivative of its monopole component, is lower than the monopole radiation temperature directly measured by FIRAS. This important finding can be referred to as ***a relativistic effect of the deviation between the temperature of the monopole and dipole components of the Cosmic Microwave Background.***

The calculation herein provides the theoretical proof of the assertion that the monopole component of the Cosmic Microwave Background is due to the Earth. If so, the WMAP satellite, located far away from the Earth, at the Lagrange 2 (L2) point in the Earth-Moon system, should be insensitive to the monopole radiation. Its instruments should register only the dipole radiation from the Universe. Therefore, the absolute and differential instruments located at the L2 point

should manifest no difference in the measured temperature of the radiation.

The WMAP satellite, unfortunately, has on board only the differential instruments (working like the DMR on COBE). However the PLANCK satellite, which will soon be launched, has on board absolute instruments. PLANCK will also be located at the L2 point, so its absolute instruments should be unable to register any signal from the monopole origination (from the Earth). This is in contrast to COBE, located near the Earth.

The above theoretical calculation and the measurement by COBE are the complete theoretical and experimental proofs of the assertion that the monopole (strong) component of the Cosmic Microwave Background is derived from the Earth, while the dipole (weak) component is the true microwave background of the Universe relative to which the Earth moves with a velocity of 365 km/sec. Due to the theoretical and experimental proofs, we expect to have a profoundly altered understanding of the Cosmic Microwave Background.

I am very thankful to Professor Pierre-Marie Robitaille who turned my attention to the systematic deviation in the Cosmic Microwave Background temperature by the FIRAS instrument on the COBE satellite, and spent much time to explain to me the details of the experiment.

First published online on November 01, 2006
Corrections posted online on December 30, 2006

References

1. Boggess N.W., et al. The COBE mission: its design and perfomance two years after lauch. *Astrophys. J.*, 1992, v. 397, 420–429. v. 397, 420–429.
2. Bennett C.L., et al. The Microwave Anisotropy Probe mission. *Astrophys. J.*, 2003, v. 583(1), 1–23.
3. Bennett C.L., et al. First-year Wilkinson Microwave Anisotropy Probe (WMAP) observations: preliminary maps and basic results. *Astrophys. J. Suppl. Ser.*, 2003, v. 148(1), 1–27.
4. Fixsen D.J., et al. The Cosmic Microwave Background spectrum from the full COBE FIRAS data set. *Astrophys. J.*, 1996, v. 473, 576–587.
5. Robitaille P.-M. On the origins of the CMB: insight from the COBE, WMAP and Relikt-1 satellites. *Progress in Physics*, 2007, v. 1, 19–23.
6. Robitaille P.-M. WMAP: a radiological analysis. *Progress in Physics*, 2007, v. 1, 3–18.
7. Smoot G.F., et al. Preliminary results from the COBE differential microwave interferometers: large angular scale isotropy of the Cosmic Microwave Background. *Astrophys. J.*, 1991, v. 371, L1–L5.
8. Tolman R. C. The theory of the relativity of motion. University of California Press, Berkeley, 1917 (reprinted by Dover Phoenix Editions, 2004).

Momentum of the Pure Radiation Field

Bo Lehnert

Alfvén Laboratory, Royal Institute of Technology, S-10044, Stockholm, Sweden
E-mail: Bo.Lehnert@ee.kth.se

The local momentum equation of the pure radiation field is considered in terms of an earlier elaborated and revised electromagnetic theory. In this equation the contribution from the volume force is found to vanish in rectangular geometry, and to become nonzero but negligible in cylindrical geometry. Consequently the radiated momentum is due to the Poynting vector only, as in conventional electrodynamics. It results in physically relevant properties of a photon model having an angular momentum (spin). The Poynting vector concept is further compared to the quantized momentum concept for a free particle, as represented by a spatial gradient operator acting on the wave function. However, this latter otherwise successful concept leads to difficulties in the physical interpretation of known and expected photon properties such as the spin, the negligible loss of transverse momentum across a bounding surface, and the Lorentz invariance.

1 Introduction

In the original and current presentation of Quantum Electrodynamics, the Poynting vector forms a basis for the quantized momentum of the pure radiation field [1, 2]. Thereby Maxwell's equations with a vanishing electric field divergence in the vacuum state are used to determine the electromagnetic field strengths and their potentials which, in their turn, are expressed by sets of quantized plane waves.

In the deduction of the Schrödinger equation, the quantized momentum for a free particle with mass has on the other hand been represented by an operator acting on the wave function and including a spatial gradient [1].

Since the individual photon can appear both as a wave and as a particle, the question may be raised whether its momentum should be represented by the Poynting vector concept, or by the spatial gradient operator concept. This question is discussed and illustrated in the present paper, in terms of a revised electromagnetic theory described in a recent review [3]. A summary of the basic equations of the theory is presented in Section 2, followed by two simple examples in Section 3 on a slab-shaped dense photon beam and on an axisymmetric model of the individual photon. A comparison between the two momentum concepts is finally made in Section 4.

2 Basic equations of the revised theory

The zero-point-energy of the vacuum state, its related electromagnetic vacuum fluctuations, the Casimir effect, and the electron-positron pair formation out of the vacuum support the hypothesis of a local electric charge density and an associated nonzero electric field divergence in such a state. On account of this, a Lorentz and gauge invariant theory has been elaborated, the details of which are given elsewhere [3–8]. The basic equations for the electric and magnetic fields $\mathbf{E}$ and $\mathbf{B}$ become

$$\operatorname{curl}\mathbf{B}/\mu_0 = \varepsilon_0(\operatorname{div}\mathbf{E})\mathbf{C} + \varepsilon_0\partial\mathbf{E}/\partial t\,, \tag{1}$$

$$\operatorname{curl}\mathbf{E} = -\partial\mathbf{B}/\partial t\,, \tag{2}$$

$$\operatorname{div}\mathbf{E} = \bar{\rho}/\varepsilon_0\,. \tag{3}$$

Here $\bar{\rho}$ is the local electric charge density in the vacuum, ε_0 and μ_0 are the conventional dielectric constant and magnetic permeability of the vacuum, $c^2 = 1/\mu_0\varepsilon_0$, and $\mathbf{C}^2 = c^2$ results from the Lorentz invariance where $\mathbf{C}$ has the character of a velocity vector. Combination of equations (1) and (2) yields the extended wave equation

$$\left(\frac{\partial^2}{\partial t^2} - c^2\nabla^2\right)\mathbf{E} + \left(c^2\nabla + \mathbf{C}\frac{\partial}{\partial t}\right)(\operatorname{div}\mathbf{E}) = 0 \tag{4}$$

for the electric field, and the associated relation

$$\left(\frac{\partial}{\partial t} + \mathbf{C}\cdot\nabla\right)(\operatorname{div}\mathbf{E}) = 0 \tag{5}$$

provided that $\operatorname{div}\mathbf{C} = 0$ which is an adopted restriction henceforth.

Using known vector identities, the basic equations (1), (2), and (3) result in the local momentum equation

$$\operatorname{div}{}^2\mathbf{S} = \mathbf{f} + \frac{\partial}{\partial t}\mathbf{g}\,, \tag{6}$$

where ${}^2\mathbf{S}$ is the electromagnetic stress tensor,

$$\mathbf{f} = \bar{\rho}\mathbf{E}' \qquad \mathbf{E}' = \mathbf{E} + \mathbf{C}\times\mathbf{B} \tag{7}$$

is the local volume force density, and

$$\mathbf{g} = \varepsilon_0\mathbf{E}\times\mathbf{B} = \frac{1}{c^2}\mathbf{S} \tag{8}$$

can be interpreted as a local electromagnetic momentum density of the radiation field, with $\mathbf{S}$ standing for the Poynting vector. Likewise a local energy equation

$$-\operatorname{div}\mathbf{S} = \bar{\rho}\,\mathbf{E}\cdot\mathbf{C} + \frac{1}{2}\,\varepsilon_0\,\frac{\partial}{\partial t}\left(\mathbf{E}^2 + c^2\mathbf{B}^2\right) \qquad (9)$$

is obtained. It is here to be observed that equations (6) and (9) are rearranged relations which do not provide more information than the original basic equations.

In the examples to be considered here, a velocity vector of the form

$$\mathbf{C} = c\,(0, \cos\alpha, \sin\alpha) \qquad (10)$$

is adopted, either in a rectangular frame (x, y, z) or in a cylindrical frame (r, φ, z). All field quantities are assumed to vary with t and z as $\exp\left[i(-\omega t + kz)\right]$ where ω and k are the corresponding frequency and wave number of an elementary normal mode. Equation (5) then results in the dispersion relation

$$\omega = kv \qquad v = c(\sin\alpha)\,. \qquad (11)$$

In order not to get in conflict with observations, such as those due to the Michelson-Morley experiments, the analysis is restricted to the condition

$$0 < \cos\alpha \equiv \delta \ll 1\,. \qquad (12)$$

With a smallness parameter $\delta \leqslant 10^{-4}$, the difference between v and c would become less than a change in the eight decimal of c.

3 Normal modes in slab-shaped and axisymmetric geometries

The first example is given by a slab-shaped dense light beam. The beam propagates in the z-direction of a rectangular frame (x, y, z), has a core region defined by $-a < x < a$, and two narrow boundary regions at $-b < x < -a$ and $a < x < b$. Within the core there is a homogeneous conventional electromagnetic wave field. This field is matched to the electromagnetic field in the inhomogeneous boundary regions as shown elsewhere [3, 8]. The analysis is here restricted to these regions within which the inhomogeneity in the x-direction requires the revised field equations to be used. In an analogous beam of circular cross-section, the source of angular momentum becomes localized to a corresponding inhomogeneous boundary region [3, 8].

The wave equation (4) now results in the relations

$$E_x = -(i/k\delta^2)\,\frac{\partial E_z}{\partial x}\,, \qquad (13)$$

$$E_y = -(\sin\alpha)\,E_z/\delta\,, \qquad (14)$$

where the field E_z plays the rôle of a generating function for the components E_x and E_y. From equation (2) the magnetic field components become

$$B_x = -E_y/c(\sin\alpha)\,, \qquad (15)$$

$$B_y = E_x/c(\sin\alpha) + \frac{i}{kc(\sin\alpha)}\,\frac{\partial E_z}{\partial x} = (\sin\alpha)E_x/c\,, \qquad (16)$$

$$B_z = -\frac{i}{kc(\sin\alpha)}\,\frac{\partial E_y}{\partial x} = -\delta E_x/c\,. \qquad (17)$$

Insertion of relations (13)–(17) into the expression (7) for the volume force then yields $\mathbf{E}' = 0$.

Further turning to the momentum density (8) of the radiation field, relations (13)–(17) give

$$g_x = 0\,, \qquad (18)$$

$$g_y = \delta\varepsilon_0\left[E_x^2 + E_y^2/(\sin\alpha)^2\right]/c\,, \qquad (19)$$

$$g_z = \varepsilon_0\left[E_x^2 + E_y^2/(\sin\alpha)^2\right]/c\,. \qquad (20)$$

Finally the power term in the energy equation (9) vanishes because relations (10), (13), and (14) combine to

$$\mathbf{E}\cdot\mathbf{C} = 0\,. \qquad (21)$$

This example thus demonstrates the following features:

- The volume force density $\mathbf{f}$ vanishes in rectangular geometry.
- The momentum density $\mathbf{g}$ of the radiation field has a primary component g_z in the direction of propagation.
- There is a secondary component g_y of the order δ, directed along the boundary and being perpendicular to the direction of propagation. This component corresponds to that which generates angular momentum (spin) in cylindrical geometry.
- There is a vanishing component g_x and no momentum is flowing across the boundary of the beam.
- The local power term in the energy equation vanishes.

The second example concerns an axisymmetric model of the individual photon. A wave or a wave packet of preserved and limited geometrical shape and undamped motion in a defined direction has then to be taken as a starting point. This leads to cylindrical geometry with propagation along z in a frame (r, φ, z). From earlier deductions based on equations (1)–(5), the electric and magnetic field components of an elementary normal mode then become [3–6]

$$E_r = -i\,g_0\,R_5/\theta\,, \qquad (22)$$

$$E_\varphi = g_0\,\delta(\sin\alpha)R_3\,, \qquad (23)$$

$$E_z = g_0\,\delta^2 R_4 \qquad (24)$$

and

$$B_r = -E_\varphi/c(\sin\alpha) = -g_0\,\delta R_3/c\,, \qquad (25)$$

$$B_\varphi = E_r(\sin\alpha)/c = -i\,g_0\,(\sin\alpha)R_5/\theta c\,, \qquad (26)$$

$$B_z = -i\,g_0\,\delta R_8/\theta c\,. \qquad (27)$$

Here we have introduced $g_0 = G_0/\delta^2$ where G_0 is the characteristic amplitude of a normalized generating function G, $\theta = kr_0$ with r_0 as a characteristic radial length, and

$$R_3 = \rho^2 DG \qquad R_4 = 1 - R_3 \tag{28}$$

$$R_5 = \frac{\partial}{\partial\rho} R_4 \qquad R_8 = \left(\frac{\partial}{\partial\rho} + \frac{1}{\rho}\right) R_3 \tag{29}$$

with $\rho = r/r_0$ and the operator D given by

$$D = \frac{\partial^2}{\partial\rho^2} + \frac{1}{\rho}\frac{\partial}{\partial\rho} - \theta^2\delta^2 \,. \tag{30}$$

For the electric field $\mathbf{E}'$ the components now reduce to

$$E'_r = -i\, g_0\, \delta^2 (R_5 + R_8)\,, /\theta \tag{31}$$

$$E'_\varphi = 0\,, \tag{32}$$

$$E'_z = g_0\, \delta^2 (R_3 + R_4) \tag{33}$$

and the momentum components of the radiation field are given by

$$c g_r/\varepsilon_0 g_0^2 = i\delta^2 (\sin\alpha)(R_4 R_5 - R_3 R_8)/\theta\,, \tag{34}$$

$$c g_\varphi/\varepsilon_0\, g_0^2 = \delta R_5 R_8/\theta^2 - \delta^3 R_3 R_4\,, \tag{35}$$

$$c g_z/\varepsilon_0\, g_0^2 = -(\sin\alpha) R_5^2/\theta^2 + \delta^2 (\sin\alpha) R_3^2 \,. \tag{36}$$

Finally the power term in the energy equation (9) becomes

$$\bar{\rho}\, \mathbf{E}\cdot\mathbf{C} = \delta^2 \bar{\rho}\, c g_0 (\sin\alpha)(R_3 + R_4) \tag{37}$$

thus being of second order in the parameter δ.

To the first order in δ the axisymmetric geometry then has features being analogous to those of the slab-shaped geometry:

- There is a negligible contribution from the volume force density $\mathbf{f}$, as well as from the radial component g_r of the radiation field.
- A secondary component g_φ of order δ gives rise to a spin of the photon model [3].
- The power term in the energy equation is negligible.

A corresponding analysis of a non-axisymmetric photon model with periodic φ-dependence and screw-shaped geometry leads to similar results [7].

The total(net) electric charge and magnetic moment of the present photon models have finally been shown to vanish through spatial integration [5–7].

4 Comparison between the momentum concepts

In the spatial gradient concept the momentum is represented by the operator

$$\mathbf{p} = -i\hbar\nabla \,. \tag{38}$$

For the normal modes being considered here, the corresponding axial component reduces to

$$p_z = \hbar k = h/\lambda = h\nu/c \tag{39}$$

which in conventional theory becomes related to a photon of energy $h\nu$, moving along z at the velocity c of light.

A comparison between the concepts of equations (8) and (38) is now made in respect to the remaining components being perpendicular to the direction of propagation, as well as in respect to the related question about Lorentz invariance.

4.1 The transverse component directed across a confining boundary

As compared to the axial component g_z, the momentum density $\mathbf{g}$ has a vanishing component g_x in slab-shaped geometry, and a nonzero but negligible component g_r in axisymmetric geometry. The corresponding relations between the momentum p_z and the components p_x and p_r are in a first approximation represented by

$$|p_x/p_z| \cong \lambda/2\pi L_x\,, \qquad |p_r/p_z| \cong \lambda/2\pi L_r \tag{40}$$

with L_x and L_r as corresponding characteristic lengths. Then the transverse components p_x and p_r cannot generally be neglected. This becomes questionable from the physical point of view when considering individual photons and light beams which have no transverse losses of momentum.

4.2 The transverse component directed along a confining boundary

With vanishing derivatives $\partial/\partial y$ or $\partial/\partial\varphi$, along a boundary in rectangular geometry or around the axis in cylindrical geometry, there are components g_y and g_φ being related to a nonzero spin. This behaviour differs from that of the momentum $\mathbf{p}$ for which the components p_y and p_φ vanish, as well as the spin. Such a behaviour appears to lack physical explanation.

When there are nonvanishing derivatives $\partial/\partial y$ and $\partial/\partial\varphi$, the concepts of $\mathbf{g}$ and $\mathbf{p}$ both result in transverse components along a boundary, but being of different forms.

4.3 The Lorentz invariance

In the present revised Lorentz invariant theory on the photon model, there is a component of the momentum $\mathbf{g}$ around the axis. This provides a spin, at the expense of the axial velocity of propagation. The latter then has to become slightly less than c, as required by the dispersion relation (11).

With the definition (38) of the momentum $\mathbf{p}$, there is a different situation. Thus equation (39) is in conventional theory consistent with an individual photon that moves at the full velocity c along the axial direction. But for the same photon also to possess a nonzero spin, it should have an additional transverse momentum p_φ, with an associated

velocity v_φ which circulates around the z-axis. For a radiation field within the volume of the photon to be considered as a self-consistent entity, the total local velocity then becomes equal to $(c^2+v_\varphi^2)^{1/2} > c$. This would represent a superluminal field configuration not being Lorentz invariant.

5 Conclusions

As expressed in terms of the present revised electromagnetic theory, the momentum concept of the pure radiation field appears to be physically relevant. The corresponding volume force density thus vanishes in rectangular geometry and is nonzero but negligible in cylindrical geometry. The momentum density is represented by the Poynting vector, as in conventional theory. Thereby its transverse components become consistent with the spin of the photon, and with a negligible loss of transverse momentum across a bounding surface.

The spatial gradient operator concept for the quantized momentum of a free particle with mass has earlier been used with success in the Schrödinger equation. However, when applying this concept to the free radiation field of the individual photon or of dense light beams, the obtained results differ from those based on the Poynting vector, and are in some cases difficult to interpret from the physical point of view. This discrepancy requires further investigation.

In this connection it should finally be mentioned that the present axisymmetric photon model [3, 6] is radially polarized. The core of a dense light beam being treated earlier [8] consists on the other hand of a linearly polarized conventional electromagnetic wave, with a boundary region having a radial gradient and leading to a spin of the beam considered as an entity.

The theory of this latter model can as well be applied to the limit of an individual photon with a linearly polarized core, a boundary region of finite radial extension, and a nonzero spin. It should thereby be kept in mind that such a model concerns the internal structure of a single photon, and therefore does not deal with the entangled quantum states of two interacting photons.

References

1. Schiff L. I. Quantum Mechanics. McGraw-Hill Book Comp. Inc., New York, 1949, Ch. XIV, Ch. II.
2. Heitler W. The quantum theory of radiation. Third edition. Clarendon Press, Oxford, 1954, Ch. II.
3. Lehnert B. Photon physics of revised electromagnetics. *Progress in Physics*, 2006, v. 2, 78–85.
4. Lehnert B., Roy S. Extended electromagnetic theory. World Scientific Publishers, Singapore, 1998.
5. Lehnert B. Optical effects of an extended electromagnetic theory. In: *Advances in Chemical Physics*, v. 119, Edited by M. W. Evans, I. Prigogine, and S. A. Rice, John Wiley and Sons, Inc., New York, 2001, 1–77.
6. Lehnert B. Photon wave and particle concepts of an extended electromagnetic theory. *Physica Scripta*, 2002, v. 66, 105–113.
7. Lehnert B. Screw-shaped light in extended electromagnetics. *Physica Scripta*, 2005, v. 72, 359–365.
8. Lehnert B. Boundary conditions and spin of a dense light beam. *Physica Scripta*, 2006, v. 74, 139–144.

New Measurement of the Earth's Absolute Velocity with the Help of the "Coupled Shutters" Experiment

Stefan Marinov*

Submitted by Erwin Schneeberger, e-mail: office@erwinschneeberger.com

An account is given of a new execution of my "coupled shutters" experiment. This time the following definite figures for the Earth's absolute velocity have been obtained: magnitude 360 ± 40 km/sec with equatorial coordinates of the apex $\delta = -24^\circ \pm 7^\circ$, $\alpha = 12.5^{\mathrm{h}} \pm 1^{\mathrm{h}}$ (for February 1984).

1 Introduction

I carried out the "coupled shutters" experiment for the first time in 1979 in Brussels [1, 2]. The precision achieved with that first experiment was not sufficient for accurately determining the Earth's absolute velocity. Thus with that experiment I could only establish that this velocity was not greater than 3,000 km/sec. The "coupled shutters" experiment is relatively very simple and cheap [1, 2], however no scientist in the world has repeated it. The general opinion expressed in numerous letters to me, in referees' comments on my papers, and in speeches at various space-time conferences which I attended or organized [3] is that my experiments are very sophisticated and difficult to execute. The *unique* discussion *in the press* on the *technical aspects* of my experiments is made by Chambers [4]. Here I should like to cite the comments of my anonymous *Foundations of Physics* referee sent to me by the editor, Prof. van der Merwe, on the 23 June 1983:

> I was informed by (name deleted) of the Department of the Air Force, Air Force Office of Scientific Research, Bolling Air Force Base, that Dr. Marinov's experiments were to be repeated by the Joint Institute for Laboratory Astrophysics. On inquiry, I learnt that JILA is not carrying out the experiments, because preliminary engineering studies had indicated that it lay beyond the expertise of the laboratory to achieve the mechanical tolerances needed to ensure a valid result.

After presenting my objections that the fact that JILA in the USA is unable to repeat my experiments cannot be considered as a ground for the rejection of my papers on the measurement of absolute velocity, Prof. van der Merwe sent me on the 24 January 1984 the following "second report" of the same referee:

> It is with regret that I cannot change my recommendation regarding Dr. Marinov's papers. In trying to justify the validity of his experimental work, Dr. Marinov highlights the points which cause the rest of the community so much concern. He states, "If I in a second-hand workshop in a fortnight for USD 500 achieve the necessary accuracy, then, I suppose, JILA can achieve it too." I know of no one in the precision measurement community who believes that measurements of the quality claimed by Dr. Marinov could be realized under such conditions and in so short a time. It will take very much more than this to change the direction of physics. I suspect that even scientists working in the most reputable laboratories in the U.S. or the world, would encounter great opposition in attempting to publish results as revolutionary as those claimed by Dr. Marinov.

In this paper I present an account of the measurement of the laboratory's absolute velocity, executed by me in Graz with the help of a new configuration of my "coupled shutters" experiment. Now the apparatus was built not in seven days but in four. As the work was "black" (a mechanician in a university workshop did it after working hours and I paid him "in the hand"), the apparatus was built predominantly over the weekend and cost 12,000 Shillings (USD 1000.–). The driving motor was taken from an old washing-machine and cost nothing.

As no scientific laboratory was inclined to offer me hospitality and the possibility to use a laser source and labora-

*Stefan Marinov (1931–1997), a Bulgarian born experimental and theoretical physicist who invented a new and highly original method to measure the anisotropy of the observable velocity of light (the "coupled shutters" experiment). He reported on the results of his experiment in a few short papers published in the peer-reviewed journals (*Physics Letters*, *General Relativity and Gravitation*, *Foundations of Physics*, etc.). After his formal education, Stefan Marinov worked from 1960 to 1974 with the research staff and also as an Assistant Professor, at the Faculty of Physics, Sofia University. Whilst there he devised and set up his first "coupled shutters" experiment and with it detected an anisotropy in the observed velocity of light. His life in Bulgaria was difficult: he was jailed in 1966/1967, 1974, and 1977, by the Bulgarian communist regime, for inappropriate "political thinking". In 1977 Marinov was deported from Bulgaria as a "political dissident". After a few years in Belgium, the USA, and Italy, he continued his research in Graz, Austria, which became his home until his tragic death in 1997. Despite the significant attention drawn to his experiment in the 1980's (many papers discussing his experiment were published in *Nature* and other journals), no other scientists attempted to repeat it. On the other hand, the experiment is simple, cheap, and can be easily repeated in any well-equipped physics laboratory. We therefore publish this detailed description of the experiment, as given by Marinov himself in *Deutsche Physik*, in 1992. The editors hope that this posthumous publication encourages and assists scientists who would like to repeat and enhance the "coupled shutters" experiment. (This paper was submitted by courtesy of Erwin Schneeberger, who was a close friend of Dr. Marinov, at Graz.)

tory mirrors, my first intention was to use as a light source, the Sun. As I earn my bread and money for continuing the scientific research, working as a groom and sleeping in a stall in a small village near Graz, I carried out the experiment in the apartment of my girl-friend. The sensitivity which I obtained with Sun's light (a perfect source of homogeneous parallel light) was good, but there were two inconveniences: (1) The motion of the Sun is considerable during the time when one makes the reversal of the axle and one cannot be sure whether the observed effect is due to the delay times of the light pulses or to the Sun's motion; (2) One can perform measurements only for a couple of hours about noon and thus there is no possibility to obtain a 24-hour "sinusoid" (explanation of the measuring procedure follows). On the other hand, at fast rotation of the axle the holed rotating disks became two sirens, so that when my apparatus began to whistle the neighbors knocked on the door, asking in dismay: "Fliegt schon der Russe über Wien?" (Is Ivan already flying over Vienna?). After a couple of altercations, my girl-friend threw out of her apartment not only my apparatus but also me.

Later, however, I found a possibility to execute the experiment in a laboratory (Fig. 1). The scheme of the experiment, its theoretical background and measuring procedure, are exactly the same as for the Brussels variation [1, 2]. Since the description is extremely simple and short, I shall also give it here, noting that the mounting of the laser and of the mirrors on the laboratory table lasted two hours.

But first, following the example of *Nature* which gives interesting quotations from its editions many years ago, I should like to also give one similarly:

> If it were possible to measure with sufficient accuracy the velocity of light without returning the ray to its starting point, the problem of measuring the first power of the relative velocity of the Earth with respect to the aether would be solved. This may not be as hopeless as might appear at first sight, since the difficulties are entirely mechanical and may possibly be surmounted in the course of time.

The names of the authors are Michelson and Morley, the year of publication is 1887. This is the paper in which Michelson and Morley give their account of the historical experiment for "measurement" of the two-way light velocity. The paper was published in two journals: *The Philosophical Magazine* and *American Journal of Science*. After giving this general opinion, Michelson and Morley proposed an experiment which is almost the *same* as my deviant "coupled mirrors" experiment [5, 6, 2]. They proposed to use a bridge method with two selenium cells where the null instrument is a telephone. I must emphasize that I could not succeed in finding a *single* paper or book treating the historic Michelson-Morley experiment, where information on their one-way proposal should be given. Let me note that in the Michelson-Morley experiment one compares the two-way light velocity in two mutually perpendicular directions, but one cannot measure its value.

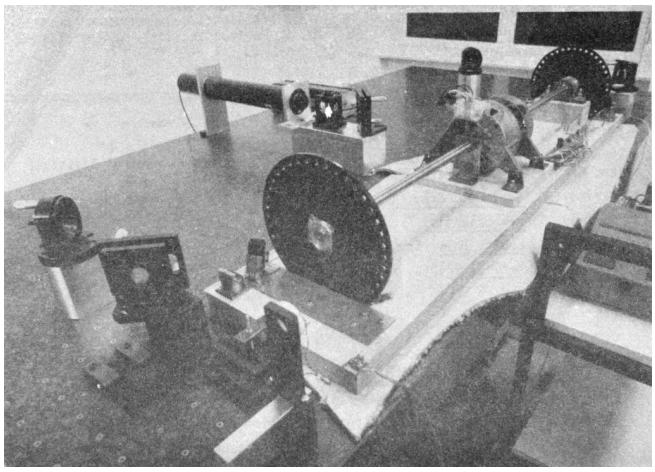

Fig. 1: The Graz "coupled shutters" experiment during preliminary measurements in the air of the laboratory; when performing measurements in vacuum the laser was mounted in parallel with the axle and the regulator for motor's velocity (to be seen between the motor and the far disk) was taken outside the evacuated space. At the left corner of the apparatus' plate one sees the socket for one of the reflecting mirrors for the case that Sun's light should be used (the socket of the other reflecting mirror is at the far right corner). The mechanician spent considerable time (and I lost money) for mastering the *adjustable* reflecting mirrors for Sun's light which have not been used in the laser arrangement, so that the price of the actually used apparatus had to be less than the half.

2 Theory of the "coupled shutters" experiment

A rotating axle driven by an electromotor, located exactly at the middle of the axle, has two holed discs at its extremities. The distance from the centres of the holes to the centre of the axle is R and the distance between the discs is d. Light from a laser is divided by a semi-transparent prism and the two beams are directed by a couple of adjustable mirrors, to the opposite ends of the rotating axle, so that the beams can pass through the discs' holes in mutually opposite directions. Any of the beams, after being chopped by the near disc and "detected" by the far disc, illuminates a photocell. By means of a galvanometer one measures the difference in the currents generated by both photocells. If covering one of the cells, one measures the current produced by the other cell.

One arranges the position of the laser beam with respect to the discs' holes in such a manner that when the axle is at rest the light of the laser which passes through the near hole illuminates *half* of the far hole. One then sets the axle in rotation, gradually increasing its speed. Since the light pulses cut by the near holes have a transit time in order to reach the far holes, with the increase of the rate of rotation less and less light will pass through the far holes, when the distant holes "escape" from the light beam positions, and,

conversely, more and more light will pass through the far holes, when the distant holes "enter" into the light beam positions. For brevity I shall call the first kind of far holes "escaping" and the second kind of far holes "entering".

If one assumes that the holes as well as the beams' cross-sections are rectangular and the illuminations homogeneous, then the current I_{hom} produced by either of the photocells will be proportional to the breadth b of the light spot measured on the surface of the photocell when the axle is rotating, i.e., $I_{hom} \sim b$. When the rotational rate of the axle increases by ΔN, the breadth of the light beam passing through the "escaping" holes will become $b - \Delta b$, while the breadth of the light beam passing through "entering" holes will become $b + \Delta b$, and the produced currents will become $I_{hom} - \Delta I \sim$ $\sim b - \Delta b$, $I_{hom} + \Delta I \sim b + \Delta b$. Thus

$$\Delta b = b\,\frac{\Delta I}{I_{hom}}\,, \tag{1}$$

where ΔI is the *half* of the *change* in the *difference of the currents* produced by the photocells.

One rotates the axle first with $\frac{\Delta N}{2}$ counter-clockwise and then with $\frac{\Delta N}{2}$ clockwise, that corresponds to a change ΔN in the rate of rotation. Since

$$\Delta b = (d/c)\,\pi\,\Delta N R\,, \tag{2}$$

for the one-way velocity of light one obtains

$$c = \frac{2\pi\,\Delta N R d}{b}\,\frac{I_{hom}}{\Delta I} \tag{3}$$

In my experiment the holes, as well as the light beams, were circular, not rectangular. Consequently, instead of the measured light spot's breadth, one has to take a certain *slightly different* "effective" breadth. As the breadth b can never be measured accurately, the discussion of the difference between real breadth and "effective" breadth is senseless. Much more important, however, was the fact that the illumination in the beams' cross-sections was not homogeneous: at the centre it was maximum and at the periphery minimum. Thus the simplified relation (1) did not correspond to reality if under I_{hom} one would understand the measured current. I shall give here a certain amelioration of formula (1), which was omitted in Ref. [1], because of a fear that the presumed referee would consider my analysis as an "artificial speculation" in a search "to adapt the observed values to the theoretical formula". Now I am no more afraid of the referee. The illumination will be assumed to increase *linearly* from zero on the periphery of the light beam to a maximum at its center where the beam is "cut" by the holes' rims. The *real* current I which one measures is proportional to a certain *middle* illumination across the whole light beam, while the *real* current ΔI is proportional to the *maximum* illumination at the centre of the light beam. On the other hand, one must take into account that when the holes let the light beam fall on the photocell, first light comes from the peripheral parts and at the end from the central parts. When half of the beam has illuminated the photocell, the "left" part of the beam begins to disappear and its "right" part begins to appear, the breadth remaining always *half* of the beam. Then the holes' rims begin to extinguish first the central parts of the beam and at the end the peripheral parts. Here, for simplicity, I suppose that the cross-sections of the beams and of the holes are the same (in reality the former were smaller than the latter). Thus during the first one-third of the time of illumination the "left" half of the light beam appears, during the second one-third of the time of illumination the "left" half goes over to the "right" half, and during the last one-third of the time of illumination the "right" half disappears. Consequently, the *real* current, I, produced by the photocell will be related to the *idealized* current, I_{hom}, corresponding to a *homogeneous illumination with the central intensity* and *generated by a light spot having the half-breadth of the measured one*, by the following connection

$$\begin{aligned} I = \frac{1}{2}\int_0^1 I_{hom}\,x\left(\frac{2}{3}-\frac{x}{3}\right)dx\,= \\ = \frac{I_{hom}}{6}\left(x^2-\frac{x^3}{3}\right)\Bigg|_0^1 = \frac{I_{hom}}{9}\,. \end{aligned} \tag{4}$$

In this formula $I_{hom}dx$ is the current produced by a strip with breadth dx of the light beam; at the periphery of the beam (where $x = 0$) the produced current is zero and at the centre (where $x = 1$) it is $I_{hom}dx$. The current $I_{hom}dx$ is produced (i.e. the corresponding photons strike the photocell) during time $\frac{2}{3} - \frac{x}{3}$; for the periphery of the beam this time is $\frac{2}{3} - \frac{0}{3} = \frac{2}{3}$ and for the centre of the beam this time is $\frac{2}{3} - \frac{1}{3} = \frac{1}{3}$. The factor $\frac{1}{2}$ before the integral is present because the *measured* breadth of the light spot over the photocell is *twice* its *working* breadth. Putting (4) into (3), one obtains

$$c = \frac{2\pi\Delta N R d}{b}\,\frac{9I}{\Delta I}\,. \tag{5}$$

According to my absolute space-time theory [2, 6, 7] (and according to anybody who is acquainted *even superficially* with the experimental evidence accumulated by humanity), if the *absolute velocity's component* of the laboratory along the direction of light propagation is v, then the velocity of light is $c - v$ along the propagation direction and $c + v$ against. For these two cases formula (5) is to be replaced by the following two

$$\begin{aligned} c - v = \frac{2\pi\Delta N R d}{b}\,\frac{9I}{\Delta I + \delta I}\,, \\ c + v = \frac{2\pi\Delta N R d}{b}\,\frac{9I}{\Delta I - \delta I}\,, \end{aligned} \tag{6}$$

where $\Delta I + \delta I$ and $\Delta I - \delta I$ are the changes of the currents generated by the photocells when the rate of rotation changes

by ΔN. Dividing the second formula (6) by the first one, one obtains

$$v = \left(\frac{\delta I}{\Delta I}\right) c\,. \qquad (7)$$

Thus the measuring method consists of the following: One changes the rotational rate by ΔN and measures the change in the current of either of the photocells, which is $\Delta I \simeq \Delta I \pm \delta I$; then one measures the difference of these two changes which is $2\delta I$. I made both these measurements by a differential method with the same galvanometer, applying to it the difference of the outputs of both photocells. To measure $2\Delta I$ I made the far holes for one of the beam "escaping" and for the other "entering". To measure $2\delta I$ I made all far holes "escaping" (or all "entering").

3 Measurement of c

In the Graz variation of my "coupled-shutters" experiment I had: $d = 120$ cm, $R = 12$ cm. The light source was an Ar laser, the photocells were silicon photocollectors, and the measuring instrument was an Austrian "Norma" galvanometer. I measured $I = 21$ mA (i.e., $I_{hom} = 189$ mA) at a rotational rate of 200 rev/sec. Changing the rotation from clockwise to counter-clockwise, i.e., with $\Delta N = 400$ rev/sec, I measured $\Delta I = 52.5\,\mu$A (i.e., the measured change in the difference current at "escaping" and "entering" far holes was $2\Delta I = 105\,\mu$A). I evaluated a breadth of the light spot $b = 4.3 \pm 0.9$ mm and thus I obtained $c = (3.0 \pm 0.6) \times 10^8$ m/sec, where error is taken as only the error in the estimation of b, because the "weights" of the errors introduced by the measurement of d, R, ΔN, I, ΔI were much smaller. I repeat, the breadth b cannot be measured exactly as the peripheries of the light spot are not sharp. As a matter of fact, I chose such a breadth in the possible uncertainty range of ± 1 mm, so that the exact value of c to be obtained. I wish once more to emphasize that the theory for the measurement of c is built on the assumption of rectangular holes and light beams cross-sections and linear increase of the illumination from the periphery to the center. These simplified assumptions do not correspond to the more complicated real situation. Let me state clearly: The "coupled shutters" experiment is not to be used for an *exact* measurement of c. It is, however, to be used for sufficiently accurate measurement of the variations of c due to the absolute velocity of the laboratory when, during the different hours of the day, the axis of the apparatus takes different orientations in absolute space due to the daily rotation of the Earth (or if one would be able to place the set-up on a rotating platform). The reader will see this now.

4 Measurement of v

The measurement of c is an *absolute*, while the measurement of v is a *relative*, taking the velocity of light c as known. According to formula (7) one has to measure only two difference currents: $2\Delta I$ (at "escaping" *and* "entering" far holes) and $2\delta I$ (at "escaping" or "entering" far holes). The measurement in the air of the laboratory had two important inconveniences: (1) Dust in the air led to very big fluctuations in the measured current differences and I had to use a big condenser in parallel with the galvanometer's entrance, making the apparatus very sluggish; (2) The shrill of the holed disks at high rotational rate could lead to the same gloomy result as when executing the experiment in the apartment of my girlfriend. Thus I covered the whole set-up with a metal cover and evacuated the air by using an oil pump (this amelioration cost an additional 9,000 Shilling, i.e. USD 700,–). The performance of the experiment in vacuum has also the advantage that those people who wish to save at any price the false dogma of the constancy of the velocity of light, cannot raise the objection that the observed effect is due to temperature disturbances.

The measurement of ΔI is a simple problem as the effect is *huge*. Moreover all existing physical schools cannot raise objections against the theory presented above. However, the measurement of δI which is with three orders lower than ΔI has certain peculiarities which must be well understood. When changing the rotation from clockwise to counter-clockwise, the current produced by the one photocell changes, say, from I_1 to $I_1 + \Delta I_1 + \delta I_1$ and of the other photocell from, say, I_2 to $I_2 + \Delta I_2 - \delta I_2$. One makes I_1 to be equal to I_2, changing the light beam positions by manipulating the reflecting mirrors micrometrically. One can with difficulty obtain an exact compensation, so that the galvanometer shows a certain residual current I'. The current change ΔI_1 will be equal to the current change ΔI_2 only if the experiment is *entirely symmetric*. But it is difficult to achieve a complete symmetry (and, of course, I could not achieve it in my experiment). There are the following disturbances: On the one hand, the distribution of the light intensities in the cross-sections of both beams and the forms of the beams are not exactly the same; thus the covering of the same geometrical parts of both beams when changing the rotation of the axle does not lead to equal changes in the light intensities of both beams and, consequently, to $\Delta I_1 = \Delta I_2$. On the other hand, although the photocells were taken from a unique Sun collector cut in two pieces, even if the changes in the illuminations should be equal, the produced currents may become different (the current gain at the different points of the photocells is not the same, the internal resistances of the cells are not equal, etc. etc.). Thus after changing the rotational rate from clockwise to counter-clockwise, I measured certain current I'', but $I'' - I'$ was *not* equal to $2\delta I$, as it *must be* for an entirely symmetric setup. However, measuring the difference $I'' - I'$ during different hours of the day, I established that it was "sinusoidally modulated". This "sinusoidal modulation" was due to the absolute velocity v. All critics of my "rotating axle" experiments vociferate

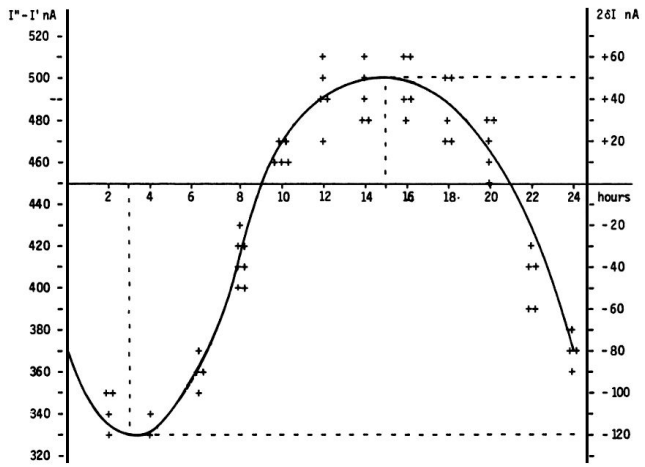

Fig. 2: Measurement of $2\delta I$. The points give the measurements at the even hours for the days from the 9th to the 13th February 1984.

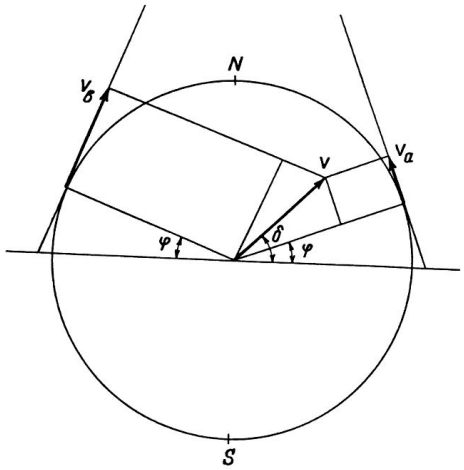

Fig. 3: The Earth and its absolute velocity at the two moments when the laboratory meridian lies in the velocity's plane.

mostly against the vibrations of the axle, asserting that these vibrations will mar the whole measurement. Meanwhile the axle caused me *absolutely no troubles*. When measuring in vacuum the axis of the apparatus pointed north/south.

I measured the "sinusoidal modulation" over 5 days, from the 9th to the 13th February 1984. As I did the experiment alone, I could not cover all 24 hours of every day. The results of the measurements are presented in Fig. 2. The most sensible scale unit of the galvanometer was 10 nA and the fluctuations were never bigger than 20 nA. The daytime hours are on the abscissa and the current differences on the left ordinate. After plotting the registered values of $I'' - I'$ and drawing the best fit curve, the "null line" (i.e., the abscissa) is drawn at such a "height" that the curve has to cut *equal* parts of the abscissa (of any 12 hours). Then on the right ordinate the current $2\delta I$ is taken positive upwards from the null line and negative downwards. Since 105 μA corresponds to a velocity 300,000 km/sec, 10 μA will correspond approximately to 30 km/sec. Considering the fluctuations of the galvanometer as a unique source of errors, I took ± 30 km/sec as the uncertainty error in the measurement of v.

When $2\delta I$ has maximum or minimum the Earth's absolute velocity lies in the plane of the laboratory's meridian (Fig. 3). The velocity components pointing to the north are taken positive and those pointing to the south negative. I always denote by v_a the component whose algebraic value is smaller. When both light beams pass through "escaping" holes, then, in the case that the absolute velocity component points to the north, the "north" photocell produces less current than the "south" photocell (with respect to the case when the absolute velocity component is perpendicular to the axis of the apparatus), while in the case that the absolute velocity component points to the south, the "north" photocell produces more current. If the light beams pass through "entering" holes, all is vice versa. Let me note that for the case shown in Fig. 3 (which does not correspond to the real situation, as in reality v_a is negative) both velocity components point to the north and both v_a and v_b are positive. In this case the "variation curve" no longer has the character of a "sinusoid"; it has 4 extrema (for 24 hours) and the "null line" must be drawn tangentially to the lowest minimum.

As can be seen from Fig. 3, the two components of the Earth's absolute velocity in the horizontal plane of the laboratory, v_a and v_b, are connected with the magnitude v of the absolute velocity by the following relations

$$v_a = v \sin(\delta - \phi), \qquad v_b = v \sin(\delta + \phi), \tag{8}$$

where ϕ is the latitude of the laboratory and δ is the declination of the velocity's apex. From these one obtains

$$v = \frac{\left\{v_a^2 + v_b^2 - 2 v_a v_b \left(\cos^2\phi - \sin^2\phi\right)\right\}^{\frac{1}{2}}}{2 \sin\phi \cos\phi}, \qquad \tan\delta = \frac{v_b + v_a}{v_b - v_a} \tan\phi. \tag{9}$$

Obviously the apex of v points to the meridian of v_a. Thus the right ascension α of the apex equaled the local sidereal time of registration of v_a. From Fig. 2 it is to be seen that this moment can be determined with an accuracy of $\pm 1^{\mathrm{h}}$. Thus it was enough to calculate (with an inaccuracy not larger than ± 5 min) the sidereal time t_{si} for the meridian where the local time is the same as the standard time t_{st} of registration, taking into account that the sidereal time at a middle midnight is as follows:

22 September	—	0^{h}	23 March	—	12^{h}
22 October	—	2^{h}	23 April	—	14^{h}
22 November	—	4^{h}	23 May	—	16^{h}
22 December	—	6^{h}	22 June	—	18^{h}
21 January	—	8^{h}	23 July	—	20^{h}
21 February	—	10^{h}	22 August	—	22^{h}.

The graph in Figure 2 shows that on the 11th February (the middle day of observation) I registered in Graz ($\phi = 47^\circ$, $\delta = 15^\circ\,26'$) the following components of the absolute velocity at the following hours (for $2(\delta I)_a = -120$nA, and $2(\delta I)_b = 50$nA)

$$\begin{aligned} v_a &= -342 \pm 30\,\text{km/sec}, \quad (t_{st})_a = 3^\text{h} \pm 1^\text{h}, \\ v_b &= +143 \pm 30\,\text{km/sec}, \quad (t_{st})_b = 15^\text{h} \pm 1^\text{h}, \end{aligned} \tag{10}$$

and formulae (9) give

$$\begin{aligned} &v = 362 \pm 40\,\text{km/sec}, \\ &\delta = -24^\circ \pm 7^\circ, \quad \alpha = (t_{si})_a = 12.5^\text{h} \pm 1^\text{h}. \end{aligned} \tag{11}$$

where the errors are calculated supposing $\phi = 45^\circ$.

The local sidereal time for the observation of v_a (i.e., the right ascension of the absolute velocity's apex) was calculated in the following manner: As for any day the sidereal time increases by 4^m (with respect to the solar time), the sidereal time at midnight on the 11th February (which follows 21 days after midnight on the 21 January) was $8^\text{h} + 1^\text{h}\,24^\text{m} = 9^\text{h}\,24^\text{m}$. At 3^h middle European (i.e., Graz) time on the 11th February the local sidereal time on the 15th meridian was $9^\text{h}\,24^\text{m} + 3^\text{h} = 12^\text{h}\,24^\text{m}$. On the Graz meridian the local sidereal time was $12^\text{h}\,24^\text{m} + 2^\text{m} = 12^\text{h}\,26^\text{m} \simeq 12.5^\text{h}$.

Important remark. I now establish that when calculating the local sidereal time of observation of v_a for my interferometric "coupled mirrors" experiment [2, 6, 8, 9], I made a very *unpleasant error*. As Sofia ($\lambda = 23^\circ\,21'$) lies westwards from the middle zonal meridian ($\lambda = 30^\circ$), I had to *subtract* the difference of $6^\circ\,39'$, which corresponds to 27^m, from the local sidereal time of the zonal meridian. Instead of doing this, I *wrongly* added. Thus the numbers given by me are to be corrected as follows:

Observation:	Wrongly calculated:	To be corrected to:
12 July 1975	$(t_{si})_a = 14^\text{h}\,23^\text{m}$	$(t_{si})_a = 13^\text{h}\,30^\text{m}$
11 January 1976	$(t_{si})_a = 14^\text{h}\,11^\text{m}$	$(t_{si})_a = 13^\text{h}\,17^\text{m}$
Right ascension of the apex of the Sun's absolute velocity	$\alpha = 14^\text{h}\,17^\text{m}$	$\alpha = 13^\text{h}\,23^\text{m}$

I beg the persons who will refer to the measurement of the Sun's absolute velocity determined by me in 1975/76 to cite *always* the corrected figures given here and not the wrongly calculated figures presented in [2, 6, 8, 9, 10, 11] and in some others of my papers.

5 Conclusions

Comparing the figures obtained now by the Graz variation of my "coupled shutters" experiment with the figures obtained some ten years ago in Sofia by the interferometric "coupled mirrors" experiment, one sees that within the limits of the supposed errors they overlap. Indeed, on the 11 January 1976 I registered in Sofia the following figures

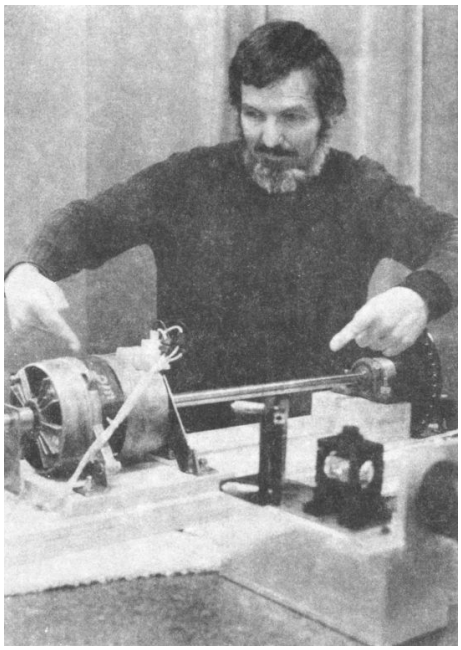

Fig. 4: February 1984. Explaining the essence of the "coupled shutters" experiment. My fingers show the ways in which both light beams go from the one perforated disk to the other. One can see on the photograph only a small part of the laser producing the initial light beam which is split by the semitransparent mirror seen in the photograph. The reflected beam goes to the left, while the refracted beam, after a reflection on the mirror seen in the photograph, goes to the right. Between the perforated disks, these two beams proceed in the opposite directions. The person who gave me a possibility to carry out my "coupled shutters" experiment in his laboratory took from me the solemn promise that I shall never say where have I carried it out. To my question, why is he so afraid, the answer was: "I do not wish one day to be poisoned by certain special services."

$$\begin{aligned} &v = 327 \pm 20\,\text{km/sec}, \\ &\delta = -21^\circ \pm 4^\circ, \quad \alpha = 13^\text{h}\,17^\text{m} \pm 20^\text{m}. \end{aligned} \tag{12}$$

As for the time of one month the figures do not change significantly, one can compare directly the figures (11) with the figures (12). The declinations are the same. As the Graz measurements were done every two hours, the registration of the right ascension was not exact enough and the difference of about one hour is not substantial. I wish to point only to the difference between the magnitudes which is 35 km/sec. I have the intuitive feeling that the figures obtained in Sofia are more near to reality. The reason is that *I profoundly believe in the mystique of the numbers,* and my Sofia measurements led to the magic number 300 km/sec for the Sun's absolute velocity (which number is to be considered together with 300,000 km/sec for light velocity and 30 km/sec for the Earth's orbital velocity). The Graz measurement destroys

this mystic harmony.

The presented account on the Graz "coupled shutters" experiment shows that the experiment is *childishly simple*, as I always asserted [1, 2]. If the scientific community refuses to accept my measurements for so many years and nobody tries to repeat them, the answer can be found in the following words of one of my *best physical and moral teachers*:

> ***Terrible is the power which an authority exerts over the world.***
>
> *Albert Einstein*

I wish to add in closing that with a letter of the 29 December 1983 I informed the Nobel committee that I am ready at any time to bring (for my account) the "coupled shutters" experiment to Stockholm and to demonstrate the registration of the Earth's absolute motion. With a letter of 28 January 1984 Dr. B. Nagel of the Physics Nobel committee informed me that my letter had been received.

References

1. Marinov S. Measurement of the one-way speed of light and the Earth's absolute velosity. *Speculations in Science and Technology*, 1980, v. 3, 57; *Proc. 2nd Marcel Grossmann Meeting on General Relativity*, Trieste, 5–11 July, 1979, North-Holland, Amsterdam & New York, 1982, p. 547–550.
2. Marinov S. Classical physics. East-West, Graz, 1981.
3. Marinov S. The thorny way of truth. East-West, Graz, 1982.
4. Chambers R. G. In: *Proceedings of ICSTA — Intern. Conference on Space-Time Absoluteness*, Genoa, July 1982, eds. S. Marinov and J. P. Wesley, East-West, Graz, 1982, p. 44.
5. Marinov S. The velocity of light is direction dependent. *Czechoslovak Journal of Physics*, 1974, v. B24, 965–970.
6. Marinov S. Eppur si muove. C.B.D.S., Brussels, 1977; 2nd and 3rd ed., East-West, Graz, 1981 and 1987 resp.; 4th edition, 2006 (*in print*).
7. Marinov S. *Foundations of Physics*, 1979, v. 9, 445.
8. Marinov S. *Abstracts of GR8 — Intern. Conference on General Relativity and Gravitation*, Waterloo, Canada, August 1977, p.244.
9. Marinov S. Measurement of the laboratory's absolute velocity. *General Relativity & Gravitation*, 1980, v. 12, 57–65.
10. Marinov S. *New Scientist*, 1976, v. 71, 662.
11. Marinov S. *Foundations of Physics*, 1976, v. 6, 571.

Upper Limit in the Periodic Table of Elements

Albert Khazan
E-mail: albkhazan@list.ru

The method of rectangular hyperbolas is developed for the first time, by which a means for estimating the upper bound of the Periodic Table is established in calculating that its last element has an atom mass of 411.663243 and an atomic number (the nuclear charge) of 155. The formulating law is given.

1 Introduction. The mathematical basis

The periodic dependence of the properties of the elements on their atomic mass, as discovered by D. I. Mendeleev in 1869, predicted the existence of new elements in appropriate locations in the Periodic Table.

Progress in synthesis and in the study of the properties of the far transuranium elements has increased interest in the question of the upper limits of the Periodic Table. G. T. Seaborg, J. L. Bloom and V. I. Goldanskii emphasized that the charge of the atomic nucleus and the position occupied by the element "define unambiguously the structure of electron jackets of its atoms and characterize the whole set of its chemical properties". They suggested the existence of nuclei containing 114, 126 and 164 protons, 184, and 258 neutrons and the Table arrangement of the relevant elements [1, 2].

The objective of this study is to determine the possible number of chemical elements, along with atomic masses and atomic numbers up to the final entry in the Periodic Table.

The calculations were performed on the basis of IUPAC [3] table data for all known elements. The basic principle resides in the idea that the proportion of the defined element Y in any chemical compound of molecular mass X should be related to its single gram-atom. In this case, if K is the atomic mass, the equation $Y = \frac{K}{X}$ would represent a rectangular hyperbola in the first quadrant ($K > 0$). Its asymptotes conform to the axis coordinates, and semi-axis $a = b = \sqrt{2\,|K|}$. The peak of the curve should occur on the virtual axis inclined at an angle of 45° to the positive direction of the abscissa axis. The necessary conditions associated with this chemical conception are: $Y \leqslant 1$ and $K \leqslant X$.

The foregoing equation differs only in the atomic mass for each element of the Periodic Table and allows calculation of the proportion of the element in any compound. Accuracy plotting the curve and the associated straight line in the logarithmic coordinates depends on the size of the steps in the denominator values, which can be entirely random but must be on the relevant hyperbola in terms of X. Consequently, it can be computed without difficulty by prescribing any value of the numerator and denominator. In Table 1a are given both known oxygen containing compounds and random data on X arranged in the order of increasing molecular mass. Fig. 1 depicts the hyperbola (the value of the approximation certainty $R^2 = 1$), calculated for 1 gram-atom of oxygen.

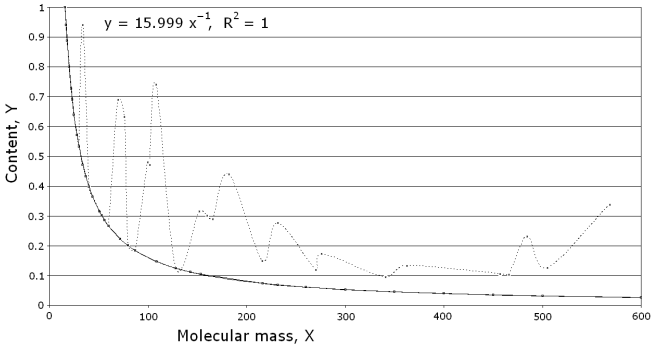

Fig. 1: Oxygen content versus the molecular mass of compounds on estimation to 1 gram-atom (hyperbola $y = k/x$) and the total amount of O (maxima, leaders). The molecular mass in the table is given according to its increase.

Estimation of the unobserved content in the chemical compound as determined by the formula is expressed on the plot by the polygonal line (Table 1b, Fig. 1). It is obvious from the Fig. 2a that the hyperbolic function of the elemental proportion in chemical compounds plotted against molecular mass, by the example of the second Group, is true ($R^2 = 1$). In the logarithmic coordinates (Fig. 2b) it is represented as the straight lines arranged in the fourth quadrant (to the right of hydrogen) all with slope 1. With the view to expansion of the basis of the arguments, this example is given for the first Group including "roentgenium" No. 111, a more recently identified element, and the predicted No. 119 and No. 155. The real axis is shown here, on which the peaks of all hyperbolas of the Periodic Table are arranged (see below).

2 Using the theorem of Lagrange

It is clear from the Fig. 2a that with the rise of the atomic mass the curvature of the hyperbola decreases (the radius of curvature increases), and the possibility to define its peak, for example, by means of graphical differentiation, becomes a problem due to errors of both subjective and objective character (instrument, vision and so on). Therefore, to estimate the curve peak of the hyperbola the mathematical method of the theorem of Lagrange was used [4].

K	X	$Y=\frac{K}{X}$	$\ln X$	$\ln Y$	Compound		Compound	X	$Y=n\frac{K}{X}$
15.9994	15.999	1	2.77255	0	O		O	15.9994	1
15.9994	17.007	0.9408	2.83363	−0.0611	$\frac{1}{2}H_2O_2$		H_2O	18.015	0.88811546
15.9994	18.015	0.8881	2.8912	−0.1187	H_2O		BeO	25.01	0.63972011
15.9994	20	0.8	2.99573	−0.2232	—		CO	28.01	0.57120314
15.9994	22	0.7272	3.09104	−0.3185	—		NO	30.006	0.53320669
15.9994	23.206	0.6895	3.14441	−0.3719	$\frac{1}{3}B_2O_3$		H_2O_2	34.01	0.94089974
15.9994	25.01	0.6397	3.21928	−0.4467	BeO		MgO	40.304	0.39698293
15.9994	28.01	0.5712	3.33256	−0.56	CO		N_2O	44.012	0.36353722
15.9994	30.006	0.5332	3.4014	−0.6288	NO		CaO	56.077	0.28532197
15.9994	33.987	0.4708	3.52598	−0.7534	$\frac{1}{3}Al_2O_3$		COS	60.075	0.26633375
15.9994	37	0.4324	3.61092	−0.8384	—		B_2O_3	69.618	0.68947686
15.9994	40.304	0.397	3.69645	−0.9239	MgO		N_2O_3	76.01	0.63149586
15.9994	44.012	0.3635	3.78446	−1.0119	N_2O		CuO	79.545	0.20114401
15.9994	50.663	0.3158	3.9252	−1.1526	$\frac{1}{3}Cr_2O_3$		Cl_2O	86.905	0.18410908
15.9994	53.229	0.3006	3.9746	−1.2021	$\frac{1}{3}Fe_2O_3$		CrO_3	99.993	0.4800336
15.9994	56.077	0.2853	4.02673	−1.2542	CaO		Al_2O_3	101.96	0.47077285
15.9994	60.075	0.2663	4.09559	−1.323	COS		N_2O_5	108.008	0.74068588
15.9994	71.844	0.2227	4.2745	−1.5019	FeO		CdO	128.41	0.12460089
15.9994	79.545	0.2011	4.37632	−1.6038	CuO		Cr_2O_3	151.99	0.31581025
15.9994	86.905	0.1841	4.46482	−1.6923	Cl_2O		Fe_2O_3	159.687	0.30058803
15.9994	108.6	0.1473	4.6877	−1.9151	$\frac{1}{3}La_2O_3$		Co_2O_3	165.86	0.2894007
15.9994	128.41	0.1246	4.85523	−2.0827	CdO		V_2O_5	181.88	0.43985045
15.9994	143.09	0.1118	4.96348	−2.1909	Cu_2O		WO_2	215.84	0.14825797
15.9994	153.33	0.1043	5.03257	−2.26	BaO		Fe_3O_4	231.53	0.27642206
15.9994	216.59	0.0739	5.37801	−2.6055	HgO		UO_2	270.027	0.11850667
15.9994	231.74	0.069	5.44562	−2.6731	Ag_2O		Ag_2CO_3	275.75	0.174064
15.9994	260	0.0615	5.56068	−2.7881	—		UO_2Cl_2	340.94	0.0938546
15.9994	300	0.0533	5.70378	−2.9312	—		Gd_2O_3	362.5	0.132409
15.9994	350	0.0457	5.85793	−3.0854	—		Tl_2O_3	456.764	0.10508709
15.9994	400	0.04	5.99146	−3.2189	—		Bi_2O_3	465.96	0.103009
15.9994	450	0.0356	6.10925	−3.3367	—		Re_2O_7	484.4	0.231205
15.9994	500	0.032	6.21461	−3.4421	—		Tl_2SO_4	504.8	0.1267781
15.9994	600	0.0267	6.39693	−3.6244	—		$Ce_2(SO_4)_3$	568.43	0.33776

Table 1: Content of oxygen Y in compounds X per gram-atom (Table 1a) left and summarized O (Table 1b) on the right.

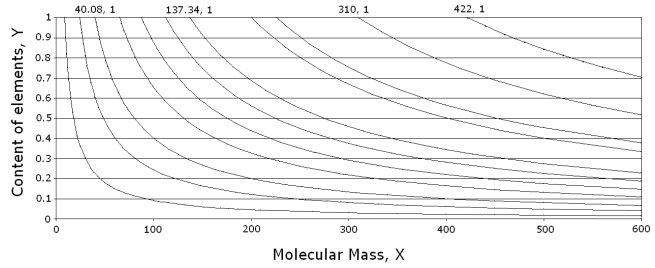

Fig. 2a: Element proportion in chemical compounds against molecular mass ($y = k/x$) on the example of the 2nd Group of the Periodic Table, plus No.126 and No.164.

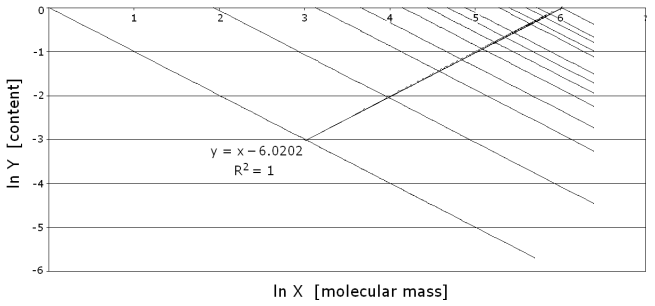

Fig. 2b: Element content versus the molecular mass in chemical compounds of the 1st Group and No.111, calculated No.119, No.155; + virtual axis.

For example, the coordinates of the peak for beryllium are as follows: $X = 60.9097$, $Y = 0.14796$, the normal equation is $Y = 0.0024292\,X$. Taking into consideration that the semiaxis of the rectangular hyperbola $a = b = \sqrt{2\,|K|}$, the coordinates of the point $X_0 = Y_0 = \sqrt{K}$.

Let us examine this fact in relation to elements with the following atomic masses (K): beryllium Be (9.0122), random Z (20), chromium Cr (51.9961), mercury Hg (200.59), No. 126 (310), random ZZ (380), No. 164 (422), random ZZZ (484). In this case $X_0 = Y_0 = \sqrt{K}$, and correspondingly, 3.00203, 4.472136, 7.210825, 14.16298, 17.606817, 19.493589, 20.54264, 22.

The obtained values are the coordinates of the rectangular hyperbola peaks ($X_0 = Y_0$), arranged along the virtual axis, the equation of which is $Y = X$ (because $\tan\alpha = 1$).

3 The point of crossing and the scaling coefficient

Our attention is focused on the point of crossing of the virtual axis with the line $Y = 1$ in Fig. 3 when the atomic mass and the molecular mass are equal, i.e. $K = X$. It is possible only in the case when the origin of the hyperbola and its peak coincide in the point with the maximum content Y according to the equation $Y = \frac{K}{X}$.

The atomic mass of this element was calculated with application of the scaling coefficient and the value of the slope of the virtual axis (the most precise mean is 0.00242917): $\tan\alpha = \frac{y}{x} = 0.00242917$, from which $x = \frac{y}{\tan\alpha}$. Due to

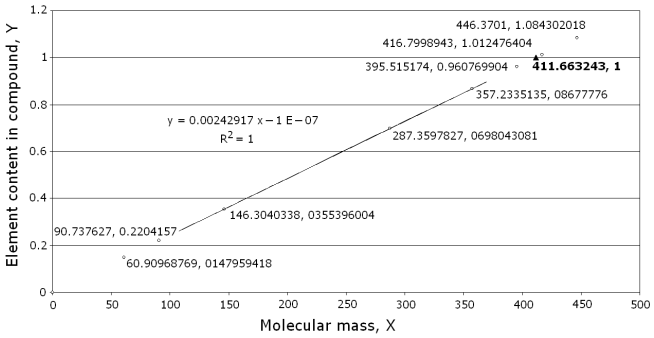

Fig. 3: The virtual axis of the hyperbolas $y = k/x$ with application of the scaling coefficient.

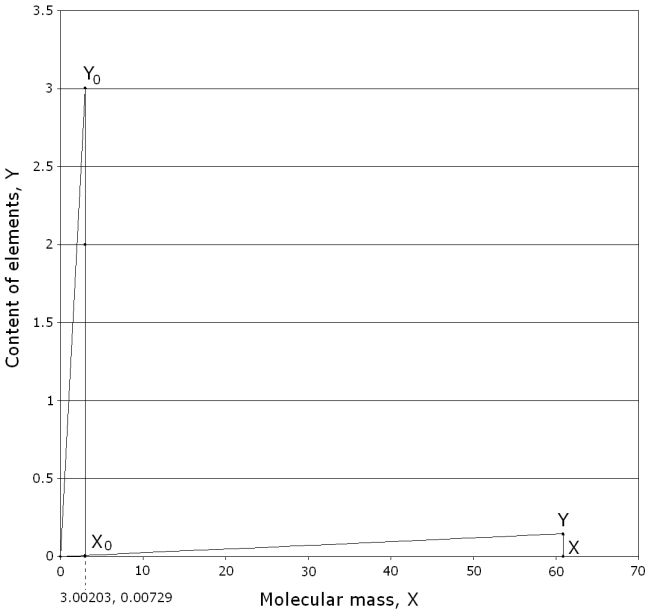

Fig. 4: Inversely proportional dependency in coordinates at calculation of the scaling coefficient.

the fact that at this point $k = x$ we have: $\frac{y}{\tan\alpha} = \frac{1}{\tan\alpha} = 411.663243$. This value is equal to the square of the scaling coefficient too: $20.2895^2 = 411.6638$, $\Delta = 0.0006$.

The coefficient was calculated from matching of the coordinates of the peak hyperbola for beryllium: $X_0 = Y_0 = \sqrt{K}$ and $X = 60.9097$, $Y = 0.14796$. Using this data to construct two triangles (Fig. 4), one easily sees an inversely proportional relationship: $\frac{X}{X_0} = \frac{Y_0}{Y}$, whence $\frac{X}{X_0} = \frac{60.9097}{3.00203} = 20.2895041$ and $\frac{Y_0}{Y} = \frac{3.00203}{0.14976} = 20.28947013$, $\Delta = 0.000034$.

The calculated value $M = 20.2895$ is the scaling coefficient. With its help the scale of system coordinates can be reorganised.

Now if one rectangular hyperbola peak is known, $X_0 = Y_0 = \sqrt{K}$, then the new coordinates will be: $X = X_0\,M$ or $X = M\sqrt{K}$, $Y = \frac{\sqrt{K}}{M}$. Furthermore, $\tan\alpha_0 = \frac{Y_0}{X_0} = 1$, so $\tan\alpha = \frac{Y}{X} = \frac{1}{M^2}$. At the same time at $Y = 1$ and $K = X$, $X = \frac{Y}{\tan\alpha}$ or $K = \frac{Y}{\tan\alpha} = \frac{1}{\tan\alpha} = M^2$.

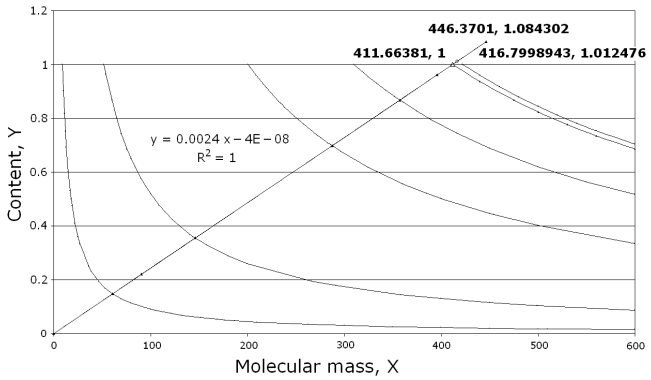

Fig. 5: Element content versus the compound's molecular mass and the hyperbola virtual axes of type $y = k/x$ for the entire Periodical Table. Additionally No.126, No.164 and that rated on (ZZZZ) are introduced.

The results obtained are plotted in Fig. 5 in comparison with the hyperbolas of such elements as Be, Cr, Hg and the hypothetical No.126 (atomic mass = 310), No.164 (atomic mass = 422), ZZZZ (atomic mass = 411.66). It is obvious that it is practically impossible to choose and calculate precisely the curve peak for an atomic mass exceeding the value 250 without the application of the mathematical method adduced herein.

The rated element ZZZZ is the last in the Periodic Table because the hyperbola No.164 after it crosses the virtual axis at the point which coordinates are: $X_0 = Y_0 = \sqrt{422} = 20.5426386$.

After scaling we have $X = 20.2895 \times 20.5426386 = 416.8$ and $Y = 20.5426386/20.2895 = 1.0125$, but this makes no sense because Y cannot exceed the value 1. In addition, the hypothetical atomic mass 422 occurred higher than the molecular mass 416.8, i.e. $X < K$, but that is absurd. Similarly, it is obvious from Fig. 2b how the virtual axis (the equation $Y = X - 6.0202$ where $Y = \ln y$, $X = \ln x$) crossing all the logarithmic straight lines at the points corresponding to the hyperbola peaks, takes the value $\ln x = 6.0202$ at $\ln y = 0$, or after taking logarithms, $X = 411.66$, $Y = 1$.

4 The atomic (ordinal) number

To determine important characteristics of the atomic number some variants of graphical functions of the atomic mass versus the nucleus of all the elements were studied, including No.126. One of them is exponential, with the equation $Y = 1.6091 e^{1.0992x}$ (where y is the atomic mass, x is $\ln$No) at $R^2 = 0.9967$. After taking the logarithm of the both sides and inserting the atomic mass of 411.66 we have No.155. The calculations also demonstrated that the ordinal No.126 should have the atomic mass 327.2 but not 310.

Finally, the following atomic masses were obtained: No.116 — 298.7, No.118 — 304.4, No.119 — 307.2, No.120 — 310, No.126 — 327.3, No.155 — 411.66.

5 The new law

Based on the foregoing, the heretofore unknown Hyperbolic law of the Periodic Table of Elements is established.

This law is due to the fact that the element content Y when estimated in relation to 1 gram-atom, in any chemical combination with molecular mass X, may be described by the adduced equations for the positive branches of the rectangular hyperbolas of the type $Y = \frac{K}{X}$ (where $Y \leqslant 1$, $K \leqslant X$), arranged in the order of increasing nuclear charge, and having the common virtual axis with their peaks tending to the state $Y = 1$ or $K = X$ as they become further removed from the origin of coordinates, reaching a maximum atomic mass designating the last element.

References

1. Seaborg G. T. and Bloom J. L. The synthetic elements. *Scientific American*, 1969, v.220(4), 56.
2. Goldanskii V. I. About connections nuclear and chemical physics. *Progress in Physical Sciences*, 1976, v. 118, issue 2.
3. IUPAC Commission on Atomic Weights and Isotopic Abundances/Atomic Weights of the Elements, 2001.
4. Weisstein E. W. Mean-value theorem. *CRC Concise Encyclopaedia of Mathematics*, 2nd edition, CRC Press, Boca Raton (FL), 2003, 1881.

Less Mundane Explanation of Pioneer Anomaly from Q-Relativity

Florentin Smarandache* and Vic Christianto†

*Department of Mathematics, University of New Mexico, Gallup, NM 87301, USA
E-mail: smarand@unm.edu

†Sciprint.org — a Free Scientific Electronic Preprint Server, http://www.sciprint.org
E-mail: admin@sciprint.org

There have been various explanations of Pioneer blueshift anomaly in the past few years; nonetheless no explanation has been offered from the viewpoint of Q-relativity physics. In the present paper it is argued that Pioneer anomalous blueshift may be caused by Pioneer spacecraft experiencing angular shift induced by similar Q-relativity effect which may also affect Jupiter satellites. By taking into consideration "aether drift" effect, the proposed method as described herein could explain Pioneer blueshift anomaly within ∼0.26% error range, which speaks for itself. Another new proposition of redshift quantization is also proposed from gravitational Bohr-radius which is consistent with Bohr-Sommerfeld quantization. Further observation is of course recommended in order to refute or verify this proposition.

1 Introduction

In the past few years, it is becoming well-known that Pioneer spacecraft has exhibited an anomalous Doppler frequency blueshifting phenomenon which cannot be explained from conventional theories, including General Relativity [1, 4]. Despite the nature of such anomalous blueshift remains unknown, some people began to argue that a post-einsteinian gravitation theory may be in sight, which may be considered as further generalisation of pseudo-Riemannian metric of general relativity theory.

Nonetheless, at this point one may ask: Why do we require a generalization of pseudo-Riemannian tensor, instead of using "patch-work" as usual to modify general relativity theory? A possible answer is: sometimes too much patch-work doesn't add up. For instance, let us begin with a thought-experiment which forms the theoretical motivation behind General Relativity, an elevator was put in free-falling motion [8a]. The passenger inside the elevator will not feel any gravitational pull, which then it is interpreted as formal analogue that "inertial acceleration equals to gravitational acceleration" (Equivalence Principle). More recent experiments (after Eötvös) suggest, however, that this principle is only applicable at certain conditions.

Further problem may arise if we ask: what if the elevator also experiences lateral rotation around its vertical axis? Does it mean that the inertial acceleration will be slightly higher or lower than gravitational pull? Similarly we observe that a disc rotating at high speed will exert out-of-plane field resemble an acceleration field. All of this seems to indicate that the thought-experiment which forms the basis of General Relativity is only applicable for some limited conditions, in particular the $F = m\frac{dv}{dt}$ part (because General Relativity is strictly related to Newtonian potential), but it may not be able to represent the rotational aspects of gravitational phenomena. Einstein himself apparently recognizes this limitation [8a, p.61]:

> "... all bodies of reference K' should be given preference in this sense, and they should be exactly equivalent to K for the formation of natural laws, provided that they are in a state of *uniform rectilinear and non-rotary motion* with respect to K." (Italic by Einstein).

Therefore, it shall be clear that the restriction of *non-rotary motion* remains a limitation for all considerations by relativity theory, albeit the *uniform rectilinear* part has been relaxed by general relativity theory.

After further thought, it becomes apparent that it is required to consider a new kind of metric which may be able to represent the rotational aspects of gravitation phenomena, and by doing so extends the domain of validity of general relativity theory.

In this regard, the present paper will discuss the aforementioned Pioneer blueshift anomaly from the viewpoint of Q-relativity physics, which has been proposed by Yefremov [2] in order to bring into application the quaternion number. Despite the use of quaternion number in physical theories is very scarce in recent years — apart of Pauli matrix — it has been argued elsewhere that using quaternion number one could expect to unify all known equations in Quantum Mechanics into the same framework, in particular via the known isomorphism between Dirac equation and Maxwell equations [5].

Another problem that was often neglected in most treatises on Pioneer spacecraft anomaly is the plausible role of aether drift effect [6]. Here it can be shown that taking this effect into consideration along with the aforementioned Q-relativity satellite's apparent shift could yield numerical prediction of Pioneer blueshift within ∼0.26% error range, which speaks for itself.

We also suggest a new kind of Doppler frequency shift which can be predicted using Nottale-type gravitational Bohr-radius, by taking into consideration varying G parameter as described by Moffat [7]. To our knowledge this proposition of new type of redshift corresponding to gravitational Bohr-radius has never been considered before elsewhere.

Further observation is of course recommended in order to verify or refute the propositions outlined herein.

2 Some novel aspects of Q-relativity physics. Pioneer blueshift anomaly

In this section, first we will review some basic concepts of quaternion number and then discuss its implications to quaternion relativity (Q-relativity) physics [2]. Then we discuss Yefremov's calculation of satellite time-shift which may be observed by precise measurement [3]. We however introduce a new interpretation here that such a satellite Q-timeshift is already observed in the form of Pioneer spacecraft blueshift anomaly.

Quaternion number belongs to the group of "very good" algebras: of real, complex, quaternion, and octonion [2]. While Cayley also proposed new terms such as quantic, it is less known than the above group. Quaternion number can be viewed as an extension of Cauchy imaginary plane to become [2]:

$$Q \equiv a + bi + cj + dk\,, \tag{1}$$

where a, b, c, d are real numbers, and i, j, k are imaginary quaternion units. These Q-units can be represented either via 2×2 matrices or 4×4 matrices [2].

It is interesting to note here that there is quaternionic multiplication rule which acquires compact form:

$$1q_k = q_k 1 = q_k\,, \quad q_j q_k = -\delta_{jk} + \varepsilon_{jkn} q_n\,, \tag{2}$$

where δ_{kn} and ε_{jkn} represent 3-dimensional symbols of Kronecker and Levi-Civita, respectively [2]. Therefore it could be expected that Q-algebra may have neat link with pseudo-Riemannian metric used by General Relativity. Interestingly, it has been argued in this regard that such Q-units can be generalised to become Finsler geometry, in particular with Berwald-Moor metric. It also can be shown that Finsler-Berwald-Moor metric is equivalent with pseudo-Riemannian metric, and an expression of Newtonian potential can be found for this metric [2a].

It may also be worth noting here that in 3D space Q-connectivity has clear geometrical and physical treatment as movable Q-basis with behaviour of Cartan 3-frame [2].

It is also possible to write the dynamics equations of Classical Mechanics for an inertial observer in constant Q-basis. $SO(3,R)$-invariance of two vectors allow to represent these dynamics equations in Q-vector form [2]:

$$m\frac{d^2}{dt^2}\left(x_k q_k\right) = F_k q_k\,. \tag{3}$$

Because of antisymmetry of the connection (generalised angular velocity) the dynamics equations can be written in vector components, by conventional vector notation [2]:

$$m\left(\vec{a} + 2\vec{\Omega}\times\vec{v} + \vec{\Omega}\times\vec{r} + \vec{\Omega}\times\left(\vec{\Omega}\times\vec{r}\right)\right) = \vec{F}\,. \tag{4}$$

Therefore, from equation (4) one recognizes known types of classical acceleration, i.e. linear, coriolis, angular, centripetal. Meanwhile it is known that General Relativity introduces Newton potential as *rigid* requirement [2a, 6b]. In other words, we can expect — using Q-relativity — to predict new effects that cannot be explained with General Relativity.

From this viewpoint one may consider a generalisation of Minkowski metric into biquaternion form [2]:

$$dz = \left(dx_k + i dt_k\right) q_k\,, \tag{5}$$

with some novel properties, i.e.:

- temporal interval is defined by imaginary vector;
- space-time of the model appears to have six dimensions (6D);
- vector of the displacement of the particle and vector of corresponding time change must always be normal to each other, or:

$$dx_k dt_k = 0\,. \tag{6}$$

It is perhaps quite interesting to note here that Einstein himself apparently once considered similar approach, by proposing tensors with Riemannian metric with Hermitian symmetry [8]. Nonetheless, there is difference with Q-relativity described above, because in Einstein's generalised Riemannian metric it has 8-dimensions, rather than 3d-space and 3d-imaginary time.

One particularly interesting feature of this new Q-relativity (or rotational relativity) is that there is universal character of motion of the bodies (including non-inertial motions), which can be described in unified manner (Hestenes also considers Classical Mechanics from similar spinor language). For instance advanced perihelion of planets can be described in term of such rotational precession [2].

Inspired by this new Q-relativity physics, it can be argued that there should be anomalous effect in planets' satellite motion. In this regard, Yefremov argues that there should be a deviation of the planetary satellite position, due to discrepancy between calculated and observed from the Earth motion magnitudes characterizing cyclic processes on this planet or near it. He proposes [2]:

$$\Delta\varphi \approx \frac{\omega V_e V_p}{c^2}\,t\,, \tag{7}$$

or

$$\Delta\varphi' \approx -\frac{\omega V_e V_p}{c^2}\,t'. \tag{8}$$

Therefore, given a satellite orbit radius r, its position shift is found in units of length $\Delta l = r\,\Delta\varphi$. His calculation

Satellites	Cycle frequency ω, 1/s	Angular shift $\Delta\varphi$, $''$/100 yrs	Linear shift Δl, km/100 yrs	Linear size a, km
Phobos (Mars)	0.00023	18.2	54	20
Deimos (Mars)	0.00006	4.6	34	12
Metis (Jupiter)	0.00025	**10.6**	431	40
Adrastea (Jupiter)	0.00024	**10.5**	429	20
Amalthea (Jupiter)	0.00015	6.3	361	189

Table 1: The following table gives values of the effect for five fast satellites of Mars and Jupiter. Orbital linear velocities are: of the Earth $V_E = 29.8$ km/s, of Mars $V_P = 24.1$ km/s, of Jupiter $V_P = 13.1$ km/s; the value of the light velocity is $c = 299\,793$ km/s; observation period is chosen 100 years. Courtesy of A. Yefremov, 2006 [3].

for satellites of Mars and Jupiter is given in Table 1. Nonetheless he gave no indication as to how to observe this anomalous effect.

In this regard, we introduce here an alternative interpretation of the aforementioned Q-satellite time-shift effect by Yefremov, i.e. this effect actually has similar effect with Pioneer spacecraft blueshift anomaly. It is known that Pioneer spacecraft exhibits this anomalous Doppler frequency while entering Jupiter orbit [1, 4], therefore one may argue that this effect is caused by Jupiter planetary gravitational effect, which also may cause similar effect to its satellites.

Despite the apparent contradiction with Yefremov's own intention, one could find that the aforementioned Q-satellite time-shift could yield a natural explanation of Pioneer spacecraft blueshift anomaly. In this regard, Taylor [9] argues that there is possibility of a mundane explanation of anomalous blueshift of Pioneer anomaly (5.99×10^{-9} Hz/sec). The all-angle formulae for relativistic Doppler shift is given by [9a, p.34]:

$$v' = v_0\gamma\,\frac{(1-\beta\cos\phi)}{\sqrt{1-\beta^2}}\,, \tag{9}$$

where $\beta = v/c$. By neglecting the $\sqrt{1-\beta^2}$ term because of low velocity, one gets the standard expression:

$$v' = v_0\gamma\,(1-\beta\cos\phi)\,. \tag{9a}$$

The derivative with respect to ϕ is:

$$\frac{dv'}{d\phi} = v_0\gamma\beta\sin\phi\,, \tag{10}$$

where $\frac{dv'}{d\phi} = 5.99\times10^{-9}$ Hz/sec, i.e. the observed Pioneer anomaly. Introducing this value into equation (10), one gets requirement of an effect to explain Pioneer anomaly:

$$d\phi = \frac{\arcsin\,(5.99\times10^{-9}\,\text{Hz})}{v_0\gamma\beta} = 1.4\times10^{-12}\,\text{deg/sec}. \tag{11}$$

Therefore, we can conclude that to explain 5.99×10^{-9} Hz/sec blueshift anomaly, it is required to find a shift of emission angle at the order 1.4×10^{-12} degree/sec only (or around $15.894''$ per 100 years).

Interestingly this angular shift can be explained with the same order of magnitude from the viewpoint of Q-satellite angular shift (see Table 1), in particular for Jupiter's Adrastea ($10.5''$ per 100 years). There is however, a large discrepancy at the order of 50% from the expected angular shift.

It is proposed here that such discrepancy between Q-satellite angular shift and expected angular shift required to explain Pioneer anomaly can be reduced if we take into consideration the "aether drift" effect [6]. Interestingly we can use experimental result of Thorndike [6, p.9], saying that the aether drift effect implies a residual apparent Earth velocity is $v_{obs} = 15 \pm 4$ km/sec. Therefore the effective V_e in equation (8) becomes:

$$V_{e.eff} = v_{obs} + V_e = 44.8\,\text{km/sec}. \tag{12}$$

Using this improved value for Earth velocity in equation (8), one will get larger values than Table 1, which for Adrastea satellite yields:

$$\Delta\varphi_{obs} = \frac{\omega V_{e.eff} V_p}{c^2}\,t = \frac{V_{e.eff}}{V_e}\Delta\varphi = 15.935''/100\,\text{yrs}. \tag{13}$$

Using this improved prediction, the discrepancy with required angular shift only ($15.894''$ per 100 years) becomes $\sim 0.26\%$, which speaks for itself. Therefore one may conclude that this less mundane explanation of Pioneer blueshift anomaly with Q-relativity may deserve further consideration.

3 A new type of redshift from gravitational Bohr radius. Possible observation in solar system.

In preceding paper [10, 11] we argued in favour of an alternative interpretation of Tifft redshift quantization from the viewpoint of quantized distance between galaxies. A method can be proposed as further test of this proposition both at solar system scale or galaxies scale, by using the known quantized Tifft redshift [14, 15, 16]:

$$\delta r \approx \frac{c}{H}\,\delta z\,. \tag{14}$$

In this regards, we use gravitational Bohr radius equation:

$$r_n = n^2\frac{GM}{v_0^2}\,. \tag{15}$$

Inserting equation (15) into (14), then one gets quantized redshift expected from gravitational Bohr radius:

$$z_n = \frac{H}{c} n^2 \frac{GM}{v_0^2} \tag{16}$$

which can be observed either in solar system scale or galaxies scale. To our present knowledge, this effect has never been described elsewhere before.

Therefore, it is recommended to observe such an accelerated Doppler-freequency shift, which for big jovian planets this effect may be detected. It is also worth noting here that according to equation (16), this new Doppler shift is quantized.

At this point one may also take into consideration a proposition by Moffat, regarding modification of Newtonian acceleration law to become [7]:

$$a(r) = -\frac{G_\infty M}{r^2} + K\frac{\exp(-\mu_\phi r)}{r^2}(1+\mu_\phi r) \tag{17}$$

where

$$G_\infty = G\left[1+\sqrt{\frac{M_0}{M}}\right]. \tag{17a}$$

Therefore equation (16) may be rewritten to become:

$$z_n \approx \frac{H}{c} n^2 \frac{GM}{v_0^2}\left[1+\sqrt{\frac{M_0}{M}}\right] \approx \chi \frac{H}{c} n^2 \frac{GM}{v_0^2} \tag{18}$$

where n is integer (1, 2, 3, ...) and:

$$\chi = \left[1+\sqrt{\frac{M_0}{M}}\right]. \tag{18a}$$

To use the above equations, one may start by using Bell's suggestion that there is fundamental redshift $z = 0.62$ which is typical for various galaxies and quasars [14]. Assuming we can use equation (16), then by setting $n = 1$, we can expect to predict the mass of quasar centre or galaxy centre. Then the result can be used to compute back how time-variation parameter affects redshift pattern in equation (18). In solar system scale, time-varying radius may be observed in the form of changing Astronomical Unit [4].

This proposition, however, deserves further theoretical considerations. Further observation is also recommended in order to verify and explore further this proposition.

4 Concluding remarks

In the present paper it is argued that Pioneer anomalous blueshift may be caused by Pioneer spacecraft experiencing angular shift induced by similar Q-relativity effect which may also affect Jupiter satellites. By taking into consideration aether drift effect, the proposed method as described herein could predict Pioneer blueshift within ~0.26% error range, which speaks for itself. Further observation is of course recommended in order to refute or verify this proposition.

Another new proposition of redshift quantization is also proposed from gravitational Bohr-radius which is consistent with Bohr-Sommerfeld quantization. It is recommended to conduct further observation in order to verify and also to explore various implications of our propositions as described herein.

Acknowledgment

The authors are would like to thank to Profs. C. Castro, E. Scholz, T. Love, and D. L. Rapoport for valuable discussions. Special thanks to Prof. A. Yefremov for sending his recent calculation of Jupiter satellite's Q-time-shift effect.

References

1. Anderson J.D., Campbell J.K., & Nieto M.M. arXiv: astro-ph/ 0608087; [1a] Nieto M.M. & Anderson J.D. arXiv: gr-qc/0507052.
2. Yefremov A. *Hypercomplex Numbers in Geometry and Physics*, 2004, v. 1(1), 105; [2a] Pavlov D. G. arXiv: math-ph/ 0609009.
3. Yefremov A. Private communication, October 2006. Email: a.yefremov@rudn.ru.
4. Laemmerzahl C. & Dittus H. Clocks and gravity, from quantum to cosmos. UCLA, 2006, http://www.physics.ucla.edu/quantum_to_cosmos/q2c06/Laemmerzahl.pdf
5. Christianto V. *EJTP*, 2006, v. 3, No. 12, http://www.ejtp.com.
6. Consoli M. arXiv: physics/0306094, p. 9; [6a] Consoli M. *et al.* arXiv: gr-qc/0306105; [6b] arXiv: hep-ph/0109215.
7. Moffat J. arXiv: astro-ph/0602607.
8. Einstein A. *Ann. Math.*, 1945, v. 46; [8a] Einstein A. Relativity: the special and general theory. Crown Trade Paperback, New York, 1951, pp. 61, 66–70.
9. Taylor S. arXiv: physics/0603074; [9a] Engelhardt W. *Apeiron*, 2003, v. 10, No. 4, 34.
10. Smarandache F. & Christianto V. *Progress in Physics*, 2006, v. 4, 27–31.
11. Smarandache F. & Christianto V. *Progress in Physics*, 2006, v. 4, 37–40.
12. Smarandache F. & Christianto V. *Progress in Physics*, 2006, v. 2, 63–67.
13. Fischer U. arXiv: cond-mat/9907457; [13a] arXiv: cond-mat/ 0004339.
14. Bell M.B. arXiv: astro-ph/0111123; [14a] Bell M.B. arXiv: astro-ph/0305112; [14b] Bell M.B. arXiv: astro-ph/0305060.
15. Humphreys R. *TJ Archive*, v. 16, http://answersingenesis.org.
16. Múnera H. *Apeiron*, 1998, v. 5, No. 3–4.
17. Zurek W. (ed.) *Proc. Euroconference in Formation and Interaction of Topological Defects*, Plenum, 1995; arXiv: cond-mat/9502119.
18. Volovik G. arXiv: cond-mat/0507454.

Study of the Matrix Effect on the Plasma Characterization of Heavy Elements in Soil Sediments using LIBS with a Portable Echelle Spectrometer

Walid Tawfik Y. Mohamed*,† and Abeer Askar*

*National Inst. of Laser Enhanced Science NILES, Dept. of Environmental Applications, Cairo University, Cairo, Egypt
†Faculty of Education for Girls, Department of Physics, Gurayyat, North of Al-gouf, Kingdom of Saudi Arabia

Corresponding author: Walid Tawfik Y. Mohamed. E-mail: Walid_Tawfik@hotmail.com

Laser-induced breakdown spectroscopy (LIBS) has been applied to perform a study of the matrix effect on the plasma characterization of soil sediment targets. The plasma is generated by focusing a pulsed Nd: YAG laser on the target in air at atmospheric pressure. The plasma emission spectrum was detected using a portable Echelle spectrometer (Mechelle 7500 — Multichannel Instruments, Stockholm, Sweden) with intensified CCD camera. Spectroscopic analysis of plasma evolution of laser produced plasmas has been characterized in terms of their spectra, and electron temperature. Four heavy elements V, Pb, Mn and Co were determined in the obtained spectra. The LTE and optically thin plasma conditions were verified for the produced plasma. The electron temperature and density were determined using the emission intensity and stark broadening, respectively, of the spectral lines of the heavy elements in the soil sediments. The electron temperature does not change with concentration. For environmental applications, the obtained results showed the capability of the proposed LIBS setup with the portable Mechelle 7500 spectrometer to be applied in-situ for real-time measurements of the variation of the matrix elemental composition of soil sediments by following up only a single element as a marker for the composition of the soil sediment without need of analysis of the other elements.

1 Introduction

The Laser Induced Breakdown Spectroscopy (LIBS) technique has been already applied to the determination of elemental concentrations in a wide range of materials in solid, liquid and gaseous phase. Measurements consist of spectral and time resolved analysis of the atomic and ionic emission lines, arising from the plasma generated by an intense laser pulse. In the case of condensed samples, the plasma is produced through laser-induced evaporation of the sample surface layer [1]. The use of laser induced breakdown spectroscopy (LIBS) in the analysis of soil and soil sediments has been studied in recent years as a technique for in-situ detection of hazardous metals [2–7]. One of the main problems in the use of LIBS is the necessity of making a calibration curve with samples possessing the same matrix composition of the samples to be analyzed. In 1998, Valery Bulatov et al. proposed a method in which the composition of a sample could be determined without the need of calibration curves [8]. However, this method is based on the measurement of the emission from all the species present in the sample, a requirement difficult to satisfy when dealing with soil sediments. The physical and chemical properties of the sample can affect the produced plasma composition, a phenomenon known as the matrix effect. The matrix effect can result in the sample being ablated differently from the target sample. The interaction between the laser and the target in LIBS is influenced significantly by the overall composition of the target, so that the intensity of the emission lines observed is a function of both the concentration of the elements of interest and the properties of the matrix that contains them. Plasma composition is dependent not only on the composition of the sample, but also on laser parameters, sample surface conditions as well as on thermal and optical properties of the sample. Previously published works studied the matrix effect under different experimental conditions to specify causes and find out the methods of correction [9–14]. The different approaches have been undertaken to discriminate between the problems resulting from the fractionation of the ablation and matrix effects. The most convenient approach is to determine elemental abundance by comparing the analyte line intensities with signals obtained from the proper reference standards having a similar matrix composition [15]. But it is not always possible to obtain such calibration curves because there are no available standard samples, or it is impossible to have an internal standard of known concentration [16]. In addition, plasma formation dynamics, sample ablation and associated processes, are highly nonlinear and not fully understood and may also play an important rôle in the matrix effect.

Recently an alternative procedure, based on the LIBS technique, for quantitative elemental analysis of solid materials has been proposed, which can, in principle, provide quantitative data with no need of calibration curves or intern-

al standards [17, 18]. The method relies on the assumption about the existence of the stoichiometric ablation and local thermodynamic equilibrium (LTE) i.e. Boltzmann distribution and Saha equation amongst the level population of any species and electron density and temperature of the plasma. However for application of this method experimentally one needs to obtain both equilibrium and thin plasma conditions, a task that may not be always possible to perform. Thus, in spite of the many advantages of LIBS the realization of a quantitative analytical method, which is able to measure the main constituents in samples from different matrices, still remains a difficult task because of the complex laser-sample and laser-plasma interaction mechanisms. As a rule, laser ablation plasma is characterized by complex spatial and temporal structures, and one meets a wide range of parameter variation during the plasma existence time.

In this paper we report on the optimized conditions for LIBS to analyze the emission spectrum of soil sediment samples with high resolution using a portable Echelle spectrometer — Mechelle 7500 — equipped with an ICCD camera. Spectroscopic analysis of plasma evolution of laser produced plasmas has been characterized in terms of their spectra, and electron temperature. Four heavy elements V, Pb, Mn and Co were determined in the obtained spectra. The electron temperature was determined using the emission intensity of the spectral lines of the heavy elements in the soil sediments. The dependence of the electron temperature on the concentrations of these heavy elements was studied.

The aim of this paper is to prove that the proposed LIBS setup could be used in the on-line environmental applications control. This could be done by following up only a single element as a marker for the composition of the soil sediment without need of analysis of the other elements.

2 Methodology

A typical LIBS experimental setup, described in detail elsewhere [3, 9, 10, 15], was used throughout the present investigations. Laser induced plasma was produced by focusing 180 mJ of a Q-switched Nd: YAG laser (surelite I, continuum, USA) operating at 1064 nm (pulse duration of 7 ns) on soil sediment samples. An energy meter (Nova 978, Ophir Optronics Ldt., USA) was employed to monitor the shot to shot pulse energy. The laser beam was focused on soil sediment samples by a 10 cm focal length quartz lens to generate the plasma. The focal point was set 5 mm below the surface of the sample in order to generate plasma of 800 μm spot diameter. This also minimized breakdown above the surface of any particles and aerosols generally present above the sample. A one meter length of used-silica optical fiber (600 μm diameter) mounted on a micro xyz-translation stage was used to collect the emission light from the plasma plume and feed it to a portable Echelle spectrometer of a 0.17 m focal length (Mechelle 7500, Multichannel instruments, Sweden). The use of a micro xyz-translation stage as a holder for fused-silica optical fibre facilitated maximum intensity of the observed emission light from the plasma plume. On the other hand, the Echelle grating spectrometers, designed for operation in high orders and high angles of incidence and diffraction, can provide high resolution in a more compact size and cover a much wider spectral range than conventional grating spectrometers [19]. This is because the Mechelle 7500 provides a constant spectral resolution (CSR) of 7500 corresponding to 4 pixels FWHM over a wavelength range 200–1000 nm displayable in a single spectrum. A gateable, intensified CCD camera, (DiCAM-Pro-12 bit, UV enhanced, 43000 channels, PCO Computer Optics, Germany) coupled to the spectrometer was used for detection of the dispersed light. The overall linear dispersion of the spectrometer camera system ranges from 0.006 (at 200 nm) to 0.033 nm/pixel (at 1000 nm). To avoid electronic interference and jitters, the intensifier high voltage was triggered optically. Echelle spectra display, control, processing and analysis were done using both Mechelle software (Multichannel Instruments, Stockholm, Sweden) and GRAMS/32 version 5.1 Spectroscopic Data Analysis Software (Galactic Industries, Salem, NH, USA).

To improve LIBS precision, spectra from several laser shots have to be averaged in order to reduce statistical error due to laser shot-to-shot fluctuation. We reproduced the measurements at four locations on the sample surface in order to avoid problems linked to sample heterogeneity. Fifty laser shots were fired at each location and saved in separated files and the average (average of 250 spectra) was computed and saved to serve as the library spectrum. For each recorded spectrum, the peak intensity, the Lorentzian curve fitting, the full width at half maximum FWHM, and the center wavelength of each line, as well as the background emission continuum were determined. Data treatment preprocessing of the averaged spectra was performed in the Microsoft Windows XP environment on a Pentium 4 PC using GRAMS/32, Excel (Microsoft office Excel 2003) and Origin software version 7.0220 (Origin Lab corporation, USA). The averages of peak tables (lists of wavelengths and intensities) of the averaged spectra were roll generated in GRAMS/32 and exported for data evaluation.

Three certified reference samples were purchased from the International Atomic Energy Agency (IAEA). The standard samples were named IAEA-SL-1, IAEA-SL-5 and IAEA-SL-7. Another three standard samples have been made by mixing of the IAEA-samples in different ratios. These samples were named Mix A, Mix B, and Mix C. The composition of Mix A, Mix B and Mix C are (37.3% of IAEA-SL-1 + 62.7% of IAEA-SL-5), (37.3% of IAEA-SL-7 + 62.7% of IAEA-SL-5) and (26.3% of IAEA-SL-1 + 73.7% of IAEA-SL-7) respectively. These mixtures were carefully blended and grounded in a ceramic grinder, then seived using a stainless steel sieve with a net grain size of 70 microns to ensure

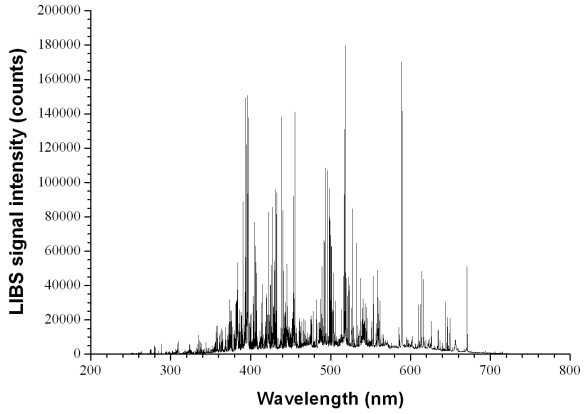

Fig. 1: Typical LIBS spectrum for soil sediment target. The laser energy was 100 mJ at wavelength 1064 nm, plasma emissions are accumulated with delay 2.5 μs, and gate width 1 μs.

Sample	Mn	Pb	Co	V
IAEA-SL-1	3460	37.7	19.8	170
IAEA-SL-5	852	129	14.8	151
IAEA-SL-7	631	60	8.9	66
Mix A	1825	95	16.6	158
Mix B	770	103.2	12.6	119.3
Mix C	1375	54.1	11.7	93.4

Table 1: The elemental concentrations of Mn, Pb, Co and V in the six standard soil sediments (in ppm).

good homogeneity and to simulate the properties of the original standard samples. The powder of each of the six standard samples was put into a stainless steel dish (30-mm diameter $\times$ 7-mm deep) to be pressed into a form of tablet at a hydraulic press weight of 20 tons/cm^2 to be suitable for handling in LIBS experiments. The elemental concentrations of Mn, Pb, Co and V in the six standard soil sediments are given in Table 1.

3 Results and discussion

3.1 LIBS spectrum

Figure 1 shows a typical plasma emission spectrum for soil sediment sample IAEA-SL-1. This spectrum is the average of 250 single shot spectra recorded at 1.5 μs delay time and 1 μs gate width.

The panoramic Echelle spectra in the spectral range 200–750 nm show the UV-visible emission lines of soil sediment samples which have a very rich spectral structure and, consequently a lot of interfering lines. In particular, soil sediment samples, made mostly of inorganic material constituents, give rise to a dense spectrum due to the contribution of heavy atom emissions in the investigated range [6]. Moreover, our observed spectra reflect the wide spectral range and the high resolution of the spectroscopic system used.

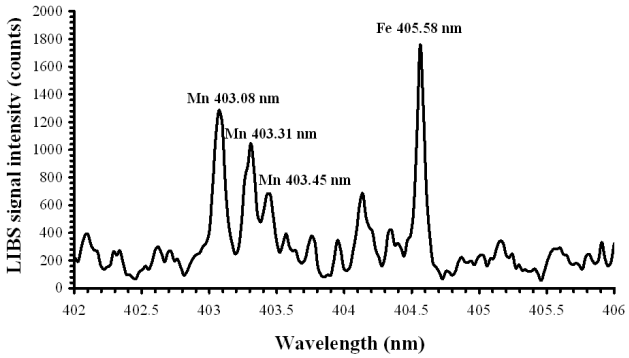

Fig. 2: Shows a high resolution spectrum of Mn with concentration of 0.346% in soil sediment sample IAEA-SL-1. Intensities ratios of the manganese triplet at wavelengths: 403.08, 403.31 and 403.45 nm are consistent with the ratios of the statistical weights of their upper level (7:5:3).

3.2 Plasma characterization

In LIBS experiments, after the initial plasma decay and during the entire observation interval, the local thermodynamic equilibrium (LTE) conditions are assumed to hold.

On the other hand, optically thin plasma has been confirmed by checking the intensity ratios of the manganese triplet at wavelengths: 403.08, 403.31 and 403.45 nm which are consistent with the ratios of the statistical weights of their upper level (7:5:3) as shown in Fig. 2 (refer to Table 2). This result indicates that the plasma was optically thin according to a procedure described previously by Simeonsson and Miziolek [20].

For optically thin plasma, the re-absorption effects of plasma emission are negligible, so the emitted spectral line intensity I is a measure of the population of the corresponding energy level of this element in the plasma. For the LTE plasma, the population of an excited level can be related to the total density $N(T)$ of neutral atom or ion of this element by Boltzmann equation as:

$$I = \frac{hc}{4\pi\lambda} N(T) \frac{A_{ki}\, g_k}{U(T)} \exp\left(-\frac{E_k}{KT}\right), \qquad (1)$$

where λ is the wavelength, A_{ki} is the transition probability, g_k is the statistical weight for the upper level, E_k is the excited level energy, T is the temperature (in LTE all temperatures are assumed to be equal, i.e. $T_e \approx T_{ion} \approx T_{plasma}$, K is Boltzmann's constant, $U(T)$ is the partition function.

The emitted spectral line intensity from a given state of excitation can be used to evaluate the plasma temperature. The lines must be well resolved for accurately evaluating their wavelengths λ, intensities I, and their transition probabilities A_{ki} must be well known [21].

Reformulating Eqn. 1 gives:

$$\ln \frac{I\,\lambda}{A_{ki}\, g_k} = -\frac{1}{KT} E_k + \ln \frac{C\,F}{U(T)}, \qquad (2)$$

Element	Wavelength, nm	A_{ki}, s^{-1}	E_k, cm^{-1}	g_k	Element	Wavelength, nm	A_{ki}, s^{-1}	E_k, cm^{-1}	g_k
Pb	240.194	2.79E+07	49439.62	3	Co	242.493	3.20E+08	41225.76	10
Pb	244.6181	2.45E+07	48686.93	3	Co	243.221	2.60E+08	41918.41	8
Pb	244.6181	2.45E+07	48686.93	3	Co	252.136	3.00E+08	39649.16	8
Pb	247.6378	3.78E+07	48188.63	5	Co	252.897	2.80E+08	40345.95	6
Pb	247.6378	3.78E+07	48188.63	5	Co	253.596	1.90E+08	40827.77	4
Pb	257.726	6.68E+07	49439.62	3	Co	254.425	3.00E+08	41101.8	2
Pb	257.726	6.68E+07	49439.62	3	Co	340.512	1.00E+08	32841.99	10
Pb	261.3655	1.87E+07	46068.44	3	Co	344.364	6.90E+07	33173.36	8
Pb	261.4175	2.35E+08	46060.84	5	Co	345.35	1.10E+08	32430.59	12
Pb	262.8262	5.59E+07	48686.93	3	Co	347.402	5.60E+07	33466.87	8
Pb	265.7094	9.91E+05	45443.17	5	Co	348.94	1.30E+08	36092.44	6
Pb	266.3154	1.01E+08	48188.63	5	Co	350.228	8.00E+07	32027.5	8
Pb	280.1995	1.08E+08	46328.67	7	Co	351.835	1.60E+08	36875.13	4
Pb	282.3189	3.04E+07	46060.84	5	Co	356.938	1.50E+08	35450.56	8
Pb	283.3053	5.92E+07	35287.22	3	Co	358.719	1.40E+08	36329.86	6
Pb	287.3311	4.15E+07	45443.17	5	Co	389.408	6.90E+07	34133.59	8
Pb	357.2729	4.08E+08	49439.62	3	V	230.785	2.60E+08	47345.94	11
Pb	363.9568	3.20E+07	35287.22	3	V	231.16	2.80E+08	47807.58	9
Pb	367.1491	1.11E+08	48686.93	3	V	231.405	2.80E+08	48151.07	7
Pb	368.3462	1.70E+08	34959.91	1	V	231.496	2.70E+08	48388.62	5
Pb	373.9935	8.30E+07	48188.63	5	V	235.341	1.90E+08	47039.27	7
Pb	401.9632	3.55E+07	46328.67	7	V	236.38	2.10E+08	46320.96	9
Pb	405.7807	9.12E+07	35287.22	3	V	237.862	1.90E+08	45378.85	9
Pb	406.2136	1.07E+08	46068.44	3	V	238.345	1.80E+08	45972.17	7
Co	231.16	2.80E+08	47807.58	9	V	238.892	2.80E+08	45197.78	11
Co	231.405	2.80E+08	48151.07	7	V	240.416	1.50E+08	46786.53	3
Co	235.341	1.90E+08	47039.27	7	V	240.725	3.60E+08	41528.53	12
Co	236.38	2.10E+08	46320.96	9	V	241.446	3.40E+08	42811.44	8
Co	237.862	1.90E+08	45378.85	9	V	241.53	3.60E+08	43199.65	6
Co	238.345	1.80E+08	45972.17	7	V	242.493	3.20E+08	41225.76	10
Co	238.892	2.80E+08	45197.78	11	V	243.221	2.60E+08	41918.41	8
Co	240.416	1.50E+08	46786.53	3	V	243.666	2.60E+08	42434.23	6
Co	240.725	3.60E+08	41528.53	12	V	243.905	2.70E+08	42796.67	4
Co	241.446	3.40E+08	42811.44	8	V	252.136	3.00E+08	39649.16	8
Co	241.53	3.60E+08	43199.65	6	V	252.897	2.80E+08	40345.95	6
V	253.596	1.90E+08	40827.77	4	Mn	404.14	7.87E+07	41789.48	10
V	254.425	3.00E+08	41101.8	2	Mn	404.88	7.50E+07	42143.57	4
V	340.512	1.00E+08	32841.99	10	Mn	405.55	4.31E+07	41932.64	8
V	344.364	6.90E+07	33173.36	8	Mn	405.89	7.25E+07	42198.56	2
V	345.35	1.10E+08	32430.59	12	Mn	406.17	1.90E+07	49415.35	6
V	347.402	5.60E+07	33466.87	8	Mn	406.35	1.69E+07	42053.73	6
V	348.94	1.30E+08	36092.44	6	Mn	407.92	3.80E+07	42143.57	4
V	350.228	8.00E+07	32027.5	8	Mn	408.29	2.95E+07	42053.73	6
V	351.835	1.60E+08	36875.13	4	Mn	408.36	2.80E+07	41932.64	8
V	356.938	1.50E+08	35450.56	8	Mn	423.51	9.17E+07	46901.13	6
V	358.719	1.40E+08	36329.86	6	Mn	441.49	2.93E+07	45940.93	6
V	389.408	6.90E+07	34133.59	8	Mn	445.16	7.98E+07	45754.27	8
Mn	401.81	2.54E+07	41932.64	8	Mn	446.20	7.00E+07	47207.28	10
Mn	403.08	1.70E+07	24802.25	8	Mn	475.40	3.03E+07	39431.31	8
Mn	403.31	1.65E+07	24788.05	6	Mn	478.34	4.01E+07	39431.31	8
Mn	403.45	1.58E+07	24779.32	4	Mn	482.35	4.99E+07	39431.31	8

Table 2: A list of the spectroscopic data of the spectral lines used for the determination of plasma temperature and density of soil sediment samples.

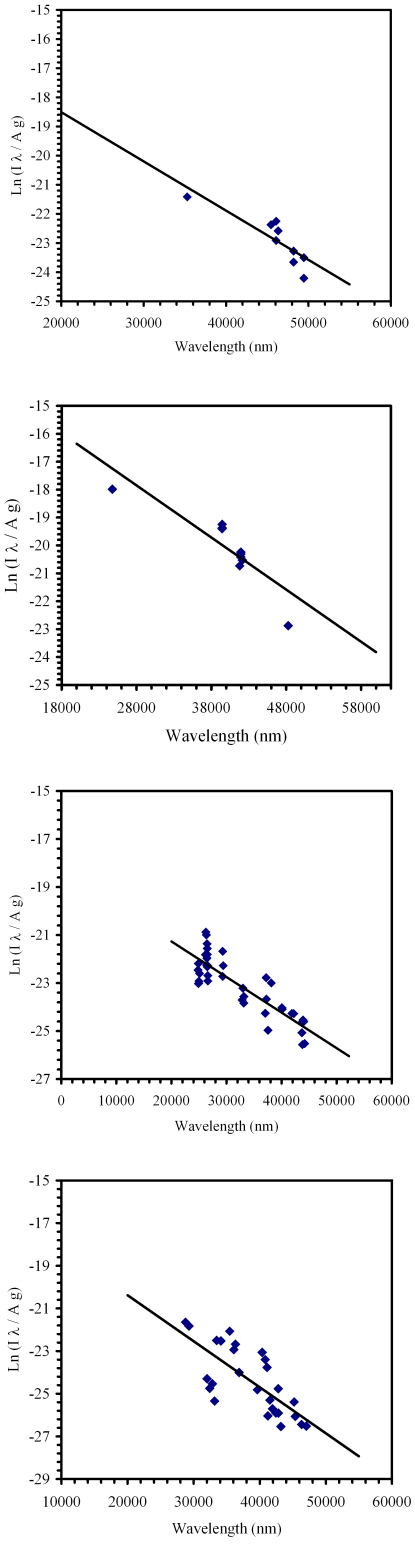

Fig. 3: Four Boltzmann plots were determined form the emission line intensities of Pb, Mn, V, and Co (shown, respectively, from up to down) observed in the laser-induced plasma of soil sediments. The slope of the plotted curves yields temperatures of for the elements 8526 K, 7700 K, 9693 K, and 6658 K respectively.

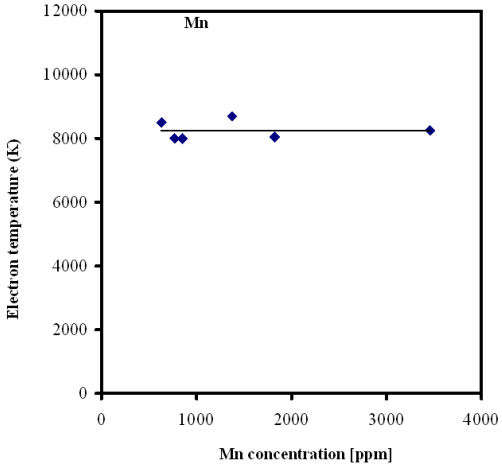

Fig. 4: Temperature measured at 2.5 μs delay time and 1 μs gate width for different concentrations of manganese in soil sediment samples.

where F is an experimental factor and C is the species concentration.

By plotting the left hand side of Eqn. 2 against the excited level energy E_k, the plasma temperature can be obtained from the slope of the resulting straight line.

The temperatures were determined form the emission line intensities of Mn, V, Co, and Pb observed in the laser-induced plasma of soil sediments. Figure 3 shows four Boltzmann plots of Eqn. 2, for each of these four trace elements where the data were fitted with the least-squares approximation. The spectral line wavelengths, energies of the upper levels, statistical weights, and transition probabilities used for each element are obtained from Griem [21], NIST [22] and Kurucz [23], and listed in Table 2. The slope of the plotted curves yields temperatures 7700 K, 9693 K, 6658 K, and 8526 K for the elements Mn, V, Co, and Pb respectively. The average value of the plasma temperature is 8000 K for soil sediment, which agrees with the value obtained by V. Lazic et al. [27] under conditions similar to ours. The difference in the plasma temperature of the four elements may be attributed to the difference in the excitation and ionization potentials between these elements.

Study of the matrix effect on the plasma temperature was done by plotting the corresponding temperature for each element against its concentration in the soil sediment samples. The variation of the plasma temperature with the concentration of the four elements was found to be about $\pm$500 K around the 8000 K as shown in Fig. 4 for Mn as an example. The figure reveals that plasma temperature has a small variation, due to some experimental errors and matrix effect, around an average value with the elemental concentration. This can be understood as follows; for optically thin plasma, increasing the element concentration returns an increasing intensity of its corresponding spectral lines with roughly the same ratio, which leads to the same slope of the Boltzmann

plot and results in the same plasma temperature.

The electrons in the plasma can perturb the energy levels of the individual ions which broaden the emission lines originating from these excited levels. Stark broadening of well-isolated lines in the plasma is, thus, useful for estimating the electron number densities provided that the Stark-broadening coefficients have been measured or calculated. The line profile for Stark broadening is well described by a Lorentzian function. The Stark line width $\Delta\lambda_{FWHM}$ can be extracted from the measured line width $\Delta\lambda_{observed}$ by subtracting the instrumental line broadening $\Delta\lambda_{instrument}$:

$$\Delta\lambda_{FWHM} = \Delta\lambda_{observed} - \Delta\lambda_{instrument}. \quad (3)$$

In our case $\Delta\lambda_{instrument}$ was 0.05 nm (determined by measuring the FWHM of the Hg lines emitted by a standard low pressure Hg lamp).

The width of Stark broadened spectral lines depends on the electron density N_e. The electron density N_e (in cm^{-3}) could be determined from the FWHM of the line from the formula [21]:

$$N_e \approx \left(\frac{\Delta\lambda_{FWHM}}{2w}\right) \times 10^{16}, \quad (4)$$

where w is the electron impact parameter (stark broadening value). This formula is generally used for calculations of plasma generated from solid targets [7, 27, 28]. Substituting the values of Stark broadening w from [21], [30], [31], and [32] in Eqn. 4, the electron density for soil sediment samples is $3\times10^{17}\,\mathrm{cm}^{-3}$. The obtained results agree with those reported by O. Samek [29].

Finally, by knowing the electron density and the plasma temperature we can determine whether the local thermodynamic equilibrium (LTE) assumption is valid by applying the criterion given by McWhirter [26].

The lower limit for electron density for which the plasma will be in LTE is:

$$N_e \geqslant 1.6\times10^{12}\,\Delta E\,T^{1/2}, \quad (5)$$

where ΔE is the largest energy transition for which the condition holds and T is the plasma temperature [20].

In the present case $\Delta E = 4.9\,\mathrm{eV}$ for Si (one of the main elements in soil sediments) and the electron density lower limit value given by Eqn. 5 is $6\times10^{15}\,\mathrm{cm}^{-3}$ (see ref. 21). The experimentally calculated densities are greater than this value, which is consistent with the assumption that the LTE prevails in the plasma.

4 Conclusion

In summary, we have carried out an accurate LIBS setup using a portable commercial Echelle spectrometer equipped with ICCD detector to study soil sediments matrix effects on the plasma characterization. Four trace heavy elements V, Pb, Mn and Co were determined in the obtained spectra. The electron density and plasma temperature were determined for the soil sediment targets. For a plasma diagnostics perspective, the target physical properties play an important role in the obtained values of the laser induced plasma temperature T_e and electron density N_e. The obtained results indicate that the produced plasma parameters (T_e, N_e) are the same for any of the elements in the same matrix composition. On the other hand, T_e and N_e are different for different matrix composition as proven previously by our group [10]. So the proposed LIBS setup could be used in on-line environmental applications control. This could be done by following up only single element as markers for the composition of the soil sediment without need of analysis of the other elements.

Acknowledgements

The authors especially acknowledge Prof. M. Abdel Harith for offering the soil sediment samples.

References

1. Piepmeier E.H. Laser ablation for atomic spectroscopy analytical application of laser. John Wiley & Sons, N.Y., 1986.
2. Davies B.E. Trace metals in the environment: retrospect and prospect. In: Adriano D.C., Ed. *Biogeochemistry of Trace Metals, Advances in Trace Substances Research*, Lewis Publishers, Boca Raton, FL, 1992, 1–17.
3. Soliman M., Tawfik W., and Harith M.A. Quantitative elemental analysis of agricultural drainage water using laser induced breakdown spectroscopy, First Cairo conference on plasma physics & applications. Cairo, Egypt, Forschungszentrum Juelich GmbH, Bilateral Seminars of the International Bureau, v. 34, 2003, 240–243.
4. Wisbrun R., Schechter I., Niessner R., and Shröder H. Laser induced breakdown spectroscopy for detection of heavy metals in environmental samples. *SPIE*, 1992, v. 1716 (SPIE, Bellingham, Washington), 2–14.
5. Colao F., Barbini R., Fantoni R., Lazic V., Palucci A., Capitelli F., and van der Steen H.J.L. Laser induced breakdown spectroscopy for semi-quantitative elemental analysis in soils and marine sediments. *EARSeL Conference Proceeding*, Dresden, Germany, 1999.
6. Barbini R., Colao F., Fantoni R., Palucci A., Ribezzo S., van der Steen H.J.L., and Angelone M. Semi-quantitative time resolved LIBS measurements. *Appl. Phys. B*, 1997, v. 65, 101–107.
7. Barbini R., Colao F., Fantoni R., Palucci A., and Capitelli F. Application of laser induced breakdown spectroscopy to the analysis of metals in soils. *Appl. Phys. A*, 1999, v. 69, 175–179.
8. Bulatov V., Krasniker R., and Schechter I. Study of matrix effects in laser plasma spectroscopy by combined multifiber spatial and temporal resolutions. *Anal. Chem.*, 1998, v. 70, 5302–5310.

9. Sabsabi M., Detalle V., Harith M.A., Tawfik W., and Imam H. Comparative study of two new commercial Echelle spectrometers equipped with intensified CCD for analysis of laser-induced breakdown spectroscopy. *Applied Optics*, 2003, v. 42, No. 30, 6094–6098.
10. Ismail M.A., Imam H., Elhassan A., Youniss W.T., and Harith M.A. LIBS limit of detection and plasma parameters of some elements in two different metallic matrices. *J. Anal. At. Spectrom.*, 2004, v. 19, 1–7.
11. Xu L., Bulatov V., Gridin V., and Schechter I. Absolute analysis of particulate materials by laser-induced breakdown spectroscopy. *Anal. Chem.*, 1997, v. 69, 2103–2108.
12. Goode S.R., Morgan S.L., Hoskins R., and Oxsher A. Identifying alloys by laser-induced breakdown spectroscopy with a time-resolved high resolution echelle spectrometer. *J. Anal. At. Spectrom.*, 2000, v. 15, 1133–1138.
13. Eppler A.S., Cremers D.A., Hickmott D.D., Ferris M.J., and Koskelo A.C. Matrix effects in the detection of Pb and Ba in soils using laser-induced breakdown spectroscopy. *Appl. Spectrosc.*, 1996, v. 50, 1175–1181.
14. Quentmeier A., Sdorra W., and Niemax K. Internal standardization in laser induced fluorescencs spectrometry of microplasms produced by laser ablation of solid samples. *Spectrochimica Acta B*, 1990, v. 45, No. 6, 5371–5379.
15. Tawfik W. Quantitative elemental analysis of seawater by laser induced breakdown spectroscopy. *Intern. J. of Pure and Applied Physics*, 2006, v. 2, No. 1, 11–21.
16. Ciucci A., Corsi M., Palleschi V., Rastelli S., Salvetti A., and Tognoni E. A new procedure for quantitative elemental analyses by laser induced plasma spectroscopy. *Applied Spectroscopy*, 1999, v. 53, 960–964.
17. Bulajic D., Corsi M., Cristoforetti G., Legnaioli S., Palleschi V., Solvetti A., and Rognoni E. A procedure for correcting self-absorption in calibration-free laser induced breakdown spectroscopy. *Spectrochim. Acta B*, 2002, v. 57, 339–353.
18. Corsi M., Palleschi V., Salvetti A., and Tognoni E. Making LIBS quantitative: a critical review of the current approaches to the problem. *Res. Adv. Appl. Spectrosc.*, 2000, v. 1, 41–47.
19. Olesik J.W. Echelle grating spectrometers for inductively coupled plasma-optical emission spectrometry. *Spectroscopy*, 1999, v. 14, No. 10, 27–30.
20. Simeonsson J.B. and Miziolek A.W. Time-resolved emission, studies of ArF laser-produced micro plasmas. *Appl. Opt.*, 1993, v. 32, 939–947.
21. Griem H.R. Plasma spectroscopy. McGraw-Hill, N.Y., 1964.
22. NIST National Institute of Standards and Technology, USA. Electronic database, http://physics.nist.gov/PhysRefData/ASD/lines_form.html.
23. Kurucz Atomic Line Database, http://www.cfa.harvard.edu/amdata/ampdata/kurucz23/sekur.html.
24. Lida Y. Effects of atmosphere on laser vaporization and excitation processes of solid samples. *Spectrochim. Acta B*, 1990, v. 45, 1353–1367.
25. Nemet B. and Kozma L. Time-resolved optical emission spectrometry of Q-switched Nd: YAG laser-induced plasmas from copper targets in air at atmospheric pressure. *Spectrochim. Acta B*, v. 50, 1869–1888.
26. Kyuseok Song, Hyungki Cha, Jongmin Lee, and Yong Lee. Investigation of the line-broadening mechanism for laser-induced copper plasma by time-resolved laser-induced breakdown spectroscopy. *Microchemical J.*, 1999, v. 63, 53–60.
27. Lazic V., Colao F., Barbini R., Fantoni R., and Palucci A. Self-absorption model in quantitative laser induced breakdown spectroscopy measurements on soils and sediments. *Spectrochimica Acta B*, 2001, v. 56, 807–820.
28. Sabsabi M. and Cielo P. Quantitative analysis of aluminum alloys by laser-induced breakdown spectroscopy and plasma characterization. *Applied Spectroscopy*, 1995, v. 49, No. 4, 499–507.
29. Samek O., Beddows D.C.S., Telle H.H., Kaiser J., Liska M., Caceres J.O., and Gonzales Urena A. Quantitative laser-induced breakdown spectroscopy analysis of calcified tissue samples. *Spectrochimica Acta B*, 2001, v. 56, 865–875.
30. Tankosic D., Popovic L.C., and Dimitrijevic M.S. The electron-impact broadening parameters for Co III spectral lines. *Astronomy and Astrophysics*, 2003, v. 399, 795–797.
31. Popovic L.C. and Dimitrijevic M.S. Tables of the electron impact broadening parameters: Mn II, Mn III, Ga III, Ge III and Ge Iv Lines. *Bull. Astron. Belgrade*, 1997, No. 156, 173–178.
32. Dunaevsky A., Chirko K., Krasik Ya. E. and Felsteiner J. Spectroscopy of a ferroelectric plasma cathode. *J. Appl. Phys.*, 2001, v. 90, No. 8, 4108–4114.

Search for Anisotropic Light Propagation as a Function of Laser Beam Alignment Relative to the Earth's Velocity Vector

C. E. Navia, C. R. A. Augusto, D. F. Franceschini, M. B. Robba and K. H. Tsui
Instituto de Física Universidade Federal Fluminense, 24210-346, Niterói, RJ, Brazil
Corresponding author: C. E. Navia. E-mail: navia@if.uff.br

A laser diffraction experiment was conducted to study light propagation in air. The experiment is easy to reproduce and it is based on simple optical principles. Two optical sensors (segmented photo-diodes) are used for measuring the position of diffracted light spots with a precision better than 0.1 μm. The goal is to look for signals of anisotropic light propagation as function of the laser beam alignment to the Earth's motion (solar barycenter motion) obtained by COBE. Two raster search techniques have been used. First, a laser beam fixed in the laboratory frame scans in space due to Earth's rotation. Second, a laser beam mounted on a turntable system scans actively in space by turning the table. The results obtained with both methods show that the course of light rays are affected by the motion of the Earth, and a predominant first order quantity with a $\Delta c/c = -\beta(1 + 2a)\cos\theta$ signature with $\bar{a} = -0.393 \pm 0.032$ describes well the experimental results. This result differs in amount of 21% from the Special Relativity Theory prediction and that supplies the value of $a = -\frac{1}{2}$ (isotropy).

1 Introduction

There are several physical reasons, theoretical and experimental, that could justify a search for anisotropies in light propagation. It is well known that Lorentz and Poincaré were the first ones to build the major part of the relativity theory on the basis of the ether concept as an inertial rest frame, and it is compatible with the Einstein's Special Relativity Theory (SRT). There are also some test theories of SRT, where the Lorentz transformations are modified. For example, an ether theory that maintains the absolute simultaneity and is kinematically equivalent to Einstein SRT was constructed [1]. These test theories are considered useful to examine potential alternatives to SRT. On the other hand, the reconstruction of the SRT, on the basis of the Lorentz-Poincaré scheme implies in an undetectable ether rest frame (non ether drift) at least in the first order [2].

This behavior of the Lorentz-Poincaré, as well as, of the Einstein theories arise because they do not govern the whole physics, for instance they do not involve gravitation. It is also well known that the presence of a gravitational field breaks the Lorentz symmetry.

On the other hand, periodic boundary conditions or close space-time topology, such as the Sagnac effect [3] where two opposite light beams travel in different time intervals the same closed path on a rotating disk, as well as the twin paradox, leads to preferred frame effects. This assumption of a preferred frame comes from an analysis made by Brans and Stewart [4] on the twin paradox, where a description of the close topology of the universe has imposed a preferred state of rest so that the principle of special relativity, although locally valid, is not globally applicable. Similar conclusion is obtained in the Wucknitz's paper [5], where standard notation of SRT using Lorentz transformations leads to coordinates which are valid locally. Periodic boundary conditions or close space-time topology, such as the Sagnac effect and the twin paradox, leads to preferred frame effects.

The above conclusion is reinforced by the generalized Sagnac effect [6] observed in a light waveguide loop consisting of linearly and circularly segments, any segment of the loop contributes to the phase difference between two counter-propagating light beams in the loop. Showing that the acceleration is not essential to take into account the effect.

A preferred frame emerge also from an analysis on the Global Positioning System (GPS) made by R. Hatch [7] and T. Van Flandern [8] where the preferred frame is not universal, but rather coincides with the local gravity field.

On the other hand, according to Fox [9], it is possible to preserve the general Lorentz Poincaré symmetry group without assuming the constancy of light speed. There are also the so called extended theories, where the SRT is modified in order to including the Planck scale parameters [10] (double relativity theories), suggesting several dispersion relations that include theories where an energy dependent speed of light [11] is claimed.

There are also evidences suggesting that the propagation of light over cosmological distances has anisotropic characteristics [12], with dependence on direction and polarization. This picture is in agreement with the interpretations of the COBE [13] measurements giving the Earth's "absolute" velocity in relation to the uniform cosmic microwave background radiation (CMBR). Of course, there are also interpretations claiming that the COBE measurements give only a velocity for the "relative" motion between the Earth and the CMBR [14]. For instance, it is possible to obtain a "virtual" image, where an isotropic distribution of CMBR with small

fluctuations ($\delta T/T \sim 10^{-5}$) can be seen, by removing the Earth motion.

So far, several tests about violation of the isotropy of the speed of light have been made. In most cases, the tests involve the so called round-trip test of light-speed isotropy like Michelson-Morley experiment and all its variants. Particularly, Miller [15, 16] has claimed a non-null results in the M-M experiments. These aspects are presented in Appendix.

On the other hand, there are also several one-way test of light isotropy experiments. In most cases, they have claimed a null result [17, 18, 19, 20]. Particularly the NASA's Deep Space Network [21] using hydrogen-maser frequency have to obtained a crude bound $\Delta c(\theta)/c < 4.5\times10^{-6}$ for the anisotropy of the one way velocity of light and refined to $\Delta c(\theta)/c < 3.5\times10^{-7}$. However, according to their own conclusions the validity of these limits rest upon the assumption that the prediction phase variations were not partially canceled. There are also experiments that have claimed success [22, 23]. Particularly, Silvertooth has claimed an experimental detection of the ether drift velocity using a device capable of detecting the beams arriving in opposite directions [23]. Silvertooth reported in 1986 a light anisotropy toward the direction of Leo constellation and compatible with COBE results. The experiment is an unusual double interferometer, an arrangement of light paths and detectors hard to be reproduced. In addition, the presence of a feedback into the laser is quite probable.

In this paper, we report results of a search for anisotropic light propagation as a function of the laser beam alignment relative to the Earth's velocity vector, using a diffraction device. The method is based on simple optical principles. Initial attempts have used digital images of the diffraction spots. However, this method was working in the limit of sensitivity. In other words, the signal's size was close to the measurement resolution. Now, our results are obtained by using the highly sensitive segmented photo-diodes to measure the position of diffracted light spots. In Section 2, the experimental setup and the basic operating principles of the diffractometer are presented. The Earth's velocity vector on the basis of the Doppler shift of the CMBR results are presents in Section 3. In Section 4, the two scanning methods and their results are presented, and finally Section 5 contains our conclusions.

2 Experimental setup and method

The diffraction experiment is installed on the campus of the Universidade Federal Fluminense, Niterói, Rio de Janeiro-Brazil at sea level. The position is given by 22°54′33″ S latitude and 43°08′39″ W longitude. The diffraction experiment is mounted on a horizontal rotating circular table.

The layout of the diffraction device is shown in Fig. 1. A laser beam transverse to a diffraction grating is diffracted in several rays. In order to determine the position of the

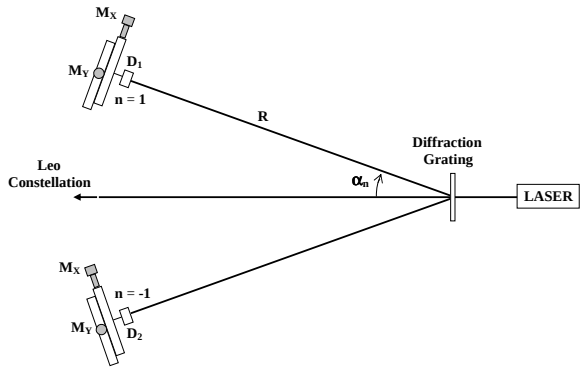

Fig. 1: General layout of the diffraction experiment. Two segmented photo-diodes (D_1 and D_2) are positioned using two vertical platforms with two positioning system (micrometers $M_x - M_y$) to detect two diffracted rays produced by a HE-Ne laser on a grating diffraction device. The relative position of a light spot with respect to the center on a segmented photo-diode is obtained by simply measuring the output current of each segment. The setup is mounted on a turntable system

light spots, we have used two segmented PSD photo-diodes divided into two segments, separated by a gap (see Fig. 2). The position of each photo-diode coincides with the positions of the maxima intensity of the diffraction images, for $n = +1$ and $n = -1$ respectively, as shown in Fig. 1. Two precision multi-axis positioning systems, and each one consist of a vertical platform with two independent (X–Y) micrometers, have been used to mount the photo-diodes.

Following Fig. 1, it is possible to see that the maxima of intensity of the diffraction images (rays) satisfy the condition

$$\sin\alpha_n = \pm n\,\frac{\lambda}{\eta\,\delta}, \quad \text{with} \quad n = 0, 1, 2, \ldots, \qquad (1)$$

where $\lambda\,(= 632.8\,\text{nm})$ is the wave length, $\delta\,(= 1/600\,\text{mm})$ is the diffraction grating step and $\eta\,(= 1.000226)$ is the refraction index of air. The wave length λ can be obtained as the ratio between the speed of light c and the light frequency ν resulting in $\lambda = c/\nu$. An expression for c as a function of the angle α can be obtained as

$$c = \frac{\eta\,\nu\,\delta}{n}\,\sin\alpha_n\,. \qquad (2)$$

Under the assumption that ν and η remain constant during the experiment, and if c depends on the direction of propagation, variations of the diffraction spot positions, α_n, for instance, as a function of the laser beam alignment, relative to the Earth's velocity vector, can be interpreted as an indication of violation of the isotropy of c. The relative variation can be expressed as

$$\frac{\Delta c}{c} = \frac{\Delta(\sin\alpha_n)}{\sin\alpha_n} = \cot\alpha_n\;\Delta\alpha_n\,. \qquad (3)$$

We look for this anisotropic light propagation signal through measurements of $\Delta\alpha_n$ as a function of the Earth's

Observer	Year	v_E, km/s	α, hour	δ, degree
Pensias & Wilson (ground) [27]	1965		I s o t r o p i c	
Conklin (ground) [28]	1969	200±100	13±2	30±30
Henry (balloon) [29]	1971	320±80	10±4	−30±25
Smoot et al. (airplane) [30]	1977	390±60	11.0±0.5	6±10
COBE (satellite) [32]	1991	371±0.5	11.20±0.01	−7.22±0.08
WMAP (satellite) [33]	2003	368±0.2	11.20±0.01	−7.22±0.08

Table 1: Vector velocity of the Earth (solar system) relative to the CMBR rest frame, measured using the anisotropy of the CMBR in several experiments.

velocity vector. The search has been made by using two independent types of scanning, and the methods as well as the results are presented in Section 4.

The determination of the position of the light spots is made by measuring the output photo-current in each segment of the photo-diodes. A symmetric spot, positioned at the center, generates equal photo-currents in the two segments. The relative position is obtained by simply measuring the output current of each segment. The position of a light spot with respect to the center on a segmented photo-diode is found by

$$\Delta l = l_0 \left(\frac{I_1 - I_2}{I_1 + I_2} \right) , \qquad (4)$$

where l_0 is a proportionality constant. The method offers position resolution better than 0.1 μm, and the angular variation can be obtained as

$$\Delta\alpha_n = \frac{\Delta l}{R} = \frac{l_0}{R} \left(\frac{I_1 - I_2}{I_1 + I_2} \right) . \qquad (5)$$

For the diffraction experiment with $R = 30.0$ cm, the angular resolution is better than 3.3×10^{-7} rad.

We have used the data acquisition system of the Tupi muon telescope [24, 25, 26], which is made on the basis of the Advantech PCI-1711/73 card. The analog output signal from each segmented photo-diodes is linked to the analog input of the PCI card. The PCI card has 16 analog input channels with a A/D conversion up to 100 kHz sampling rate. All the data manipulations such as the addition and the subtraction of currents are made via software, using the virtual instrument technique. The application programs were written using the Lab-View tools. A summary of the basic circuit is shown in Fig. 2.

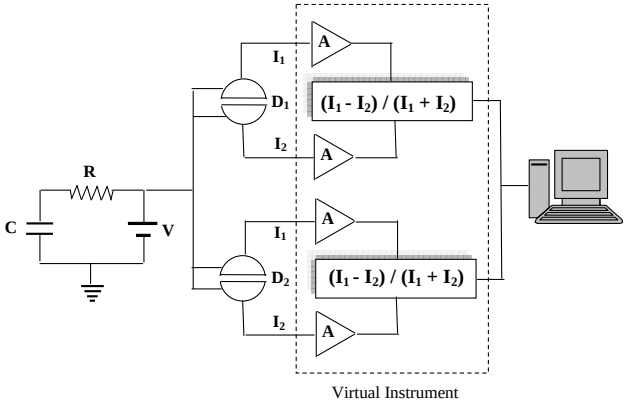

Fig. 2: Block diagram of the diffraction experiment data acquisition system. D_1 and D_2 represent the segment photo-diodes.

3 The Earth's velocity vector

The discovery of a pervasive background radiation from the universe by Penzias and Wilson [27] in 1965 is probably the strongest evidence for the hot Big Band model. The CMBR is a 2.7 Kelvin thermal black body spectrum with a peak in the micro wave range, and it is considered a relic of the Big Bang. In the past when the Universe was much smaller, the radiation was also much hotter. As the Universe expanded, it cooled down to the present level.

In Penzias-Wilson's data, the radiation appeared as highly isotropic. However, in the next round of experiments [28, 29, 30] temperature anisotropies were found. These anisotropies are expressed using the spherical harmonic expansion, and the Earth's motion with velocity $\beta = v/c$ relative to the CMBR rest frame of temperature T_0 produces a Doppler shift as

$$\frac{\Delta T}{T_0} = \beta \cos\theta + \frac{\beta^2}{2} \cos 2\theta + \mathrm{O}(\beta^3) . \qquad (6)$$

In Table 1, measurements of the velocity vector of the Earth (solar system) in several experiments in chronological order using the anisotropy of the CMBR are summarized. Southern Hemisphere airborne measurements of the anisotropy in the cosmic microwave background radiation by Smoot and Lubin [31] (1979 — Lima, Peru) are in essential agreement with previous measurements from the northern hemisphere and the first-order anisotropy is readily interpreted as resulting from a motion of the Sun relative to the background radiation.

The COBE data [32] indicate a big temperature anisotropy in the cosmic background radiation which is represented by a dipole form with an amplitude of $\Delta T/T_0 = 1.23 \times 10^{-3} = 0.123\%$. This arises from the motion of the solar system barycenter, with a velocity $v = 371 \pm 0.5$ km/s ($\beta = 0.001237 \pm 0.000002$) at 68%CL, relative to the so called

"CMBR rest frame" and towards a point whose equatorial coordinates are $(\alpha, \delta) = (11.20^{\mathrm{h}} \pm 0.01^{\mathrm{h}}, -7.22^{\circ} \pm 0.08^{\circ})$. This direction points to the Leo constellation. Recently, the WMAP [33] mission has improved the resolution of the angular power spectrum of the CMBR and has verified the COBE results.

4 Raster search techniques

We look for an anisotropy signal in the light propagation as a function of the Earth's velocity vector. At our latitude ($\sim 23^{\circ}$ S) there are two passages of the Leo constellation on the horizon every 24 hours. The first one is near the West direction, and the second is approximately 12 hours later, and it is near the East direction. Consequently it is possible to mount a laser diffraction experiment on a horizontal turntable system and point the laser beam toward the Leo constellation. The raster search can be made by using two methods as are described below.

4.1 Passive raster search system due to Earth's rotation

This method consists in to fix the laser beam direction toward the first or second passage of the Leo constellation on the horizon. As the Earth rotates, the laser beam will be aligned to the first or second passage of the Leo constellation (CMBR apex according to COBE) on the horizon over a 24 hour period.

As the laser, the diffraction grating, and the detectors are always fixed, the method is free of mechanical perturbations, which can be introduced, for instance, when the system is rotated. However, the method requires measurements over a long period of time (at least 12 hours) and several days and this introduces the so called DRIFT-long-term timing variation by aging due to temperature variations (diurnal and semi-diurnal temperature dependence). In the case of diffraction experiments, this effect is amplified due to the temperature dependence of the refraction index. Even so, the situation is not critical, because the angular variation of the diffracted rays is obtained from the ratio $(I_1 - I_2)/(I_1 + I_2)$ and the systematic effects tend to the cancel.

There is also the JITTER-timing (short term) noise due to statistical fluctuations of the signal (shot and thermal noises), and they have a "white" frequency distribution, where the spectral power densities are constant.

If the CMBR apex has an altitude, h, and an azimuth angle, θ_A, the projection of the Earth's velocity, v, on the laser beam direction is

$$v_p = v \cos(\theta_A - \theta_{beam}) \cos h \,, \tag{7}$$

where θ_{beam} is the azimuth of the laser beam and coincides with the CMBR apex azimuth when it is on the horizon. Consequently, the values $\theta_A = \theta_{beam}$ and $h = 0$ represents the CMBR apex culmination on the horizon.

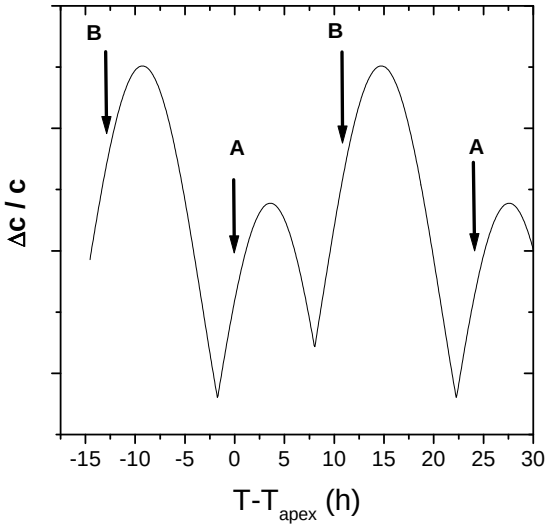

Fig. 3: Expected variation of the one way light speed anisotropy relative to the CMBR dipole direction for a period of 24 hours according to Mausouri and Sexl test theory (with $a \neq -\frac{1}{2}$) and modulated by the altitude variation of the CMBR apex due to Earth rotation. The curve was obtained for the Latitude $= 23^{\circ}$ S. The vertical arrows A and B indicates the moment of the passage of the CMBR apex for the horizon. In A (B) the laser beam is parallel (anti-parallel) to the Earth velocity vector.

On the other hand, we have analyzed the experimental data using the test theory of Mausouri and Sexl [1]. according to this test theory, the one way speed of light is anisotropic by an among

$$c(\theta) = c - v(1 + 2a) \cos\theta \,, \tag{8}$$

where θ is the angle between the velocity, v, of the moving system (i.e. the Earth motion) and the direction of light propagation. In our experiment $\theta = \theta_A - \theta_{beam}$. The value $a = -\frac{1}{2}$ correspond to the isotropic SRT prediction, and $a \neq -\frac{1}{2}$ represents an anisotropic signal in the one-way path speed of light. According to Eq. 7 in the passive raster search system, the Mausouri and Sexl equation is modulated by the altitude variation and can be expressed as

$$c(\theta, h) = c - v(1 + 2a) \cos(\theta_A - \theta_{beam}) \cos h \,, \tag{9}$$

and the relative variation is

$$\Delta c(\theta, h)/c = -\beta(1 + 2a) \cos(\theta_A - \theta_{beam}) \cos h \,, \tag{10}$$

where $\beta = v/c$. As we know the equatorial coordinates of the CMBR $(\alpha, \delta) = (11.20^{\mathrm{h}} \pm 0.01^{\mathrm{h}}, -7.22^{\circ} \pm 0.08^{\circ})$ according to COBE. The transformation from equatorial coordinate system (α, δ) to the horizontal coordinate system (θ_A, h) permits to obtain a correlation between θ_A and h as

$$h = \arcsin(\sin\phi \sin\delta + \cos\phi \cos\delta \cos H) \,, \tag{11}$$

$$\theta_A = \arcsin(-\cos\delta \sin H / \cos h) \,, \tag{12}$$

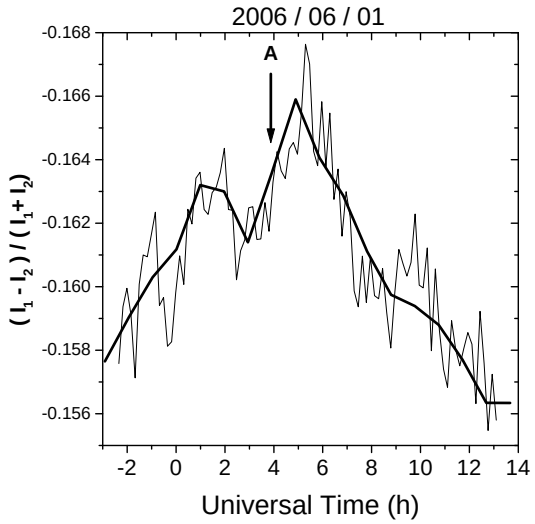

Fig. 4: Histogram obtained in the passive scan system averaging the raw data in blocks of 10 minutes The vertical arrow indicates the moment of the passage of the CMBR apex (according to COBE) for the horizon. The bold line represent a polynomial fit on the data.

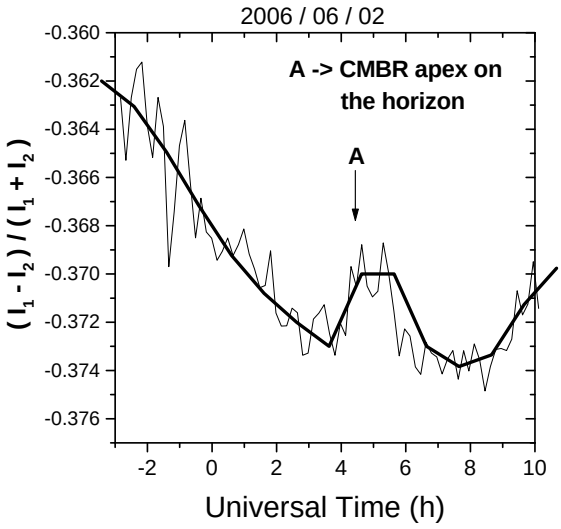

Fig. 5: The same as Fig. 4.

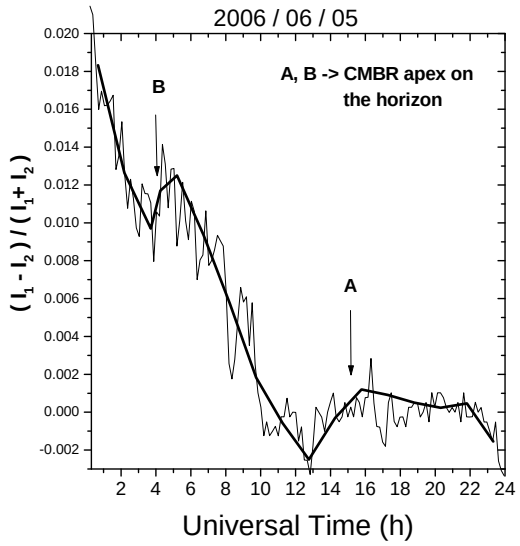

Fig. 6: The same as Fig. 4

where $\phi(=-23^\circ\ \mathrm{S})$ is the latitude and $H(=T-\alpha)$ is the hour angle and T is the sidereal time. Under this conditions, the behavior of $(\Delta c/c)$ given by the Eq. 10 is reproduced in Fig. 3, where the vertical arrows A and B indicates the moment of the passage of the CMBR apex (according to COBE) for the horizon. In A (B) the laser beam is parallel (anti-parallel) to the Earth velocity vector.

In the experiment $\Delta c/c$ is inferred from $\Delta\alpha_n$ measurements (see Eq. 3 and Eq. 5 from Section 2). Examples of raster scans (in the passive mode) were obtained in the first set of measurements (June of 2006) as shown in Fig. 4, Fig. 5 and Fig. 6. Four months after we have repeating the experiment and the result obtained on November of 2006 is shown in Fig. 7. In all cases, built-in a DRIFT-long-term it is possible to see peculiar signatures (see Fig. 3) where the culmination of the CMBR apex on the horizon is between a depression and a peak of the $\Delta c/c$.

In order to extract the Earth's velocity from these experimental data, it is necessary to remove the DRIFT-long-term timing variation, because they are obtained in different days. Meantime this procedure is not free from experimental bias. The calibration will be done in the next search with active rotation which is free of the DRIFT-long-term timing variation.

Before publication of this paper we were informed by V. Gurzadyan [34, 35] of a similar study on anisotropy of the one way velocity of light relative to the dipole of the CMBR based on the Compton edge of laser photons scattered in electron beam at GRAAL ESRF (Grenoble) accelerator, where a similar behavior in the time series was obtained (see Fig. 4 from ref. [35]). However, according to the authors this variations comes probably from temperature variations. We were also informed that is in progress an analysis with new data.

4.2 Active raster search with a turntable system

In this active system, the laser beam is first pointed toward the direction of the Leo constellation (CMBR apex) when it is exactly on the horizon. Then the turntable, upon which the entire laser diffraction experiment is mounted, is rotated in steps of 30 degrees up to 180 degrees. At every angular step, the output current of the photo-diodes is registered during one minute at a counting rate of 10 readings per second. A complete set of measurements can be done in less than ten minutes. Consequently the measurements are free from DRIFT-long-term timing variations. They are influenced only by the JITTER-timing uncertainties (noise in the system by statistical fluctuations of the signals). However, this method requires a careful rotation of the system in order to avoid mechanical perturbations. The measurements, after a gaussian fit in the raw data, are shown in Fig. 8 for seven angular

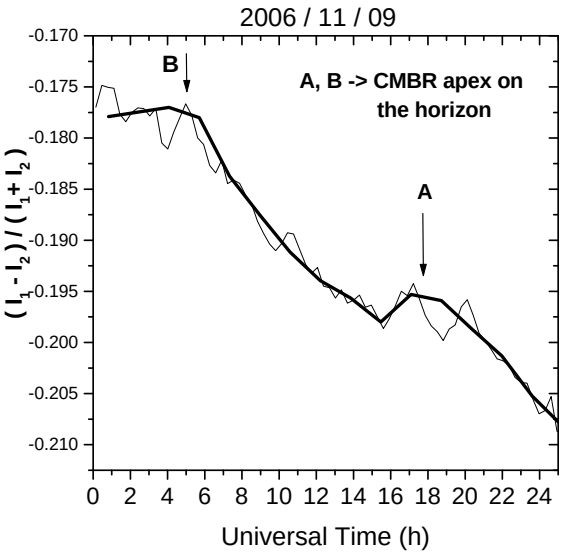

Fig. 7: The same as Fig. 4

regions, and the one-way light path anisotropy can be extracted from

$$\frac{\Delta c}{c} = \cot\alpha\,\Delta\alpha\,, \tag{13}$$

with

$$\Delta\alpha = \frac{l_0}{R}\left[\frac{I_1 - I_2}{I_1 + I_2}\right], \tag{14}$$

where the calibration factor obtained for these measurements is $l_0\,(=0.407\pm0.034\,\text{mm})$.

We have analyzed the experimental data using also the test theory of Mausouri and Sexl [1] where the one way speed of light is anisotropic by the among

$$c(\theta) = c - v(1+2a)\cos\theta\,. \tag{15}$$

The parameter a can be obtained by fitting the test theory to the experimental results using the expression

$$\frac{\Delta c}{c} = \cot\alpha\,\Delta\alpha = -\beta(1+2a)\cos\theta\,, \tag{16}$$

where $\beta(=0.001237\pm0.000002)$ is the COBE Earth's velocity parameter. The comparison between our measurements and the test theory is shown in Fig. 9, where an offset such that $(I_1 - I_2)/(I_1 + I_2) = 0$ at $\theta = 90^\circ$ has been used. The experimental results seem to agree to a $\beta(1+2a)\cos\theta_A$ signature, and the parameter a extracted from our data is

$$a = -0.4106 \pm 0.0225\,, \tag{17}$$

which differs from the $a = -\frac{1}{2}$ SRT prediction, as well as, some experimental upper limits using the Mössbauer effect [19].

The measurements above shown were made on June of 2006, they were confirmed in a new set of measurements (including a new calibration) in November of 2006 and the result is presented in Fig. 10. The parameter a extracted from this new data is $a = 0.3755\pm0.0403$ in agreement with the previous value.

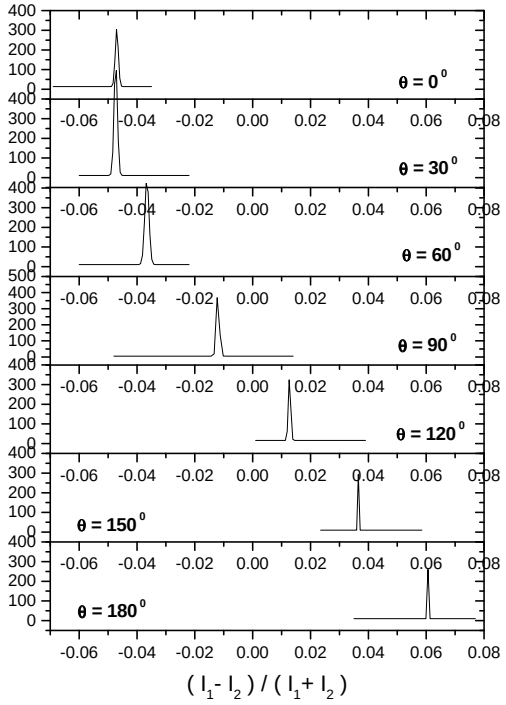

Fig. 8: Counting rate is plotted as a function of $(I_1 - I_2)/(I_1 + I_2)$ at a given laser beam alignment relative to the Earth's velocity vector obtained in June of 2006. The complete set of measurements was made in ten minutes.

5 Conclusions and remarks

The discovery of a dipole anisotropy in the CMBR is interpreted as a Doppler shift produced by the Earth's motion (solar barycenter). An experimental survey has been made in order to test if the Earth's velocity is relevant on light propagation in a quantity of first order. The measurements have been obtained by using a laser diffraction experiment mounted on turntable system. Two optic sensors (segmented photo-diodes) were used for measuring the position of diffracted light spots with a precision better than 0.1 μm. The experiment is easy to reproduce, and it is based on simple optical principles. Two raster search techniques (scan subjected to Earth's rotation and scan subjected to an active rotation) have been used to look for signals of anisotropic light propagation as a function of the laser beam alignment relative to the Earth's motion. The results obtained with both methods show that the course of the rays is affected by the motion of the Earth. They are susceptible of being interpreted by the test theory of Mausouri and Sexl [1] where the one way speed of light is anisotropic by the amount $c(\theta) = c - v(1+2a)\cos\theta$.

In the scan subjected to Earth's rotation, this pure* dependence is modulated by the variation of the altitude, h, of the CMBR apex and expressed as $\Delta c/c = -\beta(1+2a)\times$ $\times\cos(\theta_A - \theta_{beam})\cos h$. Despite of the statistical fluctua-

*This meas $\cos\theta = \cos(\theta_A - \theta_{beam})$.

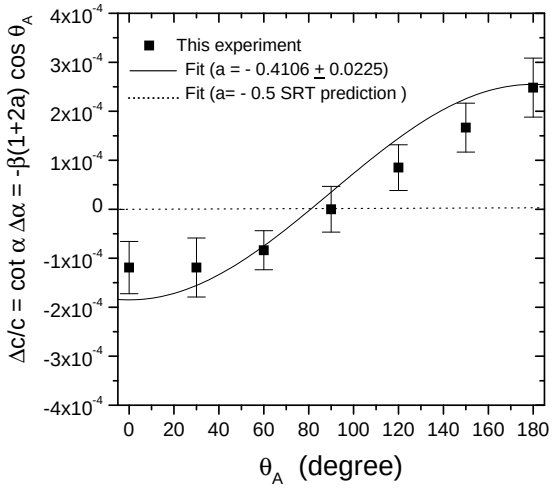

Fig. 9: Comparison between the one-way path light anisotropy $\Delta c/c = -\beta(1+2a)\cos\theta$ function, relative to the Earth's velocity vector and the experimental data obtained in June of 2006, for two different values of the fit parameter, $a = -0.4106$ and $a = -\frac{1}{2}$ respectively. Here $\theta_A = 0$ represent the laser beam pointing to the CMBR apex on the horizon.

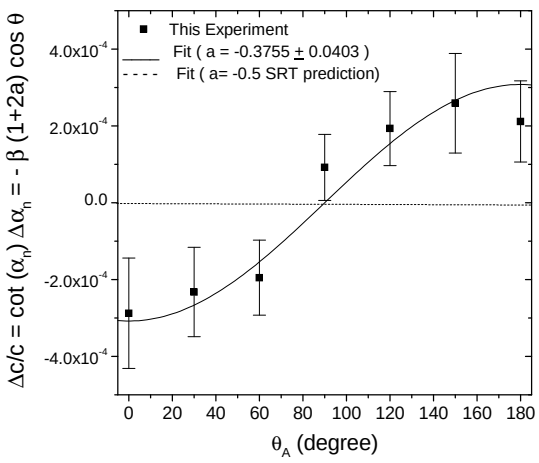

Fig. 10: The same as Fig. 9.

tions (short term noise), the results of these scans are in agreement with the prediction of the "modulated" Mousouri and Sexl test theory (with $a \neq -\frac{1}{2}$). In all cases, built-in a DRIFT-long-term it is possible to see peculiar signatures (see Fig. 3) where the culmination of the CMBR apex on the horizon is between a depression and a peak of the $\Delta c/c$.

In the scan subjected to an active rotation, the altitude of the CMBR apex is always $h = 0$, because a complete set of measurements can be done in 10 minutes. The azimuth varies from zero to 180 degree relative to the Earth's velocity direction. Consequently it is free from DRIFT-long-term timing variations. In this case, the Mausouri and Sexl parameter is extract from a fit of the data giving $a = -0.4106 \pm 0.0225$ (from data obtained on June 2006), and $a = -0.3755 \pm 0.0403$ (from data obtained on November 2006), and they differs from SRT prediction where $a = -0.5$.

We remark that the CMBR dipole is a frame dependent quantity. According to Scott and Smoot [39], we can thus determine the "absolute rest frame" of the universe as that in which the CMBR dipole would be zero. In short, our results point out that it is not possible to neglect the preferred frame imposed by cosmology.

Acknowledgements

This paper is a memorial tribute to our professor and friend C. M. G. Lattes, who introduced us the non-conventional aspects of relativity. We are thankful to all the members of the laboratory of Thin Films of IF-UFF for implementing the techniques of using segmented photo-diodes. One of the authors (C.E.N) is thankful to R. Wang for the critics and useful comments.

Appendix: The Miller's ether drift direction

According to the theories that incorporate the length contraction principle (Einstein and Lorentz-Poincaré theories), experiments where two orthogonal light paths are compared (two way speed experiments) like the Michelson-Morley interferometer and all variants are incapable of detecting the Earth's motion (no ether drift) due to the length contraction of the interferometer arm parallel to the direction of the Earth's velocity.

Strictly speaking, a null result is expected only in vacuum where the refractive index is $\eta = 1$. While, if $\eta \neq 1$ the Fresnel's drag effect in the rest frame of the medium (Σ) cancels the effect of the genuine Lorentz transformation to a moving frame (Σ'). Following the Lorentz transformation equations from Σ' with speed v to Σ, and taking into account the Fresnel relation of the speed of light in the medium $c' = c/\eta$, it is possible to obtain the so called two-way speed of light anisotropy as

$$\bar{c'}(\theta) = \frac{2c'(\theta)\,c'(\theta+\pi)}{c'(\theta)+c'(\theta+\pi)}\,, \qquad \text{(A1)}$$

and the relative variation as

$$\frac{\Delta c'(\theta)}{c} = -\frac{v^2}{c^2}\left[\frac{\eta^2-1}{\eta^2}\left(1-\frac{3}{2}\,\sin\theta^2\right)\right]. \qquad \text{(A2)}$$

We can see that the two-way speed of light anisotropy is null only in the case $\eta = 1$ (vacuum). This prediction is in agreement with modern ether drift experiments in vacuum [36, 37], using two cavity-stabilized lasers and whose value is

$$\frac{\Delta c'}{c} \sim 10^{-15}. \qquad \text{(A3)}$$

In the gaseous mode, for instance air ($\eta = 1.000226$), a maximum value of $\Delta c'/c$ happens in reference axis parallel to Earth's velocity. The tiny fringe shifts, observed in various Michelson-Morley type experiments, represent a non-null

effect for the two-way speed of light anisotropy. Dayton Miller [15, 16] was one of the first few in claiming that the Michelson-Morley data and his own data obtained in the mount Wilson are non-null results. Particularly, the mount Wilson data obtained in 1925–1926 is compatible with an obrvable Earth velocity of $v \sim 8.5 \pm 1.5$ km/s, when the data is analyzed on the basis of classical physics. While on the basis of a different calibration including the length contraction (see Eq. A2), the Miller result gives speeds for the movement of the Earth, larger than $v > 300$ km/s.

A review of the Dayton Miller's ether drift experiments made by James DeMeo [38] shows indisputable evidence that data collected by Miller was affected by the sidereal period and this is clear proof of a cosmological ether drift effect. However, the Miller's determination of the velocity direction of the Earth does not coincide with the direction obtained by COBE. The Miller's direction for the Earth velocity is almost perpendicular to the direction established by COBE, observing the CMBR anisotropy. In our opinion, Miller's result has the same problem as the first results of the CMBR survey as is shown in Table 1. For instance, both Miller and Conklin have obtained a non-null result on the two-way path light speed anisotropy and the dipole anisotropy of the CMBR, respectively. Nevertheless, both experiments have failed to obtain the coordinates of the Earth's velocity vector direction correctly.

References

1. Mansouri R. M. and Sexl R. U. *Gen. Relativ. & Gravit.*, 1977, v. 8, 497.
2. Lorentz H. A. The theory of electrons:and its applications to the phenomena of light and radiant head. Dover Phoenix Editions, 2004.
3. Sagnac G. C. R. *Acad. Sci. Paris*, 1913, v. 157, 708.
4. Brans C. H. and Stewart D. R. *Phys. Rev. D*, 1973, v. 8, 1662–1666.
5. Wucknitz O. arXiv: gr-qc/0403111.
6. Wang R., Zheng Y., and Yao A. *Phys. Rev. Lett.*, 2004, v. 93, 143901.
7. Hatch R. R. *Galilean Electrodynamic*, 2002, v. 13, 3.
8. Flandern V. T. Available in http://metaresearch.org/cosmology/gps-relativity.asp.
9. Fox V. The theory of the space-time and gravitation. Pergamon, New York, 1964.
10. Amelino-Camelia G. *Phys. Lett. B*, 2001, v. 510, 255.
11. Albrecht A. and Magueijo J. *Phys. Rev. D*, 1999, v. 59, 043516.
12. Nodland B. and Ralston J. P. *Phys. Rev. Lett.*, 1997, v. 78, 3043–3046.
13. Smoot G. F. et al. *Astrophysical Journal*, 1991, v. 371, L1–L5.
14. Yaes R. J. Reconciling COBE data with relativity. *Physics Today*, 1993, March 13.
15. Miller D. C. *Rev. Mod. Phys.*, 1933, v. 5, 203–255.
16. Cahill R. T. *Progress in Physics*, 2005, v. 3, 25.
17. Cialdea R. *Lett. Nuovo Cimento*, 1972, v. 4, 821.
18. Krisher T. P. et al. *Phys. Rev. D*, 1990, v. 42, 731.
19. Turner K. C. and Hill H. A. *Phys. Rev. B*, 1964, v. 252, 134.
20. Gagnon D. R., Torr D. G., Kolen P. T., and Chang T. *Phys. Rev. A*, 1988, v. 38, 1767.
21. Timothy P. et al. *Phys. Rev. D*, 1990, v. 42, 731.
22. Kolen P. T. and Torr D. G. *Found. Phys.*, 1982, Np. 12, 401.
23. Silvertooth E. W. *Specl. Sci. and Tech.*, 1986, v. 10, 3.
24. Navia C. E, Augusto C. R. A., Robba M. B, Malheiro M., and Shigueoka H. *Astrophysical Journal*, 2005, v. 621, 1137.
25. Augusto C. R. A., Navia C. E. and Robba M. B., *Phys. Rev. D*, 2005, v. 71, 103011.
26. Navia C. E., Augusto C. R. A., Tsui K. H. and Robba M. B. *Phys. Rev.*, 2005, v. 72, 103001.
27. Penzias A. A. and Wilson R. W. *Astrophys. Journal*, 1965, v. 142, 419.
28. Conklin E. K. *Nature*, 1969, v. 222, 971.
29. Henry P. *Nature*, 1971, v. 231, 516.
30. Smoot G. F., Gorenstein M. V., and Miller R. A. *Phys. Rev. Lett.*, 1977, v. 39, 898.
31. Smoot G. F. and Lubin P. M. *Astrophysical Journal*, Part 2 — Letters to the Editor, 1979, v. 234, L83.
32. Smoot G. F. and Scoot D. Cosmic Background Radiation. *European. Phys. J.*, 2000, No. 1–4, 145–149.
33. Bennett C. L. et al. *Astrophys. J. Supp.*, 2003, v. 148, 1.
34. Gurzadyan V. Private communication.
35. Gurzadyan V. et al. *Mod. Phys. Lett.*, 2005, v. 20, 19; arXiv: astro-ph/0410742.
36. Brillet A. and Hall J. L. *Phys. Rev. Lett.*, 1979, v. 42, 549.
37. Müller H., Hermann S., Braxmaier C., Schiller S. and Peters A. *Phys. Rev. Lett.*, 2003, v. 91, 0204001.
38. DeMeo J. Available in http://www.orgonelab.org/miller.htm.
39. Scott D. and Smoot G. F. *Journal of Physics*, 2006, v. 33, 238.

Quantization State of Baryonic Mass in Clusters of Galaxies

Franklin Potter* and Howard G. Preston†

*Sciencegems.com, 8642 Marvale Dr., Huntington Beach, CA 92646 USA
†15 Vista del Sol, Laguna Beach, CA 92651 USA

E-mail: *drpotter@lycos.com and †hpres@cox.net

The rotational velocity curves for clusters of galaxies cannot be explained by Newtonian gravitation using the baryonic mass nor does MOND succeed in reducing this discrepancy to acceptable differences. The dark matter hypothesis appears to offer a solution; however, non-baryonic dark matter has never been detected. As an alternative approach, quantum celestial mechanics (QCM) predicts that galactic clusters are in quantization states determined solely by the total baryonic mass of the cluster and its total angular momentum. We find excellent agreement with QCM for ten galactic clusters, demonstrating that dark matter is not needed to explain the rotation velocities and providing further support to the hypothesis that all gravitationally bound systems have QCM quantization states.

1 Introduction

The rotational velocity curves of galaxy clusters [1] are very similar to the rotational velocity curves of individual galaxies, with the rotational velocity value rising rapidly at very small radial distances only to quickly reach an approximately constant velocity for all greater radial distances from about 200 kpc to out beyond 1500 kpc. Newtonian gravitation using only the observed baryonic mass fails to explain the curves both for galaxies and for clusters of galaxies. In clusters, the baryonic mass is predominantly due to the hot intracluster gas that is observed by its free-free X-ray emissions. This gas fraction plus the stellar masses make up the observed baryonic mass of about 10%–15% of the dynamic mass required to explain the rotational velocity curves using Newtonian gravitation, an enormous discrepancy.

Three interesting possible explanations for galactic rotation curves have been proposed: (1) the dark matter hypothesis (DM) introduces non-baryonic matter that is insensitive to all interactions except gravitation, but there has been no detection of any possible form of dark matter; (2) a modified Newtonian dynamics (MOND) effective at all distance scales when the accelerations are less than $1.2\times10^{-10}\,\mathrm{m/s^2}$, which has been very successful in explaining the rotation and luminosity curves of individual galaxies but has large discrepancies for galaxy clusters [2] in both the cluster core and in the outer regions; (3) quantum celestial mechanics (QCM) derived [3] from the general relativistic Hamilton-Jacobi equation which dictates that all gravitationally bound systems have quantization states. The QCM states are determined by two physical quantities only — the system's total baryonic mass and its total angular momentum. QCM agrees with MOND and the baryonic Tully-Fisher relation for individual galaxies.

In this paper, we compare the QCM predictions for the baryonic mass for ten galaxy clusters to the detected baryonic masses. Our new result is that the QCM baryonic mass values agree with the measured baryonic values even where DM succeeds and MOND fails. No dark matter is required to explain the observed rotation curves. The baryonic matter in a single QCM quantization state produces the correct rotational velocity for the cluster.

2 Conceptual review of QCM

In a series of papers [3, 4, 5], we derived a Schrödinger-like scalar wave equation from the general relativistic Hamilton-Jacobi equation via a tranformation that utilizes the total angular momentum of the gravitationally bound system instead of an angular momentum proportional to Planck's constant. We have shown agreement of its quantization state solutions with the energy states of the planets of the Solar System, of the satellites of the Jovian planets, and of the disk states of galaxies. In a preliminary table-top investigation with a torsion bar system that is now being modified to minimize possible extraneous influences, the QCM predicted quantization states with quantized energy per mass and quantized angular momentum per mass have been detected. The results from the improved apparatus will be reported.

According to QCM, the quantization state energies per orbiting particle mass μ are

$$\frac{E_n}{\mu} = -\frac{G^2M^4}{2n^2H_\Sigma^2} \tag{1}$$

where G is the gravitational constant, M is the total mass of the gravitationally bound system, H_Σ is the system's total angular momentum, and n is an integer. Typically, E_n is on the order of $10^{-6}\mu c^2$. Unlike the quantum mechanics of atomic states whereby each electron is in its own quantum state, in QCM there can be billions of stars (i.e., particles)

Cluster	kT, keV	R_{200}, kpc	M_{200}, $\times 10^{14} M_\odot$	v_{kT}, $\times 10^6$ m/s	M, $\times 10^{13} M_\odot$	H_Σ, $\times 10^{70}$ kg$\times$m^2/s
A1983	2.18 ± 0.09	1100 ± 140	1.59 ± 0.61	0.65 ± 0.03	1.12 ± 0.21	5.10 ± 1.65
MKW9	2.43 ± 0.24	1006 ± 84	1.20 ± 0.30	0.68 ± 0.08	1.34 ± 0.63	7.00 ± 5.76
A2717	2.56 ± 0.06	1096 ± 44	1.57 ± 0.19	0.70 ± 0.02	1.50 ± 0.17	8.57 ± 1.71
A1991	2.71 ± 0.07	1106 ± 41	1.63 ± 0.18	0.72 ± 0.02	1.68 ± 0.19	10.4 ± 2.0
A2597	3.67 ± 0.09	1344 ± 49	3.00 ± 0.33	0.84 ± 0.02	3.11 ± 0.30	30.7 ± 5.1
A1068	4.67 ± 0.11	1635 ± 47	5.68 ± 0.49	0.95 ± 0.03	5.09 ± 0.64	72.7 ± 16.1
A1413	6.62 ± 0.14	1707 ± 57	6.50 ± 0.65	1.13 ± 0.03	10.2 ± 1.1	$245. \pm 46$
A478	7.05 ± 0.12	2060 ± 110	10.8 ± 1.8	1.16 ± 0.02	11.3 ± 0.8	$294. \pm 36$
PKS0745	7.97 ± 0.28	1999 ± 77	10.0 ± 1.2	1.24 ± 0.05	14.8 ± 2.4	$469. \pm 132$
A2204	8.26 ± 0.22	2075 ± 77	11.8 ± 1.3	1.26 ± 0.04	15.7 ± 2.0	$525. \pm 116$

Table 1: QCM predicted galactic cluster baryonic mass M and angular momentum H_Σ.

in the same QCM state. Also notice that there is no explicit distance dependence in this energy state expression, in sharp contrast to classical mechanics, because the state radial wave function extends over a large range. QCM tells us that gravitationally bound systems, such as planetary systems and galaxies, are quantized systems and that their behavior cannot be fully understood by classical general relativistic dynamics.

QCM has been used also to derive the general expression for the MOND acceleration $a_0 = 1.2 \times 10^{-10}$ m/s^2, this specific MOND value being an average value for many galaxies. Our general expression is

$$a_0 = \frac{G^3 M^7}{n^4 H_\Sigma^4}\,, \tag{2}$$

a result which suggests that a_0 would be slightly different for each galaxy instead of being taken as a universal value.

We combine these equations algebraically to solve for M and H_Σ in terms of the measured asymptotic rotational velocity and the MOND acceleration. Assuming that the virial theorem holds for galaxies, the velocity v is derived from Eq. 1 to yield

$$M = \frac{v^4}{G a_0}\,, \qquad H_\Sigma = \frac{v^7}{n G a_0^2}\,. \tag{3}$$

These expressions hold true for galaxies. In the next section they will be applied to clusters of galaxies and the predicted baryonic mass values will be compared to the dynamic mass values determined from observational data.

3 Galaxy cluster QCM masses

QCM is assumed to have universal application to isolated gravitationally bound systems. To a good approximation, clusters of galaxies are isolated gravitationally bound systems and therefore should demonstrate the quantization states dictated by QCM. In many cases the galaxy clusters have no dominant central mass, with the intragalactic gas dispersed throughout the cluster. For simplicity, we assume that the cluster system is in the $n = 1$ state, that the virial theorem applies, that $a_0 = 1.2 \times 10^{-10}$ m/s^2, and that the cluster is approximately a flattened ellipsoid similar to the Local Group [6] that includes our Galaxy and M31. The latter assumption is not strictly required but allows an easy analogy to disk galaxies where we know that QCM and MOND apply extremely well.

We use the ten galaxy clusters analyzed by Arnaud et al. [7] to determine the QCM predicted baryonic mass and angular momentum via Eqs. 3 above. Their radial distance R_{200} is the distance where inside that radius the mean mass density is 200 times the critical density of the universe, and their M_{200} is the total mass within this radius in solar masses $M_\odot$ as determined by a standard NFW universal density profile for a dark matter halo as determined by Navarro et al. [8] from N-body simulations. The kT (keV) represents the spectroscopic temperature of the $0.1 \leqslant r \leqslant 0.5 R_{200}$ region, and the velocity v_{kT} comes from these temperatures. Table 1 lists our results for the total baryonic mass M and the total angular momentum H_Σ.

4 Discussion

Our predicted QCM baryonic masses M in Table 1 for the clusters are about a factor of ten smaller (10^{13} vs. 10^{14}) than the dynamic masses M_{200} which were determined by assuming a dark matter NFW profile. There is reasonable agreement between our QCM baryonic mass values and the baryonic masses from the spectroscopic data. There is no need to invoke the gravitational consequences of DM. The galactic cluster is in a QCM quantization state. This result indicates that quantum celestial mechanics determines certain dynamic behavior of galaxies and galactic clusters.

One additional physical quantity we know now is the total baryonic angular momentum of each galactic cluster. This angular momentum value determines all the quantiza-

tion states of the system in which the gas and the individual galaxies (i.e., particles) can occupy. Particles at all radii from the cluster center are in the same angular momentum quantization state. Note that we have assumed that $n = 1$ for each cluster; however, some clusters could have baryonic mass in the $n = 2$ state as well.

QCM has been applied successfully to solar systems, galaxies and clusters of galaxies. The results strongly suggest that the known baryonic mass in each system is sufficient to explain the rotational velocity values without invoking the gravitational consequences of dark matter. As expected from QCM, these gravitationally bound systems all behave as non-classical systems exhibiting quantization states determined by the total mass and the total angular momentum.

References

1. Pointecouteau E., Arnaud M. and Pratt G. W. The structural and scaling properties of nearby galaxy clusters: I — The universal mass profile. arXiv: astro-ph/0501635.
2. Pointecouteau E. and Silk J. New constraints on MOND from galaxy clusters. arXiv: astro-ph/0505017.
3. Preston H. G. and Potter F. Exploring large-scale gravitational quantization without $\hbar$ in planetary systems, galaxies, and the Universe. arXiv: gr-qc/0303112.
4. Potter F. and Preston, H.G. Gravitational lensing by galaxy quantization states. arXiv: gr-qc/0405025.
5. Potter F. and Preston H. G. Quantum Celestial Mechanics: large-scale gravitational quantization states in galaxies and the Universe. *1st Crisis in Cosmology Conference: CCC-I*, Lerner E.J. and Almeida J. B., eds., AIP CP822, 2006, 239–252.
6. Pasetto S. and Chiosi C. Planar distribution of the galaxies in the Local Group: a statistical and dynamical analysis. arXiv: astro-ph/0611734.
7. Arnaud M., Pointecouteau E. and Pratt G. W. The structural and scaling properties of nearby galaxy clusters — II. The $M - T$ relation. *Astron. & Astrophys.*, v. 441, 2005, 893; arXiv: astro-ph/0502210.
8. Navarro J., Frenk C. S. and White S. D. M. A universal density profile from hierarchical clustering. *Astrophys. J.*, 1997, v. 490, 493.

Experimental Investigations of the Existence of a Local-Time Effect on the Laboratory Scale and the Heterogeneity of Space-Time

Victor A. Panchelyuga*, Valeri A. Kolombet*, Maria S. Panchelyuga* and Simon E. Shnoll*,†

*Institute of Theor. and Experim. Biophysics, Russian Acad. of Sciences, Pushchino, Moscow Region, 142290, Russia
†Department of Physics, Moscow State University, Moscow 119992, Russia

Corresponding authors. Victor A. Panchelyuga: panvic333@yahoo.com; Simon E. Shnoll: shnoll@iteb.ru

The main subject of this work is an experimental investigation of the existence of a local-time effect on the laboratory scale, i.e. longitudinal distances between locations of measurements from one metre to tens of metres. A short review of our investigations of the existence of a local-time effect for longitudinal distances from 500 m to 15 km is also presented. Besides investigations of the minimal spatial scale for a local-time effect, the paper presents investigations of the effect in the time domain. In this relation the structure of intervals distribution in the neighbourhood of local-time peaks was studied and splitting of the peaks was revealed. Further investigations revealed second order splitting of local-time peaks. From this result it is concluded that space-time heterogeneity, which follows from the local-time effect, probably has fractal character. The results lead to the conclusion of sharp anisotropy of space-time.

1 Introduction

Our previous works [1–4] give a detailed description of macroscopic fluctuations phenomena, which consists of regular changes in the fine structure of histogram shapes built on the basis of short samples of time series of fluctuations in different process of any nature — from biochemical reactions and noises in gravitational antennae to fluctuations in α-decay rate. From the fact that fine structure of histograms, which is the main object of macroscopic fluctuation phenomena investigations, doesn't depend on the qualitative nature of the fluctuating process, so it follows that the fine structure can be caused only by the common factor of space-time heterogeneity. Consequently, macroscopic fluctuation phenomena can be determined by gravitational interaction, or as shown in [5, 6], by gravitational wave influence.

The present work was carried out as further investigations into macroscopic fluctuation phenomena. The local time effect, which is the main subject of this paper, is synchronous in the local time appearance of pairs of histograms with similar fine structure constructed on the basis of measurements of fluctuations in processes of different nature at different geographical locations. The effect illustrates the dependence of the fine structure of the histograms on the Earth's rotation around its axis and around the Sun.

The local time effect is closely connected with space-time heterogeneity. In other words, this effect is possible only if the experimental setup consists of a pair of separated sources of fluctuations moving through heterogeneous space. It is obvious that for the case of homogeneous space the effect doesn't exist. Existence of a local-time effect for some space-time scale can be considered as evidence of space-time heterogeneity, which corresponds to this scale. Dependence of a local-time effect on the local time or longitudinal time difference between places of measurements leads to the conclusion that space heterogeneity has axial symmetry.

The existence of a local time effect was studied for different distances between places of measurement, from a hundred kilometres up to the largest distance possible on the Earth ($\sim$15000 km). The goal of the present work is an investigation of the existence of the effect for distances between places of measurements ranging from one metre up to tens of metres. Such distances we call "laboratory scale".

2 Experimental investigations of the existence of a local-time effect for longitudinal distances between places of measurements from 500 m to 15 km

The main problem of experimental investigations of a local-time effect at small distances is resolution enhancement of the macroscopic fluctuations method, which is defined by histogram duration. All investigations of a local-time effect were carried out by using α-decay rate fluctuations of ^{239}Pu sources. Histogram durations in this case are one minute. But such sources of fluctuations become uselessness for distances in tens of kilometres or less when histogram durations must be about one second or less. For this reason in work [7–8] we rejected α-decay sources of fluctuations and instead used as a source, noise generated by a semiconductor diode. Diodes give a noise signal with a frequency band of up to tens of megahertz and because of this satisfy the requirements of the present investigations.

To check the suitability of the selected diode noise source for local-time effect investigations, comparative tests were made at distances for which existence of the effect was proved by using α-decay sources of fluctuations [7]. This

work confirmed the suitability of diode semiconductor noise for studies of the local-time effect.

Below we present a short description of our experiments for investigation of a local-time effect for longitudinal distances of 500 m up to 15 km between locations of measurements. The first experiment studied the local-time effect for a longitudinal distance of 15 km between locations of measurements, the second one for a set of longitudinal distances from 500 m to 6 km. A more detailed description of these experiments is given in [8].

In the first experiment a series of synchronous measurements were carried out in Pushchino (Lat. 54°50.037′ North, Lon. 37°37.589′ East) and Bolshevik (Lat. 54°54.165′ North, Lon. 37°21.910′ East). The longitudinal difference α between places of measurements was $\alpha = 15.679'$. This value of α corresponds to a difference of local time $\Delta t = 62.7$ sec and longitudinal distance $\Delta l = 15$ km.

To study the local-time effect in Pushchino and Bolshevik, we obtained 10-minute time series by digitizing fluctuations from noise generators with a sampling frequency of 44100 Hz. From this initial time series with three different steps of 735, 147 and 14 points, we extracted single measurements and obtained three time series with equivalent frequency equal 60 Hz, 300 Hz and 3150 Hz. On the basis of this time series, in a standard way [1–3] using a 60-point sample length for the first and second time series and a 63-point sample length for third time series, we constructed three sets consisting of histograms with duration 1 sec, 0.2 sec and 0.02 sec.

Fig. 1a depicts the intervals distribution obtained after comparisons of the 1-sec histogram sets. The distribution has a peak, which corresponds to a time interval of 63 ± 1 sec, and which accurately corresponds to a local time difference $\Delta t = 62.7$ sec between places of measurements.

Local time peaks ordinarily obtained on the interval distributions are very sharp and consist of 1–2 histograms [1–3] i.e. are practically structureless. The peak in Fig. 1a can also be considered as structureless. This leads us to the further investigation of its structure.

The fact that all sets of histograms were obtained on the basis of the same initial time series on the one hand, enables enhancement of time resolution of the method of investigation, and on the other hand, eliminates necessity of very precise and expensive synchronization of spaced measurements. The intervals distribution obtained for the 1-sec histograms set allows the use of information about the location of a local-time peak alignment of time series. The alignment makes possible the use of the set of histograms of the next order of smallness.

Using the 0.2-sec histograms set increased resolution five times and allowed more detailed investigations of local-time peak structure and its position on the time axis. Since the positions of the peak on the 1-sec intervals distribution (Fig. 1a) are known, it is possible to select their neighbour-

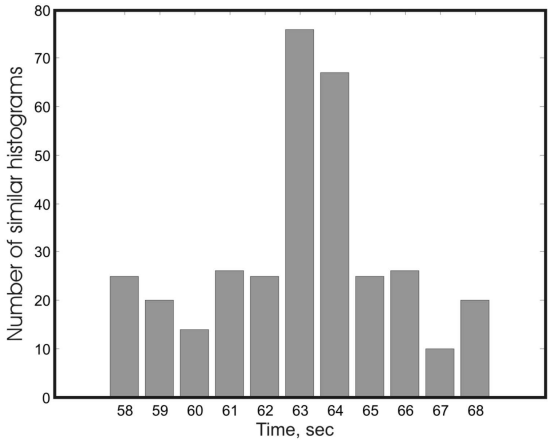

Figure 1a

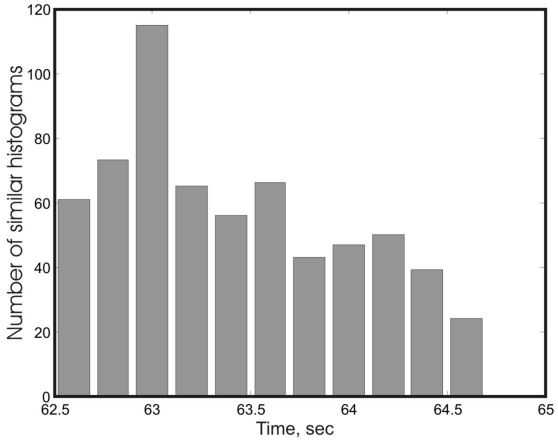

Figure 1b

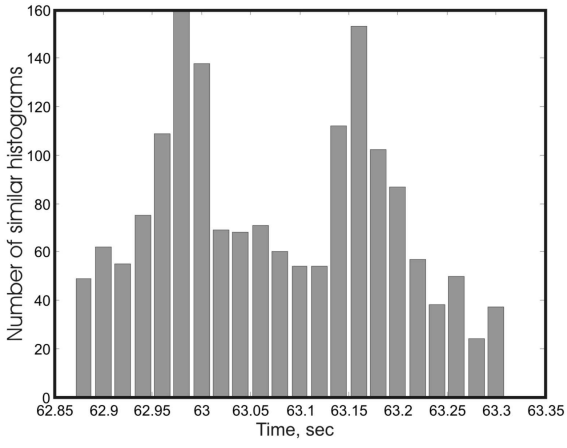

Figure 1c

Fig. 1: Intervals distributions obtained after comparisons of 1-sec (a), 0.2-sec (b), and 0.02-sec (c) histogram sets. The Y-axis depicts the number of histograms, which were found to be similar; the X-axis — time interval between pairs of histograms, sec.

hood by means of 60 sec relative shift of initial time series and prepare after this a 0.2-sec histograms set for further comparison.

The intervals distribution obtained from comparisons for the 0.2-sec histograms set is presented in Fig. 1b. One can see that maximum similarity of histogram shape occurs for pairs of histograms separated by an interval of 63 ± 0.2 sec. This value is the same as for the 1-sec histogram intervals distribution, but in the latter case it is defined with an accuracy of 0.2 sec.

It's easy to see from the intervals distribution, Fig. 1b, that after fivefold enhancement of resolution, the distribution has a single sharp peak again. So a change of time scale in this case doesn't lead to a change of intervals distribution. This means that we must enhance the time resolution yet again to study the local time peak structure. We can do this by using the 0.02-sec histograms set.

The intervals distribution for the case of 0.02-sec histograms is presented in Fig. 1c. Unlike the intervals distributions in Fig. 1a and in Fig. 1b, distribution in Fig. 1c consists of two distinct peaks. The first peak corresponds to a local time difference of 62.98 ± 0.02 sec, the second one to 63.16 ± 0.02 sec. The difference between the peaks is $\Delta t' = 0.18\pm 0.02$ sec.

Splitting of the local-time peak in Fig 1c is similar to splitting of the daily period in two peaks with periods equal to solar and sidereal days [9–11]. This result will be considered in the next section.

The experiment described above demonstrates the existence of a local-time effect for longitudinal distance between locations of measurements at 15 km, and splitting of the local-time peak corresponding to that distance. It is natural to inquire as to what is the minimum distance for the existence of a local time effect. The next step in this direction is the second experiment presented below.

In this experiment two measurement systems were used: stationary and mobile. Four series of measurements were carried out. The longitudinal differences of locations of stationary and mobile measurement systems was 6 km, 3.9 km, 1.6 km and 500 m. The method of experimental data processing used was the same as for first experiment. It was found that for each of foregoing distances, a local-time effect exists and the local-time peak splitting can be observed.

3 Second-order splitting of the local-time peak. Preliminary results

Four-minute splitting of the daily period of repetition of histogram shape on solar and stellar sub-periods was reported in [3]. In that paper the phenomenon is considered as evidence of existence of two preferential directions: towards the Sun and towards the coelosphere. After a time interval of 1436 min the Earth makes one complete revolution and the measurement system plane has the same direction in space as one stellar day before. After four minutes from this moment, the measurement system plane will be directed towards the Sun. This is the cause of a solar-day period — 1440 min.

Let us suppose that the splitting described in the present paper has the same nature as splitting of the daily period. Then from the daily period splitting $\Delta T = 4$ min it is possible to obtain a constant of proportionality k:

$$k = \frac{240\,\text{sec}}{86400\,\text{sec}} \approx 2.78\times10^{-3}. \qquad (1)$$

The longitudinal difference between places of measurements presented in the second section is $\Delta t = 62.7$ sec and we can calculate splitting of the local-time peak for this value of Δt:

$$\Delta t' = k\,\Delta t = 62.7\times2.78\times10^{-3} \approx 0.17\,\text{sec}\,. \qquad (2)$$

It is easy to see from Fig. 1c that splitting of the local-time peak is amounts to 0.18 ± 0.02 sec. This value agrees with estimation (2). Values of splitting of the local-time peak, which were obtained for the mobile experiment, are also in good agreement with values obtained by the help of formula (2).

This result allows us to consider sub-peaks of local-time peak as stellar and solar and suppose that in this case the cause of splitting is the same as for daily-period splitting. But the question about local-time peak structure remains open.

In order to further investigations of the local-time peak structure an experiment was carried out using synchronous measurements in Rostov-on-Don (Lat. $47^\circ13.85'$ North, Lon. $39^\circ44.05'$ East) and Bolshevik (Lat. $54^\circ54.16'$ North, Lon. $37^\circ21.91'$ East). The local-time difference for these locations of measurements is $\Delta t = 568.56$ sec. The value of the local-time peak splitting, according to (2), is $\Delta t' = 1.58$ sec. The method of experimental data processing was the same as described in section 2.

In Fig. 2, a summation of all results of expert comparison is presented. For the considered case we omit presentation of our results in the form of interval distributions, like those in Fig 1, because it involves multiplicity graphs.

Fig. 2 consists of four lines. At the leftmost side of each line is the duration of a single histogram in the four sets of histograms, which were prepared for comparison. So we have four sets consisting of 1-sec, 0.2-sec, 0.0286-sec and 1.36 ms histograms. The rectangle in the first line schematically shows a local-time peak, obtained as a result of comparisons for the 1-sec histograms set. Taking into account synchronization error (about one second), the result is 567 ± 2 sec. This value is in agreement with the calculated longitudinal difference of local time $\Delta t = 568.56$ sec (throughout Fig. 2, calculated values are given in parentheses).

The second line in Fig. 2 presents results for the 0.2-sec histograms set. The values in the rectangles show sidereal and solar sub-peaks of the local-time peak. The value between

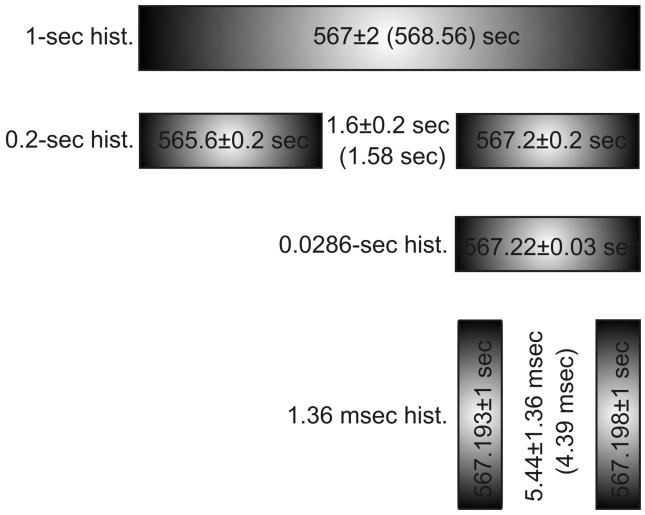

Fig. 2: Local-time peak splitting obtained in the experiment with synchronous measurements of fluctuations of a pair of semiconductor noise generators, carried out in Rostov-on-Don and Bolshevik.

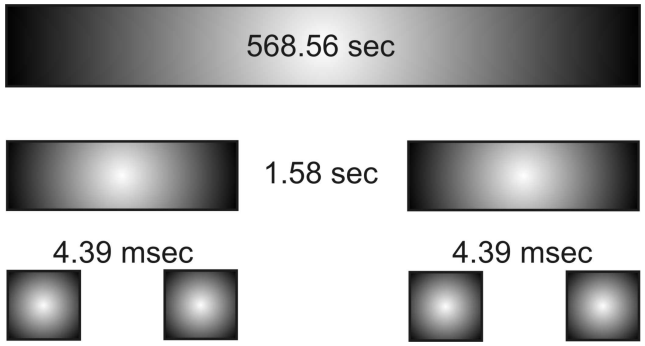

Fig. 3: Expected structure of local-time peak splitting for experiment with synchronous measurements in Rostov-on-Don and Bolshevik, calculated on the base of formula (4).

the rectangles gives the splitting of the local-time peak. The experimentally obtained splitting value is 1.6 ± 0.2 sec, which is in good agreement with the value calculated on the basis of formula (2).

The third and fourth lines of Fig.2 present the results of additional investigations of local-time peak structure. In the third line is the result of comparisons of the 0.0286-sec histograms set for intervals, which constitute the closest neighbourhood of 567.2 ± 0.2-sec peak. Using the 0.0286-sec histograms set increased resolution almost ten times and defines peak position on the intervals distribution at 567.22 ± 0.03 sec. The obtained peak is structureless. Further increase of resolution moves to the 1.36-ms histograms set, presented in fourth line. In this case resolution enhancement revealed splitting of 567.22 ± 0.03 sec peak.

The splitting presented in last line of the diagram, can be regarded as second-order splitting. It can be calculated using first-order splitting $\Delta t' = 1.58$ sec by the analogue of formula (2):

$$\Delta t'' = k\Delta t'. \tag{3}$$

It easy to see from (3) and from Fig. 2, for second-order splitting $\Delta t''$ the value of first-order splitting $\Delta t'$ plays the same rôle as the local-time value Δt for $\Delta t'$. Numerical calculations using (3) gives $\Delta t'' = 4.39$ ms, which is in good agreement with the experimentally obtained splitting value 5.44 ± 1.36 ms.

Experimental evidence for the existence of second-order splitting leads us to conjecture the possibility of n-order splitting. It easy to see from (2) and (3) that the n-order splitting value Δt^n can be obtained in the following way:

$$\Delta t^n = k^n \Delta t\,. \tag{4}$$

Fig. 3 presents an idealized structure of local-time peak splitting for the considered experiment, which was calculated on the base of formula (4). Unlike Fig. 2, the structure of local-time peak splitting in Fig. 3 is symmetrical. Studies of a possible splitting of 565.6 ± 0.2 sec peak is our immediate task. At this time the results presented in the Fig. 2 can be considered as preliminary.

4 Experimental investigations of the existence of a local-time effect for longitudinal distances between places of measurements from 1 m to 12 m

The experiments described in two previous sections demonstrate the existence of a local-time effect for a longitudinal distance of 500 m between locations of measurements, and the existence of second-order splitting of the local-time peak. The next step in our investigations is a study of the local-time effect on the laboratory scale.

The main difference between local-time effect investigations on the laboratory scale and the experiments described above is an absence of a special synchronization system. In the laboratory case the experimental setup consists of two synchronous data acquisition channels and two spaced noise generators, which are symmetrically connected to it. A LeCroy WJ322 digital storage oscilloscope was used for data acquisition. Standard record length of the oscilloscope consists of 500 kpts per channel. This allowed obtaining of two synchronous sets of 50-point histograms. The maximum length of every set is 10000 histograms.

Fig. 4 presents values of local time shift as a function of distance between two noise generators. The graph presents the results of investigations of a local-time effect for distances of 1 m, 2 m, 3 m, and 12 m. Local-time values were found with an accuracy of 9.52 ms for the 12 m experiments and with an accuracy of 1.36 ms for the 1 m, 2 m, and 3 m experiments.

An example of an intervals distribution for 1 m longitudinal distance between two noise generators is presented in

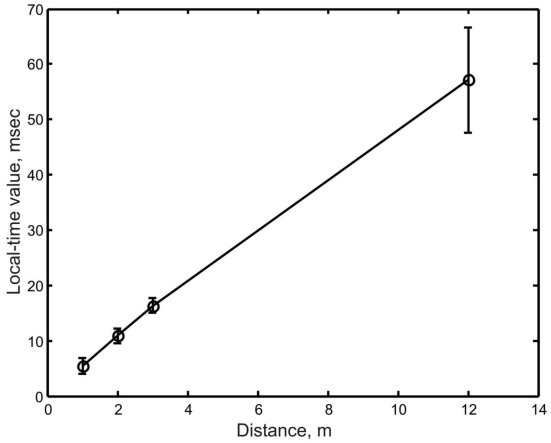

Fig. 4: Values of local time shift as a function of distance between two sources of fluctuations. The graph presents investigations of the local-time effect for distances 1 m, 2 m, 3 m, and 12 m.

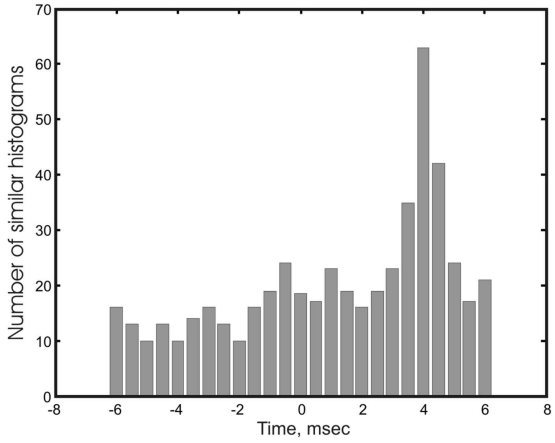

Fig. 5: Example of intervals distribution for longitudinal distance between two sources of fluctuations at one metre separation. Single histogram duration — 0.5 ms.

Fig. 5. The intervals distribution was obtained on the basis of the 0.5-ms histograms set. Using the Earth's equatorial radius value (6378245 m) and the latitude of the place of measurements (54°50.0.37′), it is possible to estimate the local-time difference for a 1m longitudinal distance. The estimated value is 3.7 ms. It is easy to see from Fig. 5 that the experimentally obtained value of local-time peak is 4 ± 0.5 ms, which is in good agreement with the theoretical value.

The results of our investigations for the laboratory scale, which are presented in this section, confirm a local-time effect for distances up to one metre. So we can state that a local-time effect exists for distances from one metre up to thousands of kilometers. This is equivalent to the statement that space heterogeneity can be observed down to the 1m scale.

5 Discussion

Local-time effect, as pointed out in [1], is linked to rotational motion of the Earth. The simplest explanation of this fact is that, due to the rotational motion of the Earth, after time Δt, measurement system No. 2 appears in the same place where system No. 1 was before. The same places cause the same shape of fine structure of histograms. Actually such an explanation is not sufficient because of the orbital motion of the Earth, which noticeably exceeds axial rotational motion. Therefore measurement system No. 2 cannot appear in the same places where system No. 1 was. But if we consider two directions defined by the centre of the Earth and two points were we conduct spaced measurement, then after time Δt measurement system No. 2 takes the same directions in space as system No. 1 before. From this it follows that similarity of histogram shapes is in some way connected with the same space directions. This conclusion also agrees with experimental results presented in [12–13].

In speaking of preferential directions we implicitly supposed that the measurement system is directional and because of this can resolve these directions. Such a supposition is quite reasonable for the case of daily period splitting, but for splitting of the local-time peak observed on the 1m scale it becomes very problematic because an angle, which must be resolved by the measurement system, is negligible. It is most likely that in this case we are dealing with space-time structure, which are in some way connected with preferential directions towards the Sun and the coelosphere. Second-order splitting of local-time peaks can also be considered as an argument confirming this supposition. Apparently we can speak of a sharp anisotropy of near-earth space-time. Existence of a local-time effect leads us to conclude that this anisotropy is axially symmetric.

The Authors are grateful to Dr. Hartmut Muller, V. P. Tikhonov and M. N. Kondrashova for valuable discussions and financial support. Special thanks go to our colleagues O. A. Mornev, R. V. Polozov, T. A. Zenchenko, K. I. Zenchenko and D. P. Kharakoz.

References

1. Shnoll S.E., Kolombet V.A., Pozharskii E.V., Zenchenko T.A., Zvereva I.M. and Konradov A.A. Realization of discrete states during fluctuations in macroscopic processes. *Physics-Uspekhi*, 1998, v. 41(10), 1025–1035.
2. Shnoll S.E., Zenchenko T.A., Zenchenko K.I., Pozharskii E.V., Kolombet V.A. and Konradov A.A. Regular variation of the fine structure of statistical distributions as a consequence of cosmophysical agents. *Physics-Uspekhi*, v. 43(2), 205–209.

3. Shnoll S.E. Periodical changes in the fine structure of statistic distributions in stochastic processes as a result of arithmetic and cosmophysical reasons. *Time, Chaos, and Math. Problems*, No. 3, University Publ. House, Moscow, 2004, 121–154.
4. Shnoll S.E. Changes in the fine structure of stochastic distributions as consequence of space-time fluctuations. *Progress in Physics*, 2006, v. 6, 39–45.
5. Panchelyuga V.A. and Shnoll S.E. Experimental investigations of gravitational-wave influence on the form of distribution function of alpha-decay rate. Abstracts of VI International Crimean Conference "Cosmos and Biosphere", Partenit, Crimea, Ukraine, September 26 – October 1, 2005, 50–51.
6. Panchelyuga V.A. and Shnoll S.E. Experimental investigation of spinning massive body influence on fine structure of distribution functions of alpha-decay rate fluctuations. In: *Space-Time Structure*, Moscow, TETRU, 2006, 328–343.
7. Panchelyuga V.A., Kolombet V.A., Kaminsky A.V., Panchelyuga M.S. and Shnoll S.E. The local time effect observed in noise processes. *Bull. of Kaluga University*, 2006, No. 2, 3–8.
8. Panchelyuga V.A., Kolombet V.A., Panchelyuga M.S. and Shnoll S.E. Local-time effect on small space-time scale. In: *Space-Time Structure*, Moscow, TETRU, 2006, 344–350.
9. Shnoll S.E. Discrete distribution patterns: arithmetic and cosmophysical origins of their macroscopic fluctuations. *Biophysics*, 2001, v. 46(5), 733–741.
10. Shnoll S.E., Zenchenko K.I. and Udaltsova N.V. Cosmophysical Effects in the structure of daily and yearly periods of changes in the shape of histograms constructed from the measurements of ^{239}Pu alpha-activity. *Biophysics*, 2004, v. 49, Suppl. 1, 155.
11. Shnoll S.E., Zenchenko K.I. and Udaltsova N.V. Cosmophysical effects in structure of the daily and yearly periods of change in the shape of the histograms constructed by results of measurements of alpha-activity Pu-239. arXiv: physics/0504092.
12. Shnoll S.E., Zenchenko K.I., Berulis I.I., Udaltsova N.V. and Rubinstein I.A. Fine structure of histograms of alpha-activity measurements depends on direction of alpha particles flow and the Earth rotation: experiments with collimators. arXiv: physics/0412007.
13. Shnoll S.E., Rubinshtejn I.A., Zenchenko K.I., Shlekhtarev V.A., Kaminsky A.V., Konradov A.A. and Udaltsova N.V. Experiments with rotating collimators cutting out pencil of alpha-particles at radioactive decay of ^{239}Pu evidence sharp anisotropy of space. *Progress in Physics*, 2005, v. 1, 81–84; arxiv: physics/0501004.

SPECIAL REPORT

A High Temperature Liquid Plasma Model of the Sun*

Pierre-Marie Robitaille

Dept. of Radiology, The Ohio State University, 130 Means Hall, 1654 Upham Drive, Columbus, Ohio 43210, USA

E-mail: robitaille.1@osu.edu

In this work, a liquid model of the Sun is presented wherein the entire solar mass is viewed as a high density/high energy plasma. This model challenges our current understanding of the densities associated with the internal layers of the Sun, advocating a relatively constant density, almost independent of radial position. The incompressible nature of liquids is advanced to prevent solar collapse from gravitational forces. The liquid plasma model of the Sun is a non-equilibrium approach, where nuclear reactions occur throughout the solar mass. The primary means of addressing internal heat transfer are convection and conduction. As a result of the convective processes on the solar surface, the liquid model brings into question the established temperature of the solar photosphere by highlighting a violation of Kirchhoff's law of thermal emission. Along these lines, the model also emphasizes that radiative emission is a surface phenomenon. Evidence that the Sun is a high density/high energy plasma is based on our knowledge of Planckian thermal emission and condensed matter, including the existence of pressure ionization and liquid metallic hydrogen at high temperatures and pressures. Prior to introducing the liquid plasma model, the historic and scientific justifications for the gaseous model of the Sun are reviewed and the gaseous equations of state are also discussed.

1 Introduction

1.1 Historical perspective

The modern theory of the Sun [1–5] can be traced back to 1870 when Lane published his discussion of the gaseous nature of this sphere [6]. At the time, of course, one could have had little idea about whether or not the Sun was really a gas. Nonetheless, Eddington [7, 8] would build on these early ideas. He believed that the laws of physics and thermodynamics could be used to deduce the internal structure of the Sun without any experimental verification [7, 8]. In 1926, he would speak hypothetically about being able to live on an isolated planet completely surrounded by clouds. Under these conditions, he still thought he could analyze the Sun without any further knowledge than its mass, its size, and the laws of physics [7, 8]. It was in this spirit that Eddington set out to expand on Lane's model of the Sun.

Eddington, more than any other person, has shaped our current understanding of the Sun. Consequently, it is fitting that a review of the current model be centered on his contributions. Some may argue that we have moved well beyond Eddington in our reasoning. However, Eddington has set a scientific course for the study of the Sun which has remained essentially unchallenged for nearly eighty years. Every new finding has been rationalized within the context of the gaseous model and no alternative starting point exists. Yet, the gaseous model is characterized by inconsistencies and physical interpretations which cannot be easily explained based on laboratory findings.

As such, the hot liquid plasma model is presented herein. The new model provides a scientific alternative in solar analysis. It is based on a reevaluation of the internal processes and structures associated with the gaseous model. The liquid model advocates a much higher photospheric density and temperature, thereby directly invoking the physics associated with high energy/high density plasmas. In addition, it completely eliminates Eddington's radiative zone and brings into question the existence of the current very high density ($150\,\mathrm{g/cm^3}$) core.

1.2 Eddington's polytrope and solar collapse

Eddington began his analysis of the Sun by assuming that Lane's gaseous model was correct [6]. The Sun was treated as a simple polytrope [3], wherein a direct relationship existed between pressure, P, and density, ρ [9]. Eddington's polytrope was of the form $\rho = K_1 P^{1/\gamma}$, where K_1 is a constant and the polytrope exponent, γ, was set to $\frac{4}{3}$. Under these conditions, the central density of the Sun was $\sim$54 times the average density and the central pressure was $1.24\times10^7\,\mathrm{dyn/cm^2}$ [3]. By having recourse to the ideal gas law and fully radiative heat transfer, Eddington deduced a central core temperature of 1.2×10^7 [3, 7, 8]. Today, this remains the range for

*This work was posted as arXiv: astro-ph/0410075, October 4, 2004. The discussion relative to the internal constitution of the stars in the introduction places a heavy emphasis on the writings of A. S. Eddington. The author wishes to also highlight the work of Nikolai Kozyrev on "Sources of Stellar Energy and the Theory of Internal Constitution of Stars" translated from the original Russian dissertation in Progress in Physics 2005, v. 3, 61–99. Kozyrev's excellent work provides additional important contributions and insight relative to the gaseous models of the stars.

the internal temperature of the Sun $\sim 1.5 \times 10^7$ K (e.g., [2–5]).

At the same time, Eddington realized that a gaseous Sun should collapse on itself [7, 8]. Specifically, the great forces of gravity should compress the mass into a much smaller sphere. Like his predecessors, Eddington pondered on why the gaseous Sun did not collapse. He solved the problem by invoking outward radiation pressure originating from the central core. Reasoning that the inside of the Sun was generating light, Eddington thought that these photons could produce the outward pressure sought. Since light quanta clearly possessed momentum, this "light pressure" kept the gaseous Sun from collapsing [7, 8]. Consequently, Eddington postulated that the inner portion of the Sun produced photons. He then deduced that these individual light quanta would sooner or later collide with a gas ion or atom and propel it against the forces of the Sun's gravity. The region of the Sun where this occurs was called the radiative zone. It remains a central portion of solar theory to this day. Importantly, however, this zone exists primarily as a result of Eddington's reasoning. For stars on the order of the solar mass, it is currently held that internal radiation pressure is not as significant as Eddington had advanced. A radiative zone is still present, but the effects of radiation pressure are downplayed. Rather, modern theory holds that the Sun is prevented from collapse due to electron gas pressure [3]. The radiation zone is still present in the Sun, but radiation pressure becomes dominating only for heavy stars on the order of 10 solar masses [3].

The modern theory of the Sun also makes use of a significant convective zone, which extends throughout the outer envelope. Convective zones extend to deeper levels as stellar masses decrease, such that small stars can be viewed as fully convective. Conversely, for stars with masses larger than the Sun, it is the core of the star which is convective [3]. The extent of the convective zone then grows towards the envelope of the star, as mass increases. Eventually, the convective zone extends to 70% of the stellar radius in stars on the order of 50 solar masses. In this case, the envelope is radiative in nature. Supermassive stars, like the smallest stars, finally become fully convective [3].

1.3 Photon shifts and opacity considerations

While Eddington believed that he properly understood a key aspect of solar structure with the creation of the radiative zone, he also wanted to know exactly how many photons the Sun could produce to support this hypothesis. Not sufficiently considering Kirchhoff's work [10], Eddington incorrectly believed that Stefan's law was universal [11]. He then applied this law to estimating the amount of photons produced. Given the dimensions involved, and the temperatures hypothesized for the solar interior, this photon output would have been tremendous. Eddington also recognized that a blackbody at millions of degrees should produce its photons at X-ray frequencies [12].

Thus, Eddington had deduced that the internal portion of the Sun was at 1.2×10^7 K. This resulted in the generation of photons at X-ray frequencies. At the same time, Langley had previously measured the solar spectrum and was setting the temperature of the photosphere at $\sim$6,000 K. In order to resolve this dilemma, Eddington simply stated that when photons are emitted, they are initially produced at X-ray frequencies [7, 8]. However, as these photons are scattered or absorbed in the collisions associated with radiation pressure, they slowly lose some of their energy. In this manner, after millions of years and many collisions, the photons emerge from the Sun's photosphere shifted to the visible region. Only a very small fraction of the total photons in the radiative zone manage to escape at any time. According to Eddington, the radiative zone is acting as a very slowly-leaking "sieve" [7, 8]. The photons traveling through this zone were thought to experience free-free, bound-free, and bound-bound absorptions along with scattering [2, 3]. The entire process would result in producing a certain opacity in the solar interior.

Eddington's model requires that these processes (scattering and free-free, bound-free, and bound-bound transitions) result in a final opacity which becomes Planckian in appearance. This was needed in order to permit the proper absorption and reemission of all photons, at all frequencies, and at all levels of the solar interior. In fact, the "opacity problem" constitutes one of the great weaknesses in a model of an interiorly radiating object. The issue is so complex that Rosseland mean opacities [2, 3], which are frequency independent, are often utilized. Such a procedure completely sidesteps the central issue. It is always possible to build an absorption or opacity profile given enough elements and weighted physical mechanisms (scattering and free-free, bound-free, and bound-bound transitions). However, the requirement that these profiles continually and systematically change throughout the interior of the Sun, while remaining blackbody in nature and yielding the proper frequency dependence, does not appeal either to simplicity or objective reality. In fact, the generation of a Planckian spectrum requires a Planckian process [10]. Such a spectrum can never be generated from the sum of many non-Planckian processes. Once again, the current gaseous model has serious shortcomings in the manner in which solar thermal emission is explained.

Unfortunately, for Langley and Eddington, the situation is even more complex than they initially believed [10]. The Sun is not in thermal equilibrium with an enclosure. In reality, enormous convection currents are present both on the solar surface and within the solar interior. These convection currents can easily act to violate the integrity of Eddington's layers. Therefore, the interior of the Sun represents a significant deviation of the requirements set forth in Kirchhoff's law (equilibrium with a perfectly absorbing enclosure [10]).

The application of the laws of thermal emission [11–13] to the Sun constitutes a violation of thermodynamic principles.

1.4 Coronal heating

Beyond Eddington, the next big step in solar theory came in the 1950's when scientists were beginning to obtain interesting data from the solar corona. It was observed that the corona possessed, within it, highly ionized ions produced at temperatures well in excess of 1.0×10^6 K [14]. The width of Lyman-α lines further demonstrates that temperatures in the corona ranged from 2.6×10^6 to 1.2×10^6 K at 1.5 and 4 solar radii, respectively [14]. These findings of very hot temperatures in the corona presented a problem for solar theory. A temperature within the corona ($>1.0\times10^6$ K) which exceeded that of the photosphere ($\sim$6,000 K) indicated a violation of the 2nd law of thermodynamics. That is, heat could not be coming from inside the Sun to heat the corona, while remaining incapable of heating the photosphere. Thus, if the photosphere was really at $\sim$6,000 K, there must be found an alternative means to heat the corona. It has now been widely accepted that the local heating in the corona occurs as a result of a process involving the flow of ions through the magnetic fields of the Sun [5].

1.5 Helioseismology

Currently, much of the support for the gaseous models of the Sun arises from helioseismology [15] or the study of solar quakes on the surface of the Sun. It is claimed that excellent agreement exists between the theoretical models and the actual seismological data. In large part, this is a direct measure of the gaseous model's ability to permit variations in density, pressure, temperature, composition, depth and opacity values throughout the solar interior. Given enough variables, good agreement with experimental data can be achieved. Nonetheless, it is interesting that despite phenomenal agreement between theory and experiment, the theoretical fits completely break down in the outer 5% of the solar disk [16]. This is not surprising since the solar photosphere currently has a hypothetical density which is lower than that present within the best vacuums achieved on earth. Since acoustic waves cannot propagate in a vacuum, it is not surprising that the theorists are unable to fit the exterior the Sun [16]. Yet, this is precisely that region of the Sun from which all the data is being collected.

1.6 Summary of the gaseous models

Eddington was concerned with the great problems of solar theory: (1) how to prevent the gaseous Sun from collapsing on itself, (2) how to set the internal temperature, and finally, (3) how to shift the frequency of photons produced at X-ray frequencies to the observed visible region. He solved these problems by invoking radiation pressure and the laws of thermal radiation. The creation of the radiative zone resulted in tremendous radiation pressure within the Sun. For Eddington, this radiation pressure exactly balanced with the gravitational forces and resulted in one of the earliest gaseous models of the Sun. The gaseous Sun had been prevented from collapsing and photons were produced appropriately in the visible range. The interior of Eddington's gaseous Sun was at very high temperatures estimated at millions of degrees. Yet, this extremely hot object was surrounded by a very cool photosphere, only $\sim$1,000 kilometers thick and at a temperature of just $\sim$6,000 K.

Regrettably, the idea that photons become the primary means of striving for internal thermal equilibrium in a star is not in accordance with our knowledge of the thermal behavior of objects [17, 18]. Rather, for all other objects, internal thermal equilibrium is achieved through thermal convection and conduction [17, 18]. In contrast, radiative heat transfer enables an object to dissipate heat and reach thermal equilibrium with the outside world (e.g., [17–20]). Astrophysical treatments of thermal radiation [21–23] minimize these arguments and, like all other textbooks, fail to state the underlying cause of the radiation [10].

Under the gaseous model, the internal temperature of the stars continues to rise, despite the fact that photons are being emitted. Stellar compression becomes an uncontrollable process. In order to cool the stars, photons must be injected into their interior. Eddington best summarizes this violation of thermodynamics and the dilemma it creates for all gaseous models [2]: "I do not see how a star which has once got into this compressed condition is ever going to get out of it. So far as we know, the close packing of matter is only possible so long as the temperature is great enough to ionize the material. When a star cools down and regains the normal density ordinarily associated with solids, it must expand and do work against gravity... Imagine a body continually losing heat but with insufficient energy to grow cold!"

Note that the second sentence in this quote is the essence of the problem. Eddington has ignored the consequences of van der Waals' equation and the incompressibility of the liquid state. He constructs a model wherein the known behavior of the condensed states of matter on Earth is discarded. The gaseous model requires production of photons at high frequency (X-ray, gamma) within the core of the Sun, which are then shifted to the visible region [7, 8]. However, the shifting of a blackbody radiation spectrum produced at one Wien's displacement temperature to another is without experimental verification. The current complexity associated with the calculations of stellar opacities hint at the unreasonableness of such conjectures. A Planckian process is required to generate a Planckian spectrum [10]. However, the gaseous stellar models are incapable of yielding a Planckian process, since they "a priori" exclude the existence of condensed matter and of a photospheric lattice.

Since modern stellar theory remains based on gaseous models, the analytical equations of state [24, 25] are founded

on the assumption that the Sun can be treated as a compressible gas. The emergence of numerical solutions [24, 25], including such refinements as the addition of partial ionization and Debye-Huckle theory, alters nothing of the underlying framework. Currently, the density of the central core is thought to be $\sim$150 g/cm^3, while that of the lower photosphere is on the order of 10^{-7} g/cm^3 [26]. Neither of the numbers, of course, can be verified by direct experimentation. The modern Sun and all of the main sequence stars remain viewed as compressible gases without lattice structure. Only the details of the local densities, temperatures, composition, opacities, radiative emission, and convection currents, are altered. For stars near the solar mass, it is advanced that electron gas pressure now acts to prevent solar collapse [2, 3]. This is true even though the mathematical analysis of electron gas pressure relies on the use of real or imaginary rigid surfaces [2] which can never exist within the stars. The stars are quite unlike the Earth's atmosphere, since the latter is resting on a distinct surface. As a result, electron gas pressure is unlikely to prevent solar collapse since the gaseous models cannot invoke rigid surfaces while maintaining the integrity of the gaseous state. Irrespective of such arguments, one cannot discount that Eddington's radiative pressure remains extremely important for the gaseous theories, especially in the more massive stars.

2 Liquids and gases

The flow of material on the surface of the Sun (e.g., [2, 3, 5, 27]) makes both the gaseous and liquid states prime candidates for discussing the nature of the photosphere. Unfortunately, the distinction between the gaseous and liquid state is often difficult to establish. Gases and liquids are often viewed simply as fluids with no further distinction, but differences do exists. Liquids are characterized by their relatively high densities and by their surface tensions [28–31]. They also have real internal structure and can be seen as possessing "fleeting lattices" with short range order [28–31]. Gases, on the other hand, fail to display a surface and have no internal structure. Liquids can boil and thereby produce the gaseous state. Gases cannot boil. Liquids, unlike gases, are essentially incompressible [28–31]. In conjunction with solids, liquids correspond to the densest form of matter detected in the laboratory. In this regard, a significant increase in the density of the liquid state would require changes within the atomic nucleus itself, as the atomic number is increased. Large changes in pressure, by themselves, are incapable of significantly altering, by orders of magnitude, the density of the liquid state [28–32]. This is quite unlike the behavior of highly compressible gases, as reflected in the ideal gas law [28, 32].

Although their exact thermal behavior remains extremely poorly documented [20], liquids can also emit continuous radiation by virtue of their continuous physical nature. Mostly liquid metals have been studied [20], and little is known about the thermal properties of nonmetallic liquids. Studies with water at microwave frequencies only add to the complexity of the problem. For instance, it is easy to establish that the oceans are not blackbody in nature. At the Nadir angle (view is normal to the water surface), the sea surface appears with a brightness temperature of less than 100 K at 1.4 GHz [33]. In addition, the brightness temperature of salt water can be relatively independent of actual temperature [33]. When larger observation angles are used, the brightness temperature of sea water rapidly rises [33], although it is always short of the correct value. Since the brightness temperature of salt water is so highly dependent on salinity, it is clear that an understanding of thermal emission processes in liquids is complex [33].

Liquids unlike gases, can support transverse wave propagation as reflected by the presence of weak phonons. The behavior of phonons has been examined in liquid helium [34]. Phonons have also been studied in superionic conductors which are characterized by liquid-like mobility of one of the ionic species [35]. The study of phonons in solids and liquids usually involves neutron scattering experiments (e.g., [34–38]). As for gases, they are unable to support transverse phonons. Neutron scattering experiments, aimed at determining structure in solids and liquids, do not exist as related to gases. Acoustic experiments with gases involve the study of longitudinal waves.

Differences clearly exist between the liquid and gaseous states [28–32]. As such, these two phases are not simply a continuum of one another, as is often assumed. Unlike the ideal gas law, the equations used in the analysis of liquids tend to be complex. Herein lies a major difficulty in advancing a liquid model of the Sun. Nonetheless, in order to discern the relative merits of a gaseous versus a liquid model, solar observations themselves, not mathematical simplicity, must guide the theorist. Thus, solar behavior must be reexamined and the most critical data remains the nature of the solar spectrum.

3 Thermal emission

3.1 Local thermal equilibrium

Modern solar models make extensive use of local thermal equilibrium in order to simplify the analysis of stellar structure [1–3]. Nonetheless, plasmas are well-known to support electronic and ionic temperatures which are not at equilibrium. Recent work [10] highlights that the Sun cannot meet the requirements for a blackbody, as set down by Kirchhoff, for the simple reason that it is not in thermal equilibrium with a perfectly absorbing enclosure [9, 19]. The analysis of the Sun is a non equilibrium problem, as manifested by the presence of convection currents, solar eruptions, solar wind, and emission of light without confinement. All transport processes, including convection, are non equilibrium pro-

cesses [29]. Planck has previously warned that the presence of convection currents is sufficient to completely destroy local thermal equilibrium arguments [39]. That local thermal equilibrium does not exist is of profound consequence to any theorist, since simplifying assumptions are removed. Despite this complication, the lack of local thermal equilibrium for the interior of the Sun is consistent with observations of non-equilibrium in the solar corona, where significantly different electronic and ionic temperatures have been detected [40]. Nonequilibrium within the corona may well be a manifestation of the state of the entire star. The photosphere is clearly not in thermal equilibrium with an enclosure (e.g., [9, 19]). Furthermore, it possesses convection currents rendering it unsuitable as a candidate in blackbody radiation [10, 39].

As such, it was improper for Langley [41, 42] to set a temperature of the photosphere at ∼6,000 K, simply because a thermal emission spectrum was present. The proper assignment of a temperature based on thermal arguments depends on the known presence of a perfectly absorbing enclosure, namely a solid graphite box [10]. Langley's use of Planckian arguments [11–13, 39, 41, 42] to set a temperature for the photosphere constitutes a violation of Kirchhoff's law of thermal emission [10, 43, 44]. The presence of local thermal equilibrium is central to the assignment of any temperature based on thermodynamic arguments [10, 39].

Eddington's need to shift the solar spectrum to lower frequencies requires that gaseous atom or ionic hydrogen or helium be able to both absorb and re-emit a blackbody spectrum. This creates essentially impossible constraints on the opacities needed inside the Sun, especially given that only scattering and free-free, bound-free, and bound-bound transitions can be considered. None of these processes are individually capable of providing the proper Planckian behavior. Only complex summations, involving many discontinuous phenomena, can lead to the required continuous opacities. The problem is so complicated that the entire task is often sidestepped. Rosseland mean opacities, which are frequency independent, are often used to deal with this issue [2, 3]. However, the use of Rosseland mean opacities is unsatisfactory. The requirements set on opacity by Eddington for the radiative zone are contrary to our knowledge of thermal emission spectra in either gases or plasmas (e.g., [45, 46]). As mentioned above, the production of a Planckian spectrum must involve a Planckian process and not the summation of many non-Planckian spectra. The "opacity problem" represents the greatest single warning sign that a gaseous model of the stars cannot be correct.

3.2 Thermal emission in liquids

Like solids, liquids possess a lattice, although this structure is often fleeting (e.g., [29–31]). This is manifested in the presence of Brownian motion within the liquid. Thus, in a liquid, not all of the energy is contained within the vibrational degrees of freedom of the lattice. This directly accounts for the inability to obtain a complete monitoring of the energy distribution within a liquid based only on its thermal emission. Indeed, most of the nonnuclear energy in a liquid may well be contained in the translational and rotational degrees of freedom. The ability of a liquid to store energy in translational degrees of freedom certainly leaves less energy than expected at a given temperature in the vibrational degrees of freedom. This is a problem for a Planckian oscillator model which does not consider translational and rotational energy [13]. As a result, it is hypothesized that the presence of translational and rotation degrees of freedom can cause a liquid to report a much lower temperature than its real temperature, when the laws of thermal emission [11–13] are utilized to monitor its emission spectrum. As mentioned above, the idea that radiation pressure is present within the Sun is not in accordance with the known mechanisms of heat transfer within objects [17]. There is no experimental basis on Earth for invoking that an object can strive for internal thermal equilibrium using thermal radiation. Conduction and convection dominate heat transfer within objects [17]. A liquid model is more apt to deal with heat transfer through these two mechanisms, since it provides increased density, facilitating both more efficient conduction and convection.

4 The liquid model of the Sun

A central tenant of the liquid plasma model is that the density within the solar interior is nearly constant. It has been well established that liquids are essentially incompressible and that their compressibility decreases quite dramatically as pressure is increased [28–31]. Therefore, in the liquid plasma model, the liquid framework is regarded as incompressible and the issue of solar collapse never arises.

There are numerous arguments supporting a liquid plasma model. These include: (1) the continuous nature of the emission spectrum, (2) the average density of the solar mass, (3) the gentle oblateness of the solar sphere, (4) the presence of a distinct solar surface, (5) the presence of surface gravity waves and helioseimology studies, (6) the known existence of hydrogen on Earth in the liquid metallic plasma state at high pressures and temperatures, (7) the existence of solar boiling, and (8) the presence of the corona, transition zone, and chromosphere. In addition, the liquid plasma model provides for the mixing of solar materials, resulting in important evolutionary consequences for the stars. At the same time, the liquid plasma model addresses the issue of coronal heating and helps to resolve the thermodynamic problems in this area.

4.1 Solar emission

The solar spectrum deviates from a blackbody in appearance in that the high frequency region is distorted. This finding

urges caution in setting a temperature to the photosphere using Planckian arguments. Based on experimental work in thermal emission, the photosphere cannot be a low density gas or plasma. Gases and plasmas, outside the confines of an enclosure, simply cannot produce a Planckian-shaped thermal emission profile as seen in the visible light of the photosphere. These issues have previously been discussed in detail [10]. The production of a continuous blackbody spectrum is incongruent with an origin from a low density source. Experimental blackbodies are exclusively solids (e.g., [47–51]).

The concept that the photosphere, as an "opaque gas", is able to emit as a blackbody is not supportable. Without exception, the approach to opaque behavior by gases or plasmas is accompanied by an increase in density and pressure. In contrast, the density advanced for the photosphere is on the order of 10^{-7} g/cm^3 [26]. No gas has been demonstrated to approach optically opaque behavior at such densities. Thus, while it is believed that, in the limit of high pressures, some gases can become opaque, it is more likely that they simply become liquids. The idea, that free gases or plasmas can become optically opaque [45, 46] and can follow Kirchhoff's law, ignores the known observation that such behavior cannot be produced outside the confines of a solid enclosure [10]. Studies in which gases or plasmas approach optically opaque behavior are always confined to enclosures at high pressure. For instance, note that the Tokamak reactors used in plasma physics are often lined with graphite [52]. This situation is exactly analogous to the experimental conditions under which Kirchhoff's law was developed [10]. Real blackbodies always involve enclosures which are either made from graphite [49, 50] or lined with soot (graphite) containing paints [47, 48, 51]. As a result, it is not surprising that, in the limit of high pressure within the confines of a Tokamak, the approach to blackbody behavior can be reached [10, 45, 52]. In any case, such a setting is completely unlike the surface of the Sun, wherein a solid enclosure is not present.

Unfortunately, it appears that the exact physical mechanism for producing a blackbody radiation spectrum has not been defined by the scientific community [10]. Nonetheless, thermal radiation must be linked to one of the simplest processes within matter, namely atomic or nuclear vibrations within the confines of a lattice structure [10]. This is reminiscent of Planck and his oscillators [13, 39]. In the final analysis, whatever physical mechanism is invoked for blackbody radiation, it should be independent of nuclear reactions, since all solids are able to emit some form of continuous thermal radiation [20].

If it is true that the frequency and amount of photons released by an object is related only to the amount of energy in the vibrational degrees of freedom of the lattice [10], it is easy to see why Langley believed that the photosphere was at a temperature of only $\sim$6,000 K. Note the well established convection currents on the surface of the Sun (e.g., [4, 5, 27]). These currents contain translational energy which is not readily available for thermal emission. However, during flares and other eruptions, it is well-known that X-rays can be released from the solar surface. These X-rays reveal brightness temperatures of millions of degrees (e.g., [4, 5, 27]). In this case, the translational energy of the liquid envelope is being converted to thermal photons in a manner revealing a stored energy bath with temperatures well in excess of 6,000 K. Such X-ray findings from the solar surface were not at the disposal of Langley when he set the photospheric temperature in the mid-1800's [41, 42].

It is therefore hypothesized that a liquid can instantaneously lower the total output of photons, at a given temperature, and release them at a frequency significantly lower than what would be predicted from their real energy content and temperature. This is simply an energy partition problem which arises in the presence of convection currents. The sea surface temperature at microwave frequencies discussed above hints to this behavior.

A liquid photosphere with a temperature of $\sim 7.0 \times 10^6$ K could be generating photons not at X-ray frequencies, as expected, but rather in the visible range. This occurs because the photosphere has convection. Since most of the energy of the photosphere is tied up in the translational (or rotational) degrees of freedom and its associated convection, it is simply not available for the generation of thermal photons. However, this energy can become available during a solar eruption which reveals that the real temperatures of the solar photosphere are well in excess of 6,000 K. The liquid phase provides a means of producing a thermal radiation curve for the Sun at a lower apparent temperature than its real temperature. All that is required is to lower the force constant in Planck's oscillators. In this regard, note that an oscillator representing a van der Waals interaction would have a much weaker force constant than one representing covalent bonds.

This hypothesis remedies the problem with Langley's temperature for the photosphere. Setting a real temperature of the photosphere at $\sim 7.0 \times 10^6$ K permits the free flow of heat throughout the outer layers of the Sun. The 2nd law of thermodynamics is no longer violated. Photons do not take millions of years to leave the Sun [7, 8]. Rather, they are solely produced and released at the photosphere using a mechanism common to all condensed objects on Earth. The radiative zone is eliminated and the need to shift high energy photons removed.

4.2 Solar densities

The Sun has an average density ($\sim$1.4 g/cm^3) which can easily support the liquid plasma model. Indeed, the gaseous model applies extremes of density which are not easily justified (150 g/cm^3 for the core and 10^{-7} g/cm^3 for the photosphere [26]). Instead, the liquid plasma model simply requires a very ordinary density throughout the body of the Sun.

The presence of a liquid structure eliminates the need for radiation pressure to prevent the Sun from collapsing on itself. The liquid alone can support the upper layers. For the gaseous models, solar collapse is prevented by having recourse to internal radiation and electron gas pressure both of which are without sound experimental justification. In a liquid model, the problem of solar collapse is simply addressed by invoking the incompressibility of liquids. Interestingly, the Jovian planets all have densities consistent with the liquid state (Jupiter: $\sim$1.33 g/cm^3; Saturn: 0.7 g/cm^3, Uranus: 1.30 g/cm^3, and Neptune 1.76 g/cm^3). For a gaseous model of the Sun, it would have been convenient if at least one of these planets had an average density consistent with the sparse gaseous states (e.g., 10^{-4}–10^{-7} g/cm^3) currently proposed for the convective zone and the photosphere (10^{-7} g/cm^3) [26]. Note that the latter density approaches the value of a reasonably good vacuum in the laboratory. The Jovian planets have high average densities (0.7–1.76 g/cm^3) despite their small size and masses relative to the Sun. As such, the sparse densities currently assigned to the outer layers of the Sun are incongruent with the high average densities of the Jovian planets, especially given that these are also constituted primarily of hydrogen and helium. This leads us to deduce that the Jovian planets are also condensed in nature and that they may have significant liquid components, both on their surface or in their interior.

The densities of materials on Earth is determined primarily by the atomic number and by the packing of the crystal lattice. As far as the existence of a solar core is concerned, there is no experimental evidence for reaching densities of $\sim$150 g/cm^3 using a hydrogen and helium framework. Without exception, high densities involve high atomic numbers. Mathematical arguments to the contrary are based exclusively on the collapse of a gaseous model of the Sun and are without experimental justification in the laboratory. Once again, the Jovian planets do not support the idea of a dense core given that they, like the Sun, possess average densities on the order of 1 g/cm^3. Unlike the gaseous model, which must have a dense core to compensate for its sparse convective zone and photosphere, the liquid model does not necessitate the presence of a dense core. Such a core may or may not be present. However, laboratory observations, with the densities achievable using helium and hydrogen, suggest that it cannot exist.

4.3 The solar surface

The Sun has a reasonably distinct surface. This point has recently been emphasized by images obtained with the Swedish Solar Telescope [53, 54]. These images reveal that the solar surface is not simply composed of clouds hovering about, but has a clear three-dimensional appearance which evolves in a manner reflecting "solar hills, valleys, and canyons" [53, 54]. Solar granulations appear to be "puffy hills billowing upwards" [53, 54]. This represents strong evidence that the solar surface is dense and has surface tension, a clear property of the liquid state.

Gases are not characterized as possessing surfaces. This accounts for the extension of the corona (which is a gaseous plasma) for millions of miles beyond the Sun without a distinct boundary. The hot liquid plasma model of the Sun helps to explain the distinct nature of the solar surface, wherein a transition is observed between the photospheric density and that of the solar atmosphere. The chromosphere is reminiscent of the critical opalescence of a gas in the vicinity of criticality [30], and the existence of such a zone is highly supportive of a liquid model. Furthermore, the surface nature of the Sun is well visualized using imaging methods, including Doppler techniques [40, 53–55]. The surface tension of a liquid provides an elegant explanation for the distinct nature of the solar surface, which is not easily available within the context of a gaseous model.

4.4 The solar oblateness

Solar oblateness, ε is a dimensionless quantity

$$\varepsilon = (R_E - R_P)/R_E$$

obtained by comparing the values of the equatorial (R_E) and the polar radii (R_P). The existence of gentle solar oblateness has been recognized for nearly thirty years. Initial values measured by Dicke and Goldberg [56] were as large as $4.51\pm0.34\times10^{-5}$. More modern values are slightly less pronounced at 8.77×10^{-6} [57]. While such oblateness appears extremely small and negligible at first glance, it provides a dilemma for the gaseous models.

In order to properly analyze solar oblateness, it is necessary to have recourse to models of rigid body rotation [57]. In this regard, the theory of rotating liquid masses is well developed and extensive discussions can be found in Littleton's classic text [58]. In addressing the oblateness of the Sun [56, 57], the density of this rotating sphere is maintained as essentially constant throughout the solar radius [57]. The model used is described by an analytical form and is able to account both for the rotation of the convective zone and for the differential rotation of the inner Sun [57]. Importantly, the rigid body model [57, 58] is not dependent on the solar density. This is in sharp contrast with the well-known equations of state for stellar structure [2, 3, 24, 25]. The latter, of course, possess a strong interdependence of density and pressure with radial distance.

Beyond the Sun, other stars also possess varying degrees of oblateness. The most significant of these, at present, appears to be the southern star Achernar, a hot B-type star with a mass currently estimated at six times the mass of the Sun. The oblateness of this star is caused by rapid rotation and is a stunning 1.56 ± 0.05 [59]. Achernar's oblateness is so severe that it is completely incompatible with the Roche model,

wherein the mass of a star is concentrated near the stellar interior [3, 59]. The oblateness of the Sun and some stars provides significant support for the liquid plasma model of the Sun and a tremendous hurdle for the gaseous models.

4.5 Surface gravity waves and helioseismology

A liquid plasma model of the Sun is also best suited to the study of helioseismology (e.g., [15]). This is because terrestrial observations of this nature are exclusively limited to the oceans and continents, materials with high densities. It would be incongruent to advance such studies for the terrestrial atmosphere. Yet, the density of the terrestrial atmosphere at sea level is $\sim$1,000 times greater than the density proposed by the gaseous models for the solar surface.

A solar seismic wave [55] was produced in association with a flare on the surface of the Sun on 9 July 1996 [40]. Such a Sun quake demonstrates that the solar surface is fully able to sustain a surface gravity (or transverse) wave extending over millions of meters. These are described as "resembling ripples from a pebble thrown on a pond" [40, 55]. The ability to sustain such a wave requires the presence of very dense materials. Indeed, sparse gases are completely unable to sustain surface gravity waves as these require the presence of condensed matter. Such Sun quakes provide powerful evidence that the solar surface is comprised of a material attaining a very high density. While a gaseous model can easily deal with longitudinal acoustic waves within the solar interior, the same cannot be said for its ability to deal with the presence of a surface gravity (or transverse) seismic wave on the surface. Once again, it is clear that the current theoretical fits fail at the solar surface [16].

The ability to conduct helioseismology studies on the Sun (e.g., [15, 40, 55]) is incongruent with a true gaseous nature. While sparse gases and plasmas are able to sustain longitudinal acoustic waves, they are unable to support transverse seismic waves. Terrestrial seismology is limited to the study of the oceans and the continents. The Earth's atmosphere is much too thin to enable such studies. The liquid plasma model of the Sun is better suited to explain the presence of seismologic activity on the surface of the Sun.

4.6 Hydrogen as a liquid metal plasma

At atmospheric temperatures and pressures, hydrogen exists as a diatomic molecular gas. At low temperatures, condensed molecular hydrogen is an insulator with a relatively wide band gap ($Eg = 15$ eV). It is noteworthy that when hydrogen is shock-compressed, and thereby submitted to extreme pressures ($>$140 GPa) and temperatures (3000 K), it is able to under pressure ionization [60]. In so doing, hydrogen assumes a liquid metallic state, as revealed by its greatly increased conductivity [60]. Similar results hold for deuterium, although the insulator to metal transition occurs under less intense conditions [61]. The existence of liquid metallic hydrogen plasmas is of tremendous importance in astrophysics and has direct consequences on the structures of Jupiter and Saturn [30, 60]. However, these findings have not been extended to the Sun, even though the Sun is able to subject hydrogen to higher temperatures and pressures.

In any case, dense liquid metallic plasmas of hydrogen provide very interesting possibilities in stellar structure which should be considered by the plasma physicist. That liquid metallic hydrogen is known to exist, directly implies that the Sun can be treated as a liquid metal plasma. The equations of magnetohydrodynamics [62] become relevant not only in the corona, but also within the entire Sun. This has tremendous consequences for stellar and plasma physics, further implying that the gaseous equations of state must be abandoned. A liquid metal plasma model of the Sun implies (1) high, nearly constant, densities, (2) a rigid body problem, and (3) the use of continuous equations of state and magnetohydrodynamics [45, 62, 63].

Liquid metallic hydrogen may also present interesting lattice characteristics to the theorist. Calculations reveal that metallic hydrogen displays an important dependence of potential energy and interatomic distance [63]. For instance, in liquid sodium, the potential well for interionic bonding has a single minimum. In contrast, for metallic hydrogen, the spatial inhomogeneity of the electron density is so important that higher order perturbations must be considered. This leads to potential functions with groups of minima rather than a single minimum [63]. These potential energy functions have important pressure dependences [63]. As a result, metallic hydrogen should be able to assume a variety of lattice structures, with varying interatomic distances, in a manner which depends primarily on temperature and pressure. It is likely that future extensions of these findings to liquid metallic hydrogen will enable the calculation of various possible structures within the liquid phase itself. This may be important in helping us understand the nature of Sunspots and stellar luminosities, particularly when magnetic field effects are added to the problem.

4.7 The displacement of solar mass

All current gaseous models of the Sun make the assumption that densities are gradually changing between the convection zone, photosphere, chromosphere, transition zone, and corona. In these models, only the opacity changes at the photosphere, in order to create the "illusion" of a surface. Nonetheless, it is clear that a phase transition is occurring between the photosphere and the chromosphere/transition zone/corona.

In the photosphere, both upward and downward radial flows are observed. These are also associated with transverse flows parallel to the surface itself. The motion of Sunspots also reminds us that transverse flows are an important com-

ponent of mass displacement in the photosphere. In sharp contrast, flows in the corona are clearly radial in nature (ignoring the effects of solar eruptions and flares). The solar wind is a manifestation of these radially pronounced flows. Consequently, the analysis of solar mass displacement, at the surface and in the corona, clearly reveals that we are dealing with an important phase transition at the photosphere. The solar corona is a gaseous plasma. Note that it has all the characteristics of a true sparse state (no surface, no continuous spectrum, not subject to seismological studies, unable to boil). It is proper to think of the corona as representing the vapor surrounding the condensed photosphere. This is typical of every liquid-gas equilibrium observed on Earth. The corona has no distinct boundary, reflecting once again that it is the true gaseous plasma, not the photosphere. As previously noted, the chromosphere is reminiscent of the critical opalescence at the gas/liquid interface near criticality [30]. This is an important observation which should not be dismissed.

4.8 The boiling action of the solar surface

Solar boiling is a well established occurrence. Indeed, it is commonplace to refer to the Sun as a "boiling gas". Gases, however, cannot boil. They are the result of such action. The act of boiling is a property of the liquid state and is directly associated with the presence of a distinct surface. To speak of the Sun as "a boiling gas", as is done in so many astrophysical texts, is an unintended contradiction relative to the current gaseous model of the Sun.

5 Advantages of the liquid plasma model

5.1 Solar mixing and nuclear reaction processes

The presence of a liquid state provides an opportunity for mixing of nuclear species within the solar sphere. The liquid state can maintain the nuclei involved in nuclear reactions in close proximity with constant mixing, thereby providing a significant advantage in achieving efficient nuclear burning. Conversely, within a solid core, the flow of reacting nuclei is greatly hindered. All solar models advocate that the bulk of the nuclear reactions in the Sun occur in the core. As the Sun evolves, it is said that the hydrogen core will slowly burn out [2, 3]. The Sun will then move to helium burning, and later to the burning of the heavier elements. In contrast, in the liquid plasma model, nuclear reactions are free to occur throughout the solar body, as a result of the nearly uniform solar density.

The energy produced in this fashion, within the solar interior, would be brought to the surface by conduction and convection. When nuclear reactions occur on the surface of the Sun, energy could be directly emitted in the form of gamma rays. That nuclear reactions can be distributed throughout the solar interior has dramatic implications for the lifetime of our Sun, since the burning out of a nuclear core would not occur. A liquid model could extend the life of our star more than 10 fold, relative to the current expectancy. This is because only 10% of the hydrogen fuel is hypothesized to be burned, in the core of the present gaseous model, before the Sun is forced to switch to helium [3]. The liquid model elegantly overcomes such limitations, by enabling the continuous free flow of reactants in nuclear processes. As a result, the composition of the photosphere becomes an important indicator of the composition of the entire star, since convection now acts to equilibrate the entire solar interior. The determination of stellar compositions is subject only to the timescale of mixing. Such reevaluations have profound implications for stellar evolution and cosmology.

5.2 Coronal heating

The eruption of solar flares and prominences are associated with the displacement of material from the solar surface. Such events often occur in conjunction with the release of strong X-ray and gamma ray flashes. These flashes point to an underlying thermal potential in the photosphere which is not expressed under normal circumstances. This provides secondary evidence for the hot photospheric liquid plasma model. In this model, the heating of the corona, by complex magnetic field interactions is still permitted, but no longer required. The primary means of internal heat transfer within the Sun once again becomes convection and conduction [17]. Since energy transfer through convection is only proportional to T and not T^4 (as was the case for thermal radiation), it can be expected that regions of non-equilibrium superheated fluid exist within the Sun. A theory based on the release of superheated fluid from the interior could help explain much of the solar activity found on the surface, including flares and prominences.

In order to simultaneously preserve Langley's temperature and respect the 2nd law of thermodynamics, the gaseous model provides two means of generating heat (e.g., [4, 5, 27]). The first of these occurs within the Sun and is thought to be thermonuclear in origin. The second occurs in the corona and is thought to be of magnetic origin. Particles moving at enormous speeds are also involved to ensure this second temperature. Furthermore, something strange must be happening relative to the photosphere. The gaseous model advances that this layer cannot be heated either by the interior of the Sun or by the corona, both of which are at much higher temperatures. This problem is overcome in the liquid plasma model by raising the true temperature of the photosphere itself, based on energy partition in liquids and on the known production of hard X-rays at the solar surface during eruptive events.

At the same time, the liquid model is quite easily extended to include the presence of Alfvén waves in the chromosphere, transition zone, and corona, much in the same way

as the current gaseous model (e.g., [4, 5, 27]). In this regard, the increased density of the photosphere in the liquid model may well help to better explain the origin and behavior of the magnetic field lines located at the surface of the Sun.

5.3 The evolution of the stars

It is clear that adopting a liquid plasma model of the Sun constitutes a significant reshaping of astrophysics with important evolutionary and cosmological consequences. These are too broad to discuss in this work. The issue at hand is simply the assignment of the proper state of matter for the Sun.

5.4 The birth of a star

Current stellar evolution theory holds that the stars are initially formed as a result of the free fall gravitational collapse of interstellar clouds [3]. A significant weakness of these models is the need for a disturbance initiating the collapse [3]. It is also difficult to conceive how many stars can form from a single cloud in such models. Nonetheless, as the collapse proceeds, the process rapidly accelerates until a quasi-steady state is reached with the ignition of nuclear reactions [3].

Relative to the formation of a liquid plasma Sun, it may be important to reconsider this question. What if stellar formation is initiated not by gravitational collapse, but rather by the slow condensation and growth of a star? Star formation would be initiated in extremely cold matter, wherein two atoms first make van der Waals contact [28]. Given the low temperatures, if their combined kinetic energy is not sufficient to overcome the force associated with the van der Waals attraction, a two-atom system is created. A third atom would then join the first two and so on, until a larger and larger mass is created.

The latent heat of condensation could be dissipated by radiative emission. Initially, of course, such seeds of stellar formation would be very subject to destruction, because a high energy atom could always come and break up the process. However, a mass could grow large enough that its van der Waals forces, and its energy of cohesion, are sufficient to deal with the kinetic energy of any single noncondensed atom. When this occurs, condensation would increase rapidly. Again, the important interaction is the van der Waals force. Eventually, a large body could be formed and gravitational forces would become important. The stellar mass would continue to grow. Hydrogen would be converted to a liquid metal plasma, when a critical value for the mass and pressure is achieved. This would correspond to a mass on the order of the Jovian planets (since they are currently theorized to be liquid metal plasmas [60]). As the forces of gravity begin to dominate, the mass of the star would grow until the internal pressure and temperatures become high enough to provoke nuclear ignition and the birth of a new star.

A significant advantage of this approach is that stellar formation takes place at low temperatures. Cold hydrogen is permitted to condense and ignition occurs only once a given stellar mass is reached.

6 Conclusions

For over one hundred years now, the gaseous model of the Sun has dominated scientific thought in solar research. Yet, the model is complex and not easily supported by scientific experimentation. Sufficient evidence is presented herein that the Sun is truly a liquid plasma. In contrast, not a single reason can be provided supporting the idea that the Sun is a gas. The argument made in advance textbooks and coursework simply rests on the observation that the Sun is “hot”. The assumption then follows that it cannot be a liquid. Such arguments completely ignore the nature of liquids and gases.

Simple extensions of the Clausius-Clapeyron equation, neglect fact that the Sun is not in a closed system. Furthermore, the gaseous model ignores the existence of liquid metallic hydrogen plasmas in the laboratory.

In reality, we have very little understanding of the pressures and temperatures associated with the Sun. As a result, the “proofs of the gaseous model” tend to be mathematical and theoretical, not experimental. That is because of the mathematical simplicity and elegance of the current equations of state [1–3]. However, as Michelson reminds us: “Everything depends on the insight with which ideas are handled before they reach the mathematical stage [32].”

It is not prudent to apply gaseous equations of state to the Sun, without allowing for experimental guidance. Current solutions relative to solar collapse, temperature, density, internal radiative emission, photon shifting, and seismology, are significant issues for which little more that theoretical arguments are advanced. In addition, all the gaseous models ignore that atoms have size. The possibility that the condensed state needs to be considered is being ignored, precisely because van der Waals’ contributions to physical phenomena have been dismissed. Real gases are not infinitely compressible. Yet, the Sun is being described as an ideal gas in many solar models, despite the fact that the ideal gas law from the onset violates van der Waals’ findings. Furthermore, the gaseous model is counter to many experimental results in the laboratory, relative to the thermal and physical behavior of gases. Unfortunately, no alternative model currently exists as a point of discussion.

In contrast to the gaseous model of the Sun, the hot liquid plasma model is extremely simple; requiring no theoretical arguments beyond those provided by the liquid state itself, even in the area of energy partition. The hot liquid plasma model addresses the problems of solar collapse and seismology with simplicity. It reconciles the violation of the 2nd

law of thermodynamics and the heating of the corona, by invoking the simple release of stored energy from the convection currents of the photosphere. It dismisses extreme densities with hydrogen and helium, by having recourse to the incompressibility of the liquid state. The liquid model eliminates radiative heat transfer as a means of striving for internal thermal equilibrium, as contrary to established thermodynamic principles. Internal thermal equilibrium within the Sun must be achieved using convection and conduction, as is the case for every other object.

The liquid plasma model also provides an alternative explanation for "photon shifting". The visible light of the photosphere is simply produced instantly as a direct manifestation of the vibrational energy contained within the liquid lattice of the solar surface. The problem of calculating internal solar opacities, which must be continually adjusted for frequency and temperature, is removed. Rather, it is argued that not a single photon is being produced within the Sun. Radiative emission remains a surface phenomenon for the Sun, as it is for every other object known to man.

As with any new model, it is clear that a great deal of effort will be required to place each solar finding in the context of a liquid framework. The gaseous equations of state had provided a mathematically elegant approach to stellar structure. In the liquid plasma model, the equations associated with magnetohydrodynamics move to the forefront. This implies that, rather than concentrate on pressure and density, we must turn our attention to thermal conductivity and viscosity. This is far from being a simple problem. Pressure and density changes can be relatively easily addressed, in the liquid plasma model, based on known rigid body solutions [58]. However, the determination of solar conductivities and viscosities poses a daunting task for plasma physics. This is especially true since thermal conductivities and viscosities are often viewed as second and fourth-order tensors, respectively.

Nonetheless, the plasma physicist may eventually gain a better understanding of these quantities as related to stellar interiors, particularly as our efforts are focused on the nature and properties of liquid metallic hydrogen.

It is certainly true that the reevaluation of stellar structure will be difficult. As the same time, the introduction of the liquid plasma model brings new and exciting dimensions in our quest to characterize the physics associated with the Sun. Prudence dictates that we consider every possibility, as we continue to explore this still mystical object in our sky.

Dedication: This work is dedicated to the memory of Jacqueline Alice Roy.

References

1. Chandrashekar S. An introduction to the study of stellar interiors. New York, Dover Publications, 1957.
2. Clayton D. D. Principles of stellar evolution and nucleosynthesis. New York, McGraw-Hill Book Company, 1968.
3. Kippenhahn R. and Weigert A. Stellar structure and evolution. 3rd ed., Berlin, Springer-Verlag, 1994.
4. Stix M. The Sun: an introduction. Berlin, Springer-Verlag, 1989.
5. Zirin H. Astrophysics of the Sun. Cambridge, Cambridge University Press, 1988.
6. Lane L. H. On the theoretical temperature of the Sun, under the hypothesis of a gaseous mass maintaining its volume by its internal heat, and depending on the laws of gases as known to terrestrial experiments. *Am. J. Sci. Arts*, 1870, Ser. 2, v. 50, 57–74.
7. Eddington A. S. The internal constitution of the stars. New York, Dover Publications, 1959.
8. Eddington A. S. Stars and atoms. New Haven, Yale University Press, 1927.
9. Landsberg P. T. Thermodynamics with quantum statistical illustrations. New York, Interscience, 1961, 250–291.
10. Robitaille P. M. L. On the validity of Kirchhoff's law of thermal emission. *IEEE Trans. Plasma Science*, 2003, v. 31(6), 1263–1267.
11. Stefan J. Ueber die Beziehung zwischen der Wärmestrahlung und der Temperature. *Sitzungsberichte der mathematischnaturwissenschaftlichen Classe der kaiserlichen Akademie der Wissenschaften*, Wien 1879, v. 79, 391–428.
12. Wien W. Ueber die Energieverteilung in Emissionspektrum eines schwarzen Körpers. *Ann. Phys.*, 1896, v. 58, 662–669.
13. Planck M. Ueber das Gesetz der energieverteilung in Normalspectrum. *Annalen der Physik*, 1901, v. 4, 553–563.
14. Livingston W. and Koutchmy S. Eclipse science results: past and present. *ASP Conference Series*, 2000, v. 205, 3–10.
15. Gough D. O. Seismology of the Sun and the distant stars. Dordrecht, D. Reidel Publishing Company, 1986.
16. Bahcall J. N., Pinsonneault M. H. and Basu S. Solar models: current epoch and time dependences, neutrinos, and helioseismological properties. *Astrophys. J.*, 2001, v. 555, 990–1012.
17. Knudsen J. G., Hottel H. C., Sarofim A. F., Wankat P. C. and Knaebel K. S. Heat tansmission. In: *Perry's Chemical Engineers' Handbook*, 7th ed., New York, The McGraw-Hill Book Company, 1997, 5:23–42.
18. Touloukian Y. S. and Ho C. Y. Thermophysical properties of matter. New York, Plenum, v. 1–8, 1970.
19. Chapman A. J. Heat transfer. New York, The Macmillan Company, 1967, 413.
20. Siegel R. and Howell J. Thermal radiation heat transfer. 4th ed., New York, Taylor and Francis, 2002.
21. Peraiah A. An introduction to radiative transfer. Cambridge, Cambridge University Press, 2002.
22. Rybicki G. B. and Lightman A. P. Radiative processes in astrophysics. New York, John Wiley and Sons, 1979.
23. Shu F. H. The physics of astrophysics: radiation. Mill Valle (CA), University Science Books, 1991.

24. Rogers F. J., Swenson F. J. and Iglesias C. A. OPAL equation-of-state tables for astrophysical applications. *Astrophys. J.*, 1996, v. 456, 902–908.
25. Saumon D., Chabrier G. and Van Horn H. M. An equation of state for low-mass stars and giant planets. *Astrophys. J. Suppl. Ser.*, 1995, v. 99, 713–741.
26. Gray D. F. The observation and analysis of stellar photospheres. 2nd ed., Cambridge, Cambridge University Press, 1992, 124.
27. Cortes T. R. and Sanchez F. The structure of the Sun. Cambridge, Cambridge University Press, 1996.
28. Atkins P. W. Physical chemistry. New York, W. H. Freeman and Company, 1990, 668–671.
29. Croxton C. A. Progess in liquid physics. Chichester (UK), John Wiley & Sons, 1978, 1–592.
30. March N. H. and Tosi M. P. Introduction to liquid state physics. New Jersey, World Scientific, 2002.
31. Mortimer R. G. Physical chemistry. New York, Harcourt Academic Press, 2000, 25–26.
32. Michelson I. The science of fluids. Van Nostrand Reinhold Company, 1970.
33. Ulaby F. T., Moore R. K. and Fung A. K. Microwave remote sensing active and passive: radar remote sensing and surface scattering and emission theory. Vol. 2, London, Addison-Wesley Publishing Company, 1982, 880–884.
34. Srivastava G. P. The physics of phonons. New York, Adam Hilger, 1990, 360–370.
35. Bruesch P. Phonons: theory and experiments. New York, Springer-Verlag, 1982, 167–199.
36. Kittel C. Introduction to solid state physics. New York, John Willey and Sons, 1986, 83–124.
37. Palmer D. W., Thompson M. W. and Townsend P. D. Atomic collision phenomena in solids. Amsterdam, North-Holland Publishing Company, 1970.
38. Reissland J. A. The physics of phonons. London, John Wiley and Sons, 1973.
39. Planck M. The theory of heat radiation. Philadelphia, P. Blakiston's Sons & Co., 1914.
40. Fleck B., Brekke P., Haugan S, Duarte L. S., Domingo V., Gurman J. B. and Poland A. I. Four years of SOHO discoveries — Some Highlighs. *ESA Bulletin*, 2000, v. 102, 68–86.
41. Langley S. P. Experimental determination of wave-lengths in the invisible spectrum. *Mem. Natl. Acad. Sci.*, 1883, v. 2, 147–162.
42. Langley S. P. On hitherto unrecognized wave-lengths. *Phil. Mag.*, 1886, v. 22, 149–173.
43. Kirchhoff G. Ueber den Zusammenhang von Emission und Absorption von Licht und Warme. *Monatsberichte der Akademie der Wissenschaften zu Berlin*, 1860, Sessions of Dec. 1859, 783–787.
44. Kirchhoff G. Ueber das Verhaltnis zwischen dem Emissionsvermogen und dem absorptionsvermogen der Körper für Waeme und Litcht. *Annalen der Physik*, 1860, v. 109, 275–301.
45. Boulos M. I, Fauchais P. and Pfender E. Thermal plasmas: fundamentals and applications. New York, Plenum Press, 1994, 377.
46. Penner S. S. Quantitative molecular spectroscopy and gas emissivities. Reading (MA), Addison-Wesley Publ. Co., 1959.
47. Fowler J. B. A third generation water bath based blackbody source. *J. Res. Natl. Inst. Stand. Technol.*, 1995, v. 100, 591–599.
48. Fowler J. B. An oil-based 293 K to 473 K blackbody source. *J. Res. Natl. Inst. Stand. Technol.*, 1996, v. 101, 629–637.
49. Murphy A. V., Tsai B. K. and Saunders R. D. Comparative calibration of heat flux sensors in two blackbody facilities. *J. Res. Natl. Inst. Stand. Technol.*, 1999, v. 104, 487–494.
50. Murphy A. V., Tsai B. K. and Saunders R. D. Transfer calibration validation tests on a heat flux sensor in the 51 mm high-temperature blackbody. *J. Res. Natl. Inst. Stand. Technol.*, 2001, v. 106, 823–831.
51. Navarro M., Bruce S. S., Johnson B. C., Murphy A. V. and Sunders R. D. Vacuum processing technique for development of primary standard blackbodies. *J. Res. Natl. Inst. Stand. Technol.*, 1999, v. 104, 253–259.
52. Burchell T. D. Thermal properties and nuclear energy applications. In: *Graphite and Its Precursors*, Sydney, Australia, Gordon and Breach Science Publishers, 2001, 87–110.
53. Roberts A. M. Solar faculae stand exposed. *Sky and Telescope*, 2003, v. 106(4), 26.
54. Scharmer G. B., Gudiksen B. V., Kiselman D., Lfdahl M. G., Rouppe van der Voort L. H. M. Dark cores in sunspot pernumbral filaments. *Nature*, 2002, v. 420, 151–153.
55. Kosovichev A. G. and Zharkova V. V. X-ray flare sparks quake inside the Sun. *Nature*, 1998, v. 393, 28.
56. Dicke R. H. and Goldenberg H. M. Solar oblateness and General Relativity. *Phys. Rev. Lett.*, 1967, v. 18(9), 313–316.
57. Godier S. and Rozelot J. P. The solar oblateness and its relationship with the structure of the tacholine and the Sun's subsurface. *Astron. & Astrophys.*, 2000, v. 355, 365–374.
58. Littleton R. A. The stability of rotating liquid masses. Cambridge, Cambridge University Press, 1953.
59. Domiciana de Souza A., Kervella P., Jankov S., Abe L., Vakili F., diFolco E. and Paresce F. The spinning-top be star achernar from VLTI-VINCI. *Astron. & Astroph.*, 2003, v. 407, L47–L50.
60. Weir S. T., Mitchell A. C and Nellis W. J. Metallization of fluid molecular hydrogen at 140 Gpa (1.4 Mbar). *Phys. Rev. Lett.*, 1996, v. 76, 1860–1863.
61. Collins G. W., DaSilva L. B., Celliers P., Gold D. M., Foord M. E., Wallace R. G., Ng A., Weber S. V., Budil K. S. and Cauble R. Measurements of the equation of state of deuterium at the fluid-insulator-metal transition. *Science*, 1998, v. 281, 1178–1181.
62. Woods L. C. Principles of magnetoplasma dynamics. Oxford, Clarendon Press, 1987.
63. Kowalenko N. P. and Krasny Y. P. Theory of equilibrium and kinetic properties of liquid metal. In: *Transport Properties in Dense Plasmas*, Basel, Birkhauser Verlag, 1984, 127–155.

The Journal on Advanced Studies in Theoretical and Experimental Physics, including Related Themes from Mathematics

PROGRESS IN PHYSICS

A quarterly issue scientific journal, registered with the Library of Congress (DC, USA). This journal is peer reviewed and included in the abstracting and indexing coverage of: Mathematical Reviews and MathSciNet (AMS, USA), DOAJ of Lund University (Sweden), Zentralblatt MATH (Germany), Referativnyi Zhurnal VINITI (Russia), etc.

Electronic version of this journal:
http://www.ptep-online.com
http://www.geocities.com/ptep_online

To order printed issues of this journal, contact the Editor-in-Chief.

ISSN: 1555-5534 (print)
ISSN: 1555-5615 (online)

Standard Address Number: 297-5092
Printed in the United States of America

APRIL 2007 **VOLUME 2**

CONTENTS

Information for Authors and Subscribers

Progress in Physics has been created for publications on advanced studies in theoretical and experimental physics, including related themes from mathematics. All submitted papers should be professional, in good English, containing a brief review of a problem and obtained results.

All submissions should be designed in LaTeX format using *Progress in Physics* template. This template can be downloaded from *Progress in Physics* home page http://www.ptep-online.com. Abstract and the necessary information about author(s) should be included into the papers. To submit a paper, mail the file(s) to Chief Editor.

All submitted papers should be as brief as possible. Commencing 1st January 2006 we accept brief papers, no larger than 8 typeset journal pages. Short articles are preferable. Papers larger than 8 pages can be considered in exceptional cases to the section *Special Reports* intended for such publications in the journal.

All that has been accepted for the online issue of *Progress in Physics* is printed in the paper version of the journal. To order printed issues, contact Chief Editor.

This journal is non-commercial, academic edition. It is printed from private donations.

The Theory of Vortical Gravitational Fields

Dmitri Rabounski
E-mail: rabounski@yahoo.com

This paper treats of vortical gravitational fields, a tensor of which is the rotor of the general covariant gravitational inertial force. The field equations for a vortical gravitational field (the Lorentz condition, the Maxwell-like equations, and the continuity equation) are deduced in an analogous fashion to electrodynamics. From the equations it is concluded that the main kind of vortical gravitational fields is "electric", determined by the non-stationarity of the acting gravitational inertial force. Such a field is a medium for traveling waves of the force (they are different to the weak deformation waves of the space metric considered in the theory of gravitational waves). Standing waves of the gravitational inertial force and their medium, a vortical gravitational field of the "magnetic" kind, are exotic, since a non-stationary rotation of a space body (the source of such a field) is a very rare phenomenon in the Universe.

1 The mathematical method

There are currently two methods for deducing a formula for the Newtonian gravitational force in General Relativity. The first method, introduced by Albert Einstein himself, has its basis in an arbitrary interpretation of Christoffel's symbols in the general covariant geodesic equations (the equation of motion of a free particle) in order to obtain a formula like that by Newton (see [1], for instance). The second method is due to Abraham Zelmanov, who developed it in the 1940's [2, 3]. This method determines the gravitational force in an exact mathematical way, without any suppositions, as a part of the gravitational inertial force derived from the non-commutativity of the differential operators invariant in an observer's spatial section. This formula results from Zelmanov's mathematical apparatus of chronometric invariants (physical observable quantities in General Relativity).

The essence of Zelmanov's mathematical apparatus [4] is that if an observer accompanies his reference body, his observable quantities are the projections of four-dimensional quantities upon his time line and the spatial section — *chronometrically invariant quantities*, via the projecting operators $b^\alpha = \frac{dx^\alpha}{ds}$ and $h_{\alpha\beta} = -g_{\alpha\beta} + b_\alpha b_\beta$, which fully define his real reference space (here b^α is his velocity relative to his real references). So the chr.inv.-projections of a world-vector Q^α are $b_\alpha Q^\alpha = \frac{Q_0}{\sqrt{g_{00}}}$ and $h^i_\alpha Q^\alpha = Q^i$, while the chr.inv.-projections of a 2nd rank world-tensor $Q^{\alpha\beta}$ are $b^\alpha b^\beta Q_{\alpha\beta} = \frac{Q_{00}}{g_{00}}$, $h^{i\alpha} b^\beta Q_{\alpha\beta} = \frac{Q^i_0}{\sqrt{g_{00}}}$, $h^i_\alpha h^k_\beta Q^{\alpha\beta} = Q^{ik}$. The principal physical observable properties of a space are derived from the fact that the chr.inv.-differential operators $\frac{{}^*\partial}{\partial t} = \frac{1}{\sqrt{g_{00}}} \frac{\partial}{\partial t}$ and $\frac{{}^*\partial}{\partial x^i} = \frac{\partial}{\partial x^i} + \frac{1}{c^2} v_i \frac{{}^*\partial}{\partial t}$ are non-commutative as $\frac{{}^*\partial^2}{\partial x^i \partial t} - \frac{{}^*\partial^2}{\partial t \partial x^i} = \frac{1}{c^2} F_i \frac{{}^*\partial}{\partial t}$ and $\frac{{}^*\partial^2}{\partial x^i \partial x^k} - \frac{{}^*\partial^2}{\partial x^k \partial x^i} = \frac{2}{c^2} A_{ik} \frac{{}^*\partial}{\partial t}$, and also that the chr.inv.-metric tensor $h_{ik} = -g_{ik} + b_i b_k$ may not be stationary. The principal physical observable characteristics are the chr.inv.-vector of the gravitational inertial force F_i, the chr.inv.-tensor of the angular velocities of the space rotation A_{ik}, and the chr.inv.-tensor of the rates of the space deformations D_{ik}:

$$F_i = \frac{1}{\sqrt{g_{00}}} \left(\frac{\partial \mathrm{w}}{\partial x^i} - \frac{\partial v_i}{\partial t} \right), \quad \mathrm{w} = c^2 \left(1 - \sqrt{g_{00}}\right), \tag{1}$$

$$A_{ik} = \frac{1}{2} \left(\frac{\partial v_k}{\partial x^i} - \frac{\partial v_i}{\partial x^k} \right) + \frac{1}{2c^2} \left(F_i v_k - F_k v_i \right), \tag{2}$$

$$D_{ik} = \frac{1}{2} \frac{{}^*\partial h_{ik}}{\partial t}, \; D^{ik} = -\frac{1}{2} \frac{{}^*\partial h^{ik}}{\partial t}, \; D = D^k_k = \frac{{}^*\partial \ln\sqrt{h}}{\partial t}, \tag{3}$$

where w is the gravitational potential, $v_i = -\frac{c\, g_{0i}}{\sqrt{g_{00}}}$ is the linear velocity of the space rotation, $h_{ik} = -g_{ik} + \frac{1}{c^2} v_i v_k$ is the chr.inv.-metric tensor, $h = \det \|h_{ik}\|$, $h\, g_{00} = -g$, and $g = \det \|g_{\alpha\beta}\|$. The observable non-uniformity of the space is set up by the chr.inv.-Christoffel symbols

$$\Delta^i_{jk} = h^{im} \Delta_{jk,m} = \frac{1}{2} h^{im} \left(\frac{{}^*\partial h_{jm}}{\partial x^k} + \frac{{}^*\partial h_{km}}{\partial x^j} - \frac{{}^*\partial h_{jk}}{\partial x^m} \right), \tag{4}$$

which are constructed just like Christoffel's usual symbols $\Gamma^\alpha_{\mu\nu} = g^{\alpha\sigma} \Gamma_{\mu\nu,\sigma}$ using h_{ik} instead of $g_{\alpha\beta}$.

A four-dimensional generalization of the chr.inv.-quantities F_i, A_{ik}, and D_{ik} is [5]

$$F_\alpha = -2c^2 b^\beta a_{\beta\alpha}\,, \tag{5}$$

$$A_{\alpha\beta} = c h^\mu_\alpha h^\nu_\beta a_{\mu\nu}\,, \tag{6}$$

$$D_{\alpha\beta} = c h^\mu_\alpha h^\nu_\beta d_{\mu\nu}\,, \tag{7}$$

where

$$a_{\alpha\beta} = \frac{1}{2} \left(\nabla_\alpha b_\beta - \nabla_\beta b_\alpha \right), \; d_{\alpha\beta} = \frac{1}{2} \left(\nabla_\alpha b_\beta + \nabla_\beta b_\alpha \right). \tag{8}$$

For instance, the chr.inv.-projections of F^α are

$$\varphi = b_\alpha F^\alpha = \frac{F_0}{\sqrt{g_{00}}} = 0\,, \qquad q^i = h^i_\alpha F^\alpha = F^i. \tag{9}$$

Proceeding from the exact formula for the gravitational inertial force above, we can, for the first time, determine vortical gravitational fields.

2 D'Alembert's equations of the force

It is a matter of fact that two bodies attract each other due to the transfer of the force of gravity. The force of gravity is absent in a homogeneous gravitational field, because the gradient of the gravitational potential $\mathfrak{w}$ is zero everywhere therein. Therefore it is reasonable to consider the field of the vector potential F^α as a medium transferring gravitational attraction via waves of the force.

D'Alembert's equations of the vector field F^α without its inducing sources

$$\Box F^\alpha = 0 \tag{10}$$

are the equations of propagation of waves traveling in the field*. The equations have two chr.inv.-projections

$$b_\sigma \Box F^\sigma = 0\,, \qquad h^i_\sigma \Box F^\sigma = 0\,, \tag{11}$$

which are the same as

$$b_\sigma\, g^{\alpha\beta}\nabla_\alpha\nabla_\beta F^\sigma = 0\,, \qquad h^i_\sigma\, g^{\alpha\beta}\nabla_\alpha\nabla_\beta F^\sigma = 0\,. \tag{12}$$

These are the chr.inv.-d'Alembert equations for the field $F^\alpha = -2c^2 a^{\cdot\alpha}_{\sigma\cdot} b^\sigma$ without its-inducing sources. To obtain the equations in detailed form isn't an easy process. Helpful here is the fact that the chr.inv.-projection of F^α upon a time line is zero. Following this path, after some algebra, we obtain the chr.inv.-d'Alembert equations (11) in the final form

$$\left.\begin{aligned}
&\frac{1}{c^2}\frac{{}^*\partial}{\partial t}\left(F_k F^k\right) + \frac{1}{c^2}F_i\frac{{}^*\partial F^i}{\partial t} + D^k_m\frac{{}^*\partial F^m}{\partial x^k} + \\
&+ h^{ik}\frac{{}^*\partial}{\partial x^i}\left[(D_{kn}+A_{kn})F^n\right] - \frac{2}{c^2}A_{ik}F^iF^k + \\
&+ \frac{1}{c^2}F_mF^mD + \Delta^m_{kn}D^k_mF^n - \\
&- h^{ik}\Delta^m_{ik}\left(D_{mn}+A_{mn}\right)F^n = 0\,, \\
&\frac{1}{c^2}\frac{{}^*\partial^2F^i}{\partial t^2} - h^{km}\frac{{}^*\partial^2F^i}{\partial x^k\partial x^m} + \frac{1}{c^2}\left(D^i_k + A^{\cdot i}_{k\cdot}\right)\frac{{}^*\partial F^k}{\partial t} + \\
&+ \frac{1}{c^2}\frac{{}^*\partial}{\partial t}\left[\left(D^i_k + A^{\cdot i}_{k\cdot}\right)F^k\right] + \frac{1}{c^2}D\frac{{}^*\partial F^i}{\partial t} + \frac{1}{c^2}F^k\frac{{}^*\partial F^i}{\partial x^k} + \\
&+ \frac{1}{c^2}\left(D^i_n + A^{\cdot i}_{n\cdot}\right)F^nD - \frac{1}{c^2}\Delta^i_{km}F^kF^m + \frac{1}{c^4}F_kF^kF^i - \\
&- h^{km}\left\{\frac{{}^*\partial}{\partial x^k}\left(\Delta^i_{mn}F^n\right) + \left(\Delta^i_{kn}\Delta^n_{mp} - \Delta^n_{km}\Delta^i_{np}\right)F^p + \right. \\
&\left. + \Delta^i_{kn}\frac{{}^*\partial F^n}{\partial x^m} - \Delta^n_{km}\frac{{}^*\partial F^i}{\partial x^n}\right\} = 0\,.
\end{aligned}\right\} \tag{13}$$

*The waves travelling in the field of the gravitational inertial force aren't the same as the waves of the weak perturbations of the space metric, routinely considered in the theory of gravitational waves.

3 A vortical gravitational field. The field tensor and pseudo-tensor. The field invariants

We introduce the tensor of the field as a rotor of its four-dimensional vector potential F^α as well as Maxwell's tensor of electromagnetic fields, namely

$$F_{\alpha\beta} = \nabla_\alpha F_\beta - \nabla_\beta F_\alpha = \frac{\partial F_\beta}{\partial x^\alpha} - \frac{\partial F_\alpha}{\partial x^\beta}\,. \tag{14}$$

We will refer to $F_{\alpha\beta}$ (14) as the *tensor of a vortical gravitational field*, because this is actual a four-dimensional vortex of an acting gravitational inertial force F^α.

Taking into account that the chr.inv.-projections of the field potential $F^\alpha = -2c^2 a^{\cdot\alpha}_{\sigma\cdot} b^\sigma$ are $\frac{F_0}{\sqrt{g_{00}}} = 0$, $F^i = h^{ik}F_k$, we obtain the components of the field tensor $F_{\alpha\beta}$:

$$F_{00} = F^{00} = 0\,, \qquad F_{0i} = -\frac{1}{c}\sqrt{g_{00}}\,\frac{{}^*\partial F_i}{\partial t}\,, \tag{15}$$

$$F_{ik} = \frac{{}^*\partial F_i}{\partial x^k} - \frac{{}^*\partial F_k}{\partial x^i} + \frac{1}{c^2}\left(v_i\frac{{}^*\partial F_k}{\partial t} - v_k\frac{{}^*\partial F_i}{\partial t}\right), \tag{16}$$

$$F^{\cdot 0}_{0\cdot} = \frac{1}{c^2}\,v^k\frac{{}^*\partial F_k}{\partial t}, \qquad F^{\cdot i}_{0\cdot} = \frac{1}{c}\sqrt{g_{00}}\,h^{ik}\frac{{}^*\partial F_k}{\partial t}, \tag{17}$$

$$\begin{aligned}
F^{\cdot 0}_{k\cdot} = \frac{1}{\sqrt{g_{00}}}\left[\frac{1}{c}\frac{{}^*\partial F_k}{\partial t} - \frac{1}{c^3}\,v_kv^m\frac{{}^*\partial F_m}{\partial t} + \right. \\
\left. + \frac{1}{c}\,v^m\left(\frac{{}^*\partial F_m}{\partial x^k} - \frac{{}^*\partial F_k}{\partial x^m}\right)\right],
\end{aligned} \tag{18}$$

$$F^{\cdot i}_{k\cdot} = h^{im}\left(\frac{{}^*\partial F_m}{\partial x^k} - \frac{{}^*\partial F_k}{\partial x^m}\right) - \frac{1}{c^2}\,h^{im}v_k\frac{{}^*\partial F_m}{\partial t}\,, \tag{19}$$

$$\begin{aligned}
F^{0k} = \frac{1}{\sqrt{g_{00}}}\left[\frac{1}{c}\,h^{km}\frac{{}^*\partial F_m}{\partial t} + \right. \\
\left. + \frac{1}{c}\,v^nh^{mk}\left(\frac{{}^*\partial F_n}{\partial x^m} - \frac{{}^*\partial F_m}{\partial x^n}\right)\right],
\end{aligned} \tag{20}$$

$$F^{ik} = h^{im}h^{kn}\left(\frac{{}^*\partial F_m}{\partial x^n} - \frac{{}^*\partial F_n}{\partial x^m}\right). \tag{21}$$

We see here two chr.inv.-projections of the field tensor $F_{\alpha\beta}$. We will refer to the time projection

$$E^i = \frac{F^{\cdot i}_{0\cdot}}{\sqrt{g_{00}}} = \frac{1}{c}\,h^{ik}\frac{{}^*\partial F_k}{\partial t}\,, \quad E_i = h_{ik}E^k = \frac{1}{c}\frac{{}^*\partial F_i}{\partial t} \tag{22}$$

as the "electric" observable component of the vortical gravitational field, while the spatial projection will be referred to as the "magnetic" observable component of the field

$$H^{ik} = F^{ik} = h^{im}h^{kn}\left(\frac{{}^*\partial F_m}{\partial x^n} - \frac{{}^*\partial F_n}{\partial x^m}\right), \tag{23}$$

$$H_{ik} = h_{im}h_{kn}H^{mn} = \frac{{}^*\partial F_i}{\partial x^k} - \frac{{}^*\partial F_k}{\partial x^i}\,, \tag{24}$$

which, after use of the 1st Zelmanov identity [2, 3] that links the spatial vortex of the gravitational inertial force to the non-stationary rotation of the observer's space

$$\frac{{}^*\partial A_{ik}}{\partial t}+\frac{1}{2}\left(\frac{{}^*\partial F_k}{\partial x^i}-\frac{{}^*\partial F_i}{\partial x^k}\right)=0\,, \qquad (25)$$

takes the form

$$H^{ik}=2h^{im}h^{kn}\frac{{}^*\partial A_{mn}}{\partial t}\,, \qquad H_{ik}=2\frac{{}^*\partial A_{ik}}{\partial t}\,. \qquad (26)$$

The "electric" observable component E^i of a vortical gravitational field manifests as the non-stationarity of the acting gravitational inertial force F^i. The "magnetic" observable component H_{ik} manifests as the presence of the spatial vortices of the force F^i or equivalently, as the non-stationarity of the space rotation A_{ik} (see formula 26). Thus, two kinds of vortical gravitational fields are possible:

1. Vortical gravitational fields of the "electric" kind ($H_{ik}=0$, $E^i\neq 0$). In this field we have no spatial vortices of the acting gravitational inertial force F^i, which is the same as a stationary space rotation. So a vortical field of this kind consists of only the "electric" component E^i (22) that is the non-stationarity of the force F^i. Note that a vortical gravitational field of the "electric" kind is permitted in both a non-holonomic (rotating) space, if its rotation is stationary, and also in a holonomic space since the zero rotation is the ultimate case of stationary rotations;
2. The "magnetic" kind of vortical gravitational fields is characterized by $E^i=0$ and $H_{ik}\neq 0$. Such a vortical field consists of only the "magnetic" components H_{ik}, which are the spatial vortices of the acting force F^i and the non-stationary rotation of the space. Therefore a vortical gravitational field of the "magnetic" kind is permitted only in a non-holonomic space. Because the d'Alembert equations (13), with the condition $E^i=0$, don't depend on time, a "magnetic" vortical gravitational field is a medium for *standing waves* of the gravitational inertial force.

In addition, we introduce the pseudotensor $F^{*\alpha\beta}$ of the field dual to the field tensor

$$F^{*\alpha\beta}=\frac{1}{2}\,E^{\alpha\beta\mu\nu}F_{\mu\nu}\,, \qquad F_{*\alpha\beta}=\frac{1}{2}\,E_{\alpha\beta\mu\nu}F^{\mu\nu}, \quad (27)$$

where the four-dimensional completely antisymmetric discriminant tensors $E^{\alpha\beta\mu\nu}=\frac{e^{\alpha\beta\mu\nu}}{\sqrt{-g}}$ and $E_{\alpha\beta\mu\nu}=e_{\alpha\beta\mu\nu}\sqrt{-g}$ transform tensors into pseudotensors in the inhomogeneous anisotropic four-dimensional pseudo-Riemannian space*.

Using the components of the field tensor $F_{\alpha\beta}$, we obtain the chr.inv.-projections of the field pseudotensor $F^{*\alpha\beta}$:

$$H^{*i}=\frac{F^{*\cdot i}_{0\cdot}}{\sqrt{g_{00}}}=\frac{1}{2}\,\varepsilon^{ikm}\left(\frac{{}^*\partial F_k}{\partial x^m}-\frac{{}^*\partial F_m}{\partial x^k}\right), \qquad (28)$$

$$E^{*ik}=F^{*ik}=-\frac{1}{c}\,\varepsilon^{ikm}\frac{{}^*\partial F_m}{\partial t}\,, \qquad (29)$$

where $\varepsilon^{ikm}=b_0\,E^{0ikm}=\sqrt{g_{00}}\,E^{0ikm}=\frac{e^{ikm}}{\sqrt{h}}$ and $\varepsilon_{ikm}=b^0E_{0ikm}=\frac{E_{0ikm}}{\sqrt{g_{00}}}=e_{ikm}\sqrt{h}$ are the chr.inv.-discriminant tensors [2]. Taking into account the 1st Zelmanov identity (25) and the formulae for differentiating ε^{ikm} and ε_{ikm} [2]

$$\frac{{}^*\partial\varepsilon_{imn}}{\partial t}=\varepsilon_{imn}\,D\,, \qquad \frac{{}^*\partial\varepsilon^{imn}}{\partial t}=-\varepsilon^{imn}D\,, \qquad (30)$$

we write the "magnetic" component H^{*i} as follows

$$H^{*i}=\varepsilon^{ikm}\frac{{}^*\partial A_{km}}{\partial t}=2\left(\frac{{}^*\partial\Omega^{*i}}{\partial t}+\Omega^{*i}D\right), \qquad (31)$$

where $\Omega^{*i}=\frac{1}{2}\,\varepsilon^{ikm}A_{km}$ is the chr.inv.-pseudovector of the angular velocity of the space rotation, while the trace $D=h^{ik}D_{ik}=D^n_n$ of the tensor D_{ik} is the rate of the relative expansion of an elementary volume permeated by the field.

Calculating the invariants of a vortical gravitational field ($J_1=F_{\alpha\beta}F^{\alpha\beta}$ and $J_2=F_{\alpha\beta}F^{*\alpha\beta}$), we obtain

$$J_1=h^{im}h^{kn}\left(\frac{{}^*\partial F_i}{\partial x^k}-\frac{{}^*\partial F_k}{\partial x^i}\right)\left(\frac{{}^*\partial F_m}{\partial x^n}-\frac{{}^*\partial F_n}{\partial x^m}\right)-\\ -\frac{2}{c^2}\,h^{ik}\frac{{}^*\partial F_i}{\partial t}\frac{{}^*\partial F_k}{\partial t}, \qquad (32)$$

$$J_2=-\frac{2}{c}\,\varepsilon^{imn}\left(\frac{{}^*\partial F_m}{\partial x^n}-\frac{{}^*\partial F_n}{\partial x^m}\right)\frac{{}^*\partial F_i}{\partial t}\,, \qquad (33)$$

which, with the 1st Zelmanov identity (25), are

$$J_1=4h^{im}h^{kn}\frac{{}^*\partial A_{ik}}{\partial t}\frac{{}^*\partial A_{mn}}{\partial t}-\frac{2}{c^2}\,h^{ik}\frac{{}^*\partial F_i}{\partial t}\frac{{}^*\partial F_k}{\partial t}\,, \qquad (34)$$

$$J_2=-\frac{4}{c}\,\varepsilon^{imn}\frac{{}^*\partial A_{mn}}{\partial t}\frac{{}^*\partial F_i}{\partial t}=\\ =-\frac{8}{c}\left(\frac{{}^*\partial\Omega^{*i}}{\partial t}+\Omega^{*i}D\right)\frac{{}^*\partial F_i}{\partial t}\,. \qquad (35)$$

By the strong physical condition of isotropy, a field is isotropic if both invariants of the field are zeroes: $J_1=0$ means that the lengths of the "electric" and the "magnetic" components of the field are the same, while $J_2=0$ means that the components are orthogonal to each other. Owning the case of a vortical gravitational field, we see that such a field is isotropic if the common conditions are true

$$\left.\begin{aligned} &h^{im}h^{kn}\frac{{}^*\partial A_{ik}}{\partial t}\frac{{}^*\partial A_{mn}}{\partial t}=\frac{1}{2c^2}\,h^{ik}\frac{{}^*\partial F_i}{\partial t}\frac{{}^*\partial F_k}{\partial t}\\ &\frac{{}^*\partial A_{mn}}{\partial t}\frac{{}^*\partial F_i}{\partial t}=0 \end{aligned}\right\} \qquad (36)$$

*Here $e^{\alpha\beta\mu\nu}$ and $e_{\alpha\beta\mu\nu}$ are Levi-Civita's unit tensors: the four-dimensional completely antisymmetric unit tensors which transform tensors into pseudotensors in a Galilean reference frame in the four-dimensional pseudo-Euclidean space [1].

however their geometrical sense is not clear.

Thus the anisotropic field can only be a mixed vortical gravitational field bearing both the "electric" and the "magnetic" components. A strictly "electric" or "magnetic" vortical gravitational field is always spatially isotropic.

Taking the above into account, we arrive at the necessary and sufficient conditions for the existence of *standing waves of the gravitational inertial force*:

1. A vortical gravitational field of the strictly "magnetic" kind is the medium for standing waves of the gravitational inertial force;
2. Standing waves of the gravitational inertial force are permitted only in a non-stationary rotating space.

As soon as one of the conditions ceases, the acting gravitational inertial force changes: the standing waves of the force transform into traveling waves.

4 The field equations of a vortical gravitational field

It is known from the theory of fields that the field equations of a field of a four-dimensional vector-potential A^α is a system consisting of 10 equations in 10 unknowns:

- Lorentz's condition $\nabla_\sigma A^\sigma = 0$ states that the four-dimensional potential A^α remains unchanged;
- the continuity equation $\nabla_\sigma j^\sigma = 0$ states that the field-inducing sources ("charges" and "currents") can not be destroyed but merely re-distributed in the space;
- two groups ($\nabla_\sigma F^{\alpha\sigma} = \frac{4\pi}{c} j^\alpha$ and $\nabla_\sigma F^{*\alpha\sigma} = 0$) of the Maxwell-like equations, where the 1st group determines the "charge" and the "current" as the components of the four-dimensional current vector j^α of the field.

This system completely determines a vector field A^α and its sources in a pseudo-Riemannian space. We shall deduce the field equations for a vortical gravitational field as a field of the four-dimensional potential $F^\alpha = -2c^2 a^{\cdot\alpha}_{\sigma\cdot} b^\sigma$.

Writing the divergence $\nabla_\sigma F^\sigma = \frac{\partial F^\sigma}{\partial x^\sigma} + \Gamma^\sigma_{\sigma\mu} F^\mu$ in the chr.inv.-form [2, 3]

$$\nabla_\sigma F^\sigma = \frac{1}{c}\left(\frac{{}^*\partial\varphi}{\partial t} + \varphi D\right) + \frac{{}^*\partial q^i}{\partial x^i} + q^i \frac{{}^*\partial \ln\sqrt{h}}{\partial x^i} - \frac{1}{c^2} F_i q^i \quad (37)$$

where $\frac{{}^*\partial \ln\sqrt{h}}{\partial x^i} = \Delta^j_{ji}$ and $\frac{{}^*\partial q^i}{\partial x^i} + q^i \Delta^j_{ji} = {}^*\nabla_i q^i$, we obtain the *chr.inv.-Lorentz condition* in a vortical gravitational field

$$\frac{{}^*\partial F^i}{\partial x^i} + F^i \Delta^j_{ji} - \frac{1}{c^2} F_i F^i = 0\,. \quad (38)$$

To deduce the Maxwell-like equations for a vortical gravitational field, we collect together the chr.inv.-projections of the field tensor $F_{\alpha\beta}$ and the field pseudotensor $F^{*\alpha\beta}$. Expressing the necessary projections with the tensor of the rate of the space deformation D^{ik} to eliminate the free h^{ik} terms, we obtain

$$E^i = \frac{1}{c} h^{ik} \frac{{}^*\partial F_k}{\partial t} = \frac{1}{c}\frac{{}^*\partial F^i}{\partial t} + \frac{2}{c} F_k D^{ik}, \quad (39)$$

$$H^{ik} = 2h^{im}h^{kn}\frac{{}^*\partial A_{mn}}{\partial t} = \\ = 2\frac{{}^*\partial A^{ik}}{\partial t} + 4\left(A^{i\cdot}_{\cdot n} D^{kn} - A^{k\cdot}_{\cdot m} D^{im}\right), \quad (40)$$

$$H^{*i} = \varepsilon^{imn}\frac{{}^*\partial A_{mn}}{\partial t} = 2\frac{{}^*\partial \Omega^{*i}}{\partial t} + 2\Omega^{*i} D\,, \quad (41)$$

$$E^{*ik} = -\frac{1}{c}\varepsilon^{ikm}\frac{{}^*\partial F_m}{\partial t}\,. \quad (42)$$

After some algebra, we obtain the *chr.inv.-Maxwell-like equations* for a vortical gravitational field

$$\left.\begin{aligned} &\frac{1}{c}\frac{{}^*\partial^2 F^i}{\partial x^i \partial t} + \frac{2}{c}\frac{{}^*\partial}{\partial x^i}\left(F_k D^{ik}\right) + \frac{1}{c}\left(\frac{{}^*\partial F^i}{\partial t} + 2F_k D^{ik}\right)\Delta^j_{ji} - \\ &\qquad - \frac{2}{c} A_{ik}\left(\frac{{}^*\partial A^{ik}}{\partial t} + A^{i\cdot}_{\cdot n} D^{kn}\right) = 4\pi\rho \\ &2\frac{{}^*\partial^2 A^{ik}}{\partial x^k \partial t} - \frac{1}{c^2}\frac{{}^*\partial^2 F^i}{\partial t^2} + 4\frac{{}^*\partial}{\partial x^k}\left(A^{i\cdot}_{\cdot n} D^{kn} - A^{k\cdot}_{\cdot m} D^{im}\right) + \\ &+ 2\left(\Delta^j_{jk} - \frac{1}{c^2} F_k\right)\left\{\frac{{}^*\partial A^{ik}}{\partial t} + 2\left(A^{i\cdot}_{\cdot n} D^{kn} - A^{k\cdot}_{\cdot m} D^{im}\right)\right\} - \\ &- \frac{2}{c^2}\frac{{}^*\partial}{\partial t}\left(F_k D^{ik}\right) - \frac{1}{c^2}\left(\frac{{}^*\partial F^i}{\partial t} + 2F_k D^{ik}\right) D = \frac{4\pi}{c} j^i \end{aligned}\right\} \text{Group I,} \quad (43)$$

$$\left.\begin{aligned} &\frac{{}^*\partial^2 \Omega^{*i}}{\partial x^i \partial t} + \frac{{}^*\partial}{\partial x^i}\left(\Omega^{*i} D\right) + \frac{1}{c^2}\Omega^{*m}\frac{{}^*\partial F_m}{\partial t} + \\ &\qquad + \left(\frac{{}^*\partial \Omega^{*i}}{\partial t} + \Omega^{*i} D\right)\Delta^j_{ji} = 0 \\ &\varepsilon^{ikm}\frac{{}^*\partial^2 F_m}{\partial x^k \partial t} + \varepsilon^{ikm}\left(\Delta^j_{jk} - \frac{1}{c^2} F_k\right)\frac{{}^*\partial F_m}{\partial t} + 2\frac{{}^*\partial^2 \Omega^{*i}}{\partial t^2} + \\ &\qquad + 4D\frac{{}^*\partial \Omega^{*i}}{\partial t} + 2\left(\frac{{}^*\partial D}{\partial t} + D^2\right)\Omega^{*i} = 0 \end{aligned}\right\} \text{Group II.} \quad (44)$$

The *chr.inv.-continuity equation* $\nabla_\sigma j^\sigma = 0$ for a vortical gravitational field follows from the 1st group of the Maxwell-like equations, and is

$$\begin{aligned} &\frac{{}^*\partial^2}{\partial x^i \partial x^k}\left(\frac{{}^*\partial A^{ik}}{\partial t}\right) - \frac{1}{c^2}\left(\frac{{}^*\partial A^{ik}}{\partial t} + A^{i\cdot}_{\cdot n} D^{kn}\right)\left(A_{ik} D + \frac{{}^*\partial A_{ik}}{\partial t}\right) - \\ &- \frac{1}{c^2}\left[\frac{{}^*\partial^2 A^{ik}}{\partial t^2} + \frac{{}^*\partial}{\partial t}\left(A^{i\cdot}_{\cdot n} D^{nk}\right)\right] A_{ik} + \frac{1}{2c^2}\left(\frac{{}^*\partial F^i}{\partial t} + 2F_k D^{ik}\right)\times \\ &\times\left(\frac{{}^*\partial \Delta^j_{ji}}{\partial t} + \frac{D}{c^2} F_i - \frac{{}^*\partial D}{\partial x^i}\right) + 2\frac{{}^*\partial^2}{\partial x^i \partial x^k}\left(A^{i\cdot}_{\cdot n} D^{kn} - A^{k\cdot}_{\cdot m} D^{im}\right) + \\ &+ \left[\frac{{}^*\partial A^{ik}}{\partial t} + 2\left(A^{i\cdot}_{\cdot n} D^{kn} - A^{k\cdot}_{\cdot m} D^{im}\right)\right]\left[\frac{{}^*\partial}{\partial x^i}\left(\Delta^j_{jk} - \frac{1}{c^2} F_k\right) + \right. \\ &\left. + \left(\Delta^j_{ji} - \frac{1}{c^2} F_i\right)\left(\Delta^l_{lk} - \frac{1}{c^2} F_k\right)\right] = 0\,. \end{aligned} \quad (45)$$

To see a simpler sense of the obtained field equations, we take the field equations in a homogeneous space ($\Delta^i_{km} = 0$)

free of deformation ($D_{ik}=0$)*. In such a space the chr.inv.-Maxwell-like equations obtained take the simplified form

$$\left.\begin{aligned} &\frac{1}{c}\frac{{}^*\partial^2 F^i}{\partial x^i \partial t}-\frac{2}{c}A_{ik}\frac{{}^*\partial A^{ik}}{\partial t}=4\pi\rho \\ &2\frac{{}^*\partial^2 A^{ik}}{\partial x^k\partial t}-\frac{2}{c^2}F_k\frac{{}^*\partial A^{ik}}{\partial t}-\frac{1}{c^2}\frac{{}^*\partial^2 F^i}{\partial t^2}=\frac{4\pi}{c}\,j^i \end{aligned}\right\}\ \text{Group I,} \tag{46}$$

$$\left.\begin{aligned} &\frac{{}^*\partial^2\Omega^{*i}}{\partial x^i\partial t}+\frac{1}{c^2}\,\Omega^{*m}\frac{{}^*\partial F_m}{\partial t}=0 \\ &\varepsilon^{ikm}\frac{{}^*\partial^2 F_m}{\partial x^k\partial t}-\frac{1}{c^2}\,\varepsilon^{ikm}F_k\frac{{}^*\partial F_m}{\partial t}+2\frac{{}^*\partial^2\Omega^{*i}}{\partial t^2}=0 \end{aligned}\right\}\ \text{Group II,} \tag{47}$$

where the field-inducing sources are

$$\rho=\frac{1}{4\pi c}\left(\frac{{}^*\partial^2 F^i}{\partial x^i\partial t}-2A_{ik}\frac{{}^*\partial A^{ik}}{\partial t}\right), \tag{48}$$

$$j^i=\frac{c}{2\pi}\left(\frac{{}^*\partial^2 A^{ik}}{\partial x^k\partial t}-\frac{1}{c^2}F_k\frac{{}^*\partial A^{ik}}{\partial t}-\frac{1}{2c^2}\frac{{}^*\partial^2 F^i}{\partial t^2}\right), \tag{49}$$

and the chr.inv.-continuity equation (45) takes the form

$$\begin{aligned}\frac{{}^*\partial^2}{\partial x^i\partial x^k}\left(\frac{{}^*\partial A^{ik}}{\partial t}\right)-\frac{1}{c^2}A_{ik}\frac{{}^*\partial^2 A^{ik}}{\partial t^2}-\frac{1}{c^2}\frac{{}^*\partial A_{ik}}{\partial t}\frac{{}^*\partial A^{ik}}{\partial t}-\\ -\frac{1}{c^2}\left(\frac{{}^*\partial F_k}{\partial x^i}-\frac{1}{c^2}F_iF_k\right)\frac{{}^*\partial A^{ik}}{\partial t}=0\,.\end{aligned} \tag{50}$$

The obtained field equations describe the main properties of vortical gravitational fields:

1. The chr.inv.-Lorentz condition (38) shows the inhomogeneity of a vortical gravitational field depends on the value of the acting gravitational inertial force F^i and also the space inhomogeneity Δ^j_{ji} in the direction the force acts;
2. The 1st group of the chr.inv.-Maxwell-like equations (43) manifests the origin of the field-inducing sources called "charges" ρ and "currents" j^i. The "charge" ρ is derived from the inhomogeneous oscillations of the acting force F^i and also the non-stationary rotation of the space (to within the space inhomogeneity and deformation withheld). The "currents" j^i are derived from the non-stationary rotation of the space, the spatial inhomogeneity of the non-stationarity, and the non-stationary oscillations of the force F^i (to within the same approximation);
3. The 2nd group of the chr.inv.-Maxwell-like equations (44) manifests the properties of the "magnetic" component H^{*i} of the field. The oscillations of the acting force F^i is the main factor making the "magnetic" component distributed inhomogeneously in the space. If there is no acting force ($F^i=0$) and the space is free of deformation ($D_{ik}=0$), the "magnetic" component is stationary.
4. The chr.inv.-continuity equation (50) manifests in the fact that the "charges" and the "currents" inducing a vortical gravitational field, being located in a non-deforming homogeneous space, remain unchanged while the space rotation remains stationary.

Properties of waves travelling in a field of a gravitational inertial force reveal themselves when we equate the field sources ρ and j^i to zero in the field equations (because a free field is a wave):

$$\frac{{}^*\partial^2 F^i}{\partial x^i\partial t}=2A_{ik}\frac{{}^*\partial A^{ik}}{\partial t}\,, \tag{51}$$

$$\frac{{}^*\partial^2 A^{ik}}{\partial x^k\partial t}=\frac{1}{c^2}F_k\frac{{}^*\partial A^{ik}}{\partial t}+\frac{1}{2c^2}\frac{{}^*\partial^2 F^i}{\partial t^2}\,, \tag{52}$$

which lead us to the following conclusions:

1. The inhomogeneous oscillations of the gravitational inertial force F^i, acting in a free vortical gravitational field, is derived mainly from the non-stationary rotation of the space;
2. The inhomogeneity of the non-stationary rotations of a space, filled with a free vortical gravitational field, is derived mainly from the non-stationarity of the oscillations of the force and also the absolute values of the force and the angular acceleration of the space.

The foregoing results show that numerous properties of vortical gravitational fields manifest only if such a field is due strictly to the "electric" or the "magnetic" kind. This fact forces us to study these two kinds of vortical gravitational fields separately.

5 A vortical gravitational field of the "electric" kind

We shall consider a vortical gravitational field strictly of the "electric" kind, which is characterized as follows

$$H_{ik}=\frac{{}^*\partial F_i}{\partial x^k}-\frac{{}^*\partial F_k}{\partial x^i}=2\frac{{}^*\partial A_{ik}}{\partial t}=0\,, \tag{53}$$

$$H^{ik}=2h^{im}h^{kn}\frac{{}^*\partial A_{mn}}{\partial t}=0\,, \tag{54}$$

$$E_i=\frac{1}{c}\frac{{}^*\partial F_i}{\partial t}\neq 0\,, \tag{55}$$

$$E^i=\frac{1}{c}\,h^{ik}\frac{{}^*\partial F_k}{\partial t}=\frac{1}{c}\frac{{}^*\partial F^i}{\partial t}+\frac{2}{c}\,F_k\,D^{ik}\neq 0\,, \tag{56}$$

$$H^{*i}=\varepsilon^{imn}\frac{{}^*\partial A_{mn}}{\partial t}=2\frac{{}^*\partial\Omega^{*i}}{\partial t}+2\Omega^{*i}D=0\,, \tag{57}$$

$$E^{*ik}=-\frac{1}{c}\,\varepsilon^{ikm}\frac{{}^*\partial F_m}{\partial t}\neq 0\,. \tag{58}$$

*Such a space has no waves of the space metric (waves the space deformation), however waves of the gravitational inertial force are permitted therein.

We are actually considering a stationary rotating space (if it rotates) filled with the field of a non-stationary gravitational inertial force without spatial vortices of the force. This is the main kind of vortical gravitational fields, because a non-stationary rotation of a space body is very rare (see the "magnetic" kind of fields in the next Section).

In this case the chr.inv.-Lorentz condition doesn't change to the general formula (38), because the condition does not have the components of the field tensor $F_{\alpha\beta}$.

The field invariants $J_1 = F_{\alpha\beta}F^{\alpha\beta}$ and $J_2 = F_{\alpha\beta}F^{*\alpha\beta}$ (34, 35) in this case are

$$J_1 = -\frac{2}{c^2}\, h^{ik}\frac{{}^*\partial F_i}{\partial t}\frac{{}^*\partial F_k}{\partial t}\,, \qquad J_2 = 0\,. \tag{59}$$

The chr.inv.-Maxwell-like equations for a vortical gravitational field strictly of the "electric" kind are

$$\left.\begin{aligned} &{}^*\nabla_i E^i = 4\pi\rho \\ &\frac{1}{c}\left(\frac{{}^*\partial E^i}{\partial t} + E^i D\right) = -\frac{4\pi}{c}\, j^i \end{aligned}\right\} \text{ Group I,} \tag{60}$$

$$\left.\begin{aligned} &E^{*ik}A_{ik} = 0 \\ &{}^*\nabla_k E^{*ik} - \frac{1}{c^2}F_k E^{*ik} = 0 \end{aligned}\right\} \text{ Group II,} \tag{61}$$

and, after E^i and E^{*ik} are substituted, take the form

$$\left.\begin{aligned} &\frac{1}{c}\frac{{}^*\partial^2 F^i}{\partial x^i \partial t} + \frac{1}{c}\left(\frac{{}^*\partial F^i}{\partial t} + 2F_k D^{ik}\right)\Delta^j_{ji} + \\ &\qquad + \frac{2}{c}\frac{{}^*\partial}{\partial x^i}\left(F_k D^{ik}\right) = 4\pi\rho \\ &\frac{1}{c^2}\frac{{}^*\partial^2 F^i}{\partial t^2} + \frac{2}{c^2}\frac{{}^*\partial}{\partial t}\left(F_k D^{ik}\right) + \\ &\qquad + \frac{1}{c^2}\left(\frac{{}^*\partial F^i}{\partial t} + 2F_k D^{ik}\right)D = -\frac{4\pi}{c}\, j^i \end{aligned}\right\} \text{ Group I,} \tag{62}$$

$$\left.\begin{aligned} &\frac{1}{c^2}\,\Omega^{*m}\frac{{}^*\partial F_m}{\partial t} = 0 \\ &\varepsilon^{ikm}\frac{{}^*\partial^2 F_m}{\partial x^k \partial t} + \varepsilon^{ikm}\left(\Delta^j_{jk} - \frac{1}{c^2}F_k\right)\frac{{}^*\partial F_m}{\partial t} = 0 \end{aligned}\right\} \text{ Group II.} \tag{63}$$

The chr.inv.-continuity equation for such a field, in the general case of a deforming inhomogeneous space, takes the following form

$$\left(\frac{{}^*\partial F^i}{\partial t} + 2F_k D^{ik}\right)\left(\frac{{}^*\partial \Delta^j_{ji}}{\partial t} - \frac{{}^*\partial D}{\partial x^i} + \frac{D}{c^2}F_i\right) = 0\,, \tag{64}$$

and becomes the identity "zero equal to zero" in the absence of space inhomogeneity and deformation. In fact, the chr. inv.-continuity equation implies that one of the conditions

$$\frac{{}^*\partial F^i}{\partial t} = -2F_k D^{ik}, \qquad \frac{{}^*\partial \Delta^j_{ji}}{\partial t} = \frac{{}^*\partial D}{\partial x^i} - \frac{D}{c^2}F_i \tag{65}$$

or both, are true in such a vortical gravitational field.

The chr.inv.-Maxwell-like equations (62, 63) in a non-deforming homogeneous space become much simpler

$$\left.\begin{aligned} &\frac{1}{c}\frac{{}^*\partial^2 F^i}{\partial x^i \partial t} = 4\pi\rho \\ &\frac{1}{c^2}\frac{{}^*\partial^2 F^i}{\partial t^2} = -\frac{4\pi}{c}\, j^i \end{aligned}\right\} \text{ Group I,} \tag{66}$$

$$\left.\begin{aligned} &\frac{1}{c^2}\,\Omega^{*m}\frac{{}^*\partial F_m}{\partial t} = 0 \\ &\varepsilon^{ikm}\frac{{}^*\partial^2 F_m}{\partial x^k \partial t} - \frac{1}{c^2}\,\varepsilon^{ikm}F_k\frac{{}^*\partial F_m}{\partial t} = 0 \end{aligned}\right\} \text{ Group II.} \tag{67}$$

The field equations obtained specify the properties for vortical gravitational fields of the "electric" kind:

1. The field-inducing sources ρ and j^i are derived mainly from the inhomogeneous oscillations of the acting gravitational inertial force F^i (the "charges" ρ) and the non-stationarity of the oscillations (the "currents" j^i);
2. Such a field is permitted in a rotating space $\Omega^{*i} \neq 0$, if the space is inhomogeneous ($\Delta^i_{kn} \neq 0$) and deforming ($D_{ik} \neq 0$). The field is permitted in a non-deforming homogeneous space, if the space is holonomic ($\Omega^{*i} = 0$);
3. Waves of the acting force F^i travelling in such a field are permitted in the case where the oscillations of the force are homogeneous and stable;
4. The sources ρ and q^i inducing such a field remain constant in a non-deforming homogeneous space.

6 A vortical gravitational field of the "magnetic" kind

A vortical gravitational field strictly of the "magnetic" kind is characterized by its own observable components

$$H_{ik} = \frac{{}^*\partial F_i}{\partial x^k} - \frac{{}^*\partial F_k}{\partial x^i} = 2\frac{{}^*\partial A_{ik}}{\partial t} \neq 0\,, \tag{68}$$

$$H^{ik} = 2h^{im}h^{kn}\frac{{}^*\partial A_{mn}}{\partial t} \neq 0\,, \tag{69}$$

$$E_i = \frac{1}{c}\frac{{}^*\partial F_i}{\partial t} = 0\,, \tag{70}$$

$$E^i = \frac{1}{c}\,h^{ik}\frac{{}^*\partial F_k}{\partial t} = \frac{1}{c}\frac{{}^*\partial F^i}{\partial t} + \frac{2}{c}\,F_k D^{ik} = 0\,, \tag{71}$$

$$H^{*i} = \varepsilon^{imn}\frac{{}^*\partial A_{mn}}{\partial t} = 2\frac{{}^*\partial \Omega^{*i}}{\partial t} + 2\Omega^{*i}D \neq 0\,, \tag{72}$$

$$E^{*ik} = -\frac{1}{c}\,\varepsilon^{ikm}\frac{{}^*\partial F_m}{\partial t} = 0\,. \tag{73}$$

Actually, in such a case, we have a non-stationary rotating space filled with the spatial vortices of a stationary gravitational inertial force F_i. Such kinds of vortical gravitational fields are exotic compared to those of the "electric"

kind, because a non-stationary rotation of a bulky space body (planet, star, galaxy) — the generator of such a field — is a very rare phenomenon in the Universe.

In this case the chr.inv.-Lorentz condition doesn't change to the general formula (38) or for a vortical gravitational field of the "electric" kind, because the condition has no components of the field tensor $F_{\alpha\beta}$.

The field invariants (34, 35) in the case are

$$J_1 = 4h^{im}h^{kn}\frac{{}^*\partial A_{ik}}{\partial t}\frac{{}^*\partial A_{mn}}{\partial t}\,, \qquad J_2 = 0\,. \tag{74}$$

The chr.inv.-Maxwell-like equations for a vortical gravitational field strictly of the "magnetic" kind are

$$\left.\begin{aligned} &\frac{1}{c}\,H^{ik}A_{ik} = -4\pi\rho \\ &{}^*\nabla_k\,H^{ik} - \frac{1}{c^2}F_k H^{ik} = \frac{4\pi}{c}\,j^i \end{aligned}\right\} \text{ Group I,} \tag{75}$$

$$\left.\begin{aligned} &{}^*\nabla_i\,H^{*i} = 0 \\ &\frac{{}^*\partial H^{*i}}{\partial t} + H^{*i}D = 0 \end{aligned}\right\} \text{ Group II,} \tag{76}$$

which, after substituting for H^{ik} and H^{*i}, are

$$\left.\begin{aligned} &\frac{1}{c}\,A^{ik}\frac{{}^*\partial A_{ik}}{\partial t} = -2\pi\rho \\ &\frac{{}^*\partial^2 A^{ik}}{\partial x^k\partial t} + 2\frac{{}^*\partial}{\partial x^k}\left(A^{i\cdot}_{\cdot n}D^{kn} - A^{k\cdot}_{\cdot m}D^{im}\right) + \left(\Delta^j_{jk} - \frac{1}{c^2}F_k\right)\times \\ &\qquad\times\left\{\frac{{}^*\partial A^{ik}}{\partial t} + 2\left(A^{i\cdot}_{\cdot n}D^{kn} - A^{k\cdot}_{\cdot m}D^{im}\right)\right\} = \frac{2\pi}{c}\,j^i \end{aligned}\right\} \text{ Group I,} \tag{77}$$

$$\left.\begin{aligned} &\frac{{}^*\partial^2\Omega^{*i}}{\partial x^i\partial t} + \frac{{}^*\partial}{\partial x^i}\left(\Omega^{*i}D\right) + \left(\frac{{}^*\partial\Omega^{*i}}{\partial t} + \Omega^{*i}D\right)\Delta^j_{ji} = 0 \\ &\frac{{}^*\partial^2\Omega^{*i}}{\partial t^2} + \frac{{}^*\partial}{\partial t}\left(\Omega^{*i}D\right) + \left(\frac{{}^*\partial\Omega^{*i}}{\partial t} + \Omega^{*i}D\right)D = 0 \end{aligned}\right\} \text{ Group II.} \tag{78}$$

The chr.inv.-continuity equation for such a field, in a deforming inhomogeneous space, is

$$\begin{aligned} &\frac{{}^*\partial^2}{\partial x^i\partial x^k}\left(\frac{{}^*\partial A^{ik}}{\partial t}\right) - \frac{1}{c^2}A^{ik}\frac{{}^*\partial^2 A_{ik}}{\partial t^2} - \frac{1}{c^2}\left(\frac{{}^*\partial A^{ik}}{\partial t} + A^{ik}D\right)\times \\ &\times\frac{{}^*\partial A_{ik}}{\partial t} + 2\frac{{}^*\partial^2}{\partial x^i\partial x^k}\left(A^{i\cdot}_{\cdot n}D^{kn} - A^{k\cdot}_{\cdot m}D^{im}\right) + \left\{\frac{{}^*\partial A^{ik}}{\partial t} + \right. \\ &\left. + 2\left(A^{i\cdot}_{\cdot n}D^{kn} - A^{k\cdot}_{\cdot m}D^{im}\right)\right\}\left\{\left(\frac{{}^*\partial\Delta^j_{jk}}{\partial x^i} - \frac{1}{c^2}\frac{{}^*\partial F_k}{\partial x^i} + \right.\right. \\ &\left.\left. + \left(\Delta^j_{jk} - \frac{1}{c^2}F_k\right)\left(\Delta^l_{li} - \frac{1}{c^2}F_i\right)\right\} = 0\,. \end{aligned} \tag{79}$$

If the space is homogeneous and free of deformation, the continuity equation becomes

$$\begin{aligned} &\frac{{}^*\partial^2}{\partial x^i\partial x^k}\left(\frac{{}^*\partial A^{ik}}{\partial t}\right) - \frac{1}{c^2}A^{ik}\frac{{}^*\partial^2 A_{ik}}{\partial t^2} - \\ &- \frac{1}{c^2}\left(\frac{{}^*\partial A_{ik}}{\partial t} + \frac{{}^*\partial F_k}{\partial x^i} - \frac{1}{c^2}F_iF_k\right)\frac{{}^*\partial A^{ik}}{\partial t} = 0\,. \end{aligned} \tag{80}$$

In such a case (a homogeneous space free of deformation) the chr.inv.-Maxwell-like equations (77, 78) become

$$\left.\begin{aligned} &\frac{1}{c}\,A^{ik}\frac{{}^*\partial A_{ik}}{\partial t} = -2\pi\rho \\ &\frac{{}^*\partial^2 A^{ik}}{\partial x^k\partial t} - \frac{1}{c^2}F_k\frac{{}^*\partial A^{ik}}{\partial t} = \frac{2\pi}{c}\,j^i \end{aligned}\right\} \text{ Group I,} \tag{81}$$

$$\left.\begin{aligned} &\frac{{}^*\partial^2\Omega^{*i}}{\partial x^i\partial t} = 0 \\ &\frac{{}^*\partial^2\Omega^{*i}}{\partial t^2} = 0 \end{aligned}\right\} \text{ Group II.} \tag{82}$$

The obtained field equations characterizing a vortical gravitational field of the "magnetic" kind specify the properties of such kinds of fields:

1. The field-inducing "charges" ρ are derived mainly from the non-stationary rotation of the space, while the field "currents" j^i are derived mainly from the non-stationarity and its spatial inhomogeneity;
2. Such a field is permitted in a non-deforming homogeneous space, if the space rotates homogeneously at a constant acceleration;
3. Waves in such a field are standing waves of the acting gravitational inertial force. The waves are permitted only in a space which is inhomogeneous ($\Delta^i_{kn} \neq 0$) and deforming ($D_{ik} \neq 0$);
4. The sources ρ and j^i inducing such a field remain unchanged in a non-deforming homogeneous space where $F^i \neq 0$.

7 Conclusions

According the foregoing results, we conclude that the main kind of vortical gravitational fields is "electric", derived from a non-stationary gravitational inertial force and, in part, the space deformation. Such a field is a medium for traveling waves of the gravitational inertial force. Standing waves of a gravitational inertial force are permitted in a vortical gravitational field of the "magnetic" kind (spatial vortices of a gravitational inertial force or, that is the same, a non-stationary rotation of the space). Standing waves of the gravitational inertial force and their medium, a vortical gravitational field of the "magnetic" kind, are exotic, due to a non-stationary rotation of a bulky space body (the source of such a field) is a very rare phenomenon in the Universe.

It is a matter of fact that gravitational attraction is an everyday reality, so the traveling waves of the gravitational inertial force transferring the attraction should be incontrovertible. I think that the satellite experiment, propounded in [6], would detect the travelling waves since the amplitudes of the lunar or the solar flow waves should be perceptible.

Submitted on September 11, 2006
Accepted on November 15, 2006

References

1. Landau L. D. and Lifshitz E. M. The classical theory of fields. Butterworth–Heinemann, 2003, 428 pages (4th edition).
2. Zelmanov A. L. Chronometric invariants. Dissertation thesis, 1944. American Research Press, Rehoboth (NM), 2006.
3. Zelmanov A. L. Chronometric invariants and co-moving coordinates in the general relativity theory. *Doklady Acad. Nauk USSR*, 1956, v. 107(6), 815 – 818.
4. Rabounski D. Zelmanov's anthropic principle and the infinite relativity principle. *Progress in Physics*, 2005, v. 1, 35 –37.
5. Zelmanov A. L. Orthometric form of monad formalism and its relations to chronometric and kinemetric invariants. *Doklady Acad. Nauk USSR*, 1976, v. 227 (1), 78–81.
6. Rabounski D. A new method to measure the speed of gravitation. *Progress in Physics*, 2005, v. 1, 3–6; The speed of gravitation. *Proc. of the Intern. Meeting PIRT-2005*, Moscow, 2005, 106–111.

Forces of Space Non-Holonomity as the Necessary Condition for Motion of Space Bodies

Larissa Borissova
E-mail: lborissova@yahoo.com

The motion of a satellite in the gravitational field of the Earth is studied. The condition of weightlessness in terms of physical observable quantities is formulated. It is shown that the motion of all planets in the Solar system satisfy this condition. The exact solution of non-null geodesic lines describing the motion of a satellite in a state of weightlessness is obtained. It is shown that two kinds of rotational forces (forces of non-holonomity) exist: the inner force is linked to a gravitational potential, the outer force changes geometric properties of a space. The latter force causes both anisotropy of the velocity of light and additional displacement of mass-bearing bodies.

1 Introduction

We continue studies commenced in [1], where, using General Relativity, the space metric along the Earth's trajectory in the Galaxy was constructed. This metric was constructed in two steps: (i) the metric along the Earth's transit in the gravitational field of the Sun; (ii) using the Lorenz transformation to change to the reference frame moving along the z-axis coinciding with the direction in which the Earth moves in the Galaxy. The behaviour of a light ray in a reference body's space described by the obtained metric was studied in [1]. It follows from exact solutions of the isotropic geodesic lines equations for the obtained metric, that an anisotropy of the velocity of light exists in the z-direction. This anisotropy is due to the motion of the Earth in the Galaxy. The Earth's motion in the Galaxy causes additional spreading of the light ray in this direction: harmonic oscillations with a 24-hour period and amplitude $\frac{\mathrm{v}}{2}$, where v is the velocity of concomitant motion of the Earth with the Solar system in the Galaxy.

The metric describing a satellite's motion around the Earth as it moves concomitantly with the Earth in the gravitational field of the Sun is applied in this paper. The motion of a satellite by means of non-isotropic (non-null) geodesic lines equations is described. The motion of a satellite in a state of weightlessness is realised. The strong mathematical definition of this state in terms of physically observed (chronometrically invariant) quantities of A. L. Zelmanov [2, 3] is formulated. It is shown that the condition of weightlessness means that gravitational-inertial forces are absent in the region in which a satellite moves. The condition of weightlessness is a *condition of a equilibrium* between the gravitational (Newtonian) force F_N attracting a satellite towards the Earth's centre and the force F_ω directing it from the Earth. We called it the *inner force of non-holonomity*. We describe this force as a vector product of two quantities: (1) a pseudo-vector of the angular velocity of the Earth's daily rotation ω; (2) a vector of the linear velocity V of orbital motion of a satellite. The result of vectorial multiplication of these quantities is a pseudo-vector, directed always in the direction opposite to the force of gravitational attraction. If the forces of attraction and rejection are not equal one to other, a satellite: (1) falls to Earth if $F_\omega < F_N$; (2) escapes Earth if $F_\omega > F_N$. It is shown that the condition of weightlessness applies to all planets of the Solar system. Moreover, it is in accordance with Kepler's third law: *the cube of the mean distance of a planet from the Sun is proportional to the square of the period of rotation of the planet around the Sun*.

We obtain the exact solution of the non-isotropic (non-null) geodesic lines equations. It follows from them that the relativistic mass of a satellite in a state of weightlessness is constant; space velocities and space displacements in the r- and z-directions include additions caused by the Earth's daily rotation; the motion in the z-direction coinciding with the Earth's motion in the Solar system includes the effect which is described by harmonic oscillations having a period of 24 hours and an amplitude of 13 cm.

The question as to why the z-direction is preferred, is studied. It is shown that motion along the z-axis is also a rotational motion, with the angular velocity Ω, around the gravitational centre of a greater body. This body attracts the studied body and the gravitational centre around which the studied body rotates with the angular velocity ω. In order that this situation can be realized it is necessary that both these motions satisfy the condition of weightlessness.

It is shown that two kinds of forces exist, linked to a rotational motion. Because rotation of a space means that this space is non-holonomic [2, 3], we called these forces the inner and the outer force of non-holonomity, respectively. They have a different physical nature. From the physical viewpoint the inner force F_ω counteracts the Newtonian force F_N, the outer force F_Ω causes the motion in the z-direction. This action is an interaction of two rotations with the angular velocities ω and Ω, respectively. From the mathematical viewpoint these forces are different, because they are included in different terms of the space-time metric.

2 The weightlessness condition in terms of physical observable quantities

We consider, using the methods of General Relativity, the space of a body which: (1) rotates on its own axis, passing through its centre of gravity; (2) moves as a whole around the centre of gravity of a greater body. For example, the Earth rotates on its axis and simultaneously rotates around the Sun. The period of one rotation of the Earth on its axis is *one astronomical day*, or 86,400 sec. The linear velocity v_{rot} of this rotation depends on geographic latitude ϕ: $\mathrm{v}_{rot} = 500\cos\phi$ m/sec ($\mathrm{v}_{rot} = 0$ at the Earth's poles). The Earth rotates around the Sun with the velocity $\mathrm{v} = 30$ km/sec. The period of this rotation is *one astronomical year*, or 365.25 of astronomical days. The Earth's radius is 6,370 km, the distance between the Earth and the Sun is 150×10^6 km, and therefore we can consider the orbital motion of the Earth approximately as a forward motion.

We will consider every parallel of the Earth as a cylinder oriented in interplanetary space along the Earth's axis, passing through its poles. Every point of the Earth: (1) rotates around the axis with a velocity depending on its geographic latitude; (2) moves together with the Earth in the Sun's space with the velocity 30 km/sec. It is necessary to note that the points of the Earth space, which are on the Earth axis, move forward only. It is evident that, not only for the Earth's poles but also for all points along this direction, the linear velocity of rotation is zero. The combined motion of every point of the Earth's space (except axial points) is a very elongated spiral [1].

This metric is applicable to the general case of one body rotating around another body, moving concomitantly with the latter in the gravitational field of a greater body. For example, the Earth rotates around the Sun with the velocity 30 km/sec and simultaneously moves together with the Sun in the galactic space with the velocity 222 km/sec. The combined motion of the Earth motion in the Galaxy is described by a very elongated spiral. This case is studied in detail in [1]. The combined motion of every point of the Earth's surface in the Galaxy is more complicated trajectory.

The metric describing the space of a body which rotates around another body (or around its own centre of gravity) and moves together with the latter in the gravitational field of a greater body is [1]:

$$ds^2 = \left(1-\frac{2GM}{c^2r}\right)c^2dt^2 + \frac{2\omega r^2}{c}cdtd\varphi - \\ -\left(1+\frac{2GM}{c^2r}\right)dr^2 - r^2d\varphi^2 + \frac{2\omega\mathrm{v}r^2}{c^2}d\varphi dz - dz^2, \tag{1}$$

where $G = 6.67\times10^{-8}$ cm^3/g$\times$sec^2 is Newton's gravitational constant, ω is the angular velocity of the rotation around the axis, v is the orbital velocity of the body, r, φ and z are cylindrical coordinates. We direct the z-axis along a direction of a forward motion. This metric describes the motion of all points of the rotating body, besides axial points.

We apply Zelmanov's theory of physically observed quantities (chronometrically invariants) [2, 3] in order to describe this gravitational field. The three-dimensional observed space of the space-time (1) has a metric h_{ik} ($i = 1, 2, 3$). Its components are

$$\begin{aligned} h_{11} &= 1+\frac{2GM}{c^2r}, \quad h_{22} = r^2\left(1+\frac{\omega^2r^2}{c^2}\right), \\ h_{23} &= -\frac{\omega r^2\mathrm{v}}{c^2}, \qquad h_{33} = 1; \\ h^{11} &= 1-\frac{2GM}{c^2r}, \quad h^{22} = \frac{1}{r^2}\left(1-\frac{\omega^2r^2}{c^2}\right), \\ h^{23} &= \frac{\omega\mathrm{v}}{c^2}, \qquad h^{33} = 1. \end{aligned} \tag{2}$$

Physically observed (chronometrically invariant) characteristics of this space are

$$F^1 = \left(\omega^2r - \frac{GM}{r^2}\right)\left(1+\frac{\omega^2r^2}{c^2}\right), \tag{3}$$

$$A^{12} = -\frac{\omega}{r}\left(1-\frac{2GM}{c^2r}+\frac{\omega^2r^2}{2c^2}\right), \quad A^{31} = \frac{\omega^2\mathrm{v}r}{c^2}, \tag{4}$$

where F^i is a vector of a gravitational-inertial force, A^{ik} is a tensor of an angular velocity of a rotation (a tensor of a non-holonomity). The third characteristic is a tensor of velocities of a deformation $D_{ik} = 0$.

Geometric space characteristics of (2) are chronometrically invariant Christoffel symbols Δ^k_{ij} of the second kind:

$$\Delta^k_{ij} = h^{km}\Delta_{ij,m} = \frac{1}{2}h^{km}\left(\frac{{}^*\partial h_{im}}{\partial x^j} + \frac{{}^*\partial h_{im}}{\partial x^i} - \frac{{}^*\partial h_{ij}}{\partial x^m}\right), \tag{5}$$

where $\Delta_{ij,m}$ are Christoffel symbols of the first kind, while $\frac{{}^*\partial}{\partial x^i} = \frac{\partial}{\partial x^i} - \frac{1}{c^2}v_i\frac{{}^*\partial}{\partial t}$ is chronometric differentiation with respect to spatial coordinates, and $\frac{{}^*\partial}{\partial t}$ is chronometric differentiation with respect to time. Because the gravitational field described by the metric (1) is stationary, we have $\frac{{}^*\partial}{\partial x^i} = \frac{\partial}{\partial x^i}$

The non-zero components of Δ^k_{ij} for (1) are

$$\begin{aligned} \Delta^1_{11} &= \frac{GM}{c^2r}, \quad \Delta^1_{22} = -r\left(1-\frac{2GM}{c^2r}+\frac{2\omega^2r^2}{c^2}\right), \\ \Delta^1_{23} &= \frac{\omega\mathrm{v}r}{c^2}, \quad \Delta^2_{12} = \frac{1}{r}\left(1+\frac{\omega^2r^2}{c^2}\right), \quad \Delta^2_{13} = -\frac{\omega\mathrm{v}}{c^2r}. \end{aligned} \tag{6}$$

Let's consider the particular case of this motion when the gravitational-inertial force is absent:

$$F^i = 0. \tag{7}$$

We rewrite it for the metric (1) in the form

$$\frac{GM}{r} = \omega^2r^2 = V^2, \tag{8}$$

where V is the linear velocity of a rotational motion.

Substituting into (8) the Earth's mass $M_\oplus = 6\times10^{27}$g and the Earth's radius $R_\oplus = 6.37\times10^8$ cm we obtain the value of a velocity of a rotation $\mathrm{V} = 7.9$ km/sec. This value is the *first space velocity*, which we denote by V_I. If we accelerate a body located on the Earth in this way, so that its velocity acquires the value 7.9 km/sec, it will move freely in the gravitational field of the Earth as an Earth satellite. This means that condition (7) is the *weightlessness condition* in General Relativity, formulated in terms of physically observed quantities.

Substituting into (8) the mass of the Sun $M_\odot = 2\times10^{33}$ g and the distance between the Earth and the Sun $r = 15\times10^{12}$ cm we obtain $\mathrm{v} = 30$ km/sec — the orbital velocity of the Earth in the gravitational field of the Sun. This means that *the Earth rotates around the Sun in the state of weightlessness*.

Analogous calculations show [4] that *the orbital motion of the Moon around the Earth and orbital motions of all planets of the Solar system satisfy the weightlessness condition*. We conclude that the weightlessness condition is the condition by which the force of Newton's attraction F_N equals the force F_ω connected with a rotational motion. It is evident that this force must be directed opposite to that of the Newtonian force. It is possible to consider this force as a vector product of two quantities: (1) a pseudo-scalar of an angular velocity of rotation ω directed along the Earth's axis; (2) a vector $V = \omega \times r$ in a direction tangential to the satellite's orbit. Thus we have

$$F_\omega = \omega \times V = \omega \times \big[\omega \times r\big]. \tag{9}$$

This force is directed opposite to the Newtonian force in a right coordinate frame. Its value is $\omega \mathrm{V} \sin\alpha$, α the angle between these vectors; it equals $\omega^2 r$ if these quantities are orthogonal to one another.

We call this force the *inner force of non-holonomity*, because it acts on a body moving in the inner gravitational field of another body. This force is included in the g_{00}-component of the fundamental metric tensor $g_{\alpha\beta}$.

It is necessary to explain why we consider ω a pseudo-vector. In general, Zelmanov defines a pseudo-vector of an angular velocity $\Omega^i = \frac{1}{2}\,\varepsilon^{imn} A_{mn}$, where ε^{imn} is a completely antisymmetric chronometrically invariant unit tensor. For it we have $\varepsilon^{123} = \frac{1}{\sqrt{h}}$, where h is the determinant of a three-dimensional fundamental metric tensor h_{ik}.

Taking (8) into account, we calculate for the metric (1):

$$h = r^2\left(1 + \frac{3\omega^2 r^2}{c^2}\right), \tag{10}$$

$$A_{12} = -\omega r\left(1 + \frac{3\omega^2 r^2}{2c^2}\right), \tag{11}$$

with the other components of A_{ik} all zero. Consequently only the component $\Omega^3 = -\omega$ is not zero for this metric.

It is easy to calculate for all planets that orbital motion satisfies Kepler's third law.

3 The motion of a satellite in the gravitational field of the Earth

We consider the motion of a satellite in the gravitational field of the Earth rotating around the its own axis and moving in the gravitational field of the Sun (rotating around its centre). This is a motion of a free body, so it is consequently described by the geodesic equations

$$\frac{d^2x^\alpha}{ds^2} + \Gamma^\alpha_{\mu\nu}\frac{dx^\mu}{ds}\frac{dx^\nu}{ds} = 0, \tag{12}$$

where $\frac{dx^\alpha}{ds}$ is a vector of a four-dimensional velocity, $\Gamma^\alpha_{\mu\nu}$ are four-dimensional Christoffel symbols. In terms of observed quantities, these equations have the form

$$\begin{aligned}&\frac{dm}{d\tau} - \frac{m}{c^2}F_iV^i + \frac{m}{c^2}D_{ik}V^iV^k = 0,\\ &\frac{d(mV^i)}{d\tau} + 2m\big(D^i_k + A^{\cdot i}_{k\cdot}\big)V^k - mF^i + m\Delta^i_{nk}V^nV^k = 0,\end{aligned} \tag{13}$$

where τ is proper (observed) time, $V^i = \frac{dx^i}{d\tau}$ is a three-dimensional observed velocity, m is the relativistic mass of a satellite. It is evident that its gravitational field is negligible.

Substituting into these equations the calculated values of A^{ik} and Δ^k_{ij} for the metric (1) and taking into account the condition of weightlessness (8), we obtain a system of equations

$$\frac{dm}{d\tau} = 0\,, \tag{14}$$

$$\begin{aligned}\frac{d}{d\tau}\left(m\frac{dr}{d\tau}\right) + 2m\omega r\left(1 - \frac{\omega^2 r^2}{2c^2}\right)\frac{d\varphi}{d\tau} + \frac{m\omega^2 r}{c^2}\left(\frac{dr}{d\tau}\right)^2 -\\ - mr\left(\frac{d\varphi}{d\tau}\right)^2 + \frac{2m\omega\mathrm{v}r}{c^2}\frac{d\varphi}{d\tau}\frac{dz}{d\tau} = 0\,,\end{aligned} \tag{15}$$

$$\begin{aligned}&\frac{d}{d\tau}\left(m\frac{d\varphi}{d\tau}\right) - \frac{2m\omega}{r}\left(1 + \frac{\omega^2 r^2}{2c^2}\right)\frac{dr}{d\tau} +\\ &+ \frac{2m}{r}\left(1 + \frac{\omega^2 r^2}{c^2}\right)\frac{dr}{d\tau}\frac{d\varphi}{d\tau} - \frac{2m\omega\mathrm{v}}{c^2 r}\frac{dr}{d\tau}\frac{dz}{d\tau} = 0\,,\end{aligned} \tag{16}$$

$$\frac{d}{d\tau}\left(m\frac{dz}{d\tau}\right) - \frac{2m\omega^2\mathrm{v}r}{c^2}\frac{dr}{d\tau} = 0. \tag{17}$$

We obtain from equation (14) that the relativistic mass of a space body is, by a condition of weightlessness, constant: $m = \mathrm{const}$. Using this condition we calculate the first integral of equation (17)

$$\dot z = \dot z_0 + \frac{\omega^2\mathrm{v}\left(r^2 - r_0^2\right)}{c^2}, \tag{18}$$

where $\dot z$ denotes differentiation with respect to τ, $\dot z_0$ and r_0 are initial values.

Taking into account that $m=\text{const}$ and also $\frac{GM}{c^2r}=\frac{\omega^2r^2}{c^2}$ (the condition of weightlessness) we rewrite (15) and (16) as

$$\ddot{r}+2\omega r\left(1-\frac{\omega^2r^2}{2c^2}\right)\dot{\varphi}+\frac{\omega^2r}{c^2}\dot{r}^2-r\dot{\varphi}^2+\frac{2\omega\mathrm{v}r}{c^2}\dot{\varphi}\dot{z}=0, \quad (19)$$

$$\ddot{\varphi}-\frac{2\omega}{r}\left(1+\frac{\omega^2r^2}{c^2}\right)\dot{r}+\frac{2}{r}\left(1+\frac{\omega^2r^2}{c^2}\right)\dot{r}\dot{\varphi}-\frac{2\omega\mathrm{v}}{c^2r}\dot{r}\dot{z}=0. \quad (20)$$

The linear velocity of the Earth's rotation around its axis, $\omega r\cos\phi$, has the maximum value, at the equator, $\omega r=$ 500 m/sec, and consequently the maximum value of $\frac{\omega^2r^2}{c^2}=$ $=6\times10^{-11}$. Substituting (18) into (19–20) and neglecting the terms $\frac{\omega^2r^2}{c^2}$ and $\frac{\omega^2r\dot{r}^2}{c^2}$, we obtain

$$\ddot{r}+2\omega r\dot{\varphi}-r\dot{\varphi}^2+\frac{2\omega\mathrm{v}r}{c^2}\dot{\varphi}\dot{z}_0=0\,, \quad (21)$$

$$\ddot{\varphi}-2\omega\frac{\dot{r}}{r}+2\dot{\varphi}\frac{\dot{r}}{r}-\frac{2\omega\mathrm{v}\dot{z}_0}{c^2}\frac{\dot{r}}{r}=0\,. \quad (22)$$

We rewrite (24) in the form

$$\ddot{\varphi}+2\left(\dot{\varphi}-\widetilde{\omega}\right)\frac{\dot{r}}{r}=0\,, \quad (23)$$

where $\widetilde{\omega}=\omega\left(1+\frac{\mathrm{v}\dot{z}_0}{c^2}\right)$. The quantity $\widetilde{\omega}$ is the angular velocity of an Earth point daily rotation containing a correction $\frac{\mathrm{v}\dot{z}_0}{c^2}$ which is due to the orbital motion of the Earth around the Sun. It is necessary that we do not neglect the term $\frac{\mathrm{v}\dot{z}_0}{c^2}$, because its order is 2.7×10^{-9}: we propose $\mathrm{v}=30$ km/sec (the orbital velocity of the Earth) and $\dot{z}_0=8$ km/sec (the initial value of the satellite velocity).

The variable in equation (23) can be separated, and therefore it is easily integrated. The first integral is

$$\dot{\varphi}=\widetilde{\omega}+\frac{\left(\dot{\varphi}_0-\widetilde{\omega}\right)r_0^2}{r^2}\,, \quad (24)$$

where $\dot{\varphi}$ and r_0 are initial values.

Substituting (24) into (21) we obtain, after transformations, the second order differential equation relative to r

$$\ddot{r}+\widetilde{\omega}^2r-\frac{\left(\dot{\varphi}_0-\widetilde{\omega}\right)r_0^4}{r^3}=0\,. \quad (25)$$

We introduce the new variable $p=\dot{r}$. Then $\ddot{r}=p\frac{dp}{dr}$ and (25) becomes

$$p\,dp=\frac{\left(\dot{\varphi}_0-\widetilde{\omega}\right)^2r_0^4}{r^3}\,dr-\widetilde{\omega}^2r\,dr=0\,, \quad (26)$$

the variables of which are also separable. It is easily integrated to

$$\dot{r}^2=\left(\frac{dr}{d\tau}\right)^2=-\omega^2r^2-\frac{\left(\dot{\varphi}_0-\widetilde{\omega}\right)^2r_0^4}{r^2}+K, \quad (27)$$

where the constant of integration K is

$$K=\dot{r}_0^2+r_0^2\left[2\widetilde{\omega}^2+\dot{\varphi}_0\left(\dot{\varphi}_0-2\widetilde{\omega}\right)\right]. \quad (28)$$

We obtain

$$\dot{r}=\frac{dr}{d\tau}=\pm\sqrt{K-\widetilde{\omega}^2r^2-\frac{\left(\dot{\varphi}_0-\widetilde{\omega}\right)^2r_0^4}{r^2}}\,. \quad (29)$$

This too is an equation with separable variables. Considering the positive sign we obtain, after elementary transformations,

$$d\tau=\frac{r\,dr}{\sqrt{-\widetilde{\omega}^2r^4+Kr^2-\left(\dot{\varphi}_0-\widetilde{\omega}\right)^2r_0^4}}\,. \quad (30)$$

Introducing the new variable $y=r^2$ we have

$$d\tau=\frac{1}{2}\frac{dy}{\sqrt{-\widetilde{\omega}^2y^2+Ky-\left(\dot{\varphi}_0-\widetilde{\omega}\right)^2r_0^4}}. \quad (31)$$

Integrating (31) and returning to the old variable r we obtain the expression for τ

$$\tau=-\frac{1}{2\widetilde{\omega}}\arcsin\frac{K-2\widetilde{\omega}^2r^2}{\sqrt{K^2-4\widetilde{\omega}^2\left(\dot{\varphi}_0-\widetilde{\omega}\right)r_0^4}}+B, \quad (32)$$

where B is a constant of integration. Calculating $B=0$ for the initial value of $\tau_0=0$ we rewrite (32) as

$$\sin2\widetilde{\omega}\tau=\frac{2\widetilde{\omega}^2\left(r^2-r_0^2\right)}{\sqrt{K^2-4\widetilde{\omega}^2\left(\dot{\varphi}_0-\omega\right)^2r_0^4}}\,, \quad (33)$$

where r_0 is the initial value of r. It is easy to express r^2 as

$$r^2=r_0^2+\frac{\sqrt{K^2-4\widetilde{\omega}^2\left(\dot{\varphi}_0-\widetilde{\omega}\right)}}{2\widetilde{\omega}^2}\sin2\widetilde{\omega}\tau. \quad (34)$$

Expressing $K^2-4\widetilde{\omega}^2B^2$ through initial values we obtain

$$r=\sqrt{r_0^2+\frac{Q}{2\widetilde{\omega}^2}\sin2\widetilde{\omega}\tau}\,, \qquad Q=\text{const}, \quad (35)$$

where $Q=\sqrt{\left(\dot{r}_0^2+r_0^2\dot{\varphi}_0^2\right)\left[\dot{r}_0^2+r_0^2(\dot{\varphi}_0+2\widetilde{\omega})^2\right]}$.

Substituting (35) into (18) and integrating the resulting expression we have

$$z=\dot{z}_0\tau+\frac{\mathrm{v}Q}{2\widetilde{\omega}c^2}\left(1-\cos2\widetilde{\omega}\tau\right)+z_0\,, \quad (36)$$

where z_0 and $\dot{z}_0$ are initial values.

Substituting (34) into (24) and integrating we obtain for φ the expression

$$\varphi=\widetilde{\omega}\tau+\frac{2\widetilde{\omega}^2r_0^2\left(\dot{\varphi}_0-\widetilde{\omega}\right)}{\sqrt{Q^2-4\widetilde{\omega}^4r_0^4}}\times \\ \times\ln\left|\frac{2\widetilde{\omega}^2r_0^2\tan\widetilde{\omega}\tau+Q-\sqrt{Q^2-4\widetilde{\omega}^4r_0^4}}{2\widetilde{\omega}^2r_0^2\tan\widetilde{\omega}\tau+Q+\sqrt{Q^2-4\widetilde{\omega}^4r_0^4}}\right|+P\,, \quad (37)$$

where the integration constant equals $P=\varphi_0-\frac{2\widetilde{\omega}^2r_0^2(\dot{\varphi}_0-\widetilde{\omega})}{Q^2-4\widetilde{\omega}^4r_0^4}\times$ $\times\ln\left|\frac{Q-\sqrt{Q^2-4\widetilde{\omega}^4r_0^4}}{Q+\sqrt{Q^2-4\widetilde{\omega}^4r_0^4}}\right|$.

We see from (35–37) that trajectories of a freely falling satellite in the Earth's gravitational field conclude corrections for the daily rotation of the Earth. Besides that, the motion in the z-direction coinciding with a forward motion of the Earth includes the velocity of the orbital motion of the Earth around the Sun. Let's estimate the correction in the z-direction caused the orbital motion of the Earth with velocity 30 km/sec. In order to estimate the value Q, we propose that the satellite moved vertically at the initial moment. This means that only the radial component of the initial velocity is not zero: $\dot{r}_0 \neq 0$. Let it be equal to the first space velocity: $\dot{r}_0 \simeq V_I = 8$ km/sec. In this case $Q = V_I^2 \simeq 64$ km^2/sec^2. Taking into account the angular velocity of the daily rotation $\omega = 8 \times 10^{-5}$ sec^{-1} we obtain the correction $\frac{\mathrm{v}Q}{2\widetilde{\omega}c^2} = 13$ cm. This means that a satellite not only moves forward with a velocity $\dot{z}_0$ in the z-direction, it also undergoes harmonic oscillations with the amplitude 13 cm during the 24-hour period.

It is necessary to take into account these corrections in relation to some experiments with satellites. For example, experiments, the aim of which is to discover gravitational waves: two geostationary satellites are considered as two free particles. Measuring changes of the distance between them by means of laser interferometer, scientists propose to discover gravitational waves emitted by different space sources. It is evident, it is necessary to take into account changes of this distance caused by motion of satellites in the gravitational field of the Sun.

Let's study in detail why the z-direction is preferred. The displacement in the z-direction includes the velocity $\mathrm{v} = 30$ km/sec of the Earth's motion in the gravitational field of the Sun. We consider this motion as a "forward" motion. On the other hand, this motion is as well rotation, because the Earth rotates around the Sun. Therefore we can consider v as a vector product of two quantities

$$\mathrm{v} = \Omega \times R\,, \tag{38}$$

where $\Omega = 2 \times 10^{-7}$ sec^{-1} is the angular velocity of the Earth's orbital rotation, $R = 150 \times 10^6$ km is the distance between the Earth and the Sun.

Now we define the *outer force of non-holonomity* F_Ω as a force of a kind different to F_ω. This definition corresponds to the case where one body rotates around another as the latter rotates around a greater body. We define this force also as a force of non-holonomity, because Zelmanov proved that a rotation of a three-dimensional space means that this space is non-holonomic. The metric of the corresponding space-time in this case necessarily includes the mixed (space-time) terms g_{0i}, because it is impossible to transform coordinates in such a way that all $g_{0i} = 0$.

We define the outer force of non-holonomity as

$$F_\Omega = \omega \times \left[\Omega \times R\right], \tag{39}$$

where ω and Ω are angular velocities of two different rotations: ω is the angular velocity of rotation of a space body around a centre of attraction; Ω is the angular velocity of rotation of the concomitant rotation of a space body and its centre of attraction around a greater space body. The interaction of both rotations produces a real force, acting on masses the fields of which are in the region of this force.

We see that this force is included in metric (1) as an off-diagonal term $\frac{\omega \mathrm{v} r^2}{c^2}$. It is also contained in the chronometrically invariant Christoffel symbols (6). Solving the null geodesic lines equations for this metric, we obtained in [1] that an anisotropy of the velocity of light exists in the z-direction. The z-axis in (1) coincides with the direction of the concomitant motion of the Earth with the Solar system. This motion realises the velocity 222 km/sec. The anisotropy correction appearing in this direction as

$$\Delta\dot{z} = \frac{\mathrm{v}}{2} \sin 2\widetilde{\omega}\tau\,, \tag{40}$$

where $\dot{z} = \frac{dz}{d\tau}$, $\widetilde{\omega}$ is the angular velocity of the Earth's orbital motion. thus the value of $\dot{z}$ is realised during one astronomic year harmonic oscillation, with the amplitude 111 km/sec.

4 Conclusion. Further perspectives

We studied in this paper the motion of a satellite in the Earth's gravitational field. This motion is realised by the condition of weightlessness, defined as a state of equilibrium between two forces: the Newtonian force of attraction F_N and the force of repulsion F_ω, caused by a rotational motion. The existence of a rotation means the existence of a field of non-holonomity, and, consequently, the existence of forces of non-holonomity. The inner force of non-holonomity F_ω is a pseudo-tensor, always directed opposite to the direction to the centre of attraction. This is a real force countering the Newtonian force F_N. The equality of these two forces means that a satellite moves around the Earth in a state of weightlessness.

A satellite moves freely, and consequently moves along non-isotropic geodesic lines. We obtain from these equations that the relativistic mass of a satellite is constant. Displacements of a satellite in the r- and φ-directions include components caused by the daily rotation of the Earth. Solving the non-null geodesic lines equations describing its motion, we obtained from formula (36)

$$\Delta\dot{z} = \frac{\mathrm{v}Q}{2c^2} \simeq \frac{\mathrm{v}V_I^2}{2c^2} = 10^{-8} \text{ km}, \tag{41}$$

where $\mathrm{v} = 30$ km/sec, $V_I = 8$ km/sec is the first space velocity. This correction is very small, but it has the same origin as the anisotropy of the velocity of light. Calculating the displacement of a satellite in the z-direction, we obtain the correction as a harmonic oscillation with the amplitude 13 cm and of 24-hour period.

The expression (36) is the exact solution of the equation (17). It is easy to see that the second term of (17) includes the quantity $m\omega \mathrm{v} = m\omega\Omega R$, where R is the distance between the Earth and the Sun. We can rewrite it as the angular momentum L of the outer force of non-holonomity

$$L = mF_{\Omega}R = m\omega\Omega R\,. \tag{42}$$

We conclude that:

1. If a body rotating around a centre of attraction also rotates with the latter around a greater origin of attraction, these fields of rotation interact.

This interaction exists only by the condition that both bodies rotate. The interaction of two fields of non-holonomity (the inner and the outer) causes an anisotropy in the velocity of light in the direction of the motion in the gravitational field of a greater body [1]. This interaction causes the displacement in this equation of a mass-bearing body (a satellite) obtained in the present paper. Both effects have the same nature: the angular moment of the outer force of non-holonomity deviates null and non-null trajectories of light-like particles and mass-bearing bodies.

We conclude that the inner and the outer forces of non-holonomity have a different nature, and therefore produce different effects on the motion of space bodies (and light).

2. The inner force of non-holonomity counters the Newtonian force of attraction. It is included in a three-dimensional potential of a gravitational field

$$\mathrm{w} = c^2\left(1 - \sqrt{g_{00}}\right) \simeq \frac{GM}{r} + \frac{\omega^2 r^2}{2}\,. \tag{43}$$

This field of non-holonomity is linked to the weightlessness condition: the motion of a space body satisfies the weightlessness condition if $\frac{\partial \mathrm{w}}{\partial r} = 0$. This result follows from the definition of a gravitational-inertial force vector

$$F_i = \frac{1}{1 - \frac{\mathrm{w}}{c^2}}\left(\frac{\partial \mathrm{w}}{\partial x^i} - \frac{\partial v_i}{\partial t}\right). \tag{44}$$

We see that if a rotation is stationary (i. e. $\frac{\partial v_i}{\partial t} = 0$) the condition of weightlessness has the form $\frac{\partial \mathrm{w}}{\partial x^i} = 0$. It is evident that if a rotation is non-stationary, the condition of the weightlessness takes the form

$$\frac{\partial \mathrm{w}}{\partial x^i} = \frac{\partial v_i}{\partial t}\,. \tag{45}$$

It is interesting to note that a stationary rotation of a three-dimensional space is linked with motions of the space-time. It is shown in [4] that a stationary rotation of a three-dimensional space is a motion of the space-time itself due to the fact that a Lie derivative for this metric is zero.

3. The outer force of non-holonomity acts on the geometry of the space of transit of a body which rotates around another body and moves with the latter in the gravitational field of a greater body. It imparts energy to a moving (rotating) system of bodies, the gravitational fields of which are part of the gravitational field. We obtain the following chain: the gravitational field of the Earth (and all other planets) is a part of the Sun's gravitational field; the gravitational field of the Sun is a part of the galactic gravitational field, etc. All these space bodies are linked by gravitational forces and forces of non-holonomity. Its equilibrium is a necessary condition of existence for the Universe.

A study of spaces with non-stationary rotation is the theme of further papers. A necessary consideration of this problem involves the microwave radiation in the observed Universe. We have shown in the second part of [1] that the space-time satisfying to metric (1) can be permeated only by matter with stationary characteristics: a density, a stream of energy, a stress tensor, etc. Proposing that the Universe is filled by an ideal fluid (gas) and electromagnetic radiation, we showed that the electromagnetic field can only be stationary. If we consider this electromagnetic field as an electromagnetic wave, we conclude that these waves can only be standing waves. But observations show that in our Universe a microwave electromagnetic radiation exists. We therefore must initially choice a non-stationary metric. Such a metric can allow non-stationary electromagnetic radiation. It is possible that microwave radiation is linked with non-stationary fields of non-holonomity. But this is a theme for further studies.

Submitted on October 18, 2006
Accepted on December 14, 2006

References

1. Borissova L. Preferred spatial directions in the Universe: a General Relativity approach. *Progress in Physics*, 2006, v. 4, 51–64.
2. Zelmanov A. L. Chronometric invariants and co-moving coordinates in the general relativity theory. *Doklady Acad. Nauk USSR*, 1956, v. 107(6), 815–818.
3. Zelmanov A. L. Chronometric invariants. Dissertation thesis, 1944. American Research Press, Rehoboth (NM), 2006.
4. Rabounski D. and Borissova L. Particles here and beyond the Mirror. Editorial URSS, Moscow, 2001; arXiv: gr-qc/0304018.

Evidence of Non-local Chemical, Thermal and Gravitational Effects

Huping Hu and Maoxin Wu

Biophysics Consulting Group, 25 Lubber Street, Stony Brook, NY 11790, USA

E-mail: hupinghu@quantumbrain.org

Quantum entanglement is ubiquitous in the microscopic world and manifests itself macroscopically under some circumstances. But common belief is that it alone cannot be used to transmit information nor could it be used to produce macroscopic non-local effects. Yet we have recently found evidence of non-local effects of chemical substances on the brain produced through it. While our reported results are under independent verifications by other groups, we report here our experimental findings of non-local chemical, thermal and gravitational effects in simple physical systems such as reservoirs of water quantum-entangled with water being manipulated in a remote reservoir. With the aids of high-precision instruments, we have found that the pH value, temperature and gravity of water in the detecting reservoirs can be non-locally affected through manipulating water in the remote reservoir. In particular, the pH value changes in the same direction as that being manipulated; the temperature can change against that of local environment; and the gravity apparently can also change against local gravity. These non-local effects are all reproducible and can be used for non-local signalling and many other purposes. We suggest that they are mediated by quantum entanglement between nuclear and/or electron spins in treated water and discuss the implications of these results.

1 Introduction

Scientific methods require that one conform one's knowledge of nature to repeatable observations. Thus, it is unscientific to reject what's observed repeatedly and consistently. With this in mind, we comment that quantum entanglement has been recently shown to be physically real in many laboratories [1, 2]. Indeed, spins of electrons, photons and nuclei have now been successfully entangled in various ways for the purposes of quantum computation and communication [3, 4]. On the other hand, we have recently observed non-local effects of chemical substances on the brain produced through quantum entanglement [5, 6] which are commonly thought to be impossible [7]. Here we report our work carried out on simple physical systems, in particular, water, using simple physical/chemical observables such as pH, temperature and gravity measured with high-precision instruments. Our motivation for measuring pH change of water in one reservoir, while manipulating water in a remote reservoir quantum-entangled with the former, is to investigate whether and how pH value in the water being measured shifts under non-local influences. Our motivation for measuring temperature variation of water in one reservoir, while manipulating water in a remote reservoir quantum-entangled with the former, is to investigate whether and how the thermodynamics of water being measured changes under non-local influences. Our motivation for measuring gravity change of one reservoir of water, while manipulating water in a remote reservoir quantum-entangled with the former, is to investigate whether gravity also change under non-local influences.

The successes of the experiments described herein were achieved with the aids of high-precision analytical instruments. They include an Ohaus Voyager Analytical Balance with capacity 210 g, resolution 0.1 mg, repeatability 0. 1mg and sensitivity drift 3PPM/°C, a Control Company traceable-calibration digital thermometer with resolution 0.001°C and repeatability 0.002°C near 25°C in liquid such as water (estimated from calibration data provided), and a Hanna microprocessor pH meter Model 213 with resolution 0.001 and repeatability 0.002. The other key apparatus is a 25-litre Dewar filled with liquid nitrogen and positioned remotely at a desired distance which not only provided the drastic changes in the water being manipulated but also served as a natural Faraday cage blocking any possible electromagnetic influence between the water being measured and the water being manipulated. Also vital to the success of the experiments described herein was the stable environment found in an underground room which shields many external noises such as mechanical vibration, air turbulence and large temperature change.

2 Materials and methods

Quantum-entangled stock water in individual volumes of 500 ml or similar quantities was prepared as described previously [5] which might then be split into smaller volumes or combined into larger ones based on needs.Briefly, in one procedure 500 ml fresh tap water in a closed plastic reservoir was exposed to microwave radiation in a 1500 W microwave oven for 2 min and then left in room temperature for 24 hours

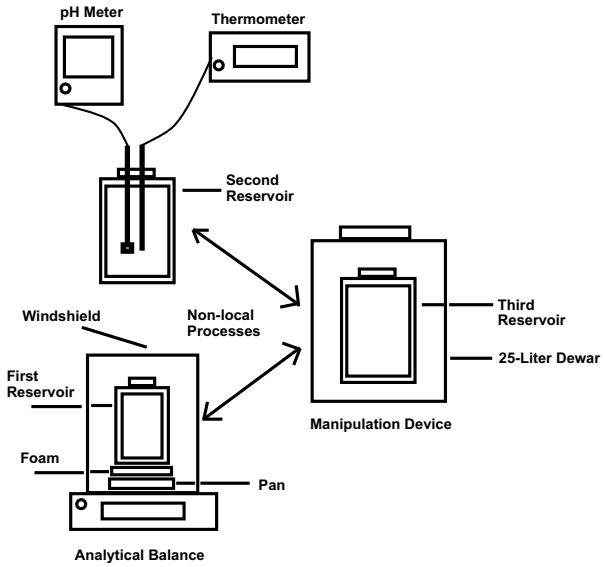

Fig. 1: Illustration of the key experimental setup. Several variations of this setup were also used in the actual experiments as described in the text. For example, in one variation, the manipulation was heating the water in the 3rd reservoir to boiling point and then cooling it down. In a second variation, the gravity measurement was eliminated and the manipulations were first adding 5 ml concentrated HCl (38%) to the third reservoir, then adding 20 g NaOH to the same and third heating the same to boiling point. In a third variation, the Dewar was located more than 500 feet away from the site of measurement. In fourth variation, the gravity and pH measurements were eliminated and the temperature measurements were carried out more than 50 miles away from the location of the Dewar.

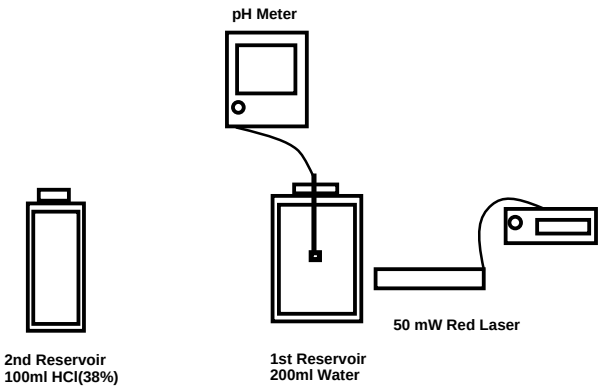

Fig. 2: Illustration of the second experimental setup which allows the measurement of pH value in the presence or absence of concentrated HCl about 500 cm away from and behind the water being measured. If no quantum entanglement is involved, the presence or absence of the HCl should not affect the pH value.

before use. In a second procedure 500 ml fresh tap water in the closed plastic reservoir was exposed to audio-frequency radiations of a 20 W magnetic coil for 30 min and then left in room temperature for 24 hours before use. In a third procedure, 500 ml bottled natural water was simply left in room temperature for at least 30 days before use. In a fourth procedure, 500 ml bottled distilled water was simply left in room temperature for at least 30 days before use. It was found previously that the stock water prepared according to these procedures is quantum-entangled [5].

Figure 1 shows a diagram of the key experimental setup. It includes (1) the analytical balance calibrated internally and stabilized in the underground room for more than one week before use and a tightly closed plastic first reservoir containing 175 ml water split from the 500 ml stock water which is placed on the wind-shielded pan of the balance with 1-inch white foam in between as insulation; (2) the digital thermometer and calibrated pH meter placed into the middle of a glass second reservoir containing 75 ml water split from the 500 ml stock water which is closed to prevent air exchange; and (3) the 25-litre Dewar containing 15–25 litres of liquid nitrogen which is located at a distant of 50 feet from the underground room and a tightly closed plastic third-reservoir containing 250 ml water split from the 500 ml stock water to be submerged into the liquid nitrogen in the Dewar at a specified time.

Experiments with the above first-setup were carried out as follows: (1) prepare the 500 ml quantum entangled stock water, divide the same into 175 ml, 75 ml and 250 ml portions and put them into their respective reservoirs described above; (2) set up the experiment according to Figure 1 and let the instruments to stabilize for 30 min before any measurements is taken; (3) record for 20 min minute-by-minute changes of pH value and temperature of the water in the first-reservoir and weight of the second reservoir with water before submerging the third reservoir into liquid nitrogen; (4) submerge the third-reservoir with water into liquid nitrogen for 15 min or another desired length of time and record the instrument readings as before; and (5) take the third-reservoir out of liquid nitrogen, thaw the same in warm water for 30 min or longer and, at the same time, record the instrument readings as before. Control experiments were carried out in same steps with nothing done to the water in the third-reservoir.

In one variation of the above setup, the closed plastic third-reservoir was replaced with a metal container and instead of freeze-thaw treatment the water in the metal container was quickly heated to boiling within 4–5 minutes and then cooled in cold water. In a second variation of the above setup, the gravity portion of the experiment was eliminated and the water in the first and second reservoirs was combined into a closed thermal flask which prevents heat exchange between the water being measured and its local environment. In a third variation of the above setup, the gravity portion of the experiment was eliminated and the water in the first and second reservoirs was combined into a fourth plastic container in which 5 ml concentrated HCl (38% by weight) was first added, then 20 g NaOH powder was added and next the same water was transferred to a metal container and heated to boiling on a stove. In a fourth

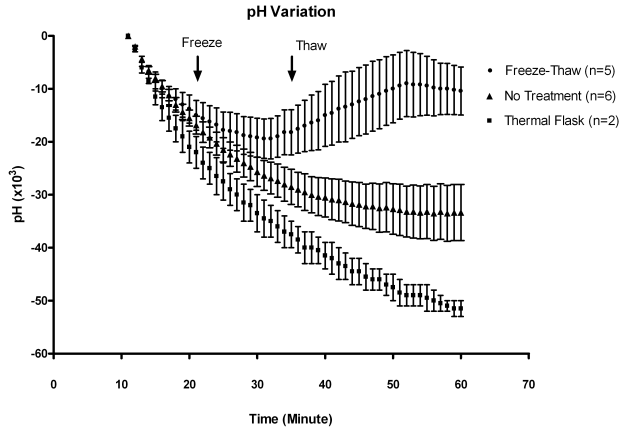

Fig. 3: pH variations under remote manipulations of water quantum-entangled with water being measured. The pH value at the starting point is set to zero and the results shown were obtained from one batch of quantum-entangled water. The difference in pH values from control in which no freeze-thaw was done at the point of thawing is about 0.010. However, if the water being measured was kept in a thermal flask to prevent energy exchange with the local environment, no effect on pH value was observed during freeze-thaw treatment of remote water. Statistical analysis on data collected after freezing for 10 min show that the results are significantly different under the different treatments/settings shown.

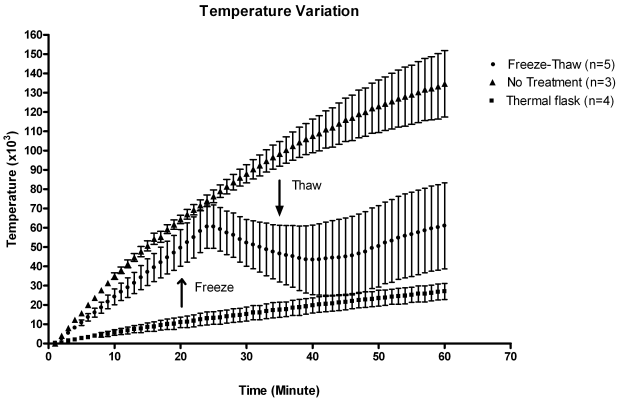

Fig. 4: Temperature variations under remote manipulations of water quantum-entangled with water being measured. The temperature at the starting point is set to zero and the results shown were obtained from one batch of quantum-entangled water. The temperature difference from control in which no freeze-thaw was done at the point of thawing is about 0.05°C. However, if the water being measured is kept in a thermal flask to prevent heat exchange with the local environment, no dropping of temperature were observed under freeze-thaw treatment. Statistical analysis performed on data collected after freezing for 10 min show that the results are significantly different under the different treatments/settings shown.

variation of the above first-setup, the 25-litre Dewar containing liquid nitrogen was replaced by a large water tank located 20-feet above the underground room which contained 200-gallon tap water sitting in room temperature for months and, instead of submersion, the water in the third-reservoir was poured into the large water tank the purpose of which was to quantum-entangle the poured water with the water in the large tank. In a fifth variation of the above setup, the gravity portion of the experiment was eliminated and the water in the first and second reservoirs was combined into a closed glass fourth-reservoir which was moved to a location more than 50 miles away from the Dewar for temperature measurement.

Figure 2 shows a diagram of the second experimental setup. It includes: (1) a red laser with a 50 mW output and wavelengths 635–675 nm placed next and pointed to a flat glass first-reservoir containing 200 ml tap water sitting in room temperature for more than a week without air exchange; (2) the calibrated pH meter and optionally the digital thermometer placed into the middle of the said flat glass reservoir which was closed to prevent air exchange; and (3) a round glass second-reservoir containing 100 ml concentrated HCl (38% by weight) to be placed 500 cm away from the first-reservoir at a specified time.

Experiments with the above second setup were carried out as follows: (1) prepare the 200 ml tap water and set up the experiment according Figure 2; turn on the laser so that the laser light first passes through the first-reservoir and then gets scattered on a nearby concrete wall, and let the instruments to stabilize for 30 min before any measurement is taken; (2) record for 10 min minute-by-minute changes of pH value and optionally temperature of the water in the first-reservoir; and (3) place the second reservoir containing 100 ml HCl on the path of the laser light and at a distance of 500 cm from the first reservoir and record for 60 min or longer instrument readings as before. Control experiments were carried out in same steps in the absence of HCl.

3 Results

Figures 3, 4 and 5 summarize the results obtained from experiments conducted with the key setup and one batch of quantum-entangled water which were simply bottled natural water with a shelf time of more than 90 days. Similar results were also obtained with water prepared according to other quantum entanglement methods mentioned above and other quantum-entangled liquid such as olive oil, alcohol and even Coca Cola as discussed later. The different distances of the Dewar from the underground room where most measurements were done made no noticeable differences with respect to the results obtained.

Figure 3 shows changes of pH value of the water in the second-reservoir during the three stages of manipulations of the water in the remote third-reservoir. As shown, within minutes after the remote third-reservoir was submerged into liquid nitrogen, during which the temperature of water being manipulated would drop from about 25°C to −193°C, the pH value of the water in the second reservoir steadily stopped dropping and then started rising, but about 20 min after the

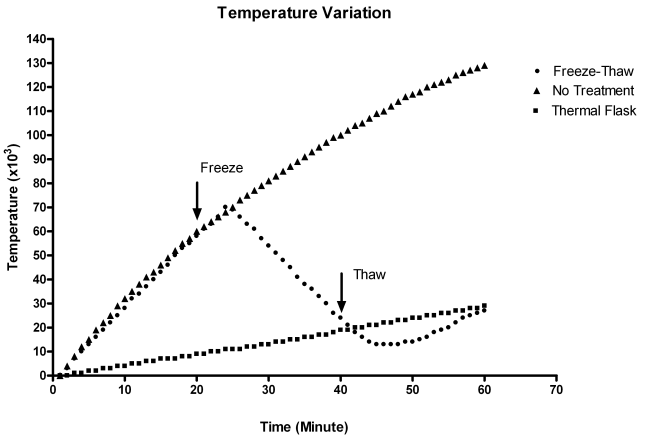

Fig 4A: One particular example detailing temperature variations under remote manipulation. The temperature difference from control at the point of thawing is about 0.08°C. However, if the water being measured is kept in a thermal flask, no dropping of temperature were observed under freeze-thaw treatment.

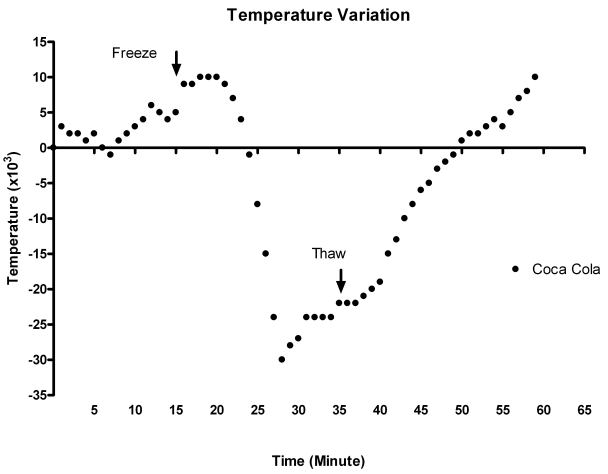

Fig 4B: One example showing temperature variation of a different liquid, Coca Cola, under remote manipulation of a portion of the said liquid quantum-entangled with another portion of the liquid being measured. Other liquids such as distilled water, olive oil and alcohol also showed similar qualitative results under the same treatment.

frozen water was taken out of liquid nitrogen and thawed in warm water the pH value of the same steadily levelled off and started dropping again. In contrast, the control experiments did not show such dynamics. It is known that the pH value of water increases as its temperature goes down to 0°C. Therefore, the pH value of water being measured goes in the same direction as the remote water when the latter is manipulated. The difference in pH values from control in which no freeze-thaw was done at the point of thawing is about 0.010. However, if the water being measured is kept in a thermal flask to prevent heat exchange with the local environment, no effect on pH value was observed under freeze-thaw treatment of the remote water. Statistical analysis performed on data collected after freezing for 10 minutes show that the results are significantly different under these different treatments/settings.

Figure 4 shows temperature variations of the water in the second-reservoir during the three stages of manipulations of the water in the remote third-reservoir. As shown, before the submersion of the remote third-reservoir into liquid nitrogen the temperature of the water in the second-reservoir rose in small increments due to, by design, the slight temperature difference between the local environment and the water inside the second reservoir; but within about 4–5 minutes after the remote third-reservoir was submerged into liquid nitrogen, during which the temperature of water being manipulated would drop from about 25°C to −193°C, the temperature of the water in the second reservoir first stopped rising and then steadily dropped in small increments; and then within about 4–5 minutes after the frozen water was taken out of liquid nitrogen and thawed in warm water the temperature of the same first stopped dropping and then steadily rose again in small increments. In contrast, the control experiments did not show such dynamics. The temperature difference from control in which no freeze-thaw was done at the point of thawing is about 0.05°C. However, if the water being measured is kept in a thermal flask to prevent heat exchange with the local environment, no dropping of temperature were observed under freeze-thaw treatment of the remote water. Statistical analysis performed on data collected after freezing for 10 minutes show that the results are significantly different under these different treatments/settings.

In addition, Figure 4A shows one particular example of temperature variations under remote manipulation of water quantum-entangled with water being measured. In this case, the temperature difference from control at the point of thawing is about 0.08°C. Further, Figure 4B shows one example of temperature variation of a different liquid, Coca Cola, under remote manipulation of a portion of the said liquid quantum-entangled with another portion being measured. Other liquids such as distilled water, olive oil and alcohol also showed similar qualitative results under the same freeze-thaw treatment. Furthermore, preliminary experiments conducted with the temperature measurement done at a location more than 50 miles way from the Dewar also show results similar to those obtained at distances of 50 and 500 feet respectively.

Figure 5 shows weight variations of the first reservation during the three stages of manipulation of the water in the remote third-reservoir. Before the submersion of the remote third-reservoir into liquid nitrogen the weight being measured drifted lower very slowly. But almost immediately after the remote third-reservoir was submerged into liquid nitrogen, during which the temperature and physical properties of water being manipulated drastically changed, the weight of the first-reservoir dropped at an increased rate, and after the

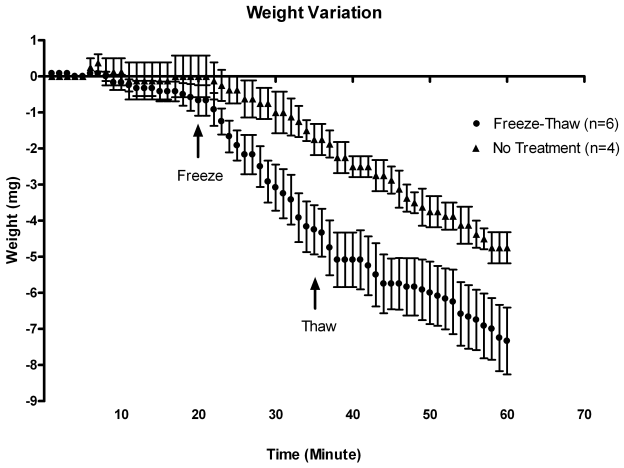

Fig 5: Weight variations under remote manipulations of water quantum-entangled with water being weighed. The weight at the starting point is set to zero and the results shown were obtained from one batch of quantum-entangled water. The weight differences from control in which no freeze-thaw was done at the point of thawing is about 2.5 mg. In some cases, the weight of the water being weighed not only briefly stop dropping for several minutes but also rose briefly for several seconds to minutes as shown in Figure5A. Also when the remote water was quickly heated to boiling on a stove instead of being frozen in liquid nitrogen, a brief rise of weight in the range of about 0.5 mg were repeated observed in one variation of the key setup. Further, when the remote water was poured into a 200-gallon water tank, small but noticeably increased weight losses were also observed in several experiments conducted to date. Statistical analysis performed on data collected after freezing for 10 min show that the results are significantly different under the different treatments/settings shown.

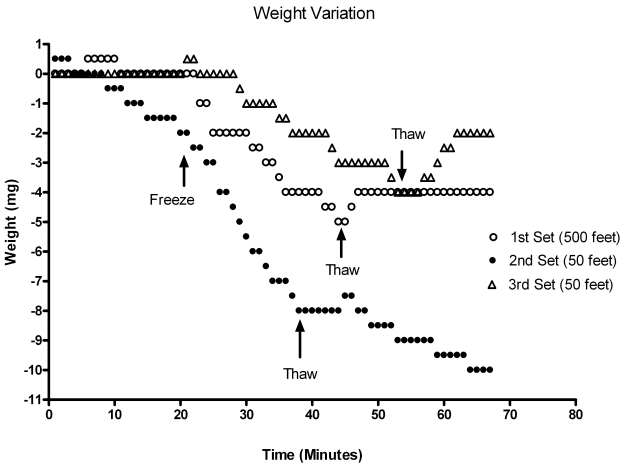

Fig 5A: Examples of weight variations under remote manipulations of water quantum-entangled with water being weighed. The onset of increased weight loss started either at the time of freezing treatment or slightly later. The signatures of thawing induced weight increases were clear for the three different thawing times. The distances shown are the respectively distances of the Dewar to the location of measurement in each experiment.

frozen water was taken out the liquid nitrogen and thawed in warm water the weight of the same first stopped dropping and, in some cases, even rose before resuming drifting lower as further discussed below. In contrast, the control experiments did not show such dynamics. The weight difference from control in which no freeze-thaw was done at the point of thawing is about 2.5 mg. Statistical analysis performed on data collected after freezing for 10 minutes show that the results are significantly different under these different treatments/settings.

As shown in Figure 5A, in some cases, the weight of the water being measured not only stopped dropping for several minutes but also rose. The signatures of freezing induced weight decreases and thawing induced weight increases for three different thawing times are very clear. In addition, Figure 5B shows one example of weight and temperature variations under the same remote manipulation of water quantum-entangled with water being weighed and measured respectively. Again, the signatures of freezing and thawing induced weight and temperature decreases and increases are respectively very clear. Further, Figure 5C shows another example of weight and temperature variations under another same remote manipulation in which the Dewar was located about 500 feet away from where the measurements were taken. The general background trend of decreasing temperature was due to environmental temperature change. Yet again, the signatures of freezing and thawing induced weight and temperature variations were respectively are very clear. Also, when the remote water was quickly heated to boiling on a stove instead of being frozen in liquid nitrogen, a brief rise of weight in the range of about 0.5 mg were repeated observed in several experiments conducted so far.

Furthermore, when the remote water was poured into the 200-gallon water tank instead of being frozen in liquid nitrogen, small but noticeably increased weight losses were repeatedly observed in the several experiments conducted to date. More specifically, before mixing of the water in the remote third-reservoir with water in the water tank the measured weight drifted lower very slowly, but within short time measured in minutes after the water in the remote third-reservoir was poured into the water tank, during which the water in the said tank got quantum-entangled with the water in the third-reservoir, the weight of the first-reservoir dropped at small but increased rate for a period of time. In contrast, the control experiments did not show such dynamics.

Figure 6 shows an example of temperature variations under the respective treatments of adding 5 ml concentrated HCl (38%) to the third reservoir, then adding 20 g NaOH to the same and third heating the same to boiling point. The signatures of these remote treatments induced temperature changes were clear and repeatedly observable in quite a few experiments conducted to date.

Figure 7 shows the variations of pH value of the water in

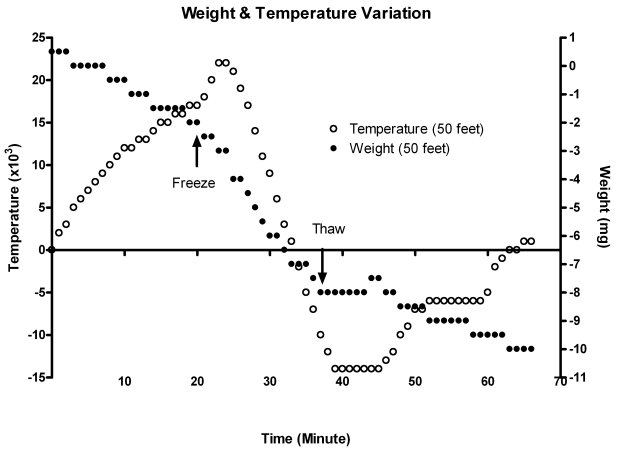

Fig 5B: One example of weight and temperature variations under the same remote manipulation of water quantum-entangled with water being weighed and measured respectively. The onset of increased weight loss started at the time of freezing treatment but the onset of temperature decrease against environmental temperature started a few minutes later after freezing treatment started. The signatures of thawing induced weight and temperature increases were clear. The distance shown is the distance of the Dewar to the location of measurement.

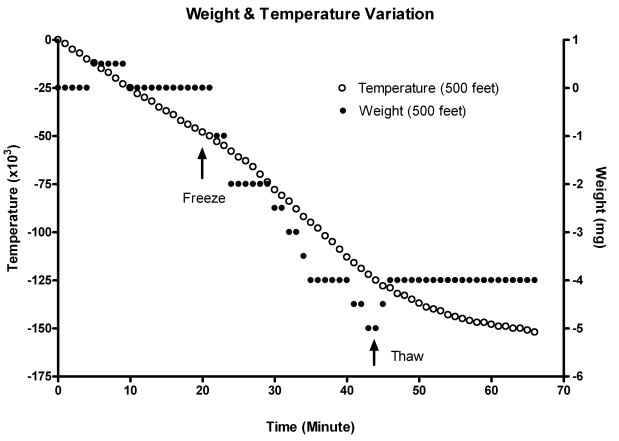

Fig 5C: Second example of weight and temperature variations under another same remote manipulation of water quantum-entangled with water being weighed and measured respectively. The general background trend of decreasing temperature was due to environmental temperature change. The onset of increased weight loss started at the time of freezing treatment but the onset of increased temperature loss started a few minutes later after freezing treatment started. The signatures of thawing induced weight increase and slow down of temperature loss were again clear. The distance shown is the distance of the Dewar to the location of measurement.

the first reservoir in experiments done with the setup in Figure 2. As shown, in about 30 min after the second-reservoir containing 100 ml concentrated HCl (38% by weight) was placed behind the first-reservoir at a distance of 500 cm and on the path of the laser beam, during which the water in the first-reservoir got quantum-entangled with the content in the second reservoir, the pH value of the water in the first-reservoir steadily decreased. In contrast, the control experiments did not show such dynamics. Also, the 50 mW red laser did not affect the temperature of the water in the first reservoir significantly during the whole treatment. The difference in pH value from control in which HCl was absence is about 0.070 after 50 min of exposure to HCl. Statistical analysis performed on data collected after exposure to HCl for 30 min show that the results are significantly different from control. Various experiments done with direct additions of HCl to the remote water also repeated showed decreases in pH value in the water being measured.

4 Discussions

With all experimental setups and their variations described herein, we have observed clear and reproducible non-local effects with the aids of high-precision analytical instruments and under well-controlled conditions. The physical observables used for measuring the non-local effects are simple ones which can be measured with high precisions. These effects are, even under the most stringent statistical analysis, significantly above and beyond what were noticeable in the control experiments.

Through careful analysis, we have likely excluded the possibility that the observed weight variation was a secondary local effect due to heat loss and/or sensitivity drift of balance associated with temperature change induced by the remote manipulation. First, during the period of remote manipulation the total temperature change was less than 0.08°C so the total heat loss for the 175 ml water in the first-reservoir is about 60 J. In contrast, the weight loss during remote manipulation was on average about 2.5 mg which is 22.5×10^9 J in energy unit. Second, the first-reservoir and the pan of the balance were separated by 1-inch white foam to prevent heat transfer to the analytic balance. Even in the highly unlikely scenario that this temperature change somehow affected the overall temperature of the balance, the associated sensitivity drift of the balance was about 0.03 mg which is 10 times smaller than what's actually observed. In addition, Figures 5A, 5B and 5C also show several other signatures of remote freeze-thaw treatment as the sole cause of the observed weight variations. Therefore, we cautiously suggest that the observed gravity variation is a genuine and direct non-local effect associated with quantum entanglement. However, as with many other important new results, replications by others are the key to independently confirm our results reported here.

We chose to use liquid nitrogen in a large Dewar placed at a distant location for manipulating water in our experiments because it can provide drastic changes in temperature and properties of water in a very short period of time. Our expectation was that, if the quantum entities inside the water being measured are able to sense the changes experienced by

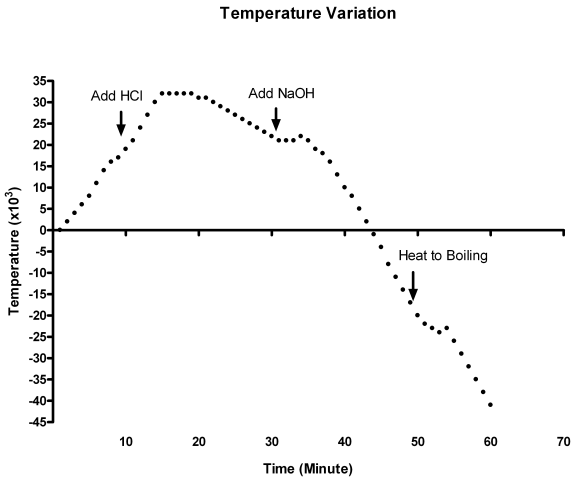

Fig 6: An example of temperature variations under the respective treatments of adding 5 ml concentrated HCl (38%) to the third reservoir, then adding 20 g NaOH to the same and third heating the same to boiling point. The signatures of these remote treatments induced temperature changes were clear and repeatedly observable in quite a few experiments conducted to date. The general background trend of the temperature first increasing, flattening and decreasing was due to environmental temperature change.

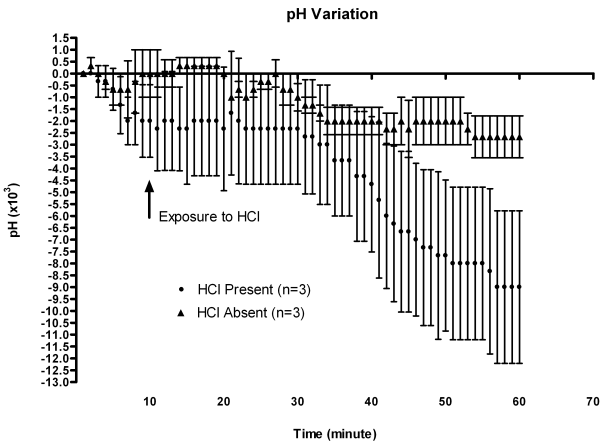

Fig 7: pH variations under laser treatment in the presence and absence of concentrated HCl with the setup in Figure 2. The pH value at the starting point is set to zero. The difference in pH value from control in which HCl was absence is about 0.07 after 50 min of exposure to HCl. Various experiments done with direct additions of HCl to the remote water also repeated showed decreases in pH value in the water being measured. Statistical analysis performed on data collected after exposure to HCl for 30 min show that the results are significant different from control.

the quantum entities in the water being manipulated through quantum entanglement and further utilize the information associated with the said changes, the chemical, thermal and even possibly gravitational properties of the water might be affected through quantum entanglement mediated non-local processes [5, 6]. The most logical explanation for these observed non-local effects is that they are the consequences of non-local processes mediated by quantum entanglement between quantum entities in the water being measured and the remote water being manipulated as more specifically illustrated below.

First, when pH value of the water in the manipulation reservoir is high or low or is changing under direct manipulation such as extreme cooling or heating or addition of acidic or alkaline chemical, the measured pH in the detecting reservoir shifts in the same direction under the non-local influence of the water in the manipulation reservoir mediated through quantum entanglement and, under the condition that the detecting reserve is able to exchange energy with its local environment, as if H+ in the latter is directly available to water in the detecting reservoir.

Second, when the temperature in the manipulation reservoir is extremely low or high or is changing under direct manipulation such as extreme cooling or heating or addition of heat-generating and/or property-changing chemical such as concentrated HCl or NaOH powder, the temperature in the detecting reservoir changes in the same direction under non-local influence of the water in the manipulation reservoir mediated through quantum entanglement and, under the condition that the detecting reserve is able to exchange heat with its local environment so that the local thermodynamic energy is conserved, as if the heat or lack of it in manipulation reservoir is directly available to the water in the detecting reservoir.

Third, when water in manipulation reservoir is manipulated though extreme cooling, heating or mixing with large quantum-entangled mass, e.g., water, such that, it is hereby cautiously suggested, the quantum entanglement of the water under manipulation with its local environment changes, the weight of the water in the detecting reservoir also changes under the presumed non-local influence of the manipulation reservoir mediated through quantum entanglement. However, independent and vigorous replications should be carried out before a definite conclusion is drawn.

We suggest here that the said quantum entities inside water are likely nuclear spins for the reasons discussed below. Water contains vast numbers of nuclear spins carried by 1H. These spins form complex intra- and inter-molecular networks through various intra-molecular J- and dipolar couplings and both short- and long-range intermolecular dipolar couplings. Further, nuclear spins have relatively long relaxation times after excitations [8]. Thus, when a nematic liquid crystal is irradiated with multi-frequency pulse magnetic fields, its 1H spins can form long-lived intra-molecular quantum coherence with entanglement for information storage [9]. Long-lived entanglement of two macroscopic electron spin ensembles in room temperature (0.05 ms) has also been achieved [1]. Furthermore, spin is a fundamental quantum process and was shown to be responsible for the quantum effects in both Hestenes and Bohmian quantum mechanics

[10, 11]. Thus, we suggest that quantum-entangled nuclear spins and/or electron spins are likely the mediators of all observed non-local effects reported here [5, 6].

5 Conclusions

Several important conclusions can be drawn from our findings. First, we have realized non-local signalling using three different physical observables, pH value, temperature and apparently gravity. Second, we have shown that the temperature of water in a detecting reservoir quantum entangled with water in a remote reservoir can change against the temperature of its local environment when the latter is manipulated under the condition that the water the detecting reservoir is able to exchange heat with its local environment. Third, we have also shown that the gravity of water in a detecting reservoir quantum entangled with water in a remote reservoir apparently also change when the latter was remotely manipulated. Our findings imply that the properties of all matters can be affected non-locally through quantum entanglement mediated processes.

Finally, with respect applications, our findings enable various quantum entanglement assisted technologies be developed. Some of these technologies can be used to manipulate and/or affect remotely various physical, chemical and/or biological systems including human bodies. Other such technologies can be used for non-local signalling and communications between remote locations of arbitrary distances in various ways. Potentially, other novel and practical applications can also be developed based on our experimental findings.

Acknowledgements

We wish to thank Yongchang Hu for assisting the authors with some of the experiments and Danielle Graham for showing her research at a 2006 conference.

Submitted on November 16, 2006
Re-submitted after revision on November 23, 2006
Accepted on November 30, 2006

References

1. Julsgaard B., Kozhekin A., Polzik E. S. Experimentally long-lived entanglement of two macroscopic objects. *Nature*, 2001, v. 413, 400–403.
2. Ghosh S., Rosenbaum T. F., Aeppli G., Coppersmith S. N. Entangled quantum state of magnetic dipoles. *Nature*, 2003, v. 425, 48–51.
3. Matsukevich D. N. and Kuzmich A. Quantum state transfer between matter and light. *Science*, 2004, v. 306, 663–666.
4. Chanelière T. et al. Storage and retrieval of single photons transmitted between remote quantum memorie. *Nature*, 2005, v. 438, 833–836.
5. Hu H. P. and Wu M. X. Nonlocal effects of chemical substances on the brain produced through quantum entanglement. *Progress in Physics*, 2006, v. 3 , 20–26; *NeuroQuantology*, 2006, v. 4, 17–31.
6. Hu H. P. and Wu M. X. Thinking outside the box: the essence and imications of quantum entanglement. *NeuroQuantology*, 2006, v. 4, 5–16; Cogprints: ID4581.
7. Eberhard P. Bell's theorem and the different concepts of locality. *Nuovo Cimento*, 2004, v. 46B, 392–419.
8. Gershenfeld N. and Chuang I. L. Bulk spin resonance quantum computation. *Science*, 1997, v. 275, 350–356.
9. Khitrin A. K., Ermakov V. L., Fung B. M. Information storage using a cluster of dipolar-coupled spins. *Chem. Phys. Lett.*, 2002, v. 360, 160–166.
10. Hestenes D. Quantum mechanics from self-interaction. *Found. Phys.*, 1983, v. 15, 63–78.
11. Salesi G. and Recami E. Hydrodynamics of spinning particles. *Phys. Rev.*, 2004, v. A57, 98–105.

On Line-Elements and Radii: A Correction

Stephen J. Crothers

Queensland, Australia
E-mail: thenarmis@yahoo.com

Using a manifold with boundary various line-elements have been proposed as solutions to Einstein's gravitational field. It is from such line-elements that black holes, expansion of the Universe, and big bang cosmology have been alleged. However, it has been proved that black holes, expansion of the Universe, and big bang cosmology are not consistent with General Relativity. In a previous paper disproving the black hole theory, the writer made an error which, although minor and having no effect on the conclusion that black holes are inconsistent with General Relativity, is corrected herein for the record.

1 Introduction

In a previous paper [1] (see page 8 therein) the writer made the following claim:

"*the ratio* $\frac{\chi}{R_p} > 2\pi$ *for all finite* R_p"

where R_p is the proper radius and χ is the circumference of a great circle. This is not correct. In fact, the ratio $\frac{\chi}{R_p}$ is greater than 2π for some values of R_p and is less than 2π for other values of R_p. Furthermore, there is a value of χ for which $\frac{\chi}{R_p} = 2\pi$, thereby making $R_p = R_c$, where R_c is the radius of curvature. Thus, if the transitional value of the circumference of a great circle is χ_e, then

$$\chi < \chi_e \Rightarrow \frac{\chi}{R_p} > 2\pi,$$

$$\chi = \chi_e \Rightarrow \frac{\chi}{R_p} = 2\pi,$$

$$\chi > \chi_e \Rightarrow \frac{\chi}{R_p} < 2\pi.$$

2 Correction — details

Consider the general static vacuum line-element

$$ds^2 = A(r)dt^2 - B(r)dr^2 - C(r)\left(d\theta^2 + \sin^2\theta\, d\varphi^2\right), \quad (1)$$

$$A(r), B(r), C(r) > 0.$$

It has been shown in [1] that the solution to (1) is

$$ds^2 = \left(1 - \frac{\alpha}{\sqrt{C(r)}}\right)dt^2 - \frac{1}{1 - \frac{\alpha}{\sqrt{C(r)}}}\, d\sqrt{C(r)}^2 - C(r)\left(d\theta^2 + \sin^2\theta\, d\varphi^2\right), \quad (2)$$

$$\alpha < \sqrt{C(r)} < \infty,$$

where, using $c = G = 1$,

$$R_c = R_c(r) = \sqrt{C(r)} = \left(\left|r - r_0\right|^n + \alpha^n\right)^{\frac{1}{n}},$$

$$R_p = R_p(r) = \sqrt{R_c(r)\left(R_c(r) - \alpha\right)} + \alpha \left|\frac{R_c(r) + \sqrt{R_c(r) - \alpha}}{\sqrt{\alpha}}\right|, \quad (3)$$

$$r \in \Re, \quad n \in \Re^+, \quad r \neq r_0,$$

and where r_0 and n are entirely arbitrary constants, and α is a function of the mass M of the source of the gravitational field: $\alpha = \alpha(M)$. Clearly, $\lim_{r \to r_0^{\pm}} R_p(r) = 0^+$ and also $\lim_{r \to r_0^{\pm}} R_c(r) = \alpha^+$ irrespective of the values of r_0 and n. Usually $\alpha = 2m \equiv 2GM/c^2$ by means of a comparision with the Newtonian potential, but this identification is rather dubious.

Setting $R_p = R_c$, one finds that this occurs only when

$$R_c \approx 1.467\alpha.$$

Then

$$\chi_e \approx 2.934\pi\alpha.$$

Thus, at χ_e the Euclidean relation $R_p = R_c$ holds. This means that when $\chi = \chi_e$ the line-element takes on a Euclidean character.

An analogous consideration applies for the case of a point-mass endowed with charge or with angular momentum or with both. In those cases α is replaced with the corresponding constant, as developed in [2].

3 Summary

The circumference of a great circle in Einstein's gravitational field is given by

$$\chi = 2\pi R_c,$$

$$2\pi\alpha < \chi < \infty.$$

In the case of the static vacuum field, the great circle with circumference $\chi = \chi_e \approx 2.934\,\pi\alpha$ takes on a Euclidean character in that $R_p = R_c \approx 1.467\,\alpha$ there, and so χ_e marks a transition from spacetime where $\frac{\chi}{R_p} < 2\pi$ to spacetime where $\frac{\chi}{R_p} > 2\pi$. Thus,

$$\lim_{r\to\infty^{\pm}} \frac{\chi}{R_p(r)} = 2\pi,$$

$$\lim_{r\to r_0^{\pm}} \frac{\chi}{R_p(r)} = \infty\,,$$

$$\lim_{\chi\to\chi_e^{\pm}} \frac{\chi}{R_p(r)} = 2\pi.$$

Similar considerations must be applied for a point-mass endowed with charge, angular momentum, or both, but with α replaced by the corresponding constant β in the expression for R_p [2],

$$\beta = \frac{\alpha}{2} + \sqrt{\frac{\alpha^2}{4} - (q^2 + a^2\cos^2\theta)}\,,$$

$$q^2 + a^2 < \frac{\alpha^2}{4}\,, \qquad a = \frac{2L}{\alpha}\,,$$

where q is the charge and L is the angular momentum, and so

$$R_c = R_c(r) = \left(\left|r - r_0\right|^n + \beta^n\right)^{\frac{1}{n}},$$

$$r \in \Re, \quad n \in \Re^+, \quad r \neq r_0,$$

where both r_0 and n are entirely arbitrary constants.

Submitted on December 26, 2006
Accepted on January 06, 2007

References

1. Crothers S. J. On the geometry of the general solution for the vacuum field of the point-mass. *Progress in Physics*, 2005, v. 2, 3–14.
2. Crothers S. J. On the ramifications of the Schwarzschild space-time metric. *Progress in Physics*, 2005, v. 1, 74–80.

Relativistic Cosmology Revisited

Stephen J. Crothers
Queensland, Australia
E-mail: thenarmis@yahoo.com

In a previous paper the writer treated of particular classes of cosmological solutions for certain Einstein spaces and claimed that no such solutions exist in relation thereto. In that paper the assumption that the proper radius is zero when the line-element is singular was generally applied. This general assumption is unjustified and must be dropped. Consequently, solutions do exist in relation to the aforementioned types, and are explored herein. The concept of the Big Bang cosmology is found to be inconsistent with General Relativity.

1 Introduction

In a previous paper [1] the writer considered what he thought was a general problem statement in relation to certain Einstein spaces, and concluded that no such solutions exist for those types. However, the problem statement treated in the aforementioned paper adopted an unjustified assumption — that the proper radius is zero when the line-element is singular. Although this occurs in the case of the gravitational field for $R_{\mu\nu}=0$, it is not a general principle and so it cannot be generally applied, even though it can be used to amplify various errors in the usual analysis of the well known cosmological models, as done in [1]. By dropping the assumption it is found that cosmological solutions do exist, but none are consistent with the alleged Big Bang cosmology.

2 The so-called "Schwarzschild — de Sitter model"

Consider the line-element

$$ds^2 = \left(1-\frac{\alpha}{R_c}-\frac{\lambda}{3}R_c^2\right)dt^2 - \\ -\left(1-\frac{\alpha}{R_c}-\frac{\lambda}{3}R_c^2\right)^{-1}dR_c^2 - R_c^2\left(d\theta^2+\sin^2\theta\, d\varphi^2\right), \tag{1}$$

where $R_c = R_c(r)$ is the radius of curvature, r a parameter, and α a function of mass. This has no solution for some function $R_c(r)$ on $R_c(r)\to\infty$ [1].

If $\alpha = 0$, (1) reduces to

$$ds^2 = \left(1-\frac{\lambda}{3}R_c^2\right)dt^2 - \\ -\left(1-\frac{\lambda}{3}R_c^2\right)^{-1}dR_c^2 - R_c^2\left(d\theta^2+\sin^2\theta\, d\varphi^2\right). \tag{2}$$

This has no solution for some function $R_c(r)$ on values $\sqrt{\frac{3}{\lambda}} < R_c(r) < \infty$ [1].

For $1-\frac{\lambda}{3}R_c^2 > 0$ and $R_c \geqslant 0$, it is required that

$$0 \leqslant R_c < \sqrt{\frac{3}{\lambda}}. \tag{3}$$

The proper radius on (2) is

$$R_p = \int \frac{dR_c}{\sqrt{1-\frac{\lambda}{3}R_c^2}} = \sqrt{\frac{3}{\lambda}}\,\arcsin\sqrt{\frac{\lambda}{3}}\,R_c^2 + K,$$

where K is a constant. $R_p = 0$ is satisfied if $R_c = 0 = K$, in accord with (3). Then

$$R_p = \sqrt{\frac{3}{\lambda}}\,\arcsin\sqrt{\frac{\lambda}{3}}\,R_c^2.$$

Now

$$\sqrt{\frac{3}{\lambda}}\,\arcsin 1 = \sqrt{\frac{3}{\lambda}}\,\frac{(1+4n)\,\pi}{2} = \\ = \lim_{R_c\to\sqrt{\frac{3}{\lambda}}^-}\sqrt{\frac{3}{\lambda}}\,\arcsin\sqrt{\frac{\lambda}{3}}\,R_c = \lim_{R_c\to\sqrt{\frac{3}{\lambda}}^-}R_p, \tag{4}$$
$$n = 0, 1, 2, \ldots$$

in accord with (3). Thus, R_p can be arbitrarily large. Moreover, R_p can be arbitrarily large for any R_c satisfying (3) since

$$R_p = \sqrt{\frac{3}{\lambda}}\,\arcsin\sqrt{\frac{\lambda}{3}}\,R_c = \sqrt{\frac{3}{\lambda}}\,(\psi+2n\pi), \\ n = 0, 1, 2, \ldots$$

where ψ is in radians, $0 \leqslant \psi < \frac{\pi}{2}$.

In the case of (1), the mutual constraints on the radius of curvature are

$$\frac{\lambda}{3}R_c^3 - R_c + \alpha < 0 \\ 0 < R_c(r). \tag{5}$$

The proper radius on (1) is

$$R_p(r) = \int \frac{dR_c}{\sqrt{1-\frac{\alpha}{R_c}-\frac{\lambda}{3}R_c^2}} + K, \tag{6}$$

where K is a constant, subject to $R_p \geqslant 0$. The difficulty here is the cubic in (5) and (6). The approximate positive roots to the cubic are α and $\sqrt{\frac{3}{\lambda}}$. These must correspond

to limiting values in the integral (6). Both $R_c(r)$ and $R_p(r)$ also contain α and λ.

In addition, it was argued in [1] that the admissible form for $R_c(r)$ in (1) must reduce, when $\lambda = 0$, to the Schwarzschild form

$$R_c(r) = \left(|r - r_0|^n + \alpha^n\right)^{\frac{1}{n}} \qquad n \in \Re^+, \quad r \in \Re, \quad r \neq r_0\,, \tag{7}$$

where r_0 and n are entirely arbitrary constants. Note that when $\alpha = 0$ and $\lambda = 0$, (1) reduces to Minkowski space and (7) reduces to the radius of curvature in Minkowski space, as necessary.

Determination of the required general parametric expression for $R_c(r)$ in relation to (1), having all the required properties, is not a simple problem. Numerical methods suggest however [1], that there may in fact be no solution for $R_c(r)$ in relation to (1), subject to the stated constraints. At this time the question remains open.

3 Einstein's cylindrical model

Consider the line-element

$$ds^2 = dt^2 - \left[1 - (\lambda - 8\pi P_0)\, R_c^2\right]^{-1} dR_c^2 - R_c^2\left(d\theta^2 + \sin^2\theta\, d\varphi^2\right). \tag{8}$$

This of course has no Lorentz signature solution in $R_c(r)$ for $\frac{1}{\sqrt{\lambda - 8\pi P_0}} < R_c(r) < \infty$ [1].

For $1 - (\lambda - 8\pi P_0)\, R_c^2 > 0$ and $R_c = R_c(r) \geqslant 0$,

$$0 \leqslant R_c < \frac{1}{\sqrt{\lambda - 8\pi P_0}}. \tag{9}$$

The proper radius is

$$R_p = \int \frac{dR_c}{\sqrt{1 - (\lambda - 8\pi P_0)\, R_c^2}} = = \frac{1}{\sqrt{\lambda - 8\pi P_0}} \arcsin\sqrt{(\lambda - 8\pi P_0)\, R_c^2} + K,$$

where K is a constant. $R_p = 0$ is satisfied for $R_c = 0 = K$, so that

$$R_p = \frac{1}{\sqrt{\lambda - 8\pi P_0}} \arcsin\sqrt{(\lambda - 8\pi P_0)\, R_c^2}\,,$$

in accord with (9).

Now

$$\frac{1}{\sqrt{\lambda - 8\pi P_0}} \arcsin 1 = \frac{(1 + 4n)\,\pi}{2\sqrt{\lambda - 8\pi P_0}} = = \lim_{R_c \to \frac{1}{\sqrt{\lambda - 8\pi P_0}}{}^-} \frac{1}{\sqrt{\lambda - 8\pi P_0}} \arcsin\sqrt{(\lambda - 8\pi P_0)\, R_c^2} \qquad n = 0, 1, 2, \ldots$$

in accord with (9). Thus R_p can be arbitrarily large. Moreover, R_p can be arbitrarily large for any R_c satisfying (9), since

$$R_p = \frac{1}{\sqrt{\lambda - 8\pi P_0}} \arcsin\sqrt{(\lambda - 8\pi P_0) R_c^2} = \frac{(\psi + 2n\pi)}{\sqrt{\lambda - 8\pi P_0}}\,, \qquad n = 0, 1, 2, \ldots$$

where ψ is in radians, $0 \leqslant \psi < \frac{\pi}{2}$.

4 De Sitter's spherical model

Consider the line-element

$$ds^2 = \left(1 - \frac{\lambda + 8\pi\rho_{00}}{3} R_c^2\right) dt^2 - \left(1 - \frac{\lambda + 8\pi\rho_{00}}{3} R_c^2\right)^{-1} dR_c^2 - R_c^2\left(d\theta^2 + \sin^2\theta\, d\varphi^2\right). \tag{10}$$

This has no Lorentz signature solution in some $R_c(r)$ on $\sqrt{\frac{3}{\lambda + 8\pi\rho_{00}}} < R_c(r) < \infty$ [1].

For $1 - \frac{\lambda + 8\pi\rho_{00}}{3} R_c^2 > 0$ and $R_c = R_c(r) \geqslant 0$,

$$0 \leqslant R_c < \sqrt{\frac{3}{\lambda + 8\pi\rho_{00}}}\,. \tag{11}$$

The proper radius is

$$R_p = \int \frac{dR_c}{\sqrt{\left(1 - \frac{\lambda + 8\pi\rho_{00}}{3}\right) R_c^2}} = = \sqrt{\frac{3}{\lambda + 8\pi\rho_{00}}} \arcsin\sqrt{\left(\frac{\lambda + 8\pi\rho_{00}}{3}\right) R_c^2} + K,$$

where K is a constant. $R_p = 0$ is satisfied for $R_c = 0 = K$, so

$$R_p = \sqrt{\frac{3}{\lambda + 8\pi\rho_{00}}} \arcsin\sqrt{\left(\frac{\lambda + 8\pi\rho_{00}}{3}\right) R_c^2}\,,$$

in accord with (11).

Now

$$\sqrt{\frac{3}{\lambda + 8\pi\rho_{00}}} \arcsin 1 = \sqrt{\frac{3}{\lambda + 8\pi\rho_{00}}} \frac{(1 + 4n)\,\pi}{2} = = \lim_{R_c \to \sqrt{\frac{3}{\lambda + 8\pi\rho_{00}}}{}^-} \sqrt{\frac{3}{\lambda + 8\pi\rho_{00}}} \arcsin\sqrt{\left(\frac{\lambda + 8\pi\rho_{00}}{3}\right) R_c^2}\,, \qquad n = 0, 1, 2, \ldots$$

in accord with (11). Thus R_p can be arbitrarily large. Moreover, R_p can be arbitrarily large for any R_c satisfying (11), since

$$R_p = \sqrt{\frac{3}{\lambda + 8\pi\rho_{00}}} \arcsin\sqrt{\left(\frac{\lambda + 8\pi\rho_{00}}{3}\right) R_c^2} = = \sqrt{\frac{3}{\lambda + 8\pi\rho_{00}}}\,(\psi + 2n\pi)\,, \qquad n = 0, 1, 2, \ldots$$

where ψ is in radians, $0 \leqslant \psi < \frac{\pi}{2}$.

5 Cosmological models of expansion

Transform (10) by

$$\bar{R}_c = \frac{R_c}{\sqrt{1-\frac{R_c^2}{W^2}}}\, e^{-\frac{t}{W}}, \quad \bar{t} = t + \frac{1}{2} W \ln\left(1-\frac{R_c^2}{W^2}\right),$$

$$W^2 = \frac{3}{\lambda + 8\pi\rho_{00}},$$

to get

$$ds^2 = d\bar{t}^2 - e^{\frac{2\bar{t}}{W}}\left(d\bar{R}_c^2 + \bar{R}_c^2 d\theta^2 + \bar{R}_c^2 \sin^2\theta\, d\varphi^2\right), \quad (12)$$

where according to (11), $0 \leqslant \bar{R}_c < \infty$. Clearly the proper radius on (12) is

$$\bar{R}_p = \lim_{\bar{R}_c\to\infty} e^{\frac{\bar{t}}{W}} \int_0^{\bar{R}_c} d\bar{R}_c = \infty\,,$$

therefore (12) describes an infinite Universe for all $\bar{t}$.

Consider the line-element

$$ds^2 = dt^2 - \frac{e^{g(t)}}{\left(1+\frac{k}{4}G^2\right)^2}\left[dG^2 + G^2(d\theta^2 + \sin^2\theta d\varphi^2)\right], \quad (13)$$

where $G = G(r)$, r a parameter. If $k = 0$ a form of (12) is obtained. If $k > 0$,

$$R_p = e^{\frac{1}{2}g(t)} \int \frac{dG}{1+\frac{k}{4}G^2} = e^{\frac{1}{2}g(t)}\left[\frac{2}{\sqrt{k}} \arctan\frac{\sqrt{k}}{2} G + K\right],$$

where K is a constant. $R_p = 0$ is satisfied by $G = 0 = K$, so

$$R_p = e^{\frac{1}{2}g(t)} \int \frac{dG}{1+\frac{k}{4}G^2} = e^{\frac{1}{2}g(t)} \frac{2}{\sqrt{k}} \arctan\frac{\sqrt{k}}{2} G.$$

Now for (13), the radius of curvature is

$$R_c = \frac{G}{1+\frac{k}{4}G^2}\,, \quad (14)$$

which is maximum when $G = \frac{2}{\sqrt{k}}$, i. e.

$$R_{c_{max}} = R_c\left(\frac{2}{\sqrt{k}}\right) = \frac{1}{\sqrt{k}}\,.$$

Also, $\lim_{G\to\infty} R_c = 0$. Therefore, on (13),

$$0 \leqslant R_c \leqslant \frac{1}{\sqrt{k}}\,, \quad (15)$$

or equivalently

$$0 \leqslant G \leqslant \frac{2}{\sqrt{k}}\,. \quad (16)$$

Now

$$R_p\left(G = \frac{2}{\sqrt{k}}\right) = e^{\frac{1}{2}g(t)} \arctan 1 = e^{\frac{1}{2}g(t)} \arctan 1 =$$

$$= e^{\frac{1}{2}g(t)} \frac{(1+4n)\,\pi}{4}, \qquad n = 0, 1, 2, \ldots$$

which is arbitrarily large. Moreover, R_p is arbitrarily large for any R_c satisfying (15), or equivalently for any G satisfying (16), since

$$R_p = e^{\frac{1}{2}g(t)} \frac{2}{\sqrt{k}}\,(\psi + n\pi)\,, \quad n = 0, 1, 2, \ldots$$

where ψ is in radians, $0 \leqslant \psi \leqslant \frac{\pi}{4}$.

If $k < 0$, set $k = -s$, $s > 0$. Then

$$R_p = e^{\frac{1}{2}g(t)} \int \frac{dG}{1+\frac{s}{4}G^2} = e^{\frac{1}{2}g(t)}\left[\frac{1}{\sqrt{s}} \ln\left|\frac{G+\frac{2}{\sqrt{s}}}{G-\frac{2}{\sqrt{s}}}\right| + K\right],$$

where K is a constant. $R_p = 0$ is satisfied for $G = 0 = K$. Then

$$R_p = e^{\frac{1}{2}g(t)} \frac{1}{\sqrt{s}} \ln\left|\frac{G+\frac{2}{\sqrt{s}}}{G-\frac{2}{\sqrt{s}}}\right|.$$

To maintain signature in (13),

$$-\frac{2}{\sqrt{s}} < G < \frac{2}{\sqrt{s}}\,.$$

However, since a negative radius of curvature is meaningless, and since on (13) the radius of curvature in this case is

$$R_c(G) = \frac{G}{1-\frac{s}{4}G^2}\,, \quad (17)$$

it is required that

$$0 \leqslant G < \frac{2}{\sqrt{s}}\,. \quad (18)$$

Now

$$\lim_{G\to\frac{2}{\sqrt{s}}^-} e^{\frac{1}{2}g(t)} \frac{1}{\sqrt{s}} \ln\left|\frac{G+\frac{2}{\sqrt{s}}}{G-\frac{2}{\sqrt{s}}}\right| = \infty,$$

in accord with (18). The proper radius of the space and the radius of curvature of the space are therefore infinite for all time t.

The usual transformation of (13) to obtain the Robertson-Walker line-element involves expressing (13) in terms of the radius of curvature of (13) instead of the quantity G, thus

$$\bar{G} = \frac{G}{1+\frac{k}{4}G^2}\,,$$

carrying (13) into

$$ds^2 = dt^2 - e^{g(t)}\left[\frac{d\bar{G}^2}{1-\frac{k}{4}\bar{G}^2} + \bar{G}^2\left(d\theta^2 + \sin^2\theta d\varphi^2\right)\right]. \quad (19)$$

If $k = 0$ a form of (12) is obtained.

Comparing $\bar{G}$ with (14) it is plain that $\bar{G} = R_c(G)$, where $0 \leqslant R_c \leqslant \frac{1}{\sqrt{k}}$ by (15), $k > 0$, and therefore $0 \leqslant \bar{G} \leqslant \frac{1}{\sqrt{k}}$. Now

$$R_p = e^{\frac{1}{2}g(t)} \int \frac{dR_c}{\sqrt{1-\frac{k}{4}R_c^2}} = e^{\frac{1}{2}g(t)}\left(\frac{2}{\sqrt{k}} \arcsin\frac{\sqrt{k}}{2} R_c + K\right),$$

where K is a constant. $R_p=0$ is satisfied for $R_c=0=K$, so

$$R_p = e^{\frac{1}{2}g(t)}\frac{2}{\sqrt{k}}\arcsin\frac{\sqrt{k}}{2}R_c\,,$$

in accord with (15).

Then

$$R_p\left(R_c=\frac{1}{\sqrt{k}}\right)=e^{\frac{1}{2}g(t)}\,\frac{2}{\sqrt{k}}\left(\frac{\pi}{6}+2n\pi\right), \qquad (20)$$
$$n=0,1,2,\ldots$$

in accord with (15), and so R_p is arbitrarily large for all time t. When making the transformation to the Robertson-Walker form the limits on the transformed coordinate cannot be ignored. Moreover, R_P is arbitrarily large for all time for any R_c satisfying (15), since

$$R_p = e^{\frac{1}{2}g(t)}\frac{2}{\sqrt{k}}\left(\psi+2n\pi\right), \qquad n=0,1,2,\ldots$$

where ψ is in radians, $0\leqslant\psi\leqslant\frac{\pi}{6}$.

If $k<0$ set $k=-s$ where $s>0$, then (19) becomes

$$ds^2=dt^2-e^{g(t)}\left[\frac{dR_c^2}{1+\frac{s}{4}R_c^2}+R_c^2\left(d\theta^2+\sin^2\theta\,d\varphi^2\right)\right]. \quad (21)$$

The proper radius is

$$R_p=e^{\frac{1}{2}g(t)}\int\frac{dR_c}{\sqrt{1+\frac{s}{4}R_c^2}}=e^{\frac{1}{2}g(t)}\left[\frac{2}{\sqrt{s}}\ln\left(R_c+\sqrt{R_c^2+\frac{4}{s}}\right)+K\right]$$

where K is a constant. $R_p=0$ is satisfied for $R_c=0$ and $K=-\frac{2}{\sqrt{s}}\ln\frac{2}{\sqrt{s}}$, in accord with (17) and (18). So

$$R_p=e^{\frac{1}{2}g(t)}\,\frac{2}{\sqrt{s}}\ln\left(\frac{R_c+\sqrt{R_c^2+\frac{4}{s}}}{\frac{2}{\sqrt{s}}}\right).$$

Now $R_p\to\infty$ as $R_c\to\infty$, in accord with (17) and (18). Thus, (21) describes an infinite Universe for any time t.

6 Conclusions

By the foregoing types of spacetimes, General Relativity permits cosmological solutions, contrary to the claims made in [1]. However, the Big Bang theory is not consistent with General Relativity, since the spacetimes permitted are all spatially infinite (arbitrarily large) for any time t.

Submitted on January 13, 2007
Re-submitted after revision on January 18, 2007
Accepted on January 19, 2007

References

1. Crothers S. J. On the general solution to Einstein's vacuum field for the point-mass when $\lambda\neq0$ and its consequences for relativistic cosmology. *Progress in Physics*, 2005, v. 3, 7–14.

Cosmological Redshift Interpreted as Gravitational Redshift

Franklin Potter* and Howard G. Preston†

*Sciencegems.com, 8642 Marvale Dr., Huntington Beach, CA 92646, USA
†15 Vista del Sol, Laguna Beach, CA 92651, USA

E-mail: *drpotter@lycos.com and †hpres@cox.net

Distant redshifted SNe1a light sources from the Universe that are usually interpreted as cosmological redshifts are shown to be universal *gravitational* redshifts seen by all observers in the quantum celestial mechanics (QCM) approach to cosmology. The increasingly negative QCM gravitational potential dictates a non-linear redshift with distance and an apparent gravitational repulsion. No space expansion is necessary. QCM is shown to pass the test of the five kinematical criteria for a viable approach to cosmology as devised by Shapiro and Turner, so the role of QCM in understanding the behavior of the Universe may be significant.

1 Introduction

The observed redshift from distant sources can be interpreted as (1) a velocity redshift called the Doppler Effect, (2) a cosmological redshift in which space itself is expanding during the transit time of the photons, and/or (3) a gravitational redshift as introduced by the General Theory of Relativity (GTR). High-z redshifts from distant SNe1a light sources in galaxies are presently being interpreted as cosmological redshifts, apparently providing observational evidence for the expansion of the Universe.

A new theory, Quantum Celestial Mechanics(QCM), developed from GTR by H. G. Preston and F. Potter [1, 2], accurately predicts the observed SNe1a redshifts from near and distant galaxies. For the Universe, there exists in QCM a previously unknown gravitational potential that is used to derive all of the observed SNe1a redshifts. In addition, QCM predicts no mass currents in any coordinate direction, i.e., no galaxies moving away anywhere. These results eliminate the need for a space expansion. The presently known average baryonic density of the Universe is sufficient for QCM to explain the critical matter/energy density of the Universe.

Observations of galaxies and distributions of galaxies are beginning to suggest conflicts with the standard concept of an expanding Universe and its interpretation of a high-z redshift as a cosmological redshift. For example, galaxies at $z = 2.5$ are reported [3] to be extremely dense when using the expanding Universe assumptions and standard galaxy modeling. However, if the Universe is not expanding, the linear scales of these galaxies would be much larger, eliminating the high density conflict and revealing galaxies much similar to galaxies seen locally.

Theoretical approaches are also beginning to inquire about what we really know about cosmic expansion and its acceleration. In an interesting paper, C. A. Shapiro and M. S. Turner [4] relax the assumption of GTR but retain the weaker assumption of an isotropic and homogeneous space-time described by a metric theory of gravity. Using the Robertson-Walker metric to describe the Universe and accepting the dimming and redshifting of a gold set of SNe1a data [5], they determine the cosmic acceleration kinematically and provide a list of five kinematical criteria that must be met by any approach to cosmology.

In this paper, we compare the QCM predictions for the state of the Universe to the five criteria provided by Shapiro and Turner. Our new result is that QCM agrees with the five criteria. Therefore, SNe1a redshifts can be interpreted as universal *gravitational* redshifts instead of cosmological redshifts. There is no need for space expansion.

2 Reviewing the QCM potential

In a series of papers [1, 2, 6] we derived and applied QCM to the Solar System, to other solar system-like systems such as the satellites of the Jovian planets and exoplanet systems, to the Galaxy, to other galaxies in general, and to clusters of galaxies [7]. In all these cases there is reasonable agreement with the observational data, i.e., the predicted QCM states of the gravitationally-bound systems were shown to be actual states of the systems without the need for dark matter. Recall that the QCM general wave equation derived from the general relativistic Hamilton-Jacobi equation is approximated by a Schrödinger-like wave equation and that a QCM quantization state is completely determined by the system's total baryonic mass M and its total angular momentum H_Σ.

These agreements with the data strongly suggest that QCM applies universally and that all gravitationally-bound systems should obey the quantization conditions dictated by QCM. Therefore, not only should the large-scale gravitationally bound systems like a solar system exhibit QCM behavior, but even a torsion balance near an attractor mass should have quantization states. And the largest gravitationally-bound system of all, the Universe, should also be describable by QCM. The QCM states of a torsion bar system will be

discussed in a future paper. In this paper we concentrate on the QCM Universe.

For gravitationally-bound smaller systems, we found that the Schwarzschild metric approximation produced an efffective gravitational potential for a particle of mass μ in orbit

$$V_{\text{eff}} = -\frac{GM}{r} + \frac{l\,(l+1)\,H^2c^2}{2r^2}\,, \qquad (1)$$

where G is the gravitational constant, c is the speed of light in vacuum, the characteristic length scale $H = H_\Sigma/Mc$, the angular momentum quantization number l originates from the θ-coordinate symmetry, and r is the r-coordinate distance from the origin in spherical coordinates. Therefore, in QCM the total angular momentum squared is $l\,(l+1)\mu^2H^2c^2$ instead of the classical Newtonian expression. Consequently, the quantization of angular momentum dictates which particular circular orbit expectation values $<r>$ in QCM correspond to equilibrium orbital radii, in contrast to Newtonian gravitation for which all radii are equilibrium radii.

In the case of the Universe we used the GTR interior metric approximation, which is directly related to the general Robertson-Walker type of metric. Omitting small terms in the r-coordinate equation, we derived a new Hubble relation that agrees with the SNe1a data. At the same time we showed that our QCM approach produced the required average matter/energy density of about 2×10^{-11} J/m^3, corresponding to the critical density $\rho_c = 8\times10^{-27}$ kg$\times$m^{-3}, with only a 5% contribution from known baryonic matter, i.e., without needing dark energy.

The QCM effective gravitational potential for all observers inside a static dust-filled, constant density universe with no pressure is

$$V_{\text{eff}} \approx -\frac{kr^2c^2}{2\,(1-kr^2)^2} + \frac{l\,(l+1)H^2c^2}{2r^2(1-kr^2)}\,, \qquad (2)$$

where $k = 8\pi G\rho_c/3c^2$. Figure 1 shows this QCM gravitational potential for an r-coordinate distance up to about 10 billion light-years.

If the total angular momentum of the Universe is zero or nearly zero, H can be ignored and then the negative gradient of the first term in V_{eff} produces an average *positive* radial acceleration

$$<\ddot{r}> = kc^2\,\frac{r\,(1+kr^2)}{(1-kr^2)^3} \qquad (3)$$

from which we derive a new Hubble relation

$$<\dot{r}> = r\,\frac{c\sqrt{k}}{1-kr^2}\,. \qquad (4)$$

For r-coordinate distances up to about one billion light-years, when $kr^2 \ll 1$, we recover the standard Hubble relation and have a Hubble constant $h \sim 2\times10^{-18}$ s^{-1}, about 62 km per second per megaparsec, an acceptable value [8]. Without the kr^2 in the denominator, $v/c \to 1$ at about 14.1 billion light-years; otherwise, the maximum visible coordinate distance $r = 8.74$ billion light-years, with more of the Universe beyond this distance.

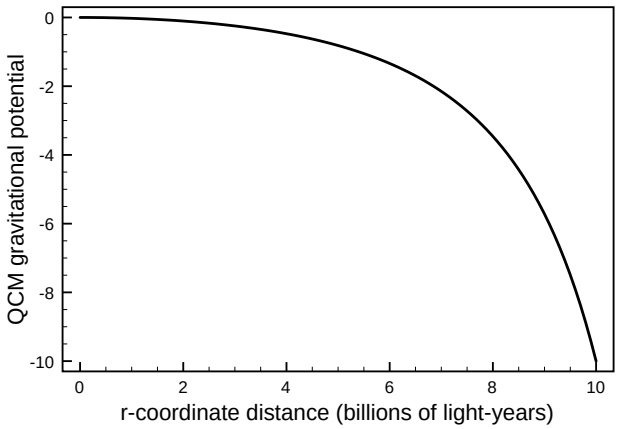

Fig. 1: QCM gravitational potential to 10 billion light-years.

Notice that the QCM effective gravitational potential is negative (when H can be ignored) but produces an apparent *repulsive* gravitational radial acceleration! Each observer anywhere in this Universe will determine that the incoming photons are redshifted. Why? Because the photons originate in a source that is in a more negative gravitational potential where the clock rates are slower than the clock rates at the observer. And this redshift increases non-linearly because the potential becomes more negative more rapidly with increasing distance away. There is no need for expansion of space and its cosmological redshift to explain the SNe1a data. There is no need for dark energy to explain the accelerated expansion.

3 The kinematical criteria

Our QCM approach to cosmology and an understanding of the behavior of the Universe must meet specific kinematical criteria. By analyzing the gold set of SNe1a data, Shapiro and Turner list these five kinematical criteria to be met by any viable approach to a cosmology:

1. Very strong evidence that the Universe once accelerated and that this acceleration is likely to have been relatively recent in cosmic history.
2. Strong evidence that the acceleration q was higher in the past and that the average dq/dz is positive, where z is the redshift.
3. Weak evidence that the Universe once decelerated, but this result may be a model-dependent feature.
4. Little or no evidence that the Universe is presently accelerating, i.e., it is difficult to constrain q for $z < 0.1$ with SNe1a data.
5. No particular models of the acceleration history provide more acceptable fits to the SNe1a data than any

others, i.e., several different kinematic models fit the data as well as the cold dark matter hypotheses called ΛCDM and wCDM.

The QCM effective gravitational potential V_{eff} and the new Hubble relation provide QCM explanations for these five criteria:

1. The light now just reaching us from farther and farther away exhibits an increasing redshift because the V_{eff} is increasingly more and more negative with increasing distance. Without QCM, the interpretation would be that the acceleration is recent.
2. The V_{eff} is increasingly more and more negative with increasing distance. Without QCM, a higher acceleration in the past is required for the space expansion approach to cosmology.
3. QCM shows no deceleration at the level of mathematical approximation we used.
4. The new Hubble relation of QCM reduces to the linear dependence of the standard Hubble relation for z small, agreeing with there being no acceleration presently.
5. Our QCM approach fits the SNe1a data as well as the other approaches, producing about a 12% increase from the linear Hubble when $kr^2 \sim 0.11$, consistent with the data.

QCM explains the five criteria in its unique way because the SNe1a redshift now originates in the properties of the static interior metric and its QCM gravitational potential. The important consequence is that QCM cannot be eliminated by any of the five criteria and must be considered as a viable approach to cosmology.

4 Final comments

The existence of a *repulsive* gravitational potential in the QCM wave equation for the Universe removes the necessity for invoking dark matter and dark energy. According to QCM, the Universe is not expanding and does not require dark energy in order for us to understand its behavior. Previously labelled cosmological redshifts are actually gravitational redshifts of the photons reaching us from distant sources in the Universe that are in greater negative gravitational potentials than the observer. Each and every observer experiences this same behavior. This static Universe is always in equilibrium.

Submitted on January 22, 2007
Accepted on January 24, 2007

References

1. Preston H. G. and Potter F. Exploring large-scale gravitational quantization without $\hbar$ in planetary systems, galaxies, and the Universe. arXiv: gr-qc/0303112.
2. Potter F. and Preston H. G. Quantum Celestial Mechanics: large-scale gravitational quantization states in galaxies and the Universe. *1st Crisis in Cosmology Conference: CCC-I*, Lerner E.J. and Almeida J.B., eds., AIP CP822, 2006, 239–252.
3. Zirm A. W. *et al.* NICMOS imaging of DRGs in the HDF-S: A relation between star-formation and size at $z \sim 2.5$. arXiv: astro-ph/0611245.
4. Shapiro C. A. and Turner M. S. What do we really know about cosmic acceleration? arXiv: astro-ph/0512586.
5. Riess A. G. *et al.* (Supernova Search Team). Observational evidence from supernovae for an accelerating universe and a cosmological constant. arXiv: astro-ph/9805201.
6. Potter F. and Preston H. G. Gravitational lensing by galaxy quantization states. arXiv: gr-qc/0405025.
7. Potter F. and Preston H. G. Quantization states of baryonic mass in clusters of galaxies. *Progress in Physics*, 2007, v. 1, 61–63.
8. Bonanos A. Z.*et al*. (DIRECT Project). The first DIRECT distance determination to a detached eclipsing binary in M33. arXiv: astro-ph/0606279.

Exact Solution of the Three-Body Santilli-Shillady Model of the Hydrogen Molecule

Raúl Pérez-Enríquez*, José Luis Marín† and Raúl Riera†

*Departamento de Física, Universidad de Sonora, Apdo. Postal 1626, Hermosillo 83000, Sonora, Mexico
E-mail: rpereze@fisica.uson.mx

†Departamento de Investigación en Física, Universidad de Sonora

The conventional representation of the H_2 molecule characterizes a 4-body system due to the independence of the orbitals of the two valence electrons as requested by quantum chemistry, under which conditions no exact solution is possible. To overcome this problem, Santilli and Shillady introduced in 1999 a new model of the H_2-molecule in which the two valence electrons are deeply bounded-correlated into a single quasi-particle they called isoelectronium that is permitted by the covering hadronic chemistry. They pointed out that their new H_2-model is a restricted 3-body system that, as such, is expected to admit an exact solution and suggested independent studies for its identification due to its relevance, e.g., for other molecules. In 2000, Aringazin and Kucherenko did study the Santilli-Shillady restricted 3-body model of the H_2 molecules, but they presented a variational solution that, as such, is not exact. In any case, the latter approach produced significant deviations from experimental data, such as a 19.6% inter-nuclear distance greater than the experimental value. In this paper we present, apparently for the first time, an exact solution of the Santilli-Shillady restricted 3-body model of the Hydrogen molecule along the lines of its originators and show that it does indeed represent correctly all basic data. Intriguingly, our solution confirms that the orbital of the isoelectronium (referred to as its charge distribution around the nuclei) must be concentrated in a limited region of space given by the Santilli-Shillady oo-shaped orbits. Our exact solution is constructed by following the Ley-Koo solution to the Schrödinger equation for a confined hydrogen molecular ion, H_2^+. We show that a confined model to the 3-body molecule reproduces the ground state curve as calculated by Kolos, Szalewics and Monkhorst with a precision up to the 4-th digit and a precision in the representation of the binding energy up to the 5-th digit.

1 Introduction

As it is well known, the conventional representation of the Hydrogen molecule characterizes a four-body system due to the independence of the orbitals of the two valence electrons as requested by quantum chemistry, under which conditions no exact solution is possible. To overcome this problem, R. M. Santilli and D. Shillady introduced in 1999 a new model of the H_2-molecule [1, 2], in which the two valence electrons are deeply bounded-correlated into a single quasi-particle they called isoelectronium that is permitted by the covering hadronic chemistry [3a].

They pointed out that their new model of Hydrogen molecule is a restricted three-body system that, as such, is expected to admit an exact solution; they suggested to carry out independent studies for its identification due to its relevance, e.g., for other molecules. In 2000, Aringazin and Kucherenko [4] did study the Santilli-Shillady restricted three-body model of the Hydrogen molecule, but they presented a variational solution that, as such, is not exact. In any case, the latter approach produced significant deviations from experimental data, such as a 19.6% inter-nuclear distance greater than the experimental value.

In this paper we present, apparently for the first time, an exact solution of the Santilli-Shillady restricted three-body model of the Hydrogen molecule along the lines of its originators and show that it does indeed represent correctly all basic data. Intriguingly, our solution confirms that the orbital of the isoelectronium (referred to as its charge distribution around the nuclei) must be concentrated in a limited region of space given by the Santilli-Shillady oo-shaped orbits. Our exact solution is constructed by following the E. Ley-Koo and A. Cruz solution to the Schrödinger equation for a confined hydrogen molecular ion, H_2^+ [5]. We show that a confined model to the three-body molecule reproduces the ground state curve as calculated by Kolos, Szalewics and Monkhorst [6] with a precision up to the 4-th digit and a precision in the representation of the binding energy up to the 5-th digit.

The suggestion that a kind of correlated state of electrons is present while they surround in closed paths the nuclei stimulates the search of a complementary quantum mechanical approach. In addition, Pérez-Enríquez [7], while working on high-Tc superconductivity, found that by using a Möbius-type orbital for Cooper pairs, there is a structural parameter in perovskite type superconductors that correlates linearly

with the critical temperature. Other contributions to the discussion about correlation between electrons were presented by Taut [8] in 1999. He reported that a one-particle representation could apply to systems with high densities of charge, based upon a pair-correlation function and density of charge for a system of two electrons in an external potential.

In our approach as it has been mentioned, we use the idea of a system under confinement as worked by E. Ley-Koo and A. Cruz for the hydrogen molecular ion and by other authors for molecules under pressure [9, 10]. Besides, previous studies related to the present discussion concerning hydrogenic impurities and excitons in quantum dots have been carried out by our team and others [11, 12, 13].

The main features of the restricted three-body Santilli-Shillady model, we discuss here, are summarized in section 2; special attention is drawn to the isoelectronium proposal. In this section, we also compare the results from this model with a standard ground state energy curve calculated by Kolos, Szalewics and Monkhorst (KSM curve) [6]. In section 3, we describe how to calculate the exact solution to the three-body model including a spheroidal confinement and a defect of mass parameters in order to reproduce the standard KSM curve, using a variational calculation. Finally, in section 4, some conclusions are made with regard to the accuracy of our results.

2 Iso-chemical model of the hydrogen molecule

The point of departure of the iso-chemical model of the hydrogen molecule, presented for the first time in 1999 by Santilli and Shillady [1], resides in the fact that the distance between nuclei is large; hence, the force binding them together comes form the orbiting electrons. The main hypothesis of the model describes how the valence electrons become involved in a binding process when they are at very short distance giving rise to a new state or quasi-particle, called isoelectronium. This particle would be responsible for the stability of the molecule and would describe a oo-shaped orbit around the nuclei "in a similar way as a planet orbits around binary stars" [1].

This hydrogen molecule model is forbidden by quantum mechanics and quantum chemistry since the proximity of electrons creates a repulsive Coulomb force between them; however, the authors assume that this difficulty can be overruled by a non-Hamiltonian interaction based on the overlapping of wave packets associated with each electron. This force surmounts the electrostatic one and allows the quasi-particle formation. They affirm that "the attractive force coming from the deep wave-overlapping does not have an equivalent in quantum mechanics and requires the new theory" [1]. This is the reason to introduce the so called iso-mechanics and iso-chemistry theories as part of hadronic mechanics [3b].

Our approach, however, uses the isoelectronium hypothesis and at the same time looks for a compatible state in the frame of quantum chemistry. We will show that there exists a state reproducing the ground state energy of the hydrogen molecule in the frame of the restricted three-body Santilli-Shillady model.

The two basic notions of hadronic chemistry that we need for understanding the iso-chemical model of the hydrogen molecule are:

(a) Hadronic horizon. The hadronic horizon is a distance between electrons, r_c, which measures one femtometer ($1\,\text{fm} = 10^{-15}\,\text{m}$). Outside this range quantum chemistry applies and within it hadronic chemistry is valid;

(b) The trigger, which is given by external (conventional) interactions, causes the identical electrons to move one toward the other and penetrate the hadronic horizon against Coulomb interaction (once inside the said horizon, the attractive hadronic force overcomes the repulsive Coulomb one), resulting in a bound state.

Santilli presented for the first time the hypothesis of a bound state between electrons in 1978 [3], while explaining the structure of a π^0 meson as a hadronic bound state of one electron and one positron. Later, Animalou [14] and Animalou and Santilli [15] extended the model to consider the Cooper pair in superconductivity as a hadronic bound state of two identical electrons.

According to Santilli, in the case of π^0 there is no need for a trigger because the involved particles have opposite charges. However, the existence of the Cooper pair requires a trigger, which Santilli and Animalou identified as the field of the copper ions. In the case of the hydrogen molecule, they conjecture that the trigger, constituted by the field between nuclei, is sufficiently intense (attractive for the electrons) enough to draw them together. They assume, essentially, that atom attraction is sufficient to cause the overlapping between wave packets, thus pushing electrons beyond the hadronic horizon.

2.1 Four-body Santilli-Shillady model

The iso-chemical model of the hydrogen molecule uses the conventional quantum model of the H_2 subject to a non-unitary transformation for the condition $r_c = r_{12}$. This inter electronic distance is small given that the electrons are inside the hadronic horizon. After using this transformation, one can reduce the problem to an equation that uses a Hulthén potential, recalling that at short distances, this behaves like a Coulomb potential,

$$\left\{-\frac{\hbar^2}{2\mu_1}\nabla_1^2-\frac{\hbar^2}{2\mu_2}\nabla_2^2-V_0\frac{e^{-r_{12}/r_c}}{1-e^{-r_{12}/r_c}}+\frac{e^2}{r_{12}}-\right.$$
$$\left.-\frac{e^2}{r_{1a}}-\frac{e^2}{r_{2a}}-\frac{e^2}{r_{1b}}-\frac{e^2}{r_{2b}}+\frac{e^2}{R}\right\}|\widehat{\psi}\rangle = E\,|\widehat{\psi}\rangle\,. \quad (1)$$

As Santilli and Shillady affirm, this equation exhibits a new explicitly attractive force among neutral atoms of the

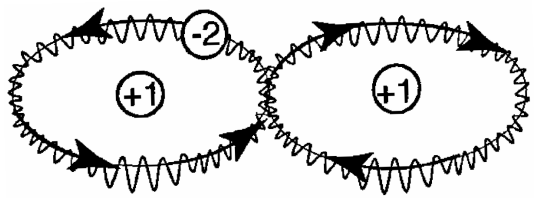

Fig. 1: Hydrogen molecule in the restricted three-body Santilli-Shillady model; a stable isoelectronium moves around nuclei in a oo-shaped orbit (figure taken from Santilli 1999, ref. [1]).

molecule in a way that is not possible within the quantum chemistry framework. They claim that Eq. (1) explains why only two hydrogen atoms make up the molecule and allows the exact representation of the binding energy in the full 4-body configuration.

A further simplification of the iso-chemical model can be introduced by making the two iso-electrons (electrons inside the hadronic horizon) be bound together into a state called isoelectronium as mentioned above. With this approximation, Equation (1) is reduced to a restricted three-body problem because one can consider $r_{1a} \approx r_{2a} = r_a$ and $r_{1b} \approx r_{2b} = r_a$ as $r_{12} \ll r_a, r_b$. In this manner, an exactly solvable problem similar to the conventional ion is obtained. One remarkable idea proposed by the authors consists in representing the isotopic model of the molecule as two H-protons at rest and the isoelectronium moving around them in a oo-shaped orbit, as it is shown in Figure 1 and described by the following structural equation:

$$\left\{ -\frac{\hbar^2}{2\mu_1}\nabla_1^2 - \frac{\hbar^2}{2\mu_2}\nabla_2^2 - V_0 \frac{e^{-r_{12}/r_c}}{1-e^{-r_{12}/r_c}} + \frac{e^2}{r_{12}} - \right. \\ \left. - \frac{2e^2}{r_a} - \frac{2e^2}{r_b} + \frac{e^2}{R} \right\} |\widehat{\psi}\rangle = E\,|\widehat{\psi}\rangle\,. \tag{2}$$

This simplification, impossible in a quantum chemistry environment, could be used to reach an exact solution of the H-molecule. At this point, it is worth mentioning that with the aid of this model, Santilli and Shillady extended their analysis to other molecules; in particular, they studied the hydrogen and oxygen atoms in order to form HO. This gave them elements to present, for the first time, an exact solution to the water molecule, treated as an HOH molecule, using an isotopic intersection of an HO and an OH [2]. They have further their research to extend their model to another type of molecular chains and molecules.

Results for the Santilli-Shillady model of molecular hydrogen were obtained by the standard Boys-Reeves model [1], using an attractive Gaussian-screened-Coulomb potential. These authors used their SASLOBE programme (Santilli-Animalou-Shillady LOBE) to calculate the energies reported in columns three and four of Table 1, which in turn are compared with the quantum chemical results (first column).

Results from Table 1 show that the energy calculated by the SASLOBE program (-1.174444 au) differs from the exact result in the 6th digit (a 3×10^{-5} error) with a 20 hours process time in a 320 MFLOPS Silicon Graphics computer. Notice that some changes in the most expensive routines in the iso-chemical model improve by a factor of 1000 the time used to compute a Boys-Reeves C.I. calculation. An important result is that with their method, they found a bound length ($R = 1.4011$ bohr) which coincides with that of the C.I. value.

Concept/species	H_2 [a)]	$\widehat{H}_2$ [b)]	$\widetilde{H}_2$ [c)]
Energy (variational)	-1.12822497	-7.61509174	*
Energy SCF (au)	1.14231305	*	-1.13291228
Energy SAS (au)	*	*	-1.174444
Energy exact[d)] (au)	-1.174474	*	-1.174474
Bond length (bohr)	1.4011	0.2592	1.4011
Isoelectronium radius (bohr)	*	*	0.01124995

Notes: [a)] Normal molecule in the quantum-chemical model
[b)] Molecule in the restricted three-body model (see)
[c)] Molecule in the iso-chemical model (stable isoelectronium)
[d)] Ground state energy by Kolos, Szalewicz and Monhorst

Table 1: Comparison of results from Iso-chemical model. Taken from Santilli 1999, ref. [1].

This new way to represent chemical bonding has allowed the opening of a whole field named Hadronic Mechanics. With this new tool, several problems of physics and chemistry have been worked, leading to new proposals that range from energetic problems to superconductivity issues [16]. Our work has not taken that road; it considers the solution of the restricted three-body in the frame of Quantum Mechanics, two protons bound by an orbiting stable isoelectronium. This approach uses the solution of an H_2^+ ion but with a charge $q = -2e$ for the quasi-particle.

2.2 Restricted three-body Santilli-Shillady model

The four-body Santilli-Shillady model, as described by Eq. (2), was modified by Aringazin and Kucherenko [4] in order to restrict it to an explicit three-body approach. Within this restricted three-body Santilli-Shillady model (M3CS-S), these authors found a set of two equations that can be solved exactly. In this section we follow the main features of their method and show some of their results to contrast them with the results from our approach. The restricted Santilli-Shillady model assumes three basic conditions:

(a) A stable isoelectronium;

(b) The size of the isoelectronium can be neglected as compared with the inter nuclear distance; and,

(c) The Born-Oppenheimer approximation is valid.

When we combine these conditions with Eq. (2), representing a four-body equation, we arrive at a couple of differential equations which can be exactly solved. Aringazin and Kucherenko assumed that:

$$\mu_1 = \mu_2 = m_e\,. \tag{3}$$

And that the isoelectronium mass and reduced mass were

$$M = \mu_1 + \mu_2\,; \qquad m = \frac{\mu_1\mu_2}{M}\,. \tag{4}$$

In order to simplify expressions, they transformed the momentum operators

$$\overline{p}_i = -i\hbar\,\frac{\partial}{\partial r_i}\,, \qquad i = 1, 2; \tag{5}$$

into generalized ones:

$$\overline{P}_M = -i\hbar\,\frac{\partial}{\partial \overline{r}_{ab}}, \qquad \overline{p}_{12} = -i\hbar\,\frac{\partial}{\partial \overline{r}_{12}}\,. \tag{6}$$

Through them, Aringazin and his colleague arrived to a new equation from which the three-body equation can be derived by a variable separation method; i.e., from equation

$$\left\{-\frac{\hbar^2}{2M}\nabla^2_{ab} - \frac{\hbar^2}{2m}\nabla^2_{12} - V_0\frac{e^{-r_{12}/r_c}}{1-e^{-r_{12}/r_c}} + \frac{e^2}{r_{12}} - \right. \\ \left. - \frac{2e^2}{r_a} - \frac{2e^2}{r_b} + \frac{e^2}{R}\right\}|\widehat{\psi}\rangle = E\,|\widehat{\psi}\rangle \tag{7}$$

they got two equations, one describing the electrons inside the hadronic horizon in terms of the distance between them:

$$-\frac{\hbar^2}{2m}\,\nabla^2_{12}\,\chi + V(r_{12})\,\chi = \varepsilon\,\chi\,; \tag{8}$$

and, the second for the isoelectronium interaction with the nuclei:

$$-\frac{\hbar^2}{2M}\,\nabla^2_{ab}\,\psi + W(r_a, r_b, R)\,\psi = (E-\varepsilon)\,\psi, \tag{9}$$

where

$$|\widehat{\psi}\rangle = \chi\,(r_{12})\,\psi(r_a, r_b) \tag{10}$$

with

$$V(r_{12}) = \frac{e^2}{r_{12}} - V_0\frac{e^{-r_{12}/r_c}}{1-e^{-r_{12}/r_c}}, \tag{11}$$

and

$$W(r_a, r_b, R) = -\frac{2e^2}{r_a} - \frac{2e^2}{r_b} + \frac{e^2}{R}\,. \tag{12}$$

The Aringazin-Kucherenko proposal, Eqs. (9) and (12), becomes the restricted three-body Santilli-Shillady Model (M3CS-S) with which we are going to compare our results. On the other hand, Eqs. (8) and (11) become the description of the electrons involved in the isoelectronium itself. They have also considered that since the size of isoelectronium is small, the energy must be near zero, $\varepsilon \approx 0$; a point we are not going to discuss here.

ν [a)]	E	R_{opt} [b)]
0.3	−1.142556	1.722645
0.307	−1.169215	1.683367
0.308	−1.173024	1.677899
0.308381[c)]	−1.174475	1.675828
0.309	−1.176832	1.672471

Notes: [a)] Mass parameter in
[b)] Optimum bond length (bohr)
[c)] Parameter to obtain best energy

Table 2: Minimum energy dependence on the mass parameter

The direct solution of these equations gives results for the energy and bond length far from the experimentally observed; for example, the minimum energy, $E = -7.614289$ au, is much lower than $E_e = -1.17447567$ au, while the bond length, $R = 0.25$ bohr, markedly differs from $R = 1.4011$ bohr.

2.3 Results from the Aringazin-Kucherenko approach

As it has just been mentioned, the application of the restricted three-body Santilli-Shillady model gives results far from the experimental values for both, energy and bond length. In order to correct this problem, Aringazin and his team have chosen a scaling method to equalize their energy value with that experimentally observed. By assuming a charge equal to $-2e$ for the isoelectronium and its mass $M = \nu m_e$, they assigned to E the formula $E = W + 1/R$ (W is isoelectronium energy) and R in Eq. (9) to get a scaling rule for their original calculated data. The summary of the scaling process is:

$$(R, W) \longrightarrow (R,\, W + 1/R) \longrightarrow \left(\frac{R}{2\nu},\, 4\nu\, W\right) \longrightarrow \\ \longrightarrow \left(\frac{R}{2\nu},\, 4\nu\, W + \frac{2\nu}{R}\right). \tag{13}$$

Values in Table 2 show energy variations with respect to mass parameter and allows the identification of as the best parameter for the estimation of energy, $E = -1.174475$ au. While we have a 7th significant digit precision to the desired energy, the correspondent bond length disagrees 19.6% from the expected value.

There are, in the literature, a great number of studies and estimates for the ground state energy of molecular hydrogen. This elemental molecule is the most studied one and has compelled researchers in this field to design tools and other quantum mechanical theories. To compare our results with those of Aringazin-Kucherenko, we are going to use as the ground state energy curve the values reported by Kolos, Szalewicz y Monkhorst [6] as reference. Though there are already other studies reporting higher precision values, up to 12 significant digits [17], for example, we will not employ them here for we do not need such precision as our method gives numbers up to the 6th significant digit. These data are going to be identified as Kolos data or KSM curve.

With the aid of the data for the electronic energy W as a function of the distance between nuclei in the molecule (we remit the reader to Table 2 in ref. [4]), it is possible to construct a curve for the molecular energy according to the M3CS-S model. In Figure 2, we present a graph comparing the corresponding curve with Kolos data. It is self evident that both curves are very different, mainly in the region $R > 2.0$, though profiles are similar for lower R values.

On the other hand, the optimum bond length, $R = 1.675828$ bohr, of this curve is deviated from the experimentally observed value by 19.6%. These observations to the M3CS-S model imply that some kind of adjustment is

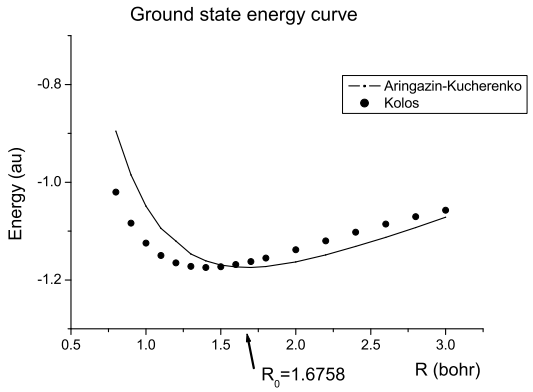

Fig. 2: Comparison between KSM's ground state energy data and scaled Aringazin-Kucherenko curve.

needed; probably a change in one of the features of the isoelectronium model could suppress these differences. In next section, we will present one such modification: the finite extension of isoelectronium.

3 Confined isoelectronium approach

We have shown until this point that the M3CS-S model satisfies the established conditions for the existence of isoelectronium with two drawbacks: it lacks the precision to represent the ground state potential energy curve of the hydrogen molecule and does not give a good approximation to its optimum bond length. In this section, we are going to introduce a condition directly related to the isoelectronium definition, a condition on the extension of isoelectronium wave function that will provide a modified three-body Santilli-Shillady model reproducing the behavior of the KSM curve in an appreciable range of distances between nuclei in the molecule.

The isoelectronium, as proposed by iso-chemistry, is a particle that brings together both electrons in the Hydrogen molecule, bound firmly (stable isoelectronium) by a Hulthén type potential. With a charge twice of the electron this quasi-particle has to orbit around protons in a very compact way. For an $M = 2m_e$ particle, the results of the calculations give very low energies and small bond length values. From this picture, we consider that the four-body problem of the hydrogen molecule can be converted into a compatible three-body approach if some aspects of the quasi-particle formation and molecule structure are taken into account. First of all, the formation of particles involves the transformation of mass into energy as it is observed for example in nuclear reactions; this means that while electrons come together to form an isoelectronium, there must be an effective mass factor present in the description of the molecule. As seen from the Schrödinger equation, this parameter would appear as a scaling factor for the energy and bond length.

This kind of scaling has been suggested in the literature before, not just by Aringazin and Kucherenko but by other authors as well. In particular, Svidzinsky and collaborators [18] have recently published a paper on the role of scaling while they attempt to represent the hydrogen molecule from Bohr's model. They make a dimensional scaling of the energy in this pre-quantum mechanical description. In our approach, scaling comes from an effective mass factor.

Another factor that must be considered in our model arises from the fact that a double charged particle surrounding both nuclei in the molecule can not extend in the same way as an electron does in the molecular ion. This small but heavily charged quasi-particle must have to limit its motion to confined orbits. Thus, the Hydrogen molecule with the isoelectronium orbiting two protons has to appear as a confined system. Therefore, as a way to improve the restricted three-body Santilli-Shillady model, a pair of conditions was introduced to understand the kind of movement an isoelectronium would describe. We have hypothesized the following additional restrictions for the isoelectronium model:

(a) The formation of the quasi-particle from the two electrons involves an effective mass transformation; i.e., the mass and charge of isoelectronium are $M = \nu m_e$ and $q = -2e$, respectively, where ν is the effective mass parameter, also called "iso-renormalization of mass"; and

(b) The spatial extension of the orbits of isoelectronium is limited to a defined region of space: the isoelectronium must orbit in a spheroidal shaped region of space.

Using these two hypotheses we have worked out two methods for the solution of the hydrogen molecule problem. First, the solution of Eq. (9) is considered in a way similar to the Ley-Koo and Cruz solution for the molecular ion confined by a spheroidal box [5]. They arrive to an exact solution for the differential equation by using separation of variables and the condition of a vanishing wave function on the spheroidal border. The second, whose results are reported here, uses a variational approach to solve Eq. (9) as it was done by Marín and Muñoz [19], with the same border condition: $\psi(\xi_0, \eta, \varphi) = 0$ and ξ_0 defines the shape of the box.

3.1 Exact solution to the confined model

Our variational approach to solve the modified three-body Santilli-Shillady model of the hydrogen molecule (modified M3CS-S) arrives to the following equation after applying the Hamiltonian for H_2^+, but including the above stated conditions on the mass, $M = \nu m_e$, where ν is the mass parameter, and the $q = -2e$ is the charge:

$$\left\{ -\frac{\hbar}{2\nu m_e} \frac{4}{\rho^2(\xi^2-\eta^2)} \left[\frac{\partial}{\partial\xi}(\xi^2-1)\frac{\partial}{\partial\xi} + \frac{\partial}{\partial\eta}(1-\eta^2)\frac{\partial}{\partial\eta} \right] + \right.$$
$$+ \frac{\xi^2-\eta^2}{(\xi^2-1)(1-\eta^2)} \frac{\partial^2}{\partial\varphi^2} - \frac{4e^2}{\rho} \frac{(Z_1+Z_2)\xi + (Z_2-Z_1)\eta}{\xi^2-\eta^2} + \quad (14)$$
$$\left. + \frac{Z_1 Z_2 e^2}{\rho} \right\} \psi(\xi,\eta,\varphi) = E' \psi(\xi,\eta,\varphi) ,$$

subject to the following restriction:

$$\psi(\xi_0, \eta, \varphi) = 0, \tag{15}$$

which specifies a spheroidal shaped region of space where the particle moves ($\xi \leqslant \xi_0$). Moreover, the wave function must vanish at the border. Due to the symmetry of the molecule in the ground state ($m = 0$), the azimuthal variable, can be suppressed so the problem is reduced to the $z - x$ plane. In addition, we introduce atomic units:

$$a_0 = \frac{\hbar^2}{m_e e^2}\,; \qquad E' = \frac{e^2}{2a_0}E\,; \qquad R = \frac{\rho}{a_0}\,.$$

Thus, the equation is rewritten as

$$\widetilde{H}\phi = E\phi$$

or

$$\left\{-\frac{4}{\nu R^2(\xi^2-\eta^2)}\left[\frac{\partial}{\partial\xi}(\xi^2-1)\frac{\partial}{\partial\xi}+\frac{\partial}{\partial\eta}(1-\eta^2)\frac{\partial}{\partial\eta}\right]-\right.$$
$$\left.-\frac{8}{R}\frac{(Z_1+Z_2)\xi+(Z_2-Z_1)\eta}{\xi^2-\eta^2}+\frac{Z_1Z_2}{R}\right\}\phi(\xi,\eta)=E\phi(\xi,\eta). \tag{16}$$

With this reduction, the above stated conditions can be met by a simple variational function considering one parameter and a cut off factor:

$$\phi(\alpha;\xi,\eta) = (\xi_0 - \xi)\big(\exp\big[-\alpha(\xi+\eta)\big]+ \\ +\exp\big[-\alpha(\xi-\eta)\big]\big)\,. \tag{17}$$

The minimum energy of this modified M3CS-S molecule can be obtained by minimization of the functional of energy

$$E(\alpha) = \frac{\langle\phi|\,\widetilde{H}\,|\phi\rangle}{\langle\phi\,|\phi\rangle} \tag{18}$$

subject to the condition

$$\left.\frac{\partial E}{\partial\alpha}\right|_{E=E_{\min}} = 0\,, \tag{19}$$

But really such a minimum energy, $E_{\min}$, will depend on several parameters

$$E_{\min} = E_{\min}(\nu, \xi_0, R)\,, \tag{20}$$

i.e., mass scale, spheroidal box and nuclei separation parameters. If we leave free all three parameters and use a simplex optimization method, a Nelder-Mead method for example [20], we will find that this energy is located at a point near the one reported by Santilli-Shillady and included here in Table 1 ($E = -7.61509174$ au and $R = 0.2592$ bohr). However, we can choose a fixed value for the mass parameter and find the minimum energy suitable for the ground state energy of free H_2.

Effectively, in order to obtain the minimum energy corresponding to a given mass parameter, ν, we have optimized the energy using the Nelder-Mead algorithm for two parameters: ξ_0 — spheroidal box shape; and, R — bond length.

ξ_0 [a)]	R [b)]	ν [c)]	E [d)]
48.46714783	1.41847181	0.37030	−1.1741987
48.46714783	1.41847181	0.37035	−1.1743573
48.46714783	1.41847181	0.37038	−1.1744523
48.46714783	1.41847181	0.37039	−1.1744840 [e)]
48.46714783	1.41847181	0.37040	−1.1745157
48.46714783	1.41847181	0.37050	−1.1748325
48.46714783	1.41847181	0.37060	−1.1751492

Notes: [a)] Shape parameter inverse of eccentricity (optimization)
[b)] Bond length parameter (optimization)
[c)] Mass parameter up to five digits (fixed)
[d)] Minimum energy (calculated by program)
[e)] Nearest value to exact energy (error)

Table 3: Minimum energy from parameter optimization for the confined model.

One relevant aspect resulting from these calculations is that for all mass parameter values the convergence of the method yields always identical values for both parameters as can be seen in Table 3 ($\xi_0 = 48.46714783$; $R = 1.41847181$ bohr). Furthermore, the minimum energy for $\nu = 0.37039$ gives an energy $E = -1.1744840$ au; that is, we have obtained the energy of the experimentally observed ground state of molecular hydrogen with a precision of 1×10^{-5} and a corresponding error in bond length of just 1.24%. This last result must be compared with the difference calculated by Aringazin and Kucherenko, 19.6%, to appreciate the importance of our finding.

Our approach to the hydrogen molecule, named from here onward as the Pérez-Marín-Riera approach to the restricted three-body Santilli-Shillady of the hydrogen molecule or M3CPM-R, encompasses more than the sole calculation of the minimum energy. With it, we can reproduce the whole set of data points of the KSM ground state curve in the $R \in [0.8, 3.2]$ interval.

3.2 Comparison of our data with KSM curve

As we have just mentioned, our approach to the isoelectronium movement provides an effective way to represent the ground state of H_2. Using the box shape and effective mass parameters found for the closest value to the exact energy of the ground state minimum, we have calculated the energy for several values of the distance between protons ranging from 0.4 to 6.0 bohr. The values obtained in this manner show a very significant behavior, a least in a defined interval $R \in [0.8, 3.2]$. We reproduce the values that Kolos and his collaborators obtained with a highly sophisticated computing method, shown with ours in Table 4 for comparison. As can be seen while reviewing the las column in the table, a difference appears in the fourth significant digit for the worst result and up to the fifth digit for the best, which is located at $R = 1.40$ bohr.

Figure 3 illustrates the values for the energy as a function of R found by Kolos (big points) together with the curve (line) representing our data. Both data sets are identical to

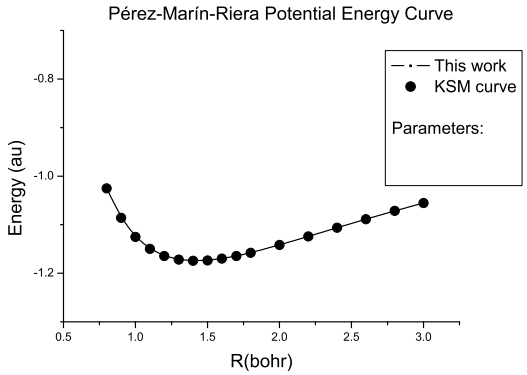

Fig. 3: Comparison between Kolos data and our exact restricted three-body model for the Hydrogen molecule (parameters are: ν - mass; ξ_0 - spheroidal shape).

each other up to the 4th significant digit; this is confirmed by a χ^2 statistical test ($\chi^2 = 1.3522$ with $gl = 17$), with a confidence level of 0.9999998 We state that by confining the isoelectronium, it is possible to reproduce the standard curve with a minimum computational calculation effort.

Again, if compare this result with that of the Aringazin-Kucherenko curve ($\chi^2 = 410.239$ with $gl = 17$), we state that the Aringazin curve differs completely from the KSM curve, as it was shown in Figure 2.

Both findings, up to six digit precision in minimum energy coincidence and whole curve reproduction, give support to our approach to the three-body Santilli-Shillady model. We can establish that the hypothesis on the isoelectronium movement is correct; that is, the orbiting of isoelectronium around both nuclei limits itself to a spheroidal region of space. Another way to express this behavior is that the formation of isoelectronium could be favored by the confinement of the molecule without changing its general properties.

The isoelectronium movement in a bound state together with the charge distribution confirms the explanation given by iso-chemistry to the following question: Why has the hydrogen molecule only two atoms? In our view, as soon as the molecule forms (isoelectronium) it becomes a bound system thus limiting the possibility of another hydrogen atom to be part of the molecule. In fact, the Pauli principle requires that the two valence electrons are correlated-bounded in a singlet state; as a result, the isoelctronium has spin zero. Consequently, no third electron can be bound via a conventional valence (see [3c] for details).

4 Conclusions

The value for the minimum energy of the ground state of the hydrogen molecule has been obtained using the three-body Santilli-Shillady model. Other parameters involved, such as the optimum bond length or energies for several distances between nuclei, can not be verified with it. We have shown that after modifying the model, by introducing a condition on

R [a]	α [b]	M3CP-M [c]	KSM [d]	Diff. [e]
0.80	0.4188965	−1.024900	−1.0200565	0.0048435
0.90	0.4585059	−1.085753	−1.0836432	0.0021098
1.00	0.4964746	−1.125001	−1.1245396	0.0004614
1.10	0.5331055	−1.149680	−1.1500574	0.0003774
1.20	0.5686328	−1.164305	−1.1649352	0.0006302
1.30	0.6032813	−1.171876	−1.1723471	0.0004711
1.40	0.6371875	−1.174438	−1.1744757	0.0000377 [f]
1.50	0.6705273	−1.173416	−1.1728550	0.0005610
1.60	0.7033789	−1.169826	−1.1685833	0.0012427
1.70	0.7358594	−1.164397	−1.1624586	0.0019384
1.80	0.7680469	−1.157664	−1.1550686	0.0025954
2.00	0.8319141	−1.141767	−1.1381329	0.0036341
2.20	0.8953906	−1.124237	−1.1201321	0.0041049
2.40	0.9589063	−1.106267	−1.1024226	0.0038444
2.60	1.0228130	−1.088534	−1.0857913	0.0027427
2.80	1.0871880	−1.071422	−1.0706831	0.0007389
3.00	1.1521880	−1.055136	−1.0573262	0.0021902
3.20	1.2179690	−1.039776	−1.0457995	0.0060235

Notes: [a] Bond length (in bohr)
[b] Non linear variational parameter
[c] Our data in the present work with $\xi_0 = 48.467148$ and $\nu = 0.37039$
[d] Kolos, Szalewicz and Monhorst data from 1986 [6]
[e] Absolute value of the difference.
[f] Best approximation up to 6th significant digit

Table 4: Energies for the M3CP-M model and KSM curve

the isoelectronium orbit, it is possible to calculate a minimum energy for the ground state coincident with the experimental values up to the sixth significant digit. Furthermore, the modified three-body model of the hydrogen molecule, a confined three-body system, enables the reproduction of the whole curve of ground state energy in the range $[0.80, 3.20]$ for the bond length. The physical interpretation to the confined isoelectronium model comprehends the isoelectronium itself, since the interaction between electrons while the quasiparticle is forming, implies its movement to be restricted to a defined region of space. The Santilli-Shillady orbits, the oo-shaped orbits, go beyond a way of speaking, they are a condition for the movement of the electron pair. This limitation in movement could be present in other states of electron pairs, such as the Cooper pairs of superconductivity, mainly in high Tc Superconductivity, for example.

The M3CP-M-R model of the hydrogen molecule introduced here represents an appropriate approach to study this molecule and gives support to the isoelectronium model introduced by Santilli and Shillady.

Acknowledgements

We want to thank Universidad de Sonora for the support given to this project; in particular, the scholarship for the PhD Student Raul Ruben Perez Enriquez. We also recognize the comments and support received from Prof. R. M. Santilli. This work was done under a CONACyT project.

Submitted on January 22, 2007
Accepted on January 29, 2007

References

1. Santilli R. M. and Shillady D. D. A new iso-chemical model of the hydrogen molecule. *Intern. J. Hydrogen Energy*, 1999, v. 24, 943–956.
2. Santilli R. M. and Shillady D. D. A new iso-chemical model of the water molecule. *Intern. J. Hydrogen Energy*, 2000, v. 25, 173–183.
3. Santilli R. R. *Hadronic J.*, 1978, v. 1, 574. [3a]; Elements of hadronic mechanics, vols. I, II (1995) and III (in press), Ukraine Acad. of Sciences, Kiev, (accessed on http://www.i-b-r.org/ Hadronic-Mechanics.htm) [3b]; Foundations of hadronic chemistry with applications to new clean energies and fuels. Kluwer Academic Publisher, the Netherlands, 2000 [3c].
4. Aringazin A. K. and Kucherenko M. G. Exact solution of the restricted three-body Santilli-Shillady model of H_2 molecule. *Hadronic J.*, 2000, v. 23, 1–76.
5. Ley-Koo E. and Cruz S. A. The hydrogen atom and the H_2^+ and HeH^{++} molecular ions inside prolate spheroidal boxes. *J. Chem. Phys.*, 1981, v. 74, 4603–4610.
6. Kolos W., Szalewicz K., Monkhorst H. J. New Bohr-Oppenheimer potential energy curve and vibrational energies for the electronic ground state of the hydrogen molecule. *J. Chem. Phys.*, 1986, v. 84, 3278–3283.
7. Pérez-Enríquez R. Structural parameter for high Tc superconductivity from an octahedral Möbius strip in RBaCuO:123 type perovskite. *Rev. Mex. Fis.*, 2002, v. 48, Supl. 1, 262–267.
8. Taut M. Two electrons in an external oscillator potential: particular analytic solutions of a Coulomb correlation problem. *Phys. Rev. A*, 1993, v. 48, 3561–3565.
9. LeSar R. and Herschbach D. R. Electronic and vibrational properties of molecules at high pressures: hydrogen molecule in a rigid spheroidal box. *J. Phys. Chem.*, 1981, v. 85, 2798–2804.
10. Corella-Madueco A., Rosas R., Marín J. L., Riera R. and Campoy G. Hydrogen molecule confined within a spheroidal box. (to be published).
11. Marín J. L., Cruz S. A. Use of the direct variational method for the study of one- and two-electron atomic systems confined by spherical penetrable boxes. *J. Phys. B: At. Mol. Opt. Phys.*, 1992, v. 25, 4365–4371.
12. Marín J. L., Campoy G. and Riera R. Simple model to study some properties of H trapped in solids. *Intern. J. Quantum Chem.*, 2003, v. 93, 271–274.
13. Valderrama E. G and Ugalde J. M. Electron correlation studies by means of local-scaling transformation and electron-pair density functions. *J. Math. Chem.*, 2005, v. 37, 211–231.
14. Animalou A. O. E. *Hadronic J.*, 1994, v. 17, 379.
15. Animalou A. O. E. and Santilli R. M. *Intern. J. Quantum Chem.*, 1995, v. 29, 175.
16. Santilli R. M. Foundations of hadronic chemistry with applications to new clean energies and fuels. Ed. IBR., Kluwer Academic Publishers 2001.
17. Sims J. S. and Hagstrom S. A. High precision variational calculations for the Born-Oppenheimer energies of the ground state of the hydrogen molecule. *J. Chem. Phys.*, 2006, v. 124, 094101.
18. Svidinsky A. A., Scully M. O. and Herschbach D. R. Simply and surprisingly accurate approach to the chemical bond obtained from dimensional scaling. *Phys. Rev. Let.*, 2005, v. 95, 080401.
19. Marín J. L. and Muñoz G. Variational calculations for enclosed quantum systems within soft spheroidal boxes: the case of H, H_2^+ and HeH_2^+. *J. Mol. Structure* (Teochem), 1993, v. 287, 281–285.
20. Wright M. H. Direct search methods: once scorned, now respectable. In: *Numerical analysis 1995*, Dundee University Press, 191–208.

Study of the Matrix Effect on the Plasma Characterization of Six Elements in Aluminum Alloys using LIBS With a Portable Echelle Spectrometer

Walid Tawfik Y. Mohamed

National Inst. of Laser Enhanced Science NILES, Dept. of Environmental Applications, Cairo University, Cairo, Egypt
Faculty of Education for Girls, Department of Physics, Gurayyat, North of Al-gouf, Kingdom of Saudi Arabia

E-mail: Walid_Tawfik@hotmail.com

Laser-induced breakdown spectroscopy (LIBS) has been applied to perform a study of the matrix effect on the plasma characterization of Fe, Mg, Be, Si, Mn, and Cu in aluminum alloy targets. The generated plasma emissions due to focusing of a 100 mj Nd: YAG pulsed laser at 1064 nm at the target surface were detected using a portable Echelle spectrometer with intensified CCD camera. Spectroscopic analysis of plasma evolution of laser produced plasmas has been characterized in terms of their spectra, electron density N_e and electron temperature T_e assuming the LTE and optically thin plasma conditions. The obtained average values of T_e and N_e were 7600 K and 3×10^{17} cm^{-3}, respectively, for the six elements in the aluminum alloy samples. The electron density increases with the element concentration while the plasma temperature does not has significance change with concentration. For industrial applications, LIBS with the portable Echelle spectrometer could be applied in the on-line production control that following up elemental concentration in metals and pharmaceuticals by only measuring N_e.

1 Introduction

Laser Induced Plasma Spectroscopy (LIPS or LIBS) is an alternative elemental analysis technology based on the optical emission spectra of the plasma produced by the interaction of high-power laser with gas, solid and liquid media. The increasing popularity of this technique is due to easiness of the experimental set-up and to the wide flexibility in the investigated material that doesn't need any pre-treatment of the sample before the analysis. Obvious tasks for LIBS are certification of metal contents in alloys, trace detection of metals for environmental pollution analysis in soils, on-line control of laser induced industrial processes (e.g. cutting and welding, thin film deposition), quick characterization of material in archaeological objects and works of art, and many others [1–5].

LIBS is based on analysis of line emission from the laser-induced plasma, obtained by focusing a pulsed laser beam onto the sample. The physical and chemical properties of the sample can affect the produced plasma composition, a phenomenon known as the matrix effect. The interaction between the laser and the target in LIBS is influenced significantly by the overall composition of the target, so that the intensity of the emission lines observed is a function of both the concentration of the elements of interest and the properties of the matrix that contains them. Plasma composition is dependent not only on composition of the sample, but also on laser parameters, sample surface conditions as well as on thermal and optical properties of the sample. Previously published works studied the matrix effect under different experimental conditions to specify causes and find out the methods of correction [6–11]. The different approaches have been undertaken to discriminate the problems resulting from the fractionation of the ablation and matrix effects. The most convenient approach is to determine elemental abundance comparing the analytic line intensities with signals obtained from the proper reference standards having the similar matrix composition. But, it is not always possible to obtain such calibration curves because there are no available standard samples, or it is impossible to have an internal standard of known concentration [12, 13]. In addition, plasma formation dynamics, sample ablation and associated processes are highly non-linear and not fully understood and may also play an important role as reasons of the matrix effect.

Recently an alternative procedure, based on the LIBS technique, for quantitative elemental analysis of solid materials has been proposed, which can, in principle, provide quantitative data with no need of calibration curves or internal standards [14, 15]. The method relies on the assumption about the existence the stoichiometric ablation and local thermodynamic equilibrium (LTE) i.e. Boltzmann distribution and Saha equation amongst the level population of any species and electron density and temperature of the plasma. However for application of this method experimentally one needs to obtain both equilibrium and thin plasma conditions, a task that may not be always possible to perform. Thus, in spite of the many advantages of LIBS the realization of a quantitative analytical method, which is able to measure main constituents in samples from different matrices, still remains a difficult task because of the complex laser-sample

and laser-plasma interaction mechanisms. As a rule, laser ablation plasma is characterized by complex spatial and temporal structures, and one meets a wide range of varying of parameters during the plasma existence time.

In this paper, we report the optimized conditions for LIBS to analyze the emission spectrum of aluminum alloy samples with high resolution using a portable Echelle spectrometer Mechelle 7500 equipped with ICCD camera. Spectroscopic analysis of plasma evolution of laser produced plasmas has been characterized in terms of their spectra, electron density and electron temperature. The LTE and optically thin plasma conditions were verified for the produced plasma. The electron temperature and density were determined using the emission intensity and stark broadening, respectively, of the spectral lines of six elements Fe, Mg, Be, Si, Mn, and Cu in the aluminum alloys. The dependence of the electron density and temperature on the concentrations of these elements was studied.

2 Experimental setup

2.1 Instrumentation

A typical LIBS experimental setup, described in details by the author elsewhere [6], is used throughout the present investigations. The plasma formation was attained with the aid of a Q-switched Nd: YAG laser (surelite I, continuum, USA) operating at 1064 nm (pulse duration of 7 ns) and repetition rate of 0.1 Hz – 10 Hz. The laser pulse energy of 100 mJ was adjusted by a suitable combination of beam splitters at constant operating high voltage (1.3 kV) and Q-switch delay (1.65 μs) to ensure spatial and temporal beam profile stability. An energy meter (Nova 978, Ophir Optronics Ldt., USA) was employed to monitor the shot to shot pulse energy. The laser beam was focused on aluminum alloy samples by a 10 cm focal length quartz lens to generate the plasma. A one meter length fused-silica optical fiber (600 μm diameter) mounted on a micro *xyz*-translation stage is used to collect the emission light from the plasma plume and feed it to a portable Echelle spectrometer of a 0.17 m focal length (Mechelle 7500, Multichannel Instruments, Sweden). The Echelle grating spectrometers designed for operation in high orders and high angles of incidence and diffraction, can provide high resolution in a more compact size and cover a much wider spectral range than conventional grating spectrometers [16]. The Mechelle 7500 provides a constant spectral resolution (CSR) of 7500 corresponding to 4 pixels FWHM over a wavelength range 200–1000 nm displayable in a single spectrum. A gateable, intensified CCD camera, (DiCAM-Pro-12 bit, UV enhanced, 43000 channels, PCO Computer Optics, Germany) coupled to the spectrometer was used for detection of the dispersed light. The overall linear dispersion of the spectrometer camera system ranges from 0.006 (at 200 nm) to 0.033 nm/pixel (at 1000 nm). To avoid the electronic interference and jitters, the intensifier high voltage was triggered optically. Echelle spectra display, control, processing and analysis were done using both Mechelle software (Multichannel Instruments, Stockholm, Sweden) and GRAMS/32 version 5.1 Spectroscopic Data Analysis Software (Galactic Industries, Salem, NH, USA).

2.2 Optimization of data acquisition procedure

Many optimization procedures were performed to improve our LIBS resolution and sensitivity and to minimize the measurements fluctuations and problems due to the sample heterogeneity.

To improve data reproducibility, and to avoid electronic jittering problem, the laser was set to single shot mode. Then, the Nd:YAG laser beam was focused onto the sample surface at 90° angle. This was done using a 25 mm diameter dichroic mirror that reflects 99% of high energy 1064 nm wavelength. This mirror placed just before the laser-focusing lens as shown in Figure 1. The focal point was set 5 mm below the surface of the sample in order to generate plasma of 800 μm spot diameter. This also minimize breakdown above the surface of any particles and aerosols generally present above the sample. Moreover, for each new sample, before spectral collection, 20 laser pulses were performed to clean the sample surface and removes surface oxides and contamination to ensure that the observed spectrum is representative of the sample composition. Furthermore, we found that enhancement of the data reproducibility can be achieved by accumulation of consecutive measured spectra for exposures of duration 1000 ns, each delayed 2500 ns from the laser pulse. These values of delay time and exposure window time (gate time) for the ICCD camera produced spectra with minimal background and signals from major lines that did not saturate the detector.

On the other hand, the use of a micro *xyz*-translation stage as a holder for fused-silica optical fiber facilities maximum intensity of the observed emission light from the plasma plume. We investigated a set of eight standard samples of aluminum alloy to study the dependence of the electron density and temperature on the concentrations of six elements Be, Mg, Si, Mn, Fe and Cu by the proposed LIBS setup. So that, these samples, which have never been treaded before using LIBS with Mechelle 7500, were selected to have the six elements with a range of concentrations. We used disk shaped standard samples of aluminum alloy provided by Alcan International Limited (0.5 cm; $\phi = 5$ cm). The concentrations of Mg, Si, Be, Cu, Mn and Fe in the aluminum alloy samples are given in Table 1.

Now, we aim to produce LIBS spectra with high precision. Precision is the measure of the degree of reproducibility of a measurement. Laser shot-to-shot variation causes differences in the plasma properties, therefore affects the magnitude of the element signal, and hence degrades the LIBS

Sample	Be	Mg	Si	Fe	Cu	Mn	Al
AL 3104	0.0011	1.15	0.21	0.42	0.17	0.92	Balance
AL 4104	0.0017	1.56	9.63	0.7	0.12	0.046	Balance
AL 5052	0.0043	2.51	0.087	0.33	0.042	0.09	Balance
AL 5182	0.0012	4.67	0.11	0.27	0.061	0.35	Balance
AL 5754	0.0022	2.54	0.22	0.35	0.1	0.29	Balance
AL 6063	0.00030	0.54	0.43	0.2	0.085	0.081	Balance
AL 7010	0.0007	2.44	0.11	0.22	1.88	0.082	Balance
AL a380.2	0.00036	0.028	9.17	0.41	3.61	0.042	Balance

Table 1: Beryllium, copper, iron, magnesium, silicon and manganese concentrations (in w/w %) in the standard aluminum alloy samples.

precision. To improve LIBS precision, spectra from several laser shots have to be averaged in order to reduce statistical error due to laser shot-to-shot fluctuation. We reproduced the measurements at five locations on the sample surface in order to avoid problems linked to sample heterogeneity. Twenty shots were fired at each location and saved in separated files and the average was computed and saved to serve as the library spectrum. For each recorded spectrum, the peak intensity, the Lorentzian curve fitting, the full width at half maximum FWHM, and the center wavelength of each line, as well as the background emission continuum are determined. Data treatment preprocessing of the averaged spectra data was performed in the Windows environment on a Pentium 4 PC using GRAMS/32, Excel (Microsoft Office Excel 2003) and Origin software version 7.0220 (Origin Lab Co., USA). The averages of peak tables (lists of wavelengths and intensities) of the averaged spectra were roll generated in GRAMS/32 and exported for data evaluation.

3 Results and discussion

3.1 LIBS spectrum

Figure 1 shows a typical plasma emission spectrum for aluminum alloy sample AL 7010. This spectrum is the average of 100 single shot spectra recorded at 2.5 μs delay time and 1 μs gate width. The panoramic Echelle spectra in the spectral range 200–700 nm show the UV emission lines of aluminum as a major element and the emission lines of Si, Cu, Be, Fe, Mn and Mg in the aluminum alloy sample. Moreover, our observed spectra reflect the wide spectral range and the high resolution of the used spectroscopic system.

3.2 Electron temperature measurements

In LIBS experiments, assuming optically thin plasma and the local thermodynamic equilibrium (LTE) conditions are hold, the re-absorption effects of plasma emission are negligible (i.e. the main ionization process is produced through impact excitation by thermal electrons). Upon these conditions, a Boltzmann population distribution can be assumed in describing the actual thermodynamics parameters of the plasma. So, the emitted spectral line intensity I is a measure of the population of the corresponding energy level of this element in the plasma. Then I corresponding to the transition between levels E_k and E_i of the atomic species α with concentration C_α, can be expressed as

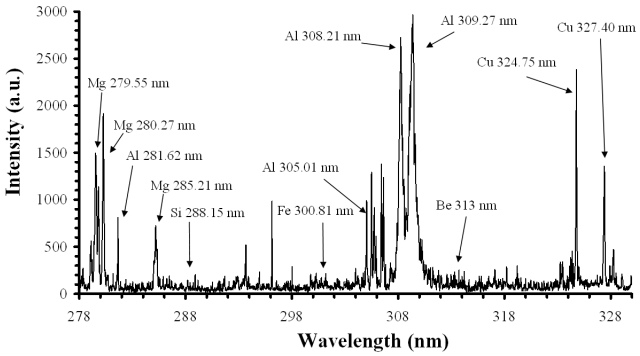

Fig. 1: Typical LIBS spectrum for aluminum alloy sample AL 7010. The laser energy was 100 mJ at wavelength 1064 nm, plasma emissions are accumulated with delay 2.5 μs, and gate width 1 μs.

$$I_\alpha^{ki} = F C_\alpha \frac{g_k A_{ki} e^{\frac{-E_k}{K_B T}}}{U_\alpha(T)}, \qquad (1)$$

where K_B is the Boltzmann constant, $U_\alpha(T)$ is the partition function, A_{ki} is the transition probability, g_k is the statistical weight for the upper level, E_k is the excited level energy, T is the temperature (in LTE all temperatures are assumed to be equal, i.e. $T_e \approx T_{ion} \approx T_{plasma}$) and F is a constant depending on experimental conditions.

Equation (1) allows also for evaluating C_α when the sample and reference plasma temperature are different, once the atomic parameters are derived from atomic databases. In order to evaluate the plasma temperature, they take the natural logarithm of Equation (1), obtaining

$$\ln\left(\frac{I_\alpha^{ki}}{g_k A_{ki}}\right) = \frac{E_k}{K_B T} + \ln\left(\frac{C_\alpha F}{U_\alpha(T_\alpha)}\right). \qquad (2)$$

In the two-dimensional Boltzmann plane identified by the left hand term of Equation (2) and by E_k, different

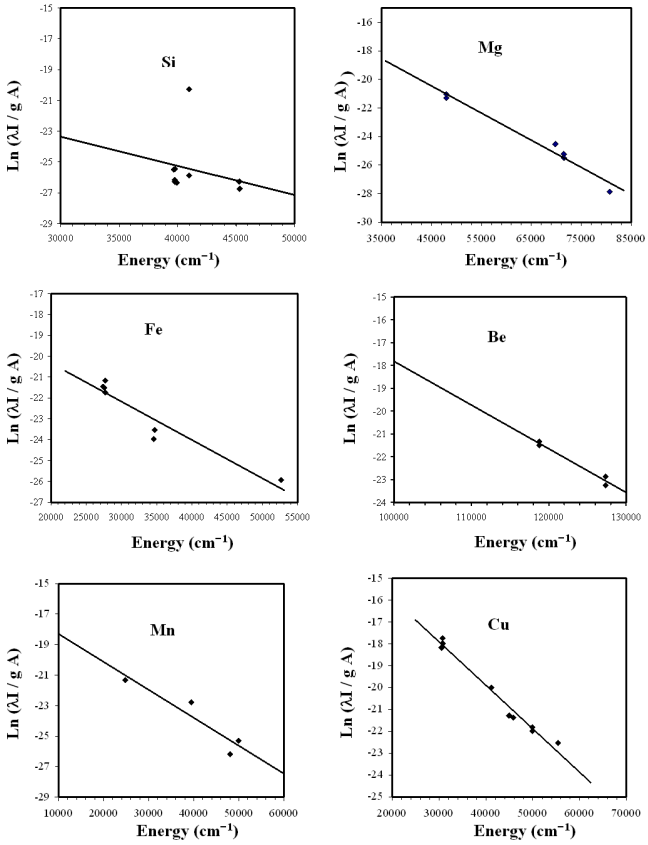

Fig. 2: Six Boltzmann plots were determined form the emission line intensities of Si, Mg, Fe, Be, Mn and Cu observed in the laser-induced plasma of aluminum alloy sample AL 7010. The slope of the plotted curves yields temperatures of 7606 K, 7562 K, 7817 K, 7511 K, 7842 K, and 7224 K for the elements Si, Mg, Fe, Be, Mn, and Cu respectively.

emission lines intensities belonging to the same element in the same spectrum lie along a straight line with a slope of $-1/K_B T$ [21].

In our experiment, the temperatures were determined form the emission line intensities of Mg, Si, Be, Cu, Mn and Fe observed in the laser-induced plasma of aluminum alloys. Figure 2 show six Boltzmann plots of Eqn. (2), for each of these six elements in the aluminum alloy sample AL 7010 where the data were fitted with the least-square approximation. The spectral lines wavelengths, energies of the upper levels, statistical weights, and transition probabilities used for each element are obtained from NIST [17] and Griem [21], and listed in Table 2. The slope of the plotted curves yields temperatures 7606 K, 7562 K, 7817 K, 7511 K, 7842 K, and 7224 K for the elements Si, Mg, Fe, Be, Mn, and Cu respectively. The average value of the plasma temperature is 7600 K which agrees with the value obtained by Sabsabi and Cielo [20] under conditions similar to ours. The difference in the plasma temperature of the six elements may be attributed to the difference in the excitation and ionization

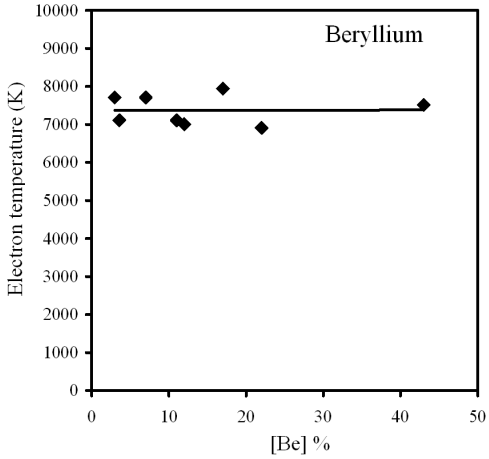

Fig. 3: Electron temperature measured at 2.5 μs delay time and 1 μs gate width using Boltzmann plot for different concentrations of beryllium in different aluminum alloy samples.

potentials between these elements.

Then the matrix effect on the plasma temperature was studied using the variety of concentrations of the six elements in the eight aluminum samples. This was done by plotting the corresponding temperature for each element versus its concentration in the aluminum alloy samples. Under our experimental conditions, no significance change was found for the plasma temperature with the concentration of the six elements, especially for low concentration elements as shown in Figure 3 as an example for Beryllium. This is could be understanding as follows; for optical thin plasma, increasing the element concentration returns an increasing of the intensity of its corresponding spectral lines with roughly the same ratio, which leads to have the same slope of Boltzmann plot and results in the same plasma temperature.

3.3 Electron density measurements

The usual method for determination of electron density is the measuring of the broadening of a suitable emission line of the laser-plasma spectrum. There are several possible mechanisms of line broadening in plasma: self-absorption, pressure broadening, Doppler broadening, Stark broadening, etc. Lida reported that the line broadening and the spectral shift of the emission line are due mainly to self-absorption phenomenon [18]. In the present study line splitting and the spectral shift, which are good evidence of self-absorption, were monitored carefully. No evidence of line splitting or spectral shift was observed.

Nemet and Kozma reported the broadening of transition lines as pressure, Stark, and Doppler broadening [19]. But pressure and Doppler broadening should not be so much different among transition lines as is the case for plasma of solids. Kyuseok Song *et al.* stated that Stark broadening may be one of the reasons since the broadening effect increases as the energy level increases [22]. Stark broadening results

Element	Wavelength (nm)	A_{ki} (s^{-1})	E_k (cm^{-1})	g_k	Stark broadening parameter w (nm)	Element	Wavelength (nm)	A_{ki} (s^{-1})	E_k (cm^{-1})	g_k	Stark broadening parameter w (nm)
Si	221.89	1.50E+06	45276.18	3	—	Fe	376.01	4.47E+06	45978.00	15	—
Si	243.87	7.40E+05	40991.88	3	—	Fe	376.38	5.44E+07	34547.21	5	—
Si	250.69	4.66E+07	39955.05	5	—	Fe	376.55	9.80E+07	52655.00	15	—
Si	251.43	6.10E+07	39760.28	3	—	Fe	376.72	6.40E+07	34692.14	3	—
Si	251.61	1.21E+08	39955.05	5	—	Fe	378.60	4.20E+06	46026.94	13	—
Si	252.41	1.81E+08	39683.16	1	—	Fe	538.33	5.6E+07	53352.98	13	5.3E-03 [29]
Si	252.85	7.70E+07	39760.28	3	—	Cu	240.00	2.00E+06	67911.85	4	4.1E-3 [21, 28]
Si	288.15	1.89E+08	40991.88	3	0.74E-3 [21]	Cu	261.84	3.07E+07	49382.95	4	—
Si	300.67	1.10E+03	33326.05	5	—	Cu	276.64	9.60E+06	49382.95	4	—
Si	302.00	3.30E+03	33326.05	5	—	Cu	282.44	7.80E+06	46598.34	6	—
Si	390.55	1.18E+07	40991.88	3	1.46E-3 [21]	Cu	296.12	3.76E+06	44963.22	8	—
Mg	277.66	1.32E+08	57873.94	5	—	Cu	306.34	1.55E+06	45879.31	4	—
Mg	277.82	1.82E+08	57833.4	3	—	Cu	319.41	1.55E+06	44544.15	4	—
Mg	277.98	4.09E+08	57873.94	5	—	Cu	324.75	1.39E+08	30783.69	4	—
Mg	278.14	5.43E+08	57812.77	1	—	Cu	327.40	1.37E+08	30535.30	2	—
Mg	278.29	2.14E+08	57833.4	3	—	Cu	333.78	3.80E+05	41153.43	8	—
Mg	279.07	4.01E+08	71491.06	4	—	Cu	402.26	1.90E+07	55387.67	4	—
Mg	279.55	2.60E+08	35760.88	4	—	Cu	406.26	2.10E+07	55391.29	6	—
Mg	279.79	4.79E+08	71490.19	6	—	Cu	427.51	3.45E+07	62403.32	8	—
Mg	280.27	2.57E+08	35669.31	2	—	Cu	465.11	3.80E+07	62403.32	8	—
Mg	281.11	1.96E+08	83520.47	5	—	Cu	510.55	2.00E+06	30783.69	4	—
Mg	281.17	2.11E+08	83511.25	3	—	Cu	515.32	6.00E+07	49935.20	4	—
Mg	285.21	4.91E+08	35051.26	3	3.6E-04 [27]	Cu	521.82	7.50E+07	49942.06	6	—
Mg	291.54	4.09E+08	80693.01	5	—	Cu	529.25	1.09E+07	62403.32	8	—
Mg	292.86	1.15E+08	69804.95	2	—	Cu	570.02	2.40E+05	30783.69	4	—
Mg	293.65	2.30E+08	69804.95	2	—	Cu	578.21	1.65E+06	30535.30	2	—
Fe	370.11	4.80E+07	51192.27	9	—	Mn	258.97	2.6E+08	38543.08	7	5.91E-03 [30]
Fe	370.56	3.22E+06	27394.69	7	—	Mn	401.81	2.54E+07	41932.64	8	—
Fe	371.99	1.62E+07	26874.55	11	—	Mn	403.08	1.70E+07	24802.25	8	—
Fe	372.26	4.97E+06	27559.58	5	—	Mn	403.31	1.65E+07	24788.05	6	—
Fe	372.71	2.00E+07	50534.39	7	—	Mn	403.45	1.58E+07	24779.32	4	—
Fe	373.33	6.20E+06	27666.35	3	—	Mn	404.14	7.87E+07	41789.48	10	—
Fe	373.53	2.40E+07	50475.29	9	—	Mn	404.88	7.50E+07	42143.57	4	—
Fe	373.71	1.42E+07	27166.82	9	—	Mn	405.55	4.31E+07	41932.64	8	—
Fe	373.83	3.80E+07	53093.52	13	—	Mn	405.89	7.25E+07	42198.56	2	—
Fe	374.56	1.15E+07	27394.69	7	—	Mn	406.17	1.90E+07	49415.35	6	—
Fe	374.59	7.33E+06	27666.35	3	—	Mn	406.35	1.69E+07	42053.73	6	—
Fe	374.83	9.15E+06	27559.58	5	—	Mn	407.92	3.80E+07	42143.57	4	—
Fe	375.82	6.34E+07	34328.75	7	—	Mn	408.29	2.95E+07	42053.73	6	—
Mn	408.36	2.80E+07	41932.64	8	—	Be	265.08	1.80E+08	59695.07	3	—
Mn	423.51	9.17E+07	46901.13	6	—	Be	313.04	1.15E+08	31935.32	4	2.81E-05 [21]
Mn	441.49	2.93E+07	45940.93	6	—	Be	313.11	1.15E+08	31928.744	2	—
Mn	445.16	7.98E+07	45754.27	8	—	Be	324.16	1.37E+07	127335.12	2	—
Mn	446.20	7.00E+07	47207.28	10	—	Be	324.18	2.73E+07	127335.12	2	—
Mn	475.40	3.03E+07	39431.31	8	—	Be	327.46	1.43E+07	118761.32	4	—
Mn	478.34	4.01E+07	39431.31	8	—	Be	327.47	1.43E+07	118760.51	2	—
Mn	482.35	4.99E+07	39431.31	8	—	Be	332.10	6.90E+06	52080.94	3	—
Be	265.05	1.08E+08	59697.08	5	—	Be	332.11	2.10E+07	52080.94	3	—
Be	265.06	1.44E+08	59695.07	3	—	Be	332.13	3.40E+07	52080.94	3	—

Table 2: A list of the spectroscopic data of the spectral lines used for the determination of plasma temperature and density of aluminum alloy samples.

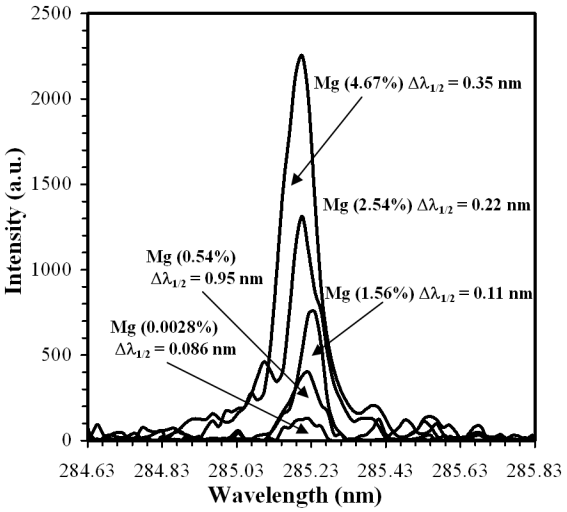

Fig. 4: The 285.21 nm line with sufficient resolution to measure the full width at half-maximum ($\lambda_{1/2}$) at different concentrations of Mg in the aluminum alloys. For each line, the data points were fitted with Lorentzian fitting function using the Origin software to determine ($\lambda_{1/2}$).

from Coulomb interactions between the radiator and the charged particles present in the plasma. Both ions and electrons induce Stark broadening, but electrons are responsible for the major part because of their higher relative velocities. Therefore, in our conditions, the profile of a line is mainly contributed to linewidths arises from the Stark effect while the contribution of other mechanisms of broadening (Doppler effect, Van der Waals broadening, and resonance broadening) can be neglected, as shown under conditions similar to ours by Sabsabi and Cielo [20].

The electrons in the plasma can perturb the energy levels of the individual ions which broaden the emission lines originating from these excited levels. Stark broadening of well-isolated lines in the plasma is, thus, useful for estimating the electron number densities provided that the Stark-broadening coefficients have been measured or calculated. The line profile for stark broadened is well described by a Lorentzian function

Since the instrumental line-broadening exhibit Gaussian shape, then the stark line width $\Delta\lambda_{FWHM}$ can be extracted from the measured line width $\Delta\lambda_{observed}$ by subtracting the instrumental line broadening $\Delta\lambda_{instrument}$:

$$\Delta\lambda_{FWHM} = \Delta\lambda_{observed} - \Delta\lambda_{instrument}\,. \qquad (3)$$

In our case $\Delta\lambda_{instrument}$ was 0.05 nm (determined by measuring the FWHM of the Hg lines emitted by a standard low pressure Hg lamp).

The width of stark broadening spectral line depends on the electron density N_e. Both the linear and the quadratic stark effect are encountered in spectroscopy. Only the hydrogen atom and H-like ion exhibit the linear stark effect. For the linear stark effect the electron density should be deduced from H line width from the formula [21]

$$N_e = C(N_e, T)\,\Delta\lambda_{FWHM}^{3/2} \qquad (4)$$

the values of the parameter $C(N_e, T)$ are tabulated in the literature [21], which determine the relative contribution of the electron collision on the electrostatic fields, and depend weakly on N_e and T.

For a non-H-like line, the electron density (in cm^{-3}) could be determined from the FWHM of the line from the formula [21]:

$$N_e \approx \left(\frac{\Delta\lambda_{FWHM}}{2w}\right) \times 10^{16}, \qquad (5)$$

where w is the electron impact parameter (stark broadening value) and it is given in Table 2. The last formula is generally used for calculations of plasma generated from solid targets [7, 8, 20].

Six lines were identified as candidates for electron-density measurements: 390.55 nm, 285.21 nm, 538.33 nm, 240.00 nm, 258.97 nm and 313.04 nm for Si, Mg, Fe, Cu, Mn and Be respectively. Figure 4 shows, as an example for Mg, the 285.21 nm line with sufficient resolution to measure the full width at half-maximum ($\lambda_{1/2}$) at different concentrations of Mg in the aluminum alloys. All the six lines data points were fitted with Lorentzian fitting function using the Origin software to determine ($\lambda_{1/2}$) as shown in Fig. 4 for Mg as an example. Substituting the values of $\lambda_{1/2}$ in Eqn. (3) and the corresponding values of stark broadening w from Table 2 in Eqn. (6) the electron density for Mg was determined. These steps were repeated for each concentration of the six elements in the eight aluminum alloy samples. Then the obtained electron density values were plotted versus the element concentration. Figure 5 shows six plots for the variation of the electron density values versus the concentrations of Mg, Si, Be, Fe, Cu and Mn in different aluminum alloy samples. These plots reveal that, in case of Mg, Si, Fe, Cu and Mn, electron density increases with the element concentration. For the case of low concentration elements like Be, the increase of the electron density with the element concentration is very weak. This result might occur because increasing the "element" concentration comprises increasing portion of the laser-target interaction volume which agrees with O. Samek [24] and Rusak *et al.* [25].

Finally, by knowing the electron density and the plasma temperature we can determine whether the local thermodynamic equilibrium (LTE) assumption is valid applying the criterion given by McWhirter [26].

The lower limit for electron density for which the plasma will be in LTE is:

$$N_e \geqslant 1.4\times10^{14}\,\Delta E^3 T^{1/2}, \qquad (6)$$

where ΔE is the largest energy transition for which the condition holds and T is the plasma temperature [23].

In the present case $\Delta E = 3.65$ eV for Al (see Ref. [20])

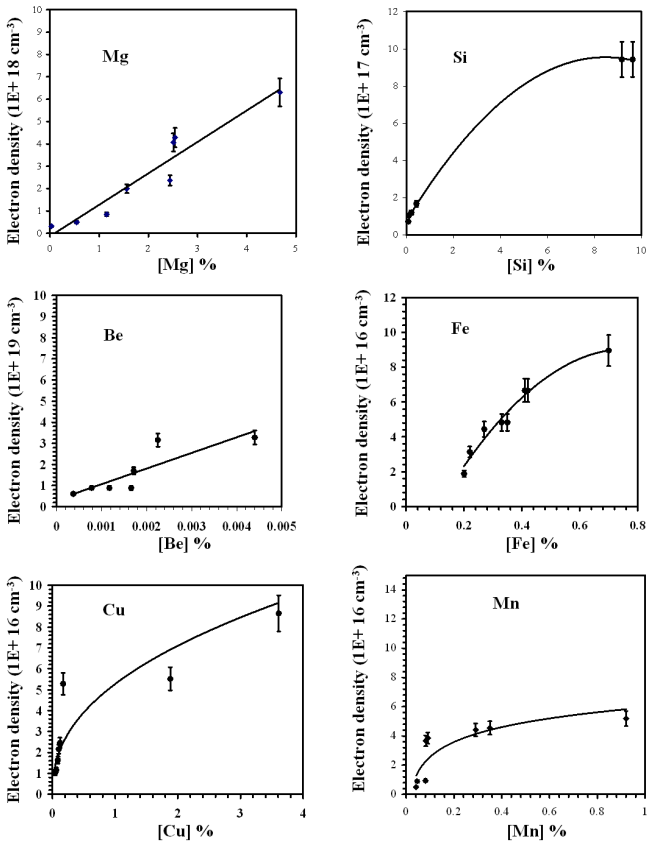

Fig. 5: Six plots for the variation of the electron density values versus the concentrations of Mg, Si, Be, Fe, Cu and Mn in different aluminum alloy samples.

and the electron density lower limit value given by Eqn. (7) is 6×10^{15} cm^{-3}. The experimentally calculated densities are greater than this value, which is consistent with the assumption that the LTE prevailing in the plasma.

4 Conclusion

In summary, we have carried out an accurate LIBS setup using portable commercial Echelle spectrometer equipped with ICCD detector to study aluminum alloys matrix effects on the plasma characterization. The electron density and plasma temperature were determined for six elements (Fe, Mg, Be, Si, Mn, and Cu) in the aluminum alloy targets. The electron density increases with the element concentration while the plasma temperature does not has significance change with the element concentration.

For a plasma diagnostics perspective, the target physical properties play an important role in the obtained values of the laser induced plasma temperature T_e and electron density N_e. For industrial application, LIBS could be applied in the on-line industrial process that following up elemental concentration in metals and pharmaceuticals by only measuring N_e of that element.

Acknowledgment

The author gratefully acknowledges the support of Prof. M. Sabsabi and Prof. M. Abdel-Harith specially for offering the standard aluminum alloy samples.

Submitted on January 20, 2007
Accepted on February 02, 2007

References

1. Radziemski L. J. Review of selected analytical applications of laser plasmas and laser ablation, 1987–1994. *Microchem. J.*, 1994, v. 50, 218–234,.
2. Rusak D. A., Castle B. C., Smith B. W. and Winefordner J. D. Fundamentals and applications of laser-induced breakdown spectroscopy. *Crit. Rev. Anal. Chem.*, 1997, v. 27, 257–290.
3. Sneddon J. and Lee Y. Novel and recent applications of elemental determination by laser-induced breakdown spectrometry. *Anal. Lett.*, 1999, v. 32, 2143–2162.
4. Tognoni E., Palleschi V., Corsi M. and Cristoforetti G. Quantitative micro-analysis by laser-induced breakdown spectroscopy: a review of the experimental approaches. *Spectrochim. Acta Part B*, 2002, v. 57, 1115–1130.
5. Majidi V. and Joseph M. R. Spectroscopic applications of laser-induced plasmas. *Crit. Rev. Anal. Chem.*, 1992, v. 23, 143–162.
6. Bulatov V., Krasniker R. and Schechter I. Study of matrix effects in laser plasma spectroscopy by combined multifiber spatial and temporal resolutions. *Anal. Chem.*, 1998, v. 70, 5302–5310.
7. Sabsabi M., Detalle V., Harith M. A., Walid Tawfik and Imam H. Comparative study of two new commercial Echelle spectrometers equipped with intensified CCD for analysis of laser-induced breakdown spectroscopy. *Applied Optics*, 2003, v. 42, No. 30, 6094–6098.
8. Ismail M. A., Imam H., Elhassan A., Walid Tawfik and Harith M. A. LIBS limit of detection and plasma parameters of some elements in two different metallic matrices. *J. Anal. At. Spectrom.*, 2004, v. 19, 1–7.
9. Xu L., Bulatov V., Gridin V. and Schechter I. Absolute analysis of particulate materials by laser-induced breakdown spectroscopy. *Anal. Chem.*, 1997, v. 69, 2103–2108.
10. Goode S. R., Morgan S. L., Hoskins R. and Oxsher A. Identifying alloys by laser-induced breakdown spectroscopy with a time-resolved high resolution echelle spectrometer. *J. Anal. At. Spectrom.*, 2000, v. 15, 1133–1138.
11. Eppler A. S., Cremers D. A., Hickmott D. D., Ferris M. J. and Koskelo A. C. Matrix effects in the detection of Pb and Ba in soils using laser-induced breakdown spectroscopy. *Appl. Spectrosc.*, 1996, v. 50, 1175–1181.
12. Quentmeier A., Sdorra W. and Niemax K. Internal standardization in laser induced fluorescencs spectrometry of microplasms produced by laser ablation of solid samples. *Spectrochimica Acta B*, 1990, v. 45, No. 6, 5371–5379.

13. Bassiotis I., Diamantopoulou A., Giannoundakos A., Roubani-Kalantzopoulou F. and Kompitsas M. Effects of experimental parameters in quantitative analysis of steel alloy by laser-induced breakdown spectroscopy. *Spectrochim. Acta Part B*, 2001, v. 56, 671–683.
14. Ciucci A., Corsi M., Palleschi V., Rastelli V., Salvetti A. and Tognoni E. A new procedure for quantitative elemental analyses by laser induced plasma spectroscopy. *Applied Spectroscopy*, 1999, v. 53, 960–964.
15. Bulajic D., Corsi M., Cristoforetti G., Legnaioli S., Palleschi V., Solvetti A. and Rognoni E. A procedure for correcting self-absorption in calibration-free laser induced breakdown spectroscopy. *Spectrochim. Acta B*, 2002, v. 57, 339–353.
16. Corsi M., Palleschi V., Salvetti A. and Tognoni T. Making LIBS quantitative: a critical review of the current approaches to the problem. *Res. Adv. Appl. Spectrosc.*, 2000, v. 1, 41–47.
17. Olesik J. W. Echelle grating spectrometers for inductively coupled plasma-optical emission spectrometry. *Spectroscopy*, 1999, v. 14, No. 10, 27–30.
18. NIST National Institute of Standards and Technology, USA, electronic database, http://physics.nist.gov/PhysRefData/ASD/lines_form.html
19. Lida Y. Effects of atmosphere on laser vaporization and excitation processes of solid samples. *Spectrochim. Acta B*, 1990, v. 45, 1353–1367.
20. Nemet B. and Kozma L. Time-resolved optical emission spectrometry of Q-switched Nd:YAG laser-induced plasmas from copper targets in air at atmospheric pressure. *Spectrochim. Acta B*, 1995, v. 50, 1869–1888.
21. Sabsabi M. and Cielo P. Quantitative analysis of aluminum alloys by laser-induced breakdown spectroscopy and plasma characterization. *Applied Spectroscopy*, 1995, v. 49, No. 4, 499–507.
22. Griem H. R. Plasma spectroscopy. McGraw-Hill, New York, 1964.
23. Kyuseok Song, Hyungki Cha, Jongmin Lee and Yong Lee. Investigation of the line-broadening mechanism for laser-induced copper plasma by time-resolved laser-induced breakdown spectroscopy. *Microchem. Journal*, 1999, v. 63, 53–60.
24. Bekefi G. Principles of laser plasmas. Wiley, New York, 1976, 550–605.
25. Samek O., Beddows D.C.S., Telle H.H., Kaiser J., Liska M., Caceres J.O. and Gonzales Urena A. Quantitative laser-induced breakdown spectroscopy analysis of calcified tissue samples. *Spectrochimica Acta Part B*, 2001, v. 56, 865–875.
26. Rusak D. A., Clara M., Austin E. E., Visser K., Niessner R., Smith B. W. and Winefordner J. D. Investigation of the effect of target water content on a laser-induced plasma. *Applied Spectroscopy*, 1997, v. 51, No. 11, 1628–1631.
27. McWhirter R.W.P. In: *Plasma Diagnostic Techniques*, ed. R. H. Huddlestone and S. L. Leonard, Academic Press, New York, 1965, Ch. 5, 206.
28. Le Drogoff B., Margotb J., Chakera M., Sabsabi M., Barthelemy O., Johnstona T.W., Lavillea S., Vidala F. and von Kaenela Y. Temporal characterization of femtosecond laser pulses induced plasma for spectrochemical analysis of aluminum alloys. *Spectrochimica Acta Part B*, 2001, v. 56, 987–1002.
29. Konjevic N. and Wiese W. L. Stark widths and shifts for spectral lines of neutral and ionized atoms. *J. Phys. Chem. Ref. Data*, 1990, v. 19, 1337.
30. Freudestien S. and Cooper J. Stark broadening of Fe I 5383 Å. *Astron. & Astrophys.*, 1979, v. 71, 283–288.
31. Popovic L. C. and Dimitrijevic M. S. Tables of the electron impact broadening parameters: Mn II, Mn III, Ga III, Ge III and Ge Iv Lines. *Bull. Astron. Belgrade*, 1997, No. 156, 173–178.

A Letter by the Editor-in-Chief:

Twenty-Year Anniversary of the Orthopositronium Lifetime Anomalies: The Puzzle Remains Unresolved

This letter gives a history of two observed anomalies of orthopositronium annihilation, of which the 20th anniversary occurs this year. The anomalies, breaking the basics of Quantum Electrodynamics, require more experimental study, in view of the recent claim of the Michigan group of experimentalists, which alleges resolution of one of the anomalies.

It is now the 20th anniversary of the observation of anomalies of orthopositronium annihilation (both discovered in 1987) in experiments conducted by two groups of researchers: one group in the USA, headed by the late Prof. Arthur Rich in the University of Michigan at Ann Arbor, and the other group in Russia, headed by Dr. Boris Levin of the Institute of Chemical Physics in Moscow, but then at the Gatchina Nuclear Centre in St. Petersburg.

The anomalies dramatically break the basics of Quantum Electrodynamics.

Recently my long-time colleague, Boris Levin, one of the discoverers of the anomalies, suggested that the last experiment of the Michigan group, by which it has claimed resolution of one of the anomalies [1], was set up so that an electric field introduced into the experiment (it accelerates the particle beam before the target) mere suppressed the anomaly despite the electric field helps to reach complete thermalization of orthopositronium in the measurement cell. As a dry rest the anomaly, remaining represented but suppressed by the field, became mere invisible in the given experiment.

Now Levin proposes a modification of the last Michigan experiment in order to demonstrate the fact that the anomaly remains. He describes his proposed experiment in his brief paper appearing in this issue of Progress in Physics.

I would give herein a brief introduction to the anomalies (otherwise dispersed throughout many particular papers in science journals).

Positronium is an atom-like orbital system that contains an electron and its anti-particle, the positron, coupled by electrostatic forces. There are two kinds of positronium: parapositronium p-Ps, in which the spins of the electron and the positron are oppositely directed so that the total spin is zero, and orthopositronium o-Ps, in which the spins are co-directed so that the total spin is one. Because a particle-anti-particle system is unstable, life span of positronium is rather small. In vacuum parapositronium decays in $\sim 1.25\times10^{-10}$ s, while orthopositronium in $\sim 1.4\times10^{-7}$ s. In a medium the life span is even shorter because positronium tends to annihilate with electrons of the medium. Due to the law of conservation of charge parity, parapositronium decays into an even number of γ-quanta (2, 4, 6, ...) while orthopositronium annihilates into an odd number of γ-quanta (3, 5, 7, ...). The older modes of annihilation are less probable and their contributions are very small. For instance, the rate of five-photon annihilation of o-Ps compared to that of three-photon annihilation is as small as $\lambda_5 \approx 10^{-6}\lambda_3$. Hence parapositronium actually decays into two γ-quanta p-Ps $\rightarrow 2\gamma$, while orthopositronium decays into three γ-quanta o-Ps $\rightarrow 3\gamma$.

In the laboratory environment positronium can be obtained by placing a source of free positrons into matter, a monatomic gas for instance. The source of positrons is β^+-decay, self-triggered decays of protons in neutron-deficient atoms $\mathrm{p} \rightarrow \mathrm{n} + \mathrm{e}^+ + \nu_\mathrm{e}$. It is also known as positron β-decay.

Some of free positrons released into a gas from a β^+-decay source quite soon annihilate with free electrons and electrons in the container's walls. Other positrons capture electrons from gas atoms thus producing orthopositronium and parapositronium (in ratio 3:1).

The time spectrum of positron annihilations (number of events vs. life span) is the basic characteristic of their annihilation in matter. In particular, in such spectra one can see parts corresponding to annihilation with free electrons and annihilation of p-Ps and o-Ps.

In inert gases the time spectrum of annihilation of quasi-free positrons generally forms an exponential curve with a plateau in its central part, known as a "shoulder" [2, 3].

In 1965 P. E. Osmon published [2] pictures of observed time spectra of annihilation of positrons in inert gases (He, Ne, Ar, Kr, Xe). In his experiments he used ^{22}NaCl as a source of β^+-decay positrons. Analyzing the results of the experiments, Levin noted that the spectrum in neon was peculiar compared to those in other monatomic gases: in neon, points in the curve were so widely scattered that the presence of a "shoulder" was uncertain. Repeated measurements of time spectra of annihilation of positrons in He, Ne, and Ar, later accomplished by Levin [4, 5], have proven the existence of anomaly in neon. A specific feature of the experiments conducted by Osmon, Levin and some other researchers is that the source of positrons was ^{22}Na, while the moment of appearance of the positron was registered according to the γ_n-quantum of decay of excited ^{22*}Ne, $^{22*}\mathrm{Ne} \rightarrow {}^{22}\mathrm{Ne} + \gamma_\mathrm{n}$, from one of the products of β^+-decay of ^{22}Na. This method is quite justified and is commonly used, because the life span of excited ^{22*}Ne is as small as $\tau \simeq 4\times10^{-12}$ s, which is a few orders of magnitude less than those of the positron and parapositronium.

In his further experiments [6, 7] Levin discovered that the peculiarity of the annihilation spectrum in neon (abnormally widely scattered points) is linked to the presence in natural neon of a substantial quantity of its isotope ^{22}Ne (around 9%). Levin called this effect the *isotope anomaly*. Time spectra were measured in neon environments of two isotopic compositions: (1) natural neon (90.88% of ^{20}Ne, 0.26% of ^{21}Ne, and 8.86% of ^{22}Ne); (2) neon with reduced content of ^{22}Ne (94.83% of ^{20}Ne, 0.26% of ^{21}Ne, and 4.91% of ^{22}Ne). Comparison of the time spectra of positron decay revealed that in natural neon (composition 1) the shoulder is fuzzy, while in neon poor in ^{22}Ne (composition 2) the shoulder is always pronounced. In the part of the spectrum to which o-Ps decay mostly contributes, the ratio between intensity of decay in ^{22}Ne-poor neon and that in natural neon (with more ^{22}Ne) is 1.85 ± 0.1 [7].

The relationship between the anomaly of positron annihilation in neon and the presence of ^{22}Ne admixture, as shown in [6, 7], hints at the existence in gaseous neon of *collective nuclear excitation* of ^{22}Ne isotopes. In the terminal stage of β^+-decay nuclear excitation of ^{22*}Ne (life time $\sim 4\times10^{-12}$ s) is somehow passed to a set of ^{22}Ne nuclei around the source of positrons and is carried away by a nuclear γ_n-quantum after a long delay in the moment of self-annihilation of orthopositronium (free positrons and parapositronium live much shorter). Hence collective excitation of ^{22}Ne atoms seems to be the reason for the isotope anomaly. On the other hand, the nature of the material carrier that passes excitation of nuclear ^{22*}Ne to the surrounding ^{22}Ne atoms is still unclear, as is the means by which orthopositronium is linked to collective excitation — collective nuclear excitation is only known in crystals (Mössbauer effect, 1958).

In 1990 Levin [8] suggested, as a result of a relationship between orthopositronium and collective nuclear excitation, that a 1-photon mode of its annihilation should be observed. But decay of o-Ps into one γ-quantum would break the laws of conservation of Quantum Electrodynamics. To justify this phenomenological conclusion without breaking QED laws, Levin, in his generalised study [9], suggested that in the specific experimental environment, annihilation of some orthopositronium atoms releases one γ-quantum into our world and two γ-quanta into a mirror Universe, placing them beyond observation. But before any experiments are designed to prove or disprove the existence of such a "1-photon" mode, or any theory is developed to explain the observed effect, the problem still requires discussion.

Another anomaly is the substantially higher measured rate of annihilation of orthopositronium (the reciprocal to its life span) compared to that predicted by QED.

Measurement of the orthopositronium annihilation rate is among the main tests aimed at experimental verification of QED. Before the mid 1980's no difference between theory and experiment was observed, as measurement precision remained at the same low level.

In 1987, thanks to new precision technology, a group of researchers based at the University of Michigan (Ann Arbor) made a breakthrough in this area. The experimental results showed a substantial gap between experiment and theory. The anomaly that the Michigan group revealed was that measured rates of annihilation at $\lambda_{T(exp)} = 7.0514\pm0.0014\ \mu s^{-1}$ and $\lambda_{T(exp)} = 7.0482\pm0.0016\ \mu s^{-1}$ (to a precision of 0.02% and 0.023% using gas and vacuum methods [10–13] were much higher compared to $\lambda_{T(theor)} = 7.00383\pm0.00005\ \mu s^{-1}$ as predicted by QED [14–17]. The 0.2% effect was ten times greater than the measurement precision, and was later called the λ_T-anomaly [9].

In 1986 Robert Holdom [18] suggested that "mixed type" particles may exist, which, being in a state of oscillation, stay for some time in our world and for some time in a mirror Universe. In the same year S. Glashow [18] gave further development to the idea and showed that in the case of 3-photon annihilation o-Ps will "mix up" with its mirror twin, thus producing two effects: (1) a higher annihilation rate due to an additional mode of decay, o-Ps$\rightarrow$nothing, because products of decay passed into the mirror Universe cannot be detected; (2) the ratio between orthopositronium and parapositronium numbers will decrease from o-Ps : p-Ps = 3:1 to 1.5:1. But because at that time (1986) no such effects were reported, Glashow concluded that no oscillation is possible between our-world and mirror-world orthopositronium.

On the other hand, by the early 1990's these theoretical studies motivated many researchers worldwide to an experimental search for various "exotic" (unexplained by QED) modes of o-Ps decay, which could shed some light on the abnormally high rate of decay. These were, to name just a few, search for o-Ps$\rightarrow$nothing mode [20], check of possible contribution from 2-photon mode [21–23] or from other exotic modes [24–26]. As a result it has been shown that no exotic modes can contribute to the anomaly, while contribution of the o-Ps$\rightarrow$nothing mode is limited to $< 5.8\times10^{-4}$ of o-Ps$\rightarrow 3\gamma$.

In a generalised study in 1995 [9] it was pointed out that the programme of critical experiments was limited to a search for the 1-photon mode o-Ps$\rightarrow\gamma\backslash 2\gamma'$ involving the mirror Universe and to a search for the mode o-Ps$\rightarrow$nothing. The situation has not changed significantly over the past five years. The most recent publication on this subject, in May 2000 [27], still focused on the Holdom-Glashow suggestion of a possible explanation of the λ_T-anomaly by interaction of orthopositronium with its mirror-world twin, and on a search for the o-Ps$\rightarrow$nothing mode. But no theory has yet been proposed to account for the possibility of such an interaction and to describe its mechanism.

The absence of a clear explanation of the λ_T-anomaly encouraged G. S. Adkins *et al.* [28] to suggest the experiments made in Japan [29] in 1995 as an alternative to the basic Michigan experiments. No doubt, the high statistical accuracy of the Japanese measurements [29] puts them on the same

level as the basic experiments [10–13]. But all the Michigan measurements possessed the property of a "full experiment", which in this particular case means no external influence could affect the wave function of positronium. Such an influence is inevitable due to the electrodynamic nature of positronium, and can be avoided only using special techniques. As was shown later, by Levin [31], this factor was not taken into account in Japanese measurements [29] and thus they do not possess property of a "full experiment".

As early as 1993 S. G. Karshenboim, one of the leaders in the theory, showed that QED had actually exhausted its theoretical capabilities to explain the orthopositronium anomalies [30]. The puzzle remains unresolved.

January 30, 2007 Dmitri Rabounski
Editor-in-Chief

References

1. Vallery R. S., Zitzewitz P. W. and Gidley D. W. Resolution of the orthopositronium-lifetime puzzle. *Phys. Rev. Lett.*, 2003, v. 90, 203402 (1–4).
2. Osmon P. E. Positron lifetime spectra in noble gases. *Phys. Rev. B*, 1965, v. 138, 216.
3. Tao S. J., Bell J. and Green J. H. Fine structure in delayed coincidence lifetime curves for positron in argon. *Proc. Phys. Soc.*, 1964, v. 83, 453.
4. Levin B. M. and Shantarovich V. P. Annihilation of positrons in gaseous neon. *High Energy Chem.*, 1977, v. 11(4), 322–323.
5. Levin B. M. Time spectra of positron annihilation in neon. *Soviet J. Nucl. Physics*, 1981, v. 34(6), 917–918.
6. Levin B. M. and Shantarovich V. P. Anomalies in the time spectra of positron in gaseous neon. *Soviet J. Nucl. Physics*, 1984, v. 39(6), 855–856.
7. Levin B. M., Kochenda L. M., Markov A. A. and Shantarovich V. P. Time spectra of annihilation of positrons (^{22}Na) in gaseous neon of various isotopic compositions. *Soviet J. Nucl. Physics*, 1987, v. 45(6), 1119–1120.
8. Levin B. M. Orthopositronium: a program for critical experiments. *Soviet J. Nucl. Physics*, 1990, v. 52(2), 342–343.
9. Levin B. M. On the kinematics of one-photon annihilation of orthopositronium. *Phys. At. Nuclei*, 1995, v. 58(2), 332–334.
10. Gidley D. W., Rich A., Sweetman E. and West D. New precision measurements of the decay rates of singlet and triplet positronium. *Phys. Rev. Lett.*, 1982, v. 49, 525–528.
11. Westbrook C.I., Gidley D.W., Conti R.S. and Rich A. New precision measurement of the orthopositronium decay rate: a discrepancy with theory. *Phys. Rev. Lett.*, 1987, v. 58, 1328–1331.
12. Westbrook C. I., Gidley D. W., Conti R. S. and Rich A. Precision measurement of the orthopositronium vacuum decay rate using the gas technique. *Phys. Rev. A*, 1989, v. 40, 5489–5499.
13. Nico J. S., Gidley D. W., Rich A. and Zitzewitz P. W. Precision measurement of the orthopositronium decay rate using the vacuum technique. *Phys. Rev. Lett.*, 1990, v. 65, 1344–1347.
14. Caswell W. E. and Lepage G. P. O(α^2-in-α)-corrections in positronium-hyperfine splitting and decay rate. *Phys. Rev. A*, 1979, v. 20, 36.
15. Adkins G. S. Radiative-corrections to positronium decay. *Ann. Phys. (N.Y.)*, 1983, v. 146, 78.
16. Adkins G. S., Salahuddin A. A. and Schalm K. E. Analytic evaluation of the self-energy and outer-vertex corrections to the decay rate of orthopositronium in the Fried-Yennie gauge. *Phys. Rev. A*, 1992, v. 45, 3333–3335.
17. Adkins G. S., Salahuddin A. A. and Schalm K. E. Order-α corrections to the decay rate of ortopositronium in the Fried-Yennie gauge. *Phys. Rev. A*, 1992, v. 45, 7774–7780.
18. Holdom B. Two U(1)'s and ϵ charge shifts. *Phys. Lett. B*, 1986, v. 166, 196–198.
19. Glashow S. L. Positronium versus the mirror Universe. *Phys. Lett. B*, 1986, v. 167, 35–36.
20. Atoyan G. S., Gninenko S. N., Razin V. I. and Ryabov Yu. V. A search for photonless annihilation of orthopositronium. *Phys. Lett. B*, 1989, v. 220, 317–320.
21. Asai S., Orito S., Sanuki T., Yasuda M. and Yokoi T. Direct search for orthopositronium decay into two photons. *Phys. Rev. Lett.*, 1991, v. 66, 1298–1301.
22. Gidley D. W., Nico J. S. and Skalsey M. Direct search for two-photon modes of orthopositronium. *Phys. Rev. Lett.*, 1991, v. 66, 1302–1305.
23. Al-Ramadhan A. H. and Gidley D. W. New precision measurement of the decay rate of singlet positronium. *Phys. Rev. Lett.*, 1994, v. 72, 1632–1635.
24. Orito S., Yoshimura K., Haga T., Minowa M. and Tsuchiaki M. New limits on exotic two-body decay of orthopositronium. *Phys. Rev. Lett.*, 1989, v. 63, 597–600.
25. Mitsui T., Fujimoto R., Ishisaki Y., Ueda Y., Yamazaki Y., Asai S. and Orito S. Search for invisible decay of orthopositronium. *Phys. Rev. Lett.*, 1993, v. 70, 2265–2268.
26. Skalsey M. and Conti R. S. Search for very weakly interacting, short-lived, C-odd bosons and the orthopositronium decay-rate problem. *Phys. Rev. A*, 1997, v. 55(2), 984.
27. Foot R. and Gninenko S. N. Can the mirror world explain the orthopositronium lifetime puzzle? *Phys. Lett. B*, 2000, v. 480, 171–175.
28. Adkins G. S., Melnikov K. and Yelkhovsky A. Virtual annihilation contribution to orthopositronium rate decay. *Phys. Rev. A*, 1999, v. 60(4), 3306–3307.
29. Asai S., Orito S. and Shinohara N. New measurement of the orthopositronium decay rate. *Phys. Lett. B*, 1995, v. 357, 475–480; Jinnouchi O., Asai S., and Koboyashi T. arXiv: hep-ex/0011011.
30. Karshenboim S. G. Corrections to hyperfine splitting in positronium. *Phys. At. Nuclei*, 1993, v. 56(12), 155–171.
31. Levin B. M. Orthopositronium-lifetime puzzle is not solved: on an effect of non-perturbative contribution. CERN E-Print, EXT-2004-016.

A Proposed Experimentum Crucis for the Orthopositronium Lifetime Anomalies

Boris M. Levin
E-mail: bormikhlev@mail.ru, bormikhlev@mail.ioffe.ru

Expansion of the Standard Model (SM) for the quantitative description of the orthopositronium lifetime anomalies allows formulation of additional experimental tests of supersymmetry in the final state of the positron beta-decay of nuclei such as ^{22}Na, ^{68}Ga, and resolution of the results of the last Michigan experiment (2003).

In 2003, at the University of Michigan (Ann Arbor), a measurement of the o-Ps annihilation rate was carried out, and the researchers reported complete agreement between the experimental value, $\lambda_{\mathrm{T}} = 7.0404(10)(8)\,\mu\mathrm{s}^{-1}$, and the value calculated in the frame of QED, $\lambda_{\mathrm{T(theor)}}$=$7.039979(11)\mu\mathrm{s}^{-1}$ [1]. These measurements were performed by a different technique, namely, a *dc* electric field of 7 kV/cm was introduced into the measurement cell. For this reason, and since they disregarded the "isotope anomaly" of o-Ps in gaseous neon in "resonance conditions" [2, 3], authors [1] could not include the *additional* action of the electric field on the observed o-Ps self-annihilation rate $\lambda_{\mathrm{T(exp)}}$ [3], notwithstanding the provisions they undertook to ensure complete o-Ps thermalization. The additional action of the electric field $E\sim$7 kV/cm oriented parallel to the force of gravity should suppress the excess $\Delta\lambda_{\mathrm{T}}\simeq 0.19\div 0.14\%$ over the calculated value $\lambda_{\mathrm{T(theor)}}$, which had been reported earlier by the Michigan group and referred to quantitatively as the *macroscopic quantum effect* (the "λ_{T}-anomaly" [3])*.

This is why rejection [1] of the conclusions drawn from the earlier high-precision λ_{T} measurements does not appear unambiguous.

The uncertainty we are presently witnessing can be resolved only by performing a program of additional measurements.

Consider the scheme of a Gedanken experiment for a measuring cell filled with a gas (Fig. 1).

Could one substantiate a program of comparative measurements which would yield as a final result the *doubling* of the parameter V to be measured with the external dc electric field orientation changed from *horizontal* to *vertical*? This would be certainly impossible within the SM. An analysis of the o-Ps anomalies within the concept of spontaneously broken complete relativity opens up such a possibility; indeed, restoration of the symmetry under discussion "should be accompanied by doubling of the space-time dimension" [4].

The uniqueness of orthopositronium dynamics (*virtual single-quantum* (!) *annihilation*, *CP*-invariance) make it an intriguing probe to double the space-time (see [5]).

*Here and so forth the sign $\div$ means that the values were obtained in the gas and vacuum experiments respectively.

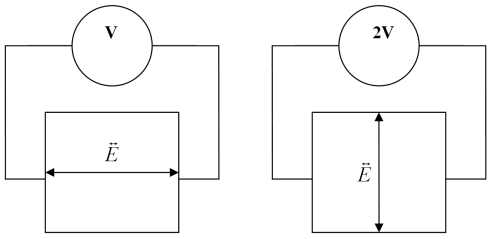

Fig. 1: Scheme and the *result* of a Gedanken experiment with an electric field in a laboratory on Earth. The measuring cell is filled with gas. $\vec{E}$ is orientation and *dc* voltage of an electric field; V is the value of the parameter to be measured.

Consider in this connection again the standard experimental technique used to measure positron/orthopositronium annihilation lifetime spectra.

Figure 2 presents a block diagram of a fast-slow lifetime spectrometer of delayed γ_{n}–γ_{a} coincidences.

Recording of *real* coincidences (in the start-stop arrangement) with a time resolution of 1.7×10^{-9} s [2] between the signal produced by a nuclear γ_{n} quantum of energy $\simeq$1.28 MeV ("start") with the signal generated by the detected γ_{a} annihilation quantum of energy $\simeq 0.34\div 0.51$ MeV ("stop", corresponding, accordingly, to 3γ and 2γ-annihilation) is accompanied by the energy (amplitude) discrimination in the slow ("side") coincidence channels (with a resolution $\delta\tau_{\mathrm{s}}\sim 10^{-6}$ s between the corresponding signals from the last-but-one dynodes of the lifetime PM tubes, an approach that cuts efficiently *random* coincidence noise.

After subtraction of the random coincidence background, the positron annihilation lifetime spectra of inert gases would represent the sums of exponentials with characteristic annihilation rate constants λ_i

$$N(t) = \sum_{i=0}^{i=2} \mathrm{I}_i\, e^{-\lambda_i t},$$

where λ_0 and I_0 are, respectively, the rate and intensity of *two-quantum* annihilation of the para-positronium component (p-Ps), λ_1 and I_1 are the components of *two-quantum* annihilation of the quasi-free positrons that have not formed positronium (with so-called "shoulder" peculiarity [5]), and

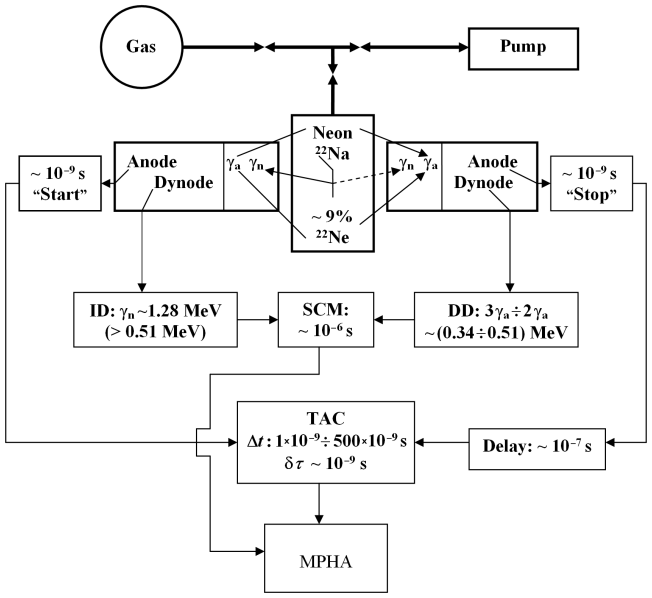

Fig. 2: Block-diagram of the lifetime spectrometer (fast-slow γ_n–γ_a coincidences). ID is for Integral Discriminator (excludes γ_a detection in the "start" channel); DD is for Differential Discriminator (restricts γ_n detection in the "stop" channel); SCM is for Slow Coincidence Module; TAC is for Time-to-Amplitude Converter ($\Delta t \rightarrow$ amplitude); MPHA is multichannel pulse-height analyzer.

λ_2 and I_2 are those of *three-quantum annihilation* of the orthopositronium component.

Experimental bounds accumulated in the two decades of intense studies of the orthopositronium problem lead one to the conclusion that the *additional single-quantum mode* of orthopositronium annihilation involves not a photon but rather a *notoph* (γ° is a zero-mass, zero-helicity particle which is complementary in properties to the photon) [7] and two *mirror photons* γ' with a negative total energy of 3.6×10^{-4} eV [3, 5]:

$$\text{o-Ps} \setminus \text{p-Ps}' \, (\text{p-Ps}') \longrightarrow \gamma^\circ \setminus 2\gamma'.$$

This was how the broadening of the framework in which the nature of the o-Ps anomalies could be analyzed (from QED to SQED) and the phenomenology of the mechanism of energy and momentum deficit compensation in a single-quantum mode were first formulated [7].

Treated from the SM standpoint, however, detection of a quantum of energy 1.022 MeV in the "stop" channel of the fast-slow coincidences is forbidden (see the "lower" and "upper" detection thresholds of $\sim 0.34 \div 0.51$ MeV, respectively, in Fig. 2).

We now come back to the principal question of *how the additional realization of supersymmetry would be established in the experiment*.

Detection of a single-notoph o-Ps annihilation mode should also be accompanied by observation of an energy

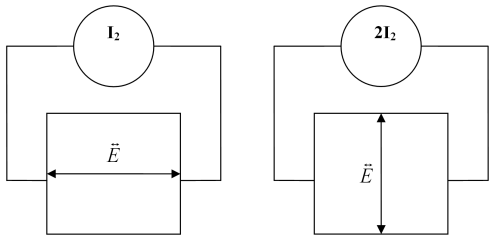

Fig. 3: Scheme of additional measurements: is there a connection between gravity and electromagnetism?

deficit in the "stop" channel of the lifetime spectrometer: indeed, *single-notoph annihilation* is identified in the scintillator by the Compton-scattered electron $\mathbf{e}$, which is bound in the *long-range atom* "shell" in a "pair" $\mathrm{e}\bar{\mathrm{e}}$ with the "electronic hole" $\bar{\mathrm{e}}$ (negative mass) in the "C-field/mirror Universe" structure. Half of the notoph energy, $\sim$0.51 MeV, is transferred to the $\mathbf{e}$ hole ($\bar{\mathrm{e}}$) and, thus, "disappears" (*anti-Compton scattering*). As a result, the additional single-notoph mode is detected by the lifetime spectrometer in the "stop" channel by Compton scattering of an electron e of energy $\leqslant 0.51$ eV.

The experiment is in agreement with the phenomenology proposed for quantitative description of the o-Ps anomalies provided we assume that the additional single-notoph annihilation mode contributes to the *instantaneous coincidence peak* [5]. This means that one half of the intensity of the long-lived lifetime spectral component obtained under "resonance conditions" for neon of natural isotope abundance (I_2) transfers to the $t \sim 0$ region. An electric field of 7 kV/cm applied parallel to the force of gravity should suppress the additional mode and double the orthopositronium component ($2I_2$). Accordingly, in the Michigan experiment (non-resonance conditions) an electric field oriented along the force of gravity would bring about complete agreement between $\lambda_{T(exp)}$ with the QED-calculated value $\lambda_{T(theor)}$; and the disagreement of about $\Delta\lambda_T/\lambda_T \simeq 0.19 \div 0.14\%$ found previously (in experiments without electric field) should again appear after the action of the electric field has been neutralized (by applying it perpendicular to the force of gravity) [3].

The term "anti-Compton scattering" has been borrowed from J. L. Synge [8]; it appears appropriate to cite here an excerpt from the abstract of this paper written by a celebrated proponent of the theory of relativity:

> "The purpose of this paper is to answer the following question in terms of concepts of classical relativistic mechanics: How is Compton scattering altered if we replace the photon by a particle of zero rest mass and *negative* energy, and apply the conservation of 4-momentum? [...] Since particles with negative energies are not accepted in modern physics, it is perhaps best to regard this work as a kinematical exercise in Minkowskian geometry, worth recording because the results are not obvious".

Observation of orthopositronium anomalies gives one physical grounds to broaden the present-day SM. It now appears appropriate to analyze "anti-Compton scattering" in connection with the detection of notoph in the proposed program of *additional measurements*, which aim at proving the existence of a connection between gravity and electromagnetism [3].

We may add that the concept of the supersymmetric version of a *spin-$^1/_2$ quasi-particle* and a hole as *supersymmetric partners* has been discussed in the literature [9].

To sum up: one should carry out additional measurements because the result, *inconceivable* in the frame of the SM, becomes an expected result in the program of *experimentum crucis* (Fig. 3).

A positive result of this crucial experiment would mean the birth of *new physics* that would be complementary to the Standard Model.

Submitted on January 24, 2007
Accepted on January 30, 2007

References

1. Vallery R. S., Gidley D. W. and Zitzewitz P. W. Resolution of orthopositronium-lifetime puzzle. *Phys. Rev. Lett.*, 2003, v. 90(20), 203402 (1–4).
2. Levin B. M., Kochenda L. M., Markov A. A. and Shantarovich V. P. Time spectra of annihilation of positron (^{22}Na) in gaseous neon of various isotopic compositions. *Sov. J. Nucl. Phys.*, 1987, v. 45(6), 1119–1120.
3. Kotov B. A., Levin B. M. and Sokolov V. I. Orthopositronium: on the possible relation of gravity to electricity. Preprint-1784, A. F. Ioffe Physical Technical Institute of Russian Academy of Sciences. St.-Petersburg, 2005; arXiv: quant-ph/0604171.
4. Andreev A. F. Spontaneously broken complete relativity. *JETF Lett.*, 1982, v. 36(3), 100.
5. Levin B. M. Orthopositronium: annihilation of positron in gaseous neon. arXiv: quant-ph/0303166.
6. Ogievetskii V. I. and Polubarinov I. V. Notoph and its possible interactions. *Sov. J. Nucl. Res.*, 1966, v. 4(1), 156.
7. Levin B. M. On the kinematics of one-photon annihilation of orthopositronium. *Phys. At. Nucl.*, 1995, v. 58 (2). 332.
8. Synge J. L. Anti-Compton scattering. *Proc. Roy. Ir. Acad.*, 1974, v.A74 (9), 67.
9. Lee C. J. Spin-$^1/_2$ particle and hole as supersymmetry partners. *Phys. Rev. A*, 1994, v.50, R4 (4–6).

Numerical Solution of Time-Dependent Gravitational Schrödinger Equation

Vic Christianto*, Diego L. Rapoport† and Florentin Smarandache‡

*Sciprint.org — a Free Scientific Electronic Preprint Server, http://www.sciprint.org
E-mail: admin@sciprint.org
†Dept. of Sciences and Technology, Universidad Nacional de Quilmes, Bernal, Argentina
E-mail: diego.rapoport@gmail.com
‡Department of Mathematics, University of New Mexico, Gallup, NM 87301, USA
E-mail: smarand@unm.edu

In recent years, there are attempts to describe quantization of planetary distance based on time-independent gravitational Schrödinger equation, including Rubcic & Rubcic's method and also Nottale's Scale Relativity method. Nonetheless, there is no solution yet for time-dependent gravitational Schrödinger equation (TDGSE). In the present paper, a numerical solution of time-dependent gravitational Schrödinger equation is presented, apparently for the first time. These numerical solutions lead to gravitational Bohr-radius, as expected. In the subsequent section, we also discuss plausible extension of this gravitational Schrödinger equation to include the effect of phion condensate via Gross-Pitaevskii equation, as described recently by Moffat. Alternatively one can consider this condensate from the viewpoint of Bogoliubov-deGennes theory, which can be approximated with coupled time-independent gravitational Schrödinger equation. Further observation is of course recommended in order to refute or verify this proposition.

1 Introduction

In the past few years, there have been some hypotheses suggesting that quantization of planetary distance can be derived from a gravitational Schrödinger equation, such as Rubcic & Rubcic and also Nottale's scale relativity method [1, 3]. Interestingly, the gravitational Bohr radius derived from this gravitational Schrödinger equation yields prediction of new type of astronomical observation in recent years, i.e. extrasolar planets, with unprecedented precision [2].

Furthermore, as we discuss in preceding paper [4], using similar assumption based on gravitational Bohr radius, one could predict new planetoids in the outer orbits of Pluto which are apparently in good agreement with recent observational finding.. Therefore one could induce from this observation that the gravitational Schrödinger equation (and gravitational Bohr radius) deserves further consideration.

In the meantime, it is known that all present theories discussing gravitational Schrödinger equation only take its time-independent limit. Therefore it seems worth to find out the solution and implication of time-dependent gravitational Schrödinger equation (TDGSE). This is what we will discuss in the present paper.

First we will find out numerical solution of time-independent gravitational Schrödinger equation which shall yield gravitational Bohr radius as expected [1, 2, 3]. Then we extend our discussion to the problem of time-dependent gravitational Schrödinger equation.

In the subsequent section, we also discuss plausible extension of this gravitational Schrödinger equation to include the effect of phion condensate via Gross-Pitaevskii equation, as described recently by Moffat [5]. Alternatively one can consider this phion condensate model from the viewpoint of Bogoliubov-deGennes theory, which can be approximated with coupled time-independent gravitational Schrödinger equation. To our knowledge this proposition of coupled time-independent gravitational Schrödinger equation has never been considered before elsewhere.

Further observation is of course recommended in order to verify or refute the propositions outlined herein.

All numerical computation was performed using Maple. Please note that in all conditions considered here, we use only gravitational Schrödinger equation as described in Rubcic & Rubcic [3], therefore we neglect the scale relativistic effect for clarity.

2 Numerical solution of time-independent gravitational Schrödinger equation and time-dependent gravitational Schrödinger equation

First we write down the time-independent gravitational Schrödinger radial wave equation in accordance with Rubcic & Rubcic [3]:

$$\frac{d^2R}{dr^2}+\frac{2}{r}\frac{dR}{dr}+\frac{8\pi m^2 E'}{H^2}R+ +\frac{2}{r}\frac{4\pi^2 GMm^2}{H^2}R-\frac{\ell(\ell+1)}{r^2}R=0\,. \tag{1}$$

When H, V, E' represents gravitational Planck constant, Newtonian potential, and the energy per unit mass of the

orbiting body, respectively, and [3]:

$$H = h\left(2\pi f \frac{Mm_n}{m_0^2}\right), \tag{2}$$

$$V(r) = -\frac{GMm}{r}, \tag{3}$$

$$E' = \frac{E}{m}. \tag{4}$$

By assuming that R takes the form:

$$R = e^{-\alpha r} \tag{5}$$

and substituting it into equation (1), and using simplified terms only of equation (1), one gets:

$$\Psi = \alpha^2 e^{-\alpha r} - \frac{2\alpha e^{-\alpha r}}{r} + \frac{8\pi GMm^2 e^{-\alpha r}}{rH^2}. \tag{6}$$

After factoring this equation (7) and solving it by equating the factor with zero, yields:

$$RR = -\frac{2\left(4\pi GMm^2 - H^2\alpha\right)}{\alpha^2 H^2} = 0, \tag{7}$$

or

$$RR = 4\pi GMm^2 - H^2\alpha = 0, \tag{8}$$

and solving for α, one gets:

$$a = \frac{4\pi^2 GMm^2}{H^2}. \tag{9}$$

Gravitational Bohr radius is defined as inverse of this solution of α, then one finds (in accordance with Rubcic & Rubcic [3]):

$$r_1 = \frac{H^2}{4\pi^2 GMm^2}, \tag{10}$$

and by substituting back equation (2) into (10), one gets [3]:

$$r_1 = \left(\frac{2\pi f}{\alpha c}\right)^2 GM. \tag{11}$$

Equation (11) can be rewritten as follows:

$$r_1 = \frac{GM}{\nu_0^2}, \tag{11a}$$

where the "specific velocity" for the system in question can be defined as:

$$\nu_0 = \left(\frac{2\pi f}{\alpha c}\right)^{-1} = \alpha_g c. \tag{11b}$$

The equations (11a)-(11b) are equivalent with Nottale's result [1, 2], especially when we introduce the quantization number: $r_n = r_1 n^2$ [3]. For complete Maple session of these all steps, see Appendix 1. Furthermore, equation (11a) may be generalised further to include multiple nuclei, by rewriting it to become: $r_1 = (GM)/v^2 \Rightarrow r_1 = (G\Sigma M)/v^2$, where ΣM represents the sum of central masses.

Solution of time-dependent gravitational Schrödinger equation is more or less similar with the above steps, except that we shall take into consideration the right hand side of Schrödinger equation and also assuming time dependent form of r:

$$R = e^{-\alpha r(t)}. \tag{12}$$

Therefore the gravitational Schrödinger equation now reads:

$$\begin{aligned}&\frac{d^2R}{dr^2} + \frac{2}{r}\frac{dR}{dr} + \frac{8\pi m^2 E'}{H^2}R + \\ &+\frac{2}{r}\frac{4\pi^2 GMm^2}{H^2}R - \frac{\ell(\ell+1)}{r^2}R = H\frac{dR}{dt},\end{aligned} \tag{13}$$

or by using Leibniz chain rule, we can rewrite equation (15) as:

$$\begin{aligned}&-H\frac{dR}{dr(t)}\frac{dr(t)}{dt} + \frac{d^2R}{dr^2} + \frac{2}{r}\frac{dR}{dr} + \frac{8\pi m^2 E'}{H^2}R + \\ &+\frac{2}{r}\frac{4\pi^2 GMm^2}{H^2}R - \frac{\ell(\ell+1)}{r^2}R = 0.\end{aligned} \tag{14}$$

The remaining steps are similar with the aforementioned procedures for time-independent case, except that now one gets an additional term for RR:

$$\begin{aligned}RR' = H^3\alpha\left(\frac{d}{dt}r(t)\right)r(t) - \alpha^2 r(t)H^2 + \\ + 8\pi GMm^2 - 2H^2\alpha = 0.\end{aligned} \tag{15}$$

At this point one shall assign a value for $\frac{d}{dt}r(t)$ term, because otherwise the equation cannot be solved. We choose $\frac{d}{dt}r(t) = 1$ for simplicity, then equation (15) can be rewritten as follows:

$$RR' := \frac{rH^3\alpha}{2} + \frac{rH^2\alpha^2}{2} + 4\pi^2 GMm^2 - H^2\alpha = 0. \tag{16}$$

The roots of this equation (16) can be found as follows:

$$\begin{aligned}a1 &:= \frac{-r^2H + 2H + \sqrt{r^4H^4 - 4H^3r + 4H^2 - 32rGMm^2\pi^2}}{2rH}, \\ a2 &:= \frac{-r^2H + 2H - \sqrt{r^4H^4 - 4H^3r + 4H^2 - 32rGMm^2\pi^2}}{2rH}.\end{aligned} \tag{17}$$

Therefore one can conclude that there is time-dependent modification factor to conventional gravitational Bohr radius (10). For complete Maple session of these steps, see Appendix 2.

3 Gross-Pitaevskii effect. Bogoliubov-deGennes approximation and coupled time-independent gravitational Schrödinger equation

At this point it seems worthwhile to take into consideration a proposition by Moffat, regarding modification of Newtonian acceleration law due to phion condensate medium, to include Yukawa type potential [5, 6]:

$$a(r) = -\frac{G_\infty M}{r^2} + K\frac{\exp(-\mu_\phi r)}{r^2}(1 + \mu_\phi r). \tag{18}$$

Therefore equation (1) can be rewritten to become:

$$\frac{d^2R}{dr^2}+\frac{2}{r}\frac{dR}{dr}+\frac{8\pi m^2E'}{H^2}R+ \\ +\frac{2}{r}\frac{4\pi^2\big(GM-K\exp(-\mu_\phi r)(1+\mu_\phi r)\big)m^2}{H^2}R- \\ -\frac{\ell(\ell+1)}{r^2}R=0, \tag{19}$$

or by assuming $\mu = 2\mu_0 = \mu_0 r$ for the exponential term, equation (19) can be rewritten as:

$$\frac{d^2R}{dr^2}+\frac{2}{r}\frac{dR}{dr}+\frac{8\pi m^2E'}{H^2}R+ \\ +\frac{2}{r}\frac{4\pi^2\big(GM-Ke^{-2\mu_0}(1+\mu_0 r)\big)m^2}{H^2}R-\frac{\ell(\ell+1)}{r^2}R=0. \tag{20}$$

Then instead of equation (8), one gets:

$$RR''=8\pi GMm^2-2H^2\alpha-8\pi^2m^2Ke^{-\mu_0}(1+\mu)=0. \tag{21}$$

Solving this equation will yield a modified gravitational Bohr radius which includes Yukawa effect:

$$r_1=\frac{H^2}{4\pi^2(GM-Ke^{-2\mu_0})m^2} \tag{22}$$

and the modification factor can be expressed as ratio between equation (22) and (10):

$$\chi=\frac{GM}{(GM-Ke^{-2\mu_0})}. \tag{23}$$

(For complete Maple session of these steps, see Appendix 3.)

A careful reader may note that this "Yukawa potential effect" as shown in equation (20) could be used to explain the small discrepancy (around $\pm 8\%$) between the "observed distance" and the computed distance based on gravitational Bohr radius [4, 6a]. Nonetheless, in our opinion such an interpretation remains an open question, therefore it may be worth to explore further.

There is, however, an alternative way to consider phion condensate medium i.e. by introducing coupled Schrödinger equation, which is known as Bogoliubov-deGennes theory [7]. This method can be interpreted also as generalisation of assumption by Rubcic-Rubcic [3] of subquantum structure composed of positive-negative Planck mass. Therefore, taking this proposition seriously, then one comes to hypothesis that there shall be coupled Newtonian potential, instead of only equation (3).

To simplify Bogoliubov-deGennes equation, we neglect the time-dependent case, therefore the wave equation can be written in matrix form [7, p.4]:

$$[A]\,[\Psi]=0, \tag{24}$$

where $[A]$ is 2×2 matrix and $[\Psi]$ is 2×1 matrix, respectively, which can be represented as follows (using similar notation with equation 1):

$$\big[A\big]=\begin{pmatrix} \dfrac{8\pi GMm^2e^{-\alpha r}}{rH^2} & \alpha^2e^{-\alpha r}-\dfrac{2\alpha e^{-\alpha r}}{r} \\ \alpha^2e^{-\alpha r}-\dfrac{2\alpha e^{-\alpha r}}{r} & -\dfrac{8\pi GMm^2e^{-\alpha r}}{rH^2} \end{pmatrix} \tag{25}$$

and

$$\big[\Psi\big]=\begin{pmatrix} f(r) \\ g(r) \end{pmatrix}. \tag{26}$$

Numerical solution of this matrix differential equation can be found in the same way with the previous methods, however we leave this problem as an exercise for the readers.

It is clear here, however, that Bogoliubov-deGennes approximation of gravitational Schrödinger equation, taking into consideration phion condensate medium will yield nonlinear effect, because it requires solution of matrix differential equation* (21) rather than standard ODE in conventional Schrödinger equation (or time-dependent PDE in 3D-condition). This perhaps may explain complicated structures beyond Jovian Planets, such as Kuiper Belt, inner and outer Oort Cloud etc. which of course these structures cannot be predicted by simple gravitational Schrödinger equation. In turn, from the solution of (21) one could expect that there are numerous undiscovered celestial objects in the Oort Cloud.

Further observation is also recommended in order to verify and explore further this proposition.

4 Concluding remarks

In the present paper, a numerical solution of time-dependent gravitational Schrödinger equation is presented, apparently for the first time. This numerical solution leads to gravitational Bohr-radius, as expected.

In the subsequent section, we also discuss plausible extension of this gravitational Schrödinger equation to include the effect of phion condensate via Gross-Pitaevskii equation, as described recently by Moffat. Alternatively one can consider this condensate from the viewpoint of Bogoliubov-deGennes theory, which can be approximated with coupled time-independent gravitational Schrödinger equation.

It is recommended to conduct further observation in order to verify and also to explore various implications of our propositions as described herein.

Acknowledgment

The writers would like to thank to Profs. C. Castro for valuable discussions.

Submitted on January 08, 2007
Accepted on January 30, 2007
After revision: March 06, 2007

*For recent articles discussing analytical solution of matrix differential equations, the reader is referred to Electronic Journal of Differential Equations (free access online on many mirrors as http://ejde.math.txstate.edu, http://ejde.math.unt.edu, http://www.emis.de/journals/EJDE etc.).

References

1. Nottale L. *et al. Astron. & Astrophys.*, 1997, v. 322, 1018.
2. Nottale L., Schumacher G. and Levefre E. T. *Astron. & Astrophys.*, 2000, v. 361, 379–389; accessed online on http://daec.obspm.fr/users/nottale.
3. Rubcic A. and Rubcic J. The quantization of solar like gravitational systems. *Fizika*, B-7, 1998, v. 1, No. 1–13.
4. Smarandache F. and Christianto V. *Progress in Physics*, 2006, v. 2, 63–67.
5. Moffat J. arXiv: astro-ph/0602607.
6. Smarandache F. and Christianto V. *Progress in Physics*, 2006, v. 4, 37–40; [6a] Christianto V. *EJTP*, 2006, v. 3, No. 12, 117–144; accessed onle on http://www.ejtp.com.
7. Lundin N. I. Microwave induced enhancement of the Josephson DC. *Chalmers University of Technology & Gotterborg University Report*, p. 4–7.
8. Griffin M. arXiv: cond-mat/9911419.
9. Tuszynski J. *et al. Physica A*, 2003, v. 325, 455–476; accessed onle on http://sciencedirect.com.
10. Toussaint M. arXiv: cs.SC/0105033.
11. Fischer U. arXiv: cond-mat/9907457; [8a] arXiv: cond-mat/0004339.
12. Zurek W. (ed.) In: *Proc. Euroconference in Formation and Interaction of Topological Defects*, Plenum Press, 1995; accessed online: arXiv: cond-mat/9502119.
13. Volovik G. arXiv: cond-mat/0507454.

Appendix 1 Time-independent gravitational Schrödinger equation

> restart;
> with (linalg);
> R:=exp(−(alpha*r));

$$R := e^{-\alpha r}$$

> D1R:=diff(R,r); D2R:=diff(D1R,r);

$$D1R := -\alpha e^{-\alpha r}$$

$$D2R := -\alpha^2 e^{-\alpha r}$$

> SCHEQ1:=D2R+D1R*2/r+8*pi^2*m*E*R/h^2+8*pi^2*G*M*m^2*R/(r*h^2)−l*(l+1)*R/r^2=0;
> XX1:=factor(SCHEQ1);
> #Using simplified terms only from equation (A*8, of Rubcic & Rubcic, 1998)
> ODESCHEQ:=D2R+D1R*2/r+8*pi^2*G*M*m^2*R/(r*h^2)=0;

$$ODESCHEQ := \alpha^2 e^{-\alpha r} - \frac{2\alpha e^{-\alpha r}}{r} + \frac{8\pi^2 GMm^2 e^{-\alpha r}}{rH^2} = 0$$

> XX2:=factor(SCHEQ2);

$$XX2 := \frac{e^{-\alpha r}\left(\alpha^2 rH^2 - 2H^2\alpha + 8\pi^2 GMm^2\right)}{rH^2} = 0$$

> RR:=solve(XX2,r);

$$RR := -\frac{2(4\pi^2 GMm^2 - H^2\alpha)}{\alpha^2 H^2}$$

> #Then solving for RR=0, yields:
> SCHEQ3:=4*pi^2*G*M*m^2−h^2*alpha=0;

$$SCHEQ3 := 4\pi^2 GMm^2 - H^2\alpha = 0$$

> a:=solve(SCHEQ3,alpha);

$$a := \frac{4\pi^2 GMm^2}{H^2}$$

> #Gravitational Bohr radius is defined as inverse of alpha:
> gravBohrradius:=1/a;

$$r_{gravBohr} := \frac{H^2}{4\pi^2 GMm^2}$$

Appendix 2 Time-dependent gravitational Schrödinger equation

> #Solution of gravitational Schrodinger equation (Rubcic, Fizika 1998);
> restart;
> #with time evolution (Hagendorn's paper);
> S:=r(t); R:=exp(−(alpha*S)); R1:=exp(−(alpha*r));

$$S := r(t)$$

$$R := e^{-\alpha r}$$

> D4R:=diff(S,t); D1R:=−alpha*exp(−(alpha*S)); D2R:=−alpha^2*exp(−(alpha*S)); D5R:=D1R*D4R;

$$D4R := \frac{d}{dt}r(t)$$

$$D1R := -\alpha e^{-\alpha r(t)}$$

$$D2R := -\alpha^2 e^{-\alpha r(t)}$$

$$D1R := -\alpha e^{-\alpha r(t)}\frac{d}{dt}r(t)$$

> #Using simplified terms only from equation (A*8)
> SCHEQ3:=−h*D5R+D2R+D1R*2/S+8*pi^2*G*M*m^2*R/(S*h^2);
> XX2:=factor(SCHEQ3);

$$XX2 := \frac{e^{-\alpha r(t)}\left(H^3\alpha\frac{dr(t)}{dt}r(t) - \alpha^2 r(t)H^2 - 2H^2\alpha + 8\pi^2 GMm^2\right)}{r(t)H^2} = 0$$

> #From standard solution of gravitational Schrodinger equation, we know (Rubcic, Fizika 1998):
> SCHEQ4:=4*pi^2*G*M*m^2−h^2*alpha;

$$SCHEQ4 := 4\pi^2 GMm^2 - H^2\alpha$$

> #Therefore time-dependent solution of Schrodinger equation may introduce new term to this gravitational Bohr radius.
> SCHEQ5:=(XX2*(S*h^2)/(exp(−(alpha*S))))−2*SCHEQ4;

$$ODESCHEQ5 := H^3\alpha\frac{dr(t)}{dt}r(t) - \alpha^2 r(t)H^2$$

> #Then we shall assume for simplicity by assigning value to d[r(t)]/dt:
> D4R:=1;
> Therefore SCHEQ5 can be rewritten as:
> SCHEQ5:= H^3*alpha*r/2+alpha^2*r*H^2/2−4*pi^2*G*M*m^2−H^2*alpha=0;

$$SCHEQ5 := \frac{rH^3\alpha}{2} + \frac{rH^2\alpha^2}{2} + 4\pi^2 GMm^2 - H^2\alpha = 0$$

> Then we can solve again SCHEQ5 similar to solution of SCHEQ4:
> a1:=solve(SCHEQ5,alpha);

$$a1 := \frac{-r^2H + 2H + \sqrt{r^4H^4 - 4H^3r + 4H^2 - 32rGMm^2\pi^2}}{2rH}$$

$$a2 := \frac{-r^2H + 2H - \sqrt{r^4H^4 - 4H^3r + 4H^2 - 32rGMm^2\pi^2}}{2rH}$$

> #Therefore one could expect that there is time-dependent change of gravitational Bohr radius.

Appendix 3 Time-independent gravitational Schrödinger equation with Yukawa potential [5]

> #Extension of gravitational Schrodinger equation (Rubcic, Fizika 1998);
> restart;
> #departure from Newton potential;
> R:=exp(−(alpha*r));

$$R := e^{-\alpha r}$$

> D1R:= diff(R,r); D2R:= diff(D1R,r);

$$D1R := -\alpha e^{-\alpha r}$$

$$D2R := -\alpha^2 e^{-\alpha r}$$

> SCHEQ2:=D2R+D1R*2/r+8*piˆ2*(G*M−K*exp(−2*mu)*(1+mu*r))*mˆ2*R/(r*hˆ2)=0;

$$ODESCHEQ := \alpha^2 e^{-\alpha r} - \frac{2\alpha e^{-\alpha r}}{r} + \\ + \frac{8\pi^2(GM - Ke^{-2\mu}(1+\mu r))m^2 e^{-\alpha r}}{rH^2} = 0$$

> XX2:=factor(SCHEQ2);
> RR1:=solve(XX2,r);

$$RR1 := -\frac{2(-H^2\alpha + 4\pi^2 GMm^2 - 4\pi^2 m^2 Ke^{-2\mu})}{-\alpha^2 H^2 + 8\pi^2 m^2 Ke^{-2\mu}}$$

> #from standard gravitational Schrodinger equation we know:
> SCHEQ3:=4*piˆ2*G*M*mˆ2−hˆ2*alpha=0;
> a:=solve(SCHEQ3, alpha);
> #Gravitational Bohr radius is defined as inverse of alpha:
> gravBohrradius:=1/a;

$$r_{gravBohr} := \frac{H^2}{4\pi^2 GMm^2}$$

> #Therefore we conclude that the new terms of RR shall yield new terms (YY) into this gravitational Bohr radius:
> PI:= (RR*(alphaˆ2*hˆ2)−(−8*piˆ2*G*M*mˆ2+2*hˆ2*alpha));
> #This new term induced by pion condensation via Gross-Pitaevskii equation may be observed in the form of long-range potential effect. (see Moffat J., arXiv: astro-ph/0602607, 2006; also Smarandache F. and Christianto V. Progress in Physics, v. 2, 2006, & v. 1, 2007, www.ptep-online.com)
> #We can also solve directly:
> SCHEQ5:=RR*(alphaˆ2*hˆ2)/2;

$$SCHEQ5 := \frac{\alpha^2 H^2(-H^2\alpha + 4\pi^2 GMm^2 - 4\pi^2 m^2 Ke^{-2\mu})}{-\alpha^2 H^2 + 8\pi^2 m^2 Ke^{-2\mu}}$$

> a1:=solve(SCHEQ5, alpha);

$$a1 := 0, 0, \frac{4\pi^2 m^2(GM - Ke^{-2\mu})}{H^2}$$

> #Then one finds modified gravitational Bohr radius in the form:
> modifgravBohrradius:=1/(4*piˆ2*(G*M−K*exp(−2*mu))*mˆ2/hˆ2);

$$r_{modified.gravBohr} := \frac{H^2}{4\pi^2 m^2(GM - Ke^{-2\mu})}$$

> #This modification can be expressed in chi-factor:
> chi:=modifgravBohrradius/gravBohrradius;

$$\chi := \frac{GM}{GM - Ke^{-2\mu}}$$

A Note on Unified Statistics Including Fermi-Dirac, Bose-Einstein, and Tsallis Statistics, and Plausible Extension to Anisotropic Effect

Vic Christianto* and Florentin Smarandache†

*Sciprint.org — a Free Scientific Electronic Preprint Server, http://www.sciprint.org
E-mail: admin@sciprint.org

†Department of Mathematics, University of New Mexico, Gallup, NM 87301, USA
E-mail: smarand@unm.edu

In the light of some recent hypotheses suggesting plausible unification of thermo-statistics where Fermi-Dirac, Bose-Einstein and Tsallis statistics become its special subsets, we consider further plausible extension to include non-integer Hausdorff dimension, which becomes realization of fractal entropy concept. In the subsequent section, we also discuss plausible extension of this unified statistics to include anisotropic effect by using quaternion oscillator, which may be observed in the context of Cosmic Microwave Background Radiation. Further observation is of course recommended in order to refute or verify this proposition.

1 Introduction

In recent years, there have been some hypotheses suggesting that the spectrum and statistics of Cosmic Microwave Background Radiation has a kind of *scale invariant* character [1], which may be related to non-integer Hausdorff dimension. Interestingly, in this regard there is also proposition sometime ago suggesting that Cantorian spacetime may have deep link with Bose condensate with non-integer Hausdorff dimension [2]. All of these seem to indicate that it is worth to investigate further the non-integer dimension effect of Bose-Einstein statistics, which in turn may be related to Cosmic Microwave Background Radiation spectrum.

In the meantime, some authors also consider a plausible generalization of known statistics, i.e. Fermi-Dirac, Bose-Einstein, and Tsallis statistics, to become more unified statistics [3, 4]. This attempt can be considered as one step forward from what is already known, i.e. to consider anyons as a generalization of bosons and fermions in two-dimensional systems [5, p. 2] Furthermore, it is known that superfluidity phenomena can also be observed in Fermi liquid [6].

First we will review the existing procedure to generalize Fermi-Dirac, Bose-Einstein, and Tsallis statistics, to become more unified statistics [3, 4]. And then we explore its plausible generalization to include fractality of Tsallis' non-extensive entropy parameter.

In the subsequent section, we also discuss plausible extension of this proposed unified statistics to include anisotropic effect, which may be observed in the context of Cosmic Microwave Background Radiation. In particular we consider possibility to introduce quaternionic momentum. To our knowledge this proposition has never been considered before elsewhere.

Further observation is of course recommended in order to verify or refute the propositions outlined herein.

2 Unified statistics including Fermi-Dirac, Bose-Einstein, and Tsallis statistics

In this section we consider a different theoretical framework to generalize Fermi-Dirac and Bose-Einstein statistics, from conventional method using anyons, [5] in particular because this conventional method cannot be generalized further to include Tsallis statistics which has attracted some attention in recent years.

First we write down the standard expression of Bose distribution [9, p. 7]:

$$\bar{n}(\epsilon_i) = \frac{1}{\exp\big(\beta(\epsilon_i - \mu)\big) - 1}\,, \tag{1}$$

where the harmonic energy levels are given by [9, p. 7]:

$$\epsilon_i = \left(n_x + n_y + n_z + \frac{3}{2}\right)\hbar\omega_0\,. \tag{2}$$

When we assume that bosons and fermions are g-ons obeying fractional exclusion statistics, then we get a very different picture. In accordance with [3], we consider the spectrum of fractal dimension (also called *generalized Renyi dimension* [11]):

$$D_q = \lim_{\delta\to 0}\frac{1}{q-1}\frac{\ln\Omega_q}{\ln\delta}\,, \tag{3}$$

(therefore the spectrum of fractal dimension is equivalent with Hausdorff dimension of the set A [11]).

Then the relation between the entropy and the spectrum of fractal dimension is given by: [3]

$$S_q = -K_B\lim_{\delta\to 0}\ln\delta D_q\,, \tag{4}$$

where K_B is the Boltzmann constant.

The spectrum of fractal dimension may be expressed in terms of p:

$$D_q \approx \frac{1}{q-1} \frac{\sum_{i=1}^{k} p_i^q - 1}{\ln \delta} . \quad (5)$$

Then, substituting equation (6) into (4), we get the Tsallis non-extensive entropy [3]:

$$S_q = -K_B \frac{\sum_{i=1}^{k} p_i^q - 1}{q-1} . \quad (6)$$

After a few more assumptions, and using g-on notation [3], i.e. $g=1$ for generalized Fermi-Dirac statistics and $g=0$ for generalised Bose-Einstein statistics, then one gets the most probable distribution for g-ons [3]:

$$\bar{n}_k(\epsilon_i, g, q) = \frac{1}{\left(1-(q-1)\beta(\epsilon_i-\mu)\right)^{\frac{1}{q-1}} + 2g - 1} , \quad (7)$$

Which gives standard Planck distribution for $\mu=0$, $g=0$ and $q=1$ [3, 9]. In other words, we could expect that g-ons gas statistics could yield more generalized statistics than anyons'.

To introduce further generality of this expression (8), one may consider the parameter q as function of another non-integer dimension, therefore:

$$\bar{n}_k(\epsilon_i, g, q, D) = \frac{1}{\left(1-(q^D-1)\beta(\epsilon_i-\mu)\right)^{\frac{1}{q^D-1}} + 2g - 1} , \quad (8)$$

where $D=1$ then equation (9) reduces to be (8).

Of course, the picture described above will be different if we introduce non-standard momentum [5, p. 7]:

$$p^2 = -\frac{d^2}{dx^2} + \frac{\lambda}{x^2} . \quad (9)$$

In the context of Neutrosophic logic as conceived by one of these writers [8], one may derive a proposition from the arguments presented herein, i.e. apart from common use of anyons as a plausible generalization of fermion and boson, perhaps an alternative method for generalization of fermion and boson can be described as follows:

1. If we denote fermion with (f) and boson with (b), then it follows that there could be a mixture composed of both (f) and (b) $\rightarrow$ (f) $\cap$ (b), which may be called as "anyons";
2. If we denote fermion with (f) and boson with (b), and because $g=1$ for generalized Fermi-Dirac statistics and $g=0$ for generalised Bose-Einstein statistics, then it follows that the wholeness of both (f) and (b) $\rightarrow$ (f) $\cup$ (b), which may be called as "g-on";
3. Taking into consideration of possibility of "neitherness", then if we denote non-fermion with ($\neg$f) and non-boson with ($\neg$b), then it follows that there shall be a mixture composed of both ($\neg$f) and also ($\neg$b) $\rightarrow$ ($\neg$f) $\cap$ ($\neg$b), which may be called as "feynmion" (after physicist the late R. Feynman);
4. Taking into consideration of possibility of "neitherness", then it follows that the wholeness of both ($\neg$f) and ($\neg$b) $\rightarrow$ ($\neg$f) $\cup$ ($\neg$b), which may be called as "anti-g-on".

Therefore, a conjecture which may follow from this proposition is that perhaps in the near future we can observe some new entities corresponding to g-on condensate or feynmion condensate.

3 Further extension to include anisotropic effect

At this section we consider the anisotropic effect which may be useful for analyzing the anisotropy of CMBR spectrum, see Fig. 1 [13].

For anisotropic case, one cannot use again equation (2), but shall instead use [7, p. 2]:

$$\epsilon_i = \left(n_x + \frac{1}{2}\right)\hbar\omega_x + \left(n_y + \frac{1}{2}\right)\hbar\omega_y + \left(n_z + \frac{1}{2}\right)\hbar\omega_z , \quad (10)$$

where n_x, n_y, n_z are integers and >0. Or by neglecting the $1/2$ parts and assuming a common frequency, one can re-write (10) as [7a, p.1]:

$$\epsilon_i = (n_x r + n_y s + n_z t)\hbar\omega_0 , \quad (11)$$

where r, s, t is multiplying coefficient for each frequency:

$$r = \frac{\omega_x}{\omega_0} , \qquad s = \frac{\omega_y}{\omega_0} , \qquad t = \frac{\omega_z}{\omega_0} . \quad (12)$$

This proposition will yield a different spectrum compared to isotropic spectrum by assuming isotropic harmonic oscillator (2). See Fig. 2 [7a]. It is interesting to note here that the spectrum produced by anisotropic frequencies yields number of peaks more than 1 (multiple-peaks), albeit this is not near yet to CMBR spectrum depicted in Fig. 1. Nonetheless, it seems clear here that one can expect to predict the anisotropy of CMBR spectrum by using of more anisotropic harmonic oscillators.

In this regard, it is interesting to note that some authors considered half quantum vortices in $p_x + ip_y$ superconductors [14], which indicates that energy of partition function may be generalized to include Cauchy plane, as follows:

$$E = p_x c + ip_y c \approx \hbar\omega_x + i\hbar\omega_y , \quad (13)$$

or by generalizing this Cauchy plane to quaternion number [12], one gets instead of (13):

$$E_{qk} = \hbar\omega + i\hbar\omega_x + j\hbar\omega_y + k\hbar\omega_z , \quad (14)$$

which is similar to standard definition of quaternion number:

$$Q \equiv a + bi + cj + dk . \quad (15)$$

Therefore the partition function with anisotropic harmon-

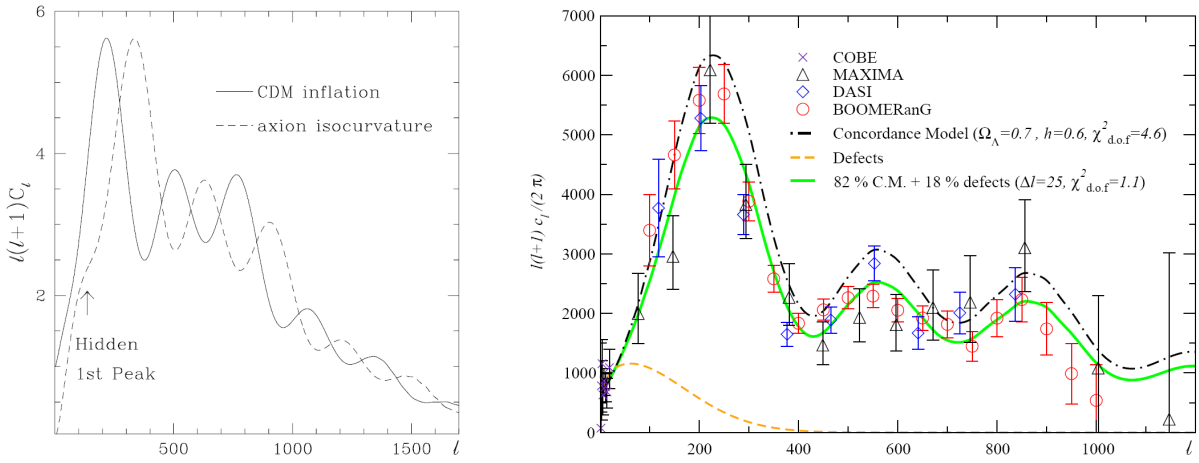

Fig. 1: Anisotropy of CMBR (after Tkachev [13]). Left panel: comparison of CMB power spectra in the models with adiabatic and isocurvature initial perturbations. Right panel: adiabatic power spectra in comparison with spectra appearing in models seeded by topological defects. In this panel some older, pre-WMAP, data are also shown.

ic potential can be written in quaternion form. Therefore instead of (11), we get:

$$\epsilon_i = \left(n_x r + n_y s + n_z t + i n_x r + j n_y s + k n_z t\right) \hbar\omega_0 , \quad (16)$$

which can be written as:

$$\epsilon_i = (1 + q_k)(n_k r_k)\hbar\omega_0 , \quad (17)$$

where $k = 1, 2, 3$ corresponding to index of quaternion number i, j, k. While we don't obtain numerical result here, it can be expected that this generalisation to anisotropic quaternion harmonic potential could yield better prediction, which perhaps may yield to exact CMBR spectrum. Numerical solution of this problem may be presented in another paper.

This proposition, however, may deserve further considerations. Further observation is also recommended in order to verify and also to explore various implications of.

4 Concluding remarks

In the present paper, we review an existing method to generalize Fermi-Dirac, Bose-Einstein, and Tsallis statistics, to become more unified statistics. And then we explore its plausible generalization to include fractality of Tsallis non-extensive entropy parameter .

Therefore, a conjecture which may follow this proposition is that perhaps in the near future we can observe some new entities corresponding to g-on condensate or feynmion condensate.

In the subsequent section, we also discuss plausible extension of this proposed unified statistics to include anisotropic effect, which may be observed in the context of Cosmic Microwave Background Radiation. In particular we consider possibility to introduce quaternionic harmonic oscillator. To our knowledge this proposition has never been considered before elsewhere.

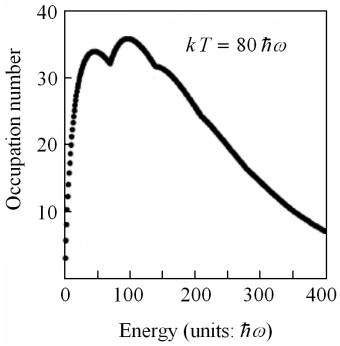

Fig. 2: Spectrum for anisotropic harmonic oscillator potential (after Ligare [7a]).

It is recommended to conduct further observation in order to verify and also to explore various implications of our propositions as described herein.

Acknowledgment

The writers would like to thank to Profs. C. Castro, A. Yefremov, D. L. Rapoport, D. Rabounski, S. Crothers and L. Borissova for valuable discussions.

Submitted on January 08, 2007
Accepted on January 30, 2007

References

1. Antoniadis I. *et al.* arXiv: astro-ph/9611208.
2. Castro C. and Granik A. Why we live in 3 dimensions. arXiv: hep-th/0004152.
3. Buyukkilic F. and Demirhan D. arXiv: hep-th/0010192.
4. Utyuzh O. V. *et al.* arXiv: hep-ph/9910355.
5. Leinaas J. M. arXiv: hep-th/9611167.
6. Pinilla M. R. Signatures of superfluidity in atomic Fermi gases. Diss. Helsinki University of Tech., Nov. 2003, 72 p.

7. Ligare M. Numerical analysis of Bose-Einstein condensation in a three dimensional harmonic oscillator potential. *Am. J. Phys.*, 1998, v. 66, No. 3, 2; [7a] Ligare M. *Am. J. Phys.*, 2002, v. 70, No. 1.
8. Smarandache F. and Christianto V. *Progress in Physics*, 2006, v. 4, 37–40.
9. Griffin A. arXiv: cond-mat/9911419.
10. Tuszynski J. *et al. Physica A*, 2003, v. 325, 455–476.
11. Batunin F. *Physics-Uspekhi*, 1995, v. 38(6), 609–623.
12. Yefremov A. Relativistic oscillator in quaternion relativity. In: *Quantization in Astrophysics, Brownian Motion, and Supersymmetry*, F. Smarandache and V. Christianto (eds.), Chennai Publisher, India, in press (Nov. 2006).
13. Tkachev I. arXiv: hep-ph/0405168, p. 17–18.
14. Stone M. *et al.* arXiv: cond-mat/0505515, p. 14–15.

On the Rate of Change of Period for Accelerated Motion and Their Implications in Astrophysics

R. Rajamohan and A. Satya Narayanan

Indian Institute of Astrophysics, Koramangala, Bangalore – 560 034, India

E-mail: satya@iiap.res.in

We have derived in this paper, the relationship that needs to be satisfied when length measurements are expressed in two different units. Interesting relationships emerge when the smaller of the two units chosen is a function of time. We relate these results to the expected periodicities in the observed data when a system of objects are revolving around a common center of mass. We find that these results are highly intriguing and can equally well account for some of the major results in the field of astrophysics.

1 Introduction

In an earlier paper (Rajamohan and Satya Narayanan [1]) we derived the condition that needs to be satisfied for signal from a relatively stationary emitter to meet an observer moving transverse to the line of sight. A receiver moving across the line of sight is equivalent of the receiver accelerating away along the line of sight from the emitter. In this paper, we have derived the period and period derivative for this equivalent situation.

It is well known that signals with uniform period P_e from an emitter will arrive at a receiver, moving with uniform relative velocity V along the line of sight, with a period P given by the equation

$$P = \frac{P_e}{(1 - V/C)},$$

where C is the signal speed. Instead if the receiver or the emitter were to be accelerating with a as the value of acceleration, it is generally assumed that the observed rate of change of period $\dot{P}$ per unit time is governed by the equation (Shklovski [2])

$$\dot{P} = \frac{aP}{C}. \qquad (1)$$

The above equation does not take into account the relationship between space intervals and time intervals properly. When acceleration is involved, the time interval Δt that corresponds to a given space interval Δx is a function of time. That is, the space interval Δx corresponds to smaller and smaller time interval (along the direction of motion) as the velocity of the accelerating receiver is a function of time.

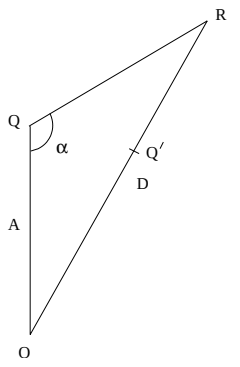

Fig. 1: Schematic representation of the observer and the emitter meeting at a point.

The space-time relationship when properly taken into account leads to an additional term which is enormously larger than that given by equation (1).

2 Relationship between time, length and the unit of length-measurement

Consider the general case when the observer is at a distance A (km) from the emitter moving with uniform velocity V at an angle α to the line of sight as shown in Figure 1. Let the emitter at position O emit signals at regular intervals of P_e seconds.

At time $t = 0$, let a signal start from O when the observer is at Q (at $t = 0$). Let this signal meet the observer at R at time t. Let the initial distance $OQ = A$ at $t = 0$ and the distance $OR = D$ at time t.

From triangle OQR

$$(OR)^2 = (OQ)^2 + (QR)^2 - 2(OQ)(QR)\cos\alpha$$

or

$$D^2 = A^2 + V^2t^2 - 2AV\cos\alpha t = A^2\left[1 + \frac{V^2t^2}{A^2} - \frac{2V\cos\alpha t}{A}\right],$$

$$D = A\left[1 + \frac{V^2t^2}{A^2} - \frac{2V\cos\alpha t}{A}\right]^{\frac{1}{2}} \approx A + \frac{1}{2}\frac{V^2t^2}{A} -$$

$$- V\cos\alpha t - \frac{1}{2}\frac{V^2t^2\cos^2\alpha}{A} = A - V\cos\alpha t + \frac{1}{2}\frac{V^2\sin^2\alpha}{A}t^2.$$

Therefore

$$D - A = -V\cos\alpha t + \frac{1}{2}\frac{V^2\sin^2\alpha}{A}t^2.$$

We can rewrite $D - A$ as

$$D - A = ut + \frac{1}{2}at^2;$$

u is positive when α is greater than 90° and negative when α is less than 90°. However, $a = V^2\sin^2\alpha/A$ is always positive. If the angle α were to be 0 or 180°, the observer will be moving uniformly along the line of sight and the signals from O will be equally spaced in time. If the observer were to move in a circular orbit around the emitter then too, the period observed would be constant. In all other cases the acceleration due to transverse component that leads to the period derivative will always be positive.

Draw a circle with A as radius. Let it intercept the line

OR at Q'. Therefore $OQ = OQ'$. Let the signal from O reach Q' at time t_e

$$D - A = Q'R = C(t - t_e) = ut + \frac{1}{2}at^2.$$

The signal from O meeting the uniformly moving observer along QR is equivalent to the same signal chasing an observer from Q' to R with initial velocity u and acceleration a

$$C(t - t_e) = ut + \frac{1}{2}at^2 =$$
$$= u\big[t_e + (t - t_e)\big] + \frac{1}{2}a\big[t_e + (t - t_e)\big]^2 =$$
$$= ut_e + \frac{1}{2}at_e^2 + (u + at_e)(t - t_e) + \frac{1}{2}a(t - t_e)^2.$$

Let $C(t - t_e) = X$ and $ut_e + \frac{1}{2}at_e^2 = X_e$. The space interval X_e contains N signals where $N = X_e/CP_e$ which will get folded in the space interval $X - X_e$ as the train of signals moving along OR will be spaced at CP_e km.

Therefore

$$t - t_e = \frac{X}{C} = \frac{X_e}{C} + \frac{u + at_e}{C}(t - t_e) + \frac{1}{2}\frac{a}{C}(t - t_e)^2.$$

Hence the average observed period in the time interval $(t - t_e)$ is

$$\bar{P} = \frac{(t - t_e)}{N} = \frac{(t - t_e)CP_e}{X_e} = \frac{X}{X_e}P_e\,,$$

$$\bar{P} = \frac{X}{X_e}P_e = P_e + \frac{u(t - t_e)CP_e}{CX_e} + \frac{at_e(t - t_e)CP_e}{CX_e} +$$
$$+ \frac{\frac{1}{2}a(t - t_e)^2CP_e}{CX_e}\,,$$

$$\bar{P} = P_e + \frac{u}{C}\frac{X}{X_e}P_e + \frac{at_e}{C}\frac{X}{X_e}P_e + \frac{1}{2}\frac{a(t - t_e)}{C}\frac{X}{X_e}P_e\,.$$

For N signals in the time interval $(t - t_e)$, we can write

$$(t - t_e) = P_iN + \frac{1}{2}\dot{P}P_iN^2,$$

where P_i is the initial period. Hence

$$\bar{P} = \frac{t - t_e}{N} = P_i + \frac{1}{2}\dot{P}P_iN\,.$$

Comparing this with

$$\bar{P} = P_e + \frac{u}{C}\frac{X}{X_e}P_e + \frac{at_e}{C}\frac{X}{X_e}P_e\left[1 + \frac{1}{2}\frac{t - t_e}{t_e}\right]$$

we derive

$$\bar{P} = P_i + \frac{at_e}{C}\frac{X}{X_e}P_e\left[1 + \frac{1}{2}\frac{(t - t_e)}{t_e}\right]$$

as $P_i = P_e/(1 - u/C)$. Hence $\frac{1}{2}\dot{P}N \approx \frac{at_e}{C}\left[1 + \frac{1}{2}\frac{(t - t_e)}{t_e}\right]$ or

$$\dot{P} = \frac{2at_e}{CN}\left[1 + \frac{1}{2}\frac{t - t_e}{t_e}\right] = \frac{2at_e(CP_e)}{CX_e}\left[1 + \frac{1}{2}\frac{t - t_e}{t_e}\right].$$

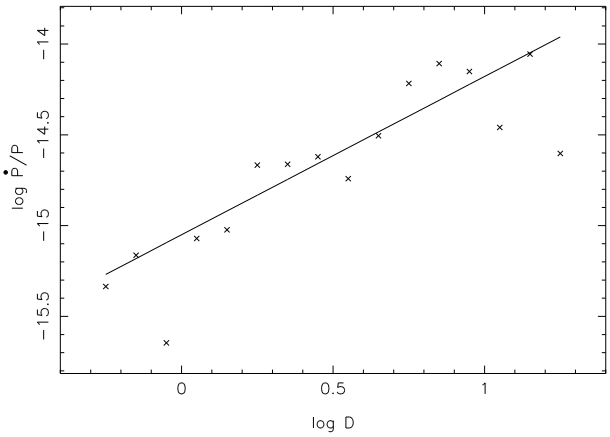

Fig. 2: $\log \dot{P}/P$ plotted as a function of $\log \mathrm{D}$.

As $|X_e| = |u|t_e + \frac{1}{2}at_e^2$,

$$\dot{P} \approx \frac{2a}{|u|} + \frac{aP_e}{C}\,.$$

The second term on the right hand side of the above equation is the Shklovski's [2] solution which is u/C times smaller than the first term

$$\dot{P} = \frac{2at_e}{X_e}P_e\Big(1 + \frac{u}{C}\Big) = \frac{2at_e}{|u|}\Big(1 + \frac{u}{C}\Big) \approx \frac{2P_e}{t_e}\Big(1 + \frac{u}{C}\Big)\,.$$

The acceleration a due to transverse component of velocity is always positive and hence $\dot{P}$ will be positive even when the observer is moving toward the emitter at an angle α less than 90°.

3 The period derivatives of pulsars

If V_τ is the relative transverse velocity between the Sun and the Pulsar, then the relative acceleration is V_τ^2/d. As $\sqrt{2}d/V_\tau = t$ is the relative time of free fall over $\frac{\pi}{2}$ radians, we can write $\dot{P} = 2P_e/t = \frac{1}{2}V_\tau/d = \frac{\pi}{2}V_\tau/d$. This is of the order of the average observed period derivate of pulsars. If we assume that an inverse square law is applicable the average observed period derivatives of pulsars must increase as a function of distance from the Sun.

Figure 2, is a plot of $\log \dot{P}/P$ versus $\log \mathrm{D}$ of all pulsars in the period range 0.1 to 3 seconds and in the distance range $\log \mathrm{D} = -0.3$ to $+1.3$. The data is taken from Taylor et al. [3]. Table 1 gives the values of $\log \dot{P}/P$ averaged in different distance bins. N is the number of pulsars in each bin. Leaving the two points that are slightly further away from the mean relationship, the best fit straight line $Y = mX + k$ gives a slope of 0.872 and the constant as -15.0506. The constant k gives the value of $\sqrt{2}V_\tau/d$ at an average distance of the Sun. In short we expect that this should more or less correspond with the accepted values for the Sun's motion around the galactic center. Taking $V_\odot = 210$ km×s^{-1} and $d_\odot = 8$ kpc , we get $\sqrt{2}V_\odot/d_\odot = 1.24\times10^{-15}$ and the value from k is 1.12×10^{-15}.

log D	log $\dot{P}/P$	N
−0.25	−15.3353	10
−0.15	−15.1632	17
−0.05	−15.6460	12
0.05	−15.0711	16
0.15	−15.0231	27
0.25	−14.6667	38
0.35	−14.6620	46
0.45	−14.6205	51
0.55	−14.7416	78
0.65	−14.5052	66
0.75	−14.2172	49
0.85	−14.1072	51
0.95	−14.1509	30
1.05	−14.4594	12
1.15	−14.0552	10
1.25	−14.6030	3

Table 1: log $\dot{P}/P$ as a function of log D and the number of pulsars in each bin.

This is given more as an illustration of the application of this effect. The real (true) spin down rates of the large majority of pulsars, may be much lower than the canonical value of 3×10^{-15}. Hence the average observed period derivatives of pulsars is due to the differential galactic rotation effect. This result is fully in conformity with the observed relationship between transverse motion and $\dot{P}$ by Anderson and Lyne [4] and Cordes [5] and that the correlation found by them cannot be accounted for purely by selection effects alone (Stollman and Van den Heuvel [6]).

4 Bending of light

As the photon angle accelerates in the gravitational field of the Sun, the angle $\Delta\phi$ at which the light from the limb of the Sun would be seen to meet the observer is the instantaneous value of the second derivative of α with respect to time at the distance of the earth. This is given by

$$\Delta\phi = \frac{\pi}{2}\,\frac{d^2\alpha}{dt^2}\,t\,(1s) = \frac{\pi}{2}\,\frac{2CV_\tau}{d^2}\,(1s)\,\frac{d}{C} = \frac{\pi V_\tau\,(1s)}{d}\,,$$

where $\frac{\pi}{2}$ is introduced as a scale factor to relate the free-fall height to the actual arc length that an object traverses in a gravitational field; V_τ is the relative transverse velocity and d is the distance between the Sun and the Earth. This will result in an observed bending of light as

$$\Delta\phi = \frac{\pi V_\tau\,(1s)}{d} = \frac{407\pi}{1.5\times10^8 \text{ radians}} = 1.76 \text{ arc sec.}$$

5 Precession of Mercury's orbit

The arrival time acceleration when not taken into account will appear as though the orbit is precessing. A good example is the precesion of Mercury's orbit. Treating Mercury as a rotating object with a period equal to its synodic period $P_s = 115.88$ days,

$$\Delta\omega = \frac{\pi V_\tau}{d} = \frac{3.14\times18.1}{0.917\times10^8} = 61.98\times10^{-8} \text{ rad},$$

which is the change per synodic period. Hence,

$$\frac{\Delta\omega}{P_s} = \frac{61.98\times10^{-8}}{115.88\times86400} = \\ = 6.19\times10^{-14} \text{ rad}\times\text{s}^{-1} = 40 \text{ arc sec/century.}$$

6 Binary pulsars

In the case of a binary pulsar, the relative transverse motion of the common centre of mass of the binary system and the Sun will lead to a secular increase in the period. Over and above this effect, the acceleration of the pulsar in the gravitational field of its companion will lead to further periodic deceleration in the arrival times. In analogy with Mercury, we can therefore expect a similar phenomenon in the case of binary pulsars. That is, the orbit might appear to precess if the arrival time delays caused by the pulsar acceleration in the gravitational field of the companion is not taken into account. The apparent precesion per pulse period P_e will be (Rajamohan and Satya Narayanan [1])

$$\Delta\omega = \frac{\pi}{4}\,\frac{V^2}{a^2}\,P_e^2\,.$$

Approximating the orbit to be circular and expressing the above equation in terms of well determined quantities,

$$\Delta\omega \approx \pi^3 P_e^2/P_b^2\,,$$

P_b is the orbital period and a is the semi-major axis of the orbit. Introducing appropriate values for PSR1913+16, we find

$$\Delta\omega \approx 1.386\times10^{-10} \text{ rad/pulse} \approx 4.24^\circ \text{ yr}^{-1},$$

which is in very good agreement with the observed value of 4.2261° yr^{-1} by Taylor and Weisberg [7]. For PSR1534+12 we find

$$\Delta\omega \approx 0.337\times10^{-10} \text{ rad/pulse} \approx 1.61^\circ \text{ yr}^{-1},$$

while the observed value is 1.756° yr^{-1} (Taylor et al. [8]).

Acknowledgements

We are thankful to Dr. Baba Verghese for his help in producing the Table and the Figures in this paper.

Submitted on February 02, 2007
Accepted on February 06, 2007

References

1. Rajamohan R. and Satya Narayanan A. *Speculations in Science and Technology*, 1995, v. 18, 51.
2. Shklovski I. S. *Soviet Astron.*, 1969, v. 13, 562.
3. Taylor J. H., Manchester R. N. and Lyne A. G. Catalogue of 706 pulsars, 1995 (http://pulsar.princeton.edu).
4. Anderson B. and Lyne A. G. *Nature*, 1983, v. 303, 597.
5. Cordes J. M. *Astrophys. J.*, 1986, v. 311, 183.
6. Stollman G. M. and Van den Heuvel E. P. J. *Astron. & Astrophys*, 1986, v. 162, 87.
7. Taylor J. H. and Weisberg J. M. *Astroph. J.*, 1982, v. 253, 908.
8. Taylor J. H., Wolszan A., Damour T. and Weisberg J. M. *Nature*, 1992, v. 355, 132.

Gravitation on a Spherically Symmetric Metric Manifold

Stephen J. Crothers

Queensland, Australia

E-mail: thenarmis@yahoo.com

The usual interpretations of solutions for Einstein's gravitational field satisfying the spherically symmetric condition contain anomalies that are not mathematically permissible. It is shown herein that the usual solutions must be modified to account for the intrinsic geometry associated with the relevant line elements.

1 Introduction

The standard interpretation of spherically symmetric line elements for Einstein's gravitational field has not taken into account the fundamental geometrical features of spherical symmetry about an arbitrary point in a metric manifold. This has led to numerous misconceptions as to distance and radius that have spawned erroneous theoretical notions.

The nature of spherical symmetry about an arbitrary point in a three dimensional metric manifold is explained herein and applied to Einstein's gravitational field.

It is plainly evident, *res ipsa locquitur*, that the standard claims for black holes and Big Bang cosmology are not consistent with elementary differential geometry and are consequently inconsistent with General Relativity.

2 Spherical symmetry of three-dimensional metrics

Denote ordinary Efcleethean* 3-space by $\mathbf{E}^3$. Let $\mathbf{M}^3$ be a 3-dimensional metric manifold. Let there be a one-to-one correspondence between all points of $\mathbf{E}^3$ and $\mathbf{M}^3$. Let the point $O \in \mathbf{E}^3$ and the corresponding point in $\mathbf{M}^3$ be O'. Then a point transformation T of $\mathbf{E}^3$ into itself gives rise to a corresponding point transformation of $\mathbf{M}^3$ into itself.

A rigid motion in a metric manifold is a motion that leaves the metric $d\ell'^2$ unchanged. Thus, a rigid motion changes geodesics into geodesics. The metric manifold $\mathbf{M}^3$ possesses spherical symmetry around any one of its points O' if each of the ∞^3 rigid rotations in $\mathbf{E}^3$ around the corresponding arbitrary point O determines a rigid motion in $\mathbf{M}^3$.

The coefficients of $d\ell'^2$ of $\mathbf{M}^3$ constitute a metric tensor and are naturally assumed to be regular in the region around every point in $\mathbf{M}^3$, except possibly at an arbitrary point, the centre of spherical symmetry $O' \in \mathbf{M}^3$.

Let a ray i emanate from an arbitrary point $O \in \mathbf{E}^3$. There is then a corresponding geodesic $i' \in \mathbf{M}^3$ issuing from the corresponding point $O' \in \mathbf{M}^3$. Let P be any point on i other than O. There corresponds a point P' on $i' \in \mathbf{M}^3$ different to O'. Let g' be a geodesic in $\mathbf{M}^3$ that is tangential to i' at P'.

Taking i as the axis of ∞^1 rotations in $\mathbf{E}^3$, there corresponds ∞^1 rigid motions in $\mathbf{M}^3$ that leaves only all the points on i' unchanged. If g' is distinct from i', then the ∞^1 rigid rotations in $\mathbf{E}^3$ about i would cause g' to occupy an infinity of positions in $\mathbf{M}^3$ wherein g' has for each position the property of being tangential to i' at P' in the same direction, which is impossible. Hence, g' coincides with i'.

Thus, given a spherically symmetric surface Σ in $\mathbf{E}^3$ with centre of symmetry at some arbitrary point $O \in \mathbf{E}^3$, there corresponds a spherically symmetric geodesic surface Σ' in $\mathbf{M}^3$ with centre of symmetry at the corresponding point $O' \in \mathbf{M}^3$.

Let Q be a point in $\Sigma \in \mathbf{E}^3$ and Q' the corresponding point in $\Sigma' \in \mathbf{M}^3$. Let $d\sigma$ be a generic line element in Σ issuing from Q. The corresponding generic line element $d\sigma' \in \Sigma'$ issues from the point Q'. Let Σ be described in the usual spherical-polar coordinates r, θ, φ. Then

$$d\sigma^2 = r^2(d\theta^2 + \sin^2\theta\, d\varphi^2), \qquad (1)$$

$$r = |\overline{OQ}|.$$

Clearly, if r, θ, φ are known, Q is determined and hence also Q' in Σ'. Therefore, θ and φ can be considered to be curvilinear coordinates for Q' in Σ' and the line element $d\sigma' \in \Sigma'$ will also be represented by a quadratic form similar to (1). To determine $d\sigma'$, consider two elementary arcs of equal length, $d\sigma_1$ and $d\sigma_2$ in Σ, drawn from the point Q in different directions. Then the homologous arcs in Σ' will be $d\sigma'_1$ and $d\sigma'_2$, drawn in different directions from the corresponding point Q'. Now $d\sigma_1$ and $d\sigma_2$ can be obtained from one another by a rotation about the axis $\overline{OQ}$ in $\mathbf{E}^3$, and so $d\sigma'_1$ and $d\sigma'_2$ can be obtained from one another by a rigid motion in $\mathbf{M}^3$, and are therefore also of equal length, since the metric is unchanged by such a motion. It therefore follows that the ratio $\frac{d\sigma'}{d\sigma}$ is the same for the two different directions irrespective of $d\theta$ and $d\varphi$, and so the foregoing ratio is a function of position, i.e. of r, θ, φ. But Q is an arbitrary point in Σ, and so $\frac{d\sigma'}{d\sigma}$ must have the same ratio for any corresponding points Q and Q'. Therefore, $\frac{d\sigma'}{d\sigma}$ is a function of r alone, thus

$$\frac{d\sigma'}{d\sigma} = H(r),$$

and so

$$d\sigma'^2 = H^2(r)\, d\sigma^2 = H^2(r) r^2 (d\theta^2 + \sin^2\theta\, d\varphi^2), \qquad (2)$$

*For the geometry due to Efcleethees, usually and abominably rendered as Euclid.

where $H(r)$ is *a priori* unknown. For convenience set $R_c = H(r) = H(r)r$, so that (2) becomes

$$d\sigma'^2 = R_c^2(d\theta^2 + \sin^2\theta\, d\varphi^2), \tag{3}$$

where R_c is a quantity associated with $\mathbf{M}^3$. Comparing (3) with (1) it is apparent that R_c is to be rightly interpreted in terms of the Gaussian curvature K at the point Q', i.e. in terms of the relation $K = \frac{1}{R_c^2}$ since the Gaussian curvature of (1) is $K = \frac{1}{r^2}$. This is an intrinsic property of all line elements of the form (3) [1, 2]. Accordingly, R_c can be regarded as a radius of curvature. Therefore, in (1) the radius of curvature is $R_c = r$. Moreover, owing to spherical symmetry, all points in the corresponding surfaces Σ and Σ' have constant Gaussian curvature relevant to their respective manifolds and centres of symmetry, so that all points in the respective surfaces are umbilic.

Let the element of radial distance from $O \in \mathbf{E}^3$ be dr. Clearly, the radial lines issuing from O cut the surface Σ orthogonally. Combining this with (1) by the theorem of Pythagoras gives the line element in $\mathbf{E}^3$

$$d\ell^2 = dr^2 + r^2(d\theta^2 + \sin^2\theta\, d\varphi^2). \tag{4}$$

Let the corresponding radial geodesic from the point $O' \in \mathbf{M}^3$ be dg. Clearly the radial geodesics issuing from O' cut the geodesic surface Σ' orthogonally. Combining this with (3) by the theorem of Pythagoras gives the line element in $\mathbf{M}^3$ as,

$$d\ell'^2 = dg^2 + R_c^2(d\theta^2 + \sin^2\theta\, d\varphi^2), \tag{5}$$

where dg is, by spherical symmetry, also a function only of R_c. Set $dg = \sqrt{B(R_c)}dR_c$, so that (5) becomes

$$d\ell'^2 = B(R_c)dR_c^2 + R_c^2(d\theta^2 + \sin^2\theta\, d\varphi^2), \tag{6}$$

where $B(R_c)$ is an *a priori* unknown function.

Setting $dR_p = \sqrt{B(R_c)}dR_c$ carries (6) into

$$d\ell'^2 = dR_p^2 + R_c^2(d\theta^2 + \sin^2\theta\, d\varphi^2). \tag{7}$$

Expression (6) is the most general for a metric manifold $\mathbf{M}^3$ having spherical symmetry about some arbitrary point $O' \in \mathbf{M}^3$ [1, 3].

Considering (4), the distance $R_p = |\overline{OQ}|$ from the point at the centre of spherical symmetry O to a point $Q \in \Sigma$, is given by

$$R_p = \int_0^r dr = r = R_c\,.$$

Call R_p the proper radius. Consequently, in the case of $\mathbf{E}^3$, R_p and R_c are identical, and so the Gaussian curvature at any point in $\mathbf{E}^3$ can be associated with R_p, the radial distance between the centre of spherical symmetry at the point $O \in \mathbf{E}^3$ and the point $Q \in \Sigma$. Thus, in this case, we have $K = \frac{1}{R_c^2} = \frac{1}{R_p^2} = \frac{1}{r^2}$. However, this is not a general relation, since according to (6) and (7), in the case of $\mathbf{M}^3$, the radial geodesic distance from the centre of spherical symmetry at the point $O' \in \mathbf{M}^3$ is not given by the radius of curvature, but by

$$R_p = \int_0^{R_p} dR_p = \int_{R_c(0)}^{R_c(r)} \sqrt{B(R_c(r))}\, dR_c(r) = \int_0^r \sqrt{B(R_c(r))}\, \frac{dR_c(r)}{dr}\, dr\,,$$

where $R_c(0)$ is *a priori* unknown owing to the fact that $R_c(r)$ is *a priori* unknown. One cannot simply assume that because $0 \leqslant r < \infty$ in (4) that it must follow that in (6) and (7) $0 \leqslant R_c(r) < \infty$. In other words, one cannot simply assume that $R_c(0) = 0$. Furthermore, it is evident from (6) and (7) that R_p determines the radial geodesic distance from the centre of spherical symmetry at the arbitrary point O' in $\mathbf{M}^3$ (and correspondingly so from O in $\mathbf{E}^3$) to another point in $\mathbf{M}^3$. Clearly, R_c does not in general render the radial geodesic length from the centre of spherical symmetry to some other point in a metric manifold. Only in the particular case of $\mathbf{E}^3$ does R_c render both the Gaussian curvature and the radial distance from the centre of spherical symmetry, owing to the fact that R_p and R_c are identical in that special case.

It should also be noted that in writing expressions (4) and (5) it is implicit that $O \in \mathbf{E}^3$ is defined as being located at the origin of the coordinate system of (4), i.e. O is located where $r = 0$, and by correspondence O' is defined as being located at the origin of the coordinate system of (5), i.e. using (7), $O' \in \mathbf{M}^3$ is located where $R_p = 0$. Furthermore, since it is well known that a geometry is completely determined by the form of the line element describing it [4], expressions (4) and (6) share the very same fundamental geometry because they are line elements of the same form.

Expression (6) plays an important rôle in Einstein's gravitational field.

3 The standard solution

The standard solution in the case of the static vacuum field (i.e. no deformation of the space) of a single gravitating body, satisfying Einstein's field equations $R_{\mu\nu} = 0$, is (using $G = c = 1$),

$$ds^2 = \left(1 - \frac{2m}{r}\right) dt^2 - \left(1 - \frac{2m}{r}\right)^{-1} dr^2 - r^2(d\theta^2 + \sin^2\theta\, d\varphi^2)\,, \tag{8}$$

where m is allegedly the mass causing the field, and upon which it is routinely claimed that $2m < r < \infty$ is an exterior region and $0 < r < 2m$ is an interior region. Notwithstanding the inequalities it is routinely allowed that $r = 2m$ and $r = 0$ by which it is also routinely claimed that $r = 2m$ marks a "removable" or "coordinate" singularity and that $r = 0$ marks a "true" or "physical" singularity [5].

The standard treatment of the foregoing line-element proceeds from simple inspection of (8) and thereby upon the following assumptions:

(a) that there is only one radial quantity defined on (8);

(b) that r can approach zero, even though the line-element (8) is singular at $r = 2m$;

(c) that r is the radial quantity in (8) ($r = 2m$ is even routinely called the "Schwarzschild radius" [5]).

With these unstated assumptions, but assumptions nonetheless, it is usual procedure to develop and treat of black holes. However, all three assumptions are demonstrably false at an elementary level.

4 That assumption (a) is false

Consider standard Minkowski space (using $c = G = 1$) described by

$$ds^2 = dt^2 - dr^2 - r^2 d\Omega^2, \qquad (9)$$
$$0 \leqslant r < \infty\,,$$

where $d\Omega^2 = d\theta^2 + \sin^2\theta\, d\varphi^2$. Comparing (9) with (4) it is easily seen that the spatial components of (9) constitute a line element of $\mathbf{E}^3$, with the point at the centre of spherical symmetry at $r_0 = 0$, coincident with the origin of the coordinate system.

In relation to (9) the *calculated* proper radius R_p of the sphere in $\mathbf{E}^3$ is,

$$R_p = \int_0^r dr = r\,, \qquad (10)$$

and the radius of curvature R_c is

$$R_c = r = R_p\,. \qquad (11)$$

Calculate the surface area of the sphere:

$$A = \int_0^{2\pi}\int_0^{\pi} r^2 \sin\theta\, d\theta\, d\varphi = 4\pi r^2 = 4\pi R_p^2 = 4\pi R_c^2\,. \qquad (12)$$

Calculate the volume of the sphere:

$$V = \int_0^{2\pi}\int_0^{\pi}\int_0^{r} r^2 \sin\theta\, dr\, d\theta\, d\varphi = \frac{4}{3}\pi r^3 = \frac{4}{3}\pi R_p^3 = \frac{4}{3}\pi R_c^3\,. \qquad (13)$$

Then for (9), according to (10) and (11),

$$R_p = r = R_c\,. \qquad (14)$$

Thus, for Minkowski space, R_p and R_c are identical. This is because Minkowski space is pseudo-Efcleethean.

Now comparing (8) with (6) and (7) is is easily seen that the spatial components of (8) constitute a spherically symmetric metric manifold $\mathbf{M}^3$ described by

$$d\ell'^2 = \left(1 - \frac{2m}{r}\right)^{-1} dr^2 + r^2 d\Omega^2,$$

and which is therefore in one-to-one correspondence with $\mathbf{E}^3$. Then for (8),

$$R_c = r\,,$$
$$R_p = \int \sqrt{\frac{r}{r-2m}}\, dr \neq r = R_c\,.$$

Hence, $R_P \neq R_c$ in (8) in general. This is because (8) is non-Efcleethean (it is pseudo-Riemannian). Thus, assumption (a) is false.

5 That assumption (b) is false

On (8),

$$R_p = R_p(r) = \int \sqrt{\frac{r}{r-2m}}\, dr = \\ = \sqrt{r\,(r-2m)} + 2m \ln\left|\sqrt{r} + \sqrt{r-2m}\right| + K, \qquad (15)$$

where K is a constant of integration.

For some r_0, $R_p(r_0) = 0$, where r_0 is the corresponding point at the centre of spherical symmetry in $\mathbf{E}^3$ to be determined from (15). According to (15), $R_p(r_0) = 0$ when $r = r_0 = 2m$ and $K = -m \ln 2m$. Hence,

$$R_p(r) = \sqrt{r\,(r-2m)} + 2m \ln\left(\frac{\sqrt{r} + \sqrt{r-2m}}{\sqrt{2m}}\right). \qquad (16)$$

Therefore, $2m < r < \infty \Rightarrow 0 < R_p < \infty$, where $R_c = r$. The inequality is required to maintain Lorentz signature, since the line-element is undefined at $r_0 = 2m$, which is the only possible singularity on the line element. Thus, assumption (b) is false.

It follows that the centre of spherical symmetry of $\mathbf{E}^3$, in relation to (8), is located not at the point $r_0 = 0$ in $\mathbf{E}^3$ as usually assumed according to (9), but at the point $r_0 = 2m$, which corresponds to the point $R_p(r_0 = 2m) = 0$ in the metric manifold $\mathbf{M}^3$ that is described by the spatial part of (8). In other words, the point at the centre of spherical symmetry in $\mathbf{E}^3$ in relation to (8) is located at any point Q in the spherical surface Σ for which the radial distance from the centre of the coordinate system at $r = 0$ is $r = 2m$, owing to the one-to-one correspondence between all points of $\mathbf{E}^3$ and $\mathbf{M}^3$. It follows that (8) is not a generalisation of (9), as usually claimed. The manifold $\mathbf{E}^3$ of Minkowski space corresponding to the metric manifold $\mathbf{M}^3$ of (8) is not described by (9), because the point at the centre of spherical symmetry of (9), $r_0 = 0$, does not coincide with that required by (15) and (16), namely $r_0 = 2m$.

In consequence of the foregoing it is plain that the expression (8) is not general in relation to (9) and the line element (8) is not general in relation to the form (6). This is due to the incorrect way in which (8) is usually derived from (9), as pointed out in [6, 7, 8]. The standard derivation of (8) from (9) unwittingly shifts the point at the centre of spheriacly symmetry for the $\mathbf{E}^3$ of Minkowski space from $r_0 = 0$

to $r_0 = 2m$, with the consequence that the resulting line element (8) is misinterpreted in relation to $r = 0$ in the $\mathbf{E^3}$ of Minkowski space as described by (9). This unrecognised shift actually associates the point $r_0 = 2m \in \mathbf{E^3}$ with the point $R_p(2m) = 0$ in the $\mathbf{M^3}$ of the gravitational field. The usual analysis then incorrectly associates $R_p = 0$ with $r_0 = 0$ instead of with the correct $r_0 = 2m$, thereby conjuring up a so-called "interior", as typically alleged in [5], that actually has no relevance to the problem — a completely meaningless manifold that has nothing to do with the gravitational field and so is disjoint from the latter, as also noted in [6, 9, 10, 11]. The point at the centre of spherical symmetry for Einstein's gravitational field is $R_p = 0$ and is also the origin of the coordinate system for the gravitational field. Thus the notion of an "interior" manifold under some other coordinate patch (such as the Kruskal-Szekeres coordinates) is patently false. This is clarified in the next section.

6 That assumption (c) is false

Generalise (9) so that the centre of a sphere can be located anywhere in Minkowski space, relative to the origin of the coordinate system at $r = 0$, thus

$$\begin{aligned} ds^2 &= dt^2 - \left(d\,|r - r_0|\right)^2 - |r - r_0|^2\, d\Omega^2 = \\ &= dt^2 - \frac{(r - r_0)^2}{|r - r_0|^2} dr^2 - |r - r_0|^2\, d\Omega^2 = \\ &= dt^2 - dr^2 - |r - r_0|^2\, d\Omega^2, \end{aligned} \tag{17}$$

$$0 \leqslant |r - r_0| < \infty\,,$$

which is well-defined for all real r. The value of r_0 is arbitrary. The spatial components of (17) describe a sphere of radius $D = |r - r_0|$ centred at some *point* r_0 on a common radial line through r and the origin of coordinates at $r = 0$ (i.e. centred at the *point* of orthogonal intersection of the common radial line with the spherical surface $r = r_0$). Thus, the arbitrary point r_0 is the centre of spherical symmetry in $\mathbf{E^3}$ for (17) in relation to the problem of Einstein's gravitational field, the spatial components of which is a spherically symmetric metric manifold $\mathbf{M^3}$ with line element of the form (6) and corresponding centre of spherical symmetry at the point $R_p(r_0) = 0 \,\forall\, r_0$. If $r_0 = 0$, (9) is recovered from (17). One does not need to make $r_0 = 0$ so that the centre of spherical symmetry in $\mathbf{E^3}$, associated with the metric manifold $\mathbf{M^3}$ of Einstein's gravitational field, coincides with the origin of the coordinate system itself, at $r = 0$. Any point in $\mathbf{E^3}$, relative to the coordinate system attached to the arbitrary point at which $r = 0$, can be regarded as a point at the centre of spherical symmetry in relation to Einstein's gravitational field. Although it is perhaps desirable to make the point $r_0 = 0$ the centre of spherical symmetry of $\mathbf{E^3}$ correspond to the point $R_p = 0$ at the centre of symmetry of $\mathbf{M^3}$ of the gravitational field, to simplify matters somewhat, this has not been done in the usual analysis of Einstein's gravitational field, despite appearances, and in consequence thereof false conclusions have been drawn owing to this fact going unrecognised in the main.

Now on (17),

$$\begin{aligned} R_c &= |r - r_0|\,, \\ R_p &= \int_0^{|r-r_0|} d\,|r - r_0| = \int_{r_0}^{r} \frac{(r - r_0)}{|r - r_0|} dr = |r - r_0| \equiv R_c, \end{aligned} \tag{18}$$

and so $R_p \equiv R_c$ on (17), since (17) is pseudo-Efcleethean. Setting $D = |r - r_0|$ for convenience, generalise (17) thus,

$$ds^2 = A\big(C(D)\big)\, dt^2 - B\big(C(D)\big)\, d\sqrt{C(D)}^{\,2} - C(D)\, d\Omega^2, \tag{19}$$

where $A\big(C(D)\big)$, $B\big(C(D)\big)$, $C(D) > 0$. Then for $R_{\mu\nu} = 0$, metric (19) has the solution,

$$\begin{aligned} ds^2 = &\left(1 - \frac{\alpha}{\sqrt{C(D)}}\right) dt^2 - \\ &- \frac{1}{1 - \frac{\alpha}{\sqrt{C(D)}}} d\sqrt{C(D)}^{\,2} - C(D)\, d\Omega^2, \end{aligned} \tag{20}$$

where α is a function of the mass generating the gravitational field [3, 6, 7, 9]. Then for (20),

$$\begin{aligned} R_c &= R_c(D) = \sqrt{C(D)}, \\ R_p &= R_p(D) = \int \sqrt{\frac{\sqrt{C(D)}}{\sqrt{C(D)} - \alpha}}\, d\sqrt{C(D)} = \\ &= \int \sqrt{\frac{R_c(D)}{R_c(D) - \alpha}}\, dR_c(D) = \sqrt{R_c(D)\big(R_c(D) - \alpha\big)} + \\ &+ \alpha \ln\left(\frac{\sqrt{R_c(D)} + \sqrt{R_c(D) - \alpha}}{\sqrt{\alpha}}\right), \end{aligned} \tag{21}$$

where $R_c(D) \equiv R_c\left(|r - r_0|\right) = R_c(r)$. Clearly r is a parameter, located in Minkowski space according to (17).

Now $r = r_0 \Rightarrow D = 0$, and so by (21), $R_c(D = 0) = \alpha$ and $R_p(D = 0) = 0$. One must ascertain the admissible form of $R_c(D)$ subject to the conditions $R_c(D = 0) = \alpha$ and $R_p(D = 0) = 0$ and $dR_c(D)/dD > 0$ [6, 7], along with the requirements that $R_c(D)$ must produce (8) from (20) at will, must yield Schwarzschild's [12] original solution at will (which is *not* the line element (8) with r down to zero), must produce Brillouin's [13] solution at will, must produce Droste's [14] solution at will, and must yield an infinite number of equivalent metrics [3]. The only admissible form satisfying these conditions is [7],

$$R_c = R_c(D) = \left(D^n + \alpha^n\right)^{\frac{1}{n}} \equiv \left(|r - r_0|^n + \alpha^n\right)^{\frac{1}{n}} = R_c(r), \tag{22}$$

$$D > 0, \quad r \in \Re, \quad n \in \Re^+, \quad r \neq r_0,$$

where r_0 and n are entirely arbitrary constants.

Choosing $r_0 = 0$, $r > 0$, $n = 3$,

$$R_c(r) = \left(r^3 + \alpha^3\right)^{\frac{1}{3}}, \tag{23}$$

and putting (23) into (20) gives Schwarzschild's original solution, defined on $0 < r < \infty$.

Choosing $r_0 = 0$, $r > 0$, $n = 1$,

$$R_c(r) = r + \alpha, \tag{24}$$

and putting (24) into (20) gives Marcel Brillouin's solution, defined on $0 < r < \infty$.

Choosing $r_0 = \alpha$, $r > \alpha$, $n = 1$,

$$R_c(r) = (r - \alpha) + \alpha = r, \tag{25}$$

and putting (25) into (20) gives line element (8), but defined on $\alpha < r < \infty$, as found by Johannes Droste in May 1916. Note that according to (25), and in general by (22), r is not a radial quantity in the gravitational field, because $R_c(r) = (r-\alpha)+\alpha = D+\alpha$ is really the radius of curvature in (8), defined for $0 < D < \infty$.

Thus, assumption (c) is false.

It is clear from this that the usual line element (8) is a restricted form of (22), and by (22), with $r_0 = \alpha = 2m$, $n = 1$ gives $R_c = |r - 2m| + 2m$, which is well defined on $-\infty < r < \infty$, i.e. on $0 \leqslant D < \infty$, so that when $r = 0$, $R_c(0) = 4m$ and $R_P(0) > 0$. In the limiting case of $r = 2m$, then $R_c(2m) = 2m$ and $R_p(2m) = 0$. The latter two relationships hold for any value of r_0.

Thus, if one insists that $r_0 = 0$ to match (9), it follows from (22) that,

$$R_c = \left(|r|^n + \alpha^n\right)^{\frac{1}{n}},$$

and if one also insists that $r > 0$, then

$$R_c = \left(r^n + \alpha^n\right)^{\frac{1}{n}}, \tag{26}$$

and for $n = 1$,

$$R_c = r + \alpha,$$

which is the simplest expression for R_c in (20) [6, 7, 13].

Expression (26) has the centre of spherical symmetry of $\mathbf{E}^3$ located at the point $r_0 = 0 \,\forall\, n \in \Re^+$, corresponding to the centre of spherical symmetry of $\mathbf{M}^3$ for Einstein's gravitational field at the point $R_p(0) = 0 \;\forall\; n \in \Re^+$. Then taking $\alpha = 2m$ it follows that $R_p(0) = 0$ and $R_c(0) = \alpha = 2m$ for all values of n.

There is no such thing as an interior solution for the line element (20) and consequently there is no such thing as an interior solution on (8), and so there can be no black holes.

7 That the manifold is inextendable

That the singularity at $R_p(r_0) \equiv 0$ is insurmountable is clear by the following ratio,

$$\lim_{r \to r_0^{\pm}} \frac{2\pi R_c(r)}{R_p(r)} = \lim_{r \to r_0^{\pm}} \frac{2\pi \left(|r - r_0|^n + \alpha^n\right)^{\frac{1}{n}}}{R_p(r)} = \infty,$$

since $R_p(r_0) = 0$ and $R_c(r_0) = \alpha$ are invariant.

Hagihara [15] has shown that all radial geodesics that do not run into the boundary at $R_c(r_0) = \alpha$ (i.e. that do not run into the boundary at $R_p(r_0) = 0$) are geodesically complete.

Doughty [16] has shown that the acceleration a of a test particle approaching the centre of mass at $R_p(r_0) = 0$ is given by,

$$a = \frac{\sqrt{-g_{00}}\left(-g^{11}\right)|g_{00,1}|}{2g_{00}}.$$

By (20) and (22), this gives,

$$a = \frac{\alpha}{2R_c^{\frac{3}{2}}\sqrt{R_c(r) - \alpha}}.$$

Then clearly as $r \to r_0^{\pm}$, $a \to \infty$, independently of the value of r_0.

J. Smoller and B. Temple [10] have shown that the Oppenheimer-Volkoff equations do not permit gravitational collapse to form a black hole and that the alleged interior of the Schwarzschild spacetime (i.e. $0 \leqslant R_c(r) \leqslant \alpha$) is therefore *disconnected* from Schwarzschild spacetime and so does not form part of the solution space.

N. Stavroulakis [17, 18, 19, 20] has shown that an object cannot undergo gravitational collapse into a singularity, or to form a black hole.

Suppose $0 \leqslant \sqrt{C(D(r))} < \alpha$. Then (20) becomes

$$ds^2 = -\left(\frac{\alpha}{\sqrt{C}} - 1\right) dt^2 + \left(\frac{\alpha}{\sqrt{C}} - 1\right)^{-1} d\sqrt{C}^2 - C\left(d\theta^2 + \sin^2\theta\, d\varphi^2\right),$$

which shows that there is an interchange of time and length. To amplify this set $r = \bar{t}$ and $t = \bar{r}$. Then

$$ds^2 = \left(\frac{\alpha}{\sqrt{C}} - 1\right)^{-1} \frac{\dot{C}^2}{4C}\, d\bar{t}^2 - \left(\frac{\alpha}{\sqrt{C}} - 1\right) d\bar{r}^2 - C\left(d\theta^2 + \sin^2\theta\, d\varphi^2\right),$$

where $C = C(\bar{t})$ and the dot denotes $d/d\bar{t}$. This is a time dependent metric and therefore bears no relation to the problem of a static gravitational field.

Thus, the Schwarzschild manifold described by (20) with (22) (and hence (8)) is inextendable.

8 That the Riemann tensor scalar curvature invariant is everywhere finite

The Riemann tensor scalar curvature invariant (the Kretschmann scalar) is given by $f = R_{\mu\nu\rho\sigma}R^{\mu\nu\rho\sigma}$. In the general case of (20) with (22) this is

$$f = \frac{12\alpha^2}{R_c^6(r)} = \frac{12\alpha^2}{\left(|r - r_0|^n + \alpha^n\right)^{\frac{6}{n}}}.$$

A routine attempt to justify the standard assumptions on (8) is the *a posteriori* claim that the Kretschmann scalar

must be unbounded at a singularity [5, 21]. Nobody has ever offered a proof that General Relativity necessarily requires this. That this additional *ad hoc* assumption is false is clear from the following ratio,

$$f(r_0) = \frac{12\alpha^2}{\left(|r - r_0|^n + \alpha^n\right)^{\frac{6}{n}}} = \frac{12}{\alpha^4} \; \forall \, r_0 \, .$$

In addition,

$$\lim_{r\to\pm\infty} \frac{12\alpha^2}{\left(|r - r_0|^n + \alpha^n\right)^{\frac{6}{n}}} = 0 \, ,$$

and so the Kretschmann scalar is finite everywhere.

9 That the Gaussian curvature is everywhere finite

The Gaussian curvature K of (20) is,

$$K = K\big(R_c(r)\big) = \frac{1}{R_c^2(r)} \, ,$$

where $R_c(r)$ is given by (22). Then,

$$K(r_0) = \frac{1}{\alpha^2} \; \forall \, r_0 \, ,$$

and

$$\lim_{r\to\pm\infty} K(r) = 0 \, ,$$

and so the Gaussian curvature is everywhere finite.

Furthermore,

$$\lim_{\alpha\to 0} \frac{1}{\alpha^2} = \infty,$$

since when $\alpha = 0$ there is no gravitational field and empty Minkowski space is recovered, wherein R_p and R_c are identical and $0 \leqslant R_p < \infty$. A centre of spherical symmetry in Minkowski space has an infinite Gaussian curvature because Minkowski space is pseudo-Efcleethean.

10 Conclusions

Using the spherical-polar coordinates, the general solution to $R_{\mu\nu} = 0$ is (20) with (22), which is well-defined on

$$-\infty < r_0 < \infty,$$

where r_0 is entirely arbitrary, and corresponds to

$$0 < R_p(r) < \infty, \quad \alpha < R_c(r) < \infty,$$

for the gravitational field. The only singularity that is possible occurs at $g_{00} = 0$. It is impossible to get $g_{11} = 0$ because there is no value of the parameter r by which this can be attained. No interior exists in relation to (20) with (22), which contain the usual metric (8) as a particular case.

The radius of curvature $R_c(r)$ does not in general determine the radial geodesic distance to the centre of spherical symmetry of Einstein's gravitational field and is only to be interpreted in relation to the Gaussian curvature by the equation $K = 1/R_c^2(r)$. The radial geodesic distance from the point at the centre of spherical symmetry to the spherical geodesic surface with Gaussian curvature $K = 1/R_c^2(r)$ is given by the proper radius, $R_p(R_c(r))$. The centre of spherical symmetry in the gravitational field is invariantly located at the point $R_p(r_0) = 0$.

Expression (20) with (22), and hence (8) describes only a centre of mass located at $R_p(r_0) = 0$ in the gravitational field, $\forall \, r_0$. As such it does not take into account the distribution of matter and energy in a gravitating body, since $\alpha(M)$ is indeterminable in this limited situation. One cannot generally just utilise a potential function in comparison with the Newtonian potential to determine α by the weak field limit because α is subject to the distribution of the matter of the source of the gravitational field. The value of α must be calculated from a line-element describing the interior of the gravitating body, satisfying $R_{\mu\nu} - \frac{1}{2} R g_{\mu\nu} = \kappa T_{\mu\nu} \neq 0$. The interior line element is necessarily different to the exterior line element of an object such as a star. A full description of the gravitational field of a star therefore requires two line elements [22, 23], not one as is routinely assumed, and when this is done, there are no singularities anywhere. The standard assumption that one line element is sufficient is false. Outside a star, (20) with (22) describes the gravitational field in relation to the centre of mass of the star, but α is nonetheless determined by the interior metric, which, in the case of the usual treatment of (8), has gone entirely unrecognised, so that the value of α is instead determined by a comparison with the Newtonian potential in a weak field limit.

Black holes are not predicted by General Relativity. The Kruskal-Szekeres coordinates do not describe a coordinate patch that covers a part of the gravitational manifold that is not otherwise covered - they describe a completely different pseudo-Riemannian manifold that has nothing to do with Einstein's gravitational field [6, 9, 11]. The manifold of Kruskal-Szekeres is not contained in the fundamental one-to-one correspondence between the $\mathbf{E}^3$ of Minkowski space and the $\mathbf{M}^3$ of Einstein's gravitational field, and is therefore a spurious augmentation.

It follows in similar fashion that expansion of the Universe and the Big Bang cosmology are inconsistent with General Relativity, as is easily demonstrated [24, 25].

Submitted on February 03, 2007
Accepted on February 09, 2007

References

1. Levi-Civita T. The Absolute Differential Calculus, Dover Publications Inc., New York, 1977.
2. O'Neill B. Semi-Riemannian geometry with applications to Relativity, Academic Press, San Deigo, 1983.
3. Eddington A. S. The mathematical theory of relativity. Cambridge University Press, Cambridge, 2nd edition, 1960.
4. Tolman R. C. Relativity, thermodynamics and cosmology. Dover Publications Inc., Mineola (NY), 1987.

5. Misner C. W., Thorne K. S. and Wheeler J. A. Gravitation. W. H. Freeman and Company, New York, 1973.
6. Abrams L. S. Black holes: the legacy of Hilbert's error. *Can. J. Phys.*, v. 67, 919, 1989; arXiv: gr-qc/0102055.
7. Crothers S. J. On the geometry of the general solution for the vacuum field of the point-mass. *Progress in Physics*, 2005, v. 2, 3–14.
8. Antoci S. David Hilbert and the origin of the "Schwarzschild" solution. arXiv: physics/0310104.
9. Loinger A. On black holes and gravitational waves. La Goliardica Paves, Pavia, 2002.
10. Smoller S. and Temple B. On the Oppenheimer-Volkoff equations in General Relativity. *Arch. Rational Mech. Anal.*, v. 142, 177–191, Springer-Verlag, 1998.
11. Crothers S. J. On the Regge-Wheeler tortoise and the Kruskal-Szekeres coordinates. *Progress in Physics*, 2006, v. 3, 30–34.
12. Schwarzschild K. On the gravitational field of a mass point according to Einstein's theory. *Sitzungsber. Preuss. Akad. Wiss., Phys. Math. Kl*., 1916, 189; arXiv: physics/9905030.
13. Brillouin M. The singular points of Einstein's Universe. *Journ. Phys. Radium*, 1923, v. 23, 43; accessed online on http://www.geocities.com/theometria/brillouin.pdf.
14. Droste J. The field of a single centre in Einstein's theory of gravitation, and the motion of a particle in that field. *Ned. Acad. Wet., S. A.*, 1917, v. 19, 197; accessed online on http://www.geocities.com/theometria/Droste.pdf.
15. Hagihara Y. *Jpn. J. Astron. Geophys.*, 1931, v. 8, 97.
16. Doughty N. *Am. J. Phys.*, 1981, v. 49, 720.
17. Stavroulakis N. A statical smooth extension of Schwarzschild's metric. *Lett. Nuovo Cim.*, Ser.2, 1974, v.11, No.8, 427–430; http://www.geocities.com/theometria/Stavroulakis-3.pdf.
18. Stavroulakis N. On the principles of General Relativity and the $\Theta(4)$-invariant metrics. *Proceedings of the* 3^{rd} *Panhellenic Congress of Geometry*, Athens, 1997, 169–182; assessed online on http://www.geocities.com/theometria/Stavroulakis-2.pdf.
19. Stavroulakis N. On a paper by J. Smoller and B. Temple. *Annales Fond. Louis de Broglie*, 2002, v. 27, No. 3, 511–521; http://www.ptep-online.com/theometria/Stavroulakis-1.pdf.
20. Stavroulakis N. Non-Euclidean geometry and gravitation. *Progress in Physics*, 2006, v. 2, 68–75.
21. Kruskal M. D. Maximal extension of Schwarzschild metric. *Phys. Rev.*, 1960, v. 119, 1743.
22. Schwarzschild K. On the gravitational field of a sphere of incompressible fluid according to Einstein's theory. *Sitzungsber. Preuss. Akad. Wiss., Phys. Math. Kl.*, 1916, 424; arXiv: physics/9912033.
23. Crothers S. J. On the vacuum field of a sphere of incompressible fluid. *Progress in Physics*, 2005, v. 2, 76–81.
24. Crothers S. J. On the general solution to Einstein's vacuum field for the point-mass when $\lambda \neq 0$ and its consequences for relativistic cosmology. *Progress in Physics*, 2005, v. 3, 7–18.
25. Crothers S. J. Relativistic cosmology revisited. *Progress in Physics*, 2007, v. 2, 27–30.

On the Propagation of Gravitation from a Pulsating Source

Nikias Stavroulakis
Solomou 35, 15233 Chalandri, Greece
E-mail: nikias.stavroulakis@yahoo.fr

According to an idea underlying the classical relativity, a pulsating (or simply expanding or simply contracting) spherical source does not generate an external dynamical (i.e. non-stationary) gravitational field. The relativists believe that this idea is well based on account of the so-called Birkhoff's theorem, which, contrary to the fundamental principles of general relativity, states that the external gravitational field of a non-stationary spherical mass is necessarily static. However, as shown in several papers [2, 3, 4, 7, 8], Birkhoff's theorem is, in fact, a vicious circle arising from the introduction of inadmissible implicit transformations which eliminate in advance the boundary conditions defining the radial motion of the sphere bounding the matter, namely the boundary conditions inducing the non-stationary states of the gravitational field. In the present paper we deal with the rigorous mathematical theory of the subject and put forward the corresponding form of the spacetime metric in order to prepare a thorough study of the equations of gravitation related to the dynamical states of the gravitational field.

1 S$\Theta(4)$-invariant metrics and gravitational disturbances

Let us first consider a general spacetime metric

$$\sum_{i,j=0}^{3} g_{ij} dx_i dx_j \tag{1.1}$$

namely a form of signature $(+1,-1,-1,-1)$ on a open set $U \subset \mathbb{R}\times\mathbb{R}^3$. In order that the local time and the proper time of the observes be definable, the timelike character of x_0 must be clearly indicared together with its distinction from the spacelike character of the coordinates x_1, x_2, x_3. This is why, according to Levi-Civita [l], the components g_{00}, g_{11}, g_{22}, g_{33} of the metric tensor must satisfy the conditions $g_{00}>0$, $g_{11}<0$, $g_{22}<0$, $g_{33}<0$.

Our investigation of an $S\Theta(4)$-invariant (or $\Theta(4)$-invariant) metric follows Levi-Civita's point of view by allowing at the same time a slight generalization which will be fully justified. More precisely, an allowable $S\Theta(4)$-invariant (or $\Theta(4)$-invariant) metric will satisfy the conditions $g_{00}>0$, $g_{11}\leqslant 0$, $g_{22}\leqslant 0$, $g_{33}\leqslant 0$. We recall [9] the explicit form of such a metric

$$ds^2 = \left(f dx_0 + f_1 (x dx)\right)^2 - \ell_1^2 dx^2 - \frac{\ell^2-\ell_1^2}{\rho^2}(x dx)^2,$$
$$x_0 = t, \ell(t,0) = \ell_1(t,0),$$

which is invariant by the action of the group $S\Theta(4)$ consisting of the matrices of the form

$$\begin{pmatrix} 1 & O_H \\ O_V & A \end{pmatrix}, \quad O_H = (0,0,0), \quad O_V = \begin{pmatrix} 0 \\ 0 \\ 0 \end{pmatrix},$$
$$A \in SO(3)$$

as well as by the action of the group $\Theta(4)$ consisting of the matrices of the same form for which $A \in O(3)$. Note that the given form of the metric does not contain the important functions

$$h = \rho f_1 = \rho f_1(t,\rho), \qquad g = \rho\ell_1 = \rho\ell_1(t,\rho),$$

because they are not C^∞ on the subspace $\mathbb{R}\times\{(0,0,0)\}$. However, as already noted [9], on account of their geometrical and physical significance, it is very convenient to insert them into the metric, thus obtaining

$$ds^2 = \left(f dx_0 + \frac{h}{\rho}(x dx)\right)^2 - \left(\frac{g}{\rho}\right)^2 dx^2 - \\ - \frac{1}{\rho^2}\left(\ell^2 - \left(\frac{g}{\rho}\right)^2\right)(x dx)^2 \tag{1.2}$$

and then

$$g_{00} = f^2, \qquad g_{ii} = \left(h^2-\ell^2\right)\frac{x_i^2}{\rho^2} - \left(\frac{g}{\rho}\right)^2\left(1-\frac{x_i^2}{\rho^2}\right),$$
$$(i=1,2,3).$$

We contend that $g_{ii}\leqslant 0$, $(i=1,2,3)$, if and only if $|h|\leqslant\ell$. In fact, if $|h|\leqslant\ell$, we have obviously $g_{ii}\leqslant 0$, $(i=1,2,3)$. On the other hand, if $|h|>\ell$, by choosing $x_1=\rho$, $x_2=x_3=0$, we have $g_{11}=h^2-\ell^2>0$.

The $S\Theta(4)$ -invariant metric (1.2), considered with the condition $|h|\leqslant\ell$, is assumed to represent the gravitational field generated by a spherical isotropic non-rotating, in general pulsating, distribution of matter. This field is related intuitively to a radial uniform propagation of spherical gravitational (and possibly electromagnetic) disturbances issuing from the matter and governed by the time according to the following rule:

> The emission of a disturbance takes place at a given instant from the entirety of the sphere bounding the matter (namely from the totality of the points of this sphere) and reaches the totality of any other sphere $S_\rho : \| x \| = \rho > 0$ outside the matter at another instant.

The assignment of a given instant t to every point of the sphere S_ρ means that we consider an infinity of simultaneous events $\{(t, x) \,|x \in S_\rho\}$ related to S_ρ. This conception of simultaneity is restricted to the considered sphere S_ρ and cannot be extended radially (for greater or less values of ρ). So the present situation differs radically from that encountered in special relativity. In particular, the synchronization of clocks in S_ρ cannot be carried out by the standard method put forward by Einstein, because there are no null geodesies of the metric associated with curves lying on S_ρ. The idea of synchronization in $S_\rho : \| x \| = \rho > 0$ is closely related to the very definition of the $S\Theta(4)$-invariant field: For any fixed value of time t, the group $S\Theta(4)$ sends the subspace $\{t\} \times S_\rho$ of $\mathbb{R} \times \mathbb{R}^3$ onto itself, so that the group $S\Theta(4)$ assigns the value of time t to every point of the sphere S_ρ. Specifically, given any two distinct points x and y of S_ρ, there exists an operation of $S\Theta(4)$ sending (t, x) onto (t, y). This operation appears as an abstract mathematical mapping and must be clearly distinguished from a rotation in $\mathbb{R}^3$ in the sense of classical mechanics. Such a rotation in $\mathbb{R}^3$ is a motion defined with respect to a pre-existing definition of time, whereas the assignment of the value of time t to every point of S_ρ, is an "abstract operation" introducing the time in the metric.

Let S_m be the sphere bounding the matter. As will be shown later on, the "synchronization" in S_m induces the synchronization in any other sphere S_ρ outside the matter by means of the propagation process of gravitation. In a stationary state, the radius of S_m reduces to a constant, say σ, and every point of S_m can be written as $x = \alpha\sigma$ where $\alpha = (\alpha_1, \alpha_2, \alpha_3) \in S_1$, S_1 being the unit sphere:

$$S_1 = \Big\{\alpha = (\alpha_1, \alpha_2, \alpha_3) \in \mathbb{R}^3 \big| \\ \| \alpha \| = \sqrt{\alpha_1^2 + \alpha_2^2 + \alpha_3^2} = 1\Big\}.$$

Now, in a non-stationary state, the radius of S_m will be a function of time, say $\sigma(t)$, and the equation of S_m can be written as $x = \alpha\sigma(t)$ with $\alpha \in S_1$. So each value of time t defines both the radius $\sigma(t)$ and the "simultaneous events" $\{(t, \alpha\sigma(t)) \,|\, \alpha \in S_1\}$. This simultaneity is also closely related to the definition of the $S\Theta(4)$ invariant field: $\{(t, \alpha\sigma(t)) \,| \, \alpha \in S_1\}$ remains invariant by the action of $S\Theta(4)$. From these considerations it follows that the first principles related to the notion of time must be introduced axiomatically on the basis of the very definition of the $S\Theta(4)$-invariance. Their physical justification is to be sought a posteriori by taking into account the results provided by the theory itself.

This being said, according to our assumptions, it makes sense to consider as a function of time the curvature radius $g(t, \rho) = \rho\ell_1(t, \rho)$ of a sphere $\|x\| = \rho = \text{const} > 0$ outside the matter. The same assumptions allow to define, as functions of time, the radius $\sigma(t)$ and the curvature radius, denoted by $\zeta(t)$, of the sphere bounding the matter. These positive functions, $\sigma(t)$ and $\zeta(t)$, constitute the boundary conditions at finite distance for the non-stationary field outside the pulsating source. They are assumed to be C^∞, but they cannot be analytic, because the vanishing of $|\sigma'(t)|+|\zeta'(t)|$ on certain compact time intervals does not imply its vanishing on $\mathbb{R}$.

Since the internal field extends to the external one through the sphere $\|x\| = \sigma(t)$, the non-stationary (dynamical) states of the gravitational field outside the pulsating source are induced by the radial motion of this sphere, namely by the motion defined mathematically by the boundary conditions $\sigma(t)$ and $\zeta(t)$. So, it is reasonable to assume that, if $\sigma'(t) = \\ = \zeta'(t) = 0$ on a compact interval of time $[t_1, t_2]$, no propagation of gravitational disturbances takes place in the external space during $[t_1, t_2]$ (at least if there is no diffusion of disturbances). It follows that the gravitational radiation in the external space depends on the derivatives $\sigma'(t)$ and $\zeta'(t)$, so that we may identify their pair with the gravitational disturbance inducing the dynamical states outside the matter. More precisely, the non-stationary-states are generated by the propagation of the gravitational disturbance in the exterior space, so that we have first to clarify the propagation process. Our intuition suggests that the propagation of gravitation is closely related to the radial propagation of light, and this is why we begin by defining the function governing the radial propagation of light from the sphere bounding the matter.

2 Radial null geodesics

We recall that a curve $x(v) = (x_0(v), x_1(v), x_2(v), x_3(v))$ is a geodesic line with respect to (1.1) if

$$\frac{D}{dv}\frac{dx(v)}{dv} = q(v)\frac{dx(v)}{dv}\,.$$

So we are led to introduce the vector

$$Y^j = \frac{d^2x_j}{dv^2} + \sum_{k,\ell=0}^{3} \Gamma^j_{k\ell}\frac{dx_k}{dv}\frac{dx_\ell}{dv} - q(v)\frac{dx_j}{dv}, \quad (j = 0, 1, 2, 3),$$

which allows to write the equations of a geodesic in their general form

$$Y^0 = 0\,, \qquad Y^1 = 0\,, \qquad Y^2 = 0\,, \qquad Y^3 = 0\,.$$

On the other hand, a null line (not necessarily geodesic) is defined by the condition

$$\sum_{i,j=0}^{3} g_{ij}\frac{dx_i}{dv}\frac{dx_j}{dv} = 0\,, \qquad (v \neq s),$$

which implies

$$\sum g_{ij}\frac{dx_i}{dv}\frac{d^2x_j}{dv^2}+\sum\Gamma_{i,k\ell}\frac{dx_i}{dv}\frac{dx_k}{dv}\frac{dx_\ell}{dv}=0$$

so that by setting

$$X_j=\sum g_{ij}\frac{dx_i}{dv}$$

we deduce by an easy computation the relation

$$\sum_{j=0}^{3}X_jY^j=0$$

which is valid for every null line.

Now, let

$$d_t=\big\{x_1=\alpha_1\rho,\ \ x_2=\alpha_2\rho,\ \ x_3=\alpha_3\rho,\\ \alpha_1^2+\alpha_2^2+\alpha_3^2=1,\ \ \rho\geqslant\sigma(t)\big\}$$

be a half-line issuing from a point of the sphere $\|x\|=\sigma(t)$. The vanishing of (1.2) on d_t gives rise to two radial null lines defined respectively by the equations

$$\frac{dt}{d\rho}=\frac{-h(t,\rho)+\ell(t,\rho)}{f(t,\rho)} \tag{2.1}$$

$$\frac{dt}{d\rho}=\frac{-h(t,\rho)-\ell(t,\rho)}{f(t,\rho)} \tag{2.2}$$

Proposition 2.1. *The above defined null lines are null geodesics.*

Proof. By using a transformation defined by an element of the group $S\Theta(4)$, we may assume, without restriction of generality, that d_t is defined by the equations $x_1=\rho$, $x_2=0$, $x_3=0$, where $\rho\geqslant\sigma(t)$. Then taking into account the expressions of the Christoffel symbols [9], we see that

$$\Gamma^2_{00}=\Gamma^2_{01}=\Gamma^2_{11}=0,\qquad \Gamma^3_{00}=\Gamma^3_{01}=\Gamma^3_{11}=0,$$

so that the equations $Y^2=0$, $Y^3=0$ are identically verified. Moreover $x_2=x_3=0$ imply

$$Y^0=\frac{d^2t}{dv^2}+\Gamma^0_{00}\left(\frac{dt}{dv}\right)^2+\Gamma^0_{11}\left(\frac{d\rho}{dv}\right)^2+\\ +2\Gamma^0_{01}\frac{dt}{dv}\frac{d\rho}{dv}-q(v)\frac{dt}{dv},$$

$$Y^1=\frac{d^2\rho}{dv^2}+\Gamma^1_{00}\left(\frac{dt}{dv}\right)^2+\Gamma^1_{11}\left(\frac{d\rho}{dv}\right)^2+\\ +2\Gamma^1_{01}\frac{dt}{dv}\frac{d\rho}{dv}-q(v)\frac{d\rho}{dv}.$$

Now, let $t=\xi(\rho)$ be a solution of (2.1) and take $v=\rho$. Then the equation $Y^1=0$ gives

$$\Gamma^1_{00}\big(\xi(\rho),\rho\big)\big(\xi'(\rho)\big)^2+\Gamma^1_{11}\big(\xi(\rho),\rho\big)+\\ +2\Gamma^1_{01}\big(\xi(\rho),\rho\big)\xi'(\rho)=q(\rho)$$

so that it defines the function $q(\rho)$. Next, since the equations $Y^1=0$, $Y^2=0$, $Y^3=0$ are fulfilled, the condition $\sum_{j=0}^3X_jY^j=0$ reduces to $X_0Y^0=0$, and since

$$X_0=g_{00}\frac{dt}{dv}+g_{01}\frac{dx_1}{dv}=f^2\frac{dt}{d\rho}+fh=\\ =f^2\left(\frac{-h+\ell}{f}\right)+fh=f\ell>0,$$

it follows also that $Y^0=0$. In the same way taking into account that $-f\ell<0$, we prove the assertion regarding (2.2).

Corollary 2.1. *The equation (2.1), resp. (2.2), defines the radial motion of the photons issuing from (resp. approaching to) the pulsating spherical mass.*

In fact, since $|h|\leqslant\ell$, we have $-h+\ell\geqslant0$, which impies $dt/d\rho\geqslant0$, and $-h-\ell\leqslant0$ which implies $dt/d\rho\leqslant0$.

Remark 2.1. The condition $|h|\leqslant\ell$ has been introduced in order to ensure the physical validity of the spacetime metric. Now we see that it is absolutely indispensable in order to define the radial motion of light. In fact, if $h>\ell$ (resp. $-h>\ell$), the photons issuing from (resp. approaching to) the spherical mass would be inexistent for the metric. A detailed discussion of the inconsistencies resulting from the negation of the condition $|h|\leqslant\ell$ is given in the paper [6].

Remark 2.2. As already remarked, the propagation of the gravitation from the pulsating source is closely related to the radial propagation of te outgoing light which is defined by (2.1). Regarding the equation (2.2), which defines the radial propagation of the incoming light, it is not involved in our study, because there are no gravitational disturbances coming from the "infinity".

3 On the solutions of (2.1)

Let us consider a photon emitted radially at an instant u from the sphere bounding the matter. Its velocity at this instant, namely

$$\frac{d\rho}{dt}=\frac{f\big(u,\sigma(u)\big)}{\ell\big(u,\sigma(u)\big)-h\big(u,\sigma(u)\big)}$$

is greater than the radial velocity $|\sigma'(u)|$ of this sphere, whence the condition

$$\frac{\ell\big(u,\sigma(u)\big)-h\big(u,\sigma(u)\big)}{f\big(u,\sigma(u)\big)}\,|\sigma'(u)|<1$$

which implies in particular the validity of the condition

$$\frac{\ell\big(u,\sigma(u)\big)-h\big(u,\sigma(u)\big)}{f\big(u,\sigma(u)\big)}\,\sigma'(u)<1 \tag{3.1}$$

which is trivially valid if $\sigma'(u)\leqslant0$.

This being said, let us consider the open set

$$U=\big\{(t,\rho)\in\mathbb{R}^2\,|\,\rho>\sigma(t)\big\}$$

and denote by F its frontier:

$$F=\big\{(t,\rho)\in\mathbb{R}^2\,|\,\rho=\sigma(t)\big\}.$$

Since the equation (2.1) is conceived on the closed set $\overline{U} = U \cup F$, the functions f, h, ℓ are defined on $\overline{U}$. However, since we have to define the solutions of (2.1) by using initial conditions in F, we are led to extend the function

$$\alpha(t,\rho) = \frac{-h(t,\rho)+\ell(t,\rho)}{f(t,\rho)}$$

to a C^∞ function $\hat{\alpha}(t,\rho) \geqslant 0$ on an open set W containing $\overline{U}$. It is not necessary to indicate a precise extension on W because its values on $W-\overline{U}$ play an auxiliary part and are not involved in the final result.

This remark applies also to the derivatives of the functions f, h, ℓ at the points of F. In fact, although the definition of these derivatives takes into account the extension $\hat{\alpha}(t,\rho)$, their values on F, on account of the continuity, are defined uniquely by their values on U.

This being said, for each fixed point $(u,\sigma(u)) \in F$, the differential equation

$$\frac{dt}{d\rho} = \hat{\alpha}(t,\rho)$$

possesses a unique local solution $t = \hat{\xi}(u,\rho)$ taking the value u for $\rho = \sigma(u)$. Let $]\,\rho_1(u), \rho_2(u)\,[$ be the maximal interval of validity of this local solution $(\rho_1(u) < \sigma(u) < \rho_2(u))$.

Lemma 3.1. *There exists a real number $\epsilon > 0$ such that $\sigma(u) < \epsilon < \rho_2(u)$ and $(\hat{\xi}(u,\rho),\rho) \in U$ for every $\rho \in]\,\sigma(u), \epsilon\,]$.*

Proof. Assume that such a number does not exist. Then we can find a sequence of values $\rho_n > \sigma(u)$ converging to $\sigma(u)$ and such that $(\hat{\xi}(u,\rho_n),\rho_n) \notin U$, which means that $\sigma(\hat{\xi}(u,\rho_n)) \geqslant \rho_n$, and implies, in particular $\hat{\xi}(u,\rho_n) \neq u$. It follows that

$$\frac{\hat{\xi}(u,\rho_n)-u}{\rho_n-\sigma(u)} \cdot \frac{\sigma\big(\hat{\xi}(u,\rho_n)\big)-\sigma(u)}{\hat{\xi}(u,\rho_n)-u} = \frac{\sigma\big(\hat{\xi}(u,\rho_n)\big)-\sigma(u)}{\rho_n-\sigma(u)} \geqslant 1$$

and since $\hat{\xi}(u,\sigma(u)) = u$, $\rho_n \to \sigma(u)$, we obtain

$$\frac{\partial\hat{\xi}\big(u,\sigma(u)\big)}{\partial\rho}\,\sigma'(u) \geqslant 1\,,$$

or

$$\frac{-h\big(u,\sigma(u)\big)+\ell\big(u,\sigma(u)\big)}{f\big(u,\sigma(u)\big)}\,\sigma'(u) \geqslant 1$$

which contradicts (3.1). This contradiction proves our assertion.

Lemma 3.2. *We also have $(\hat{\xi}(u,\rho),\rho) \in U$ for every $\rho \in]\,\epsilon, \rho_2(u)\,[$.*

Proof. If not, the set of values $\rho \in]\,\epsilon, \rho_2(u)\,[$ for which $\sigma(\hat{\xi}(u,\rho)) = \rho$ is not empty. Let ρ_0 be the greatest lower bound of this set. Then $\sigma(\hat{\xi}(u,\rho_0)) = \rho_0$. Let $\hat{\xi}(u,\rho_0) = t_0$ and let $\psi(t_0,\rho)$ be the local solution of the differential equation

$$\frac{dt}{d\rho} = \hat{\alpha}(t,\rho)$$

for which $\psi(t_0,\rho_0) = t_0$. The uniqueness of the solution implies obviously that $\psi(t_0,\rho) = \hat{\xi}(u,\rho)$. On the other hand, for every $\rho \in]\,\sigma(u), \rho_0\,[$, we have $\sigma(\hat{\xi}(u,\rho)) < \rho$. Moreover $\hat{\xi}(u,\rho_0) \neq \hat{\xi}(u,\rho)$ because the equality $\hat{\xi}(u,\rho_0) = \hat{\xi}(u,\rho)$ would imply

$$\rho_0 = \sigma\big(\hat{\xi}(u,\rho_0)\big) = \sigma\big(\hat{\xi}(u,\rho)\big) < \rho$$

contradicting the choice of ρ. On the other hand

$$\sigma\big(\hat{\xi}(u,\rho_0)\big) - \sigma\big(\hat{\xi}(u,\rho)\big) = = \rho_0 - \sigma\big(\hat{\xi}(u,\rho)\big) > \rho_0 - \rho > 0$$

so that we can write

$$\frac{\hat{\xi}(u,\rho_0)-\hat{\xi}(u,\rho)}{\rho_0-\rho} \cdot \frac{\sigma\big(\hat{\xi}(u,\rho_0)\big)-\sigma\big(\hat{\xi}(u,\rho)\big)}{\hat{\xi}(u,\rho_0)-\hat{\xi}(u,\rho)} = = \frac{\sigma\big(\hat{\xi}(u,\rho_0)\big)-\sigma\big(\hat{\xi}(u,\rho)\big)}{\rho_0-\rho} \geqslant 1$$

or

$$\frac{\psi(t_0,\rho_0)-\psi(t_0,\rho)}{\rho_0-\rho} \cdot \frac{\sigma(t_0)-\sigma\big(\psi(t_0,\rho)\big)}{t_0-\psi(t_0,\rho)} \geqslant 1$$

and for $\rho \to \rho_0$ we find

$$\frac{\partial\psi(t_0,\rho_0)}{\partial\rho}\,\sigma'(t_0) \geqslant 1$$

or

$$\frac{-h\big(t_0,\sigma(t_0)\big)+\ell\big(t_0,\sigma(t_0)\big)}{f(t_0,\sigma(t_0))}\,\sigma'(t_0) \geqslant 1$$

which contradicts (3.1). This contradiction proves our assertion.

Proposition 3.1. *Let $\xi(u,\rho)$ be the restriction of the solution $\hat{\xi}(u,\rho)$ to the interval $[\,\sigma(u), \rho_2(u)\,[$. Then $\xi(u,\rho)$ does not depend on the extension $\hat{\alpha}(t,\rho)$ of $\alpha(t,\rho)$, so that it is the unique local solution of (2.1) in $\overline{U}$ satisfying the condition $\xi(u,\sigma(u)) = u$.*

In fact, since $\hat{\xi}(u,\sigma(u)) = u$ and $(\hat{\xi}(u,\rho),\rho) \in U$ for $\rho > \sigma(u)$, the definition of $\xi(u,\rho)$ on $[\,\sigma(u), \rho_2(u)[$ depends uniquely on the function $\alpha(t,\rho)$ which is defined on $\overline{U}$

In general, the obtained solution $\xi(u,\rho)$ is defined on a bounded interval $[\,\sigma(u), \rho_2(u)\,[$. However the physical conditions of the problem require that the emitted photon travel to infinity. In fact, the pulsating source (whenever it is expanding) can not overtake the photon emitted radially at the instant u. Consequently the functions f, h, ℓ involved in the metric must be such that, for each value of $u \in \mathbb{R}$, the solution $\xi(u,\rho)$ of (2.1) be defined on the half-line $[\,\sigma(u), +\infty\,[$, so that $\rho_2(u) = +\infty$ and $(\xi(u,\rho),\rho) \in U$ for every $\rho \in]\,\sigma(u), +\infty\,[$. Then the corresponding curves $(\xi(u,\rho),\rho)$ issuing from the points of F are the leaves of a foliation of $\overline{U}$ representing the paths of the photons emitted radially from the sphere bounding the matter (see Figure 1 shown in Page 79).

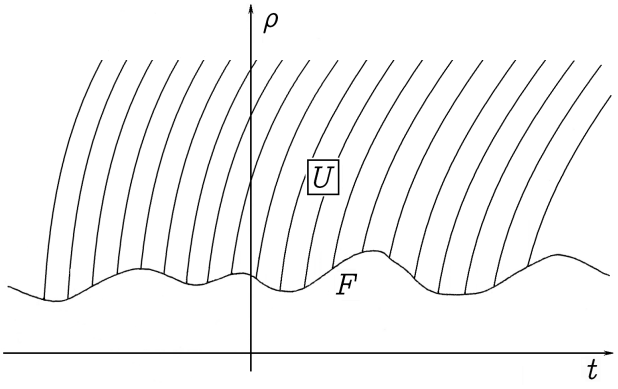

Fig. 1: Foliation representing the paths of the photons emitted radially from the sphere bounding the matter.

4 Propagation function of light and canonical metric

The solution $\xi(u,\rho)$ appears as a function of two variables: On the one hand the time $u \in \mathbb{R}$ on the sphere bounding the matter, and on the other hand the radial coordinate $\rho \in [\sigma(u), +\infty[$.

Proposition 4.1. *The function $\xi(u,\rho)$, $(u,\rho) \in \overline{U}$, fulfils the conditions*

$$\frac{\partial \xi(u,\rho)}{\partial u} > 0, \quad \frac{\partial \xi(u,\rho)}{\partial \rho} \geqslant 0$$

the first of which allows to solve with respect to u the equation $t = \xi(u,\rho)$, where $\xi(u,\sigma(u)) = u$, and obtain thus the instant u of the radial emission of a photon as a function of (t,ρ): $u = \pi(t,\rho)$. The so obtained function $\pi(t,\rho)$ on $\overline{U}$ satisfies the conditions

$$\frac{\partial \pi(t,\rho)}{\partial t} > 0\,, \qquad \frac{\partial \pi(t,\rho)}{\partial \rho} \leqslant 0\,, \qquad \pi\big(t,\sigma(t)\big) = t\,.$$

Proof. Since $-h + \ell \geqslant 0$, the condition $\xi(u,\rho)/\partial\rho \geqslant 0$ is obvious on account of (2.1). On the other hand, taking the derivatives of both sides of the identity $\xi(u,\sigma(u)) = u$ we obtain

$$\frac{\partial \xi\big(u,\sigma(u)\big)}{\partial u} + \frac{\partial \xi\big(u,\sigma(u)\big)}{\partial \rho}\,\sigma'(u) = 1$$

or

$$\frac{\partial \xi\big(u,\sigma(u)\big)}{\partial u} + \frac{-h\big(u,\sigma(u)\big) + \ell\big(u,\sigma(u)\big)}{f\big(u,\sigma(u)\big)}\,\sigma'(u) = 1$$

whence, on account of (3.1),

$$\frac{\partial \xi\big(u,\sigma(u)\big)}{\partial u} > 0$$

for every $u \in \mathbb{R}$. It remains to prove that, for each fixed value $u_0 \in \mathbb{R}$, and for each fixed value $\rho_0 > \sigma(u_0)$, we have $\partial\xi(u_0,\rho_0)/\partial u > 0$.

Now, $\rho_0 > \sigma(u_0)$ implies that there exists a straight line segment

$$\big[-\epsilon_1 + \xi(u_0,\rho_0), \epsilon_1 + \xi(u_0,\rho_0)\big] \times \{\rho_0\}\,, \epsilon_1 > 0,$$

contained in U. Let us denote by L_1, L_0, L_2 respectively the leaves containing the points

$$\big(-\epsilon_1 + \xi(u_0,\rho_0),\, \rho_0\big),\ \big(\xi(u_0,\rho_0),\, \rho_0\big),\ \big(\epsilon_1 + \xi(u_0,\rho_0),\, \rho_0\big).$$

L_0 is defined by the solution $\xi(u_0,\rho)$ of (2.1), whereas L_1 and L_2 are defined respectively by two solutions $\xi(u_1,\rho)$ and $\xi(u_2,\rho)$ with convenient values u_1 and u_2. Since $L_1 \cap L_0 = \emptyset$, $L_0 \cap L_2 = \emptyset$, it follows obviously that $u_1 < u_0$ and $u_0 < u_2$. The same reasoning shows that, if $u_1 < u' < u_0 < u'' < u_2$, then

$$\xi(u_1,\rho_0) < \xi(u',\rho_0) < \xi(u_0,\rho_0) < \xi(u'',\rho_0) < \xi(u_2,\rho_0),$$

so that $\xi(u,\rho_0)$ is a strictly increasing function of u on the interval $[u_1,u_2]$. It follows that $\partial\xi(u_0,\rho_0)/\partial u > 0$ as asserted. Regarding the last assertion, it results trivially from the identity $\xi(\pi(t,\rho),\rho) = t$, which implies

$$\frac{\partial \xi}{\partial u}\cdot\frac{\partial \pi}{\partial t} = 1\,, \qquad \frac{\partial \xi}{\partial u}\cdot\frac{\partial \pi}{\partial \rho} + \frac{\partial \xi}{\partial \rho} = 0\,.$$

Remark. Let u_1 and u_2 be two instants such that $u_1 < u_2$, and let ρ be a positive length. If the values $\xi(u_1,\rho)$ and $\xi(u_2,\rho)$ are both definable, which implies, in particular, $\xi(u_1,\rho) \geqslant u_1$ and $\xi(u_2,\rho) \geqslant u_2$, then $\xi(u_1,\rho) < \xi(u_2,\rho)$.

The function $\pi(t,\rho)$ characterizes the radial propagation of light and will be called *propagation function*. Its physical significance is the following : If a photon reaches the sphere $\|x\| = \rho$ at the instant t, then $\pi(t,\rho)$ is the instant of its radial emission from the sphere bounding the matter.

Proposition 4.2 *If a photon emitted radially from the sphere bounding the matter reaches the sphere $\|x\| = \rho$ at the instant t, then its radial velocity at this instant equals*

$$-\frac{\partial \pi(t,\rho)/\partial t}{\partial \pi(t,\rho)/\partial \rho}\,.$$

In fact, since

$$\frac{dt}{d\rho} = \frac{-h+\ell}{f} = \frac{\partial \xi(u,\rho)}{\partial \rho},$$

the velocity in question equals

$$\frac{d\rho}{dt} = \left(\frac{\partial \xi(u,\rho)}{\partial \rho}\right)^{-1} = -\left(\frac{\partial \xi(u,\rho)}{\partial u}\,\frac{\partial \pi(t,\rho)}{\partial \rho}\right)^{-1} = -\frac{\partial \pi(t,\rho)/\partial t}{\partial \pi(t,\rho)/\partial \rho}\,.$$

Remark. The preceding formula applied to the classical propagation function $t - \frac{\rho}{c}$, gives the value c.

Since the parameter u appearing in the solution $\xi(u,\rho)$ represents the time on the sphere bounding the matter and describes the real line, we are led to define a mapping $\Gamma\colon \overline{U} \to \overline{U}$, by setting $\Gamma(t,\rho) = (\pi(t,\rho),\rho) = (u,\rho)$.

Proposition 4.3. *The mapping Γ is a diffeomorphism which reduces to the identity on the frontier F of U. Moreover it transforms the leaf $\{(t,\rho)\in\overline{U}\,|\,t=\xi(u,\rho)\}$ issuing from a point $(u,\sigma(u))\in F$ into a half-line issuing from the same point and parallel to the ρ-axis. Finally it transforms the general $\Theta(4)$ invariant metric (1.2) into another $\Theta(4)$-invariant metric for which $h=\ell$, so that the new propagation function is identical with the new time coordinate.*

Proof. The mapping Γ is one-to-one and its jacobian determinant $\partial\pi(t,\rho)/\partial t$ is strictly positive everywhere. Consequently Γ is a diffeomorphism. Moreover, since each leaf is defined by a fixed value of u, its transform in the new coordinates (u,ρ) is actually a half-line parallel to the ρ-axis. Finally, since $t=\xi(u,\rho)$ and $\partial\xi/\partial\rho=(-h+\ell)/f$, it follows that

$$\begin{aligned} f\,dt+\frac{h}{\rho}\,(x\,dx) &= \left(f\,\frac{\partial\xi}{\partial u}\right)du+\left(f\,\frac{\partial\xi}{\partial\rho}\right)d\rho+h\,d\rho \\ &= \left(f\,\frac{\partial\xi}{\partial u}\right)du+\left(f\left(\frac{-h+\ell}{f}\right)+h\right)d\rho \\ &= \left(f\,\frac{\partial\xi}{\partial u}\right)du+\ell\,d\rho \\ &= \left(f\,\frac{\partial\xi}{\partial u}\right)du+\ell\,\frac{(x\,dx)}{\rho} \end{aligned}$$

with

$$f=f\big(\xi(u,\rho),\rho\big),\quad h=h\big(\xi(u,\rho),\rho\big),\quad \ell=\ell\big(\xi(u,\rho),\rho\big).$$

So the remarkable fact is that, in the transformed $\Theta(4)$-invariant metric, the function h equals ℓ. The corresponding equation (2.1) reads

$$\frac{du}{d\rho}=0$$

whence $u=\text{const}$, so that the new propagation function is identified with the time coordinate u. (This property follows also from the fact that the transform of $\pi(t,\rho)$ is the function $\pi(\xi(u,\rho),\rho)=u$.)

The Canonical Metric. In order to simplify the notations, we write $f(u,\rho)$, $\ell(u,\rho)$, $g(u,\rho)$ respectively instead of

$$f\big(\xi(u,\rho),\rho\big)\frac{\partial\xi(u,\rho)}{\partial u}\,,\quad \ell\big(\xi(u,\rho),\rho\big)\,,\quad g\big(\xi(u,\rho),\rho\big)$$

so that the transformed metric takes the form

$$\begin{aligned} ds^2 &= \left(f(u,\rho)\,du+\ell(u,\rho)\,\frac{(x\,dx)}{\rho}\right)^2- \\ &-\left[\left(\frac{g(u,\rho)}{\rho}\right)^2dx^2+\left(\big(\ell(u,\rho)\big)^2-\left(\frac{g(u,\rho)}{\rho}\right)^2\right)\frac{(x\,dx)^2}{\rho^2}\right] \end{aligned} \tag{4.1}$$

which will be termed Canonical.

The equality $h=\ell$ implies important simplifications: Since the propagation function of light is identified with the new time coordinate u, it does not depend either on the unknown functions f, ℓ, g involved in the metric or on the boundary conditions at finite distance $\sigma(u)$, $\zeta(u)$. The radial motion of a photon emitted radially at an instant u_0 from the sphere $\|x\|=\sigma(u)$ will be defined by the equation $u=u_0$, which, when u_0 describes $\mathbb{R}$, gives rise to a foliation of $\overline{U}$ by half-lines issuing from the points of F and parallel to the ρ-axis (Figure 2). This property makes clear the physical significance of the new time coordinate u. Imagine that the photon emitted radially at the instant u_0 is labelled with the indication u_0. Then, as it travels to infinity, it assigns the value of time u_0 to every point of the corresponding ray. This conception of time differs radically from that introduced by special relativity. In this last theory, the equality of values of time at distinct points is defined by means of the process of synchronization. In the present situation the equality of values of time along a radial half-line is associated with the radial motion of a single photon. The following proposition is obvious (although surprising at first sight).

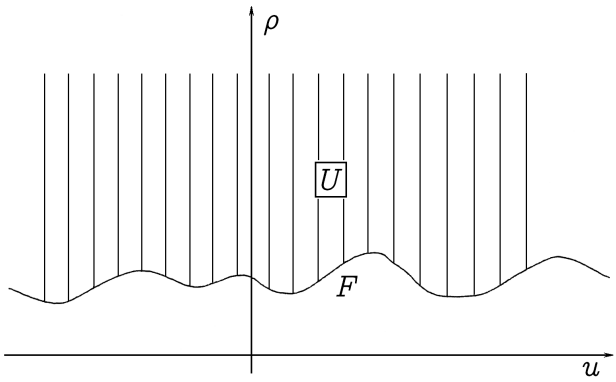

Fig. 2: The rise to a foliation of $\overline{U}$ by half-lines issuing from the points of F and parallel to the ρ-axis.

Proposition 4.4. *With respect to the canonical metric, the radial velocity of propagation of light is infinite.*

Note that the classical velocity of propagation of light, namely c, makes sense only with respect to the time defined by synchronized clocks in an inertial system.

We emphasize that the canonical metric is conceived on the closed set $\{(u,x)\in\mathbb{R}\times\mathbb{R}^3\,|\,\|x\|\geqslant\sigma(u)\}$ namely on the exterior of the matter, and it is not possible to assign to it a universal validity on $\mathbb{R}\times\mathbb{R}^3$. In fact, ℓ is everywhere strictly positive, whereas h vanishes for $\rho=0$, so that the equality $h(t,\,\|x\|)=\ell(t,\,\|x\|)$ cannot hold on a neighbourhood of the origin. It follows that the canonical metric is incompatible with the idea of a punctual source.

5 Propagation function of gravitational disturbances

We recall that, $\sigma(u)$ and $\zeta(u)$ being respectively the radius and the curvature radius of the sphere bounding the matter, we are led to identify the pair of derivatives $(\sigma'(u),\zeta'(u))$ with the gravitational disturbance produced at the instant u on the entirety of the sphere in question. This local disturbance induces a radial propagation process with propagation

paths identified with the radial geodesies and wave fronts covering successively the spheres $\|x\| = \rho = \text{const}$. This process modifies step by step the field outside the matter and thus gives rise to a non-stationary (dynamical) state of the gravitational field. It follows that apart from any theory aimed at determining the gravitational field, we have first to elucidate the propagation process of the gravitational disturbance. In order to carry out this investigation, we refer constantly to the canonical metric (4.1) which, without restriction of generality, gives rise to significant simplifications. This being said, the gravitational disturbance being produced at the instant u on the sphere bounding the matter, let us consider the instant $t = \psi(u, \rho)$ at which it reaches the sphere $\|x\| = \rho$, so that we have, in particular, $\psi(u, \sigma(u)) = u$. We assume naturally that the pulsating source does not hinder the propagation of gravitation outside the matter. In other words, every time that the sphere bounding the matter is expanding, it can not overtake the advancing gravitational disturbance. This is the case if and only if $(\psi(u, \rho), \rho) \in U$ for every $\rho > \sigma(u)$. On the other hand, on account of the physical conditions of the problem, the derivative $\dfrac{\partial \psi(u, \rho)}{\partial \rho}$ cannot be negative, so that the equation $t = \psi(u, \rho)$ defines non decreasing functions of ρ giving rise to a foliation of $\overline{U}$ by curves issuing from the points of F. Because of this foliation, we have the condition

$$\frac{\partial \psi(u, \rho)}{\partial u} > 0 \tag{5.1}$$

which allows to solve the equation $t = \psi(u, \rho)$ with respect to u, thus obtaining the propagation function of the gravitational disturbance $u = e(t, \rho)$ relative to the canonical metric (4.1). Note that, on account of (5.1), by setting $\Delta(u, \rho) = (\psi(u, \rho), \rho) = (t, \rho)$, we define a diffeomorphism $\Delta : \overline{U} \to \overline{U}$, the restriction of which to F is the identity.

Proposition 5.1 *If the gravitational disturbance emitted at the instant u reaches the sphere $\|x\| = \rho$ at the instant t, then its radial velocity at this instant equals*

$$-\frac{\partial e(t, \rho)/\partial t}{\partial e(t, \rho)/\partial \rho}\,.$$

Proof. The velocity in question equals

$$\frac{d\rho}{dt} = \frac{1}{dt/d\rho} = \frac{1}{\partial \psi(u, \rho)/\partial \rho}$$

and since the derivation of the identity

$$e\big(\psi(u, \rho), \rho\big) = u$$

with respect to ρ gives

$$\frac{\partial e}{\partial t}\frac{\partial \psi}{\partial \rho} + \frac{\partial e}{\partial \rho} = 0\,,$$

we obtain

$$\frac{1}{\partial \psi(u, \rho)/\partial \rho} = -\frac{\partial e(t, \rho)/\partial t}{\partial e(t, \rho)/\partial \rho}$$

as asserted.

Remark. Since the radial velocity of propagation of light is infinite with respect to the canonical metric (4.1), the velocity of radial propagation of the gravitational disturbance is necessarily less than (or possibly equal to) that of light. In fact, we can establish the identity of the two propagation functions on the basis of a hypothesis which suggests itself quite naturally.

Proposition 5.2. *If the diffeomorphism Δ transforms the canonical metric (4.1) into another physically admissible $\Theta(4)$-invariant metric on $\overline{U}$, then the propagation function of the gravitational disturbance is identical with the propagation function of light.*

Proof. In order to transform (4.1) by means of Δ, we have simply to replace u in (4.1) by $e(t, \rho)$ thus obtaining the $\Theta(4)$-invariant metric

$$\begin{aligned} ds^2 = &\left(F dt + \frac{H}{\rho}(x dx)\right)^2 - \\ &- \left[\left(\frac{G}{\rho}\right)^2 dx^2 + \left(L^2 - \left(\frac{G}{\rho}\right)^2\right)\frac{(x dx)^2}{\rho^2}\right] \end{aligned} \tag{5.2}$$

where

$$F = F(t, \rho) = f\big(e(t, \rho), \rho\big)\frac{\partial e(t, \rho)}{\partial t}\,, \tag{5.3}$$

$$H = H(t, \rho) = f\big(e(t, \rho), \rho\big)\frac{\partial e(t, \rho)}{\partial \rho} + \ell\big(e(t, \rho), \rho\big), \tag{5.4}$$

$$G = G(t, \rho) = g\big(e(t, \rho), \rho\big),$$

$$L = L(t, \rho) = \ell\big(e(t, \rho), \rho\big).$$

In the new metric (5.2), each value of $t = \psi(u, \rho)$ is the instant at which the disturbance emitted at the instant u reaches the sphere $\|x\| = \rho$. Consequently $e(t, \rho)$ is also the propagation function of the gravitational disturbance with respect to (5.2).

We now prove that the derivative $\partial e(t, \rho)/\partial \rho$ vanishes identically on $\overline{U}$.

We argue by contradiction. If this derivative does not vanish, the propagation function $e(t, \rho)$ of the gravitational disturbance is distinct from the propagation function of light with respect to (4.1), hence also with respect to the transformed metric (5.2). This last being admissible, according to our assumption, it satisfies the condition

$$|H(t, \rho)| \leqslant L(t, \rho)\,,$$

so that the radial motion of the photons issuing from the matter is defined by the equation

$$\frac{dt}{d\rho} = \frac{-H(t, \rho) + L(t, \rho)}{F(t, \rho)}\,.$$

On account of (5.3) and (5.4), we have

$$\frac{-H(t, \rho) + L(t, \rho)}{F(t, \rho)} = -\frac{\partial e(t, \rho)/\partial \rho}{\partial e(t, \rho)/\partial t}$$

so that the preceding equation reads

$$\frac{\partial e(t,\rho)}{\partial t}\,dt + \frac{\partial e(t,\rho)}{\partial \rho}\,d\rho = 0$$

whence $e(t,\rho) = \text{const}$ and since $e(t,\sigma(t)) = t$, $e(t,\rho)$ is the propagation function of light with respect to (5.2) contrary to our assumptions. This contradiction proves our assertion, namely that $\partial e(t,\rho)/\partial\rho = 0$ on $\overline{U}$.

This being proved, since the condition $\psi(e(t,\rho),\rho) = t$ implies

$$\frac{\partial \psi}{\partial u}\frac{\partial e}{\partial \rho} + \frac{\partial \psi}{\partial \rho} = 0\,,$$

the derivative $\partial\psi/\partial\rho$ vanishes identically on $\overline{U}$. In other words, $\psi(t,\rho)$ does not depend on ρ, so that

$$\psi(u,\rho) = \psi\big(u,\sigma(u)\big) = u$$

for every $\rho \geqslant \sigma(u)$. It follows that the propagation function of the gravitational disturbance is the same as that of light with respect to (4.1), hence also with respect to any admissible transformation of (4.1).

From now on we will not distinguish the propagation function of gravitational disturbances from that of light. So we can begin by the consideration of the canonical metric (4.1) for the study of the equations of gravitation related to a spherical pulsating source. This investigation will be carried out in another paper.

Submitted on February 09, 2007
Accepted on February 14, 2007

References

1. Levi-Civita T. On the analytic expression that must be given to the gravitational tensor in Einstein's theory. arXiv: physics/9906004, translation and foreword by S. Antoci and A. loinger (originally, in: *Rendiconti della Reale Accademia dei Lincei*, 1917, v. 26, 381).
2. Stavroulakis N. Exact solution for the field of a pulsating source, *Abstracts of Contributed Papers For the Discussion Groups, 9th International Conference on General Relativity and Gravitation*, July 14–19, 1980, Jena, Volume 1, 74–75.
3. Stavroulakis N. Mathématiques et trous noirs, *Gazette des mathématiciens*, No. 31, Juillet 1986, 119–132.
4. Stavroulakis N. Solitons and propagation d'actions suivant la relativité générale (première partie). *Annales Fond. Louis de Broglie*, 1987, v. 12, No. 4, 443–473.
5. Stavroulakis N. Solitons and propagation d'actions suivant la relativité générale (deuxième partie). *Annales Fond. Louis de Broglie*, 1988, v. 13, No. 1, 7–42.
6. Stavroulakis N. Sur la fonction de propagation des ébranlements gravitationnels. *Annales Fond. Louis de Broglie*, 1995, v. 20, No. 1, 1–31.
7. Stavroulakis N. On the principles of general relativity and the $S\Theta(4)$-invariant metrics. *Proc. 3^{rd} Panhellenic Congr. Geometry*, Athens 1997, 169–182.
8. Stavroulakis N. Vérité scientifique et trous noirs (première partie). Les abus du formalisme. *Annales Fond. Louis de Broglie*, 1999, v. 24, No. 1, 67–109.
9. Stavroulakis N. Non-Euclidean geometry and gravitation, *Progress in Physics*, 2006, v. 2, 68–75.

Effect from Hyperbolic Law in Periodic Table of Elements

Albert Khazan
E-mail: albkhazan@list.ru

Hyperbola curves $Y = K/X$ and $Y = (mx+n)/(px+q)$ at determination of the upper limit of the Periodic System have been studied. Their interdependence is shown by the example of mathematical calculations in chemistry.

1 Introduction. Mathematical basis

Our previous article shows that the Y content of any element K in a chemical compound is decreasing in case molecular mass X is increasing in the range from 1 up to any desired value in compliance with rectangular hyperbole law $Y = \frac{K}{X}$. Simultaneously, fraction $(1-Y)$ is increasing in inverse proportion in compliance with formula $1-Y = \frac{K}{X}$ or

$$Y = \frac{X-K}{X}\,. \tag{1}$$

It is known that the function

$$y = \frac{ax+b}{cx+d} \tag{2}$$

is called a linear-fractional function [2]. If $c = 0$ and $d \neq 0$, then we get linear dependence $y = \frac{a}{d}x + \frac{b}{d}$. If $c \neq 0$, then

$$y = \frac{a}{c} + \frac{\frac{bc-ad}{c^2}}{x+\frac{d}{c}}\,. \tag{3}$$

Supposing that $X = x + \frac{d}{c}$, $\frac{bc-ad}{c^2} = k \neq 0$, $Y = y - \frac{a}{c}$, we get $Y = \frac{K}{X}$, i.e. rectangular hyperbole formula which center is shifted from coordinates origin to point $C\left(-\frac{d}{c}; \frac{a}{c}\right)$.

As we can see, formula (1) is a special case of the function (2), cause coefficient $d = 0$. Then, determinant $D(ad-bc)$ degenerates into $-bc$. There exists a rule: when $D < 0$, $(K > 0)$, real axis together with X axis (abscissa axis) makes an angle $+45°$; and if $D > 0$, then the angle is $-45°$. In our case $D = a \times 0 - (-K) \times 1 = K$. Therefore, real axis, on which tops of all new hyperboles will be located, shall be in perpendicular position to the axis $y = \frac{k}{x}$. At that, the center is shifted from the coordinates origin $C(0;0)$ to the point $C(0;1)$. That means, in our case, semi-axes

$$a = b = \sqrt{\frac{2|D|}{c^2}} = \sqrt{2K}\,. \tag{4}$$

Then the coordinates of the top of the other hyperbole Beryllium will be: $X_0 = Y_0 = \sqrt{K} = \sqrt{9.0122} = 3.00203$ and $X' = 60.9097$, $Y' = 1 - Y = 1 - 0.14796 = 0.85204$.

In order to avoid possible mistakes let us use the following terminology: hyperbole of $y = \frac{k}{x}$ kind is called straight, and linear-fractional — an adjoining one.

Figure 1 demonstrates these curves which represent five elements from different groups: chlorine (No. 17), zirconium (No. 40), wolfram (No. 74), mendelevium (No. 101), and the last one (No. 155). Peculiarity of the diagrams is symmetry axis at content of elements equal to 0.5. It is clear that both hyperboles of the last element and ordinate axis limit the existence area of all chemical compounds related to one gram-atom.

Previously [1], we proved that all the elements of Periodic System can be described by means of rectangular hyperbole formulas. That is why, it is quite enough to present several diagrams in order to illustrate this or that dependence. The same is valid for linear-fractional functions which curves are directed bottom-up. If we put the picture up by symmetry axis, we shall see that they fully coincide with straight hyperboles. At the cross point of straight and adjoining hyperboles on this line, abscissa is equal to doubled atomic mass of the element. Coordinates of another cross points for each pair of hyperboles have the following parameters: X is equal to the sum of atomic mass of two elements $(K_1 + K_2)$, and Y has two values $\frac{K_1}{K_1+K_2}$ and $\frac{K_2}{K_1+K_2}$. Mentioned above is valid up to the upper bound of Periodic System inclusive.

As we can see on Figure 2, (A00) and (B01) are real axes of straight and adjoining hyperboles accordingly; and, AC and BD, (00E) and (01E) are tangents to them. Real axes are perpendicular to each other and to tangents. And all of them are equal to each other. Diagonals (00D) and (01C) divide straights AE and BE in halves.

There are formulas of mentioned lines. Cross points of these lines are also calculated. Abscissa of cross sections are values divisible by atomic mass of the last element: 0; 205.83; 274.44; 329.328; 411.66; 548.88; 617.49; 823.32 (0; 0.5; 0.667; 0.8; 1.0; 1.333; 1.5; 2.0).

For reference, Figure 3 demonstrates graphical construction for tungsten.

We can see, that knowing real axes (normal to the top of hyperboles), it is very easy to build up tangents to any element, if required, in order to check accuracy of chosen tops. For that, it is necessary to calculate formula of the straight which passes through the point $\mathrm{M}_1(x_1; y_1)$ and parallel $y = ax + b$:

$$y - y_1 = a(x - x_1)\,. \tag{5}$$

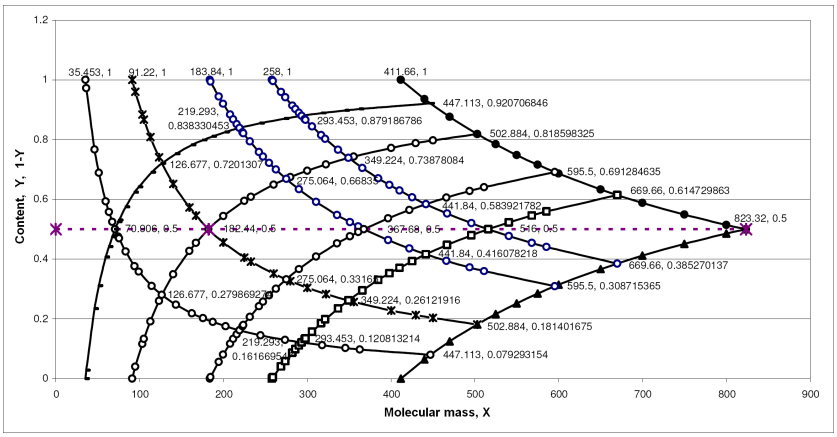

Fig. 1: Dependence of Y and $1-Y$ content from molecular mass in straight and adjoining hyperboles accordingly.

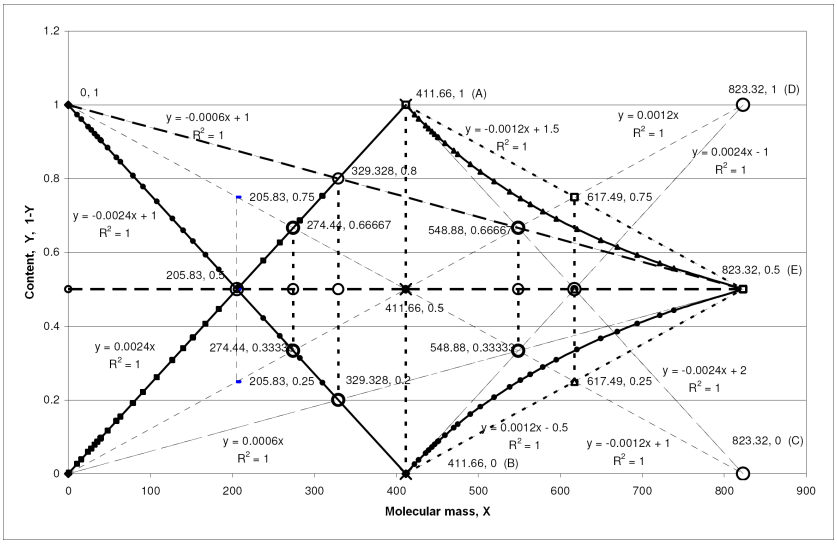

Fig. 2: Main lines of straight and adjoining hyperboles of the last element: real axes, tangents, diagonals etc.

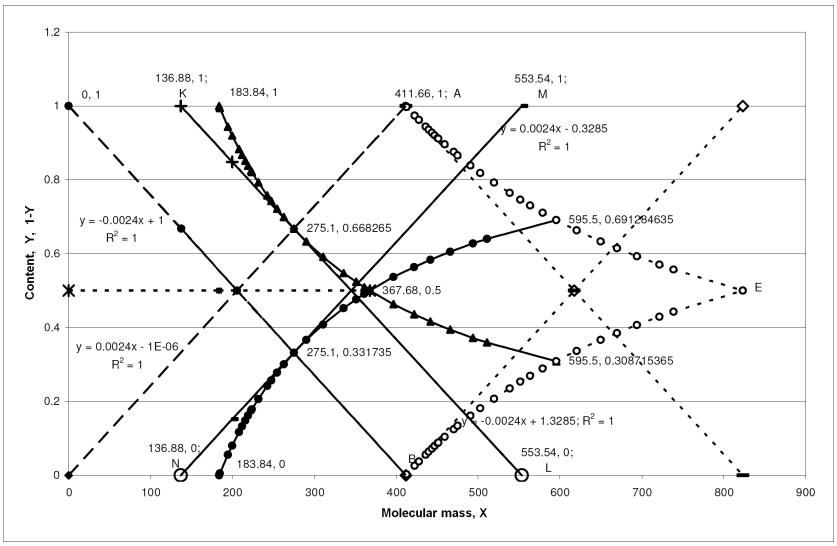

Fig. 3: Hyperboles of the last element and tungsten, their cross points and tangents.

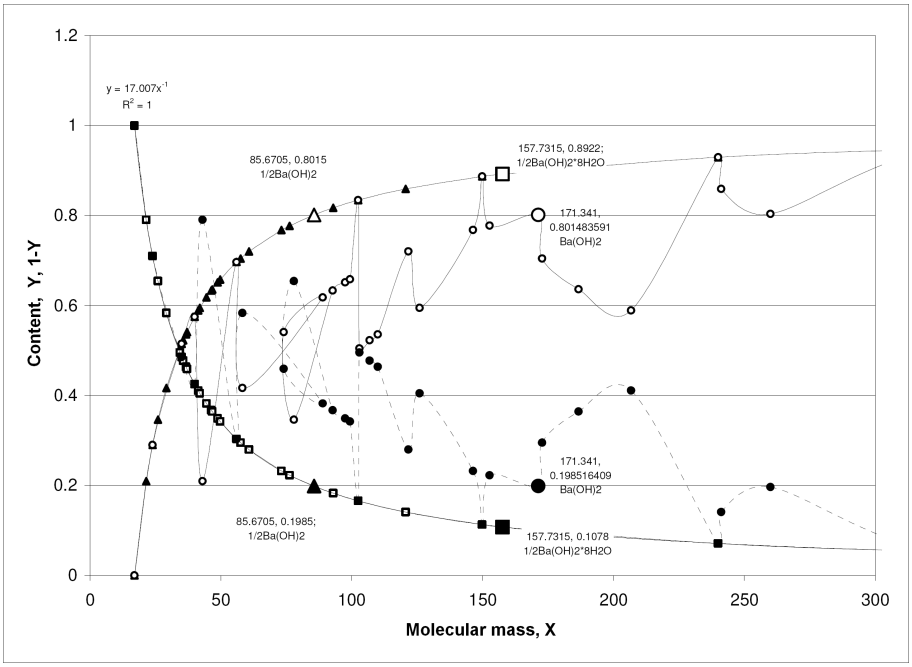

Fig. 4: Dependence of content of Y (OH) and $1-Y$ in hydroxides from their molecular mass counting on 1 gram-mole OH (of hyperbole). Broken curves are overall (summarized) content of OH in a substance.

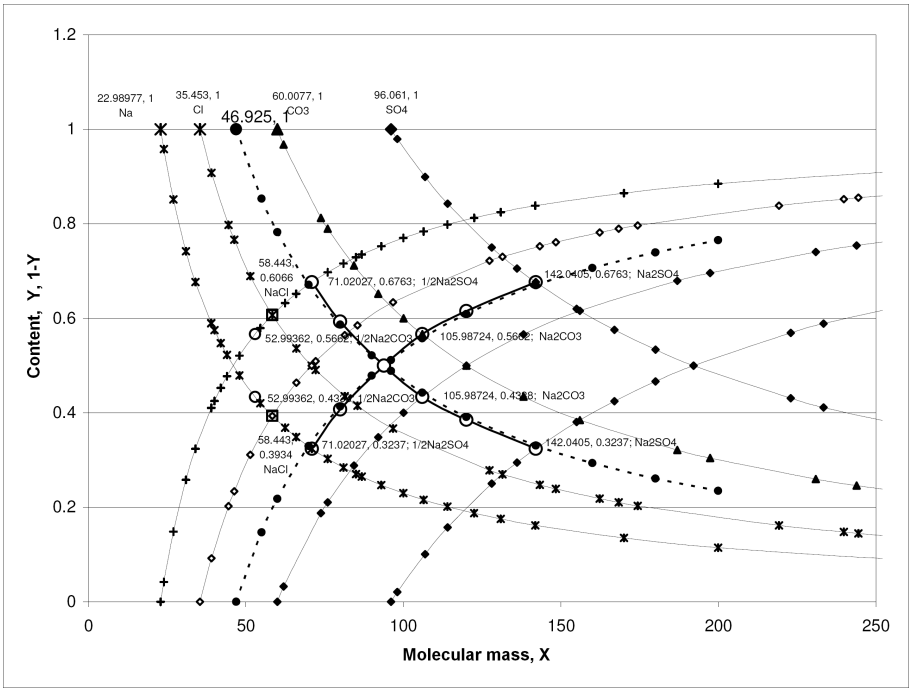

Fig. 5: Application of mathematic methods at calculating of the diagram containing hyperboles of sodium, chlorine and groups CO_3, SO_4. Building up of a new hyperbole based on these data.

2 Application of law of hyperboles for chemical compounds

As it has already been mentioned above, the law is based on the following: the content of the element we are determining in the substance should be referred to its gram-atom. It was shown in detail by the example of oxygen. In compliance with the formula $y = \frac{k}{x}$ element is a numerator, and any compound is a denominator. For example, in order to determine content of sodium (Na) in compounds with molecular mass NaOH (39.9967), Na_2CO_3 (105.9872), Na_3PO_4 (163.941), NaCl (58.443), Na_2SO_4 (142.0406) it is necessary, before the formula, to put coefficients, reducing amount of sodium in it to a unit: 1, $\frac{1}{2}$, $\frac{1}{3}$, 1, $\frac{1}{2}$, accordingly. Then, numerically, part of element (Y) will be: 0.5748, 0.4338, 0.4207, 0.3934, and 0.3237. I.e. it is in one range with decreasing, and value $(1-Y)$ with increasing. Both these curves (in pairs) which are built based on these data are referred to one element.

Method of rectangular hyperboles is worked out in order to determine the last element of the Periodic System of D. I. Mendeleev. But its capabilities are much bigger.

Let us build straight and adjoining hyperboles for sodium, chlorine and also for groups CO_3 and SO_4, which form, accordingly, carbonates and sulphates. As we can see in formula $y = \frac{k}{x}$ they replace elements in a numerator. In our last work, we said that hyperboles can by formed by any numbers within location of their tops on a real axis. However, there is a rule for groups, similar to that of 1 gram-atom of the element: their quantity in calculated compounds should not exceed a unit. Otherwise we get a situation shown on Figure 4.

As we can see, it is necessary to put coefficient $\frac{1}{2}$ before the formula of hydroxide at bivalent barium. Then, his compounds will be on hyperboles. In case of non-observance of this rule, their points will be on broken line (circle).

Now we can start to solve a problem of building up new hyperboles, based on existing ones (Figure 5).

Let's mark on them several general points related to the known compounds. On sodium curves there are two points (on each curve) $\frac{1}{2}Na_2CO_3$ and $\frac{1}{2}Na_2SO_4$, which are also located on respective hyperboles but without the coefficient $\frac{1}{2}$ (Na_2CO_3 and Na_2SO_4). Thus, the point $\frac{1}{2}Na_2SO_4$, located on the straight hyperbole of sodium, and its cross points with hyperboles CO_3 and SO_4 form imaginary broken line located between chlorine and CO_3.

In a similar manner it works with adjoining hyperboles. Let's build a formula (by three points) $Y = 63.257\,X^{-1.0658}$ of a power function (or $\ln y = 4.1472 - 1.0658 \ln x$). With the help of mentioned formula we will find some more coordinates, including (obligatory) their crossing center (93.85; 0.5). Then we divide the abscissa of this point by 2 (straight and adjoining hyperboles cross at doubled value of atomic mass) we get X, equal to 46.925, and that is a numerator in a formula of new hyperboles ($y = \frac{46.925}{x}$).

3 Conclusion

Method of rectangular hyperboles makes it possible to do the following:

- to create mathematical basis for using hyperboles of the kind $y = 1 - \frac{k}{x}$ in chemistry;
- to determine existence area of the chemical compounds;
- to calculate formulas of the main lines and cross points of all the hyperboles, including the last element;
- to show the possibility of building up hyperboles whose numerator is a group of elements, including the rule of 1 gram-atom (in this case it is 1 gram-mole);
- to calculate and to build unknown in advance hyperboles by several data of known chemical compounds located on respective curves;
- to control (with high accuracy) the content of synthesized substances;
- to design chemical compounds.

Due to the fact that it is inconvenient to call each time the element 155 (that we calculated in this paper) "the last element" and by the right of the discoverer we decided to call it **KHAZANIUM (Kh)**.

Submitted on February 13, 2007
Accepted on February 19, 2007

References

1. Khazan A. Upper limit in the Periodic System of Elements. *Progress in Physics*, 2007, v. 1, 38–41.
2. Vigotskiy M. Handbook on higher mathematics. Moscow, Nauka, 2004, page 991.

Fast LIBS Identification of Aluminum Alloys

Walid Tawfik Y. Mohamed

National Inst. of Laser Enhanced Science NILES, Dept. of Environmental Applications, Cairo University, Cairo, Egypt
Faculty of Education for Girls, Department of Physics, Gurayyat, North of Al-gouf, Kingdom of Saudi Arabia

E-mail: Walid_Tawfik@hotmail.com

Laser-induced breakdown spectroscopy (LIBS) has been applied to analysis aluminum alloy targets. The plasma is generated by focusing a 300 mJ pulsed Nd: YAG laser on the target in air at atmospheric pressure. Such plasma emission spectrum was collected using a one-meter length wide band fused-silica optical fiber connected to a portable Echelle spectrometer with intensified CCD camera. Spectroscopic analysis of plasma evolution of laser produced plasmas has been characterized in terms of their spectra, electron density and electron temperature assuming the LTE and optically thin plasma conditions. The LIBS spectrum was optimized for high S/N ratio especially for trace elements. The electron temperature and density were determined using the emission intensity and stark broadening, respectively, of selected aluminum spectral lines. The values of these parameters were found to change with the aluminum alloy matrix, i.e. they could be used as a fingerprint character to distinguish between different aluminum alloy matrices using only one major element (aluminum) without needing to analysis the rest of elements in the matrix. Moreover, It was found that the values of T_e and N_e decrease with increasing the trace elements concentrations in the aluminum alloy samples. The obtained results indicate that it is possible to improve the exploitation of LIBS in the remote on-line industrial monitoring application, by following up only the values of T_e and N_e for aluminum in aluminum alloys as a marker for the correct alloying using an optical fiber probe.

1 Introduction

The interaction of high-power pulsed laser light with a target or solid samples has been an active topic not only in plasma physics but also in the field of analytical chemistry. During the paste decade, the use of Laser Induced Plasma Spectroscopy (LIBS) as an alternative elemental analysis technology based on the optical emission spectra of the plasma produced by the interaction of high-power laser with a target has been studied by several authors [1–7]. Because of the lack of pretreatment of the material as well as the speed of analysis, not mentioning the possibility of in situ analysis, this technique offers an attractive solution for a wide range of industrial applications. However, the existent commercial instruments are still not sufficient to guarantee reproducibility and precise quantitative results. In fact, the analytical performance of the LIBS technique depends strongly on the choice of experimental conditions that influence the laser-produced plasma characteristics [8]. The main parameters affecting the performance of LIBS results are as follows: laser intensity, excitation wavelength, laser pulse duration, and the surrounding atmosphere [9]. Moreover, the physical and chemical properties of the sample can affect the produced plasma composition, a phenomenon known as the matrix effect. The interaction between the laser and the target in LIBS is influenced significantly by the overall composition of the target, so that the intensity of the emission lines observed is a function of both the concentration of the elements of interest and the properties of the matrix that contains them. The author published works studied the matrix effect under different experimental conditions to specify causes and find out the methods of correction [4, 6, 7].

On the other hand, from a more fundamental point of view, LIBS diagnostic studies of electron temperature T_e and number density N_e have all been based on assumptions, most importantly those of the existence of local thermodynamic equilibrium LTE conditions and of optically thin plasma [10]. Ciucci et al. [11] have discussed the possibility of devising a calibration free method, i.e. some kind of an "absolute analysis" approach. The success of such approach heavily relies upon the accurate knowledge of the parameters and the validity of the assumptions cited above. Apparently LIBS plasmas fulfill LTE conditions even though during the measurement time, the plasma parameters rapidly change due to expansion. In this connection, one needs to determine the conditions for expanding high density plasmas to be in an equilibrium state as well as of the time duration for the existence of such equilibrium. The aim of the present paper is to study the variation of the plasma parameters with aluminum lines in different aluminum alloy matrices. This will help not only clarifying the constraints to be taken into account when measuring T_e and N_e but also using the matrix effect to distinguish different aluminum alloy matrices.

Sample	Be	Mg	Si	Fe	Cu	Ca	Mn	Al
AL 6063	0.00030	0.54	0.43	0.2	0.085	0.0021	0.081	Balance
AL 4104	0.0017	1.56	9.63	0.7	0.12	0.0021	0.046	Balance
AL 5754	0.0022	2.54	0.22	0.35	0.1	0.0011	0.29	Balance
AL 3104	0.0011	1.15	0.21	0.42	0.17	0.0031	0.92	Balance

Table 1: Beryllium, Copper, iron, magnesium, silicon, calcium and manganese concentrations (in w/w %) in the standard aluminum alloy samples.

2 Experimental setup

A typical LIBS experimental setup, described in details by the author elsewhere [4, 6], is used throughout the present investigations. The plasma formation was attained with the aid of a Q-switched Nd: YAG laser (NY81.30, continuum, USA) operating at 1064 nm (pulse duration of 7 ns) and repetition rate of 0.1 Hz–30 Hz. The laser pulse energy of 100–300 mJ was adjusted by a suitable combination of beam splitters at constant operating high voltage (1.3 kV) and Q-switch delay (1.65 μs) to ensure spatial and temporal beam profile stability. An energy meter (Nova 978, Ophir Optronics Ldt., USA) was employed to monitor the shot to shot pulse energy. The laser beam was focused on aluminum alloy samples by a 10 cm focal length quartz lens to generate the plasma. The emitted light from the plasma plume is collected via a one-meter length wide band fused-silica optical fiber connected to a 0.17 m focal length Echelle spectrometer (Mechelle 7500, Multichannel Instruments, Sweden). The Mechelle 7500 provides a constant spectral resolution of 7500 corresponding to 4 pixels FWHM, over a wavelength range 200–1000 nm displayable in a single spectrum. A gateable, intensified CCD camera, (DiCAM-Pro, PCO Computer Optics, Germany) coupled to the spectrometer was used for detection of the dispersed light. The overall linear dispersion of the spectrometer-camera system ranges from 0.006 nm/pixel (at 200 nm) to 0.033 nm/pixel (at 1000 nm). To avoid the electronic interference and jitters, the CCD intensifier high voltage was triggered optically. The ICCD camera control was performed via Mechelle software (Multichannel Instruments, Stockholm, Sweden). The emission spectra display, processing and analysis were done using 2D- and 3D-GRAMS/32 version 5.1 spectroscopic data analysis software (Galactic Industries, Salem, NH, USA). To improve data reproducibility, and to avoid electronic jittering problem, the laser was set to single shot mode. Then, the Nd:YAG laser beam was focused onto the sample surface at 90° angle. This was done using a 25 mm diameter dichroic mirror that reflects 99% of high energy 1064 nm wavelength. The focal point was set 5 mm below the surface of the sample in order to generate plasma of 800 μm spot diameter. This also minimize breakdown above the surface of any particles and aerosols generally present above the sample. Moreover, for each new sample, before spectral collection, 20 laser pulses were performed to clean the sample surface and removes surface oxides and contamination to ensure that the observed spectrum is representative of the sample composition.

On the other hand, the use of a micro xyz-translation stage as a holder for fused-silica optical fiber facilities maximum intensity of the observed emission light from the plasma plume. Now, we aim to produce LIBS spectra with high precision. Precision is the measure of the degree of reproducibility of a measurement. Laser shot-to-shot variation causes differences in the plasma properties, therefore affects the magnitude of the element signal, and hence degrades the LIBS precision. To improve LIBS precision, spectra from several laser shots have to be averaged in order to reduce statistical error due to laser shot-to-shot fluctuation. We reproduced the measurements at five locations on the sample surface in order to avoid problems linked to sample heterogeneity. Twenty shots were fired at each location and saved in separated files and the average was computed and saved to serve as the library spectrum. For each recorded spectrum, the peak intensity, the Lorentzian curve fitting, the full width at half maximum FWHM, and the center wavelength of each line, as well as the background emission continuum are determined. Data treatment preprocessing of the averaged spectra data was performed in the Windows environment on a Pentium 4 PC using GRAMS/32, Excel (Microsoft Office Excel 2003) and Origin software version 7.0220 (Origin Lab Corp., USA). The averages of peak tables (lists of wavelengths and intensities) of the averaged spectra were roll generated in GRAMS/32 and exported for data evaluation.

We investigated a set of five standard samples of aluminum alloy to study the dependence of the electron density and temperature on the matrix effect. So that, these samples were selected to have trace elements with a range of concentrations. We used disk shaped standard samples of aluminum alloy provided by Alcan international limited (0.5 cm; $\phi = 5$ cm). The concentrations of the trace elements "Mg, Si, Be, Cu, Mn, Fe, Ca" in the aluminum alloy samples are given in Table 1.

3 Results and discussion

3.1 Optimizing LIBS spectrum

Optimizing LIBS for a high resolution aluminum alloy was done by optimizing the experimental conditions including the time delay, the gate delay (the integration time) and the laser irradiance. In fact, the timing of the recorded signal

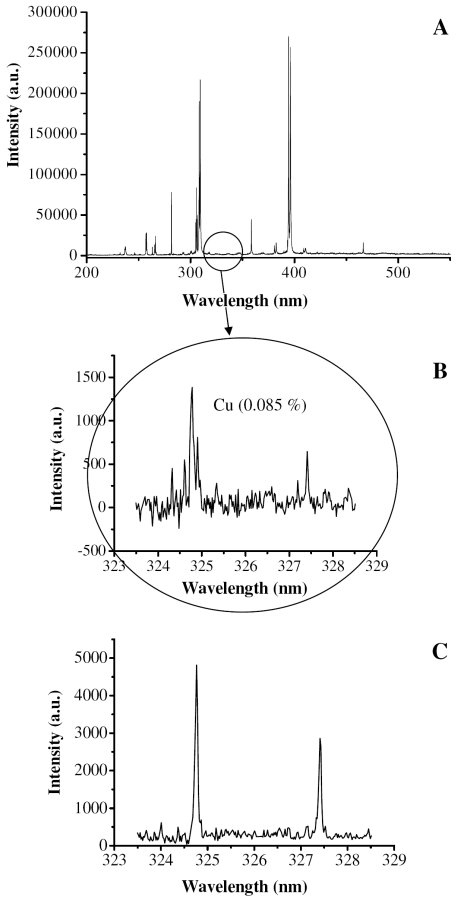

Fig. 1: The figure contains three spectra as follows: A — the panoramic LIBS spectrum in the spectral range 200–700 nm shows the UV-visible emission lines of aluminum as a major element and the emission lines of the trace elements in the aluminum alloy sample AL 6063. B — a zoomed segment showing the copper lines 324.7 nm and 327.4 nm in the UV region recorded at 1.5 μs delay time and 1 μs gate width using laser irradiance of 10^8 W/cm^2 for sample AL 6063 containing copper concentration of 0.085% (w/w) where S/N = 8. C — the same copper lines using the optimized conditions of 2.5 μs delay time and 1.5 μs gate width at 10^{10} W/cm^2 laser irradiance where S/N = 25.

depend on the laser energy and wavelength, so we firstly increased the laser energy from 70 mJ, as used before by the author [6], to 300 mJ. In this case, the laser irradiance increased from $\approx 10^8$ W/cm^2 to $\approx 10^{10}$ W/cm^2 which found to be suitable for the case of aluminum alloy samples having trace elements with concentrations in the ppm range. Then under the late laser irradiance, the delay time, at which the spectrum is recorded from the laser start, was optimized by scanning the delay time with the signal intensity as done previously by the author [6]. It was found that the optimized conditions are 2.5 μs delay time and 1.5 μs gate width at 10^{10} W/cm^2 laser irradiance at the sample surface. The gate delay was limited to 1.5 μs to avoid saturation of the detector. Optimizing LIBS spectrum was done in order to reduce the background signal and increase the signal to noise ratio (S/N). Figure 1 shows a typical plasma emission spectrum for aluminum alloy sample AL 6063. The figure contains three spectra as follows: A — the panoramic LIBS spectrum in the spectral range 200–700 nm shows the UV-visible emission lines of aluminum as a major element and the emission lines of the trace elements in the aluminum alloy sample. B — a zoomed segment showing the copper lines 324.7 nm and 327.4 nm in the UV region recorded at 1.5 μs delay time and 1 μs gate width using laser irradiance of 10^8 W/cm^2 for sample AL 6063 containing copper concentration of 0.085% (w/w) where S/N = 8. C — the same copper lines using the optimized conditions of 2.5 μs delay time and 1.5 μs gate width at 10^{10} W/cm^2 laser irradiance where S/N = 25. This, of course, makes LIBS to be a very high-resolution spectroscopic system for the trace elements with concentrations in the ppm range.

3.2 Plasma parameters and matrix effect

The main factors that influence the light emitted by the plasma are its temperature, the number density of the emitting species, and the electronic density. The number density of the emitting species (e.g. atoms, ions, etc) depends on the total mass ablated by the laser, the plasma temperature, and the degree of the excitation and/or ionization of the plasma. The vaporized amount, in turn, depends on the absorption of the incident laser radiation by the surface, the plasma shielding [12], which is related to the electron density of the plasma, and the laser fluence. Therefore, the knowledge of the plasma temperature and the density of plasma species are vital for the understanding of the dissociation–atomization, excitation, and ionization processes occurring in the plasma. For this reason, study the variation of these plasma parameters with aluminum lines in different aluminum alloy matrices. This will help not only clarifying the constraints to be taken into account when measuring T_e and N_e but also using the matrix effect to distinguish different aluminum alloy matrices.

For plasma in local thermodynamic equilibrium (LTE), the population density of atomic and ionic electronic states is described by a Boltzmann distribution. For optically thin plasma, the re-absorption effects of plasma emission are negligible. So, the emitted spectral line intensity I is a measure of the population of the corresponding energy level of this element in the plasma. For the LTE plasma, the population of an excited level can be related to the total density $N(T)$ of neutral atom or ion of this element by Boltzmann equation [13] as:

$$I = \frac{hc}{4\pi\lambda} N(T) \frac{A_{ki}\, g_k}{U(T)} \exp\left(-\frac{E_k}{KT}\right), \qquad (1)$$

where λ is the wavelength, A_{ki} is the transition probability, g_k is the statistical weight for the upper level, E_k is the

Wavelength (nm)	A_{ki} (s^{-1})	E_k (cm^{-1})	g_k	Stark broadening parameter W (nm)
281.62	3.83E+08	95351	1	4.2900E-04
308.85	1.50E+07	139289.2	5	—
364.92	1.50E+07	132823	3	—
364.92	1.50E+07	132823	3	—
365.11	2.10E+07	132822.8	5	—
365.11	2.10E+07	132822.8	5	—
365.50	2.70E+07	132822.9	7	—
365.50	2.70E+07	132822.9	7	—
370.32	3.80E+07	133916.4	5	—
373.20	4.30E+06	132215.5	3	—
373.39	1.30E+07	132215.5	3	—
373.80	2.10E+07	132215.5	3	—
386.62	3.70E+07	132778.6	1	—
390.07	4.80E+05	85481.35	5	—
559.33	1.10E+08	124794.1	5	—
624.34	1.10E+08	121483.5	7	—

Table 2: A list of the spectroscopic data of the aluminum spectral lines used for the determination of plasma temperature and density of aluminum alloy samples.

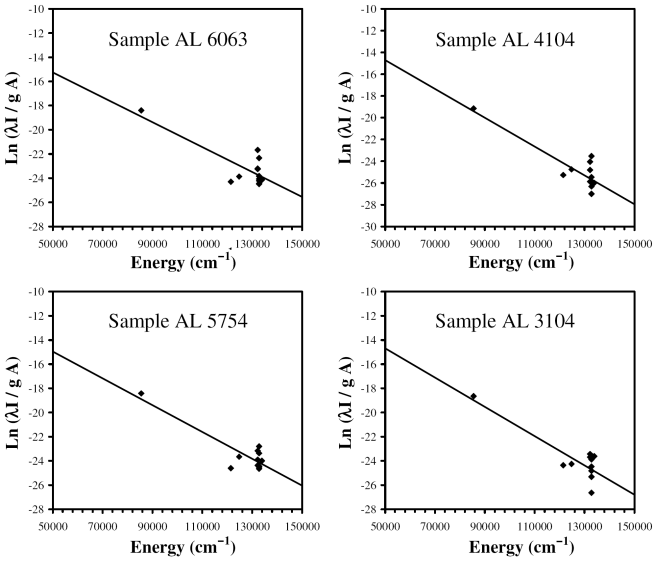

Fig. 2: Four Boltzmann plots were determined form the emission line intensities of aluminum observed in the laser-induced plasma of aluminum alloys. The slope of the plotted curves yields temperatures 13960 K, 12974 K, 11871 K, and 10841 K for the samples AL 6063, AL 5754, AL 3104 and AL 4104 respectively.

excited level energy, T is the temperature (in LTE all temperatures are assumed to be equal, i.e. $T_e \approx T_{ion} \approx T_{plasma}$), K is the Boltzmann constants, $U(T)$ is the partition function.

The emitted spectral line intensity from a given state of excitation can be used to evaluate the plasma temperature. The lines must be well resolved for accurately evaluating their wavelengths λ, intensities I, and their transition probabilities A_{ki} must be know.

Reformulating Eqn. (1) gives;

$$\ln \frac{I\lambda}{A_{ki}\, g_k} = -\frac{1}{KT} E_k + \ln \frac{C\, F}{U(T)}\,, \qquad (2)$$

where F is an experimental factor and C is the species concentration.

By plotting the left hand side of Eqn. (2) vs. the excited level energy E_k, the plasma temperature can be obtained from the slope of obtained straight line.

During the early stages of plasma formation, the emitted spectrum is dominated by an intense continuum (Bremsstrahlung radiation), on which several heavily broadened ionic lines of the elements present are superimposed. The broadening of the ionic lines is due to the high electron densities occurring at this initial period (Stark broadening). At the same time, the excited neutral atoms' spectral lines are relatively weak; they are superimposed on the continuum and often overlap with the ionic lines. Hence, they cannot be easily isolated and measured. As a consequence, the measurement of their intensity for the construction of Boltzmann plots becomes problematic at early times (e.g. the first few hundred nanoseconds) and the use of time delay is compulsory. However, each spectral line exhibits different temporal evolution that is element and atomic energy level specific. Under our experimental conditions, a delay time of 2.5 μs delay time and 1.5 μs gate width at 10^{10} W/cm^2 laser irradiance have been determined as optimum conditions (as described in Section 3.1 before). Under these experimental conditions, the plasma temperatures were determined form the emission line intensities of sixteen selected aluminum lines (see Table 2) observed in the laser-induced plasma of different aluminum alloy targets. Figure 2 show four Boltzmann plots of Eqn. (2), for these lines where the data were fitted with the least-square approximation. The spectral lines wavelengths, energies of the upper levels, statistical weights, and transition probabilities used for these lines were obtained from NIST [14] and Griem [13], and listed in Table 3. The slope of the plotted curves yields temperatures 13960 K, 12974 K, 11871 K, and 10841 K for the samples AL 6063, AL 5754, AL 3104 and AL 4104 respectively as listed in Table 3).

On the other hand, the electron number density can be obtained from the Stark-broadening of the emission lines [15]. This is because, Stark-broadening results from Coulomb interactions between the radiator and the charged particles present in the plasma. Both ions and electrons induce Stark broadening, but electrons are responsible for the major part because of their higher relative velocities. The electrons in the plasma can perturb the energy levels of the individual ions which broaden the emission lines originating from these excited levels. Stark broadening of well-isolated lines in the

Plasma parameters	Sample AL6063	Sample AL 5754	Sample AL 3104	Sample AL 4104
Electron Temperature (Kelvin)	13960	12974	11871	10841
Electron Density (cm^{-3})	7.28×10^{18}	4.28×10^{18}	4.44×10^{18}	2.28×10^{18}

Table 3: The plasma electron temperature T_e and density N_e determined from aluminum spectral lines in the four standard aluminum alloy samples.

plasma is, thus, useful for estimating the electron number densities provided that the Stark-broadening coefficients have been measured or calculated. The line profile for stark broadened is well described by a Lorentzian function. Since the instrumental line-broadening exhibit Gaussian shape, then the stark line width $\Delta\lambda_{FWHM}$ can be extracted from the measured line width $\Delta\lambda_{observed}$ by subtracting the instrumental line broadening $\Delta\lambda_{instrument}$:

$$\Delta\lambda_{FWHM} = \Delta\lambda_{observed} - \Delta\lambda_{instrument}\,. \qquad (3)$$

In our case $\Delta\lambda_{instrument}$ was 0.05 nm (determined by measuring the FWHM of the Hg lines emitted by a standard low pressure Hg lamp).

The width of stark broadening spectral line depends on the electron density N_e. Both the linear and the quadratic stark effect are encountered in spectroscopy. Only the hydrogen atom and H-like ion exhibit the linear stark effect. For the linear stark effect the electron density should be deduced from H line width from the formula [13]

$$N_e = C(N_e, T)\,\Delta\lambda_{FWHM}^{3/2} \qquad (4)$$

the values of the parameter $C(N_e, T)$ are tabulated in the literature [13], which determine the relative contribution of the electron collision on the electrostatic fields, and depend weakly on N_e and T.

For a non-H-like line, the electron density (in cm^{-3}) could be determined from the FWHM of the line from the formula [13]:

$$N_e \approx \left(\frac{\Delta\lambda_{FWHM}}{2W}\right)\times 10^{16}, \qquad (5)$$

W is the electron impact parameter (stark broadening value) and it is given in Table 2). The last formula is generally used for calculations of plasma generated from solid targets [7, 12].

The aluminum line 281.62 nm was identified as candidate for electron-density measurements. Figure 3 shows, the 281.62 nm line with sufficient resolution to measure the full width at half-maximum ($\lambda_{1/2}$) at four different aluminum alloy samples. All the data points were fitted with Lorentzian fitting function using the Origin software to determine ($\lambda_{1/2}$) as shown in Fig. 3 and found to be 0.113 nm, 0.070 nm, 0.092 nm and 0.088 nm for the samples AL6063, AL 4104, AL 5754, and AL 3104 respectively. Substituting the values of $\lambda_{1/2}$ in Eqn. (3) and the corresponding value of stark broadening W (4.29×10^{-4} nm from Griem [13] at plasma temperature of 10000 K) in Eqn. (5) the electron density values of 7.28×10^{18}, 4.28×10^{18}, 4.44×10^{18}, and 2.28×10^{18}

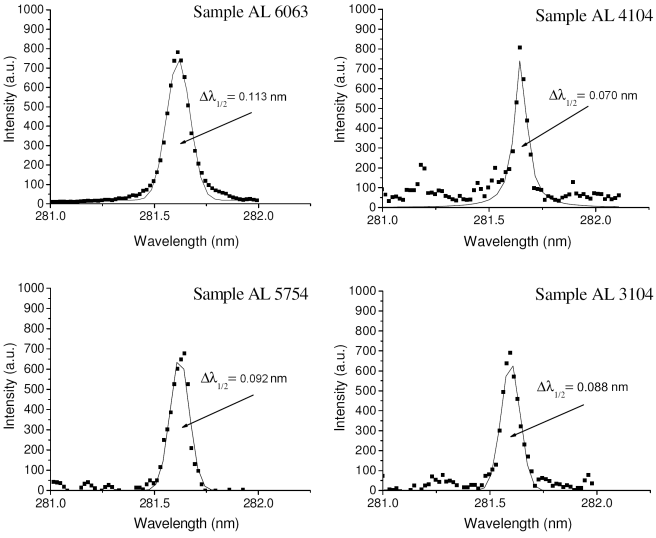

Fig. 3: The 281.62 nm line with sufficient resolution to measure the full width at half-maximum ($\lambda_{1/2}$) at four different aluminum alloy samples. All the data points were fitted with Lorentzian fitting function using the Origin software and the values of $\lambda_{1/2}$ found to be 0.113 nm, 0.070 nm, 0.092 nm and 0.088 nm for the samples AL6063 , AL 4104, AL 5754, and AL 3104 respectively.

were obtained for the samples AL 6063, AL 5754, AL 3104 and AL 4104 respectively as listed in Table 3.

The above obtained results reveal that plasma parameters (T_e, N_e) change with changing the aluminum alloy matrix i.e. matrix dependent. Moreover, by comparing the results of the four samples in Table 3 with the concentrations of the trace elements in Table 1, one could recognized that while the concentrations of trace elements increase both values of T_e and N_e decrease. This is well clear by comparing the two samples AL 6063 and AL 4104 thus while all the trace elements, except Mn, increase (silicon concentration increases from 0.43% to 9.63%), both values of T_e and N_e decrease from 13960 K, $7.28\times10^{18}cm^{-3}$ to 10841 K, $2.28\times10^{18}cm^{-3}$, respectively. This result might occur because increasing the "trace element" concentration comprises increasing portion of the laser-target interaction volume of that trace element and decreases the laser-target interaction volume of the major element (aluminum). Moreover, aluminum "the major element" species are easy to be ionized than the species of the seven trace elements which leads to higher electron density for aluminum alloy samples with low trace elements concentrations than for relatively high trace elements concentrations. Moreover, this is clear since,

the ionization potential of Al, Ca, Be, Mg, Si, Mn, Fe, and Cu are (in eV) 5.98, 6.11, 9.32, 7.64, 8.15, 7.43, 7.87 and 7.72 respectively. The last observed result agrees with previously observed results obtained by O. Samek [15] and Rusak et al. [16].

Finally, by knowing the electron density and the plasma temperature we can determine whether the local thermodynamic equilibrium (LTE) assumption is valid applying the criterion given by McWhirter [17], Bekefi [18] where the lower limit for electron density for which the plasma will be in LTE is:

$$N_e \geqslant 1.4\times10^{14}\Delta E^3\, T^{1/2}, \qquad (6)$$

ΔE is the largest energy transition for which the condition holds and T is the plasma temperature.

In the present case $\Delta E = 4.34$ eV for Mg (see Ref. [13]) and the highest temperature is 1.2 eV (13960 K), then the electron density lower limit value given by Eqn. (6) is 1.25×10^{16} cm^{-3}. The experimentally calculated densities are greater than this value, which is consistent with the assumption that the LTE prevailing in the plasma.

4 Conclusion

LIBS technique has been used to analysis different aluminum alloy samples. The LIBS spectrum was optimized for high S/N ratio especially for trace elements. The characteristic plasma parameters (T_e, N_e) were determined using selected aluminum spectral lines. The values of these parameters were found to change with the aluminum alloy matrix, i.e. they could be used as a fingerprint character to distinguish between different aluminum alloy matrices using only one major element (aluminum) without needing to analysis the rest of elements in the matrix. Moreover, It was found that the values of T_e and N_e decrease with increasing the trace elements concentrations in the aluminum alloy samples.

For industrial application, LIBS could be applied in the on-line industrial process that following up elemental concentration in aluminum alloys by only measuring T_e and N_e for the aluminum using an optical fiber probe. This could be done by building a database containing the determined values of T_e and N_e for a range of standard aluminum alloy matrices. Then the unknown aluminum alloy sample could be identified just by comparing its measured T_e and N_e values with the previously stored values in our database.

Acknowledgment

The author gratefully acknowledges the support of Prof. Mohamed Abel-Harith and Prof. M. Sabsabi specially for offering the aluminum alloy samples.

Submitted on February 07, 2007
Accepted on March 06, 2007
Revised version received on March 15, 2007

References

1. Radziemski L. J. Review of selected analytical applications of laser plasmas and laser ablation, 1987–1994. *Microchem. J.*, 1994, v. 50, 218–234.
2. Rusak D. A., Castle B. C., Smith B. W., and Winefordner J. D. Fundamentals and applications of laser-induced breakdown spectroscopy. *Crit. Rev. Anal. Chem.*, 1997, v. 27, 257–290.
3. Radziemski L. From LASER to LIBS, the path of technology development. *Spectrochim. Acta B*, 2002, v. 57, 1109–1113.
4. Sabsabi M., Detalle V., Harith M. A., Walid Tawfik and Imam H. Comparative study of two new commercial Echelle spectrometers equipped with intensified CCD for analysis of laser-induced breakdown spectroscopy. *Applied Optics*, 2003, v. 42, No. 30, 6094–6098.
5. Soliman M., Walid Tawfik and Harith M. A. Quantitative elemental analysis of agricultural drainage water using laser induced breakdown spectroscopy. *First Cairo Conference on Plasma Physics & Applications*, 2003, Cairo, Egypt, Forschungszentrum Juelich GmbH, Bilateral Seminars of the International Bureau, v. 34, 240–243.
6. Ismail M. A., Imam H., Elhassan A., Walid Tawfik and Harith M. A. LIBS limit of detection and plasma parameters of some elements in two different metallic matrices. *J. Anal. At. Spectrom.*, 2004, v. 19, 1–7.
7. Walid Tawfik and Abeer Askar. Study of the matrix effect on the plasma characterization of heavy elements in soil sediments using LIBS with a portable Echelle spectrometer. *Progress in Physics*, 2007, v. 1, 47–53.
8. Castle B., Talabardon K., Smith B. W. and Winefordner J. D. *Appl. Spectrosc.*, 1998, v. 52, 649–657.
9. Tognoni E., Palleschi V., Corsi M. and Cristoforetti G. *Spectrochim. Acta Part B*, 2002, v. 57, 1115–1130.
10. Yalcin S., Crosley D. R., Smith G. P. and Faris G. W. *Appl. Phys. B*, 1999, v. 68, 121–130.
11. Ciucci A., Corsi M., Palleschi V., Rastelli S., Salvetti A. and Tognoni E. *Applied Spectroscopy*, 1999, v. 53, 960-964.
12. Le Drogoff B., Margotb J., Chakera M., Sabsabi M., Barthelemy O., Johnstona T. W., Lavillea S., Vidala F. and von Kaenela Y. *Spectrochimica Acta Part B*, 2001, v. 56, 987–1002.
13. Griem H. R. Plasma Spectroscopy. McGraw-Hill, N.Y., 1964.
14. NIST National Institute of Standards and Technology, USA, electronic database, http://physics.nist.gov/PhysRefData/ASD/lines_form.html
15. Samek O., Beddows D. C. S., Telle H. H., Kaiser J., Liska M., Caceres J. O. and Gonzales Urena A. *Spectrochimica Acta Part B*, 2001, v. 56, 865–875.
16. Rusak D. A., Clara M., Austin E. E., Visser K., Niessner R., Smith B. W. and Winefordner J. D. *Applied Spectroscopy*, 1997, v. 51, No. 11, 1628–1631.
17. McWhirter R. W. P. In: *Plasma Diagnostic Techniques*, Academic Press, New York, 1965, Ch. 5, 206.
18. Bekefi G. Principles of laser plasmas. Wiley, New York, 1976, 550–605.

Notes on Pioneer Anomaly Explanation by Sattellite-Shift Formula of Quaternion Relativity: Remarks on "Less Mundane Explanation of Pioneer Anomaly from Q-Relativity"

Alexander Yefremov

Institute of Gravitation and Cosmology, Peoples' Friendship University of Russia, Miklukho-Maklaya Str. 6, Moscow 117198, Russia

E-mail: a.yefremov@rudn.ru

Use of satellite shift formula emerging in Quaternion (Q-) model of relativity theory for explanation of Pioneer anomaly [1] is critically discussed. A cinematic scheme more suitable for the case is constructed with the help of Q-model methods. An appropriate formula for apparent deceleration resulting from existence of observer-object relative velocity is derived. Preliminary quantitative assessments made on the base of Pioneer 10/11 data demonstrate closure of the assumed "relativistic deceleration" and observed "Doppler deceleration" values.

1 Introduction. Limits of satellite-shift formula

Recently [1] there was an attempt to give an explanation of Pioneer anomaly essentially using formula for relativistic shift of planet's fast satellites observed from the Earth. This formula was derived within framework of Q-method developed to calculate relativistic effects using $\mathrm{SO}(1,2)$ form-invariant quaternion square root from space-time interval rather than the interval itself [2]; in particular this advantageously permits to describe relativistic motions of any non-inertial frames. The last option was used to find mentioned formula that describes cinematic situation comprising three Solar System objects: the Earth (with observer on it), a planet, and its satellite revolving with comparatively large angular velocity. Due to existence of Earth-planet relative velocity, not great though and variable but permanent, the cycle frequency of satellite rotation (observed from the Earth) is apparently less that in realty, i.e. the "planet's clock" is slowing down, and calculation shows that the gap is growing linearly with time. Visually it looks that the satellite position on its orbit is apparently behind an expected place. For very fast satellites (like Jupiter's Metis and Adrastea) and for sufficiently long period of time the effect can probably be experimentally detected. Same effect exists of course for Mars's satellites and it is computed that monthly apparent shift on its orbit of e.g. Phobos is about 50 meters (that is by the way can be important and taken into account when planning expedition of spacecraft closely approaching the moon).

In paper of F. Smarandache and V. Christianto [1] the discussed formula was used to describe famous Pioneer effect, implying that the last great acceleration the space probe received when approached very close to Jupiter; in particular data concerning Adrastea, whose location was as close to Jupiter as the space probe, were cited in [1]. Combined with ether drift effect the formula gives good coincidence (up to 0.26%) with value of emission angle shift required to explain observation data of Pioneer's signal Doppler residuals [3].

This surprisingly exact result nevertheless should not lead to understanding that obtained by Q-method mathematical description of a specific mechanical model can bear universal character and fit to arbitrary relativistic situation. One needs to recognize that Pioneer cinematic scheme essentially differs from that of the Earth-planet-satellite model; but if one tries to explain the Pioneer effect using the same relativistic idea as for satellite shift then an adequate cinematic scheme should be elaborated. Happily the Q-method readily offers compact and clear algorithm for construction and description of any relativistic models. In Section 2 a model referring observed frequency shift of Pioneer spacecraft signals to purely relativistic reasons is regarded; some quantitative assessments are made as well as conclusions on ability of the model to explain the anomaly. In Section 3 a short discussion is offered.

2 Earth-Pioneer Q-model and signal frequency shift

Paper [3] enumerates a number of factors attracted to analyze radio data received from Pioneer 10/11 spacecraft, among them gravitational planetary perturbations, radiation pressure, interplanetary media, General Relativity*, the Earth's precession and nutation. It is worth noting here that one significant factor, time delay caused by relative probe-observer motion, is not distinguished in [3]. The fact is understandable: relative motion of spacecraft and observer on the Earth is utterly non-inertial one; Special Relativity is not at all able to cope with the case while General Relativity methods involving specific metric and geodesic lines construction

*Unfortunately paper [3] does not indicate to what depth General Relativity is taken into account: whether only Newtonian gravity is modified by Schwarzschild, Kerr (or other) metrics, or cinematic effects are regarded too.

(with all curvature tensor components zero) or additional vector transport postulates are mathematically difficult. Contrary to this the Q-relativity method easily allows building of any non-inertial relativistic scheme; an example describing a spacecraft (probe) and an Earth's observer is given below.

Assume that Pioneer anomaly is a purely relativistic effect caused by existence of Earth-Pioneer relative velocity, variable but permanent. Construct respective model using the Q-method algorithm. Choose Q-frames. Let $\Sigma = (\mathbf{q}_1, \mathbf{q}_2, \mathbf{q}_3)$ be the Earth's frame whose Cartesian directing vectors are given by quaternion "imaginary" units $\mathbf{q}_k$ obeying the multiplication rule*

$$1\,\mathbf{q}_k = \mathbf{q}_k\,1 = \mathbf{q}_k\,, \qquad \mathbf{q}_k\,\mathbf{q}_l = -\delta_{kl} + \varepsilon_{klj}\,\mathbf{q}_j\,. \quad (1)$$

Let Q-frame $\Sigma' = \{\mathbf{q}_{k'}\}$ belong to a probe. Suppose for simplicity that vectors $\mathbf{q}_2$, $\mathbf{q}_3$ are in the ecliptic plane as well as (approximately) the probe's trajectory. Assume that vector $\mathbf{q}_2$ of Σ is always parallel to Earth-probe relative velocity V. Now one is able to write rotational equation, main relation of Q-relativity, which ties two frames

$$\Sigma' = O_1^{-i\psi}\,\Sigma\,, \quad (2)$$

here $O_1^{-i\psi}$ is 3×3 orthogonal matrix of rotation about axis No. 1 at imaginary angle $-i\psi$

$$O_1^{-i\psi} = \begin{pmatrix} \cos(i\psi) & -\sin(i\psi) & 0 \\ \sin(-i\psi) & \cos(i\psi) & 0 \\ 0 & 0 & 1 \end{pmatrix} = \begin{pmatrix} \cosh\psi & -i\sinh\psi & 0 \\ i\sinh\psi & \cosh\psi & 0 \\ 0 & 0 & 1 \end{pmatrix}$$

thus "converting" frame Σ into Σ'. The first row in the matrix equation (2)

$$\mathbf{q}_{1'} = \mathbf{q}_1\cosh\psi - \mathbf{q}_2\,i\sinh\psi$$

after straightforward algebra

$$\mathbf{q}_{1'} = \cosh\psi\,(\mathbf{q}_1 - \mathbf{q}_2\,i\tanh\psi) \;\Rightarrow\; \mathbf{q}_{1'} = \frac{dt}{dt'}\,(\mathbf{q}_1 - \mathbf{q}_2\,iV\psi)$$

with usual relativistic relations

$$V = \tanh\psi, \qquad dt = dt'\cosh\psi \quad (3)$$

acquires the form of basic cinematic space-time object of Q-relativity

$$idt'\,\mathbf{q}_{1'} = idt\,\mathbf{q}_1 + dr\,\mathbf{q}_2\,,$$

a specific quaternion square root from space-time interval of Special Relativity

$$(idt'\,\mathbf{q}_{1'})(idt'\,\mathbf{q}_{1'}) = (idt\,\mathbf{q}_1 + dr\,\mathbf{q}_2)(idt\,\mathbf{q}_1 + dr\,\mathbf{q}_2) \;\Rightarrow$$
$$\Rightarrow\; dt'^2 = dt^2 - dr^2,$$

dt' being proper time segment of the probe. Eq. (3) yields ratio for probe-Earth signal period (small compared to time of observation) $T = T'\cosh\psi$, i.e. observed from Earth the period is apparently longer than it really is. Vice versa, observed frequency $f = 1/T$ is smaller than the real one f'

$$f = \frac{1}{T} = \frac{1}{T\cosh\psi} = \frac{f'}{\cosh\psi} = f'\sqrt{1-(V/c)^2}, \quad (4)$$

or for small relative velocity

$$f \cong f'\left(1 - \frac{V^2}{2c^2}\right).$$

This means that there exists certain purely apparent relativistic shift of the probe's signal detected by the Earth observer

$$\Delta f = f' - f = f'\,\frac{V^2}{2c^2}\,, \quad \text{or} \quad \frac{\Delta f}{f'} = \frac{V^2}{2c^2} = \frac{\varepsilon}{c^2}\,, \quad (5)$$

ε being the probe's kinetic energy per unit mass computed in a chosen frame. Contrary to pure Doppler effect the shift given by Eq. (5) does not depend on the direction of relative velocity of involved objects since in fact it is just another manifestation of relativistic delay of time. Light coming to observer from any relatively (and arbitrary) moving body is universally "more red" than originally emitted signal; as well all other frequencies attributed to observed moving bodies are smaller then original ones, and namely this idea was explored for derivation of satellite shift formula.

Experimental observation of the frequency change (5) must lead to conclusion that there exists respective "Doppler velocity" V_D entering formula well known from Special Relativity

$$f = \frac{f'}{\sqrt{1-(V_D/c)^2}}\left(1 - \frac{V_D}{c}\cos\beta\right), \quad (6)$$

β being angle between velocity vector and wave vector of emitted signal. If $\beta = 0$ and smaller relativistic correction are neglected then Eq. (6) can be rewritten in the form similar to Eq. (5)

$$\frac{\Delta f}{f'} \cong \frac{V_D}{c^2}\,; \quad (7)$$

comparison of Eqs. (7) and (5) yields very simple formula for calculated (and allegedly existent) "Doppler velocity" corresponding to observed relativistic frequency change

$$V_D \cong \frac{\varepsilon}{c}\,. \quad (8)$$

Estimation of the value of V_D can be done using picture of Pioneer 10/11 trajectories (Fig.1) projected upon ecliptic plane (provided in NASA report [4]); other spacecraft traces are also shown, the Earth's orbit radius too small to be indicated.

Schematically the cinematic situation for Pioneer 10 is shown at Fig. 2 where the trajectory looks as a straight line inclined at constant angle λ to axis $\mathbf{q}_2$, while the Earth's position on its orbit is determined by angle $\alpha = \Omega t$, $\Omega = 3.98\times10^{-7}\,s^{-1}$ being the Earth's orbital angular velocity. Vectors of the probe's and Earth's velocities in Solar Ecliptic

*Latin indices are 3-dimensional (3D), δ_{kl} is 3D Kroneker symbol, ε_{jkl} is 3D Levi-Civita symbol; summation convention is assumed.

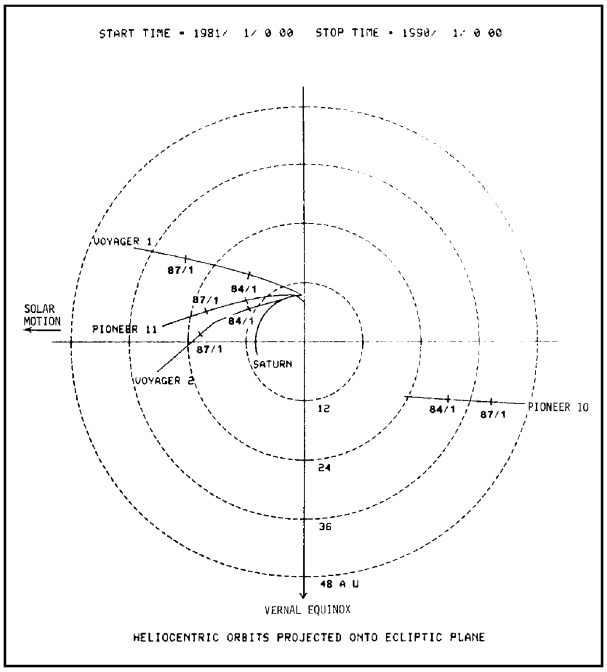

Fig. 1: Spacecraft trajectories on the ecliptic plane. (After NASA original data [4]. Used by permission.)

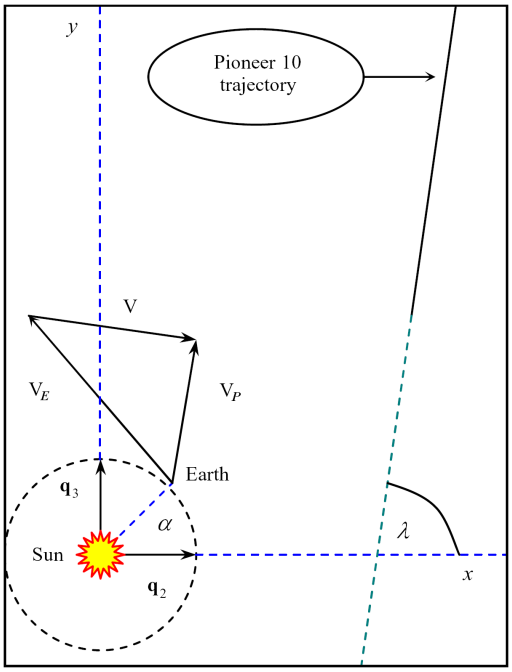

Fig. 2: Earth-Pioneer 10 cinematic scheme, where the trajectory looks as a straight line inclined at constant angle λ to axis $\mathbf{q}_2$.

(SE) coordinate system* are respectively denoted as $\mathbf{V}_P$ and $\mathbf{V}_E$; their vector subtraction gives relative Earth-probe velocity $\mathbf{V} = \mathbf{V}_P - \mathbf{V}_E$ so that

$$V_D(t) = \frac{V^2}{2c} = \frac{V_P^2 + V_E^2 - 2V_P V_E \cos(\Omega t - \lambda)}{2c}, \qquad (9)$$

and respective "Doppler acceleration" is

$$a_D = \dot{V}_D(t) = \\ = \frac{V_P \dot{V}_P - \dot{V}_P V_E \cos(\Omega t - \lambda) + \Omega V_P V_E \sin(\Omega t - \lambda)}{c}. \qquad (10)$$

In Eq. (10) the first term in the numerator claims existence of secular deceleration, since escaping from the Sun's and Jupiter's gravity the probe is permanently decelerated, $\dot{V}_p < 0$; the result is that the frequency gap shrinks giving rise to pure relativistic blue shift. Other sign-changing terms in right-hand-side of Eq. (10) are periodic (annual) ones; they may cause blue shift as well as red shift. Thus Eq. (10) shows that, although relative probe-Earth velocity incorporates into difference between real and observed frequency, nevertheless secular change of the difference is to be related only to relative probe-Sun velocity. Distinguish this term temporary ignoring the annual modulations; then the secular deceleration formula is reduced as

$$a_{SD} \cong \frac{\dot{V}_P V_P}{c}. \qquad (11)$$

*The SE is a heliocentric coordinate system with the z-axis normal to and northward from the ecliptic plane. The x-axis extends toward the first point of Aries (Vernal Equinox, i.e. to the Sun from Earth in the first day of Spring). The y-axis completes the right handed set.

Below only radial components of the probe's velocity and acceleration in Newtonian gravity are taken into account in Eq. (11); it is quite a rough assessment but it allows to conceive order of values. The probe's acceleration caused by the Sun's Newtonian gravity is

$$\dot{V}_P = -\frac{GM_\odot}{R^2}, \qquad (12)$$

$G = 6.67\times10^{-11}\,\mathrm{m^3/kg\times s^2}$, $M_\odot = 1.99\times10^{30}\,\mathrm{kg}$ are respectively gravitational constant and mass of the Sun. NASA data [5] show that in the very middle part (1983–1990) of the whole observational period of Pioneer 10 its radial distance from the Sun changes from $R \cong 28.8\,\mathrm{AU} = 4.31\times10^{12}\,\mathrm{m}$ to $R \cong 48.1\,\mathrm{AU} = 7.2\times10^{12}\,\mathrm{m}$, while year-mean radial velocity varies from $V_P = 15.18\times10^3\,\mathrm{m/s}$ to $V_P = 12.81\times10^3\,\mathrm{m/s}$. Respective values of the secular "relativistic deceleration" values for this period computed with the help of Eqs. (11), (12) vary from $a_{SD} = -3.63\times10^{-10}\,\mathrm{m/s^2}$ to $a_{SD} = -1.23\times10^{-10}\,\mathrm{m/s^2}$. It is interesting (and surprising as well) that these results are very close in order to anomalous "Doppler deceleration" of the probe $a_P = -(8\pm3)\times10^{-10}\,\mathrm{m/s^2}$ cited in [3].

Analogous computations for Pioneer 11, as checking point, show the following. Full time of observation of Pioneer 11 is shorter so observational period is taken from 1984 to 1989, with observational data from the same source [5]. Radial distances for beginning and end of the period are $R \cong 15.1\,\mathrm{AU} = 2.26\times10^{12}\,\mathrm{m}$, $R \cong 25.2\,\mathrm{AU} = 3.77\times10^{12}\,\mathrm{m}$; respective year-mean radial velocities are $V_P = 11.86\times10^3\,\mathrm{m/s}$, $V_P = 12.80\times10^3\,\mathrm{m/s}$. Computed "relativistic deceleration" values for this period are then $a_{SD} = -10.03\times10^{-10}\,\mathrm{m/s^2}$,

$a_{SD} = -5.02 \times 10^{-10}$ m/s^2: this is even in much better correlation (within limits of the cited error) with experimental value of a_P.

3 Discussion

Quantitative estimations presented above allow to conclude: additional blue shift, experimentally registered in Pioneer 10 and 11 signals, and interpreted as Sun-directed acceleration of the spacecraft to some extent, support the assumption of pure relativistic nature of the anomaly. Of course one notes that while Pioneer 11 case shows good coincidence of observed and calculated values of deceleration, values of a_{SD} for Pioneer 10 constitute only (45–15)% of observed Doppler residual; moreover generally in this approach "relativistic deceleration" is a steadily decreasing function, while experimentally (though not directly) detected deceleration a_P is claimed nearly constant. These defects could find explanation first of all in the fact that a primitive "Newtonian radial model" was used for assessments. Preliminary but more attentive reference to NASA data allows noticing that observed angular acceleration of the probes too could significantly incorporate to values of "relativistic deceleration". This problem remains to be regarded elsewhere together with analysis of the angular acceleration itself.

Acknowledgments

The author would like to thank Profs. F. Smarandache and V. Christianto for attention to his quaternion approach aimed to calculate relativistic effects of non-inertial motions. Special thanks to V. Christianto for given information on Pioneer anomaly and numerous helpful discussions.

Submitted on March 01, 2007
Accepted on March 05, 2007

References

1. Smarandache F. and Christianto V. *Progr. in Phys.*, 2007, v. 1, 42–45.
2. Yefremov A. *Grav. & Cosmol.*, 1996, v. 2, No. 4, 335–341.
3. Anderson J. D. et al. arXiv: gr-qc/9808081.
4. http://cohoweb.gsfc.nasa.gov/helios/book1/b1_62.html
5. http://cohoweb.gsfc.nasa.gov/helios/book2/b2_03.html

Single Photon Experiments and Quantum Complementarity

Danko Dimchev Georgiev

Kanazawa University Graduate School of Natural Science and Technology,
Kakuma-machi, Kanazawa-shi, Ishikawa-ken 920-1192, Japan

E-mail: danko@p.kanazawa-u.ac.jp

Single photon experiments have been used as one of the most striking illustrations of the apparently nonclassical nature of the quantum world. In this review we examine the mathematical basis of the principle of complementarity and explain why the Englert-Greenberger duality relation is not violated in the configurations of Unruh and of Afshar.

1 Introduction

In classical physics if we have two distinct physical states $\psi_1 \neq \psi_2$ of a physical system and we know that $\psi_1 \,\mathrm{OR}\, \psi_2$ is a *true* statement we can easily deduce that $\psi_1 \,\mathrm{XOR}\, \psi_2$ is a true statement too. In Quantum Mechanics however we encounter a novel possibility for *quantum coherent superposition*. It has been verified in numerous experiments that a qubit can be prepared in a linear combination of two orthogonal states, and this parallel existence in the quantum realm, in the form $\psi_1 \,\mathrm{AND}\, \psi_2$, is what requires caution when we draw conclusions from a given set of premises — the truth of $\psi_1 \,\mathrm{OR}\, \psi_2$ now does not lead to the truth of $\psi_1 \,\mathrm{XOR}\, \psi_2$.* If a qubit at point x is in a state $\psi_1 \mathrm{XOR} \psi_2$ then ψ_1 and ψ_2 are called *distinguishable states*. Logically, if the qubit at point x is in a state $\psi_1 \mathrm{XNOR} \psi_2$ the two states ψ_1 and ψ_2 will be *indistinguishable*. From the requirement for mathematical consistency it follows that two states ψ_1 and ψ_2 cannot be both *distinguishable* and *indistinguishable* at the same time.

The concept of distinguishability is intimately tied with the notion of quantum complementarity. While the quantum amplitudes evolve linearly according to the Schrödinger equation, the physical observables are obtained from the underlying quantum amplitudes through nonlinearity prescribed by Born's rule.

Thus if quantum states $\psi_1(x) \neq 0$ and $\psi_2(x) \neq 0$ are *indistinguishable* at a point x (coherent superposition), that is $\psi_1(x) \,\mathrm{AND}\, \psi_2(x)$, the probability distribution (observed intensity) is given by $P = |\psi_1(x) + \psi_2(x)|^2$. The *density matrix* of the setup is a pure type one, $\hat{\rho} = \begin{pmatrix} |\psi_1|^2 & \psi_1\psi_2^* \\ \psi_2\psi_1^* & |\psi_2|^2 \end{pmatrix}$, and $\hat{\rho} = \hat{\rho}^2$ holds. The two quantum states do quantum mechanically interfere. In Hilbert space the two functions are not orthogonal and the overlap integral is not *zero* (Vedral [12]):

$$\int \psi_1^*(x)\, \psi_2(x)\, dx \neq 0\,. \tag{1}$$

Alternatively, if quantum states $\psi_1(x)$ and $\psi_2(x)$ are *distinguishable* at a point x (incoherent superposition), that is $\psi_1(x) \mathrm{XOR} \psi_2(x)$, then the probability distribution is given by $\mathcal{P} = |\psi_1(x)|^2 + |\psi_2(x)|^2$. The *(reduced) density matrix* is mixed type one, $\hat{\rho} = \begin{pmatrix} |\psi_1|^2 & 0 \\ 0 & |\psi_2|^2 \end{pmatrix}$, and $\hat{\rho} \neq \hat{\rho}^2$. The two quantum states do not quantum mechanically interfere but just sum classically. In Hilbert space the two functions are orthogonal and the overlap integral is *zero*:

$$\int \psi_1^*(x)\, \psi_2(x)\, dx = 0\,. \tag{2}$$

The observable value given by $\mathcal{P}$ should not necessarily describe an incoherently superposed state. It might as well describe a fictious statistical average of two single amplitude experiments in which either only $\psi_1(x)$ or only $\psi_2(x)$ participates. In this case however $\psi_1(x)$ and $\psi_2(x)$ should be separately normalized to 1, and as elements in the main diagonal of the density matrix must be taken the *statistical probabilities* defining the mixture (Zeh [14]).

Next, despite the fact that qubits generally might take more than one path in a coherent superposition (Feynman and Hibbs [7]), we will still show that the "which way" claims ("*welcher weg*", in German) can be derived rigourously within the quantum mechanical formalism. The "which way" claim will be defined as an existent *one-to-one correspondence (bijection) between elements of two sets* (typically input state and observable).

ψ_1	ψ_2	XOR output	ψ_1	ψ_2	XNOR output
0	0	0	0	0	1
0	1	1	0	1	0
1	0	1	1	0	0
1	1	0	1	1	1

Table 1: Distinguishable –vs– indistinguishable states

*Such a direct interpretation of the AND gate as having corresponding quantum coherent superposed reality is consistent with the prevailing view among working physicists that resembles Everett's many worlds interpretation (MWI) of Quantum Mechanics in many ways (Tegmark and Wheeler [11]). However, the reality of quantum superposition is not a characteristic feature only of MWI. The transactional interpretation (TI) proposed by Cramer [4] and quantum gravity induced objective reduction (OR) proposed by Penrose [8] both admit of the reality of superposed quantum waves, respectively superposed space-times.

$$\overset{\mathfrak{L}_1}{[|\psi\rangle]} \rightarrow \overset{\text{path 1}}{\left[i\frac{1}{\sqrt{2}}|\psi_1\rangle\right]} + \overset{\text{path 2}}{\left[\frac{1}{\sqrt{2}}|\psi_2\rangle\right]} \rightarrow \overset{\text{path 3}}{\left[-\frac{1}{\sqrt{2}}|\psi_1\rangle\right]} + \overset{\text{path 4}}{\left[i\frac{1}{\sqrt{2}}|\psi_2\rangle\right]} \rightarrow \overset{\mathfrak{D}_1}{\left[-\frac{1}{2}|\psi_1\rangle - \frac{1}{2}|\psi_2\rangle\right]} + \overset{\mathfrak{D}_2}{\left[-i\frac{1}{2}|\psi_1\rangle + i\frac{1}{2}|\psi_2\rangle\right]} \quad (3)$$

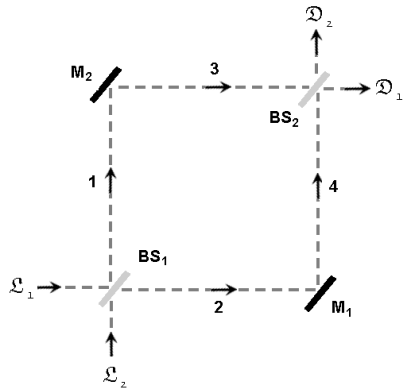

Fig. 1: *Mach-Zehnder interferometer*. Incoming photon at $\mathfrak{L}_1$ quantum mechanically *self-interferes* in order to produce its own full cancelation at detector $\mathfrak{D}_2$ and recover itself entirely at detector $\mathfrak{D}_1$. The opposite holds for the photon entering at $\mathfrak{L}_2$. Legend: BS, beam splitter, M, fully silvered mirror.

2 The Mach-Zehnder interferometer

In order to illustrate the "which way" concept let us introduce the *Mach-Zehnder interferometer*, from which more complicated interferometers can be built up. The setup is symmetric and contains two half-silvered and two fully silvered mirrors positioned at angle $\frac{\pi}{4}$ to the incoming beam (Fig. 1). The action of the beam splitter (half-silvered mirror) will be such as to transmit forward without phase shift $\frac{1}{\sqrt{2}}\psi$ of the incoming quantum amplitude ψ, while at the same time reflects perpendicularly in a coherent superposition $i\frac{1}{\sqrt{2}}\psi$ of it. The action of the fully silvered mirrors will be such as to reflect perpendicularly all of the incoming amplitude ψ with a phase shift of $\frac{\pi}{2}$, which is equivalent to multiplying the state by $e^{i\frac{\pi}{2}} = i$ (Elitzur and Vaidman [6]; Vedral [12]).

In this relatively simple setup it can be shown that a photon entering at $\mathfrak{L}_1$ will always be detected by detector $\mathfrak{D}_1$, whilst a photon entering at $\mathfrak{L}_2$ will always be detected by detector $\mathfrak{D}_2$. It is observed that the photon quantum mechanically *destructively self-interferes* at one of the detectors, whilst it quantum mechanically *constructively self-interferes* at the other detector, creating a one-to-one correspondence between the entry point and the exit point in the Mach-Zehnder interferometer.

Let the incoming amplitude Ψ at $\mathfrak{L}_1$ be normalized so that $|\Psi|^2 = 1$. The evolution of the wave package in the interferometer branches is described by formula (3), where $|\psi_1\rangle$ refers to passage along path 1 and $|\psi_2\rangle$ refers to passage along path 2.

Since the two interferometer paths are indistinguishable one easily sees that at $\mathfrak{D}_1$ one gets *constructive quantum interference*, while at $\mathfrak{D}_2$ one gets *destructive quantum interference*. The inverse will be true if the photon enters at $\mathfrak{L}_2$. Therefore we have established a one-to-one correspondence (bijection) between the entry points and detector clicks. The *indistinguishability* of ψ_1 and ψ_2 allows for *quantum self-interference* of Ψ at the detectors. Insofar as we don't specify which path of the interferometer has been traversed, allow quantum interference of amplitudes at the exit gates coming from both interferometer paths, so ψ_1 AND ψ_2 (*indistinguishable* ψ_1 and ψ_2), we will maintain the one-to-one correspondence between entry points and detectors (*distinguishable* $\mathfrak{D}_1$ and $\mathfrak{D}_2$).

If we however block one of the split beams ψ_1 or ψ_2, or we label ψ_1 and ψ_2, e.g. by different polarization filters, **V** (vertical polarization) and **H** (horizontal polarization), we will lose the quantum interference at the exit gates and the one-to-one correspondence between entry points and exit points will be lost. Thus we have encountered the phenomenon of *complementarity.* We can determine which of the interferometer paths has been taken by the photon, hence ψ_1 XOR ψ_2 (*distinguishable* ψ_1 and ψ_2), and destroy the one-to-one correspondence between entry points and exit gates (*indistinguishable* $\mathfrak{D}_1$ and $\mathfrak{D}_2$). A photon entering at $\mathfrak{L}_1$ (or $\mathfrak{L}_2$) will not self-interfere and consequently could be detected by either of the detectors with probability of $\frac{1}{2}$.

Thus we have shown that quantum coherent superposition of photon paths itself does not preclude the possibility for one to establish one-to-one correspondence (bijection) between two observables (entry and exit points). However, it will be shown that the bijection $\mathfrak{L}_1 \rightarrow \mathfrak{D}_1$, $\mathfrak{L}_2 \rightarrow \mathfrak{D}_2$ is valid for the discussed mixed case in which we have input $\mathfrak{L}_1$ XOR $\mathfrak{L}_2$, yet might not be true in the case where the input points $\mathfrak{L}_1$ and $\mathfrak{L}_2$ are in quantum coherent superposition ($\mathfrak{L}_1$ AND $\mathfrak{L}_2$) as is the case in Unruh's setup.

3 Unruh's interferometer

Unruh's thought experiment is an arrangement that tries to create a more understandable version of Afshar's experiment, which will be discussed later. Unruh's interferometer is essentially a multiple pass interferometer with two elementary building blocks of the Mach-Zehnder type. In Fig. 2 each arm of the interferometer is labelled with a number, and a photon enters at $\mathfrak{L}_1$.

Application of Feynman's *sum over histories* approach leads us to the correct quantum mechanical description of the experiment. Expression (4) is *Dirac's ket notation* for the quantum states evolving in the interferometer arms.

$$\overset{\mathfrak{L}_1}{[|\psi\rangle]} \rightarrow \overset{\text{path 1}}{\left[i\frac{1}{\sqrt{2}}|\psi_1\rangle\right]} + \overset{\text{path 2}}{\left[\frac{1}{\sqrt{2}}|\psi_2\rangle\right]} \rightarrow \overset{\text{path 3}}{\left[-\frac{1}{\sqrt{2}}|\psi_1\rangle\right]} + \overset{\text{path 4}}{\left[i\frac{1}{\sqrt{2}}|\psi_2\rangle\right]} \rightarrow$$

$$\rightarrow \overset{\text{path 5}}{\left[-i\frac{1}{2}|\psi_1\rangle + i\frac{1}{2}|\psi_2\rangle\right]} + \overset{\text{path 6}}{\left[-\frac{1}{2}|\psi_1\rangle - \frac{1}{2}|\psi_2\rangle\right]} \rightarrow \overset{\text{path 7}}{\left[\frac{1}{2}|\psi_1\rangle - \frac{1}{2}|\psi_2\rangle\right]} + \overset{\text{path 8}}{\left[-i\frac{1}{2}|\psi_1\rangle - i\frac{1}{2}|\psi_2\rangle\right]} \rightarrow \tag{4}$$

$$\rightarrow \left[\overset{\mathfrak{D}_1}{\left[\frac{1}{\sqrt{8}}|\psi_1\rangle - \frac{1}{\sqrt{8}}|\psi_2\rangle\right]} + \left[\frac{1}{\sqrt{8}}|\psi_1\rangle + \frac{1}{\sqrt{8}}|\psi_2\rangle\right]\right] + \left[\overset{\mathfrak{D}_2}{\left[i\frac{1}{\sqrt{8}}|\psi_1\rangle - i\frac{1}{\sqrt{8}}|\psi_2\rangle\right]} + \left[-i\frac{1}{\sqrt{8}}|\psi_1\rangle - i\frac{1}{\sqrt{8}}|\psi_2\rangle\right]\right]$$

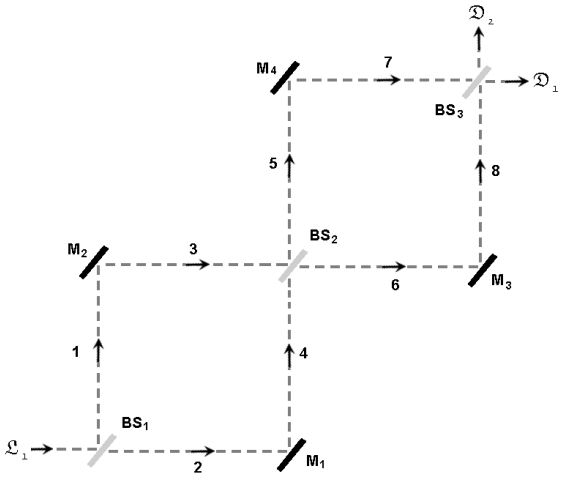

Fig. 2: Unruh's version of a multiple pass interferometer setup that captures the essence of Afshar's experiment. It is composed of two elementary building blocks described in the text, and the incoming photon at $\mathfrak{L}_1$ has an equal chance to end either at $\mathfrak{D}_1$, or at $\mathfrak{D}_2$.

3.1 Unruh's "which way" claim

Unruh obstructed path 1 and correctly argues that the photons coming from the source that pass the first half-silvered mirror and take path 2 (that is they are not reflected to be absorbed by the obstruction located in path 1) will all reach detector $\mathfrak{D}_2$. These are exactly 50% of the initial photons. The explanation is the one provided in the analysis of the Mach-Zehnder interferometer. So Unruh shows that there is a one-to-one corespondence between path 2 and detector $\mathfrak{D}_2$ when path 1 is blocked. Similarly he argues that in the inverted setup with the obstruction in path 2, all the photons that take path 1 (that is they are not absorbed by the obstruction located in path 2) will reach detector $\mathfrak{D}_1$. This suggests a one-to-one correspondence between path 1 and detector $\mathfrak{D}_1$ when path 2 is blocked.

Note at this stage that Unruh investigates a statistical mixture of two single path experiments. Therefore the case is $\psi_1\,\mathrm{XOR}\,\psi_2$, both paths ψ_1 and ψ_2 are *distinguishable* because of the *existent obstruction*, and ψ_1 and ψ_2 do not quantum *cross-interfere* with each other in the second block of the interferometer (in the first block they are separated spatially, in the second branch they are separated temporally). Thus in the mixed setup there is a one-to-one correspondence between paths and exit gates due to the *distinguishability* of ψ_1 and ψ_2, that is, there is no quantum interference between ψ_1 and ψ_2 in the second building block of Unruh's interferometer.

Unruh then unimpedes both paths ψ_1 and ψ_2, and considering the statistical mixture of the two single path experiments argues that photons that end up at detector $\mathfrak{D}_1$ have taken path ψ_1, while those ending at detector $\mathfrak{D}_2$ come from path ψ_2. The logic is that the second building block of the interferometer has both of its arms open, and the one-to-one correspondence is a result of *self-interference* of ψ_1 and *self-interference* of ψ_2 respectively.

The problem now is to secure the conclusion that "which way" information in the form of a one-to-one correspondence between paths ψ_1 and ψ_2 and the two detectors still "remains" when both paths 1 and 2 are unimpeded? The only way to justify the existence of the bijection is to take the following two statements as axioms: (i) ψ_1 and ψ_2 do not *quantum cross-interfere* with each other; (ii) ψ_1 and ψ_2 *can only quantum self-interfere*. Concisely written together, both statements reduce to one logical form, $\psi_1\,\mathrm{XOR}\,\psi_2$ i.e. ψ_1 and ψ_2 are orthogonal states. Thus Unruh's "which way" statement when both paths of the interferometer are unimpeded is equivalent to the statement that the density matrix of the photons at the detectors is a *mixed one*. Thus stated Unruh's "which way" claim, which is mathematically equivalent with the claim for a mixed state density matrix of the setup, is subject to experimental test. Quantum mechanically one may perform experiments to find whether or not two incoming beams are quantum coherent (pure state) or incoherent (mixed state). Hence Unruh's thesis is experimentally disprovable, and in order to keep true his thesis Unruh must immunize it against experimental test by postulating that one cannot experimentally distinguish the mixed state from the pure state. Otherwise one may decide to let the two beams (led away from the detectors) cross each other. If an interference pattern is build up then one will have experimental verification that the density matrix of the setup is not of the *mixed type* ($\psi_1\,\mathrm{XOR}\,\psi_2$, $\hat{\rho} \neq \hat{\rho}^2$), but one of *pure type* ($\psi_1\,\mathrm{AND}\,\psi_2$, $\hat{\rho} = \hat{\rho}^2$). It is not conventional to think that

the mixed state cannot be experimentally distinguished from the pure state, and that is why Unruh's "which way" claim for the double path coherent setup is incorrect. One notices however that if each of the paths 1 and 2 is labelled by different polarization filters, e.g. **V** and **H**, then the density matrix of the setup will be a *mixed one* (incoherent superposition in the second interferometer block), and the "which way" claim will be correct because the different polarizations will convert ψ_1 and ψ_2 into orthogonal states. If the two beams lead away from the detectors and cross, they will not produce an interference pattern.

3.2 Correct "no which way" thesis

We have already shown that if one argues that there is "which way" correspondence, he must accept that ψ_1 and ψ_2 are *distinguishable*, and hence that they will not be able to cross-interfere at arms 5–8 of the interferometer.

Now we will show the opposite; that postulating "unmeasured destructive interference" in arms 5 and 7 of the interferometer, regardless of the fact that the interference is not measured, is sufficient to erase completely the "which way" information. Postulating quantum interference in arms 5–8 is equivalent to postulating *indistinguishability* (quantum coherent superposition) of ψ_1 and ψ_2, which is equivalent to saying that ψ_1 and ψ_2 can annihilate each other.

The quantum amplitude at $\mathfrak{D}_1$ is:

$$\mathfrak{D}_1 : \left[\frac{1}{\sqrt{8}}|\psi_1\rangle - \frac{1}{\sqrt{8}}|\psi_2\rangle\right] + \left[\frac{1}{\sqrt{8}}|\psi_1\rangle + \frac{1}{\sqrt{8}}|\psi_2\rangle\right]. \quad (5)$$

The first two members in the expression have met each other earlier, so they annihilate each other. What remains is $\frac{1}{\sqrt{8}}|\psi_1\rangle + \frac{1}{\sqrt{8}}|\psi_2\rangle$ and when squared gives $\frac{1}{2}|\Psi|^2$, where ψ_1 and ψ_2 contribute equally to the observed probability of detecting a photon. Now is clear why one cannot hold consistently both the existence of "which way" one-to-one correspondence and existent but undetected interference at paths 5 and 6.

- If one postulates ψ_1 XOR ψ_2 then $\frac{1}{\sqrt{8}}|\psi_2\rangle - \frac{1}{\sqrt{8}}|\psi_2\rangle$ will interfere at the exit and the resulting observable intensity $\frac{1}{2}|\Psi|^2$ will come from squaring $\frac{1}{\sqrt{8}}|\psi_1\rangle + + \frac{1}{\sqrt{8}}|\psi_1\rangle$ i.e. only from path 1.
- If one postulates ψ_1 AND ψ_2 then $\frac{1}{\sqrt{8}}|\psi_1\rangle - \frac{1}{\sqrt{8}}|\psi_2\rangle$ will interfere first, and the resulting observable intensity $\frac{1}{2}|\Psi|^2$ will come from squaring $\frac{1}{\sqrt{8}}|\psi_1\rangle + \frac{1}{\sqrt{8}}|\psi_2\rangle$ i.e. both paths 1 and 2.

The "mixing of the two channels" at $\mathfrak{D}_2$ is analogous.

$$\mathfrak{D}_2: \left[i\frac{1}{\sqrt{8}}|\psi_1\rangle - i\frac{1}{\sqrt{8}}|\psi_2\rangle\right] + \left[-i\frac{1}{\sqrt{8}}|\psi_1\rangle - i\frac{1}{\sqrt{8}}|\psi_2\rangle\right]. \quad (6)$$

- If one postulates ψ_1 XOR ψ_2 then $i\frac{1}{\sqrt{8}}|\psi_1\rangle - i\frac{1}{\sqrt{8}}|\psi_1\rangle$ will interfere at the exit and the obtained observable intensity $\frac{1}{2}|\Psi|^2$ will come from squaring $-i\frac{1}{\sqrt{8}}|\psi_2\rangle - - i\frac{1}{\sqrt{8}}|\psi_2\rangle$ i.e. only from path 2.
- If one postulates ψ_1 AND ψ_2 then $i\frac{1}{\sqrt{8}}|\psi_1\rangle - i\frac{1}{\sqrt{8}}|\psi_2\rangle$ will interfere first, and the obtained observable intensity $\frac{1}{2}|\Psi|^2$ will come from squaring of $-i\frac{1}{\sqrt{8}}|\psi_1\rangle - - i\frac{1}{\sqrt{8}}|\psi_2\rangle$ i.e. both paths 1 and 2.

3.3 Inconsistent interpretation: "which way" + pure state density matrix

It has been suggested in web blogs and various colloquia, that only measurement of the interference at arms 5–8 disturbs the "which way" interpretation, and if the destructive quantum interference is not measured it can peacefully coexist with the "which way" claim. Mathematically formulated the claim is that there is "which way" one-to-one correspondence between paths 1 and 2, and $\mathfrak{D}_1$ and $\mathfrak{D}_2$ respectively, while at the same time the whole setup is described by a pure state density matrix. Afshar [1–3] claims an equivalent statement for his setup insisting on a "which way" + pure state density matrix.

We will *prove* that assuming a "which way" + pure state density matrix leads to mathematical inconsistency. In order to show *where the inconsistency arises* we should rewrite the expressions of the quantum amplitudes at the two detectors in a fashion where each of the wavefunctions ψ_1 and ψ_2 is written as a superposition of its own branches $|\psi_{15}\rangle, |\psi_{16}\rangle$ and $|\psi_{25}\rangle, |\psi_{26}\rangle$, respectively, where the second subscript 5 or 6 denotes a branch in the second building block of Unruh's interferometer:

$$\mathfrak{D}_1 : \frac{1}{\sqrt{8}}|\psi_{15}\rangle - \frac{1}{\sqrt{8}}|\psi_{25}\rangle + \frac{1}{\sqrt{8}}|\psi_{16}\rangle + \frac{1}{\sqrt{8}}|\psi_{26}\rangle \quad (7)$$

$$\mathfrak{D}_2 : i\frac{1}{\sqrt{8}}|\psi_{15}\rangle - i\frac{1}{\sqrt{8}}|\psi_{25}\rangle - i\frac{1}{\sqrt{8}}|\psi_{16}\rangle - i\frac{1}{\sqrt{8}}|\psi_{26}\rangle. \quad (8)$$

From the "which way" claim it follows that the contributions to the final intensity (squared amplitude) detected at $\mathfrak{D}_1$ or $\mathfrak{D}_2$ must come from ψ_1 or ψ_2 only. This is possible *if and only if* the individual branches 5 or 6 of each function are *indistinguishable*, so that the claim mathematically yields quantum destructive interference (annihilation) between ψ_{15} and ψ_{16}, and between ψ_{25} and ψ_{26}, respectively.

However to postulate at the same time that the density matrix is a pure type one i.e. there is "*undetected negative quantum cross-interference*" at branch 5 between ψ_1 and ψ_2 (self-interference of Ψ) is equivalent to saying that paths 5 and 6 are *distinguishable*. We have arrived at a logical inconsistency.

Paths 5 and 6 cannot be both *distinguishable* and *indistinguishable* for the quantum state Ψ — this is what the complementarity principle says.

Due to basic arithmetic axiom ψ_{15} cannot entirely annihilate both ψ_{16} and ψ_{25}. Thus the complementarity principle

itself is a manifestation of the underlying mathematical formalism and one ends up with an XOR bifurcation of two inconsistent with each other outcomes. The two alternative outcomes do not "complement" each other instead they logically exclude each other.

We have therefore proved that within standard Quantum Mechanics one cannot claim both "which way" and pure state of the density matrix at the same time. Whether the quantum interference at branch 5 is measured or not does not matter. Its consistent postulation is sufficient to rule out the "which way information".

3.4 Retrospective reconstructions and complementarity

Now notice that arguing that photons possess "which way" information implies that the photon density matrix at detectors is that of a *mixed type*. We have denoted the quantum amplitude through path 1 by ψ_1, and the quantum amplitude through path 2 by ψ_2. Therefore when we *retrospectively reconstruct* the photon probability distribution function we should use the correct complementarity rule $\mathcal{P} = |\psi_1|^2 + |\psi_2|^2$, and we must logically and consistently argue that there is no negative interference at path 5 — simply, we do not just add ψ_1 to ψ_2 but first square each of those amplitudes. Basically, if the two paths ψ_1 and ψ_2 are *distinguishable*, then the interference terms must be *zero*, and the (reduced) density matrix will be of *mixed type* i.e. one with off-diagonal elements being *zeroes*. To accept that there is "which way" information is equivalent to accepting that the setup with both paths unobstructed is a statistical mixture of the two single path setups with obstructions so the complementarity rule for making retrospective predictions is $\mathcal{P} = |\psi_1|^2 + |\psi_2|^2$. This alternative formulation of the principle of complementarity is in a form of instruction as to how to make the correct retrospective reconstruction of a *mixed state* setup — it says that *mixed state setups* should be retrospectively reconstructed with $\mathcal{P} = |\psi_1|^2 + |\psi_2|^2$ distribution.

However, if the beams along paths 1 and 2 interfere so that no photons are expected along path 5, the setup is a "no which way" *pure state* setup. In this case the retrospective photon probability distribution should be calculated as $P = |\psi_1 + \psi_2|^2$. Thus the alternative formulation of the principle of complementarity in a form of instruction as to how to make the correct retrospective reconstruction of *pure state* setup is — *pure state setups* should be retrospectively reconstructed with the $P = |\psi_1 + \psi_2|^2$ distribution.

Taken together the above two instructions provide a clear idea of complementarity — one cannot retrospectively recover a given setup with both types of probability distributions $\mathcal{P} = |\psi_1|^2 + |\psi_2|^2$ and $P = |\psi_1 + \psi_2|^2$ at the same time, because otherwise you will produce a mathematical inconsistency.

One sees that, in some special cases for a given point x both probability distributions coincide, so $\mathcal{P}(x) = P(x)$, and if one observes only the point x the choice of how to retrospectively reconstruct the setup might be tricky. It is unwise to retrospectively reconstruct a *pure state* setup with $\mathcal{P} = |\psi_1|^2 + |\psi_2|^2$ probability distribution. One will not arrive at a direct experimental contradiction if he looks only within the region where $\mathcal{P}(x) = P(x)$. Yet, any measurement outside this region will reveal the improper retrospective reconstruction.

4 Afshar's setup

In Afshar's setup, light generated by a laser passes through two closely spaced circular pinholes. After the dual pinholes, a lens refocuses the light so that *each image of a pinhole* is received by a separate photo-detector. Considering a mixture of single pinhole trials Afshar argues that a photon that goes through *pinhole 1* impinges only on detector $\mathfrak{D}_1$, and similarly, if it goes through *pinhole 2* impinges only on detector $\mathfrak{D}_2$. Exactly as in Unruh's setup, Afshar investigates a statistical mixture $\psi_1 \,\mathrm{XOR}\, \psi_2$ and after that draws *non sequitur* conclusions for the $\psi_1 \,\mathrm{AND}\, \psi_2$ setup. Thus according to Afshar, there is a one-to-one correspondence between pinholes and the corresponding images even when the light coherently passes through both pinholes. While in classical optics this is a straightforward conclusion, in quantum coherent setups we will shortly prove that each image of a pinhole in the coherent dual pinhole setup is counter-intuitively assembled by light coming from both pinholes at once.

Afshar [1, 2] claimed (erroneously) that Unruh's setup (originally intended to disprove Afshar's reasoning) is not equivalent to Afshar's setup, and therefore that the *"plane constructed by Unruh has no wings"*. At first glance one might argue that in Afshar's setup at *image 1* comes only quantum amplitude from *pinhole 1*, and *zero* amplitude from *pinhole 2*, and at *image 2* comes amplitude from *pinhole 2* and *zero* from *pinhole 1*. The putative difference between Unruh's setup and Afshar's setup at first glance seems to be this:

- *Afshar's setup: image 1*: $\frac{1}{\sqrt{2}}\psi_1 + 0 \times \psi_2$ and *image 2*: $\frac{1}{\sqrt{2}}\psi_2 + 0 \times \psi_1$. The *zero* looks "physically unstructured", not a result of negative interference of positive and negative amplitudes contributed from the alternative pinhole.
- *Unruh's setup:* $\mathfrak{D}_1$: $\frac{1}{\sqrt{2}}\psi_1 + \left[\frac{1}{\sqrt{8}}\psi_2 - \frac{1}{\sqrt{8}}\psi_2\right]$ and $\mathfrak{D}_2$: $\frac{1}{\sqrt{2}}\psi_2 + \left[\frac{1}{\sqrt{8}}\psi_1 - \frac{1}{\sqrt{8}}\psi_1\right]$. In this case the *zero* manifests "with physical structure", and is a result of negative interference of positive and negative amplitudes contributed from the alternative path.

If one shows that the "no which way" proof applied to Unruh's setup is not applicable to Afshar's setup, he will also show that Unruh's plane is indeed without wings. If in contrast, one can prove that in Afshar's setup the zero pinhole amplitude contribution at the opposite image is gene-

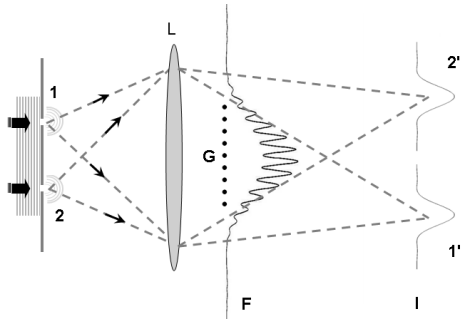

Fig. 3: Action of a lens in a dual pinhole setup — pinholes 1 and 2 create two peak images, $1'$ and $2'$, F denotes the focal plane of the lens, I denotes the image planes of the lens, G is the grid that can be used to verify the existence of an interference pattern in the coherent setup when both pinholes are open. The image is released under GNU free documentation licence by A. Drezet.

rated by *negative quantum interference*, he will show that Unruh's setup is completely equivalent to Afshar's setup. Thus our criticism of Afshar will be the same as in Unruh's case — logical fallacy and mathematical error in claiming both *pure state* and "which way".

It will now be shown that Afshar's setup is equivalent to Unruh's setup. In brief Afshar has dual pinholes, a lens, and detectors that record photons streaming away from the pinhole images created at the image plane of the lens (Afshar [3]). Analogously to Unruh's setup one closes *pinhole 1* and sees that light goes only to *image 2*, then closes *pinhole 2* and sees that light goes only to *image 1*. One may, analogously to Unruh's setup, *inconsistently postulate* "which way" + *pure state density matrix*. However, one should note that, in the single pinhole experiments, at the image plane of the lens the *zero* light intensity outside the central Airy disc of the pinhole image is a result of *destructive quantum interference*. There are many faint higher order maxima and minima outside the central Airy disc resulting from quantum interference. In order for the two pinhole images to be *resolvable** the image of the second pinhole must be outside the central Airy disc, and located in the first negative Airy ring of the first pinhole image (or further away). Therefore in the case of open *pinhole 2* at *image 1* there are destructively interfering quantum amplitudes contributed by *pinhole 2* because *image 1* resides in an Airy minimum of *image 2*. In contrast at *image 2* the waves from *pinhole 2* will constructively interfere. If both pinholes are open and some of the waves coming from *pinhole 1* cross-interfere with waves coming from *pinhole 2* in the space before the lens, there will remain a contribution by *pinhole 2* at *image 1* that will compensate exactly the decrease of quantum waves contributed by *pinhole 1* at *image 1*. Now one has to "choose" which amplitudes will annihilate, and which will remain to be squared. If one postulates the existent interference in the space before the lens (or after the lens as is the case at the focal plane of the lens) then the annihilation between ψ_1 and ψ_2 at the dark fringes will be equivalent to the interference at path 5 of Unruh's setup, and the final observed intensities at the detectors cannot be claimed to come only from one of the pinholes. Thus Afshar is wrong to say that *"Unruh's plane is without wings"*. Afshar's setup is equivalent to Unruh's setup. The treatment of complementarity is analogous. In the case with both pinholes open there is no "which way" information in Afshar's experiment. Counter-intuitively *each image of a pinhole* is assembled from light coming by half from both pinholes.

*One should cautiously note that *resolvable* images of a pinhole is not equivalent with *distinguishable* pinholes. *Resolvable* means that the two images of a pinhole are separated and not fused into a single spot. The *distinguishability* of the pinholes has to be proven by existent bijection between an image and a pinhole.

An exact calculation is adduced by Qureshi [9] where he shows that the quantum state at the overlap region where the dark interference fringes are detected can be written as

$$\psi(y,t) = aC(t)\, e^{-\frac{y^2+y_0^2}{\Omega(t)}}\left[\cosh\frac{2yy_0}{\Omega(t)} + \sinh\frac{2yy_0}{\Omega(t)}\right] + \\ + bC(t)\, e^{-\frac{y^2+y_0^2}{\Omega(t)}}\left[\cosh\frac{2yy_0}{\Omega(t)} - \sinh\frac{2yy_0}{\Omega(t)}\right], \tag{9}$$

where $C(t) = \frac{1}{(\pi/2)^{1/4}\sqrt{\epsilon+2i\hbar t/m\epsilon}}$, $\Omega(t) = \epsilon^2 + 2i\hbar t/m$, a is the amplitude contribution from *pinhole 1*, b is the amplitude contribution from *pinhole 2*, ϵ is the width of the wave-packets, $2y_0$ is the slit separation.

For Afshar's setup $a = b = \frac{1}{\sqrt{2}}$ so the sinh terms cancel out at the dark fringes and what is left is

$$\psi(y,t) = \frac{1}{2}\, aC(t)\left[e^{-\frac{(y-y_0)^2}{\Omega(t)}} + e^{-\frac{(y+y_0)^2}{\Omega(t)}}\right] + \\ + \frac{1}{2}\, bC(t)\, e^{-\frac{y+y_0^2}{\Omega(t)}}\left[e^{-\frac{(y-y_0)^2}{\Omega(t)}} + e^{-\frac{(y+y_0)^2}{\Omega(t)}}\right]. \tag{10}$$

If a lens is used, after the interference has occurred, to direct the $e^{-\frac{(y-y_0)^2}{\Omega(t)}}$ part into one detector and the part $e^{-\frac{(y+y_0)^2}{\Omega(t)}}$ into the other detector, one easily sees that the amplitudes from each slit evolve into a superposition of two parts that go to both detectors. Note that the coefficient of the part from a slit to each of the detectors becomes exactly $\frac{1}{\sqrt{8}}$ as we have obtained via analysis of Unruh's setup.

5 Englert-Greenberger duality relation

Afshar claimed he has violated the Englert-Greenberger duality relation $V^2 + D^2 \leqslant 1$, where V stands for *visibility* and D stands for *distinguishability* and are defined as:

$$D = \frac{\big||\psi_1|^2 - |\psi_2|^2\big|}{|\psi_1|^2 + |\psi_2|^2}, \tag{11}$$

$$V = \frac{2|\psi_1||\psi_2|}{|\psi_1|^2 + |\psi_2|^2}. \tag{12}$$

Since the duality relation is a mathematically true statement (theorem) then it cannot be disproved by experiment and certainly means that Afshar's arguments, through which he violates the duality relation, are inconsistent. Indeed the calculation of V and D depends on the principle of complementarity and distinguishability of the states ψ_1 and ψ_2. The calculation of V and D in Unruh's and Afshar's setup is different for pure state and mixed state setups.

5.1 Mixed state setup

In view of the foregoing explanation for Unruh's claim with *mixed density matrix*, the calculation simply yields $D = 1$ and $V = 0$. This will be true if we label the paths by different polarization filters, or if we investigate a statistical mixture of two single path/slit experiments.

$\mathfrak{D}_1$: $|\psi_1| = \frac{1}{\sqrt{2}}$, $|\psi_2| = 0$,

$\mathfrak{D}_2$: $|\psi_1| = 0$, $|\psi_2| = \frac{1}{\sqrt{2}}$.

Thus the two paths 1 and 2 are *distinguishable* and they *do not quantum mechanically cross-interfere*. This cannot be said for the quantum coherent setup with both paths/slits unimpeded.

5.2 Pure state setup

The correct analysis of Unruh's and Afshar's setup suggests a *pure state density matrix*, and amplitudes for each of the exit gates being $|\psi_1| = |\psi_2| = \frac{1}{\sqrt{8}}$. Thus one gets $D = 0$ and $V = 1$:

$\mathfrak{D}_1$:$|\psi_1| = \frac{1}{\sqrt{8}}$, $|\psi_2| = \frac{1}{\sqrt{8}}$,

$\mathfrak{D}_2$:$|\psi_1| = \frac{1}{\sqrt{8}}$, $|\psi_2| = \frac{1}{\sqrt{8}}$.

The two paths 1 and 2 are *indistinguishable*, and they *quantum mechanically cross-interfere*.

6 Conclusions

It is wrongly believed that the lens at the image plane always provides "which way" information (Afshar [1, 2]; Drezet [5]). However we have shown that Afshar's analysis is inconsistent, and that the distinguishability and visibility in Afshar's setup are erroneously calculated by Afshar *and colleagues* [3]. The two peak image at the image plane in Afshar's setup, even without wire grid in the path of the photons, is an interference pattern and does not provide any "which way" information. Exact calculations for the lens setup have been performed by Qureshi [9] and Reitzner [10], showing that once the two paths interfere the interference cannot be undone, and the "which way" information cannot be regained. The probability distribution can look like the one in a mixed setup, but the retrospective reconstruction of the setup for times before the detector click must be done with interfering waves which do not carry the "which way" information. Afshar's mathematics is inconsistent, hence Afshar's setup does not disprove MWI, or any other rival interpretation of Quantum Mechanics that opposes the standard Copenhagen paradigm.

Submitted on March 01, 2007
Accepted on March 05, 2007
After correction: March 20, 2007

References

1. Afshar S. S. Violation of the principle of complementarity, and its implications. *Proceedings of SPIE*, 2005, v. 5866, 229–244; arXiv: quant-ph/0701027.
2. Afshar S. S. Violation of Bohr's complementarity: one slit or both? *AIP Conference Proceedings*, 2006, v. 810, 294–299; arXiv: quant-ph/0701039.
3. Afshar S. S., Flores E., McDonald K. F. and Knoesel E. Paradox in wave-particle duality. *Foundations of Physics*, 2007, v. 37(2), 295–305; arXiv: quant-ph/0702188.
4. Cramer J. G. The transactional interpretation of quantum mechanics. *Reviews of Modern Physics*, 1986, v. 58, 647–688.
5. Drezet A. Complementarity and Afshar's experiment. arXiv: quant-ph/0508091.
6. Elitzur A. C. and Vaidman L. Is it possible to know about something without ever interacting with it? *Vistas in Astronomy*, 1993, v. 37, 253–256.
7. Feynman R. P. and Hibbs A. R. Quantum physics and path integrals. McGraw-Hill, New York, 1965.
8. Penrose R. On gravity's role in quantum state reduction. *General Relativity and Gravitation*, 1996, v. 28(5), 581–600.
9. Qureshi T. Complementarity and the Afshar experiment. arXiv: quant-ph/0701109.
10. Reitzner D. Comment on Afshar's expriment. arXiv: quant-ph/0701152.
11. Tegmark M. and Wheeler J. A. 100 years of the quantum. *Scientific American*, 2001, v. 284, 68–75; arXiv: quant-ph/0101077.
12. Vedral V. Modern foundations of quantum optics. Imperial College Press, London (UK), 2001.
13. Unruh W. Quantum rebel. 2004, http://axion.physics.ubc.ca/rebel.html.
14. Zeh H. D. The meaning of decoherence. Lecture Notes in Physics, 2000, v. 538, 19–42; arXiv: quant-ph/ 9905004.

Upper Limit of the Periodic Table and Synthesis of Superheavy Elements

Albert Khazan
E-mail: albkhazan@list.ru

For the first time, using the heaviest possible element, the diagram for known nuclides and stable isotopes is constructed. The direction of search of superheavy elements is indicated. The Periodic Table with an eighth period is tabulated.

1 Shell construction of a nucleus, magic numbers

The nucleus of an atom is the central part of the atom, consisting of positively charged protons (Z) and electrically neutral neutrons (N). They interact by means of the strong interaction.

If a nucleus of an atom is consider as a particle with a certain number of protons and neutrons it is called a nuclide. A nuclide is that version of an atom defined by its mass number ($A = Z + N$), its atomic number (Z) and a power condition of its nucleus. Nuclei with identical numbers of protons but different numbers of neutrons are isotopes. The majority of isotopes are unstable. They can turn into other isotopes or elements due to radioactive disintegration of the nucleus by one of the following means: β-decay (emission of electron or positron), α-decay (emission of particles consisting of two protons and two neutrons) or spontaneous nuclear fission of an isotope. If the product of disintegration is also unstable, it too breaks up in due course, and so on, until a stable product is formed.

It has been shown experimentally that a set of these particles becomes particularly stable when the nuclei contain "magic" number of protons or neutrons. The stable structure can be considered as shells or spherical orbits which are completely filled by the particles of a nucleus, by analogy with the filled electronic shells of the noble gases. The numbers of particles forming such a shell are called "magic" numbers. Nuclei with magic number of neutrons or protons are unusually stable and in nuclei with one proton or other than a magic number, the neutron poorly binds the superfluous particle. The relevant values of these numbers are 2, 8, 20, 28, 50, 82, and 126, for which there exists more stable nuclei than for other numbers. Calculations indicate existence of a nucleus with filled shell at $Z = 114$ and $N = 184$ ($^{298}114$) which would be rather stable in relation to spontaneous division. There is experimental data for the connexion of magic numbers to a nucleus with $Z = 164$ [1, 2]. J. Oganesyan [3] has alluded to a Rutherford-model atom which assumes existence of heavy nuclei with atomic numbers within the limits of $Z \sim 170$. At the same time there is a point of view holding that superheavy elements (SHEs) cannot have $Z > 125$ [4]. In October 2006 in was reported that element 118 had been synthesized in Dubna (Russia), with atomic weight 293 [5]. (It is known however, that this weight is understated, owing to technical difficulties associated with the experiments.)

2 The N-Z diagram of nuclei, islands of stability

The search for superheavy nuclei, both in the Nature and by synthesis as products of nuclear reactions, has intensified. In the 1970's 1200 artificially produced nuclei were known [6]. Currently the number is $\sim$3000, and it is estimated that this will increase to $\sim$6500 [7].

In Fig. 1 the neutron-proton diagram of nuclei of stable and artificial isotopes [8–10] is presented.

Light stable or long-lived nuclei which arrangement can be arranged in a valley of stability as shown by small circles. The top set of border points represents a line of proton stability and bottom a line of neutron stability. Beyond these limits begins the so-called, "sea of instability". There is apparently only a narrow strip of stability for which there exists a quite definite parity, N/Z. For nuclei with atomic weight below 40, the numbers of protons and neutrons are approximately identical. With increase in the quantity of neutrons the ratio increases, and in the field of $A = (N + Z) = 250$ it reaches 1.6. The growth in the number of neutrons advances the quantity of protons in heavy nuclei, which in this case become energetically more stable. To the left of the stable nuclei are proton excess nuclei, and on the right neutron excess nuclei. These and others are called exotic nuclei.

The diagram terminates in the last element from the table IUPAC [11] at No. 114, with mass number 289, while scientists suspect nucleus No. 114–298. Such isotopes should possess the increased stability and lifetime of superheavy elements.

This diagram is specially constructed, only on the basis of tabulated data, but augmented by the theoretical upper limit of the Periodic Table [12]. Up to the $Z \sim 60$ the line of trend approaches the middle of a valley of stability, with $N/Z \sim 1.33$. Furthermore, N/Z increases steadily to $\sim$1.5 up to $Z \sim 100$. The equation of the line of trend represents a polynomial of the fourth degree. It is noteworthy that this implies rejection of the upper magic number for neutrons heretofore theoretically supposed.

It is particularly evident from Fig. 2, in which small fragment of the N–Z diagram is amplified and augmented with

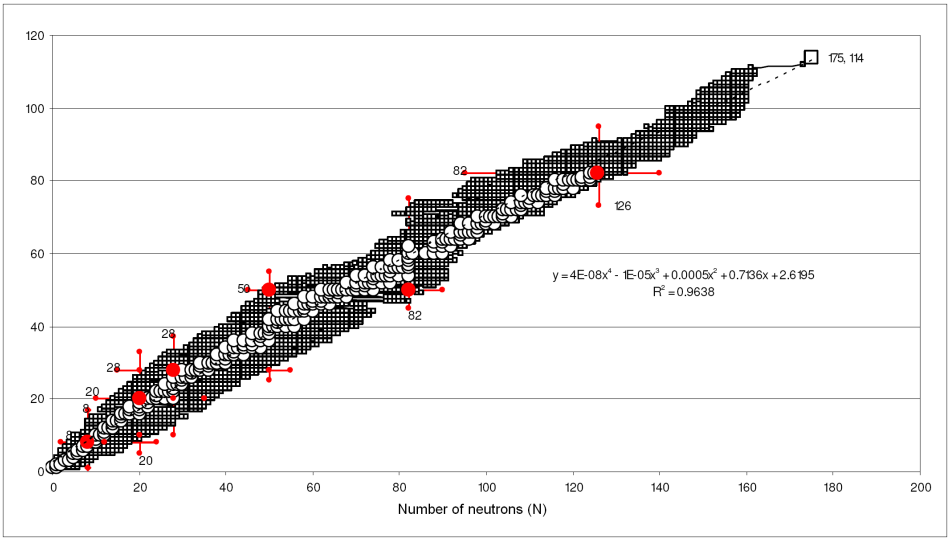

Fig. 1: N–Z diagram of nuclides.

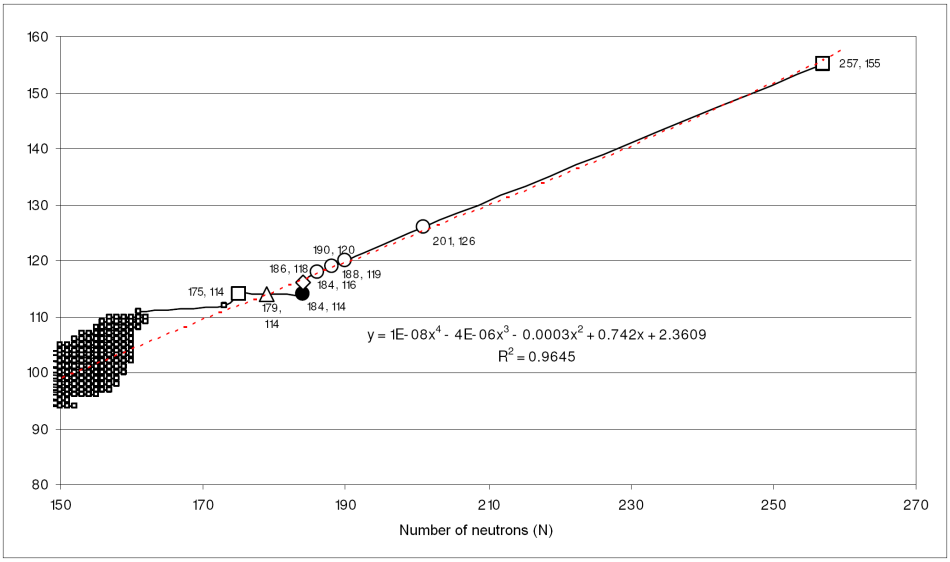

Fig. 2: N–Z diagram of nuclides with elements. For increase in scale the diagram is reduced after carrying out of a line of a trend.

some theoretically determined nuclei, including the heaviest element Z = 155, that the equations of lines of trend and the values of R^2 are practically identical in both Figures. When the line of trend for Fig. 1, without element 155, is extrapolated beyond Z = 114, it passes through the same point in Fig. 2 for Z = 155, indicating that element 155 is correctly placed by theory.

The predicted element No. 114–184 is displaced from the line of a trend. With a nuclear charge of 114 it should have 179 neutrons (A = 293) whereas 184 neutrons has atomic number 116. In the first case there is a surplus 5 neutrons, in the second a deficit of 2 protons. For an element 126 (on hypothesis) the mass number should be 310, but by our data it is 327. The data for mass number 310 corresponds to Z = 120.

It is important to note that there is a close relation between the mass number and the atomic weight. The author's formulation of the Periodic law of D. I. Mendeleev stipulates that the properties of elements (and of simple compounds) depend upon periodicity in mass number. It was established in 1913, in full conformity with the hypothesis of Van den Brook, that the atomic numbers of the chemical elements directly reflect the nuclear charge of their atoms. This law now has the following formulation: "properties of elements and simple substances have a periodic dependence on the nuclear charge of the atoms of elements".

In the Periodic Table the last, practically stable element is bismuth, Z = 83. The six following elements (No.'s 84 to 89) are radioactive and exist in Nature in insignificant quantities, and are followed by the significant radioactive ele-

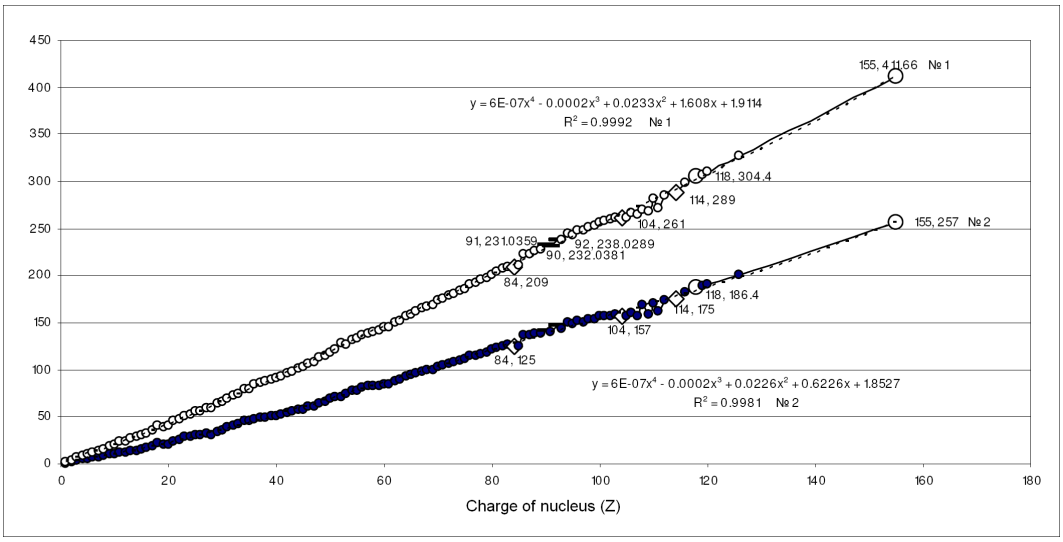

Fig. 3: Dependence of element mass number (1) and corresponding numbers of neutrons (2) on the atomic number in the Periodic Table.

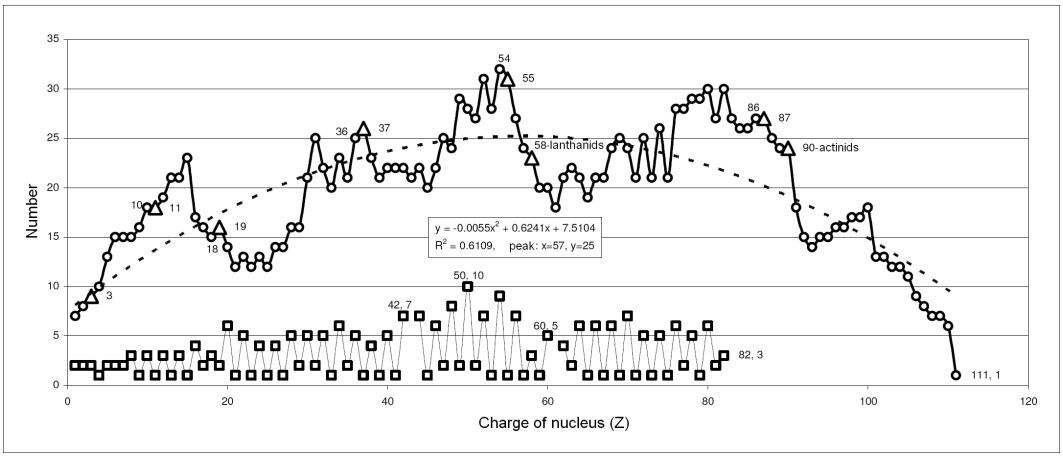

Fig. 4: Dependence of total isotopes (circle) and stable elements (square) on atomic number. The triangle designates the beginning of the periods.

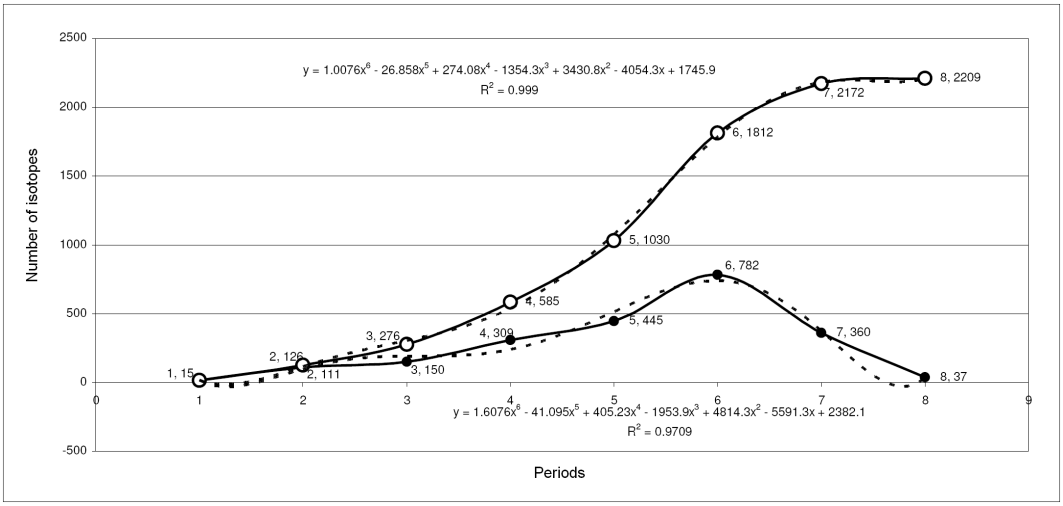

Fig. 5: Distribution of isotopes on the periods: an S-shaped summarizing curve, lower-quantity at each point.

1 H	2A 2											3A 13	4A 14	5A 15	6A 16	7A 17	2 He
3 Li	4 Be											5 B	6 C	7 N	8 O	9 F	10 Ne
11 Na	12 Mg	3B 3	4B 4	5B 5	6B 6	7B 7	8 8	8 9	8 10	1B 11	2B 12	13 Al	14 Si	15 P	16 S	17 Cl	18 Ar
19 K	20 Ca	21 Sc	22 Ti	23 V	24 Cr	25 Mn	26 Fe	27 Co	28 Ni	29 Cu	30 Zn	31 Ga	32 Ge	33 As	34 Se	35 Br	36 Kr
37 Rb	38 Sr	39 Y	40 Zr	41 Nb	42 Mo	43 Tc	44 Ru	45 Rh	46 Pd	47 Ag	48 Cd	49 In	50 Sn	51 Sb	52 Te	53 I	54 Xe
55 Cs	56 Ba	57 La	72 Hf	73 Ta	74 W	75 Re	76 Os	77 Ir	78 Pt	79 Au	80 Hg	81 Tl	82 Pb	83 Bi	84 Po	85 At	86 Rn
87 Fr	88 Ra	89 Ac	104 Rf	105 Db	106 Sg	107 Bh	108 Hs	109 Mt	110 Ds	111 Rg	112 Uub	113 Uut	114 Uuq	115 Uup	116	117	118

Table 1: The standard table of elements (long) with addition of the theoretical eighth period.

58 Ce	59 Pr	60 Nd	61 Pm	62 Sm	63 Eu	64 Gd	65 Tb	66 Dy	67 Ho	68 Er	69 Tm	70 Yb	71 Lu
90 Th	91 Pa	92 U	93 Np	94 Pu	95 Am	96 Cm	97 Bk	98 Cf	99 Es	100 Fm	101 Md	102 No	103 Lr

Table 2: Lanthanides (upper line) and actinides (lower line).

122	123	124	125	126	127	128	129	130	131	132	133	134	135	136	137	138	139
		140	141	142	143	144	145	146	147	148	149	150	151	152	153		

Table 3: The eight period: super actinides (18g and 14f elements)

119	120	121	154	**155** **Kh**

Table 4: The eight period: s-elements (No. 119, 120), g–elements (No. 121), d–elements (No. 154, 155). Element No. 155 must be analogous to Ta, as Db.

119	120	121	122	123	124	125	126	127	128	129	130	131	132	133	134	135	136
137	138	139	154	**155**													

140	141	142	143	144	145	146	147	148	149	150	151	152	153

Table 5: Variation of the Periodic Table of D. I. Mendeleev with heaviest element in the eighth period. A structure for super actinides is offered in a series in work [2].

ments thorium, protactinium and uranium (Z = 90, 91, and 92 respectively). The search for synthetic elements (No.'s 93 to 114) continues. In the IUPAC table, mass numbers for elements which do not have stable nuclides, are contained within square brackets, owing to their ambiguity.

It is clear in Fig. 3 that the reliability (R^2) of approximation for both lines of trend is close to 1. However, in the field of elements No. 104 to No. 114, fluctuations of mass number, and especially the number of neutrons, are apparent.

According to the table, the most long-lived isotope of an element violates the strict law of increase in mass number with increase in atomic number. To check the validity of element No. 155 in the general line of trend of elements for all known and theoretical [12] elements, the two following schedules are adduced:

1. For element numbers 1 to 114, $y = 1.6102\,x^{1.099}$ at $R^2 = 0.9965$;
2. For element numbers 1 to 155, $y = 1.6103\,x^{1.099}$ at $R^2 = 0.9967$.

Upon superposition there is a full overlapping line of trend that testifies to a uniform relation of dependences. Therefore, in analyzing products of nuclear reactions and in statement of experiment it is necessary to consider an element No. 155 for clarification of results.

3 The eighth period of the Periodic Table of elements

Our theoretical determination of the heaviest element at Z = 155 allows for the first time in science a presentation of Mendeleev's Table with an eighth period. Without going into details, we shall note that at the transuranium elements, electrons are located in seven shells (shells 1 to 7 inclusive), which in turn contain the subshells s, p, d, f. In the eighth period there is an 8th environment and a subshell g.

G. T. Seaborg and V. I. Goldanski, on the basis of the quantum theory, have calculated in the eighth period internal transitive superactinoid a series containing 5g-subshells for elements No. 121 to No. 138 and 6f subshells for No. 139 to No. 152. By analogy with the seventh period, No. 119 should be alkaline, No. 120 a alkaline ground metal, No. 121 similar to actinium and lanthanium, No. 153 to No. 162 contain a 7d subshell, and No. 163 to No. 168 an 8p subshell [2]. The latter class resulted because these scientists assumed the presence not only of an 8th, but also a 9th periods, with 50 elements in each.

However, distribution of isotopes depending on a atomic number of the elements (Fig. 4) looks like a parabola, in which branch Y sharply decreases, reaching the value 1 at the end of the seventh period. It is therefore, hardly possible to speak about the probability of 100 additional new elements when in the seventh period there is a set of unresolved problems.

Our problem consisted not so much in development of methods for prediction of additional elements, but in an explanation as to why their number should terminate No. 155. Considering the complexities of synthesis of heavy elements, we have hypothesized that their quantity will not be more than one for each atomic. Then, from Fig. 5 it can be seen that the S-figurative summarizing curve already in the seventh period starts to leave at a horizontal, and the eighth reaches a limit. The bottom curve shows that after a maximum in the sixth period the quantity of isotopes starts to decrease sharply. This provides even more support for our theoretical determination [12] of the heaviest possible element at Z = 155.

In July 2003 an International conference took place in Canada, resulting in publication [13], wherein it is asked, "Has the Periodic Table a limit?"

The head of research on synthesis of elements in Dubna (Russia), J. Oganesyan, has remarked that the question of the number of chemical elements concerns fundamental problems of science, and therefore the question, what is the atomic number of the heaviest element?

Despite the fact that hundreds of versions of the Periodic Table have been offered of the years, none have designated the identity of the heaviest element. The heaviest element is offered in Tables shown in Page 107.

4 Conclusions

With this **third paper** in a series on the upper limit of the Periodic Table of the Elements, the following are concluded.

1. As the fact of the establishment of the upper limit in Periodic Table of Elements until now is incontestable (on October, 25th 2005 appeared the first publication on the Internet), it is obviously necessary to make some correction to quantum-mechanical calculations for electronic configurations in the eighth period.
2. In modern nuclear physics and work on the synthesis of superheavy elements it is necessary to consider the existence of a heaviest element at Z = 155 with the certain mass number that follows from the neutron-proton diagram.
3. For discussion of the number of the periods and elements in them it is necessary to carry out further research into the seventh period.
4. From the schedules for distribution of isotopes, it is apparent that the end of the seventh period of elements is accounted for in units because of technical difficulties: No. 94 to No. 103 have been known for 20 years, and No. 104 to No. 116 for 40. Hence, to speak about construction of the Table of Elements with the eighth and ninth periods (100 elements), even for this reason, is not meaningful.

5. The variants of the Periodic Table of Mendeleev constructed herein with inclusion of the heaviest element No. 155 opens a creative path for theoretical physicists and other scientists for further development of the Table.

Submitted on March 01, 2007
Accepted on March 07, 2007

References

1. Maria Goeppert Mayer. Nuclear shell structure. In: *Modern Physics for the Engineer*, McGraw Hill, 1961, p. 40.
2. Seaborg G. T. and Bloom J. L. The synthetic elements. *Scientific American*, 1969, v. 220, No. 4, 56.
3. Oganesyan Y. Islands of stability. *The World of Science*, March 2005, No. 3.
4. Giacobbe F. W. Relativistic effects in limiting the atomic number of superheavy elements. *EJTR*, 2004, v. 1, 1–8.
5. *The Moscow News*, No. 40(1357), 20–26 October 2006.
6. James Rayford Nix. Prediction for superheavy nuclei. *Phys. Today*, 1972, v. 25(4), 30.
7. Ishhanov B. S. and Kebin E. I. Exotic nuclei. Moscow University Press, Moscow, 2002.
8. Brookhaven National Laboratory. Table of Nuclides. http://en.wikipedia.org/wiki/Tables_of_nuclides; http://en.wikipedia.org/wiki/Isotope_table_divided.
9. Tsypenyak Y. A valley of nuclear stability. *Sorovsky Educational Magazine*, 1999, v. 5, 85–90.
10. Tsypenyak Y. Division of nuclei. *Sorovsky Educational Magazine*, 1999, v. 6, 90–96.
11. Atomic weights of the elements 2001. *IUPAC — Commission on Atomic Weights and Isotopic Abundance.*
12. Khazan A. Upper limit in the Periodic System of Elements. *Progress in Physics*, 2007, v. 1, 38–41.
13. The Periodic Table: Into the 21st Century. D. H. Rouvray and R. B. King (Eds.), Research Studies Press, Baldock (UK).

The Journal on Advanced Studies in Theoretical and Experimental Physics, including Related Themes from Mathematics

PROGRESS IN PHYSICS

A quarterly issue scientific journal, registered with the Library of Congress (DC, USA). This journal is peer reviewed and included in the abstracting and indexing coverage of: Mathematical Reviews and MathSciNet (AMS, USA), DOAJ of Lund University (Sweden), Zentralblatt MATH (Germany), Referativnyi Zhurnal VINITI (Russia), etc.

To order printed issues of this journal, contact the Editors.

Electronic version of this journal can be downloaded free of charge from the web-resources:
http://www.ptep-online.com
http://www.geocities.com/ptep_online

Postal address for correspondence:

Chair of the Department
of Mathematics and Science,
University of New Mexico,
200 College Road,
Gallup, NM 87301, USA

ISSN: 1555-5534 (print)
ISSN: 1555-5615 (online)

Standard Address Number: 297-5092
Printed in the United States of America

JULY 2007 **VOLUME 3**

CONTENTS

Information for Authors and Subscribers

Progress in Physics has been created for publications on advanced studies in theoretical and experimental physics, including related themes from mathematics and astronomy. All submitted papers should be professional, in good English, containing a brief review of a problem and obtained results.

All submissions should be designed in LaTeX format using *Progress in Physics* template. This template can be downloaded from *Progress in Physics* home page http://www.ptep-online.com. Abstract and the necessary information about author(s) should be included into the papers. To submit a paper, mail the file(s) to the Editor-in-Chief.

All submitted papers should be as brief as possible. Commencing 1st January 2006 we accept brief papers, no larger than 8 typeset journal pages. Short articles are preferable. Papers larger than 8 pages can be considered in exceptional cases to the section *Special Reports* intended for such publications in the journal. Letters related to the publications in the journal or events among the science community can be applied to the section *Letters to Progress in Physics*.

All that has been accepted for the online issue of *Progress in Physics* is printed in the paper version of the journal. To order printed issues, contact the Editors.

This journal is non-commercial, academic edition. It is printed from private donations. (Look for the current author fee in the online version of the journal.)

On the Earth Microwave Background: Absorption and Scattering by the Atmosphere

Pierre-Marie Robitaille

Dept. of Radiology, The Ohio State University, 130 Means Hall, 1654 Upham Drive, Columbus, Ohio 43210, USA

E-mail: robitaille.1@osu.edu

The absorption and scattering of microwave radiation by the atmosphere of the Earth is considered under a steady state scenario. Using this approach, it is demonstrated that the microwave background could not have a cosmological origin. Scientific observations in the microwave region are explained by considering an oceanic source, combined with both Rayleigh and Mie scattering in the atmosphere in the absence of net absorption. Importantly, at high frequencies, Mie scattering occurs primarily with forward propagation. This helps to explain the lack of high frequency microwave background signals when radio antennae are positioned on the Earth's surface.

1 Introduction

The absorption of radiation by the atmosphere of the Earth has been highly studied and exploited [1–3]. In the visible region, atmospheric absorption accounts for significant deviations of the solar spectrum from the thermal lineshape. These deviations are removed when viewing the spectrum from the outer atmosphere. Under these conditions, the solar spectrum now differs from the ideal lineshape only slightly. The remaining anomalies reflect processes associated with the photosphere itself.

In the microwave region, absorption of radiation is primarily associated with reversible quantum transitions in the vibrational-rotational states of gaseous molecules, particularly oxygen and water. Intense absorption occurs in several bands. The high frequency microwave bands are consequently less suited for signal transmission to, or from, satellites [1].

2 The Microwave Background

The microwave background [4] is currently believed to be of cosmic origin. The Earth is viewed as immersed in a bath of signal arising continuously from every possible direction, without directional preference. This is an intriguing physical problem in that it represents a steady state condition, not previously considered relative to atmospheric absorption. Indeed, all other atmospheric absorption problems involve sources which are temporally and spatially dependent. Such sources are radically different from the steady state.

Since the microwave background is temporally continuous and spatially isotropic, and since the vibrational-rotational transitions of gases are reversible, the steady state scenario leads to the absence of net absorption of microwave radiation in the atmosphere. An individual absorbing species, such as molecular oxygen or water, acts simply as a scatterer of radiation. Any radiation initially absorbed will eventually be re-emitted. There can be no net absorption over time. Only the effects of direct transmission and/or scattering can exist. Herein lies the problem for assigning the microwave background to a cosmic origin. The steady state results in a lack of net absorption by the atmosphere. Thus, if the signal was indeed of cosmic origin, there could be no means for the atmosphere to provide signal attenuation at high frequency. Assuming frequency independent scattering, a perfect thermal spectrum should have been received, even on Earth. Nonetheless, the high frequency components of the microwave background, on the ground, are seriously attenuated. Only at the position of the COBE satellite has a nearly perfect thermal spectrum been recorded [5].

3 Oceanic origin of the Microwave Background

It has previously been advanced that the microwave background is of oceanic origin [6–8]. Under this hypothesis, the oceans of the Earth are emitting a signal which mimics a blackbody source. This radiation is being emitted over all possible angles. The path length that radiation travels through the atmosphere can therefore be quite substantial, especially at the lower emission angles. Arguably, this oceanic signal, with its 2.7 K apparent temperature, indirectly reflects the presence of translational and rotational degrees of freedom in the liquid. The weak hydrogen bonds between water molecules, and their associated vibrational degrees of freedom, are likely to be the underlying physical oscillators fundamentally responsible for this spectrum.

At low frequencies, oceanic radiation travels into the atmosphere where Rayleigh scattering may occur. This results in a substantial fraction of backscattering, since Rayleigh scattering is multidirectional. Consequently, the low frequency signals can easily be detected on Earth. However, at high microwave frequencies, Mie scattering dominates increasingly. Mie scattering, at the elevated frequencies, results primarily in forward propagation of the incident signal. The presence of forward scattering accounts for the lack of high frequency signals detected for the microwave background on

Earth. Forward scattering produces a preferential directionality away from the surface of the Earth. The variation of atmosperic density with elevation may also contribute to this observation. As a result, the high frequency portion of the microwave background is not well detected from the Earth. Since the problem is once again in the steady state regimen, there can be no net absorption in the atmosphere. Given sufficient scattering at all frequencies, at the position of COBE [5], the signal examined must be isotropic. At elevated frequencies, perfect scattering of the oceanic signals is being ensured by the absorption and re-emission of radiation by atmospheric gases. These processes follow substantial forward scattering. Of course, Rayleigh scattering is also being produced by small matter and scatterers in the lower atmosphere, particularly for the lower frequencies.

4 Conclusion

Given steady state, there can be no net absorption of microwave signals by the atmosphere. Yet, on Earth, the microwave background cannot be properly detected in the high frequency region. This directly implies that the microwave background cannot arise from the cosmos. Conversely, if one considers that the signal is oceanic in nature, the observed behavior of the microwave background on Earth is easily explained using a combination of absorption, re-emission, Rayleigh and Mie scattering, wherein forward propagation is also invoked. An oceanic signal followed by scattering also helps to explain the phenomenal signal to noise observed by the COBE FIRAS instrument [5]. Powerful signals imply proximal sources. This constitutes further evidence that the microwave background [4] is of Earthly origin [6–8]. We will never know the temperature of the Universe.

Dedication

This work is dedicated to Patricia Anne Robitaille.

Submitted on March 14, 2007
Accepted on March 16, 2007
First published online on March 17, 2007

References

1. Ulaby F. T., Moore R. K. and Fung A. K. Microwave remote sensing active and passive. Volume 1–3. London, Artech House, 1981–1986.
2. Janssen M. A. Atmospheric remote sensing by microwave radiometry. John Wiley, New York, 1993.
3. Iribane J. V. and Cho H.-R. Atmospheric physics. D. Reidel, Dodrecht, Holland, 1980.
4. Penzias A. A. and Wilson R. W. A measurement of excess antenna temperature at 4080 Mc/s. *Astrophys. J.* 1965, v. 1, 419–421.
5. Fixen D. L., Gheng E. S., Gales J. M., Mather J. C., Shafer R. A. and Wright E. L. The Cosmic Microwave Background spectrum from the full COBE FIRAS data set. *Astrophys. J.*, 1996, v. 473, 576–587.
6. Robitaille P.-M. L. The collapse of the Big Bang and the gaseous Sun. *New York Times*, March 17, 2002 (accessed online from http://www.thermalphysics.org/pdf/times.pdf).
7. Robitaille P.-M. L. On the origins of the CMB: insight from the COBE, WMAP, and Relikt-1 Satellites. *Progr. in Phys.*, 2007, v. 1, 19–23.
8. Rabounski D. The relativistic effect of the deviation between the CMB temperatures obtained by the COBE satellite. *Progr. in Phys.*, 2007, v. 1, 24–26.

Phase-Variation Enhancement on Deuteron Elastic Scattering from Nuclei at Intermediate Energies

A. S. Shalaby* and M. M. H. El-Gogary†

*Physics Department, Faculty of Science, Beni Suef University, Egypt
†Physics Department, Faculty of Science, Cairo University, Egypt
All correspondence should be made to A. S. Shalaby. E-mail: Ashalaby15@yahoo.com

Within the modified formalism of Glauber's multiple scattering theory, we have studied the elastic scattering of deuteron with nuclei in the mass region $6 \leqslant B \leqslant 72$ at intermediate energies. We have calculated the differential cross-section with and without invoking the phase-variation parameter into the nucleon-nucleon (NN) scattering amplitude and compared our results with the corresponding experimental data. We found that the presence of the phase-variation improves our results, especially at the minima of the diffraction patterns.

1 Introduction

In the interaction of a light ion with nuclei, elastic scattering is the largest of all partial cross sections. For projectile energies sufficiently above the Coulomb barrier, the elastic angular distribution is dominated by a diffractionlike pattern. It was realized [1] that this phenomenon is due to the finite size of the nucleus and the fact that nuclei are "partially trnsparent". One of the most important approaches used to describe such collisions is the Glauber's multiple scattering theory (GMST) [2–4]. The theory is based on high-energy approximation, in which the interacting particles are almost frozen in their instantaneous positions during the passage of the projectile through the target. As a result, the nucleon-nucleus and nucleus-nucleus scattering amplitudes are simply expressed in terms of the free nucleon-nucleon (NN) ones. The preliminary applications of this theory were found to have great successes in reproducing the hadron-nucleus scattering data [5–13]. The confidence in this theory encouraged the extension of its application to nucleus-nucleus collisions but this was faced with computational difficulties [14–19] for collisions between two nuclei of mass numbers A, $B \geqslant 4$. The series describing these collisions contains numerous $(2^{A\times B}-1)$ terms so that its complete summation is extensive. Moreover, the higher order multiple scatterings involve multi-dimensional integrals, which are cumbersome to be evaluated, even if one uses simple Gaussian forms for the nuclear densities and NN scattering amplitudes. These drawbacks were overcomed in the works of many authors like Yin et al. [20, 21], Franco and Tekou [14], Huang [22] and El-Gogary et al. [23–25]. Their results describe more satisfactorily the scattering data for the elastic collisions considered there except smaller shifts were found to exist around the diffraction patterns.

Our previous works dealt with studies the elastic scattering of hadrons either with stable nuclei [26, 27] or exotic nuclei [28]. The results are found to be good except around the diffraction pattern (as the previous authors showed) where overall shifts are still persists. It is of special interest to probe the validity of the Glauber multiple scattering theory for the elastic scattering of deuterons (which are weakly bound composite particles) with nuclei.

The essential feature of the presently proposed method is the use of a phase variation of the nucleon-nucleon elastic scattering amplitude which agrees with the empirical amplitude at low q's at the appropriate energy and its large-q behaviour is left adjustable in terms of one free parameter. The effect of the phase variation is to eliminate minima or to make them shallower and to generally increase cross-sections even at the momentum transfers where no minima originally occurred [29, 30]. Franco and Yin [31, 32] have suggested that the phase of the NN scattering amplitude should vary with the momentum transfer. So far the physical origin of this phase variation has not been settled. This phase modifies the ratio of the real part to the imaginary part of the forward amplitude and makes the diffraction pattern shallower.

Our present work is directed toward two ways; first, we have studied the elastic scattering of deuteron with nuclei in the mass region $6 \leqslant B \leqslant 72$ using the GMST where both the full multiple scattering series of the Glauber amplitude and the consistent treatment of the center-of-mass (c.m.) correlations are simultaneously employed. Second, as a result of the shifts appeared around the diffraction patterns in the previous works mentioned above, it is helpful to study the role of the phase-variation parameter of the NN scattering amplitude as invoked in this work. The theoretical formulas used to do the above calculations are given in Section 2. Section 3 includes the results and their discussions. The conclusion is summarized in Section 4. The orbits, lengths and Δ-matrices required for carrying out the above calculations are exhibited in the appendix.

2 Theoretical framework

This section is devoted to obtain the expression for the angular distribution ($\frac{d\sigma}{d\Omega}$ or $\frac{\sigma}{\sigma_{RUTH}}$) for the elastic scattering of deuteron with medium-weighted nuclei using Glauber's multiple scattering theory. This expression is developed by

taking into account both the full series expansion of the Glauber amplitude and the consistent treatment of the center-of-mass correlation.

In this theory, the elastic scattering amplitude between deuteron of mass number A and a target nucleus of mass number B and atomic number Z_B is given as [16]

$$F_{dB}(\vec{q}) = \frac{ik}{2\pi}\,\Theta(\vec{q})\int d\vec{b}\exp(i\vec{q}\cdot\vec{b})\Big\{1-\exp\big(i\chi_{dB}(\vec{b})\big)\Big\} \quad (1)$$

where, $\vec{q}$ is the momentum transferred from the deuteron to the target nucleus B, $\vec{k}$ is the incident momentum of the deuteron, and $\vec{b}$ is the impact parameter vector. $\Theta(\vec{q})$ arising from the effect of the center-of-mass correlations [16] and it was found to has an exponential form of q-squared [17]. $\chi_{dB}(\vec{b})$ is the nuclear phase-shift function resulting from the interaction between the deuteron and a target nucleus B and it is given by,

$$\begin{aligned}\exp\big[i\chi_{dB}(\vec{b})\big] = &< \Psi_d(\{\vec{r}_i'\})\,\Psi_B(\{\vec{r}_j'\})\\ &\big|\exp\big[i\chi_{dB}(\vec{b},\{\vec{s}_i'\},\{\vec{s}_j'\})\big]\big|\ \Psi_d\Psi_B>,\end{aligned} \quad (2)$$

where, $\Psi_d(\{\vec{r}_i'\})\lfloor\Psi_B(\{\vec{r}_j'\})\rfloor$ is the deuteron (target) wave functions that depends on the position vectors $\{\vec{r}_i\}\lfloor\{\vec{r}_j'\}\rfloor$ of the deuteron (target) nucleons whose projections on the impact parameter plane are $\{\vec{s}_i\}\lfloor\{\vec{s}_j'\}\rfloor$.

In Eq. (1), the effect of the center-of-mass correlation is treated as a global correction (denoted by $\Theta(\vec{q})$) multiplied by the scattering amplitude. Because $\Theta(\vec{q})$ leads to unphysical divergence as q goes to high values, Franco and Tekou [14] have overcomed this drawback by incorporating it in each order of the optical phase-shift expansion. Such treatment has modified the phase-shift function to a new form, which is simply expressed in terms of the uncorrelated one.

Thus, Eq. (1) becomes

$$F_{dB}(\vec{q}) = \frac{ik}{2\pi}\int d\vec{b}\exp(i\vec{q}\cdot\vec{b})\Big\{1-\exp\big(i\bar{\chi}_{dB}(\vec{b})\big)\Big\}, \quad (3)$$

where the modified phase-shift function $\bar{\chi}_{dB}(\vec{b})$ (which is referred here by adding a bar sign on the corresponding uncorrelated one) can be written in terms of the uncorrelated one, $\chi_{dB}(\vec{b})$, as [16, 17]

$$\begin{aligned}&\exp\big[i\bar{\chi}_{dB}(\vec{b})\big] =\\ &=\int_0^\infty J_0(qb)\Theta(q)qdq\int_0^\infty J_0(qb')\exp\big[i\bar{\chi}_{dB}(\vec{b}')\big]b'db',\end{aligned} \quad (4)$$

By taking into account the Coulomb phase-shift function in addition to the nuclear one, we can write

$$\begin{aligned}\bar{\chi}_{dB}(\vec{b}) &= \bar{\chi}_n(\vec{b}) + \bar{\chi}_C(\vec{b}) =\\ &= \bar{\chi}_n(\vec{b}) + \bar{\chi}_C^{pt}(\vec{b}) + \bar{\chi}_C^{E}(\vec{b}),\end{aligned} \quad (5)$$

where $\bar{\chi}_C^{pt}(\vec{b})$ is the modified point charge correction to the Coulomb phase-shift function, which is equal to $2n\ln\left(\frac{b}{2a}\right)$, a is equal to $\frac{1}{2k}$, $n=\frac{Z_B e^2}{\hbar v}$ is the usual Coulomb parameter and $\bar{\chi}_C^{E}(\vec{b})$ is the modified extended charge correction to the Coulomb phase shift function. $\bar{\chi}_n(\vec{b})$ is the modified nuclear interaction phase-shift function.

From Eqs. (3) and (5), we find [16, 25]

$$\begin{aligned}F_{dB}(\vec{q}) = f_C^{pt}(q) + i\int_0^\infty (kb)^{2in+1}\times\\ \times\Big\{1-\exp\big(i\bar{\chi}_C^{E}(\vec{b})+i\bar{\chi}_n(\vec{b})\big)\Big\}\,J_0(qb)db\,.\end{aligned} \quad (6)$$

Assuming the projectile (deuteron) and target ground state wave functions to have the form:

$$\Psi_{i=d,B}(\{\vec{r}_j\}) = \xi_i(\vec{R}_i)\,\Phi_i(\{\vec{r}_j^{\,int}\}),\vec{r}_j^{\,int} = \vec{r}_j - \vec{R}_i, \quad (7)$$

where $\xi_i(\vec{R}_i)$, where $i=d,B$, are the wave functions describing the center-of- mass motions of the deuteron and target nucleons, respectively. Accordingly, the center-of-mass correlation function $\Theta(\vec{q})$ is found to has the form

$$\Theta(\vec{q}) = \Big[<\xi_d(\vec{R}_d)\,\xi_B(\vec{R}_B)\,|\,e^{i\vec{q}(\vec{R}_d-\vec{R}_B)}|\,\xi_d\xi_B>\Big]^{-1}, \quad (8)$$

Now, we need to describe the wave function of the system to perform the integrations of Eqs. (2) and (8). Consider the approximation in which the nucleons inside any cluster and the clusters themselves inside the nucleus are completely uncorrelated. Then, we can write

$$|\Psi_d\Psi_B|^2 = \Pi_{i=1}^{M_A}\Pi_{\alpha=1}^{M_N}\rho_d(\vec{r}_{i\alpha})\,\Pi_{j=1}^{M_B}\Pi_{\delta=1}^{M_N}\rho_B(\vec{r}_{j\delta}'), \quad (9)$$

where ρ_d and ρ_B are the normalized single particle density functions and are chosen in the present work to be of the single-Gaussian density which is given as [25, 26, 28]

$$\rho_\gamma(\vec{r}) = \left(\frac{\alpha_\gamma^2}{\pi}\right)^{3/2}\exp(-\alpha_\gamma^2 r^2), \quad \gamma = d, B, \quad (10)$$

where α_γ is related to the rms radius by

$$\alpha_\gamma = \sqrt{\frac{3}{2}}\left(\frac{1}{<r_\gamma^2>^{1/2}}\right).$$

With the aid of the NN scattering amplitude, $f_{NN}(\vec{q})$, which is given as [22, 32]

$$f_{NN}(\vec{q}) = \frac{k_N\sigma}{4\pi}(i+\rho)\exp\left(\frac{-aq^2}{2}\right), \quad (11)$$

where, k_N is the momentum of the incident particle, σ, is the total cross-section and ρ is the ratio of the real to the imaginary parts of the forward scattering amplitude. a is taken to be complex; $a=\beta^2+i\gamma^2$, where β^2 is the slope parameter of the elastic scattering differential cross-section, and γ^2 is a free parameter introducing a phase variation of the elemental scattering amplitude, adopting the wave function (9) with the density (10) and following the same procedures as that given in Ref. [25], we can perform the

integrations in Eqs. (8) and (2) analytically and get

$$\Theta_s(q) = \exp\left[\frac{q^2}{4}\left(\frac{1}{A\alpha_d^2}+\frac{1}{B\alpha_B^2}\right)\right] \tag{12}$$

and

$$\exp\big[i\chi_n(b)\big] = 1+\sum_{\mu_1=1}^{M_1}\sum_{\lambda_{\mu_1}} T_1(\mu_1,\lambda_{\mu_1})\times \\ \times\,\Pi_{i=1}^{M_A}\Pi_{j=1}M_B\{Z_S\}^{\Delta_{ij}(\mu_1,\lambda_{\mu_1})}, \tag{13}$$

where Z_S has the reduced form

$$Z_S = C_{dB}\sum_{\mu_2=1}^{M_2}\sum_{\lambda_{\mu_2}} T_2(\mu_2,\lambda_{\mu 2})[-g]^{\mu_2}\times \\ \times\, R_S[\mu_2,\lambda_{\mu 2},\Delta(\mu_2,\lambda_{\mu 2}),0,0,\ldots]\times \\ \times\left(\exp\{-W_S[\mu_2,\lambda_{\mu 2},\Delta(\mu_2,\lambda_{\mu 2}),0,0,\ldots]\,b^2\}\right),$$

with

$$C_{dB} = \left[\frac{\alpha_d^2\,\alpha_B^2}{\pi^2}\right]^{M_N}$$

The various functions (Θ, Z, R and W) are marked by the subscript s to refer to the employed single-Gaussian density. Incorporating the c.m. correlation, the modified phase-shift function $\bar{\chi}_n(\vec{b})$ can be expressed as

$$\exp\big[i\bar{\chi}_n(b)\big] = 1+\sum_{\mu_1=1}^{M_1}\sum_{\lambda_{\mu_1}} T_1(\mu_1,\lambda_{\mu_1})\times \\ \times\,\Pi_{i=1}^{M_A}\Pi_{j=1}^{M_B}\{\bar{Z}_S\}^{\Delta_{ij}(\mu_1,\lambda_{\mu_1})}, \tag{14}$$

The form of $\bar{Z}_S$ is obtained by inserting the expressions of Z_S and $\Theta_S(\vec{q})$ into Eq. (4), yielding

$$\bar{Z}_S = C_{dB}\sum_{\mu_2=1}^{M_2}\sum_{\lambda_{\mu_2}} T_2(\mu_2,\lambda_{\mu 2})[-g]^{\mu_2}\times \\ \times\,\bar{R}_S[\mu_2,\lambda_{\mu 2},\Delta(\mu_2,\lambda_{\mu 2}),0,0,\ldots]\times \\ \times\left(\exp\{-\bar{W}_S[\mu_2,\lambda_{\mu 2},\Delta(\mu_2,\lambda_{\mu 2}),0,0,\ldots]\,b^2\}\right), \tag{15}$$

with

$$\bar{W}_s = \left[\frac{1}{W_s}-\left(\frac{1}{A\alpha_d^2}+\frac{1}{B\alpha_B^2}\right)\right]^{-1} \text{ and } \bar{R}_s = \frac{R_s\times\bar{W}_s}{W_s}$$

Finally, the modified extended charge correction to the Coulomb phase — shift, $\bar{\chi}_C^E(b)$, has already been derived analytically in Ref. [16] for a single-Gaussian density where it was found to have the form

$$\bar{\chi}_C^E(b) = nE_1(b^2/\bar{R}^2) \tag{16}$$

where $E_1(z)$ is the exponential integral function and,

$$\bar{R}^2 = R_d^2(1-A^{-1})+R_B^2(1-B^{-1}),\ \ R_d^2=\frac{1}{\alpha_d^2},\ \ R_B^2=\frac{1}{\alpha_B^2}.$$

With the results of Eqs. (14), (15) and (16), the scattering amplitude $F_{dB}(q)$ can be obtained by performing the integration in Eq. (6) numerically. Whence, the angular distribution of the elastic scattering is given by

$$\frac{d\sigma(q)}{d\Omega} = \big|F_{dB}(q)\big|^2. \tag{17}$$

The point change approximation of the coulomb amplitude $f_c^{pt}(\vec{q})$, is given as [33]

$$f_c^{pt}(q) = -2nkq^{-2}\times \\ \times\,\exp\big\{-i\big[2n\ln(qa)-2\arg\Gamma(1+in)\big]\big\}. \tag{18}$$

The Rutherford formula for the differential cross section, σ_{RUTH} is then given by

$$\sigma_{RUTH} = |f_c^{pt}(q)|^2 = 4n^2k^2q^{-4}, \tag{19}$$

where a, n, k, q have the same definitions that given above.

E/A (MeV/nucleon)	σ_{NN} (fm^2)	ρ_{NN}	β^2 (fm^2)
25	24.1	0.85	0.8258599
40	13.5	0.9	0.4861189
60	9.15	1.1725	0.3755747
85	6.1	1.0	0.2427113
342.5	2.84	0.26	0.045

Table 1: Parameters of the Nucleon-Nucleon amplitude [34, 35].

3 Results and discussion

To examine the simple analysis presented in the above section, we have calculated the differential cross section for a set of elastic nuclear reactions, like, d-$_3$Li^6, d-$_8$O^{16}, d-$_{23}$V^{50}, d-$_{32}$Ge^{70} and d-$_{32}$Ge^{72} at incident energies 171 MeV, d-$_6$C^{12} at 110, 120 and 170 MeV, d-$_{16}$S^{32} at 52 and 171 MeV, d-$_{20}$Ca^{40} at 52 and 700 MeV, d-$_{28}$Ni^{58} at 80, 120 and 170 MeV and d-$_{12}$Mg^{24} at 170MeV. The ingredients needed to perform these calculations are the parameters associated with the NN scattering amplitude and the nuclear densities as well as the orbits, lengths and Δ-matrices of the groups $G_1 = S_{M_A}\otimes S_{M_B}$ and $G_2 = S_{M_N}\otimes S_{M_N}$. For the above energies, we used the values of the NN parameters given in Table 1.

The values of the parameters α_γ, after correcting for the effects of the finite proton-size and the c.m. recoil, are [16]

$$\alpha_\gamma^2 = \frac{3}{2}\left(\frac{1-\frac{1}{\gamma}}{<r_\gamma^2>-<r_p^2>}\right), \qquad \gamma = A, B,$$

where $<r_\gamma^2>$ and $<r_p^2>$ are the mean square radii of the deuteron, target nucleus and the proton, respectively. The values of the rms radii we have used for the present nuclei and the proton are given in Table 2.

The cluster structure specific to the considered reactions and the corresponding orbits, lengths and Δ-matrices are exhibited in Appendix.

The results obtained from these calculations for the considered reactions are shown as dashed curves in Figs. 1–16. Fig. 1 contains the result obtained for d-$_3$Li^6 reaction at incident energy 171 MeV. We can see from this figure that the predicted angular distribution satisfactorily agree the scatter-

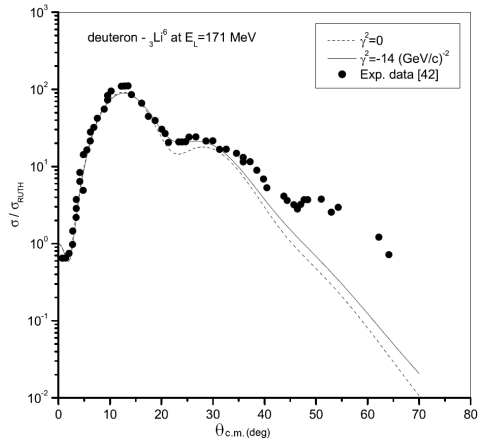

Fig. 1: Plots the elastic differential cross section (σ/σ_{RUTH}) versus scattering angle for the deuteron-$_3Li^6$ reaction at incident energy 171 MeV. The dashed curve is the constant phase result ($\gamma^2 = 0$) while the solid curve is obtained with phase variation ($\gamma^2 = -14$ (GeV/c)$^{-2}$). The dots are the experimental data [42].

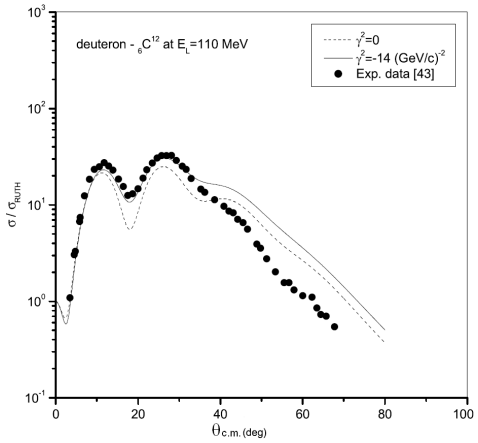

Fig. 2: Plots the elastic differential cross section (σ/σ_{RUTH}) versus scattering angle for the deuteron-$_6C^{12}$ reaction at incident energy 110 MeV. The dashed curve is the constant phase result ($\gamma^2 = 0$) while the solid curve is obtained with phase variation ($\gamma^2 = -14$ (GeV/c)$^{-2}$). The dots are the experimental data [43].

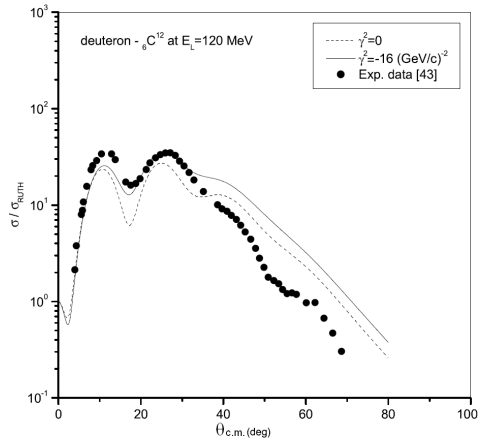

Fig. 3: Plots the elastic differential cross section (σ/σ_{RUTH}) versus scattering angle for the deuteron-$_6C^{12}$ reaction at incident energy 120 MeV. The dashed curve is the constant phase result ($\gamma^2 = 0$) while the solid curve is obtained with phase variation ($\gamma^2 = -16$ (GeV/c)$^{-2}$). The dots are the experimental data [43].

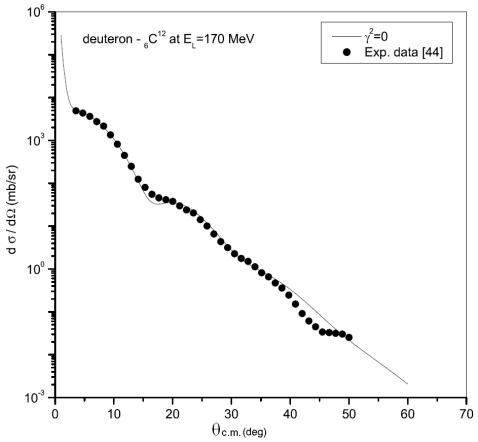

Fig. 4: Plots the elastic differential cross section ($d\sigma/d\Omega$) versus scattering angle for the deuteron-$_6C^{12}$ reaction at incident energy 170 MeV. The solid curve is the constant phase result ($\gamma^2 = 0$). The dots are the experimental data [44].

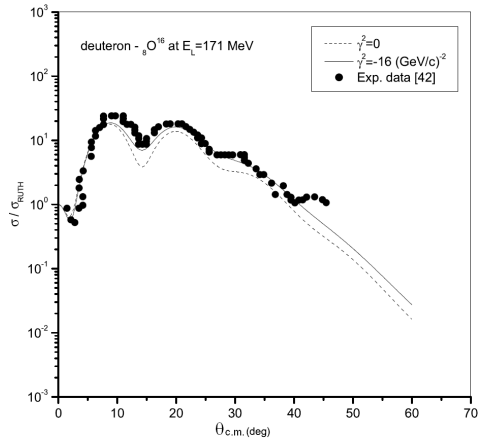

Fig. 5: Plots the elastic differential cross section (σ/σ_{RUTH}) versus scattering angle for the deuteron-$_8O^{16}$ reaction at incident energy 171 MeV. The dashed curve is the constant phase result ($\gamma^2 = 0$) while the solid curve is obtained with phase variation ($\gamma^2 = -16$ (GeV/c)$^{-2}$). The dots are the experimental data [42].

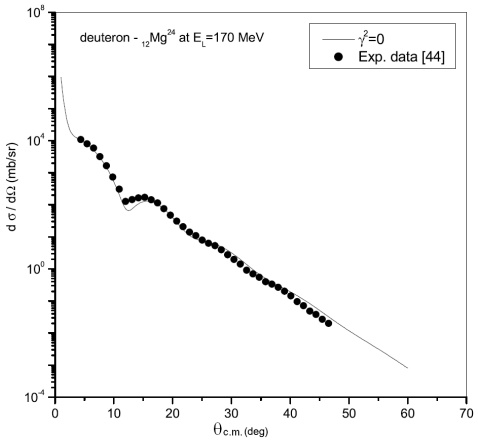

Fig. 6: Plots the elastic differential cross section ($d\sigma/d\Omega$) versus scattering angle for the deuteron-$_{12}Mg^{24}$ reaction at incident energy 170 MeV. The solid curve is the constant phase result ($\gamma^2 = 0$). The dots are the experimental data [44].

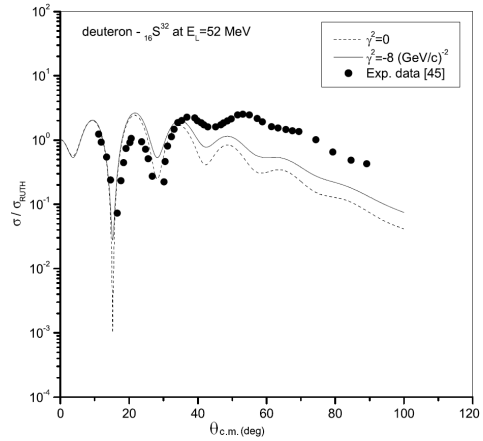

Fig. 7: Plots the elastic differential cross section (σ/σ_{RUTH}) versus scattering angle for the deuteron-$_{16}S^{32}$ reaction at incident energy 52 MeV. The dashed curve is the constant phase result ($\gamma^2 = 0$) while the solid curve is obtained with phase variation ($\gamma^2 = -8$ (GeV/c)$^{-2}$). The dots are the experimental data [45]

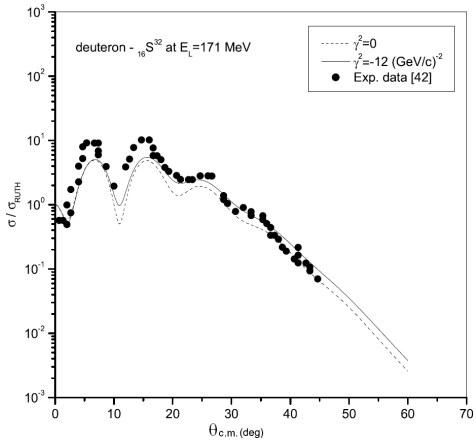

Fig. 8: Plots the elastic differential cross section (σ/σ_{RUTH}) versus scattering angle for the deuteron-$_{16}S^{32}$ reaction at incident energy 171 MeV. The dashed curve is the constant phase result ($\gamma^2 = 0$) while the solid curve is obtained with phase variation ($\gamma^2 = -12$ (GeV/c)$^{-2}$). The dots are the experimental data [42].

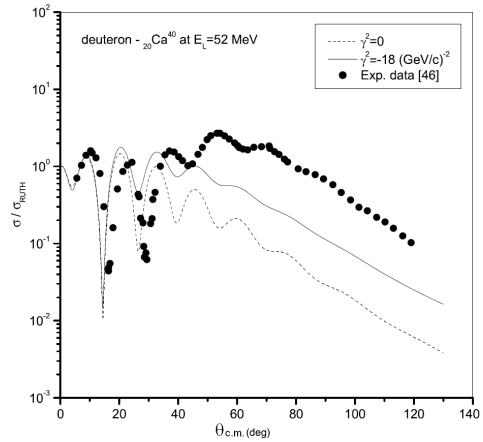

Fig. 9: Plots the elastic differential cross section (σ/σ_{RUTH}) versus scattering angle for the deuteron- $_{20}Ca^{40}$ reaction at incident energy 52 MeV. The dashed curve is the constant phase result ($\gamma^2 = 0$) while the solid curve is obtained with phase variation ($\gamma^2 = -18$ (GeV/c)$^{-2}$). The dots are the experimental data [46].

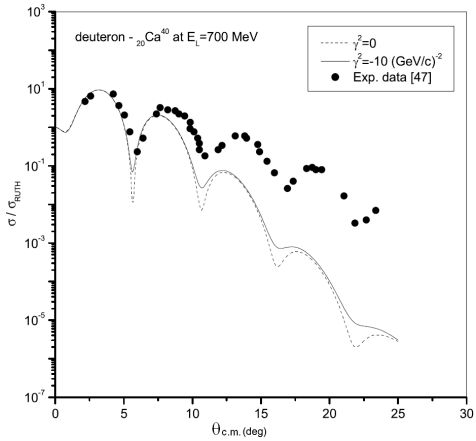

Fig. 10: Plots the elastic differential cross section (σ/σ_{RUTH}) versus scattering angle for the deuteron-$_{20}Ca^{40}$ reaction at incident energy 700 MeV. The dashed curve is the constant phase result ($\gamma^2 = 0$) while the solid curve is obtained with phase variation ($\gamma^2 = -10$ (GeV/c)$^{-2}$). The dots are the experimental data [47].

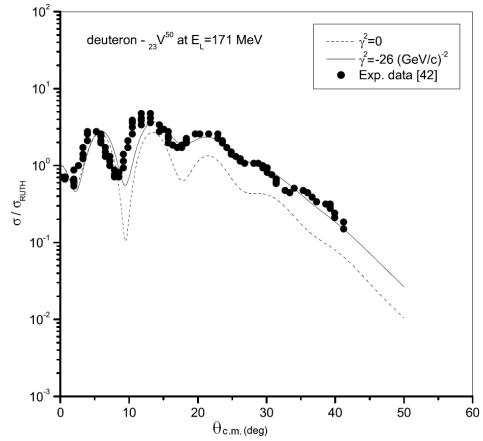

Fig. 11: Plots the elastic differential cross section (σ/σ_{RUTH}) versus scattering angle for the deuteron-$_{23}V^{50}$ reaction at incident energy 171 MeV. The dashed curve is the constant phase result ($\gamma^2 = 0$) while the solid curve is obtained with phase variation ($\gamma^2 = -26$ (GeV/c)$^{-2}$). The dots are the experimental data [42].

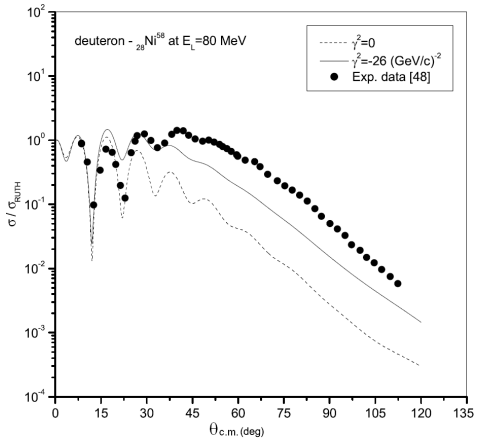

Fig. 12: Plots the elastic differential cross section (σ/σ_{RUTH}) versus scattering angle for the deuteron-$_{28}Ni^{58}$ reaction at incident energy 80 MeV. The dashed curve is the constant phase result ($\gamma^2 = 0$) while the solid curve is obtained with phase variation ($\gamma^2 = -26$ (GeV/c)$^{-2}$). The dots are the experimental data [48].

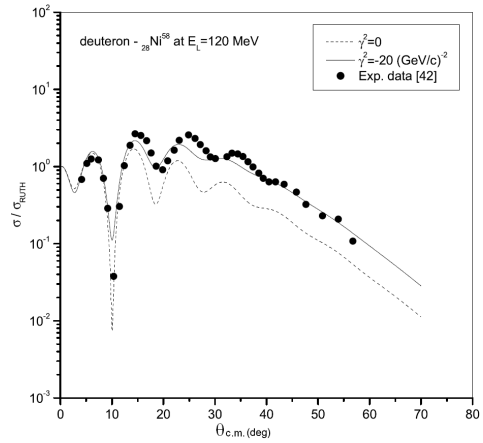

Fig. 13: Plots the elastic differential cross section (σ/σ_{RUTH}) versus scattering angle for the deuteron-$_{28}Ni^{58}$ reaction at incident energy 120 MeV. The dashed curve is the constant phase result ($\gamma^2 = 0$) while the solid curve is obtained with phase variation ($\gamma^2 = -20$ (GeV/c)$^{-2}$). The dots are the experimental data [42].

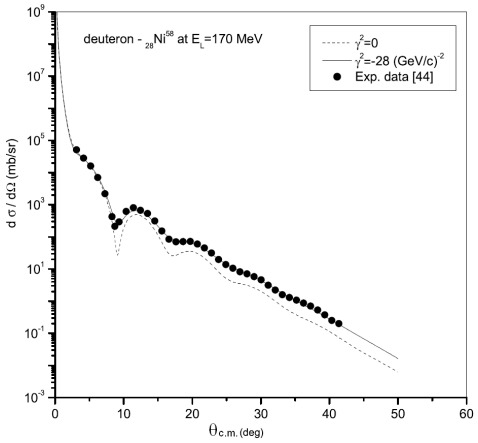

Fig. 14: Plots the elastic differential cross section ($d\sigma/d\Omega$) versus scattering angle for the deuteron-$_{28}Ni^{58}$ reaction at incident energy 170 MeV. The dashed curve is the constant phase result ($\gamma^2 = 0$) while the solid curve is obtained with phase variation ($\gamma^2 = -28$ (GeV/c)$^{-2}$). The dots are the experimental data [44].

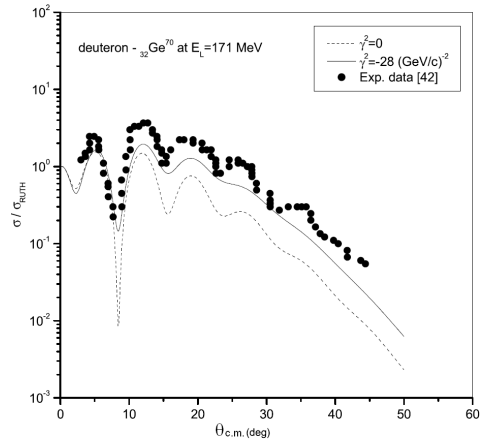

Fig. 15: Plots the elastic differential cross section (σ/σ_{RUTH}) versus scattering angle for the deuteron-$_{32}Ge^{70}$ reaction at incident energy 171 MeV. The dashed curve is the constant phase result ($\gamma^2 = 0$) while the solid curve is obtained with phase variation ($\gamma^2 = -28$ (GeV/c)$^{-2}$). The dots are the experimental data [42].

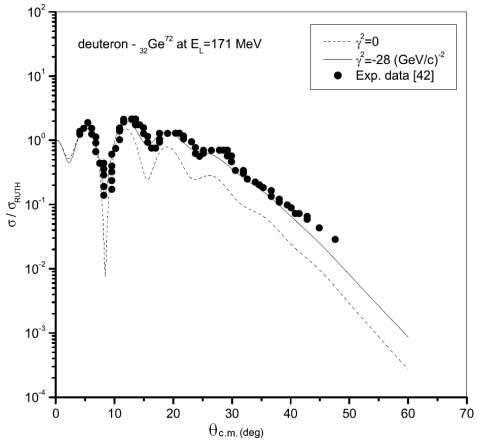

Fig. 16: Plots the elastic differential cross section (σ/σ_{RUTH}) versus scattering angle for the deuteron-$_{32}Ge^{72}$ reaction at incident energy 171 MeV. The dashed curve is the constant phase result ($\gamma^2 = 0$) while the solid curve is obtained with phase variation ($\gamma^2 = -28$ (GeV/c)$^{-2}$). The dots are the experimental data [42].

Nucleus	P	d	Li^6	C^{12}	O^{16}	Mg^{24}
$\sqrt{<r^2>}$ (fm)	0.810	2.170	2.450	2.453	2.710	2.980
Ref.	16	16	36	16	16	16
Nucleus	S^{32}	Ca^{40}	V^{50}	Ni^{58}	Ge^{70}	Ge^{72}
$\sqrt{<r^2>}$ (fm)	3.239	3.486	3.615	3.790	4.070	4.050
Ref.	37	16	37	16	37	37

Table 2: Nuclear rms radii.

ing data except a smaller shift is found at the minimum. The predicted angular distribution for d-$_6C^{12}$ elastic collision at the energies 110, 120 and 170 MeV is shown in Figs. 2–4 respectively. The scattering data is well reproduced in the last case (at 170 MeV) rather than in the other two cases (110 and 120 MeV) where smaller shifts are still appeared around the diffraction patterns. For d-$_8O^{16}$ reaction, Fig. 5, the predicted angular distribution is in good agreement with the corresponding experimental data. In Fig. 6 we presented the case of the d-$_{12}Mg^{24}$ reaction at bombarding energy 170 MeV. One can easily see from this figure that the predicted angular distribution give an excellent account to the experimental data over the whole range of the scattering angles. The calculated angular distribution for the d-$_{16}S^{32}$ reaction at energies 52 and 171 MeV are shown in Figs. 7–8. We observe from these figures that the predicted angular distribution for the 171 MeV is much better in reproducing the scattering data than that obtained at 52 MeV and smaller shifts are found around the minima in both of them. The results for the angular distribution of the elastic scattering of 52 and 700 MeV deuteron on $_{20}Ca^{40}$ nuclei are shown in Figs. 9–10. The calculations reproduce reasonably the scattering data up to the angular range ($\theta \leqslant 35^\circ$) for the first reaction and up to ($\theta \leqslant 10^\circ$) for the second reaction, while for larger angles just the qualitative trend is accounted for. For

d-$_{23}V^{50}$ reaction, Fig. 11, the data are reasonably reproduced with a smaller shift away from the forward angles. Enlarging the mass of the target nucleus as in the d-$_{28}Ni^{58}$ reaction, Figs. 12–14, one can easily see that the predicted angular distribution in the later case are twofold better in reproducing the experimental data than in the others with smaller shifts still found in all of them. For Germanium target nuclei as in the case of d-$_{32}Ge^{70}$ and d-$_{32}Ge^{72}$ reactions, Figs. 15–16, the data are quantitatively represented at the forward angles and qualitatively reproduced at the backward angles.

On discussing these results, the positive picture obtained at smaller values of momentum transfer is expected because the Glauber theory is a very good approximation at forward angles. But at larger angles poorer fits are obtained as the energy increases was not expected.

However, we should keep in mind that at these energies the input NN cross sections parameters are strongly dependent on energy as shown in Table 1. Therefore, the scattering would be very sensitive to the large q-details of the density distributions and the elemental scattering amplitudes.

In the vie of the analysis made by several authors [30, 38–41], the question about the influence of invoking a phase-variation in the NN scattering amplitude is investigated in our calculations. To investigate how the q-dependent phase $\exp\frac{-i\gamma^2q^2}{2}$ affects the deuteron-nucleus elastic scattering, we have carried out extensive numerical calculations for most of our considered reactions (where smaller shifts are found around their diffraction patterns), at various nonzero values of the phase parameter γ^2. The calculations showed that for a given value of the ratio parameter ρ, the variation of γ^2 leads to either overall increase or decrease in the estimated values of the cross sections. Indeed, we found that such change in the cross section takes place depending on the signs of ρ and γ^2, i.e. if ρ is positive, the negative value of γ^2 increases the cross section while the positive value decreases it and vice versa. Hence, a nonzero value for ρ implies a single nonzero value for γ^2 as well. This in fact agrees with what was predicted before by Ahmad and Alvi [39] from potential model calculation. However, the best results of the present calculations are shown by the solid curves in our figures. On comparing the solid curve (at $\gamma^2 \neq 0$) with the dashed curve (at $\gamma^2 = 0$) in each figure, we can note that the influence of the phase is obvious only at the minima and is roughly notable at the momentum transfers where no minima originally occurred. In general, taking this phase into account gives better agreement with the scattering data, Figs. 5, 11, 13, 14 and 16, while the improvement is confined at the minima of the results obtained for the other reactions presented in the Figs. 1–3, 7–10, 12 and 15.

4 Conclusion

In the framework of Glauber's multiple scattering theory which takes into account both the full multiple scattering series of the Glauber amplitude and a consistent treatment of the center-of-mass correlation, we have studied the elastic scattering of deuteron with different nuclei like, $_3Li^6$, $_6C^{12}$, $_8O^{16}$, $_{12}Mg^{24}$, $_{16}S^{32}$, $_{20}Ca^{40}$, $_{23}V^{50}$, $_{28}Ni^{58}$, $_{32}Ge^{70}$ and $_{32}Ge^{72}$ at intermediate energies ($25 \leqslant E/A \leqslant 342.5$). We have calculated the angular distribution ($\frac{\sigma}{\sigma_{RUTH}}$ or $\frac{d\sigma}{d\Omega}$) for the above considered reactions and compared our results with the corresponding experimental data. It was shown that, in general, a smaller shift is appeared around the minimum in most of the theoretical results and a disagreement at large scattering angles is also exist there. Trial to overcome these drawbacks is made by investigating the effect of invoking a phase-variation in the NN scattering amplitude. Although the results show that a better agreement with the experimental data is obtained, especially at the minima of the diffraction patterns in comparison with the free-phase calculations, the introduction of such phase alone is not sufficient to bring the Glauber model prediction closer to the experimental data, except for a few number of the considered energies. The reason for the insignificance of this phase at large scatteing angles may be attributed to the followings: First, The complicated eclipse occurred from the multiple scattering collisions between nucleons which are not simple (linear) in its dependence on q^2 as that taken here. Second, the utilized bare NN parameters that neglecting the in-medium effect. Thus, for serious phase effect investigation, one should use a more realistic density distribution for the deuteron and effective NN parameters that account for the density dependence and the medium effect. This will be the subject of our future work.

Submitted on March 12, 2007
Accepted on March 16, 2007

References

1. Feshbach H., Porter C. E. and Weisskopf V. E. *Phys. Rev.*, 1965, v. 96, 448.
2. R. J. Glauber lectures in theoretical physics. Edited by W. E. Brittin and L. G. Dunham, Wiley, New York, 1959, v. 1, p. 315.
3. Franco V. and Glauber R. J. *Phys. Rev.*, 1966, v. 142, 1195.
4. Glauber R. J. and Franco V. *Phys. Rev.*, 1967, v. 156, 1685.
5. Glauber R. J. and Mathiae G. *Nucl. Phys. B*, 1970, v. 21, 135.
6. Wilikin C. *Nuovo Cimento Lett.*, 1970, v. 4, 491.
7. Lesniak H. and Lesniak L. *Nucl. Phys. B*, 1972, v. 38, 221.
8. Auger J. P. and Lombard R. J. *Phys. Lett.*, 1973, v. B45, 115; Igo G. In: *High-Energy Physics and Nuclear Structure*, Edited by D. E. Nagle et al., AIP, New York, 1975, p. 63.
9. Franco V. *Phys. Rev. C*, 1974, v. 8, 1690.
10. Czyz W. *Adv. Nucl. Phys.*, 1971, v. 4, 61.
11. Bassel R. H. and Wilikin C. *Phys. Rev.*, 1968, v. 174, 1179.
12. Glauber R. J. In: *Proceeding of the Second International Conference on High-Energy Physics and Nuclear Structure*,

Rehovoth, 1967, Edited by G. Alexander, North-Holland, Amsterdam, 1967, p. 311.

13. Glauber R. J. In: *Proceeding of the Third International Conference on High-Energy Physics and Nuclear Structure*, Colubia, 1967, Edited by S. Devons, Plenum, New York, 1970, p. 207.
14. Franco V. and Tekou A. *Phys. Rev. C*, 1977, v. 16, 658.
15. Varma G. K. *Nucl. Phys. A*, 1978, v. 294, 465.
16. Franco V. and Varma G. K. *Phys. Rev. C*, 1978, v. 18, 349.
17. Czyz W. and Maximon L. C. *Ann. Phys.* (N.Y.), 1969, v. 52, 59.
18. Hynes M. V. *et al. Phys. Rev. C*, 1985, v. 31, 1438.
19. Kofoed-Hansen O. *Nuovo Cimento A*, 1969, v. 60, 621.
20. Yichun Yin *et al. Nucl. Phys. A*, 1985, v. 440, 685.
21. Yin Y. *et al. Chinese Phys.*, 1986, v. 6, 93; *Phys. Ener. Fort. Phys. Nucl.*, 1985, v. 9, 569.
22. Huang Xiang Zhong. *Phys. Rev. C*, 1985, v. 51, 2700.
23. Shalaby A. S. *et al. Phys. Rev. C*, 1997, v. 56, 2889.
24. El-Gogary M.M.H. *et al. Phys. Rev. C*, 1998, v. 58, 3513.
25. El-Gogary M.M.H. *et al. Phys. Rev. C*, 2000, v. 61, 044604.
26. Shalaby A. S. *Egypt. J. Phys.*, 2004, v. 35, No. 1, 163.
27. Shalaby A. S. *Balkan Physics Letters*, 2005, v. 13, No. 3, 111.
28. Shalaby A. S. *Egypt. J. Phys.*, 2004, v. 35, No. 3, 481.
29. Raman S. *et al. At. Data Nucl. Data Tables*, 1987, v. 36, 1.
30. Spear R. H. *et al. At. Data Nucl. Data Tables*, 1989, v. 42, 55.
31. Franco V. and Yin Y. *Phys. Lett.*, 1985, v. 55, 1059.
32. Franco V. and Yin Y. *Phys. Rev. C*, 1986, v. 34, 608.
33. Shalaby A. S. M. Sc. thesis. Cairo University, 1993.
34. Hostachy J. Y. These d'Etat. I.S.N. 87–65, Université de Grenoble (unpublished); B. Abu-Ibrahim *et al. Nucl. Phys. A*, 1999, v. 657, 391.
35. Lenzi S. M., Vitturi A. and Zardi F. *Phys. Rev. C*, 1989, v. 40, 2114.
36. Barret R. G. and Jackson D. F. Nuclear sizes and structure. Clarendon, Oxford, 1977.
37. Patterson J. D. and Peterson R. J. *Nucl. Phys. A*, 2003, v. 717, 235.
38. Lombard R. J. and Moillet J. P. *Phys. Rev. C*, 1990, v. 41, R1348.
39. Ahmad I. and Alvi M. A. *Phys. Rev. C*, 1993, v. 48, 3126.
40. Ruan Wenying and Liu Youyan. *J. Phys. G. Nucl. Part. Phys.*, 1995, v. 21, 537.
41. Ji-feng Liu, Yu-shun Zhang, Chano-yun Yang, Jun-feng Shen and Robson B. A. *Phys. Rev. C*, 1996, 54, 2509.
42. Korff A. *et al. Phys. Rev. C*, 2004, v. 70, 067601.
43. Betker A. C. *et al. Phys. Rev. C*, 1993, v. 48, 2085.
44. Baumer C. *et al. Phys. Rev. C*, 2001, v. 63, 037601.
45. Daehnick W. W., Childs J. D. and Vrcelj Z. *Phys. Rev. C*, 1980, v. 21, 2253.
46. Ermer M. *et al. Phys. Lett. B*, 1987, v. 188, 17.
47. Nguyen Van Sen *et al. Phys. Lett. B*, 1985, v. 156, 185.
48. Stephenson E. J. *et al. Nucl. Phys. A*, 1981, v. 359, 316.

Appendix

This appendix contains the tables of the orbits, lengths and Δ-matrices employed in our calculations. We obtained them by enumerating and investigating all the possible combinations of collisions according to their pertation [20]. In the present work, the elastic collisions, d-$_3$Li^6, d-$_6$C^{12}, d-$_8$O^{16}, d-$_{12}$Mg^{24}, d-$_{16}$S^{32}, d-$_{20}$Ca^{40}, d-$_{23}$V^{50}, d-$_{28}$Ni^{58}, d-$_{32}$Ge^{70} and d-$_{32}$Ge^{72} have been studied according to their cluster and nucleon structures. The orbits, lengths and Δ-matrices of the groups $G_1 = S_{M_A} \otimes S_{M_B}$ and $G_2 = = S_{M_N} \otimes S_{M_N}$ (defined in Section 2) corresponding to these reactions depend on the assumed cluster and nucleon configurations.

The numbers (M_A, M_B, M_N), determining the cluster and nucleon structures assumed in each system are taken as follows: $M_A = 1$, $M_N = 2$ while M_B is different for each reaction and it is equal to $B/2$, where B is the mass number of the target nucleus.

For the sake of brevity, we give only the tables of the non-similar groups.

μ	λ_μ	$T(\mu, \lambda_\mu)$	$\Delta(\mu, \lambda_\mu)$
1	1	29	10000000000000000000000000000
2	1	406	11000000000000000000000000000
3	1	3654	11100000000000000000000000000
4	1	23751	11110000000000000000000000000
5	1	118755	11111000000000000000000000000
6	1	475020	11111100000000000000000000000
7	1	1560780	11111110000000000000000000000
8	1	4292145	11111111000000000000000000000
9	1	10015005	11111111100000000000000000000
10	1	20030010	11111111110000000000000000000
11	1	34597290	11111111111000000000000000000
12	1	51895935	11111111111100000000000000000
13	1	67863915	11111111111110000000000000000
14	1	77558760	11111111111111000000000000000

Table 3: Orbits, lengths and Δ-matrices for $G = S_1 \otimes S_{29}$. Total number of orbits (including the orbits not shown) $= 29$.

μ	λ_μ	$T(\mu, \lambda_\mu)$	$\Delta(\mu, \lambda_\mu)$
1	1	29	10000000000000000000000000000
2	1	190	11000000000000000000000000000
3	1	1140	11100000000000000000000000000
4	1	4845	11110000000000000000000000000
5	1	15504	11111000000000000000000000000
6	1	38760	11111100000000000000000000000
7	1	77520	11111110000000000000000000000
8	1	125970	11111111000000000000000000000
9	1	167960	11111111100000000000000000000
10	1	184756	11111111110000000000000000000

Table 4: Orbits, lengths and — matrices for $G = S_1 \otimes S_{20}$. Total number of orbits (including the orbits not shown) $= 20$.

μ	λ_μ	$T(\mu, \lambda_\mu)$	$\Delta(\mu, \lambda_\mu)$
1	1	25	10000000000000000000000000000
2	1	300	11000000000000000000000000000
3	1	2300	11100000000000000000000000000
4	1	12650	11110000000000000000000000000
5	1	53130	11111000000000000000000000000
6	1	177100	11111100000000000000000000000
7	1	480700	11111110000000000000000000000
8	1	1081575	11111111000000000000000000000
9	1	2042975	11111111100000000000000000000
10	1	3268760	11111111110000000000000000000
11	1	4457400	11111111111000000000000000000
12	1	5200300	11111111111100000000000000000

Table 5: Orbits, lengths and Δ-matrices for $G = S_1 \otimes S_{25}$. Total number of orbits (including the orbits not shown) $= 25$.

μ	λ_μ	$T(\mu,\lambda_\mu)$	$\Delta(\mu,\lambda_\mu)$
1	1	3	100

Table 6: Orbits, lengths and Δ-matrices for $G = S_1 \otimes S_3$. Total number of orbits (including the orbits not shown) $= 3$.

μ	λ_μ	$T(\mu,\lambda_\mu)$	$\Delta(\mu,\lambda_\mu)$
1	1	35	10000000000000000000000000000000
2	1	595	11000000000000000000000000000000
3	1	6545	11100000000000000000000000000000
4	1	52360	11110000000000000000000000000000
5	1	324632	11111000000000000000000000000000
6	1	1623160	11111100000000000000000000000000
7	1	6724520	11111110000000000000000000000000
8	1	23535820	11111111000000000000000000000000
9	1	70607460	11111111100000000000000000000000
10	1	1.835794E8	11111111110000000000000000000000
11	1	4.172259E8	11111111111000000000000000000000
12	1	8.344518E8	11111111111100000000000000000000
13	1	1.4763378E9	11111111111110000000000000000000
14	1	2.3199594E9	11111111111111000000000000000000
15	1	3.2479432E9	11111111111111100000000000000000
16	1	4.0599289E9	11111111111111110000000000000000
17	1	4.5375676E9	11111111111111111000000000000000

Table 7: Orbits, lengths and Δ-matrices for $G = S_1 \otimes S_{35}$. Total number of orbits (including the orbits not shown) $= 35$.

μ	λ_μ	$T(\mu,\lambda_\mu)$	$\Delta(\mu,\lambda_\mu)$
1	1	36	10000000000000000000000000000000
2	1	630	11000000000000000000000000000000
3	1	7140	11100000000000000000000000000000
4	1	58905	11110000000000000000000000000000
5	1	376992	11111000000000000000000000000000
6	1	1947792	11111100000000000000000000000000
7	1	8347680	11111110000000000000000000000000
8	1	302660340	11111111000000000000000000000000
9	1	94143280	11111111100000000000000000000000
10	1	2.5418686E8	11111111110000000000000000000000
11	1	6.008053E8	11111111111000000000000000000000
12	1	1.2516777E9	11111111111100000000000000000000
13	1	2.3107896E9	11111111111110000000000000000000
14	1	3.7962972E9	11111111111111000000000000000000
15	1	5.5679026E9	11111111111111100000000000000000
16	1	7.3078721E9	11111111111111110000000000000000
17	1	8.5974966E9	11111111111111111000000000000000
18	1	9.0751353E9	11111111111111111100000000000000

Table 8: Orbits, lengths and Δ-matrices for $G = S_1 \otimes S_{36}$. Total number of orbits (including the orbits not shown) $= 36$.

In these tables, the first column represents the order of multiple scattering μ which ranges from 1 to $1 \times n$ while λ_μ in the second column represents the serial index used to number the orbits of order μ. The third column represents the length of the orbit $T(\mu,\lambda_\mu)$. In the fourth column the $(1 \times n)$-digit binary numbers give the Δ-matrices of the group $G = S_1 \otimes S_n$. The n-digits are the elements Δ_{1i}, where $i = 1, 2, \ldots, n$.

By symmetry, the orbits, lengths and Δ-matrices for $\mu's$ which are not shown in our tables could be easily deduced from the Tables. This is carried out by using the results for order $\mu' = m \times n - \mu$ and interchanging the $0's$ and $1's$ of $\Delta(\mu',\lambda_{\mu'})$. The indices λ_μ and $\lambda_{\mu'}$ are the same and the lengths $T(\mu,\lambda_\mu)$ and $T(\mu',\lambda_{\mu'})$ are equal. The matrix $\Delta(n,1)$ has elements Δ_{1j} equal to 1.

The orbits, lengths and Δ-matrices of the groups $G = S_2 \otimes S_2$ [24] & $S_1 \otimes S_6$ & $S_1 \otimes S_{12}$ & $S_1 \otimes S_{16}$ [26] and $S_1 \otimes S_8$ [28] are also used to carry out our present calculations in addition to what was listed above.

Funnel's Fluctuations in Dyonic Case: Intersecting D1–D3 Branes

Jamila Douari* and Arafa H. Ali*†

*Center for Advanced Mathematical Sciences, American University of Beirut, Beirut, Lebanon
†Department of Physics, Chonnam National University, Gwangju, Korea

All correspondence should be made to A. H. Ali. E-mail: arafa16@yahoo.com
Permanent address: Department of Physics, Faculty of Sciences, Beni-suef University, Egypt

The fluctuations of funnel solutions of intersecting D1 and D3 branes are quite explicitly discussed by treating different modes and different directions of the fluctuation at the presence of world volume electric field. The boundary conditions are found to be Neumann boundary conditions.

1 Introduction

D-branes described by Non-abelian Born-Infeld (BI) action [1] have many fascinating features. Among these there is the possibility for D-branes to morph into other D-branes of different dimensions by exciting some of the scalar fields [2, 3]. It's known in the literature that there are many different but physically equivalent descriptions of how a D1-brane may end on a D3-brane. From the point of view of the D3 brane the configuration is described by a monopole on its world volume. From the point of view of the D1-brane the configuration is described by the D1-brane opening up into a D3-brane where the extra three dimensions form a fuzzy two-sphere whose radius diverges at the origin of the D3-brane. These different view points are the stringy realization of the Nahm transformation [4, 5]. Also the dynamics of the both bion spike [2, 6] and the fuzzy funnel [5, 7, 8] were studied by considering linearized fluctuations around the static solutions.

The present work is devoted to study the fluctuations of funnel solutions in the presence of a world-volume electric field. By discussing the solutions and the potentials for this particular case we end by the system D1⊥D3 branes gets a special property because of the presence of electric field; the system is divided to two regions corresponding to small and large electric field. Consequently, the system has Neumann boundary conditions and the end of open string can move freely on the brane which is agree with its dual discussed in [9] considering Born-Infeld action dealing with the fluctuation of the bion skipe in D3⊥D1-case.

The paper is organized as follows: In section 2, we start by a brief review on D1⊥D3 branes in dyonic case by using the non-Born-Infeld action. Then, we discuss the fluctuations of the fuzzy funnel in section 3 for zero and high modes. We give the solutions of the linearized equations of motion of the fluctuations for both cases the overall transverse and the relative one. We also discuss the solutions and the potential depending on the presence of electric field which is leading to Neumann boundary conditions as special property of the system. Then the waves on the brane cause the fuzzy funnel to freely oscillate.

2 D1⊥D3 branes with electric field swished on

In this section, we review in brief the funnel solutions for D1⊥D3 branes from D3 and D1 branes points of view. First, using abelian BI action for the world-volume gauge field and one excited transverse scalar in dyonic case, we give the funnel solution. It was showed in [10] that the BI action, when taken as the fundamental action, can be used to build a configuration with a semi-infinite fundamental string ending on a D3-brane [11]. The dyonic system is given by using D-string world-volume theory and the fundamental strings introduced by adding a $U(1)$ electric field. Thus the system is described by the following action

$$\begin{aligned} S &= \int dt L = \\ &= -T_3 \int d^4\sigma \sqrt{-\det(\eta_{ab} + \lambda^2\,\partial_a\phi^i\,\partial_b\phi^i + \lambda F_{ab})} = \\ &= -T_3 \int d^4\sigma \Big[1 + \lambda^2\Big(|\nabla\phi|^2 + B^2 + E^2\Big) + \\ &+ \lambda^4\big((B\cdot\nabla\phi)^2 + (E\cdot B)^2 + |E\wedge\nabla\phi|^2\big)\Big]^{\frac{1}{2}} \end{aligned} \tag{1}$$

in which F_{ab} is the field strength and the electric field is denoted as $F_{09} = EI_{ab}$, (I_{ab} is $N\times N$ matrix). σ^a ($a = 0, \ldots, 3$) denote the world volume coordinates while ϕ^i ($i = 4, \ldots, 9$) are the scalars describing transverse fluctuations of the brane and $\lambda = 2\pi\ell_s^2$ with ℓ_s is the string length. In our case we excite just one scalar so $\phi^i = \phi^9 \equiv \phi$. Following the same process used in the reference [10] by considering static gauge, we look for the lowest energy of the system. Accordingly to (1) the energy of dyonic system is given as

$$\begin{aligned} \Xi = T_3 \int d^3\sigma \Big[&\lambda^2|\nabla\phi + \vec{B} + \vec{E}|^2 + (1 - \lambda^2\,\nabla\phi\cdot\vec{B})^2 - \\ &- 2\lambda^2\vec{E}\cdot(\vec{B} + \nabla\phi) + \lambda^4\Big((\vec{E}\cdot\vec{B})^2 + |\vec{E}\wedge\nabla\phi|^2\Big)\Big]^{\frac{1}{2}}, \end{aligned} \tag{2}$$

then if we require $\nabla\phi + \vec{B} + \vec{E} = 0$, Ξ reduces to $\Xi_0 \geqslant 0$ and we find

$$\begin{aligned} \Xi_0 = T_3 \int d^3\sigma \Big[&\big(1 - \lambda^2\,(\nabla\phi)\cdot\vec{B}\big)^2 + 2\lambda^2\vec{E}\cdot\vec{E} + \\ &+ \lambda^4\left((\vec{E}\cdot\vec{B})^2 + |\vec{E}\Lambda\nabla\phi|^2\right)\Big]^{\frac{1}{2}} \end{aligned} \tag{3}$$

as minimum energy. By using the Bianchi identity $\nabla\cdot B=0$ and the fact that the gauge field is static, the funnel solution is then

$$\phi=\frac{N_m+N_e}{2r}\,, \tag{4}$$

with N_m is magnetic charge and N_e electric charge.

Now we consider the dual description of the $D1\perp D3$ from D1 branes point of view. To get D3-branes from D-strings, we use the non-abelian BI action

$$\begin{aligned} S &= -T_1\int d^2\sigma\times \\ &\times \mathrm{Str}\Big[-\det(\eta_{ab}+\lambda^2\,\partial_a\phi^i\,Q^{-1}_{ij}\,\partial_b\phi^j)\det Q^{ij}\Big]^{\frac{1}{2}} \end{aligned} \tag{5}$$

where $Q_{ij}=\delta_{ij}+i\lambda\big[\phi_i,\phi_j\big]$. Expanding this action to leading order in λ yields the usual non-abelian scalar action

$$\begin{aligned} S &\cong -T_1\int d^2\sigma\times \\ &\times\Big[N+\lambda^2\,\mathrm{tr}\,\big(\partial_a\phi^i+\tfrac{1}{2}\big[\phi_i,\phi_j\big]\big[\phi_j,\phi_i\big]\big)+\dots\Big]^{\frac{1}{2}}. \end{aligned}$$

The solutions of the equation of motion of the scalar fields ϕ_i, $i=1,2,3$ represent the D-string expanding into a D3-brane analogous to the bion solution of the D3-brane theory [2, 3]. The solutions are

$$\phi_i=\pm\frac{\alpha_i}{2\sigma},\qquad \big[\alpha_i,\alpha_j\big]=2i\epsilon^{ijk}\alpha_k,$$

with the corresponding geometry is a long funnel where the cross-section at fixed σ has the topology of a fuzzy two-sphere.

The dyonic case is taken by considering (N,N_f)-strings. We have N D-strings and N_f fundamental strings [5]. The theory is described by the action

$$\begin{aligned} S &= -T_1\int d^2\sigma\times \\ &\times\mathrm{Str}\Big[-\det(\eta_{ab}+\lambda^2\partial_a\phi^iQ^{-1}_{ij}\partial_b\phi^j+\lambda E\,I_{ab})\det Q^{ij}\Big]^{\frac{1}{2}} \end{aligned} \tag{6}$$

in which we replaced the field strength F_{ab} by EI_{ab} (I_{ab} is $N\times N$-matrix) meaning that the fundamental string is introduced by adding a $U(1)$ electric field E.

The action can be rewritten as

$$S=-T_1\int d^2\sigma\,\mathrm{Str}\Big[-\det\begin{pmatrix}\eta_{ab}+\lambda EI_{ab} & \lambda\partial_a\phi^j\\ -\lambda\partial_b\phi^i & Q^{ij}\end{pmatrix}\Big]^{\frac{1}{2}}, \tag{7}$$

then the bound states of D-strings and fundamental strings are made simply by introducing a background $U(1)$ electric field on D-strings, corresponding to fundamental strings dissolved on the world-sheet. By computing the determinant, the action becomes

$$\begin{aligned} S &= -T_1\int d^2\sigma\times \\ &\times\mathrm{Str}\Big[(1-\lambda^2E^2+\alpha_i\alpha_i\hat{R}'^2)(1+4\lambda^2\alpha_j\alpha_j\hat{R}^4)\Big]^{\frac{1}{2}}, \end{aligned} \tag{8}$$

where the following ansatz were inserted

$$\phi_i=\hat{R}\alpha_i\,. \tag{9}$$

Hence, we get the funnel solution for dyonic string by solving the equation of variation of $\hat{R}$, as follows

$$\phi_i=\frac{\alpha_i}{2\sigma\sqrt{1-\lambda^2E^2}}. \tag{10}$$

3 Fluctuations of dyonic funnel solutions

In this section, we treat the dynamics of the funnel solutions. We solve the linearized equations of motion for small and time-dependent fluctuations of the transverse scalar around the exact background in dyonic case.

We deal with the fluctuations of the funnel (10) discussed in the previous section. By plugging into the full $(N-N_f)$ string action (6, 7) the "overall transverse" $\delta\phi^m(\sigma,t)=$ $=f^m(\sigma,t)\,I_N$, $m=4,\dots,8$ which is the simplest type of fluctuation with I_N the identity matrix, together with the funnel solution, we get

$$\begin{aligned} S &= -T_1\int d^2\sigma\,\mathrm{Str}\bigg[(1+\lambda E)\Big(1+\frac{\lambda^2\alpha^i\alpha^i}{4\sigma^4}\Big)\times \\ &\times\bigg(\Big(1+\frac{\lambda^2\alpha^i\alpha^i}{4\sigma^4}\Big)\big(1+(\lambda E-1)\,\lambda^2(\partial_t\delta\phi^m)^2\big)+ \\ &+\lambda^2(\partial_\sigma\delta\phi^m)^2\bigg)\bigg]^{\frac{1}{2}}\approx -NT_1\int d^2\sigma H\bigg[(1+\lambda E)- \\ &-(1-\lambda^2E^2)\frac{\lambda^2}{2}(\dot{f}^m)^2+\frac{(1+\lambda E)\lambda^2}{2H}(\partial_\sigma f^m)^2+\dots\bigg] \end{aligned} \tag{11}$$

where

$$H=1+\frac{\lambda^2C}{4\sigma^4}$$

and $C=\mathrm{tr}\,\alpha^i\alpha^i$. For the irreducible $N\times N$ representation we have $C=N^2-1$. In the last line we have only kept the terms quadratic in the fluctuations as this is sufficient to determine the linearized equations of motion

$$\Big((1-\lambda E)\Big(1+\lambda^2\,\frac{N^2-1}{4\sigma^4}\Big)\partial_t^2-\partial_\sigma^2\Big)f^m=0\,. \tag{12}$$

In the overall case, all the points of the fuzzy funnel move or fluctuate in the same direction of the dyonic string by an equal distance δx^m. First, the funnel solution is $\phi^i=$ $=\frac{1}{2\sqrt{1-\lambda^2E^2}}\frac{\alpha^i}{\sigma}$ and the fluctuation f^m waves in the direction of x^m;

$$f^m(\sigma,t)=\Phi(\sigma)\,e^{-iwt}\delta x^m. \tag{13}$$

With this ansatz the equation of motion is

$$\Big((1-\lambda E)Hw^2+\partial_\sigma^2\Big)\Phi(\sigma)=0\,, \tag{14}$$

then the problem is reduced to finding the solution of a single scalar equation.

Thus, we remark that the equation (14) is an analog one-dimensional Schrödinger equation and it can be rewritten as

$$\Big(-\partial_\sigma^2 + V(\sigma)\Big)\,\Phi(\sigma) = w^2\,(1-\lambda E)\,\Phi(\sigma), \qquad (15)$$

with

$$V(\sigma) = w^2(\lambda E - 1)\,\lambda^2\,\frac{N^2-1}{4\sigma^4}.$$

We notice that, if the electric field dominates $E \gg 1$, the potential goes to $w^2\lambda^3 E\frac{N^2}{4\sigma^4}$ for large N and if $E \ll 1$ we find $V = -\,w^2\,\lambda^2\,\frac{N^2}{4\sigma^4}$. This can be seen as two separated systems depending on electric field so we have Neumann boundary condition separating the system into two regions $E \gg 1$ and $E \ll 1$.

Now, let's find the solution of a single scalar equation (14). First, the equation (14) can be rewritten as follows

$$\left(\frac{1}{w^2(1-\lambda E)}\,\partial_\sigma^2 + 1 + \frac{\lambda^2 N^2}{4\sigma^4}\right)\Phi(\sigma) = 0\,, \qquad (16)$$

for large N. If we suggest $\tilde{\sigma} = w\sqrt{1-\lambda E}\,\sigma$ the latter equation becomes

$$\left(\partial_{\tilde{\sigma}}^2 + 1 + \frac{\kappa^2}{\tilde{\sigma}^4}\right)\Phi(\tilde{\sigma}) = 0\,, \qquad (17)$$

with the potential is

$$V(\tilde{\sigma}) = \frac{\kappa^2}{\tilde{\sigma}^4}\,, \qquad (18)$$

and $\kappa = \frac{\lambda N w^2}{2}(1-\lambda E)$. This equation is a Schrödinger equation for an attractive singular potential $\propto \tilde{\sigma}^{-4}$ and depends on the single coupling parameter κ with constant positive Schrödinger energy. The solution is then known by making the following coordinate change

$$\chi(\tilde{\sigma}) = \int_{\sqrt{\kappa}}^{\tilde{\sigma}} dy\,\sqrt{1+\frac{\kappa^2}{y^4}}\,, \qquad (19)$$

and

$$\Phi = \left(1+\frac{\kappa^2}{\tilde{\sigma}^4}\right)^{-\frac{1}{4}}\tilde{\Phi}\,. \qquad (20)$$

Thus, the equation (17) becomes

$$\Big(-\partial_\chi^2 + V(\chi)\Big)\tilde{\Phi} = 0\,, \qquad (21)$$

with

$$V(\chi) = \frac{5\kappa^2}{\left(\tilde{\sigma}^2 + \frac{\kappa^2}{\tilde{\sigma}^2}\right)^3}\,. \qquad (22)$$

Then, the fluctuation is found to be

$$\Phi = \left(1+\frac{\kappa^2}{\tilde{\sigma}^4}\right)^{-\frac{1}{4}} e^{\pm i\chi(\tilde{\sigma})}. \qquad (23)$$

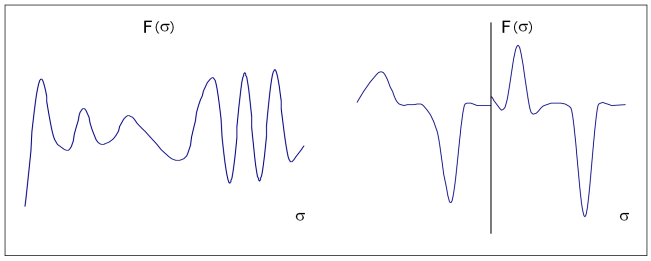

Fig. 1: Left hand curve represents the overall fluctuation wave in zero mode and low electric field. Right hand curve shows the scattering of the overall fluctuation wave in zero mode and high electric field. This latter caused a discontinuitity of the wave which means Neumann boundary condition.

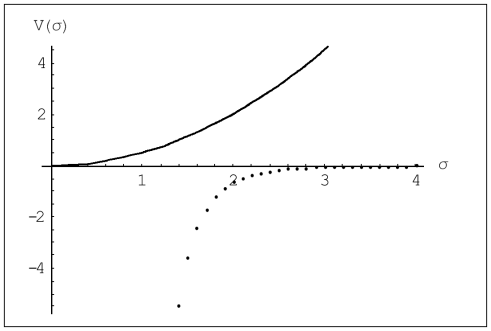

Fig. 2: The up line shows the potential in zero mode of the overall funnel's fluctuations at the absence of electric field E and the dots represent the potential in the same mode at the presence of E. The presence of E is changing the potential totally to the opposite.

This fluctuation has the following limits; at large σ, $\Phi \sim e^{\pm i\chi(\tilde{\sigma})}$ and if σ is small $\Phi = \frac{\sqrt{\kappa}}{\tilde{\sigma}}e^{\pm i\chi(\tilde{\sigma})}$. These are the asymptotic wave function in the regions $\chi \to \pm\infty$, while around $\chi \sim 0$; i.e. $\tilde{\sigma} \sim \sqrt{\kappa}$, $f^m \sim 2^{-\frac{1}{4}}e^{-iwt}\delta x^m$ (Fig. 1).

The potential (22) in large and small limits of electric field becomes (Fig. 2):

- $E \gg 1$, $V(\chi) \sim \frac{-5\lambda N^2}{E\sigma^6}$;
- $E \ll 1$, $V(\chi) \sim \frac{5\lambda^2 N^2 w^2}{4\left(w^2\sigma^2 + \frac{\lambda^2 N^2 w^2}{4\sigma^2}\right)}$.

At the presence of electric field we remark that around $\sigma \sim 0$ there is a symmetric potential which goes to zero very fast and more fast as electric field is large $\sim \frac{-1}{E\sigma^2}$. As discussed above, again we get the separated systems in different regions depending on the values of electric field. Also if we have a look at the fluctuation (23) we find that f^m in the case of $E \gg 1$ is different from the one in $E \ll 1$ case and as shown in the Fig. 1 the presence of electric field causes a discontinuity of the fluctuation wave which means free boundary condition. Contrarily, at the absence of electric field the fluctuation wave is continue. Then, this is seen as Neumann boundary condition from non-Born-Infeld dynamics separating the system into two regions $E \gg 1$ and $E \ll 1$ which is agree with its dual discussed in [9].

The fluctuations discussed above could be called the zero mode $\ell = 0$ and for high modes $\ell \geqslant 0$, the fluctuations are

$$\delta\phi^m(\sigma,t) = \sum_{\ell=0}^{N-1} \psi^m_{i_1\dots i_\ell}\alpha^{i_1}\dots\alpha^{i_\ell}$$

with $\psi^m_{i_1\dots i_\ell}$ are completely symmetric and traceless in the lower indices.

The action describing this system is

$$\begin{aligned} S \approx -NT_1 \int d^2\sigma \Big[& (1+\lambda E)H - (1-\lambda^2E^2)\times \\ & \times H\frac{\lambda^2}{2}(\partial_t\delta\phi^m)^2 + \frac{(1+\lambda E)\lambda^2}{2H}(\partial_\sigma\delta\phi^m)^2 - \\ & -(1-\lambda^2E^2)\frac{\lambda^2}{2}\big[\phi^i,\delta\phi^m\big]^2 - \frac{\lambda^4}{12}\big[\partial_\sigma\phi^i,\partial_t\delta\phi^m\big]^2 + \dots\Big] \end{aligned} \tag{24}$$

Now the linearized equations of motion are

$$\begin{aligned} & \Big[(1+\lambda E)H\partial_t^2 - \partial_\sigma^2\Big]\delta\phi^m + (1-\lambda^2E^2)\times \\ & \times\big[\phi^i,\big[\phi^i,\delta\phi^m\big]\big] - \frac{\lambda^2}{6}\big[\partial_\sigma\phi^i,\big[\partial_\sigma\phi^i,\partial_t^2\delta\phi^m\big]\big] = 0\,. \end{aligned} \tag{25}$$

Since the background solution is $\phi^i \propto \alpha^i$ and we have $\big[\alpha^i,\alpha^j\big] = 2i\epsilon_{ijk}\alpha^k$, we get

$$\begin{aligned} \big[\alpha^i,\big[\alpha^i,\delta\phi^m\big]\big] &= \sum_{\ell<N}\psi^m_{i_1\dots i_\ell}\big[\alpha^i,\big[\alpha^i,\alpha^{i_1}\dots\alpha^{i_\ell}\big]\big] \\ &= \sum_{\ell<N} 4\ell(\ell+1)\psi^m_{i_1\dots i_\ell}\alpha^{i_1}\dots\alpha^{i_\ell} \end{aligned} \tag{26}$$

To obtain a specific spherical harmonic on 2-sphere, we have

$$\begin{aligned} \big[\phi^i,\big[\phi^i,\delta\phi^m_\ell\big]\big] &= \frac{\ell(\ell+1)}{\sigma^2}\,\delta\phi^m_\ell, \\ \big[\partial_\sigma\phi^i,\big[\partial_\sigma\phi^i,\partial_t^2\delta\phi^m\big]\big] &= \frac{\ell(\ell+1)}{\sigma^4}\,\partial_t^2\delta\phi^m_\ell. \end{aligned} \tag{27}$$

Then for each mode the equations of motion are

$$\begin{aligned} \Bigg[\bigg((1+\lambda E)\Big(1+\lambda^2\frac{N^2-1}{4\sigma^4}\Big) - \frac{\lambda^2\ell(\ell+1)}{6\sigma^4}\bigg)\partial_t^2 - \\ -\partial_\sigma^2 + (1-\lambda^2E^2)\frac{\ell(\ell+1)}{\sigma^2}\Bigg]\delta\phi^m_\ell = 0\,. \end{aligned} \tag{28}$$

The solution of the equation of motion can be found by taking the following proposal. Let's consider $\phi^m_\ell = f^m_\ell(\sigma)e^{-iwt}\delta x^m$ in direction m with $f^m_\ell(\sigma)$ is some function of σ for each mode ℓ.

The last equation can be rewritten as

$$\Big[-\partial_\sigma^2 + V(\sigma)\Big]f^m_\ell(\sigma) = w^2(1+\lambda E)\,f^m_\ell(\sigma), \tag{29}$$

with

$$\begin{aligned} V(\sigma) = -w^2\bigg((1+\lambda E)\frac{\lambda^2N^2}{4\sigma^4} - \frac{\lambda^2\ell(\ell+1)}{6\sigma^4}\bigg) + \\ + (1-\lambda^2E^2)\frac{\ell(\ell+1)}{\sigma^2}\,. \end{aligned}$$

Let's write the equation (29) in the following form

$$\begin{aligned} \Bigg[w^2\bigg((1+\lambda E)H - \frac{\lambda^2\ell(\ell+1)}{6\sigma^4}\bigg) - \\ -(1-\lambda^2E^2)\frac{\ell(\ell+1)}{\sigma^2} + \partial_\sigma^2\Bigg]f^m_\ell(\sigma) = 0\,. \end{aligned} \tag{30}$$

and again as

$$\begin{aligned} \Bigg[1+\frac{1}{\sigma^4}\bigg(\lambda^2\frac{N^2-1}{4} - \frac{\lambda^2\ell(\ell+1)}{6(1+\lambda E)}\bigg) - \\ -(1-\lambda E)\frac{\ell(\ell+1)}{w^2\sigma^2} + \frac{1}{w^2(1+\lambda E)}\partial_\sigma^2\Bigg]f^m_\ell(\sigma) = 0\,. \end{aligned} \tag{31}$$

We define new coordinate $\tilde\sigma = w\sqrt{1+\lambda E}\,\sigma$ and the latter equation becomes

$$\Big[\partial_{\tilde\sigma}^2 + 1 + \frac{\kappa^2}{\tilde\sigma^4} + \frac{\eta}{\tilde\sigma^2}\Big]f^m_\ell(\sigma) = 0\,, \tag{32}$$

where

$$\begin{aligned} \kappa^2 &= w^2(1+\lambda E)\bigg(\lambda^2\frac{N^2-1}{4} - \frac{\lambda^2\ell(\ell+1)}{6(1+\lambda E)}\bigg)^{\frac{1}{2}}, \\ \eta &= -(1-\lambda^2E^2)\,\ell(\ell+1) \end{aligned}$$

such that

$$N > \sqrt{\frac{2\ell(\ell+1)}{3(1+\lambda E)} + 1}\,.$$

For simplicity we choose small σ, then the equation (32) is reduced to

$$\Big[\partial_{\tilde\sigma}^2 + 1 + \frac{\kappa^2}{\tilde\sigma^4}\Big]f^m_\ell(\sigma) = 0\,, \tag{33}$$

as we did in zero mode, we get the solution by using the steps (19–22) with new κ. Since we considered small σ we get

$$V(\chi) = \frac{5\tilde\sigma^6}{\kappa^4}\,,$$

then

$$f^m_\ell = \frac{\tilde\sigma}{\sqrt{\kappa}}\,e^{\pm i\chi(\tilde\sigma)}\,. \tag{34}$$

This fluctuation has two different values at large E and small E (Fig. 3) and a closer look at the potential at large and fixed N in large and small limits of electric field leads to

- $E \gg 1$, $V(\chi) \sim \frac{20w^2E\sigma^6}{\lambda N^2}$;
- $E \ll 1$, $V(\chi) \sim \frac{5w^2\sigma^6}{\lambda^2\left(\frac{N^2}{4} - \frac{\ell(\ell+1)}{6}\right)}$.

The potential in the first case is going fast to infinity than the one in the second case because of the electric field if $\sigma \ll 1$ (Fig. 4).

For large σ the equation of motion (30) of the fluctuation becomes

$$\Big[-\partial_\sigma^2 + \tilde V(\sigma)\Big]f^m_\ell(\sigma) = w^2(1+\lambda E)f^m_\ell(\sigma)\,, \tag{35}$$

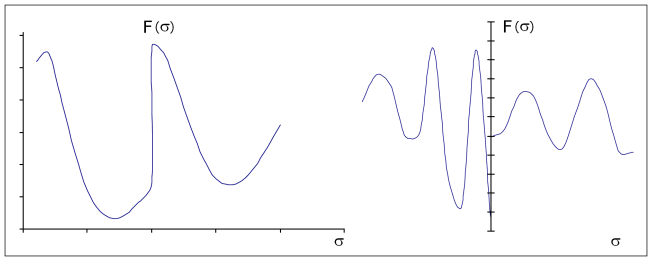

Fig. 3: The left figure shows the continuity of the fluctuation wave in high mode of the overall fluctuation at the absence of electric field E. The right figure shows the discontinuity of the wave at the presence of E in high mode meaning free boundary condition.

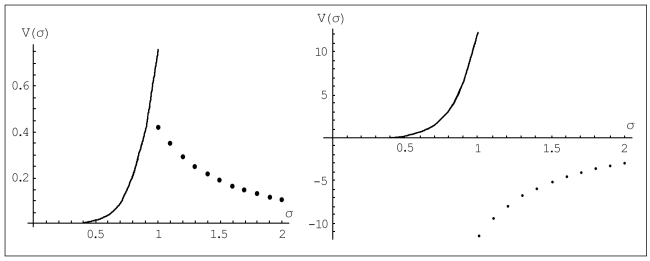

Fig. 4: The line represents the potential for small σ and dots for large σ in both figures. In high mode of overall fluctuations at the absence of electric field E, the left figure shows high potential at some stage of σ where the two curves meet. The right figure shows a critical case. The curves represent the potentials at the presence of E for small and large σ. As a remark, there is no intersecting point for theses two potentials! At some stage of σ there is a singularity.

with $\tilde{V}(\sigma)=\frac{(1-\lambda^2E^2)\,\ell(\ell+1)}{\sigma^2}$ and f_ℓ^m is now a Sturm-Liouville eigenvalue problem (Fig. 3). We found that the fluctuation has discontinuity at the presence of electric field meaning free boundary condition. Also we remark that the potential has different values in the different regions of electric field $E\gg 1$ and $E\ll 1$ and this time for large σ. In this side, the potential drops with opposite sign from one case to other and as shown in (Fig. 4). The presence of E is changing the potential totally to the opposite in both cases zero and high modes.

Consequently, by discussing explicitly the fluctuations and the potential of intersecting D1-D3 branes in D1-brane world volume theory we found that the system has Neumann boundary conditions and the end of the string can move freely on the brane for both zero and high modes of the overall transverse fluctuations case.

3.1 Relative Transverse Fluctuations

Now if we consider the "relative transverse" $\delta\phi^i(\sigma,t)=$ $=f^i(\sigma,t)\,I_N$, $i=1,2,3$ the action is

$$S=-T_1\int d^2\sigma\times \\ \times\,\mathrm{Str}\left[-\det\begin{pmatrix}\eta_{ab}+\lambda E I_{ab} & \lambda\partial_a(\phi^j+\delta\phi^j)\\ -\lambda\partial_b(\phi^i+\delta\phi^i) & Q^{ij}_*\end{pmatrix}\right]^{\frac{1}{2}}, \tag{36}$$

with $Q^{ij}_*=Q^{ij}+i\lambda\big([\phi_i,\delta\phi_j]+[\delta\phi_i,\phi_j]+[\delta\phi_i,\delta\phi_j]\big)$. As before we keep only the terms quadratic in the fluctuations and the action becomes

$$S\approx -NT_1\int d^2\sigma\Big[(1-\lambda^2E^2)\,H- \\ -(1-\lambda E)\frac{\lambda^2}{2}(\dot{f}^i)^2+\frac{(1+\lambda E)\lambda^2}{2H}(\partial_\sigma f^i)^2+\ldots\Big]. \tag{37}$$

Then the equations of motion of the fluctuations are

$$\left(-\partial_\sigma^2-w^2\frac{1-\lambda E}{1+\lambda E}\,\lambda^2\,\frac{N^2-1}{4\sigma^4}\right)f^i=w^2\frac{1-\lambda E}{1+\lambda E}f^i. \tag{38}$$

If we write $f^i=\Phi^i(\sigma)\,e^{-iwt}\delta x^i$ in the direction of x^i, the potential will be

$$V(\sigma)=-\frac{1-\lambda E}{1+\lambda E}\,\lambda^2\,\frac{N^2-1}{4\sigma^4}\,w^2.$$

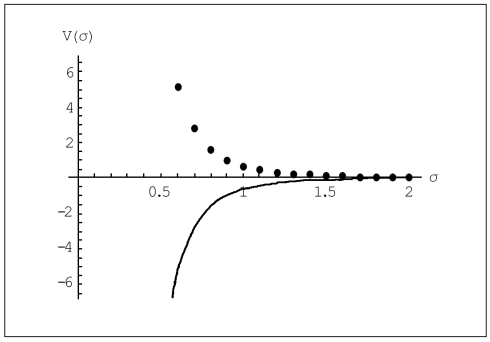

Fig. 5: The line shows the potential in zero mode of the relative funnel's fluctuations at the absence of electric field E and the dots represent the potential in the same mode at the presence of E. The presence of E is changing the potential totally to the opposite.

Let's discuss the cases of electric field:

- $E\ll 1$, $V(\sigma)\sim-\lambda^2\frac{N^2-1}{4\sigma^4}w^2$;
- $E\gg 1$, $V(\sigma)\sim\lambda^2\frac{N^2-1}{4\sigma^4}w^2$.

Also in the relative case, this is Neumann boundary condition (Fig. 5) which can be also shown by finding the solution of (38) for which we follow the same way as above by making a coordinate change suggested by WKB. This case is seen as a zero mode of what is following so we will treat this in general case by using this coordinate change for high modes.

Now let's give the equation of motion of relative transverse fluctuations of high ℓ modes with $(N-N_f)$ strings intersecting D3-branes. The fluctuation is given by

$$\delta\phi^i(\sigma,t)=\sum_{\ell=1}^{N-1}\psi^i_{i_1\ldots i_\ell}\alpha^{i_1}\ldots\alpha^{i_\ell}$$

with $\psi^i_{i_1\ldots i_\ell}$ are completely symmetric and traceless in the lower indices.

The action describing this system is

$$S \approx -NT_1 \int d^2\sigma \Big[(1-\lambda^2 E^2)\, H - \\ -(1-\lambda E) H \frac{\lambda^2}{2} (\partial_t \delta\phi^i)^2 + \frac{(1+\lambda E)\lambda^2}{2H} (\partial_\sigma \delta\phi^i)^2 - \\ -(1-\lambda E)\frac{\lambda^2}{2} \big[\phi^i, \delta\phi^i\big]^2 - \frac{\lambda^4}{12} \big[\partial_\sigma \phi^i, \partial_t \delta\phi^i\big]^2 + \dots \Big]. \quad (39)$$

The equation of motion for relative transverse fluctuations in high mode is as follows

$$\left[\frac{1-\lambda E}{1+\lambda E} H \partial_t^2 - \partial_\sigma^2\right] \delta\phi^i + (1-\lambda E)\big[\phi^i, \big[\phi^i, \delta\phi^i\big]\big] - \\ -\frac{\lambda^2}{6}\big[\partial_\sigma \phi^i, \big[\partial_\sigma \phi^i, \partial_t^2 \delta\phi^i\big]\big] = 0\,. \quad (40)$$

By the same way as done for overall transverse fluctuations the equation of motion for each mode is

$$\left[-\partial_\sigma^2 + \left(\frac{1-\lambda E}{1+\lambda E}\left(1+\lambda^2 \frac{N^2-1}{4\sigma^4}\right) - \frac{\lambda^2 \ell(\ell+1)}{6\sigma^4}\right)\partial_t^2 + \right. \\ \left. + (1-\lambda E)\frac{\ell(\ell+1)}{\sigma^2}\right] \delta\phi_\ell^i = 0\,. \quad (41)$$

We take $\delta\phi_\ell^i = f_\ell^i\, e^{-iwt}\delta x^i$, then the equation (41) becomes

$$\left[-\partial_\sigma^2 - \left(\frac{1-\lambda E}{1+\lambda E}\left(1+\lambda^2 \frac{N^2-1}{4\sigma^4}\right) - \frac{\lambda^2 \ell(\ell+1)}{6\sigma^4}\right) w^2 + \right. \\ \left. + (1-\lambda E)\frac{\ell(\ell+1)}{\sigma^2}\right] f_\ell^i = 0\,. \quad (42)$$

To solve the equation we choose for simplicity the boundaries of σ; For small σ, the equation is reduced to

$$\left[-\partial_\sigma^2 - \left(\frac{1-\lambda E}{1+\lambda E}\left(1+\lambda^2 \frac{N^2-1}{4\sigma^4}\right) - \right. \right. \\ \left. \left. - \frac{\lambda^2 \ell(\ell+1)}{6\sigma^4}\right) w^2\right] f_\ell^i = 0\,, \quad (43)$$

which can be rewritten as follows

$$\left[-\frac{1+\lambda E}{1-\lambda E}\partial_\sigma^2 - \left(\left(1+\lambda^2 \frac{N^2-1}{4\sigma^4}\right) - \right. \right. \\ \left. \left. - \frac{1+\lambda E}{1-\lambda E}\frac{\lambda^2 \ell(\ell+1)}{6\sigma^4}\right) w^2\right] f_\ell^i = 0\,. \quad (44)$$

We change the coordinate to $\tilde\sigma = \sqrt{\frac{1-\lambda E}{1+\lambda E}}\, w\sigma$ and the equation (44) becomes

$$\left[\partial_{\tilde\sigma}^2 + 1 + \frac{\kappa^2}{\tilde\sigma^4}\right] f_\ell^i(\tilde\sigma) = 0\,, \quad (45)$$

with

$$\kappa^2 = w^4\lambda^2\, \frac{3(1-\lambda E)^2(N^2-1) - 2(1-\lambda^2 E^2)\,\ell(\ell+1)}{12(1+\lambda E)^2}\,.$$

Then we follow the suggestions of WKB by making a coordinate change;

$$\beta(\tilde\sigma) = \int_{\sqrt{\kappa}}^{\tilde\sigma} dy \sqrt{1+\frac{\kappa^2}{y^4}}\,, \quad (46)$$

and

$$f_\ell^i(\tilde\sigma) = \left(1+\frac{\kappa^2}{\tilde\sigma^4}\right)^{-\frac{1}{4}} \tilde f_\ell^i(\tilde\sigma)\,. \quad (47)$$

Thus, the equation (45) becomes

$$\Big(-\partial_\beta^2 + V(\beta)\Big)\tilde f^i = 0\,, \quad (48)$$

with

$$V(\beta) = \frac{5\kappa^2}{\left(\tilde\sigma^2 + \frac{\kappa^2}{\tilde\sigma^2}\right)^3}\,. \quad (49)$$

Then

$$f_\ell^i = \left(1+\frac{\kappa^2}{\tilde\sigma^4}\right)^{-\frac{1}{4}} e^{\pm i\beta(\tilde\sigma)}\,. \quad (50)$$

The discussion is similar to the overall case; so the obtained fluctuation has the following limits; at large σ, $f_\ell^i \sim$ $\sim e^{\pm i\beta(\tilde\sigma)}$ and if σ is small $f_\ell^i = \frac{\sqrt{\kappa}}{\tilde\sigma} e^{\pm i\beta(\tilde\sigma)}$. These are the asymptotic wave function in the regions $\beta \to \pm\infty$, while around $\beta \sim 0$; i.e. $\tilde\sigma \sim \sqrt{\kappa}$, $f_\ell^i \sim 2^{-\frac{1}{4}}$.

Then let's have a look at the potential in various limits of electric field:

- $E \sim \frac{1}{\lambda}$, $V(\beta) \sim 0$;
- $E \gg 1$, $\kappa^2 \equiv \kappa_+^2 \sim w^4\lambda^2 \frac{3(N^2-1)+2\ell(\ell+1)}{12}$, then $\sigma \sim 0$ $\Rightarrow V(\beta) \sim \frac{5\tilde\sigma^6}{\kappa_+^4}$;
- $E \ll 1$, $\kappa^2 \equiv \kappa_-^2 \sim w^4\lambda^2 \frac{3(N^2-1)-2\ell(\ell+1)}{12}$; for this case we get $\sigma \sim 0 \Rightarrow V(\beta) \sim \frac{5\tilde\sigma^6}{\kappa_-^4}$;

this means that we have a Neumann boundary condition with relative fluctuations at small σ (Fig. 6).

Now, if σ is too large the equation of motion (42) becomes

$$\left[-\partial_\sigma^2 + (1-\lambda E)\frac{\ell(\ell+1)}{\sigma^2}\right] f_\ell^i = \frac{1-\lambda E}{1+\lambda E} w^2 f_\ell^i\,. \quad (51)$$

We see, the associated potential $V(\sigma) = (1-\lambda E)\frac{\ell(\ell+1)}{\sigma^2}$ goes to $-\epsilon$ in the case of $E \gg 1$ and to $+\epsilon$ if $E \ll 1$ since σ is too large with $\epsilon \sim 0$, (Fig. 6). We get the same remark as before by dealing with the fluctuations for small and large σ (50) and solving (51) respectively, at the presence of electric field that we have two separated regions depending on the electric field (Fig. 7).

We discussed quite explicitly through this section the fluctuation of the funnel solution of D1$\perp$D3 branes by treating different modes and different directions of the fluctuation. We found that the system got an important property because of the presence of electric field; the system has Neumann boundary condition.

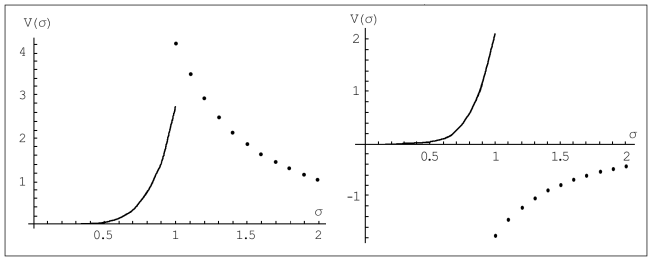

Fig. 6: As we saw in high mode of overall fluctuations, also for relative case we get high potential at some stage of σ where the the tow curves meet representing potentials for small and large σ at the absence of electric field E in the left figure. Right figure shows again a singularity this time in relative case because of the presence of E.

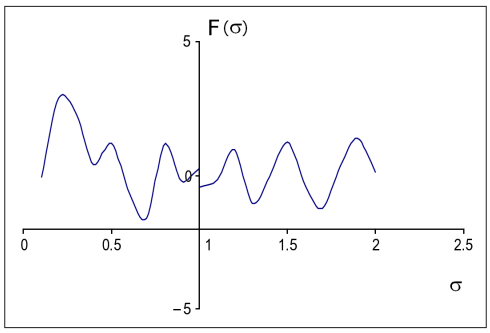

Fig. 7: The presence of electric field E causes a discontinuity of the wave in high mode of relative case meaning free boundary condition.

4 Conclusion

We have investigated the intersecting D1-D3 branes through a consideration of the presence of electric field. We have treated the fluctuations of the funnel solutions and we have discussed explicitly the potentials in both systems. We found a specific feature of the presence of electric field. When the electric field is going up and down the potential of the system is changing and the fluctuations of funnel solutions as well which cause the division of the system to tow regions. Consequently, the end point of the dyonic strings move on the brane which means we have Neumann boundary condition.

The present study is in flat background and there is another interesting investigation is concerning the perturbations propagating on a dyonic string in the supergravity background [12, 5] of an orthogonal 3-brane. Then we can deal with this important case and see if we will get the same boundary conditions by treating the dyonic fluctuations.

Acknowledgements

This work was supported by a grant from the Arab Fund for Economic and Social Development.

Submitted on March 07, 2007
Accepted on March 12, 2007

References

1. Polchinski J. Tasi lectures on D-branes. arXiv: hep-th/9611050; Leigh R. *Mod. Phys. Lett.*, 1989, v. A4, 2767.
2. Callan C. G. and Maldacena J. M. *Nucl. Phys. B*, 1998, v. 513, 198; arXiv: hep-th/9708147.
3. Gibbons G. W. *Nucl. Phys. B*, 1998, v. 514, 603; arXiv: hep-th/9709027; Howe P. S., Lambert N. D. and West P. C. *Nucl. Phys. B*, 1998, v. 515, 203; arXiv: hep-th/9709014; Banks T., Fischler W., Shenker S. H. and Susskind L. *Phys. Rev. D*, 1997, v. 55, 5112; arXiv: hepth/9610043; Kabat D. and Taylor W. *Adv. Theor. Math. Phys.*, 1998, v. 2, 181; arXiv: hep-th/9711078; Rey S. arXiv: hep-th/9711081; Myers R. C. *JHEP*, 1999, v. 9912, 022; arXiv: hep-th/9910053.
4. Brecher D. *Phys. Lett. B*, 1998, v. 442, 117; arXiv: hep-th/9804180; Cook P., de Mello Koch R. and Murugan J. *Phys. Rev. D*, 2003, v. 68, 126007; arXiv: hep-th/0306250; Barrett J. K. and Bowcock P. arXiv: hep-th/0402163.
5. Constable N. R., Myers R. C. and Tafjord O. *Phys. Rev. D*, 2000, v. 61, 106009; arXiv: hep-th/9911136.
6. Rey S.-J. and Yee J.-T. *Nucl. Phys. B*, 1998, v. 52, 229; arXiv: hep-th/9711202; Lee S., Peet A. and Thorlacius L. *Nucl. Phys. B*, 1998, v. 514, 161; arXiv: hep-th/9710097; Kastor D. and Traschen J. *Phys. Rev. D*, 2000, v. 61, 024034; arXiv: hep-th/9906237; Rey S.-J. and Yee J.-T. *Eur. Phys. J. C*, 2001, v. 22, 379; arXiv: hep-th/9803001.
7. Bhattacharyya R. and de Mello Koch R. arXiv: hep-th/0508131; Papageorgakis C., Ramgoolam S. and Toumbas N. *JHEP*, 2006, v. 0601, 030; arXiv: hep-th/0510144; Bak D., Lee J. and Min H. *Phys. Rev. D*, 1999, v. 59, 045011; arXiv: hep-th/9806149.
8. Castelino J., Lee S. and Taylor W. *Nucl. Phys. B*, 1998, v. 526, 334; arXiv: hep-th/9712105; Grosse H., Klimcik C. and Presnajder P. *Commun. Math. Phys.*, 1996, v. 180, 429; arXiv: hepth/9602115.
9. Savvidy K. G. and Savvidy G. K. *Nucl. Phys. B*, 1999, v. 561, 117; arXiv: hep-th/9902023.
10. Constable N. R., Myers R. C. and Tafjord O. *JHEP*, 2001, v. 0106, 023; arXiv: hep-th/0102080.
11. Gibbons G. W. *Nucl.Phys. B*, 1998, v. 514, 603–639; arXiv: hep-th/9709027.
12. Lee S., Peet A. and Thorlacius L. *Nucl. Phys. B*, 1998, v. 514, 161; arXiv: hep-th/9710097; Kastor D. and Traschen J. *Phys. Rev. D*, 2000, v. 61, 024034; arXiv: hep-th/9906237.

On the Possibility of Nuclear Synthesis During Orthopositronium Formation by β^+-Decay Positrons in Deuterium

Boris A. Kotov, Boris M. Levin* and Vladimir I. Sokolov†

*E-mail: bormikhlev@mail.ru, bormikhlev@mail.ioffe.ru; †E-mail: v.sokolov@mail.ioffe.ru

Observations of the "isotopic anomaly" of positron (^{22}Na) annihilation lifetime spectra in samples of gaseous neon of various isotopic abundance, the independent observations of the orthopositronium lifetime anomaly, and comparison of unique experimental data on the positron's annihilation lifetime spectra in condensed deuterium (D_2) and protium (H_2), suggest a hypothesis on synthesis of ^{4}He during the orthopositronium formation in deuterium. The decisive experiment is offered.

1 Introduction

When a muon replaces an electron in a two-centre "molecular ion" of light nuclei (e.g. $[d\,\mu^-\,d]^+$, where d is the deuteron), the structure of the ion is changed in a qualitative way — it is converted into a one-centre "compound ion" $[^{4*}He\ \mu^-]^+$ owing to a two order increase in lepton mass. Energy is then released as a result of fragmentation* and the liberation of a muon (μ catalysis).

There is the possibility that conversions of this sort occur in processes involving light diatomic molecules (in particular, D_2) as they interact with positrons in the process of production of orthopositronium [o-Ps, $^T\text{Ps} \equiv {}^3(e^+e^-)_1$]. This suggestion is based primarily on the results of independent measurements which have established lifetime anomalies in o-Ps annihilation (deviations from QED), on the "isotopic anomaly" [1] and the "λ_T-anomaly" [2, 3].

"Positronium, the bound state of the electron and positron, is a purely leptonic state — it is effectively free of hadronic and weak-interaction effects" [2], and its annihilation is calculated with high precision in QED. Observation of the "isotopic anomaly" [1] was the basis for careful study this assertion. This relationship sets up a new perspective which merits further studies.

In this connexion there is special interest in the results on lifetime annihilation spectra of positrons (orthopositronium) in liquid and solid deuterium [4] and comparison of these results with corresponding results on protium [5]. In particular, Liu and Roberts [4] have measured the short-lived components in the time-resolved spectra: $\tau_1 = 0.83 \pm 0.03$ ns (liquid D_2, 20.4 K) and $\tau_1 = 0.74 \pm 0.03$ ns (solid D_2, 13 K). However, there are no data on a long-lived component (o-Ps). The results for H_2 are $\tau_1 = 0.92 \pm 0.04$ ns (20.4 K) and $\tau_1 = 0.80 \pm 0.03$ ns (13 K). In contrast with the D_2 case, data were reported on o-Ps ($\tau_2 = 28.6 \pm 2.3$ ns at 20.4 K and 14.6 ± 1.2 ns at 13 K [5]).

Clearly, o-Ps is formed in condensed deuterium in the same way as in condensed protium. We are thus led to ask whether o-Ps is indeed absent from the time-resolved annihilation spectra in condensed deuterium. The single corresponding study [4] has failed to answer this question unambiguously.

2 Background of the hypothesis and the first attempt of its verification (a cumulative method of identification of products of nuclear synthesis)

If this difference between the time-resolved positron annihilation spectra in the condensed states of H_2 and D_2 is confirmed, then the absence of the o-Ps-component in liquid and solid deuterium could be explained on the basis that it is quenched by radiolysis products with net charge and spin, in a "blast hole" of charged products of nuclear synthesis which carry off a total energy of a few MeV per event. These products of radiolysis suppress the long-living component of the lifetime spectra (*quenching* of o-Ps [6]).

For an explanation and quantitative description of the orthopositronium anomalies [1–3] the hypothesis of representation of the β^+-decay of the nuclei ^{22}Na, ^{68}Ga, etc. ($\Delta J^\pi = 1^+$) as a *topological quantum transition* in a limited (macroscopic) "volume" of space-time is justified. The limited "volume" ("*defect*") of space-time, i.e. *vacuum-like state of matter* with positive Planckian mass $+M_{Pl}$, is the *long-range atom* having a full number of sites $N^{(3)} = 1.302 \times 10^{19}$. All its charges (baryon charge among them) are compensated for by a discrete scalar *C-field* (the "mirror Universe" with negative Planckian mass $-M_{Pl}$). A "defect" of space-time becomes some "background" where orthopositronium is within of macroscopic "*long-range atom nucleus*" with the number of sites $\bar{n} = 5.2780 \times 10^4$ in oscillation [7–12].

"Let there be a certain probability for disturbances in vacuum to alter its topology. If we now visualize some sort of 'handedness' such that at the entrance the particle is right-handed, and at the exit it is left-handed, then we have a certain probability for a right-left particle transition, which

*In the neutron channel ^{3}He (0.82 MeV) + n (2.45 MeV), or in the tritium channel, T (1.01 MeV) + p (3.02 MeV).

means that the particles have a rest mass" [13].

The aforementioned oscillations between the observable Universe and the "mirror Universe" are responsible for an additional mode of the orthopositronium annihilations

$$\text{o-Ps}\backslash\text{o-Ps}'(\text{p-Ps}') \to \gamma^{\circ}\backslash 2\gamma',$$

where γ° is a notoph, a massless particle with zero helicity, in addition to the properties to the photon (helicity ± 1); in interactions the notoph, as well as the photon, transfers spin 1 [14]. These oscillations can also cause an additional mass for electrons e_*^- that can result in nuclear synthesis during o-Ps formation by

$$e_\beta^+ + \left[d e^- e^- d\right] \to {}^3(e_\beta^+ e_*^-)_1 \left[d e_*^- d\right]^+ \to$$
$$\to \left[{}^{4*}\text{He}\, e^-\right] \to \begin{bmatrix} {}^3\text{He} + \text{n} \\ \text{T} + \text{p} \end{bmatrix}.$$

Thus, the orthopositronium anomalies (as manifestation of its connexion with the "mirror Universe") permit the formulation of a hypothesis about effective o-Ps topological mass ($\sim 200\, m_e$) and, accordingly, a two-way connexion of an electron in $[d e_*^- d]^+$ (owing to an exchange interaction at the moment of o-Ps formation), along with an experimental programme for studying this hypothesis [15].

Amongst the products of reaction we focus on ^{3}He, since (on the one hand) it is formed directly in the neutron channel, and (on the other) it accumulates, because of the decay $\text{T} \to {}^3\text{He} + e^- + \tilde{\nu}$ from the tritium channel. The accumulation method with exposition time $t_{exp} \sim 0.32$ years and a high-sensitivity *magnetic resonant mass-spectrometer* for the analysis, ^{3}He and ^{4}He have established a *negative result* concerning the products of fragmentation of a compound ion $[{}^{4*}\text{He}\, e^-]^+$ not only by the neutron channel, but also by the tritium channel [15].

However these results do not rule out the overall hypothesis which we consider: there is a possibility that nuclear synthesis involving o-Ps is cut off in the stage of formation of the "compound ion" $[{}^{4*}\text{He}\, e^-]^+$, with subsequent relaxation of nuclear excitation energy (23.85 MeV) as kinetic energy of an "α-particle", as the "long-range atom" through an "atomic nucleus" can relinquish its non-recoil energy. Now there are no data on quantum energy excitation structure of the "nucleus" and "long-range atom" as a whole. Because of the disproportionately large mass of an "atom" (M_{Pl}) in comparison with the mass of an "α-particle", the latter can practically carry away all energy of excitation and formation in a final state, after delay and recombination, as follows,

$$e_\beta^+ + [d e^- e^- d] \to {}^3(e_\beta^+ e_*^-)_1 [d e_*^- d]^+ \to$$
$$\to \left[{}^{4*}\text{He}\, e^-\right] \to {}^4\text{He} + e^- + Q\,(23.85\,\text{MeV}),$$

but part of energy can be transferred to the "lattice" of the *vacuum-like state of matter*.

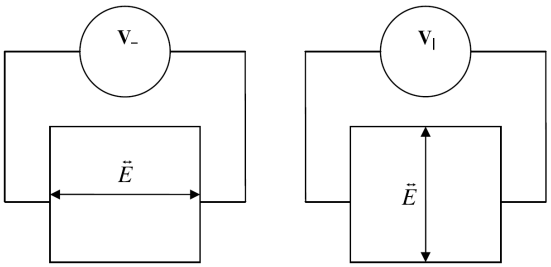

Fig. 1: V_- and $V_|$ are electric breakdown thresholds of the gas when the dc electric field is oriented horizontally and vertically respectively. A decrease in the electric breakdown threshold of deuterium (D_2) is anticipated for perpendicular orientation of electric field to gravity, under other identical conditions ($V_- < V_|$). For H_2 the electric breakdown thresholds in these measurements cannot significantly differ ($V_- \equiv V_|$). (A conventional criterion: $\vec{E} > 6.7$ kV/cm [16].)

3 The electric field opens an opportunity of direct check of a hypothesis

The latest work of the Michigan group has created a new situation for the hypothesis adduced herein. It is necessary to emphasize that the result of the last set of Michigan measurements, after introduction of a dc electric field up to $\sim$7 kV/cm in a measuring cell [16], we treat as the first observation of a connexion between gravitation and electricity [11, 12]. The introduction of an electric field in the final Michigan experiment can have other (additional) consequences to those given by authors for o-Ps thermalization [16]. According to the hypothesis, manifestation of the "isotopic anomaly" [1] and the λ_T-anomaly [2, 3] as *macroscopic quantum effects* is the generalized "displacement currents" in the final state of the topological quantum transition for nuclei ^{22}Na, ^{68}Ga, etc. The electric field probably counteracts the generalized displacement currents and has led to suppression of macroscopic quantum effects [10, 12]. The Michigan experiment [16] was set up in such a way that an electric field introduced into the experiment (it accelerates the particle beam before the target) merely suppressed the anomaly, despite the fact that the electric field helps achieve complete thermalization of orthopositronium in the measurement cell. Consequently, the anomaly, present but suppressed by the field, merely became obscured in the given experiment.

In work [12] the analysis of the mechanism of suppression of macroscopic quantum effects by an electric field is presented, from which it follows that comparative measurements of a threshold of electric breakdown in a cell with a source of positrons (^{22}Na) alternately filled by dense gases (D_2, H_2), and (for each gas) with change of orientation of an electric field (parallel and perpendicular to gravity) can be a more sensitive tool for identification of *macroscopic quantum effects* in comparison with the accumulation method [15]. At sufficiently high pressures of D_2 the activity of a

source of stationary concentrations of positrons of the radiolysis products in a field $\vec{E} > 6.7$ kV/cm, the background level created by cosmic and other casual sources of radiations can be repeatedly exceeded. In these conditions the threshold of electric breakdown of a gas oriented parallel to gravity ($V_{|}$) will be higher than the electric breakdown threshold of gas oriented perpendicular to gravity (V_{-}), under other identical conditions ($V_{|} > V_{-}$).

The experiment suggested herein, with introduction of an electric field $\vec{E} > 7$ kV/cm into a measuring cell, provided that a field $\vec{E} > 6.7$ kV/cm is still under the electric breakdown threshold of the gas (see Fig. 1), is the *decisive experiment*.

Dedication

This paper is dedicated to the memory of our long-time coauthor Dr. Boris Aleksandrovich Kotov (October 8, 1938 — April 10, 2005).

B. M. Levin and V. I. Sokolov

Submitted on March 23, 2007
Accepted on April 05, 2007

References

1. Levin B.M., Kochenda L.M., Markov A.A. and Shantarovich V.P. Time spectra of annihilation of positrons (^{22}Na) in gaseous neon of various isotopic compositions. *Sov. J. Nucl. Phys.*, 1987, v. 45 (6), 1119.
2. Westbrook C.I., Gidley D.W., Conti R.S. and Rich A. New Precision Measurement of the orthopositronium decay rate: a discrepancy with theory. *Phys. Rev. Lett.*, 1987, v. 58 (13), 1328; Precision measurement of the orthopositronium decay rate using the gas technique. *Phys. Rev. A*, v. 40 (10), 5489.
3. Nico J.S., Gidley D.W., Rich A. and Zitzewitz P.W. Precision measurement of the orthopositronium decay rate using the vacuum technique. *Phys. Rev. Lett.*, 1990, v. 65 (11), 1344.
4. Liu D.C. and Roberts W.K. Positron annihilation in condensed gases. *Phys. Rev.*, 1963, v. 130 (6), 2322.
5. Liu D.C. and Roberts W.K. Free-positron annihilation mean life in diatomic and rare gases in liquid and solid states. *Phys. Rev.*, 1963, v. 132 (4), 1633.
6. Goldanskii V.I. Physical chemistry of the positron and positronium. In: *Atomic Energy Review*, v. VI, No. 1, IAEA, Vienna, 1968.
7. Holdom B. Two U(1)'s and ε charge shifts. *Phys. Lett. B*, 1986, v. 166 (2), 196.
8. Glashow S.L. Positronium versus the mirror Universe. *Phys. Lett. B*, 1986, v. 167 (1), 35.
9. Levin B.M. On the kinematics of one-photon annihilation of orthopositronium. *Phys. At. Nucl.*, 1995, v. 58, 332.
10. Levin B.M. Orthopositronium: annihilation of positron in gaseous neon. arXiv: quant-ph/0303166.
11. Levin B.M. and Sokolov V.I. On an additional realization of supersymmetry in orthopositronium lifetime anomalies. arXiv: quant-ph/0702063.
12. Kotov B.A., Levin B.M. and Sokolov V.I. Orthopositronium: on the possible relation of gravity to electricity. Preprint-1784, A. F. Ioffe Physical Technical Institute of the Russian Academy of Sciences. St Petersburg, 2005; arXiv: quant-ph/0604171.
13. Zeldovich Y.B. Gravity, charges, cosmology and coherence. *Physics-Uspekhi*, 1977, v. 123, 502.
14. Ogievetskii V.I. and Polubarinov I.V. Notoph and its possible interactions. *Sov. J. Nucl. Phys.*, 1966, v. 4 (1), 216.
15. Kotov B.A. and Levin B.M. Orthopositronium, mirror Universe and cold fusion. Preprint LSFF/91-01, January 5, 1991; Levin B.M., Sokolov V.I., Khabarin L.V. and V.S.Yudenich. Comparative measurements of the isotopic composition of trace amounts of helium in deuterium after bombardment with positrons from ^{22}Na decay. *Sov. J. Nucl. Phys.*, 1992, v. 55 (10), 1452; Levin B.M, Borissova L.B. and Rabounski D.D. Orthopositronium and space-time effects. Moscow-St.Petersburg, Lomonosov Workshop, 1999, p.59.
16. Vallery R.S., Gidley D.W. and Zitzewitz P.W. Resolution of orthopositronium-lifetime puzzle. *Phys. Rev. Lett.*, 2003, v. 90 (20), 203402.

Reply to "Notes on Pioneer Anomaly Explanation by Satellite-Shift Formula of Quaternion Relativity"

Vic Christianto* and Florentin Smarandache†

*Sciprint.org — a Free Scientific Electronic Preprint Server, http://www.sciprint.org
E-mail: admin@sciprint.org

†Department of Mathematics, University of New Mexico, Gallup, NM 87301, USA
E-mail: smarand@unm.edu

In the present article we would like to make a few comments on a recent paper by A. Yefremov in this journal [1]. It is interesting to note here that he concludes his analysis by pointing out that using full machinery of Quaternion Relativity it is possible to explain Pioneer XI anomaly with excellent agreement compared with observed data, and explain around 45% of Pioneer X anomalous acceleration. We argue that perhaps it will be necessary to consider extension of Lorentz transformation to Finsler-Berwald metric, as discussed by a number of authors in the past few years. In this regard, it would be interesting to see if the use of extended Lorentz transformation could also elucidate the long-lasting problem known as Ehrenfest paradox. Further observation is of course recommended in order to refute or verify this proposition.

1 Introduction

We are delighted to read A. Yefremov's comments on our preceding paper [3], based on his own analysis of Pioneer anomalous "apparent acceleration" [1]. His analysis made use of a method called Quaternion Relativity, which essentially is based on $\mathrm{SO}(1,2)$ form invariant quaternion square root from space-time interval rather than the interval itself [1, 2]. Nonetheless it is interesting to note here that he concludes his analysis by pointing out that using full machinery of Quaternion Relativity it is possible to explain Pioneer XI anomaly with excellent agreement compared with observed data, and explain around 45% of Pioneer X anomalous acceleration [1].

In this regard, we would like to emphasize that our preceding paper [3] was based on initial "conjecture" that in order to explain Pioneer anomaly, it would be necessary to generalize pseudo-Riemann metric of General Relativity theory into broader context, which may include Yefremov's Quaternion Relativity for instance. It is interesting to note here, however, that Yefremov's analytical method keeps use standard Lorentz transformation in the form Doppler shift effect (Eq. 6):

$$f = \frac{f'}{\sqrt{1-\left(\frac{v_D}{c}\right)^2}}\left(1-\frac{v_D}{c}\cos\beta\right). \qquad (1)$$

While his method using relativistic Doppler shift a la Special Relativity is all right for such a preliminary analysis, in our opinion this method has a drawback that it uses "standard definition of Lorentz transformation" based on 2-dimensional problem of *rod-on-rail* as explained in numerous expositions of relativity theory [5]. While this method of rod-on-rail seems sufficient to elucidate why "simultaneity" is ambiguous term in physical sense, it does not take into consideration 3-angle problem in more general problem. This is why we pointed out in our preceding paper that apparently General Relativity inherits the same drawback from Special Relativity [3].

Another problem of special relativistic definition of Lorentz transformation is known as "reciprocity postulate", because in Special Relativity it is assumed that: $x \leftrightarrow x'$, $t \leftrightarrow t'$, $v \leftrightarrow -v'$ [6]. This is why Doppler shift can be derived without assuming reciprocity postulate (which may be regarded as the "third postulate" of Special Relativity) and without special relativistic argument, see [7]. Nonetheless, in our opinion, Yefremov's Quaternion Relativity is free from this "reciprocity" drawback because in his method there is difference between moving-observer and static-observer [2].

An example of implications of this drawback of 1-angle problem of Lorentz transformation is known as Ehrenfest paradox, which can be summarized as follows: "According to Special Relativity, a moving rod will exhibit apparent length-reduction. This is usually understood to be an observational effect, but if it is instead considered to be a real effect, then there is a paradox. According to Ehrenfest, the perimeter of a rotating disk is like a sequence of rods. So does the rotating disk shatter at the rim?" Similarly, after some thought Klauber concludes that "*The second relativity postulate does not appear to hold for rotating systems*" [8].

While it is not yet clear whether Quaternion-Relativity is free from this Ehrenfest paradox, we would like to point out that an alternative metric which is known to be nearest to Riemann metric is available in literature, and known as Finsler-Berwald metric. This metric has been discussed adequately by Pavlov, Asanov, Vacaru and others [9–12].

2 Extended Lorentz-transformation in Finsler-Berwald metric

It is known that Finsler-Berwald metric is subset of Finslerian metrics which is nearest to Riemannian metric [12], therefore it is possible to construct pseudo-Riemann metric based on Berwald-Moor geometry, as already shown by Pavlov [4]. The neat link between Berwald-Moor metric and Quaternion Relativity of Yefremov may also be expected because Berwald-Moor metric is also based on analytical functions of the H4 variable [4].

More interestingly, there was an attempt in recent years to extend 2d-Lorentz transformation in more general framework on H4 of Finsler-Berwald metric, which in limiting cases will yield standard Lorentz transformation [9, 10]. In this letter we will use extension of Lorentz transformation derived by Pavlov [9]. For the case when all components but one of the velocity of the new frame in the old frame coordinates along the three special directions are equal to zero, then the transition to the frame moving with velocity V_1 in the old coordinates can be expressed by the new frame as [9, p.13]:

$$\begin{pmatrix} x_0 \\ x_1 \\ x_2 \\ x_3 \end{pmatrix} = \begin{bmatrix} [F] & [0] \\ [0] & [F] \end{bmatrix} = \begin{pmatrix} x'_0 \\ x'_1 \\ x'_2 \\ x'_3 \end{pmatrix} \qquad (2)$$

where the transformation matrix for Finsler-Berwald metric is written as follows [9, p.13]:

$$[F] = \begin{pmatrix} \frac{1}{\sqrt{1-V_1^2}} & \frac{V_1}{\sqrt{1-V_1^2}} \\ \frac{V_1}{\sqrt{1-V_1^2}} & \frac{1}{\sqrt{1-V_1^2}} \end{pmatrix} \qquad (3)$$

and

$$[0] = \begin{pmatrix} 0 & 0 \\ 0 & 0 \end{pmatrix}. \qquad (4)$$

Or

$$x_0 = \frac{x'_0 + V x'_1}{\sqrt{1-V_1^2}}\, x_1 = \frac{V x'_0 + x'_1}{\sqrt{1-V_1^2}}\,, \qquad (5)$$

and

$$x_2 = \frac{x'_2 + V x'_3}{\sqrt{1-V_1^2}}\, x_3 = \frac{V x'_2 + x'_3}{\sqrt{1-V_1^2}}. \qquad (6)$$

It shall be clear that equation (5) $(x'_0, x'_1) \leftrightarrow (x_0, x_1)$ coincides with the corresponding transformation of Special Relativity, while the transformation in equation (6) differs from the corresponding transformation of Special Relativity where $x_2 = x'_2$, $x_3 = x'_3$ [9].

While we are not yet sure whether the above extension of Lorentz transformation could explain Pioneer anomaly better than recent analysis by A. Yefremov [1], at least it can be expected to see whether Finsler-Berwald metric could shed some light on the problem of Ehrenfest paradox. This proposition, however, deserves further theoretical considerations.

In order to provide an illustration on how the transformation keeps the Finslerian metric invariant, we can use Maple algorithm presented by Asanov [10, p.29]:

```
> c1:=cos(tau);c2:=cos(psi);c3:=cos(phi);
> u1:=sin(tau);u2:=sin(psi);u3:=sin(phi);
> l1:=c2*c3−c1*u2*u3;l2:=−c2*u3−c1*u2*c3;l3:=u1*u2;
> m1:=u2*c3+c1*c2*u3;m2:=−u2*u3+c1*c2*c3;m3:=−u1*c2;
> n1:=u1*u3; u1*c3; c1;
> F1:=(e1)^((l1+m1+n1+l2+m2+n2+l3+m3+n3+1)/4)*
(e2)^((−l1−m1−n1+l2+m2+n2−l3−m3−n3+1)/4)*
(e3)^((l1+m1+n1−l2−m2−n2−l3−m3−n3+1)/4)*
(e4)^((−l1−m1−n1−l2−m2−n2+l3+m3+n3+1)/4):
> F2:=(e1)^((−l1+m1−n1−l2+m2−n2−l3+m3−n3+1)/4)*
(e2)^((l1−m1+n1−l2+m2−n2+l3−m3+n3+1)/4)*
(e3)^((−l1+m1−n1+l2−m2+n2+l3−m3+n3+1)/4)*
(e4)^((l1−m1+n1+l2−m2+n2−l3+m3−n3+1)/4):
> F3:=(e1)^((l1−m1−n1+l2−m2−n2+l3−m3−n3+1)/4)*
(e2)^((−l1+m1+n1+l2−m2−n2−l3+m3+n3+1)/4)*
(e3)^((l1−m1−n1−l2+m2+n2−l3+m3+n3+1)/4)*
(e4)^((−l1+m1+n1−l2+m2+n2+l3−m3−n3+1)/4):
> F4:=(e1)^((−l1−m1+n1−l2−m2+n2−l3−m3+n3+1)/4)*
(e2)^((l1+m1−n1−l2−m2+n2+l3+m3−n3+1)/4)*
(e3)^((−l1−m1+n1+l2+m2−n2+l3+m3−n3+1)/4)*
(e4)^((l1+m1−n1+l2+m2−n2−l3−m3+n3+1)/4):
> a:=array(1..4,1..4):
for i from 1 to 4
do
for j from 1 to 4
do
a[i,j]:=diff(F||i,e||j);
end do:
end do:
> b:=array(1..4,1..4):
for i from 1 to 4
do
for j from 1 to 4
do
b[i,j]:=simplify(add(1/F||k*diff(a[k,i],e||j),k=1..4),symbolic);
end do:
end do:
> print(b);
```

The result is as follows:

$$\begin{bmatrix} 0 & 0 & 0 & 0 \\ 0 & 0 & 0 & 0 \\ 0 & 0 & 0 & 0 \\ 0 & 0 & 0 & 0 \end{bmatrix}.$$

This result showing that all the entries of the matrix are zeroes support the argument that the metricity condition is true [10].

3 Concluding remarks

In the present paper we noted that it is possible to generalise standard Lorentz transformation into H4 framework of Finsler-Berwald metric. It could be expected that this extended Lorentz transformation could shed some light not only to Pioneer anomaly, but perhaps also to the long-lasting problem of Ehrenfest paradox which is also problematic in General Relativity theory, or by quoting Einstein himself:

> "... Thus all our previous conclusions based on general relativity would appear to be called in question. In reality we must make a subtle detour in order to be able to apply the postulate of general relativity exactly" [5].

This reply is not intended to say that Yefremov's preliminary analysis is not in the right direction, instead we only highlight a possible way to improve his results (via extending Lorentz transformation). Furthermore, it also does not mean to say that Finsler-Berwald metric could predict better than Quaternion Relativity. Nonetheless, further observation is of course recommended in order to refute or verify this proposition.

Acknowledgment

The writers would like to thank to Profs. C. Castro for citing the Vacaru *et al.*'s book [11]. We are also grateful for discussion with Profs. A. Yefremov, G. Asanov and Z. Szabo.

Submitted on April 06, 2007
Accepted on April 12, 2007

References

1. Yefremov A. Notes on Pioneer anomaly explanation by satellite-shift formula of Quaternion Relativity. *Progress in Physics*, 2007, v. 3, 93–96.
2. Yefremov A. Quaternions: algebra, geometry and physical theories. *Hypercomplex Numbers in Geometry and Physics*, 2004, v. 1(1), 105.
3. Smarandache F. and Christianto V. Less mundane explanation of Pioneer anomaly from Q-relativity. *Progress in Physics*, 2007, v. 1, 42–45.
4. Pavlov D. G. Construction of the pseudo Riemannian geometry on the base of the Berwald-Moor geometry. arXiv: math-ph/0609009.
5. Einstein A. Relativity: the special and general theory. Crown Trade Paperback, New York, 1951, 66–70 (quoted from the ebook version, p. 97: http://www.ibiblio.org/ebooks/Einstein/Einstein_Relativity.pdf); [5a] Janssen M. http://www.tc.umn.edu/∼janss011/pdf%20files/appendix-SR.pdf; [5b] http://www.ph.utexas.edu/∼gleeson/NotesChapter11.pdf.
6. De Lange O. L. Comment on Space-time exchange invariance: Special relativity as a symmetry principle. *Am. J. Phys.*, 2002, v. 70, 78–79.
7. Engelhardt W. Relativistic Doppler effect and the principle of relativity. *Apeiron*, 2003, v. 10, No. 4, 29–49.
8. Klauber R. Toward a consistent theory of relativistic rotation. In: *Relativity in Rotating Frames*, Kluwer Academic, 2004; arXiv: physics/0404027.
9. Pavlov D. *et al.* he notions of distance and velocity modulus in the linear Finsler spaces. *Hypercomplex Numbers in Geometry and Physics*, 2005, v. 1(3), 13.
10. Asanov G. S. Finslerian metric function of totally anisotropic type. Relativistic aspects. arXiv: math-ph/0510007; [10a] Asanov G. S. arXiv: math-ph/0510049.
11. Vacaru S., Stavrinos P., Gaburov E. and Gonta D. Clifford and Riemann-Finsler structures in geometric mechanics and gravity. Geometry Balkan Press, 2005; arXiv: gr-qc/0508023, p. 39.
12. Szabo Z. Berwald metrics constructed by Chevalley's polynomials. arXiv: math.DG/0601522.
13. Weber T. Measurements on a rotating frame in relativity. *Am. J. Phys.*, 1997, v. 65, 946–953.

Comment on "Single Photon Experiments and Quantum Complementarity" by D. Georgiev

William G. Unruh

CIAR Cosmology and Gravity Program, Dept. of Physics, University of B. C., Vancouver V6T 1Z1, Canada
E-mail: unruh@physics.ubc.ca

The paper "Single Photon Experiments and Quantum Complementarity" by Georgiev misrepresents my position on the Afshar "which path/interference" debate.

D. Georgiev has recently published a paper [1] in which he argues that my interpretation [2] of a "complementarity" experiment based on Afshar's original suggestion [3] is incoherent and wrong. Unfortunately his interpretation of my model distorted what I say.

The Afshar experiment is one in which it is claimed one can both determine both which path a photon has followed and that the photon self interfered in one and same experiment, violating Bohr's complementarity principle, that complementary aspects of a system cannot simultaneously be measured. I have suggested a more stark experiment than Afshar's which throws the issues into greater relief, one whose setup Georgiev describes well in his paper.

However, he then implies that I hold certain positions about the interpretation of the experiment, interpretations which I neither hold not are contained in my description.

Referring to Georgiev's diagram, I demonstrate that **if** the photon is known to have traveled down arm 1 of the interferometer (for example by blocking arm 2, or by any other means, then the detector D1 will always register the photon. If the photon is known to have gone down arm 2, then detector D2 always clicks. The crucial question is what happens if the photon is in an arbitrary state. This raises a variety of questions, including the question as to whether one can ever infer anything about a system being measured from the outcomes reported on the measuring instrument. One could of course take the position of no. That the readings on measurement instruments tell one only about that measuring instrument and cannot be used to infer anything about the system being measured. While a defensible position, it is also one which would make experimental physics impossible. My position follows that of von Neuman, that one can make inferences from the reading on the measurement instruments to the system being measured. IF there is a 100% correlation between the apparatus outcome and the system when the system is known to be in a certain state, and if orthogonal states for the system lead to different outcomes in the apparatus, then one can make inferences from the outcome of the apparatus to the attribute of the system. In this case, the 100% correlation between which detector registers the photon to the known path the photon followed (1 or 2) allows one to infer that IF the detector D1 registers the photon, then that photon has the property that it followed path 1. This is true no matter what the state of the photon was — pure or mixed or something else. Readings on apparatus, if properly designed DO allow one to infer values for attributes of the system at earlier time.

Note the key point I made in my paper was that **if** one places an absorber into path 5 or 6, then even if those absorbers do not ever actually absorb any photons, they do destroy that correlation between the reading on the detectors and the the path, 1 or 2, the photon follows. Because in this case, if we know that the photon was on path 1, either detector D1 or D2 will register, with 50% probability or if the photon was detected by detector D1, the photon could have come from either path 1 or 2. One cannot any longer infer from the apparatus (the detectors) which path of the photon took, precisely because one was also trying to determine in the two paths interfered. The change in the experimental situation destroys the critical correlation required to make those inferences.

Georgiev then claims to prove that such an interpretation is incoherent and disagrees with the mathematics. He bases this on his equations 7 and 8 in which he ascribes a state to the photon both passing along arm 1 or 2 and arm 5 or 6. In no conventional quantum formalism do such states exist. Certainly amplitudes for the particle traveling along both path 1 and 5, say, exist, but amplitudes are just complex numbers. They are not states. And complex numbers can be added and subtracted no matter where they came from.

Submitted on March 09, 2007
Accepted on April 12, 2007

References

1. Georgiev D. *Prog. Phys.*, 2007, v. 2, 97–103.
2. Unruh W. Quantum Rebel. http://www.theory.physics.ubc.ca/rebel.html
3. Afshar S. *Found. Physics*, 2007, v. 37, 295–305, and arXiv: quant-ph/0702188.
4. von Neuman J. Mathematical foundations of quantum mechanics. Princeton Univ. Press, 1934.

Exact Mapping of Quantum Waves between Unruh's and Afshar's Setup (Reply to W. Unruh)

Danko Dimchev Georgiev

Kanazawa University Graduate School of Natural Science and Technology, Kakuma-machi, Kanazawa-shi, Ishikawa-ken 920-1192, Japan

E-mail: danko@p.kanazawa-u.ac.jp

In a recent letter, Unruh argued that I have misrepresented his position and I have "*put words into his mouth*" which distort Unruh's original analysis of Unruh's setup. Unfortunately such a complaint is ungrounded. I have presented a mathematical argument that Unruh's which way claim for the discussed setup is equivalent to the claim for a mixed density matrix of the experiment. This is a mathematical proof, and has nothing to do with misrepresentation. Unruh clearly accepts the existence of the interference pattern at paths 5 and 6, accepts that the setup is described by pure state density matrix, and at the same time insists on existing which way bijection, therefore his position is provably mathematically inconsistent.

1 Direct calculation of detector states

Unruh in [6, 7] clearly has accepted the existence of unmeasured destructive interference at path 5 (pure state density matrix) plus a direct which way claim stating that $|\psi_1\rangle$ and $|\psi_2\rangle$ are respectively eigenstates of the detectors $\mathfrak{D}_1$ and $\mathfrak{D}_2$, thus it is easy for one to show that Unruh's analysis is mathematically inconsistent [2]. Despite of the fact that the mathematical analysis in my previous paper is rigorous, it was based on retrospective discussion deciding which waves shall annihilate, and which shall remain to be squared according to Born's rule. The choice for such a purely mathematical discussion was done in order to provide insight *why* Unruh's confusion arises. In this comment I will present concise physical description of the evolution of the photon based on direct forward-in-time calculation of Unruh's setup described in detail in [2], and will spot several troublesome claims made by Unruh, which appear to be severe mathematical misunderstandings.

For a coherent setup the quantum state in Unruh's interferometer after exit of beamsplitter 2 (BS2) is $|\Psi(t_1)\rangle = = -1|\psi_6\rangle$, where $|\psi_6\rangle$ denotes the wavefunction evolving along path 6.* After reflection at mirror 3 (M3) the state evolves into $|\Psi(t_2)\rangle = -\imath|\psi_6\rangle$, which meets BS3 and splits into coherent superposition of two parts each going to one of the detectors

$$|\Psi(t_3)\rangle = \left(\frac{1}{\sqrt{2}} - \frac{1}{\sqrt{2}}\,\imath\right)|\psi_6\rangle = \frac{1}{\sqrt{2}}|\mathfrak{D}_1\rangle - \frac{1}{\sqrt{2}}\,\imath|\mathfrak{D}_2\rangle \quad (1)$$

from which follows that $|\mathfrak{D}_1\rangle = |\mathfrak{D}_2\rangle = |\psi_6\rangle$. Since $|\psi_6\rangle = = \frac{1}{2}\left(|\psi_1\rangle + |\psi_2\rangle\right)$ it is obvious that $|\psi_1\rangle$ and $|\psi_2\rangle$ are *not* eigenstates of the detectors $\mathfrak{D}_1$ and $\mathfrak{D}_2$. That is why there is no which way information in coherent version of Unruh's setup. To suggest that the BS3 can selectively only reflect or only transmit the components $|\psi_1\rangle$ and $|\psi_2\rangle$ in a fashion preserving the which way correspondence is *mathematically equivalent* to detect photons at path 6, and then determine just a single path 1 or 2 along which the photon has arrived. Since it is impossible for one to distinguish the $|\psi_1\rangle$ component from the $|\psi_2\rangle$ component of a photon detected at path 6 it is perfectly clear that the BS3 cannot distinguish these components either, so standard QM prediction is that BS3 will "see" photon coming at path 6 but BS3 will not make any difference for $|\psi_1\rangle$ or $|\psi_2\rangle$ component of the photon state. BS3 will reflect both $|\psi_1\rangle$ and $|\psi_2\rangle$ to both detectors. The evolution of the state $-\imath|\psi_6\rangle$ into a coherent superposition going to both detectors providing no which way information is straightforward and can be characterized as "back-of-an-envelope calculation".†

Now let us investigate why if one prevents the interference along path 5 by converting the setup into a mixed one, the which way information will be preserved and the states $|\psi_1\rangle$ and $|\psi_2\rangle$ *will be* eigenstates of the corresponding detectors. First, one must keep in mind how the quantum entanglements (correlations) work in QM — due to the fact the photon wavefunction is entangled with the state of external system it is possible if one investigates only the reduced density matrix of the photon to see mixed state with all off-diagonal elements being zeroes, hence no interference effects manifested. This is the essence of Zeh's decoherence theory which does not violate Schrödinger equation and one

*Here explictly should be noted that $|\psi_6\rangle$ is not just eigenstate of the position operator describing location at path 6, it is a wavefunction describing the photon state including its energy (wavelength), position, momentum, etc., that evolves in time and which may be represented as a vector (ket) in Hilbert space. As we speak about arbitrary photon with arbitrary energy, etc., the definition of the vector $|\psi_6\rangle$ is left flexible with the comprehension that it must describe fully the characteristics of the real photon. Also $|\psi_6\rangle$ is an unit vector, and as easily can be seen it must be multiplied by -1 in order for one to get the real state of the qubit at path 6.

†This expression was used by Prof. Tabish Qureshi (Jamia Millia Islamia, New Delhi, India) to describe how in just a few lines one can disprove Afshar's analysis and the calculation can be performed on the back side of an envelope for letters.

ends up with states that are not true classical mixtures, but have the same mathematical description satisfying the XOR gate. Thus let us put vertical polarizator **V** on path 1 and horizontal polarizator **H** on path 2. The state after BS2 will have non-zero component at path 5

$$|\Psi(t_1)\rangle = \left[-\frac{1}{2}\imath|\psi_1\rangle|\mathrm{V}\rangle + \frac{1}{2}\imath|\psi_2\rangle|\mathrm{H}\rangle\right] + \\ + \left[-\frac{1}{2}|\psi_1\rangle|\mathrm{V}\rangle - \frac{1}{2}|\psi_2\rangle|\mathrm{H}\rangle\right]. \quad (2)$$

Now as both wavefunctions ψ_1 and ψ_2 are orthogonal and distinguishable because of spatial separation (no overlap) in the interferometer arms 1 and 2, and because they get entangled with orthogonal states of the two different polarizators **V** and **H**, in the future spatial overlapping of the wavefunctions ψ_1 and ψ_2 cannot convert them into non-orthogonal states. Due to entanglement with polarizators the photon state is such that as if for ψ_1 the wavefunction ψ_2 does not exist, hence ψ_1 cannot overlap with ψ_2, and the state will be $\psi_1 \mathrm{XOR} \psi_2$.* At the detectors due to destructive quantum interference the ψ_2 waves will self-annihilate at $\mathfrak{D}_1$ and ψ_1 waves will self-annihilate at $\mathfrak{D}_2$. Thus $|\psi_1\rangle|\mathrm{V}\rangle$ and $|\psi_2\rangle|\mathrm{H}\rangle$ *will be* eigenstates of the corresponding detectors $\mathfrak{D}_1$ and $\mathfrak{D}_2$ (see details in [2]). This which way information is only existent because of the existent which way label which is the mixed state of photon polarization due to entanglements with the polarizators. In Unruh's single path setups the mixture of the photon states is result of obstacles on one of the interferometer paths, and then taking fictitious statistical average i.e. photons from the two alternative setups run in two distinguishable time intervals t_1 vs t_2. So in the classical mixture of two single path trials investigated by Unruh the time intervals t_1 and t_2 have the equivalent function of $|\mathrm{V}\rangle$ and $|\mathrm{H}\rangle$ entanglements. In order to complete the analogy one may explicitly write entanglements with orthogonal kets $|t_1\rangle$ and $|t_2\rangle$ describing the *interferometer quantum state* with obstacles on one of the two paths 1 or 2. Thus actually in the classical mixture discussed by Unruh it is $|\psi_1\rangle|t_1\rangle$ and $|\psi_2\rangle|t_2\rangle$ that are the eigenstates of the detectors. Destroying the mixture leads to loss of the which way information at the detectors.

Where was the essential step in the mixed setup that allowed us to recover the which way information? It was exactly the nonzero value of path 5. If in a coherent setup one allows for a state $0|\psi_5\rangle$ it is obvious that the vector $|\psi_5\rangle$ cannot be recovered without division to *zero*. Recovering of the which way information requires components included in the vector $|\psi_5\rangle$, thus one will be mathematically inconsistent if keeps the which way claim, and also claims that the state at path 5 is $0|\psi_5\rangle$ i.e. from that moment $|\psi_5\rangle$ is erased. It is obvious that in any QM calculation one can write the real state as a sum of infinite number of such terms of arbitrary vector states multiplied by *zero* without changing anything e.g. $|\Psi\rangle = |\Psi\rangle + 0|\Lambda\rangle + \cdots + 0|\Theta\rangle$. However all these *zeroed* components do not have physical significance.

And last but not least, it is clear that puting obstacle on place where the quantum amplitudes are expected to be *zero* does not change the mathematical description of the setup. Formally one may think as if having *Renninger negative-result experiment* [4] with the special case of measuring at place where the probability is *zero*. This is the only QM measurement that does not collapse the wavefunction of the setup! Analogously one may put obstacles in the space outside of the Unruh's interferometer. As the photon wavefunction is *zero* outside the interferometer it is naive one to expect that the photon wavefunction inside the interferometer is collapsed by the obstacles located around the interferometer. So puting obstacle or not, at place where the quantum amplitudes are *zero*, does not change the mathematical description. As this is always true, Unruh's idea that having obstacle or not at the negative interference area at path 5 will change the final conclusions of the which way information is wrong. As we have defined the which way information as provable bijection, it is unserious for one to believe that from a difference that has no effect on photon's wavefunction and does not change the mathematical description, one may change a mathematical proof of existent bijection.

2 Which way information as provable bijection

Now we will show that the naive statement that which way information and quantum interference are incompatible with each other is generally *false*. First one must define the which way information as a *provable bijection* between at least two distinguishable wavefunctions and two observables. Alternatively no which way information will be *disprovable bijection* i.e. the bijection is provably *false*. Then one can only say that *if* the bijection is *true* then quantum *cross-interference* of the two wavefunctions did not occur, yet *self-interference* is always possible! This was explicitly formulated in [2] however in the text bellow we discuss the idea in depth with the proposed Georgiev's four-slit experiment.

Let us us have four equally spaced identical slits A, B, C, D, and let us detect the interference pattern of photon at the *far-field Fraunhofer limit*. In case of coherent setup one will have coherent wavefunction $\Phi \equiv \Psi_A + \Psi_B + \Psi_C + \Psi_D$ and will observe a single four-slit interference $P = |\Psi_A + \\ + \Psi_B + \Psi_C + \Psi_D|^2$. This is a no which way distribution as far as we know that the photon amplitudes have passed through all four slits at once in quantum superposition.

Now let us put **V** polarizators on slits A and B, and **H** polarizators on slits C and D. There will be no *cross-interference* between the wavefunctions $\Phi_1 \equiv \Psi_A + \Psi_B$ and $\Phi_2 \equiv \Psi_C + \Psi_D$ and the observed intensity distribution will be mixed one $\mathcal{P} = |\Psi_A + \Psi_B|^2 + |\Psi_C + \Psi_D|^2$. In this case one can establish provable bijection $\Phi_1 \to P_1 \equiv |\Psi_A + \Psi_B|^2$,

*If however one erases the polarization the spatial overlap of the two waves will manifest interference and will erase the which way information.

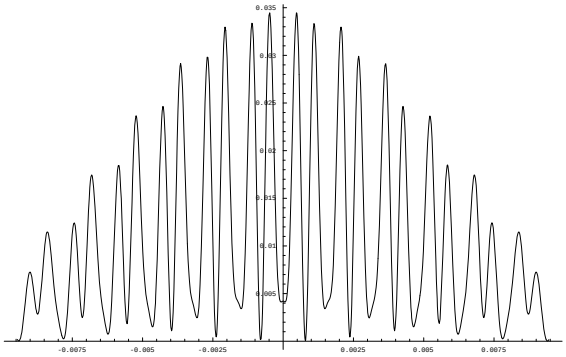

Fig. 1: The four slit interference pattern $P = |\Psi_A + \Psi_B + \Psi_C + \Psi_D|^2$ of non-polarized or identically polarized photons.

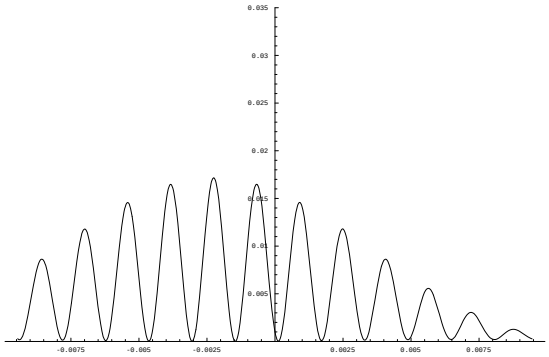

Fig. 2: Shifted to the left $P_1 = |\Psi_A + \Psi_B|^2$ double-slit interference pattern of vertically polarized photons.

$\Phi_2 \to P_2 \equiv |\Psi_C + \Psi_D|^2$. Thus there is which way information $\Phi_1 \to P_1$, $\Phi_2 \to P_2$ only because there is no cross-interference between Φ_1 and Φ_2. The self-interferences of Φ_1 and Φ_2 are always there e.g. the cross-interference between Ψ_A and Ψ_B does not allows us to further prove existent bijection in which only slit A wavefunction, or only slit B wavefunction participates. In order to illustrate the discussion we have performed numerical plotting with *Wolfram's Mathematica 5.2* for photons with wavelength $\lambda = 850\text{nm}$, slit width $s = 0.25\text{mm}$, interslit distance $d = 2\text{mm}$, at the Fraunhofer limit $z = 4.2\,\text{m}$ behind the four slits. Results are presented in Figures 1–3.

This section on the which way information as existent provable bijection was added for clarity. From the presented details it does *not* follow that Bohr's complementarity principle is wrong, we have just explicitly reformulated the principle providing strict definitions for *which way claims* as *bijections*, and have clarified the useful terms *self-interference* and *cross-interference*. If one investigates existent bijection then self-interference is always there, only certain cross-interferences are ruled out.

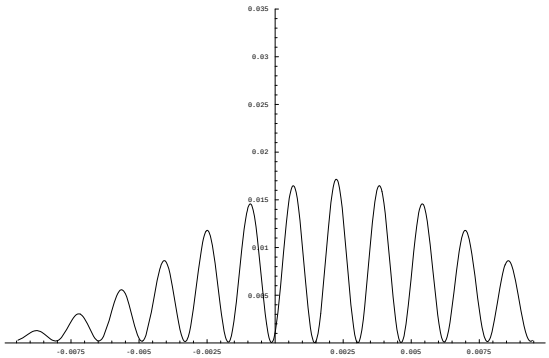

Fig. 3: Shifted to the right $P_2 = |\Psi_C + \Psi_D|^2$ double-slit interference pattern of horizontally polarized photons.

3 Quantum states as vectors

In this section we point out that QM can be approached in three ways. One way is to use wave equations with the prototype being the *Schrödinger equation*. One may write down a wave function $\Psi(x, t)$ that evolves both in space and time, where x is defined in $\mathbb{R}^3$. It is clear that the *history* of such mathematical function can be "traced" in time t, because the very defining of the wavefunction should be done by specifying its temporal evolution. Every wavefunction can be represented as a vector (ket) in Hilbert space. This is just second equivalent formulation, and changes nothing to the above definition. As the wavefunction evolves in time, it is clear that the vector representing the function will evolve in time too. It is the wavefunction that is referred to as *quantum state*, and it is the equivalent vector representing the wavefunction that is called *state vector*. Third way to represent the quantum state is with the use of *density matrices*. In the previous work [2] we have used all three representations in order to provide more clear picture of Unruh's setup.

Namely, we have shown that the different wavefunctions if they manifest cross-interference are no more described by orthogonal vectors in Hilbert space. What is more the wavefunctions were "traced" in time in order for one to prove possible bijections. Surprisingly Unruh makes the following claim:

> "*Certainly amplitudes for the particle travelling along both path 1 and 5, say, exist, but amplitudes are just complex numbers. They are not states. And complex numbers can be added and subtracted no matter where they came from.*"

Such a misunderstanding of mathematical notation is not tolerable. As written in Eqs. 7–8 in [2] the usage of Dirac's ket notation is clear. All kets denote vectors (wavefunctions), hence all these are quantum states, and nowhere I have discussed only the quantum amplitude itself.

First, one should be aware that all kets are time dependent, as for example instead of writing $|\psi_1(t_1)\rangle$, $|\psi_1(t_2)\rangle$, $|\psi_1(t_3)\rangle, \cdots$ the notation was concisely written as $|\psi_1\rangle$ with the understanding that the state is a function of time. Even for two different points along the same interferometer arm, the spread of the laser beam (or the single photon wave-

packet) is different, yet this time dependence should be kept in mind without need for explicitly stating it. It is the time dependence of the state vectors that has been overlooked by Unruh. If one rejects the possibility to "trace" the history of the discussed wavefunctions in time, then he must accept the bizarre position that it is meaningless for one to speak about bijections and which way correspondences at first place.

Another target of Unruh's comment is the reality of the states $|\psi_{15}\rangle$, $|\psi_{16}\rangle$, $|\psi_{25}\rangle$, $|\psi_{26}\rangle$ in Eqs. 7–8 in [2].

> "[*Georgiev in*] *his equations 7 and 8 ascribes a state to the photon both passing along arm 1 or 2 and arm 5 or 6. In no conventional quantum formalism do such states exist.*"

Unfortunately this is wrong. Mathematically one can always represent a wavefunction as a sum of suitably defined functions. As it was clearly stated in [2] e.g. the state $|\psi_{15}\rangle$ is a wavefunction (vector, and not a scalar as erroneously argued by Unruh) which is branch of the wavefunction ψ_1 that evolves at arm 5. Therefore the mathematical definition is rigorous $\psi_1 = \alpha(t)(\psi_{15} + \psi_{16})$. One may analitically continue both functions ψ_{15} and ψ_{16} along path 1 as well, in this case the two functions are indistinguishable for times before BS2 with $\alpha = \frac{1}{2}$, while after BS2 the wavefunctions become distinguishable with $\alpha = \frac{1}{\sqrt{2}}$. The time dependence of $\alpha(t)$ is because the orthogonality of the two states is function of time. The usage of the same Greek letter with different numerical index as a *name* of a new function is standard mathematical practice in order to keep minimum the numer of various symbols used. The fact that the vector $|\psi_{15}\rangle$ is not orthogonal with the vector $|\psi_{25}\rangle$ in the coherent version of Unruh's setup is not a valid argument that it is not a valid quantum state. Mathematically it is well defined and whether it can be observed directly is irrelevant. Analogously, at path 6 the wavefunctions ψ_1 and ψ_2 are indistinguishable however mathematically they are still valid quantum states. Indistinguishability of states does not mean their non-existence as argued by Unruh. Indeed exactly because the two quantum functions $|\psi_{15}\rangle$ and $|\psi_{25}\rangle$ are defined in different way and have different time history, one may make them orthogonal by physical means. Simply putting obstacle at path 2, and then registering photon at path 5 one observes photons with intensity distribution $P_{15} = |\psi_{15}|^2$ which are solely contributed by ψ_{15}. And each photon only manifests "*passing along arm 1 and arm 5*". The other method to create mixed state where one can have bijective association of observables to each of the states $|\psi_{15}\rangle$, $|\psi_{16}\rangle$, $|\psi_{25}\rangle$, $|\psi_{26}\rangle$ is to put different polarizators **V** and **H** on paths 1 and 2, and then detect photons at paths 5 and 6. Due to polarizator entanglements there will be four observables and provable bijection $\psi_{15} \to P_{15}$, $\psi_{16} \to P_{16}$, $\psi_{25} \to P_{25}$, $\psi_{26} \to P_{26}$, where each probability distribution P is defined by the corresponding wavefunction squared and polarization of the photon dependent on the passage either through path 1 or path 2.

If Unruh's argument were true then it obviously can be applied to Unruh's own analysis, disproving the reality of the states $|\psi_1\rangle$ and $|\psi_2\rangle$ after BS2. As noted earlier, in the mixed state discussed by Unruh the state of the photon is either $|\psi_1\rangle|t_1\rangle$ or $|\psi_2\rangle|t_2\rangle$, where by $|t_1\rangle$ and $|t_2\rangle$ we denote two different distinguishable states of the Unruh's interferometer one with obstacle at path 2, and one with obstacle at path 1. It is exactly these entanglements with the external system being the interferometer itself and the obstacles that make the states $|\psi_1\rangle$ and $|\psi_2\rangle$ orthogonal at the detectors. If Unruh's logic were correct then removing the obstacles and making the two states not orthogonal at path 6 should be interpreted as non-existence for the two states. Fortunately, we have shown that Unruh's thesis is incorrect as is based on misunderstanding the difference between vector and scalar in the ket notation. All mentioned wavefunctions in [2] are well-defined mathematically and they are valid quantum states, irrespective of whether they are orthogonal with other states or not.

4 Classical language and complementarity

Unruh's confusion concerning the reality of quantum states, is grounded on some early *antirealist* misunderstandings of QM formalism. Still in some QM textbooks one might see expressions such as "*if the position of a qubit is precisely measured the momentum is largely unknown*", or "*if in the double slit setup a photon is detected at the Fraunhofer limit one will observe interference pattern but will not know which slit the photon has passed*". Such expressions are based on simple logical error — knowledge that "*the photon has not passed either only through slit 1, or only through slit 2*" is *not* mathematically equivalent to "*lack of knowledge which slit the photon has passed*".

Let us discuss a statistical mixture of two single slit experiments with shutter on one of the slits. What knowledge do we have? Certainly this is XOR knowledge, which means either one slit, or the other one, but not both! The truth-table was given in Table 1 in [2]. It is clear that exactly one of the statements "*passage through slit 1*" or "*passage through slit 2*" is *true*.

Now investigate the logical negation of the XOR gate. This essentially describes two possibilities. The first one is trivial with both slits *closed*. The photon does not pass through any slit, so no detection will occur at the Fraunhofer limit. A photon passed through slit 1 will be indistinguishable from photon passed through slit 2, but this is *vacuously true*. Simply no such photons exist! Much more interesting is however the coherent setup in which both slits are open. Logically one proves that the photon has passed through both slits at once. This is the essence of the quantum superposition and is described by AND logical gate. The statements "*passage through slit 1*" and "*passage through slit 2*" are

simultaneously *true*, and it is ruled out that only one of them is true but not the other. Therefore the *antirealist* position based on classical physical intuition, and/or classical langauge is erroneous when it comes to describe superposed state. The logical negation (NOT gate) of the XOR gate i.e. the XOR gate is *false*, is wrongly interpreted as "*lack of knowledge on the slit passage*" i.e. XOR gate possibly might be *true* or might be *false*. As this lack of knowledge is contradicting the QM formalism one runs directly into inconsistency with the theory.

Let us now see the implications for Unruh's objection e.g. against the ψ_{15} state. As in a coherent setup this state is superposed with the ψ_{25} state along path 5, Unruh argues that they are both nonexistent. This conclusion is *non sequitur*, because the quantum superposition is described by AND logical gate and this means that ψ_{15} and ψ_{25} are both true, hence existent states. Unruh relies on von Neumann formulation of QM, which is *antirealist* one, and rejects to accept the reality of quantum superposed states. This is untenable position because the antirealist vision interpreted as lack of precise knowledge of one of two non-commuting observables is mathematically inconsistent with the underlying mathematical formalism. It exactly the opposite — if one knows precisely the spatial region of the localization of qubit (having XOR knowledge ruling out other possible localizations) then mathematically it will follow that the momentum will be spread widely amongst numerous possible values (hence having AND knowledge). What is the reality of the AND state is outside the scope of the present article and depends on the interpretation - in MWI the superposed states reside in different Universes, in Penrose's OR model the quantum coherent state resides in a single Universe with superposed space-time curvatures, etc.

From the preceding discussion follows that expressions as "*which way information*" and "*no which way information*" are just *names* and have precise mathematical definitions as provable bijection b, and respectively disprovable bijection $\neg b$. Also we have logically proved that non-commuting observables are always existent and well-defined mathematically. However in contrast with classical intuition necessarily at least one of the two non-commuting observables should be described by AND gate, hence being quantum superposed.

5 Qureshi's waves mapped onto Georgiev's waves

One of the major differences between works of Georgiev [2] and Qureshi [4] is that in our previous paper we have introduced explicitly the idea of XOR and AND states in QM, and we have explicitly formulated the need of provable bijection. Otherwise Qureshi's argument is identical to the presented here forward-in-time calculation. Yet for the sake of clarity, we will provide one-to-one mapping of *Qureshi's waves for Afshar's setup* with *Georgiev's waves for Unruh's setup*. This one-to-one mapping is mathematically clear evidence for existence of the quantum waves (states) described by Georgiev in [2] and leave no other alternative but one in which Unruh must confess his confusion in the complementarity debate.

As shown in [2] in retrospective discussion on wave annihilation, there will be eight waves that shall interfere. This is purely mathematical method, because mathematical truth is atemporal, and as explained before one either chooses self-interference of ψ_1 and self-interference of ψ_2 at detectors, or chooses destructive cross-interference between ψ_1 and ψ_2 at earlier times (path 5). Here we will show that the canceled sinh terms in Qureshi's calculation provide four more waves that go to both detectors and that one-to-one mapping exists with Georgiev's waves.

Let us denote all eight waves in Georgiev's description of Unruh's setup with ψ_{151}, ψ_{152}, ψ_{161}, ψ_{162}, ψ_{251}, ψ_{252}, ψ_{261}, ψ_{262}. As these are only *names*, the precise meaning for each one should be explicitly defined e.g. ψ_{151} is wavefunction whose history traced in time is passage along path 1, then passage along path 5, and ending at detector 1. Definitions for rest of the waves is analogous.

Now let us write again the Qureshi's equation for Afshar's setup

$$\Psi(y,t) = aC(t)\, e^{-\frac{y^2+y_0^2}{\Omega(t)}} \left[\cosh\frac{2yy_0}{\Omega(t)} + \sinh\frac{2yy_0}{\Omega(t)}\right] + \\ + bC(t)\, e^{-\frac{y^2+y_0^2}{\Omega(t)}} \left[\cosh\frac{2yy_0}{\Omega(t)} - \sinh\frac{2yy_0}{\Omega(t)}\right]$$

where $C(t) = \frac{1}{(\pi/2)^{1/4}\sqrt{\epsilon+2\imath\hbar t/m\epsilon}}$, $\Omega(t) = \epsilon^2 + \frac{2\imath\hbar t}{m}$, a is the amplitude contribution from pinhole 1, b is the amplitude contribution from pinhole 2, ϵ is the width of the wavepackets, $2y_0$ is the slit separation. Qureshi's analysis continues directly with annihilation of four of the waves contributed by the sinh terms i.e. for Afshar's setup $a = b = \frac{1}{\sqrt{2}}$ so the sinh terms cancel out at the dark fringes. What is left at the bright fringes are the cosh terms, which can be expanded as a sum of exponential functions, namely $\cosh x = \\ = \frac{1}{2}\left(e^x + e^{-x}\right)$, and after simplification we arrive at*:

$$\Psi(y,t) = \frac{1}{2}\, aC(t)\left[e^{-\frac{(y-y_0)^2}{\Omega(t)}} + e^{-\frac{(y+y_0)^2}{\Omega(t)}}\right] + \\ + \frac{1}{2}\, bC(t)\left[e^{-\frac{(y-y_0)^2}{\Omega(t)}} + e^{-\frac{(y+y_0)^2}{\Omega(t)}}\right].$$

If a lens is used after the cross-interference has ocurred to take the $e^{-\frac{(y-y_0)^2}{\Omega(t)}}$ part to detector 1, and the part $e^{-\frac{(y+y_0)^2}{\Omega(t)}}$ to detector 2, one easily sees that the amplitudes from each slit evolve into a superposition of two *identical parts* that go to both detectors. The waves that shall be responsible for which way information in *mixed setups* and make possible the bijection $a \to \mathfrak{D}_1$, $b \to \mathfrak{D}_2$ are hidden in the erased sinh

*The following equation actually is the intended Eq. 10 in [2], where unfortunately *typesetting error* occurred.

terms. Taking into account that $\sinh x = \frac{1}{2}(e^x - e^{-x})$, one may recover the four zeroed sinh components in the form:

$$0 = \frac{1}{2} aC(t) \left[e^{-\frac{(y-y_0)^2}{\Omega(t)}} - e^{-\frac{(y+y_0)^2}{\Omega(t)}} \right] + \\ + \frac{1}{2} bC(t) \left[-e^{-\frac{(y-y_0)^2}{\Omega(t)}} + e^{-\frac{(y+y_0)^2}{\Omega(t)}} \right].$$

If the eight interfering Qureshi's waves are denoted with Q, where Q_{1-4} arise from the cosh terms and Q_{5-8} arise from the sinh terms, then the one-to-one mapping with the eight Georgiev's waves is

$$Q_1 \equiv \frac{1}{2} aC(t)\, e^{-\frac{(y-y_0)^2}{\Omega(t)}} \to \psi_{161} \quad (3)$$

$$Q_2 \equiv \frac{1}{2} aC(t)\, e^{-\frac{(y+y_0)^2}{\Omega(t)}} \to \psi_{162} \quad (4)$$

$$Q_3 \equiv \frac{1}{2} bC(t)\, e^{-\frac{(y-y_0)^2}{\Omega(t)}} \to \psi_{261} \quad (5)$$

$$Q_4 \equiv \frac{1}{2} bC(t)\, e^{-\frac{(y+y_0)^2}{\Omega(t)}} \to \psi_{262} \quad (6)$$

$$Q_5 \equiv \frac{1}{2} aC(t)\, e^{-\frac{(y-y_0)^2}{\Omega(t)}} \to \psi_{151} \quad (7)$$

$$Q_6 \equiv -\frac{1}{2} aC(t)\, e^{-\frac{(y+y_0)^2}{\Omega(t)}} \to \psi_{152} \quad (8)$$

$$Q_7 \equiv -\frac{1}{2} bC(t)\, e^{-\frac{(y-y_0)^2}{\Omega(t)}} \to \psi_{251} \quad (9)$$

$$Q_8 \equiv \frac{1}{2} bC(t)\, e^{-\frac{(y+y_0)^2}{\Omega(t)}} \to \psi_{252} \quad (10)$$

To our knowledge this is the first exact one-to-one mapping between Unruh's setup and Afshar's setup, all previous discussions were much more general and based on analogy [2, 6]. Now one can explicitly verify that a and b terms in Qureshi's calculation have the same meaning as path 1 and path 2 in Unruh's setup; sinh and cosh terms have the meaning of the path 5 and path 6, and $e^{-\frac{(y-y_0)^2}{\Omega(t)}}$ and $e^{-\frac{(y+y_0)^2}{\Omega(t)}}$ terms have the meaning of detection at $\mathfrak{D}_1$ or $\mathfrak{D}_2$. The provided exact mapping between Qureshi's and Georgiev's work is clear evidence that Unruh's complaint for Georgiev's waves not being valid quantum states is invalid. None of the proposed by Georgiev states is being *zero*. Only couples of Georgiev's states can be collectively zeroed, but which members will enter in the zeroed couples depends on the density matrix of the setup. And this is just the complementarity in disguise.

6 Conclusions

In recent years there has been heated debate whether complementarity is more fundamental than the uncertainty principle [5, 8], which ended with conclusion that complementarity is enforced by quantum entanglements and not by uncertainty principle itself [1]. Indeed the analysis of the proposed here Georgiev's four-slit experiment, as well as the analysis of Unruh's and Afshar's setups, show that which way claims defined as provable bijections are just another mathematical expression of the underlying density matrix of the setup, and as discussed earlier diagonalized mixed density matrices in standard Quantum Mechanics are possible only if one considers quantum entanglements in the context of Zeh's decoherence theory [9].

Unruh's error is that he uses results from mixed state setup to infer which way correspondence in coherent setup, overlooking the fact that bijections must be mathematically proved. Therefore it is not necessary for one to measure the interference in order to destroy the which way claim, it is sufficient only to *know* the interference is existent in order to disprove the claimed bijection. Indeed in the presented calculations for Unruh's setup we have proved that Unruh's which way bijection is *false*. Hence Unruh's analysis is mathematically inconsistent.

Submitted on April 23, 2007
Accepted on May 01, 2007

References

1. Dürr S., Nonn T. and Rempe G. Origin of quantum-mechanical complementarity probed by a "which-way" experiment in an atom interferometer. *Nature*, 1998, v. 395, 33–37.
2. Georgiev D. D. Single photon experiments and quantum complementarity. *Progress in Physics*, 2007, v. 2, 97–103.
3. Qureshi T. Complementarity and the Afshar experiment. 2007, arXiv: quant-ph/0701109.
4. Renninger M. Messungen ohne storung des messobjekts. *Zeitschrift für Physik*, 1960, v. 158, 417–421.
5. Scully M. O., Englert B. G. and Walther H. Quantum optical tests of complementarity. *Nature*, 1991, v. 351, 111–116.
6. Unruh W. G. Shahriar Afshar — quantum rebel? 2004, http://axion.physics.ubc.ca/rebel.html.
7. Unruh W. G. Comment to "Single photon experiments and quantum complementarity" by D. Georgiev. *Progress in Physics*, 2007, v. 3, 39.
8. Wiseman H. and Harrison F. Uncertainty over complementarity? *Nature*, 1995, v. 377, 584.
9. Zeh H. D. Roots and fruits of decoherence. *Séminaire Poincaré*, 2005, v. 2, 1–19; arXiv: quant-ph/0512078.

The Algebraic Rainich Conditions

José Héctor Caltenco Franca, José Luis López-Bonilla and Raúl Peña-Rivero

Sección de Estudios de Posgrado e Investigación, Escuela Superior de Ingeniería Mecánica y Eléctrica, Instituto Politécnico Nacional

Postal address: Edif. Z-4, 3er Piso, Col. Lindavista, CP 07738 México DF, Mexico

E-mail: joseluis.lopezbonilla@gmail.com

In the literature, the algebraic Rainich conditions are obtained using special methods such as spinors, duality rotations, an eigenvalue problem for certain 4×4 matrices or artificial tensors of 4th order. We give here an elementary procedure for deducing an identity satisfied by a determined class of second order tensors in arbitrary $\Re^4$, from which the Rainich expressions are immediately obtained.

1 Introduction

Rainich [1–5] proposed a unified field theory for the geometrization of the electromagnetic field, whose basic relations can be obtained from the Einstein-Maxwell field equations:

$$R_{ij}-\frac{1}{2}\,R\,g_{ij}=-8\pi\left(F_{ib}F_{j\cdot}^{\cdot b}-\frac{1}{4}\,F_{ab}F^{ab}g_{ij}\right), \quad (1)$$

where $R_{ac}=R_{ca}$, $R=R_{\cdot b}^{b\cdot}$ and $F_{ac}=-F_{ca}$ are the Ricci tensor, scalar curvature and Faraday tensor [6], respectively.

If in (1) we contract i with j we find that:

$$R=0 \quad (2)$$

then (1) adopts the form:

$$R_{ij}=2\pi\,F_{ab}F^{ab}g_{ij}-8\pi\,F_{ib}F_{j\cdot}^{\cdot b} \quad (3)$$

used by several authors [1, 2, 5, 7, 8] to obtain the identity:

$$R_{ic}\,R_{j\cdot}^{\cdot c}=\frac{1}{4}\left(R_{ab}R^{ab}\right)g_{ij}\,. \quad (4)$$

If F_{ar} is known, then (3) is an equation for g_{ij} and our situation belongs to general relativity. The Rainich theory presents the inverse process: To search for a solution of (2) and (4) (plus certain differential restrictions), and after with (3) to construct the corresponding electromagnetic field; from this point of view F_{ar} is a consequence of the spacetime geometry.

In the next Section we give an elementary proof of (4), without resorting to duality rotations [2], spinors [7], eigenvalue problems [8] or fourth order tensors [9, 10].

2 The algebraic Rainich conditions

The structure of (3) invites us to consider tensors with the form:

$$C_{ij}=A\,g_{ij}+B_{ik}F_{j\cdot}^{\cdot k} \quad (5)$$

where A is a scalar and B_{ac}, F_{ij} are arbitrary antisymmetric tensors. Then from (5) it is easy to deduce the expression:

$$C_{ia}C_{\cdot j}^{a\cdot}-\frac{C}{2}\,C_{ij}-\frac{1}{4}\left(C_{ab}C^{ba}-\frac{C^2}{2}\right)g_{ij}=D_{ij} \quad (6)$$

with $C=C_{\cdot r}^{r\cdot}$ and

$$D_{ij}=B_{ik}F^{ak}B_{am}F_{j\cdot}^{\cdot m}-\frac{1}{2}\left(B^{nm}F_{nm}\right)B_{ib}F_{j\cdot}^{\cdot b}+ +\frac{1}{8}\left[\left(B^{nm}F_{nm}\right)^2-2B_{bk}F_{\cdot k}^{a\cdot}B_{a\cdot}^{\cdot m}\right]g_{ij}\,. \quad (7)$$

But in four dimensions we have the following identities between antisymmetric tensors and their duals [11–13]:

$$B_{\cdot c}^{m\cdot}F^{ic}-{}^*B^{ic}\,{}^*F_{\cdot c}^{m\cdot}=\frac{1}{2}\left(B_{cd}F^{cd}\right)g^{im},$$
$$B_{\cdot r}^{k\cdot}\,{}^*B^{ir}=\frac{1}{4}\left(B_{ab}\,{}^*B^{ab}\right)g^{ik}. \quad (8)$$

With (7) and (8) it is simple to prove that $D_{ij}=0$. Therefore (6) implies the identity:

$$C_{ia}C_{\cdot j}^{a\cdot}-\frac{C}{2}\,C_{ij}=\frac{1}{4}\left(C_{ab}C^{ba}-\frac{C^2}{2}\right)g_{ij}\,. \quad (9)$$

If now we consider the particular case:

$$A=2\pi\,F_{ab}F^{ab}, \qquad B_{ij}=-8\pi\,F_{ij}\,, \quad (10)$$

then (5) reproduces (3) and $C=R=0$, and thus (9) leads to (4), q.e.d.

Our procedure shows that the algebraic Rainich conditions can be deduced without special techniques.

Submitted on April 30, 2007
Accepted on May 01, 2007

References

1. Rainich G. Y. Electrodynamics in the general relativity theory. *Trans. Amer. Math. Soc.*, 1925, v. 27, 106.
2. Misner C. W. and Wheeler J. A. Classical Physics as geometry. *Ann. of Phys.*, 1957, v. 2, 525.

3. Farrell E. J. Uniqueness of the electromagnetic field in the Rainich unified field theory. *Tensor N. S.*, 1962, v. 12, 263.
4. Klotz A. H. and Lynch J. L. Is Rainich's theory tenable? *Lett. Nuovo Cim.*, 1970, v. 4, 248.
5. Kramer D., Stephani H., MacCallum M. and Herlt E. Exact solutions of Einstein's field equations. Cambridge University Press, 1980, Chap. 5.
6. López-Bonilla J., Ovando G. and Rivera J. Intrinsic geometry of curves and the Bonnor's equation. *Proc. Indian Acad. Sci.* (Math. Sci.), 1997, v. 107, 43.
7. Witten L. Geometry of gravitation and electromagnetism. *Phys. Rev.*, 1959, v. 115, 206.
8. Adler R., Bazin M. and Schiffer M. Introduction to general relativity. Mc. Graw-Hill, N.Y. 1965.
9. Lovelock D. The Lanczos identity and its generalizations. *Atti. Accad. Naz. Lincei Rend.*, 1967, v. 42, 187.
10. Lovelock D. The algebraic Rainich conditions. *Gen. Rel. and Grav.*, 1973, v. 4, 149.
11. Plebański J. On algebraical properties of skew tensors. *Bull. Acad. Polon. Sci. Cl.*, 1961, v. 9, 587.
12. Wheeler J. A. Geometrodynamics. Academic Press, N.Y., 1962.
13. Penney R. Duality invariance and Riemannian geometry. *J. Math. Phys.*, 1964, v. 5, 1431.

The Spacetime Structure of Open Quantum Relativity

Giuseppe Basini* and Salvatore Capozziello†

*Laboratori Nazionali di Frascati, INFN, Via E. Fermi C.P. 13, I-0044 Frascati (Roma) Italy

†Dipartimento di Scienze Fisiche, Università di Napoli "Federico II", and INFN, Sez. di Napoli
Complesso Universitario di Monte S. Angelo, Via Cinthia, Edificio N-I-80126 Napoli, Italy

Corresponding author, e-mail: capozziello@na.infn.it

In the framework of the Open Quantum Relativity, we discuss the geodesic and chronological structures related to the embedding procedure and dimensional reduction from 5D to 4D spacetime. The emergence of an extra-force term, the deduction of the masses of particles, two-time arrows and closed time-like solutions are considered leading to a straightforward generalization of causality principle.

1 Introduction

Open Quantum Relativity [1] is a theory based on a dynamical unification scheme [2] of fundamental interactions achieved by assuming a 5D space which allows that the conservation laws are always and absolutely valid as a natural necessity. What we usually describe as violations of conservation laws can be described by a process of embedding and dimensional reduction, which gives rise to an induced-matter theory in the 4D space-time by which the usual masses, spins and charges of particles, naturally spring out. At the same time, it is possible to build up a covariant symplectic structure directly related to general conservation laws [3, 4]. Finally, the theory leads to a dynamical explanation of several paradoxes of modern physics (*e.g.* entanglement of quantum states, quantum teleportation, gamma ray bursts origin, black hole singularities, cosmic primary antimatter absence and a self-consistent fit of all the recently observed cosmological parameters [2, 5, 7, 8, 9]). A fundamental rôle in this approach is the link between the geodesic structure and the field equations of the theory *before* and *after* the dimensional reduction process. The emergence of an Extra Force term in the reduction process and the possibility to recover the masses of particles, allow to reinterpret the Equivalence Principle as a dynamical consequence which naturally "selects" geodesics from metric structure and vice-versa the metric structure from the geodesics. It is worth noting that, following Schrödinger [10], in the Einstein General Relativity, geodesic structure is "imposed" by choosing a Levi-Civita connection [12] and this fact can be criticized considering a completely "affine" approach like in the Palatini formalism [13]. As we will show below, the dimensional reduction process gives rise to the generation of the masses of particles which emerge both from the field equations and the embedded geodesics. Due to this result, the coincidence of chronological and geodesic structure is derived from the embedding and a new dynamical formulation of the Equivalence Principle is the direct consequence of dimensional reduction. The dynamical structure is further rich since two time arrows and closed time-like paths naturally emerge. This fact leads to a reinterpretation of the standard notion of causality which can be, in this way, always recovered, even in the case in which it is questioned (like in entanglement phenomena and quantum teleportation [5, 6]), because it is generalized to a *forward* and a *backward causation*.

The layout of the paper is the following. In Sec.2, we sketch the 5D approach while in Sec.3 we discuss the rôle of conservation laws. Sec.4 is devoted to the discussion of geodesic structure and to the emergence of the Extra Force term. The field equations, the masses of the particles and time-like solutions are discussed in Sec.5. Conclusions are drawn in Sec.6.

2 The 5D-field equations

Open Quantum Relativity can be framed in a 5D space-time manifold and the 4D reduction procedure induces a scalar-tensor theory of gravity where conservation laws (*i.e.* Bianchi identities) play a fundamental rôle into dynamics. The 5D-manifold which we are taking into account is a Riemannian space provided with a 5D-metric of the form

$$dS^2 = g_{AB}\, dx^A dx^B\,, \tag{1}$$

where the Latin indexes are $A, B = 0, 1, 2, 3, 4$. We do not need yet to specify the 5D signature, because, in 4D, it is dynamically fixed by the reduction procedure as we shall see below. The curvature invariants, the field equations and the conservation laws in the 5D-space can be defined as follows. In general, we ask for a space which is a singularity free, smooth manifold, where conservation laws are always valid [7]. The 5D-Riemann tensor is

$$R^D_{ABC} = \partial_B \Gamma^D_{AC} - \partial_C \Gamma^D_{AB} + \Gamma^D_{EB}\Gamma^E_{AC} - \Gamma^D_{EC}\Gamma^E_{AB} \tag{2}$$

and the Ricci tensor and scalar are derived from the contractions

$$R_{AB} = R^C_{ACB}\,, \qquad {}^{(5)}R = R^A_A\,. \tag{3}$$

The field equations can be obtained from the 5D-action

$$^{(5)}\mathcal{A} = -\frac{1}{16\pi\,{}^{(5)}G}\int d^5x\sqrt{-g^{(5)}}\left[{}^{(5)}R\right], \qquad (4)$$

where $^{(5)}G$ is the 5D-gravitational coupling and $g^{(5)}$ is the determinant of the 5D-metric [2]. The 5D-field equations are

$$G_{AB} = R_{AB} - \frac{1}{2}\,g_{AB}\,{}^{(5)}R = 0\,, \qquad (5)$$

so that at least the Ricci-flat space is always a solution. Let us define now a 5D-stress-energy tensor for a scalar field Φ:

$$T_{AB} = \nabla_A\Phi\,\nabla_B\Phi - \frac{1}{2}\,g_{AB}\,\nabla_C\Phi\,\nabla^C\Phi\,, \qquad (6)$$

where only the kinetic terms are present. As standard, such a tensor can be derived from a variational principle

$$T^{AB} = \frac{2}{\sqrt{-g^{(5)}}}\frac{\delta\left(\sqrt{-g^{(5)}}\,\mathcal{L}_\Phi\right)}{\delta g_{AB}}\,, \qquad (7)$$

where $\mathcal{L}_\Phi$ is a Lagrangian density related to the scalar field Φ. Because of the definition of 5D space itself, based on the conservation laws [7], it is important to stress now that no self-interaction potential $U(\Phi)$ has to be taken into account so that T_{AB} is a completely symmetric object and Φ is, by definition, a cyclic variable. In this situation the Noether theorem always holds for T_{AB}. With these considerations in mind, the field equations can assume the form

$$R_{AB} = \chi\left(T_{AB} - \frac{1}{2}\,g_{AB}\,T\right), \qquad (8)$$

where T is the trace of T_{AB} and $\chi = 8\pi\,{}^{(5)}G$.

3 The rôle of conservation laws

Eqs. (8) are useful to put in evidence the rôle of the scalar field Φ, if we are not simply assuming Ricci-flat 5D-spaces. Due to the symmetry of the stress-energy tensor T_{AB} and the Einstein field equations G_{AB}, the contracted Bianchi identities

$$\nabla_A\,T^A_B = 0\,, \qquad \nabla_A\,G^A_B = 0\,, \qquad (9)$$

must always hold. Developing the stress-energy tensor, we obtain

$$\nabla_A\,T^A_B = \Phi_B\,{}^{(5)}\Box\Phi\,, \qquad (10)$$

where $^{(5)}\Box$ is the 5D d'Alembert operator defined as $\nabla_A\Phi^{\mathcal{A}} \equiv$ $\equiv g^{AB}\Phi_{,A;B} \equiv {}^{(5)}\Box\Phi$. The general result is that the conservation of the stress-energy tensor T_{AB} (*i.e.* the contracted Bianchi identities) implies the Klein-Gordon equation which assigns the dynamics of Φ, that is

$$\nabla_A\,T^A_B = 0 \qquad \Longleftrightarrow \qquad {}^{(5)}\Box\Phi = 0\,. \qquad (11)$$

Let us note again the absence of self-interactions due to the absence of potential terms. The relations (11) give a physical meaning to the fifth dimension. Splitting the 5D-problem in a $(4+1)$-description, it is possible to generate the mass of particles in 4D. Such a result can be deduced both from Eq. (11) and from the analysis of the geodesic structure, as we are going to show.

4 The 5D-geodesics and the Extra Force

The geodesic structure of the theory can be derived considering the action

$$\mathcal{A} = \int dS\left(g_{AB}\frac{dx^A}{dS}\frac{dx^B}{dS}\right)^{1/2}, \qquad (12)$$

whose Euler-Lagrange equations are the geodesic equations

$$\frac{d^2x^A}{dS^2} + \Gamma^A_{BC}\frac{dx^B}{dS}\frac{dx^C}{dS} = 0\,. \qquad (13)$$

Γ^A_{BC} are the 5D-Christoffel symbols. Eq. (13) can be split in the $(4+1)$ form

$$\begin{aligned} 2g_{\alpha\mu}\left(\frac{dx^\alpha}{ds}\right)\left(\frac{d^2x^\mu}{ds^2} + \Gamma^\mu_{\beta\gamma}\frac{dx^\beta}{ds}\frac{dx^\gamma}{ds}\right) + \\ + \frac{\partial g_{\alpha\beta}}{dx^4}\frac{dx^4}{ds}\frac{dx^\alpha}{ds}\frac{dx^\beta}{ds} = 0\,, \end{aligned} \qquad (14)$$

where the Greek indexes are $\mu,\nu = 0,1,2,3$ and $ds^2 =$ $= g_{\alpha\beta}dx^\alpha dx^\beta$. Clearly, in the 4D reduction (*i.e.* in the usual spacetime) we ordinarily experience only the standard geodesics of General Relativity, *i.e.* the 4D component of Eq. (14)

$$\frac{d^2x^\mu}{ds^2} + \Gamma^\mu_{\beta\gamma}\frac{dx^\beta}{ds}\frac{dx^\gamma}{ds} = 0\,, \qquad (15)$$

so that, under these conditions, the last part of the representation given by Eq. (14) is not detectable in 4D. In other words, for standard laws of physics, the metric $g_{\alpha\beta}$ does not depend on x^4 in the embedded 4D manifold. On the other hand, the last component of Eq. (14) can be read as an "Extra Force" which gives the motion of a 4D frame with respect to the fifth coordinate x^4. This fact shows that the fifth dimension has a *real physical meaning* and any embedding procedure scaling up in 5D-manifold (or reducing to 4D spacetime) has a dynamical description. The Extra Force

$$\mathcal{F} = \frac{\partial g_{\alpha\beta}}{dx^4}\frac{dx^4}{ds}\frac{dx^\alpha}{ds}\frac{dx^\beta}{ds}\,, \qquad (16)$$

is related to the mass of moving particles in 4D and to the motion of the whole 4D frame. This means that the emergence of this term in Eq. (14), leaving the 5D-geodesic equation verified, gives a new interpretation to the Equivalence Principle in 4D as a dynamical consequence. Looking at Eqs. (14) and (15), we see that in the ordinary 4D spacetime no term, in Eq. (15), is directly related to the masses which

are, on the contrary, existing in Eq. (14). In other words, it is the quantity $\mathcal{F}$, which gives the masses to the particles, and this means that the Equivalence Principle can be formulated on a dynamical base by an embedding process. Furthermore the massive particles are different but massless in 5D while, for the physical meaning of the fifth coordinate, they assume mass in 4D thanks to Eq. (16).

Let us now take into account a 5D-null path given by

$$dS^2 = g_{AB}\, dx^A dx^B = 0\,. \tag{17}$$

Splitting Eq. (17) into the 4D part and the fifth component, gives

$$dS^2 = ds^2 + g_{44}\left(dx^4\right)^2 = 0\,. \tag{18}$$

An inspection of Eq. (18) tells that a null path in 5D can result, in 4D, in a time-like path, a space-like path, or a null path depending on the sign and the value of g_{44}. Let us consider now the 5D-vector $u^A = dx^A/dS$. It can be split as a vector in the ordinary 3D-space v, a vector along the ordinary time axis w and a vector along the fifth dimension z. In particular, for 5D null paths, we can have the velocity $v^2 = w^2 + z^2$ and this should lead, in 4D, to super-luminal speed, explicitly overcoming the Lorentz transformations. The problem is solved if we consider the 5D-motion as *a-luminal*, because all particles and fields have the same speed (being massless) and the distinction among super-luminal, luminal and sub-luminal motion (the standard causal motion for massive particles) emerges only *after* the dynamical reduction from 5D-space to 4D spacetime. In this way, the fifth dimension is the entity which, by assigning the masses, is able to generate the different dynamics which we perceive in 4D. Consequently, it is the process of mass generation which sets the particles in the 4D light-cone. Specifically, let us rewrite the expression (16) as

$$\mathcal{F} = \frac{\partial g_{\mu\nu}}{\partial x^4}\frac{dx^4}{ds}\, u^\mu u^\nu. \tag{19}$$

As we said, seen in 4D, this is an Extra Force generated by the motion of the 4D frame with respect to the extra coordinate x^4. This fact shows that all the different particles are massless in 5D and acquire their rest masses m_0 in the dynamical reduction from the 5D to 4D. In fact, considering Eqs. (14) and (18), it is straightforward to derive

$$\mathcal{F} = u^\mu u^\nu\, \frac{\partial g_{\mu\nu}}{\partial x^4}\frac{dx^4}{ds} = \frac{1}{m_0}\frac{dm_0}{ds} = \frac{d\ln(m_0)}{ds}\,, \tag{20}$$

where m_0 has the rôle of a rest mass in 4D, being, from General Relativity,

$$\frac{dx^\mu}{ds} - \frac{1}{2}\frac{\partial g_{\alpha\beta}}{\partial x^\mu}\, u^\alpha u^\beta = 0 \tag{21}$$

and

$$p^\mu = m_0 u^\mu, \qquad p_\mu p^\mu = m_0^2\,, \tag{22}$$

which are, respectively, the definition of linear momentum and the mass-shell condition. Then, it is

$$d\ln(m_0) = \frac{\partial g_{\mu\nu}}{\partial x^4}\, u^\mu u^\nu dx^4 \tag{23}$$

that is

$$m_0 = \exp\int\left(\frac{\partial g_{\mu\nu}}{\partial x^4}\, u^\mu u^\nu dx^4\right) = \exp\int\left(\mathcal{F}dx^4\right). \tag{24}$$

In principle, the term $\int\left(\frac{\partial g_{\mu\nu}}{\partial x^4}\, u^\mu u^\nu dx^4\right)$ never gives a zero mass. However, this term can be less than zero and, with large absolute values, it can asymptotically produce a m_0 very close to zero. In conclusion the Extra Force induced by the reduction from the 5D to the 4D is equal to the derivative of the natural logarithm of the rest mass of a particle with respect to the $(3+1)$ line element and the expression

$$\int\left(\frac{\partial g_{\mu\nu}}{\partial x^4}u^\mu u^\nu dx^4\right) = \int\left(\mathcal{F}dx^4\right) \tag{25}$$

can be read as the total "work" capable of generating masses in the reduction process from 5D to 4D.

5 The field structure and the chronological structure

The results of previous section assume a straightforward physical meaning considering the fifth component of the metric as a scalar field. In this way, the pure "geometric" interpretation of the Extra Force can be framed in a "material" picture. In order to achieve this goal, let us consider the Campbell theorem [15] which states that it is always possible to consider a 4D Riemannian manifold, defined by the line element $ds^2 = g_{\alpha\beta}\, dx^\alpha dx^\beta$, embedded in a 5D one with $dS^2 = g_{AB}\, dx^A dx^B$. We have $g_{AB} = g_{AB}\left(x^\alpha, x^4\right)$ with x^4 the extra coordinate. The metric g_{AB} is covariant under the group of 5D coordinate transformations $x^A \to \overline{x}^A(x^B)$, but not under the restricted group of 4D transformations $x^\alpha \to \overline{x}^\alpha(x^\beta)$. This means, from a physical point of view, that the choice of the 5D coordinate can be read as the *gauge* which specifies the 4D physics. On the other hand, the signature and the value of the fifth coordinate is related to the dynamics generated by the physical quantities which we observe in 4D (mass, spin, charge). Let us start considering the variational principle

$$\delta\int d^{(5)}x\sqrt{-g^{(5)}}\left[{}^{(5)}R + \lambda(g_{44} - \epsilon\Phi^2)\right] = 0\,, \tag{26}$$

derived from (4) where λ is a Lagrange multiplier, Φ a generic scalar field and $\epsilon = \pm 1$. This procedure allows to derive the physical gauge for the 5D metric. The above 5D metric can be immediately rewritten as

$$\begin{aligned} dS^2 = g_{AB}\, dx^A dx^B = g_{\alpha\beta}dx^\alpha dx^\beta + g_{44}\left(dx^4\right)^2 = \\ = g_{\alpha\beta}\, dx^\alpha dx^\beta + \epsilon\,\Phi^2\left(dx^4\right)^2, \end{aligned} \tag{27}$$

where the signature $\epsilon = -1$ can be interpreted as "particle like" solutions while $\epsilon = +1$ gives rise to wave-like solutions. The physical meaning of these distinct classes of solutions, as we will see below, is crucial. Assuming a standard signature $(+\ -\ -\ -)$ for the 4D component of the metric, the 5D metric can be written as the matrix

$$g_{AB} = \begin{pmatrix} g_{\alpha\beta} & 0 \\ 0 & \epsilon\,\Phi^2 \end{pmatrix}, \tag{28}$$

and the 5D Ricci curvature tensor is

$$\begin{aligned} {}^{(5)}R_{\alpha\beta} = R_{\alpha\beta} - \frac{\Phi_{,\alpha;\beta}}{\Phi} + \frac{\epsilon}{2\Phi^2}\left(\frac{\Phi_{,4}\, g_{\alpha\beta,4}}{\Phi} - \right. \\ \left. - g_{\alpha\beta,44} + g^{\lambda\mu} g_{\alpha\lambda,4}\, g_{\beta\mu,4} - \frac{g^{\mu\nu} g_{\mu\nu,4}\, g_{\alpha\beta,4}}{2}\right) \end{aligned} \tag{29}$$

where $R_{\alpha\beta}$ is the 4D Ricci tensor. After the projection from 5D to 4D, $g_{\alpha\beta}$, derived from g_{AB}, no longer explicitly depends on x^4, and then the 5D Ricci scalar assumes the remarkable expression:

$${}^{(5)}R = R - \frac{1}{\Phi}\,\Box\Phi\,, \tag{30}$$

where the $\Box$ is now the 4D d'Alembert operator. The action in Eq. (26) can be recast in a 4D Brans-Dicke form

$$\mathcal{A} = -\frac{1}{16\pi G_N}\int d^4x\sqrt{-g}\,\left[\Phi R + \mathcal{L}_\Phi\right], \tag{31}$$

where the Newton constant is given by

$$G_N = \frac{{}^{(5)}G}{2\pi l} \tag{32}$$

where l is a characteristic length in 5D. Defining a generic function of a 4D scalar field φ as

$$-\frac{\Phi}{16\pi G_N} = F(\varphi) \tag{33}$$

we get a 4D general action in which gravity is nonminimally coupled to a scalar field [2, 16, 17]:

$$\begin{aligned} \mathcal{A} = \int_{\mathcal{M}} d^4x \times \\ \times\sqrt{-g}\left[F(\varphi)R + \frac{1}{2}\,g^{\mu\nu}\varphi_{;\mu}\,\varphi_{;\nu} - V(\varphi) + \mathcal{L}_m\right] \end{aligned} \tag{34}$$

$F(\varphi)$ and $V(\varphi)$ are a generic coupling and a self interacting potential respectively. The field equations can be derived by varying with respect to the 4D metric $g_{\mu\nu}$

$$R_{\mu\nu} - \frac{1}{2}\,g_{\mu\nu}R = \tilde{T}_{\mu\nu}\,, \tag{35}$$

where

$$\begin{aligned} \tilde{T}_{\mu\nu} = \frac{1}{F(\varphi)}\left\{-\frac{1}{2}\,\varphi_{;\mu}\varphi_{;\nu} + \frac{1}{4}\,g_{\mu\nu}\varphi_{;\alpha}\varphi^{;\alpha} - \right. \\ \left. - \frac{1}{2}\,g_{\mu\nu}V(\varphi) - g_{\mu\nu}\Box F(\varphi) + F(\varphi)_{;\mu\nu}\right\} \end{aligned} \tag{36}$$

is the effective stress–energy tensor containing the nonminimal coupling contributions, the kinetic terms and the potential of the scalar field φ. By varying with respect to φ, we get the 4D Klein-Gordon equation

$$\Box\varphi - RF'(\varphi) + V'(\varphi) = 0\,, \tag{37}$$

where primes indicate derivatives with respect to φ.

Eq. (37) is the contracted Bianchi identity demonstrating the recovering of conservation laws also in 4D [2]. This feature means that the effective stress-energy tensor at right hand side of (35) is a zero-divergence tensor and this fact is fully compatible with Einstein theory of gravity also starting from a 5D space. Specifically, the reduction procedure from 5D to 4D preserves all the features of standard General Relativity. In order to achieve the physical identification of the fifth dimension, let us recast the generalized Klein-Gordon equation (37) as

$$\left(\Box + m_{\text{eff}}^2\right)\varphi = 0\,, \tag{38}$$

where

$$m_{\text{eff}}^2 = \left[\,V'(\varphi) - RF'(\varphi)\right]\varphi^{-1} \tag{39}$$

is the effective mass, *i.e.* a function of φ, where self-gravity contributions $RF'(\varphi)$ and scalar field self interactions $V'(\varphi)$ are taken into account [18]. This means that a natural way to generate the masses of particles can be achieved starting from a 5D picture and the concept of *mass* can be recovered as a geometric derivation according to the Extra Force of previous section. In other words, the chronological structure and the geodesic structure of the reduction process from 5D to 4D naturally coincide since the the masses generated in both cases are equivalent. From an epistemological point of view, this new result clearly demonstrates why geodesic structure and chronological structure can be assumed to coincide in General Relativity using the Levi-Civita connection in both the Palatini and the metric approaches [13]. Explicitly the 5D d'Alembert operator can be split, considering the 5D metric in the form (27) for particle-like solutions:

$${}^{(5)}\Box = \Box - {\partial_4}^2\,. \tag{40}$$

This means that we are considering $\epsilon = -1$. We have then

$${}^{(5)}\Box\Phi = \left[\,\Box - {\partial_4}^2\right]\Phi = 0\,. \tag{41}$$

Separating the variables and splitting the scalar field Φ into two functions

$$\Phi = \varphi(t,\vec{x})\,\chi(x^4)\,, \tag{42}$$

the field φ depends on the ordinary space-time coordinates, while χ is a function of the fifth coordinate x^4. Inserting (42) into Eq. (41), we get

$$\frac{\Box\varphi}{\varphi} = \frac{1}{\chi}\left[\frac{d^2\chi}{dx_4^2}\right] = -k_n^2 \tag{43}$$

where k_n is a constant. From Eq. (43), we obtain the two field equations

$$\left(\Box + k_n^2\right)\varphi = 0\,, \tag{44}$$

and

$$\frac{d^2\chi}{dx_4^2} + k_n^2\,\chi = 0\,. \tag{45}$$

Eq. (45) describes a harmonic oscillator whose general solution is

$$\chi(x_4) = c_1 e^{-ik_n x^4} + c_2 e^{ik_n x^4}\,. \tag{46}$$

The constant k_n has the physical dimension of the inverse of a length and, assigning boundary conditions, we can derive the eigenvalue relation

$$k_n = \frac{2\pi}{l}\,n\,, \tag{47}$$

where n is an integer and l a length which we have previously defined in Eq. (32) related to the gravitational coupling. As a result, in standard units, we can recover the physical lengths through the Compton lengths

$$\lambda_n = \frac{\hbar}{2\pi m_n c} = \frac{1}{k_n} \tag{48}$$

which always assign the masses to the particles depending on the number n. It is worth stressing that, in this case, we have achieved a dynamical approach because the eigenvalues of Eq. (45) are the masses of particles which are generated by the process of reduction from 5D to 4D. The solution (46) is the superposition of two mass eigenstates. The 4D evolution is given by Eq. (38) or, equivalently, (44). Besides, the solutions in the coordinate x^4 give the associated Compton lengths from which the effective physical masses can be derived. Specifically, different values of n fix the families of particles, while, for any given value n, different values of parameters $c_{1,2}$ select the different particles within a family. With these considerations in mind, the effective mass can be obtained integrating the modulus of the scalar field Φ along the x^4 coordinate. It is

$$m_{\text{eff}} \equiv \int |\Phi| dx^4 = \int |\Phi\,(dx^4/ds)|\,ds \tag{49}$$

where ds is the 4D affine parameter used in the derivation of geodesic equation. This result means that the rest mass of a particle is derived by integrating the Extra Force along x^4 (see Eq. 24) while the effective mass is obtained by integrating the field Φ along x^4. In the first case, the mass of the particle is obtained starting from the geodesic structure of the theory, in the second case, it comes out from the field structure. In other words, the coincidence of geodesic structure and chronological structure (the causal structure), supposed as a principle in General Relativity, is due to the fact that masses are generated in the reduction process.

At this point, from the condition (42), the field 5D Φ results to be

$$\Phi(x^\alpha, x^4) = \sum_{n=-\infty}^{+\infty}\left[\varphi_n(x^\alpha)e^{-ik_n x^4} + \varphi_n^*(x^\alpha)e^{ik_n x^4}\right], \tag{50}$$

where φ and φ^* are the 4D solutions combined with the fifth-component solutions $e^{\pm ik_n x^4}$. In general, every particle mass can be selected by solutions of type (46). The number $k_n x^4$, *i.e.* the ratio between the two lengths x^4/λ_n, fixes the interaction scale. Geometrically, such a scale is related to the curvature radius of the embedded 4D spacetime where particles can be identified and, in principle, detected. In this sense, Open Quantum Relativity is an *induced-matter* theory, where the extra dimension cannot be simply classified as "compactified" since it yields all the 4D dynamics giving origin to the masses. Moreover, Eq. (50) is not a simple "tower of mass states" but a spectrum capable of explaining the hierarchy problem [7]. On the other hand, gravitational interaction can be framed in this approach considering as its fundamental scale the Planck length

$$\lambda_P = l = \left(\frac{\hbar G_N}{c^3}\right)^{1/2}, \tag{51}$$

instead of the above Compton length. It fixes the vacuum state of the system ant the masses of all particles can be considered negligible if compared with the Planck scales. Finally, as we have seen, the reduction mechanism can select also $\epsilon = 1$ in the metric (27). In this case, the 5D-Klein Gordon equation (11), and the 5D field equations (5) have wave-like solutions of the form

$$\begin{aligned} dS^2 = dt^2 - \Omega\,(t, x_1)\left(dx^1\right)^2 - \Omega\,(t, x_2)\left(dx^2\right)^2 - \\ - \Omega\,(t, x_3)\left(dx^3\right)^2 + \left(dx^4\right)^2, \end{aligned} \tag{52}$$

where

$$\Omega\,(t, x_j) = \exp i(\omega t + k_j x^j)\,, \quad j = 1, 2, 3\,. \tag{53}$$

In this solution, the necessity of the existence of two times arrows naturally emerges and, as a direct consequence, due to the structure of the functions $\Omega\,(t, x_j)$, closed time-like paths (*i.e.* circular paths) are allowed. The existence of closed time-like paths means that Anti-De Sitter [14] and Gödel [11] solutions are naturally allowed possibilities in the dynamics.

6 Discussion and conclusions

In this paper, we have discussed the reduction process which allows to recover the 4D spacetime and dynamics starting from the 5D manifold of Open Quantum Relativity. Such a theory needs, to be formulated, a *General Conservation Principle*. This principle states that conservation laws are always and absolutely valid also when, to maintain such a validity, phenomena as topology changes and entanglement

can emerge in 4D. In this way, we have a theory without singularities (like conventional black holes) and unphysical spacetime regions are naturally avoided [8, 6]. The dimensional reduction can be considered from the geodesic structure and the field equations points of view. In the first case, starting from a 5D metric, it is possible to generate an Extra Force term in 4D which is related to the rest masses of particles and then to the Equivalence Principle. In fact, masses can be dynamically generated by the fifth component of the 5D space and the relation between inertial mass and gravitational mass is not an assumed principle, as in standard physics [10], but the result of the dynamical process of embedding. It is worth noting that an "amount of work" is necessary to give the mass to a particle. An effective mass is recovered also by splitting the field equations in a $(4+1)$ formalism. The fifth component of the metric can be interpreted as a scalar field and the embedding as the process by which the mass of particles emerges. The fact that particles acquire the mass from the embedding of geodesics and from the embedding of field equations is the reason why the chronological and geodesic structures of the 4D spacetime are the same: they can be both achieved from the same 5D metric structure which is also the solution of the 5D field equations. By taking into account such a result in 4D, the result itself naturally leads to understand why the metric approach of General Relativity, based on Levi-Civita connections, succeed in the description of spacetime dynamics even without resorting to a more general scheme as the Palatini-affine approach where connection and metric are, in principle, considered distinct. The reduction process leads also to a wide class of time solutions including two-time arrows and closed time-like paths. As a consequence, we can recover the concept of causality questioned by the EPR effect [6] thanks to the necessary introduction of backward and forward causation [1]. As a final remark, we can say that Open Quantum Relativity is an approach which allows to face Quantum Mechanics and Relativity under the same dynamical standard (a covariant symplectic structure [3]): this occurrence leads to frame several paradoxes of modern physics under the same dynamical scheme by only an assumption of the absolute validity of conservation laws and the generalization of the causal structure of spacetime.

Submitted on May 14, 2007
Accepted on May 21, 2007

References

1. Basini G., Capozziello S. *Gen. Relativ. Grav.*, 2005, v. 37, 115.
2. Basini G., Capozziello S. *Gen. Relativ. Grav.*, 2003, v. 35, 2217.
3. Basini G., Capozziello S. *Mod. Phys. Lett.*, 2005, v. A20, 251.
4. Basini G., Capozziello S. *Int. Journ. Mod. Phys.*, 2006, v. D15, 583.
5. Basini G., Capozziello S. *Europhys. Lett.*, 2003, v. 63, 166.
6. Basini G., Capozziello S. and Longo G. *Gen. Relativ. Grav.*, 2003, v. 35, 189.
7. Basini G., Capozziello S. and Longo G. *Phys. Lett.*, 2003, v. 311A, 465.
8. Basini G., Capozziello S. and Longo G. *Astrop. Phys.*, 2004, v. 20, 457.
9. Basini G., Bongiorno F. and Capozziello S. *Int. Journ. Mod. Phys.*, 2004, v. D13, 717.
10. Schrödinger E. Space-time structure. Cambridge Univ. Press, Cambridge, 1960.
11. Gödel K. *Rev. Mod. Phys.*, 1949, v. 21, 447.
12. Weinberg S. Gravitation and cosmology. Wiley, New York, 1972.
13. Palatini A. *Rend. Circ. Mat. Palermo*, 1919, v. 43, 203.
14. Satinger D. H., Weaver O. L. Lie groups and algebras with applications to physics, geometry and mechanics. Springer-Verlag, Berlin, 1986.
15. Campbell J. E. A course of differential geometry. Clarendon, Oxford, 1926.
16. Basini G., Capozziello S. *Prog. Phys.*, 2006, v. 4, 65.
17. Smarandache F. A unifying field in logics: neutrosophic logic. Neutrosophy, neutrosophic set, neutrosophic probability. 3rd edition, American Research Press, Rehoboth, 2003 (recent editions occured in 1999 and 2000).
18. Birrell N., Davies P. C. Quantum fields in curved space. Cambridge Univ. Press, Cambridge, 1984.

Yang-Mills Field from Quaternion Space Geometry, and Its Klein-Gordon Representation

Alexander Yefremov*, Florentin Smarandache† and Vic Christianto‡

*Institute of Gravitation and Cosmology, Peoples' Friendship University of Russia, Miklukho-Maklaya Str. 6, Moscow 117198, Russia
E-mail: a.yefremov@rudn.ru

†Chair of the Dept. of Mathematics and Science, University of New Mexico, Gallup, NM 87301, USA
E-mail: smarand@unm.edu

‡Sciprint.org — a Free Scientific Electronic Preprint Server, http://www.sciprint.org
E-mail: admin@sciprint.org

Analysis of covariant derivatives of vectors in quaternion (Q-) spaces performed using Q-unit spinor-splitting technique and use of SL(2C)-invariance of quaternion multiplication reveals close connexion of Q-geometry objects and Yang-Mills (YM) field principle characteristics. In particular, it is shown that Q-connexion (with quaternion non-metricity) and related curvature of 4 dimensional (4D) space-times with 3D Q-space sections are formally equivalent to respectively YM-field potential and strength, traditionally emerging from the minimal action assumption. Plausible links between YM field equation and Klein-Gordon equation, in particular via its known isomorphism with Duffin-Kemmer equation, are also discussed.

1 Introduction

Traditionally YM field is treated as a gauge, "*auxiliary*", field involved to compensate local transformations of a 'main' (e.g. spinor) field to keep invariance of respective action functional. Anyway there are a number of works where YM-field features are found related to some geometric properties of space-times of different types, mainly in connexion with contemporary gravity theories.

Thus in paper [1] violation of $SO(3,1)$-covariance in gauge gravitation theory caused by distinguishing time direction from normal space-like hyper-surfaces is regarded as spontaneous symmetry violation analogous to introduction of mass in YM theory. Paper [2] shows a generic approach to formulation of a physical field evolution based on description of differential manifold and its mapping onto "model" spaces defined by characteristic groups; the group choice leads to gravity or YM theory equations. Furthermore it can be shown [2b] that it is possible to describe altogether gravitation in a space with torsion, and electroweak interactions on 4D real spacetime C^2, so we have in usual spacetime with torsion a unified theory (modulo the non treatment of the strong forces).

Somewhat different approach is suggested in paper [3] where gauge potentials and tensions are related respectively to connexion and curvature of principle bundle, whose base and gauge group choice allows arriving either to YM or to gravitation theory. Paper [4] dealing with gravity in Riemann-Cartan space and Lagrangian quadratic in connexion and curvature shows possibility to interpret connexion as a mediator of YM interaction.

In paper [5] a unified theory of gravity and electroweak forces is built with Lagrangian as a scalar curvature of space-time with torsion; if trace and axial part of the torsion vanish the Lagrangian is shown to separate into Gilbert and YM parts. Regardless of somehow artificial character of used models, these observations nonetheless hint that there may exist a deep link between supposedly really physical object, YM field and pure math constructions. A surprising analogy between main characteristics of YM field and mathematical objects is found hidden within geometry induced by quaternion (Q-) numbers.

In this regard, the role played by Yang-Mills field cannot be overemphasized, in particular from the viewpoint of the Standard Model of elementary particles. While there are a number of attempts for describing the Standard Model of hadrons and leptons from the viewpoint of classical electromagnetic Maxwell equations [6, 7], nonetheless this question remains an open problem. An alternative route toward achieving this goal is by using quaternion number, as described in the present paper. In fact, in Ref. [7] a somewhat similar approach with ours has been described, i.e. the generalized Cauchy-Riemann equations contain 2-spinor and C-gauge structures, and their integrability conditions take the form of Maxwell and Yang-Mills equations.

It is long ago noticed that Q-math (algebra, calculus and related geometry) naturally comprise many features attributed to physical systems and laws. It is known that quaternions describe three "imaginary" Q-units as unit vectors directing axes of a Cartesian system of coordinates (it was initially developed to represent subsequent telescope motions in astronomical observation). Maxwell used the fact to write his

equations in the most convenient Q-form. Decades later Fueter discovered a formidable coincidence: a pure math Cauchy-Riemann type condition endowing functions of Q-variable with analytical properties turned out to be identical in shape to vacuum equations of electrodynamics [9].

Later on other surprising Q-math — physics coincidences were found. Among them: "automatic" appearance of Pauli magnetic field-spin term with Bohr magneton as a coefficient when Hamiltonian for charged quantum mechanical particle was built with the help of Q-based metric [10]; possibility to endow "imaginary" vector Q-units with properties of not only stationary but movable triad of Cartan type and use it for a very simple description of Newtonian mechanics in rotating frame of reference [11]; discovery of inherited in Q-math variant of relativity theory permitting to describe motion of non-inertial frames [12]. Preliminary study shows that YM field components are also formally present in Q-math.

In Section 2 notion of Q-space is given in necessary detail. Section 3 discussed neat analogy between Q-geometric objects and YM field potential and strength. In Section 4 YM field and Klein-Gordon correspondence is discussed. Concluding remarks can be found in Section 5.

Part of our motivation for writing this paper was to explicate the hidden electromagnetic field origin of YM fields. It is known that the Standard Model of elementary particles lack systematic description for the mechanism of quark charges. (Let alone the question of whether quarks do exist or they are mere algebraic tools, as Heisenberg once puts forth: *If quarks exist, then we have redefined the word "exist".*) On the other side, as described above, Maxwell described his theory in quaternionic language, therefore it seems natural to ask whether it is possible to find neat link between quaternion language and YM-fields, and by doing so provide one step toward describing mechanism behind quark charges.

Further experimental observation is of course recommended in order to verify or refute our propositions as described herein.

2 Quaternion spaces

Detailed description of Q-space is given in [13]; shortly but with necessary strictness its notion can be presented as following.

Let U_N be a manifold, a geometric object consisting of points $M \in U_N$ each reciprocally and uniquely corresponding to a set of N numbers-coordinates $\{y^A\} : M \leftrightarrow \{y^A\}$, $(A = 1, 2 \dots N)$. Also let the sets of coordinates be transformed so that the map becomes a homeomorphism of a class C_k. It is known that U_N may be endowed with a proper tangent manifold T_N described by sets of orthogonal unite vectors $\mathbf{e}_{(A)}$ generating in T_N families of coordinate lines $M \to \{X^{(A)}\}$, indices in brackets being numbers of frames' vectors. Differentials of coordinates in U_N and T_N are tied as $dX^{(A)} = g_B^{(A)} dy^B$, with Lamé coefficients $g_B^{(A)}$, functions of y^A, so that $X^{(A)}$ are generally non-holonomic. Irrespectively of properties of U_N each its point may be attached to the origin of a frame, in particular presented by "imaginary" Q-units $\mathbf{q}_k$, this attachment accompanied by a rule tying values of coordinates of this point with the triad orientation $M \leftrightarrow \{y^A, \Phi_\xi\}$. All triads $\{\mathbf{q}_k\}$ so defined on U_N form a sort of "tangent" manifold $T(U, \mathbf{q})$, (really tangent only for the base U_3). Due to presence of frame vectors $\mathbf{q}_k(y)$ existence of metric and at least proper (quaternionic) connexion $\omega_{jkn} = -\omega_{jnk}$, $\partial_j \mathbf{q}_k = \omega_{jkn}\mathbf{q}_n$, is implied, hence one can tell of $T(U, \mathbf{q})$ as of a Q-tangent space on the base U_N. Coordinates x_k defined along triad vectors $\mathbf{q}_k$ in $T(U, \mathbf{q})$ are tied with non-holonomic coordinates $X^{(A)}$ in proper tangent space T_N by the transformation $dx_k \equiv h_{k(A)} dX^{(A)}$ with $h_{k(A)}$ being locally depending matrices (and generally not square) of relative $\mathbf{e}_{(A)} \leftrightarrow \mathbf{q}_k$ rotation. Consider a special case of unification $U \oplus T(U, \mathbf{q})$ with 3-dimensional base space $U = \mathbf{U}_3$. Moreover, let quaternion specificity of T_3 reflects property of the base itself, i.e. metric structure of $\mathbf{U}_3$ inevitably requires involvement of Q-triads to initiate Cartesian coordinates in its tangent space. Such 3-dimensional space generating sets of tangent quaternionic frames in each its point is named here "quaternion space" (or simply Q-space). Main distinguishing feature of a Q-space is non-symmetric form of its metric tensor* $\mathbf{g}_{kn} \equiv \mathbf{q}_k \mathbf{q}_n = -\delta_{kn} + \varepsilon_{knj}\mathbf{q}_j$ being in fact multiplication rule of "imaginary" Q-units. It is easy to understand that all tangent spaces constructed on arbitrary bases as designed above are Q-spaces themselves. In most general case a Q-space can be treated as a space of affine connexion $\Omega_{jkn} = \Gamma_{jkn} + Q_{jkn} + S_{jkn} + \omega_{jnk} + \sigma_{jkn}$ comprising respectively Riemann connexion Γ_{jkn}, Cartan contorsion Q_{jkn}, segmentary curvature (or ordinary non-metricity) S_{jkn}, Q-connexion ω_{jnk}, and Q-non-metricity σ_{jkn}; curvature tensor is given by standard expression $R_{knij} = \partial_i \Omega_{j\,kn} - \partial_j \Omega_{i\,kn} + \Omega_{i\,km}\Omega_{j\,mn} - \Omega_{j\,nm}\Omega_{i\,mk}$. Presence or vanishing of different parts of connexion or curvature results in multiple variants of Q-spaces classification [13]. Further on only Q-spaces with pure quaternionic characteristics (Q-connexion and Q-non-metricity) will be considered.

3 Yang-Mills field from Q-space geometry

Usually Yang-Mills field $A_{B\mu}$ is introduced as a gauge field in procedure of localized transformations of certain field, e.g. spinor field [14, 15]

$$\psi_a \to U(y^\beta)\,\psi_a\,. \tag{1}$$

If in the Lagrangian of the field partial derivative of ψ_a is changed to "covariant" one

$$\partial_\beta \to D_\beta \equiv \partial_\beta - gA_\beta\,, \tag{2}$$

*Latin indices are 3D, Greek indices are 4D; δ_{kn}, ε_{knj} are Kronecker and Levi-Civita symbols; summation convention is valid.

$$A_\beta \equiv i A_{C\,\beta}\,\mathbf{T}_C\,, \tag{3}$$

where g is a real constant (parameter of the model), $\mathbf{T}_C$ are traceless matrices (Lie-group generators) commuting as

$$[\mathbf{T}_B,\,\mathbf{T}_C] = i f_{BCD}\,\mathbf{T}_D \tag{4}$$

with structure constants f_{BCD}, then

$$D_\beta U \equiv (\partial_\beta - g A_\beta)\,U = 0\,, \tag{5}$$

and the Lagrangian keeps invariant under the transformations (1). The theory becomes "self consistent" if the gauge field terms are added to Lagrangian

$$L_{YM} \sim F^{\alpha\beta} F_{\alpha\beta}\,, \tag{6}$$

$$F_{\alpha\beta} \equiv F_{C\,\alpha\beta}\,\mathbf{T}_C\,. \tag{7}$$

The gauge field intensity $F_B^{\mu\nu}$ expressed through potentials $A_{B\mu}$ and structure constants as

$$F_{C\,\alpha\beta} = \partial_\alpha A_{C\,\beta} - \partial_\beta A_{C\,\alpha} + f_{CDE}\,A_{D\,\alpha}\,A_{E\,\beta}\,. \tag{8}$$

Vacuum equations of the gauge field

$$\partial_\alpha F^{\alpha\beta} + \left[A_\alpha, F^{\alpha\beta}\right] = 0 \tag{9}$$

are result of variation procedure of action built from Lagrangian (6).

Group Lie, e.g. SU(2) generators in particular can be represented by "imaginary" quaternion units given by e.g. traceless 2×2-matrices in special representation (Pauli-type) $i\mathbf{T}_B \to \mathbf{q}_{\tilde{k}} = -i\sigma_k$ (σ_k are Pauli matrices),

Then the structure constants are Levi-Civita tensor components $f_{BCD} \to \varepsilon_{knm}$, and expressions for potential and intensity (strength) of the gauge field are written as:

$$A_\beta = g\,\frac{1}{2}\,A_{\tilde{k}\,\beta}\,\mathbf{q}_{\tilde{k}}\,, \tag{10}$$

$$F_{k\,\alpha\beta} = \partial_\alpha A_{k\,\beta} - \partial_\beta A_{k\,\alpha} + \varepsilon_{kmn}\,A_{m\,\alpha}\,A_{n\,\beta}\,. \tag{11}$$

It is worthnoting that this conventional method of introduction of a Yang-Mills field type essentially exploits *heuristic base* of theoretical physics, first of all the postulate of minimal action and formalism of Lagrangian functions construction. But since description of the field optionally uses quaternion units one can assume that some of the above relations are appropriate for Q-spaces theory and may have geometric analogues. To verify this assumption we will use an example of 4D space-time model with 3D spatial quaternion section.

Begin with the problem of 4D space-time with 3D spatial section in the form of Q-space containing only one geometric object: proper quaternion connexion. Q-covariant derivative of the basic (frame) vectors $\mathbf{q}_m$ identically vanish in this space:

$$\tilde{D}_\alpha\,\mathbf{q}_k \equiv (\delta_{mk}\,\partial_\alpha + \omega_{\alpha\,mk})\,\mathbf{q}_m = 0\,. \tag{12}$$

This equation is in fact equivalent to definition of the proper connexion $\omega_{\alpha\,mk}$. If a transformation of Q-units is given by spinor group (leaving quaternion multiplication rule invariant)

$$\mathbf{q}_k = U(y)\,\mathbf{q}_{\tilde{k}}\,U^{-1}(y) \tag{13}$$

($\mathbf{q}_{\tilde{k}}$ are constants here) then Eq. (12) yields

$$\partial_\alpha U\,\mathbf{q}_{\tilde{k}}\,U^{-1} + U\,\mathbf{q}_{\tilde{k}}\,\partial_\alpha U^{-1} = \omega_{\alpha kn}\,U\,\mathbf{q}_{\tilde{n}}\,U^{-1}. \tag{14}$$

But one can easily verify that each "imaginary" Q-unit $\mathbf{q}_{\tilde{k}}$ can be always represented in the form of tensor product of its eigen-functions (EF) $\psi_{(\tilde{k})}$, $\varphi_{(\tilde{k})}$ (no summation convention for indices in brackets):

$$\mathbf{q}_{\tilde{k}}\,\psi_{(\tilde{k})} = \pm i\psi_{(\tilde{k})}, \qquad \varphi_{(\tilde{k})}\mathbf{q}_{\tilde{k}} = \pm i\varphi_{(\tilde{k})} \tag{15}$$

having spinor structure (here only EF with positive parity (with sign +) are shown)

$$\mathbf{q}_{\tilde{k}} = i(2\psi_{(\tilde{k})}\varphi_{(\tilde{k})} - 1); \tag{16}$$

this means that left-hand-side (lhs) of Eq. (14) can be equivalently rewritten in the form

$$\begin{aligned}&\frac{1}{2}\,(\partial_\alpha U\,\mathbf{q}_{\tilde{k}}\,U^{-1} + U\,\mathbf{q}_{\tilde{k}}\,\partial_\alpha U^{-1}) = \\ &\quad = (\partial_\alpha U\,\psi_{(\tilde{k})})\,\varphi_{(\tilde{k})}U^{-1} + U\,\psi_{(\tilde{k})}\,(\varphi_{(\tilde{k})}\partial_\alpha U^{-1})\end{aligned} \tag{17}$$

which strongly resembles use of Eq. (1) for transformations of spinor functions.

Here we for the first time underline a remarkable fact: *form-invariance of multiplication rule of Q-units under their spinor transformations gives expressions similar to those conventionally used to initiate introduction of gauge fields of Yang-Mills type.*

Now in order to determine mathematical analogues of these "physical fields", we will analyze in more details Eq. (14). Its multiplication (from the right) by combination $U\,\mathbf{q}_{\tilde{k}}$ with contraction by index $\tilde{k}$ leads to the expression

$$-3\,\partial_\alpha U\; + U\,\mathbf{q}_{\tilde{k}}\,\partial_\alpha U^{-1} U\mathbf{q}_{\tilde{k}} = \omega_{\alpha kn}\,U\,\mathbf{q}_{\tilde{n}}\,\mathbf{q}_{\tilde{k}}\,. \tag{18}$$

This matrix equation can be simplified with the help of the always possible development of transformation matrices

$$U \equiv a\; + b_k\,\mathbf{q}_{\tilde{k}}\,, \qquad U^{-1} = a\; - b_k\,\mathbf{q}_{\tilde{k}}\,, \tag{19}$$

$$UU^{-1} = a^2\; + b_k\,b_k = 1\,, \tag{20}$$

where a, b_k are real scalar and 3D-vector functions, $\mathbf{q}_{\tilde{k}}$ are Q-units in special (Pauli-type) representation. Using Eqs. (19), the second term in lhs of Eq. (18) after some algebra is reduced to remarkably simple expression

$$\begin{aligned}&U\,\mathbf{q}_{\tilde{k}}\,\partial_\alpha U^{-1} U\mathbf{q}_{\tilde{k}} = \\ &= (a + b_n\mathbf{q}_{\tilde{n}})\,\mathbf{q}_{\tilde{k}}(\partial_\alpha a - \partial_\alpha b_m\mathbf{q}_{\tilde{m}})\,(a + b_l\,\mathbf{q}_{\tilde{l}})\,\mathbf{q}_{\tilde{k}} = \\ &= \partial_\alpha(a + b_n\mathbf{q}_{\tilde{n}}) = -\partial_\alpha U\end{aligned} \tag{21}$$

so that altogether lhs of Eq. (18) comprises $-4\,\partial_\alpha U$ while right-hand-side (rhs) is

$$\omega_{\alpha kn}\,U\,\mathbf{q}_{\tilde{n}}\mathbf{q}_{\tilde{k}} = -\,\varepsilon_{knm}\omega_{\alpha kn}\,U\,\mathbf{q}_{\tilde{m}}\,; \tag{22}$$

then Eq. (18) yields

$$\partial_\alpha U - \frac{1}{4}\,\varepsilon_{knm}\omega_{\alpha kn}\,U\,\mathbf{q}_{\tilde{m}} = 0\,. \tag{23}$$

If now one makes the following notations

$$A_{k\,\alpha} \equiv \frac{1}{2}\,\varepsilon_{knm}\,\omega_{\alpha kn}\,, \tag{24}$$

$$A_\alpha \equiv \frac{1}{2}\,A_n\mathbf{q}_{\tilde{n}}\,, \tag{25}$$

then notation (25) exactly coincides with the definition (10) (provided $g=1$), and Eq. (23) turns out equivalent to Eq. (5)

$$U\overleftarrow{D}_\alpha \equiv U(\overleftarrow{\partial}_\alpha - A_\alpha) = 0\,. \tag{26}$$

Expression for "covariant derivative" of inverse matrix follows from the identity:

$$\partial_\alpha U\,U^{-1} = -\,U\partial_\alpha U^{-1}. \tag{27}$$

Using Eq. (23) one easily computes

$$-\,\partial_\alpha U^{-1} - \frac{1}{4}\,\varepsilon_{knm}\,\omega_{\alpha kn}\,\mathbf{q}_{\tilde{m}}U^{-1} = 0 \tag{28}$$

or

$$D_\alpha U^{-1} \equiv (\partial_\alpha + A_\alpha)\,U^{-1} = 0\,. \tag{29}$$

Direction of action of the derivative operator is not essential here, since the substitution $U^{-1}\to U$ и $U\to U^{-1}$ is always possible, and then Eq. (29) exactly coincides with Eq. (5).

Now let us summarize first results. We have a remarkable fact: form-invariance of Q-multiplication has as a corollary "covariant constancy" of matrices of spinor transformations of vector Q-units; moreover one notes that proper Q-connexion (contracted in skew indices by Levi-Civita tensor) plays the role of "gauge potential" of some Yang-Mills-type field. By the way the Q-connexion is easily expressed from Eq. (24)

$$\omega_{\alpha kn} = \varepsilon_{mkn}A_{m\,\alpha}\,. \tag{30}$$

Using Eq. (25) one finds expression for the gauge field intensity (11) (contracted by Levi-Civita tensor for convenience) through Q-connexion

$$\begin{aligned}
&\varepsilon_{kmn}F_{k\,\alpha\beta} = \\
&= \varepsilon_{kmn}(\partial_\alpha A_{k\,\beta} - \partial_\beta A_{k\,\alpha}) + \varepsilon_{kmn}\varepsilon_{mlj}A_{l\,\alpha}A_{j\,\beta} = \\
&= \partial_\alpha\omega_{\beta\,mn} - \partial_\beta\omega_{\alpha\,mn} + A_{m\,\alpha}A_{n\,\beta} - A_{m\beta}A_{n\alpha}\,.
\end{aligned} \tag{31}$$

If identically vanishing sum

$$-\delta_{mn}A_{j\,\alpha}A_{j\,\beta} + \delta_{mn}A_{j\beta}A_{j\alpha} = 0 \tag{32}$$

is added to rhs of (31) then all quadratic terms in the right hand side can be given in the form

$$\begin{aligned}
&A_{m\,\alpha}A_{n\,\beta} - A_{m\beta}A_{n\,\alpha} - \delta_{mn}A_{j\,\alpha}A_{j\,\beta} + \delta_{mn}A_{j\beta}A_{j\alpha} = \\
&= (\delta_{mp}\delta_{qn} - \delta_{mn}\delta_{qp})(A_{p\,\alpha}A_{q\,\beta} - A_{p\beta}A_{q\,\alpha}) = \\
&= \varepsilon_{kmq}\varepsilon_{kpn}(A_{p\,\alpha}A_{q\,\beta} - A_{p\beta}A_{q\,\alpha}) = \\
&= -\,\omega_{\alpha\,kn}\,\omega_{\beta\,km} + \omega_{\beta\,kn}A_{\alpha\,km}\,.
\end{aligned}$$

Substitution of the last expression into Eq. (31) accompanied with new notation

$$R_{mn\,\alpha\beta} \equiv \varepsilon_{kmn}F_{k\,\alpha\beta} \tag{33}$$

leads to well-known formula:

$$\begin{aligned}
R_{mn\,\alpha\beta} = \partial_\alpha\omega_{\beta\,mn} - \partial_\beta\omega_{\alpha\,mn} + \\
+\,\omega_{\alpha\,nk}\,\omega_{\beta\,km} - \omega_{\beta\,nk}\,\omega_{\alpha\,km}\,.
\end{aligned} \tag{34}$$

This is nothing else but curvature tensor of Q-space built out of proper Q-connexion components (in their turn being functions of 4D coordinates). By other words, Yang-Mills field strength is mathematically (geometrically) identical to quaternion space curvature tensor. But in the considered case of Q-space comprising only proper Q-connexion, all components of the curvature tensor are identically zero. So Yang-Mills field in this case has potential but no intensity.

The picture absolutely changes for the case of quaternion space with Q-connexion containing a proper part $\omega_{\beta\,kn}$ and also Q-non-metricity $\sigma_{\beta\,kn}$

$$\Omega_{\beta\,kn}(y^\alpha) = \omega_{\beta\,kn} + \sigma_{\beta\,kn} \tag{35}$$

so that Q-covariant derivative of a unite Q-vector with connexion (35) does not vanish, its result is namely the Q-non-metricity

$$\hat{D}_\alpha\mathbf{q}_k \equiv (\delta_{mk}\partial_\alpha + \Omega_{\alpha\,mk})\,\mathbf{q}_m = \sigma_{\alpha\,mk}\,\mathbf{q}_k\,. \tag{36}$$

For this case "covariant derivatives" of transformation spinor matrices may be defined analogously to previous case definitions (26) and (29)

$$U\hat{\overleftarrow{D}}_\alpha \equiv \hat{U}(\overleftarrow{\partial}_\alpha - \hat{A}_\alpha), \quad \hat{D}_\alpha U^{-1} \equiv (\partial_\alpha + \hat{A}_\alpha)U\,. \tag{37}$$

But here the "gauge field" is built from Q-connexion (35)

$$\hat{A}_{k\,\alpha} \equiv \frac{1}{2}\,\varepsilon_{knm}\Omega_{\alpha kn}, \qquad \hat{A}_\alpha \equiv \frac{1}{2}\,\hat{A}_n\mathbf{q}_{\tilde{n}}\,. \tag{38}$$

It is not difficult to verify whether the definitions (37) are consistent with non-metricity condition (36). Action of the "covariant derivatives" (37) onto a spinor-transformed unite Q-vector

$$\begin{aligned}
&\hat{D}_\alpha\,\mathbf{q}_k \to (\hat{D}_\alpha U)\,\mathbf{q}_{\tilde{k}}\,\partial_\alpha U^{-1} + U\,\mathbf{q}_{\tilde{k}}\,(\hat{D}_\alpha U^{-1}) = \\
&= \left(U\overleftarrow{D}_\alpha - \frac{1}{4}\,\varepsilon_{jnm}\Omega_{\alpha\,nm}U\mathbf{q}_{\tilde{j}}\,\mathbf{q}_{\tilde{k}}\right)U^{-1} + \\
&+ U\,\mathbf{q}_{\tilde{k}}\left(D_\alpha U^{-1} + \frac{1}{4}\,\varepsilon_{jnm}\Omega_{\alpha\,nm}\,\mathbf{q}_{\tilde{j}}U^{-1}\right)
\end{aligned}$$

together with Eqs. (26) and (29) demand:

$$U\overleftarrow{D}_\alpha = D_\alpha U^{-1} = 0 \tag{39}$$

leads to the expected results

$$\hat{D}_\alpha \mathbf{q}_k \to \frac{1}{2}\varepsilon_{jnm}\sigma_{\alpha\,nm} U \varepsilon_{jkl}\mathbf{q}_{\tilde{l}}\, U^{-1} = \\ = \sigma_{\alpha\,kl} U \mathbf{q}_{\tilde{l}}\, U^{-1} = \sigma_{\alpha\,kl}\,\mathbf{q}_l$$

i.e. "gauge covariant" derivative of any Q-unit results in Q-non-metricity in full accordance with Eq. (36).

Now find curvature tensor components in this Q-space; it is more convenient to calculate them using differential forms. Given Q-connexion 1-form

$$\Omega_{\,kn} = \Omega_{\beta\,kn} dy^\beta \tag{40}$$

from the second equation of structure

$$\frac{1}{2}\hat{R}_{kn\alpha\beta}\, dy^\alpha \wedge dy^\beta = d\Omega_{kn} + \Omega_{km}\wedge\Omega_{mn} \tag{41}$$

one gets the curvature tensor component

$$\hat{R}_{kn\alpha\beta} = \partial_\alpha\Omega_{\beta\,kn} - \partial_\beta\Omega_{\alpha\,kn} + \\ + \Omega_{\alpha\,km}\Omega_{\beta\,mn} - \Omega_{\alpha\,nm}\Omega_{\beta\,mk} \tag{42}$$

quite analogously to Eq. (34). Skew-symmetry in 3D indices allows representing the curvature part of 3D Q-section as 3D axial vector

$$\hat{F}_{m\,\alpha\beta} \equiv \frac{1}{2}\varepsilon_{knm}\hat{R}_{kn\alpha\beta} \tag{43}$$

and using Eq. (38) one readily rewrites definition (43) in the form

$$\hat{F}_{m\,\alpha\beta} = \partial_\alpha\hat{A}_{m\,\beta} - \partial_\beta\hat{A}_{m\,\alpha} + \varepsilon_{knm}\hat{A}_{k\,\alpha}\hat{A}_{n\,\beta} \tag{44}$$

which exactly coincides with conventional definition (11). QED.

4 Klein-Gordon representation of Yang-Mills field

In the meantime, it is perhaps more interesting to note here that such a neat linkage between Yang-Mills field and quaternion numbers is already known, in particular using Klein-Gordon representation [16]. In turn, this neat correspondence between Yang-Mills field and Klein-Gordon representation can be expected, because both can be described in terms of $\mathrm{SU}(2)$ theory [17]. In this regards, quaternion decomposition of $\mathrm{SU}(2)$ Yang-Mills field has been discussed in [17], albeit it implies a different metric from what is described herein:

$$ds^2 = d\alpha_1^2 + \sin^2\alpha_1\, d\beta_1^2 + d\alpha_2^2 + \sin^2\alpha_2\, d\beta_2^2\,. \tag{45}$$

However, the $\mathrm{O}(3)$ non-linear sigma model appearing in the decomposition [17] looks quite similar (or related) to the Quaternion relativity theory (as described in the Introduction, there could be neat link between Q-relativity and $\mathrm{SO}(3,1)$).

Furthermore, sometime ago it has been shown that four-dimensional coordinates may be combined into a quaternion, and this could be useful in describing supersymmetric extension of Yang-Mills field [18]. This plausible neat link between Klein-Gordon equation, Duffin-Kemmer equation and Yang-Mills field via quaternion number may be found useful, because both Duffin-Kemmer equation and Yang-Mills field play some kind of significant role in description of standard model of particles [16].

In this regards, it has been argued recently that one can derive standard model using Klein-Gordon equation, in particular using Yukawa method, without having to introduce a Higgs mass [19, 20]. Considering a notorious fact that Higgs particle has not been observed despite more than three decades of extensive experiments, it seems to suggest that an alternative route to standard model of particles using (quaternion) Klein-Gordon deserves further consideration.

In this section we will discuss a number of approaches by different authors to describe the (quaternion) extension of Klein-Gordon equation and its implications. First we will review quaternion quantum mechanics of Adler. And then we discuss how Klein-Gordon equation leads to hypothetical imaginary mass. Thereafter we discuss an alternative route for quaternionic modification of Klein-Gordon equation, and implications to meson physics.

4.1 Quaternion Quantum Mechanics

Adler's method of quaternionizing Quantum Mechanics grew out of his interest in the Harari-Shupe's rishon model for composite quarks and leptons [21]. In a preceding paper [22] he describes that in quaternionic quantum mechanics (QQM), the Dirac transition amplitudes are quaternion valued, i.e. they have the form

$$q = r_0 + r_1 i + r_2 j + r_3 k \tag{46}$$

where r_0, r_1, r_2, r_3 are real numbers, and i, j, k are quaternion imaginary units obeying

$$i^2 = j^2 = k^2 = -1, \quad ij = -ji = k, \\ jk = -kj = i, \qquad ki = -ik = j\,. \tag{47}$$

Using this QQM method, he described composite fermion states identified with the quaternion real components [23].

4.2 Hypothetical imaginary mass problem in Klein-Gordon equation

It is argued that dynamical origin of Higgs mass implies that the mass of W must always be pure imaginary [19, 20]. Therefore one may conclude that a real description for (composite) quarks and leptons shall avoid this problem, i.e. by not including the problematic Higgs mass.

Nonetheless, in this section we can reveal that perhaps the problem of imaginary mass in Klein-Gordon equation is not completely avoidable. First we will describe an elemen-

tary derivation of Klein-Gordon from electromagnetic wave equation, and then by using Bakhoum's assertion of total energy we derive alternative expression of Klein-Gordon implying the imaginary mass.

We can start with 1D-classical wave equation as derived from Maxwell equations [24, p.4]:

$$\frac{\partial^2 E}{\partial x^2} - \frac{1}{c^2}\frac{\partial^2 E}{\partial t^2} = 0\,. \tag{48}$$

This equation has plane wave solutions:

$$E(x,t) = E_0 e^{i(kx-\omega t)} \tag{49}$$

which yields the relativistic total energy:

$$\varepsilon^2 = p^2c^2 + m^2c^4. \tag{50}$$

Therefore we can rewrite (48) for non-zero mass particles as follows [24]:

$$\left(\frac{\partial^2}{\partial x^2} - \frac{1}{c^2}\frac{\partial^2}{\partial t^2} - \frac{m^2c^2}{\hbar^2}\right)\Psi e^{\frac{i}{\hbar}(px-Et)} = 0\,. \tag{51}$$

Rearranging this equation (51) we get the Klein-Gordon equation for a free particle in 3-dimensional condition:

$$\left(\nabla - \frac{m^2c^2}{\hbar^2}\right)\Psi = \frac{1}{c^2}\frac{\partial^2\Psi}{\partial t^2}\,. \tag{52}$$

It seems worthnoting here that it is more proper to use total energy definition according to Noether's theorem in lieu of standard definition of relativistic total energy. According to Noether's theorem [25], the total energy of the system corresponding to the time translation invariance is given by:

$$E = mc^2 + \frac{cw}{2}\int_0^\infty \left(\gamma^2\, 4\pi r^2\, dr\right) = k\mu c^2 \tag{53}$$

where k is *dimensionless* function. It could be shown, that for low-energy state the total energy could be far less than $E = mc^2$. Interestingly Bakhoum [25] has also argued in favor of using $E = mv^2$ for expression of total energy, which expression could be traced back to Leibniz. Therefore it seems possible to argue that expression $E = mv^2$ is more generalized than the standard expression of special relativity, in particular because the total energy now depends on actual velocity [25].

From this new expression, it is possible to rederive Klein-Gordon equation. We start with Bakhoum's assertion that it is more appropriate to use $E = mv^2$, instead of more convenient form $E = mc^2$. This assertion would imply [25]:

$$H^2 = p^2c^2 - m_0^2c^2v^2. \tag{54}$$

A bit remark concerning Bakhoum's expression, it does not mean to imply or to interpret $E = mv^2$as an assertion that it implies zero energy for a rest mass. Actually the problem comes from "mixed" interpretation of what we mean with "velocity". In original Einstein's paper (1905) it is defined as "kinetic velocity", which can be measured when standard "steel rod" has velocity approximates the speed of light. But in quantum mechanics, we are accustomed to make use it deliberately to express "photon speed" $= c$. Therefore, in special relativity 1905 paper, it should be better to interpret it as "speed of free electron", which approximates c. For hydrogen atom with 1 electron, the electron occupies the first excitation (quantum number $n = 1$), which implies that their speed also approximate c, which then it is quite safe to assume $E \sim mc^2$. But for atoms with large number of electrons occupying large quantum numbers, as Bakhoum showed that electron speed could be far less than c, therefore it will be more exact to use $E = mv^2$, where here v should be defined as "average electron speed" [25].

In the first approximation of relativistic wave equation, we could derive Klein-Gordon-type relativistic equation from equation (54), as follows. By introducing a new parameter:

$$\zeta = i\,\frac{v}{c}\,, \tag{55}$$

then we can use equation (55) in the known procedure to derive Klein-Gordon equation:

$$E^2 = p^2c^2 + \zeta^2 m_0^2 c^4, \tag{56}$$

where $E = mv^2$. By using known substitution:

$$E = i\hbar\,\frac{\partial}{\partial t}\,, \qquad p = \frac{\hbar}{i}\,\nabla\,, \tag{57}$$

and dividing by $(\hbar c)^2$, we get Klein-Gordon-type relativistic equation [25]:

$$-c^{-2}\,\frac{\partial\Psi}{\partial t} + \nabla^2\Psi = k_0^{'2}\,\Psi\,, \tag{58}$$

where

$$k_0^{'} = \frac{\zeta m_0 c}{\hbar}\,. \tag{59}$$

Therefore we can conclude that imaginary mass term appears in the definition of coefficient $k_0^{'}$ of this new Klein-Gordon equation.

4.3 Modified Klein-Gordon equation and meson observation

As described before, quaternionic Klein-Gordon equation has neat link with Yang-Mills field. Therefore it seems worth to discuss here how to quaternionize Klein-Gordon equation. It can be shown that the resulting modified Klein-Gordon equation also exhibits imaginary mass term.

Equation (52) is normally rewritten in simpler form (by asserting $c = 1$):

$$\left(\nabla - \frac{\partial^2}{\partial t^2}\right)\Psi = \frac{m^2}{\hbar^2}\,. \tag{60}$$

Interestingly, one can write the Nabla-operator above in quaternionic form, as follows:

A. Define quaternion-Nabla-operator as analog to quaternion number definition above (46), as follows [25]:

$$\nabla^q = -i\frac{\partial}{\partial t} + e_1\frac{\partial}{\partial x} + e_2\frac{\partial}{\partial y} + e_3\frac{\partial}{\partial z}\,, \tag{61}$$

where e_1, e_2, e_3 are quaternion imaginary units. Note that equation (61) has included partial time-differentiation.

B. Its quaternion conjugate is defined as follows:

$$\bar{\nabla}^q = -i\frac{\partial}{\partial t} - e_1\frac{\partial}{\partial x} - e_2\frac{\partial}{\partial y} - e_3\frac{\partial}{\partial z}\,. \tag{62}$$

C. Quaternion multiplication rule yields:

$$\nabla^q\,\bar{\nabla}^q = -\frac{\partial^2}{\partial t^2} + \frac{\partial^2}{\partial^2 x} + \frac{\partial^2}{\partial^2 y} + \frac{\partial^2}{\partial^2 z}\,. \tag{63}$$

D. Then equation (63) permits us to rewrite equation (60) in quaternionic form as follows:

$$\nabla^q\bar{\nabla}^q\Psi = \frac{m^2}{\hbar^2}\,. \tag{64}$$

Alternatively, one used to assign standard value $c=1$ and also $\hbar=1$, therefore equation (60) may be written as:

$$\left(\frac{\partial^2}{\partial t^2} - \nabla^2 + m^2\right)\varphi(x,t) = 0\,, \tag{65}$$

where the first two terms are often written in the form of square Nabla operator. One simplest version of this equation [26]:

$$-\left(\frac{\partial S_0}{\partial t}\right)^2 + m^2 = 0 \tag{66}$$

yields the known solution [26]:

$$S_0 = \pm mt + \text{constant}\,. \tag{67}$$

The equation (66) yields wave equation which describes a particle at rest with positive energy (lower sign) or with negative energy (upper sign). Radial solution of equation (66) yields Yukawa potential which predicts meson as observables.

It is interesting to note here, however, that numerical 1-D solution of equation (65), (66) and (67) each yields slightly different result, as follows. (All numerical computation was performed using Mathematica [28].)

- For equation (65) we get:

(−D[#,x,x]+mˆ2+D[#,t,t])&[y[x,t]]==

$$m^2 + y^{(0,2)}[x,t] - y^{(2,0)}[x,t] = 0$$

DSolve[%,y[x,t],{x,t}]

$$\left\{\left\{y[x,t] \to \frac{m^2x^2}{2} + C[1][t-x] + C[2][t+x]\right\}\right\}$$

- For equation (66) we get:

(mˆ2−D[#,t,t])&[y[x,t]]==

$$m^2 + y^{(0,2)}[x,t] = 0$$

DSolve[%,y[x,t],{x,t}]

$$\left\{\left\{y[x,t] \to \frac{m^2t^2}{2} + C[1][x] + tC[2][x]\right\}\right\}$$

One may note that this numerical solution is in quadratic form $\frac{m^2t^2}{2}$ + constant, therefore it is rather different from equation (67) in [26].

In the context of possible supersymetrization of Klein-Gordon equation (and also PT-symmetric extension of Klein-Gordon equation [27, 29]), one can make use biquaternion number instead of quaternion number in order to generalize further the differential operator in equation (61):

E. Define a new "diamond operator" to extend quaternion-Nabla-operator to its biquaternion counterpart, according to the study [25]:

$$\begin{aligned}\diamondsuit = \nabla^q + i\,\nabla^q = &\left(-i\frac{\partial}{\partial t} + e_1\frac{\partial}{\partial x} + e_2\frac{\partial}{\partial y} + e_3\frac{\partial}{\partial z}\right) + \\ &+ i\left(-i\frac{\partial}{\partial T} + e_1\frac{\partial}{\partial X} + e_2\frac{\partial}{\partial Y} + e_3\frac{\partial}{\partial Z}\right),\end{aligned} \tag{68}$$

where e_1, e_2, e_3 are quaternion imaginary units. Its conjugate can be defined in the same way as before.

To generalize Klein-Gordon equation, one can generalize its differential operator to become:

$$\left[\left(\frac{\partial^2}{\partial t^2} - \nabla^2\right) + i\left(\frac{\partial^2}{\partial t^2} - \nabla^2\right)\right]\varphi(x,t) = -m^2\varphi(x,t), \tag{69}$$

or by using our definition in (68), one can rewrite equation (69) in compact form:

$$\left(\diamondsuit\bar{\diamondsuit} + m^2\right)\varphi(x,t) = 0, \tag{70}$$

and in lieu of equation (66), now we get:

$$\left[\left(\frac{\partial S_0}{\partial t}\right)^2 + i\left(\frac{\partial S_0}{\partial t}\right)^2\right] = m^2. \tag{71}$$

Numerical solutions for these equations were obtained in similar way with the previous equations:

- For equation (70) we get:

(−D[#,x,x]+D[#,t,t]−I*D[#,x,x]+I*D[#,t,t]+mˆ2)
&[y[x,t]]==

$$m^2 + (1+i)\,y^{(0,2)}[x,t] - (1+i)\,y^{(2,0)}[x,t] = 0$$

DSolve[%,y[x,t],{x,t}

$$\left\{\left\{y[x,t] \to \left(\frac{1}{4} - \frac{i}{4}\right)m^2x^2 + C[1][t-x] + C[2][t+x]\right\}\right\}$$

- For equation (71) we get:

$$(-\text{m}\hat{}2+\text{D}[\#,\text{t},\text{t}]+\text{I}*\text{D}[\#,\text{t},\text{t}])\&[\text{y}[\text{x},\text{t}]]==$$

$$m^2 + (1+i)\, y^{(0,2)}[x,t] = 0$$

$$\text{DSolve}[\%,\text{y}[\text{x},\text{t}],\{\text{x},\text{t}\}]$$

$$\left\{\left\{y[x,t] \to \left(\frac{1}{4} - \frac{i}{4}\right) m^2 x^2 + C[1][x] + t\,C[2][x]\right\}\right\}$$

Therefore, we may conclude that introducing biquaternion differential operator (in terms of "diamond operator") yield quite different solutions compared to known standard solution of Klein-Gordon equation [26]:

$$y(x,t) = \left(\frac{1}{4} - \frac{i}{4}\right) m^2 t^2 + \text{constant}\,. \qquad (72)$$

In other word: we can infer hat $t = \pm \frac{1}{m}\sqrt{y/\left(\frac{1}{4} - \frac{i}{4}\right)}$, therefore it is likely that there is imaginary part of time dimension, which supports a basic hypothesis of the aforementioned BQ-metric in Q-relativity.

Since the potential corresponding to this biquaternionic KGE is neither Coulomb, Yukawa, nor Hulthen potential, then one can expect to observe a new type of matter, which may be called "*supersymmetric-meson*". If this new type of particles can be observed in near future, then it can be regarded as early verification of the new hypothesis of PT-symmetric QM and CT-symmetric QM as considered in some recent reports [27, 29]. In our opinion, its presence may be expected in particular in the process of breaking of Coulomb barrier in low energy schemes.

Nonetheless, further observation is recommended in order to support or refute this proposition.

5 Concluding remarks

If 4D space-time has for its 3D spatial section a Q-space with Q-connexion $\Omega_{\beta\, kn}$ containing Q-non-metricity $\sigma_{\beta\, kn}$, then the Q-connexion, geometric object, is algebraically identical to Yang-Mills potential

$$\hat{A}_{k\alpha} \equiv \frac{1}{2}\,\varepsilon_{knm}\Omega_{\alpha kn}\,,$$

while respective curvature tensor $\hat{R}_{kn\alpha\beta}$, also a geometric object, is algebraically identical to Yang-Mills "physical field" strength

$$\hat{F}_{m\alpha\beta} \equiv \frac{1}{2}\,\varepsilon_{knm}\hat{R}_{kn\alpha\beta}\,.$$

Thus Yang-Mills gauge field Lagrangian

$$L_{YM} \sim \hat{F}_k^{\alpha\beta}\hat{F}_{k\alpha\beta} = \frac{1}{4}\,\varepsilon_{kmn}\varepsilon_{kjl}\,\hat{R}_{mn}^{\alpha\beta}\hat{R}_{jl\alpha\beta} = \frac{1}{2}\,\hat{R}_{mn}^{\alpha\beta}\hat{R}_{mn\alpha\beta}$$

can be geometrically interpreted as a Lagrangian of "nonlinear" or "quadratic" gravitational theory, since it contains quadratic invariant of curvature Riemann-type tensor contracted by all indices. Hence Yang-Mills theory can be regarded as a theory of pure geometric objects: Q-connexion and Q-curvature with Lagrangian quadratic in curvature (as: Einstein's theory of gravitation is a theory of geometrical objects: Christoffel symbols and Riemann tensor, but with linear Lagrangian made of scalar curvature).

Presence of Q-non-metricity is essential. If Q-non-metricity vanishes, the Yang-Mills potential may still exist, then it includes only proper Q-connexion (in particular, components of Q-connexion physically manifest themselves as "forces of inertia" acting onto non-inertially moving observer); but in this case all Yang-Mills intensity components, being in fact components of curvature tensor, identically are equal to zero.

The above analysis of Yang-Mills field from Quaternion Space geometry may be found useful in particular if we consider its plausible neat link with Klein-Gordon equation and Duffin-Kemmer equation. We discuss in particular a biquaternionic-modification of Klein-Gordon equation. Since the potential corresponding to this biquaternionic KGE is neither Coulomb, Yukawa, nor Hulthen potential, then one can expect to observe a new type of matter. Further observation is recommended in order to support or refute this proposition.

Acknowledgment

Special thanks to Profs. C. Castro and D. Rapoport for numerous discussions.

Submitted on May 26, 2007
Accepted on May 29, 2007

References

1. Antonowitcz M. and Szczirba W. Geometry of canonical variables in gravity theories. *Lett. Math. Phys.*, 1985, v. 9, 43–49.
2. Rapoport D. and Sternberg S. On the interactions of spin with torsion. *Annals of Physics*, 1984, v. 158, no. 11, 447–475. MR 86e:58028; [2a] Rapoport D. and Sternberg S. Classical Mechanics without lagrangians nor hamiltoneans. *Nuovo Cimento A*, 1984, v. 80, 371–383, MR 86c:58055; [2b] Rapoport D. and Tilli M. Scale Fields as a simplicity principle. *Proceedings of the Third International Workshop on Hadronic Mechanics and Nonpotential Interactions*, Dept. of Physics, Patras Univ., Greece, A. Jannussis (ed.), in *Hadronic J. Suppl.*, 1986, v. 2, no. 2, 682–778. MR 88i:81180.
3. Chan W. K. and Shin F. G. Infinitesimal gauge transformations and current conservation in Yang theory of gravity. *Meet. Frontier Phys.*, Singapore, 1978, v. 2.
4. Hehl F. M. and Sijacki D. To unify theory of gravity and strong interactions? *Gen. Relat. and Grav.*, 1980, v. 12(1), 83.
5. Batakis N. A. Effect predicted by unified theory of gravitational and electroweak fields. *Phys. Lett. B*, 1985, v. 154(5–6), 382–392.
6. Kyriakos A. Electromagnetic structure of hadrons. arXiv: hep-th/0206059.

7. Kassandrov V. V. Biquaternion electrodynamics and Weyl-Cartan geometry of spacetime. *Grav. and Cosmology*, 1995, v. 1, no. 3, 216–222; arXiv: gr-qc/0007027.
8. Smarandache F. and Christianto V. Less mundane explanation of Pioneer anomaly from Q-relativity. *Progress in Physics*, 2007, v. 1, 42–45.
9. Fueter R. *Comm. Math. Helv.*, 1934–1935, v. B7, 307–330.
10. Yefremov A. P. *Lett. Nuovo. Cim.*, 1983, v. 37(8), 315–316.
11. Yefremov A. P. *Grav. and Cosmology*, 1996, v. 2(1), 77–83.
12. Yefremov A. P. *Acta Phys. Hung.*, Series — Heavy Ions, 2000, v. 11(1–2), 147–153.
13. Yefremov A. P. *Gravitation and Cosmology*, 2003, v. 9(4), 319–324. [13a] Yefremov A. P. Quaternions and biquaternions: algebra, geometry, and physical theories. arXiv: math-ph/0501055.
14. Ramond P. Field theory, a modern primer. The Benjamin/Cumming Publishing Co., ABPR Massachussetts, 1981.
15. Huang K. Quarks, leptons and gauge fields. World Scientific Publishing Co., 1982.
16. Fainberg V. and Pimentel B. M. Duffin-Kemmer-Petiau and Klein-Gordon-Fock equations for electromagnetic, Yang-Mills and external gravitational field interactions: proof of equivalence. arXiv: hep-th/0003283, p. 12.
17. Marsh D. The Grassmannian sigma model in SU(2) Yang-Mills theory. arXiv: hep-th/07021342.
18. Devchand Ch. and Ogievetsky V. Four dimensional integrable theories. arXiv: hep-th/9410147, p. 3.
19. Nishikawa M. Alternative to Higgs and unification. arXiv: hep-th/0207063, p. 18.
20. Nishikawa M. A derivation of the electro-weak unified and quantum gravity theory without assuming a Higgs particle. arXiv: hep-th/0407057, p. 22.
21. Adler S. L. Adventures in theoretical physics. arXiv: hep-ph/0505177, p. 107.
22. Adler S. L. Quaternionic quantum mechanics and Noncommutative dynamics. arXiv: hep-th/9607008.
23. Adler S. L. Composite leptons and quarks constructed as triply occupied quasiparticles in quaternionic quantum mechanics. arXiv: hep-th/9404134.
24. Ward D. and Volkmer S. How to derive the Schrödinger equation. arXiv: physics/0610121.
25. Christianto V. A new wave quantum relativistic equation from quaternionic representation of Maxwell-Dirac equation as an alternative to Barut-Dirac equation. *Electronic Journal of Theoretical Physics*, 2006, v. 3, no. 12.
26. Kiefer C. The semiclassical approximation of quantum gravity. arXiv: gr-qc/9312015.
27. Znojil M. PT-symmetry, supersymmetry, and Klein-Gordon equation. arXiv: hep-th/0408081, p. 7–8; [27a] arXiv: math-ph/0002017.
28. Toussaint M. Lectures on reduce and maple at UAM-I, Mexico. arXiv: cs.SC/0105033.
29. Castro C. The Riemann hypothesis is a consequence of CT-invariant Quantum Mechanics. Submitted to *JMPA*, Feb. 12, 2007.

On the Dependence of a Local-Time Effect on Spatial Direction

Victor A. Panchelyuga* and Simon E. Shnoll*,†

*Institute of Theor. and Experim. Biophysics, Russian Acad. of Sciences, Pushchino, Moscow Region, 142290, Russia
†Department of Physics, Moscow State University, Moscow 119992, Russia

Corresponding authors. Victor A. Panchelyuga: panvic333@yahoo.com; Simon E. Shnoll: shnoll@iteb.ru

This paper addresses further investigations of local-time effects on the laboratory scale. We study dependence of the effect on spatial directions defined by a pair of sources of fluctuations. The results show that the effect appears in the neighborhood of directions North-South and East-West. Only for these directions are the experimental results in excellent agreement with theoretically predicted local-time values. The results reveal the character of near-Earth space heterogeneity and lead to the conclusion that at the laboratory scale, local-time effects cannot be caused by some axial-symmetric structure, which has permanent properties along an Earth meridian. Appearance of the effect along an Earth parallel is linked to rotational motion of the Earth. Observed properties of local-time effects in the direction of an Earth meridian can be linked to motion of the Earth in this direction.

1 Introduction

The results of many years of investigation of macroscopic fluctuation phenomena can be considered as evidence of an essential heterogeneity and anisotropy of space-time. This statement is based upon the results of studies of α-decay-rate fluctuations of ^{239}Pu sources measured by plane semiconductor detectors and detectors with collimators cutting α-particle beams, carried out in the years 1985–2005 [1–6]. For reasons of methodology, the time resolution reached in those years was about one minute, and the studied spatial scale about a hundred kilometers. This work presents results of further investigations of macroscopic fluctuations phenomena with time resolution to 0.5 milliseconds.

Such resolution allows studies of local time effects for distances down to one metre between sources of fluctuations [7, 8]. On the one hand, this result has an independent importance as a lower scale end for the existence of macroscopic fluctuations phenomena, but on the other hand, it has great methodological importance due to the possibility of systematic laboratory investigations, which were previously unavailable because of very large spatial distances between places of measurement. One such investigation is the dependence of local-time effects as function of spatial directions, which is the main subject of this paper.

2 Experiment description and results

A functional diagram of the experimental setup is presented in Fig. 1b). It consists of two sources of fluctuations, which are fixed to a wooden base. The distance between the sources was 1.36 m. The base, with the sources of fluctuations, can revolve on its axis and can be positioned in any desired direction. A two-channel LeCroy WJ322 digital storage oscilloscope (DSO in Fig. 1b) was used for data acquisition.

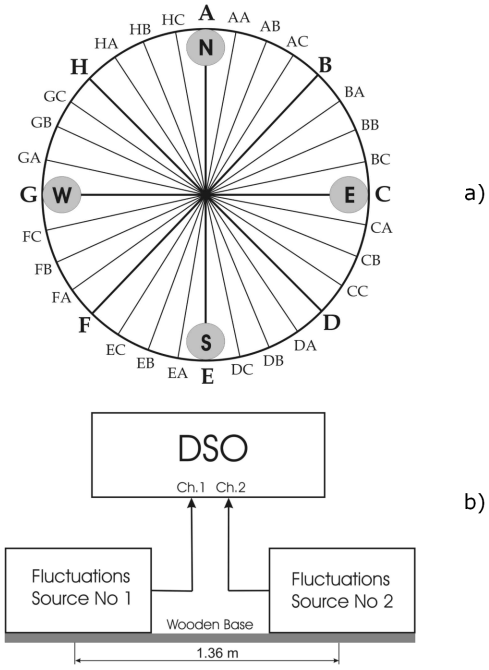

Fig. 1: Diagram of spatial directions, which was examined in experiments with fixed spatial base 1.36 m (a) and functional diagram of the experimental setup (b).

The digitizing frequency used for all series of measurements was 100 kHz. Consequently, the duration of 50-point histograms, which were used in the experiment, is 0.5 milliseconds. This means that all local-time values in the experiment are defined with an accuracy of ± 0.5 milliseconds.

Fig. 1a) depicts the spatial directions which were examined in the experiment. In Fig. 1a) every one of these directions is denoted by letters outside the circle. For example, direction AA means that the base with the sources of fluctuations is

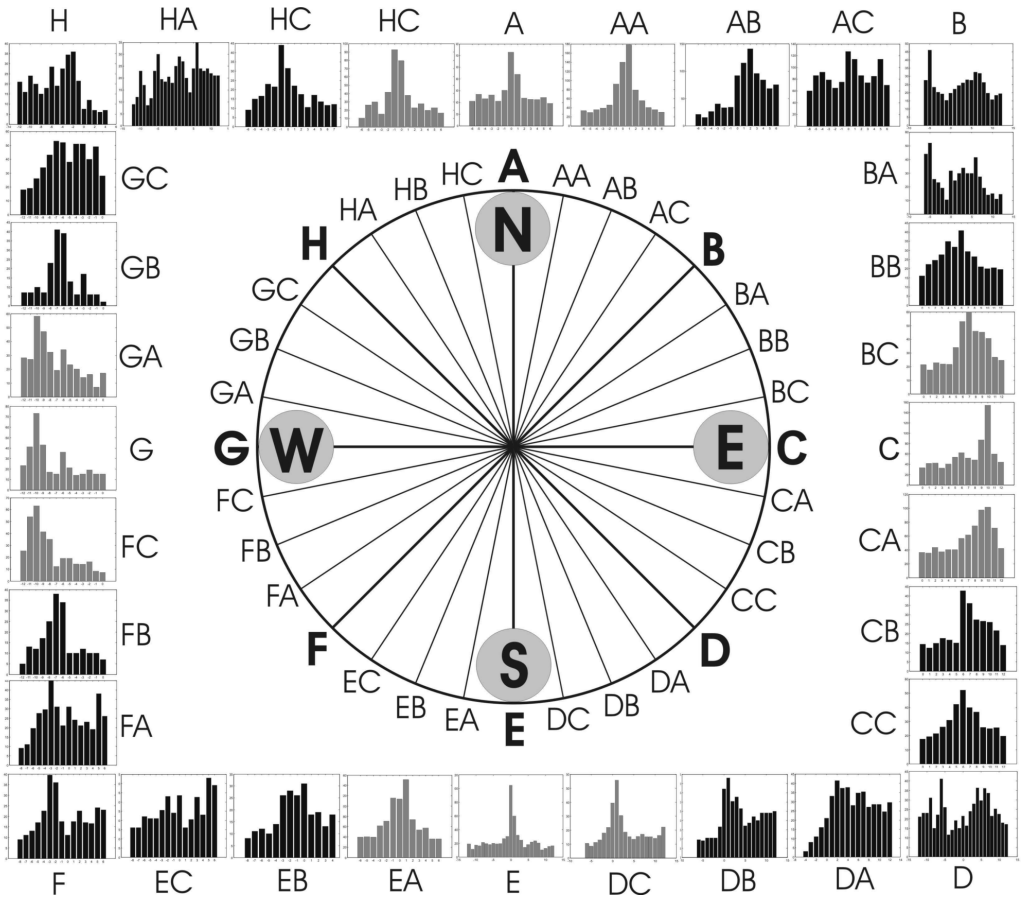

Fig. 2: Averaged interval distributions obtained for every spatial direction.

aligned in the EA-AA direction in such a way that source No 1 is placed on the AA end of the base and source No 2 is placed on the EA end. Correspondingly, direction EA means that source No 1 is on the EA end, and source No 2 is on the opposite end. Letters N, S, E, and W denote directions to the North, South, East, and West respectively. Directions A and E lie on an Earth meridian, and directions G and C lie on an Earth parallel.

The angular difference between two neighboring directions is 11.25°, so we have 32 spatial directions. To examine all the directions one series of measurements must include 32 pairs of synchronous records. Every record consists of 500,000 points. This allowed acquisition of two synchronous sets of 50-point histograms for every direction. Every set contains 10,000 histograms. The experimental results, which are presented below, are based on 8 series of measurements.

It is important to note that pairs of directions presented in Fig. 1a), for example, A-E and E-A, are actually the same because the pair of fluctuations sources used in the experiment are non-directional. For this reason the total number of directions examined is half that denoted by letters in Fig. 1a). The second measurement in an opposite pair of directions can be considered as a control. The data processing procedure used in the experiment is described in detail in [2, 9].

Fig. 2 shows the interval distributions obtained for each of the 32 spatial directions. Every one of these distributions is averaged through the interval distributions from all of the series of measurements for every one of the spatial directions. The circle inside Fig. 2 is the same as in Fig. 1a) and shows spatial directions in relation to the presented interval distributions.

All the distributions presented in Fig. 2 can be divided into two distinct groups. The first group consists of distributions in the neighbourhoods (approximately $\pm 11.25°$ of the directions A-E and C-G; labeled as A, E, C, and G. To the first group also can be related distributions that are closest to A, E, C, and G: HC, AA, BC, CA, DC, EA, FC, GA. To the second group can be related all remaining distributions. The distribution from the first group we call 'non-diagonal', and from the second, 'diagonal'. The first group in Fig. 2 is highlighted by the gray color.

The main difference between the two groups lies in the following: non-diagonal distributions always have a single peak, which corresponds to the same interval value in all series of measurements. In the case of the non-diagonal distributions, every spatial direction can be characterized by a

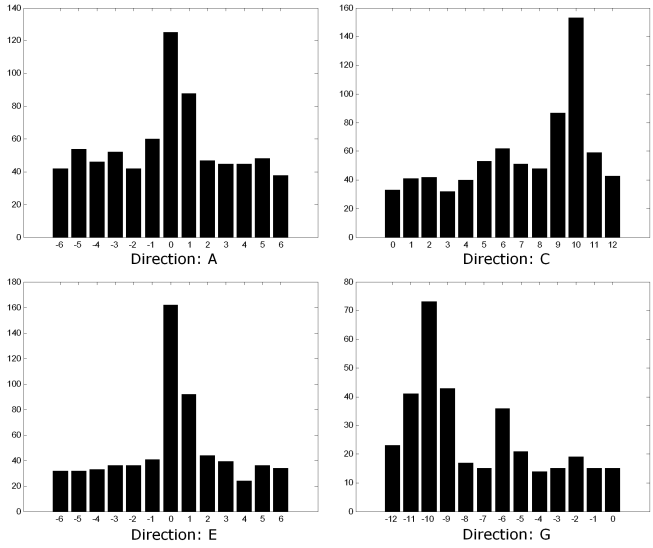

Fig. 3: Non-diagonal interval distributions for meridian (North-South) directions A and E, and for parallel (East-West) directions C and G.

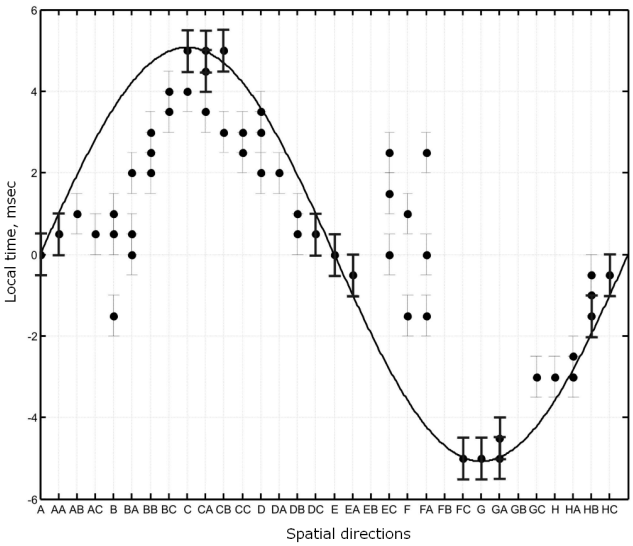

Fig. 4: Theoretical estimation (solid line) and experimentally obtained local-time values. Points with bold error bars show local-time values for non-diagonal directions.

stable, reproducible pattern of interval distribution. Contrary to non-diagonal distributions, a diagonal distribution is multi-peaked and cannot ordinarily be characterized by a stable, reproducible pattern.

Non-diagonal interval distributions are presented in Fig. 3. For Earth meridian directions (A and E), patterns of interval distributions always have a stable peak at zero intervals. In the case of Earth parallel directions (C and G), interval distributions have a peak at the interval that is equal to the local-time-difference for the spatial base of 1.36 m. This difference has the same magnitude but different sign for opposite directions. It is easy to see from Fig. 3 that interval distributions for directions C and G have peaks at the intervals 10 and -10.

3 Value of local-time-difference

As follows from previous investigations [1–6] the value of the local-time effect depends only on the longitudinal difference between places of measurements, not on latitudinal distance. From this it follows that the factor which determines the shape of fine structure of histograms must be axial-symmetric. Longitudinal dependence of local-time effect phenomenology can be considered as dependence of shape of the fine structure of histograms on spatial directions defined by the centre of the Earth and the two points where measurements are taken [8]. In this case the results of measurements depend on the solid angle between two planes defined by the axis of the Earth and the two points of measurement; such angle depends on the longitudinal difference, not on the latitudinal difference.

But for the case of separated measurements with fixed spatial base $\triangle L_0 = \text{const}$, the results of the experiment become dependent on latitude, θ. Really, the time $\triangle t$, after which fluctuation source No 2 will define the same direction as source No 1 before, depends on the velocity of the measurement system $\nu(\theta, h)$:

$$\triangle t = \frac{\triangle L_0}{\nu(\theta, h)} \sin\alpha\,, \tag{1}$$

where $\alpha \in [0, 2\pi]$ is an angle, counter-clockwise from the direction to the North (direction A). It is important to note that the theoretical estimation of the longitudinal difference is given by (1) obtained on the assumption that the factor determining the fine structure of histograms is axial-symmetric.

The value $\nu(\theta, h)$ is determined by:

$$\nu(\theta, h) = \frac{2\pi}{T}\left(\sqrt{\frac{R_p^2}{\frac{R_p^2}{R_e^2} + \tan^2\theta}} + h\right), \tag{2}$$

where $R_p = 6356863$ m and $R_e = 6378245$ m are the values of the polar and equatorial radii of the Earth [10] respectively, $T = 86160$ sec is the period of the Earth's revolution. For the place of measurements (Pushchino, Moscow region) we have latitude $\theta_p = 54°50.037'$ and height above sea level $h_p = 170$ m. So the velocity of the measurement system is $\nu(\theta_p, h_p) = 268$ m/sec. For near-equatorial regions $\nu(\theta, h)$ can exceed $\nu(\theta_p, h_p)$ by almost twice the latter. Consequently, for measurements with a fixed spatial base we have sufficiently strong dependence of local-time-difference (1) on latitude θ.

The value of the velocity $\nu(\theta_p, h_p)$ allows, on the basis of (1), calculation of the local-time-difference $\triangle t(\alpha)$ as function of spatial directions examined in the experiment. The solid line in Fig. 4 shows the results of this calculation.

Points with error bars in Fig. 4 show local-time values obtained for all series of measurements.

4 Discussions

It is easy to see from Fig. 4 that the experimental results are in excellent agreement with the theoretically predicted local-time values only for a narrow neighbourhood around the directions North-South (directions A and E) and East-West (directions C and G) i.e. for non-diagonal directions. At the same time, for diagonal directions, the experimental results in most cases don't follow the theoretical predictions. Results presented in Fig. 4 are in agreement with results summarized in Fig. 2, and linked to the dependence of local-time effect on spatial directions.

The results reveal the character of near-Earth space anisotropy. As pointed out above, the theoretical estimation of local-time effect values in Fig. 4 were obtained under the hypothesis that the effect is caused by some axial-symmetric structure, which has permanent properties along an Earth meridian. According to this hypothesis, the dependence of local-time effect must be the same for all spatial directions, and local-time values obtained in the experiment must follow the theoretically predicted values. But the fact that the diagonal directions experimental results don't confirm this hypothesis leads to the conclusion that at the laboratory scale local-time effects cannot be caused by some axial-symmetric structure.

Evidently, dependence of local-time effects in East-West directions is linked to the rotational motion of the Earth. In this case, after the time interval $\triangle t$, which is equal to local-time difference for the spatial base used, the position of the 'West' source of fluctuations will be exactly the same as the position of 'East' previously. In the case of diagonal spatial directions such a coincidence is absent. However, for North-South direction such an explanation is inapplicable.

Dependence of the local-time effect in the direction of a meridian is probably linked to the velocity component along the path of the Solar System in the Galaxy. This hypothesis is preliminary and may possibly change in consequence of future investigations.

The authors are grateful to V. P. Tikhonov, Dr. Hartmut Muller, Victor Tsyganov, and M. N. Kondrashova for valuable discussions and financial support.

Submitted on May 03, 2007
Accepted on May 21, 2007

References

1. Shnoll S.E., Kolombet V.A., Pozharskii E.V., Zenchenko T.A., Zvereva I.M. and Konradov A.A. Realization of discrete states during fluctuations in macroscopic processes. *Physics-Uspekhi*, 1998, v. 41(10), 1025–1035.
2. Shnoll S.E., Zenchenko T.A., Zenchenko K.I., Pozharskii E.V., Kolombet V.A. and Konradov A.A. Regular variation of the fine structure of statistical distributions as a consequence of cosmophysical agents. *Physics-Uspekhi*, 2000, v. 43(2), 205–209.
3. Shnoll S. E. Periodical changes in the fine structure of statistic distributions in stochastic processes as a result of arithmetic and cosmophysical reasons. *Time, Chaos, and Math. Problems*, No. 3, University Publ. House, Moscow, 2004, 121–154.
4. Shnoll S. E. Changes in the fine structure of stochastic distributions as consequence of space-time fluctuations. *Progress in Physics*, 2006, v. 6, 39–45.
5. Shnoll S.E., Zenchenko K.I., Berulis I.I., Udaltsova N.V. and Rubinstein I.A. Fine structure of histograms of alpha-activity measurements depends on direction of alpha particles flow and the Earth rotation: experiments with collimators. arXiv: physics/0412007.
6. Shnoll S.E., Rubinshtejn I.A., Zenchenko K.I., Shlekhtarev V.A., Kaminsky A.V., Konradov A.A. and Udaltsova N.V. Experiments with rotating collimators cutting out pencil of α-particles at radioactive decay of ^{239}Pu evidence sharp anisotropy of space. *Progress in Physics*, 2005, v. 1, 81–84; arXiv: physics/0501004.
7. Panchelyuga V. A., Kolombet V. A., Panchelyuga M. S. and Shnoll S. E. Local-time effect on small space-time scale. *Space-time Structure. Algebra and Geometry*, Lilia-Print, Moscow, 2007, 531–537.
8. Panchelyuga V. A., Kolombet V. A., Panchelyuga M. S. and Shnoll S. E. Experimental investigations of the existence of local-time effect on the laboratory scale and the heterogeneity of space-time. *Progress in Physics*, 2007, v. 1, 64–69.
9. Panchelyuga V. A. and Shnoll S. E. Experimental investigation of spinning massive body influence on fine structure of distribution functions of alpha-decay rate fluctuations. *Space-Time Structure*, (Collected papers), TETRU, Moscow, 2006, 328–343.
10. Physical values. Reference book. Nauka, Moscow, 1991.

A Study of a Local Time Effect on Moving Sources of Fluctuations

Victor A. Panchelyuga* and Simon E. Shnoll*,†

*Institute of Theor. and Experim. Biophysics, Russian Acad. of Sciences, Pushchino, Moscow Region, 142290, Russia
†Department of Physics, Moscow State University, Moscow 119992, Russia

Corresponding authors: V. A. Panchelyuga, e-mail: panvic333@yahoo.com; S. E. Shnoll, e-mail: shnoll@iteb.ru

This work presents an experimental investigation of a possible mechanism causing local time effects, with the aid of moving sources of fluctuations. The results show that the measurement system, consisting of two separated sources of fluctuations moving in a near-Earth space, can detect its own motion in form of a local time effect, or in other words, we can determine uniform and rectilinear motion of an isolated system on the basis of measurements made inside the system.

1 Introduction

If at any two places on the Globe we make two synchronous records of fluctuations in any natural processes, then by a standard method [1-4] we can find that shape of the fine structure of histograms, constructed on the basis of short segments of time series, is most similar for such pairs, that are separated by a time interval equal to the local time difference for the places of measurements. Because of this the phenomenon is called the local time effect. At the present time it is known that the effect exists for any distances between places of measurements, ranging from the highest possible on the Earth down to one metre [5, 6]. The local time or longitudinal difference implies dependence of the fine structure of the histograms on the Earth's rotation around its axis. In relation to ambient space this means that after a time interval equal to the local time difference measurement, system No. 2 appears in the same place where system No. 1 was located previously, or that measurement system No. 2 will be oriented in the same direction as system No. 1 was oriented before. The same places or directions mean that the same conditions prevail and, consequently, a similar shape for the histograms.

The existence of a local time effect is closely connected with space-time heterogeneity. Really the effect is possible only if the experimental setup, consisting of a pair of separated sources of fluctuations, moves through heterogeneous invariable space. It is obvious that for the case of homogeneous space the effect cannot exist. Existence of a local-time effect for some space scale can be considered as evidence of space-time heterogeneity, which corresponds to this scale.

So, to observe the local time effect we need *heterogeneous invariable* space and a pair of fluctuation sources on a fixed spatial base, which *moves synchronously* through that space. All phenomenology of the local time effect was obtained due to rotational motion of the Earth. The present investigation studies the local time effect for the case of the measurement system moving independently of the rotational motion of the Earth. In other words, we try to ascertain if an isolated measurement system, consisting of two separated sources of fluctuations, can detect its own motion in the form of a local time effect.

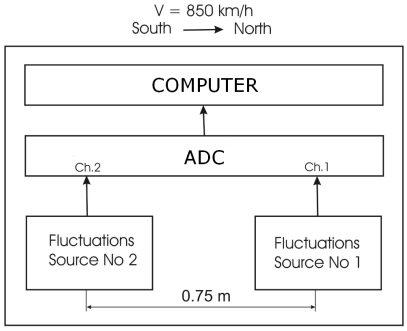

Fig. 1: Simplified diagram of the experiment with moving sources of fluctuations.

2 Experiment description and results

A simplified diagram of the experiment with moving sources of fluctuations is presented in Fig. 1. The measurement system consists of two separated sources of fluctuations, which are oriented in the line of the velocity vector of the plane in such a way that source No. 2 follows source No. 1. The sources are separated by the fixed distance of 0.75 m. Signals of fluctuations were digitized by means of an analogue-to-digital converter (ADC) via a USB interface connected to a personal computer running appropriate data acquisition software. The whole system was mounted inside the plane moving with a velocity of $V = 850$ km/h along an Earth meridian from South to North.

The digitizing frequency used for all series of measurements was 100 kHz. One record consists of 500 kpts per channel. This allowed acquisition of two synchronous sets of 50-point histograms. The maximum length of each set was 10,000 histograms. Consequently, the duration of a 50-point histogram is 0.5 ms, so that all local-time values in the experiment can be determined to an accuracy of ± 0.5 ms.

The local time value $\triangle t$ for the experiment is the time

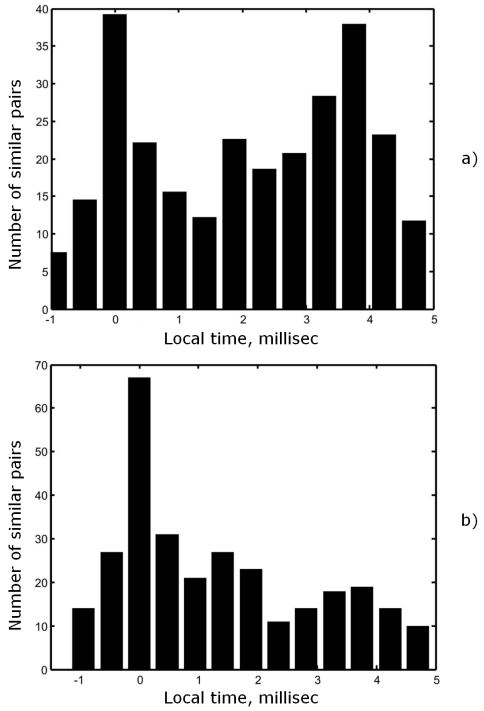

Fig. 2: a) Interval distributions for moving, and b) motionless ground-based measurement systems. Measurements were carried out at the same time each day and at the same spatial orientation of the measurement systems (South-North).

interval in which the plane can travel a distance of 0.75 m. Calculation shows that this value is $\triangle t = 3.18$ ms.

Along with the moving experiment, a motionless ground-based one was carried out. For this experiment we used the same experimental setup and exactly the same orientation of fluctuation sources. The motionless measurements were carried out at the same daytime as for measurements with the moving system.

The intervals distribution for the motionless ground-based experiment is presented in Fig. 2b). The distribution has a single peak at the zero interval. The pattern of this distribution is exactly the same as that reported in work [7] for a meridian direction.

The interval distribution for the moving measurement system is shown in Fig. 2a). Like the distribution in Fig. 2b), in this case we also have zero-peak, except this peak on the distribution has a maximum at 3.5 ± 0.5 ms, which is in good agreement with the calculated local time value $\triangle t = 3.18$ ms and can be linked to motion of the measurement system.

Both interval distributions presented in Fig. 2 represent an average of five series of measurements. Ordinates in Fig. 2 are defined to 7–10%.

3 Conclusions

The results confirm the hypothesis that a local time effect is caused by motion of the measurement system in heterogeneous invariable space. The opposite statement also is true: a measurement system moving in near-Earth space can detect its own motion in the form of a local time effect. It is interesting to note that by means of the method described above, it is possible to determine uniform and rectilinear motion of an isolated system on the basis of measurements made inside the system.

The zero-peak for both interval distributions in Fig. 2, aren't linked to plane motion and are caused only by the spatial orientation of the measurement system [7]. Investigation of the nature of the zero-peak is one of our immediate tasks.

The Authors are grateful to D. G. Pavlov, Oleg B. Khavroshkin, Ruvfet Urdukhanov, Hartmut Muller, Victor Tsyganov, Valery A. Kolombet, and Maria N. Kondrashova for valuable discussions and financial support. Special thanks go to Dmitri Maslennikov for hospitality and great assistance in taking measurements in Cairo.

Submitted on May 03, 2007
Accepted on May 21, 2007

References

1. Shnoll S.E., Kolombet V.A., Pozharskii E.V., Zenchenko T.A., Zvereva I.M. and Konradov A.A. Realization of discrete states during fluctuations in macroscopic processes. *Physics-Uspekhi*, 1998, v. 41(10), 1025–1035.
2. Shnoll S.E., Zenchenko T.A., Zenchenko K.I., Pozharskii E.V., Kolombet V.A. and Konradov A.A. Regular variation of the fine structure of statistical distributions as a consequence of cosmophysical agents. *Physics-Uspekhi*, 2000, v. 43(2), 205–209.
3. Shnoll S. E. Periodical changes in the fine structure of statistic distributions in stochastic processes as a result of arithmetic and cosmophysical reasons. *Time, Chaos, and Math. Problems*, No. 3, University Publ. House, Moscow, 2004, 121–154.
4. Panchelyuga V. A. and Shnoll S. E. Experimental investigation of spinning massive body influence on fine structure of distribution functions of alpha-decay rate fluctuations. *Space-Time Structure*, (Collected papers), TETRU, Moscow, 2006, 328–343.
5. Panchelyuga V. A., Kolombet V. A., Panchelyuga M. S. and Shnoll S. E. Local-time effect on small space-time scale. *Space-Time Structure. Algebra and Geometry.* Lilia-Print, Moscow, 2007, 531–537.
6. Panchelyuga V. A., Kolombet V. A., Panchelyuga M. S. and Shnoll S. E. Experimental investigations of the existence of local-time effect on the laboratory scale and the heterogeneity of space-time. *Progress in Physics*, 2007, v. 1, 64–69.
7. Panchelyuga V. A. and Shnoll S. E. On the dependence of local-time effects on spatial direction. *Progress in Physics*, 2007, v. 3, 51–54.

SPECIAL REPORT

A Theory of the Podkletnov Effect based on General Relativity: Anti-Gravity Force due to the Perturbed Non-Holonomic Background of Space

Dmitri Rabounski and Larissa Borissova
E-mail: rabounski@yahoo.com; lborissova@yahoo.com

We consider the Podkletnov effect — the weight loss of an object located over a superconducting disc in air due to support by an alternating magnetic field. We consider this problem using the mathematical methods of General Relativity. We show via Einstein's equations and the geodesic equations in a space perturbed by a disc undergoing oscillatory bounces orthogonal to its own plane, that there is no rôle of superconductivity; the Podkletnov effect is due to the fact that the field of the background space non-holonomity (the basic non-othogonality of time lines to the spatial section), being perturbed by such an oscillating disc produces energy and momentum flow in order to compensate the perturbation in itself. Such a momentum flow is directed above the disc in Podkletnov's experiment, so it works like negative gravity (anti-gravity). We propose a simple mechanical system which, simulating the Podkletnov effect, is an experimental test of the whole theory. The theory allows for other "anti-gravity devices", which simulate the Podkletnov effect without use of very costly superconductor technology. Such devices could be applied to be used as a cheap source of new energy, and could have implications to air and space travel.

Contents

1 Introducing Podkletnov's experiment

In 1992, Eugene Podkletnov and his team at the Tampere Institute of Technology (Finland) tested the uniformity of a unique bulky superconductor disc, rotating at high speed via a magnetic field [1]. The 145×6-mm superconductor disc was horizontally oreinted in a cryostat and surrounded by liquid helium. A small current was initiated in the disc by outer electromagnets, after which the medium was cooled to 20–70 K. As the disc achieved superconductivity, and the state became stable, another electromagnet located under the cryostat was switched on. Due to the Meissner-Ochsenfeld effect the magnetic field lifted the disc into the air. The disc was then driven by the outer electromagnets to 5000 rpm.

A small non-conducting and non-magnetic sample was suspended over the cryostat where the rotating disc was contained. The weight of the sample was measured with high precision by an electro-optical balance system. "The sample with the initial weight of 5.47834 g was found to lose about 0.05% of its weight when placed over the levitating disc without any rotation. When the rotation speed of the disc increased, the weight of the sample became unstable and gave fluctuations from −2.5 to +5.4% of the initial value. [. . .] The levitating superconducting disc was found to rise by up to 7 mm when its rotation moment increased. Test measurements without the superconducting shielding disc but with all operating solenoids connected to the power supply, had no effect on the weight of the sample" [1].

Additional results were obtained by Podkletnov in 1997, with a larger disc (a 275/80×10-mm toroid) run under

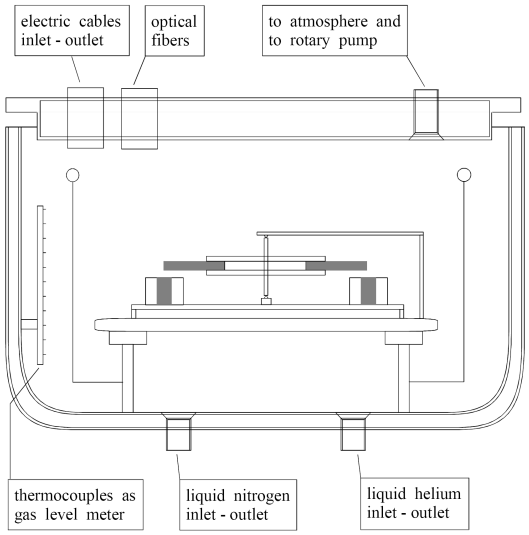

Fig. 1: Cryogenic system in Podkletnov's experiment [2]. Courtesy of E. Podkletnov. Used by permission.

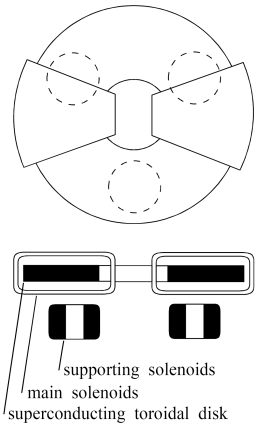

Fig. 2: Supporting and rotating solenoids in Podkletnov's experiment [2]. Courtesy of E. Podkletnov. Used by permission.

similar conditions [2]: "The levitating disc revealed a clearly measurable shielding effect against the gravitational force even without rotation. In this situation, the weight-loss values for various samples ranged from 0.05 to 0.07%. [...] Samples made from the same material and of comparable size, but with different masses, lost the same fraction of their weight. [...] Samples placed over the rotating disc initially demonstrated a weight loss of 0.3–0.5%. When the rotation speed was slowly reduced by changing the current in the solenoids, the shielding effect became considerably higher and reached 1.9–2.1% at maximum" [2].

Two groups of researchers supported by Boeing and NASA, and also a few other research teams, have attempted to replicate the Podkletnov experiment in recent years [3–7]. The main problem they encountered was the reproduction of the technology used by Podkletnov in his laboratory to produce sufficiently large superconductive ceramics. The technology is very costly: according to Podkletnov [8] this requires tens of millions of dollars. Therefore the aforementioned organisations tested discs of much smaller size, about 1″ diameter; so they produced controversial results at the boundary of precision measurement. As was pointed out by Podkletnov in his recent interview (April, 2006), the NASA team, after years of unsuccessful attempts, made a 12″ disc of superconductive ceramic. However, due to the crude internal structure (this is one of the main problems in making such discs), they were unable to use the disc to replicate his experiment [8].

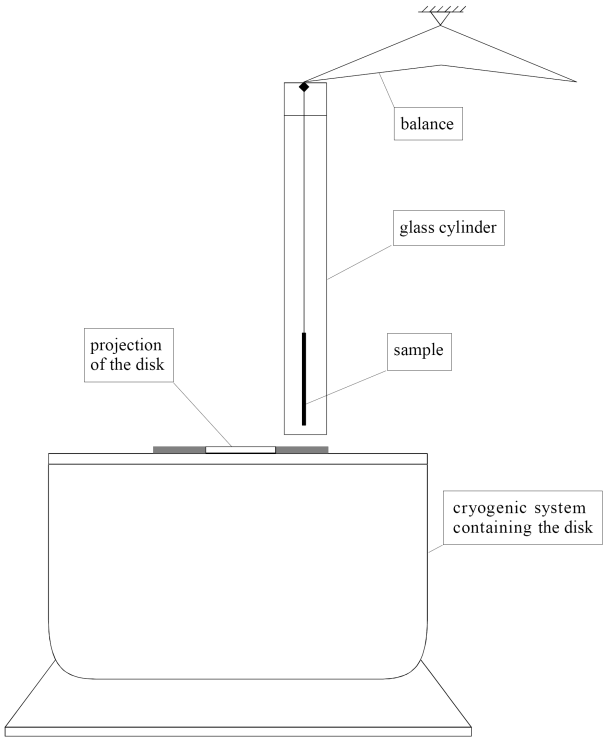

Fig. 3: Weight and pressure measurement in Podkletnov's experiment [2]. Courtesy of E. Podkletnov. Used by permission.

Podkletnov also recently reported on a "gravity field generator" [8, 9] constructed in his laboratory in recent years, on the basis of the earlier observed phenomenon.

In a nutshell, the aforementioned phenomenon is as follows. We will refer to this as the *Podkletnov effect*:

> When a disc of superconductive ceramic, being in the state of superconductivity, is suspended in air by an alternating magnetic field due to an electromagnet located under the disc, the disc is the source of a radiation. This radiation, traveling like a plane wave above the disc, acts on other bodies like a negative gravity. The radiation becomes stronger with larger discs, so it depends on the disc's mass and radius. When the disc rotates uniformly, the radiation remains the same. During acceleration/braking of the disc's rotation, the radiation essentially increases.

Podkletnov claimed many times that he discovered the effect by chance, not by any theoretical prediction. Being

an experimentalist who pioneered this field of research, he continued his experiments blindfolded: in the absence of a theoretical reason, the cause of the observed weight loss was unclear. This is why neither Podkletnov nor his followers at Boeing and NASA didn't develop a new experiment by which the weight loss effect substantially increased.

For instance, Podkletnov still believes that the key to his experiment is that special state which is specific to the electron gas inside superconductive materials in the state of superconductivity [8]. He and all the others therefore focused attention on low temperature superconductive ceramics, production of which, taking the large size of the discs into account, is a highly complicated and very costly process, beyond most laboratories. In fact, during the last 15 years only Podkletnov's laboratory has had the ability to produce such the discs with sufficient quality.

We propose a purely theoretical approach to this problem. We consider Podkletnov's experiment using the mathematical methods of General Relativity, in the Einstenian sense: we represent all essential components of the experiment as a result of the geometrical properties of the laboratory space such as the space non-uniformity, rotation, deformation, and curvature. We build a complete theory of the Podkletnov effect on the basis of General Relativity.

By this we will see that there is no rôle for superconductivity; Podkletnov's effect has a purely mechanical origin due in that the vertical oscillation of the disc, produced by the supporting alternating magnetic field, and the angular acceleration/braking of the disc's rotation, perturb a homogeneous field of the basic non-holonomity of the space (the basic non-othogonality of time lines to the spatial section, known from the theory of non-holonomic manifolds). As a result the non-holonomity field, initially homogeneous, is locally stressed, which is expressed by a change of the left side of Einstein's equations (geometry) and, through the conservation law, a corresponding change of the right side — the energy-momentum tensor for distributed matter (the alternating magnetic field, in this case). In other words, the perturbed field of the space non-holonomity produces energy-momentum in order to compensate for the local perturbation in itself. As we will see, the spatial momentum is directed above the disc in Podkletnov's experiment, so it works like negative gravity.

Owing to our theory we know definitely the key parameters ruling the weight loss effect. Therefore, following our calculation, it is easy to propose an experiment wherein the weight loss substantially increases.

For example, we describe a new experiment where the Podkletnov effect manifests via simple electro-mechanical equipment, without costly superconductor technology. This new experiment can be replicated in any physics laboratory.

We therefore claim thta with our mathematical theory of the Podkletnov effect, within the framework of General Relativity, we can calculate the factors ruling the weight loss. This gives us an opportunity to construct actual working devices which could revolutionize air and space travel. Such new technology, which uses high frequency electromagnetic generators and mechanical equipment instead of costly superconductors, can be the subject of further research on a commercial basis (due to the fact that applied research is outside academia).

Besides, additional energy-momentum produced by the space non-holonomity field in order to compensate for a local perturbation in itself, means that the Podkletnov effect can be used to produce new energy.

By our advanced study (not included in this paper), of our mathematical theory, that herein gives the key factors which rule the new energy, lends itself to the construction of devices which generate the new energy, powered by strong electromagnetic fields, not nuclear reactions and atomic fuel. Therefore this technology, free of radioactive waste, can be a source of clean energy.

2 The non-holonomic background space

2.1 Preliminary data from topology

In this Section we construct a space metric which includes a basic (primordial) non-holonomity, i.e. a basic field of the non-orthogonality of the time lines to the three-dimensional spatial section.

Here is some information from topology Each axis of a Euclidean space can be represented as the element of a circle with infinite radius [10]. An n-dimensional torus is the topological product of n circles. The volume of an n-dimensional torus is completely equivalent to the surface of an $(n+1)$-dimensional sphere. Any compact metric space of n dimensions can be mapped homeomorphicly into a subset of a Euclidean space of $2n+1$ dimensions.

Sequences of stochastic transitions between configurations of different dimensions can be considered as stochastic vector quantities (fields). The extremum of a distribution function for frequencies of the stochastic transitions dependent on n gives the most probable number of the dimensions, and, taking the mapping $n \to 2n+1$ into account, the most probable configuration of the space. This function was first studied in the 1960's by di Bartini [11, 12, 13]. He found that the function has extrema at $2n+1 = \pm 7$ that is equivalent to a 3-dimensional vortical torus coaxial with another, the same vortical torus, mirrored with the first one. Each of the torii is equivalent to a $(3+1)$-dimensional sphere. Its configuration can be easy calculated, because such formations were studied by Lewis and Larmore. A vortical torus has no breaks if the current lines coincide with the trajectory of the vortex core. Proceeding from the continuity condition, di Bartini found the most probable configuration of the vortical torus is it characterized by the ratio $E = \frac{D}{r} = \frac{1}{4} e^{6.9996968} = 274.074996$ between the torus diameter D and the radius of torus circulation r.

We apply di Bartini's result from topology to General Relativity. The time axis is represented as the element of the circle of radius $R=\frac{1}{2}D$, while the spatial axes are the elements of three small circles of radii r (the topological product of which is the 3-dimensional vortical torus). In a "metric" representation by a Minkowski diagram, the torus is a 3-dimensional spatial section of the given (3+1)-space while the time lines have some *inclination* to the the spatial section. In order for the torus (the 3-dimensional space of our world) to be uniform without break, all the time lines have the *same inclination* to the spatial section at each point of the section.

Cosines of the angles between the coordinate axes, in Riemannian geometry, are represent by the components of the fundamental metric tensor $g_{\alpha\beta}$ [14]. If the time lines are everywhere orthogonal to the spatial section, all g_{0i} are zero: $g_{0i}=0$. Such a space is called *holonomic*. If not ($g_{0i}\neq 0$), the space is said to be *non-holonomic*. As was shown in the 1940's by Zelmanov [15, 16, 17], a field of the space non-holonomity (inclinations of the time lines to the spatial section) manifests as a rotation of the space with a 3-dimensional velocity $v_i=-\frac{c\,g_{0i}}{\sqrt{g_{00}}}$. The mathematical proof is given in Appendix 1.

So a field with the same inclination of the time lines to the spatial section is characterized, in the absence of gravitational fields, by $v_i=-c\,g_{0i}=\text{const}$ at each point of the spatial section. In other words, this is a field of the *homogeneous non-holonomity* (rotation) of the whole space. It is hard to explain such a field by everyday analogy, because it has zero angular speed, and also no centre of rotation. However owing to the space-time representation by a Minkowski diagram, it appears very simply as a field of which the time arrows pierce the hyper-surface of the spatial section with the same inclination at each point.

After di Bartini's result, we therefore conclude that the most probable configuration of the basic space (space-time) of General Relativity is represented by a primordially non-holonomic (3+1)-dimensional pseudo-Riemannian space, where the non-holonomic background field is homogeneous, which manifests in the spatial section (3-dimensional space) as the presence of two fundamental drift-fields:

1. A homogeneous field of the constant linear velocity of the background space rotation

$$\bar{v}=c\,\frac{r}{R}=\frac{2c}{E}=\text{const}=2.187671\times10^{8}\ \text{cm/sec} \quad (1)$$

which originates from the fact that, given the non-holonomic space, the time-like spread R depends on the spatial-like spread r as $\frac{R}{r}=\frac{1}{2}E=137.037498$. The background space rotation, with $\bar{v}=2{,}187.671$ km/sec at each point of the space, is due to the continuity condition everywhere inside the torus;

2. A homogeneous drift-field of the constant dipole-fit linear velocity

$$\bar{\mathrm{v}}=\frac{\bar{v}}{2\pi}=\text{const}=3.481787\times10^{7}\ \text{cm/sec} \quad (2)$$

which characterizes a spatial linear drift of the non-holonomic background relative to any given observer. The field of the spatial drift with $\bar{\mathrm{v}}=348.1787$ km/sec is also present at each point of the space.

In the spatial section the background space rotation with $\bar{v}=2{,}187.671$km/sec is observed as absolute motion. This is due to the fact that a rotation due to the space non-holonomity is relative to time, not the spatial coordinates. Despite this, as proven by Zelmanov [15, 16, 17], such a rotation relates to spatial rotation, if any.

2.2 The space metric which includes a non-holonomic background

We are going to derive the metric of a non-holonomic space, which has the aforementioned most probable configuration for the (3+1)-space of General Relativity. To do this we consider an element of volume of the space (the elementary volume).

We consider the pseudo-Riemannian (3+1)-space of General Relativity. Let it be non-holonomic so that the non-holonomity field is homogeneous, i.e. manifests as a homogeneous space-time rotation with a linear velocity v, which has the same numerical value along all three spatial axes at each point of the space. The elementary 4-dimensional interval in such a space is

$$ds^2=c^2dt^2+\frac{2v}{c}\,cdt\,(dx+dy+dz)-\\ -dx^2-dy^2-dz^2, \quad (3)$$

where the second term is not reduced, for clarity.

We denote the numerical coefficient, which characterize the space rotation (see the second term on the right side), as $\alpha=v/c$. We mean, consider the most probable configuration of the (3+1)-space, $v=\bar{v}=2{,}187.671$km/sec and also $\alpha=\bar{v}/c=1/137.037498$. The ratio $\alpha=\bar{v}/c$ specific to the space (it characterizes the background non-holonomity of the space), coincides with the analytical value of Sommerfeld's fine-structure constant [11, 12, 13], connected to electromagnetic interactions.*

Given the most probable configuration of the space, each 3-dimensional volume element rotates with the linear velocity $\bar{v}=2{,}187.671$km/sec and moves with the velocity $\bar{\mathrm{v}}=\frac{\bar{v}}{2\pi}=348.1787$ km/sec relative toward any observer located in the space. The metric (3) contains the space rotation only. To modify the metric for the most probable configura-

*Tests based on the quantum Hall effect and the anomalous magnetic moment of the electron, give different experimental values for Sommerfeld's constant, close to the analytical value. For instance, the latest tests (2006) gave $\alpha\simeq 1/137.035999710(96)$ [18].

$$ds^2 = c^2dt^2 + \frac{2v\,(\cos\varphi+\sin\varphi)}{c}\,cdt\,dr + \frac{2vr\,(\cos\varphi-\sin\varphi)}{c}\,cdt\,d\varphi + \frac{2v}{c}\,cdt\,dz - \\ - dr^2 + \frac{2v\mathrm{v}\,(\cos\varphi+\sin\varphi)}{c^2}\,dr\,dz - r^2d\varphi^2 + \frac{2v\mathrm{v}r\,(\cos\varphi-\sin\varphi)}{c^2}\,d\varphi\,dz - dz^2 \qquad (7)$$

tion, we should apply Lorentz' transformation along the direction of the space motion.

We choose the z-axis for the direction of space motion. For clarity of further calculation, we use the cylindrical coordinates r, φ, z

$$x = r\cos\varphi\,, \qquad y = r\sin\varphi\,, \qquad z = z\,, \qquad (4)$$

so the metric (3) in the new coordinates takes the form

$$ds^2 = c^2dt^2 + \frac{2v}{c}\,(\cos\varphi+\sin\varphi)\,cdt\,dr + \\ + \frac{2vr}{c}\,(\cos\varphi-\sin\varphi)\,cdt\,d\varphi + \frac{2v}{c}\,cdt\,dz - \\ - dr^2 - r^2d\varphi^2 - dz^2. \qquad (5)$$

Substituting the quantities $\tilde{t}$ and $\tilde{z}$ of Lorentz' transformations

$$\tilde{t} = \frac{t+\frac{\mathrm{v}z}{c^2}}{\sqrt{1-\frac{\mathrm{v}^2}{c^2}}}\,, \qquad \tilde{z} = \frac{z+\mathrm{v}t}{\sqrt{1-\frac{\mathrm{v}^2}{c^2}}}\,, \qquad (6)$$

for t and z in the metric (5), we obtain the metric for a volume element which rotates with the constant velocity $\bar{v} = \alpha c$ and approaches with the constant velocity $\mathrm{v} = \bar{\mathrm{v}}$ with respect to any observer located in the space. This is formula (7) shown on the top of this page. In that formula

$$\frac{1}{\sqrt{1-\frac{\mathrm{v}^2}{c^2}}} = \frac{1}{\sqrt{1-\frac{\bar{\mathrm{v}}^2}{c^2}}} = \mathrm{const} \simeq 1\,, \qquad (8)$$

due to that fact that, in the framework of this problem, $\mathrm{v} \ll c$. Besides there is also $v \ll c$, so that the second order terms reduce each other. We still do not reduce the numerical coefficient c of the non-diagonal space-time terms so that they are easily recognized in the metric.

Because the non-holonomic metric (7) satisfies the most probable configuration for such a $(3+1)$-space, we regard it as the *background metric of the world*.

2.3 Study of the background metric. The main characteristics of the background space

We now calculate the main characteristics of the space which are invariant within a fixed three-dimensional spatial section, connected to an observer. Such quantities are related to the chronometric invariants, which are the physical observable quantities in General Relativity [15, 16, 17] (see Appendix 2).

After the components of the fundamental metric tensor $g_{\alpha\beta}$ are obtained from the background metric (7), we calculate the main observable characteristics of the space (see Appendix 2). It follows that in the space:

$$\frac{v}{c} = \frac{\bar{v}}{c} = \alpha = \mathrm{const}, \quad \frac{v\mathrm{v}}{c^2} = \frac{\alpha\bar{\mathrm{v}}}{c} = \frac{\bar{v}^2}{2\pi c^2} = \mathrm{const}\,, \qquad (9)$$

the gravitational potential w is zero

$$g_{00} = 1\,, \qquad \mathrm{w} = c^2\big(1-\sqrt{g_{00}}\big) = 0\,, \qquad (10)$$

the linear velocity of the space rotation $v_i = -\frac{c\,g_{0i}}{\sqrt{g_{00}}}$ is

$$\left.\begin{aligned} v_1 &= -\bar{v}\,(\cos\varphi+\sin\varphi) \\ v_2 &= -\bar{v}r\,(\cos\varphi-\sin\varphi) \\ v_3 &= -\bar{v} \end{aligned}\right\} \qquad (11)$$

the relativistic multiplier is unity (within the number of significant digits)

$$\frac{1}{\sqrt{1-\frac{\bar{\mathrm{v}}^2}{c^2}}} = \frac{1}{0.9999993} = 1\,, \qquad (12)$$

the gravitational inertial force F_i, the angular velocity of the space rotation A_{ik}, the space deformation D_{ik}, and the space curvature C_{ik} are zero

$$F_i = 0\,, \quad A_{ik} = 0\,, \quad D_{ik} = 0\,, \quad C_{ik} = 0\,, \qquad (13)$$

while of all the chr.inv.-Christoffel symbols Δ^i_{km}, only two components are non-zero,

$$\Delta^1_{22} = -r\,, \qquad \Delta^2_{12} = \frac{1}{r}\,. \qquad (14)$$

The non-holonomic background space is free of distributed matter, so the energy-momentum tensor is zero therein. Hence, as seen from the chr.inv.-Einstein equations (see Appendix 2), the background space necessarily has

$$\lambda = 0\,, \qquad (15)$$

i.e. it is also free of physical vacuum (λ-field). In other words, the non-holonomic background space is *empty*.

We conclude for the background space exposed by the non-holonomic background metric (7), that

> The non-holonomic background space satisfying the most probable configuration of the $(3+1)$-space of General Relativity is a flat pseudo-Riemannian space with the 3-dimensional Euclidean metric and a constant space-time rotation. The background space is empty; it permits neither distributed matter or vacuum (λ-field). The background space is not one an Einstein space (where $R_{\alpha\beta} = k\,g_{\alpha\beta}$, $k = \mathrm{const}$) due to the fact that Einstein's equations have $k=0$ in the background space. To be an Einstein space, the background space should be perturbed.

Read about Einstein spaces and their formal determination in *Einstein Spaces* by A. Z. Petrov [19].

It should be noted that of the fact that the 3-dimensional Euclidean metric means only $F_i = 0$, $A_{ik} = 0$, $D_{ik} = 0$ and $C_{ik} = 0$. The Christoffel symbols can be $\Delta^i_{mn} \neq 0$ due to the curvilinear coordinates.

$$ds^2 = \left(1 - \frac{2GM}{c^2 z}\right) c^2 dt^2 + \frac{2v\,(\cos\varphi + \sin\varphi)}{c}\, c\,dt\,dr + \frac{2vr\,(\cos\varphi - \sin\varphi)}{c}\, c\,dt\,d\varphi + \frac{2v}{c}\, c\,dt\,dz - \\ - dr^2 + \frac{2v\mathrm{v}\,(\cos\varphi + \sin\varphi)}{c^2}\, dr\,dz - r^2 d\varphi^2 + \frac{2v\mathrm{v}r\,(\cos\varphi - \sin\varphi)}{c^2}\, d\varphi\,dz - \left(1 + \frac{2GM}{c^2 z}\right) dz^2 \qquad (20)$$

2.4 Perturbation of the non-holonomic background

How does a gravitational field and local rotation (the gravitational field of the Earth and the rotation of a disc, for instance) affect the metric? This we now describe.

The ratio v/c, according to the continuity condition in the space (see §2), equals Sommerfeld's fine-structure constant $\alpha = \bar{v}/c = 1/137.037498$ only if the non-holonomic background metric is *unperturbed* by a local rotation, so the space non-holonomity appears as a homogeneous field of the constant linear velocity of the space rotation $\bar{v}$, which is 2,187.671 km/sec. The gravitational potential w appears in General Relativity as $\mathrm{w} = c^2(1 - \sqrt{g_{00}})$, i.e. connected to g_{00}. So the presence of a gravity field changes the linear velocity of the space rotation $v_i = -\frac{c\,g_{0i}}{\sqrt{g_{00}}}$. For an Earth-bound laboratory, we have $\frac{\mathrm{w}}{c^2} = \frac{GM}{c^2 z} \simeq 7\times10^{-10}$. This numerical value is so small that perturbations of the non-holonomic background through g_{00}, by the Earth's gravitational field, are weak. Another case — local rotations. A local rotation with a linear velocity $\tilde{v}$ or a gravitational potential w perturbs the homogeneous field of the space non-holonomity, the ratio v/c in that area changes from the initial value $\alpha = \bar{v}/c = 1/137.037498$ to a new, perturbed value

$$\frac{v}{c} = \frac{\bar{v} + \tilde{v}}{c} = \alpha + \frac{\tilde{v}}{\bar{v}}\,\alpha\,. \qquad (16)$$

This fact should be taken into account in all formulae which include v or the derivatives.

Consider a high speed gyro used in aviation navigation: a 250 g rotor of 1.65″ diameter, rotating with an angular speed of 24,000 rpm. With modern equipment this is almost the uppermost speed for such a mechanically rotating system*. In such a case the background field of the space non-holonomity is perturbed near the giro as $\tilde{v} \approx 53$ m/sec, that is 2.4×10^{-5} of the background $\bar{v} = 2{,}187.671$ km/sec. Larger effects are expected for a submarine gyro, where the rotor and, hence, the linear velocity of the rotation is larger. In other words, the non-holonomic background can be substantially perturbed near such a mechanically rotating system.

2.5 The background metric perturbed by a gravitational field

The formula for the linear velocity of the space rotation

$$v_i = -c\,\frac{g_{0i}}{\sqrt{g_{00}}}\,, \qquad (17)$$

was derived by Zelmanov [15, 16, 17], due to the space non-holonomity, and originating in it. It is evident that if the same numerical value $v_i = \mathrm{const}$ remains unchanged everywhere in the spatial section (i.e. ${}^*\nabla_i\, v^i = 0$)†

$$\left.\begin{aligned} v_i &= \mathrm{const} \\ {}^*\nabla_i\, v^i &= 0 \end{aligned}\right\} \qquad (18)$$

there is a *homogeneous field of the space non-holonomity*. By the formula (17), given a homogeneous field of the space non-holonomity, any local rotation of the space (expressed with g_{0i}) and also a gravitational potential (contained in g_{00}) perturb the homogeneous non-holonomic background.

We modify the background metric (7) to that case where the homogeneous non-holonomic background is perturbed by a weak gravitational field, produced by a bulky point mass M, that is usual for observations in a laboratory located on the Earth's surface or near orbit. The gravitational potential in General Relativity is $\mathrm{w} = c^2(1 - \sqrt{g_{00}})$. We assume gravity acting in the z-direction, i.e. $\mathrm{w} = \frac{GM}{z}$, and we omit terms of higher than the second order in c, following the usual approximation in General Relativity (see Landau and Lifshitz [20] for instance). We substitute

$$g_{00} = \left(1 - \frac{\mathrm{w}}{c^2}\right)^2 = \left(1 - \frac{GM}{c^2 z}\right)^2 \simeq 1 - \frac{2GM}{c^2 z} \neq 1 \qquad (19)$$

into the first term of the initial metric (5). After Lorentz' transformations, we obtain a formula for the non-holonomic background metric (7) perturbed by such a field of gravity. This is formula (20) displayed on the top of this page.

2.6 The background metric perturbed by a local oscillation and gravitational field

A superconducting disc in air under the influence of an alternating magnetic field of an electromagnet located beneath it, undergoes oscillatory bounces with the frequency of the current, in a vertical direction (the same that of the Earth's gravity — the z-direction in our cylindrical coordinates).

We set up a harmonic transformation of the z-coordinate

$$\tilde{z} = z + z_0 \cos\frac{\Omega}{c}\,u\,, \qquad u = ct + z\,, \qquad (21)$$

where z_0 is the initial deviation (the amplitude of the oscillation), while Ω is the frequency. After calculating $d\tilde{z}$ and $d\tilde{z}^2$ (22), and using these instead of dz and dz^2 in the non-holonomic background metric (7), we obtain the background metric (7) perturbed by the local oscillation and gravitational field. This is formula (23) shown above.

*Mechanical gyros used in aviation and submarine navigation technology have rotations in the range 6,000–30,000 rpm. The upper speed is limited by problems due to friction.

†See Appendix 2 for the chr.inv.-differentiation symbol ${}^*\nabla$.

$$\left.\begin{aligned} d\tilde{z} &= \left(1-\frac{\Omega z_0}{c}\sin\frac{\Omega}{c}u\right)dz-\left(\frac{\Omega z_0}{c}\sin\frac{\Omega}{c}u\right)cdt \\ d\tilde{z}^2 &= \left(1-\frac{\Omega z_0}{c}\sin\frac{\Omega}{c}u\right)^2dz^2-\frac{2\Omega z_0}{c}\sin\frac{\Omega}{c}u\left(1-\frac{\Omega z_0}{c}\sin\frac{\Omega}{c}u\right)cdt\,dz+\left(\frac{\Omega^2 z_0^2}{c^2}\sin^2\frac{\Omega}{c}u\right)c^2dt^2 \end{aligned}\right\} \tag{22}$$

$$\begin{aligned} ds^2 &= \left[1-\frac{2GM}{c^2\left(z+z_0\cos\frac{\Omega}{c}u\right)}-\frac{2v\Omega z_0}{c^2}\sin\frac{\Omega}{c}u-\frac{\Omega^2 z_0^2}{c^2}\sin^2\frac{\Omega}{c}u\right]c^2dt^2+ \\ &+\frac{2v\left(\cos\varphi+\sin\varphi\right)}{c}\left(1-\frac{\Omega z_0\mathrm{v}}{c^2}\sin\frac{\Omega}{c}u\right)cdt\,dr+\frac{2vr\left(\cos\varphi-\sin\varphi\right)}{c}\left(1-\frac{\Omega z_0\mathrm{v}}{c^2}\sin\frac{\Omega}{c}u\right)cdt\,d\varphi+ \\ &+\frac{2}{c}\left(1-\frac{\Omega z_0\mathrm{v}}{c^2}\sin\frac{\Omega}{c}u\right)\left\{v+\Omega z_0\sin\frac{\Omega}{c}u\left[1+\frac{2GM}{c^2\left(z+z_0\cos\frac{\Omega}{c}u\right)}\right]\right\}cdt\,dz-dr^2+ \\ &+\frac{2v\mathrm{v}\left(\cos\varphi+\sin\varphi\right)}{c^2}\left(1-\frac{\Omega z_0}{c^2}\sin\frac{\Omega}{c}u\right)dr\,dz-r^2d\varphi^2+\frac{2v\mathrm{v}r\left(\cos\varphi-\sin\varphi\right)}{c^2}\left(1-\frac{\Omega z_0}{c}\sin\frac{\Omega}{c}u\right)d\varphi\,dz- \\ &-\left[1+\frac{2GM}{c^2\left(z+z_0\cos\frac{\Omega}{c}u\right)}\right]\left(1-\frac{\Omega z_0}{c}\sin\frac{\Omega}{c}u\right)^2dz^2 \end{aligned} \tag{23}$$

$$\begin{aligned} ds^2 &= \left(1-\frac{2GM}{c^2z}-\frac{2\Omega z_0 v}{c^2}\sin\frac{\Omega}{c}u\right)c^2dt^2+\frac{2v\left(\cos\varphi+\sin\varphi\right)}{c}cdt\,dr+\frac{2vr\left(\cos\varphi-\sin\varphi\right)}{c}cdt\,d\varphi+ \\ &+\frac{2}{c}\left(v+\Omega z_0\sin\frac{\Omega}{c}u\right)cdt\,dz-dr^2-r^2d\varphi^2-dz^2 \end{aligned} \tag{25}$$

3 The space of a suspended, vertically oscillating disc

3.1 The main characteristics of the space

Metric (23) is very difficult in use. However, under the physical conditions of a real experiment, many terms vanish so that the metric reduces to a simple form. We show how.

Consider a system like that used by Podkletnov in his experiment: a horizontally oriented disc suspended in air due to an alternating high-frequent magnetic field generated by an electromagnet located beneath the disc. Such a disc undergoes an oscillatory bounce along the vertical axis with a frequency which is the same as that of the alternating magnetic field. We apply metric (23) to this case, i.e. the metric of the space near such a disc.

First, because the initial deviation of such a disc from the rest point is very small ($z_0 \ll z$), we have

$$\frac{2GM}{c^2\left(z+z_0\cos\frac{\Omega}{c}u\right)}\simeq\frac{2GM}{c^2z}\left(1-\frac{z_0}{z}\cos\frac{\Omega}{c}u\right)\simeq\frac{2GM}{c^2z}. \tag{24}$$

Second, the relativistic square is $K=1$. Third, under the conditions of a real experiment like Podkletnov's, the terms $\frac{\Omega^2 z_0^2}{c^2}$, $\frac{\Omega^2 z_0}{c}$, $\frac{\Omega z_0}{c}$, $\frac{v^2}{c^2}$ and $\frac{v}{c}$ have such small numerical values that they can be omitted from the equations. The metric (23) then takes the much simplified form, shown as expression (25) at the top of this page. In other words, the expression (25) represents the metric of the space of a disc which undergoes an oscillatory bounce orthogonal to its own plane, in the conditions of a real experiment. This is the *main metric* which will be used henceforth in our study for the Podkletnov effect.

We calculate the main observable characteristics of such a space according to Appendix 2.

In such a space the gravitational potential w and the components of the linear velocity of the space rotation v_i are

$$\mathrm{w}=\frac{GM}{z}+\left(\Omega z_0\sin\frac{\Omega}{c}u\right)v\,, \tag{26}$$

$$\left.\begin{aligned} v_1 &= -v\left(\cos\varphi+\sin\varphi\right) \\ v_2 &= -vr\left(\cos\varphi-\sin\varphi\right) \\ v_3 &= -v-\Omega z_0\sin\frac{\Omega}{c}u \end{aligned}\right\}. \tag{27}$$

The components of the gravitational inertial force F_i acting in such a space are

$$\left.\begin{aligned} F_1 &= \left(\Omega z_0\sin\frac{\Omega}{c}u\right)v_r+\left(\cos\varphi+\sin\varphi\right)v_t \\ F_2 &= \left(\Omega z_0\sin\frac{\Omega}{c}u\right)v_\varphi+r\left(\cos\varphi-\sin\varphi\right)v_t \\ F_3 &= \left(\Omega z_0\sin\frac{\Omega}{c}u\right)v_z-\frac{GM}{z^2}+v_t+ \\ &\qquad +\Omega^2 z_0\cos\frac{\Omega}{c}u \end{aligned}\right\}, \tag{28}$$

where the quantities v_r, v_φ, v_z, v_t denote the respective partial derivatives of v.

In such a space the components of the tensor of the angular velocities of the space rotation A_{ik} are

$$\left.\begin{aligned} A_{12} &= \frac{1}{2}\left(\cos\varphi+\sin\varphi\right)v_\varphi-\frac{r}{2}\left(\cos\varphi-\sin\varphi\right)v_r \\ A_{23} &= \frac{r}{2}\left(\cos\varphi-\sin\varphi\right)v_z-\frac{1}{2}\,v_\varphi \\ A_{13} &= \frac{1}{2}\left(\cos\varphi+\sin\varphi\right)v_z-\frac{1}{2}\,v_r \end{aligned}\right\}. \quad (29)$$

Because we omit all quantities proportional to $\frac{v^2}{c^2}$, the chr.inv.-metric tensor $h_{ik}=-g_{ik}+\frac{1}{c^2}v_iv_k$ (the observable 3-dimensional metric tensor) becomes $h_{ik}=-g_{ik}$. Its components for the metric (25) are

$$\left.\begin{aligned} &h_{11}=1\,, \quad h_{22}=r^2, \quad h_{33}=1 \\ &h^{11}=1\,, \quad h^{22}=\frac{1}{r^2}\,, \quad h^{33}=1 \\ &h=\det\|h_{ik}\|=r^2, \quad \frac{\partial\ln\sqrt{h}}{\partial x^1}=\frac{1}{r} \end{aligned}\right\}. \quad (30)$$

For the tensor of the space deformation D_{ik} we obtain

$$D_{33}=D^{33}=0\,, \qquad D=h^{ik}D_{ik}=0\,. \quad (31)$$

Among the chr.inv.-Christoffel symbols Δ^i_{km} within the framework of our approximation, only two components are non-zero,

$$\Delta^1_{22}=-r\,, \qquad \Delta^2_{12}=\frac{1}{r}\,, \quad (32)$$

so, despite the fact that the observable curvature tensor C_{ik} which possesses all the properties of Ricci's tensor $R_{\alpha\beta}$ on the 3-dimensional spatial section (see Appendix 2) isn't zero in the space, but within the framework of our assumption it is meant to be zero: $C_{ik}=0$. In other words, although the space curvature isn't zero, it is so small that it is negligible in a real experiment such as we are considering.

These are the physical observable characteristics of a space volume element located in an Earth-bound laboratory, where the non-holonomic background of the space is perturbed by a disc which undergoes oscillatory bounces orthogonal to its own plane.

We have now obtained all the physical observable characteristics of space required by Einstein's equations. Einstein's equations describe flows of energy, momentum and matter. Using the derived equations, we will know in precisely those flows of energy and momentum near a disc which undergoes an oscillatory bounce orthogonal to its own plane. So if there is any additional energy flow or momentum flow generated by the disc, Einstein's equations show this.

3.2 Einstein's equations in the space. First conclusion about the origin of the Podkletnov effect

Einstein's equations, in terms of the physical observable quantities given in Appendix 2, were derived in the 1940's by Zelmanov [15, 16, 17] as the projections of the general covariant (4-dimensional) Einstein equations

$$R_{\alpha\beta}-\frac{1}{2}\,g_{\alpha\beta}R=-\kappa T_{\alpha\beta}+\lambda g_{\alpha\beta} \quad (33)$$

onto the time line and spatial section of an observer.

We omit the λ-term due to its negligible effect. In considering a real situation like Podkletnov's experiment, we assume the same approximation as in the previous Section. We also take into account those physical observable characteristics of the space which are zero according to our calculation.

Einstein's equations expressed in the terms of the physical observable quantities (see Appendix 2 for the complete equations) then take the following simplified form

$$\left.\begin{aligned} &\frac{\partial F^i}{\partial x^i}-A_{ik}A^{ik}+\frac{\partial\ln\sqrt{h}}{\partial x^i}\,F^i=-\frac{\kappa}{2}\left(\rho c^2+U\right) \\ &\frac{\partial A^{ij}}{\partial x^j}+\frac{\partial\ln\sqrt{h}}{\partial x^j}\,A^{ij}=-\kappa J^i \\ &2A_{ij}A^{\cdot j}_{k\cdot}+\frac{1}{2}\left(\frac{\partial F_i}{\partial x^k}+\frac{\partial F_k}{\partial x^i}-2\Delta^m_{ik}F_m\right)= \\ &\qquad\qquad =\frac{\kappa}{2}\left(\rho c^2-U\right)h_{ik}+\kappa U_{ik} \end{aligned}\right\} \quad (34)$$

where $\rho=\frac{T_{00}}{g_{00}}$, $J^i=\frac{cT^i_0}{\sqrt{g_{00}}}$ and $U^{ik}=c^2T^{ik}$ are the observable projections of the energy-momentum tensor $T_{\alpha\beta}$ of distributed matter on the right side of Einstein's equations (the right side determines distributed matter which fill the space, while the left side determines the geometrical properties of the space). By their physical sense, ρ is the observable density of the energy of the matter field, J^i is the observable density of the field momentum, U^{ik} is the observable stress-tensor of the field.

In relation to Podkletnov's experiment, $T_{\alpha\beta}$ is the sum of the energy-momentum tensor of an electromagnetic field, generated by an electromagnet located beneath the disc, and also that of the other fields filling the space. We therefore attribute the energy-momentum tensor $T_{\alpha\beta}$ and its observable components ρ, J^i, U^{ik} to the common field.

Is there additional energy and momentum produced by the field of the background space non-holonomity in order to compensate for a perturbation therein, due to a disc undergoing oscillatory bounces orthogonal to its own pane? This is easy to answer using Einstein's equations, owing to the fact that given the unperturbed field of the background space non-holonomity, the linear velocity of the space rotation v isn't a function of the spatial coordinates and time $v\neq$ $\neq f(r,\varphi,z,t)$. After F_i, A_{ik}, D_{ik}, and Δ^i_{kn} specific to the space of a suspended, vertically oscillating disc are substituted into Einstein's equations (34), the left side of the equations should contain additional terms dependent on the derivatives of v by the spatial coordinates r, φ, z, and time t. The additional terms, appearing in the left side, build

$$
\left.
\begin{array}{l}
(\cos\varphi+\sin\varphi)\,v_{tr}+(\cos\varphi-\sin\varphi)\,\dfrac{v_{t\varphi}}{r}+v_{tz}-(1-\cos\varphi\sin\varphi)\,v_r^2-v_z^2- \\
-(1+\cos\varphi\sin\varphi)\,\dfrac{v_\varphi^2}{r^2}+\left(\cos^2\varphi-\sin^2\varphi\right)\dfrac{v_rv_\varphi}{r}+(\cos\varphi+\sin\varphi)\,v_rv_z+ \\
+(\cos\varphi-\sin\varphi)\,\dfrac{v_\varphi v_z}{r}+\dfrac{2GM}{z^3}+\left(\Omega z_0\sin\dfrac{\Omega}{c}u\right)\left(v_{rr}+\dfrac{v_{\varphi\varphi}}{r^2}+v_{zz}+\dfrac{v_r}{r}\right)=-\dfrac{\kappa}{2}\left(\rho c^2+U\right) \\
\dfrac{(\cos\varphi-\sin\varphi)}{2r}\left(v_{r\varphi}-\dfrac{v_\varphi}{r}\right)-\dfrac{(\cos\varphi+\sin\varphi)}{2}\left(\dfrac{v_{\varphi\varphi}}{r^2}+v_{zz}+\dfrac{v_r}{r}\right)+\dfrac{1}{2}\,v_{rz}=\kappa J^1 \\
\dfrac{1}{2r^2}\left[v_{\varphi z}+(\cos\varphi+\sin\varphi)\left(v_{r\varphi}-\dfrac{v_\varphi}{r}\right)-r\,(\cos\varphi-\sin\varphi)\,(v_{rr}+v_{zz})\right]=\kappa J^2 \\
\dfrac{(\cos\varphi+\sin\varphi)}{2}\,v_{rz}+\dfrac{(\cos\varphi-\sin\varphi)}{2}\dfrac{v_{\varphi z}}{r}-\dfrac{1}{2}\left(v_{rr}+\dfrac{v_{\varphi\varphi}}{r^2}+\dfrac{v_r}{r}\right)=\kappa J^3 \\
(1-\cos\varphi\sin\varphi)\,v_r^2-\left(\cos^2\varphi-\sin^2\varphi\right)\dfrac{v_rv_\varphi}{r}+\dfrac{(1+2\cos\varphi\sin\varphi)}{2}\left(\dfrac{v_\varphi^2}{r^2}+v_z^2\right)+ \\
+\,(\cos\varphi+\sin\varphi)\,v_{tr}-(\cos\varphi+\sin\varphi)\,v_rv_z+\left(\Omega z_0\sin\dfrac{\Omega}{c}u\right)v_{rr}=\dfrac{\kappa}{2}\left(\rho c^2-U\right)+\kappa U_{11} \\
\dfrac{1}{2}\Bigg[r\left(\cos^2\varphi-\sin^2\varphi\right)v_z^2+v_rv_\varphi-r\,(\cos\varphi-\sin\varphi)\,v_rv_z-(\cos\varphi+\sin\varphi)\,v_\varphi v_z+ \\
+(\cos\varphi+\sin\varphi)\,v_{t\varphi}+r\,(\cos\varphi-\sin\varphi)\,v_{tr}+2\left(\Omega z_0\sin\dfrac{\Omega}{c}u\right)\left(v_{r\varphi}-\dfrac{v_\varphi}{r}\right)\Bigg]=\kappa U_{12} \\
\dfrac{1}{2}\Bigg[v_{tr}+(\cos\varphi+\sin\varphi)\,v_{tz}-(\cos\varphi-\sin\varphi)\,\dfrac{v_rv_\varphi}{r}+(1-2\cos\varphi\sin\varphi)\,v_rv_z+ \\
+(\cos\varphi+\sin\varphi)\,\dfrac{v_\varphi^2}{r^2}-\left(\cos^2\varphi-\sin^2\varphi\right)\dfrac{v_\varphi v_z}{r}+2\left(\Omega z_0\sin\dfrac{\Omega}{c}u\right)v_{rz}\Bigg]=\kappa U_{13} \\
\dfrac{(1-2\cos\varphi\sin\varphi)}{2}\left(v_r^2+v_z^2\right)-\left(\cos^2\varphi-\sin^2\varphi\right)\dfrac{v_rv_\varphi}{r}+(1+\cos\varphi\sin\varphi)\,\dfrac{v_\varphi^2}{r^2}+ \\
+(\cos\varphi-\sin\varphi)\,\dfrac{v_{t\varphi}}{r}-(\cos\varphi-\sin\varphi)\,\dfrac{v_\varphi v_z}{r}+\left(\Omega z_0\sin\dfrac{\Omega}{c}u\right)\left(\dfrac{v_{\varphi\varphi}}{r^2}+\dfrac{v_r}{r}\right)=\dfrac{\kappa}{2}\left(\rho c^2-U\right)+\dfrac{\kappa U_{22}}{r^2} \\
\dfrac{1}{2}\Bigg[v_{t\varphi}+r\,(\cos\varphi-\sin\varphi)\,v_{tz}+r\,(\cos\varphi-\sin\varphi)\,v_r^2-(\cos\varphi+\sin\varphi)\,v_rv_\varphi- \\
-\,r\left(\cos^2\varphi-\sin^2\varphi\right)v_rv_z+(1+2\cos\varphi\sin\varphi)\,v_\varphi v_z+2\left(\Omega z_0\sin\dfrac{\Omega}{c}u\right)v_{\varphi z}\Bigg]=\kappa U_{23} \\
\dfrac{v_r^2}{2}+v_z^2-(\cos\varphi+\sin\varphi)\,v_rv_z+\dfrac{v_\varphi^2}{2r^2}-(\cos\varphi-\sin\varphi)\,\dfrac{v_\varphi v_z}{r}+v_{tz}+\dfrac{2GM}{z^3}+ \\
+\left(\Omega z_0\sin\dfrac{\Omega}{c}u\right)v_{zz}=\dfrac{\kappa}{2}\left(\rho c^2-U\right)+\kappa U_{33}
\end{array}
\right\}
\qquad (35)
$$

respective additions to the energy and momentum of the acting electromagnetic field on the right side of the equations.

Following this line, we are looking for the energy and momentum produced by the field of the background space non-holonomity due to perturbation therein.

We substitute F_i (28), A_{ik} (29), D_{ik} (31), and Δ^i_{kn} (32), specific to the space of such an oscillating disc, into the chr.inv.-Einstein equations (34), and obtain the Einstein equations as shown in formula (35). These are actually Einstein's equations for the initial homogeneous non-holonomic space perturbed by such a disc.

As seen from the left side of the Einstein equations (35), a new energy-momentum field appears near the disc due to the appearance of a non-uniformity of the field of the background space non-holonomity (i.e. due to the functions v of the coordinates and time):

1. The field bears additional energy to the electromagnetic field energy represented in the space (see the scalar Einstein equation);
2. The field has momentum flow J^i. The momentum flow spreads from the outer space toward the disc in the r-direction, twists around the disc in the φ-direction, then rises above the disc in the z-direction (see the vectorial Einstein equations which describe the momentum flow J^1, J^2, and J^3 toward r, φ, and z-direction respectively). This purely theoretical finding explains the Podkletnov effect. According to Eugene Podkletnov, a member of his experimental team smoked a pipe a few meters away from the cryostat with the superconducting disc, during operation. By a stroke of luck, Podkletnov noticed that the tobacco smoke was attracted towards the cryostat, then twisted around it and rose above it. Podkletnov then applied a high precision balance, which immediately showed a weight loss over the cryostat. Now it is clear that the tobaccosmoke revealed the momentum flow produced by the background space non-holonomity field perturbed near the vertically oscillating disc;
3. The field has distributed stresses which are expressed by an addition to the electromagnetic field stress-tensor (see the Einstein tensor equations).

In the simplest case where Podkletnov's experiment is run in a completely holonomic space ($v = 0$) the Einstein equations (35) take the simplest form

$$\left.\begin{array}{l} \dfrac{2GM}{z^3} = -\kappa\rho c^2 \\ J^1 = 0\,,\quad J^2 = 0\,,\quad J^3 = 0 \\ U_{11} = 0\,,\ U_{12} = 0\,,\ U_{13} = 0\,,\ U_{22} = 0\,,\ U_{23} = 0 \\ \dfrac{2GM}{z^3} = \kappa U_{33} \end{array}\right\} \qquad (36)$$

This is also true in another case, where the space is non-holonomic ($v \neq 0$) but v isn't function of the spatial coordinates and time $v \neq f(r, \varphi, z, t)$, that is the unperturbed homogeneous field of the background space non-holonomity. We see that in both cases there is no additional energy and momentum flow near the disc; only the electromagnetic field flow is put into equilibrium by the Earth's gravity, directed vertically along the z-axis.

So Einstein's equations show clearly that:

> The Podkletnov effect is due to the fact that the field of the background space non-holonomity, being perturbed by a suspended, vertically oscillating disc, produces energy and momentum flow in order to compensate for the perturbation therein.

3.3 Complete geometrization of matter

Looking at the right side of the Einstein equations (35), which determine distributed matter, we see that ρ and U are included only in the scalar (first) equation and also three tensor equations with the indices 11, 22, 33 (the 5th, 8th, and 10th equations). We can therefore find a formula for U. Then, substituting the formula back into the Einstein equations for ρ and U_{11}, U_{22}, U_{33}, we can express the characteristics of distributed matter through only the physical observable characteristics of the space. This fact, coupled with the fact that the other characteristics of distributed matter (J^1, J^2, J^3, U_{12}, U_{13}, U_{13}) are expressed through only the physical observable characteristics of the space by the 2nd, 3rd, 4th, 6th, 7th, and 9th equations of the Einstein equations (35), means that considering a space in which the homogeneous non-holonomic background is perturbed by an oscillating disc, we can obtain a *complete geometrization of matter*.

Multiplying the 1st equation of (35) by the 3rd, then summing with the 5th, 8th, and 10th equations, we eliminate ρ. Then, because $U = h^{ik}U_{ik} = U_{11} + \frac{U_{22}}{r^2} + U_{33}$, we obtain a formula for U expressed only via the physical observable characteristics of the space. Substituting the obtained formula for κU into the 1st equation, we obtain a formula for ρ. After that it is easy to obtain $\rho c^2 + U$ and $\rho c^2 - U$. Using these in the three Einstein tensor equations with the diagonal indices 11, 22, 33, we obtain formulae for U_{11}, U_{22}, U_{33}, all expressed only in terms of the physical observable characteristics of the space.

The resulting equations, coupled with those of the Einstein equations (35) which determine J^1, J^2, J^3, U_{12}, U_{13}, and U_{13}, build the system of the equations (37), which completely determine the properties of distributed matter — the density of the energy ρ, the density of the momentum flow J^I, and the stress-tensor U_{ik} — only in terms of the physical observable characteristics of the space. So:

> Matter which fills the space, where a homogeneous non-holonomic background is perturbed by an oscillating disc *is completely geometrized*.

$$
\left.
\begin{aligned}
&\kappa U = \frac{(1-\cos\varphi\sin\varphi)}{2}\,v_r^2 + \frac{(1+\cos\varphi\sin\varphi)}{2}\,\frac{v_\varphi^2}{r^2} + \frac{v_z^2}{2} - \frac{\left(\cos^2\varphi-\sin^2\varphi\right)}{2}\,\frac{v_r v_\varphi}{r} - \\
&- \frac{(\cos\varphi-\sin\varphi)}{2}\,\frac{v_\varphi v_z}{r} - \frac{(\cos\varphi+\sin\varphi)}{2}\,v_r v_z - 2\,(\cos\varphi+\sin\varphi)\,v_{tr} - \\
&- 2\,(\cos\varphi-\sin\varphi)\,\frac{v_{t\varphi}}{r} - 2\,v_{tz} - \frac{4GM}{z^3} - 2\left(\Omega z_0 \sin\frac{\Omega}{c}u\right)\left(v_{rr} + \frac{v_{\varphi\varphi}}{r^2} + v_{zz} + \frac{v_r}{r}\right) \\
&\kappa\rho c^2 = \frac{3}{2}\left[(1-\cos\varphi\sin\varphi)\,v_r^2 + (1+\cos\varphi\sin\varphi)\,\frac{v_\varphi^2}{r^2} + v_z^2 - \right. \\
&\left. - \left(\cos^2\varphi-\sin^2\varphi\right)\frac{v_r v_\varphi}{r} - (\cos\varphi-\sin\varphi)\,\frac{v_\varphi v_z}{r} - (\cos\varphi+\sin\varphi)\,v_r v_z\right] \\
&\frac{\kappa}{2}\left(\rho c^2 - U\right) = \frac{(1-\cos\varphi\sin\varphi)}{2}\,v_r^2 + \frac{(1+\cos\varphi\sin\varphi)}{2}\,\frac{v_\varphi^2}{r^2} + \frac{v_z^2}{2} - \frac{\left(\cos^2\varphi-\sin^2\varphi\right)}{2}\,\frac{v_r v_\varphi}{r} - \\
&- \frac{(\cos\varphi-\sin\varphi)}{2}\,\frac{v_\varphi v_z}{r} - \frac{(\cos\varphi+\sin\varphi)}{2}\,v_r v_z + (\cos\varphi+\sin\varphi)\,v_{tr} + (\cos\varphi-\sin\varphi)\,\frac{v_{t\varphi}}{r} + \\
&+ v_{tz} + \frac{2GM}{z^3} + \left(\Omega z_0 \sin\frac{\Omega}{c}u\right)\left(v_{rr} + \frac{v_{\varphi\varphi}}{r^2} + v_{zz} + \frac{v_r}{r}\right) \\
&\kappa J^1 = \frac{(\cos\varphi-\sin\varphi)}{2r}\left(v_{r\varphi} - \frac{v_\varphi}{r}\right) - \frac{(\cos\varphi+\sin\varphi)}{2}\left(\frac{v_{\varphi\varphi}}{r^2} + v_{zz} + \frac{v_r}{r}\right) + \frac{1}{2}\,v_{rz} \\
&\kappa J^2 = \frac{1}{2r^2}\left[v_{\varphi z} + (\cos\varphi+\sin\varphi)\left(v_{r\varphi} - \frac{v_\varphi}{r}\right) - r\,(\cos\varphi-\sin\varphi)\,(v_{rr}+v_{zz})\right] \\
&\kappa J^3 = \frac{(\cos\varphi+\sin\varphi)}{2}\,v_{rz} + \frac{(\cos\varphi-\sin\varphi)}{2}\,\frac{v_{\varphi z}}{r} - \frac{1}{2}\left(v_{rr} + \frac{v_{\varphi\varphi}}{r^2} + \frac{v_r}{r}\right) \\
&\kappa U_{11} = \frac{(1-\cos\varphi\sin\varphi)}{2}\,v_r^2 + (\cos\varphi\sin\varphi)\left(\frac{v_\varphi^2}{2r^2} + v_z^2\right) - \frac{\left(\cos^2\varphi-\sin^2\varphi\right)}{2}\,\frac{v_r v_\varphi}{r} - \frac{(\cos\varphi+\sin\varphi)}{2}\,v_r v_z + \\
&+ \frac{(\cos\varphi-\sin\varphi)}{2}\,\frac{v_\varphi v_z}{r} - (\cos\varphi-\sin\varphi)\,\frac{v_{t\varphi}}{r} - v_{tz} - \frac{2GM}{z^3} - \left(\Omega z_0 \sin\frac{\Omega}{c}u\right)\left(\frac{v_{\varphi\varphi}}{r^2} + v_{zz} + \frac{v_r}{r}\right) \\
&\kappa U_{12} = \frac{1}{2}\left[r\left(\cos^2\varphi-\sin^2\varphi\right)v_z^2 + v_r v_\varphi - r\,(\cos\varphi-\sin\varphi)\,v_r v_z - (\cos\varphi+\sin\varphi)\,v_\varphi v_z + \right. \\
&\left. + (\cos\varphi+\sin\varphi)\,v_{t\varphi} + r\,(\cos\varphi-\sin\varphi)\,v_{tr} + 2\left(\Omega z_0 \sin\frac{\Omega}{c}u\right)\left(v_{r\varphi} - \frac{v_\varphi}{r}\right)\right] \\
&\kappa U_{13} = \frac{1}{2}\left[v_{tr} + (\cos\varphi+\sin\varphi)\,v_{tz} - (\cos\varphi-\sin\varphi)\,\frac{v_r v_\varphi}{r} + (1-2\cos\varphi\sin\varphi)\,v_r v_z + \right. \\
&\left. + (\cos\varphi+\sin\varphi)\,\frac{v_\varphi^2}{r^2} - \left(\cos^2\varphi-\sin^2\varphi\right)\frac{v_\varphi v_z}{r} + 2\left(\Omega z_0 \sin\frac{\Omega}{c}u\right)v_{rz}\right] \\
&\frac{\kappa U_{22}}{r^2} = -(\cos\varphi\sin\varphi)\left(\frac{v_r^2}{2} + v_z^2\right) + \frac{(1+\cos\varphi\sin\varphi)}{2}\,\frac{v_\varphi^2}{r^2} - \frac{\left(\cos^2\varphi-\sin^2\varphi\right)}{2}\,\frac{v_r v_\varphi}{r} - \\
&- \frac{(\cos\varphi-\sin\varphi)}{2}\,\frac{v_\varphi v_z}{r} + \frac{(\cos\varphi+\sin\varphi)}{2}\,v_r v_z - (\cos\varphi+\sin\varphi)\,v_{tr} - v_{tz} - \frac{2GM}{z^3} - \left(\Omega z_0 \sin\frac{\Omega}{c}u\right)(v_{rr}+v_{zz}) \\
&\kappa U_{23} = \frac{1}{2}\left[v_{t\varphi} + r\,(\cos\varphi-\sin\varphi)\,v_{tz} + r\,(\cos\varphi-\sin\varphi)\,v_r^2 - (\cos\varphi+\sin\varphi)\,v_r v_\varphi - \right. \\
&\left. - r\left(\cos^2\varphi-\sin^2\varphi\right)v_r v_z + (1+2\cos\varphi\sin\varphi)\,v_\varphi v_z + 2\left(\Omega z_0 \sin\frac{\Omega}{c}u\right)v_{\varphi z}\right] \\
&\kappa U_{33} = \frac{(\cos\varphi\sin\varphi)}{2}\left(v_r^2 - \frac{v_\varphi^2}{r^2}\right) + \frac{v_z^2}{2} - \frac{(\cos\varphi+\sin\varphi)}{2}\,v_r v_z + \frac{\left(\cos^2\varphi-\sin^2\varphi\right)}{2}\,\frac{v_r v_\varphi}{r} - \\
&- \frac{(\cos\varphi-\sin\varphi)}{2}\,\frac{v_\varphi v_z}{r} - (\cos\varphi+\sin\varphi)\,v_{tr} - (\cos\varphi-\sin\varphi)\,\frac{v_{t\varphi}}{r} - \left(\Omega z_0 \sin\frac{\Omega}{c}u\right)\left(v_{rr} + \frac{v_{\varphi\varphi}}{r^2} + \frac{v_r}{r}\right)
\end{aligned}
\right\} \quad (37)
$$

There is just one question still to be answered. What is the nature of the matter?

Among the matter different from the gravitational field, only the isotropic electromagnetic field was previously geometrized — that for which the metric is determined by the Rainich condition [23, 24, 25]

$$R = 0\,, \qquad R_{\alpha\rho}R^{\rho\beta} = \frac{1}{4}\,\delta^{\beta}_{\alpha}\left(R_{\rho\sigma}R^{\rho\sigma}\right) = 0 \tag{38}$$

and the Nordtvedt-Pagels condition [26]

$$\eta_{\mu\varepsilon\gamma\sigma}\left(R^{\delta\gamma;\sigma}R^{\varepsilon\tau} - R^{\delta\varepsilon;\sigma}R^{\gamma\tau}\right) = 0\,. \tag{39}$$

The Rainich condition and the Nordtvedt-Pagels condition, being applied to the left side of Einstein's equations, completely determine the properties of the isotropic electromagnetic field on the right side. In other words, the aforementioned conditions determine both the geometric properties of the space and the properties of a pervading isotropic electromagnetic field.

An isotropic electromagnetic field is such where the field invariants $F_{\alpha\beta}F^{\alpha\beta}$ and $F_{*\alpha\beta}F^{\alpha\beta}$, constructed from the electromagnetic field tensor $F_{\alpha\beta}$ and the field pseudo-tensor $F^{*\alpha\beta} = \frac{1}{2}\,\eta^{\alpha\beta\mu\nu}F_{\mu\nu}$ dual, are zero

$$F_{\alpha\beta}F^{\alpha\beta} = 0\,, \qquad F_{*\alpha\beta}F^{\alpha\beta} = 0\,, \tag{40}$$

so the isotropic electromagnetic field has a structure truncated to that of an electromagnetic field in general.

In our case we have no limitation on the structure of the electromagnetic field, so we use the energy-momentum tensor of the electromagnetic field in the general form [20]

$$T_{\alpha\beta} = \frac{1}{4\pi}\left(-F_{\alpha\sigma}F^{\ \ \sigma}_{\beta\cdot} + \frac{1}{4}\,F_{\mu\nu}F^{\mu\nu}g_{\alpha\beta}\right), \tag{41}$$

whence the observable density of the field energy $\rho = \frac{T_{00}}{g_{00}}$ and the trace $U = h^{ik}U_{ik}$ of the observable stress-tensor of the field $U^{ik} = c^2T^{ik}$ are connected by the relation

$$\rho c^2 = U\,. \tag{42}$$

In other words, if besides the gravitational field there is be only an electromagnetic field, we should have $\rho c^2 = U$ for distributed matter in the Einstein equations.

However, as seen in the 2nd equation of the system (37), $\rho c^2 - U \neq 0$ in the Einstein equations, for the only reason that, in the case we are considering, the laboratory space is filled not only by the Earth's gravitational field and an alternating magnetic field which supports the disc in air, but also another field appeared due to the fact that the oscillating disc perturbs the non-holonomic background of the space. The perturbation field, as shown in the previous Section, bears energy and momentum*, so it can be taken as a field of distributed matter. In other words,

> We have obtained a complete geometrization of matter consisting of an arbitrary electromagnetic field and a perturbation field of the non-holonomic background of the space.

3.4 The conservation law

When considering the geodesic equations in a space, the hon-holonomic background of which is perturbed by a disc undergoing oscillatory bounces orthogonal to its own plane, we need to know the space distribution of the perturbation, i.e. some relations between the functions $v_t = \frac{\partial v}{\partial t}$, $v_r = \frac{\partial v}{\partial r}$, $v_\varphi = \frac{\partial v}{\partial \varphi}$, $v_z = \frac{\partial v}{\partial z}$, which are respective partial derivatives of the value v of the linear velocity of the space rotation v_i.

The functions v_t, v_r, v_φ, v_z are contained in the left side (geometry) of the Einstein equations we have obtained. Therefore, from a formal point of view, to find the functions we should integrate the Einstein equations. However the Einstein equations are represented in a non-empty space, so the right side of the equations is not zero, but occupied by the energy-momentum tensor $T_{\alpha\beta}$ of distributed matter which fill the space. Hence, to obtain the functions v_t, v_r, v_φ, v_z from the Einstein equations, we should express the right side of the equations — the energy-momentum tensor of distributed matter $T_{\alpha\beta}$ — through the functions as well.

Besides, in our case, $T_{\alpha\beta}$ represents not only the energy-momentum of the electromagnetic field but also the energy-momentum produced by the field of the background space non-holonomity compensating the perturbation therein. Yet we cannot divide one energy-momentum tensor by another. So we must consider the energy-momentum tensor for the common field, which presents a problem, because we have no formulae for the components of the energy-momentum tensor of the common field. In other words, we are enforced to operate with the components of $T_{\alpha\beta}$ as merely some quantities ρ, J^i, and U^{ik}.

How to express $T_{\alpha\beta}$ through the functions v_t, v_r, v_φ, v_z, aside for by the Einstein equations? In another case we would be led to a dead end. However, our case of distributed matter is completely geometrized. In other words, the geometrical structure of the space and the space distribution of the energy-momentum tensor $T_{\alpha\beta}$ are the same things. We can therefore find the functions v_t, v_r, v_φ, v_z from the space distribution of $T_{\alpha\beta}$, via the equations of the conservation law

$$\nabla_\sigma T^{\alpha\sigma} = 0\,. \tag{43}$$

The conservation law in the chr.inv.-form, i.e. represented as the projections of equation (43) onto the time line and spatial section of an observer, is [15]

$$\left.\begin{aligned} &\frac{{}^*\partial\rho}{\partial t} + D\rho + \frac{1}{c^2}D_{ij}U^{ij} + \left({}^*\nabla_i - \frac{1}{c^2}F_i\right)J^i - \frac{1}{c^2}F_i\,J^i = 0\\ &\frac{{}^*\partial J^k}{\partial t} + 2\left(D^k_i + A^{\cdot k}_{i\cdot}\right)J^i + \left({}^*\nabla_i - \frac{1}{c^2}F_i\right)U^{ik} - \rho F^k = 0 \end{aligned}\right\} \tag{44}$$

*The fact that the space non-holonomity field bears energy and momentum was first shown in the earlier publication [27], where the field of a reference body was considered.

$$\left.\begin{aligned}
&\frac{\partial\rho}{\partial t}+\frac{\partial J^1}{\partial r}+\frac{\partial J^2}{\partial\varphi}+\frac{\partial J^3}{\partial z}+\frac{1}{r}J^1=0\\
&\frac{\partial J^1}{\partial t}-\left[(\cos\varphi+\sin\varphi)\,v_\varphi-r\,(\cos\varphi-\sin\varphi)\,v_r\right]J^2-\left[(\cos\varphi+\sin\varphi)\,v_z-v_r\right]J^3+\\
&+\frac{\partial U_{11}}{\partial r}+\frac{1}{r^2}\frac{\partial U_{12}}{\partial\varphi}+\frac{\partial U_{13}}{\partial z}+\frac{1}{r}\left(U_{11}-\frac{U_{22}}{r^2}\right)-\rho\left[\left(\Omega z_0\sin\frac{\Omega}{c}u\right)v_r+(\cos\varphi+\sin\varphi)\,v_t\right]=0\\
&\frac{\partial J^2}{\partial t}-\left[(\cos\varphi+\sin\varphi)\,\frac{v_\varphi}{r^2}-(\cos\varphi-\sin\varphi)\,\frac{v_r}{r}\right]J^1-\left[(\cos\varphi-\sin\varphi)\,\frac{v_z}{r}-\frac{v_\varphi}{r^2}\right]J^3+\\
&+\frac{\partial}{\partial r}\left(\frac{U_{12}}{r^2}\right)+\frac{1}{r^2}\left(\frac{1}{r^2}\frac{\partial U_{22}}{\partial\varphi}+\frac{\partial U_{23}}{\partial z}+\frac{3}{r}U_{12}\right)-\rho\left[\left(\Omega z_0\sin\frac{\Omega}{c}u\right)\frac{v_\varphi}{r^2}+\frac{(\cos\varphi-\sin\varphi)}{r}\,v_t\right]=0\\
&\frac{\partial J^3}{\partial t}+\left[(\cos\varphi+\sin\varphi)\,v_z-v_r\right]J^1+\left[r\,(\cos\varphi-\sin\varphi)\,v_z-v_\varphi\right]J^2+\\
&+\frac{\partial U_{13}}{\partial r}+\frac{1}{r^2}\frac{\partial U_{23}}{\partial\varphi}+\frac{\partial U_{33}}{\partial z}+\frac{1}{r}U_{13}-\rho\left[\left(\Omega z_0\sin\frac{\Omega}{c}u\right)v_z-\frac{GM}{z^2}+v_t+\Omega^2 z_0\cos\frac{\Omega}{c}u\right]=0
\end{aligned}\right\}\qquad(46)$$

where $\rho=\frac{T_{00}}{g_{00}}$, $J^i=\frac{cT_0^i}{\sqrt{g_{00}}}$ and $U^{ik}=c^2T^{ik}$ are the observable projections of the energy-momentum tensor $T_{\alpha\beta}$ of distributed matter. The chr.inv.-conservation equations, taking our assumptions for real experiment into account, take the simplified form

$$\left.\begin{aligned}
&\frac{\partial\rho}{\partial t}+\frac{\partial J^i}{\partial x^i}+\frac{\partial\ln\sqrt{h}}{\partial x^i}J^i=0\\
&\frac{\partial J^k}{\partial t}+2A^{\,k}_{i\cdot}J^i+\frac{\partial U^{ik}}{\partial x^i}+\frac{\partial\ln\sqrt{h}}{\partial x^i}U^{ik}+\\
&\qquad+\Delta^k_{im}U^{im}-\rho F^k=0
\end{aligned}\right\}.\qquad(45)$$

Substituting into the equations the formulae for D, D^k_i, $A^{\,k}_{i\cdot}$, $\frac{\partial\ln\sqrt{h}}{\partial x^i}$, Δ^k_{im}, and F^k, we obtain a system of the conservation equations (46) wherein we should substitute ρ, J^i, and U^{ik} from the Einstein equations (37) then, reducing similar terms, arrive at some relations between the functions v_t, v_r, v_φ, v_z. The Einstein equations (37) substituted into (46) evidently result in intractable equations. It seems that we will have no chance of solving the resulting equations without some simplification according to real experiment. We should therefore take the simplification into account from the beginning.

First, the scalar equation of the conservation law (44) under the conditions of a real experiment takes the form of (45), which in another notation is

$$\frac{\partial\rho}{\partial t}+{}^*\nabla_i\,J^i=0\,.\qquad(47)$$

The 2nd equation of (37) determines ρ: the quantity is $\rho\sim\frac{1}{c^2}$. Omitting the term proportional to $\frac{1}{c^2}$ as its effect is negligible in a real experiment, we obtain the scalar equation of the conservation law in the form*

$${}^*\nabla_i\,J^i=0\,,\qquad(48)$$

i.e. the chr.inv.-derivative of the common flow of the spatial momentum of distributed matter is zero to within the approximation of a first-order experiment. This finding has a very important meaning:

> Given a space, the non-holonomic background of which is perturbed by an oscillating disc, the common flow of the momentum of distributed matter on the spatial section of such a space is conserved in a first-order experiment.

Second, there are three states of the disc in Podkletnov's experiment: (1) uniform rotation; (2) non-uniform rotation (acceleration/deceleration); (3) non-rotating disc. To study the case of a rotating disc we should introduce, into the metric (25), additional terms which take the rotation into account. We don't do this now, for two reasons: (1) the additional terms introduced into the metric (25) make the equations of the theory too complicated; (2) the case of a non-rotating disc is that main case where, according Podkletnov's experiments, the weight-loss effect appears in the basic form; accelerating/decelerating rotation of the disc produces only additions to the basic weight-loss. So, to understand the origin of the weight-loss phenomenon it is most reasonable to first consider perturbation of the background field of the space non-holonomity by a non-rotating disc. Because such a disc lies horizontally in the plane $r\varphi$ (horizontal plane), we should assume $v_z=0$, while the fact that there $v_r\neq0$ and $v_\varphi\neq0$ means freedom for oscillation in the plane $r\varphi$ (accelerating or decelerating twists in the plane) as a result of vertical oscillation of such a disc (otherwise, for no oscillation in the plane $r\varphi$, the conservation equations would become zero). The fact that $\varphi\neq\text{const}$ in the equations means the same.

As a result, the conservation equations (46), with the aforementioned assumptions taken into account, take the form (49). The characteristics of distributed matter such as the momentum flow J^i and the stress-tensor U^{ik}, resulting from

*The chr.inv.-differential operators are completely determined, according to [15, 16], in Appendix 2.

$$\left.\begin{aligned}
&\frac{\partial J^1}{\partial t}-\left[(\cos\varphi+\sin\varphi)\,v_\varphi-r\,(\cos\varphi-\sin\varphi)\,v_r\right]J^2+v_r\,J^3+\frac{\partial U_{11}}{\partial r}+\frac{1}{r^2}\frac{\partial U_{12}}{\partial\varphi}+\frac{1}{r}\left(U_{11}-\frac{U_{22}}{r^2}\right)=0\\
&\frac{\partial J^2}{\partial t}-\left[(\cos\varphi+\sin\varphi)\,\frac{v_\varphi}{r^2}-(\cos\varphi-\sin\varphi)\,\frac{v_r}{r}\right]J^1+\frac{v_\varphi}{r^2}\,J^3+\frac{\partial}{\partial r}\left(\frac{U_{12}}{r^2}\right)+\frac{1}{r^2}\left(\frac{1}{r^2}\frac{\partial U_{22}}{\partial\varphi}+\frac{3}{r}\,U_{12}\right)=0\\
&\frac{\partial J^3}{\partial t}-v_r\,J^1-v_\varphi\,J^2+\frac{\partial U_{13}}{\partial r}+\frac{1}{r^2}\frac{\partial U_{23}}{\partial\varphi}+\frac{1}{r}\,U_{13}=0
\end{aligned}\right\}\qquad(49)$$

$$\left.\begin{aligned}
&\kappa J^1=\frac{(\cos\varphi-\sin\varphi)}{2r}\left(v_{r\varphi}-\frac{v_\varphi}{r}\right)-\frac{(\cos\varphi+\sin\varphi)}{2}\left(\frac{v_{\varphi\varphi}}{r^2}+\frac{v_r}{r}\right)\\
&\kappa J^2=\frac{1}{2r^2}\left[(\cos\varphi+\sin\varphi)\left(v_{r\varphi}-\frac{v_\varphi}{r}\right)-r\,(\cos\varphi-\sin\varphi)\;v_{rr}\right]\\
&\kappa J^3=-\frac{1}{2}\left(v_{rr}+\frac{v_{\varphi\varphi}}{r^2}+\frac{v_r}{r}\right)\\
&\kappa U_{11}=\frac{(\cos\varphi-\sin\varphi)}{2}\,v_r^2+(\cos\varphi\sin\varphi)\,\frac{v_\varphi^2}{2r^2}-\frac{\left(\cos^2\varphi-\sin^2\varphi\right)}{2}\,\frac{v_rv_\varphi}{r}-(\cos\varphi-\sin\varphi)\,\frac{v_{t\varphi}}{r}-\\
&-\frac{2GM}{z^3}-\left(\Omega z_0\sin\frac{\Omega}{c}u\right)\left(\frac{v_{\varphi\varphi}}{r^2}+\frac{v_r}{r}\right)\\
&\kappa U_{12}=\frac{1}{2}\left[v_rv_\varphi+(\cos\varphi+\sin\varphi)\,v_{t\varphi}+r\,(\cos\varphi-\sin\varphi)\,v_{tr}+2\left(\Omega z_0\sin\frac{\Omega}{c}u\right)\left(v_{r\varphi}-\frac{v_\varphi}{r}\right)\right]\\
&\kappa U_{13}=\frac{1}{2}\left[v_{tr}-(\cos\varphi-\sin\varphi)\,\frac{v_rv_\varphi}{r}+(\cos\varphi+\sin\varphi)\,\frac{v_\varphi^2}{r^2}\right]\\
&\frac{\kappa U_{22}}{r^2}=-(\cos\varphi\sin\varphi)\,\frac{v_r^2}{2}+\frac{(\cos\varphi+\sin\varphi)}{2}\,\frac{v_\varphi^2}{r^2}-\frac{\left(\cos^2\varphi-\sin^2\varphi\right)}{2}\,\frac{v_rv_\varphi}{r}-(\cos\varphi+\sin\varphi)\,v_{tr}-\\
&-\frac{2GM}{z^3}-\left(\Omega z_0\sin\frac{\Omega}{c}u\right)v_{rr}\\
&\kappa U_{23}=\frac{1}{2}\left[v_{t\varphi}+r\,(\cos\varphi-\sin\varphi)\,v_r^2-(\cos\varphi+\sin\varphi)\,v_rv_\varphi\right]\\
&\kappa U_{33}=\frac{\cos\varphi\sin\varphi}{2}\left(v_r^2-\frac{v_\varphi^2}{r^2}\right)+\frac{\left(\cos^2\varphi-\sin^2\varphi\right)}{2}\,\frac{v_rv_\varphi}{r}-(\cos\varphi+\sin\varphi)\,v_{tr}-(\cos\varphi-\sin\varphi)\,\frac{v_{t\varphi}}{r}-\\
&-\left(\Omega z_0\sin\frac{\Omega}{c}u\right)\left(v_{rr}+\frac{v_{\varphi\varphi}}{r^2}+\frac{v_r}{r}\right)
\end{aligned}\right\}\qquad(50)$$

the Einstein equations (37), were collected in complete form into the system (37). Under the aforementioned assumptions they take the form (50).

We substitute the respective components of J^i and U^{ik} (50) into the conservation equations (49). After algebra, reducing similar terms, the first two equations of (49) become identically zero, while the third equation takes the form:

$$v_r=\frac{v_\varphi}{r}\,,\qquad(51)$$

The solution $v_r=\frac{v_\varphi}{r}$ we have obtained from the conservation equations satisfies by the function

$$v=B(t)\,r\,e^{\varphi},\qquad(52)$$

where $B(t)$ is a function of time t. Specific formula for the function $B(t)$ should be determined by nature of the phenomenon or the conditions of the experiment.

The solution indicates a dependency between the distributions of v in the r-direction and φ-direction in the space, if the non-holonomic background is perturbed by a disc lying in the $r\varphi$ plane and oscillating in the z-direction.

In other words, the conservation equations in common with the Einstein equations we have obtained mean that:

> A disc, oscillating orthogonally to its own plane, perturbs the field of the background non-holonomity of the space. Such a motion of a disc places a limitation on the geometric structure of the space. The limitation is manifested as a specific distribution of the linear velocity of the space rotation. This distribution means that such a disc should also have small twists in its own plane due to the perturbed non-holonomic background.

$$\left.\begin{aligned}
&\ddot{r}-\left[(\cos\varphi+\sin\varphi)\,v_\varphi-r\,(\cos\varphi-\sin\varphi)\,v_r\right]\dot{\varphi}-\left[(\cos\varphi+\sin\varphi)\,v_z-v_r\right]\dot{z}-\\
&-(\cos\varphi+\sin\varphi)\,v_t-r\dot{\varphi}^2-\left(\Omega z_0\sin\frac{\Omega}{c}u\right)v_r=0\\
&\ddot{\varphi}+\left[(\cos\varphi+\sin\varphi)\,\frac{v_\varphi}{r^2}-(\cos\varphi-\sin\varphi)\,\frac{v_r}{r}\right]\dot{r}-\left[(\cos\varphi-\sin\varphi)\,\frac{v_z}{r}-\frac{v_\varphi}{r^2}\right]\dot{z}-\\
&-(\cos\varphi-\sin\varphi)\,\frac{v_t}{r}+\frac{2\dot{r}}{r}\,\dot{\varphi}-\left(\Omega z_0\sin\frac{\Omega}{c}u\right)\frac{v_\varphi}{r^2}=0\\
&\ddot{z}+\left[(\cos\varphi+\sin\varphi)\,v_z-v_r\right]\dot{r}+\left[r\,(\cos\varphi-\sin\varphi)\,v_z-v_\varphi\right]\dot{\varphi}-\\
&+\frac{GM}{z^2}-v_t-\left(\Omega z_0\sin\frac{\Omega}{c}u\right)v_z-\Omega^2 z_0\cos\frac{\Omega}{c}u=0
\end{aligned}\right\}\qquad(60)$$

3.5 The geodesic equations in the space. Final conclusion about the forces driving the Podkletnov effect

This is the final part of our mathematical theory of the Podkletnov effect. Here, using the Einstein equations and the equations of the conservation law we have developed, we deduce an additional force that produces the weight-loss effect in Podkletnov's experiment, i.e. the weight-loss over a superconducting disc which is supported in air by an alternating magnetic field.

As is well known, motion in a gravitational field of a free test-particle of rest-mass m_0 is described by the equations of geodesic lines (the geodesic equations). The geodesic equations are, from a purely mathematical viewpoint, the equations of parallel transfer of the four-dimensional vector of the particle's momentum $P^\alpha = m_0\frac{dx^\alpha}{ds}$ along the particle's 4-dimensional trajectory

$$\frac{dP^\alpha}{ds}+\Gamma^\alpha_{\mu\nu}P^\mu\frac{dx^\nu}{ds}=0\,,\qquad(53)$$

where $\Gamma^\alpha_{\mu\nu}$ are Christoffel's symbols of the 2nd kind, while ds is the 4-dimensional interval along the trajectory.

The geodesic equations (53), being projected onto the time line and spatial section of an observer, and expressed through the physical observable characteristics of a real laboratory space of a real observer, are known as the chr.inv.-geodesic equations. They were deduced in 1944 by Zelmanov [15, 16]. The related scalar equation is the projection onto the time line of the observer, while the 3-dimensional vector equation is the projection onto his spatial section, and manifests the 3rd Newtonian law for the test-particle:

$$\left.\begin{aligned}
&\frac{dm}{d\tau}-\frac{m}{c^2}F_i\mathrm{v}^i+\frac{m}{c^2}D_{ik}\mathrm{v}^i\mathrm{v}^k=0\\
&\frac{d(m\mathrm{v}^i)}{d\tau}+2m\left(D^i_k+A^{\cdot i}_{k\cdot}\right)\mathrm{v}^k-mF^i+m\Delta^i_{nk}\mathrm{v}^n\mathrm{v}^k=0
\end{aligned}\right\}\qquad(54)$$

where m is the relativistic mass of the particle, v^i is the 3-dimensional observable velocity of the particle, and τ is the physical observable or proper time* [15, 16]

$$m=\frac{m_0}{\sqrt{1-\mathrm{v}^2/c^2}}\,,\qquad \mathrm{v}^i=\frac{dx^i}{d\tau}\,,\qquad(55)$$

$$d\tau=\sqrt{g_{00}}\,dt+\frac{g_{0i}}{c\sqrt{g_{00}}}\,dx^i=\sqrt{g_{00}}\,dt-\frac{1}{c^2}\,v_i\,dx^i.\qquad(56)$$

With the simplifications for the real experiment we are considering, the chr.inv.-geodesic equations (54) take the form

$$\left.\begin{aligned}
&\frac{dm}{d\tau}=0\\
&\frac{d(m\mathrm{v}^i)}{d\tau}+2mA^{\cdot i}_{k\cdot}\mathrm{v}^k-mF^i+m\Delta^i_{nk}\mathrm{v}^n\mathrm{v}^k=0
\end{aligned}\right\}\qquad(57)$$

that is, in component notation,

$$\left.\begin{aligned}
&\frac{dm}{d\tau}=0\\
&\frac{d}{d\tau}\left(m\frac{d\mathrm{v}^1}{d\tau}\right)+2mA^{\cdot 1}_{k\cdot}\mathrm{v}^k-mF^1+m\Delta^1_{22}\mathrm{v}^2\mathrm{v}^2=0\\
&\frac{d}{d\tau}\left(m\frac{d\mathrm{v}^2}{d\tau}\right)+2mA^{\cdot 2}_{k\cdot}\mathrm{v}^k-mF^2+2m\Delta^2_{12}\mathrm{v}^1\mathrm{v}^2=0\\
&\frac{d}{d\tau}\left(m\frac{d\mathrm{v}^3}{d\tau}\right)+2mA^{\cdot 3}_{k\cdot}\mathrm{v}^k-mF^3=0
\end{aligned}\right\}\qquad(58)$$

which are actual chr.inv.-equations of motion of a free test-body in the space, whose non-holonomic homogeneous background is perturbed by an oscillating disc.

The scalar geodesic equation of (58) says

$$m=\mathrm{const}\,,\qquad(59)$$

so taking this fact into account and introducing the notation $\mathrm{v}^1=\frac{dr}{d\tau}=\dot{r}$, $\mathrm{v}^2=\frac{d\varphi}{d\tau}=\dot{\varphi}$, $\mathrm{v}^3=\frac{dz}{d\tau}=\dot{z}$, we obtain a system of three vector equations of motion of the test-body (60), wherein $v_t=\frac{\partial v}{\partial t}$, $v_r=\frac{\partial v}{\partial r}$, $v_\varphi=\frac{\partial v}{\partial\varphi}$, $v_z=\frac{\partial v}{\partial z}$.

*This is that real time which is registered by the observer in his real laboratory space. Intervals of the physical observable time $d\tau$ and the observable spatial coordinates dx^i are determined, by the theory of physical observable quantities (chronometric invariants) as the projections of the interval of the 4-dimensional coordinates dx^α onto the time line and spatial section of an observer, i.e.: $b_\alpha dx^\alpha = cd\tau$, $h^i_\alpha dx^\alpha = dx^i$ [15, 16]. See Appendix 2 for the details of such a projection.

Because the terms containing z_0 in equations (60) are very small, they can be considered to be small harmonic corrections. Such equations can always be solved using the small parameter method of Poincaré. The Poincaré method is also known as the perturbation method, because we consider the right side as a perturbation of a harmonic oscillation described by the left side. The Poincaré method is related to exact solution methods, because a solution produced with the method is a power series expanded by a small parameter (see Lefschetz, Chapter XII, §2 of [21]).

However our task is much simpler. We are looking for an approximate solution of the system of the vector equations of motion in order to see the main forces acting in the basic Podkletnov experiment. We therefore simplify the equations as possible. First we take into account that, in the condition of Podkletnov's experiment, the suspended test-body has freedom to move only in the z-direction (i.e. up or down in a vertical direction, which is the direction of the acting force of gravity). In other words, concerning a free test-body falling from above the disc, we take $\dot{r} = 0$ and $\dot{\varphi} = 0$ despite the forces $\ddot{r}$ and $\ddot{\varphi}$ acting it in the r-direction and the φ-direction are non-zero. Second, rotational oscillation of the disc in the $r\varphi$–plane is very small. We therefore regard φ as a small quantity, so $\sin\varphi \simeq \varphi$ and $\cos\varphi \simeq 1$. Third, by the conservation equations, $v_\varphi = r\, v_r$.

Taking all the assumptions into account, the equations of motion (60) take the much simplified form

$$\left.\begin{aligned} &\ddot{r} + v_r \dot{z} - (1+\varphi)\, v_t - \left(\Omega z_0 \sin\frac{\Omega}{c} u\right) v_r = 0 \\ &\ddot{\varphi} + \frac{v_r}{r}\, \dot{z} - (1-\varphi)\, v_t - \left(\Omega z_0 \sin\frac{\Omega}{c} u\right) \frac{v_r}{r} = 0 \\ &\ddot{z} + g - v_t - \Omega^2 z_0 \cos\frac{\Omega}{c} u = 0 \end{aligned}\right\} \qquad (61)$$

where $g = \frac{GM}{z^2}$ is the acceleration produced by the Earth's force of gravity, remaining constant for the experiment.

For Podkletnov's experiment, $v_t = \text{const}$, and this value depends on the specific parameters of the vertically oscillating disc, such as its diameter, the frequency and amplitude of its vibration. The harmonic term in the third equation is a small correction which can only shake a test-body in the z-direction; this term cannot be a source of a force acting in just one direction. Besides, the harmonic term has a very small numerical value, and so it can be neglected. In such a case, the third equation of motion takes the simple form

$$\ddot{z} + g - v_t = 0\,, \qquad (62)$$

where the last term is a correction to the acting force of gravity due to the perturbed field of the background space non-holonomity.

Integrating the equation $\ddot{z} = -g + v_t$, we obtain

$$z = -\frac{g - v_t}{2}\,\tau^2 + C_1\tau + C_2\,, \qquad (63)$$

where the initial moment of time is $\tau_0 = 0$, the constants of integration are $C_1 = \dot{z}_0$ and $C_2 = z_0$. As a result, if the test-body is at rest at the initial moment of time ($\dot{z}_0 = 0$), its vertical coordinate z at another moment of observable time is

$$z = z_0 - \frac{g\tau^2}{2} + \frac{v_t\tau^2}{2}\,. \qquad (64)$$

The result we have obtained isn't trivial because the additional forces obtained within the framework of our theory originate in the field of the background space non-holonomity perturbed by the disc. As seen from the final equation of motion along the z-axis (62), such an additional force acts everywhere against the force of gravity. So it works like "negative gravity", a truly *anti-gravity force*.

Within the framework of Classical Mechanics we have no space-time, hence there are no space-time terms in the metrics which determine the non-holonomity of space. So such an anti-gravity force is absent in Classical Mechanics.

Such an anti-gravity force vanishes in particular cases of General Relativity, where the pseudo-Riemannian space is holonomic, and also in Special Relativity, where the pseudo-Riemannian space is holonomic by definition (in addition to the absence of curvature, gravitation, and deformation).

So the obtained anti-gravity force appears only in General Relativity, where the space is non-holonomic.

It should be noted that the anti-gravity force $F = m v_t$ isn't related to a family of forces of inertia. Inertial forces are fictitious forces unrelated to a physical field; an inertial force appears only in mechanical contact with that physical body which produces it, and disappears when the mechanical connexion ceases. On the contrary, the obtained anti-gravity force originates from a real physical field — a field of the space non-holonomity, — and is produced by the field in order to compensating for the perturbation therein. So the anti-gravity force obtained within the framework of our theory is a real physical force, in contrast to forces of inertia.

Concerning Podkletnov's experiment, we should take into account the fact that a balance suspended test-body isn't free, due to the force of reaction of the pier of the balance which completely compensates for the common force of attraction of the test-body towards the Earth (the body's weight). As a result such a test-body moves along a non-geodesic world-trajectory, so the equations of motion of such a particle have non-zero right side containing the force of the reaction of the pier. In the state of static weight, the common acceleration of the test-body in the z-direction is zero ($\ddot{z} = 0$), hence its weight Q is

$$Q = mg - m v_t\,. \qquad (65)$$

The quantity v_t contained in the additional anti-gravity force $F = m v_t$ is determined by the parameters of the small twists of the disc in the horizontal plane, the frequency of which is the same as the frequency Ω of vertical oscillation of the disc, while the amplitude depends on parameters of the

disc, such as its radius r and the amplitude z_0 of the oscillation. (A calculation for such an anti-gravity force in the condition of a real experiment is given in the next Section. As we will see, our theory gives good coincidence with the weight-loss effect as measured in Podkletnov's experiment.)

The geodesic equation we have obtained in the field of an oscillating disc allows us to draw a final conclusion about the origin of the forces which drive the weight-loss effect in Podkletnov's experiment:

> A force produced by the field of the background space non-holonomity, compensating for a perturbation therein, works like *negative gravity* in the condition of an Earth-bound experiment. Being produced by a real physical field that bears its own energy and momentum, such an anti-gravity force is a real physical force, in contrast to fictitious forces of inertia which are unrelated to physical fields.
>
> In the conditions of Podkletnov's experiment, a horizontally placed superconducting disc, suspended in air due to an alternating magnetic field, undergoes oscillatory bounces in a vertical direction (orthogonal to the plane of the disc) with the same frequency of the magnetic field. Such an oscillation perturbs the field of the background space non-holonomity, initially homogeneous. As a result the background non-holonomity field is perturbed in three spatial directions, including the horizontal plane (the plane of the disc), resulting in small amplitude oscillatory twists about the vertical direction. The oscillatory twists determine the *anti-gravity force*, produced by the perturbed field of the background space non-holonomity, and act in the vertical directing against the force of gravity. Any test-body, placed in the perturbed non-holonomity field above such a vertically oscillating disc, should experience a loss in its weight, the numerical value of which is determined by the parameters of the disc and its oscillatory motion in the vertical direction. If such a disc rotates with acceleration, this should be the source of an addition perturbation of the background non-holonomity field and, hence, a substantial addition to the weight-loss effect should be observed in experiment. (Uniform rotation of the disc should give no effect.)

Herein we have been concerned with only a theory of a phenomenon discovered by Podkletnov (we refer to this as the *Podkletnov effect*, to fix the term in scientific terminology).

According to our theory, superconductor technology accounts in Podkletnov's experiment only for levitation of the disc and driving it into small amplitude oscillatory motion in the vertical direction. However, it is evident that this isn't the only way to achieve such a state for the disc.

Furthermore, we show that there are also both mechanical and nuclear systems which can simulate the Podkletnov effect and, hence, be the sources of continuous and explosive energy from the field of the background space non-holonomity.

Such a mechanical system, simulating the conditions of the Podkletnov effect, provides a possibile means of continuous production of energy from the space non-holonomity field. At the same time we cannot achieve high numerical values of the oscillatory motion in a mechanical system, so the continuous production of energy might be low (althopugh it may still reach useful values).

On the contrary, processes of nuclear decay and synthesis, due to the instant change of the spin configuration among nucleons inside nuclei, should have high numerical values of v_t, and therefore be an explosive source of energy from the field of the background space non-holonomity.

Both mechanical and nuclear simulations of the Podkletnov effect can be achieved in practice.

4 A new experiment proposed on the basis of the theory

4.1 A simple test of the theory of the Podkletnov effect (alternative to superconductor technology)

According our theory, the Podkletnov effect has a purely mechanical origin, unrelated to superconductivity — the field of the background space non-holonomity being perturbed by a disc which undergoes oscillatory bounces orthogonal to its own plane, produces energy and momentum flow in order to compensate for the perturbation therein. Owing to this, we propose a purely mechanical experiment which reproduces the Podkletnov effect, equivalent to Podkletnov's original superconductor experiment, which would be a cheap alternative to costly superconductor technology, and also be a simple mechanical test of the whole theory of the effect.

What is the arrangement of such a purely mechanical system, which could enable reproduction of the Podkletnov effect? Searching the scientific literature, we found such a system. This is the *vibration balance* [22], invented and tested in the 1960–1970's by N. A. Kozyrev, a famous astronomer and experimental physicist of the Pulkovo Astronomical Observatory (St. Petersburg, Russia). Below is a description of the balance, extracted from Kozyrev's paper [22]:

"The vibration balance is an equal-shoulder balance, where the pier of the central prism is connected to a vibration machine. This vibration machine produces vertical vibration of the pier. The acceleration of the vibration is smaller than the acceleration of the Earth's gravitation. Therefore the prism doesn't lose contact with the pier, only alternating pressure results. Thus the distance between the centre of gravity and the cone of the prism remains constant while the weight and the balance don't change their own measurement precision. The vertical guiding rods, set up along the pier, exclude the possibility of horizontal motion of the pier. One of two samples of the same mass is rigidly suspended by the yoke of the balance, while the second sample is suspended by an elastic material. Here the force required to lift the yoke is just a small percentage of the force required to lift the rigidly fixed sample. Therefore, during vibration of the balance, there is stable kinematic of the yoke, where the point O (the point of hard suspension)

doesn't participate in vibration, while the point A (the point of elastic suspension) has maximal amplitude of oscillation which is double the amplitude of the central prism C. Because the additional force, produced during vibration, is just a few percent more than the static force, the yoke remains fixed without inner oscillation, i.e. without twist, in accordance with the requirement of static weight.

We tested different arrangements of balances under vibration. The tested balances had different sensitivities, while the elastic material was tried with rubber, a spring, etc. Here is detailed a description of the vibration balance which is currently in use. This is a technical balance of the second class of sensitivity, with a maximum payload of 1 kg. A 1 mm deviation of the measurement arrow, fixed on the yoke, shows a weight of 10 mg. The centre of gravity of the yoke is located $\sim$1 cm below the pier of the central prism. The length of the shoulders of the yoke is: OC = CA = l = = 16 cm. The amplitude of vibration is $a \approx 0.2$ mm. Thus the maximum speed of the central prism is $v = \frac{2\pi}{T} a \simeq 2$ cm/sec, while its maximum acceleration $\left(\frac{2\pi}{T}\right)^2 a = 2 \times 10^2$ is about 20% of the acceleration of the Earth's gravitation. We regularly used samples of 700 g. One of the samples was suspended by a rubber, the strain of which for 1 cm corresponds 100 g weight. So, during vibration, the additional force on the yoke is less than 10 g and cannot destroy the rigidity of the yoke. The elastic rubber suspension absorbs vibration so that the sample actually rests.

This balance, as well as all recently tested systems, showed each time the increase of the weight of the elastically suspended sample. This additional force $\triangle Q$ is proportional to the weight of the sample Q, besides $\triangle Q/Q = 3 \times 10^{-5}$. Hence, having $Q = 700$ g, $\triangle Q = 21$ mg and the force momentum twisting the yoke is 300 dynes$\times$cm.

[. . .] From first view one can think that, during such a vibration, the pier makes twists around the resting point O. In a real situation the points of the pier are carried into more complicated motion. The central prism doesn't lose contact with the pier; they are connected, and move only linearly. Therefore the central part of the yoke, where its main mass is concentrated, has no centrifugal acceleration. What is about the point O, this point in common with the rigidly suspended sample is fixed in only the vertical direction, but it can move freely in the horizontal direction. These horizontal displacements of the point O are very small. Naturally, they are $\frac{a^2}{2l}$, i.e. ~ 0.1 μm in our case. Despite that, the small displacements result a very specific kinematic of the yoke. During vibration, each point of the yoke draws an element of an ellipse, a small axis of which lies along the yoke (in the average position of it). The concavities of the elements in the yoke's sections O–C and C–A are directed opposite to each other; they produce oppositely directed centrifugal forces. Because $\bar{v}^2$ is greater in the section C–A, the centrifugal forces don't compensate each other completely: as a result there in the yoke a centrifugal force acts in the A-direction (the direction at the point of the elastically suspended sample). This centrifugal acceleration has maximum value at the point A. We have $\bar{v}^2 = \frac{4\pi^2}{T^2} a^2 = 6$ cm^2/sec^2. From here we obtain the curvature radius of the ellipse: $\rho = 4l = 60$ cm. So the centrifugal acceleration is $\frac{\bar{v}^2}{\rho} = 0.1$ cm/sec^2."

Such a vibration balance is shown in the upper picture of Fig. 4. An analogous vibration balance is shown in the lower picture of Fig. 4: there the vibration machine is connected

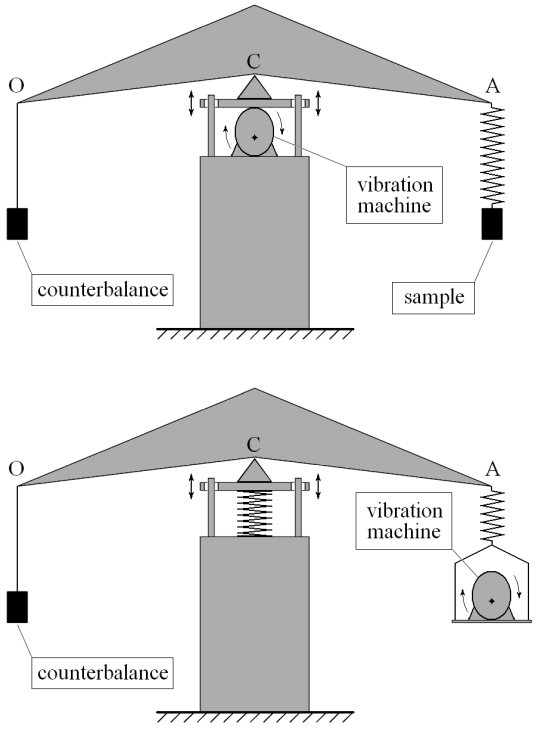

Fig. 4: The vibration balance — a mechanical test of the whole theory of the Podkletnov effect (a simple alternative to costly superconductor technology).

not to the pier of the central prism, but to he elastic suspension, while the prism's pier is supported by a spring; such a system should produce the same effect.

To understand how the Podkletnov effect manifests with the vibration balance, we consider the operation of the balance in detail (see Fig. 5).

The point O of the yoke undergoes oscillatory bounces in the r-direction with the amplitude d, given by

$$d = l - l\cos\alpha = l - l\sqrt{1 - \sin^2\alpha} = \\ = l - l\sqrt{1 - \frac{a^2}{l^2}} \simeq l - l\left(1 - \frac{a^2}{2l^2}\right) \simeq \frac{a^2}{2l}\,, \qquad (66)$$

while b is

$$b = d\tan\alpha = d\,\frac{a}{l\cos\alpha} \simeq \frac{a^3}{2l^2\left(1 - \frac{a^2}{2l^2}\right)} \simeq \frac{a^3}{2l^2 - a^2}\,. \qquad (67)$$

The point A undergoes oscillatory bounces in the z-direction with the amplitude $2a$, while its oscillatory motion in the r-direction has the amplitude

$$c = 2l - 2l\cos\alpha - d = d\,. \qquad (68)$$

The oscillatory bouncing of the points O and A along the elements of an ellipse is an accelerating/decelerating rotational motion around the focus of the ellipse. In such a case, by definition of the space non-holonomity as the non-orthogonality of time lines to the spatial section, manifest

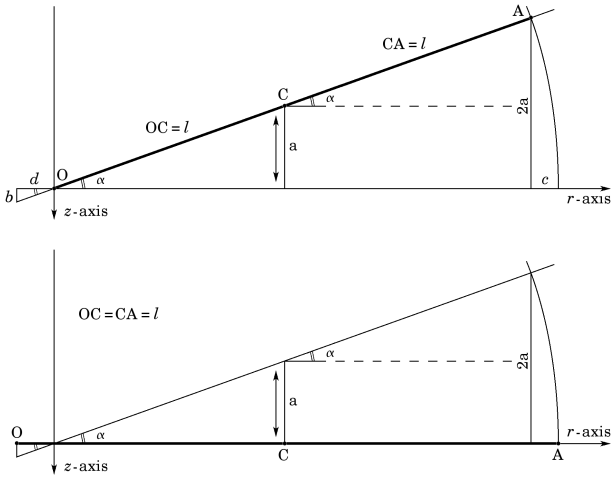

Fig. 5: The yoke of the vibration balance in operation. The yoke OA is indicated by the bold line. The double arrow shows the oscillatory bouncing motion of the point C, which is the point of connexion of the central prism and the central point of the yoke. The lower picture shows the yoke in its initial horizontal position. The upper picture shows the yoke in the upper position, at maximum deviation from the state of equilibrium.

as a three-dimensional rotation, points O and A during the oscillatory motion along respective elliptic elements, are the *source of a local field of the space non-holonomity*. Respective tangential accelerations $\bar{v}_t$ at the points O and A determine the sources.

Given that the background space is non-holonomic, such a field of the local non-holonomity is a *perturbation field* in the non-holonomic background. In other words, points O and A, in common with the respective samples mechanically connected to the points, are the sources of respective perturbation fields in the background field of the space non-holonomity.

Each point of the yoke, being carried into such an oscillatory motion, is the source of such a perturbation field. On the other hand, the average tangential acceleration of the motion, $\bar{v}_t$, takes its maximum value at the point A, then substantially decreases to the point O where it is negligible. Therefore such a yoke can be approximated as a non-symmetric system, where the end-point A is the source of a perturbation field in the non-holonomic background, while the end-point O isn't such a source.

According to the Einstein equations we have obtained in (35), the energy and momentum of a perturbation field in the non-holonomic background are produced by the whole field of the background space non-holonomity in order to compensate for the perturbation therein*. So the energy produced on a test-body in such a perturbation field isn't limited by the energy of the source of the perturbation (an oscillator, for instance), but can increase infinitely.

According to the geodesic equations (61) we have obtained in a perturbed non-holonomic field, the momentum of such a perturbation field manifests as the additional forces which act in all three directions r, φ, z relative to the source of the perturbation. If considering a free test-body constrained to move only along only the Earth's gravitational field-lines (falling freely in the z-direction), such an add-on force is expressed in the geodesic equation along the z-axis (62)

$$\ddot{z} + g - v_t = 0 \qquad (69)$$

as $F = m v_t$, and works against the force of gravity mg. In the situation of a static weight the total acceleration of such a sample is zero, $\ddot{z} = 0$, while the other forces are put into equilibrium by the weight of the sample (65)

$$Q = mg - m v_t = Q_0 - \triangle Q\,. \qquad (70)$$

A source of perturbation cannot be an object of application of a force produced due to the perturbation. Therefore the sample O is the object of application of an anti-gravity force $F = m v_t$ due to a field of the anti-gravity accelerations v_t, a source of which is the oscillatory bouncing system of the point A in common with the elastically suspended sample, while the point A itself in common with the sample has no such anti-gravity force applied to it. As a result the weight of the sample rigidly suspended at the end-point O, decreases as $\triangle Q = m v_t$, while the weight of the sample A remains the same:

$$Q_{\mathrm{O}} = mg - m v_t\,, \qquad Q_{\mathrm{A}} = mg\,. \qquad (71)$$

As a result, such a balance, during its vibration, should demonstrate a weight-loss of the rigidly suspended sample O and, respectively, a twist of the balance's yoke to the elastically suspended sample A. Such a weight-loss effect on the rigidly suspended sample, which is a fictitious increase of the weight of the elastically suspended sample, was first observed during the years 1960–1970's in the pioneering experiment of Kozyrev [22].

The half-length horizontal section of a superconducting disc suspended in air by an alternating magnetic field in Podkletnov's experiment (see Fig. 2) can be approximated by the yoke of the aforementioned vibrational balance. This is because the vertical oscillation of such a disc by an alternating magnetic field isn't symmetric in the disc's plane, so such a disc has a small oscillatory twisting motion in the vertical plane to the yoke of the vibration balance†.

*Note that we deduced the Einstein equations (35) for a space pervaded not only by an electromagnetic field, but also by distributed matter characterised by arbitrary properties. If only an electromagnetic field, there would be $\rho c^2 = U$. However $\rho c^2 - U \neq 0$ in the Einstein equations (35). This can be due to a number of reasons, the presence of an elastic force which compresses a spring, for instance. Therefore the Einstein equations we have obtained (35) are applicable to a laboratory space containing such a vibration balance.

†This is despite the fact that such a disc has so small an amplitude and so high a frequency of oscillatory twisting motion, that it seems to be levitating when almost at rest.

As a result, such a disc should experience the anti-gravity force $F = m v_t$ at the end-points of the disc, along the whole perimeter. Common action of the forces should produce:

1. The weight-loss effect $\triangle Q = m v_t$ on the disc itself. The weight-loss of the disc should increase if the disc has accelerating/decelerating rotation;
2. Respective weight-loss effect on any test-body located over the disc along the vertical axis z, according to the field of anti-gravity accelerations v_t.

Therefore the disc in Podkletnov's experiment and a vibration balance of the aforementioned type are equivalent systems. So both the superconductor experiment and the vibration balance should be described by the same theory we have adduced herein, and produce the same weight-loss effect as predicted by the theory.

The numerical value of such an anti-gravity acceleration, v_t, can also be calculated within the framework of our theory of the Podkletnov effect, and thus checked in experiment.

According to our theory, the value v of the perturbation isn't dependent on the vertical direction (the z-direction in our coordinates). Therefore only the horizontal oscillatory bouncing motion of point A (in common with the sample rigidly suspended there) perturbs the background field of the space non-holonomity. According to Fig. 5, the tangential acceleration of the point A in its oscillatory motion with amplitude $2a$ along an ellipse with the radius $\rho = 4l$, is directed in the z-direction. So the tangential acceleration cannot perturb the non-holonomic background. However there is another tangential acceleration of the point A, which results from the oscillatory motion of the point with the amplitude c (numerically $c = d$) around the upper location of the point A. This tangential acceleration is directed along the r-axis, so it is the source of a local perturbation in the non-holonomic background. The angle of the small twist at the point A during such an oscillation is $\varphi = \frac{d}{2\pi a} = \frac{a}{4\pi l}$, so the average angular acceleration of the motion is $\bar{\ddot{\varphi}} = \frac{1}{2}\ddot{\varphi} = \frac{\Omega^2 a}{8\pi l}$. The average tangential acceleration of the motion, directed in the r-direction, is $\bar{v}_t = 2a\bar{\ddot{\varphi}}$, i.e.

$$\bar{v}_t = \frac{\Omega^2 a^2}{4\pi l} = \frac{\pi \nu^2 a^2}{l}\,, \qquad (72)$$

which characterizes, according to the definition of the space non-holonomity, the local perturbation in the background field of the space non-holonomity.

Consider a vibration balance like that in Kozyrev's original experiment [22]. Each shoulder of the yoke has the length $l = 16$ cm, so the total length of the yoke is 32 cm. Let the central prism of the balance undergo oscillatory bounces in the vertical direction with an amplitude of $a = 0.020$ cm, so the amplitude of the point A is $2a = 0.040$ cm. One of the samples is rigidly suspended at point O of the yoke, while the other sample is suspended at point A by an elastic medium. Both samples have the same mass: 700 g. According to our theory, the Podkletnov effect should appear in the balance as a weight loss $\triangle Q$ of the sample O, dependent on the frequency as follows:

ν, Hz	v_t, cm/sec^2	$\triangle Q/Q$	$\triangle Q$, mg	$\triangle Q_{\text{exp}}$, mg
30	0.071	7.2×10^{-5}	50	
25	0.049	5.0×10^{-5}	35	
20	0.031	3.2×10^{-5}	22	21
15	0.018	1.8×10^{-5}	13	
10	0.0079	8.0×10^{-6}	5.6	

Table 1: The weight-loss effect, calculated with our theory of the Podkletnov effect, for a vibration balance with the same characteristics as that of Kozyrev's pioneering experiment [22]. The last column gives the numerical value of the weight-loss effect observed in Kozyrev's experiment, at a constant frequency of 20 Hz.

Kozyrev measured $\triangle Q = 21$ mg at a fixed frequency of $\nu = 20$ Hz in his experiment [22]. This corresponds with $\triangle Q = 22$ mg predicted by our theory*.

For Podkletnov's experiment, we haven't enough data for the amplitude of oscillatory bouncing motion of the superconductor disc. Despite this, we can verify our theory of the phenomenon in another way, due to the fact that Podkletnov observed a dependence of the weight-loss effect on the oscillation frequency.

Although dependency on frequency was observed in each of Podkletnov's experiments, we only have detailed data for the 1997 experiment, from publication [2]. We give in Table 2 Podkletnov's experimental values of $\triangle Q/Q$, measured on a sample located in the field of a $275/80\times10$ mm superconductor toroid at vibration frequencies of the toroid from 3.1 MHz to 3.6 MHz and the constant rotation speed 4300 rpm. The last column gives the increasing values of $\triangle Q/Q$, calculated by our theory where the weight-loss effect should be dependent on the square of the vibration frequency:

ν, MHz	$(\triangle Q/Q)_{\text{exp}}$	$(\triangle Q/Q)_{\text{theor}}$
3.1	2.2×10^{-3}	
3.2	2.3×10^{-3}	2.3×10^{-3}
3.3	2.4×10^{-3}	2.5×10^{-3}
3.4	2.6×10^{-3}	2.6×10^{-3}
3.5	2.9×10^{-3}	2.8×10^{-3}
3.6	3.2×10^{-3}	3.0×10^{-3}

Table 2: The increase of the weight-loss effect $(\triangle Q/Q)_{\text{exp}}$ with vibration frequency ν, measured in Podkletnov's experiment of 1997 [2], in comparison to the value $(\triangle Q/Q)_{\text{theor}}$ calculated by our theory of the phenomenon.

*We should also add that, coming from the geodesic equation along the z-axis, which is the third equation of (61), to the simplified form (62) thereof, we omitted the harmonic term from consideration. If the term is included, the vibration balance experiment should reveal not only an increase of the weight-loss effect with the frequency, but also resonant levels in it. The resonant levels, in further experiment, would be an additional verification of our theory.

We see that our theory is in very close accord with Podkletnov's experimental data. Furthermore, according to Podkletnov [2], despite the high measurement precision of the balance used in his experiment, some error sources produced systematic error in the order of 10^{-3} during the experiment. Taking this into account, we conclude that our theory is *sufficiently coincident* with Podkletnov's experimental data.

Podkletnov observed a decrease of the air pressure over the working device in the laboratory, and also a force distributed in a radial direction. We point out that the geodesic equations (61) obtained within the framework of our theory show forces, aside for the vertically acting anti-gravity force (i.e. acting in the z-direction), acting in the directions r and φ as well, produced by the perturbed field of the space non-holonomity. We therefore interpret Podkletnov's observations as a qualitative verification of our theory.

Podkletnov measured a much greater weight-loss effect over a disc during its accelerating/braking rotation. We haven't developed a theory for a rotating disc yet. Despite that, by analogy with our theory for a non-rotating disc, we can qualitatively predict that a field of the anti-gravity acceleration v_t produced by a rotating disc should be proportional to the radius of the disc and its angular acceleration, in accordance with the fact that Podkletnov's experiment is very difficult to reproduce on small discs, diameter about $1''$. Following Podkletnov, the weight-loss effect will be surely measured on a disc of at least $5''$ diameter.

Finally, complete verification of our theory of the Podkletnov effect should usher in new experimental checks for the frequency dependency of the weight-loss, which should appear in both the vibration balance and the Podkletnov superconductor device. With a new vibration balance experiment and a superconductor experiment confirming the frequency dependency according to (72), our theory of the Podkletnov effect would be completely verified.

4.2 New energy sources and applications to space travel

Due to the predictions of our theory, we have the possibility of the Podkletnov effect on such a simple device as the vibration balance, which is a thousand times cheaper and accessible than superconductor technology. In other words, being armed with the theory, it is more reasonable to use the weight-loss effect in practice with other devices which, working on principles other than the Podkletnov superconductor device, could easily reproduce the effect in both an Earth-bound laboratory and in space.

On the basis of our theory, new engineering applications such as anti-gravity devices and devices which could be used as new sources of energy, might be developed.

Anti-gravity engines for air and space travel. There can be at least two kinds of such engines, projected on the basis of our theory:

1. Land-based engines, which produce a strong anti-gravity acceleration field due to the Podkletnov effect. The anti-gravity acceleration field doesn't depend on the vertical distance from the disc, which generates it in Podkletnov's experiment. Due to this fact, a land-based engine, producing a beam of the anti-gravity acceleration field focused on a flying apparatus, can be used by the flying vehicle as a power station. The anti-gravity acceleration in the beam becomes the same as the acceleration of free fall. There can be limitation only from the scattering of the beam with distance. So such a land-based engine is suitable for short distances used in air travel*;
2. Engines located on board of a flying vehicle, that can be more suitable for both air and space travel. Such an engine, being the source of a field of the anti-gravity acceleration, cannot be the subject of application of the anti-gravity force produced in the field. However the force applies to the other parts of the apparatus, as in the vibration balance experiment or Podkletnov's experiment.

We note that in both cases, it isn't necessary to use a purely mechanical kernel for such an engine, as for the vibration balance experiment and Podkletnov's experiment considered in this paper. Naturally, using a mechanical oscillatory bouncing motion or accelerating/braking rotation, the maximum acceleration in the generated anti-gravity field is limited by the shock resistance of the mechanical aspects of the engine. This substantial limitation can be overcome if instead of solid bodies, liquids (liquid metal like mercury, for instance) or liquid crystals are driven into such motion by high frequency electromagnetic fields.

Devices which could be the source of new energy. This is another application of our theory, the experimental realization of which differs from the vibration balance experiment and Podkletnov's experiment. According to our theory, the coupling energy between the nucleons in a nucleus should be different due to the Podkletnov effect depending on the common orientation of the nucleons' spins in the nucleus. As a result, we could have a large explosive production of energy during not only self-decay of heavy elements like uranium and the trans-uraniums, but also by destroying the nuclei of the lightweight elements located in the middle of the Periodic Table of Elements. Of course, not just any nucleus will be the source of such energy production, but only those where, by our theory, the Podkletnov effect works, due to the specific orientation of the spins in the strong interaction amongst the nucleons.

Such an energy source, being free of deadly radiation or radioactive waste, could be a viable alternative to nuclear power plants.

*This kind of anti-gravity engine was first proposed in 2006 by Eugene Podklenov, in his interview [8].

Acknowledgements

We dedicate this research to the memory of Prof. Kyril Stanyukovich (1916–1989) and Dr. Abraham Zelmanov (1913–1987), ours teachers, and also Prof. Nikolai Kozyrev (1908–1983) and Dr. Roberto di Bartini (1897–1974) whose influence on our scientific views has been so great.

We also are very thankful to Delyan Zhelyazov for a few typing mistakes found by him in the formulae when this issue was sent to print.

Submitted on May 21, 2007
Accepted on May 31, 2007
Corrected online on December 08, 2007

References

1. Podkletnov E. and Nieminen R. A possibility of gravitational force shielding by bulk $YBa_2Cu_3O_{7-x}$ superconductor. *Physica C*, v. 203, 1992, 441–444.
2. Podkletnov E. Weak gravitation shielding properties of composite bulk $YBa_2Cu_3O_{7-x}$ superconductor below 70 K under e. m. field. arXiv: cond-mat/9701074.
3. Seife C. NASA is spending over half a million dollars on bizarre antigravity research. *New Scientist Magazine*, Issue 2172, February 06, 1999.
4. Wertheim M. Defying the shackles of gravity is a dream enshrined in myth and the human psyche. Now NASA will test a machine to determine if it is also real science. *Los Angeles Times*, March 24, 2002.
5. Boeing tries to defy gravity: an anti-gravity device would revolutionise air travel. *BBC News*, Monday, July 29, 2002.
6. Cohen D. Anti-gravity research on the rise. *New Scientist News*, July 30, 2002.
7. Ball Ph. Antigravity craft slips past patent officers: "Impossible" device gets seal of approval. *Nature*, v. 438, November 10, 2005, 139.
8. Ventura T. Interview with Dr. Eugene Podkletnov, April 10, 2006. It is accessed on http://www.americanantigravity.com/documents/Podkletnov-Interview.pdf
9. Podkletnov E. and Modanese G. Impulse gravity generator based on charged $YBa_2Cu_3O_{7-y}$ superconductor with composite crystal structure. arXiv: physics/0108005.
10. Alexandrov P. S. Combinatorial topology. Dover Publications, Mineola (NY), 1998 (rep. from the first edition of 1947).
11. Oros di Bartini R. Some relations between physical constants. *Doklady Acad. Nauk USSR*, 1965, v. 163, No. 4, 861–864.
12. Oros di Bartini R. Relations between physical constants. *Problems of the Theory of Gravitation and Elementary Particles*, Ed. by K. P. Stanyukovich and H. A. Sokolik, Moscow, Atomizdat, 1966, 249–266.
13. Oros di Bartini R. Relations between physical constants. *Progress in Physics*, 2005, v. 3, 34–40.
14. Raschewski P. K. Riemannsche Geometrie und Tensoranalysis. Deutsche Verlag der Wissenschaften, Berlin, 1959.
15. Zelmanov A. L. Chronometric invariants. Dissertation thesis, 1944. American Research Press, Rehoboth (NM), 2006.
16. Zelmanov A. L. Chronometric invariants and co-moving coordinates in the general relativity theory. *Doklady Acad. Nauk USSR*, 1956, v. 107(6), 815–818.
17. Rabounski D. Zelmanov's anthropic principle and the infinite relativity principle. *Progress in Physics*, 2005, v. 1, 35–37.
18. Gabrielse G., Hanneke D., Kinoshita T., Nio M. and Odom B. New determination of the fine structure constant from the electron g value and QED. *Phys. Rev. Lett.*, 2006, v. 97, 030802.
19. Petrov A. Z. Einstein spaces. Pergamon Press, Oxford, 1969, 411 pages (transl. by R. F. Kelleher, ed. by J. Woodrow).
20. Landau L. D. and Lifshitz E. M. The classical theory of fields. Butterworth–Heinemann, 2003, 428 pages (4th edition).
21. Lefschetz S. Differential equations: geometric theory. Interscience Publishers, New York, 1957.
22. Kozyrev N. A. The vibration balance and analysis of its operation. *Problems of Research of the Universe*, v. 7: "Astrometry and Celestial Mechanics", Moscow-Leningrad, 1978, 582–584.
23. Peres A. On geometrodynamics and null fields. *Annals of Physics* (N.Y.), 1961, v. 14(1), 419–439.
24. Wheeler J. A. Geometrodynamics. Academic Press, N.Y., 1962.
25. Caltenco Franca J. H., López-Bonilla J. L. and Peña-Rivero R. The algebraic Rainich conditions. *Progress in Physics*, 2007, v. 3, 50–51.
26. Nordtvedt K. and Pagels H. Electromagnetic plane wave solutions in general relativity. *Annals of Physics* (N.Y.), 1962, v. 17(3), 426–435.
27. Rabounski D. A theory of gravity like electrodynamics. *Progress in Physics*, 2005, v. 2, 15–29.

Appendix 1 The space non-holonomity as rotation

How is the non-orthogonality of the coordinate axes expressed by the components of the fundamental metric tensor $g_{\alpha\beta}$? To show this there are a few ways [14]. We use a formal method developed by Zelmanov [15]. First, we introduce a *locally geodesic reference frame* at a given point of the Riemannian space. Within infinitesimal vicinities of any point of such a reference frame the fundamental metric tensor is

$$\tilde{g}_{\alpha\beta} = g_{\alpha\beta} + \frac{1}{2}\left(\frac{\partial^2 \tilde{g}_{\alpha\beta}}{\partial \tilde{x}^\mu \partial \tilde{x}^\nu}\right)(\tilde{x}^\mu - x^\mu)(\tilde{x}^\nu - x^\nu) + \dots ,$$

i. e. the components at a point, and in its vicinity, are different from those at the point of reflection to within only the higher order terms, the values of which can be neglected. Therefore, at any point of a locally geodesic reference frame the fundamental metric tensor can be considered constant, while the first derivatives of the metric (the Christoffel symbols) are zero.

As a matter of fact, within infinitesimal vicinities of any point located in a Riemannian space, a locally geodesic reference frame can be set up. At the same time, at any point of this locally geodesic reference frame a tangentially flat Euclidean space can be set up so that this reference frame, being locally geodesic for the Riemannian space, is the global geodesic for that tangential flat space.

The fundamental metric tensor of a flat Euclidean space is constant, so the values of $\tilde{g}_{\mu\nu}$, taken in the vicinity of a point of the Riemannian space,

converge to the values of the tensor $g_{\mu\nu}$ in the flat space tangential at this point. Actually, this means that we can build a system of basis vectors $\vec{e}_{(\alpha)}$, located in this flat space, tangential to curved coordinate lines of the Riemannian space.

In general, coordinate lines in Riemannian spaces are curved, inhomogeneous, and are not orthogonal to each other. So the lengths of the basis vectors may sometimes be very different from unity.

We denote a four-dimensional infinitesimal displacement vector by $d\vec{r}=(dx^0, dx^1, dx^2, dx^3)$, so that $d\vec{r}=\vec{e}_{(\alpha)}dx^\alpha$, where components of the basis vectors $\vec{e}_{(\alpha)}$ tangential to the coordinate lines are $\vec{e}_{(0)}=\{e^0_{(0)}, 0, 0, 0\}$, $\vec{e}_{(1)}=\{0, e^1_{(1)}, 0, 0\}$, $\vec{e}_{(2)}=\{0, 0, e^2_{(2)}, 0\}$, $\vec{e}_{(3)}=\{0, 0, 0, e^2_{(3)}\}$. The scalar product of the vector $d\vec{r}$ with itself is $d\vec{r}d\vec{r}=ds^2$. On the other hand, the same quantity is $ds^2=g_{\alpha\beta}\,dx^\alpha dx^\beta$. As a result we have

$$g_{\alpha\beta}=\vec{e}_{(\alpha)}\vec{e}_{(\beta)}=e_{(\alpha)}e_{(\beta)}\cos\left(x^\alpha;x^\beta\right),$$

so we obtain

$$g_{00}=e^2_{(0)},$$
$$g_{0i}=e_{(0)}e_{(i)}\cos\left(x^0;x^i\right),$$
$$g_{ik}=e_{(i)}e_{(k)}\cos\left(x^i;x^k\right).$$

The gravitational potential is $\mathrm{w}=c^2(1-\sqrt{g_{00}})$. So the time basis vector $\vec{e}_{(0)}$ tangential to the time line $x^0=ct$, having the length

$$e_{(0)}=\sqrt{g_{00}}=1-\frac{\mathrm{w}}{c^2},$$

is smaller than unity the greater the gravitational potential w.

The space rotation linear velocity $v_i=-\frac{c\,g_{0i}}{\sqrt{g_{00}}}$ and, according to it, the chr.inv.-metric tensor $h_{ik}=-g_{ik}+\frac{g_{0i}\,g_{0k}}{g_{00}}$ gives

$$v_i=-c\,e_{(i)}\cos\left(x^0;x^i\right),$$
$$h_{ik}=e_{(i)}e_{(k)}\Big[\cos\left(x^0;x^i\right)\cos\left(x^0;x^k\right)-\cos\left(x^i;x^k\right)\Big].$$

Appendix 2 A short tour of chronometric invariants

Determination of physical observable quantities in General Relativity isn't a trivial problem. For instance, for a four-dimensional vector Q^α we may heuristically assume that its three spatial components form a three-dimensional observable vector, while the temporal component is an observable potential of the vector field (which generally doesn't prove they can be actually observed). However a contravariant tensor of the 2nd rank $Q^{\alpha\beta}$ (as many as 16 components) makes the problem much more indefinite. For tensors of higher rank the problem of heuristic determination of observable components is more complicated. Besides, there is an obstacle related to definition of observable components of covariant tensors (in which the indices are subscripts) and of mixed tensors, which have both subscripts and superscripts. Therefore the most reasonable way out of the labyrinth of heuristic guesses is to create a strict mathematical theory to enable calculation of observable components for any tensor quantities.

A complete mathematical apparatus to calculate physical observable quantities for a four-dimensional pseudo-Riemannian space was completed in 1944 by Abraham Zelmanov [15]: that is the strict solution of the problem. He called the apparatus the *theory of chronometric invariants*. Many researchers were working on the problem in the 1930–1940's. Even Landau and Lifshitz in their famous book *The Classical Theory of Fields* (1939) introduced observable time and the observable three-dimensional interval similar to those introduced by Zelmanov. But they limited themselves only to this particular case and did not arrive at general mathematical methods to define physical observable quantities in pseudo-Riemannian spaces.

The essence of Zelmanov's theory is that if an observer accompanies his physical reference body, his observable quantities are projections of four-dimensional quantities on his time line and the spatial section — *chronometrically invariant quantities*, made by projecting operators

$$b^\alpha=\frac{dx^\alpha}{ds},\qquad h_{\alpha\beta}=-g_{\alpha\beta}+b_\alpha b_\beta,$$

which fully define his real reference space (here b^α is his velocity with respect to his real references). Thus, the chr.inv.-projections of a world-vector Q^α are

$$b_\alpha Q^\alpha=\frac{Q_0}{\sqrt{g_{00}}},\qquad h^i_\alpha Q^\alpha=Q^i,$$

while chr.inv.-projections of a world-tensor of the 2nd rank $Q^{\alpha\beta}$ are

$$b^\alpha b^\beta Q_{\alpha\beta}=\frac{Q_{00}}{g_{00}},\quad h^{i\alpha}b^\beta Q_{\alpha\beta}=\frac{Q^i_0}{\sqrt{g_{00}}},\quad h^i_\alpha h^k_\beta Q^{\alpha\beta}=Q^{ik}.$$

Physically observable properties of the space are derived from the fact that chr.inv.-differential operators

$$\frac{{}^*\partial}{\partial t}=\frac{1}{\sqrt{g_{00}}}\frac{\partial}{\partial t},\qquad \frac{{}^*\partial}{\partial x^i}=\frac{\partial}{\partial x^i}+\frac{1}{c^2}v_i\frac{{}^*\partial}{\partial t}$$

are non-commutative

$$\frac{{}^*\partial^2}{\partial x^i\,\partial t}-\frac{{}^*\partial^2}{\partial t\,\partial x^i}=\frac{1}{c^2}F_i\frac{{}^*\partial}{\partial t},\quad \frac{{}^*\partial^2}{\partial x^i\partial x^k}-\frac{{}^*\partial^2}{\partial x^k\partial x^i}=\frac{2}{c^2}A_{ik}\frac{{}^*\partial}{\partial t},$$

and also from the fact that the chr.inv.-metric tensor

$$h_{ik}=-g_{ik}+\frac{g_{0i}\,g_{0k}}{g_{00}}=-g_{ik}+\frac{1}{c^2}v_i\,v_k,$$

which is the chr.inv.-projection of the fundamental metric tensor $g_{\alpha\beta}$ onto the spatial section $h^\alpha_i h^\beta_k g_{\alpha\beta}=-h_{ik}$, may not be stationary. The main observable characteristics are the chr.inv.-vector of gravitational inertial force F_i, the chr.inv.-tensor of angular velocities of the space rotation A_{ik}, and the chr.inv.-tensor of rates of the space deformations D_{ik}, namely

$$F_i=\frac{1}{\sqrt{g_{00}}}\left(\frac{\partial \mathrm{w}}{\partial x^i}-\frac{\partial v_i}{\partial t}\right),$$
$$A_{ik}=\frac{1}{2}\left(\frac{\partial v_k}{\partial x^i}-\frac{\partial v_i}{\partial x^k}\right)+\frac{1}{2c^2}\left(F_i v_k-F_k v_i\right),$$
$$D_{ik}=\frac{1}{2}\frac{{}^*\partial h_{ik}}{\partial t},\quad D^{ik}=-\frac{1}{2}\frac{{}^*\partial h^{ik}}{\partial t},\quad D=D^k_k=\frac{{}^*\partial\ln\sqrt{h}}{\partial t},$$

where w is the gravitational potential

$$\mathrm{w}=c^2\left(1-\sqrt{g_{00}}\right),$$

and v_i is the linear velocity of the space rotation

$$v_i=-c\,\frac{g_{0i}}{\sqrt{g_{00}}},\quad v^i=-c\,g^{0i}\sqrt{g_{00}},\quad v_i=h_{ik}v^k,$$

while $h=\det\|h_{ik}\|$, $h\,g_{00}=-g$, $g=\det\|g_{\alpha\beta}\|$. Observable inhomogeneity of the space is set up by the chr.inv.-Christoffel symbols

$$\Delta^i_{jk}=h^{im}\Delta_{jk,m}=\frac{1}{2}\,h^{im}\left(\frac{{}^*\partial h_{jm}}{\partial x^k}+\frac{{}^*\partial h_{km}}{\partial x^j}-\frac{{}^*\partial h_{jk}}{\partial x^m}\right),$$

which are built just like Christoffel's usual symbols

$$\Gamma^\alpha_{\mu\nu}=g^{\alpha\sigma}\,\Gamma_{\mu\nu,\sigma}=\frac{1}{2}\,g^{\alpha\sigma}\left(\frac{\partial g_{\mu\sigma}}{\partial x^\nu}+\frac{\partial g_{\nu\sigma}}{\partial x^\mu}-\frac{\partial g_{\mu\nu}}{\partial x^\sigma}\right)$$

using h_{ik} instead of $g_{\alpha\beta}$. Components of the usual Christoffel symbols are linked to the chr.inv.-Christoffel symbols and other chr.inv.-chractersitics of the accompanying reference space of the given observer by the relations

$$D^i_k+A^{\cdot i}_{k\cdot}=\frac{c}{\sqrt{g_{00}}}\left(\Gamma^i_{0k}-\frac{g_{0k}\Gamma^i_{00}}{g_{00}}\right),$$
$$F^k=-\frac{c^2\,\Gamma^k_{00}}{g_{00}},\qquad g^{i\alpha}g^{k\beta}\,\Gamma^m_{\alpha\beta}=h^{iq}h^{ks}\Delta^m_{qs}.$$

Zelmanov had also found that the chr.inv.-quantities F_i and A_{ik} are linked to one another by two identities

$$\frac{{}^*\partial A_{ik}}{\partial t}+\frac{1}{2}\left(\frac{{}^*\partial F_k}{\partial x^i}-\frac{{}^*\partial F_i}{\partial x^k}\right)=0,$$
$$\frac{{}^*\partial A_{km}}{\partial x^i}+\frac{{}^*\partial A_{mi}}{\partial x^k}+\frac{{}^*\partial A_{ik}}{\partial x^m}+\frac{1}{2}\left(F_iA_{km}+F_kA_{mi}+F_mA_{ik}\right)=0$$

which are known as *Zelmanov's identities*.

Zelmanov deduced chr.inv.-formulae for the space curvature. He followed that procedure by which the Riemann-Christoffel tensor was built: proceeding from the non-commutativity of the second derivatives of an arbitrary vector

$$^*\nabla_i\,^*\nabla_k Q_l - {}^*\nabla_k\,^*\nabla_i Q_l = \frac{2A_{ik}}{c^2}\frac{^*\partial Q_l}{\partial t} + H_{lki.}^{\cdots\ \ j} Q_j\,,$$

he obtained the chr.inv.-tensor

$$H_{lki.}^{\cdots\ \ j} = \frac{^*\partial\Delta_{il}^j}{\partial x^k} - \frac{^*\partial\Delta_{kl}^j}{\partial x^i} + \Delta_{il}^m\,\Delta_{km}^j - \Delta_{kl}^m\,\Delta_{im}^j$$

which is similar to Schouten's tensor from the theory of non-holonomic manifolds. The tensor $H_{lki}^{\cdots\ \ j}$ differs algebraically from the Riemann-Christoffel tensor because of the presence of the space rotation A_{ik} in the formula. Nevertheless its generalization gives the chr.inv.-tensor

$$C_{lkij} = \frac{1}{4}\left(H_{lkij} - H_{jkil} + H_{klji} - H_{iljk}\right),$$

which possesses all the algebraic properties of the Riemann-Christoffel tensor in this three-dimensional space and, at the same time, the property of chronometric invariance. Therefore Zelmanov called C_{iklj} the *chr.inv.-curvature tensor* the tensor of the observable curvature of the observer's spatial section. Its successive contraction

$$C_{kj} = C_{kij.}^{\cdots\ \ i} = h^{im}C_{kimj}\,, \qquad C = C_j^j = h^{lj}C_{lj}$$

gives the chr.inv.-scalar C, which is the *observable three-dimensional curvature* of this space.

Chr.inv.-projections of the Riemann-Christoffel tensor

$$X^{ik} = -c^2\frac{R_{0\cdot0\cdot}^{i\cdot\ \ k}}{g_{00}}\,, \quad Y^{ijk} = -c\,\frac{R_{0\cdots}^{\cdot\ \ ijk}}{\sqrt{g_{00}}}\,, \quad Z^{ijkl} = c^2R^{ijkl},$$

after substituting the necessary components of the Riemann-Christoffel tensor and lowering indices, are

$$X_{ij} = \frac{^*\partial D_{ij}}{\partial t} - \left(D_i^l + A_{i.}^{\cdot\ \ l}\right)(D_{jl}+A_{jl}) + \frac{1}{2}(^*\nabla_i F_j + {}^*\nabla_j F_i) - \frac{1}{c^2}F_iF_j\,,$$
$$Y_{ijk} = {}^*\nabla_i\left(D_{jk}+A_{jk}\right) - {}^*\nabla_j\left(D_{ik}+A_{ik}\right) + \frac{2}{c^2}A_{ij}F_k\,,$$
$$Z_{iklj} = D_{ik}D_{lj} - D_{il}D_{kj} + A_{ik}A_{lj} - A_{il}A_{kj} + 2A_{ij}A_{kl} - c^2C_{iklj}\,,$$

where we have $Y_{(ijk)} = Y_{ijk} + Y_{jki} + Y_{kij} = 0$, just like the Riemann-Christoffel tensor. Successive contraction of the spatial observable projection Z_{iklj} gives

$$Z_{il} = D_{ik}D_l^k - D_{il}D + A_{ik}A_{l.}^{\cdot\ \ k} + 2A_{ik}A_{l.}^{k\cdot} - c^2C_{il}\,,$$
$$Z = h^{il}Z_{il} = D_{ik}D^{ik} - D^2 - A_{ik}A^{ik} - c^2C\,.$$

Accordingly, Einstein's equations in the case where matter is arbitrarily distributed throughout the space have the chr.inv.-projections (the chr.inv.-Einstein equations)

$$\frac{^*\partial D}{\partial t} + D_{jl}D^{jl} + A_{jl}A^{lj} + \left({}^*\nabla_j - \frac{1}{c^2}F_j\right)F^j = -\frac{\kappa}{2}\left(\rho c^2 + U\right) + \lambda c^2,$$
$$^*\nabla_j\left(h^{ij}D - D^{ij} - A^{ij}\right) + \frac{2}{c^2}F_j\,A^{ij} = \kappa J^i,$$
$$\frac{^*\partial D_{ik}}{\partial t} - (D_{ij}+A_{ij})\left(D_k^j + A_{k\cdot}^{\cdot\ \ j}\right) + D\,D_{ik} + 3A_{ij}A_{k\cdot}^{\cdot\ \ j} - \frac{1}{c^2}F_iF_k +$$
$$+\frac{1}{2}(^*\nabla_iF_k + {}^*\nabla_kF_i) - c^2C_{ik} = \frac{\kappa}{2}\left(\rho c^2h_{ik} + 2U_{ik} - Uh_{ik}\right) + \lambda c^2h_{ik}\,.$$

where $^*\nabla_j$ denotes the chr.inv.-derivative, for instance

$$^*\nabla_i\,q_k = \frac{^*\partial q_k}{dx^i} - \Delta_{ik}^l q_l\,, \quad {}^*\nabla_i\,q^k = \frac{^*\partial q^k}{dx^i} + \Delta_{il}^k q^l,$$
$$^*\nabla_i\,q_{jk} = \frac{^*\partial q_{jk}}{dx^i} - \Delta_{ij}^l q_{lk} - \Delta_{ik}^l q_{jl}\,,$$
$$^*\nabla_i\,q_j^k = \frac{^*\partial q_j^k}{dx^i} - \Delta_{ij}^l q_l^k + \Delta_{il}^k q_j^l\,,$$
$$^*\nabla_i\,q^{jk} = \frac{^*\partial q^{jk}}{dx^i} + \Delta_{il}^j q^{lk} + \Delta_{il}^k q^{jl},$$
$$^*\nabla_i\,q^i = \frac{^*\partial q^i}{dx^i} + \Delta_{ji}^j q^i = \frac{^*\partial q^i}{dx^i} + \frac{^*\partial\ln\sqrt{h}}{\partial x^i}\,q^i,$$
$$^*\nabla_i\,q^{ji} = \frac{^*\partial q^{ji}}{dx^i} + \Delta_{il}^j q^{il} + \frac{^*\partial\ln\sqrt{h}}{\partial x^i}\,q^{ji},$$

while the quantities

$$\rho = \frac{T_{00}}{g_{00}}\,, \qquad J^i = \frac{cT_0^i}{\sqrt{g_{00}}}\,, \qquad U^{ik} = c^2T^{ik}$$

(from which we have $U = h^{ik}U_{ik}$) are the chr.inv.-components of the energy-momentum tensor $T_{\alpha\beta}$ of distributed matter: the physical observable density of the field energy ρ, the physical observable density of the field momentum vector J^i, and the physical observable stress-tensor U^{ik}. For instance, the energy-momentum tensor of the electromagnetic field has the form [20]

$$T_{\alpha\beta} = \frac{1}{4\pi}\left(-F_{\alpha\sigma}F_{\beta\cdot}^{\cdot\ \ \sigma} + \frac{1}{4}\,F_{\mu\nu}F^{\mu\nu}g_{\alpha\beta}\right),$$

where $F_{\alpha\beta}$ is the electromagnetic field tensor (so-called Maxwell's tensor). (It follows that the field density ρ is connected to the quantity $U = h^{ik}U_{ik}$ by $\rho c^2 = U$.)

In this way, for any quantity or equation obtained using general covariant methods, we can calculate their physically observable projections on the time line and the spatial section of any particular reference body and formulate the projections in terms of their real physically observable properties, from which we obtain equations containing only quantities measurable in practice.

LETTERS TO PROGRESS IN PHYSICS

Comment on the "Declaration of the Academic Freedom" by D. Rabounski

Marian Apostol

Department of Theoretical Physics, Institute of Atomic Physics, Magurele-Bucharest MG-6, PO Box MG-35, Romania
E-mail: apoma@theory.nipne.ro

At least four major misconceptions gravely affect science and technology today, and the progress of scientific and technological research. These misconceptions are related to a utilitarian view of science, whereby large-scale collaborations and institutions of higher learning are conceived of as the only means for developing science and technology, where scientific publication is the sole aim of scientific research, within a commercial view of the nature of these human endeavours and activities. It is revealed herein just how abusive and destructive these misconceptions are, and to what great extent they now plague society. In complementing D. Rabounski's recent Declaration of the Academic Freedom, scientific and technological research should reaffirm its free, universal and critical nature, as a source of human dignity and honour, honesty and lucidity. Unfortunately, a despicable vulgarization of science and technology has led nowadays to a widely held relativism and uncertainty, which is employed as a theoretical ideology for manipulation and domination, placing human society in great peril.

Science and technology has changed human life essentially and irreversibly, both personal and social, the environment, and created a new, artificial world with profound cultural implications at the level of human behaviour, psychology and mentality. Human society today depends essentially on science and technology, to the point that life on Earth can be irreversibly damaged by the loss of science and technology. The only thing today that still remains outside the scope of science and technology is the creation of life, although basic modification of life is already present, and destroying life by science and technology is routine. Today's science and technology teaches us that the planet Earth, the Solar System, and perhaps the whole Universe, are very likely casual, and perhaps not eternal. It is therefore much more sensible to do everything possible to preserve life, for as long as possible.

Science and technology are now in great peril, not only due to social and political changes, and not only by a very uncontrollable economic activity, but also by various misconceptions. The latter are the most pernicious, because the human world is indeed a "matter of will and representation" (Schopenhauer). There are at least four plagues which the vulgarization of science and technology have generated in our modern society: relativism, indeterminacy, utilitarianism, manipulation and domination, and which now collectively turn against science and technology.

I adduce herein a series of current injurious misconceptions related to science and technology.

It is wrong, but widely held today, that science must satisfy any immediate desire or need, either physical or mental, as whimsical as may be, and that technology must satisfy as soon and most economically as possible. This is profoundly wrong. Science responds only to our intellectual impulse, this is its nature, to "accommodate in the most economical way our sensations to our ideas, which is a basic need for our survival" (Planck). It is indeed a deep wonder, which nobody could have ever explained, and probably cannot ever, that answering our intellectual questions may sometimes result in practical, technological applications that make our life more comfortable. History shows this, without explanation, but it also definitely shows that the way from science to technology is not direct, but a very mediated one. To bring scientific discoveries into practical life one needs commitment, investment, patience, competence, a lot of work, and, especially, the acceptance of the possibility that it may never happen at all. Science teaches us basically that its technological applications are in fact a matter of good luck, and we must accept this point as a scientific statement, as strange as it may sound. It reveals the autonomy and the freedom of science, which bears upon its profound nature. The politicians and policy-makers of today must accept that it is not they who should direct science and technology, but instead precisely the opposite, it is science and technology which should direct them, if life is going to be preserved and cultivated. Admittedly, it is difficult to accept that science would not be "scientific". Actually, as a matter of fact, science is nothing else but that endeavour that makes human the mysteries of the natural world, as the history of Mankind testifies.

Another common misconception about science nowadays is that science must be done exclusively in collaboration, and, as such, the broader the collaboration, the better — it is the only possible way to achieve scientific advances.

This is wrong. First, history proves the contrary. Newton worked alone, Maxwell similarly, Boltzmann worked alone and much against the current wisdom, Einstein likewise notoriously, the quantum physicists in the first half of the 20th century worked in a restricted cooperation, etc, etc. Feynman used to talk a lot with people around and about, find problems and work them for himself, alone. There is no other way. Similar examples occur in sciences other than physics. No profound scientific discovery has ever been made by many people, but always by one or, occasionally, by a few at any time. This is not only a historical fact, but a logical one too. If a discovery emerged in the heads of many, then it would not be something new, nor revolutionary, but instead, it would be a routine, trivial thing, by definition. Another, positive argument, without resorting to the *demonstratio per absurdum*, is the following. Suppose that for one scientific problem there would be many, most valuable contributors. Since the problem is one and these contributors are many it follows that each of them brings only a small contribution. Then, the problem is never solved by any one of them, but by one, who synthesized the work of the many. That does not mean that many workers in science or technology are not desirable, or that they would be superfluous. On the contrary, they make a valuable research environment, their work is the fuel of great discoveries, but it is only the coal in the scientific furnace. It is not science, it is only the probable way toward science. Science is what a few do based on the work of many. As such, the opinion of the many in science is useless, and always dangerous, because they do not know. They are non-scientific, they are only the material used in scientific and technological discoveries. Democracy in science and technology is a most dangerous thing, because it is contrary to the scientific spirit and to the nature of these endeavours. In contrast with political and social life, where today democracy is the accepted way of making mistakes, in science and technology the only acceptable medium of making mistakes along the way to the correct answer is the scientific and technical aristocracy. Only the latter "knows what knows and what does not know" (Socrates), which is its claim to competence. The former, people at large, do not know what knows, or what they don't. In its endeavour to acquire positive knowledge, *i.e.* that knowledge which is so probable to be taken as granted and warranted, science must only use lucidity and honesty, and cannot afford any inconsequential talk. This points again towards a basic feature of science and technology, that of creativity, which comes from their profound freedom and autonomy, a sense of honour generated exclusively by honesty and lucidity. Our attention nowadays is insistently and ideologically forced, by politics and the media, towards great scientific and technological organizations, as the only way of developing science and technology. This is a dishonest enterprise, the content of such actions is anti-scientific. Such people say one thing but mean the opposite. They abuse science, falsify and manipulate it, for image and political ends. Science and technology can only be achieved in an adequate environment, and the institutions of research of today are more than welcome, the larger the better. But we must be aware that they are there only for the purpose of an act of scientific or technological discovery, and not for becoming ends in themselves. Scientists must not, by necessity, belong to any such large organizations, in order to be scientists, or engineers. The requirement of an institutional enrollment for scientists and engineers is an abusive plague upon our mentality nowadays, with profound negative consequences. Today, scientific work can be carried out by electronic means as an individual, building upon the work of smaller or larger scientific and technical organizations. The factual reality shows that any discovery in science and technology was made by individuals, who used the work of many, sometimes of hordes. The big organizations of scientific research and technology are necessary, but not sufficient, by no means. They are just disposable means. Since the means should not dictate our aims, democracy must not be permitted to decide upon scientific and technological matters. It must be fully and for ever banished from science and technology. In science and technology we do not know the solutions. But certainly the "solutions" of the many are wrong, especially because they do not know what they do not know. This is why the opinion of those who "know that they do not know" is by far preferable, and history proves this point. In political and social life democracy may be a convenient instrument, especially when and where the majority is meager. Then, we have a permanent civil war in society, without a very definite outcome, which gains time for social life.

Another misconception which produces much damage to scientific research is related to scientific publications. Scientific publications are a means of doing scientific research, and they do occur naturally in the process of research. They are meant to present results of scientific research to the scientific public, in order to help science advance. The aim of scientific research is to get scientific results, which naturally are materialized in scientific publications. If we define, as is the case today, that scientific publications are the aim and the goal of scientific research, we confound the means for the aim, thereby falsifying scientific research and impeding the progress of science. Scientific authors of today no longer publish for a scientific aim, they publish instead only for the number of "papers". The great pressure of "publish or perish" placed today upon scientific researchers by various political and administrative bodies, by the research institutional organizations and universities, has definitely turned the attention of the researchers from science to publications. The scientific literature has been invaded by an enormous amount of publications, at a tremendously increasing rate, which contains no scientific result, which nobody reads, and which is completely useless. Such publications are merely

"progress reports", which mean only that "time has passed" (Oppenheimer), and reveal only that the research funds have been spent. They have been spent indeed, but not on research. They have been spent on useless publications, and the costs obviously do not match the output. The requirement of publications as an end *per se* is one of the greatest attacks the political and administrative media are now mounting against scientific research, its freedom, liberty, and its very nature. It has deliberately misled contemporary scientific research along a false path, and locked genuine scientific individuals outside the social organization of scientific research. Mankind is losing and wasting one of its most valuable natural resources, scientific creativity. Moreover, influential political and administrative bodies and organizations with a commercial orientation have defined a number of scientific journals as the "main stream", according to their rate of citations, in the "impact factor", in complete disregard for their scientific contents. Research which is not in this "main stream" perishes, it is not funded, whilst those which belong to such influential organizations are published, funded and run forever, without any scientific result: producing only with a massive literature, good for nothing. Because the frequent citation of such literature is improper, there is no reference to the scientific content, which is absent, because it is just a formality, a ritual of the publications industry. The "impact factor" is defined by these organizations as the ratio of the number of citations to the number of published papers, so the scientific journals of today publish only those papers which are most likely to be cited, *i.e.* those which come precisely from the same influential organizations which define the impact factor. This is a self-approving type of institutional activity, which is closed in itself, permits no criticism, no contrary opinion, and, as such, is typical of underground, criminal, terrorist-like, dictatorial, secret societies and organizations. In fact, the secret character of these organizations is obvious in their practice of the "anonymous peer review" procedure. These "main stream" journals have in fact a quite notorious and ignominious past: they have rejected from publication authors like Einstein, Schwinger, Fermi and also Feynman. Many articles published today by the foremost "main stream" scientific journals are withdrawn soon thereafter by the authors, which reflects conflict within those organizations, very similar to the fights and wars between rival criminal mobs. Moreover, if the "impact factor" was instead referred to the number of papers in the sold copies according to declared users, we would have a very different picture, and the "main stream" would be seen immediately to be in fact a "mean stream", because there are a lot of declared-users sold copies of these journals which nobody reads. Research funds are spent not only to produce such journals, but to buy them, without being read or used. This is a vicious activity which falsifies scientific research, and to impose the "main stream" upon scientific activity is another great attack upon the freedom of scientific research. To exclude from publication people who do not belong to those influential organizations is an attack upon the universality of science. In 1920 Sommerfeld established a new scientific journal, which soon became the famous Zeitschrift für Physik. This journal never had reviewers, let alone "anonymous reviewers". The scientific articles were published under the sole scientific and moral authority of Sommerfeld. This real freedom permitted the birth of quantum mechanics, nuclear and solid-state physics and all the other branches of modern Physics. Of course, not all of the papers published in Zeit Phys were good, and Sommerfeld did not understand them all. But he was a professional of science, and where his professional expertise could not help him, he exercised his honesty and lucidity. This is competence in science.

Another misconception regarding the scientific research of today is that it must be self sustaining, as any commercial activity. This is a nonsense. The nature of scientific "products", which are the scientific results, is such that not only does nobody buy them, but they are also offered freely. These "products" have no immediate practical utility. The best we can expect is to bring them to the attention of as many learned people as possible, and even to society at large, in order to get new ideas, visions, perspectives, etc., and to make apparent possible practical applications. The latter depend on technological skills and means, which is an undertaking in its own right. It does not only make use of the scientific results, but it provides scientific research with new suggestions and ideas. As such, both scientific research and technological development, which aims at practical applications of the scientific results, must be funded by society with no regard to immediate commercial reward. In comparison with other social costs, and in regard to its enormous benefits, as proved by history, the funding of scientific and technological research is modest; the highest spending today on science and technology does not exceed about 3–4% of GDP in the most developed countries. Scientific and technological research is funded today by government or corporations, by universities and private companies, and to a much less extent by sponsors, benefactors, philanthropists or a sort of "mecena". In all of these situations the misconceptions described above prevail and dominate, mixed up with a misleading financial "reasoning". First, the notion of "project funding" tends to be generalized up to the point that researchers get their salaries exclusively on an "competition" basis. This is nonsense: one cannot expect honest work from a worker who is not paid a regular salary. Consequently, "project competition" generates corruption, it is "lobby and lottery", it provides only an occasional, temporary and irregular income. Scientific researchers turn their attention from their real work to the process of getting funded through such a "competition" basis. "Project funding" was originally restricted to temporary jobs for PhD students or post-doctoral researchers, until these beginners secured a stable research, teaching, or technical position, and was mainly limited to

universities as a form of further education and instruction, facilitating social insertion. Today, this "competition of project funding" tends to be generalized, destroying scientific research and scientific education. Indeed, it is almost universally accepted today that university professors should no longer concentrate upon their teaching mission, but should instead do research. This is a grave diversion, which explains why scientific education has degraded and declined so much in our modern society. As for research funding from sponsors or other individuals, this is a naive conception. Almost nobody gives personal money without asking for something rewarding in return. Scientific results produce satisfaction only when one takes part in getting them. Otherwise, such sorts of things are absurd. According to an old joke, "I love work. I would sit and watch it for hours". Such sponsors, benefactors, philanthropists and various "mecena", desire in fact publicity and image for their money to use these for getting in turn even more money. But image and publicity gained by scientific research means diverting the latter from its nature, and, in fact, abusing it. This is another grave injury inflicted upon scientific research by our modern society. A man who relatively recently invested $50,000.00 in a private research institute, took twice as much from government and public funds, and acquired 3 or 4 permanent staff. The institute now accommodates many visitors, whose expenses are paid by their respective institutional employers, and who deliver public lectures on nonsense such as black holes, the Big Bang, conscience, etc., etc. This is nice, to "scientize" the public at large, but it is pseudo-science. In addition, that fellow became an influential member of various government and academic bodies, from which he draws a big salary, which overcompensates by far the original $50,000.00, for his vulgarization of scientific research and his "great service" to society. Such are the methods of modern society for destroying science.

Funding scientific and technological research without asking for an immediate revenue, according to the nature of these activities, does not mean that these activities are unaccountable. On the contrary. But first let us remark that their products are not physical, but intellectual. As such, the printed paper, or the electronic archives, which embody the present scientific literature cannot be mistaken for the scientific results. Not even the experimental setups or apparatus produced by technological research should be mistaken for the result of this research, because they only serve to represent physically an idea. Scientific and technological research is accountable by its scientific and technical results, which are essentially spiritual, or intellectual, objects. This accountability is realized by the scientists themselves, who are able to speak clearly, logically and, especially, critically about their own work. The democratic vote of the majority is nonsense in this enterprise. (I have witnessed, at a degraded nuclear laboratory, the neutron lifetime established by majority vote; they decided about 1 second.) The responsible political, administrative and social elements are afraid of being trumped by scientists in this process of accountability. I can assure them that they wouldn't. But of course, these people must try to become a little literate in science and technology. And finally, what is not risky today in any enterprise? A sure and safe business either does not exist or it is illegal. The fact that we do not know does not give us the right to abuse and destroy scientific research, nor to falsify it. The latter is illegal, and deserves legal punishment, the former is bad and irreversibly damaging for us, for our children and for the whole future of Mankind. It is morally culpable.

The Declaration of Academic Freedom, or Scientific Freedom, is quite welcome, and essentially declares the following Rights.

According to its nature, scientific research has the Right of doing Science; it has the Right of doing it in perfect Freedom and Universality, aiming exclusively at spiritual and intellectual results, without interference from political, administrative or social organizations, to publish its scientific results wherever, whenever and in whatever way it considers appropriate. It has the Right of discussing openly, freely and critically, whatever the result declared as being scientific, and society must warrant this Right and facilitate its exercise. It has the Right of being funded appropriately by society and the Right of accounting for its own results according to its own criteria, ways, methods and procedures. Scientific and technological research has the Right of dismissing as abusive, intruding and falsifying, the use of democracy in scientific matters, the "main stream" publications and "impact factor" as means of evaluation, "project competition" as a means of funding. It has the Right of being Free and Autonomous, and to give account of its results to the whole of society, according to its own methods, practices, procedures, historically established. The Right to Scientific Research is a Fundamental Human Right.

Submitted on April 12, 2007
Accepted on April 16, 2007

LETTERS TO PROGRESS IN PHYSICS

Is Classical Statistical Mechanics Self-Consistent?

(A paper in honour of C. F. von Weizsäcker, 1912–2007)

Peter Enders

Ahornallee 11, D-15754 Senzig, Germany
E-mail: enders@dekasges.de

In addition to his outstanding achievements in physics and activities in policy, C.-F. von Weizsäcker is famous for his talks, given as a member of the Academy Leopoldina. Due to the latter, I could learn quite a lot from his methodological writings. In particular, he is the only modern thinker I'm aware of who has pointed to the difference between Newton's and Laplace's notions of state. But this difference is essential for the relationship between classical and quantum physics. Moreover it is the clue to overcoming Gibbs' paradox within classical statistical mechanics itself.

1 Introduction

With Carl-Friedrich Freiherr von Weizsäcker (1912–2007) an outstanding physicist, philosopher and human being passed away. Born into a family with long traditions of widespread interests, activities and education — his father was a highly ranked diplomat, his younger brother Richard was President of Western Germany — he showed from the very beginning a strong interest in both physics and philosophy. His talks as a member of the German Academy of Sciences Leopoldina are famous not only by their original content, but also by his humour. His books on methodological and historical issues display his broad scope, and are full of wise insights. As a master, he acknowledged the masters of the past; one can learn from him how to learn from the masters, then and now. Notably, I remember his reference to Euler's (1707–1783) reasoning on the equivalence of causal (differential equations) and teleological descriptions (minimum principles), and his pointing to the difference between the notions of state as used by Newton (1643–1727), and today, respectively [1]. As the latter has profound implications even for modern physics, I would like to honour von Weizsäcker through outlining its relevance for statistical and quantum physics.

2 State and motion

2.1 Conservation laws vs laws of motion

Descartes (1596–1650), Huygens (1629–1695), Newton and Euler started their exposition of the basic laws with the conservation of (stationary) state. This is followed by the change of state and eventually by the change of location (equation of motion). The location of a body is not a state variable, because it changes even without the action of an external force, i.e., without reason. The latter kind of reasoning was abandoned at the end of 18th century as part of scholastics ([1], p. 235). The centre of the Lagrange (1736–1813) formalism is occupied by the Lagrangian equation of motion, i.e., equations for the non-state variable location (represented by the generalized coordinates).

On the other hand, this equation of motion indicates at once the conservation of (generalized) momentum for the force-free motion of a body in a homogeneous space. Indeed, there is a very tight interconnection of symmetries and conserved quantities in general, as stated in Noether's (1882–1935) theorem, the mechanical and field-theoretical applications of which being usually expressed by means of the Lagrange formalism. The principle of least action containing the Lagrange function is often even placed at the pinnacle of mechanics.

This development has strengthened the focus of physicists on the equations of motion and weakened their attention on the laws of state conservation, despite the extraordinary rôle of energy in quantum mechanics and Bohr's (1885–1962) emphasis on the fundamental rôle of the principles of state conservation and of state change [2]. Indeed, there are derivations of Newton's equation of motion from the energy law, e.g., in [3, 4, 5]; a deduction of Hamilton's (1805–1865) equation of motion from Euler's principles of classical mechanics can be found in [6, 7].

Thus, there are two traditional lines of thought,

- the "physics of conserved quantities": Parmenides (ca. 515 BC — ca. 445 BC) — Descartes — Leibniz (1646–1716), and
- the "physics of laws of change": Heraclites (ca. 388 BC — ca. 315 BC) — Galileo (1564–1642) — Newton.

In the end, both lines are equivalent, leading eventually to the same results, as first shown by Daniel Bernoulli (1700–1782) [8].

2.2 Motion vs stationary states

In classical mechanics, if an external force ceases to act upon a body or conservative system, the latter remains in that stationary state it has assumed at that moment. Non-

stationary motion is a continuous sequence of stationary states. Consequently, the set of stationary states of a system determines both its stationary and its non-stationary motions and, in particular, its set of possible configurations. For instance, the turning points of a pendulum are determined by its energy.

In quantum mechanics, the situation is somewhat more complicated. The set of stationary states is (quasi-)discontinuous. The external influence vanishes most likely at an instant, when the wave function of the system is *not* equal to one of the stationary states. However, it can be constructed from the stationary wave functions. According to Schrödinger (1887–1961) [9], the transition between two states is characterized by contributions to the wave function from both states. It's like climbing a staircase without jumping, i.e., the one foot leaves the lower step only after the other foot has reached the higher step. In this sense, the fashionable term "quantum leap" is a fiction. Therefore, the quantum motion, too, is largely determined by the stationary states.

2.3 State variables vs quantum numbers

A freely moving body exhibits 3 Newtonian state variables (e.g., the 3 components of its momentum vector; c.f. Laws 1 and 2), but 6 Laplacian state variables (e.g., the 6 components of its velocity and position vectors; c.f. Laplace's demon [10]). A freely moving spinless quantum particle exhibits 3 quantum numbers (e.g., the 3 components of its momentum vector).

The planets revolving around the sun à la Kepler (1571–1630) exhibit 3 Newtonian state variables (e.g., the total energy and 2 components of the angular momentum), but 6 Laplacian state variables (e.g., those of free bodies, given above). Neglecting spin, the one-electron states of atoms are labeled by 3 quantum numbers (1 for the energy plus 2 for the angular momentum). The same applies to the three-dimensional classical and quantum oscillators, respectively.

The example of these three basic systems of mechanics, both classical and quantum, clearly demonstrates that the Newtonian notion of state — corresponding largely to the modern notion of stationary states — is much more appropriate for comparing classical and quantum systems than the Laplacian notion of state. It should be enlightening to draw these parallels for field theory.

3 (In)Distinguishability

3.1 Permutation symmetry of Newtonian state functions

Two classical bodies are equal if they possess the same mass, size, charge, etc. [11]. A simple example is given by the red balls of snooker (a kind of billiards; I abstract, of course, from deviations caused by the production process). Due to the unique locus of a body, they can be distinguished by their locations and, thus, are not identical. For the outcome of a snooker game, however, this does not play any rôle. Similarly, for recognizing a player of the own team, only the color of the tricot is important, not its size. In other words, it is not the totality of properties that matters, but just that subset which is important for the current situation.

The Hamilton function of a system of equal bodies is invariant under the interchange of two bodies (permutation of the space and momentum variables). More generally, given only the Newtonian state variables of a system, the classical (!) bodies in it are indistinguishable. This allows for discussing the issue of (in)distinguishability within classical dynamics. Equal quantum particles are also not identical, if they can be distinguished through their localization.

3.2 Distribution functions vs energy spectrum

In his 1907 paper "Planck's theory of radiation and the theory of specific heat of solids" [12], Einstein (1879–1955) not only founded the quantum theory of solids, but demonstrated also, that the differences between the classical and quantum occupation of states result from the different character of the energy spectra of classical and quantum systems, respectively; and he defined quantization as a selection problem [6, 7].

Wien's (1864–1928) classical distribution law he obtained by using the continuous energy spectrum of a classical oscillator, while Planck's (1858–1947) non-classical distribution law emerges from the discrete energy spectrum of a quantum oscillator.

In a perfect crystal, the atoms oscillate around localized lattice positions and, therefore, are distinguishable. Their interaction, however, leads to collective oscillations called normal modes. In these common states, the individual lattice atoms become indistinguishable. It is these normal modes that were actually used by Einstein. However, due to the use of Newton's notion of state Einstein was able to derive Planck's distribution law by means of "classical" arguments.

3.3 Gibbs' paradox

Consider a box filled uniformly with a gas in thermal equilibrium. When putting a slide sufficiently slowly into it, dividing the box into two parts, no macroscopic quantity of the box as a whole should change. However, within conventional classical statistical mechanics, the entropy changes drastically, because the interchange of two molecules from now different parts of the box is regarded as being significant. This is called Gibbs' (1839–1903) paradox [13]. In conventional representations, it is argued that, actually, the molecules are quantum particles and, thus, indistinguishable; the double counting is corrected ad hoc.

Now, as outlined above, if Newton's rather than Laplace's notion of state is used, an interchange of any two molecules of the same part or of different parts of the box, does not affect the state. Therefore, the artifact of Gibbs' paradox

can be avoided from the very beginning when working with Newton's notion of state, as can be seen from Einstein's 1907 paper discussed above.

4 Summary and discussion

Contrary to Einstein's results, Ehrenfest (1880–1933) [14] and Natanson (1864–1937) [15] explained the difference between the classical and quantum radiation laws by means of different counting rules for distinguishable and indistinguishable particles ([16], §1.4; [17], vol. 1, pt. 2, sect. V.3). Apparently supported by the uncertainty relation, in particular, after its "iconization" as the "uncertainty principle", this view prevailed for most of the 20th century. Only at its end was it realized more and more that it is not the (in)distinguishability of particles that matters, but that of the states (e.g. [18], sects. 1 and 2.1; [19], sect. 4.1). Using Newton's rather than Laplace's notion of state, the statistical reasoning in [18, 19] can be physically-dynamically substantiated.

It needs, perhaps, a congenial mixing of physics and philosophy, like that of von Weizsäcker, to recognize and stress the importance of notions within physics. As the notions are the tools of our thinking, the latter cannot be more accurate than the former.

Both Newton's and Laplace's notions of state exhibit advantages [20]. The proper use of them makes classical statistical mechanics self-consistent.

Acknowledgement

I'm thankful to the Academy Leopoldina for keeping a tight relationship with its members in Western Germany during the Cold War, and also for a grant after unification. I'm indebted to Dr. D. Rabounski and Prof. J. L. López-Bonilla for encouraging the writing of this contribution.

Submitted on May 14, 2007
Accepted on May 16, 2007

References

1. von Weizsäcker C. F. *Aufbau der Physik*, München, 2002; The structure of physics. Springer, Heidelberg, 2006.
2. Bohr N. On the constitution of atoms and molecules. *Phil. Mag.*, 1913, v. 26, 1–25
3. Violle J. Lehrbuch der Physik. Vol. 1: Mechanik. Springer, Berlin, 1892–1893.
4. Schütz J. R. Das Prinzip der absoluten Erhaltung der Energie. *Gött. Nachr.*, Math.-phys. Kl., 1897, 110.
5. Hamel G. Mechanik I: Grundbegriffe der Mechanik. Teubner, Leipzig/Berlin, 1921.
6. Enders P. & Suisky D. Quantization as selection problem. *Int. J. Theor. Phys.*, 2005, v. 44, 161–194.
7. Enders P. Von der klassischen Physik zur Quantenphysik. Eine historisch-kritische deduktive Ableitung mit Anwendungsbeispielen aus der Festkörperphysik. Springer, Heidelberg, 2006.
8. Bernoulli D. Examen principorum mechanicae et demonstrationes geometricae de compositione et resolutione virium. *Comment. Acad. Petrop.*, Febr. 1726, 126–142; cited after Grigor'jan A. T. & Kowaljow B. T. Daniil Bernulli. Nauka, Moskau, 1981, Ch. 5.
9. Schrödinger E. Quantisierung als Eigenwertproblem. Dritte Mitteilung. *Ann. Phys.*, 1926, v. 80, 437–490.
10. de Laplace P. S. Essai Philosophique sur la Probabilité. Paris, 1814, p. 2.
11. von Helmholtz H. Einleitung zu den Vorlesungen über Theoretische Physik. *Vorlesungen über Theoretische Physik*, v. I/1, ed. by A. König & C. Runge, Barth, Leipzig, 1903.
12. Einstein A. Die Plancksche Theorie der Strahlung und die Theorie der spezifischen Wärme. *Ann. Phys.*, 1907, v. 22, 180–190.
13. Gibbs J. W. Elementary principles in statistical mechanics developed with especial reference to the rational foundation of thermodynamics. Scribner, New York, 1902.
14. Ehrenfest P. Welche Züge der Lichtquantenhypothese spielen in der Theorie der Wärmestrahlung eine wesentliche Rolle? *Ann. Phys.*, 1911, v. 36, 91–118.
15. Natanson L. On the statistical theory of radiation. *Bull. l'Acad. Sci. Cracovie (A)*, 1911, 134–148; Über die statistische Theorie der Strahlung. *Phys. Z.*, 1911, v. 12, 659–666.
16. Jammer M. The conceptual development of quantum mechanics. McGraw-Hill, New York etc., 1967, Ch. 1, Fn. 205.
17. Mehra J. & Rechenberg H. The historical development of quantum theory. Springer, New York, 1982.
18. Bach A. Indistinguishable classical particles. Springer, Berlin etc., 1997.
19. Glazer M. & Wark J. Statistical mechanics. A survival guide. Oxford Univ. Press, Oxford, 2001.
20. Enders P. Equality and identity and (in)distinguishability in classical and quantum mechanics from the point of view of Newton's notion of state. *Proc. Int. Symp. "Frontiers of Fundamental and Computational Physics (FFP6)"*, Udine (Italien), 26–29.09.2004, B. G. Sidharth, F. Honsell & A. De Angelis (Eds.), Klower, Dordrecht, 2006, 239–245.

Carl Friedrich von Weizsäcker, 1983.

Biography*

Carl Friedrich Freiherr (Baron) von Weizsäcker (June 28, 1912, Kiel – April 28, 2007, Säcking near Starnberg) was a German physicist and philosopher. He was the longest-living member of the research team which tried, and failed, to develop a nuclear weapon in Germany during the Second World War.

Weizsäcker was born in Kiel, Germany, the son of the German diplomat Ernst von Weizsäcker. He was the elder brother of the former German President Richard von Weizsäcker, father of the physicist and environmental researcher Ernst Ulrich von Weizsäcker and father-in-law of the former General Secretary of the World Council of Churches Konrad Raiser.

From 1929 to 1933, Weizsäcker studied physics, mathematics and astronomy in Berlin, Göttingen and Leipzig supervised by and in cooperation, e.g., with Werner Heisenberg and Niels Bohr. The supervisor of his doctoral thesis was Friedrich Hund.

His special interest as a young researcher was the binding energy of atomic nuclei, and the nuclear processes in stars. Together with Hans Bethe he found a formula for the nuclear processing in stars, called the Bethe-Weizsäcker formula and the cyclic process of fusion in stars (Bethe-Weizsäcker process, published in 1937).

Note regarding personal names: *Freiherr* is a title, translated as *Baron*, not a first or middle name. (The female forms are *Freifrau* and *Freiin*.)

During the Second World War, he joined the German nuclear energy project, participating in efforts to construct an atomic bomb. As a protegee of Heisenberg, he was present at a crucial meeting at the Army Ordinance headquarters in Berlin on 17 September 1939, at which the German atomic weapons program was launched. In July 1940 he was co-author of a report to the Army on the possibility of "energy production" from refined uranium, and which also predicted the possibility of using plutonium for the same purpose. He was later based at Strasbourg, and it was the American capture of his laboratory and papers there in December 1944 that revealed to the Western Allies that the Germans had not come close to developing a nuclear weapon.

Historians have been divided as to whether Heisenberg and his team were sincerely trying to construct a nuclear weapon, or whether their failure reflected a desire not to succeed because they did not want the Nazi regime to have such a weapon. This latter view, largely based on postwar interviews with Heisenberg and Weizsäcker, was put forward by Robert Jungk in his 1957 book *Brighter Than a Thousand Suns*. Weizsäcker states himself that Heisenberg, Wirtz and he had a private agreement to study nuclear fission to the fullest possible in order to "decide" themselves how to proceed with its technical application. "There was no conspiracy, not even in our small three-men-circle, with certainty not to make the bomb. Just as little, there was no passion to make the bomb . . . " (cited from: C. F. von Weizsäcker, *letter to Mark Walker*, August 5, 1990).

The truth about this question was not revealed until 1993, when transcripts of secretly recorded conversations among ten top German physicists, including Heisenberg and Weizsäcker, detained at Farm Hall, near Cambridge in late 1945, were published. The *Farm Hall Transcript* revealed that Weizsäcker had taken the lead in arguing for an agreement among the scientists that they would claim that they had never wanted to develop a German nuclear weapon. This story, which they knew was untrue, was called among themselves *die Lesart* (the Version). Although the memorandum which the scientists drew up was drafted by Heisenberg, one of those present, Max von Laue, later wrote: "The leader in all these discussions was Weizsäcker. I did not hear any mention of any ethical point of view" (cited from: John Cornwell, *Hitler's Scientists*, Viking, 2003, p. 398). It was this version of events which was given to Jungk as the basis of his book.

Weizsäcker was allowed to return to Germany in 1946 and became director of a department for theoretical physics in the Max Planck Institut for Physics in Göttingen (successor of Kaiser Wilhelm Institut). From 1957 to 1969, Weizsäcker was professor of philosophy at the University of Hamburg. In 1957 he won the Max Planck medal. In 1970 he formulated a *Weltinnenpoltik* (world internal policy). From 1970 to 1980, he was head of the Max Planck Institute for the Research of Living Conditions in the Modern World, in Starnberg. He researched and published on the danger of nuclear war, what he saw as the conflict between the first world and the third world, and the consequences of environmental destruction. In the 1970's he founded, together with the Indian philosopher Pandit Gopi Krishna, a research foundation "for western sciences and eastern wisdom". After his retirement in 1980 he became a Christian pacifist, and intensified his work on the conceptual definition of quantum physics, particularly on the Copenhagen Interpretation.

His experiences in the Nazi era, and with his own behavior in this time, gave Weizsäcker an interest in questions on ethics and responsibility. He was one of the Gättinger 18 — 18 prominent German physicists — who protested in 1957 against the idea that the Bundeswehr should be armed with tactical nuclear weapons. He further suggested that West Germany should declare its definitive abdication of all kinds of nuclear weapons. However he never accepted his share of responsibility for the German scientific community's efforts to build a nuclear weapon for Nazi Germany, and continued to repeat the version of these events agreed on at Farm Hill. Some others believe this version to be a deliberate falsehood.

In 1963 Weizsäcker was awarded the Friedenspreis des Deutschen Buchhandels (peace award of the German booksellers). In 1989, he won the Templeton Prize for Progress in Religion. He also received the Order Pour le Mérite. There is a Gymnasium named after him, in the town of Barmstedt, which lies northwest of Hamburg, in Schleswig-Holstein, the Carl Friedrich von Weizsäcker Gymnasium im Barmstedt.

Main books by C. F. von Weizsäcker

1. Zum Weltbild der Physik. Leipzig, 1946. Translated into English as The World View of Physics, Londres, 1952; in French — Le Monde vu par la Physique, Paris, 1956.
2. Die Geschichte der Natur. Göttingen, 1948.
3. Die Einheit der Natur. München, 1971. Translated into English as The Unity of Nature, N.Y., 1980.
4. Wege in der Gefahr. München, 1976. Translated into English as The Politics of Peril, N.Y., 1978.
5. Der Garten des Menschlichen. München, 1977. Translated as The Ambivalence of Progress: Essays on Historical Anthropology, N.Y., 1988.
6. Introduction to The Biological Basis of Religion and Genius, by Gopi Krishna, N.Y., 1971, 1972 (the introduction takes half the book).
7. Aufbau der Physik. München, 1985. Translated as The Structure of Physics, Heidelberg, 2006.
8. Der Mensch in seiner Geschichte. München, 1991.
9. Zeit und Wissen. München, 1992.
10. Grosse Physiker. München, 1999.

*The biography and foto are included into the issue, from the *Wikipedia*, by the Editors of *Progress in Physics*. The *Wikipedia* texts and images are under the GNU free documentation license. The Editors of *Progress in Physics* are thankful to the *Wikipedia*.

LETTERS TO PROGRESS IN PHYSICS

Zelmanov's Anthropic Principle and Torah

Betzalel Avraham Feinstein

Baltimore, Maryland, USA

E-mail: cafeinst@msn.com; http://chidusheibetzalel.blogspot.com

According to Jewish Kabbalistic tradition, nothing is real except for G-d. In this brief letter, originally addressed to Torah scholars, we demonstrate how Zelmanov's Anthropic Principle is consistent with this tradition by analyzing the famous question in philosophy, "If a tree falls in a forest and no one is around to hear it, does it make a sound?"

There is a famous question in philosophy: "If a tree falls in a forest and no one is around to hear it, does it make a sound?" Philosophers have been debating this question for centuries. The philosophers who answer "No", called idealists, are of the opinion that reality is whatever we perceive it to be. And the philosophers who answer "Yes', called realists, are of the opinion that reality exists independently of observers.

In the 1940's, the prominent cosmologist Abraham Zelmanov introduced his Anthropic Principle:

"The Universe has the interior we observe, because we observe the Universe in this way. It is impossible to divorce the Universe from the observer. The observable Universe depends on the observer and the observer depends on the Universe. If the contemporary physical conditions in the Universe change then the observer is changed. And vice versa, if the observer is changed then he will observe the world in another way. So the Universe he observes will be also changed. If no observers exist then the observable Universe as well does not exist" [1, 2].

The Anthropic Principle answer to the above question is both "Yes" and "No". "Yes", since the observer is dependent upon the observable Universe for his or her existence, so it is possible for sound, which is part of the observable Universe, to exist without an observer. And "No", since the observable Universe is dependent upon the observer for its existence, so it is impossible for sound to exist without an observer. So the Anthropic Principle seems to be logically contradictory. But Zelmanov's Anthropic Principle is nevertheless consistent with Torah. How is this possible?

According to our Torah sages of blessed memory, only G-d is real, since only G-d has an independent existence that is not subject to change from external factors.* The question, "If a tree falls in a forest and no one is around to hear it, does it make a sound?", is based upon the assumption that either the observer or the observable Universe is real. Thus according to the reasoning of our Torah sages of blessed memory, the question, "If a tree falls in a forest and no one is around to hear it, does it make a sound?", is based upon a false premise, since both the observer and the observable universe are not real (according to the sages' definition of "real"). Hence, it is possible for the answer to the question, "If a tree falls in a forest and no one is around to hear it, does it make a sound?" to be both "Yes" and "No" and still be consistent with Torah.

Submitted on May 16, 2007
Accepted on May 21, 2007

*One of the best references for the claim that Torah tradition says that only G-d is real is the book entitled *Tanya*, by Rabbi Shneur Zalman of Liadi [3]. Book 2 of Tanya, entitled *Sha'ar ha-Yichud ve'ha'Emunah* (translated as *The Gateway of Unity and Belief*) explains this principle in detail.

References

1. Rabounski D. Zelmanov's Anthropic Principle and the Infinite Relativity Principle. *Progress in Physics*, 2006, v. 1, 35–37.
2. Zelmanov A. L. Chronometric invariants. Dissertation thesis, 1944. American Research Press, Rehoboth (NM), 2006.
3. Rabbi Shneur Zalman of Liadi. Lessons in Tanya. (The English translation of Tanya, with comments.) Translated by Rabbi Levy Wineberg and Rabbi Sholom B. Wineberg. Edited by Uri Kaploun. Comments by Rabbi Yosef Wineberg. Kehot Publication Society, New York, 1998, 1970 pages in 5 vols.

Open Letter by the Editor-in-Chief: Declaration of Academic Freedom (Scientific Human Rights)
*The Bulgarian Translation**

Декларация за Академична Свобода

(Научни Човешки Права)

Клауза 1: Предисловие

Началото на 21-ви век отразява по-силно от всякога в историята на човечеството, дълбочината и значимостта на ролята, която науката и технологиите имат в човешките дела.

Мощното нахлуване на модерната наука и технологии в различни отрасли дава общопритето впечатление, че бъдещи ключови открития са възможни принципно и единствено от големи правителствени или корпоративно финансирани изследователски групи, които имат достъп до изключително скъпа апаратура и орда от помощен персонал.

Това общоприето впечатление обаче е митично, и не отразява истинската природа на това как се правят научни открития. Големи и скъпи технологични проекти, без значение колко сложни, са всъщност резултат на приложението на проницателни научни прозрения на малка група от отдадени на науката изследователи или самостоятелни учени, често работещи в изолация. Учен, който работи сам, сега и в бъдеще, точно както и в миналото, ще може да прави открития, които значимо могат да повлияят на съдбата на човечеството и да променят лицето на цялата планета, която ние толкова незначително обитаваме.

Фундаментални открития по правило се правят от индивиди, които работят в подчинени позиции в правителствени агенции, изследователски и образователни институции, или комерсиални предприятия. Следователно изследователят често е подтискан от институционните или корпоративни директори, които работещи под друга агенда (дневен ред), се опитват да поемат контрол и да прилагат научните открития за лична или корпоративна изгода, или себевъзвеличаване.

Историята на научните открития е пълна със случаи на подтискане и подигравки към учения дръзнал да се противопостави на установените догми, но в които през следващите години правотата на учения е била доказана чрез неумолимия марш на практическата необходимост и жаждата за интелектуално развитие. Също така историята е пълна и със случаи на мръсен и петнящ плагиаризъм и преднамерено фалшиво представяне на факти, престъпно извършено поради безскруполност, мотивирана от завист и користолюбие. Така е и днес!

Целта на тази Декларация е да подкрепи и развие фундаменталната доктрина защитаваща, че научните изследвания трябва да са независими от скрито или открито подтискащо влияние от бюрократични, политически, религиозни или наказателни директиви, и че създаването на наука е човешко право не по-малко от други основни човешки права, които вече са разискани в различни международни спогодби и международни закони.

Всички учени с подобно мислене нека се придържат към тази Декларация в знак на солидарност с международната научна общност, и нека уважат правото на населението на Земята на неоковано от догми създаване на наука, всеки според собствените индивидуални възможности и предпочитания, за да може да се развива науката, и всеки, като порядъчен гражданин в този непорядъчен свят, да има шанс да допринесе максимална полза за човечеството.

Клауза 2: Кой е учен

Учен е всеки човек, който прави наука. Всеки човек, който сътрудничи с учен в развитието и представянето на идеи и данни в научните изследвания или прилагането им, е също учен. Наличието на професионална квалификация не е пререквизит за да може човек да бъде учен.

Клауза 3: Къде се прави наука

Научни изследвания могат да бъдат извършвани абсолютно навсякъде, например на работното място, в процес на образование, по време на спонсорирана академична програма, в научни групи, или самостоятелно вкъщи провеждайки собствено проучване.

Клауза 4: Свобода на избор на изследователска тема

Много учени работещи за високи научни звания или в други изследователски програми на научни институции като университети и институти за напреднали изследвания, биват възпрепятствани да работят по изследователска тема по собствен избор от висши академични и/или административни представители, не поради липса на необходимата техника, а поради това че академичната йерархия и/или други органи просто не одобряват проучва-

*Original text published in English: *Progress in Physics*, 2006, v. 1, 57–60. Online — http://www.ptep-online.com/

Автор на оригиналния текст е Димитри Рабунски, главен редактор на списание *Progress in Physics*. E-mail: rabounski@yahoo.com

Преводът на Български език е направен от Данко Димчев Георгиев. E-mail: dankomed@gmail.com

ниятa, които могат да се противопоставят на общоприетата догма, любима теория, или поради финансирането на други проекти, които иначе биха могли да бъдат дискредитирани от предложеното проучване. Авторитетът на ортодоксалното мнозинство често бива използван за да потопи начинанията за дадено научно проучване, само и само за да не бъде разстроен бюджета. Тази общоприета практика на обмислено подтискане на свободната научна мисъл е ненаучна в своята екстремност, а освен това е и престъпна. Тя не може да бъде толерирана.

Учен работещ за някаква академична институция, власт или агенция, трябва да бъде абсолютно свободен да избира изследователска тема, ограничена само от материалната база и интелектуални възможности, които могат да бъдат предоставени от институцията, агенцията или властта. Ако учен провежда изследвания като част от сътрудническа група, ръководителите на проекта и водачите на група трябва да бъдат ограничени само до съвещателна и консултативна роля във връзка с избора на подходяща изследователска тема от учен в групата.

Клауза 5: Свобода на избор на изследователски методи

Често бива оказван натиск върху учения от административния персонал или по-старши академици във връзка с дадена изследователска програма провеждана в академична среда, за да се принуди учения да използва други методи от тези които той е избрал, без друга причина освен лични предпочитания, пристрастие, институционна политика, редакторска диктатура, или колективна власт. Тази практика, която е доста разпространена, е преднамерено отричане на свободата на мисълта и не може да бъде разрешена.

Некомерсиален или академичен учен има правото да развива изследователска тема по всеки рационален начин, който учения смята за най-ефективен. Финансовите решения относно това как ще се обезпечи изследването са собствен проблем на учения.

Ако некомерсиален или академичен учен работи като член на колаборативен некомерсиален или академичен колектив от учени, то лидерите на проекта и ръководителите на изследването трябва да имат само съвещателна или консултативна роля и не трябва да повлияват, променят или ограничават изследователските методи или изследователската тема на учен от групата.

Клауза 6: Свобода на участие и сътрудничество в научните изследвания

Налице е значим елемент на институционално съперничество в практиката на съвременната наука, съпътствано от елементи на лична завист или запазване на репутацията на всяка цена, независимо от научната действителност. Това често възпрепятства учените да отблязват помощта на компетентни колеги от съперничещи институции или такива без академично работно място. Подобна практика също е преднамерено възпрепятстване на научния прогрес.

Ако некомерсиален учен иска помощ от друг човек, и този човек е съгласен, то ученият има свободата да покани този човек и да използва всякаква и цялостна помощ, при положение, че помощта е в рамките на предоставения изследователски бюджет. Ако помощта не зависи от предоставения бюджет, то учения има правото да наеме като асистент даден човек по собствена преценка, свободен от възпрепятстване от който и да е било.

Клауза 7: Свобода за несъгласие в научна дискусия

В резултат на скрита завист или направени капиталовложения, модерната наука ненавижда откритата научна дискусия и с желание забранява тези учени, които поставят под въпрос ортодоксалните възгледи. Много често учени с доказани качества, които показват проблеми в общоприета теория или интерпретация на данни, биват наричани ненормални, за да могат техните възгледи да бъдат игнорирани. Те биват подложени на присмех публично или в частна кореспонденция, систематично не биват допускани за участие в научни конгреси, семинари или колоквиуми, за да не могат техните идеи да имат слушатели. Преднамерена фалшификация на данни или изопачаване на дадена теория, сега са често оръжие в арсенала на тези които безскруполно целят подтискането на определени научни или исторически факти. Формирани международни комитети съставени от научни мерзавци сега провеждат и оглавяват научни конгреси на които могат да участват само последователи, които представят статии без значение от качеството на съдържанието им. Тези комитети използват крупни суми от обществения бюджет за да спонсорират собствените си проекти употребявайки измама и лъжи. Всяко възражение към техните предложения, което е базирано на научни аргументи бива заглушавано с всички налични средства, за да могат парите да продължават да текат в собствените научноизследователски сметки, по този начин гарантирайки им добре платено собствено работно място. По тяхна повеля част от противопоставилите се учени биват изхвърляни от работното място, други биват възпрепятствани от успешно уговаряне на научни мероприятия чрез изградена мрежа от корумпирани съучастници. В някои ситуации учени биват изхвърляни от конкурси за висши образователни програми, например докторантури, за това че са изразили идеи които подкопават дадена модна теория, независимо от това колко е отдавнашна тази ортодоксална теория. Фундаментален факт е, че никоя научна теория е непоклатима или неприкосновена, следователно всяка теория е отворена за дискусия и повторно оценяване. Това обаче е забравено от споменатите

международни комитети. Те също така игнорират факта, че даден феномен може да има множество правдоподобни обяснения, и злостно дискредитират всяко обяснение което не е в унисон с тяхното ортодоксално мнение като без да се колебаят използват ненаучни аргументи за да оправдаят пристрастните си убеждения.

Всички учени трябва да бъдат свободни да обсъждат собствените си изследвания както и изследванията на други учени без страх от публично или лично безпричинно осмиване, без страх от това да бъдат обвинени, очернени, поставени под съмнение, или да бъдат дискредитирани по друг начин от безпочвени твърдения. Никой учен не бива да бъде поставян в положение в което прехраната или репутацията му да бъдат рискувани само заради изказването на научно мнение. Свободата за научно изразяване трябва да е първостепенна. Употребата на власт за отхвърлянето на научен аргумент е ненаучна и не трябва да бъде използвана за заблуда, потискане, заплашване, отлъчване от обществото, или по друг начин насилва или оковава учения. Преднамереното потискане на научните факти или аргументи, както чрез действие така и чрез бездействие, а също и преднамереното подправяне на фактите за да подкрепят аргумент или дискредитират противопоставящ се възглед, е научна измама, която е равна на научно престъпление. Принципите на доказване трябва да водят всяка научна дискусия, независимо дали доказателтсвото е физично, теоретично (математическо), или комбинация от двете споменати.

Клауза 8: Свобода на публикуване на научни резултати

Окаяно и жалко цензориране на научни статии сега се е превърнало в стандартна практика на редакторските бордове на важни списания и електронни архиви, и тяхната банда от набедени експертни рецензенти. Рецензентите в голяма част са предпазени от гарантираната анонимност така че авторът не може да е сигурен в тяхната компетентност. Статии сега рутинно се отхвърлят поради това, че авторът не е съгласен или се противопоставя на общоприето предпочитана теория или преобладаваща правоверност. Много статии сега се отхвърлят автоматично само защото сред авторите се появява името на учен, който е имал пререкания с редакторите на списанието, рецензентите, или други експертни цензори, като въобще и не се поглежда съдържанието на отхвърлената статия. Съществуват "черни листи" на инакомислещи учени и този лист се разпространява между редакторските бордове на списания които имат един и същ участващ редактор. Всичко това спомага за голямо пристрастие и престъпно потискане на свободната мисъл, и би трябвало да бъдат заклеймени от международната научна общност.

Всички учени трябва да имат право да представят техните научни резултати, изцяло или частично, на съответни научни конференции, както и да ги публикуват в отпечатвани научни списания, електронни архиви, или всякаква друга медия. Никой учен не трябва да получава отказ за публикуване на изпратена от него работа просто защото е подложил на въпрос мнението на сегашното мнозинство, съществува конфликт с мнението на редакторския борд, подкопава устоите на текущи или планирани от други учени изследвания, е в конфликт с някаква политическа догма, религиозно изповедание, или личното мнение на някого, и никой учен не трябва да бъде поставян в "черна листа", цензуриран или недопускан да публикува поради някого си. Никой учен не бива да блокира, модифицира, или по друг начин възпрепятства публикацията на работа на друг учен поради какъвто и да е било обещан подкуп.

Клауза 9: Съавторство на научни статии

Слабо пазена тайна в научните кръгове е, че много съавтори на научни статии всъщност имат малък или даже никакъв принос относно докладваните в публикацията резултати. Много ръководители на докторанти например нямат нищо против да си поставят името заедно с автора на който те са ръководители. В много от случаите човекът, който пише статията е интелектуално понапред от формалния си ръководител. В други случаи, отново заради желание за именитост, репутация, пари, престиж и други подобни, не участвали в проучването хора биват включвани в статията като съавтори. По този начин действителния автор може да отговаря на противопоставени алтернативни възгледи но само с риск след това да бъде наказан по някакъв начин, или рискува да не получи научната си степен. Много всъщност биват изхвърлени и не завършват научната си степен поради тази причина. Такава безобразна практика не може да бъде толерирана. Само хора, които са отговорни за изследването трябва да бъдат официално обявени за съавтори.

Никой учен не трябва да кани друг човек да бъде включен и никой учен не бива да позволява да бъде включен като съавтор на научна статия, ако те не са допринесли значимо за резултатите публикувани в статията. Никой учен не бива да позволява да бъде насилен от представител на дадена академична институция, корпорация, правителствена агенция, или друг човек, за да бъдат имената на тези хора включени като съавтор в изследване проведено от учения в което те не са допринесли значимо, както и учения не бива да предоставя името си за употреба като съавтор в замяна на подаръци или друг подкуп. Никой човек не бива да убеждава или да се опитва да убеждава учен, по какъвто и да е било начин, за да може името на учения да бъде включено като съавтор на научна статия относно резултати за които учения не е допринесъл значимо.

Клауза 10: Независимост на учения от връзки с институция

Много учени сега биват наемани с краткотрайни договори. С прекратяване на трудовия договор се прекратява и академичната връзка с дадена институция. Честа политика на редакторските бордове на списания е да не публикуват статии на хора без връзка с академична или комерсиална институция. Поради липсата на връзка с институция много възможности остават недостъпни за учения, а също така шансовете му да представя лекции и статии на конференции биват редуцирани. Това е порочна практика, която трябва да бъде спряна. Науката не признава връзките с институция.

Нито един учен не бива да бъде възпрепятстван да представя статии на конференции, колоквиуми или семинари, да публикува резултатите си във всякаква медия, да има достъп до академични библиотеки или научни публикации, да посещава научни срещи, да чете лекции, да иска връзка с дадена академична институция, научен институт, правителствена или комерсиална лаборатория, или друга организация.

Клауза 11: Отворен достъп до научна информация

Повечето специализирани книги относно научна информация, както и много научни списания, имат малка или не носят никаква печалба, така че комерсиални издателски къщи не желаят да публикуват такива творби без да им се заплати от академичната институция, правителствена агенция, филантропска фондация, или други подобни. При такива обстоятелства комерсиалните издателски къщи трябва да предоставят свободен достъп до електронните версии на публикуваните научни материали, и да се борят да редуцират цената на отпечатаните от тях публикации до минимум.

Нека всички учени се борят за осигуряване на неплатен достъп до техните научни публикации, или ако това не е възможно, то достъпът да е на минимална цена. Всички учени трябва да предприемат активни мерки, за да могат техните специализирани книги да бъдат достъпни на възможно най-малка цена по този начин правейки научната информация широко достъпна за международното научно общество.

Клауза 12: Морална отговорност на учените

Историята ни учи, че научните открития се използват както за добро така и за зло, за полза на едни и разоряване на други. Тъй като прогресът на науката и технологията не може да бъде спрян, то трябва да бъдат предприети мерки за ограничаване на потенциални злосторни приложения. Само демократично избрано правителство, свободно от религиозни, расистки или други предразсъдъци, може да охранява цивилизацията. Единствено демократично избрано правителство, трибунал или комитет могат да охраняват правото на свобода на научно създаване. Днес, различни недемократични страни или тоталитарни режими активно провеждат изследвания в областта на ядрената физика, химия, вирусология, генетично инжинерство, и други науки, за да могат да продуцират ядрено, химическо или биологическо оръжие. Нито един учен не бива да сътрудничи на недемократични страни или тоталитарни режими. Всеки учен принуден да работи за разработка на оръжие на такива страни трябва да намери начин и средства да забави развитието на изследователските програми и да редуцира научната производителност, за да може цивилизацията и демокрацията да възтържествуват.

Всички учени носят морална отговорност за собствените научни разработки и открития. Нито един учен не бива доброволно да се въвлича в дизайн или конструкция на каквито и да е било оръжия за недемократични страни или тоталитарни режими, или да позволява неговите научни умения и знание да бъдат приложени за разработване на нещо което може да навреди на човечеството. Ученият трябва да живее с мисълта, че всяко недемократично правителство или незачитане на човешките права е престъпление.

Март 12, 2007

Open Letter by the Editor-in-Chief: Declaration of Academic Freedom (Scientific Human Rights)
*The Romanian Translation**

Declaraţie asupra Libertăţii Academice

(Drepturile Omului în Domeniul Ştiinţific)

Articolul 1: Introducere

Inceputul secolului al 21-lea reflectă mai mult decât oricând în istoria omenirii, rolul adânc şi significant al ştiinţei şi tehnologiei în activităţile umane.

Natura atotpătrunzătoare şi universală a ştiinţei şi tehnologiei moderne a dat naştere unei percepţii comune că viitoarele descoperiri importante pot fi făcute, în principal sau în exclusivitate, numai de grupuri mari de cercetare finanţate de guvernări sau de firme mari, care au access la instrumente foate scumpe precum şi la un număr mare de personal de support.

Această percepţie comună, este totuşi nerealistă şi contrazice modul adevărat în care sunt făcute descoperirile ştiinţifice. Proiecte tehnologice mari şi scumpe, oricât de complexe, sunt numai rezultatul aplicării profundei intuiţii ştiinţifice a unor grupuri mici de cercetători dedicaţi sau a unor oameni de ştiinţă solitari, care de multe ori lucrează izolaţi. Un om de ştiinţă care lucrează singur, este, acum precum şi în viitor, aşa cum a fost şi în trecut, capabil să facă o descoperire, care poate influenţa substanţial soarta omenirii şi poate schimba faţa întegii planete pe care o locuim pentru aşa de puţin timp.

Descoperirile cele mai importante sunt făcute de persoane care lucreaza ca subalterni în diverse agenţii guvernamentale, instituţii de învăţământ şi cercetare, sau intreprinderi comerciale. În consecinţă, cercetătorul este foare frecvent forţat sau umbrit de directorii instituţiilor şi firmelor, care, având planuri diferite, caută să controleze şi să aplice descoperirile ştiintifice şi cercetările pentru profit personal sau pentru organizaţie, sau prestigiu personal.

Recordul istoric al decoperirilor ştiinţifice abundă în cazuri de represiune şi ridiculizare făcute de cei la putere, dar în ultimii ani acestea au fost dezvăluite si corectate de către inexorabilul progres al necesităţii practice şi iluminare intelectuală. Tot aşa de rău arată şi istoria distrugerii şi degradării produse prin plagiarism şi denaturare intenţionată, făcute de necinstiţi, motivaţi de invidie şi lăcomie. Şi aşa este şi azi.

Intenţia acestei Declaraţii este să sprijine şi să dezvolte doctrina fundamentală că cercetarea ştiinţifică trebuie să fie liberă de influenţa ascunsă şi făţiş represivă a directivelor birocratice, politice, religioase, pecuniare şi, de asemenea, creaţia ştiinţifică este un drept al omului, nu mai mic decât alte drepturi similare şi speranţe disperate care sunt promulgate in acorduri şi legi internaţionale.

Toţi oamenii de ştiinţă care sunt de acord vor trebui să respecte aceasta Declaraţie, ca o indicaţie a solidarităţii cu comunitatea ştiinţifică internaţională care este preocupată de acest subiect, şi să asigure drepturile cetăţenilor lumii la creaţie ştiinţifică fără amestec, în acordanţă cu talentul şi dispoziţia fiecăruia, pentru progresul ştiinţei şi conform abilităţii lor maxime ca cetăţeni decenţi într-o lume indecentă, în avantajul Omenirii. Stiinţa şi tehnologia au fost pentru prea multă vreme servanţii asupririi.

Articolul 2: Cine este un cercetător ştiinţific

Un cercetător ştiinţific este orice persoană care se preocupă de ştiinţă. Orice persoană care colaborează cu un cercetător în dezvoltarea şi propunerea ideilor şi a informaţiilor într-un project sau aplicaţie, este de asemenea un cercetător. Deţinerea unor calificări formale nu este o cerinţă prealabilă pentru ca o persoană să fie un cercetător ştiinţific.

Articolul 3: Unde este produsă ştiinţa

Cercetarea ştiinţifică poate să aibă loc oriunde, de exemplu, la locul de muncă, în timpul studiilor, în timpul unui program academic sponsorizat, în grupuri, sau ca o persoană singură acasă făcând o cercetare independentă.

Articolul 4: Libertatea de a alege o temă de cercetare

Mulţi cercetători care lucrează pentru nivele mai avansate de cercetare sau în alte programe de cercetare la instituţii academice, cum sunt universităţile şi facultăţile de studii avansate, sunt descurajaţi, de personalul de conducere academic sau de oficiali din administraţie, de a lucra în domeniul lor preferat de cercetare, şi aceasta nu din lipsa mijloacelor de suport, ci din cauza ierarhiei academice sau a altor oficialităţi, care pur şi simplu nu aprobă o direcţie de cercetare să se dezvolte la potenţialul ei, ca să nu deranjeze dogma convenţională, teoriile favorite, sau subvenţionarea altor proiecte care ar putea fi discreditate de cercetarea propusă. Autoritatea majorităţii ortodoxe este destul de frecvent invocată ca să stopeze un proiect de cercetare, astfel încât autorităţile şi bugetul să nu fie deranjate. Această practică

*Original text published in English: *Progress in Physics*, 2006, v. 1, 57–60. Online — http://www.ptep-online.com/

Textul originar în limba engleză de Dmitri Rabounski, Redactor Şef al revistei *Progress in Physics*. E-mail: rabounski@yahoo.com

Traducere autorizată în limba romană de Florentin Smarandache. E-mail: smarand@unm.edu

comună este o obstrucţie deliberată a gândirii libere, este neştiinţifică la extrem, şi este criminală. Aceasta nu poate fi tolerată.

Un cercetător care lucrează pentru orice instituţie academică, organizaţie, sau agenţie trebuie să fie complet liber în alegerea unei teme de cercetare şi să fie limitat doar de suportul material şi de expertiza intelectuală care poate fi oferită de instituţia academică, organizaţia, sau agenţia respectivă. Dacă un cercetător îşi desfăsoară activitatea lui de cercetare fiind membru al unui grup de cercetători, atunci directorii de cercetare şi liderii grupului îşi vor limita rolul lor doar la capacitatea de recomandare şi consultanţă în ceea ce priveşte alegerea unei teme de cercetare relevante de către un cercetător din grup.

Articolul 5: Libertatea de alegere a metodelor de cercetare

În multe cazuri personalul administrativ sau academic de conducere impune o anumită presiune asupra unor cercetători, care fac parte dintr-un program de cercetare care se desfăşoară într-un mediu academic, ca să-i forţeze să adopte alte metode de cercetare decât acelea alese de ei, motivul fiind nu altul decât o preferinţă personală, o prejudecată, o procedură instituţională, ordine editorială, ori autoritate colectivă. Această practică, care este destul de răspândită, este o eliminare deliberată a libertăţii de gândire, şi această nu poate fi permisă.

Un cercetator academic sau dintr-o instituţie care nu lucrează pentru profit are dreptul să dezvolte o temă de cercetare în orice mod rezonabil, utilizând orice mijloace rezonabile pe care el le consieră că vor fi cele mai eficiente. Doar cercetătorul însuşi ia decizia finală asupra modului cum cercetarea va fi efectuată.

Dacă un cercetator academic, sau dintr-o instituţie care nu lucrează pentru profit, lucrează ca un membru al unui grup de cercetători academici, sau dintr-o instituţie care nu lucrează pentru profit, conducătorii de proiect şi directorii de cercetare vor avea doar un rol de îndrumători şi consultanţi şi nu trebuie în nici un fel să influenţeze, să intervină, sau să limiteze metodele de cercetare sau tema de cercetare ale unui cercetător din grup.

Articolul 6: Libertatea de participare şi colaborare în cercetare

În practicarea ştiinţei moderne există un element semnificant de rivalitate instituţională, concomitent cu elemente de invidie personală şi de prezervare a reputaţiei cu orice preţ, indiferent de realităţile ştiinţifice. Aceasta de multe ori a condus la faptul că cercetătorii au fost împiedicaţi să nominalizeze asistenţa colegilor competenţi care fac parte din instituţii rivale sau alţii care nu au nici o afiliaţie academică. Această practică este de asemenea o obstrucţie deliberată a progresului ştiinţific.

Dacă un cercetator ştiinţific dintr-o instituţie care nu lucrează pentru profit cere asistenţa unui alt cercetător şi dacă acel cercetător este de accord, cercetătorul are libertatea de a invita celălalt cercetător să-i ofere orice asistenţă, cu condiţia ca asistenţa să fie în cadrul bugetului de cercetare stabilit. Dacă asistenţa este independentă de buget, cercetătorul are libertatea să angajeze cercetătorul colaborator la discreţia lui, fără absolut nici o intervenţie din partea nici unei alte persoane.

Articolul 7: Libertatea de a nu fi de accord în discuţii ştiinţifice

Datorită invidiei ascunse şi a intereselor personale, ştiinţa modernă nu apreciază discuţii deschise şi nu acceptă în mod categoric pe acei cercetători care pun la îndoială teoriile ortodoxe. Deseori, cercetători cu abilităţi deosebite, care arată deficienţele într-o teorie actuală sau într-o interpretare a datelor, sunt denumiţi excentrici, astfel ca vederile lor să poată fi ignorate cu uşurinţă. Ei sunt făcuţi de râs în public şi în discuţii personale şi sunt opriţi în mod sistematic de a participa la convenţii, seminarii, sau colocvii ştiinţifice, astfel ca ideile lor să nu poată să găsească o audienţă. Falsificări deliberate ale datelor şi reprezentarea greşită a teoriei sunt acum unelte frecvente ale celor fără scrupule, în eliminarea dovezilor, atât tehnice cât şi istorice. Comitete internaţionale de cercetători rău-intenţionaţi au fost formate şi aceste comitete organizează şi conduc convenţii internaţionale, unde numai cei care sunt de accord cu ei sunt admişi să prezinte lucrări, indiferent de calitatea acestora. Aceste comitete extract sume mari de bani din bugetul public ca să suporte proiectele lor preferate, folosind falsităţi şi minciuni. Orice obiecţiune la propunerile lor, pe baze ştiinţifice, este trecută sub tăcere prin orice mijloace la dispoziţia lor, aşa ca banii să poată să continue să se verse la conturile proiectelor lor şi să le garanteze posturi bine plătite. Cercetătorii care s-au opus au fost daţi afară la cererea acestor comitete, alţii au fost împiedicaţi, de către o reţea de complici corupţi, de a obţine posturi academice. În alte situaţii unii au fost daţi afară de la candidatura pentru titluri academice avansate, cum ar fi doctoratul, pentru că şi-au exprimat idei care nu sunt de accord cu teoria la modă, chiar dacă această teorie ortodoxă la modă este în vigoare de multă vreme. Ei ignoră complet faptul fundamental că nici o teorie ştiinţifică nu este definitivă şi inviolabilă, şi prin urmare este deschisă pentru discuţii şi re-examinare. De asemenea ei ignoră faptul că un fenomen ar putea să aibă mai multe explicaţii plauzibile, şi în mod răutăcios discreditează orice explicaţie care nu este de acord cu opinia ortodoxă, folosind fără nici o restricţie argumente neştiinţifice să explice opiniile lor părtinitoare.

Toţi cercetătorii trebuie să fie liberi să discute cercetările lor şi cercetările altora, fără frica de a fi ridiculizaţi, fără nici o bază materială, în public sau în discuţii particulare,

sau să fie acuzaţi, criticaţi, nerespectaţi sau discreditaţi în alte feluri, cu afirmaţii nesubstanţiate. Nici un cercetător nu trebuie să fie pus într-o poziţie în care situaţia sau reputaţia lui vor fi riscate, datorită exprimării unei opinii ştiinţifice. Libertatea de exprimare ştiinţifică trebuie să fie supremă. Folosirea autorităţii în respingerea unui argument ştiinţific este neştiinţifică şi nu trebuie să fie folosită ca să oprească, să anuleze, să intimideze, să ostracizeze, sau să reducă la tăcere ori să interzică în orice fel un cercetător. Înterzicerea deliberată a faptelor sau argumentelor ştiinţifice, fie prin fapte sau prin omitere, şi falsificarea deliberată a datelor, ca să suporte un argument sau ca să discrediteze un punct de vedere opus, este o decepţie ştiinţifică, care poate fi numită crimă ştiinţifică. Principiile de evidenţă trebuie să fie călăuza discuţiei ştiinţifice, fie că acea evidenţa este fizică sau teoretică sau o combinaţie a lor.

Articolul 8: Libertatea de a publica rezultate ştiinţifice

O cenzură deplorabilă a articolelor ştiinţifice a devenit acum practica standard a editorilor multor jurnale de specialitate şi arhive electronice, şi a grupurilor lor de aşa zişi referenţi experţi. Referenţii sunt, în majoritate, protejaţi prin anonimitate aşa încât un autor nu le poate verifica aşa zisa lor expertiză. Lucrările sunt acum de obicei respinse dacă autorul nu este de accord sau contrazice teorii preferate şi ortodoxia majoritară. Multe lucrări sunt acum respinse în mod automat bazat pe faptul că în bibliografie apare citat un cercetător care nu este în graţiile editorilor, referenţilor, sau al altor cenzori experţi, cu nici un fel de consideraţie faţă de conţinutul lucrării. Există o listă neagră a cercetătorilor care sunt în opoziţie şi această listă este comunicată între conducerile editurilor. Toate acestea duc la o crasă prejudecare şi o represiune greşită împotriva gândirii libere şi trebuie condamnate de comunitatea internaţională a cercetătorilor.

Toţi cercetătorii trebuie să aibă dreptul să prezinte rezultatele cercetărilor lor ştiinţifice, în totalitate sau parţial, la conferinţe ştiinţifice relevante, şi să le publice în jurnale ştiinţifice tipărite, arhive electronice sau in altă media. Cercetătorilor nu trebuie să li se respingă lucrările sau rapoartele lor când sunt prezentate spre publicare în jurnale ştiinţifice, arhive electronice, sau in altă media, numai pentru motivul că lucrările lor pun sub semn de întrebare opinia majoritară curentă, este în contradicţie cu opiniile unei conduceri editoriale, zdruncină bazele altor proiecte de cercetare prezente sau de viitor ale altor cercetători, este în conflict cu orice dogmă politică sau doctrină religioasă, sau cu opinia personală a cuiva, şi nici un cercetător ştiinţific nu trebuie să fie pe lista neagră sau cenzurat şi împiedicat de la publicare de nici o altă persoană. Nici un cercetător ştiinţific nu trebuie să blocheze, modifice, sau să se amestece în orice mod la publicarea lucrării unui cercetător deoarece îi sunt promise cadouri sau alte favoruri.

Artiolul 9: Publicând articole ştiinţifice în calitate de co-autor

In cercurile ştiinţifice este un secret bine cunoscut, că mulţi co-autori ai lucrărilor de cercetare au foarte puţin sau nimic în comun cu rezultatele prezentate. Mulţi conducători de teze ale studenţilor, de exemplu, nu au nici o problemă să-şi pună numele pe lucrările candidaţilor pe care numai formal îi coordonează. În multe cazuri dintre acestea, persoana care de fapt scrie lucrarea are o inteligenţă superioară celei a coordinatorului. In alte situaţii, din nou, pentru motive de notorietate, reputaţie, bani, prestigiu, şi altele, neparticipanţi sunt incluşi în lucrare în calitate de co-autori. Adevăraţii autori ai acestor lucrări pot să obiecteze numai cu riscul de a fi penalizaţi mai târziu într-un mod sau altul, sau chiar riscând să fie excluşi de la candidatura pentru grade superioare de cercetare sau din grupul de cercetare. Mulţi au fost de fapt eliminaţi din aceste motive. Această teribilă practică nu poate fi tolerată. Numai acele persone responsabile pentru cercetare trebuie să fie creditaţi ca autori.

Cercetatorii nu trebuie să invite alte persoane să fie co-autori şi nici un cercetător nu ar trebui să admită ca numele lui să fie inclus în calitate de co-autor la o lucrare ştiinţifică, dacă nu au avut o contribuţie substanţială la cercetarea prezentată în lucrare. Nici un cercetător nu trebuie să se lase forţat de nici un reprezentant al unei instituţii academice, firmă, agenţie guvernamentală, sau orice altă persoană să devină co-autor la o lucrare, dacă ei nu au avut o contribuţie significantă pentru acea lucrare, şi nici un cercetător nu trebuie să accepte să fie co-autor în schimb pentru pentru cadouri sau alte gratuităţi. Nici o persoană nu trebuie să încurajeze sau să încerce să încurajeze un cercetător, în orice modalitate, să admită ca numele său să fie inclus în calitate de co-autor al unei lucrări ştiinţifice pentru care ei nu au adus o contribuţie semnificativă.

Articolul 10: Independenţa afiliaţiei

Mulţi cercetători sunt angajaţi prin contracte de scurtă durată. Odată cu terminarea contractului se termină şi afiliaţia academică. Este frecventă practica conducerii editurilor ca persoanelor fără afiliaţie academică sau comercială să nu li se publice lucrările. Când cercetătorul nu este afiliat, el nu are resurse şi deci are oportunităţi reduse să participe şi să prezinte lucrări la conferinţe. Aceasta este o practică vicioasă care trebuie stopată. Ştiinţa nu recunoaşte afiliaţie.

Nici un cercetător nu trebuie să fie împiedicat de la prezentarea de lucrări la conferinţe, colocvii sau seminarii, de la publicarea în orice media, de la acces la biblioteci academice sau publicaţii ştiinţifice, de la participarea la şedinţe academice, sau de la prezentarea de prelegeri, din cauză că nu are o afiliere cu instituţii academice, institute de cercetare, laboratoare guvernamentale sau comericale, sau cu orice altă organizaţie.

Articolul 11: Acces deschis la informaţia ştiinţifică

Multe cărţi ştiinţifice de specialitate şi multe jurnale ştiinţifice au un profit mic sau nici un profit, de aceea editorii refuză să le publice fără o contribuţie monetară de la instittţiile academice, agenţii guvernamentale, fundaţii filantropice, şi altele. În aceste circumstanţe editorii ar trebui să dea acces liber la versiunile electronice ale publicaţiilor, şi să se străduiască să menţină costul pentru tipărirea materialului la minim.

Toţi cercetătorii trebuie să se străduiască să se asigure ca lucrările lor să fie gratuite şi accesibile la comunitatea ştiinţifică internaţională, sau, dacă nu este posibil, la un preţ modest. Toţi cercetătorii trebuie să ia măsuri active ca să ofere cărţile lor tehnice la cel mai mic preţ posibil, pentru ca informaţia ştiinţifică să devină accesibilă marii comunităţi ştiinţifice internaţionale.

Articolul 12: Responsabiltatea etică a cercetătorilor

Istoria este martoră că descoperirile ştiinţifice sunt folosite în ambele direcţii, bune şi rele, pentru binele unora şi pentru distrugerea altora. Deoarece progresul ştiinţei şi tehnologiei nu poate fi oprit, trebuie să avem metode de control asupra applicaţiilor rău făcătoare. Doar guvernele alese democratic, eliberate de religie, de rasism şi alte prejudicii, pot să protejeze civilizaţia. Doar guvernele, tribunalele şi comitetele alese democratic pot proteja dreptul la o creaţie ştiinţifică liberă. Astăzi, diferite state nedemocratice şi regime totalitare performă o activă cercetare în fizica nucleară, chimie, virologie, inginerie genetică, etc. ca să producă arme nucleare, chimice şi biologice. Nici un cercetător nu trebebuie să colaboreze voluntar cu state nedemocratice sau regime totalitare. Orice cercetător forţat să lucreze în crearea de arme pentru astfel de state trebuie să găsească mijloace de a încetini progresul programelor de cercetare şi să reducă rezultatele ştiinţifice, astfel încât civilizaţia şi democraţia în cele din urmă să triumfe.

Toţi cercetătorii au o responsabilitate morală pentru descoperirile şi rezultatele lor ştiinţifice. Nici un cercetător să nu se angajeze de bună voie în proiectarea sau construcţia a nici unui fel de armament pentru state cu regimuri nedemocratice sau totalitare sau să accepte ca talentele şi cunoştiinţele lor să fie aplicate în crearea de arme care vor conduce la distrugerea Omenirii. Un cercetător ştiinţific trebuie să trăiască aplicând dictonul că toate guvernele nedemocratice şi violarea drepturilor umane sunt crime.

14 martie, 2007

Open Letter by the Editor-in-Chief: Declaration of Academic Freedom (Scientific Human Rights)
*The French Translation**

Déclaration de la Liberté Académique

(Les Droits de l'Homme dans le Domaine Scientifique)

Article 1: Préambule

Le début du 21ème siècle reflète, plus qu'aucun autre temps de l'histoire, la profondeur et l'importance de la science et la technologie dans les affaires humaines.

La nature puissante et influente de la science et la technologie modernes a fait naître une perception commune voulant que les prochaines grandes découvertes ne peuvent être faites principalement ou entièrement que par des groupes de recherche qui sont financés par des gouvernements ou des sociétés et ont accès à une instrumentation dispendieuse et à des hordes de personnel de soutien.

Cette perception est cependant mythique et donne une fausse idée de la façon dont des découvertes scientifiques sont faites. Les grands et coûteux projets technologiques, aussi complexes qu'ils soient, ne sont que le résultat de l'application de la perspicacité des petits groupes de recherche ou d'individus dévoués, travaillant souvent seuls ou séparément. Un scientifique travaillant seul est, maintenant et dans le futur, comme dans le passé, capable de faire une découverte qui pourrait influencer le destin de l'humanité.

Les découvertes les plus importantes sont généralement faites par des individus qui sont dans des positions subalternes au sein des organismes gouvernementaux, des établissements de recherche et d'enseignement, ou des entreprises commerciales. Par conséquent, le rechercheur est trop souvent restraint par les directeurs d'établissements ou de la société, qui ont des ambitions différentes, et veulent contrôler et appliquer les découvertes et la recherche pour leur bien-être personnel, leur agrandissement, ou pour le bien-être de leur organisation.

L'histoire est remplie d'exemples de suppression et de ridicule par l'établissement. Pourtant, plus tard, ceux-ci ont été exposés et corrigés par la marche inexorable de la nécessité pratique et de l'éclaicissement intellectuel. Tristement, la science est encore marquée par la souillure du plagiat et l'altération délibérée des faits par les sans-scrupules qui sont motivés par l'envie et la cupidité; cette pratique existe encore aujourd'hui.

L'intention de cette Déclaration est de confirmer et promouvoir la doctrine fondamentale de la recherche scientifique; la recherche doit être exempte d'influences suppressive, latente et manifeste, de directives bureaucratiques, politiques, religieuses et pécuniaires. La création scientifique doit être un droit de l'homme, tout comme les droits et espérances tels que proposés dans les engagements internationaux et le droit international.

Tous les scientifiques doivent respecter cette Déclaration comme étant signe de la solidarité dans la communauté scientifique internationale. Ils défendront les droits à la création scientifique libre, selon leurs différentes qualifications, pour l'avancement de la science et, à leur plus grande capacité en tant que citoyens honnêtes dans un monde malhonnête, pour permettre un épanouissement humain. La science et la technologie ont été pendant trop longtemps victimes de l'oppression.

Article 2: Qu'est-ce qu'un scientifique

Un scientifique est une personne qui travaille en science. Toute personne qui collabore avec un scientifique en développant et en proposant des idées et des informations dans la recherche, ou son application, est également un scientifique. Une formation scientifique formelle n'est pas un prérequis afin d'être un scientifique.

Article 3: Le domaine de la science

La recherche scientifique existe n'importe où, par exemple, au lieu de travail, pendant un cours d'éducation formel, pendant un programme universitaire commandité, dans un groupe, ou en tant qu'individu à sa maison conduisant une recherche indépendante.

Article 4: Liberté du choix du thème de recherche

Plusieurs scientifiques qui travaillent dans des échelons plus élevés de recherche tels que les établissements académiques, les universités et les institutions, sont empêchés de choisir leurs sujets de recherche par l'administration universitaire, les scientifiques plus haut-placés ou par des fonctionnaires administratifs. Ceci n'est pas par manque d'équipements, mais parce que la hiérarchie académique et/ou d'autres fonctionnaires n'approuvent pas du sujet d'une enquête qui pourrait déranger le dogme traditionnel, les théories favorisées, ou influencer négativement d'autres projets déjà proposés. L'autorité plutôt traditionnelle est souvent suscitée pour

*Original text published in English: *Progress in Physics*, 2006, v. 1, 57–60. Online — http://www.ptep-online.com/

Le texte originaire en anglais par Dmitri Rabounski, rédacteur en chef de la revue *Progress in Physics*. E-mail: rabounski@yahoo.com

Traduction autorisée en français par Florentin Smarandache (New Mexico, USA), e-mail: smarand@unm.edu. Edition par Stéphanie Robitaille-Trzcinski (Nova Scotia, Canada), e-mail: str@ns.sympatico.ca.

faire échouer un projet de recherche afin de ne pas déranger l'autorité et les budgets. Cette pratique commune est une obstruction délibérée à la science, ainsi que la pensée scientifique et démontre un élément anti-scientifique à l'extrême; ces actions sont criminelles et ne peuvent pas être tolérées.

Un scientifique dans n'importe quel établissement académique, institution ou agence, doit être complètement libre quant au choix d'un thème de recherche. Il peut être limité seulement par l'appui matériel et les qualifications intellectuelles offertes par l'établissement éducatif, l'agence ou l'institution. Quand un scientifique effectue de la recherche collaborative, les directeurs de recherche et les chefs d'équipe seront limités aux rôles de consultation et de recommandation par rapport au choix d'un thème approprié pour un scientifique dans leur groupe.

Article 5: Liberté de choisir ses méthodes et ses techniques de recherche

Souvent les scientifiques sont forcés par le personnel administratif ou académique à adopter des méthodes de recherches contraires à celles que le scientifique préfère. Cette pression exercée sur un scientifique contre son gré est à cause de la préférence personnelle, le préjugé, la politique institutionnelle, les préceptes éditoriaux, ou même l'autorité collective. Cette pratique répandue va à l'encontre la liberté de pensée et ne peut pas être permise ni toléreé.

Un scientifique travaillant à l'extérieur du secteur commercial doit avoir le droit de développer un thème de recherche de n'importe quelle manière et moyens raisonnables qu'il considère les plus efficaces. La décision finale sur la façon dont la recherche sera executée demeure celle du scientifique lui-même.

Quand un scientifique travaille en collaboration, il doit avoir l'indépendance de choisir son thème et ses méthodes de recherche, tandis que les chefs de projets et les directeurs auront seulement des droits de consultatition et de recommandation, sans influencer, atténuer ou contraindre les méthodes de recherches ou le thème de recherche d'un scientifique de leur groupe.

Article 6: Liberté de participation et de collaboration en recherche

La rivalité entre les différentes institutions dans la science moderne, la jalousie personnelle et le désir de protéger sa réputation à tout prix empêchent l'entraide parmi des scientifiques qui sont aussi compétents les uns que les autres mais qui travaillent dans des établissements rivaux. Un scientifique doit avoir recours à ses collègues dans un autre centre de recherche.

Quand un premier scientifique qui n'a aucune affiliation commerciale a besoin de l'aide et qu'il invite un autre scientifique, ce deuxième est libre d'accepter d'aider le premier si l'aide demeure à l'intérieur du budget déjà établi. Si l'aide n'est pas dépendante des considérations budgetaires, le premier scientifique a la liberté d'engager le deuxième à sa discrétion sans l'interposition des autres. Le scientifique pourra ainsi rémunérer le deuxième s'il le désire, et cette décision demeure à sa discrétion.

Article 7: Liberté du désaccord dans la discussion scientifique

À cause de la jalousie et des intérêts personnels, la science moderne ne permet pas de discussion ouverte et bannit obstinément ces scientifiques qui remettent en cause les positions conventionnelles. Certains scientifiques de capacité exceptionnelle qui précisent des lacunes dans la théorie ou l'interprétation courante des données sont étiquetés comme cinglés, afin que leurs opinions puissent être facilement ignorées. Ils sont raillés en public et en privé et sont systématiquement empêchés de participer aux congrès scientifiques, aux conférences et aux colloques scientifiques, de sorte que leurs idées ne puissent pas trouver une audience. La falsification délibérée des données et la présentation falsifiée des théories sont maintenant les moyens utlilisés habituellement par les sans-scrupules dans l'étouffement des faits, soit techniques soit historiques. Des comités internationaux de mécréants scientifiques ont été formés et ces mêmes comités accueillent et dirigent des conventions internationales auxquelles seulement leurs acolytes sont autorisés à présenter des articles sans tenir compte de la qualité du travail. Ces comités amassent de grandes sommes d'argent de la bourse publique et placent en premier leurs projets commandités et fondés par la déception et le mensonge. N'importe quelle objection à leurs propositions, pour protéger l'intégrité scientifique, est réduite au silence par tous leur moyens, de sorte que l'argent puisse continuer à combler leurs comptes et leur garantir des emplois bien payés. Les scientifiques qui s'y opposent se font renvoyer à leur demande; d'autres ont été empêchés de trouver des positions académiques par ce réseau de complices corrompus. Dans d'autres situations certains ont vu leur candidature expulsée des programmes d'études plus élevés, tels que le doctorat, après avoir ébranlé une théorie à la mode, même si une théorie plus conventionnelle existe depuis plus longtemps. Le fait fondamental qu'aucune théorie scientifique est ni définitive ni inviolable, et doit être ré-ouverte, dicutée et ré-examinée, ils l'ignorent complètement. Souvent ils ignorent le fait qu'un phénomène peut avoir plusieurs explications plausibles, et critiquent avec malveillance n'importe quelle explication qui ne s'accorde pas avec leur opinion. Leur seul recours est l'utilisation d'arguments non scientifiques pour justifier leurs avis biaisés.

Tous les scientifiques seront libres de discuter de leur recherche et la recherche des autres sans crainte d'être ridiculisés, sans fondement matériel, en public ou en privé, et sans êtres accusés, dénigrés, contestés ou autrement critiqués

par des allégations non fondées. Aucun scientifique ne sera mis dans une position dans laquelle sa vie ou sa réputation sera en danger, dû à l'expression de son opinion scientifique. La liberté d'expression scientifique sera primordiale. L'autorité ne sera pas employée dans la réfutation d'un argument scientifique pour bâillonner, réprimer, intimider, ostraciser, ou autrement pour contraindre un scientifique à l'obéissance ou lui faire obstacle. La suppression délibérée des faits ou des arguments scientifiques, par acte volontaire ou par omission, ainsi que la modification délibérée des données pour soutenir un argument ou pour critiquer l'opposition constitue une fraude scientifique qui s'élève jusqu'à un crime scientifique. Les principes de l'évidence guideront toutes discussions scientifiques, que cette évidence soit concrète, théorique ou une combinaison des deux.

Article 8: Liberté de publier des résultats scientifiques

La censure déplorable des publications scientifiques est maintenant devenue la norme des bureaux de rédaction, des journaux et des archives électroniques, et leurs bandes de soit-dits arbitres qui prétent être experts. Les arbitres sont protégés par l'anonymat, de sorte qu'un auteur ne puisse pas vérifier l'expertise prétendue. Des publications sont maintenant rejetées si l'auteur contredit, ou est en désaccord avec, la théorie préférée et la convention la plus acceptée. Plusieurs publications sont rejetées automatiquement parce qu'il y a un des auteurs dans la liste qui n'a pas trouvé faveur avec les rédacteurs, les arbitres, ou d'autres censureurs experts, sans respect quelconque pour le contenu du document. Les scientifiques discordants sont mis sur une liste noire et cette liste est communiquée entre les bureaux de rédaction des participants. Cet effet culmine en un penchant biaisé et une suppression volontaire de la libre pensée, et doit être condamné par la communauté scientifique internationale.

Tous les scientifiques doivent avoir le droit de présenter leurs résultats de recherche, en entier ou en partie, aux congrès scientifiques appropriés, et d'éditer ceux-ci dans les journaux scientifiques, les archives électroniques, et tous les autres médias. Aucun scientifique ne se fera rejeter ses publications ou rapports quand ils seront soumis pour publication dans des journaux scientifiques, des archives électroniques, ou d'autres médias, simplement parce que leur travail met en question l'opinion populaire de la majorité, fait conflit avec les opinions d'un membre de rédaction, contredit les prémisses de bases d'autres recherche ou futurs projets de recherche prévus par d'autres scientifiques, sont en conflit avec quelque sorte de dogme politique, religieuse, ou l'opinion personnelle des autres. Aucun scientifique ne sera mis sur une liste noire, ou sera autrement censuré pour empêcher une publication par quiconque. Aucun scientifique ne bloquera, modifiera, ou interfèrera autrement avec la publication du travail d'un scientifique sachant qu'il aura des faveurs ou bénifices en le faisant.

Article 9: Les publications à co-auteurs

C'est un secret mal gardé parmi les scientifiques que beaucoup de co-auteurs de publications ont réellement peu, ou même rien, en rapport avec la recherche présentée. Les dirigeants de recherche des étudiants diplômés, par exemple, préfèrent leurs noms inclus avec celui des étudiants sous leur surveillance. Dans de tels cas, c'est l'élève diplômé qui a une capacité intellectuelle supérieure à son dirigeant. Dans d'autres situations, pour des fins de notoriété et de réputation, d'argent, de prestige et d'autres raisons malhonnêtes, des personnes qui n'ont rien contribué sont incluses en tant que co-auteurs. Les vrais auteurs peuvent s'y opposer, mais seront pénalisés plus tard d'une manière quelconque, voir même l'expulsion de leur candidature pour un diplôme plus élevé, ou une mise à pied d'une équipe de recherche. C'est un vécu réel de plusieurs co-auteurs dans ces circonstances. Cette pratique effroyable ne doit pas être tolérée. Pour maintenir l'intégrité de la science, seulement les personnes chargées de la recherche devraient être reconnues en tant qu'auteurs.

Aucun scientifique n'invitera quiconque n'a pas collaboré avec lui à être inclus en tant que co-auteur, de même, aucun scientifique ne permettera que son nom soit inclus comme co-auteur d'une publication scientifique sans y avoir contribué de manière significative. Aucun scientifique ne se laissera contraindre par les représentants d'un établissement académique, par une société, un organisme gouvernemental, ou qui que ce soit à inclure leur nom comme co-auteur d'une recherche s'il n'y a pas contribué de manière significative. Un scientifique n'acceptera pas d'être co-auteur en échange de faveurs ou de bénéfices malhonnêtes. Aucune personne ne forcera un scientifique d'aucune manière à mettre son nom en tant que co-auteur d'une publication si le scientifique n'y a pas contribué de manière significative.

Article 10: L'indépendance de l'affiliation

Puisque des scientifiques travaillent souvent à contrats à court terme, quand le contrat est terminé, l'affiliation académique du scientifique est aussi terminée. C'est souvent la politique des bureaux de rédaction que ceux sans affiliation académique ou commerciale ne peuvent pas être publiés. Sans affiliation, beaucoup de ressources ne sont pas disponibles au scientifiques, aussi les occasions de présenter des entretiens et des publications aux congrès sont réduites. Cette pratique vicieuse doit être arrêtée. La science se déroule indépendamment de toutes affiliations.

Aucun scientifique ne sera empêché de présenter des publications aux congrès, aux colloques ou aux séminaires; un scientifique pourra publier dans tous les médias, aura accès aux bibliothèques académiques ou aux publications scientifiques, pourra assister à des réunions scientifiques, donner des conférences, et ceci même sans affiliation avec un établissement académique, un institut scientifique, un

laboratoire gouvernemental ou commercial ou tout autre organisation.

Article 11: L'accès à l'information scientifique

La plupart des livres de science et les journaux scientifiques ne font pas de profits, donc les éditeurs sont peu disposés à les éditer sans une contribution financière des établissements académiques, des organismes gouvernementaux, des fondations philanthropiques et leur semblables. Dans ces cas, les éditeurs commerciaux doivent permettre le libre accès aux versions électroniques des publications et viser à garder le coût d'imprimerie à un minimum.

Les scientifiques s'efforceront d'assurer la disponibilité de leurs ouvrages à la communauté internationale gratuitement, ou à un coût minimum. Tous les scientifiques doivent faire en sorte que les livres de techniques soient disponibles à un coût minimum pour que l'information scientifique puisse être disponible à une plus grande communauté scientifique internationale.

Article 12: La responsabilité morale des scientifiques

L'histoire a démontré que des découvertes scientifiques sont parfois utilisées à des fins extrèmes, soit bonnes, soit mauvaises, au profit de certains et à la ruine des autres. Puisque l'avancement de la science et de la technologie continue toujours, des moyens d'empêcher son application malveillante doivent être établis. Puisqu'un gouvernement élu de manière démocratique, sans biais religieux, racial ou autres biais peut sauvegarder la civilisation, ainsi seulement le gouvernement, les tribunaux et les comités élu de manière démocratique peuvent sauvegarder le droit de la création scientifique libre et intègre. Aujourd'hui, divers états anti-démocratiques et régimes totalitaires font de la recherche active en physique nucléaire, en chimie, en virologie, en génétique, etc. afin de produire des armes nucléaires, chimiques ou biologiques. Aucun scientifique ne devrait volontairement collaborer avec les états anti-démocratiques ou les régimes totalitaires. Un scientifique qui est contraint à travailler au développement des armes pour de tels états doit trouver des moyens pour ralentir le progrès de cette recherche et réduire son rendement, de sorte que la civilisation et la démocratie puissent finalement régner.

Tous les scientifiques ont la responsabilité morale de leurs créations et découvertes. Aucun scientifique ne prendra volontairement part dans les ébauches ou la construction d'armes pour des états anti-démocratiques et/ou des régimes totalitaires, et n'appliquera ni ses connaissances ni son talent au développement d'armes nuisibles à l'humanité. Un scientifique suivra le maxime que tous les gouvernements anti-démocratiques et l'abus des droits de l'homme sont des crimes.

Le 10 avril, 2007

Open Letter by the Editor-in-Chief: Declaration of Academic Freedom (Scientific Human Rights)
*The Russian Translation**

Декларация Академической Свободы

(Права Человека в Научной Деятельности)

Статья 1: Преамбула

Начало 21-го *столетия больше, чем любая* другая эпоха в истории человечества, проявляет глубину и значение роли науки и техники в человеческих делах.

Интенсивное развитие современной науки и техники явилось причиной банального мнения, что все дальнейшие ключевые открытия в науке могут быть сделаны преимущественно или исключительно крупными исследовательскими группами (коллективами), финансируемыми исключительно на уровне государства или крупной корпорации, и, соответственно, имеющими доступ к очень дорогому экспериментальному оборудованию и большому количеству вспомогательного обслуживающего персонала.

Эта обычная точка зрения, однако, является мифом, и противоречит истинному положению дел с теоретическими и экспериментальными исследованиями в современной науке. В действительности крупные и дорогие технологические проекты — это всего лишь результат приложения фундаментальных научных знаний, полученных небольшими группами исследователей или вообще индивидуалами, часто работающими в отрыве от крупных научных коллективов и институтов. Ученый, работающий в одиночку — ныне, так же как и в прошлом — способен сделать открытие, которое может существенно повлиять на судьбу человечества и изменить лицо всей нашей планеты.

Большинство инновационных открытий вообще сделаны индивидуумами, работающими, в зависимости от специфики исследования, в научно-исследовательских институтах, ВУЗах или лабораториях промышленных предприятий. В такой ситуации, будучи непосредственно зависимым от начальства, исследователь очень часто сдерживается или даже подавляется самой бюрократической структурой учреждения или его директором, которые стремятся монополизировать научное открытие или иные результаты исследования ученого для своей личной выгоды или прибыли предприятия.

Мировая история научных открытий переполнена случаями подавления и просто издевательств и насмешек по отношению к реальным ученым-исследователям со стороны их непосредственного начальства и бюрократов, руководивших учреждениями, где эти ученые работали. Таких случаев, иногда закончившихся трагически, — множество: как в прошлом науки так и в настоящем. В том числе, сами результаты оригинального исследования часто губятся преднамеренными искажениями и откровенным плагиатом со стороны недобросовестных, завистливых, и алчных коллег. Такие “коллеги”, будучи не в состоянии сделать что-то новое в науке, пытаются использовать труды своих более талантливых подчиненных, а если это не получается по ряду организационных причин, то просто подавить или не дать ходу этим исследованиям, чтобы эти блестящие научные результаты не оттеняли их собственные бездарные попытки имитации научной деятельности. Эта порочная практика продолжается почти повсеместно и поныне.

Цель этой Декларации состоит в том, чтобы установить фундаментальную доктрину: научное исследование должно быть свободно от скрытого и откровенного репрессивного влияния бюрократических, политических, религиозных и финансовых директив; научное творчество является фундаментальным правом человека не меньше, чем другие фундаментальные права человека. Эта доктрина несомненно должна быть предметом обсуждения международных договоров, и отражена в международном праве.

Главы всех государств и правительств, претендующих на причастность к демократическому мировому сообществу, должны соблюдать и всячески поддерживать эту Декларацию как признак солидарности с заинтересованным международным сообществом ученых, и дать право всем народам нашей планеты Земля к свободному неограниченному научному творчеству на благо всего человечества. Творчество в науке и технике слишком долго были объектом притеснения. Этой порочной практике должен быть положен конец.

Статья 2: Кто такой ученый

Ученый — это любой человек, кто производит научные исследования. Любой человек, кто сотрудничает с ученым в обсуждении и развитии идеи его исследования — также ученый. Проведение формальной квалификации (как-то выдача диплома о специальном образовании, при-

*Original text published in English: *Progress in Physics*, 2006, v. 1, 57–60. Online — http://www.ptep-online.com/

Автор оригинального текста Декларации на английском языке — Дмитрий Рабунский, Главный редактор журнала *Progress in Physics*. E-mail: rabounski@yahoo.com

Перевод Декларации на русский язык — Эльмира Исаева. E-mail: el_max63@yahoo.com; elmira@physics.ab.az

своение ученой степени и т.п.) — еще не повод для того, чтобы считать кого-то ученым.

Статья 3: Где делается наука

Научное исследование может быть выполнено в любом месте вообще, например, на рабочем месте, в течение формального курса образования, в течение спонсируемой академической программы, в группах, или также индивидуумом у себя дома.

Статья 4: Свобода выбора темы для научного исследования

Многие ученые, работающие по программе получения ученой степени или в рамках других исследовательских программ, в ВУЗах, таких как университеты или колледжи расширенного обучения, не имеют реальной возможности собственного выбора темы их исследовательской работы. Как правило, им предлагается сделать выбор только из некого списка "разрешенных" тем, предоставляемого администрацией или начальством, которое руководит данной программой. Это происходит потому, что академическая иерархия и/или другие академические начальники, администрирующие науку, просто не одобряют самостоятельную линию поведения ученых в науке, боясь что новые оригинальные исследования и возможные неожиданные результаты могут быть намного ярче и успешней их собственной научной деятельности и, таким образом, дискредитировать их собственный авторитет в науке (и, как следствие, они сильно рискуют лишиться получаемых в течении многих лет грантов и другого финансирования, которое может быть передано более успешным ученым). Кроме того, есть риск, что принципиально новые исследования могут опровергнуть какую-либо научную догму, поддерживаемую данной научной школой, что было бы на руку другим научным школам, которые эту догму не признают. Власть ортодоксального большинства, ведомого отнюдь не интересом к поиску новых научных знаний, а элементарными корыстными интересами, жаждой денег и власти, весьма часто срывает научную работу, если становится видна перспектива принципиально нового прорыва в науке. Эта банальная практика — преднамеренное препятствие свободной научной мысли — не имеет ничего общего с наукой, и является преступной. Этой порочной практике должен быть положен конец.

Ученый, работающий для любого ВУЗа, научного института или агентства, должен быть полностью свободен в выборе исследовательской темы. Какие-то ограничения могут происходить только из-за реалий недостаточности материальной поддержки, и ничего более относящегося к собственно теме или предмету научного исследования. Если же ученый выполняет исследование как член рабочей группы, проводящей некоторое исследование по совместной тематике, то выбор должен быть результатом совместных консультаций в данной рабочей группе.

Статья 5: Свобода выбора исследовательских методов

Часто имеет место тот факт, что ученый, проводящий исследование в рамках некоторой академической среды (научного института, ВУЗа или корпорации), вынужден принимать исследовательские методы отличные от тех, которые он избрал в начале своего исследования. Чаще всего это происходит из-за корпоративных предубеждений, навязываемых индивидуалу, а также элементарного лоббирования и корысти получить оплату за аренду оборудования данной лаборатории или института. Эта практика весьма широко распространена, и является по сути преднамеренным препятствием свободы научного творчества. Этой порочной практике должен быть положен конец.

Ученый, работающий по некоммерческой или академической программе, имеет право развивать свою исследовательскую тему любым разумным способом и любыми разумными средствами, которые он считает необходимыми и наиболее эффективными для его исследования. Окончательное решение о том, каким образом и на каком оборудовании будет проводиться данное исследование, должно быть сделано самим ученым.

Если же ученый выполняет исследование в составе рабочей группы, объединенной общей тематикой, руководители проекта имеют право только на консультацию и не должны влиять или ограничивать исследовательские методы или исследовательскую тему ученого в пределах группы.

Научное сообщество — это не армия, а свободное объединение людей, занимающихся научным творчеством на благо человечества и научного прогресса.

Статья 6: Свобода сотрудничества в научном исследовании

Существует немалый элемент конкуренции в практике современной науки. Этому сопутствуют обстоятельства с элементами личной зависти и сохранения репутации академического начальства любой ценой, независимо от научных фактов. Это часто приводит к тому, что ученый, проводящий реальные исследования ведущие к принципиально новым результатам в науке, становится безработным. Эта порочная практика — также преднамеренное препятствование свободе научного прогресса.

Если ученому требуется помощь в исследовании от какого-то другого (любого) человека, который согласен помочь, тогда ученый волен пригласить этого человека для участия в своем исследовании независимо от мнения

на эту тему его академического начальства. Ученый также волен предоставлять свою посильную помощь любому другому исследователю, если эта помощь находится в пределах бюджета его исследовательской программы.

Статья 7: Свобода разногласий в научной дискуссии

Вследствие скрытой ревности и жажды личного обогащения, в современном научном сообществе, разделенном корпоративными интересами и закулисной борьбой научных школ, получила широкое распространение ненависть к открытому обсуждению научных результатов а также порочная практика преднамеренно исключать из дискуссии тех ученых, кто подвергает сомнению ортодоксальные догмы, принятые и отстаиваемые той или иной научной школой. Очень часто, ученые способные указать на неточности в текущей теории или интерпретации данных, объявляются сумасшедшими для того, чтобы было удобно игнорировать их мнение и идеи. Они высмеиваются публично и конфиденциально, и систематически получают отказ от научных конференций, семинаров и коллоквиумов так, чтобы препятствовать свободному обсуждению их идей и научных результатов. Преднамеренная фальсификация данных и искажение существующих теорий — теперь частые средства для подавления и скрытия "неугодных" научных фактов. Многие научные комитеты, журналы и академические фонды были сформированы таким образом, чтобы только их руководителям, их помошникам и связанным с ними ученым, им и только им было позволено использовать финансовые ресурсы, публиковать свои научные работы (независимо от качества содержания) и т.п. Эти комитеты часто расходуют огромные суммы денег простых налогоплательщиков, чтобы финансировать исключительно свои собственные проекты, что в конечном итоге ведет к коррупции, обману и лжи. Любое возражение на их проекты, имеющее серьезное научное обоснование, сразу подвергается травле со стороны находящихся под их контролем научных журналов и других средств массовой информации. Единственная цель такой порочной политики — это сделать так, чтобы деньги продолжали по-прежнему течь на банковские счета руководителей этих проектов и их помошников, гарантируя им и членам их семей хорошо обеспеченное будущее, а их друзьям из среды ученых — высоко оплачиваемые рабочие места. Под авторитарным и финансовым давлением этих руководителей, их научные оппоненты увольняются или отстраняются от проведения научных работ и экспертиз, а несогласные ученики отстраняются от PhD программ; на их место назначаются совсем другие люди из числа коррумпированных сообщников. Это все — не наука. Для описания всего этого есть только одно подходящее слово — мафия.

Фундаментальный факт, что никакая научная теория не является абсолютно определенной и неприкосновенной и поэтому открыта для обсуждения и развития, часто игнорируется в академической среде. Также игнорируется тот факт, что одно и тоже явление может иметь несколько равноправных объяснений (как, например, корпускулярная и волновая теория света). Злонамеренно дискредитируется любое объяснение, которое не согласовывается с ортодоксальным мнением, при этом без колебания используются любые ненаучные методы, чтобы одержать верх в дискуссии и получить желаемый грант, субсидию или другую финансовую помощь.

Все ученые должны быть свободны в обсуждении их собственных исследований и исследований других ученых, без опасения публичных насмешек, обвинений, унижений, или необоснованной критики, что совершенно недопустимо в научной дискуссии. Ни один ученый не должен быть поставлен в такое положение, в котором его средства к существованию или репутация будут в опасности вследствие выражения его научного мнения. Свобода научного выражения должна быть главной. Использование административной власти в опровержении научных результатов не имеет ничего общего с нормальным научным процессом и не должно использоваться, чтобы завязывать рот, подавлять, или запугивать ученого. Преднамеренное сокрытие научных фактов и подавление научного мнения — это научное мошенничество, и является составом преступления. Все научные обсуждения экспериментальных или теоретических результатов должны вести к принципу очевидности.

Статья 8: Свобода публикации результатов научного исследования

Цензура научных документов ныне стала стандартной практикой редакций основных научных журналов и электронных архивов. Рецензенты защищены, главным образом, анонимностью так, чтобы автор не смог проверить их предполагаемую экспертизу. Статьи теперь обычно отклоняются, если автор не соглашается или противоречит точке зрения научной школы, которая монополизировала данный научный журнал. Много статей теперь отклоняются автоматически на основании присутствия в списке авторов какого-либо ученого, к которому не расположены редакторы или рецензенты журнала, или который принадлежит к "враждебной" научной школе, придерживающейся иной точки зрения на исследуемое явление природы. Все это не имеет вообще никакого отношения к содержанию поданной научной статьи. Существует также порочная практика составления "черных списков" в которые заносят имена ученых, неугодных данной редакции или рецензентам. Статьи ученых, имена которых занесены в такой "черный список", отклоняются без рассмотрения, по чисто формальным поводам.

Применяющие эту и подобные порочные методы, виновны в подавлении свободного мышления, что является

преступлением против прав человека и должно быть осуждено международным научным сообществом.

Все ученые должны иметь право представлять свои научные исследовательские результаты, полностью или частично, на соответствующих научных конференциях и издавать в научных журналах, электронных архивах и любых других средствах массовой информации. Ни один ученый не должен получить отказ в публикации в научном журнале, электронном архиве или других средствах массовой информации, на том основании, что его научно обоснованное мнение или результаты исследования находятся в конфликте с мнением большинства, мнением редакции журнала, или опровергают какую-либо догму, поддерживаемую научной школой, монополизировавшей данный журнал. Ни один ученый не должен быть помещен в "черный список" нежелательных авторов, или блокирован любым другим формальным образом от возможности публиковать результаты своих научных исследований.

Только фактические ошибки в расчетах или эксперименте, или несоответствие тематике данного издания могут быть причиной отказа в публикации поданной научной работы.

Статья 9: Соавторство в научном исследовании

В научных кругах прекрасно известно: многие из соавторов научных публикаций фактически имеют небольшой или вообще никакого вклада в данное исследование. Например, — научные руководители PhD студентов. Во многих таких случаях, человек, который фактически проводит научное исследование и пишет по его результатам научную статью, имеет интеллект и способности, намного выше своего номинального начальника. Тем не менее, номинальные начальники и другие люди, от которых зависит продолжение финансирования научной работы, получение ученой степени, и т.п. чаще всего включаются как соавторы в научную публикацию. Фактические авторы не могут даже возразить против этого, опасаясь что впоследствии могут будут лишены финансирования, возможности получить ученую степень, отстранены от работы в исследовательской группе, и т.п. Известно множество случаев, когда ученые, реально проводившие исследования и писали научные статьи, были вообще исключены их начальством из списка соавторов под угрозой увольнения или прочих репрессивных мер. Эта ужасная практика является преступлением, и не может более продолжаться. Только те люди, кто реально проводил научное исследование, могут быть аккредитованы как соавторы итоговой научной публикации.

Ни один ученый не должен включать другого человека в список соавторов своей научной публикации, если этот человек не внес значительного вклада в данное исследование. Ни один ученый не должен позволять себе быть принужденным любым представителем ВУЗа, корпорации, правительственного агентства или любого другого человека включать их имена в список соавторов исследования, которое они не делали. Ни один ученый не должен позволять использовать свое имя в списке соавторов научной работы как предмет торговли или обмена на любые подарки, ученую степень, или финансовую помощь. Ни один человек не должен стимулировать или пытаться стимулировать ученого в том, что тот включил его в список соавторов научного исследования или публикации, в которую он не внес значительного научного вклада.

Статья 10: Независимость от аффилиации

В настоящее время значительная доля ученых работает по краткосрочным контрактам, тогда как в промежутках между контрактами или грантами (это может длиться годами), они формально не заняты в научной индустрии. В рамках любого контракта существует такое понятие – академическая аффилиация. Вместе с тем, часто политика редакций научных журналов такова, что научные работы исследователей не имеющих академической аффилиации не принимаются к публикации, а часто даже просто не рассматриваются. Кроме того, не имея академической аффилиации, ученый лишен доступа ко многим научным ресурсам, а также возможности представлять свои работы на конференциях. Это — порочная практика, которой должен быть положен конец. Наука не подразумевает наличие академической аффилиации.

Никто, ни одна организация или группа людей администрирующие науку, не должны устанавливать правила препятствующие ученым, не имеющим академической аффилиации, представлять свои научные труды и разработки на конференциях, коллоквиумах или семинарах, а также публиковать их в любых средствах массовой информации. Никто не должен устанавливать правила, препятствующие ученым, не имеющим академической аффилиации, получать свободный доступ к академическим библиотекам или научным публикациям, к посещению научных встреч или лекций в ВУЗах, научных институтах, правительственных или коммерческих лабораториях или любой другой организации.

Статья 11: Открытый доступ к научной информации

Специализированная научная литература и подавляющее большинство научных журналов дают очень маленькую прибыль или вообще убыточны. Поэтому издатели не желают издавать их на коммерческой основе и, естественно, требуют от ученых денег. Оплата такой литературы, чаще всего, поступает от исследовательских институтов, где работают данные ученые, а также ВУЗов, академических фондов и организаций, филантропов-

индивидуалов и т.п. При таких обстоятельствах коммерческие издатели должны предоставлять свободный доступ к электронным версиям публикаций и по возможности стремиться свести стоимость напечатанных материалов к минимуму.

Все ученые должны способствовать и стремиться к тому, чтобы их публикации и исследовательские документы были доступны международному научному сообществу бесплатно, или в альтернативе, если этого нельзя избежать, по минимальной стоимости. Все ученые должны предпринять активные меры для того, чтобы сделать их книги и журналы доступными по самой низкой возможной цене так, чтобы научная информация могла быть доступна самому широкому международному научному сообществу.

Статья 12: Морально-этическая ответственность ученого

История свидетельствует: в конечном счете научные открытия очень часто используются в разрушительных целях, во вред и даже уничтожение цивилизации и человечества в целом. Так как научно-технический прогресс не может быть остановлен, необходимо установить ряд средств, препятствующих такому деструктивному применению результатов научных исследований и технических разработок. Прежде всего, необходимо помнить: только демократически избранное гражданское правительство, свободное от религиозных, расовых и других предрассудков, может сохранить цивилизацию. Только демократически избранные правительства и комитеты могут сохранить право на свободное научное творчество. Ныне мы видим: различные недемократические государства и тоталитарные режимы проводят активные исследования и технические разработки в ядерной физике, химии, вирусологии, генной инженерии и т.п., с целью производства ядерного, химического и биологического оружия массового поражения. Ни один ученый не должен добровольно сотрудничать с недемократическими правительствами или тоталитарными режимами. Если же ученый был силой привлечен к работам по созданию вооружений в таком государстве, он должен постараться найти способы замедлить продвижение своей исследовательской программы в этой области так, чтобы данный тоталитарный режим не смог воспользоваться полученными результатами его исследования и цивилизованные страны, несущие всему миру принципы демократии и прогресса, смогли бы в конечном счете победить тоталитарное зло.

Все ученые несут моральную ответственность за результаты их научных работ и открытий. Ни один ученый не должен добровольно участвовать в проектировании или создании оружия любого вида для недемократических государств или тоталитарных режимов, или позволять применить его знания или научные навыки к развитию технологий, опасных для человечества. Каждый ученый должен иметь в виду, что деятельность любого недемократического правительства, а также нарушение прав человека являются преступлением.

14 мая 2007

The Journal on Advanced Studies in Theoretical and Experimental Physics, including Related Themes from Mathematics

PROGRESS IN PHYSICS

A quarterly issue scientific journal, registered with the Library of Congress (DC, USA). This journal is peer reviewed and included in the abstracting and indexing coverage of: Mathematical Reviews and MathSciNet (AMS, USA), DOAJ of Lund University (Sweden), Zentralblatt MATH (Germany), Referativnyi Zhurnal VINITI (Russia), etc.

To order printed issues of this journal, contact the Editors.

Electronic version of this journal can be downloaded free of charge from the web-resources:
http://www.ptep-online.com
http://www.geocities.com/ptep_online

Postal address for correspondence:

Chair of the Department
of Mathematics and Science,
University of New Mexico,
200 College Road,
Gallup, NM 87301, USA

This journal is powered by LaTeX

A variety of books can be downloaded free from the Digital Library of Science:
http://www.gallup.unm.edu/∼smarandache

ISSN: 1555-5534 (print)
ISSN: 1555-5615 (online)

Standard Address Number: 297-5092
Printed in the United States of America

OCTOBER 2007 **VOLUME 4**

CONTENTS

Information for Authors and Subscribers

Progress in Physics has been created for publications on advanced studies in theoretical and experimental physics, including related themes from mathematics and astronomy. All submitted papers should be professional, in good English, containing a brief review of a problem and obtained results.

All submissions should be designed in LaTeX format using *Progress in Physics* template. This template can be downloaded from *Progress in Physics* home page http://www.ptep-online.com. Abstract and the necessary information about author(s) should be included into the papers. To submit a paper, mail the file(s) to the Editor-in-Chief.

All submitted papers should be as brief as possible. We usually accept brief papers, no larger than 8–10 typeset journal pages. Short articles are preferable. Large papers can be considered in exceptional cases to the section *Special Reports* intended for such publications in the journal. Letters related to the publications in the journal or to the events among the science community can be applied to the section *Letters to Progress in Physics*.

All that has been accepted for the online issue of *Progress in Physics* is printed in the paper version of the journal. To order printed issues, contact the Editors.

This journal is non-commercial, academic edition. It is printed from private donations. (Look for the current author fee in the online version of the journal.)

On the Gravitational Field of a Pulsating Source

Nikias Stavroulakis

Solomou 35, 15233 Chalandri, Greece

E-mail: nikias.stavroulakis@yahoo.fr

Because of the pseudo-theorem of Birkhoff, the important problem related to the dynamical gravitational field of a non-stationary spherical mass is ignored by the relativists. A clear formulation of this problem appears in the paper [5], which deals also with the establishment of the appropriate form of the spacetime metric. In the present paper we establish the corresponding equations of gravitation and bring out their solutions.

1 Introduction

As is shown in the paper [5], the propagation of gravitation from a spherical pulsating source is governed by a function $\pi(t,\rho)$, termed *propagation function*, satisfying the following conditions

$$\frac{\partial\pi(t,\rho)}{\partial t}>0,\quad \frac{\partial\pi(t,\rho)}{\partial\rho}\leqslant 0,\quad \pi(t,\sigma(t))=t,$$

where $\sigma(t)$ denotes the time-dependent radius of the sphere bounding the matter. The propagation function is not uniquely defined. Any function fulfilling the above conditions characterizes the propagation of gravitation according to the following rule: If the gravitational disturbance reaches the sphere $\|x\|=\rho$ at the instant t, then $\tau=\pi(t,\rho)$ is the instant of its radial emission from the entirety of the sphere bounding the matter. Among the infinity of possible choices of $\pi(t,\rho)$, we distinguish principally the one identified with the time coordinate, namely the propagation function giving rise to the *canonical* $\Theta(4)$*-invariant metric*

$$\begin{aligned} ds^2 &= \left(f(\tau,\rho)d\tau+\ell(\tau,\rho)\,\frac{x\,dx}{\rho}\right)^2- \\ &-\left[\left(\frac{g(\tau,\rho)}{\rho}\right)^2 dx^2+\left(\big(\ell(\tau,\rho)\big)^2-\left(\frac{g(\tau,\rho)}{\rho}\right)^2\right)\frac{(x\,dx)^2}{\rho^2}\right] \end{aligned} \tag{1.1}$$

(here τ denotes the time coordinate instead of the notation u used in the paper [5]).

Any other $\Theta(4)$-invariant metric results from (1.1) if we replace τ by a conveniently chosen propagation function $\pi(t,\rho)$. Consequently the general form of a $\Theta(4)$-invariant metric outside the matter can be written as

$$\begin{aligned} ds^2 &= \left[\left(f\big(\pi(t,\rho),\rho\big)\frac{\partial\pi(t,\rho)}{\partial t}\right)dt+\right. \\ &\left.+\left(f\big(\pi(t,\rho),\rho\big)\frac{\partial\pi(t,\rho)}{\partial\rho}+\ell\big(\pi(t,\rho),\rho\big)\right)\frac{x\,dx}{\rho}\right]^2- \\ &-\left[\left(\frac{g\big(\pi(t,\rho),\rho\big)}{\rho}\right)^2 dx^2+\left(\big(\ell(\pi(t,\rho),\rho)\big)^2-\right.\right. \\ &\left.\left.-\left(\frac{g\big(\pi(t,\rho),\rho\big)}{\rho}\right)^2\right)\frac{(x\,dx)^2}{\rho^2}\right]. \end{aligned} \tag{1.2}$$

The equations of gravitation related to (1.2) are very complicated, but we do not need to write them explicitly, because the propagation function occurs in them as an arbitrary function. So their solution results from that of the equations related to (1.1) if we replace τ by a general propagation function $\pi(t,\rho)$. It follows that the investigation of the $\Theta(4)$-invariant gravitational field must by based on the canonical metric (1.1). The metric (1.2) indicates the dependence of the gravitational field upon the general propagation function $\pi(t,\rho)$, but it is of no interest in dealing with specific problems of gravitation for the following reason. Each allowable propagation function is connected with a certain conception of time, so that the infinity of allowable propagation functions introduces an infinity of definitions of time with respect to the general $\Theta(4)$-invariant metric. This is why the notion of time involved in (1.2) is not clear.

On the other hand, the notion of time related to the canonical metric, although unusual, is uniquely defined and conceptually easily understandable.

This being said, from now on we will confine ourselves to the explicit form of the canonical metric, namely

$$\begin{aligned} ds^2 &= \big(f(\tau,\rho)\big)^2 d\tau^2+2f(\tau,\rho)\,\ell(\tau,\rho)\frac{(x\,dx)}{\rho}\,d\tau- \\ &-\left(\frac{g(\tau,\rho)}{\rho}\right)^2 dx^2+\left(\frac{g(\tau,\rho)}{\rho}\right)^2\frac{(x\,dx)^2}{\rho^2} \end{aligned} \tag{1.3}$$

which brings out its components:

$$\begin{aligned} &g_{00}=\big(f(\tau,\rho)\big)^2,\qquad g_{0i}=f(\tau,\rho)\,\ell(\tau,\rho)\frac{x_i}{\rho},\\ &g_{ii}=-\left(\frac{g(\tau,\rho)}{\rho}\right)^2+\left(\frac{g(\tau,\rho)}{\rho}\right)^2\frac{x_i^2}{\rho^2},\\ &g_{ij}=\left(\frac{g(\tau,\rho)}{\rho}\right)^2\frac{x_i x_j}{\rho^2},\qquad (i,j=1,2,3;\ i\neq j). \end{aligned}$$

Note that, since the canonical metric, on account of its own definition, is conceived outside the matter, we have not to bother ourselves about questions of differentiability on the subspace $\mathbb{R}\times\{(0,0,0)\}$ of $\mathbb{R}\times\mathbb{R}^3$. It will be always understood that the spacetime metric is defined for $(\tau,\rho)\in\overline{U}$, $\rho=\|x\|$, $\overline{U}$ being the closed set $\{(\tau,\rho)\in\mathbb{R}^2|\rho\geq\sigma(\tau)\}$.

2 Summary of auxiliary results

We recall that the Christoffel symbols of second kind related to a given $\Theta(4)$-invariant spacetime metric [3] are the components of a $\Theta(4)$-invariant tensor field and depend on ten functions $B_\alpha = B_\alpha(t,\rho)$, $(\alpha = 0,1,\dots,9)$, according to the following formulae

$$\Gamma^0_{00} = B_0,\ \ \Gamma^0_{0i} = \Gamma^0_{i0} = B_1 x_i,\quad \Gamma^i_{00} = B_2 x_i,$$

$$\Gamma^0_{ii} = B_3 + B_4 x_i^2,\ \ \Gamma^0_{ij} = \Gamma^0_{ji} = B_4 x_i x_j,$$

$$\Gamma^i_{i0} = \Gamma^i_{0i} = B_5 + B_6 x_i^2,\ \ \Gamma^i_{j0} = \Gamma^i_{0j} = B_6 x_i x_j,$$

$$\Gamma^i_{ii} = B_7 x_i^3 + (B_8 + 2B_9)x_i,$$

$$\Gamma^i_{jj} = B_7 x_i x_j^2 + B_8 x_i,\quad \Gamma^j_{ij} = \Gamma^j_{ji} = B_7 x_i x_j^2 + B_9 x_i,$$

$$\Gamma^i_{jk} = B_7 x_i x_j x_k,\quad (i,j,k = 1,2,3;\ i \neq j \neq k \neq i).$$

We recall also that the corresponding Ricci tensor is a symmetric $\Theta(4)$-invariant tensor defined by four functions Q_{00}, Q_{01}, Q_{11}, Q_{22}, the computation of which is carried out by means of the functions B_α occurring in the Christoffel symbols:

$$Q_{00} = \frac{\partial}{\partial t}(3B_5 + \rho^2 B_6) - \rho\frac{\partial B_2}{\partial \rho} -$$
$$- B_2(3 + 4\rho^2 B_9 - \rho^2 B_1 + \rho^2 B_8 + \rho^2 B_7) -$$
$$- 3B_0 B_5 + 3B_5^2 + \rho^2 B_6(-B_0 + 2B_5 + \rho^2 B_6),$$

$$Q_{01} = \frac{\partial}{\partial t}(\rho^2 B_7 + B_8 + 4B_9) - \frac{1}{\rho}\frac{\partial B_5}{\partial \rho} - \rho\frac{\partial B_6}{\partial \rho} +$$
$$+ B_2(B_3 + \rho^2 B_4) - 2B_6(2 + \rho^2 B_9) -$$
$$- B_1(3B_5 + \rho^2 B_6),$$

$$Q_{11} = -\frac{\partial B_3}{\partial t} - \rho\frac{\partial B_8}{\partial \rho} - (B_0 + B_5 + \rho^2 B_6)B_3 +$$
$$+ (1 - \rho^2 B_8)(B_1 + \rho^2 B_7 + B_8 + 2B_9) - 3B_8,$$

$$Q_{22} = -\frac{\partial B_4}{\partial t} + \frac{1}{\rho}\frac{\partial}{\partial \rho}(B_1 + B_8 + 2B_9) + B_1^2 + B_8^2 -$$
$$- 2B_9^2 - 2B_1 B_9 + 2B_3 B_6 + (-B_0 - B_5 + \rho^2 B_6)B_4 +$$
$$+ \big(-3 + \rho^2(-B_1 + B_8 - 2B_9)\big)B_7.$$

3 The Ricci tensor related to the canonical metric (1.3)

In order to find out the functions B_α, $(\alpha = 0,1,\dots,9)$, resulting from the metric (1.3), we have simply to write down the explicit expressions of the Christoffel symbols Γ^0_{00}, Γ^0_{01}, Γ^1_{00}, Γ^0_{11}, Γ^1_{01}, Γ^1_{12}, Γ^1_{22}, thus obtaining

$$B_0 = \frac{1}{f}\frac{\partial f}{\partial \tau} + \frac{1}{\ell}\frac{\partial \ell}{\partial \tau} - \frac{1}{\ell}\frac{\partial f}{\partial \rho},\qquad B_1 = 0,$$

$$B_2 = -\frac{f}{\rho\ell^2}\frac{\partial \ell}{\partial \tau} + \frac{f}{\rho\ell^2}\frac{\partial f}{\partial \rho},$$

$$B_3 = \frac{g}{\rho^2 f\ell}\frac{\partial g}{\partial \rho},\qquad B_4 = -\frac{g}{\rho^4 f\ell}\frac{\partial g}{\partial \rho},$$

$$B_5 = \frac{1}{g}\frac{\partial g}{\partial \tau},\qquad B_6 = \frac{1}{\rho^2\ell}\frac{\partial f}{\partial \rho} - \frac{1}{\rho^2 g}\frac{\partial g}{\partial \tau},$$

$$B_7 = -\frac{g}{\rho^5 f\ell}\frac{\partial g}{\partial \tau} + \frac{1}{\rho^3 f}\frac{\partial f}{\partial \rho} + \frac{1}{\rho^4} + \frac{g}{\rho^5\ell^2}\frac{\partial g}{\partial \rho} +$$
$$+ \frac{1}{\rho^3\ell}\frac{\partial \ell}{\partial \rho} - \frac{2}{\rho^3 g}\frac{\partial g}{\partial \rho},$$

$$B_8 = \frac{g}{\rho^3 f\ell}\frac{\partial g}{\partial \tau} + \frac{1}{\rho^2} - \frac{g}{\rho^3\ell^2}\frac{\partial g}{\partial \rho},$$

$$B_9 = -\frac{1}{\rho^2} + \frac{1}{\rho g}\frac{\partial g}{\partial \rho}.$$

The conditions $B_1 = 0$, $B_3 + \rho^2 B_4 = 0$ imply several simplifications. Moreover an easy computation gives

$$Q_{11} + \rho^2 Q_{22} = 2\rho\frac{\partial B_9}{\partial \rho} -$$
$$- 2(1 + \rho^2 B_9)(B_8 + B_9 + \rho^2 B_7) + 4B_9.$$

Replacing now everywhere the functions B_α, $(\alpha = 0,1,\dots,9)$, by their expressions, we obtain the four functions defining the Ricci tensor.

Proposition 3.1 *The functions Q_{00}, Q_{01}, Q_{11}, Q_{22} related to (1.3) are defined by the following formulae.*

$$\begin{aligned} Q_{00} &= \frac{1}{\ell}\frac{\partial^2 f}{\partial\tau\partial\rho} - \frac{f}{\ell^2}\frac{\partial^2 f}{\partial\rho^2} + \frac{f}{\ell^2}\frac{\partial^2 \ell}{\partial\tau\partial\rho} + \frac{2}{g}\frac{\partial^2 g}{\partial\tau^2} - \\ &- \frac{f}{\ell^3}\frac{\partial\ell}{\partial\tau}\frac{\partial\ell}{\partial\rho} + \frac{f}{\ell^3}\frac{\partial f}{\partial\rho}\frac{\partial\ell}{\partial\rho} + \frac{2f}{\ell^2 g}\frac{\partial\ell}{\partial\tau}\frac{\partial g}{\partial\rho} - \\ &- \frac{2f}{\ell^2 g}\frac{\partial f}{\partial\rho}\frac{\partial g}{\partial\rho} - \frac{2}{fg}\frac{\partial f}{\partial\tau}\frac{\partial g}{\partial\tau} - \frac{2}{\ell g}\frac{\partial\ell}{\partial\tau}\frac{\partial g}{\partial\tau} + \\ &+ \frac{2}{\ell g}\frac{\partial f}{\partial\rho}\frac{\partial g}{\partial\tau} - \frac{1}{f\ell}\frac{\partial f}{\partial\tau}\frac{\partial f}{\partial\rho}, \end{aligned} \tag{3.1}$$

$$\begin{aligned} \rho Q_{01} &= \frac{\partial}{\partial\tau}\left(\frac{1}{f\ell}\frac{\partial(f\ell)}{\partial\rho}\right) - \frac{\partial}{\partial\rho}\left(\frac{1}{\ell}\frac{\partial f}{\partial\rho}\right) + \\ &+ \frac{2}{g}\frac{\partial^2 g}{\partial\tau\partial\rho} - \frac{2}{\ell g}\frac{\partial f}{\partial\rho}\frac{\partial g}{\partial\rho}, \end{aligned} \tag{3.2}$$

$$\begin{aligned} \rho^2 Q_{11} &= -1 - \frac{2g}{f\ell}\frac{\partial^2 g}{\partial\tau\partial\rho} + \frac{g}{\ell^2}\frac{\partial^2 g}{\partial\rho^2} - \frac{2}{f\ell}\frac{\partial g}{\partial\tau}\frac{\partial g}{\partial\rho} - \\ &- \frac{g}{\ell^3}\frac{\partial\ell}{\partial\rho}\frac{\partial g}{\partial\rho} + \frac{1}{\ell^2}\left(\frac{\partial g}{\partial\rho}\right)^2 + \frac{g}{f\ell^2}\frac{\partial f}{\partial\rho}\frac{\partial g}{\partial\rho}, \end{aligned} \tag{3.3}$$

$$Q_{11}+\rho^2 Q_{22}=\frac{2}{g}\left(\frac{\partial^2 g}{\partial\rho^2}-\frac{\partial g}{\partial\rho}\frac{1}{f\ell}\frac{\partial(f\ell)}{\partial\rho}\right). \tag{3.4}$$

Note that from (3.1) and (3.2) we deduce the following useful relation

$$\begin{aligned}\ell Q_{00}-f\rho Q_{01}=&\frac{2\ell}{g}\frac{\partial^2 g}{\partial\tau^2}+\frac{2f}{\ell g}\frac{\partial\ell}{\partial\tau}\frac{\partial g}{\partial\rho}-\\&-\frac{2\ell}{fg}\frac{\partial f}{\partial\tau}\frac{\partial g}{\partial\tau}-\frac{2}{g}\frac{\partial\ell}{\partial\tau}\frac{\partial g}{\partial\tau}+\frac{2}{g}\frac{\partial f}{\partial\rho}\frac{\partial g}{\partial\tau}-\frac{2f}{g}\frac{\partial^2 g}{\partial\tau\partial\rho}.\end{aligned} \tag{3.5}$$

4 Reducing the system of the equations of gravitation

In order to clarify the fundamental problems with a minimum of computations, we will assume that the spherical source is not charged and neglect the cosmological constant. The charge of the source and the cosmological constant do not add difficulties in the discussion of the main problems, so that they may be considered afterwards.

Of course, the equations of gravitation outside the pulsating source are obtained by writing simply that the Ricci tensor vanishes, namely

$$Q_{00}=0,\quad Q_{01}=0,\quad Q_{11}=0,\quad Q_{11}+\rho^2 Q_{22}=0.$$

The first equation $Q_{00}=0$ is to be replaced by the equation

$$\ell Q_{00}-f\rho Q_{01}=0$$

which, on account of (3.5), is easier to deal with.

This being said, in order to investigate the equations of gravitation, we assume that the dynamical states of the gravitational field alternate with the stationary ones without diffusion of gravitational waves.

We begin with the equation $Q_{11}+\rho^2 Q_{22}=0$, which, on account of (3.4), can be written as

$$\frac{\partial}{\partial\rho}\left(\frac{1}{f\ell}\frac{\partial g}{\partial\rho}\right)=0$$

so that

$$\frac{\partial g}{\partial\rho}=\beta f\ell$$

where β is a function depending uniquely on the time τ.

Let us consider a succession of three intervals of time,

$$[\tau_1,\tau_2]\quad]\tau_2,\tau_3[\quad [\tau_3,\tau_4],$$

such that the gravitational field is stationary during $[\tau_1,\tau_2]$ and $[\tau_3,\tau_4]$ and dynamical during $]\tau_2,\tau_3[$.

When τ describes $[\tau_1,\tau_2]$ and $[\tau_3,\tau_4]$, the functions f, ℓ, g depend uniquely on ρ, so that β reduces then necessarily to a constant, which, according to the known theory of the stationary vacuum solutions, equals $\frac{1}{c}$, c being the classical constant (which, in the present situation, does not represent the velocity of propagation of light in vacuum). It follows that, if β depends effectively on τ during $]\tau_2,\tau_3[$, then it appears as a boundary condition at finite distance, like the radius and the curvature radius of the sphere bounding the matter. However, we cannot conceive a physical situation related to such a boundary condition. So we are led to assume that β is a universal constant, namely $\frac{1}{c}$, keeping this value even during the dynamical states of the gravitational field. However, before accepting finally the universal constancy of β, it is convenient to investigate the equations of gravitation under the assumption that β depends effectively on time during the interval $]\tau_2,\tau_3[$.

We first prove that $\beta=\beta(\tau)$ does not vanish in $]\tau_2,\tau_3[$. We argue by contradiction, assuming that $\beta(\tau_0)=0$ for some value $\tau_0\in]\tau_2,\tau_3[$. Then $\frac{\partial g}{\partial\rho}$ and $\frac{\partial^2 g}{\partial\rho^2}=\beta\frac{\partial(f\ell)}{\partial\rho}$ vanish for $\tau=\tau_0$, whereas $\frac{\partial^2 g}{\partial\tau\partial\rho}=(f\ell)\beta'+\beta\frac{\partial(f\ell)}{\partial\tau}$ reduces to $(f\ell)\beta'(\tau_0)$ for $\tau=\tau_0$. Consequently the equation $\rho^2 Q_{11}=0$ reduces to the condition $1+2g\beta'(\tau_0)=0$ whence $\beta'(\tau_0)<0$ (since $g>0$). It follows that $\beta(\tau)$ is strictly decreasing on a certain interval $[\tau_0-\varepsilon,\tau_0+\varepsilon]\subset]\tau_2,\tau_3[$, $\varepsilon>0$, so that $\beta(\tau)<0$ for every $\tau\in]\tau_0,\tau_0+\varepsilon]$. Let τ_{00} be the least upper bound of the set of values $\tau\in]\tau_0+\varepsilon,\tau_3[$ for which $\beta(\tau)=0$ (This value exists because $\beta(\tau)=\frac{1}{c}>0$ on $[\tau_3,\tau_4]$). Then $\beta(\tau_{00})=0$ and $\beta(\tau)>\tau_{00}$ for $\tau>\tau_{00}$. But, according to what has just been proved, the condition $\beta(\tau_{00})=0$ implies that $\beta(\tau)<0$ on a certain interval $]\tau_{00},\tau_{00}+\eta]$, $\eta>0$, giving a contradiction. It follows that the function $\beta(\tau)$ is strictly positive on $]\tau_2,\tau_3[$, hence also on any interval of non-stationarity, and since $\beta(\tau)=\frac{1}{c}$ on the intervals of stationarity, it is strictly positive everywhere. Consequently we are allowed to introduce the inverse function $\alpha=\alpha(\tau)=\frac{1}{\beta(\tau)}$ and write

$$f\ell=\alpha\frac{\partial g}{\partial\rho} \tag{4.1}$$

and

$$f=\frac{\alpha}{\ell}\frac{\partial g}{\partial\rho}. \tag{4.2}$$

Inserting this expression of f into the equation $\rho^2 Q_{11}=0$ and then multiplying throughout by $\frac{\partial g}{\partial\rho}$, we obtain an equation which can be written as

$$\frac{\partial}{\partial\rho}\left(-\frac{2g}{\alpha}\frac{\partial g}{\partial\tau}+\frac{g}{\ell^2}\left(\frac{\partial g}{\partial\rho}\right)^2-g\right)=0$$

whence

$$-\frac{2g}{\alpha}\frac{\partial g}{\partial\tau}+\frac{g}{\ell^2}\left(\frac{\partial g}{\partial\rho}\right)^2-g=-2\mu=\text{function of }\tau,$$

and

$$\frac{\partial g}{\partial\tau}=\frac{\alpha}{2}\left(-1+\frac{2\mu}{g}+\frac{1}{\ell^2}\left(\frac{\partial g}{\partial\rho}\right)^2\right). \tag{4.3}$$

It follows that

$$\frac{\partial^2 g}{\partial\tau\partial\rho}=\alpha\left(-\frac{\mu}{g^2}\frac{\partial g}{\partial\rho}-\frac{1}{\ell^3}\frac{\partial\ell}{\partial\rho}\left(\frac{\partial g}{\partial\rho}\right)^2+\frac{1}{\ell^2}\frac{\partial g}{\partial\rho}\frac{\partial^2 g}{\partial\rho^2}\right) \tag{4.4}$$

and

$$\frac{\partial^3 g}{\partial\tau\partial\rho^2} = \alpha\left(\frac{2\mu}{g^3}\left(\frac{\partial g}{\partial\rho}\right)^2 - \frac{\mu}{g^2}\frac{\partial^2 g}{\partial\rho^2} + \right.$$
$$+ \frac{3}{\ell^4}\left(\frac{\partial\ell}{\partial\rho}\right)^2\left(\frac{\partial g}{\partial\rho}\right)^2 - \frac{1}{\ell^3}\frac{\partial^2\ell}{\partial\rho^2}\left(\frac{\partial g}{\partial\rho}\right)^2 - \tag{4.5}$$
$$\left. - \frac{4}{\ell^3}\frac{\partial\ell}{\partial\rho}\frac{\partial g}{\partial\rho}\frac{\partial^2 g}{\partial\rho^2} + \frac{1}{\ell^2}\left(\frac{\partial^2 g}{\partial\rho^2}\right)^2 + \frac{1}{\ell^2}\frac{\partial g}{\partial\rho}\frac{\partial^3 g}{\partial\rho^3}\right).$$

On the other hand, since $f\ell = \alpha\frac{\partial g}{\partial\rho}$, the expression (3.2) is transformed as follows

$$\rho Q_{01} = \frac{1}{\left(\frac{\partial g}{\partial\rho}\right)^2}\left(\frac{\partial g}{\partial\rho}\frac{\partial^3 g}{\partial\tau\partial\rho^2} - \frac{\partial^2 g}{\partial\rho^2}\frac{\partial^2 g}{\partial\tau\partial\rho}\right) +$$
$$+\alpha\left(-\frac{3}{\ell^4}\left(\frac{\partial\ell}{\partial\rho}\right)^2\frac{\partial g}{\partial\rho} + \frac{1}{\ell^3}\frac{\partial^2\ell}{\partial\rho^2}\frac{\partial g}{\partial\rho} + \right.$$
$$\left. + \frac{3}{\ell^3}\frac{\partial\ell}{\partial\rho}\frac{\partial^2 g}{\partial\rho^2} - \frac{1}{\ell^2}\frac{\partial^3 g}{\partial\rho^3} - \frac{2\mu}{g^3}\frac{\partial g}{\partial\rho}\right)$$

and replacing in it $\frac{\partial^2 g}{\partial\tau\partial\rho}$ and $\frac{\partial^3 g}{\partial\tau\partial\rho^2}$ by their expressions (4.4) and (4.5), we find $\rho Q_{01} = 0$. Consequently the equation of gravitation $\rho Q_{01} = 0$ is verified. It remains to examine the equation $\ell Q_{00} - f\rho Q_{01} = 0$. We need some preliminary computations. First we consider the expression of $\frac{\partial^2 g}{\partial\tau^2}$ resulting from the derivation of (4.3) with respect to τ, and then replacing in it $\frac{\partial g}{\partial\tau}$ and $\frac{\partial^2 g}{\partial\tau\partial\rho}$ by their expressions (4.3) and (4.4), we obtain

$$2\frac{\partial^2 g}{\partial\tau^2} = -\frac{d\alpha}{d\tau} + 2\frac{d\alpha}{d\tau}\frac{\mu}{g} + \frac{1}{\ell^2}\frac{d\alpha}{d\tau}\left(\frac{\partial g}{\partial\rho}\right)^2 +$$
$$+\frac{2\alpha}{g}\frac{d\mu}{d\tau} - \frac{2\alpha^2\mu^2}{g^3} + \frac{\alpha^2\mu}{g^2} - \frac{2\alpha}{\ell^3}\frac{\partial\ell}{\partial\tau}\left(\frac{\partial g}{\partial\rho}\right)^2 - \tag{4.6}$$
$$- 3\frac{\alpha^2\mu}{\ell^2 g^2}\left(\frac{\partial g}{\partial\rho}\right)^2 - \frac{2\alpha^2}{\ell^5}\frac{\partial\ell}{\partial\rho}\left(\frac{\partial g}{\partial\rho}\right)^3 + \frac{2\alpha^2}{\ell^4}\left(\frac{\partial g}{\partial\rho}\right)^2\frac{\partial^2 g}{\partial\rho^2}.$$

Next, because of (4.2), we have

$$\frac{\partial f}{\partial\rho} = -\frac{\alpha}{\ell^2}\frac{\partial\ell}{\partial\rho}\frac{\partial g}{\partial\rho} + \frac{\alpha}{\ell}\frac{\partial^2 g}{\partial\rho^2} \tag{4.7}$$

and

$$\frac{\partial f}{\partial\tau} = \frac{1}{\ell}\frac{d\alpha}{d\tau}\frac{\partial g}{\partial\rho} - \frac{\alpha}{\ell^2}\frac{\partial\ell}{\partial\tau}\frac{\partial g}{\partial\rho} + \frac{\alpha}{\ell}\frac{\partial^2 g}{\partial\tau\partial\rho}.$$

Lastly taking into account (4.4), we obtain

$$\frac{\partial f}{\partial\tau} = \frac{1}{\ell}\frac{d\alpha}{d\tau}\frac{\partial g}{\partial\rho} - \frac{\alpha}{\ell^2}\frac{\partial\ell}{\partial\tau}\frac{\partial g}{\partial\rho} - \frac{\alpha^2\mu}{\ell g^2}\frac{\partial g}{\partial\rho} -$$
$$- \frac{\alpha^2}{\ell^4}\frac{\partial\ell}{\partial\rho}\left(\frac{\partial g}{\partial\rho}\right)^2 + \frac{\alpha^2}{\ell^3}\frac{\partial g}{\partial\rho}\frac{\partial^2 g}{\partial\rho^2}. \tag{4.8}$$

Now inserting (4.2), (4.3), (4.4), (4.6), (4.7), (4.8) into (3.5), we obtain, after cancelations, the very simple expression

$$\ell Q_{00} - f\rho Q_{01} = \frac{2\alpha\ell}{g^2}\frac{d\mu}{d\tau}.$$

Consequently the last equation of gravitation, namely $\ell Q_{00} - f\rho Q_{01} = 0$, implies that $\frac{d\mu}{d\tau} = 0$, namely that μ reduces to a constant.

Finally the system of the equations of gravitation is reduced to a system of two equations, namely (4.1) and (4.3), where μ is a constant valid whatever is the state of the field, and α is a strictly positive function of time reducing to the constant c during the stationary states of the field. As already remarked, if α depends effectively on τ during the dynamical states, then it plays the part of a boundary condition the origin of which is indefinable. The following reasoning, which is allowed according to the principles of General Relativity, corroborates the idea that α must be taken everywhere equal to c.

Since $\alpha(\tau) > 0$ everywhere, we can introduce the new time coordinate

$$u = \frac{1}{c}\int_{\tau_0}^{\tau}\alpha(v)dv$$

which amounts to a change of coordinate in the sphere bounding the matter. The function

$$\psi(\tau) = \frac{1}{c}\int_{\tau_0}^{\tau}\alpha(v)dv$$

being strictly increasing, its inverse $\tau = \varphi(u)$ is well defined and $\varphi' = \frac{1}{\psi'} = \frac{c}{\alpha}$. Instead of $\ell(\tau,\rho)$ and $g(\tau,\rho)$ we have now the functions $L(u,\rho) = \ell(\varphi(u),\rho)$ and $G(u,\rho) = g(\varphi(u),\rho)$,

Moreover, since $fd\tau = f\varphi' du$, $f(\tau,\rho)$ is replaced by the function $F(u,\rho) = \varphi'(u)f(\varphi(u),\rho) = \frac{c}{\alpha}f(\varphi(u),\rho)$.

It follows that

$$FL = \varphi' f\ell = \frac{c}{\alpha}\,\alpha\,\frac{\partial g}{\partial\rho} = c\,\frac{\partial G}{\partial\rho} \tag{4.9}$$

and

$$\frac{\partial G}{\partial u} = \frac{\partial g}{\partial\tau}\frac{d\tau}{du} = \frac{\alpha}{2}\left(-1 + \frac{2\mu}{g} + \frac{1}{\ell^2}\left(\frac{\partial g}{\partial\rho}\right)^2\right)\frac{c}{\alpha} =$$
$$= \frac{c}{2}\left(-1 + \frac{2\mu}{G} + \frac{1}{L^2}\left(\frac{\partial G}{\partial\rho}\right)^2\right). \tag{4.10}$$

Writing again $f(\tau,\rho), \ell(\tau,\rho), g(\tau,\rho)$ respectively instead of $F(u,\rho), L(u,\rho), G(u,\rho)$, we see that the equations (4.9) and (4.10) are rewritten as

$$f\ell = c\,\frac{\partial g}{\partial\rho} \tag{4.11}$$

$$\frac{\partial g}{\partial\tau} = \frac{c}{2}\left(-1 + \frac{2\mu}{g} + \frac{1}{\ell^2}\left(\frac{\partial g}{\partial\rho}\right)^2\right). \tag{4.12}$$

So (4.1) and (4.3) preserve their form, but the function α is now replaced by the constant c. Finally we are allowed to dispense with the function α and deal subsequently with the equations (4.11) and (4.12).

5 Stationary and non-stationary solutions

If the field is stationary during a certain interval of time, then the derivative $\frac{\partial g}{\partial \tau}$ vanishes on this interval. The converse is also true. In order to clarify the situation, consider the succession of three intervals of time $]\tau_1, \tau_2[$, $[\tau_2, \tau_3]$, $]\tau_3, \tau_4[$ such that $]\tau_1, \tau_2[$ and $]\tau_3, \tau_4[$ be maximal intervals of non-stationarity, and $\frac{\partial g}{\partial \tau} = 0$ on $[\tau_2, \tau_3]$. Then we have on $[\tau_2, \tau_3]$ the equation

$$-1 + \frac{2\mu}{g} + \frac{1}{\ell^2}\left(\frac{\partial g}{\partial \rho}\right)^2 = 0$$

from which it follows that ℓ does not depend either on τ. On account of (4.11), this property is also valid for f. Consequently the vanishing of $\frac{\partial g}{\partial \tau}$ on $[\tau_2, \tau_3]$ implies the establishment of a stationary state.

During the stationary state we are allowed to introduce the radial geodesic distance

$$\delta = \int_0^\rho \ell(v)dv$$

and investigate subsequently the stationary equations in accordance with the exposition appearing in the paper [4]. Since

$$\delta = \beta(\rho)$$

is a strictly increasing function of ρ, the inverse function $\rho = \gamma(\delta)$ is well defined and allows to consider as function of δ every function of ρ. In particular the curvature radius $G(\delta) = g(\gamma(\delta))$ appears as a function of the geodesic distance δ and gives rise to a complete study of the stationary field. From this study it follows that the constant μ equals $\frac{km}{c^2}$ and that the solution $G(\delta)$ possesses the greatest lower bound 2μ. Moreover $G(\delta)$ is defined by the equation

$$\int_{2\mu}^{G} \frac{du}{\sqrt{1 - \frac{2\mu}{u}}} = \delta - \delta_0 \qquad (5.1)$$

where δ_0 is a new constant unknown in the classical theory of gravitation. This constant is defined by means of the radius δ_1 and the curvature radius $\zeta_1 = G(\delta_1)$ of the sphere bounding the matter:

$$\delta_0 = \delta_1 - \sqrt{G(\delta_1)(G(\delta_1) - 2\mu)} - 2\mu \ln\left(\sqrt{\frac{G(\delta_1)}{2\mu}} + \sqrt{\frac{G(\delta_1)}{2\mu} - 1}\right).$$

So the values δ_1 and $\zeta_1 = G(\delta_1)$ constitute the boundary conditions at finite distance. Regarding $F = F(\delta) = f(\gamma(\delta))$, it is defined by means of G:

$$F = cG' = c\sqrt{1 - \frac{2\mu}{G}}, \quad (G \geqslant 2\mu).$$

The so obtained solution does not extend beyond the interval $[\tau_2, \tau_3]$ and even its validity for $\tau = \tau_2$ and $\tau = \tau_3$ is questionable. The notion of radial geodesic distance does not make sense in the intervals of non-stationarity such as $]\tau_1, \tau_2[$ and $]\tau_3, \tau_4[$. Then the integral

$$\int_0^\rho \ell(\tau, v)dv$$

depends on the time τ and does not define an invariant length. As a way out of the difficulty we confine ourselves to the consideration of the radical coordinate related to the manifold itself, namely $\rho = \|x\|$.

Regarding the curvature radius $\zeta(\tau)$, it is needed in order to conceive the solution of the equations of gravitation. The function $g(\tau, \rho)$ must be so defined that $g(\tau, \sigma(\tau)) = \zeta(\tau)$. The functions $\sigma(\tau)$ and $\zeta(\tau)$ are the boundary conditions at finite distance for the non-stationary field. They are not directly connected with the boundary conditions of the stationary field defined by means of the radial geodesic distance.

6 On the non-stationary solutions

According to very strong arguments summarized in the paper [2], the relation $g \geqslant 2\mu$ is always valid outside the matter whatever is the state of the field. This is why the first attempt to obtain dynamical solutions was based on an equation analogous to (5.1), namely

$$\int_{2\mu}^{g} \frac{du}{\sqrt{1 - \frac{2\mu}{u}}} = \gamma(\tau, \rho)$$

where $\gamma(\tau, \rho)$ is a new function satisfying certain conditions. This idea underlies the results presented briefly in the paper [1]. However the usefulness of introduction of a new function is questionable. It is more natural to deal directly with the functions f, ℓ, g involved in the metric. In any case we have to do with two equations, namely (4.11) and (4.12), so that we cannot expect to define completely the three unknown functions. Note also that, even in the considered stationary solution, the equation (5.1) does not define completely the function G on account of the new unknown constant δ_0. In the general case there is no way to define the function $g(\tau, \rho)$ by means of parameters and simpler functions. The only available equation, namely (4.12), a partial differential equation including the unknown function $\ell(\tau, \rho)$, is, in fact, intractable. As a way out of the difficulties, we propose to consider the function $g(\tau, \rho)$ as a new entity required by the non-Euclidean structure involved in the dynamical gravitational field. In the present state of our knowledge, we confine ourselves to put forward the main features of $g(\tau, \rho)$ in the closed set

$$\overline{U} = \{(\tau, \rho) \in \mathbb{R}^2 | \rho \geqslant \sigma(\tau)\}.$$

Since the vanishing of f or ℓ would imply the degeneracy of the spacetime metric, these two functions are necessarily strictly positive on $\overline{U}$. Then from the equation (4.11) it fol-

lows that

$$\frac{\partial g(\tau,\rho)}{\partial \rho} > 0 \tag{6.1}$$

on the closed set $\overline{U}$. On the other hand, since (4.12) can be rewritten as

$$\frac{2}{c}\frac{\partial g}{\partial \tau} + 1 - \frac{2\mu}{g} = \frac{1}{\ell^2}\left(\frac{\partial g}{\partial \rho}\right)^2$$

we have also

$$\frac{2}{c}\frac{\partial g}{\partial \tau} + 1 - \frac{2\mu}{g} > 0 \tag{6.2}$$

on the closed set $\overline{U}$. Now, on account of (6.1) and (6.2), the equations (4.11) and (4.12) define uniquely the functions f and ℓ by means of g:

$$f = c\sqrt{\frac{2}{c}\frac{\partial g}{\partial \tau} + 1 - \frac{2\mu}{g}} \tag{6.3}$$

$$\ell = \frac{\partial g/\partial \rho}{\sqrt{\frac{2}{c}\frac{\partial g}{\partial \tau} + 1 - \frac{2\mu}{g}}}\,. \tag{6.4}$$

It is now obvious that the curvature radius $g(\tau,\rho)$ plays the main part in the conception of the gravitational field. Although it has nothing to do with coordinates, the relativists have reduced it to a so-called radial coordinate from the beginnings of General Relativity. This glaring mistake has given rise to intolerable misunderstandings and distorted completely the theory of the gravitational field.

Let $]\tau_1,\tau_2[$ be a maximal bounded open interval of non-stationarity. Then $\frac{\partial g}{\partial \tau} = 0$ for $\tau = \tau_1$ and $\tau = \tau_2$, but $\frac{\partial g}{\partial \tau} \neq 0$ on an open dense subset of $]\tau_1,\tau_2[$. So $\frac{\partial g}{\partial \tau}$ appears as a gravitational wave travelling to infinity, and it is natural to assume that $\frac{\partial g}{\partial \tau}$ tends uniformly to zero on $[\tau_1,\tau_2]$ as $\rho \to +\infty$. Of course the behaviour of $\frac{\partial g}{\partial \tau}$ depends on the boundary conditions which do not appear in the obtained general solution. They are to be introduced in accordance with the envisaged problem. In any case the gravitational disturbance plays the fundamental part in the conception of the dynamical gravitation, but the state of the field does not follow always a simple rule.

In particular, if the gravitational disturbance vanishes during a certain interval of time $[\tau_1,\tau_2]$, the function $g(\tau,\rho)$ does not depend necessarily only on ρ during $[\tau_1,\tau_2]$. In other words, the gravitational field does not follow necessarily the Huyghens principle contrary to the solutions of the classical wave equation in $\mathbb{R}^3$.

We deal briefly with the case of *a Huyghens type field*, namely a $\Theta(4)$-invariant gravitational field such that the vanishing of the gravitational disturbance on a time interval implies the establishment of a universal stationary state. Then the time is involved in the curvature radius by means of the boundary conditions $\sigma(\tau)$, $\zeta(\tau)$, so that $g(\tau,\rho)$ is in fact a function of $(\sigma(\tau),\zeta(\tau),\rho) : g(\sigma(\tau),\zeta(\tau),\rho)$. The corresponding expressions for f and ℓ result from (6.3) and (6.4):

$$f = c\sqrt{\frac{2}{c}\left(\frac{\partial g}{\partial \sigma}\sigma'(\tau) + \frac{\partial g}{\partial \zeta}\zeta'(\tau)\right) + 1 - \frac{2\mu}{g}}$$

$$\ell = \frac{\frac{\partial g}{\partial \rho}}{\sqrt{\frac{2}{c}\left(\frac{\partial g}{\partial \sigma}\sigma'(\tau) + \frac{\partial g}{\partial \zeta}\zeta'(\tau)\right) + 1 - \frac{2\mu}{g}}}$$

where g denotes $g(\sigma(\tau),\zeta(\tau),\rho)$.

If $\sigma'(\tau) = \zeta'(\tau) = 0$ during an interval of time, the boundary conditions $\sigma(\tau)$, $\zeta(\tau)$ reduce to positive constants σ_0, ζ_0 on this interval, so that the curvature radius defining the stationary states depends on the constants $\sigma_0,\zeta_0 : g(\sigma_0,\zeta_0,\rho)$. It is easy to write down the conditions satisfied by $g(\sigma_0,\zeta_0,\rho)$, considered as function of three variables.

Submitted on June 12, 2007
Accepted on June 13, 2007

References

1. Stavroulakis N. Exact solution for the field of a pulsating source. Abstracts of Contributed Papers for the Discussion Groups, *9th International Conference on General Relativity and Gravitation*, July 14–19, 1980, Jena, Volume 1, 74–75.
2. Stavroulakis N. Particules et particules test en relativité générale. *Annales Fond. Louis de Broglie*, 1991, v. 16, No. 2, 129–175.
3. Stavroulakis N. Vérité scientifique et trous noirs (troisième partie) Equations de gravitation relatives à une métrique $\Theta(4)$-invariante. *Annales Fond. Louis de Broglie*, 2001, v. 26, No. 4, 605–631.
4. Stavroulakis N. Non-Euclidean geometry and gravitation. *Progress in Physics*, 2006, v. 2, 68–75.
5. Stavroulakis N. On the propagation of gravitation from a pulsating source. *Progress in Physics*, 2007, v. 2, 75–82.

Dynamical 3-Space: Supernovae and the Hubble Expansion — the Older Universe without Dark Energy

Reginald T. Cahill

School of Chemistry, Physics and Earth Sciences, Flinders University, Adelaide 5001, Australia
E-mail: Reg.Cahill@flinders.edu.au

We apply the new dynamics of 3-space to cosmology by deriving a Hubble expansion solution. This dynamics involves two constants; G and α — the fine structure constant. This solution gives an excellent parameter-free fit to the recent supernova and gamma-ray burst redshift data without the need for "dark energy" or "dark matter". The data and theory together imply an older age for the universe of some 14.7Gyrs. The 3-space dynamics has explained the bore hole anomaly, spiral galaxy flat rotation speeds, the masses of black holes in spherical galaxies, gravitational light bending and lensing, all without invoking "dark matter" or "dark energy". These developments imply that a new understanding of the universe is now available.

1 Introduction

There are theoretical claims based on observations of Type Ia supernova (SNe Ia) redshifts [1, 2] that the universe expansion is accelerating. The cause of this acceleration has been attributed to an undetected "dark energy". Here the dynamical theory of 3-space is applied to Hubble expansion dynamics, with the result that the supernova and gamma-ray burst redshift data is well fitted without an acceleration effect and without the need to introduce any notion of "dark energy". So, like "dark matter", "dark energy" is an unnecessary and spurious notion. These developments imply that a new understanding of the universe is now available.

1.1 Dynamical 3-Space

At a deeper level an information-theoretic approach to modelling reality, *Process Physics* [3, 4], leads to an emergent structured "space" which is 3-dimensional and dynamic, but where the 3-dimensionality is only approximate, in that if we ignore non-trivial topological aspects of the space, then it may be embedded in a 3-dimensional geometrical manifold. Here the space is a real existent discrete fractal network of relationships or connectivities, but the embedding space is purely a mathematical way of characterising the 3-dimensionality of the network. Embedding the network in the embedding space is very arbitrary; we could equally well rotate the embedding or use an embedding that has the network translated or translating. These general requirements then dictate the minimal dynamics for the actual network, at a phenomenological level. To see this we assume at a coarse grained level that the dynamical patterns within the network may be described by a velocity field $\mathbf{v}(\mathbf{r}, t)$, where $\mathbf{r}$ is the location of a small region in the network according to some arbitrary embedding. The 3-space velocity field has been observed in at least 8 experiments [3, 4]. For simplicity we assume here that the global topology of the network is not significant for the local dynamics, and so we embed in an E^3, although a generalisation to an embedding in S^3 is straightforward and might be relevant to cosmology. The minimal dynamics is then obtained by writing down the lowest-order zero-rank tensors, of dimension $1/t^2$, that are invariant under translation and rotation, giving

$$\nabla\cdot\left(\frac{\partial\mathbf{v}}{\partial t}+(\mathbf{v}\cdot\nabla)\mathbf{v}\right)+\frac{\alpha}{8}\left((\mathrm{tr}D)^2-\mathrm{tr}(D^2)\right)=-4\pi G\rho\,, \quad (1)$$

$$D_{ij}=\frac{1}{2}\left(\frac{\partial v_i}{\partial x_j}+\frac{\partial v_j}{\partial x_i}\right), \quad (2)$$

where $\rho(\mathbf{r}, t)$ is the effective matter density. The embedding space coordinates provide a coordinate system or frame of reference that is convenient to describing the velocity field, but which is not real. In *Process Physics* quantum matter are topological defects in the network, but here it is sufficient to give a simple description in terms of an effective density. G is Newton's gravitational constant, and describes the rate of non-conservative flow of space into matter, and data from the bore hole g anomaly and the mass spectrum of black holes reveals that α is the fine structure constant $\approx 1/137$, to within experimental error [5, 6, 7].

Now the acceleration $\mathbf{a}$ of the dynamical patterns in the 3-space is given by the Euler or convective expression

$$\mathbf{a}(\mathbf{r},t)=\lim_{\Delta t\to 0}\frac{\mathbf{v}\big(\mathbf{r}+\mathbf{v}(\mathbf{r},t)\Delta t, t+\Delta t\big)-\mathbf{v}(\mathbf{r},t)}{\Delta t}=\\ =\frac{\partial\mathbf{v}}{\partial t}+(\mathbf{v}\cdot\nabla)\mathbf{v}\,. \quad (3)$$

As shown in [8] the acceleration $\mathbf{g}$ of quantum matter is identical to the acceleration of the 3-space itself, apart from vorticity and relativistic effects, and so the gravitational acceleration of matter is also given by (3). Eqn. (1) has black hole solutions for which the effective masses agree with observational data for spherical star systems [5, 6, 7]. Theses black holes also explain the flat rotation curves in spiral galaxies [9].

2 Supernova and gamma-ray burst data

The supernovae and gamma-ray bursts provide standard candles that enable observation of the expansion of the universe. The supernova data set used herein and shown in Figs. 2 and 3 is available at [10]. Quoting from [10] we note that Davis *et al.* [11] combined several data sets by taking the ESSENCE data set from Table 9 of Wood–Vassey *et al.* (2007) [13], using only the supernova that passed the light-curve-fit quality criteria. They took the HST data from Table 6 of Riess *et al.* (2007) [12], using only the supernovae classified as gold. To put these data sets on the same Hubble diagram Davis *et al.* used 36 local supernovae that are in common between these two data sets. When discarding supernovae with $z < 0.0233$ (due to larger uncertainties in the peculiar velocities) they found an offset of 0.037 ± 0.021 magnitude between the data sets, which they then corrected for by subtracting this constant from the HST data set. The dispersion in this offset was also accounted for in the uncertainties. The HST data set had an additional 0.08 magnitude added to the distance modulus errors to allow for the intrinsic dispersion of the supernova luminosities. The value used by Wood–Vassey *et al.* (2007) [13] was instead 0.10 mag. Davis *et al.* adjusted for this difference by putting the Gold supernovae on the same scale as the ESSENCE supernovae. Finally, they also added the dispersion of 0.021 magnitude introduced by the simple offset described above to the errors of the 30 supernovae in the HST data set. The final supernova data base for the distance modulus $\mu_{obs}(z)$ is shown in Figs. 2 and 3. The gamma-ray burst (GRB) data is from Schaefer [14].

3 Expanding 3-space — the Hubble solution

Suppose that we have a radially symmetric density $\rho(r,t)$ and that we look for a radially symmetric time-dependent flow $\mathbf{v}(\mathbf{r},t) = v(r,t)\hat{\mathbf{r}}$ from (1). Then $v(r,t)$ satisfies the equation, with $v' = \frac{\partial v(r,t)}{\partial r}$,

$$\frac{\partial}{\partial t}\left(\frac{2v}{r} + v'\right) + vv'' + 2\frac{vv'}{r} + (v')^2 + \\ + \frac{\alpha}{4}\left(\frac{v^2}{r^2} + \frac{2vv'}{r}\right) = -4\pi G\rho(r,t)\,. \tag{4}$$

Consider first the zero energy case $\rho = 0$. Then we have a Hubble solution $v(r,t) = H(t)r$, a centreless flow, determined by

$$\dot{H} + \left(1 + \frac{\alpha}{4}\right)H^2 = 0 \tag{5}$$

with $\dot{H} = \frac{dH}{dt}$. We also introduce in the usual manner the scale factor $R(t)$ according to $H(t) = \frac{1}{R}\frac{dR}{dt}$. We then obtain the solution

$$H(t) = \frac{1}{(1+\frac{\alpha}{4})t} = H_0\frac{t_0}{t};\quad R(t) = R_0\left(\frac{t}{t_0}\right)^{4/(4+\alpha)} \tag{6}$$

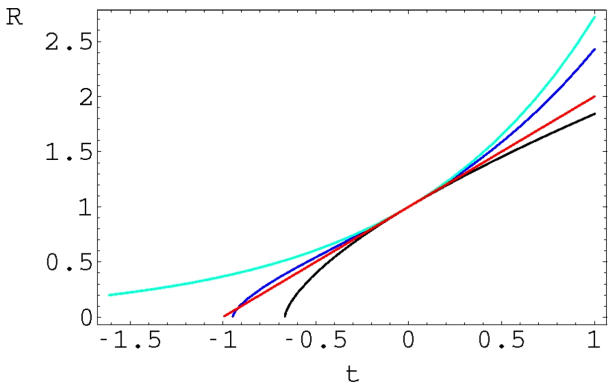

Fig. 1: Plot of the scale factor $R(t)$ vs t, with $t = 0$ being "now" with $R(0) = 1$, for the four cases discussed in the text, and corresponding to the plots in Figs. 2 and 3: (i) the upper curve (green) is the "dark energy" only case, resulting in an exponential acceleration at all times, (ii) the bottom curve (black) is the matter only prediction, (iii) the 2nd highest curve (to the right of $t = 0$) is the best-fit "dark energy" plus matter case (blue) showing a past deceleration and future exponential acceleration effect. The straight line plot (red) is the dynamical 3-space prediction showing a slightly older universe compared to case (iii). We see that the best-fit "dark energy"-matter curve essentially converges on the dynamical 3-space result. All plots have the same slope at $t = 0$, i.e. the same value of H_0. If the age of the universe is inferred to be some 14Gyrs for case (iii) then the age of the universe is changed to some 14.7Gyr for case (iv).

where $H_0 = H(t_0)$ and $R_0 = R(t_0)$. We can write the Hubble function $H(t)$ in terms of $R(t)$ via the inverse function $t(R)$, i.e. $H(t(R))$ and finally as $H(z)$, where the redshift observed now, t_0, relative to the wavelengths at time t, is $z = R_0/R - 1$. Then we obtain

$$H(z) = H_0(1+z)^{1+\alpha/4}. \tag{7}$$

We need to determine the distance travelled by the light from a supernova before detection. Using a choice of coordinate system with $r = 0$ at the location of a supernova the speed of light relative to this embedding space frame is $c + v(r(t),t)$, i.e. c wrt the space itself, where $r(t)$ is the distance from the source. Then the distance travelled by the light at time t after emission at time t_1 is determined implicitly by

$$r(t) = \int_{t_1}^{t} dt'\left(c + v\big(r(t'),t'\big)\right), \tag{8}$$

which has the solution on using $v(r,t) = H(t)r$

$$r(t) = cR(t)\int_{t_1}^{t}\frac{dt'}{R(t')}\,. \tag{9}$$

Expressed in terms of the observable redshift z this gives

$$r(z) = c(1+z)\int_0^z \frac{dz'}{H(z')}\,. \tag{10}$$

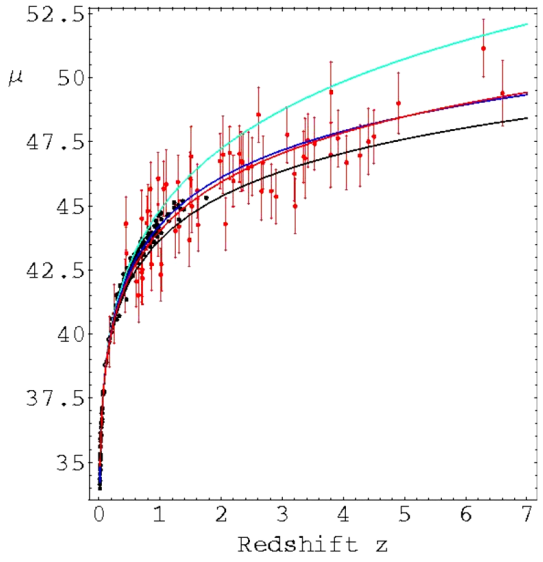

Fig. 2: Hubble diagram showing the combined supernovae data from Davis *et al.* [11] using several data sets from Riess *et al.* (2007) [12] and Wood-Vassey *et al.* (2007) [13] (dots without error bars for clarity — see Fig. 3 for error bars) and the Gamma-Ray Bursts data (with error bars) from Schaefer [14]. Upper curve (green) is "dark energy" only $\Omega_\Lambda = 1$, lower curve (black) is matter only $\Omega_m = 1$. Two middle curves show best-fit of "dark energy"-matter (blue) and dynamical 3-space prediction (red), and are essentially indistinguishable. However the theories make very different predictions for the future and for the age of the universe. We see that the best-fit 'dark energy'-matter curve essentially converges on the dynamical 3-space prediction.

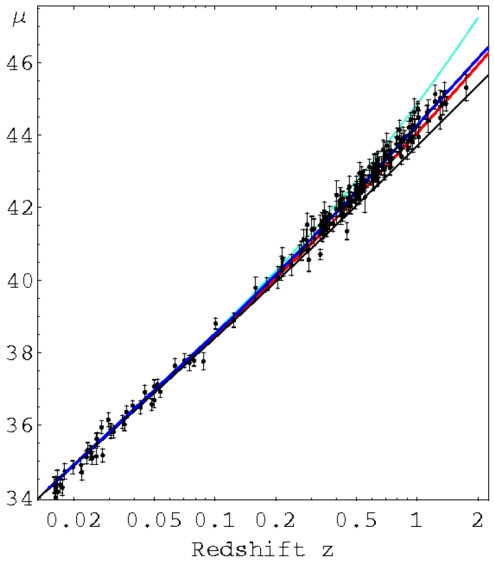

Fig. 3: Hubble diagram as in Fig. 2 but plotted logarithmically to reveal details for $z < 2$, and without GRB data. Upper curve (green) is "dark-energy" only, next curve down (blue) is best fit of "dark energy"-matter. Lower curve (black) is matter only $\Omega_m = 1$. Lower of two middle curves (red) is dynamical 3-space parameter-free prediction.

The effective dimensionless distance is given by

$$d(z) = (1+z)\int_0^z \frac{H_0 dz'}{H(z')} \tag{11}$$

and the theory distance modulus is then defined by

$$\mu_{th}(z) = 5\log_{10}\big(d(z)\big) + m\,. \tag{12}$$

Because all the selected supernova have the same absolute magnitude, m is a constant whose value is determined by fitting the low z data.

Using the Hubble expansion (7) in (11) and (12) we obtain the middle curves (red) in Figs. 2 and the 3, yielding an excellent agreement with the supernovae and GRB data. Note that because $\frac{\alpha}{4}$ is so small it actually has negligible effect on these plots. Hence the dynamical 3-space gives an immediate account of the universe expansion data, and does not require the introduction of a cosmological constant or "dark energy", but which will be nevertheless discussed next.

When the energy density is not zero we need to take account of the dependence of $\rho(r,t)$ on the scale factor of the universe. In the usual manner we thus write

$$\rho(r,t) = \frac{\rho_m}{R(t)^3} + \frac{\rho_r}{R(t)^4} + \Lambda \tag{13}$$

for matter, EM radiation and the cosmological constant or "dark energy" Λ, respectively, where the matter and radiation is approximated by a spatially uniform (i.e independent of r) equivalent matter density. We argue here that Λ — the dark energy density, like dark matter, is an unnecessary concept. Then (4) becomes for $R(t)$

$$\frac{\ddot{R}}{R} + \frac{\alpha}{4}\frac{\dot{R}^2}{R^2} = -\frac{4\pi G}{3}\left(\frac{\rho_m}{R^3} + \frac{\rho_r}{R^4} + \Lambda\right) \tag{14}$$

giving

$$\dot{R}^2 = \frac{8\pi G}{3}\left(\frac{\rho_m}{R} + \frac{\rho_r}{R^2} + \Lambda R^2\right) - \frac{\alpha}{2}\int \frac{\dot{R}^2}{R} dR\,. \tag{15}$$

In terms of $\dot{R}^2$ this has the solution

$$\dot{R}^2 = \frac{8\pi G}{3}\left(\frac{\rho_m}{(1-\frac{\alpha}{2})R} + \frac{\rho_r}{(1-\frac{\alpha}{4})R^2} + \frac{\Lambda R^2}{(1+\frac{\alpha}{4})} + bR^{-\frac{\alpha}{2}}\right) \tag{16}$$

which is easily checked by substitution into (15), where b is an arbitrary integration constant. Finally we obtain from (16)

$$t(R) = \int_{R_0}^{R} \frac{dR}{\sqrt{\frac{8\pi G}{3}\left(\frac{\rho_m}{R} + \frac{\rho_r}{R^2} + \Lambda R^2 + bR^{-\alpha/2}\right)}} \tag{17}$$

where now we have re-scaled parameters $\rho_m \to \rho_m/(1-\frac{\alpha}{2})$, $\rho_r \to \rho_r/(1-\frac{\alpha}{4})$ and $\Lambda \to \Lambda/(1+\frac{\alpha}{4})$. When $\rho_m = \rho_r = \Lambda = 0$, (17) reproduces the expansion in (6), and so the density terms in (16) give the modifications to the dominant purely spatial

expansion, which we have noted above already gives an excellent account of the data.

From (17) we then obtain

$$H(z)^2 = {H_0}^2(\Omega_m(1+z)^3 + \Omega_r(1+z)^4 + \\ + \Omega_\Lambda + \Omega_s(1+z)^{2+\alpha/2}) \quad (18)$$

with

$$\Omega_m + \Omega_r + \Omega_\Lambda + \Omega_s = 1\,. \quad (19)$$

Using the Hubble function (18) in (11) and (12) we obtain the plots in Figs. 2 and 3 for four cases:

(i) $\Omega_m = 0$, $\Omega_r = 0$, $\Omega_\Lambda = 1$, $\Omega_s = 0$, i.e a pure "dark energy" driven expansion,

(ii) $\Omega_m = 1$, $\Omega_r = 0$, $\Omega_\Lambda = 0$, $\Omega_s = 0$ showing that a matter only expansion is not a good account of the data,

(iii) from a least squares fit with $\Omega_s = 0$ we find $\Omega_m = 0.28$, $\Omega_r = 0$, $\Omega_\Lambda = 0.68$ which led to the suggestion that the "dark energy" effect was needed to fix the poor fit from (ii), and finally

(iv) $\Omega_m = 0$, $\Omega_r = 0$, $\Omega_\Lambda = 0$, $\Omega_s = 1$, as noted above, that the spatial expansion dynamics alone gives a good account of the data.

Of course the EM radiation term Ω_r is non-zero but small and determines the expansion during the baryogenesis initial phase, as does the spatial dynamics expansion term because of the α dependence. If the age of the universe is inferred to be some 14Gyrs for case (iii) then, as seen in Fig. 1, the age of the universe is changed to some 14.7Gyr for case (iv). We see that the one-parameter best-fit "dark energy"-matter curve essentially converges on the no-parameter dynamical 3-space result.

4 Conclusions

There is extensive evidence for a dynamical 3-space, with the minimal dynamical equation now known and confirmed by numerous experimental and observational data. As well we have shown that this equation has a Hubble expanding 3-space solution that in a parameter-free manner manifestly fits the recent supernova data, and in doing so reveals that "dark energy", like "dark matter", is an unnecessary notion. The Hubble solution leads to a uniformly expanding universe, and so without acceleration: the claimed acceleration is merely an artifact related to the unnecessary "dark energy" notion. This result gives an older age for the universe of some 14.7Gyr, and resolves as well various problems such as the fine tuning problem, the horizon problem and other difficulties in the current modelling of the universe.

Submitted on June 20, 2007
Accepted on June 25, 2007

References

1. Riess A.G. *et al. Astron. J.*, 1998, v. 116, 1009.
2. Perlmutter S. *et al. Astrophys. J.*, 1999, v. 517, 565,.
3. Cahill R. T. Process physics: from information theory to quantum space and matter, Nova Science Pub., New York, 2005.
4. Cahill R. T. Dynamical 3-space: a review. arXiv: 0705.4146.
5. Cahill R. T. Gravity, 'dark matter' and the fine structure constant. *Apeiron*, 2005, v. 12 (2), 144–177.
6. Cahill R. T. "Dark matter" as a quantum foam in-flow effect. In: *Trends in Dark Matter Research*, ed. J. Val Blain, Nova Science Pub., New York, 2005, 96–140.
7. Cahill R. T. Black holes and quantum theory: the fine structure constant connection. *Progress in Physics*, 2006, v. 4, 44–50.
8. Cahill R. T. Dynamical fractal 3-space and the generalised Schrödinger equation: equivalence principle and vorticity effects. *Progress in Physics*, 2006, v. 1, 27–34.
9. Cahill R. T. Black holes in elliptical and spiral galaxies and in globular clusters. *Progress in Physics*, 2005, v. 3, 51–56.
10. http://dark.dark-cosmology.dk/∼tamarad/SN/
11. Davis T., Mortsell E., Sollerman J. and ESSENCE. Scrutinizing exotic cosmological models using ESSENCE supernovae data combined with other cosmological probes. arXiv: astro-ph/0701510.
12. Riess A. G. *et al.* New Hubble Space Telescope discoveries of type Ia supernovae at $z > 1$: narrowing constraints on the early behavior of dark energy. arXiv: astro-ph/0611572.
13. Wood-Vassey W. M. *et al. Observational constraints on the nature of the dark energy: first cosmological results from the ESSENCE supernovae survey*. arXiv: astro-ph/0701041.
14. Schaefer B. E. The Hubble diagram to redshift > 6 from 69 gamma-ray bursts. *Ap. J.*, 2007, v. 660, 16–46.

Dynamical 3-Space: Alternative Explanation of the "Dark Matter Ring"

Reginald T. Cahill

School of Chemistry, Physics and Earth Sciences, Flinders University, Adelaide 5001, Australia
E-mail: Reg.Cahill@flinders.edu.au

NASA has claimed the discovery of a "Ring of Dark Matter" in the galaxy cluster CL 0024+17, see Jee M.J. *et al.* arXiv:0705.2171, based upon gravitational lensing data. Here we show that the lensing can be given an alternative explanation that does not involve "dark matter". This explanation comes from the new dynamics of 3-space. This dynamics involves two constant G and α — the fine structure constant. This dynamics has explained the bore hole anomaly, spiral galaxy flat rotation speeds, the masses of black holes in spherical galaxies, gravitational light bending and lensing, all without invoking "dark matter", and also the supernova redshift data without the need for "dark energy".

1 Introduction

Jee *et al.* [1] claim that the analysis of gravitational lensing data from the HST observations of the galaxy cluster CL 0024+17 demonstrates the existence of a "dark matter ring". While the lensing is clearly evident, as an observable phenomenon, it does not follow that this must be caused by some undetected form of matter, namely the putative "dark matter". Here we show that the lensing can be given an alternative explanation that does not involve "dark matter". This explanation comes from the new dynamics of 3-space [2, 3, 4, 5, 6]. This dynamics involves two constant G and α — the fine structure constant. This dynamics has explained the bore hole anomaly, spiral galaxy flat rotation speeds, the masses of black holes in spherical galaxies, gravitational light bending and lensing, all without invoking "dark matter". The 3-space dynamics also has a Hubble expanding 3-space solution that explains the supernova redshift data without the need for "dark energy" [8]. The issue is that the Newtonian theory of gravity [9], which was based upon observations of planetary motion in the solar system, missed a key dynamical effect that is not manifest in this system. The consequences of this failure has been the invoking of the fix-ups of "dark matter" and "dark energy". What is missing is the 3-space self-interaction effect. Experimental and observational data has shown that the coupling constant for this self-interaction is the fine structure constant, $\alpha \approx 1/137$, to within measurement errors. It is shown here that this 3-space self-interaction effect gives a direct explanation for the reported ring-like gravitational lensing effect.

2 3-space dynamics

As discussed elsewhere [2, 8] a deeper information — theoretic *Process Physics* has an emergent structured 3-space, where the 3-dimensionality is partly modelled at a phenomenological level by embedding the time- dependent structure in an E^3 or S^3 embedding space. This embedding space is not real — it serves to coordinatise the structured 3-space, that is, to provide an abstract frame of reference. Assuming the simplest dynamical description for zero-vorticity spatial velocity field $\mathbf{v}(\mathbf{r}, t)$, based upon covariant scalars we obtain at lowest order [2]

$$\nabla \cdot \left(\frac{\partial \mathbf{v}}{\partial t} + (\mathbf{v} \cdot \nabla)\mathbf{v} \right) + \frac{\alpha}{8} \big((\mathrm{tr} D)^2 - \mathrm{tr}(D^2) \big) = -4\pi G \rho, \quad (1)$$

$$\nabla \times \mathbf{v} = \mathbf{0}\,, \qquad D_{ij} = \frac{1}{2} \left(\frac{\partial v_i}{\partial x_j} + \frac{\partial v_j}{\partial x_i} \right), \quad (2)$$

where $\rho(\mathbf{r}, t)$ is the matter and EM energy density expressed as an effective matter density. In Process Physics quantum matter are topological defects in the structured 3-spaces, but here it is sufficient to give a simple description in terms of an effective density.

We see that there are two constants G and α. G turns out to be Newton's gravitational constant, and describes the rate of non-conservative flow of 3-space into matter, and α is revealed by experiment to be the fine structure constant. Now the acceleration $\mathbf{a}$ of the dynamical patterns of 3-space is given by the Euler convective expression

$$\mathbf{a}(\mathbf{r}, t) = \lim_{\Delta t \to 0} \frac{\mathbf{v}\big(\mathbf{r} + \mathbf{v}(\mathbf{r}, t)\Delta t, t + \Delta t\big) - \mathbf{v}(\mathbf{r}, t)}{\Delta t} = \\ = \frac{\partial \mathbf{v}}{\partial t} + (\mathbf{v} \cdot \nabla)\mathbf{v} \quad (3)$$

and this appears in the first term in (1). As shown in [3] the acceleration of quantum matter $\mathbf{g}$ is identical to this acceleration, apart from vorticity and relativistic effects, and so the gravitational acceleration of matter is also given by (3). Eqn. (1) is highly non-linear, and indeed non-local. It exhibits a range of different phenomena, and as has been shown the α term is responsible for all those effects attributed to the undetected and unnecessary "dark matter". For example, outside of a spherically symmetric distribution of matter, of total

mass M, we find that one solution of (1) is the velocity in-flow field

$$\mathbf{v}(\mathbf{r}) = -\hat{\mathbf{r}}\sqrt{\frac{2GM(1+\frac{\alpha}{2}+\ldots)}{r}} \tag{4}$$

and then the the acceleration of (quantum) matter, from (3), induced by this in-flow is

$$\mathbf{g}(\mathbf{r}) = -\hat{\mathbf{r}}\,\frac{GM(1+\frac{\alpha}{2}+\ldots)}{r^2} \tag{5}$$

which is Newton's Inverse Square Law of 1687 [9], but with an effective mass $M(1+\frac{\alpha}{2}+\ldots)$ that is different from the actual mass M.

In general because (1) is a scalar equation it is only applicable for vorticity-free flows $\nabla\times\mathbf{v}=\mathbf{0}$, for then we can write $\mathbf{v}=\nabla u$, and then (1) can always be solved to determine the time evolution of $u(\mathbf{r},t)$ given an initial form at some time t_0. The α-dependent term in (1) and the matter acceleration effect, now also given by (3), permits (1) to be written in the form

$$\nabla\cdot\mathbf{g} = -4\pi G\rho - 4\pi G\rho_{DM}\,, \tag{6}$$

$$\rho_{DM}(\mathbf{r},t) \equiv \frac{\alpha}{32\pi G}\big((\mathrm{tr}\,D)^2 - \mathrm{tr}(D^2)\big)\,, \tag{7}$$

which is an effective "matter" density that would be required to mimic the α-dependent spatial self-interaction dynamics. Then (6) is the differential form for Newton's law of gravity but with an additional non-matter effective matter density. So we label this as ρ_{DM} even though no matter is involved [4, 5]. This effect has been shown to explain the so-called "dark matter" effect in spiral galaxies, bore hole g anomalies, and the systematics of galactic black hole masses.

The spatial dynamics is non-local. Historically this was first noticed by Newton who called it action-at-a-distance. To see this we can write (1) as an integro-differential equation

$$\frac{\partial\mathbf{v}}{\partial t} = -\nabla\left(\frac{\mathbf{v}^2}{2}\right) + \\ + G\int d^3r'\,\frac{\rho_{DM}(\mathbf{r}',t)+\rho(\mathbf{r}',t)}{|\mathbf{r}-\mathbf{r}'|^3}\,(\mathbf{r}-\mathbf{r}')\,. \tag{8}$$

This shows a high degree of non-locality and non-linearity, and in particular that the behaviour of both ρ_{DM} and ρ manifest at a distance irrespective of the dynamics of the intervening space. This non-local behaviour is analogous to that in quantum systems and may offer a resolution to the horizon problem.

2.1 Spiral galaxy rotation anomaly

Eqn (1) gives also a direct explanation for the spiral galaxy rotation anomaly. For a non-spherical system numerical solutions of (1) are required, but sufficiently far from the centre, where we have $\rho=0$, we find an exact non-perturbative two-parameter class of analytic solutions

$$\mathbf{v}(\mathbf{r}) = -\hat{\mathbf{r}}\,K\left(\frac{1}{r}+\frac{1}{R_s}\left(\frac{R_s}{r}\right)^{\frac{\alpha}{2}}\right)^{1/2} \tag{9}$$

where K and R_s are arbitrary constants in the $\rho=0$ region, but whose values are determined by matching to the solution in the matter region. Here R_s characterises the length scale of the non-perturbative part of this expression, and K depends on α, G and details of the matter distribution. From (5) and (9) we obtain a replacement for the Newtonian "inverse square law"

$$\mathbf{g}(\mathbf{r}) = -\hat{\mathbf{r}}\,\frac{K^2}{2}\left(\frac{1}{r^2}+\frac{\alpha}{2rR_s}\left(\frac{R_s}{r}\right)^{\frac{\alpha}{2}}\right). \tag{10}$$

The 1st term, $1/r^2$, is the Newtonian part. The 2nd term is caused by a "black hole" phenomenon that (1) exhibits. This manifests in different ways, from minimal supermassive black holes, as seen in spherical star systems, from globular clusters to spherical galaxies for which the black hole mass is predicted to be $M_{BH}=\alpha M/2$, as confirmed by the observational datas [2, 4, 5, 6, 7], to primordial supermassive black holes as seen in spiral galaxies as described by (9); here the matter spiral is caused by matter in-falling towards the primordial black hole.

The spatial-inflow phenomenon in (9) is completely different from the putative "black holes" of General Relativity — the new "black holes" have an essentially $1/r$ force law, up to $\mathrm{O}(\alpha)$ corrections, rather than the usual Newtonain and

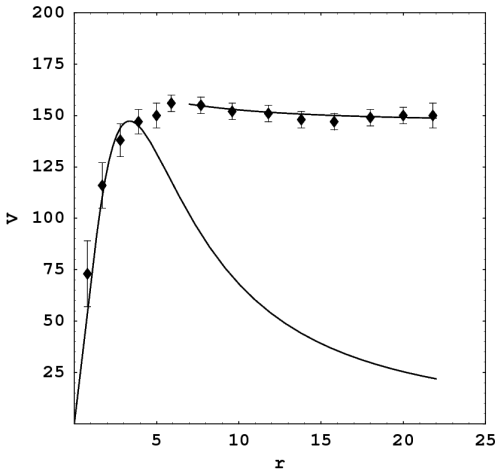

Fig. 1: Data shows the non-Keplerian rotation-speed curve v_O for the spiral galaxy NGC 3198 in km/s plotted against radius in kpc/h. Lower curve is the rotation curve from the Newtonian theory for an exponential disk, which decreases asymptotically like $1/\sqrt{r}$. The upper curve shows the asymptotic form from (11), with the decrease determined by the small value of α. This asymptotic form is caused by the primordial black holes at the centres of spiral galaxies, and which play a critical role in their formation. The spiral structure is caused by the rapid in-fall towards these primordial black holes.

Fig. 2: The "dark matter" density extracted by deconvolution of the gravitational lensing data for galaxy cluster CL 0024+17, see Jee M.J. *et al.* arXiv:0705.2171. Picture credit: NASA, ESA, M.J. Jee and H.C. Ford (John Hopkins University). The "dark matter" density has been superimposed on a HST image of the cluster. The axis of "symmetry" is perpendicular to the planer of this image. The gravitational lensing is caused by two galaxy clusters that have undergone collision. It is claimed herein that the lensing is associated with the 3-space interaction of these two "nearby" galaxy clusters, and not by the fact that they had collided, as claimed in [1]. The effect it is claimed, herein, is caused by the spatial in-flows into the black holes within the galaxies.

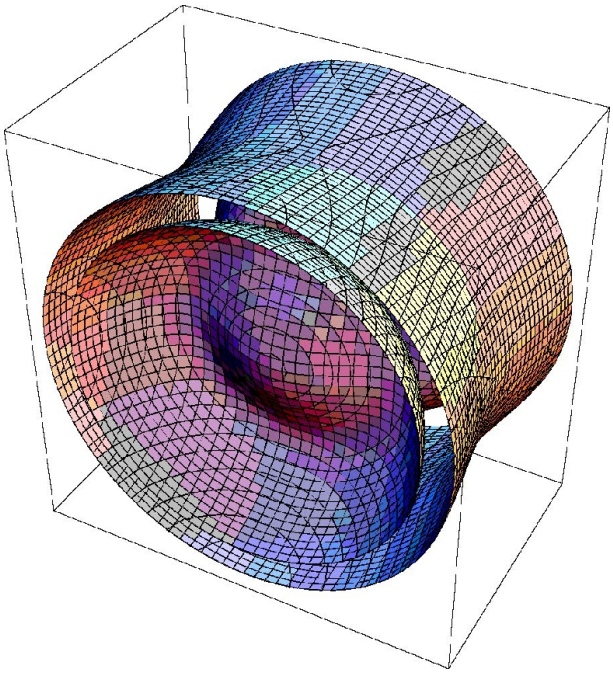

Fig. 3: Plot showing two constant value surfaces of $\Delta\rho_{DM}(\mathbf{r})$ from (19). We have modelled the system with two galaxies located on the axis of symmetry, but outside of the range of the plot. This plot shows the effects of the interfering spatial in-flows generating an effective "dark matter" density, as a spatial self-interaction effect. This "dark matter" density is that required to reproduce the gravitational acceleration if we used Newton's law of gravity. This phenomenon is caused by the α-dependent dynamics in (1), essentially a quantum-space effect. Viewed along the axis of symmetry this shell structure would appear as a ring-like structure, as seen in Fig. 2.

GR $1/r^2$ law. The centripetal acceleration relation for circular orbits $v_{\circ}(r) = \sqrt{rg(r)}$ gives a "universal rotation-speed curve"

$$v_{\circ}(r) = \frac{K}{2}\left(\frac{1}{r} + \frac{\alpha}{2R_s}\left(\frac{R_s}{r}\right)^{\frac{\alpha}{2}}\right)^{1/2}. \qquad (11)$$

Because of the α dependent part this rotation-velocity curve falls off extremely slowly with r, as is indeed observed for spiral galaxies. An example is shown in Fig. 1. It was the inability of the Newtonian and Einsteinian gravity theories to explain these observations that led to the notion of "dark matter".

For the spatial flow in (9) we may compute the effective dark matter density from (7)

$$\tilde{\rho}_{DM}(r) = \frac{(1-\alpha)\alpha}{16\pi G}\frac{K^2}{R_s^3}\left(\frac{R_s}{r}\right)^{2+\alpha/2}. \qquad (12)$$

It should be noted that the Newtonian component of (9) does not contribute, and that $\tilde{\rho}_{DM}(\mathbf{r})$ is exactly zero in the limit $\alpha \to 0$. So supermassive black holes and the spiral galaxy rotation anomaly are all α-dynamics phenomena.

2.2 Gravitational lensing

The spatial velocity field may be observed on the cosmological scale by means of the light bending and lensing effect. But first we must generalise the Maxwell equations so that the electric and magnetic fields are excitations of the dynamical 3-space, and not of the embedding space:

$$\nabla\times\mathbf{E} = -\mu\left(\frac{\partial\mathbf{H}}{\partial t} + \mathbf{v}\cdot\nabla\mathbf{H}\right), \quad \nabla\cdot\mathbf{E} = \mathbf{0}, \qquad (13)$$

$$\nabla\times\mathbf{H} = \epsilon\left(\frac{\partial\mathbf{E}}{\partial t} + \mathbf{v}\cdot\nabla\mathbf{E}\right), \quad \nabla\cdot\mathbf{H} = \mathbf{0}, \qquad (14)$$

which was first suggested by Hertz in 1890, but with $\mathbf{v}$ being a constant vector field. As easily determined the speed of EM radiation is $c = \frac{1}{\sqrt{\epsilon\mu}}$ wrt to the dynamical space, and not wt to the embedding space as in the original form of Maxwell's equations, and as light-speed anisotropy experiment have indicated [2]. The time-dependent and inhomogeneous velocity field causes the refraction of EM radiation. This can be computed by using the Fermat least-time approximation. Then the EM trajectory $\mathbf{r}(t)$ is determined by minimising the elapsed

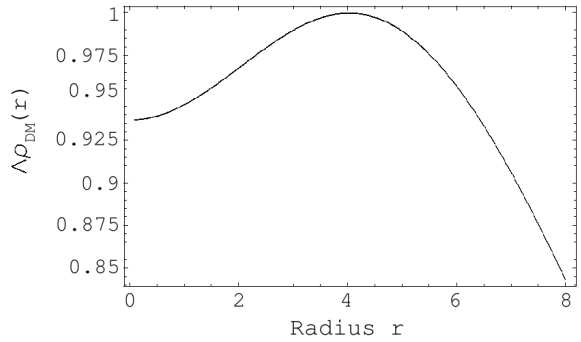

Fig. 4: Plot of $\Delta\rho_{DM}(\mathbf{r})$ from (19) in a radial direction from a midpoint on the axis joining the two galaxies.

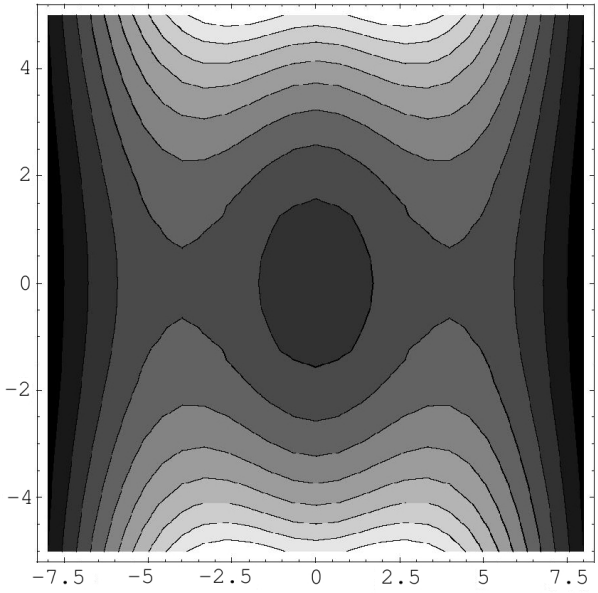

Fig. 5: Plot of $\Delta\rho_{DM}(\mathbf{r})$ from (19) in the plane containing the two galaxies. The two galaxies are located at +10 and -10, i.e above and below the vertical in this contour plot. This plot shows the effects of the interfering in-flows.

travel time:

$$\tau = \int_{s_i}^{s_f} \frac{ds\,\left|\frac{d\mathbf{r}}{ds}\right|}{\left|c\,\hat{\mathbf{v}}_R(s) + \mathbf{v}\big(\mathbf{r}(\mathbf{s}),\mathbf{t}(\mathbf{s})\big)\right|} \qquad (15)$$

$$\mathbf{v}_R = \left(\frac{d\mathbf{r}}{dt} - \mathbf{v}(\mathbf{r},\mathbf{t})\right) \qquad (16)$$

by varying both $\mathbf{r}(s)$ and $t(s)$, finally giving $\mathbf{r}(t)$. Here s is a path parameter, and $\mathbf{v}_R$ is a 3-space tangent vector for the path. As an example, the in-flow in (4), which is applicable to light bending by the sun, gives the angle of deflection

$$\delta = 2\,\frac{v^2}{c^2} = \frac{4GM(1+\frac{\alpha}{2}+\ldots)}{c^2 d} + \ldots \qquad (17)$$

where v is the in-flow speed at distance d and d is the impact parameter. This agrees with the GR result except for the α correction. Hence the observed deflection of 8.4×10^{-6} radians is actually a measure of the in-flow speed at the sun's surface, and that gives $v = 615$ km/s. These generalised Maxwell equations also predict gravitational lensing produced by the large in-flows from (9) associated with the new "black holes" in galaxies. So again this effect permits the direct observation of the these black hole effects with their non inverse-square-law accelerations.

3 Galaxy Cluster lensing

It is straightforward to analyse the gravitational lensing predicted by a galaxy cluster, with the data from CL 0024+17 of particular interest. However rather than compute the actual lensing images, we shall compute the "dark matter" effective density from (7), and compare that with the putative "dark matter" density extracted from the actual lensing data in [1]. To that end we need to solve (1) for two reasonably close galaxies, located at positions $\mathbf{R}$ and $-\mathbf{R}$. Here we look for a perturbative modification of the 3-space in-flows when the two galaxies are nearby. We take the velocity field in 1st approximation to be the superposition

$$\mathbf{v}(\mathbf{r}) \approx \mathbf{v}(\mathbf{r}-\mathbf{R}) + \mathbf{v}(\mathbf{r}+\mathbf{R})\,, \qquad (18)$$

where the RHS $\mathbf{v}$'s are from (9).

Substituting this in (1) will then generate an improved solution, keeping in mind that (1) is non-linear, and so this superposition cannot be exact. Indeed it is the non-linearity effect which it is claimed herein is responsible for the ring-like structure reported in [1]. Substituting (18) in (7) we may compute the change in the effective "dark matter" density caused by the two galaxies interfering with the in-flow into each separately, i.e.

$$\Delta\rho_{DM}(\mathbf{r}) = \rho_{DM}(\mathbf{r}) - \tilde{\rho}_{DM}(\mathbf{r}-\mathbf{R}) - \tilde{\rho}_{DM}(\mathbf{r}+\mathbf{R}) \qquad (19)$$

$\tilde{\rho}_{DM}(\mathbf{r}\pm\mathbf{R})$ are the the effective "dark matter" densities for one isolated galaxy in (12). Several graphical representations of $\Delta\rho_{DM}(\mathbf{r})$ are given in Figs. 3, 4 and 5. We seen that viewed along the line of the two galaxies the change in the effective "dark matter" density has the form of a ring, in particular one should compare the predicted effective "dark matter" density in Fig. 3 with that found by deconvoluting the gravitaitaional lensing data shown in shown Fig. 2.

4 Conclusions

We have shown that the dynamical 3-space theory gives a direct account of the observed gravitational lensing caused by two galaxy clusters, which had previously collided, but that the ring-like structure is not related to that collision, contrary to the claims in [1]. The distinctive lensing effect is caused by interference between the two spatial in-flows, resulting in EM refraction which appears to be caused by the presence

of a "matter" having the form of a ringed-shell structure, exactly comparable to the observed effect. This demonstrates yet another success of the new dynamical theory of 3-space, which like the bore hole, black hole and spiral galaxy rotation effects all reveal the dynamical consequences of the α-dependent term in (1). This amounts to a totally different understanding of the nature of space, and a completely different account of gravity. As shown in [3] gravity is a quantum effect where the quantum waves are refracted by the 3-space, and that analysis also gave a first derivation of the equivalence principle. We see again that "dark matter" and "dark energy" are spurious concepts required only because Newtonian gravity, and *ipso facto* GR, lacks fundamental processes of a dynamical 3-space — they are merely *ad hoc* fix-ups. We have shown elsewhere [7] that from (1) and the generalised Dirac equation we may show that a curved spacetime formalism may be introduced that permits the determination of the quantum matter geodesics, but that in general the spacetime metric does not satisfy the Hilbert-Einstein equations, as of course GR lacks the α-dependent dynamics. This induced spacetime has no ontological significance. At a deeper level the occurrence of α in (1) suggests that 3-space is actually a quantum system, and that (1) is merely a phenomenological description of that at the "classical" level. In which case the α-dependent dynamics amounts to the detection of quantum space and quantum gravity effects, although clearly not of the form suggested by the quantisation of GR.

Submitted on May 21, 2007
Accepted on June 25, 2007

References

1. Jee M. J. *et al.* Discovery of a ring-like dark matter structure in the core of the Galaxy Cluster CL 0024+17. arXiv: 0705.2171, to be published in *The Astrophysical Journal*.
2. Cahill R. T. Process physics: from information theory to quantum space and matter. Nova Science Pub., New York, 2005.
3. Cahill R. T. Dynamical fractal 3-space and the generalised Schrödinger equation: equivalence principle and vorticity effects. *Progress in Physics*, 2006, v.,1, 27–34.
4. Cahill R. T. Gravity, "dark matter" and the fine structure constant. *Apeiron*, 2005, v. 12 (2), 144–177.
5. Cahill R. T. "Dark matter" as a quantum foam in-flow effect. In *Trends in Dark Matter Research*, ed. J. Val Blain, Nova Science Pub., New York, 2005, 96-140.
6. Cahill R. T. Black holes in elliptical and spiral galaxies and in globular clusters. *Progress in Physics*, 2005, v. 3, 51–56.
7. Cahill R. T. Black holes and quantum theory: the fine structure constant connection. *Progress in Physics*, 2006, v. 4, 44–50.
8. Cahill R.,T. Dynamical 3-space: supernova and the Hubble expansion — the older universe without dark energy. *Progress in Physics*. 2007, v. 4, 9–12.
9. Newton I. Philosophiae Naturalis Principia Mathematica. 1687.

Quantum Spin Transport in Mesoscopic Interferometer

Walid A. Zein, Adel H. Phillips and Omar A. Omar

Faculty of Engineering, Ain Shams University, Cairo, Egypt
E-mail: adel_phillips@yahoo.com

Spin-dependent conductance of ballistic mesoscopic interferometer is investigated. The quantum interferometer is in the form of ring, in which a quantum dot is embedded in one arm. This quantum dot is connected to one lead via tunnel barrier. Both Aharonov-Casher and Aharonov-Bohm effects are studied. Our results confirm the interplay of spin-orbit coupling and quantum interference effects in such confined quantum systems. This investigation is valuable for spintronics application, for example, quantum information processing.

1 Introduction

The flexibility offered by semiconductor spintronics [1] is anticipated to lead to novel devices and may eventually become used for quantum information processing. Another advantage offered by spin systems in semiconductors is their long coherence times [2, 3]. In recent years, much attention has been devoted towards the interplay of the spin-orbit interaction and quantum interference effects in confined semiconductor heterostructures [4, 5, 6]. Such interplay can be exploited as a mean to control and manipulate the spin degree of freedom at mesoscopic scale useful for phase-coherent spintronics applications.

Since the original proposal of the spin field effect transistor (SFET) [7] by Datta and Das, many proposals have appeared based on intrinsic spin splitting properties of semiconductors associated with the Rashba spin-orbit interaction [8, 9, 10].

In the present paper, a quantum interference effect in coherent Aharonov-Casher ring is investigated. In such devices quantum effects are affecting transport properties.

2 The model

The mesoscopic device proposed in the present paper is in the form of quantum dot embedded in one arm of the Aharonov-Casher interferometer. This interferometer is connected to two conducting leads. The form of the confining potential in such spintronics device is modulated by an external gate electrode, allowing for direct control of the electron spin-orbit interaction. The main feature of the electron transport through such device is that the difference in the Aharonov-Casher phase of the electrons traveling clockwise and counterclockwise directions produces spin-sensitive interference effects [11, 12]. The quantum transport of the electrons occurs in the presence of Rashba spin-orbit coupling [13] and the influence of an external magnetic field. With the present proposed mesoscopic device, we can predict that the spin polarized current through such device is controlled via gate voltage.

The Hamiltonian, $\hat{H}$, describing the quantum transport through the present studied device could be written in the form as [14]

$$\hat{H} = \frac{P^2}{2m^*} + V(r) + \hat{H}_{soc}\,, \tag{1}$$

where $\hat{H}_{soc}$ is the Hamiltonian due to the spin-orbit coupling and is expressed as

$$\hat{H}_{soc} = \frac{\hbar^2}{2m^*a^2}\left(-i\,\frac{\partial}{\partial\varphi} + \frac{\omega_{soc}\,m^*a^2}{\hbar}\,\sigma_r\right), \tag{2}$$

where $\omega_{soc} = \frac{\alpha}{\hbar a}$ and it is called the frequency associated with the spin-orbit coupling, α is the strength of the spin-orbit coupling, a is the radius of the Aharonov-Casher ring and σ_r is the radial part of the Pauli matrices which expressed in the components of Pauli matrices σ_x, σ_y as

$$\begin{aligned}\sigma_r &= \sigma_x\cos\varphi + \sigma_y\sin\varphi\,,\\ \sigma_\varphi &= \sigma_y\cos\varphi - \sigma_x\sin\varphi\,.\end{aligned} \tag{3}$$

The parameter φ, Eq. (3) represents the phase difference of electrons passing through the upper and the lower arms of the ring. In Eq. (1), $V(r)$ is the effective potential for transmission of electrons through the quantum dot which depends, mainly, on the tunnel barrier between the quantum dot and the lead. Applying external magnetic field, B, normal to the plane of the device, then the Aharonov-Bohm phase picked up by an electron encircling this magnetic flux is given by

$$\Phi_{AB} = \frac{\pi\,e\,B\,a^2}{\hbar}\,. \tag{4}$$

Then the Hamiltonian, $\hat{H}_{soc}$, due to the spin-orbit coupling Eq. (2) will take the form

$$H'_{soc} = \frac{\hbar^2}{2m^*a^2}\left(-i\,\frac{\partial}{\partial\varphi} - \frac{\Phi_{AB}}{2\pi} - \frac{\omega_{soc}\,m^*a^2}{\hbar}\,\sigma_r\right). \tag{5}$$

Now in order to study the transport properties of the present quantum system, we have to solve Schrödinger equation and finding the eigenfunctions for this system as follows

$$\hat{H}\,\Psi = E\,\Psi\,. \tag{6}$$

The solution of Eq. (6) consists of four eigenfunctions [14], where $\Psi_L(x)$ is the eigenfunction for transmission through the left lead, $\Psi_R(x)$-for the right lead, $\Psi_{up}(\theta)$-for the upper arm of the ring and $\Psi_{low}(\theta)$-for the lower arm of the ring. Their forms will be as

$$\Psi_L(x) = \sum_{\sigma}\left[A\,e^{ikx} + B\,e^{-ikx}\right]\,\chi^{\sigma}(\pi)\,, \quad x\in[-\infty,0]\,, \tag{7a}$$

$$\Psi_R(x) = \sum_{\sigma}\left[C\,e^{ikx'} + D\,e^{-ikx'}\right]\,\chi^{\sigma}(0)\,, \quad x\in[0,\infty]\,, \tag{7b}$$

$$\Psi_{up}(\varphi) = \sum_{\sigma,\mu} F_{\mu}\,e^{in'^{\sigma}_{\mu}\varphi}\,\chi^{\sigma}(\varphi)\,, \quad \varphi\in[0,\pi]\,, \tag{7c}$$

$$\Psi_{low}(\varphi) = \sum_{\sigma,\mu} G_{\mu}\,e^{in^{\sigma}_{\mu}\varphi}\,\chi^{\sigma}(\varphi)\,, \quad \varphi\in[\pi,2\pi]\,. \tag{7d}$$

The mutually orthogonal spinors $\psi^{\sigma}_{n}(\varphi)$ are expressed in terms of the eigenvectors $\binom{1}{0}$, $\binom{0}{1}$ of the Pauli matrix σ_z as

$$\chi^{(1)}_{n}(\varphi) = \begin{pmatrix} \cos\frac{\theta}{2} \\ e^{i\varphi}\sin\frac{\theta}{2} \end{pmatrix}, \tag{7}$$

$$\chi^{(2)}_{n}(\varphi) = \begin{pmatrix} \sin\frac{\theta}{2} \\ -e^{i\varphi}\cos\frac{\theta}{2} \end{pmatrix}, \tag{8}$$

where the angle θ [15] is given by

$$\theta = 2\tan^{-1}\frac{\Omega - \sqrt{\Omega^2+\omega^2_{soc}}}{\omega_{soc}} \tag{9}$$

in which Ω is given by

$$\Omega = \frac{\hbar}{2\,m^*\,a^2}\,. \tag{10}$$

The parameters n'^{σ}_{μ} and n^{σ}_{μ} are expressed respectively as

$$n'^{\sigma}_{\mu} = \mu\,k'a - \varphi + \frac{\Phi_{AB}}{2\pi} + \frac{\Phi^{\sigma}_{AC}}{2\pi}\,, \tag{11}$$

$$n^{\sigma}_{\mu} = \mu\,k a - \varphi + \frac{\Phi_{AB}}{2\pi} + \frac{\Phi^{\sigma}_{AC}}{2\pi}\,, \tag{12}$$

where $\mu=\pm1$ corresponding to the spin up and spin down of transmitted electrons, Φ_{AB} is given by Eq. (4). The term Φ_{AC} represents the Aharonov-Casher phase and is given by

$$\Phi^{(\mu)}_{AC} = -\pi\left[1 + \frac{(-1)^{\mu}(\omega^2_{soc}+\Omega^2)^{1/2}}{\Omega}\right]. \tag{13}$$

The wave numbers k', k are given respectively by

$$k' = \sqrt{\frac{2m^*E}{\hbar^2}}\,, \tag{14}$$

$$k = \sqrt{\frac{2m^*}{\hbar^2}\left(V_d + e\,V_g + \frac{N^2e^2}{2C} + E_F - E\right)}\,, \tag{15}$$

where V_d is the barrier height, V_g is the gate voltage, N is the number of electrons entering the quantum dot, C is the total capacitance of the quantum dot, m^* is the effective mass of electrons with energy, E, and charge, e, and E_F is the Fermi energy.

The conductance, G, for the present investigated device will be calculated using landauer formula [16] as

$$G = \frac{2e^2\sin\varphi}{h}\sum_{\mu=1,2}\int dE\left(-\frac{\partial f_{FD}}{\partial E}\right)|\Gamma_{\mu}(E)|^2\,, \tag{16}$$

where f_{FD} is the Fermi-Dirac distribution is function and $|\Gamma_{\mu}(E)|^2$ is tunneling probability. This tunneling probability could be obtained by applying the Griffith boundary conditions [15, 17, 18], which states that the eigenfunctions (Eqs. 7a, 7b, 7c, 7d) are continuous and that the current density is conserved at each intersection. Then the expression for $\Gamma_{\mu}(E)$ is given by

$$\Gamma_{\mu}(E) = \frac{8i\,\cos\frac{\Phi_{AB}+\Phi^{(\mu)}_{AC}}{2}\,\sin(\pi ka)}{4\cos(2\pi k'a)+4\cos\left(\Phi_{AB}+\Phi^{(\mu)}_{AC}\right)+4i\sin(2\pi k'a)}\,. \tag{17}$$

3 Results and discussion

In order to investigate the quantum spin transport characteristics through the present device, we solve Eqs. (17, 18) numerically. We use the heterostructures as InGaAs/InAlAs.

We calculate the conductance, G, at different both magnetic field and the ω_{soc} which depends on the Rashba spin-orbit coupling strength. The main features of our obtained results are:

1. Figs. 1 and Fig. 2 show the dependence of the conductance on the magnetic field, B, for small and large values of B at different ω_{soc}.
2. Fig. 3 shows the dependence of the conductance on the parameter ω_{soc} at different values of B.

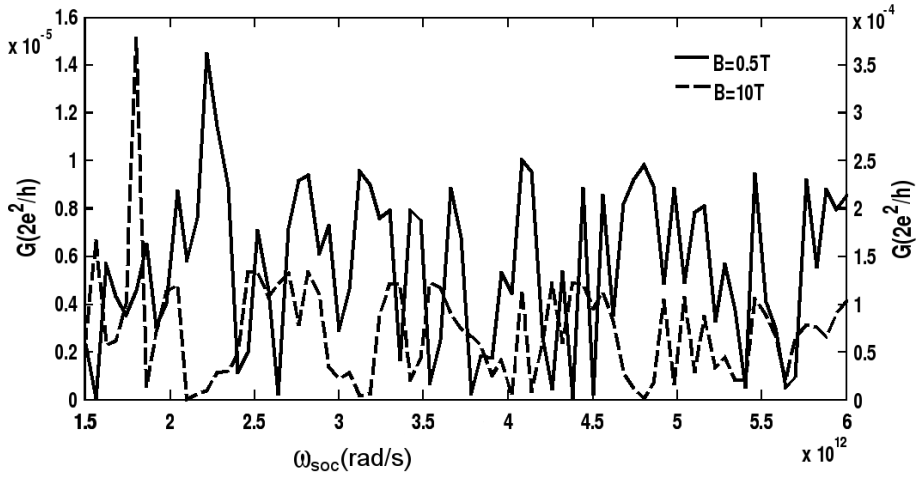

Fig. 3: The dependence of conductance on ω_{soc} at different values of B.

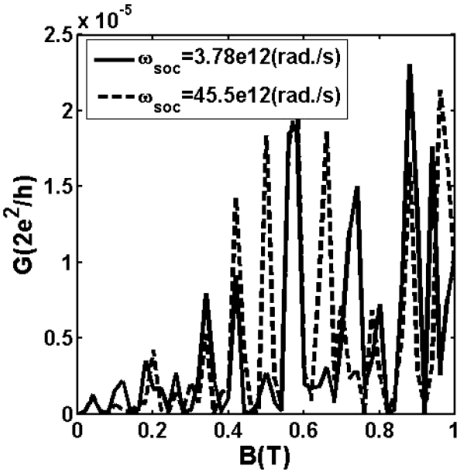

Fig. 1: The dependence of conductance on B at different ω_{soc} (small B).

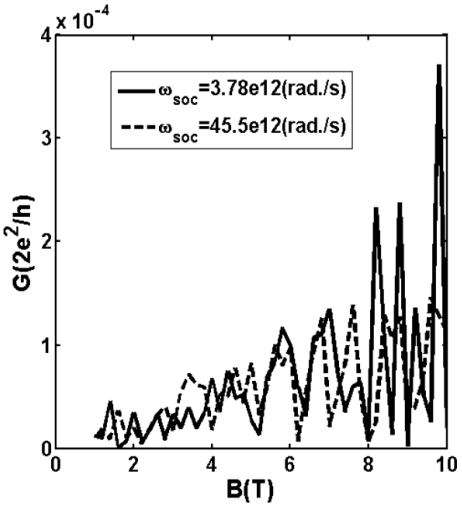

Fig. 2: The dependence of conductance on B at different ω_{soc} (large B).

From the figures we observe a quasi-periodic oscillations in the conductance (Fig. 1), and takes the form of satellite peaks. While for large values of B, the oscillations behave completely different from those in case of small values of B. The oscillatory behavior of $G(\omega_{soc})$ shows a wide peaks and in some ranges of ω_{soc}, there is a splitting in the peaks.

The obtained results could be explained as follows: The oscillatory behavior of the conductance with B and ω_{soc} could be due to spin-sensitive quantum-interference effects caused by the difference in the Aharonov-Casher phase accumulated by the opposite spin states. Also the quantum interference effects in the present device could be due to Aharonov-Bohm effect. Our results are found concordant with those in the literatures [4, 5, 15, 19].

4 Conclusions

In the present paper an expression for the conductance has been deduced for the investigated mesoscopic device. The spin transport in such coherent device is investigated taking into consideration both Aharonov-Casher and Aharonov-Bohm effects in the quantum dot connected to conducting lead via a tunnel barrier. The present results are valuable for employing such devices in phase coherent spintronics applications.

Submitted on August 15, 2007
Accepted on August 20, 2007

References

1. Zutic I., Fabian J. and Das Sarma S. *Review of Modern Physics*, 2004, v. 76, 323.
2. Perel V. I., Tarasenko S. A. and Yassievich I. N. *Phys. Rev. B*, 2003, v. 67, 201304(R).
3. Awadalla A. A., Aly A. H., Phillips A. H. *International Journal of Nanoscience*, 2007, v. 6(1), 41.

4. Nitta J., Meijer F. E., and Takayanagi H. *Appl. Phys. Lett.*, 1999, v. 75, 695.
5. Molnar B., Vasilopoulos P., and Peeters F. M. *Appl. Phys. Lett.*, 2004, v. 85, 612.
6. Rashba E. I. *Phys. Rev. B*, 2000, v. 62, R16267.
7. Datta S. and Das B. *Appl. Phys. Lett.*, 1990, v. 56, 665.
8. Meijer P. E., Morpurgo A. F. and Klapwijk T. M. *Phys. Rev. B*, 2002, v. 66, 033107.
9. Grundler D. *Phys. Rev. Lett.*, 2000, v. 84, 6074.
10. Kiselev A. A. and Kim K. W. *J. Appl. Phys.*, 2003, v. 94, 4001.
11. Aharonov Y. and Casher A. *Phys. Rev. Lett.*, 1984, v. 53, 319.
12. Yau J. B., De Pootere E. P., and Shayegan M. *Phys. Rev. Lett.*, 2003, v. 88, 146801.
13. Rashba E. I. *Sov. Phys. Solid State*, 1960, v. 2, 1109.
14. Hentschel M., Schomerus H., Frustaglia D. and Richter K. *Phys. Rev. B*, 2004, v. 69, 155326.
15. Molnar B., Peeters F. M. and Vasilopoulos P. *Phys. Rev. B*, 2004, v. 69, 155335.
16. Datta S. Electronic transport in mesoscopis systems. Cambridge Unversity Press, Cambridge, 1997.
17. Griffith S. *Trans. Faraday Soc.*, 1953, v. 49, 345.
18. Xia J. B. *Phys. Rev. B*, 1992, v. 45, 3593.
19. Citro R., Romeo F. and Marinaro M. *Phys. Rev. B*, 2006, v. 74, 115329.

Some Remarks on Ricci Flow and the Quantum Potential

Robert Carroll

University of Illinois, Urbana, IL 61801, USA

E-mail: rcarroll@math.uiuc.edu

We indicate some formulas connecting Ricci flow and Perelman entropy to Fisher information, differential entropy, and the quantum potential. There is a known relation involving the Schroedinger equation in a Weyl space where the Weyl-Ricci curvature is proportional to the quantum potential. The quantum potential in turn is related to Fisher information which is given via the Perelman entropy functional arising from a differential entropy under Ricci flow. These relations are written out and seem to suggest connections between quantum mechanics and Ricci flow.

1 Formulas involving Ricci flow

Certain aspects of Perelman's work on the Poincaré conjecture have applications in physics and we want to suggest a few formulas in this direction; a fuller exposition will appear in a book in preparation [8]. We go first to [13, 24–28, 33, 39] and simply write down a few formulas from [28, 39] here with minimal explanation. Thus one has Perelman's functional ($\dot{\mathcal{R}}$ is the Riemannian Ricci curvature)

$$\mathfrak{F} = \int_M (\dot{\mathcal{R}} + |\nabla f|^2)\exp(-f)dV \tag{1.1}$$

and a so-called Nash entropy $(\mathbf{1A})$ $N(u) = \int_M u\log(u)dV$ where $u = \exp(-f)$. One considers Ricci flows with $\delta g \sim \partial_t g = h$ and for $(\mathbf{1B})$ $\square^* u = -\partial_t u - \Delta u + \dot{\mathcal{R}}u = 0$ (or equivalently $\partial_t f + \Delta f - |\nabla f|^2 + \dot{\mathcal{R}} = 0$) it follows that $\int_M \exp(-f)dV = 1$ is preserved and $\partial_t N = \mathfrak{F}$. Note the Ricci flow equation is $\partial_t g = -2Ric$. Extremizing $\mathfrak{F}$ via $\delta\mathfrak{F} \sim$ $\sim \partial_t \mathfrak{F} = 0$ involves $Ric + Hess(f) = 0$ or $R_{ij} + \nabla_i\nabla_j f = 0$ and one knows also that

$$\begin{aligned} \partial_t N &= \int_M (|\nabla f|^2 + \dot{\mathcal{R}})\exp(-f)\,dV = \mathfrak{F}; \\ \partial_t \mathfrak{F} &= 2\int_M |Ric + Hess(f)|^2 \exp(-f)\,dV. \end{aligned} \tag{1.2}$$

2 The Schrödinger equation and WDW

Now referring to [3–5, 7–12, 15, 16, 18–23, 29–32, 35–38, 40] for details we note first the important observation in [39] that $\mathfrak{F}$ is in fact a Fisher information functional. Fisher information has come up repeatedly in studies of the Schrödinger equation (SE) and the Wheeler-deWitt equation (WDW) and is connected to a differential entropy correspondingto the Nash entropy above (cf. [4, 7, 18, 19]). The basic ideas involve (using 1-D for simplicity) a quantum potential Q such that $\int_M PQ\,dx \sim \mathfrak{F}$ arising from a wave function $\psi =$ $= R\exp(iS/\hbar)$ where $Q = -(\hbar^2/2m)(\Delta R/R)$ and $P \sim |\psi|^2$ is a probability density. In a WDW context for example one can develop a framework

$$\left.\begin{aligned} &Q = cP^{-1/2}\,\partial(GP^{1/2}); \\ &\int QP = c\int P^{1/2}\,\partial(GP^{1/2})\,\mathfrak{D}h\,dx \;\to \\ &\to -c\int \partial P^{1/2} G\,\partial P^{1/2}\,\mathfrak{D}h\,dx \end{aligned}\right\} \tag{2.1}$$

where G is an expression involving the deWitt metric $G_{ijk\ell}(h)$. In a more simple minded context consider a SE in 1-D $i\hbar\partial_t\psi = -(\hbar^2/2m)\partial_x^2\psi + V\psi$ where $\psi = R\exp(iS/\hbar)$ leads to the equations

$$\left.\begin{aligned} &S_t + \frac{1}{2m}S_x^2 + Q + V = 0; \\ &\partial_t R^2 + \frac{1}{m}(R^2 S_x)_x = 0 : \; Q = -\frac{\hbar^2}{2m}\frac{R_{xx}}{R}. \end{aligned}\right\} \tag{2.2}$$

In terms of the exact uncertainty principle of Hall and Reginatto (see [21, 23, 34] and cf. also [4, 6, 7, 31, 32]) the quantum Hamiltonian has a Fisher information term $c\int dx\,(\nabla P\cdot\nabla P/2mP)$ added to the classical Hamiltonian (where $P = R^2 \sim |\psi|^2$) and a simple calculation gives

$$\begin{aligned} \int PQ\,d^3x \sim -\frac{\hbar^2}{8m}\int \left[2\Delta P - \frac{1}{P}|\nabla P|^2\right] d^3x \;= \\ = \frac{\hbar^2}{8m}\int \frac{1}{P}|\nabla P|^2\,d^3x\,. \end{aligned} \tag{2.3}$$

In the situation of (2.1) the analogues to Section 1 involve ($\partial \sim \partial_x$)

$$\left.\begin{aligned} &P \sim e^{-f}; \qquad P' \sim P_x \sim -f'e^{-f}; \\ &Q \sim e^{f/2}\,\partial(G\,\partial e^{-f/2}); \;\; PQ \sim e^{-f/2}\,\partial(G\,\partial e^{-f/2}); \\ &\int PQ \to -\int \partial e^{-f/2}\,G\,\partial e^{-f/2} \sim -\int \partial P^{1/2} G\,\partial P^{1/2}. \end{aligned}\right\} \tag{2.4}$$

In the context of the SE in Weyl space developed in [1, 2, 4, 7, 10, 11, 12, 35, 36, 40] one has a situation $|\psi|^2 \sim R^2 \sim \sim P \sim \hat{\rho} = \rho/\sqrt{g}$ with a Weyl vector $\vec{\phi} = -\nabla \log(\hat{\rho})$ and a quantum potential

$$Q \sim -\frac{\hbar^2}{16m}\left[\dot{\mathcal{R}} + \frac{8}{\sqrt{\hat{\rho}}}\frac{1}{\sqrt{g}}\partial_i\left(\sqrt{g}\,g^{ik}\partial_k\sqrt{\hat{\rho}}\right)\right] = \\ = -\frac{\hbar^2}{16m}\left[\dot{\mathcal{R}} + \frac{8}{\sqrt{\hat{\rho}}}\Delta\sqrt{\hat{\rho}}\right] \tag{2.5}$$

(recall $\operatorname{div}\operatorname{grad}(U) = \Delta U = (1/\sqrt{g})\,\partial_m(\sqrt{g}\,g^{mn}\partial_n U)$. Here the Weyl-Ricci curvature is $(\mathbf{2A})$ $\mathcal{R} = \dot{\mathcal{R}} + \mathcal{R}_w$ where

$$\mathcal{R}_w = 2\,|\vec{\phi}|^2 - 4\nabla\cdot\vec{\phi} = 8\,\frac{\Delta\sqrt{\hat{\rho}}}{\sqrt{\hat{\rho}}} \tag{2.6}$$

and $Q = -(\hbar^2/16m)\mathcal{R}$. Note that

$$-\nabla\cdot\vec{\phi} \sim -\Delta\log(\hat{\rho}) \sim -\frac{\Delta\hat{\rho}}{\hat{\rho}} + \frac{|\nabla\hat{\rho}|^2}{\hat{\rho}^2} \tag{2.7}$$

and for $\exp(-f) = \hat{\rho} = u$

$$\int \hat{\rho}\,\nabla\cdot\vec{\phi}\,dV = \int\left[-\Delta\hat{\rho} + \frac{|\nabla\hat{\rho}|^2}{\hat{\rho}}\right]dV \tag{2.8}$$

with the first term in the last integral vanishing and the second providing Fisher information again. Comparing with Section 1 we have analogues $(\mathbf{2B})$ $G \sim (R + |\vec{\phi}|^2)$ with $\vec{\phi} = = -\nabla\log(\hat{\rho}) \sim \nabla f$ to go with (2.4). Clearly $\hat{\rho}$ is basically a probability concept with $\int\hat{\rho}\,dV = 1$ and Quantum Mechanics (QM) (or rather perhaps Bohmian mechanics) seems to enter the picture through the second equation in (2.2), namely $(\mathbf{2C})$ $\partial_t\hat{\rho} + (1/m)\operatorname{div}(\hat{\rho}\nabla S) = 0$ with $p = mv = \nabla S$, which must be reconciled with $(\mathbf{1B})$ (i.e. $(1/m)\operatorname{div}(u\nabla S) = = \Delta u - \dot{\mathcal{R}}u$). In any event the term $G = \dot{\mathcal{R}} + |\vec{\phi}|^2$ can be written as $(\mathbf{2D})$ $\dot{\mathcal{R}} + \mathcal{R}_w + (|\vec{\phi}|^2 - \mathcal{R}_w) = \alpha Q + (4\nabla\cdot\vec{\phi} - |\vec{\phi}|^2)$ which leads to $(\mathbf{2E})$ $\mathfrak{F} \sim \alpha\int_M QP\,dV + \beta\int|\vec{\phi}|^2 P dV$ putting Q directly into the picture and suggesting some sort of quantum mechanical connection.

REMARK 2.1. We mention also that Q appears in a fascinating geometrical role in the relativistic Bohmian format following [3, 15, 37, 38] (cf. also [4, 7] for survey material). Thus e.g. one can define a quantum mass field via

$$\mathfrak{M}^2 = m^2\exp(Q) \sim m^2(1+Q); \\ Q \sim \frac{-\hbar^2}{c^2m^2}\frac{\Box(\sqrt{\rho})}{\sqrt{\rho}} \sim \frac{\alpha}{6}\mathcal{R}_w \tag{2.9}$$

where ρ refers to an appropriate mass density and $\mathfrak{M}$ is in fact the Dirac field β in a Weyl-Dirac formulation of Bohmian quantum gravity. Further one can change the 4-D Lorentzian metric via a conformal factor $\Omega^2 = \mathfrak{M}^2/m^2$ in the form $\tilde{g}_{\mu\nu} = = \Omega^2 g_{\mu\nu}$ and this suggests possible interest in Ricci flows etc. in conformal Lorentzian spaces (cf. here also [14]). We refer to [3, 15] for another fascinating form of the quantum potential as a mass generating term and intrinsic self energy. ■

NOTE. Publication information for items below listed by archive numbers can often be found on the net listing. ■

Submitted on June 27, 2007
Accepted on June 29, 2007

References

1. Audretsch J. *Phys. Rev. D*, 1983, v. 27, 2872–2884.
2. Audretsch J., Gähler F. and Straumann N., *Comm. Math. Phys.*, 1984, v. 95, 41–51.
3. Bertoldi G., Faraggi A. and Matone M. *Class. Quant. Grav.*, 2000, v. 17, 3965; arXiv: hep-th/9909201.
4. Carroll R. Fluctuations, information, gravity, and the quantum potential. Springer, 2006.
5. Carroll R. arXiv: physics/0511076 and 0602036.
6. Carroll R. arXiv: gr-qc/0512146.
7. Carroll R. arXiv: math-ph/0701077.
8. Carroll R. On the quantum potential. (Book in preparation.)
9. Carroll R. *Teor. Mat. Fizika*, (to appear).
10. Carroll R. *Found. Phys.*, 2005, v. 35, 131–154.
11. Castro C. *Found. Phys.*, 1992, v. 22, 569–615; *Found. Phys. Lett.*, 1991, v. 4, 81.
12. Castro C. and Mahecha J. *Prog. Phys.*, 2006, v. 1, 38–45.
13. Chow B. and Knopf D. The Ricci flow: An introduction. *Amer. Math. Soc.*, 2004.
14. Crowell L. Quantum fluctuations of spacetime. World Scientific, 2005.
15. Faraggi A. and Matone M. *Inter. Jour. Mod. Phys. A*, 2000, v. 15, 1869–2017; arXiv: hep-th/9809127.
16. Frieden B. Physics from Fisher information. Cambridge Univ. Press, 1998.
17. Fujii Y. and Maeda K. The scalar tensor theory of gravitation. Cambridge Univ. Press, 2003.
18. Garbaczewski P. arXiv: cond-mat/0211362 and 0301044.
19. Garbaczdwski P. arXiv: quant-ph/0408192; *Jour. Stat. Phys.*, 2006, v. 123, 315–355.
20. Garbaczewski P. arXiv: cond-mat/0604538; quant-ph/0612151.
21. Hall M. arXiv: gr-qc/0408098.
22. Hall M., Kumar K. and Reginatto M. arXiv: quant-ph/0103041.
23. Hall M., Kumar K. and Reginatto M. *Jour. Phys. A*, 2003, v. 36, 9779–9794; arXiv: hep-th/0206235 and 0307259.
24. Jost J. Riemannian geometry and geometric analysis. Springer, 2002.
25. Kholodenko A. arXiv: gr-qc/0010064; hep-th/0701084.
26. Kholodenko A. and Ballard E. arXiv: gr-qc/0410029.
27. Kholodenko A. and Freed K. *Jour. Chem. Phys.*, 1984, v. 80, 900–924.

28. Müller R. Differential Harnack inequalities and the Ricci flow. Eur. Math. Soc. Pub. House, 2006.
29. Nikolić H. *Euro. Phys. Jour. C*, 2005, v. 421, 365–374; arXiv: hep-th/0407228; gr-qc/9909035 and 0111029; hep-th/0202204 and 0601027.
30. Nikolić H. arXiv: gr-qc/0312063; hep-th/0501046; quant-ph/0603207 and 0512065.
31. Parwani R. arXiv: quant-ph/0408185 and 0412192; hep-th/0401190.
32. Parwani R. arXiv: quant-ph/0506005 and 0508125.
33. Perelman G. arXiv: math.DG/0211159, 0303109, and 0307245.
34. Reginatto M. arXiv: quant-ph/9909065.
35. Santamato E. *Phys. Rev. D*, 1984, v. 29, 216–222.
36. Santamato E. *Phys. Rev. D*, 1985, v. 32, 2615–26221; *Jour. Math. Phys.*, 1984, v. 25, 2477–2480.
37. Shojai F. and Shojai A. arXiv: gr-qc/0306099.
38. Shojai F. and Shojai A. arXiv: gr-qc/0404102.
39. Topping P. Lectures on the Ricci flow. Cambridge Univ. Press, 2006.
40. Wheeler J. *Phys. Rev. D*, 1990, v. 41, 431–441; 1991, v. 44, 1769–1773.

The Little Heat Engine: Heat Transfer in Solids, Liquids and Gases

Pierre-Marie Robitaille

Dept. of Radiology, The Ohio State University, 130 Means Hall, 1654 Upham Drive, Columbus, Ohio 43210, USA
E-mail: robitaille.1@osu.edu

In this work, an introductory exposition of the laws of thermodynamics and radiative heat transfer is presented while exploring the concepts of the ideal solid, the lattice, and the vibrational, translational, and rotational degrees of freedom. Analysis of heat transfer in this manner helps scientists to recognize that the laws of thermal radiation are strictly applicable only to the ideal solid. On the Earth, such a solid is best represented by either graphite or soot. Indeed, certain forms of graphite can approach perfect absorption over a relatively large frequency range. Nonetheless, in dealing with heat, solids will eventually sublime or melt. Similarly, liquids will give way to the gas phase. That thermal conductivity eventually decreases in the solid signals an inability to further dissipate heat and the coming breakdown of Planck's law. Ultimately, this breakdown is reflected in the thermal emission of gases. Interestingly, total gaseous emissivity can decrease with increasing temperature. Consequently, neither solids, liquids, or gases can maintain the behavior predicted by the laws of thermal emission. Since the laws of thermal emission are, in fact, not universal, the extension of these principles to non-solids constitutes a serious overextension of the work of Kirchhoff, Wien, Stefan and Planck.

The question now is wherein the mistake consists and how it can be removed.

Max Planck, Philosophy of Physics, 1936.

While it is true that the field of thermodynamics can be complex [1–8] the basic ideas behind the study of heat (or energy) transfer remain simple. Let us begin this study with an ideal solid, S_1, in an empty universe. S_1 contains atoms arranged in a regular array called a "lattice" (see Figure 1). Bonding electrons may be present. The nuclei of each atom act as weights and the bonding electrons as springs in an oscillator model. Non-bonding electrons may also be present, however in an ideal solid these electrons are not involved in carrying current. By extension, S_1 contains no electronic conduction bands. The non-bonding electrons may be involved in Van der Waals (or contact) interactions between atoms. Given these restraints, it is clear that S_1 is a non-metal.

Ideal solids do not exist. However, graphite provides a close approximation of such an object. Graphite is a black, carbon-containing, solid material. Each carbon atom within graphite is bonded to 3 neighbors. Graphite is black because it very efficiently absorbs light which is incident upon its surface. In the 1800's, scientists studied objects made from graphite plates. Since the graphite plates were black, these objects became known as "blackbodies". By extension, we will therefore assume that S_1, being an ideal solid, is also a perfect blackbody. That is to say, S_1 can perfectly absorb any light incident on its surface.

Let us place our ideal solid, S_1, in an imaginary box. The walls of this box have the property of not permitting any heat to be transferred from inside the box to the outside world and vice versa. When an imaginary partition has the property of not permitting the transfer of heat, mass, and light, we say that the partition is adiabatic. Since, S_1 is alone inside the adiabatic box, no light can strike its surface (sources of light do not exist). Let us assume that S_1 is in the lowest possible energy state. This is the rest energy, E_{rest}. For our ideal solid, the rest energy is the sum of the relativistic energy, E_{rel}, and the energy contained in the bonds of the solid, E_{bond}. The relativistic energy is given by Einstein's equation, $E = mc^2$. Other than relativistic and bonding energy, S_1 contains no other energy (or heat). Simplistically speaking, it is near 0 Kelvin, or absolute zero.

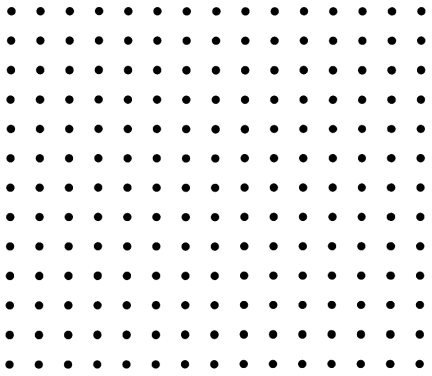

Fig. 1: Schematic representation of the ideal solid, S_1. The atoms are arranged in a regular array, or "lattice".

That absolute zero exists is expressed in the form of the 3rd law of thermodynamics, the last major law of heat transfer to be formulated. This law is the most appropriate starting point for our discussion. Thus, an ideal solid contain-

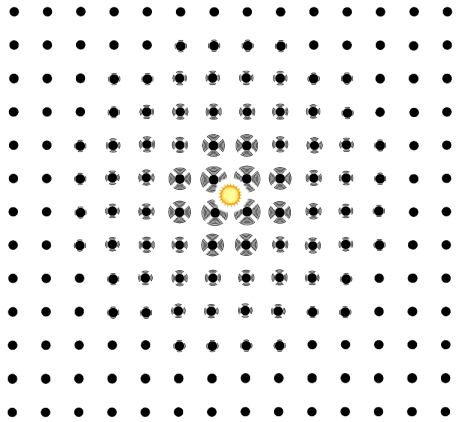

Fig. 2: Depiction of the Little Heat Engine at the center of the lattice. The atoms near this heat source move about their absolute location, such that they experience no net displacement over time. The vibrational degrees of freedom are slowly being filled.

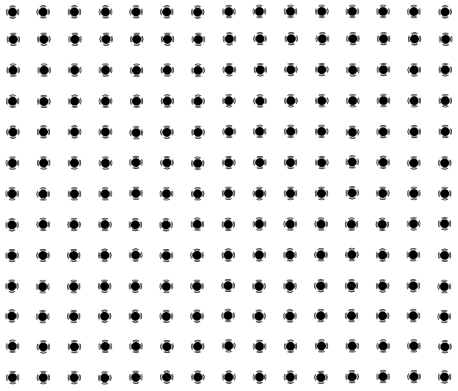

Fig. 3: The Little Heat Engine is turned off and the heat introduced into the lattice begins to equilibrate throughout the solid.

ing no heat energy is close to absolute zero as defined by the 3rd law of thermodynamics. In such a setting, the atoms that make up the solid are perfectly still. Our universe has a total energy (E_{total}) equal to the rest mass of the solid: $E_{total} = E_{solid} = E_{rest} = E_{rel} + E_{bond}$.

Now, let us imagine that there is a hypothetical little heat engine inside S_1. We chose an engine rather than a source to reflect the fact that work is being done as we ponder this problem. However, to be strictly correct, a source of heat could have been invoked. For now, we assume that our little heat engine is producing hypothetical work and it is also operating at a single temperature. It is therefore said to be isothermal. As it works, the little heat engine releases heat into its environment.

It is thus possible to turn on this hypothetical little heat engine and to start releasing heat inside our solid. However, where will this heat go? We must introduce some kind of "receptacle" to accept the heat. This receptacle will be referred to as a "degree of freedom". The first degrees of freedom that we shall introduce are found in the vibration of the atoms about their absolute location, such that there is no net displacement of the atoms over time. The heat produced by our little heat engine will therefore begin to fill the vibrational degrees of freedom and the atoms in its vicinity will start vibrating. When this happens, the bonds of the solid begin to act as little springs. Let us turn on the heat engine for just a little while and then turn it off again. Now we have introduced a certain quantity of heat (or energy) inside the solid. This heat is in the immediate vicinity of the little heat engine (see Figure 2). As a result, the atoms closest to the heat engine begin to vibrate reflecting the fact that they have been heated. The total amount of energy contained in the vibrational degrees of freedom will be equal to E_{vib}.

Since the little heat engine has been turned off, the heat produced will now start to equilibrate within the solid (see Figure 3). Thus, the area nearest the little heat engine becomes colder (the atoms nearest the heat engine slow down their vibration) and the areas away from our little engine heat up (they increase their vibration). As this happens, S_1 is moving towards thermal equilibrium. That is, it is becoming isothermal — moving to a single uniform temperature. In this state, all the atoms in S_1 share equally in the energy stored in the vibrational degrees of freedom. The driving force for reaching this thermal equilibrium is contained in the 2nd law of thermodynamics. This law states that heat must always move from hotter to colder regions in an irreversible manner.

That heat flows in an irreversible manner is the central theme of the 2nd law of thermodynamics. Indeed, no matter what mechanism will be invoked to transfer heat in nature, it will always be true that the macroscopic transfer of heat occurs in an irreversible manner.

So far, S_1 is seeking to reach a uniform temperature or thermal equilibrium. For our ideal solid, thermal equilibrium can only be achieved through thermal conduction which in turn is supported by energy contained in the vibrational degrees of freedom. Thermal conduction is the process whereby heat energy is transferred within an object without the absolute displacement of atoms or molecules. If the little heat engine was kept on, then thermal conduction would constantly be trying to bring our solid to thermal equilibrium. If there were no processes other than thermal conduction, and the engine was turned off, eventually one would think that the entire solid would come to a single new temperature and thermal equilibrium would be achieved. At this stage, our universe would have a total energy equal to that contained in the rest energy ($E_{rel} + E_{bond}$) and in the vibrational degrees of freedom ($E_{total} = E_{solid} = E_{rest} + E_{vib}$).

However, even though our little heat engine has been turned off, thermal equilibrium cannot be reached in this scenario. This is because there is another means of dissipating heat available to the solid. Thus, as the solid is heated, it dissipates some of the energy contained in its vibrational degrees of freedom into our universe in an effort to cool down. This is accomplished by converting some of the energy contained

in the vibrational degrees of freedom into light!

The light that objects emit in an attempt to cool down is called thermal radiation. The word thermal comes in because we are dealing with heat. The word radiation comes from the fact that it is light (or radiation) which is being emitted.

This light is emitted at many different frequencies (see Figure 4). We represent the total amount of energy in this emission as E_{em}. Emission of light provides another means of dealing with heat. Thus, the emission of light joins vibration in providing for our stationary non-metallic solid the only degrees of freedom to which it can ever have access. However, the energy of emission becomes a characteristic of our universe and not of the solid. Thus, the universe now has a total energy given by $E_{total} = E_{solid} + E_{em}$. As for the solid, it still has an energy equal only to that stored as rest energy and that contained in the vibrational degrees of freedom, $E_{solid} = E_{rest} + E_{vib}$. However, note that since all the heat energy of the solid was initially contained in its vibrational degrees of freedom, the energy of emission (E_{em}) must be related to the energy contained in E_{vib} at the time of emission.

As stated above, light has the property that it cannot cross an adiabatic partition. Consequently, the light produced by heating the solid becomes trapped in our virtual box. If we kept our adiabatic walls close to the solid, eventually thermal equilibrium would be achieved between the solid and the radiation. In this scenario, the solid would be constantly emitting and absorbing radiation. Under a steady state regimen, all of the atoms in the solid would be sharing equally in the energy contained in the vibrational degrees of freedom. However, let us make the box large for now, so that it will take the light many years to reach the walls of the box and be reflected back towards the solid. For all purposes then, the light that the solid emits cannot return and hit the surface of the solid.

Up to this point, by turning on our little heat engine, we have been able to discuss two important processes. The first is thermal conduction. Thermal conduction is that process which tries to bring the internal structure of the solid to thermal equilibrium. In our ideal solid, the vibrations of the atoms are the underlying support for this process. The second process is thermal radiation (also called radiative emission). Through radiative emission, the solid is trying to come to thermal equilibrium with the outside world. There are only two means for an ideal solid to deal with heat. It can strive to achieve internal thermal equilibrium through thermal conduction supported by the vibrations of its atoms and it can dissipate some of the energy contained in its vibrational degrees of freedom to the outside world through thermal radiation.

For an ideal solid, the light emitted in an attempt to reach or maintain thermal equilibrium will contain a continuous range of frequencies (see Figure 4). The intensity of the light at any given frequency will be given by the well known

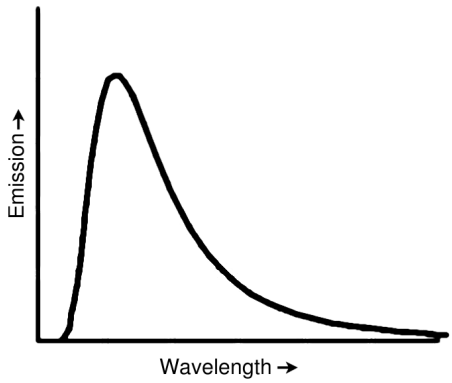

Fig. 4: The light that objects emit in an attempt to cool down is called thermal radiation. Emission of light provides another means of dealing with heat. The emission is continuous over all frequencies for our ideal solid, S_1.

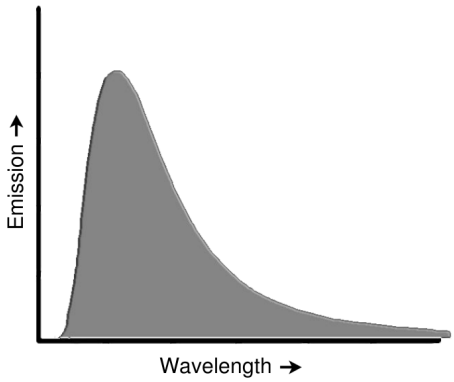

Fig. 5: For the ideal solid, S_1, the total emission (area under the curve) is proportional to the fourth power of the temperature as dictated by Stefan's law of thermal emission.

Planckian relation [9]

$$B_\nu(T) = \frac{\varepsilon_\nu}{\kappa_\nu} = \frac{2h\nu^3}{c^2}\frac{1}{e^{h\nu/kT}-1}\,.$$

Planck's equation states that the light produced, at a frequency ν, by a blackbody (or an ideal solid), B_ν, depends only on two variables: temperature, T, and the frequency, ν. All the other terms in this equation are constants (h = Planck's constant, k = Boltzman's constant, c = speed of light). This equation tells us that the nature of light produced is dependent only on the temperature of the solid and on the frequency of interest. The fact that the light emitted by an ideal solid was dependent only on temperature and frequency was first highlighted by Gustav Robert Kirchhoff in the mid-1800's. Kirchhoff's formulation became know as Kirchhoff's Law of Thermal Radiation [10, 11]

$$B_\nu(T) = \frac{\varepsilon_\nu}{\kappa_\nu}\,.$$

In this equation, ε_ν represents the ability of the blackbody to emit light (emissivity) and κ_ν represents its ability

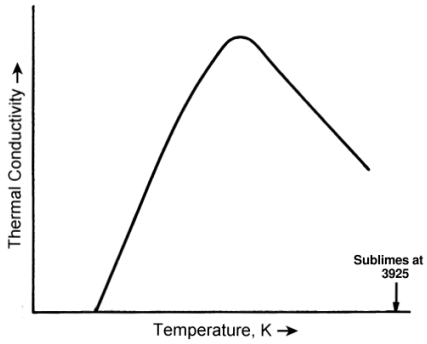

Fig. 6: Thermal conductivity for pyrolytic graphite (parallel to the layer planes) increases to a maximum and then begins to decrease. Eventually, graphite sublimes at 3925 K. Adapted from reference 15, volume 2, *Thermal Conductivity of Nonmetallic Solids*, 1970.

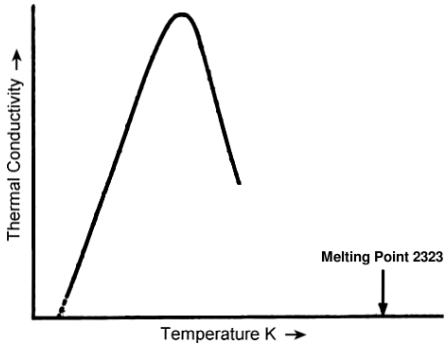

Fig. 7: Thermal conductivity for sapphire (Al_2O_3) increases to a maximum and then decreases. Eventually, sapphire melts at 2323 K. Adapted from reference 15, volume 2, *Thermal Conductivity of Nonmetallic Solids*, 1970.

to absorb light (opacity) at a given frequency. As mentioned above, an ideal solid is a blackbody, or a perfect absorber of light ($\kappa_\nu = 1$). As such, this equation states that the manner in which a blackbody emits or absorbs light at a given frequency depends exclusively on its temperature. The function, f, contained in Kirchhoff's Law $B_\nu = \frac{\varepsilon_\nu}{\kappa_\nu} = f(T, \nu)$ was elucidated by Max Planck as shown in the first equation above. It is for this reason that Kirchhoff's equation constitutes the left hand portion of Planck's equation [9]. As a result, any work by Kirchhoff on this topic is critical to our understanding of Planck's work [9, 10, 11].

It has also been observed that the amount of light that our ideal solid will produce, or the total emission (see the area under the curve in Figure 5), is proportional to the fourth power of the solid's temperature. This is known as Stefan's law of emission ($\varepsilon = \sigma T^4$), where ε represents total emission and Stefan's constant, σ , is equal to 5.67051×10^{-8} Watts/(m^2K^4) [12]. Note that Stefan's law of emission reveals a pronounced increase in the production of light, with temperature. Thus, as the temperature of the solid increases, thermal radiation can greatly increase to accommodate the increased requirement for heat dissipation. If the solid is at room temperature, this light will be emitted at infrared frequencies, that is, just below the portion of the electromagnetic spectrum that is visible to the human eye. Indeed, this emitted light at room temperatures can be viewed with a thermal or infrared camera of the type used by the military to see at night.

Interestingly for S_1, the frequency of light at which the maximal emission occurs (ν_{max}) is directly related to the temperature $\nu_{max}/c = T$). This is known as Wien's law of displacement [13].

Let us turn on our little heat engine once again. As the little heat engine releases more heat into solid, it becomes apparent that thermal conductivity increases only approximately linearly with temperature. In fact, as temperature is increased for many real solids, thermal conductivity actually may initially increase to a maximum and then suddenly begin to decrease (see Figure 6 for graphite and Figure 7 for sapphire or Al_2O_3) [14]. Since the vibrational degrees of freedom are central to both thermal conduction and emission, one can only gather that the vibrational degrees of freedom simply become incapable of dealing with more heat (see Figure 8). Herein lies a problem for maintaining the solid phase. As temperature is increased, there is a greater difficulty of dealing with the internal flow of heat within the solid. The solid must begin to search for a new degree of freedom.

The next available means of dealing with heat lies in breaking bonds that link up the atoms forming the ideal solid. As these bonds begin to break, the atoms (or the molecules) gain the ability to change their average location. New degrees of freedom are born, namely, the translational and rotational degrees of freedom. Interestingly, these new degrees of freedom are associated with both the flow of heat and mass.

With the arrival of the translational and rotational degrees of freedom, S_1 is transformed into one of two possibilities. It can either melt — giving rise to the liquid phase, L_1; or, it can sublime — giving rise directly to the gas phase, G_1. Graphite, perhaps the closest material to an ideal solid, sublimes (see Figure 6) and never melts. Whereas sapphire or Al_2O_3 melts (see Figure 7). In any case, as a solid is being converted to a liquid or a gas, the absolute amount of rest energy is changing, because bonds are being broken ($E_{bond} \to 0$).

Since many solids melt giving rise to L_1, let us turn our attention first to this situation. We assume that unlike graphite, our ideal solid can in fact melt. Thus, as more heat is pumped into S_1, the temperature will no longer rise. Rather, the solid S_1 will simply slowly be converted to the liquid L_1. The melting point has been reached (see Figure 9 and Figure 10) and the liquid created (see Figure 11).

Since L_1 has just been created, let us turn off our little heat engine once again. The liquid L_1 at this stage, much like S_1 of old, is still capable of sustaining thermal conduction as an internal means of trying to reach thermal equilibrium through the vibrational degrees of freedom. However, the absolute level of thermal conduction is often more than 100 times lower than in the solid [8, 15]. The liquid L_1 also

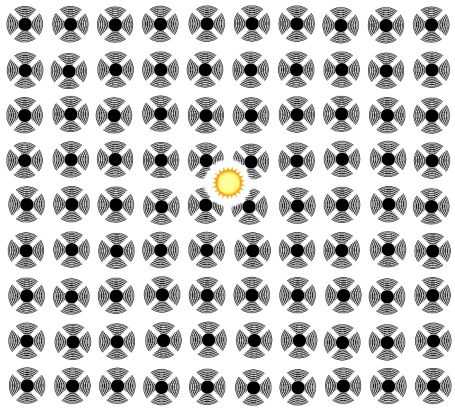

Fig. 8: The Little Heat Engine has introduced so much heat into the lattice that the vibrational degrees of freedom become full. The solid must search for a new way to deal with the continued influx of heat.

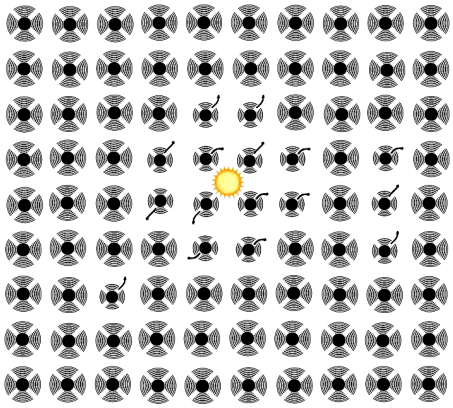

Fig. 9: As The Little Heat Engine continues to heat the lattice, the melting point is eventually reached. The solid, S_1, begins to melt as the translational and rotational degrees of freedom start to be filled.

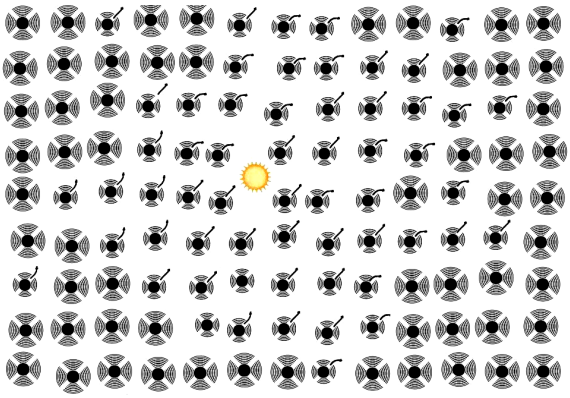

Fig. 10: As The Little Heat Engine continues to heat the lattice, melting continues. The regular array of the solid lattice is being replaced by the fleeting lattice of the liquid.

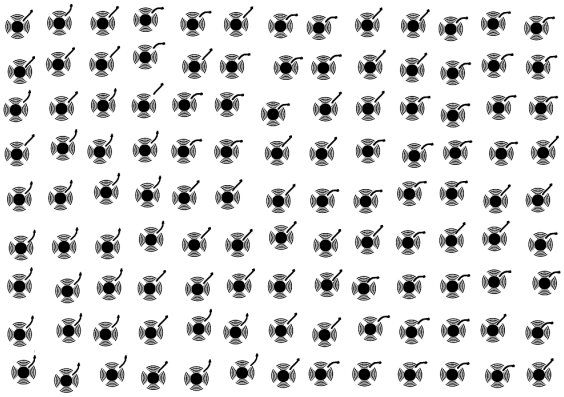

Fig. 11: The Little Heat Engine is turned off and melting of S_1 into L_1 is completed. The regular solid lattice is now completely replaced with the fleeting lattice of the liquid. The individual atoms now experience absolute displacement in position over time.

has access to thermal radiation as a means of dissipating heat to the outside world.

However, within L_1, a new reality has taken hold. The requirements placed on conduction and radiative emission for heat dissipation have now been relaxed for the liquid and, mass transfer becomes a key means of dissipating heat within such an object. Indeed, internal convection, the physical displacement (or flow) of atoms or molecules, can now assist thermal conduction in the process of trying to reach internal thermal equilibrium. Convection is a direct result of the arrival of the translational degrees of freedom. The driving force for this process once again is the 2nd law of thermodynamics and the physical phenomenon involved is expressed in kinetic energy of motion. Thus, through internal convection, currents are set up within the liquid, whose sole purpose is an attempt at thermal equilibrium. As convection currents form, the bonds that make up the liquid are constantly in the process of breaking and reforming. Like thermal conduction, the process of internal convection changes approximately linearly with temperature. For its part, L_1 now has three means of dealing with heat transfer: conduction, convection (internal), and thermal radiation (external). The total energy of the universe is now expressed as $E_{total} = E_{liquid} + E_{emission}$. The energy within the liquid is divided between the rest energy and the energy flowing through the vibrational, translational, and rotational degrees of freedom, $E_{liquid} = E_{rest} + E_{vib} + + E_{trans} + E_{rot}$. Thermal conduction and radiative emission remain tied to the energy associated with the vibrational degrees of freedom, while convection becomes associated with the energy within the translational and rotational degrees of freedom. The added heat energy contained within the liquid is now partitioned amongst three separate degrees of freedom: $E_{vib} + E_{trans} + E_{rot}$.

At this stage, the little heat engine can be turned on again. Very little is known regarding thermal emission from liquids. However, it appears that when confronted with increased inflow of heat, the liquid responds in a very different way. Indeed, this is seen in its thermal emission. Thus, while thermal emission in the solid increased with the fourth power of the temperature, thermal emissivity in a liquid increases little, if

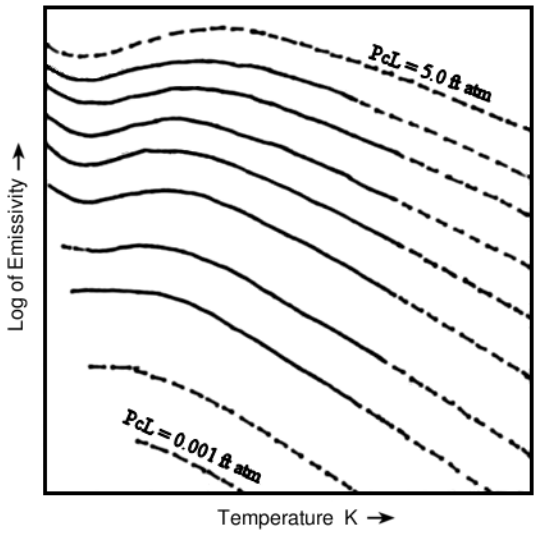

Fig. 12: The total emissivity for CO_2 at 1 atmosphere for various pressure path lengths. Note that emissivity can actually drop significantly with increasing temperature. Gases are unable to follow Stefan's Law. Adapted from reference 17.

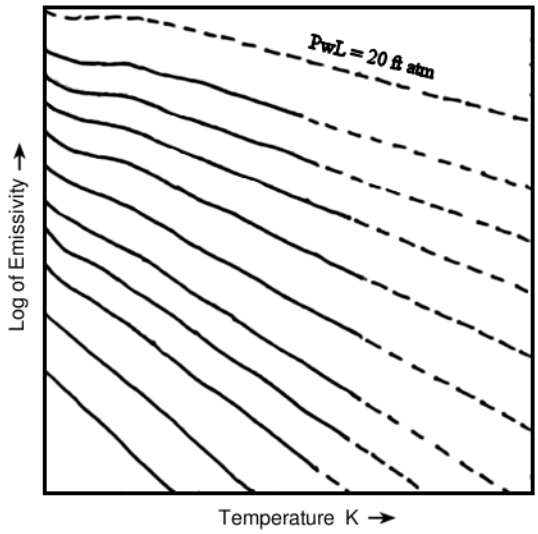

Fig. 13: The total emissivity of water vapor for various pressure path lengths. Note that the total emissivity can actually drop significantly with increasing temperature. Gases are unable to follow Stefan's Law. Adapted from reference 17.

at all, with temperature [8, 15]. Indeed, total thermal emission may actually decrease. Stefan's law does not hold in a liquid. That is because new degrees of freedom, namely the translational and rotational degrees of freedom (and its associated convection), have now been introduced into the problem. Since the vibrational degrees of freedom are no longer exclusively in control of the situation, Stefan's law fails.

It has already been noted that thermal conduction is eventually unable to deal with increased heat in the solid. In liquids, it is often observed that thermal conductivity changes only slightly with temperature and often decreases [8, 14, 15]. At the same time, it is clear that thermal radiation does not increase with temperature in the liquid. One can only surmise that convection rapidly becomes a dominant means of dealing with heat transfer in the liquid phase. This can be seen by examining the viscosity of the liquid. Thus, the viscosity of liquids decreases with temperature and the liquid flows better at higher temperature [14]. This is a direct reflection that an increasing percentage of bonds within the liquid are being broken in order to accommodate the increased flow of heat, or energy, into the translational degrees of freedom.

Let us now return to our little heat engine. Since the little heat engine has been left on, as it continues to heat L_1, a point will be reached where internal conduction and convection along with thermal radiation can no longer accommodate the increase in heat. At that point, a new process must arise to carry heat away. Thus, with an internal structure weakened by broken bonds, individual atoms or molecules are now free to carry mass and heat directly away from the liquid in the form of kinetic energy of motion. The liquid L_1 enters the gas phase becoming G_1. This is exactly analogous to what occurred previously for the solid with sublimation. The liquid L_1 has now reached the boiling point. While it boils, its temperature will no longer increase. Rather, it is simply being slowly converted from the liquid L_1 to the gas G_1. According to the kinetic theory of gases, the molecules of the gas are traveling at a particular average velocity related to the temperature of the gas at a given pressure. It is our adiabatic partitions that have ensured that we can speak of pressure. The fact that the gas molecules are moving is a reflection of the convection within the gas which, in turn, is an expression of the translational degrees of freedom. Let us turn off our little heat engine for a moment in order to analyze what has just transpired.

In the gas G_1, individual molecules are not attached to each other but are free to move about. This is once again a reflection of the translational degrees of freedom. G_1 can have either a molecular nature (it is made up of individual molecules) or an atomic nature (it is made up of individual atoms). For now, let us make the assumption that S_1 was selected such that a diatomic molecular gas, G_1, is produced. Let us also assume that our diatomic molecular gas will be made up of two different types of atoms. Note that we are deviating slightly from the requirements of an ideal solid in order to deal with molecular gases. Once in the gas phase, the molecular gas can also invoke rotational degrees of freedom. Therefore, the molecular gas G_1 has energy partitioned amongst its available degrees of freedom, $E_{gas} = E_{rest} + E_{vib} + E_{trans} + E_{rot}$. Note that in the molecular gas the E_{rest} term decreases, reflecting the breakdown of S_1 and L_1 into the gas G_1 (less energy is now contained in E_{bond}). From above, we now see that the total energy in the universe is $E_{total} = E_{gas} + E_{em} = E_{rest} + E_{vib} + E_{trans} + + E_{rot} + E_{em}$. The molecular gas will still be able to emit ra-

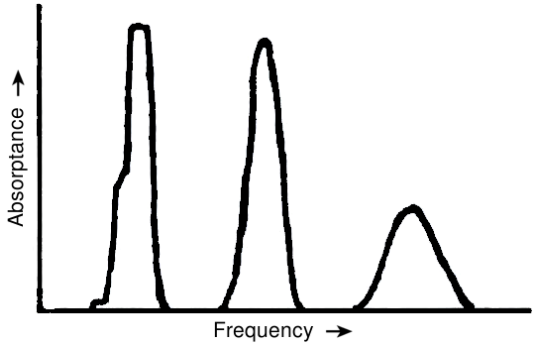

Fig. 14: Schematic representation of the absorptance for CO_2 at 830 K and 10 atmospheres for a path length of 0.388 meters. The gas absorbs in discrete bands and not in a continuous fashion as previously observed for a solid. Adapted from reference 8.

diation, typically in the microwave or infrared region of the electromagnetic spectrum.

It is now time to turn our little heat engine on again. As more heat is generated, the gas will increase the average kinetic energy of motion of its constituent molecules. Nonetheless, thermal conduction within G_1 is now at least 10 times lower than was the case for the liquid [15]. Most importantly the total radiative emissivity for the molecular gas at constant pressure actually begins to drop dramatically with increased temperature [7, 16]. We can speak of constant pressure when we do not permit the adiabatic walls of our imaginary box to move. If we now move in our adiabatic walls we increase the pressure on the gas and the emissivity will increase, corresponding to a higher apparent temperature.

Nonetheless, it should be noted that the total emissivity for a gas at constant pressure can actually drop significantly with increasing temperature (see Figure 12 and Figure 13). Consequently, we can see that Stefan's law does not hold for gases [7]. In fact, thermal emission for the diatomic gas (like CO and NO) occurs in discrete bands of the electromagnetic spectrum and in a manner not simply related to temperature (see Figure 14, Figure 15 and Figure 16) [8, 16]. The situation becomes even more interesting if the gas is not molecular, but rather monatomic in nature (like Ar or He for instance). In that case, when moving from the liquid to the gas phase, G_1 looses both its rotational, and more importantly, its vibrational, degrees of freedom, $E_{bond} = E_{vib} = E_{rot} = 0$. Neglecting electronic emission, which typically occurs in the ultra violet or visible range, a monatomic gas cannot emit significant radiation in the microwave and infrared regions. Indeed, for such a gas, Stefan's law no longer has any real meaning.

It is now clear that relative to S_1 (and even L_1), the molecular gas G_1 is unable to dissipate its heat effectively to the outside world in response to increased temperature. Indeed, since thermal emission can drop dramatically with temperature for molecular gases, as temperature is increased, a greater fraction of the heat energy must be dealt with by the translational and rotational degrees of freedom. If the gas is made up of molecules as is the case for G_1, then as more heat is pumped into the gas by our little engine, the gas molecules will eventually break apart into their constituent atoms. The gas then adopts the nature of monatomic gases as mentioned above with $E_{bond} = E_{vib} = E_{rot} = 0$. As more heat is pumped into the system, electronic transitions within each atom becomes more and more important. If the little heat engine is not stopped, much like what happened in the case of the solid and the liquid, the atomic gas will no longer be able to deal with the increased heat. Eventually, the electrons gain enough energy to start emitting radiation in the visible or ultra-violet range. As the little heat engine continues to generate heat, the electrons will gain enough energy to become free of the nucleus and a final new state is born — the plasma. The discussion of heat flow in plasmas is beyond our scope at this stage. Suffice it to say that if the little heat engine continues to operate, still another process would occur, namely nuclear reactions.

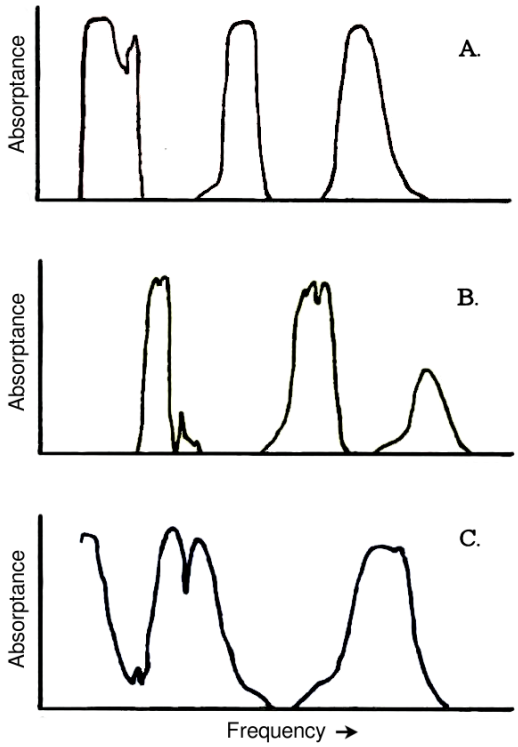

Fig. 15: Schematic representation of the absorptance for carbon dioxide (A: CO_2 partial pressure path product = 3.9 atm m, temperature = 1389 K, total pressure = 10 atm, partial pressure = 10 atm), water (B: H_2O partial pressure path product = 3.9 atm m, temperature = 1389 K, total pressure = 10 atm, partial pressure = 10 atm), and methane (C: CH_4 partial pressure path product = 3.9 atm m, temperature = 1389 K, total pressure = 10 atm, partial pressure = 10 atm). Note that for gases absorbance is not continuous and occurs in discrete bands. Adapted from reference 8.

It is now time to finally turn off our little heat engine. We have learned a lot with this little device and so it is somewhat

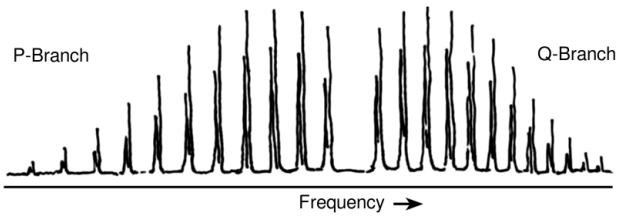

Fig. 16: Vibrational-rotational spectrum of hydrochloric acid at room temperature. The spectrum reveals the presence of the two isotropic form, $H^{35}Cl$ and $H^{37}Cl$. Adapted from reference 18.

sad to state that it can live only in our imagination. This is because our little heat engine violates the 1st law of thermodynamics. That law states that there must be conservation of energy. Namely, energy cannot be created or destroyed. However, when Einstein introduced relativity he demonstrated that $E = mc^2$. Thus, it is actually possible to convert mass into energy and vise versa. As a result, after Einstein, the 1st law of thermodynamics had to be modified. Consequently, the 1st law of thermodynamics now states that there must be conservation of mass and energy. Theoretically, these two entities could be freely interchanged with one another.

For a moment in closing however, let us return to our initial solid S_1. Of course, in the real world our solid is not in an isolated universe. Other solids, liquids (like our oceans) and gases (like our atmosphere) also exist. How do these affect our solid? In order to understand this, let us now bring two other solids into our adiabatic box. We will assume that these two solids, denoted "S_2" and "S_3", are in thermal equilibrium with each other. That is to say that, if "S_2" is placed in direct contact with "S_3" no net heat will flow between these objects. Now, if we now place solid "S_1" in contact with solid "S_2", we will discover one of two things. Either solid "S_1" is in thermal equilibrium with solid "S_2", or it is not in equilibrium. If it is in equilibrium with S_2, then by the 0th law of thermodynamics, it must also be in equilibrium with S_3. If on the other hand the solid S_1 it is not in equilibrium with S_2, then S_1, S_2 and S_3 will all move to a new thermal equilibrium with each other. If they are not in direct physical contact, this can only occur through thermal emission. However, if they are in direct contact, then they can use the much more efficient means of conduction to reach thermal equilibrium. If in turn we substitute a liquid or a gas for one of the solids, then convection can also be used to reach thermal equilibrium amongst all the objects. This is provided of course that the solids remain in physical contact with the gas or liquid. In the real universe therefore, all of the matter is simultaneously trying to reach thermal equilibrium with all other matter. The 2nd law of thermodynamics is governing this flow of heat. Most importantly, this process on a macroscopic scale is irreversible.

But now what of our little heat engine? Would it not be nice to bring it back? Perhaps we can! That is because, for our solar system, it is our Sun, and its internal energy, which is the ultimate source of energy. Therefore our Sun becomes for us a local little heat engine. As for the stars, they become other local heat engines, in a universe constantly striving for thermal equilibrium.

Author's comment on The Little Heat Engine:

The Little Heat Engine is telling us that the internal processes involved in heat transfer cannot be ignored. However, modern courses in classical thermodynamics often neglect the internal workings of the system. In large part, this is because the fathers of thermodynamics (men like Kirchhoff, Gibbbs and Claussius) did not yet have knowledge of the internal workings of the system. As such, they had no choice but to treat the entire system.

In this essay, it becomes apparent that Stefan's Law of thermal emission does not hold for liquids and gases. This is a reflection that these two states of matter have other available degrees of freedom. For instance, if Stefan's Law had held, solids would have no need to melt. They could keep dealing with heat easily, simply by emitting photons in a manner proportional with the fourth power of the temperature. However, the drop in thermal conductivity observed in the solid heralds the breakdown of Stefan's law and the ensuing change in phase. The Little Heat Engine is telling us that statistical thermodynamics must be applied when dealing with thermal emission. The Little Heat Engine is a constant reminder that universality does not exist in thermal radiation. The only materials which approach the blackbody on the Earth are generally made of either graphite or soot. The application, by astrophysics, of the laws of blackbody radiation [9–13] to the Sun [19, 20] and to unknown signals [21] irrespective of the phase of origin constitutes a serious overextension of these laws. Experimental physics has well established that there is no universality and that the laws of thermal radiation are properly restricted to the solid [22, 23].

Acknowledgments

The author acknowledges Karl Bedard and Luc Robitaille for assistance in preparing the figures and Christophe Robitaille is recognized for his computing skills.

Submitted on June 29, 2007
Accepted on July 02, 2007

References

1. Lansdsberg P. T. Thermodynamics. Interscience Publishers, New York, NY, 1961.
2. Chapman A. J. Heat transfer. The MacMillan Company, New York, NY, 1967.
3. Truesdell C. The tragicomical history of thermodynamics 1822–1854. Springer-Verlag, New York, NY. 1980.
4. Nash L. K. Elements of statistical thermodynamics. Addison-Wesley Publishing Company. Menlo Park, CA, 1968.

5. Buchdahl H. A. Twenty lectures on thermodynamics. Pergamon Press, Oxford, UK, 1975.
6. Wilson A. H. Thermodynamics and statistical mechanics. Cambridge University Press, Cambridge, UK, 1961.
7. Knudsen J. G., Bell K. J., Holt A. D., Hottel H. C., Sarofim A. F., Standiford F. C., Stuhlbarg D. and Uhl V. W. Heat transmission. In: *Perry's Chemical Engineer's Handbook Sixth Edition* (R. H. Perry, D. W. Green and J. O. Maloney, Eds.) McGraw-Hill Book Company, New York, p. 10.1–10.68, 1984.
8. Siegel R. and Howell J. R. Thermal radiation heat transfer (3rd Edition). Hemisphere Publishing Corporation, Washington, DC, 1992.
9. Planck M. Ueber das Gesetz der Energieverteilung in Normalspectrum. *Annalen der Physik*, 1901, v. 4, 553–563.
10. Kirchhoff G. Ueber den Zusammenhang von Emission und Absorption von Licht und Wärme. *Monatsberichte der Akademie der Wissenschaften zu Berlin*, sessions of Dec. 1859, 783–787.
11. Kirchhoff G. Ueber das Verhaltnis zwischen dem Emissionsvermögen und dem Absorptionsvermögen der Körper für Wärme und Licht. *Annalen der Physik*, 1860, v. 109, 275–301.
12. Stefan J. Ueber die Beziehung zwischen der Warmestrahlung und der Temperatur. *Wein. Akad. Sitzber.*, 1879, v. 79, 391–428.
13. Wien W. Uber die Energieverteilung im Emissionspektrum eines schwarzen Körpers. *Annalen der Physik*, 1896, v. 58, 662–669.
14. Touloukian Y. S. and Ho C. Y. Thermophysical Properties of Matter (vols. 1–8). Plenum, New York, 1970.
15. Vargaftik N. B., Filippov L. D., Tarzimanov A. A. and Totskii E. E. Handbook of thermal conductivities of liquids and gases. CRC Press, Boca Raton, FL, 1994.
16. Penner S. S. Quantitative molecular spectroscopy and gas emissivities. Addison-Wesley Publishing Company Inc., Reading, MA, 1959.
17. DeWitt D. P. and Nutter G. D. Theory and practice of radiation thermometry. John Wiley and Sons Inc., New York, NY, 1988.
18. Gasser R. P. H. and Richards W. G. An introduction to statistical thermodynamics. World Scientific, London, UK, 1995.
19. Langley S. P. Experimental determination of wave-lengths in the invisible spectrum. *Mem. Natl. Acad. Sci.*, 1883, v. 2, 147–162.
20. Langley S. P. On hitherto unrecognized wave-lengths. *Phil. Mag.*, 1886, v. 22, 149–173.
21. Penzias A. A. and Wilson R. W. A measurement of excess antenna temperature at 4080 Mc/s. *Astrophysical J.*, 1965, v. 1, 419–421.
22. Robitaille P.-M. L. On the validity of Kirchhoff's law of thermal emission. *IEEE Trans. Plasma Sci.*, 2003, v. 31 (6), 1263.
23. Robitaille P.-M. L. An analysis of universality in blackbody radiation. *Progr. Phys.*, 2006, v. 2, 22–23.

SPECIAL REPORT

A Four-Dimensional Continuum Theory of Space-Time and the Classical Physical Fields

Indranu Suhendro

Department of Physics, Karlstad University, Karlstad 651 88, Sweden
E-mail: spherical_symmetry@yahoo.com

In this work, we attempt to describe the classical physical fields of gravity, electromagnetism, and the so-called intrinsic spin (chirality) in terms of a set of fully geometrized constitutive equations. In our formalism, we treat the four-dimensional space-time continuum as a deformable medium and the classical fields as intrinsic stress and spin fields generated by infinitesimal displacements and rotations in the space-time continuum itself. In itself, the unifying continuum approach employed herein may suggest a possible unified field theory of the known classical physical fields.

1 Introduction

Many attempts have been made to incorporate the so-called standard (Hookean) linear elasticity theory into general relativity in the hope to describe the dynamics of material bodies in a fully covariant four-dimensional manner. As we know, many of these attempts have concentrated solely on the treatment of material bodies as linearly elastic continua and not quite generally on the treatment of space-time itself as a linearly elastic, deformable continuum. In the former case, taking into account the gravitational field as the only intrinsic field in the space-time continuum, it is therefore true that the linearity attributed to the material bodies means that the general consideration is limited to weakly gravitating objects only. This is because the curvature tensor is in general quadratic in the the so-called connection which can be said to represent the displacement field in the space-time manifold. However, in most cases, it is enough to consider an infinitesimal displacement field only such that the linear theory works perfectly well. However, for the sake of generality, we need not assume only the linear behavior of the properly-stressed space-time continuum (and material bodies) such that the possible limiting consequences of the linear theory can be readily overcome whenever it becomes necessary. Therefore, in the present work, we shall both consider both the linear and nonlinear formulations in terms of the response of the space-time geometry to infinitesimal deformations and rotations with intrinsic generators.

A few past attempts at the full description of the elastic behavior of the space-time geometry in the presence of physical fields in the language of general relativity have been quite significant. However, as standard general relativity describes only the field of gravity in a purely geometric fashion, these past attempts have generally never gone beyond the simple reformulation of the classical laws of elasticity in the presence of gravity which means that these classical laws of elasticity have merely been referred to the general four-dimensional curvilinear coordinates of Riemannian geometry, nothing more. As such, any possible interaction between the physical fields (e.g., the interaction between gravity and electromagnetism) has not been investigated in detail.

In the present work, we develop a fully geometrized continuum theory of space-time and the classical physical fields in which the actions of these physical fields contribute directly to the dynamics of the space-time geometry itself. In this model, we therefore assume that a physical field is directly associated with each and every point in the region of space-time occupied by the field (or, a material body in the case of gravity). This allows us to describe the dynamics of the space-time geometry solely in terms of the translational and rotational behavior of points within the occupied region. Consequently, the geometric quantities (objects) of the space-time continuum (e.g., curvature) are directly describable in terms of purely kinematic variables such as displacement, spin, velocity, acceleration, and the particle symmetries themselves.

As we have said above, at present, for the sake of simplicity, we shall assume the inherently elastic behavior of the space-time continuum. This, I believe, is adequate especially in most cosmological cases. Such an assumption is nothing but intuitive, especially when considering the fact that we do not fully know the reality of the constituents of the fabric of the Universe yet. As such, the possible limitations of the present theory, if any, can be neglected considerably until we fully understand how the fabric of the space-time continuum is actually formed and how the properties of individual elementary particles might contribute to this formation.

2 The fundamental geometric properties of a curved manifold

Let us present the fundamental geometric objects of an n-dimensional curved manifold. Let $\omega_a = \frac{\partial X^i}{\partial x^a} E_i = \partial_a X^i E_i$ (the Einstein summation convention is assumed throughout

this work) be the covariant (*frame*) basis spanning the n-dimensional base manifold $\mathbb{C}^\infty$ with local coordinates $x^a = = x^a\left(X^k\right)$. The contravariant (*coframe*) basis θ^b is then given via the orthogonal projection $\left\langle \theta^b, \omega_a \right\rangle = \delta^b_a$, where δ^b_a are the components of the Kronecker delta (whose value is unity if the indices coincide or null otherwise). The set of linearly independent local directional derivatives $E_i = \frac{\partial}{\partial X^i} = \partial_i$ gives the coordinate basis of the locally flat tangent space $\mathbb{T}_x(\mathbb{M})$ at a point $x \in \mathbb{C}^\infty$. Here $\mathbb{M}$ denotes the topological space of the so-called n-tuples $h(x) = h\left(x^1, \ldots, x^n\right)$ such that relative to a given chart $(U, h(x))$ on a neighborhood U of a local coordinate point, our $\mathbb{C}^\infty$-differentiable manifold itself is a topological space. The dual basis to E_i spanning the locally flat cotangent space $\mathbb{T}^*_x(\mathbb{M})$ will then be given by the differential elements dX^k via the relation $\left\langle dX^k, \partial_i \right\rangle = \delta^k_i$. In fact and in general, the *one-forms* dX^k indeed act as a linear map $\mathbb{T}_x(\mathbb{M}) \to \mathbb{R}$ when applied to an arbitrary vector field $F \in \mathbb{T}_x(\mathbb{M})$ of the explicit form $F = F^i \frac{\partial}{\partial X^i} = f^a \frac{\partial}{\partial x^a}$. Then it is easy to see that $F^i = F\, X^i$ and $f^a = F\, x^a$, from which we obtain the usual transformation laws for the contravariant components of a vector field, i.e., $F^i = \partial_a X^i f^a$ and $f^i = \partial_i x^a F^i$, relating the localized components of F to the general ones and vice versa. In addition, we also see that $\left\langle dX^k, F \right\rangle = F X^k = F^k$.

The components of the symmetric metric tensor $g = = g_{ab}\, \theta^a \otimes \theta^b$ of the base manifold $\mathbb{C}^\infty$ are readily given by

$$g_{ab} = \langle \omega_a, \omega_b \rangle$$

satisfying

$$g_{ac}\, g^{bc} = \delta^b_a$$

where $g^{ab} = \left\langle \theta^a, \theta^b \right\rangle$. It is to be understood that the covariant and contravariant components of the metric tensor will be used to raise and the (component) indices of vectors and tensors.

The components of the metric tensor

$$g\left(x_N\right) = \eta_{ik}\, dX^i \otimes dX^k$$

describing the locally flat tangent space $\mathbb{T}_x(\mathbb{M})$ of rigid frames at a point $x_N = x_N\left(x^a\right)$ are given by

$$\eta_{ik} = \langle E_i, E_k \rangle = \mathrm{diag}\left(\pm 1, \pm 1, \ldots, \pm 1\right).$$

In four dimensions, the above may be taken to be the components of the Minkowski metric tensor, i.e., $\eta_{ik} = \langle E_i, E_k \rangle = = \mathrm{diag}\,(1, -1, -1, -1)$.

Then we have the expression

$$g_{ab} = \eta_{ik}\, \partial_a X^i\, \partial_b X^k.$$

The line-element of $\mathbb{C}^\infty$ is then given by

$$ds^2 = g = g_{ab}\left(\partial_i x^a\, \partial_k x^b\right) dX^i \otimes dX^k$$

where $\theta^a = \partial_i x^a dX^i$.

Given the existence of a local coordinate transformation via $x^i = x^i\left(\bar{x}^\alpha\right)$ in $\mathbb{C}^\infty$, the components of an arbitrary tensor field $T \in \mathbb{C}^\infty$ of rank (p, q) transform according to

$$T^{ab\ldots g}_{cd\ldots h} = T^{\alpha\beta\ldots\lambda}_{\mu\nu\ldots\eta}\, \partial_\alpha x^a\, \partial_\beta x^b \ldots \partial_\lambda x^g\, \partial_c \bar{x}^\mu\, \partial_d \bar{x}^\nu \ldots \partial_h \bar{x}^\eta.$$

Let $\delta^{i_1 i_2 \ldots i_p}_{j_1 j_2 \ldots j_p}$ be the components of the generalized Kronecker delta. They are given by

$$\delta^{i_1 i_2 \ldots i_p}_{j_1 j_2 \ldots j_p} = \in_{j_1 j_2 \ldots j_p} \in^{i_1 \ldots i_p} = \det \begin{pmatrix} \delta^{i_1}_{j_1} & \delta^{i_2}_{j_1} & \ldots & \delta^{i_p}_{j_1} \\ \delta^{i_1}_{j_2} & \delta^{i_2}_{j_2} & \ldots & \delta^{i_p}_{j_2} \\ \ldots & \ldots & \ldots & \ldots \\ \delta^{i_1}_{j_p} & \delta^{i_2}_{j_p} & \ldots & \delta^{i_p}_{j_p} \end{pmatrix}$$

where $\in_{j_1 j_2 \ldots j_p} = \sqrt{\det(g)}\, \epsilon_{j_1 j_2 \ldots j_p}$ and $\in^{i_1 i_2 \ldots i_p} = \frac{\epsilon^{i_1 i_2 \ldots i_p}}{\sqrt{\det(g)}}$ are the covariant and contravariant components of the completely anti-symmetric Levi-Civita permutation tensor, respectively, with the ordinary permutation symbols being given as usual by $\epsilon_{j_1 j_2 \ldots j_q}$ and $\epsilon^{i_1 i_2 \ldots i_p}$. Again, if ω is an arbitrary tensor, then the object represented by

$${}^*\omega_{j_1 j_2 \ldots j_p} = \frac{1}{p!}\, \delta^{i_1 i_2 \ldots i_p}_{j_1 j_2 \ldots j_p}\, \omega_{i_1 i_2 \ldots i_p}$$

is completely anti-symmetric.

Introducing a generally asymmetric connection Γ via the covariant derivative

$$\partial_b \omega_a = \Gamma^c_{ab} \omega_c$$

i.e.,

$$\Gamma^c_{ab} = \langle \theta^c, \partial_b \omega_a \rangle = \Gamma^c_{(ab)} + \Gamma^c_{[ab]}$$

where the round index brackets indicate symmetrization and the square ones indicate anti-symmetrization, we have, by means of the local coordinate transformation given by $x^a = = x^a\left(\bar{x}^\alpha\right)$ in $\mathbb{C}^\infty$

$$\partial_b e^\alpha_a = \Gamma^c_{ab} e^\alpha_c - \bar{\Gamma}^\alpha_{\beta\lambda}\, e^\beta_a\, e^\lambda_b$$

where the tetrads of the *moving frames* are given by $e^\alpha_a = = \partial_a \bar{x}^\alpha$ and $e^a_\alpha = \partial_\alpha x^a$. They satisfy $e^a_\alpha e^\alpha_b = \delta^a_b$ and $e^\alpha_a e^a_\beta = = \delta^\alpha_\beta$. In addition, it can also be verified that

$$\partial_\beta e^a_\alpha = \bar{\Gamma}^\lambda_{\alpha\beta}\, e^a_\lambda - \Gamma^a_{bc}\, e^b_\alpha\, e^c_\beta\,,$$

$$\partial_b e^a_\alpha = e^a_\lambda\, \bar{\Gamma}^\lambda_{\alpha\beta}\, e^\beta_b - \Gamma^a_{cb}\, e^c_\alpha\,.$$

We know that Γ is a non-tensorial object, since its components transform as

$$\Gamma^c_{ab} = e^c_\alpha\, \partial_b e^\alpha_a + e^c_\alpha\, \bar{\Gamma}^\alpha_{\beta\lambda}\, e^\beta_a\, e^\lambda_b\,.$$

However, it can be described as a kind of displacement field since it is what makes possible a comparison of vectors from point to point in $\mathbb{C}^\infty$. In fact the relation $\partial_b \omega_a = \Gamma^c_{ab} \omega_c$

defines the so-called metricity condition, i.e., the change (during a displacement) in the basis can be measured by the basis itself. This immediately translates into

$$\nabla_c\, g_{ab} = 0$$

where we have just applied the notion of a covariant derivative to an arbitrary tensor field T:

$$\nabla_m T^{ab\ldots g}_{cd\ldots h} = \partial_m T^{ab\ldots g}_{cd\ldots h} + \Gamma^a_{pm} T^{pb\ldots g}_{cd\ldots h} + \Gamma^b_{pm} T^{ap\ldots g}_{cd\ldots h} + \ldots$$
$$\ldots + \Gamma^g_{pm} T^{ab\ldots p}_{cd\ldots h} - \Gamma^p_{cm} T^{ab\ldots g}_{pd\ldots h} - \Gamma^p_{dm} T^{ab\ldots g}_{cp\ldots h} - \ldots$$
$$\ldots - \Gamma^p_{hm} T^{ab\ldots g}_{cd\ldots p}$$

such that $(\partial_m T)^{ab\ldots g}_{cd\ldots h} = \nabla_m\, T^{ab\ldots g}_{cd\ldots h}$.

The condition $\nabla_c g_{ab} = 0$ can be solved to give

$$\Gamma^c_{ab} = \frac{1}{2}\, g^{cd} \left(\partial_b\, g_{da} - \partial_d\, g_{ab} + \partial_a\, g_{bd}\right) + \\ + \Gamma^c_{[ab]} - g^{cd} \left(g_{ae} \Gamma^e_{[db]} + g_{be} \Gamma^e_{[da]}\right)$$

from which it is customary to define

$$\Delta^c_{ab} = \frac{1}{2}\, g^{cd} \left(\partial_b\, g_{da} - \partial_d\, g_{ab} + \partial_a\, g_{bd}\right)$$

as the Christoffel symbols (symmetric in their two lower indices) and

$$K^c_{ab} = \Gamma^c_{[ab]} - g^{cd} \left(g_{ae} \Gamma^e_{[db]} + g_{be} \Gamma^e_{[da]}\right)$$

as the components of the so-called cotwist tensor (antisymmetric in the first two mixed indices).

Note that the components of the twist tensor are given by

$$\Gamma^a_{[bc]} = \frac{1}{2}\, e^a_\alpha \left(\partial_c\, e^\alpha_b - \partial_b\, e^\alpha_c + e^\beta_b\, \bar{\Gamma}^\alpha_{\beta c} - e^\beta_c\, \bar{\Gamma}^\alpha_{\beta b}\right)$$

where we have set $\bar{\Gamma}^\alpha_{\beta c} = \bar{\Gamma}^\alpha_{\beta\lambda} e^\lambda_c$, such that for an arbitrary scalar field Φ we have

$$\left(\nabla_a \nabla_b - \nabla_b \nabla_a\right) \Phi = 2\Gamma^c_{[ab]} \nabla_c\, \Phi\,.$$

The components of the curvature tensor R of $\mathbb{C}^\infty$ are then given via the relation

$$\left(\nabla_q \nabla_p - \nabla_p \nabla_q\right) T^{ab\ldots s}_{cd\ldots r} = T^{ab\ldots s}_{wd\ldots r} R^w{}_{cpq} + T^{ab\ldots s}_{cw\ldots r} R^w{}_{dpq} +$$
$$+ \ldots + T^{ab\ldots s}_{cd\ldots w} R^w{}_{rpq} - T^{wb\ldots s}_{cd\ldots r} R^a{}_{wpq} - T^{aw\ldots s}_{cd\ldots r} R^b{}_{wpq} -$$
$$- \ldots - T^{ab\ldots w}_{cd\ldots r} R^s{}_{wpq} - 2\Gamma^w_{[pq]} \nabla_w\, T^{ab\ldots s}_{cd\ldots r}$$

where

$$R^d{}_{abc} = \partial_b \Gamma^d_{ac} - \partial_c \Gamma^d_{ab} + \Gamma^e_{ac} \Gamma^d_{eb} - \Gamma^e_{ab} \Gamma^d_{ec}$$
$$= B^d{}_{abc}\left(\Delta\right) + \hat{\nabla}_b\, K^d_{ac} - \hat{\nabla}_c\, K^d_{ab} + K^e_{ac} K^d_{eb} - K^e_{ab} K^d_{ec}\,,$$

where $\hat{\nabla}$ denotes covariant differentiation with respect to the Christoffel symbols alone, and where

$$B^d{}_{abc}\left(\Delta\right) = \partial_b \Delta^d_{ac} - \partial_c \Delta^d_{ab} + \Delta^e_{ac} \Delta^d_{eb} - \Delta^e_{ab} \Delta^d_{ec}$$

are the components of the Riemann-Christoffel curvature tensor of $\mathbb{C}^\infty$.

From the components of the curvature tensor, namely, $R^d{}_{abc}$, we have (using the metric tensor to raise and lower indices)

$$R_{ab} \equiv R^c{}_{acb} = B_{ab}\left(\Delta\right) + \hat{\nabla}_c K^c_{ab} - K^c_{ad} K^d_{cb} - \\ - 2\hat{\nabla}_b\, \Gamma^c_{[ac]} + 2K^c_{ab} \Gamma^d_{[cd]}$$

$$R \equiv R^a{}_a = B\left(\Delta\right) - 4\, g^{ab}\, \hat{\nabla}_a\, \Gamma^c_{[bc]} - \\ - 2\, g^{ac}\, \Gamma^b_{[ab]} \Gamma^d_{[cd]} - K_{abc} K^{acb}$$

where $B_{ab}\left(\Delta\right) \equiv B^c_{acb}\left(\Delta\right)$ are the components of the symmetric Ricci tensor and $B\left(\Delta\right) \equiv B^a_a\left(\Delta\right)$ is the Ricci scalar. Note that $K_{abc} \equiv g_{ad} K^d_{bc}$ and $K^{acb} \equiv g^{cd} g^{be} K^a_{de}$.

Now since

$$\Gamma^b_{ba} = \Delta^b_{ba} = \Delta^b_{ab} = \partial_a \left(\ln \sqrt{\det\left(g\right)}\right)$$

$$\Gamma^b_{ab} = \partial_a \left(\ln \sqrt{\det\left(g\right)}\right) + 2\Gamma^b_{[ab]}$$

we see that for a continuous metric determinant, the so-called homothetic curvature vanishes:

$$H_{ab} \equiv R^c{}_{cab} = \partial_a\, \Gamma^c_{cb} - \partial_b\, \Gamma^c_{ca} = 0\,.$$

Introducing the traceless Weyl tensor W, we have the following decomposition theorem:

$$R^d{}_{abc} = W^d{}_{abc} + \frac{1}{n-2}\left(\delta^d_b R_{ac} + g_{ac} R^d{}_b - \delta^d_c R_{ab} - g_{ab} R^d{}_c\right) + \\ + \frac{1}{\left(n-1\right)\left(n-2\right)}\left(\delta^d_c\, g_{ab} - \delta^d_b\, g_{ac}\right) R$$

which is valid for $n > 2$. For $n = 2$, we have

$$R^d{}_{abc} = K_G \left(\delta^d_b\, g_{ac} - \delta^d_c\, g_{ab}\right)$$

where

$$K_G = \frac{1}{2}\, R$$

is the Gaussian curvature of the surface. Note that (in this case) the Weyl tensor vanishes.

Any n-dimensional manifold (for which $n > 1$) with constant sectional curvature R and vanishing twist is called an Einstein space. It is described by the following simple relations:

$$R^d{}_{abc} = \frac{1}{n(n-1)}\left(\delta^d_b\, g_{ac} - \delta^d_c\, g_{ab}\right) R\,,$$

$$R_{ab} = \frac{1}{n}\, g_{ab}\, R\,.$$

In the above, we note especially that

$$R^{d}{}_{abc} = B^{d}{}_{abc}(\Delta),$$

$$R_{ab} = B_{ab}(\Delta),$$

$$R = B(\Delta).$$

Furthermore, after some lengthy algebra, we obtain, in general, the following *generalized* Bianchi identities:

$$R^{a}{}_{bcd} + R^{a}{}_{cdb} + R^{a}{}_{dbc} = -2\big(\partial_d \Gamma^{a}_{[bc]} + \partial_b \Gamma^{a}_{[cd]} + \\ + \partial_c \Gamma^{a}_{[db]} + \Gamma^{a}_{eb}\Gamma^{e}_{[cd]} + \Gamma^{a}_{ec}\Gamma^{e}_{[db]} + \Gamma^{a}_{ed}\Gamma^{e}_{[bc]}\big),$$

$$\nabla_e R^{a}{}_{bcd} + \nabla_c R^{a}{}_{bde} + \nabla_d R^{a}{}_{bec} = \\ = 2\big(\Gamma^{f}_{[cd]} R^{a}{}_{bfe} + \Gamma^{f}_{[de]} R^{a}{}_{bfc} + \Gamma^{f}_{[ec]} R^{a}{}_{bfd}\big),$$

$$\nabla_a \left(R^{ab} - \frac{1}{2} g^{ab} R \right) = 2 g^{ab} \Gamma^{c}_{[da]} R^{d}{}_{c} + \Gamma^{a}_{[cd]} R^{cdb}{}_{a}$$

for any metric-compatible manifold endowed with both curvature and twist.

In the last of the above set of equations, we have introduced the generalized Einstein tensor, i.e.,

$$G_{ab} \equiv R_{ab} - \frac{1}{2} g_{ab} R$$

In particular, we also have the following specialized identities, i.e., the *regular* Bianchi identities:

$$B^{a}{}_{bcd} + B^{a}{}_{cdb} + B^{a}{}_{dbc} = 0,$$

$$\hat{\nabla}_e B^{a}{}_{bcd} + \hat{\nabla}_c B^{a}{}_{bde} + \hat{\nabla}_d B^{a}{}_{bec} = 0,$$

$$\hat{\nabla}_a \left(B^{ab} - \frac{1}{2} g^{ab} B \right) = 0.$$

In general, these hold in the case of a symmetric, metric-compatible connection. Non-metric differential geometry is beyond the scope of our present consideration.

We now define the so-called Lie derivative which can be used to define a diffeomorphism invariant in $\mathbb{C}^{\infty}$. for a vector field U and a tensor field T, both arbitrary, the invariant derivative represented (in component notation) by

$$L_U T^{ab\ldots g}_{cd\ldots h} = \partial_m T^{ab\ldots g}_{cd\ldots h} U^m + T^{ab\ldots g}_{md\ldots h} \partial_c U^m + \\ + T^{ab\ldots g}_{cm\ldots h} \partial_d U^m + \ldots + T^{ab\ldots g}_{cd\ldots m} \partial_h U^m - \\ - T^{mb\ldots g}_{cd\ldots h} \partial_m U^a - T^{am\ldots g}_{cd\ldots h} \partial_m U^b - \ldots - T^{ab\ldots m}_{cd\ldots h} \partial_m U^g$$

defines the Lie derivative of T with respect to U. With the help of the twist tensor and the relation

$$\partial_b U^a = \nabla_b U^a - \Gamma^{a}_{cb} U^c = \nabla_b U^a - \big(\Gamma^{a}_{bc} - 2\Gamma^{a}_{[bc]}\big) U^c$$

we can write

$$L_U T^{ab\ldots g}_{cd\ldots h} = \nabla_m T^{ab\ldots g}_{cd\ldots h} U^m + T^{ab\ldots g}_{md\ldots h} \nabla_c U^m + \\ + T^{ab\ldots g}_{cm\ldots h} \nabla_d U^m + \ldots + T^{ab\ldots g}_{cd\ldots m} \nabla_h U^m - T^{mb\ldots g}_{cd\ldots h} \nabla_m U^a - \\ - T^{am\ldots g}_{cd\ldots h} \nabla_m U^b - \ldots - T^{ab\ldots m}_{cd\ldots h} \nabla_m U^g + \\ + 2\Gamma^{a}_{[mp]} T^{mb\ldots g}_{cd\ldots h} U^p + 2\Gamma^{b}_{[mp]} T^{am\ldots g}_{cd\ldots h} U^p + \\ \ldots + 2\Gamma^{g}_{[mp]} T^{ab\ldots m}_{cd\ldots h} U^p - 2\Gamma^{m}_{[cp]} T^{ab\ldots g}_{md\ldots h} U^p + \\ + 2\Gamma^{m}_{[dp]} T^{ab\ldots g}_{cm\ldots h} U^p - \ldots - 2\Gamma^{m}_{[hp]} T^{ab\ldots g}_{cd\ldots m} U^p.$$

Hence, noting that the components of the twist tensor, namely, $\Gamma^{i}_{[kl]}$, indeed transform as components of a tensor field, it is seen that the $L_U T^{ij\ldots s}_{kl\ldots r}$ do transform as components of a tensor field. Apparently, the beautiful property of the Lie derivative (applied to an arbitrary tensor field) is that it is connection-independent even in a curved manifold.

We will need the identities derived in this Section later on.

3 The generalized four-dimensional linear constitutive field equations

We shall now present a four-dimensional linear continuum theory of the classical physical fields capable of describing microspin phenomena in addition to the gravitational and electromagnetic fields. By microspin phenomena, we mean those phenomena generated by rotation of points in the four-dimensional space-time manifold (continuum) $\mathbb{S}^4$ with local coordinates x^{μ} in the manner described by the so-called Cosserat continuum theory.

We start with the following constitutive equation in four dimensions:

$$T^{\mu\nu} = C^{\mu\nu}{}_{\rho\sigma} D^{\rho\sigma} = \frac{1}{\kappa} \left(R^{\mu\nu} - \frac{1}{2} g^{\mu\nu} R \right)$$

where now the Greek indices run from 0 to 3. In the above equation, $T^{\mu\nu}$ are the contravariant components of the generally asymmetric energy-momentum tensor, $C^{\mu\nu}_{\rho\sigma}$ are the mixed components of the generalized four-dimensional elasticity tensor, $D^{\rho\sigma}$ are the contravariant components of the four-dimensional displacement gradient tensor, $R^{\mu\nu}$ are the contravariant components of the generalized (asymmetric) four-dimensional Ricci curvature tensor, $\kappa = -8\pi$ is the Einstein coupling constant (in geometrized units), and $R = R^{\mu}_{\mu}$ is the generalized Ricci four-dimensional curvature scalar.

Furthermore, we can decompose our four-dimensional elasticity tensor into its holonomic and anholonomic parts as follows:

$$C^{\mu\nu}{}_{\rho\sigma} = A^{\mu\nu}{}_{\rho\sigma} + B^{\mu\nu}{}_{\rho\sigma}$$

where

$$A^{\mu\nu}{}_{\rho\sigma} = A^{(\mu\nu)}{}_{(\rho\sigma)} = A^{\mu\nu}{}_{\rho\sigma}$$

$$B^{\mu\nu}{}_{\rho\sigma} = B^{[\mu\nu]}{}_{[\rho\sigma]} = B^{\mu\nu}{}_{\rho\sigma}$$

such that

$$C^{\mu\nu}{}_{\rho\sigma} = C_{\rho\sigma}{}^{\mu\nu} .$$

Therefore, we can express the fully covariant components of the generalized four-dimensional elasticity tensor in terms of the covariant components of the symmetric metric tensor $g_{\mu\nu}$ (satisfying, as before, $g_{\nu\sigma}g^{\mu\sigma} = \delta^{\mu}_{\nu}$) as

$$C_{\mu\nu\rho\sigma} = \alpha\, g_{\mu\nu}g_{\rho\sigma} + \beta g_{\mu\rho}g_{\nu\sigma} + \gamma\, g_{\mu\sigma}g_{\nu\rho} =$$
$$= \alpha g_{\mu\nu}g_{\rho\sigma} + \lambda\left(g_{\mu\rho}g_{\nu\sigma} + g_{\mu\sigma}g_{\nu\rho}\right) + \omega\left(g_{\mu\rho}g_{\nu\sigma} - g_{\mu\sigma}g_{\nu\rho}\right)$$

where $\alpha, \beta, \gamma, \lambda$, and ω are constitutive invariants that are not necessarily constant. It is therefore seen that

$$A_{\mu\nu\rho\sigma} = \alpha\, g_{\mu\nu}g_{\rho\sigma} + \lambda\left(g_{\mu\rho}g_{\nu\sigma} + g_{\mu\sigma}g_{\nu\rho}\right)$$

$$B_{\mu\nu\rho\sigma} = \omega\left(g_{\mu\rho}g_{\nu\sigma} - g_{\mu\sigma}g_{\nu\rho}\right)$$

An infinitesimal displacement (diffeomorphism) in the space-time manifold $\mathbb{S}^4$ from an initial point P to a neighboring point Q is given as usual by

$$x^{\mu}(Q) = x^{\mu}(P) + \xi^{\mu}$$

where ξ^{μ} are the components of the four-dimensional infinitesimal displacement field vector. The generally asymmetric four-dimensional displacement gradient tensor is then given by

$$D_{\mu\nu} = \nabla_{\nu}\,\xi_{\mu} .$$

The decomposition $D_{\mu\nu} = D_{(\mu\nu)} + D_{[\mu\nu]}$ and the supplementary infinitesimal point-rotation condition $\Gamma^{\alpha}_{[\mu\nu]}\xi^{\mu} = 0$ allow us to define the symmetric four-dimensional displacement ("dilation") tensor by

$$\Phi_{\mu\nu} = D_{(\mu\nu)} = \frac{1}{2}\left(\nabla_{\mu}\xi_{\nu} + \nabla_{\nu}\xi_{\mu}\right) = \frac{1}{2}\,L_{\xi}\,g_{\mu\nu}$$

from which the "dilation" scalar is given by

$$\Phi = \Phi^{\mu}{}_{\mu} = D^{\mu}{}_{\mu} = \frac{1}{2}\,g^{\mu\nu}\,L_{\xi}\,g_{\mu\nu} = \nabla_{\mu}\,\xi^{\mu}$$

as well as the anti-symmetric four-dimensional intrinsic spin (vorticity) tensor by

$$\omega_{\mu\nu} = D_{[\mu\nu]} = \frac{1}{2}\left(\nabla_{\nu}\,\xi_{\mu} - \nabla_{\mu}\,\xi_{\nu}\right) .$$

Let us now decompose the four-dimensional infinitesimal displacement field vector as follows:

$$\xi^{\mu} = \partial^{\mu} F + \psi^{\mu} .$$

Here the continuous scalar function F represents the integrable part of the four-dimensional macroscopic displacement field vector while the remaining parts are given by ψ^{μ} via

$$\psi^{\mu} = \sigma^{\mu} + \phi^{\mu} + 2\,\bar{e}\,\varphi^{\mu}$$

where σ^{μ} are the components of the non-integrable four-dimensional macroscopic displacement field vector, ϕ^{μ} are the components of the four-dimensional microscopic (micropolar) intrinsic spin vector, $\bar{e}$ is a constant proportional to the electric charge, and φ^{μ} are the components of the electromagnetic four-potential vector. We assume that in general σ^{μ}, ϕ^{μ}, and φ^{μ} are linearly independent of each other.

The intrinsic four-dimensional macroscopic spin ("angular momentum") tensor is then given by

$$\Omega_{\mu\nu} = \frac{1}{2}\left(\nabla_{\nu}\,\sigma_{\mu} - \nabla_{\mu}\,\sigma_{\nu}\right) .$$

Likewise, the intrinsic four-dimensional microscopic (micropolar) spin tensor is given by

$$S_{\mu\nu} = \frac{1}{2}\left(\nabla_{\nu}\,\phi_{\mu} - \nabla_{\mu}\,\phi_{\nu}\right) .$$

Note that this tensor vanishes when the points are not allowed to rotate such as in conventional (standard) cases.

Meanwhile, the electromagnetic field tensor is given by

$$F_{\mu\nu} = \nabla_{\nu}\,\varphi_{\mu} - \nabla_{\mu}\,\varphi_{\nu} .$$

In this case, we especially note that, by means of the condition $\Gamma^{\alpha}_{[\mu\nu]}\xi^{\mu} = 0$, the above expression reduces to the usual Maxwellian relation

$$F_{\mu\nu} = \partial_{\nu}\varphi_{\mu} - \partial_{\mu}\varphi_{\nu} .$$

We can now write the intrinsic spin tensor as

$$\omega_{\mu\nu} = \Omega_{\mu\nu} + S_{\mu\nu} + \bar{e}F_{\mu\nu} .$$

Hence the full electromagnetic content of the theory becomes visible. We also see that our space-time continuum can be considered as a dynamically polarizable medium possessing chirality. As such, the gravitational and electromagnetic fields, i.e., the familiar classical fields, are intrinsic geometric objects in the theory.

Furthermore, from the cotwist tensor, let us define a geometric spin vector via

$$A_{\mu} \equiv K^{\sigma}_{\mu\sigma} = 2\Gamma^{\sigma}_{[\mu\sigma]} .$$

Now, in a somewhat restrictive case, in connection with the spin fields represented by σ^{μ}, ϕ^{μ}, and φ^{μ}, the selection

$$A_{\mu} = c_1\sigma_{\mu} + c_2\phi_{\mu} + 2\,\bar{e}\,c_3\varphi_{\mu} = \in \psi_{\mu}$$

i.e.,

$$\in = \frac{c_1\sigma_{\mu} + c_2\phi_{\mu} + 2\,\bar{e}\,c_3\varphi_{\mu}}{\sigma_{\mu} + \phi_{\mu} + 2\,\bar{e}\,\varphi_{\mu}}$$

will directly attribute the cotwist tensor to the intrinsic spin fields of the theory. However, we would in general expect the intrinsic spin fields to remain in the case of a semi-symmetric connection, for which $A_{\mu} = 0$ and so we cannot carry this proposition any further.

At this point, we see that the holonomic part of the generalized four-dimensional elasticity tensor given by $A_{\mu\nu\rho\sigma}$ is responsible for (centrally symmetric) gravitational phenomena while the anholonomic part given by $B_{\mu\nu\rho\sigma}$ owes its existence to the (con)twist tensor which is responsible for the existence of the intrinsic spin fields in our consideration.

Furthermore, we see that the components of the energy-momentum tensor can now be expressed as

$$T_{\mu\nu} = \alpha\, g_{\mu\nu}\Phi + \beta\, D_{\mu\nu} + \gamma\, D_{\nu\mu}\,.$$

In other words,

$$T_{(\mu\nu)} = \alpha\, g_{\mu\nu}\Phi + (\beta+\gamma)\,\Phi_{\mu\nu}\,,$$

$$T_{[\mu\nu]} = (\beta-\gamma)\,\omega_{\mu\nu}\,.$$

Alternatively,

$$T_{(\mu\nu)} = \frac{1}{2}\,\alpha\, g_{\mu\nu} g^{\alpha\beta} L_\xi\, g_{\alpha\beta} + \frac{1}{2}\,(\beta+\gamma)\, L_\xi\, g_{\mu\nu}\,,$$

$$T_{[\mu\nu]} = (\beta-\gamma)\,(\Omega_{\mu\nu} + S_{\mu\nu} + \bar{e}\, F_{\mu\nu})\,.$$

We may note that, in a sense analogous to that of the ordinary mechanics of continuous media, the generally asymmetric character of the energy-momentum tensor means that a material object in motion is generally subject to distributed body couples.

We also have

$$T = T^{\mu}{}_{\mu} = (4\alpha + \beta + \gamma)\,\Phi = -\frac{1}{\kappa}\,R.$$

Let us briefly relate our description to the standard material description given by general relativity. For this purpose, let us assume that the intrinsic spin fields other than the electromagnetic field are negligible. If we denote the material density and the pressure by ρ and p, respectively, then it can be directly verified that

$$\Phi = \frac{\rho - 4p}{4\alpha + \beta + \gamma}$$

is a solution to the ordinary expression

$$T_{(\mu\nu)} = \rho\, u_\mu u_\nu - p g_{\mu\nu} - \\ - \frac{1}{4\pi}\left(F_{\mu\sigma}F^{\sigma}{}_{\nu} - \frac{1}{4}\, g_{\mu\nu} F_{\alpha\beta}F^{\alpha\beta}\right)$$

where u_μ are the covariant components of the unit velocity vector. This is true whether the electromagnetic field is present or not since the (symmetric) energy-momentum tensor of the electromagnetic field given by

$$J_{\mu\nu} = -\frac{1}{4\pi}\left(F_{\mu\sigma}F^{\sigma}{}_{\nu} - \frac{1}{4}\, g_{\mu\nu} F_{\alpha\beta}F^{\alpha\beta}\right)$$

is traceless.

At this point, however, we may note that the covariant divergence

$$\nabla_\mu T^{\mu\nu} = g^{\mu\nu}\nabla_\mu(\alpha\Phi) + \beta\nabla_\mu D^{\mu\nu} + \\ + \gamma\nabla_\mu D^{\nu\mu} + D^{\mu\nu}\nabla_\mu\beta + D^{\nu\mu}\nabla_\mu\gamma$$

need not vanish in general since

$$\nabla_\mu T^{\mu\nu} = \frac{1}{\kappa}\nabla_\mu\left(R^{\mu\nu} - \frac{1}{2}\, g^{\mu\nu} R\right) = \\ = \frac{1}{\kappa}\left(2\, g^{\mu\nu}\Gamma^{\rho}_{[\sigma\mu]} R^{\sigma}_{\rho} + \Gamma^{\lambda}_{[\rho\sigma]} R^{\rho\sigma\nu}{}_{\lambda}\right).$$

In an isotropic, homogeneous Universe, for which the constitutive invariants $\alpha, \beta, \gamma, \lambda$, and ω are constant, the above expression reduces to

$$\nabla_\mu T^{\mu\nu} = \alpha\, g^{\mu\nu}\nabla_\mu\,\Phi + \beta\nabla_\mu D^{\mu\nu} + \gamma\nabla_\mu D^{\nu\mu}.$$

If we require the above divergence to vanish, however, we see that the motion described by this condition is still more general than the pure geodesic motion for point-particles.

Still in the case of an isotropic, homogeneous Universe, possibly on large cosmological scales, then our expression for the energy-momentum tensor relates the generalized Ricci curvature scalar directly to the "dilation" scalar. In general, we have

$$R = -\kappa\,(4\alpha + \beta + \gamma)\,\Phi = -\kappa\Lambda\Phi = -\frac{1}{2}\,\kappa\Lambda\, g^{\mu\nu} L_\xi\, g_{\mu\nu}\,.$$

Now, for the generalized Ricci curvature tensor, we obtain the following asymmetric constitutive field equation:

$$R_{\mu\nu} = \kappa\left(T_{\mu\nu} - \frac{1}{2}\, g_{\mu\nu}\, T\right) = \kappa\,(\theta\, g_{\mu\nu} + \beta\, D_{\mu\nu} + \gamma)$$

where

$$\theta = -\frac{1}{2}\,(2\alpha + \beta + \gamma)\,\Phi\,.$$

In other words,

$$R_{(\mu\nu)} = \kappa\big(\theta g_{\mu\nu} + (\beta+\gamma)\,\Phi_{\mu\nu}\big),$$

$$R_{[\mu\nu]} = \kappa\,(\beta-\gamma)\,\omega_{\mu\nu}\,.$$

Inserting the value of κ, we can alternatively write

$$R_{(\mu\nu)} = -8\pi\left(\theta\, g_{\mu\nu} + \frac{1}{2}\,(\beta+\gamma)\, L_\xi g_{\mu\nu}\right)$$

$$R_{[\mu\nu]} = -8\pi\,(\beta-\gamma)\,(\Omega_{\mu\nu} + S_{\mu\nu} + \bar{e}\, F_{\mu\nu})\,.$$

Hence, the correspondence between the generalized Ricci curvature tensor and the physical fields in our theory becomes complete. The present theory shows that in a curved space-time with a particular spherical symmetry and in a flat Minkowski space-time (both space-times are solutions to the equation $\Phi_{\mu\nu} = 0$, i.e., $L_\xi\, g_{\mu\nu} = 0$) it is in general still possible for the spin fields to exist. One possible geometry that

complies with such a space-time symmetry is the geometry of distant parallelism with vanishing space-time curvature (but non-vanishing Riemann-Christoffel curvature) and non-vanishing twist.

Now let us recall that in four dimensions, with the help of the Weyl tensor W, we have the decomposition

$$R_{\mu\nu\rho\sigma} = W_{\mu\nu\rho\sigma} + \\ + \frac{1}{2}\left(g_{\mu\rho}R_{\nu\sigma} + g_{\nu\sigma}R_{\mu\rho} - g_{\mu\sigma}R_{\nu\rho} - g_{\nu\rho}R_{\mu\sigma}\right) + \\ + \frac{1}{6}\left(g_{\mu\sigma}g_{\nu\rho} - g_{\mu\rho}g_{\nu\sigma}\right)R\,.$$

We obtain, upon setting $\bar{\alpha} = \frac{1}{2}\kappa\theta$, $\bar{\beta} = \frac{1}{2}\kappa\beta$, $\bar{\gamma} = \frac{1}{2}\kappa\gamma$, and $\bar{\lambda} = \frac{1}{6}\kappa\Lambda$

$$R_{\mu\nu\rho\sigma} = W_{\mu\nu\rho\sigma} + 2\bar{\alpha}\left(g_{\mu\rho}g_{\nu\sigma} - g_{\mu\sigma}g_{\nu\rho}\right) + \\ + \bar{\beta}\left(g_{\mu\rho}D_{\nu\sigma} + g_{\nu\sigma}D_{\mu\rho} - g_{\mu\sigma}D_{\nu\rho} - g_{\nu\rho}D_{\mu\sigma}\right) + \\ + \bar{\gamma}\left(g_{\mu\rho}D_{\sigma\nu} + g_{\nu\sigma}D_{\rho\mu} - g_{\mu\sigma}D_{\rho\nu} - g_{\nu\rho}D_{\sigma\mu}\right) + \\ + \bar{\lambda}\left(g_{\mu\rho}g_{\nu\sigma} - g_{\mu\sigma}g_{\nu\rho}\right)\Phi\,.$$

Therefore, in terms of the anholonomic part of the generalized elasticity tensor, we have

$$R_{\mu\nu\rho\sigma} = W_{\mu\nu\rho\sigma} + 2\frac{\bar{\alpha}}{\omega}B_{\mu\nu\rho\sigma} + \\ + \bar{\beta}\left(g_{\mu\rho}D_{\nu\sigma} + g_{\nu\sigma}D_{\mu\rho} - g_{\mu\sigma}D_{\nu\rho} - g_{\nu\rho}D_{\mu\sigma}\right) + \\ + \bar{\gamma}\left(g_{\mu\rho}D_{\sigma\nu} + g_{\nu\sigma}D_{\rho\mu} - g_{\mu\sigma}D_{\rho\nu} - g_{\nu\rho}D_{\sigma\mu}\right) + \\ + \bar{\lambda}\left(g_{\mu\rho}g_{\nu\sigma} - g_{\mu\sigma}g_{\nu\rho}\right)\Phi\,.$$

In the special case of a pure gravitational field, the twist of the space-time continuum vanishes. In this situation our intrinsic spin fields vanish and consequently, we are left simply with

$$R_{\mu\nu\rho\sigma} = W_{\mu\nu\rho\sigma} + \\ + \frac{1}{2}\left(\bar{\beta} + \bar{\gamma}\right)\left(g_{\mu\rho}D_{\nu\sigma} + g_{\nu\sigma}D_{\mu\rho} - g_{\mu\sigma}D_{\nu\rho} - g_{\nu\rho}D_{\mu\sigma}\right) + \\ + \bar{\lambda}\left(g_{\mu\rho}g_{\nu\sigma} - g_{\mu\sigma}g_{\nu\rho}\right)\Phi\,.$$

In standard general relativity, this gives the explicit form of the Riemann-Christoffel curvature tensor in terms of the Lie derivative $L_\xi\, g_{\mu\nu} = 2\Phi_{\mu\nu}$. For a space-time satisfying the symmetry $L_\xi\, g_{\mu\nu} = 0$, we simply have $R_{\mu\nu\rho\sigma} = W_{\mu\nu\rho\sigma}$, i.e., the space-time is devoid of material sources or "empty". This condition is relatively weaker than the case of a space-time with constant sectional curvature, $R = \text{const.}$ for which the Weyl tensor vanishes.

4 The generalized four-dimensional non-linear constitutive field equations

In reference to the preceding section, let us now present, in a somewhat concise manner, a non-linear extension of the formulation presented in the preceding section. The resulting non-linear constitutive field equations will therefore not be limited to weak fields only. In general, it can be shown that the full curvature tensor contains terms quadratic in the displacement gradient tensor and this gives us the reason to express the energy-momentum tensor which is quadratic in the displacement gradient tensor.

We start with the non-linear constitutive field equation

$$T^{\mu\nu} = C^{\mu\nu}{}_{\rho\sigma}D^{\rho\sigma} + K^{\mu\nu}{}_{\rho\sigma\lambda\eta}D^{\rho\sigma}D^{\lambda\eta} = \frac{1}{\kappa}\left(R^{\mu\nu} - \frac{1}{2}g^{\mu\nu}R\right)$$

where

$$K_{\mu\nu\rho\sigma\lambda\eta} = a_1\, g_{\mu\nu}g_{\rho\sigma}g_{\lambda\eta} + a_2\, g_{\mu\nu}g_{\rho\lambda}g_{\sigma\eta} + \\ + a_3 g_{\mu\nu}g_{\rho\eta}g_{\sigma\lambda} + a_4\, g_{\rho\sigma}g_{\mu\lambda}g_{\nu\eta} + a_5\, g_{\rho\sigma}g_{\mu\eta}g_{\nu\lambda} + \\ + a_6\, g_{\lambda\eta}g_{\mu\rho}g_{\nu\sigma} + a_7\, g_{\lambda\eta}g_{\mu\sigma}g_{\nu\rho} + a_8\, g_{\mu\lambda}g_{\nu\rho}g_{\sigma\eta} + \\ + a_9\, g_{\mu\lambda}g_{\nu\sigma}g_{\rho\eta} + a_{10}\, g_{\mu\eta}g_{\nu\rho}g_{\sigma\lambda} + a_{11}\, g_{\mu\eta}g_{\nu\sigma}g_{\rho\lambda} + \\ + a_{12}\, g_{\nu\lambda}g_{\mu\rho}g_{\sigma\eta} + a_{13}\, g_{\nu\lambda}g_{\mu\sigma}g_{\rho\eta} + a_{14}\, g_{\nu\eta}g_{\mu\rho}g_{\sigma\lambda} + \\ + a_{15}\, g_{\nu\eta}g_{\mu\sigma}g_{\rho\lambda}$$

where the fifteen constitutive invariants a_1, a_2, ..., a_{15} are not necessarily constant.

We shall set

$$K_{\mu\nu\rho\sigma\lambda\eta} = K_{\rho\sigma\mu\nu\lambda\eta} = K_{\lambda\eta\mu\nu\rho\sigma} = K_{\mu\nu\lambda\eta\rho\sigma}\,.$$

Letting

$$K_{\mu\nu\rho\sigma\lambda\eta} = P_{\mu\nu\rho\sigma\lambda\eta} + Q_{\mu\nu\rho\sigma\lambda\eta}\,,$$

$$P_{\mu\nu\rho\sigma\lambda\eta} = P_{(\mu\nu)(\rho\sigma)(\lambda\eta)}\,,$$

$$Q_{\mu\nu\rho\sigma\lambda\eta} = Q_{[\mu\nu][\rho\sigma][\lambda\eta]}\,,$$

we have

$$P_{\mu\nu\rho\sigma\lambda\eta} = P_{\rho\sigma\mu\nu\lambda\eta} = P_{\lambda\eta\mu\nu\rho\sigma} = P_{\mu\nu\lambda\eta\rho\sigma}\,,$$

$$Q_{\mu\nu\rho\sigma\lambda\eta} = Q_{\rho\sigma\mu\nu\lambda\eta} = Q_{\lambda\eta\mu\nu\rho\sigma} = Q_{\mu\nu\lambda\eta\rho\sigma}\,.$$

Introducing the eleven constitutive invariants b_1, b_2, ..., b_{11}, we can write

$$K_{\mu\nu\rho\sigma\lambda\eta} = b_1 g_{\mu\nu}g_{\rho\sigma}g_{\lambda\eta} + b_2 g_{\mu\nu}\left(g_{\rho\lambda}g_{\sigma\eta} + g_{\rho\eta} + g_{\sigma\lambda}\right) + \\ + b_3 g_{\mu\nu}\left(g_{\rho\lambda}g_{\sigma\eta} - g_{\rho\eta}g_{\sigma\lambda}\right) + b_4 g_{\rho\sigma}\left(g_{\mu\lambda}g_{\nu\eta} + g_{\mu\eta}g_{\nu\lambda}\right) + \\ + b_5 g_{\rho\sigma}\left(g_{\mu\lambda}g_{\nu\eta} - g_{\mu\eta}g_{\nu\lambda}\right) + b_6 g_{\lambda\eta}\left(g_{\mu\rho}g_{\nu\sigma} + g_{\mu\sigma}g_{\nu\rho}\right) + \\ + b_7 g_{\lambda\eta}\left(g_{\mu\rho}g_{\nu\sigma} - g_{\mu\sigma}g_{\nu\rho}\right) + b_8 g_{\mu\lambda}\left(g_{\upsilon\rho}g_{\sigma\eta} + g_{\nu\sigma}g_{\rho\eta}\right) + \\ + b_9 g_{\mu\lambda}\left(g_{\nu\rho}g_{\sigma\eta} - g_{\nu\sigma}g_{\rho\eta}\right) + b_{10} g_{\nu\lambda}\left(g_{\mu\rho}g_{\sigma\eta} + g_{\mu\sigma}g_{\rho\eta}\right) + \\ + b_{11} g_{\nu\lambda}\left(g_{\mu\rho}g_{\sigma\eta} - g_{\mu\sigma}g_{\rho\eta}\right).$$

The energy-momentum tensor is therefore given by

$$T_{\mu\nu} = \left(\alpha\,\Phi + b_1\,\Phi^2 + 2\,b_2\,\Phi_{\rho\sigma}\,\Phi^{\rho\sigma} + 2\,b_3\,\omega_{\rho\sigma}\,\omega^{\rho\sigma}\right)g_{\mu\nu} + \\ + \beta\, D_{\mu\nu} + \gamma\, D_{\nu\mu} + 2\left(b_4 + b_6\right)\Phi\,\Phi_{\mu\nu} + \\ + 2\left(b_5 + b_7\right)\Phi\,\omega_{\mu\nu} + 2\,b_8\,D^{\rho}{}_{\mu}\,\Phi_{\nu\rho} + 2\,b_9\,D^{\rho}{}_{\mu}\,\omega_{\nu\rho} + \\ + 2\,b_{10}\,D^{\rho}{}_{\nu}\,\Phi_{\mu\rho} + 2\,b_{11}\,D^{\rho}{}_{\nu}\,\omega_{\mu\rho}\,.$$

In other words,

$$T_{(\mu\nu)} = \left(\alpha\,\Phi + b_1\,\Phi^2 + 2b_2\,\Phi_{\rho\sigma}\,\Phi^{\rho\sigma} + 2b_3\,\omega_{\rho\sigma}\,\omega^{\rho\sigma}\right) g_{\mu\nu} +$$
$$+ \left(\beta + \gamma\right)\Phi_{\mu\nu} 2\left(b_4 + b_6\right)\Phi\,\Phi_{\mu\nu} + \left(b_8 + b_{10}\right) \times$$
$$\times \left(D^{\rho}{}_{\mu}\,\Phi_{\nu\rho} + D^{\rho}{}_{\nu}\,\Phi_{\mu\rho}\right) + \left(b_9 + b_{11}\right)\left(D^{\rho}{}_{\mu}\,\omega_{\nu\rho} + D^{\rho}{}_{\nu}\,\omega_{\mu\rho}\right),$$

$$T_{[\mu\nu]} = \left(\beta - \gamma\right)\omega_{\mu\nu} + 2\left(b_4 + b_6\right)\Phi\,\omega_{\mu\nu} + \left(b_8 + b_{10}\right) \times$$
$$\times \left(D^{\rho}{}_{\mu}\,\Phi_{\nu\rho} - D^{\rho}{}_{\nu}\,\Phi_{\mu\rho}\right) + \left(b_9 + b_{11}\right)\left(D^{\rho}{}_{\mu}\,\omega_{\nu\rho} - D^{\rho}{}_{\nu}\,\omega_{\mu\rho}\right).$$

We also have

$$T = \mu_1\,\Phi + \mu_2\,\Phi^2 + \mu_3\,\Phi_{\mu\nu}\,\Phi^{\mu\nu} + \mu_4\,\omega_{\mu\nu}\,\omega^{\mu\nu}$$

where we have set

$$\mu_1 = 4\alpha + \beta + \gamma\,,$$
$$\mu_2 = 4b_1 + 2\left(b_4 + b_6\right),$$
$$\mu_3 = 8b_2 + 2\left(b_8 + b_{10}\right),$$
$$\mu_4 = 8b_3 + 2\left(b_9 - b_{11}\right),$$

for the sake of simplicity.

For the generalized Ricci curvature tensor, we obtain

$$R_{\mu\nu} = \kappa\left\{\left(c_1\Phi + c_2\,\Phi^2 + c_3\,\Phi_{\rho\sigma}\,\Phi^{\rho\sigma} + c_4\omega_{\rho\sigma}\omega^{\rho\sigma}\right) g_{\mu\nu} +\right.$$
$$+ c_5\,D_{\mu\nu} + c_6\,D_{\nu\mu} + c_7\Phi\,\Phi_{\mu\nu} + c_8\,\Phi\omega_{\mu\nu} + c_9\,D^{\rho}{}_{\mu}\,\Phi_{\nu\rho} +$$
$$\left. + c_{10}\,D^{\rho}{}_{\mu}\omega_{\nu\rho} + c_{11}\,D^{\rho}{}_{\nu}\,\Phi_{\mu\rho} + c_{12}\,D^{\rho}{}_{\nu}\omega_{\mu\rho}\right\}$$

where

$$c_1 = -\frac{1}{2}\left(2\alpha + \beta + \gamma\right), \qquad c_7 = 2\left(b_4 + b_6\right),$$
$$c_2 = -\left(b_1 + b_4 + b_6\right), \qquad c_8 = 2\left(b_5 + b_7\right),$$
$$c_3 = -\left(2b_2 + b_8 + b_{10}\right), \qquad c_9 = 2b_8\,,$$
$$c_4 = -\left(2b_3 + b_9 - b_{11}\right), \qquad c_{10} = 2b_9\,,$$
$$c_5 = \beta\,, \qquad c_{11} = 2b_{10}\,,$$
$$c_6 = \gamma\,, \qquad c_{12} = 2b_{11}\,,$$

i.e.,

$$R_{(\mu\nu)} = \kappa\left\{\left(c_1\Phi + c_2\,\Phi^2 + c_3\,\Phi_{\rho\sigma}\,\Phi^{\rho\sigma}\right.\right. +$$
$$\left. + c_4\omega_{\rho\sigma}\omega^{\rho\sigma}\right) g_{\mu\nu} + \left(c_5 + c_6\right)\Phi_{\mu\nu} + c_7\Phi\,\Phi_{\mu\nu} +$$
$$+ \frac{1}{2}\left(c_9 + c_{11}\right)\left(D^{\rho}{}_{\mu}\,\Phi_{\nu\rho} + D^{\rho}{}_{\nu}\,\Phi_{\mu\rho}\right) +$$
$$\left. + \frac{1}{2}\left(c_{10} + c_{12}\right)\left(D^{\rho}{}_{\mu}\,\omega_{\nu\rho} + D^{\rho}{}_{\nu}\,\omega_{\mu\rho}\right)\right\},$$

$$R_{[\mu\nu]} = \kappa\left\{\left(c_5 - c_6\right)\omega_{\mu\nu} + c_8\,\Phi\,\omega_{\mu\nu} +\right.$$
$$+ \frac{1}{2}\left(c_9 + c_{11}\right)\left(D^{\rho}{}_{\mu}\,\Phi_{\nu\rho} - D^{\rho}{}_{\nu}\,\Phi_{\mu\rho}\right) +$$
$$\left. + \frac{1}{2}\left(c_{10} + c_{11}\right)\left(D^{\rho}{}_{\mu}\,\omega_{\nu\rho} - D^{\rho}{}_{\nu}\,\omega_{\mu\rho}\right)\right\}.$$

The generalized Ricci curvature scalar is then

$$R = \kappa\left(h_1\,\Phi + h_2\,\Phi^2 + h_3\,\Phi_{\mu\nu}\,\Phi^{\mu\nu} + h_4\,\omega_{\mu\nu}\,\omega^{\mu\nu}\right)$$

where

$$h_1 = 4c_1 + c_5 + c_6\,,$$
$$h_2 = 4c_2 + c_5\,,$$
$$h_3 = 4c_3 + c_9 + c_{11}\,,$$
$$h_4 = 4c_4 + c_{10} + c_{12}\,.$$

Finally, we obtain, for the curvature tensor, the following expression:

$$R_{\mu\nu\rho\sigma} = W_{\mu\nu\rho\sigma} +$$
$$+ \left(f_1\,\Phi + f_2\,\Phi^2 + f_3\,\Phi_{\lambda\eta}\,\Phi^{\lambda\eta} + f_4\,\omega_{\lambda\eta}\omega^{\lambda\eta}\right) \times$$
$$\times \left(g_{\mu\rho}g_{\nu\sigma} - g_{\mu\sigma}g_{\nu\rho}\right) + \left(\bar{\beta} + f_5\,\Phi\right)\left(g_{\mu\rho}\,\Phi_{\nu\sigma} + g_{\nu\sigma}\,\Phi_{\mu\rho} -\right.$$
$$- g_{\mu\sigma}\,\Phi_{\nu\rho} - g_{\nu\rho}\,\Phi_{\mu\sigma}\Big) + \left(\bar{\beta} + f_6\,\Phi\right)\left(g_{\mu\rho}\omega_{\nu\sigma} + g_{\nu\sigma}\omega_{\mu\rho} -\right.$$
$$- g_{\mu\sigma}\omega_{\nu\rho} - g_{\nu\rho}\omega_{\mu\sigma}\Big) + \bar{\gamma}\left(g_{\mu\rho}\,D_{\sigma\nu} + g_{\nu\sigma}\,D_{\rho\mu} -\right.$$
$$- g_{\mu\sigma}\,D_{\rho\nu} - g_{\nu\rho}\,D_{\sigma\mu}\Big) + f_7\left(D^{\lambda}{}_{\nu}\,\Phi_{\sigma\lambda}\,g_{\mu\rho} +\right.$$
$$+ D^{\lambda}{}_{\mu}\,\Phi_{\rho\lambda}\,g_{\nu\sigma} - D^{\lambda}{}_{\nu}\,\Phi_{\rho\lambda}\,g_{\mu\sigma} - D^{\lambda}{}_{\mu}\,\Phi_{\sigma\lambda}\,g_{\nu\rho}\Big) +$$
$$+ f_8\left(D^{\lambda}{}_{\nu}\,\omega_{\sigma\lambda}\,g_{\mu\rho} + D^{\lambda}{}_{\mu}\,\omega_{\rho\lambda}\,g_{\nu\sigma} - D^{\lambda}{}_{\nu}\,\omega_{\rho\lambda}\,g_{\mu\sigma} -\right.$$
$$- D^{\lambda}{}_{\mu}\,\omega_{\sigma\lambda}\,g_{\nu\rho}\Big) + f_9\left(D^{\lambda}{}_{\sigma}\,\Phi_{\nu\lambda}\,g_{\mu\rho} + D^{\lambda}{}_{\rho}\,\Phi_{\mu\lambda}\,g_{\nu\sigma} -\right.$$
$$- D^{\lambda}{}_{\rho}\,\Phi_{\nu\lambda}\,g_{\mu\sigma} - D^{\lambda}{}_{\sigma}\,\Phi_{\mu\lambda}g_{\nu\rho}\Big) + f_{10}\left(D^{\lambda}{}_{\sigma}\,\omega_{\nu\lambda}\,g_{\mu\rho} +\right.$$
$$\left. + D^{\lambda}{}_{\rho}\,\omega_{\mu\lambda}\,g_{\nu\sigma} - D^{\lambda}{}_{\rho}\,\omega_{\nu\lambda}\,g_{\mu\sigma} - D^{\lambda}{}_{\sigma}\,\omega_{\mu\lambda}\,g_{\nu\rho}\right)$$

where

$$f_1 = c_1 = \bar{\alpha} + \bar{\lambda}\,, \qquad f_6 = c_8\,,$$
$$f_2 = \left(1 - \frac{2}{3}\,\kappa\right)c_2 + \frac{1}{6}\,\kappa\,c_7\,, \qquad f_7 = c_9\,,$$
$$f_3 = \left(1 - \frac{2}{3}\,\kappa\right)c_3 + \frac{1}{6}\,\kappa\left(c_9 + c_{11}\right), \qquad f_8 = c_{10}\,,$$
$$f_4 = \left(1 - \frac{2}{3}\,\kappa\right)c_4 + \frac{1}{6}\,\kappa\left(c_{10} - c_{12}\right), \qquad f_9 = c_{11}\,,$$
$$f_5 = c_7\,, \qquad f_{10} = c_{12}\,.$$

At this point, the apparent main difficulty lies in the fact that there are too many constitutive invariants that need to be exactly determined. As such, the linear theory is comparatively preferable since it only contains three constitutive invariants. However, by presenting the most general structure of the non-linear continuum theory in this section, we have acquired a quite general picture of the most general behavior of the space-time continuum in the presence of the classical fields.

5 The equations of motion

Let us now investigate the local translational-rotational motion of points in the space-time continuum $\mathbb{S}^4$. Consider an infinitesimal displacement in the manner described in the preceding section. Keeping the initial position fixed, the unit velocity vector is given by

$$u^\mu = \frac{d\xi^\mu}{ds} = \frac{dx^\mu}{ds},$$

$$1 = g_{\mu\nu} u^\mu u^\nu,$$

such that, at any proper time given by the world-line s, the parametric representation

$$d\xi^\mu = u^\mu \left(x^\alpha, s\right) ds$$

describes space-time curves whose tangents are everywhere directed along the direction of a particle's motion. As usual, the world-line can be parametrized by a scalar ς via $s = a\varsigma + b$, where a and b are constants of motion.

The local equations of motion along arbitrary curves in the space-time continuum $\mathbb{S}^4$ can be described by the quadruplet of unit space-time vectors (u, v, w, z) orthogonal to each other where the first three unit vectors, or the triplet (u, v, w), may be defined as (a set of) local tangent vectors in the (three-dimensional) hypersurface $\Sigma(t)$ such that the unit vector z is normal to it. More explicitly, the hypersurface $\Sigma(t)$ is given as the time section $t = x^0 = \text{const}$ of $\mathbb{S}^4$. This way, the equations of motion will be derived by generalizing the ordinary Frenet equations of orientable points along an arbitrary curve in three-dimensional Euclidean space, i.e., by recasting them in a four-dimensional manner. Of course, we will also include effects of microspin generated by the twist of space-time.

With respect to the anholonomic space-time basis $\omega_\mu = \omega_\mu\left(x^\alpha(X^k)\right) = e^i_\mu \frac{\partial}{\partial X^i}$, we can write

$$u = u^\mu \omega_\mu,$$
$$v = v^\mu \omega_\mu,$$
$$w = w^\mu \omega_\mu,$$
$$z = z^\mu \omega_\mu,$$

we obtain, in general, the following set of equations of motion of points, i.e., point-like particles, along an arbitrary curve ℓ in the space-time continuum $\mathbb{S}^4$:

$$\frac{Du^\mu}{Ds} = \phi v^\mu,$$
$$\frac{Dv^\mu}{Ds} = \tau w^\mu - \phi u^\mu,$$
$$\frac{Dw^\mu}{Ds} = \tau v^\mu + \varphi z^\mu,$$
$$\frac{Dz^\mu}{Ds} = \varphi w^\mu,$$

where the operator $\frac{D}{Ds} = u^\mu \nabla_\mu$ represents the absolute covariant derivative. In the above equations we have introduced the following invariants:

$$\phi = \left(g_{\mu\nu} \frac{Du^\mu}{Ds} \frac{Du^\nu}{Ds}\right)^{1/2},$$

$$\tau = \in_{\mu\nu\rho\sigma} u^\mu v^\nu \frac{Dv^\rho}{Ds} z^\sigma,$$

$$\varphi = \left(g_{\mu\nu} \frac{Dz^\mu}{Ds} \frac{Dz^\nu}{Ds}\right)^{1/2}.$$

In particular, we note that, the twist scalar τ measures the twist of the curve ℓ in $\mathbb{S}^4$ due to microspin.

At this point, we see that our equations of motion describe a "minimal" geodesic motion (with intrinsic spin) when $\phi = 0$. In other words, if

$$\frac{Du^\mu}{Ds} = 0,$$
$$\frac{Dv^\mu}{Ds} = \tau w^\mu,$$
$$\frac{Dw^\mu}{Ds} = \tau v^\mu + \varphi z^\mu,$$
$$\frac{Dz^\mu}{Ds} = \varphi w^\mu.$$

However, in general, any material motion in $\mathbb{S}^4$ will not follow the condition $\phi = 0$. This is true especially for the motion of a physical object with structure. In general, any physical object can be regarded as a collection of points (with different orientations) obeying our general equations of motion. It is therefore clear that $\phi \neq 0$ for a moving finite physical object (with structure) whose material points cannot be homogeneously oriented.

Furthermore, it can be shown that the gradient of the unit velocity vector can be decomposed according to

$$\nabla_\nu u_\mu = \alpha_{\mu\nu} + \beta_{\mu\nu} + \frac{1}{6} h_{\mu\nu} \bar{\theta} + u_\nu a_\mu$$

where

$$h_{\mu\nu} = g_{\mu\nu} - u_\mu u_\nu,$$

$$\alpha_{\mu\nu} = \frac{1}{4} h^\alpha_\mu h^\beta_\nu \left(\nabla_\alpha u_\beta + \nabla_\beta u_\alpha\right) =$$
$$= \frac{1}{4} h^\alpha_\mu h^\beta_\nu \left(\hat{\nabla}_\alpha u_\beta + \hat{\nabla}_\beta u_\alpha\right) - \frac{1}{2} h^\alpha_\mu h^\beta_\nu K^\sigma_{(\alpha\beta)} u_\sigma,$$

$$\beta_{\mu\nu} = \frac{1}{4} h^\alpha_\mu h^\beta_\nu \left(\nabla_\alpha u_\beta - \nabla_\beta u_\alpha\right) =$$
$$= \frac{1}{4} h^\alpha_\mu h^\beta_\nu \left(\hat{\nabla}_\alpha u_\beta - \hat{\nabla}_\beta u_\alpha\right) - \frac{1}{2} h^\alpha_\mu h^\beta_\nu K^\sigma_{[\alpha\beta]} u_\sigma,$$

$$\bar{\theta} = \nabla_\mu u^\mu,$$

$$a_\mu = \frac{Du_\mu}{Ds}.$$

Note that

$$h_{\mu\nu}\,u^{\nu} = \alpha_{\mu\nu}\,u^{\nu} = \beta_{\mu\nu}\,u^{\nu} = 0\,,$$

$$K^{\sigma}_{(\alpha\beta)} = -g^{\sigma\lambda}\left(g_{\alpha\eta}\,\Gamma^{\eta}_{[\lambda\beta]} + g_{\beta\eta}\,\Gamma^{\eta}_{[\lambda\alpha]}\right),$$

$$K^{\sigma}_{[\alpha\beta]} = \Gamma^{\sigma}_{[\alpha\beta]}\,.$$

Meanwhile, with the help of the identities

$$u^{\lambda}\nabla_{\nu}\nabla_{\lambda}\,u_{\mu} = \nabla_{\nu}\left(u^{\lambda}\nabla_{\lambda}\,u_{\mu}\right) - \left(\nabla_{\nu}\,u_{\lambda}\right)\left(\nabla^{\lambda}u_{\mu}\right) =$$

$$= \nabla_{\nu}\,a_{\mu} - \left(\nabla_{\nu}\,u_{\lambda}\right)\left(\nabla^{\lambda}u_{\mu}\right),$$

$$u^{\lambda}\left(\nabla_{\nu}\,\nabla_{\lambda} - \nabla_{\lambda}\nabla_{\nu}\right)u_{\mu} = R^{\sigma}{}_{\mu\lambda\nu}\,u_{\sigma}\,u^{\lambda} - 2\Gamma^{\sigma}_{[\lambda\nu]}u^{\lambda}\nabla_{\sigma}u_{\mu}\,,$$

we obtain

$$\frac{D\bar{\theta}}{Ds} = \nabla_{\mu}a^{\mu} - (\nabla_{\mu}u^{\nu})(\nabla_{\nu}u^{\mu}) - R_{\mu\nu}u^{\mu}u^{\nu} + 2\Gamma^{\sigma}_{[\mu\nu]}u^{\mu}\nabla_{\sigma}u^{\nu}$$

for the "rate of shear" of a moving material object with respect to the world-line.

6 The variational principle for the theory

Let us now derive the field equations of the present theory by means of the variational principle. Considering thermodynamic effects, in general, our theory can best be described by the following Lagrangian density:

$$\bar{L} = \bar{L}_1 + \bar{L}_2 + \bar{L}_3$$

where

$$\bar{L}_1 = \frac{1}{\kappa}\sqrt{\det(g)}\,\times$$

$$\times\left(R^{\mu\nu}\left(\nabla_{\nu}\,\xi_{\mu} - D_{\mu\nu}\right) - \frac{1}{2}\left(\Phi - D^{\mu}{}_{\mu}\right)R\right),$$

$$\bar{L}_2 = \sqrt{\det(g)}\left(\frac{1}{2}\,C^{\mu\nu}{}_{\rho\sigma}\,D_{\mu\nu}D^{\rho\sigma} + \right.$$

$$\left. + \frac{1}{3}\,K^{\mu\nu}{}_{\rho\sigma\lambda\eta}\,D_{\mu\nu}D^{\rho\sigma}D^{\lambda\eta} - \Theta D^{\mu}{}_{\mu}\Delta T\right),$$

$$\bar{L}_3 = \sqrt{\det(g)}\,u^{\mu}\left(\nabla_{\mu}\,\xi_{\nu}\right)\left(f\xi^{\nu} - \rho u^{\nu}\right),$$

where Θ is a thermal coefficient, ΔT is (the change in) the temperature, and f is a generally varying scalar entity. Note that here we have only explicitly assumed that $\Phi = \nabla_{\mu}\,\xi^{\mu}$.

Alternatively, we can express $\bar{L}$ as follows:

$$\bar{L}_1 = \frac{1}{\kappa}\sqrt{\det(g)}\left(R^{\mu\nu} - \frac{1}{2}\,g^{\mu\nu}R\right)\left(\nabla_{\nu}\,\xi_{\mu} - D_{\mu\nu}\right).$$

Hence we have

$$\bar{L} = \sqrt{\det(g)}\left\{T^{\mu\nu}\left(\nabla_{\nu}\,\xi_{\mu} - D_{\mu\nu}\right) + \right.$$

$$+ \frac{1}{2}\,C^{\mu\nu}{}_{\rho\sigma}\,D_{\mu\nu}D^{\rho\sigma} + \frac{1}{3}\,K^{\mu\nu}{}_{\rho\sigma\lambda\eta}\,D_{\mu\nu}D^{\rho\sigma}D^{\lambda\eta} -$$

$$\left. - \Theta D^{\mu}{}_{\mu}\Delta T + u^{\mu}\left(\nabla_{\mu}\,\xi_{\nu}\right)\left(f\xi^{\nu} - \rho u^{\nu}\right)\right\}.$$

We then arrive at the following invariant integral:

$$I = \int\limits_{\mathbb{S}^4}\left\{T^{\mu\nu}\left(\nabla_{(\nu}\,\xi_{\mu)} - \Phi_{\mu\nu}\right) + T^{\mu\nu}\left(\nabla_{(\nu}\,\xi_{\mu)} - \omega_{\mu\nu}\right) + \right.$$

$$+ \frac{1}{2}\,A^{\mu\nu}{}_{\rho\sigma}\Phi_{\mu\nu}\Phi^{\rho\sigma} + \frac{1}{2}\,B^{\mu\nu}{}_{\rho\sigma}\omega_{\mu\nu}\,\omega^{\rho\sigma} +$$

$$+ \frac{1}{3}\,P^{\mu\nu}{}_{\rho\sigma\lambda\eta}\,\Phi_{\mu\nu}\,\Phi^{\rho\sigma}\,\Phi^{\lambda\eta} + \frac{1}{3}\,Q^{\mu\nu}{}_{\rho\sigma\lambda\eta}\omega_{\mu\nu}\omega^{\rho\sigma}\,\omega^{\lambda\eta} -$$

$$\left. - \Theta D^{\mu}{}_{\mu}\,\Delta T + u^{\mu}\left(\nabla_{\mu}\,\xi_{\nu}\right)\left(f\,\xi^{\nu} - \rho\,u^{\nu}\right)\right\}d\Sigma$$

where $d\Sigma = \sqrt{\det(g)}\;dx^0dx^1dx^2dx^3$ is the proper four-dimensional differential volume.

Writing $\bar{L} = \sqrt{\det(g)}\,L$ and employing the variational principle, we then have

$$\delta I = \int\limits_{\mathbb{S}^4}\left\{\frac{\partial L}{\partial T^{\mu\nu}}\,\delta T^{\mu\nu} + \frac{\partial L}{\partial\Phi^{\mu\nu}}\,\delta\Phi^{\mu\nu} + \frac{\partial L}{\partial\omega^{\mu\nu}}\,\delta\omega^{\mu\nu} + \right.$$

$$\left. + \frac{\partial L}{\partial\left(\nabla_{\mu}\,\xi_{\nu}\right)}\,\delta\left(\nabla_{\mu}\,\xi_{\nu}\right)\right\}d\Sigma = 0\,.$$

Now

$$\int\limits_{\mathbb{S}^4}\frac{\partial L}{\partial\left(\nabla_{\mu}\,\xi_{\nu}\right)}\,\delta\left(\nabla_{\mu}\,\xi_{\nu}\right)d\Sigma = \int\limits_{\mathbb{S}^4}\nabla_{\mu}\left(\frac{\partial L}{\partial\left(\nabla_{\mu}\,\xi_{\nu}\right)}\,\delta\xi_{\nu}\right)d\Sigma -$$

$$-\int\limits_{\mathbb{S}^4}\nabla_{\mu}\left(\frac{\partial L}{\partial\left(\nabla_{\mu}\,\xi_{\nu}\right)}\right)\delta\xi_{\nu}d\Sigma = -\int\limits_{\mathbb{S}^4}\nabla_{\mu}\left(\frac{\partial L}{\partial\left(\nabla_{\mu}\,\xi_{\nu}\right)}\right)\delta\xi_{\nu}\,d\Sigma$$

since the first term on the right-hand-side of the first line is an absolute differential that can be transformed away on the boundary of integration by means of the divergence theorem. Hence we have

$$\delta I = \int\limits_{\mathbb{S}^4}\left\{\frac{\partial L}{\partial T^{\mu\nu}}\,\delta T^{\mu\nu} + \frac{\partial L}{\partial\Phi^{\mu\nu}}\,\delta\Phi^{\mu\nu} + \frac{\partial L}{\partial\omega^{\mu\nu}}\,\delta\omega^{\mu\nu} - \right.$$

$$\left. - \nabla_{\mu}\left(\frac{\partial L}{\partial\left(\nabla_{\mu}\,\xi_{\nu}\right)}\right)\delta\xi_{\nu}\right\}d\Sigma = 0$$

where each term in the integrand is independent of the others. We may also note that the variations $\delta T^{\mu\nu}$, $\delta\Phi^{\mu\nu}$, $\delta\omega^{\mu\nu}$, and $\delta\xi_{\nu}$ are arbitrary.

From $\frac{\partial L}{\partial T^{\mu\nu}} = 0$, we obtain

$$\Phi_{\mu\nu} = \nabla_{(\nu}\,\xi_{\mu)}\,,$$

$$\omega_{\mu\nu} = \nabla_{[\nu}\,\xi_{\mu]}\,,$$

i.e., the covariant components of the "dilation" and intrinsic spin tensors, respectively.

From $\frac{\partial L}{\partial\Phi^{\mu\nu}} = 0$, we obtain

$$T^{(\mu\nu)} = \frac{1}{\kappa}\left(R^{(\mu\nu)} - \frac{1}{2}\,g^{\mu\nu}R\right) =$$

$$= A^{\mu\nu}{}_{\rho\sigma}\Phi^{\rho\sigma} + P^{\mu\nu}{}_{\rho\sigma\lambda\eta}\Phi^{\rho\sigma}\Phi^{\lambda\eta} - \Theta g^{\mu\nu}\Delta T$$

i.e., the symmetric contravariant components of the energy-momentum tensor.

In other words,

$$T^{\mu\nu} = \frac{1}{\kappa}\left(R^{\mu\nu} - \frac{1}{2}\,g^{\mu\nu}R\right) =$$

$$= C^{\mu\nu}{}_{\rho\sigma}\,D^{\rho\sigma} + K^{\mu\nu}{}_{\rho\sigma\lambda\eta}\,D^{\rho\sigma}D^{\lambda\eta} - \Theta g^{\mu\nu}\Delta T\,.$$

Finally, we now show in detail that the fourth variation yields an important equation of motion. We first see that

$$\frac{\partial L}{\partial\left(\nabla_\mu\,\xi_\nu\right)} = T^{\mu\nu} + u^\mu\left(f\xi^\nu - \rho u^\nu\right).$$

Hence

$$\nabla_\mu\left(\frac{\partial L}{\partial\left(\nabla_\mu\,\xi_\nu\right)}\right) = \nabla_\mu T^{\mu\nu} + \nabla_\mu\left(f\,u^\mu\right)\xi^\nu +$$

$$+ f\,u^\mu\,\nabla_\mu\,\xi^\nu - \nabla_\mu\left(\rho\,u^\mu\right)u^\nu - \rho u^\mu\nabla_\mu\,u^\nu.$$

Let us define the "extended" shear scalar and the mass current density vector, respectively, via

$$l = \nabla_\mu\left(fu^\mu\right),$$

$$J^\mu = \rho\,u^\mu.$$

We can now readily identify the acceleration vector and the body force per unit mass, respectively, by

$$a^\mu = u^\nu\,\nabla_\nu\,a^\mu = \frac{Du^\mu}{Ds}\,,$$

$$b^\mu = \frac{1}{\rho}\left(l\,\xi^\mu + f\left(1 - \nabla_\nu\,J^\nu\right)u^\mu\right).$$

In the conservative case, the condition $\nabla_\mu\,J^\mu = 0$ gives

$$\frac{D\rho}{Ds} = -\,\rho\,\nabla_\mu\,u^\mu.$$

In the weak-field limit for which $u^\mu = \left(1, u^A\right)$ (where $A = 1, 2, 3$) we obtain the ordinary continuity equation,

$$\frac{\partial\rho}{\partial t} + \nabla_A\left(\rho\,u^A\right) = 0\,.$$

Finally, we have

$$\int\limits_{\mathbb{S}^4}\left(\nabla_\mu T^{\mu\nu} + \rho\,b^\nu - \rho\,a^\nu\right)\delta\xi_\nu d\Sigma = 0$$

i.e., the equation of motion

$$\nabla_\mu\,T^{\mu\nu} = \rho\,\left(a^\nu - b^\nu\right)$$

or

$$\nabla_\mu\left(R^{\mu\nu} - \frac{1}{2}\,g^{\mu\nu}R\right) = \kappa\rho\left(a^\nu - b^\nu\right).$$

If we restrict our attention to point-like particles, the body force vanishes since it cannot act on a structureless (zero-dimensional) object. And since the motion is geodesic, i.e., $a^\mu = 0$, we have the conservation law

$$\nabla_\mu\,T^{\mu\nu} = 0\,.$$

In this case, this conservation law is true regardless of whether the energy-momentum tensor is symmetric or not.

Let us now discuss the so-called couple stress, i.e., the couple per unit area which is also known as the distributed moment. We denote the couple stress tensor by the second-rank tensor field M. In analogy to the linear constitutive relations relating the energy-momentum tensor to the displacement gradient tensor, we write

$$M^{\mu\nu} = J^{\mu\nu}{}_{\rho\sigma}\,L^{\rho\sigma} + H^{\mu\nu}{}_{\rho\sigma\lambda\eta}\,L^{\rho\sigma}L^{\lambda\eta}$$

where

$$J_{\mu\nu\rho\sigma} = E_{\mu\nu\rho\sigma} + F_{\mu\nu\rho\sigma}\,,$$

$$H_{\mu\nu\rho\sigma\lambda\eta} = U_{\mu\nu\rho\sigma\lambda\eta} + V_{\mu\nu\rho\sigma\lambda\eta}\,.$$

These are assumed to possess the same symmetry properties as $C_{\mu\nu\rho\sigma}$ and $K_{\mu\nu\rho\sigma\lambda\eta}$, respectively, i.e., $E_{\mu\nu\rho\sigma}$ have the same symmetry properties as $A_{\mu\nu\rho\sigma}$, $F_{\mu\nu\rho\sigma}$ have the same symmetry properties as $B_{\mu\nu\rho\sigma}$, $U_{\mu\nu\rho\sigma\lambda\eta}$ have the same symmetry properties as $P_{\mu\nu\rho\sigma\lambda\eta}$, and $V_{\mu\nu\rho\sigma\lambda\eta}$ have the same symmetry properties as $Q_{\mu\nu\rho\sigma\lambda\eta}$.

Likewise, the asymmetric tensor given by

$$L_{\mu\nu} = L_{(\mu\nu)} + L_{[\mu\nu]}$$

is comparable to the displacement gradient tensor.

Introducing a new infinitesimal spin potential via ϕ_μ, let the covariant dual form of the intrinsic spin tensor be given by

$$\bar{\omega}_{\mu\nu} = \frac{1}{2}\in_{\mu\nu\rho\sigma}\omega^{\rho\sigma} = \frac{1}{2}\left(\nabla_\nu\,\phi_\mu - \nabla_\mu\,\phi_\nu\right).$$

Let us now introduce a completely anti-symmetric third-rank spin tensor via

$$S^{\mu\nu\rho} = -\frac{1}{2}\left(\beta - \gamma\right)\in^{\mu\nu\rho\sigma}\phi_\sigma\,.$$

As a direct consequence, we see that

$$\nabla_\rho\,S^{\mu\nu\rho} = \left(\beta - \gamma\right)\omega^{\mu\nu}$$

In other words,

$$\nabla_\rho\,S^{\mu\nu\rho} = T^{[\mu\nu]} - N^{\mu\nu} = \frac{1}{\kappa}\left(R^{[\mu\nu]} - \Lambda^{\mu\nu}\right)$$

where

$$N^{\mu\nu} = 2\left(b_4 + b_6\right)\Phi\,\omega^{\mu\nu} + \left(b_8 + b_{10}\right)\times$$

$$\times\left(D^{\mu\rho}\Phi^\nu{}_\rho - D^{\nu\rho}\Phi^\mu{}_\rho\right) + \left(b_9 + b_9\right)\left(D^{\mu\rho}\omega^\nu{}_\rho - D^{\nu\rho}\omega^\mu{}_\rho\right),$$

$$\Lambda^{\mu\nu} = c_8\Phi\,\omega^{\mu\nu} + \frac{1}{2}\left(c_9 + c_{11}\right)\left(D^{\mu\rho}\Phi^\nu{}_\rho - D^{\nu\rho}\Phi^\mu{}_\rho\right) +$$

$$+\frac{1}{2}\left(c_{10} + c_{11}\right)\left(D^{\mu\rho}\omega^\nu{}_\rho - D^{\nu\rho}\omega^\mu{}_\rho\right).$$

We can now form the second Lagrangian density of our theory as

$$\bar{H} = \sqrt{\det(g)}\Big\{ M^{\mu\nu}\left(\nabla_\nu \phi_\mu - L_{\mu\nu}\right) + \frac{1}{2} J^{\mu\nu}{}_{\rho\sigma} L_{\mu\nu} L^{\rho\sigma} + \\ + \frac{1}{3} H^{\mu\nu}{}_{\rho\sigma\lambda\eta} L_{\mu\nu} L^{\rho\sigma} L^{\lambda\eta} - \in^{\mu}{}_{\rho\sigma\lambda} \left(\nabla_\nu \phi_\mu\right) S^{\rho\sigma\nu} u^\lambda + \\ + u^\mu \left(\nabla_\mu \phi_\nu\right)\left(h\phi^\nu - I\rho s^\nu\right)\Big\}$$

where h is a scalar function, I is the moment of inertia, and s^ν are the components of the angular velocity vector.

Letting $L_{(\mu\nu)} = X_{\mu\nu}$ and $L_{[\mu\nu]} = Z_{\mu\nu}$, the corresponding action integral is

$$J = \int\limits_{\mathbb{S}^4} \Big\{ M^{\mu\nu}\left(\nabla_{(\nu}\phi_{\mu)} - X_{\mu\nu}\right) + M^{\mu\nu}\left(\nabla_{[\nu}\phi_{\mu]} - Z_{\mu\nu}\right) + \\ + \frac{1}{2} E^{\mu\nu}{}_{\rho\sigma} X_{\mu\nu} X^{\rho\sigma} + \frac{1}{2} F^{\mu\nu}{}_{\rho\sigma} Z_{\mu\nu} Z^{\rho\sigma} + \\ + \frac{1}{3} U^{\mu\nu}{}_{\rho\sigma\lambda\eta} X_{\mu\nu} X^{\rho\sigma} X^{\lambda\eta} + \frac{1}{3} V^{\mu\nu}{}_{\rho\sigma\lambda\eta} Z_{\mu\nu} Z^{\rho\sigma} Z^{\lambda\eta} - \\ - \in^{\mu}{}_{\rho\sigma\lambda}\left(\nabla_\nu \phi_\mu\right) S^{\rho\sigma\nu} u^\lambda + u^\mu\left(\nabla_\mu \phi_\nu\right)\left(h\phi^\nu - I\rho s^\nu\right)\Big\} d\Sigma\,.$$

As before, writing $\bar{H} = \sqrt{\det(g)}H$ and performing the variation $\delta J = 0$, we have

$$\delta J = \int\limits_{\mathbb{S}^4} \Big\{ \frac{\partial H}{\partial M^{\mu\nu}} \delta M^{\mu\nu} + \frac{\partial H}{\partial X^{\mu\nu}} \delta X^{\mu\nu} + \\ + \frac{\partial H}{\partial Z^{\mu\nu}} \delta Z^{\mu\nu} - \nabla_\mu \left(\frac{\partial H}{\partial\left(\nabla_\mu \phi_\nu\right)} \right) \delta\phi_\nu \Big\} d\Sigma = 0$$

with arbitrary variations $\delta M^{\mu\nu}$, $\delta X^{\mu\nu}$, $\delta Z^{\mu\nu}$, and $\delta\phi_\nu$.

From $\frac{\partial H}{\partial M^{\mu\nu}} = 0$, we obtain

$$X_{\mu\nu} = \nabla_{(\nu}\phi_{\mu)}\,,$$

$$Z_{\mu\nu} = \nabla_{[\nu}\phi_{\mu]}\,.$$

From $\frac{\partial H}{\partial X^{\mu\nu}} = 0$, we obtain

$$M^{(\mu\nu)} = E^{\mu\nu}{}_{\rho\sigma} X^{\rho\sigma} + U^{\mu\nu}{}_{\rho\sigma\lambda\eta} X^{\rho\sigma} X^{\lambda\eta}\,.$$

From $\frac{\partial H}{\partial Z^{\mu\nu}} = 0$, we obtain

$$M^{[\mu\nu]} = F^{\mu\nu}{}_{\rho\sigma} Z^{\rho\sigma} + V^{\mu\nu}{}_{\rho\sigma\lambda\eta} Z^{\rho\sigma} Z^{\lambda\eta}\,.$$

We therefore have the constitutive relation

$$M^{\mu\nu} = J^{\mu\nu}{}_{\rho\sigma} L^{\rho\sigma} + H^{\mu\nu}{}_{\rho\sigma\lambda\eta} L^{\rho\sigma} L^{\lambda\eta}\,.$$

Let us investigate the last variation

$$-\int\limits_{\mathbb{S}^4} \nabla_\mu \left(\frac{\partial H}{\partial\left(\nabla_\mu \phi_\nu\right)} \right) \delta\phi_\nu \, d\Sigma = 0$$

in necessary detail.

Firstly,

$$\frac{\partial H}{\partial\left(\nabla_\mu \phi_\nu\right)} = M^{\mu\nu} - \in^{\nu}{}_{\lambda\rho\sigma} S^{\lambda\rho\mu} u^\sigma + u^\mu\left(h\phi^\nu - I\rho s^\nu\right).$$

Then we see that

$$\nabla_\mu \left(\frac{\partial H}{\partial\left(\nabla_\mu \phi_\nu\right)} \right) = \nabla_\mu M^{\mu\nu} - \\ - \in^{\nu}{}_{\mu\rho\sigma} T^{[\mu\rho]} u^\sigma - \in^{\nu}{}_{\lambda\rho\sigma} S^{\lambda\rho\mu} \nabla_\mu u^\sigma + \nabla_\mu\left(hu^\mu\right)\phi^\nu + \\ + h u^\mu \nabla_\mu \phi^\nu - I\nabla_\mu\left(\rho u^\mu\right) s^\nu - I\rho u^\mu \nabla_\mu s^\nu.$$

We now define the angular acceleration by

$$\alpha^\mu = u^\nu \nabla_\nu s^\mu = \frac{Ds^\mu}{Ds}$$

and the angular body force per unit mass by

$$\beta^\mu = \frac{1}{\rho}\left(\bar{l}\,\phi^\mu + h\frac{D\phi^\mu}{Ds} - I\left(\nabla_\nu J^\nu\right) s^\mu \right)$$

where $\bar{l} = \nabla_\mu\left(hu^\mu\right)$.

We have

$$\int\limits_{\mathbb{S}^4} \Big\{ \nabla_\mu M^{\mu\nu} - \in^{\nu}_{\mu\rho\sigma} \left(T^{[\mu\rho]} u^\sigma + S^{\mu\rho\lambda}\nabla_\lambda u^\sigma \right) + \\ + \rho\beta^\nu - I\rho\alpha^\nu \Big\} \delta\phi_\nu \, d\Sigma = 0\,.$$

Hence we obtain the equation of motion

$$\nabla_\mu M^{\mu\nu} = \in^{\nu}{}_{\mu\rho\sigma} \times \\ \times \left\{ \left(T^{[\mu\rho]} - N^{\mu\rho} \right) u^\sigma + S^{\mu\rho\lambda}\nabla_\lambda u^\sigma \right\} + \rho\left(I\alpha^\nu - \beta^\nu\right)$$

i.e.,

$$\nabla_\mu M^{\mu\nu} = \in^{\nu}{}_{\mu\rho\sigma} \times \\ \times \left\{ \frac{1}{\kappa}\left(R^{[\mu\rho]} - \Lambda^{\mu\rho} \right) u^\sigma + S^{\mu\rho\lambda}\nabla_\lambda u^\sigma \right\} + \rho\left(I\alpha^\nu - \beta^\nu\right).$$

7 Final remarks

We have seen that the classical fields of physics can be unified in a simple manner by treating space-time itself as a four-dimensional finite (but unbounded) elastic medium capable of undergoing extensions (dilations) and internal point-rotations in the presence of material-energy fields. In the present framework, the classical physical fields indeed appear on an equal footing as they are of purely geometric character. In addition, we must note that this apparent simplicity still leaves the constitutive invariants undetermined. At the moment, we leave this aspect of the theory to more specialized

attempts. However, it can be said, in general, that we expect the constitutive invariants of the theory to be functions of the known physical properties of matter such as material density, energy density, compressibility, material symmetry, etc. This way, we have successfully built a significant theoretical framework that holds in all classical physical situations.

We would also like to remark that once the constitutive invariants are determined and incorporated into the possible equations of state, the fully non-linear formulation of the present theory should be very satisfactory for describing the dynamics of astrophysical objects especially various fluids which exhibit the characteristics of non-degenerate relativistic and non-Newtonian fluids.

We have seen that the general dynamical behavior of a material body as determined by the equations of motion given in Section 5, is intrinsically related to the underlying geometry of the space-time continuum which in turn is largely determined by the constitutive relations given in Sections 3 and 4. In Section 6, we have also constructed a framework in which the motion of a point-like particle is always subject to the conservation law of matter and energy regardless of the particle's intrinsic spin.

We also note that a material body in our continuum representation of space-time can be regarded as the three-dimensional boundary of a so-called world-tube such that outside the world-tube the region is said to be free or empty. This three-dimensional boundary can be represented by a time-like hypersurface. Such hypersurfaces can be seen as disturbances in the space-time continuum. Furthermore, such disturbances are equivalent to three-dimensional representations of material waves (not necessarily gravitational waves). In this context, one may formulate the dynamic discontinuity conditions as purely geometric and kinematic compatibility conditions over the hypersurfaces.

In common with standard general relativity, a region of the space-time continuum is said to be statical if it can be covered by a space-time coordinate system relative to which the components of the metric tensor are independent of time. It may be that such a region can be covered by one or more such coordinate systems. As such, material waves are propagated into a fixed (three-dimensional) curved space along trajectories normal to the family of hypersurfaces given by the successive positions of a material body in the fixed space. In various cases, such trajectories can be represented as curves of zero length in the space-time continuum.

The microscopic substructure of the space-time continuum provides us room for additional degrees of freedom. In other words, there exist intrinsic length scales associated with these additional degrees of freedom. Correspondingly, one may define the so-called microrotational inertial field. In fact, the internal rotation of the points in the space-time continuum is seen as representing the intrinsic spin of elementary particles. On microscopic scales, the structure of the space-time continuum can indeed appear to be granular. Due to possible effects arising from this consideration, it is often not sufficient to model the space-time continuum itself as continuous, isotropic, and homogeneous. Furthermore, the rather predominant presence of twisting paths may give rise to particles exhibiting micropolar structure.

In geometrizing microspin phenomena, we emphasize that the initial microspin variables are not to be freely chosen to be included in the so-called elasticity scalar functional of the space-time continuum which is equivalent to a Lagrangian density. Rather, one must first identify them with the internal geometric properties of the space-time continuum. In other words, one must primarily unfold their underlying geometric existence in the space-time continuum itself. This is precisely what we have done in this work.

Finally, we note that geometric discontinuities can also be incorporated into the present theory. Such discontinuities can be seen as topological defects in the space-time continuum. Holographic four-dimensional continua with cellular, fibrous, or foamy structure may indeed represent admissible semi-classical models of the Universe which can be realized in the framework of the present theory. In such a case, the metric must therefore be quantized. It remains to be seen how this might correspond to any conventional quantum description of the space-time continuum.

Acknowledgements

I would like to sincerely thank D. Rabounski and S. J. Crothers for their kind assistance and the numerous discussions devoted to making this work appear in a somewhat more readable form.

Submitted on June 22, 2007
Accepted on July 04, 2007

References

1. Landau L. D. and Lifshitz E. M. Theory of elasticity. Pergamon, 1975.
2. Forest S. Mechanics of Cosserat media — an introduction. Ecole des Mines de Paris, Paris, 2005.
3. Sakharov A. D. *Dokl. Akad. Nauk USSR*, 1967, v. 177, 70.
4. Sokolov S. N. *Gen. Rel. Grav.*, 1995, v. 27, 1167.

SPECIAL REPORT

A New Semi-Symmetric Unified Field Theory of the Classical Fields of Gravity and Electromagnetism

Indranu Suhendro

Department of Physics, Karlstad University, Karlstad 651 88, Sweden
E-mail: spherical_symmetry@yahoo.com

We attempt to present a classical theoretical framework in which the gravitational and electromagnetic fields are unified as intrinsic geometric objects in the space-time manifold. For this purpose, we first present the preliminary geometric considerations dealing with the metric differential geometry of Cartan connections. The unified field theory is then developed as an extension of the general theory of relativity based on a semi-symmetric Cartan connection which is meant to be as close as possible structurally to the symmetric connection of the Einstein-Riemann space-time.

1 Introduction

It is now well-known that there are various paths available, provided by geometry alone, to a unified description of physical phenomena. The different possibilities for the interpretation of the underlying nature and fabric of the Universe in a purely geometric fashion imply that there is a deep underlying structural reason for singular harmony that lies in the depths of Nature's unity. It appears that the Universe is a self-descriptive continuum which connects what seem to be purely intrinsic mathematical objects to physical observables. It is the belief that analytical geometry alone is able to provide the profoundest description of the complexity and harmony of our structured Universe that has led generations of mathematicians and physicists to undertake the task of geometrizing the apparently systematic laws of Nature. Indeed this is, as Einstein once described, the effect of the sense of universal causation on the inquisitive mind.

The above-mentioned wealth of the inherent mathematical possibility for the geometrization of physics has resulted in the myriad forms of unified field theory which have been proposed from time to time, roughly since 1918 when H. Weyl's applied his so-called purely infinitesimal geometry which was a relaxation of the geometry of Riemann spaces to the task of geometrizing the electromagnetic field in the hope to unify it with the already geometrized gravitational field of general relativity [6]. However, often for want of simplicity, this fact which basically gives us a vision of a solid, reified reality may also lead us to think that the Universe of phenomena must be ultimately describable in the somewhat simplest and yet perhaps most elegant mathematical (i.e., geometric) formalism. Furthermore, when one is exposed to the different forms of unified field theory, especially for the first time, I believe it is better for one to see a less complicated version, otherwise one might get overloaded mentally and it follows that there is a chance that such a thing will just prevent one from absorbing the essence of our desired simplicity which is intuitively expected to be present in any objective task of unification.

Given the freedom of choice, we do not attempt, in this work, to speak about which version of unified field theory out of many is true, rather we shall present what I believe should qualify among the logically simplest geometric descriptions of the classical fields of gravity and electromagnetism. Indeed, for the reason that we may not still be fully aware of the many hidden aspects of the Universe on the microscopic (quantum) scales, at present we shall restrict our attention to the unification and geometrization of the classical fields alone.

As we know, there are many types of differential geometry, from affine geometry to non-affine geometry, from metric (i.e., metric-compatible) geometry to non-metric geometry. However, the different systems of differential geometry that have been developed over hundreds of years can be most elegantly cast in the language of Cartan geometry. The geometric system I will use throughout this physical part of our work is a metric-compatible geometry endowed with a semi-symmetric Cartan connection. It therefore is a variant of the so-called Riemann-Cartan geometry presented in Sections 1.1-1.6. As we know, the standard form of general relativity adopts the symmetric, twist-free, metric-compatible Christoffel connection. We are also aware that the various extensions of standard general relativity [7] tend to employ more general connections that are often asymmetric (e.g., the Sciama-Kibble theory [8, 9]) and even non-metric in general (e.g., the Weyl theory [6]). However, in the present work, we shall insist on logical simplicity and on having meaningful physical consequences. Once again, we are in no way interested in pointing out which geometric system is most relevant to physics, rather we are simply concerned with describing in detail what appears to be among the most consistent and accurate views of the physical world. We only wish to construct a unified field theory on the common foundation of beauty, simplicity, and observational accuracy without having to deal

with unnecessarily complex physical implications that might dull our perspective on the workings of Nature. I myself have always been fond of employing the most general type of connection for the purpose of unification. However, after years of poring over the almost universally held and (supposedly) objectively existing physical evidence, I have come to the conclusion that there is more reason to impose a simpler geometric formulation than a more general type of geometry such as non-metric geometry. In this work, it is my hope to dovetail the classical fields of gravity and electromagnetism with the conventional Riemann-Cartan geometry in general and with a newly constructed semi-symmetric Cartan connection in particular. Our resulting field equations are then just the distillation of this motive, which will eventually give us a penetrating and unified perspective on the nature of the classical fields of gravity and electromagnetism as *intrinsic* geometric fields, as well as on the possible interaction between the translational and rotational symmetries of the space-time manifold.

I believe that the semi-symmetric nature of the present theory (which keeps us as close as possible to the profound, observable physical implications of standard general relativity) is of great generality such that it can be applied to a large class of problems, especially problems related to the more general laws of motion for objects with structure.

2 A comprehensive evaluation of the differential geometry of Cartan connections with metric structure

The splendid, profound, and highly intuitive interpretation of differential geometry by E. Cartan, which was first applied to Riemann spaces, has resulted in a highly systematic description of a vast range of geometric and topological properties of differentiable manifolds. Although it possesses a somewhat abstract analytical foundation, to my knowledge there is no instance where Riemann-Cartan geometry, cast in the language of differential forms (i.e., exterior calculus), gives a description that is in conflict with the classical tensor analysis as formalized, e.g., by T. Levi-Civita. Given all its successes, one might expect that any physical theory, which relies on the concept of a field, can be elegantly built on its rigorous foundation. Therefore, as long as the reality of metric structure (i.e., metric compatibility) is assumed, it appears that a substantial modified geometry is not needed to supersede Riemann-Cartan geometry.

A common overriding theme in both mathematics and theoretical physics is that of unification. And as long as physics can be thought of as geometry, the geometric objects within Riemann-Cartan geometry (such as curvature for gravity and twist for intrinsic spin) certainly help us visualize and conceptualize the essence of unity in physics. Because of its intrinsic unity and its breadth of numerous successful applications, it might be possible for nearly all the laws governing physical phenomena to be combined and written down in compact form via the structural equations. By the intrinsic unity of Riemann-Cartan geometry, I simply refer to its tight interlock between algebra, analysis, group representation theory, and geometry. At least in mathematics alone, this is just as close as one can get to a "final" unified description of things. I believe that the unifying power of this beautiful piece of mathematics extends further still.

I'm afraid the title I have given to this first part of our work (which deals with the essential mathematics) has a somewhat narrow meaning, unlike the way it sounds. In writing this article, my primary goal has been to present Riemann-Cartan geometry in a somewhat simpler, more concise, and therefore more efficient form than others dealing with the same subject have done before [1, 4]. I have therefore had to drop whatever mathematical elements or representations that might seem somewhat highly counterintuitive at first. After all, not everyone, unless perhaps he or she is a mathematician, is familiar with abstract concepts from algebra, analysis, and topology, just to name a few. Nor is he or she expected to understand these things. But one thing remains essential, namely, one's ability to catch at least a glimpse of the beauty of the presented subject via deep, often simple, real understanding of its basics. As a non-mathematician (or simply a "dabbler" in pure mathematics), I do think that pure mathematics as a whole has grown extraordinarily "strange", if not complex (the weight of any complexity is really relative of course), with a myriad of seemingly separate branches, each of which might only be understood at a certain level of depth by the pure mathematicians specializing in that particular branch themselves. As such, a comparable complexity may also have occurred in the case of theoretical physics itself as it necessarily feeds on the latest formalism of the relevant mathematics each time. Whatever may be the case, the real catch is in the *essential understanding* of the basics. I believe simplicity alone will reveal it without necessarily having to diminish one's perspectives at the same time.

2.1 A brief elementary introduction to the Cartan (-Hausdorff) manifold $\mathbb{C}^\infty$

Let $\omega_a = \frac{\partial X^i}{\partial x^a} E_i = \partial_a X^i E_i$ (summation convention employed throughout this article) be the covariant (*frame*) basis spanning the n-dimensional base manifold $\mathbb{C}^\infty$ with local coordinates $x^a = x^a\left(X^k\right)$. The contravariant (*coframe*) basis θ^b is then given via the orthogonal projection $\left\langle \theta^b, \omega_a \right\rangle = \delta^b_a$, where δ^b_a are the components of the Kronecker delta (whose value is unity if the indices coincide or null otherwise). Now the set of linearly independent local directional derivatives $E_i = \frac{\partial}{\partial X^i} = \partial_i$ gives the coordinate basis of the locally flat tangent space $\mathbb{T}_x(M)$ at a point $x \in \mathbb{C}^\infty$. Here $\mathbb{M}$ denotes the topological space of the so-called n-tuples $h(x) = h\left(x^1, \ldots, x^n\right)$ such that relative to a given chart $\left(U, h(x)\right)$ on a neighborhood U of a local coordinate point, our $\mathbb{C}^\infty$-differentiable manifold itself is a topological space. The dual basis to E_i spanning the locally flat cotangent space $\mathbb{T}^*_x(\mathbb{M})$ will then

be given by the differential elements dX^k via the relation $\langle dX^k, \partial_i \rangle = \delta^k_i$. In fact and in general, the *one-forms* dX^k indeed act as a linear map $\mathbb{T}_x(\mathbb{M}) \to \mathbb{R}$ when applied to an arbitrary vector field $F \in \mathbb{T}_x(\mathbb{M})$ of the explicit form $F = F^i \frac{\partial}{\partial X^i} = f^a \frac{\partial}{\partial x^a}$. Then it is easy to see that $F^i = FX^i$ and $f^a = Fx^a$, from which we obtain the usual transformation laws for the contravariant components of a vector field, i.e., $F^i = \partial_a X^i f^a$ and $f^i = \partial_i x^a F^i$, relating the localized components of F to the general ones and vice versa. In addition, we also see that $\langle dX^k, F \rangle = FX^k = F^k$.

The components of the metric tensor $g = g_{ab}\theta^a \otimes \theta^b$ of the base manifold $\mathbb{C}^\infty$ are readily given by

$$g_{ab} = \langle \omega_a, \omega_b \rangle .$$

The components of the metric tensor $g(x_N) = \eta_{ik} dX^i \otimes dX^k$ describing the locally flat tangent space $\mathbb{T}_x(\mathbb{M})$ of rigid frames at a point $x_N = x_N(x^a)$ are given by

$$\eta_{ik} = \langle E_i, E_k \rangle = \operatorname{diag}(\pm 1, \pm 1, \ldots, \pm 1).$$

In four dimensions, the above may be taken to be the components of the Minkowski metric tensor, i.e., $\eta_{ik} = \langle E_i, E_k \rangle = \operatorname{diag}(1, -1, -1, -1)$.

Then we have the expression

$$g_{ab} = \eta_{ik}\, \partial_a X^i \partial_b X^k$$

satisfying

$$g_{ac} g^{bc} = \delta^b_a$$

where $g^{ab} = \langle \theta^a, \theta^b \rangle$.

The manifold $\mathbb{C}^\infty$ is a metric space whose line-element in this formalism of a differentiable manifold is directly given by the metric tensor itself, i.e.,

$$ds^2 = g = g_{ab} \left(\partial_i x^a \partial_k x^b \right) dX^i \otimes dX^k,$$

where the coframe basis is given by the one-forms $\theta^a = \partial_i x^a dX^i$.

2.2 Exterior calculus in n dimensions

As we know, an arbitrary tensor field $T \in \mathbb{C}^\infty$ of rank (p, q) is the object

$$T = T^{i_1 i_2 \ldots i_q}_{j_1 j_2 \ldots j_p} \omega_{i_1} \otimes \omega_{i_2} \otimes \ldots \otimes \omega_{i_q} \otimes \theta^{j_1} \otimes \theta^{j_2} \otimes \ldots \otimes \theta^{j_p}.$$

Given the existence of a local coordinate transformation via $x^i = x^i(\bar{x}^\alpha)$ in $\mathbb{C}^\infty$, the components of $T \in \mathbb{C}^\infty$ transform according to

$$T^{ij\ldots s}_{kl\ldots r} = T^{\alpha\beta\ldots\lambda}_{\mu\nu\ldots\eta} \partial_\alpha x^i \partial_\beta x^j \ldots \partial_\lambda x^s \partial_k \bar{x}^\mu \partial_l \bar{x}^\nu \ldots \partial_r \bar{x}^\eta.$$

Taking a local coordinate basis $\theta^i = dx^i$, a Pfaffian p-form ω is the completely anti-symmetric tensor field

$$\omega = \omega_{i_1 i_2 \ldots i_p} dx^{i_1} \wedge dx^{i_2} \wedge \ldots \wedge dx^{i_p},$$

where

$$dx^{i_1} \wedge dx^{i_2} \wedge \ldots \wedge dx^{i_p} \equiv \frac{1}{p!} \delta^{i_1 i_2 \ldots i_p}_{j_1 j_2 \ldots j_p} dx^{j_1} \otimes dx^{j_2} \otimes \ldots \otimes dx^{j_p}.$$

In the above, the $\delta^{i_1 i_2 \ldots i_p}_{j_1 j_2 \ldots j_p}$ are the components of the generalized Kronecker delta. They are given by

$$\delta^{i_1 i_2 \ldots i_p}_{j_1 j_2 \ldots j_p} = \in_{j_1 j_2 \ldots j_p} \in^{i_1 \ldots i_p} = \det \begin{pmatrix} \delta^{i_1}_{j_1} & \delta^{i_2}_{j_1} & \ldots & \delta^{i_p}_{j_1} \\ \delta^{i_1}_{j_2} & \delta^{i_2}_{j_2} & \ldots & \delta^{i_p}_{j_2} \\ \ldots & \ldots & \ldots & \ldots \\ \delta^{i_1}_{j_p} & \delta^{i_2}_{j_p} & \ldots & \delta^{i_p}_{j_p} \end{pmatrix}$$

where $\in_{j_1 j_2 \ldots j_p} = \sqrt{\det(g)}\, \epsilon_{j_1 j_2 \ldots j_p}$ and $\in^{i_1 i_2 \ldots i_p} = \frac{\epsilon^{i_1 i_2 \ldots i_p}}{\sqrt{\det(g)}}$ are the covariant and contravariant components of the completely anti-symmetric Levi-Civita permutation tensor, respectively, with the ordinary permutation symbols being given as usual by $\epsilon_{j_1 j_2 \ldots j_q}$ and $\epsilon^{i_1 i_2 \ldots i_p}$.

We can now write

$$\omega = \frac{1}{p!} \delta^{i_1 i_2 \ldots i_p}_{j_1 j_2 \ldots j_p} \omega_{i_1 i_2 \ldots i_p} dx^{j_1} \wedge dx^{j_2} \wedge \ldots \wedge dx^{j_p}.$$

such that for a null p-form $\omega = 0$ its components satisfy the relation $\delta^{i_1 i_2 \ldots i_p}_{j_1 j_2 \ldots j_p} \omega_{i_1 i_2 \ldots i_p} = 0$.

By meticulously moving the dx^i from one position to another, we see that

$$dx^{i_1} \wedge dx^{i_2} \wedge \ldots \wedge dx^{i_{p-1}} \wedge dx^{i_p} \wedge dx^{j_1} \wedge dx^{j_2} \wedge \ldots$$
$$\ldots \wedge dx^{j_q} = (-1)^p dx^{i_1} \wedge dx^{i_2} \wedge \ldots \wedge dx^{i_{p-1}} \wedge dx^{j_1} \wedge$$
$$\wedge dx^{j_2} \wedge \ldots \wedge dx^{j_q} \wedge dx^{i_p}$$

and

$$dx^{i_1} \wedge dx^{i_2} \wedge \ldots \wedge dx^{i_p} \wedge dx^{j_1} \wedge dx^{j_2} \wedge \ldots \wedge dx^{j_q} =$$
$$= (-1)^{pq} dx^{j_1} \wedge dx^{j_2} \wedge \ldots \wedge dx^{j_q} \wedge dx^{i_1} \wedge dx^{i_2} \wedge \ldots$$
$$\ldots \wedge dx^{i_p}.$$

Let ω and π be a p-form and a q-form, respectively. Then, in general, we have the following relations:

$$\omega \wedge \pi = (-1)^{pq} \pi \wedge \omega = \omega_{i_1 i_2 \ldots i_p} \pi_{j_1 j_2 \ldots j_q} dx^{i_1} \wedge dx^{i_2} \wedge \ldots$$
$$\ldots \wedge dx^p \wedge dx^{j_1} \wedge dx^{j_2} \wedge \ldots \wedge dx^{j_q}$$

$$d(\omega + \pi) = d\omega + d\pi$$

$$d(\omega \wedge \pi) = d\omega \wedge \pi + (-1)^p \omega \wedge d\pi$$

Note that the mapping $d : \omega = d\omega$ is a $(p+1)$-form. Explicitly, we have

$$d\omega = \frac{(-1)^p}{(p+1)!} \delta^{i_1 i_2 \ldots i_p}_{j_1 j_2 \ldots j_p} \frac{\partial \omega_{i_1 i_2 \ldots i_p}}{\partial x^{i_{p+1}}} dx^{j_1} \wedge dx^{j_2} \wedge \ldots$$
$$\ldots \wedge dx^{j_p} \wedge dx^{i_{p+1}}.$$

For instance, given a (continuous) function f, the one-form $df = \partial_i f dx^i$ satisfies $d^2 f \equiv ddf = \partial_k \partial_i f dx^k \wedge dx^i = 0$. Likewise, for the one-form $A = A_i dx^i$, we have $dA = \partial_k A_i dx^k \wedge dx^i$ and therefore $d^2 A = \partial_l \partial_k A_i dx^l \wedge dx^k \wedge dx^i = 0$, i.e., $\delta^{ikl}_{rst} \partial_l \partial_k A_i = 0$ or $\partial_l \partial_k A_i + \partial_k \partial_i A_l + \partial_i \partial_l A_k = 0$. Obviously, the last result holds for arbitrary p-forms $\Pi^{ij\ldots s}_{kl\ldots r}$, i.e.,

$$d^2 \Pi^{ij\ldots s}_{kl\ldots r} = 0 .$$

Let us now consider a simple two-dimensional case. From the transformation law $dx^i = \partial_\alpha x^i d\bar{x}^\alpha$, we have, upon employing a positive definite Jacobian, i.e., $\frac{\partial (x^i, x^j)}{\partial (\bar{x}^\alpha, \bar{x}^\beta)} > 0$, the following:

$$dx^i \wedge dx^j = \partial_\alpha x^i \partial_\beta x^j d\bar{x}^\alpha \wedge d\bar{x}^\beta = \frac{1}{2} \frac{\partial \left(x^i, x^j\right)}{\partial \left(\bar{x}^\alpha, \bar{x}^\beta\right)} d\bar{x}^\alpha \wedge d\bar{x}^\beta .$$

It is easy to see that

$$dx^1 \wedge dx^2 = \frac{\partial \left(x^1, x^2\right)}{\partial \left(\bar{x}^1, \bar{x}^2\right)} d\bar{x}^1 \wedge d\bar{x}^2 .$$

which gives the correct transformation law of a surface element.

We can now elaborate on the so-called *Stokes theorem*. Given an arbitrary function f, the integration in a domain D in the manifold $\mathbb{C}^\infty$ is such that

$$\iint\limits_D f\left(x^i\right) dx^1 \wedge dx^2 = \iint\limits_D f\left(x^i\left(\bar{x}^\alpha\right)\right) \frac{\partial \left(x^1, x^2\right)}{\partial \left(\bar{x}^1, \bar{x}^2\right)} d\bar{x}^1 d\bar{x}^2 .$$

Generalizing to n dimensions, for any $\psi^i = \psi^i\left(x^k\right)$ we have

$$d\psi^1 \wedge d\psi^2 \wedge \ldots \wedge d\psi^n = \frac{\partial \left(\psi^1, \psi^2, \ldots, \psi^n\right)}{\partial \left(x^1, x^2, \ldots, \bar{x}^n\right)} dx^1 \wedge dx^2 \wedge \ldots \wedge dx^n .$$

Therefore (in a particular domain)

$$\iint \ldots \int f d\psi^1 \wedge d\psi^2 \wedge \ldots \wedge d\psi^n = \iint \ldots \int f\left(x^i\right) \frac{\partial \left(\psi^1, \psi^2, \ldots, \psi^n\right)}{\partial \left(x^1, x^2, \ldots, x^n\right)} dx^1 \wedge dx^2 \wedge \ldots \wedge dx^n .$$

Obviously, the value of this integral is independent of the choice of the coordinate system. Under the coordinate transformation given by $x^i = x^i\left(\bar{x}^\alpha\right)$, the Jacobian can be expressed as

$$\frac{\partial \left(\psi^1, \psi^2, \ldots, \psi^n\right)}{\partial \left(x^1, x^2, \ldots, x^n\right)} = \frac{\partial \left(\psi^1, \psi^2, \ldots, \psi^n\right)}{\partial \left(\bar{x}^1, \bar{x}^2, \ldots, \bar{x}^n\right)} \frac{\partial \left(\bar{x}^1, \bar{x}^2, \ldots, \bar{x}^n\right)}{\partial \left(x^1, x^2, \ldots, x^n\right)} .$$

If we consider a $(n-m)$-dimensional subspace (hypersurface) $\mathbb{S} \in \mathbb{C}^\infty$ whose local coordinates u^A parametrize the coordinates x^i, we have

$$\iint \ldots \int f d\psi^1 \wedge d\psi^2 \wedge \ldots \wedge d\psi^n = \iint \ldots \int f\left(x^i\left(u^A\right)\right) \times \frac{\partial \left(\psi^1\left(x^i\left(u^A\right)\right), \psi^2\left(x^i\left(u^A\right)\right), \ldots, \psi^n\left(x^i\left(u^A\right)\right)\right)}{\partial \left(u^1, u^2, \ldots, u^{n-m}\right)} \times du^1 du^2 \ldots du^{n-m} .$$

2.3 Geometric properties of a curved manifold

Let us recall a few concepts from conventional tensor analysis for a while. Introducing a generally asymmetric connection Γ via the covariant derivative

$$\partial_b \omega_a = \Gamma^c_{ab} \omega_c$$

i.e.,

$$\Gamma^c_{ab} = \langle \theta^c, \partial_b \omega_a \rangle = \Gamma^c_{(ab)} + \Gamma^c_{[ab]}$$

where the round index brackets indicate symmetrization and the square ones indicate anti-symmetrization, we have, by means of the local coordinate transformation given by $x^a = x^a\left(\bar{x}^\alpha\right)$ in $\mathbb{C}^\infty$

$$\partial_b e^\alpha_a = \Gamma^c_{ab} e^\alpha_c - \bar{\Gamma}^\alpha_{\beta\lambda} e^\beta_a e^\lambda_b ,$$

where the tetrads of the *moving frames* are given by $e^\alpha_a = \partial_a \bar{x}^\alpha$ and $e^a_\alpha = \partial_\alpha x^a$. They satisfy $e^a_\alpha e^\alpha_b = \delta^a_b$ and $e^\alpha_a e^a_\beta = \delta^\alpha_\beta$. In addition, it can also be verified that

$$\partial_\beta e^a_\alpha = \bar{\Gamma}^\lambda_{\alpha\beta} e^a_\lambda - \Gamma^a_{bc} e^b_\alpha e^c_\beta \partial_b e^a_\alpha = e^a_\lambda \bar{\Gamma}^\lambda_{\alpha\beta} e^\beta_b - \Gamma^a_{cb} e^c_\alpha .$$

From conventional tensor analysis, we know that Γ is a non-tensorial object, since its components transform as

$$\Gamma^c_{ab} = e^c_\alpha \partial_b e^\alpha_a + e^c_\alpha \bar{\Gamma}^\alpha_{\beta\lambda} e^\beta_a e^\lambda_b .$$

However, it can be described as a kind of displacement field since it is what makes possible a comparison of vectors from point to point in $\mathbb{C}^\infty$. In fact the relation $\partial_b \omega_a = \Gamma^c_{ab} \omega_c$ defines the so-called metricity condition, i.e., the change (during a displacement) in the basis can be measured by the basis itself. This immediately translates into

$$\nabla_c g_{ab} = 0 ,$$

where we have just applied the notion of a covariant derivative to an arbitrary tensor field T:

$$\nabla_k T^{ij\ldots s}_{lm\ldots r} = \partial_k T^{ij\ldots s}_{lm\ldots r} + \Gamma^i_{pk} T^{pj\ldots s}_{lm\ldots r} + \Gamma^j_{pk} T^{ip\ldots s}_{lm\ldots r} + \ldots + \Gamma^s_{pk} T^{ij\ldots p}_{lm\ldots r} - \Gamma^p_{lk} T^{ij\ldots s}_{pm\ldots r} - \Gamma^p_{mk} T^{ij\ldots s}_{lp\ldots r} - \ldots - \Gamma^p_{rk} T^{ij\ldots s}_{lm\ldots p}$$

such that $\left(\partial_k T\right)^{ij\ldots s}_{lm\ldots r} = \nabla_k T^{ij\ldots s}_{lm\ldots r}$.

The condition $\nabla_c g_{ab} = 0$ can be solved to give

$$\Gamma^c_{ab} = \frac{1}{2} g^{cd} \left(\partial_b g_{da} - \partial_d g_{ab} + \partial_a g_{bd}\right) + \Gamma^c_{[ab]} - \\ - g^{cd} \left(g_{ae}\Gamma^e_{[db]} + g_{be}\Gamma^e_{[da]}\right)$$

from which it is customary to define

$$\Delta^c_{ab} = \frac{1}{2} g^{cd} \left(\partial_b g_{da} - \partial_d g_{ab} + \partial_a g_{bd}\right)$$

as the Christoffel symbols (symmetric in their two lower indices) and

$$K^c_{ab} = \Gamma^c_{[ab]} - g^{cd} \left(g_{ae}\Gamma^e_{[db]} + g_{be}\Gamma^e_{[da]}\right)$$

as the components of the so-called contwist tensor (antisymmetric in the first two mixed indices).

Note that the components of the twist tensor are given by

$$\Gamma^a_{[bc]} = \frac{1}{2} e^a_\alpha \left(\partial_c e^\alpha_b - \partial_b e^\alpha_c + e^\beta_b \bar{\Gamma}^\alpha_{\beta c} - e^\beta_c \bar{\Gamma}^\alpha_{\beta b}\right)$$

where we have set $\bar{\Gamma}^\alpha_{\beta c} = \bar{\Gamma}^\alpha_{\beta\lambda} e^\lambda_c$, such that for an arbitrary scalar field Φ we have

$$\left(\nabla_a \nabla_b - \nabla_b \nabla_a\right) \Phi = 2\Gamma^c_{[ab]} \nabla_c \Phi \,.$$

The components of the curvature tensor R of $\mathbb{C}^\infty$ are then given via the relation

$$\left(\nabla_q \nabla_p - \nabla_p \nabla_q\right) T^{ab\ldots s}_{cd\ldots r} = T^{ab\ldots s}_{wd\ldots r} R^w_{\ cpq} + T^{ab\ldots s}_{cw\ldots r} R^w_{\ dpq} + \\ \ldots + T^{ab\ldots s}_{cd\ldots w} R^w_{\ rpq} - T^{wb\ldots s}_{cd\ldots r} R^a_{\ wpq} - T^{aw\ldots s}_{cd\ldots r} R^b_{\ wpq} - \ldots \\ - T^{ab\ldots w}_{cd\ldots r} R^s_{\ wpq} - 2\Gamma^w_{[pq]} \nabla_w T^{ab\ldots s}_{cd\ldots r}$$

where

$$R^d_{\ abc} = \partial_b \Gamma^d_{ac} - \partial_c \Gamma^d_{ab} + \Gamma^e_{ac}\Gamma^d_{eb} - \Gamma^e_{ab}\Gamma^d_{ec} = \\ = B^d_{\ abc}\left(\Delta\right) + \hat{\nabla}_b K^d_{\ ac} - \hat{\nabla}_c K^d_{\ ab} + K^e_{\ ac} K^d_{\ eb} - K^e_{\ ab} K^d_{\ ec}$$

where $\hat{\nabla}$ denotes covariant differentiation with respect to the Christoffel symbols alone, and where

$$B^d_{\ abc}\left(\Delta\right) = \partial_b \Delta^d_{ac} - \partial_c \Delta^d_{ab} + \Delta^e_{ac}\Delta^d_{eb} - \Delta^e_{ab}\Delta^d_{ec}$$

are the components of the Riemann-Christoffel curvature tensor of $\mathbb{C}^\infty$.

From the components of the curvature tensor, namely, $R^d_{\ abc}$, we have (using the metric tensor to raise and lower indices)

$$R_{ab} \equiv R^c_{\ acb} = B_{ab}\left(\Delta\right) + \hat{\nabla}_c K^c_{ab} - K^c_{ad} K^d_{cb} - \\ - 2\hat{\nabla}_b \Gamma^c_{[ac]} + 2K^c_{ab}\Gamma^d_{[cd]}$$

$$R \equiv R^a_{\ a} = B\left(\Delta\right) - 4g^{ab}\hat{\nabla}_a \Gamma^c_{[bc]} - \\ - 2g^{ac}\Gamma^b_{[ab]}\Gamma^d_{[cd]} - K_{abc} K^{acb}$$

where $B_{ab}\left(\Delta\right) \equiv B^c_{\ acb}\left(\Delta\right)$ are the components of the symmetric Ricci tensor and $B\left(\Delta\right) \equiv B^a_{\ a}\left(\Delta\right)$ is the Ricci scalar. Note that $K_{abc} \equiv g_{ad} K^d_{bc}$ and $K^{acb} \equiv g^{cd} g^{be} K^a_{de}$.

Now since

$$\Gamma^b_{ba} = \Delta^b_{ba} = \Delta^b_{ab} = \partial_a \left(\ln \sqrt{\det\left(g\right)}\right)$$

$$\Gamma^b_{ab} = \partial_a \left(\ln \sqrt{\det\left(g\right)}\right) + 2\Gamma^b_{[ab]}$$

we see that for a continuous metric determinant, the so-called homothetic curvature vanishes:

$$H_{ab} \equiv R^c_{\ cab} = \partial_a \Gamma^c_{cb} - \partial_b \Gamma^c_{ca} = 0$$

Introducing the traceless Weyl tensor C, we have the following decomposition theorem:

$$R^d_{\ abc} = C^d_{\ abc} + \frac{1}{n-2}\left(\delta^d_b R_{ac} + g_{ac} R^d_{\ b} - \delta^d_c R_{ab} - g_{ab} R^d_{\ c}\right) + \\ + \frac{1}{(n-1)(n-2)}\left(\delta^d_c g_{ab} - \delta^d_b g_{ac}\right) R$$

which is valid for $n > 2$. For $n = 2$, we have

$$R^d_{\ abc} = K_G \left(\delta^d_b g_{ac} - \delta^d_c g_{ab}\right)$$

where

$$K_G = \frac{1}{2} R$$

is the Gaussian curvature of the surface. Note that (in this case) the Weyl tensor vanishes.

Any n-dimensional manifold (for which $n > 1$) with constant sectional curvature R and vanishing twist is called an Einstein space. It is described by the following simple relations:

$$R^d_{\ abc} = \frac{1}{n(n-1)}\left(\delta^d_b g_{ac} - \delta^d_c g_{ab}\right) R$$

$$R_{ab} = \frac{1}{n} g_{ab} R \,.$$

In the above, we note especially that

$$R^d_{\ abc} = B^d_{\ abc}\left(\Delta\right),$$

$$R_{ab} = B_{ab}\left(\Delta\right),$$

$$R = B\left(\Delta\right).$$

Furthermore, after some elaborate (if not tedious) algebra, we obtain, in general, the following *generalized* Bianchi identities:

$$R^a_{\ bcd} + R^a_{\ cdb} + R^a_{\ dbc} = -2\big(\partial_d \Gamma^a_{[bc]} + \\ + \partial_b \Gamma^a_{[cd]} + \partial_c \Gamma^a_{[db]} + \Gamma^a_{eb}\Gamma^e_{[cd]} + \Gamma^a_{ec}\Gamma^e_{[db]} + \Gamma^a_{ed}\Gamma^e_{[bc]}\big)$$

$$\nabla_e R^a_{\ bcd} + \nabla_c R^a_{\ bde} + \nabla_d R^a_{\ bec} = \\ = 2\left(\Gamma^f_{[cd]} R^a_{\ bfe} + \Gamma^f_{[de]} R^a_{\ bfc} + \Gamma^f_{[ec]} R^a_{\ bfd}\right)$$

$$\nabla_a \left(R^{ab} - \frac{1}{2} g^{ab} R\right) = 2g^{ab}\Gamma^c_{[da]} R^d_{\ c} + \Gamma^a_{[cd]} R^{cdb}_{\ \ a}$$

for any metric-compatible manifold endowed with both curvature and twist.

In the last of the above set of equations, we have introduced the generalized Einstein tensor, i.e.,

$$G_{ab} \equiv R_{ab} - \frac{1}{2} g_{ab} R .$$

In particular, we also have the following specialized identities, i.e., the *regular* Bianchi identities:

$$B^a{}_{bcd} + B^a{}_{cdb} + B^a{}_{dbc} = 0 ,$$

$$\hat{\nabla}_e B^a{}_{bcd} + \hat{\nabla}_c B^a{}_{bde} + \hat{\nabla}_d B^a{}_{bec} = 0$$

$$\hat{\nabla}_a \left(B^{ab} - \frac{1}{2} g^{ab} B \right) = 0 .$$

In general, these hold in the case of a symmetric, metric-compatible connection. Non-metric differential geometry is beyond the scope of our present consideration. We will need the identities presented in this section in the development of our semi-symmetric, metric-compatible unified field theory.

2.4 The structural equations

The results of the preceding section can be expressed in the language of exterior calculus in a somewhat more compact form.

In general, we can construct arbitrary p-forms $\omega^{ab\ldots e}_{cd\ldots f}$ through arbitrary $(p-1)$ forms $\alpha^{ab\ldots e}_{cd\ldots f}$, i.e.,

$$\omega^{ab\ldots e}_{cd\ldots f} = d\alpha^{ab\ldots e}_{cd\ldots f} = \frac{\partial \alpha^{ab\ldots e}_{cd\ldots f}}{\partial x^h} \wedge dx^h .$$

The covariant exterior derivative is then given by

$$D\omega^{ab\ldots e}_{cd\ldots f} = \nabla_h \omega^{ab\ldots e}_{cd\ldots f} \wedge dx^h$$

i.e.,

$$D\omega^{ab\ldots e}_{cd\ldots f} = d\omega^{ab\ldots e}_{cd\ldots f} + (-1)^p \left(\omega^{hb\ldots e}_{cd\ldots f} \wedge \Gamma^a_h + \right.$$
$$+ \omega^{ah\ldots e}_{cd\ldots f} \wedge \Gamma^b_h + \ldots + \omega^{ab\ldots h}_{cd\ldots f} \wedge \Gamma^e_h - \omega^{ab\ldots e}_{hd\ldots f} \wedge \Gamma^h_c -$$
$$\left. - \omega^{ab\ldots e}_{ch\ldots f} \wedge \Gamma^h_d - \ldots - \omega^{ab\ldots e}_{cd\ldots h} \wedge \Gamma^h_f \right)$$

where we have defined the connection one-forms by

$$\Gamma^a_b \equiv \Gamma^a_{bc} \theta^c$$

with respect to the coframe basis θ^a.

Now we write the twist two-forms τ^a as

$$\tau^a = D\theta^a = d\theta^a + \Gamma^a_b \wedge \theta^b .$$

This gives the first structural equation. With respect to another local coordinate system (with coordinates $\bar{x}^\alpha$) in $\mathbb{C}^\infty$ spanned by the basis $\epsilon^\alpha = e^\alpha_a \theta^a$, we see that

$$\tau^a = -e^a_\alpha \bar{\Gamma}^\alpha_{[\beta\lambda]} \varepsilon^\beta \wedge \varepsilon^\lambda .$$

We shall again proceed to define the curvature tensor. For a triad of arbitrary vectors u, v, w, we may define the following relations with respect to the frame basis ω_a:

$$\nabla_u \nabla_v w \equiv u^c \nabla_c \left(v^b \nabla_b w^a \right) \omega_a$$

$$\nabla_{[u,v]} w \equiv \nabla_b w^a \left(u^c \nabla_c v^b - v^c \nabla_c u^b \right)$$

where ∇_u and ∇_v denote covariant differentiation in the direction of u and of v, respectively.

Then we have

$$\left(\nabla_u \nabla_v - \nabla_v \nabla_u \right) w = {}^*R^a{}_{bcd} w^b u^c v^d \omega_a .$$

Note that

$${}^*R^a{}_{bcd} = \partial_c \Gamma^a_{bd} - \partial_d \Gamma^a_{bc} + \Gamma^e_{bd} \Gamma^a_{ec} - \Gamma^e_{bc} \Gamma^a_{ed} +$$
$$+ 2\Gamma^e_{[cd]} \Gamma^a_{be} = R^a{}_{bcd} + 2\Gamma^e_{[cd]} \Gamma^a_{be}$$

are the components of the extended curvature tensor ${}^*R$.

Define the curvature two-forms by

$${}^*R^a{}_b \equiv \frac{1}{2} {}^*R^a{}_{bcd} \theta^c \wedge \theta^d .$$

The second structural equation is then

$${}^*R^a{}_b = d\Gamma^a_b + \Gamma^a_c \wedge \Gamma^c_b .$$

The third structural equation is given by

$$d^2 \Gamma^a_b = d\,{}^*R^a{}_b - {}^*R^a{}_c \wedge \Gamma^c_b + \Gamma^a_c \wedge {}^*R^c{}_b = D\,{}^*R^a{}_b$$

which is equivalent to the generalized Bianchi identities given in the preceding section.

In fact the second and third structural equations above can be directly verified using the properties of exterior differentiation given in Section 1.2.

Now, as we have seen, the covariant exterior derivative of arbitrary one-forms ϕ^a is given by $D\phi^a = d\phi^a + \Gamma^a_b \wedge \phi^b$. Then

$$DD\phi^a = d\left(D\phi^a\right) + \Gamma^a_b \wedge D\phi^b =$$
$$= d\left(d\phi^a + \Gamma^a_b \wedge \phi^b \right) + \Gamma^a_c \wedge \left(d\phi^c + \Gamma^c_d \wedge \phi^d \right) =$$
$$= d\Gamma^a_b \wedge \phi^b - \Gamma^a_b \wedge \Gamma^b_c \wedge \phi^c =$$
$$= \left(d\Gamma^a_b + \Gamma^a_c \wedge \Gamma^c_b \right) \wedge \phi^b$$

where we have used the fact that the $D\phi^a$ are two-forms. Therefore, from the second structural equation, we have

$$DD\phi^a = {}^*R^a{}_b \wedge \phi^b .$$

Finally, taking $\phi^a = \theta^a$, we give the fourth structural equation as

$$DD\theta^a = D\tau^a = {}^*R^a{}_b \wedge \theta^b$$

or,

$$d\tau^a = {}^*R^a{}_b \wedge \theta^b - \Gamma^a_b \wedge \tau^b .$$

Remarkably, this is equivalent to the first generalized Bianchi identity given in the preceding section.

2.5 The geometry of distant parallelism

Let us now consider a special situation in which our n-dimensional manifold $\mathbb{C}^\infty$ is embedded *isometrically* in a flat n-dimensional (pseudo-)Euclidean space $\mathbb{E}^n$ (with coordinates $v^{\bar{m}}$) spanned by the constant basis $e_{\bar{m}}$ whose dual is denoted by $s^{\bar{n}}$. This embedding allows us to globally cover the manifold $\mathbb{C}^\infty$ in the sense that its geometric structure can be parametrized by the Euclidean basis $e_{\bar{m}}$ satisfying

$$\eta_{\bar{m}\bar{n}} = \langle e_{\bar{m}}, e_{\bar{n}} \rangle = \mathrm{diag}\,(\pm 1, \pm 1, \ldots, \pm 1)\,.$$

It is important to note that this situation is different from the one presented in Section 1.1, in which case we may refer the structural equations of $\mathbb{C}^\infty$ to the locally flat tangent space $\mathbb{T}_x(\mathbb{M})$. The results of the latter situation (i.e., the *localized* structural equations) should not always be regarded as globally valid since the tangent space $\mathbb{T}_x(\mathbb{M})$, though ubiquitous in the sense that it can be defined everywhere (at any point) in $\mathbb{C}^\infty$, cannot cover the whole structure of the curved manifold $\mathbb{C}^\infty$ without changing orientation from point to point.

One can construct geometries with special connections that will give rise to what we call *geometries with parallelism*. Among others, the geometry of *distant parallelism* is a famous case. Indeed, A. Einstein adopted this geometry in one of his attempts to geometrize physics, and especially to unify gravity and electromagnetism [5]. In its application to physical situations, the resulting field equations of a unified field theory based on distant parallelism, for instance, are quite remarkable in that the so-called energy-momentum tensor appears to be geometrized via the twist tensor. We will therefore dedicate this section to a brief presentation of the geometry of distant parallelism in the language of Riemann-Cartan geometry.

In this geometry, it is possible to orient vectors such that their directions remain invariant after being displaced from a point to some distant point in the manifold. This situation is made possible by the vanishing of the curvature tensor, which is given by the integrability condition

$$R^d{}_{abc} = e^d_{\bar{m}}\,(\partial_b \partial_c - \partial_c \partial_b)\, e_a^{\bar{m}} = 0$$

where the connection is now given by

$$\Gamma^c_{ab} = e^c_{\bar{m}}\, \partial_b e_a^{\bar{m}}$$

where $e_a^{\bar{m}} = \partial_a \xi^{\bar{m}}$ and $e^a_{\bar{m}} = \partial_{\bar{m}} x^a$.

However, while the curvature tensor vanishes, one still has the twist tensor given by

$$\Gamma^a_{[bc]} = \frac{1}{2}\, e^a_{\bar{m}} \left(\partial_c e_b^{\bar{m}} - \partial_b e_c^{\bar{m}}\right)$$

with the $e_a^{\bar{m}}$ acting as the components of a spin "potential". Thus the twist can now be considered as the primary geometric object in the manifold $\mathbb{C}^\infty_p$ endowed with distant parallelism.

Also, in general, the Riemann-Christoffel curvature tensor is non-vanishing as

$$B^d{}_{abc} = \hat{\nabla}_c K^d_{ab} - \hat{\nabla}_b K^d_{ac} + K^e_{ab} K^d_{ec} - K^e_{ac} K^d_{eb}\,.$$

Let us now consider some facts. Taking the covariant derivative of the tetrad $e_a^{\bar{m}}$ with respect to the Christoffel symbols alone, we have

$$\hat{\nabla}_b\, e_a^{\bar{m}} = \partial_b e_a^{\bar{m}} - e_d^{\bar{m}} \Delta^d_{ab} = e_c^{\bar{m}} K^c_{ab}$$

i.e.,

$$K^c_{ab} = e^c_{\bar{m}} \hat{\nabla}_b\, e_a^{\bar{m}} = -e_a^{\bar{m}} \hat{\nabla}_b\, e^c_{\bar{m}}\,.$$

In the above sense, the components of the contwist tensor give the so-called *Ricci rotation coefficients*. Then from

$$\hat{\nabla}_c \hat{\nabla}_b\, e_a^{\bar{m}} = e_d^{\bar{m}} \left(\hat{\nabla}_c\, K^d_{ab} + K^e_{ab} K^d_{ec}\right)$$

it is elementary to show that

$$\left(\hat{\nabla}_c \hat{\nabla}_b - \hat{\nabla}_b \hat{\nabla}_c\right) e_a^{\bar{m}} = e_d^{\bar{m}} B^d{}_{abc}\,.$$

Likewise, we have

$$\tilde{\nabla}_b\, e_a^{\bar{m}} = \partial_b e_a^{\bar{m}} - e_d^{\bar{m}} K^d_{ab} = e_c^{\bar{m}} \Delta^c_{ab}$$

$$\Delta^c_{ab} = e^c_{\bar{m}} \tilde{\nabla}_b\, e_a^{\bar{m}} = -e_a^{\bar{m}} \tilde{\nabla}_b\, e^c_{\bar{m}}$$

where now $\tilde{\nabla}$ denotes covariant differentiation with respect to the Ricci rotation coefficients alone. Then from

$$\tilde{\nabla}_c \tilde{\nabla}_b e_a^{\bar{m}} = e_d^{\bar{m}} \left(\tilde{\nabla}_c \Delta^d_{ab} + \Delta^e_{ab} \Delta^d_{ec}\right)$$

we get

$$\left(\tilde{\nabla}_c \tilde{\nabla}_b - \tilde{\nabla}_b \tilde{\nabla}_c\right) e_a^{\bar{m}} = -e_d^{\bar{m}} \big(B^d{}_{abc} - 2\Delta^d_{ae} \Gamma^e_{[bc]} - \\ - \Delta^e_{ab} K^d_{ec} + \Delta^e_{ac} K^d_{eb} - K^e_{ab} \Delta^d_{ec} + K^e_{ac} \Delta^d_{eb}\big)\,.$$

In this situation, one sees, with respect to the coframe basis $\theta^a = e^a_{\bar{m}} s^{\bar{m}}$, that

$$d\theta^a = -\Gamma^a_b \wedge \theta^b \equiv T^a$$

i.e.,

$$T^a = \Gamma^a_{[bc]} \theta^b \wedge \theta^c.$$

Thus the twist two-forms of this geometry are now given by T^a (instead of τ^a of the preceding section). We then realize that

$$D\theta^a = 0\,.$$

Next, we see that

$$d^2\theta^a = dT^a = -d\Gamma^a_b \wedge \theta^b + \Gamma^a_b \wedge d\theta^b = \\ = -\left(d\Gamma^a_b + \Gamma^a_c \wedge \Gamma^c_b\right) \wedge \theta^b = \\ = -{}^*R^a{}_b \wedge \theta^b.$$

But, as always, $d^2\theta^a = 0$, and therefore we have

$$^*R^a{}_b \wedge \theta^b = 0$$

Note that in this case, $^*R^a{}_b \neq 0$ (in general) as

$$^*R^a{}_{bcd} = 2\Gamma^e_{[cd]}\Gamma^a_{be}$$

will not vanish in general. We therefore see immediately that

$$^*R^a{}_{bcd} + {}^*R^a{}_{cdb} + {}^*R^a{}_{dbc} = 0$$

giving the integrability condition

$$\Gamma^e_{[cd]}\Gamma^a_{be} + \Gamma^e_{[db]}\Gamma^a_{ce} + \Gamma^e_{[bc]}\Gamma^a_{de} = 0\,.$$

Meanwhile, the condition

$$dT^a = 0$$

gives the integrability condition

$$\partial_d\Gamma^a_{[bc]} + \partial_b\Gamma^a_{[cd]} + \partial_c\Gamma^a_{[db]} = 0\,.$$

Contracting, we find

$$\partial_c\Gamma^c_{[ab]} = 0\,.$$

It is a curious fact that the last two relations somehow remind us of the algebraic structure of the components of the electromagnetic field tensor in physics.

Finally, from the contraction of the components $B^d{}_{abc}$ of the Riemann-Christoffel curvature tensor (the Ricci tensor), one defines the regular Einstein tensor by

$$\hat{G}_{ab} \equiv B_{ab} - \frac{1}{2}\,g_{ab}B \equiv kE_{ab}$$

where k is a physical coupling constant and E_{ab} are the components of the so-called energy-momentum tensor. We therefore see that

$$E_{ab} = \frac{1}{k}\left(K^c_{ad}K^d_{cb} - \hat{\nabla}_c K^c_{ab} + 2\hat{\nabla}_b\Gamma^c_{[ac]} - 2K^c_{ab}\Gamma^d_{[cd]}\right) - \\ - \frac{1}{2k}\,g_{ab}\left(4g^{cd}\hat{\nabla}_c\Gamma^e_{[de]} + 2g^{ce}\Gamma^d_{[cd]}\Gamma^f_{[ef]} + K_{cde}K^{ced}\right).$$

In addition, the following two conditions are satisfied:

$$E_{[ab]} = 0\,,$$

$$\hat{\nabla}_a E^{ab} = 0\,.$$

We have now seen that, in this approach we have applied here, the energy-momentum tensor (matter field) is fully geometrized. This way, gravity arises from twistal (spin) interaction (possibly, on the microscopic scales) and becomes an emergent phenomenon rather than a fundamental one. This seems rather speculative. However, it may have profound consequences.

2.6 Spin frames

A spin frame is described by the anti-symmetric tensor product

$$\Omega^{ik} = \frac{1}{2}\left(\theta^i \otimes \theta^k - \theta^k \otimes \theta^i\right) = \theta^i \wedge \theta^k \equiv \frac{1}{2}\left[\theta^i, \theta^k\right].$$

In general, then, for arbitrary vector field fields A and B, we can form the commutator

$$[A, B] = A \otimes B - B \otimes A\,.$$

Introducing another vector field C, we have the so-called Jacobi identity

$$[A, [B, C]] + [B, [C, A]] + [C, [A, B]] = 0\,.$$

With respect to the local coordinate basis elements $E_i = \partial_i$ of the tangent space $\mathbb{T}_x(\mathbb{M})$, we see that, astonishingly enough, the anti-symmetric product $[A, B]$ is what defines the Lie (exterior) derivative of B with respect to A:

$$L_A B \equiv [A, B] = \left(A^i\partial_i B^k - B^i\partial_i A^k\right)\frac{\partial}{\partial X^k}\,.$$

(Note that $L_A A = [A, A] = 0$.) The terms in the round brackets are just the components of our Lie derivative which can be used to define a diffeomorphism invariant (i.e., by taking $A^i = \xi^i$ where ξ represents the displacement field in a neighborhood of coordinate points).

Furthermore, for a vector field U and a tensor field T, both arbitrary, we have (in component notation) the following:

$$L_U T^{ij\ldots s}_{kl\ldots r} = \partial_m T^{ij\ldots s}_{kl\ldots r}U^m + T^{ij\ldots s}_{ml\ldots r}\partial_k U^m + \\ + T^{ij\ldots s}_{km\ldots r}\partial_l U^m + \ldots + T^{ij\ldots s}_{kl\ldots m}\partial_r U^m - T^{mj\ldots s}_{kl\ldots r}\partial_m U^i - \\ - T^{im\ldots s}_{kl\ldots r}\partial_m U^j - \ldots - T^{ij\ldots m}_{kl\ldots r}\partial_m U^s$$

It is not immediately apparent whether these transform as components of a tensor field or not. However, with the help of the twist tensor and the relation

$$\partial_k U^i = \nabla_k U^i - \Gamma^i_{mk}U^m = \nabla_k U^i - \left(\Gamma^i_{km} - 2\Gamma^i_{[km]}\right)U^m$$

we can write

$$L_U T^{ij\ldots s}_{kl\ldots r} = \nabla_m T^{ij\ldots s}_{kl\ldots r}U^m + T^{ij\ldots s}_{ml\ldots r}\nabla_k U^m + \\ + T^{ij\ldots s}_{km\ldots r}\nabla_l U^m + \ldots + T^{ij\ldots s}_{kl\ldots m}\nabla_r U^m - T^{mj\ldots s}_{kl\ldots r}\nabla_m U^i - \\ - T^{im\ldots s}_{kl\ldots r}\nabla_m U^j - \ldots - T^{ij\ldots m}_{kl\ldots r}\nabla_m U^s + \\ + 2\Gamma^i_{[mp]}T^{mj\ldots s}_{kl\ldots r}U^p + 2\Gamma^j_{[mp]}T^{im\ldots s}_{kl\ldots r}U^p + \ldots \\ + 2\Gamma^s_{[mp]}T^{ij\ldots m}_{kl\ldots r}U^p - 2\Gamma^m_{[kp]}T^{ij..s}_{ml\ldots r}U^p - \\ - 2\Gamma^m_{[lp]}T^{ij\ldots s}_{km\ldots r}U^p - \ldots - 2\Gamma^m_{[rp]}T^{ij\ldots s}_{kl\ldots m}U^p.$$

Hence, noting that the components of the twist tensor, namely, $\Gamma^i_{[kl]}$, indeed transform as components of a tensor

field, it is seen that the $L_U T^{ij\ldots s}_{kl\ldots r}$ do transform as components of a tensor field. Apparently, the beautiful property of the Lie derivative (applied to an arbitrary tensor field) is that it is connection-independent even in a curved manifold.

If we now apply the commutator to the frame basis of the base manifold $\mathbb{C}^\infty$ itself, we see that (for simplicity, we again refer to the coordinate basis of the tangent space $\mathbb{T}_x(\mathbb{M})$)

$$[\omega_a, \omega_b] = \left(\partial_a X^i \, \partial_i \partial_b X^k - \partial_b X^i \, \partial_i \partial_a X^k\right) \frac{\partial}{\partial X^k} \, .$$

Again, writing the tetrads simply as $e^i_a = \partial_a X^i$, $e^a_i = \partial_i x^a$, we have

$$[\omega_a, \omega_b] = \left(\partial_a e^k_b - \partial_b e^k_a\right) \frac{\partial}{\partial X^k}$$

i.e.,

$$[\omega_a, \omega_b] = -2\Gamma^c_{[ab]} \omega_c \, .$$

Therefore, in the present formalism, the components of the twist tensor are by themselves proportional to the so-called *structure constants* Ψ^c_{ab} of our rotation group:

$$\Psi^c_{ab} = -2\Gamma^c_{[ab]} = -e^c_i \left(\partial_a e^i_b - \partial_b e^i_a\right) .$$

As before, here the tetrad represents a spin potential.

Also note that

$$\Psi^d_{ab}\Psi^e_{dc} + \Psi^d_{bc}\Psi^e_{da} + \Psi^d_{ca}\Psi^e_{db} = 0 \, .$$

We therefore observe that, as a consequence of the present formalism of differential geometry, spin fields (*objects of anholonomicity*) in the manifold $\mathbb{C}^\infty$ are generated *directly* by the twist tensor.

3 The new semi-symmetric unified field theory of the classical fields of gravity and electromagnetism

In this part, we develop our semi-symmetric unified field theory on the foundations of Riemann-Cartan geometry presented in Sections 1.1–1.6. We shall concentrate on physical events in the four-dimensional space-time manifold $\mathbb{S}^4$ with the usual Lorentzian signature. As we will see, the choice of a semi-symmetric Cartan twist will lead to a set of physically meaningful field equations from which we will obtain not only the generally covariant Lorentz equation of motion of a charged particle, but also its generalizations.

We are mainly concerned with the dynamical equations governing a cluster of individual particles and their multiple field interactions and also the possibility of defining geometrically and phenomenologically conserved currents in the theory. We will therefore not assume dimensional (i.e., structural) homogeneity with regard to the particles. Classically, a point-like (i.e., structureless) particle which characterizes a particular physical field is only a mere idealization which is not subject, e.g., to any possible dilation when interacting with other particles or fields. Still within the classical context, we relax this condition by assigning a structural configuration to each individual particle. Therefore, the characteristic properties of the individual particles allow us to describe a particle as a field in a physically meaningful sense. In this sense, the particle-field duality is abolished on the phenomenological level as well. In particular, this condition automatically takes into account both the rotational and reflectional symmetries of individual particles which have been developed separately. As such, without having to necessarily resort to particle isotropy, the symmetry group in our theory is a general one, i.e., it includes all rotations about all possible axes and reflections in any plane in the space-time manifold $\mathbb{S}^4$.

The presence of the semi-symmetric twist causes any local (hyper)surface in the space-time manifold $\mathbb{S}^4$ to be *non-orientable* in general. As a result, the trajectories of individual particles generally depend on the twisted path they trace in $\mathbb{S}^4$. It is important to note that this twist is the generator of the so-called microspin, e.g., in the simplest case, a spinning particle is simply a point-rotation in the sense of the so-called Cosserat continuum theory [10]. As usual, the semi-symmetric twist tensor enters the curvature tensor as an integral part via the general (semi-symmetric) connection. This way, all classical physical fields, not just the gravitational field, are intrinsic to the space-time geometry.

3.1 A semi-symmetric connection based on a semi-simple (transitive) rotation group

Let us now work in *four* space-time dimensions (since this number of dimensions is most relevant to physics). For a semi-simple (transitive) rotation group, we can show that

$$[\omega_a, \omega_b] = -\gamma \in_{abcd} \varphi^c \, \theta^d$$

where $\in_{abcd} = \sqrt{\det(g)}\, \epsilon_{abcd}$ are the components of the completely anti-symmetric four-dimensional Levi-Civita permutation tensor and φ is a vector field normal to a three-dimensional space (hypersurface) $\sum(t)$ defined as the time section $ct = x^0 = \text{const}$. (where c denotes the speed of light in vacuum) of $\mathbb{S}^4$ with local coordinates z^A. It satisfies $\varphi_a \varphi^a = = \gamma = \pm 1$ and is given by

$$\varphi_a = \frac{1}{6} \, \gamma \in_{abcd} \in^{ABC} \lambda^b_A \lambda^c_B \lambda^d_C$$

where

$$\lambda^a_A \equiv \partial_A x^a, \qquad \lambda^A_a \equiv \partial_a z^A,$$

$$\lambda^b_A \lambda^A_a = \delta^b_a - \gamma \varphi_a \varphi^b,$$

$$\lambda^a_A \lambda^B_a = \delta^B_A \, .$$

More specifically,

$$\in_{ABC} \varphi_d = \in_{abcd} \lambda^a_A \lambda^b_B \lambda^c_C$$

from which we find

$$\in_{abcd} = \in_{ABC} \lambda^A_a \lambda^B_b \lambda^C_c \varphi_d + \Lambda_{abcd}$$

where

$$\Lambda_{abcd} = \gamma\left(\in_{ebcd}\varphi_a + \in_{aecd}\varphi_b + \in_{abed}\varphi_c\right)\varphi^e .$$

Noting that $\Lambda_{abcd}\varphi^d = 0$, we can define a completely anti-symmetric, three-index, four-dimensional "permutation" tensor by

$$\Phi_{abc} \equiv \in_{abcd}\varphi^d = \gamma \in_{ABC} \lambda^A_a \lambda^B_b \lambda^C_c .$$

Obviously, the hypersurface $\sum(t)$ can be thought of as representing the position of a material body at any time t. As such, it acts as a boundary of the so-called world-tube of a family of world-lines covering an arbitrary four-dimensional region in $\mathbb{S}^4$.

Meanwhile, in the most general four-dimensional case, the twist tensor can be decomposed according to

$$\Gamma^c_{[ab]} = \frac{1}{3}\left(\delta^c_b\Gamma^d_{[ad]} - \delta^c_a\Gamma^d_{[bd]}\right) + \\ + \frac{1}{6}\in^c{}_{abd}\in^d{}_{pqr} g^{qs}g^{rt}\Gamma^p_{[st]} + g^{cd}Q_{dab} ,$$

$$Q_{abc} + Q_{bca} + Q_{cab} = 0 ,$$

$$Q^a_{ab} = Q^a_{ba} = 0 .$$

In our special case, the twist tensor becomes completely anti-symmetric (in its three indices) as

$$\Gamma^c_{[ab]} = -\frac{1}{2}\gamma g^{ce} \in_{abed}\varphi^d$$

from which we can write

$$\varphi^a = -\frac{1}{3}\in^{abcd}\Gamma_{b[cd]}$$

where, as usual, $\Gamma_{b[cd]} = g_{be}\Gamma^e_{[cd]}$. Therefore, at this point, the full connection is given by (with the Christoffel symbols written explicitly)

$$\Gamma^c_{ab} = \frac{1}{2}g^{cd}\left(\partial_b g_{da} - \partial_d g_{ab} + \partial_a g_{bd}\right) - \frac{1}{2}\gamma\in^c{}_{abd}\varphi^d .$$

We shall call this special connection "*semi-symmetric*". This gives the following simple conditions:

$$\Gamma^c_{(ab)} = \Delta^c_{ab} = \frac{1}{2}g^{cd}\left(\partial_b g_{da} - \partial_d g_{ab} + \partial_a g_{bd}\right) ,$$

$$K^c_{ab} = \Gamma^c_{[ab]} = -\frac{1}{2}\gamma\in^c_{abd}\varphi^d ,$$

$$\Gamma^b_{[ab]} = 0 ,$$

$$\Gamma^b_{ab} = \Gamma^b_{ba} = \partial_a\left(\ln\sqrt{\det(g)}\right) .$$

Furthermore, we can extract a projective metric tensor ϖ from the twist (via the structure constants) as follows:

$$\varpi_{ab} = g_{ab} - \gamma\varphi_a\varphi_b = 2\Gamma^c_{[ad]}\Gamma^d_{[cb]} .$$

In three dimensions, the above relation gives the so-called Cartan metric.

Finally, we are especially interested in how the existence of twist affects a coordinate frame spanned by the basis ω_a and its dual θ^b in a geometry endowed with distant parallelism. Taking the *four-dimensional curl* of the coframe basis θ^b, we see that

$$[\nabla, \theta^a] = 2d\theta^a = 2T^a \\ = -\gamma\in^{\bar{m}\bar{n}\bar{p}\bar{q}}\left(\partial_{\bar{m}}e^a_{\bar{n}}\right)\varphi_{\bar{p}}e_{\bar{q}}$$

where $\nabla = \theta^b\nabla_b = s^{\bar{m}}\partial_{\bar{m}}$ and $\in^{abcd} = \frac{1}{\sqrt{\det(g)}}\epsilon^{abcd}$. From the metricity condition of the tetrad (with respect to the basis of E^n), namely, $\nabla_b e^{\bar{m}}_a = 0$, we have

$$\partial_b e^{\bar{m}}_a = \Gamma^c_{ab}e^{\bar{m}}_c ,$$

$$\partial^{\bar{n}}e^{\bar{m}}_a = \eta^{\bar{n}\bar{p}}e^b_{\bar{p}}\partial_b e^{\bar{m}}_a = e^{\bar{m}}_c\Gamma^c_{ab}e^{\bar{n}b} .$$

It is also worthwhile to note that from an equivalent metricity condition, namely, $\nabla_a e^b_{\bar{m}} = 0$, one finds

$$\partial_{\bar{n}}e^a_{\bar{m}} = -\Gamma^a_{bc}e^b_{\bar{m}}e^c_{\bar{n}} .$$

Thus we find

$$[\nabla, \theta^a] = -\gamma\in^{bcde}\Gamma^a_{[bc]}\varphi_d\omega_e .$$

In other words,

$$T^a = d\theta^a = -\frac{1}{2}\gamma\in^{bcde}\Gamma^a_{[bc]}\varphi_d\omega_e .$$

For the frame basis, we have

$$[\nabla, \omega_a] = -\gamma\in^{bcde}\Gamma_{a[bc]}\varphi_d\omega_e .$$

At this point it becomes clear that the presence of twist in $\mathbb{S}^4$ rotates the frame and coframe bases themselves. The basics presented here constitute the reality of the so-called *spinning frames*.

3.2 Construction of the semi-symmetric field equations

In the preceding section, we have introduced the semi-symmetric connection

$$\Gamma^c_{ab} = \frac{1}{2}g^{cd}\left(\partial_b g_{da} - \partial_d g_{ab} + \partial_a g_{bd}\right) - \frac{1}{2}\gamma\in^c{}_{abd}\varphi^d$$

based on the semi-simple rotation group

$$[\omega_a, \omega_b] = -\gamma\in_{abcd}\varphi^c\theta^d .$$

Now we are in a position to construct a classical unified field theory of gravity and electromagnetism based on this connection. We shall then call the resulting field equations semi-symmetric, hence the name semi-symmetric unified field theory. (Often the terms "symmetric" and "asymmetric" refer to the metric rather than the connection.)

Using the results we have given in Section 1.3, we see that the curvature tensor built from our semi-symmetric connection is given by

$$R^{d}{}_{abc} = B^{d}{}_{abc} - \frac{1}{2}\,\gamma\left(\in^{d}{}_{ace}\,\hat{\nabla}_b\varphi^e - \in^{d}{}_{abe}\,\hat{\nabla}_c\varphi^e\right) + \\ + \frac{3}{2}\,\gamma\left(g_{eb}\,\delta^{def}_{acg} - g_{ec}\,\delta^{def}_{abg}\right)\varphi_f\,\varphi^g .$$

As before, the generalized Ricci tensor is then given by the contraction $R_{ab} = R^{c}{}_{acb}$, i.e.,

$$R_{ab} = B_{ab} - \frac{1}{2}\,(g_{ab} - \gamma\,\varphi_a\varphi_b) - \frac{1}{2}\,\gamma\in^{cd}{}_{ab}\,\hat{\nabla}_c\varphi_d .$$

Then we see that its symmetric and anti-symmetric parts are given by

$$R_{(ab)} = B_{ab} - \frac{1}{2}\,(g_{ab} - \gamma\,\varphi_a\,\varphi_b)$$

$$R_{[ab]} = -\frac{1}{2}\,\gamma\in^{cd}{}_{ab}\,F_{cd}$$

where

$$F_{ab} = \frac{1}{2}\,(\partial_a\varphi_b - \partial_b\varphi_a)$$

are the components of the intrinsic spin tensor of the first kind in our unified field theory. Note that we have used the fact that $\hat{\nabla}_a\varphi_b - \hat{\nabla}_b\varphi_a = \partial_a\varphi_b - \partial_b\varphi_a$.

Note that if

$$\varphi^a = \gamma\,\delta^a_0$$

then the twist tensor becomes covariantly constant throughout the space-time manifold, i.e.,

$$\nabla_d\,\Gamma^c_{[ab]} = \hat{\nabla}_d\,\Gamma^c_{[ab]} = 0 .$$

This special case may indeed be anticipated as in the present theory, the two fundamental geometric objects are the metric and twist tensors.

Otherwise, in general let us define a vector-valued gravo-electromagnetic potential A via

$$\varphi^a = \lambda A^a$$

where

$$\lambda = \left(\frac{\gamma}{A_a A^a}\right)^{1/2} .$$

Letting $\in = \lambda^2\gamma$, we then have

$$R_{ab} = B_{ab} - \frac{1}{2}\,(g_{ab} - \in A_a A_b) - \frac{1}{2}\,\gamma\in^{cd}{}_{ab}\left(\lambda\bar{F} + H_{cd}\right)$$

where

$$\bar{F}_{ab} = \frac{1}{2}\,(\partial_a A_b - \partial_b A_a) ,$$

$$H_{ab} = -\frac{1}{2}\,(A_a\,\partial_b\lambda - A_b\,\partial_a\lambda) .$$

We may call $\bar{F}_{ab}$ the components of the intrinsic spin tensor of the second kind. The components of the anti-symmetric field equation then take the form

$$R_{[ab]} = -\frac{1}{2}\,\gamma\in^{cd}{}_{ab}\,\left(\lambda\bar{F}_{cd} + H_{cd}\right) .$$

Using the fact that

$$\partial_a F_{bc} + \partial_b F_{ca} + \partial_c F_{ab} = 0$$

we obtain

$$\nabla_a R^{[ab]} = 0 .$$

The dual of the anti-symmetric part of the generalized Ricci tensor is then given by

$$\tilde{R}_{[ab]} = \frac{1}{2}\,\in_{abcd} R^{[cd]} = -\frac{1}{2}\,(\partial_a\varphi_b - \partial_b\varphi_a)$$

i.e.,

$$\tilde{R}_{[ab]} = -\left(\lambda\bar{F}_{ab} + H_{ab}\right) .$$

We therefore see that

$$\partial_a\tilde{R}_{[bc]} + \partial_b\tilde{R}_{[ca]} + \partial_c\tilde{R}_{[ab]} = 0 .$$

At this point, the components of the intrinsic spin tensor take the following form:

$$\bar{F}_{ab} = -\frac{1}{2\lambda}\left(\in_{abcd} R^{[cd]} + 2H_{ab}\right) .$$

The generalized Einstein field equation is then given by

$$G_{ab} = R_{ab} - \frac{1}{2}\,g_{ab}\,R = kT_{ab}$$

where k is a coupling constant, $R = R^a{}_a = B - \frac{3}{2}$ (in our geometrized units) is the generalized Ricci scalar, and T_{ab} are the components of the energy-momentum tensor of the coupled matter and spin fields. Taking the covariant divergence of the generalized Einstein tensor with the help of the relations

$$\nabla_a R^{ab} = \hat{\nabla}_a R^{ab} - \Gamma^b_{[ac]} R^{[ac]} ,$$

$$\nabla_a R = \partial_a R = \partial_a B ,$$

$$F_{ab}\varphi^b = -\frac{1}{2}\,\varphi^b\hat{\nabla}_b\varphi_a ,$$

we obtain

$$\nabla_a G^{ab} = \hat{\nabla}_a G^{ab} - \gamma\,F^b{}_a\varphi^a .$$

On the other hand, using the integrability condition

$$\in^{abcd}\hat{\nabla}_b\hat{\nabla}_c\varphi_d = \in^{abcd}\partial_b\partial_c\varphi_d = 0$$

we have

$$\hat{\nabla}_a R^{ab} = \hat{\nabla}_a B^{ab} - \frac{1}{2}\,\gamma\hat{\nabla}_a\left(\varphi^a\varphi^b\right) .$$

Therefore

$$\nabla_a G^{ab} = \hat{\nabla}_a \hat{G}^{ab} + \frac{1}{2}\gamma\left(\varphi^b \hat{\nabla}_a \varphi^a + \varphi^a \hat{\nabla}_a \varphi^b\right) - \gamma F^b{}_a \varphi^a$$

where, as before, $\hat{G}_{ab} = B_{ab} - \frac{1}{2} g_{ab} B$. But as $\hat{\nabla}_a \hat{G}^{ab} = 0$, we are left with

$$\nabla_a G^{ab} = \frac{1}{2}\gamma\left(\varphi^b \hat{\nabla}_a \varphi^a + \varphi^a \hat{\nabla}_a \varphi^b\right) - \gamma F^b{}_a \varphi^a .$$

We may notice that in general the above divergence does not vanish.

We shall now seek a possible formal correspondence between our present theory and both general relativistic gravitomagnetism and Maxwellian electrodynamics. We shall first assume that particles do not necessarily have point-like structure. Now let the rest (inertial) mass of a particle and the speed of light in vacuum (again) be denoted by m and c, respectively. Also, let ϕ represent the scalar gravoelectromagnetic potential and let g_a and B_a denote the components of the gravitational spin potential and the electromagnetic four-potential, respectively. We now make the following ansatz:

$$\lambda = \text{const} = -\frac{\bar{g}}{2mc^2} ,$$

$$A_a = \partial_a \phi + v\, g_{0a} = \partial_a \phi + g_a + B_a ,$$

where v is a constant and

$$\bar{g} = (1+m)\, n + 2(1+s_\pi)\, e$$

is the *generalized gravoelectromagnetic charge*. Here n is the structure constant (i.e., a volumetric number) which is different from zero for structured particles, s_π is the spin constant, and e is the electric charge (or, more generally, the electromagnetic charge).

Now let the gravitational vorticity tensor be given by

$$\omega_{ab} = \frac{1}{2}(\partial_a g_b - \partial_b g_a)$$

which vanishes in spherically symmetric (i.e., centrally symmetric) situations. Next, the electromagnetic field tensor is given as usual by

$$f_{ab} = \partial_b B_a - \partial_a B_b .$$

The components of the intrinsic spin tensor can now be written as

$$\bar{F}_{ab} = \omega_{ab} - \frac{1}{2} f_{ab} .$$

As a further consequence, we have $H_{ab} = 0$ and therefore

$$\bar{F}_{ab} = -\frac{1}{2\lambda} \in_{abcd} R^{[cd]} = \frac{mc^2}{\bar{g}} \in^{cd}{}_{ab} R_{[cd]} .$$

The electromagnetic field tensor in our unified field theory is therefore given by

$$f_{ab} = -2\left(\frac{mc^2}{\bar{g}} \in^{cd}{}_{ab} R_{[cd]} - \omega_{ab}\right) .$$

Here we see that when the gravitational spin is present, the electromagnetic field does interact with the gravitational field. Otherwise, in the presence of a centrally symmetric gravitational field we have

$$f_{ab} = -\frac{2mc^2}{\bar{g}} \in^{cd}{}_{ab} R_{[cd]}$$

and there is no physical interaction between gravity and electromagnetism.

3.3 Equations of motion

Now let us take the unit vector field φ to represent the unit velocity vector field, i.e.,

$$\varphi^a = u^a = \frac{dx^a}{ds}$$

where ds is the (infinitesimal) world-line satisfying

$$1 = g_{ab} \frac{dx^a}{ds} \frac{dx^b}{ds} .$$

This selection defines a general material object in our unified field theory as a hypersurface $\sum(t)$ whose world-velocity u is normal to it. Indeed, we will soon see some profound physical consequences.

Invoking this condition, we immediately obtain the following equation of motion:

$$\nabla_a G^{ab} = \frac{1}{2}\gamma\left(u^b \nabla_a u^a + \frac{Du^b}{Ds}\right) - \gamma F^b{}_a \varphi^a$$

where we have used the following relations:

$$\Gamma^c_{(ab)} = \Delta^c_{ab}$$

$$\Gamma^c_{[ab]} = -\frac{1}{2}\gamma \in^c{}_{abd} u^d$$

$$\frac{Du^a}{Ds} = u^b \nabla_b u^a = \frac{du^a}{ds} + \Gamma^a_{(bc)} u^b u^c = \\ = \frac{du^a}{ds} + \Delta^a_{bc} u^b u^c = u^b \hat{\nabla}_a u^a .$$

What happens now if we insist on guaranteeing the conservation of matter and spin? Letting

$$\nabla_a G^{ab} = 0$$

and inserting the value of λ, we obtain the equation of motion

$$\frac{Du^a}{Ds} = -\frac{\bar{g}}{mc^2} \bar{F}^a{}_b u^b - u^a \nabla_b u^b$$

i.e., the *generalized* Lorentz equation of motion

$$\frac{Du^a}{Ds} = \frac{\bar{g}}{2mc^2}\left(f^a{}_b - 2\omega^a{}_b\right) u^b - u^a \nabla_b u^b .$$

From the above equation of motion we may derive special equations of motion such as those in the following cases:

1. For an electrically charged, non-spinning, incompressible, structureless (point-like) particle moving in a static, centrally symmetric gravitational field, we have $m \neq 0$, $e \neq 0$, $s_\pi = 0$, $n = 0$, $\nabla_a u^a = 0$, $f_{ab} \neq 0$, $\omega_{ab} = 0$. Therefore its equation of motion is given by
$$\frac{Du^a}{Ds} = \frac{e}{mc^2} f^a{}_b u^b$$
which is just the standard, relativistically covariant Lorentz equation of motion.
2. For an electrically charged, spinning, incompressible, structureless particle moving in a non-static, spinning gravitational field, we have $m \neq 0$, $e \neq 0$, $s_\pi \neq 0$, $n = 0$, $\nabla_a u^a = 0$, $f_{ab} \neq 0$, $\omega_{ab} \neq 0$. Therefore its equation of motion is given by
$$\frac{Du^a}{Ds} = \frac{(1+s_\pi)}{mc^2} e \left(f^a{}_b - 2\omega^a{}_b\right) u^b.$$
3. For a neutral, non-spinning, incompressible, structureless particle moving in a static, centrally symmetric gravitational field, we have $m \neq 0$, $e = 0$, $s_\pi = 0$, $n = 0$, $\nabla_a u^a = 0$, $f_{ab} = 0$, $\omega_{ab} = 0$. Therefore its equation of motion is given by the usual geodesic equation of motion
$$\frac{Du^a}{Ds} = 0\,.$$
In general, this result does not hold for arbitrary incompressible bodies with structure.
4. For a neutral, static, non-spinning, compressible body moving in a static, non-spinning, centrally symmetric gravitational field, we have $m \neq 0$, $e = 0$, $s_\pi = 0$, $n \neq 0$, $\nabla_a u^a \neq 0$, $f_{ab} = 0$, $\omega_{ab} = 0$. Therefore its equation of motion is given by
$$\frac{Du^a}{Ds} = -u^a \nabla_b u^b$$
which holds for non-Newtonian fluids in classical hydrodynamics.
5. For an electrically charged, non-spinning, compressible body moving in a static, non-spinning, centrally symmetric gravitational field, we have $m \neq 0$, $e \neq 0$, $s_\pi = 0$, $n \neq 0$, $\nabla_a u^a \neq 0$, $f_{ab} \neq 0$, $\omega_{ab} = 0$. Therefore its equation of motion is given by
$$\frac{Du^a}{Ds} = \frac{n(1+m)}{mc^2} e f^a{}_b u^b - u^a \nabla_b u^b$$
which holds for a variety of classical Maxwellian fluids.
6. For a neutral, spinning, compressible body moving in a non-static, spinning gravitational field, the parametric (structural) condition is given by $m \neq 0$, $e = 0$, $s_\pi, \neq 0$, $n \neq 0$, $\nabla_a u^a \neq 0$, $f_{ab} = 0$, $\omega_{ab} \neq 0$. Therefore its equation of motion is given by
$$\frac{Du^a}{Ds} = -\frac{n(1+m)}{mc^2} \omega^a{}_b u^b - u^a \nabla_b u^b.$$

Note that the exact equation of motion for massless, neutral particles cannot be directly extracted from the general form of our equation of motion.

We now proceed to give the most general form of the equation of motion in our unified field theory. Using the general identity (see Section 1.3)
$$\nabla_a G^{ab} = 2g^{ab}\Gamma^c_{[da]} R^d{}_c + \Gamma^a_{[cd]} R^{cdb}{}_a$$
we see that
$$\nabla_a G^{ab} = \gamma \left(\in^b{}_{cda} R^{[cd]} + \frac{1}{2} \in_{cdea} R^{cdeb} \right) u^a.$$
After some algebra, we can show that the above relation can also be written in the form
$$\frac{Du^a}{Ds} = - \in^a{}_{bcd} R^{[bc]} u^d.$$
Note that the above general equation of motion is true whether the covariant divergence of the generalized Einstein tensor vanishes or not. Otherwise, let $\Phi^a = \nabla_b G^{ba}$ represent the components of the non-conservative vector of the coupled matter and spin fields. Our equation of motion can then be written alternatively as
$$\frac{Du^a}{Ds} = \frac{1}{2} \in_{bcde} R^{bcda} u^e - \gamma \Phi^a.$$
Let us once again consider the conservative case, in which $\Phi^a = 0$. We now have the relation
$$\frac{1}{2} \in_{bcde} R^{bcda} u^e = -\frac{2\bar{g}}{mc^2} \bar{F}^a{}_b u^b - u^a \nabla_b u^b$$
i.e.,
$$\frac{1}{2} \left(\in_{cdhb} R^{cdha} + \frac{4\bar{g}}{mc^2} \bar{F}^a{}_b \right) u^b = -u^a \nabla_b u^b.$$
For a structureless spinning particle, we are left with
$$\left(\in_{cdhb} R^{cdha} + \frac{4(1+s_\pi)}{mc^2} e \bar{F}^a{}_b \right) u^b = 0$$
for which the general solution may read
$$\bar{F}_{ab} = e \frac{mc^2}{4(1+s_\pi)} \left(\in_{acde} R_b{}^{cde} - \in_{bcde} R_a{}^{cde} \right) + S_{ab}$$
where $S_{ab} \neq 0$ are the components of a generally asymmetric tensor satisfying
$$S_{ab} u^b = -e \frac{mc^2}{4(1+s_\pi)} \in_{acde} R_b{}^{cde} u^b.$$
In the case of a centrally symmetric gravitational field, this condition should again allow us to determine the electromagnetic field tensor from the curvature tensor alone.

Now, with the help of the decomposition
$$R^d{}_{abc} = C^d{}_{abc} + \frac{1}{2} \left(\delta^d_b R_{ac} + g_{ac} R^d{}_b - \delta^d_c R_{ab} - g_{ab} R^d{}_c \right) + \\ + \frac{1}{6} \left(\delta^d_c g_{ab} - \delta^d_b g_{ac} \right) R$$

we obtain the relation

$$\in_{bcde} R^{bcda} = \in_{bcde} \left(C^{bcda} + \frac{1}{2} \left(g^{ac} R^{[bd]} - g^{ab} R^{[cd]} \right) \right) .$$

However, it can be shown that the last two terms in the above relation cancel each other, since

$$\in_{bcde} g^{ac} R^{[bd]} = \in_{bcde} g^{ab} R^{[cd]} = -\gamma\, g^{ac} \left(\partial_e u_c - \partial_c u_e \right)$$

therefore we are left with the simple relation

$$\in_{bcde} R^{bcda} = \in_{bcde} C^{bcda} .$$

If the space-time under consideration is conformally flat (i.e., $C^{d}_{\ abc} = 0$), we obtain the following integrability condition for the curvature tensor:

$$\in_{bcde} R^{bcda} = 0 .$$

It is easy to show that this is generally true if the components of the curvature tensor are of the form

$$R_{abcd} = \frac{1}{12} \left(g_{ac} g_{bd} - g_{ad} g_{bc} \right) B + P_{abcd}$$

where

$$P_{abcd} = \varepsilon \left(g_{ac} g_{bd} - g_{ad} g_{bc} \right) \bar{F}_{rs} \bar{F}^{rs}$$

with ϵ being a constant of proportionality. In this case, the generalized Ricci tensor is completely symmetric, i.e.,

$$R_{(ab)} = \frac{1}{4} g_{ab} \left(B + 12\, \varepsilon\, \bar{F}_{rs} \bar{F}^{rs} \right) \oplus$$

$$R_{[ab]} = 0 .$$

We also have

$$R = B + 12\, \varepsilon\, \bar{F}_{ab} \bar{F}^{ab}$$

such that the variation $\delta S = 0$ of the action integral

$$S = \iiiint \sqrt{\det(g)}\, R\, d^4x = \iiiint \sqrt{\det(g)} \left(B + 12\, \varepsilon\, \bar{F}_{ab} \bar{F}^{ab} \right) d^4x$$

where $dV = \sqrt{\det(g)}\, dx^0 dx^1 dx^2 dx^3 = \sqrt{\det(g)}\, d^4x$ defines the elementary four-dimensional volume, gives us a set of generalized Einstein-Maxwell equations. Note that in this special situation, the expression for the curvature scalar is true irrespective of whether the Ricci scalar B is constant or not. Furthermore, this gives a generalized Einstein space endowed with a generally non-vanishing spin density. Electromagnetism, in this case, appears to be inseparable from the gravitational vorticity and therefore becomes an emergent phenomenon. Also, the motion then becomes purely geodesic:

$$\frac{du^a}{ds} + \Delta^{a}_{bc} u^b u^c = 0 ,$$

$$\bar{F}_{ab} u^b = 0 .$$

3.4 The conserved gravoelectromagnetic currents of the theory

Interestingly, we can obtain more than one type of conserved gravoelectromagnetic current from the intrinsic spin tensor of the present theory.

We have seen in Section 2.2 that the intrinsic spin tensor in the present theory is given by

$$\bar{F}_{ab} = \frac{mc^2}{\bar{g}} \in^{cd}_{\ ab} R_{[cd]} .$$

We may note that

$$\widehat{j}^a \equiv \widehat{\nabla}_b \bar{F}^{ba} = 0$$

which is a covariant "source-free condition" in its own right.

Now, we shall be particularly interested in obtaining the conservation law for the gravoelectromagnetic current in the most general sense.

Define the absolute (i.e., global) gravoelectromagnetic current via the total covariant derivative as follows:

$$j^a \equiv \nabla_b \bar{F}^{ba} = \frac{mc^2}{\bar{g}} \in^{abcd} \nabla_d R_{bc} .$$

Now, with the help of the relation

$$\nabla_c \bar{F}_{ab} + \nabla_a \bar{F}_{bc} + \nabla_b \bar{F}_{ca} = -2 \left(\Gamma^{d}_{[ab]} \bar{F}_{cd} + \Gamma^{d}_{[bc]} \bar{F}_{ad} + \Gamma^{d}_{[ca]} \bar{F}_{bd} \right)$$

we see that

$$j^a = -\frac{6mc^2}{\bar{g}} g^{ce} \delta^{ab}_{cd} R_{[be]} u^d .$$

Simplifying, we have

$$j^a = \frac{6mc^2}{\bar{g}} R^{[ab]} u_b .$$

At this moment, we have nothing definitive to say about gravoelectromagnetic charge confinement. We cannot therefore speak of a globally admissible gravoelectromagnetic current density yet. However, we can show that our current is indeed conserved. As a start, it is straightforward to see that we have the relative conservation law

$$\hat{\nabla}_a j^a = 0 .$$

Again, this is not the most desired conservation law as we are looking for the most generally covariant one.

Now, with the help of the relations

$$\in^{abcd} \nabla_c F_{ab} = - \in^{abcd} \left(\Gamma^{e}_{[ac]} F_{eb} + \Gamma^{e}_{[bc]} F_{ae} \right)$$

$$\Gamma^{a}_{[bc]} = -\frac{1}{2} \gamma \in^{a}_{\ bcd} u^d$$

we obtain

$$\nabla_a R^{[ab]} = -2 F^{ab} u_a .$$

Therefore

$$u_b \nabla_a R^{[ab]} = 0 \,.$$

Using this result together with the fact that

$$R^{[ab]} \nabla_a u_b = -\frac{1}{2}\,\gamma \in^{abcd} F_{ab} F_{cd} = 0$$

we see that

$$\nabla_a j^a = \frac{6mc^2}{\bar{g}} \left(u_b \nabla_a R^{[ab]} + R^{[ab]} \nabla_a u_b \right) = 0$$

i.e., our gravoelectromagnetic current is conserved in a fully covariant manner.

Let us now consider a region in our space-time manifold in which the gravoelectromagnetic current vanishes. We have, from the boundary condition $j^a = 0$, the governing equation

$$R_{[ab]} u^b = 0$$

which is equivalent to the following integrability condition:

$$\in^{abcd} u_a \left(\partial_c u_d - \partial_d u_c \right) = 0 \,.$$

In three dimensions, if in general $\mathrm{curl} u \neq 0$, this gives the familiar integrability condition

$$u \cdot \mathrm{curl}\, u = 0$$

where the dot represents three-dimensional scalar product.

We are now in a position to define the phenomenological gravoelectromagnetic current density which shall finally allow us to define gravoelectromagnetic charge confinement. However, in order to avoid having extraneous sources, we do not in general expect such confinement to hold globally. From our present perspective, what we need is a relative (i.e., local) charge confinement which can be expressed solely in geometric terms.

Therefore we first define the spin tensor density (of weight $+2$) as

$$\bar{f}^{ab} \equiv \det(g)\, \bar{F}^{ab} = \frac{mc^2}{\bar{g}}\, \sqrt{\det(g)}\, \varepsilon^{abcd} R_{[cd]} \,.$$

The phenomenological (i.e., relative) gravoelectromagnetic current density is given here by

$$\bar{j}^a = \partial_b \bar{f}^{ab} = \frac{mc^2}{\bar{g}} \left(\partial_b \sqrt{\det(g)} \right) \varepsilon^{abcd} R_{[cd]}$$

i.e.,

$$\bar{j}^a = \frac{mc^2}{2\bar{g}}\, \varepsilon^{abcd} g^{rs} \left(\partial_b g_{rs} \right) R_{[cd]} \,.$$

Meanwhile, using the identity

$$\partial_a g^{bc} = -g^{br} g^{cs} \partial_a g_{rs}$$

we see that

$$\left(\partial_a g^{rs} \right) \left(\partial_b g_{rs} \right) = \left(\partial_a g_{rs} \right) \left(\partial_b g^{rs} \right) .$$

Using this result and imposing continuity on the metric tensor, we finally see that

$$\partial_a \bar{j}^a = \frac{mc^2}{2\bar{g}}\, \varepsilon^{abcd} \times$$

$$\times \left(\frac{1}{2}\, g^{rs} g^{pq} \left(\partial_a g_{rs} \right) \left(\partial_b g_{pq} \right) - \left(\partial_a g^{rs} \right) \left(\partial_b g_{rs} \right) \right) R_{[cd]} = 0$$

which is the desired local conservation law. In addition, it is easy to show that

$$\hat{\nabla}_a \bar{j}^a = 0 \,.$$

Unlike the geometric current represented by j^a, the phenomenological current density given by $\bar{j}^a$ corresponds directly to the hydrodynamical analogue of a gravoelectromagnetic current density if we set

$$\bar{j}^a \;=\; \det(g)\; \rho\, u^a$$

which defines charge confinement in our gravoelectrodynamics. Combining this relation with the previously given equivalent expression for j^a, we obtain

$$\rho \;=\; \frac{mc^2}{2\bar{g}} \;\in^{abcd}\; u_a\, g^{rs}\; \left(\partial_b\, g_{rs} \right)\; R_{[cd]}$$

i.e.,

$$\rho \;=\; \frac{mc^2}{\bar{g}} \;\in^{abcd}\; u_a\, \Gamma^h_{hb}\, R_{[cd]}$$

for the gravoelectromagnetic charge density. Note that this is a pseudo-scalar.

At this point, it becomes clear that the gravoelectromagnetic charge density is generated by the properties of the curved space-time itself, i.e., the non-unimodular character of the space-time geometry, for which $\sqrt{\det(g)} = 1$ and $\Gamma^h_{hb} \neq 0$, and the twist (intrinsic spin) of space-time which in general causes material points (whose characteristics are given by $\bar{g}$) to rotate on their own axes such that in a finite region in the space-time manifold, an "individual" energy density emerges. Therefore, in general, a material body is simply a collection of individual material points confined to interact gravoelectrodynamically with each other in a finite region in our curved space-time. More particularly, this can happen in the absence of either the electromagnetic field or the gravitational vorticity, but not in the absence of both fields. To put it more simply, it requires both local curvature and twist to generate a material body out of an energy field.

4 Final remarks

At this point, we may note that we have not considered the conditions for the balance of spin (intrinsic angular momentum) in detail. This may be done, in a straightforward manner, by simply expressing the anti-symmetric part of the generalized Ricci tensor in terms of the so-called spin density tensor as well as the couple stress tensor. This can then be used to develop a system of equations governing the balance of energy-momentum in our theory. Therefore, we also need

to obtain a formal representation for the energy-momentum tensor in terms of the four-momentum vector. This way, we obtain a set of constitutive equations which characterize the theory.

This work has simply been founded on the feeling that it *could* be physically correct as a unified description of physical phenomena due to its manifest simplicity. Perhaps there remains nothing more beyond the simple appreciation of that possibility. It is valid for a large class of particles and (space-time) continua in which the coordinate points themselves are allowed to rotate and translate. Since the particles are directly related to the coordinate points, they are but intrinsic objects in the space-time manifold, just as the fields are.

It remains, therefore, to consider a few physically meaningful circumstances in greater detail for the purpose of finding particular solutions to the semi-symmetric field equations of our theory.

Acknowledgements

I am indebted to my dear friends S. J. Crothers and D. Rabounski and also Prof. B. Suhendro, Prof. S. Hwang, and Prof. S. Antoci for the enlightening discussions in a large number of seemingly separate theoretical and experimental disciplines. I would also like to sincerely express my gratitude for their continuous moral support.

Submitted on July 02, 2007
Accepted on July 16, 2007

References

1. Cartan E. Les systémes différentials extérieurs et leurs applications géométriques. *Actualités scientifiques*, v. 994, Paris, 1945.
2. Rund H. The differential geometry of Finsler spaces. Springer, Berlin-Copenhagen-Heidelberg, 1959.
3. Cartan E. Formes différentielles. Hermann, Paris, 1967.
4. Greub W., Halperin S. and Vanstone R. Connections, curvature and cohomology. Vol. I. Academic Press, New York, 1972.
5. Einstein A. Zür enheitlichen Feldtheorie. Prussian Academy, Berlin, 1929.
6. Weyl H. Gravitation and electricity. Sitz. Berichte d. Preuss. Akad d. Wissenschaften, 1918.
7. Hehl F. W., von der Heyde P., Kerlick G. D. and Nester J. M. General relativity with spin and twist: foundations and prospects. *Rev. Mod. Phys.*, 1976, v. 48, 393–416.
8. Kibble T. W. B. Lorentz invariance and the gravitational field. *J. Math. Phys.*, 1961, v. 2, 212–221.
9. Sciama D. W. On the analogy between charge and spin in general relativity. In: *Recent Developments in General Relativity*, Pergamon Press, Oxford, 1962, 415–439.
10. Forest S. Mechanics of Cosserat media — an introduction. Ecole des Mines de Paris, Paris, 2005.

Optical-Fiber Gravitational Wave Detector: Dynamical 3-Space Turbulence Detected

Reginald T. Cahill

School of Chemistry, Physics and Earth Sciences, Flinders University, Adelaide 5001, Australia
E-mail: Reg.Cahill@flinders.edu.au

Preliminary results from an optical-fiber gravitational wave interferometric detector are reported. The detector is very small, cheap and simple to build and operate. It is assembled from readily available opto-electronic components. A parts list is given. The detector can operate in two modes: one in which only instrument noise is detected, and data from a 24 hour period is reported for this mode, and in a 2nd mode in which the gravitational waves are detected as well, and data from a 24 hour period is analysed. Comparison shows that the instrument has a high S/N ratio. The frequency spectrum of the gravitational waves shows a pink noise spectrum, from 0 to 0.1 Hz.

1 Introduction

Preliminary results from an optical-fiber gravitational wave interferometric detector are reported. The detector is very small, cheap and simple to build and operate, and is shown in Fig. 1. It is assembled from readily available opto-electronic components, and is suitable for amateur and physics undergraduate laboratories. A parts list is given. The detector can operate in two modes: one in which only instrumental noise is detected, and the 2nd in which the gravitational waves are detected as well. Comparison shows that the instrument has a high S/N ratio. The frequency spectrum of the gravitational waves shows a pink noise spectrum, from essentially 0 to 0.1 Hz. The interferometer is 2nd order in v/c and is analogous to a Michelson interferometer. Michelson interferometers in vacuum mode cannot detect the light-speed anisotropy effect or the gravitational waves manifesting as light-speed anisotropy fluctuations. The design and operation as well as preliminary data analysis are reported here so that duplicate detectors may be constructed to study correlations over various distances. The source of the gravitational waves is unknown, but a 3D multi-interferometer detector will soon be able to detect directional characteristics of the waves.

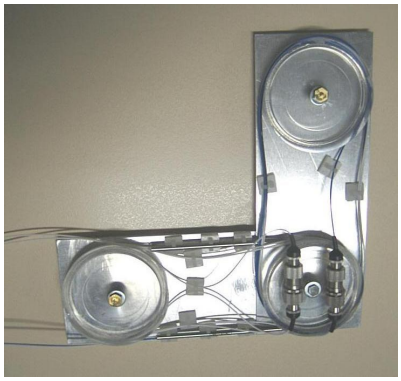

Fig. 1: Photograph of the detector showing the fibers forming the two orthogonal arms. See Fig. 2 for the schematic layout. The beam splitter and joiner are the two small stainless steel cylindrical tubes. The two FC to FC mating sleeves are physically adjacent, and the fibers can be re-connected to change from Mode A (Active detector — gravitational wave and device noise detection) to Mode B (Background — device noise measurements only). The overall dimensions are 160mm×160mm. The 2×2 splitter and joiner each have two input and two output fibers, with one not used.

2 Light speed anisotropy

In 2002 it was reported [1, 2] that light-speed anisotropy had been detected repeatedly since the Michelson-Morley experiment of 1887 [3]. Contrary to popular orthodoxy they reported a light-speed anisotropy up to 8 km/s based on their analysis of their observed fringe shifts. The Michelson-Morley experiment was everything except *null*. The deduced speed was based on Michelson's Newtonian-physics calibration for the interferometer. In 2002 the necessary special relativity effects and the effects of the air present in the light paths were first taken into account in calibrating the interferometer. This reanalysis showed that the actual observed fringe shifts corresponded to a very large light-speed anisotropy, being in excess of 1 part in 1000 of $c = 300{,}000$ km/s. The existence of this light-speed anisotropy is not in conflict with the successes of Special Relativity, although it is in conflict with Einstein's postulate that the speed of light is invariant. This large light-speed anisotropy had gone unnoticed throughout the twentieth century, although we now know that it was detected in seven experiments, ranging from five 2nd order in v/c gas-mode Michelson-interferometer experiments [3–7] to two 1st order in v/c one-way RF coaxial cable travel-speed measurements using atomic clocks [8, 9]. In 2006 another RF travel time coaxial cable experiment was performed [10]. All eight light-speed anisotropy experiments agree [11, 12]. Remarkably five of these experiments [3, 4, 8, 9, 10] reveal pronounced *gravitational wave* effects, where the meaning of this term is explained below. In particular detailed analysis of

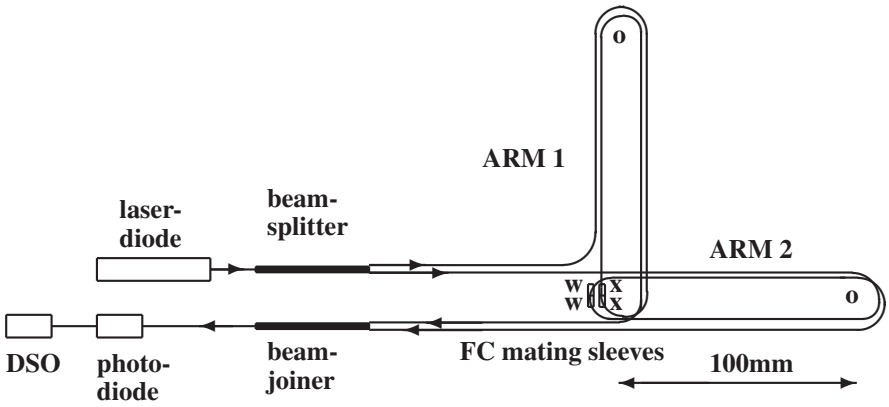

Fig. 2: Schematic layout of the interferometric optical-fiber light-speed anisotropy/gravitational wave detector (in Mode **A**). Actual detector is shown in Fig.1, with ARM2 located to the left, so as to reduce lengths of fiber feeds and overall size. Coherent 650 nm light from the laser diode is split into two 1m length single-mode polarisation preserving fibers by the beam splitter. The two fibers take different directions, ARM1 and ARM2, after which the light is recombined in the beam joiner, which also has 1m length fibers, in which the phase differences lead to interference effects that are indicated by the outgoing light intensity, which is measured in the photodiode, and then recorded in the Digital Storage Oscilloscope (DSO). In Mode **A** the optical fibers are joined $x - x$ and $w - w$ at the FC to FC mating sleeves, as shown. In the actual layout the fibers make four loops in each arm, and the length of one straight section is 100 mm, which is the center to center spacing of the plastic turners, having diameter = 52 mm, see Fig. 1. The two FC to FC mating sleeves are physically adjacent and by re-connecting the fibers as $x - w$ and $w - x$ the light paths can be made symmetrical wrt the arms, giving Mode **B**, which only responds to device noise — the **B**ackground mode. In Mode **A** the detector is **A**ctive, and responds to both flowing 3-space and device noise. The relative travel times, and hence the output light intensity, are affected by the fluctuating speed and direction of the flowing 3-space, by affecting differentially the speed of the light, and hence the net phase difference between the two arms.

the Michelson-Morley fringe shift data shows that they not only detected a large light-speed anisotropy, but that their data also reveals large wave effects [12]. The reason why their interferometer could detect these phenomena was that the light paths passed through air; if a Michelson interferometer is operated in vacuum then changes in the geometric light-path lengths exactly cancel the Fitzgerald-Lorentz arm-length contraction effects. This cancellation is incomplete when a gas is present in the light paths. So modern vacuum Michelson interferometers are incapable of detecting the large light-speed anisotropy or the large gravitational waves. Here we detail the construction of a simple optical-fiber light-speed anisotropy detector, with the main aim being to record and characterise the gravitational waves. These waves reveal a fundamental aspect to reality that is absent in the prevailing models of reality.

3 Dynamical 3-Space and gravitational waves

The light-speed anisotropy experiments reveal that a dynamical 3-space exists, with the speed of light being c only wrt to this space: observers in motion "through" this 3-space detect that the speed of light is in general different from c, and is different in different directions. The notion of a dynamical 3-space is reviewed in [11, 12]. The dynamical equations for this 3-space are now known and involve a velocity field $\mathbf{v}(\mathbf{r}, t)$, but where only relative velocities are observable. The coordinates $\mathbf{r}$ are relative to a non-physical mathematical embedding space. These dynamical equations involve Newton's gravitational constant G and the fine structure constant α. The discovery of this dynamical 3-space then required a generalisation of the Maxwell, Schrödinger and Dirac equations. In particular these equations showed that the phenomenon of gravity is a wave refraction effect, for both EM waves and quantum matter waves [12, 13]. This new physics has been confirmed by explaining the origin of gravity, including the Equivalence Principle, gravitational light bending and lensing, bore hole g anomalies, spiral galaxy rotation anomalies (so doing away with the need for dark matter), black hole mass systematics, and also giving an excellent parameter-free fit to the supernovae and gamma-ray burst Hubble expansion data [14] (so doing away with the need for dark energy). It also predicts a novel spin precession effect in the GPB satellite gyroscope experiment [15]. This physics gives an explanation for the successes of the Special Relativity formalism, and the geodesic formalism of General Relativity. The wave effects already detected correspond to fluctuations in the 3-space velocity field $\mathbf{v}(\mathbf{r}, t)$, so they are really 3-space turbulence or wave effects. However they are better known, if somewhat inappropriately as "gravitational waves" or "ripples" in "spacetime". Because the 3-space dynamics gives a deeper understanding of the spacetime formalism, we now know that the metric of the induced spacetime, merely a mathematical construct having no ontological significance, is related to $\mathbf{v}(\mathbf{r}, t)$ according to [11, 12]

$$ds^2 = dt^2 - \frac{\big(d\mathbf{r} - \mathbf{v}(\mathbf{r}, t)dt\big)^2}{c^2} = g_{\mu\nu}\, dx^\mu dx^\nu . \qquad (1)$$

The gravitational acceleration of matter, and of the structural patterns characterising the 3-space, is given by [12, 13]

$$\mathbf{g} = \frac{\partial \mathbf{v}}{\partial t} + (\mathbf{v} \cdot \nabla)\mathbf{v} \qquad (2)$$

and so fluctuations in $\mathbf{v}(\mathbf{r}, t)$ may or may not manifest as a gravitational force. The general characteristics of $\mathbf{v}(\mathbf{r}, t)$ are now known following the detailed analysis of the eight experiments noted above, namely its average speed, over an hour or so, of some 420 ± 30 km/s, and direction RA $= 5.5 \pm 2^{\text{hr}}$, Dec $= 70 \pm 10^{\circ}$ S, together with large wave/turbulence effects. The magnitude of this turbulence depends on the timing resolution of each particular experiment, and here we report that the speed fluctuations are very large, as also seen in [10] Here we employ a new detector design that enables a detailed study of $\mathbf{v}(\mathbf{r}, t)$, and with small timing resolutions. A key experimental test of the various detections of $\mathbf{v}(\mathbf{r}, t)$ is that the data shows that the time-averaged $\mathbf{v}(\mathbf{r}, t)$ has a direction that has a specific Right Ascension and Declination as given above, i.e. the time for say a maximum averaged speed depends on the local sidereal time, and so varies considerably throughout the year, as do the directions to all astronomical processes/objects. This sidereal effect constitutes an absolute proof that the direction of $\mathbf{v}(\mathbf{r}, t)$ and the accompanying wave effects are real "astronomical" phenomena, as there is no known earth-based effect that can emulate the sidereal effect.

4 Gravitational wave detector

To measure $\mathbf{v}(\mathbf{r}, t)$ has been difficult until now. The early experiments used gas-mode Michelson interferometers, which involved the visual observation of small fringe shifts as the relatively large devices were rotated. The RF coaxial cable experiments had the advantage of permitting electronic recording of the RF travel times, over 500 m [8] and 1.5km [9], by means of two or more atomic clocks, although the experiment reported in [10] used a novel technique that enable the coaxial cable length to be reduced to laboratory size. The new detector design herein has the advantage of electronic recording as well as high precision because the travel time differences in the two orthogonal fibers employ light interference effects, with the interference effects taking place in an optical beam-joiner, and so no optical projection problems arise. The device is very small, very cheap and easily assembled from readily available opto-electronic components. The schematic layout of the detector is given in Fig. 2, with a detailed description in the figure caption. The detector relies on the phenomenon where the 3-space velocity $\mathbf{v}(\mathbf{r}, t)$ affects differently the light travel times in the optical fibers, depending on the projection of $\mathbf{v}(\mathbf{r}, t)$ along the fiber directions. The differences in the light travel times are measured by means of the interference effects in the beam joiner. However at present the calibration constant k of the device is not yet known, so it is not yet known what speed corresponds to the measured time difference Δt, although comparison with the earlier experiments gives a guide. In general we expect

Parts	**Thorlabs** http://www.thorlabs.com/
1x Si Photodiode Detector/ Amplifier/Power Supply	PDA36A or PDA36A-EC select for local AC voltage
1xFiber Adaptor for above	SM1FC
1xFC Fiber Collimation Pkg	F230FC-B
1xLens Mounting Adaptor	AD1109F
2xFC to FC Mating Sleeves	ADAFC1
2x 2x2 Beam Splitters	FC632-50B-FC
Fiber Supports	PFS02
	Midwest Laser Products http://www.midwest-laser.com/
650nm Laser Diode Module	VM65003
LDM Power Supply/3VDC	**Local Supplier or Batteries**
BNC 50Ω coaxial cable	**Local Supplier**
	PoLabs
PoScope USB DSO	http://www.poscope.com/

Table 1: List of parts and possible suppliers for the detector. The FC Collimation Package and Lens Mounting Adaptor together permit the coupling of the Laser Diode Module to the optical fiber connector. This requires unscrewing the lens from the Laser Diode Module and screwing the diode into above and making judicious adjustment to maximise light coupling. The coaxial cable is required to connect the photodiode output to the DSO. Availability of a PC to host the USB DSO is assumed. The complete detector will cost ≈ $1100 US dollars.

$$\Delta t = k^2 \frac{L v_P^2}{c^3} \cos\big(2(\theta - \psi)\big) \qquad (3)$$

where k is the instrument calibration constant. For gas-mode Michelson interferometers k is known to be given by $k^2 \approx \approx n^2 - 1$, where n is the refractive index of the gas. Here $L = 4 \times 100$ mm is the effective arm length, achieved by having four loops of the fibers in each arm, and v_P is the projection of $\mathbf{v}(\mathbf{r}, t)$ onto the plane of the detector. The angle θ is that of the arm relative to the local meridian, while ψ is the angle of the projected velocity, also relative to the local meridian. A photograph of the prototype detector is shown in Figure 1.

A key component is the light source, which can be the laser diode listed in the Table of parts. This has a particularly long coherence length, unlike most cheap laser diodes, although the data reported herein used a more expensive He-Ne laser. The other key components are the fiber beam splitter/joiner, which split the light into the fibers for each arm, and recombine the light for phase difference measurements by means of the fiber-joiner and photodiode detector and amplifier. A key feature of this design is that the detector can oper-

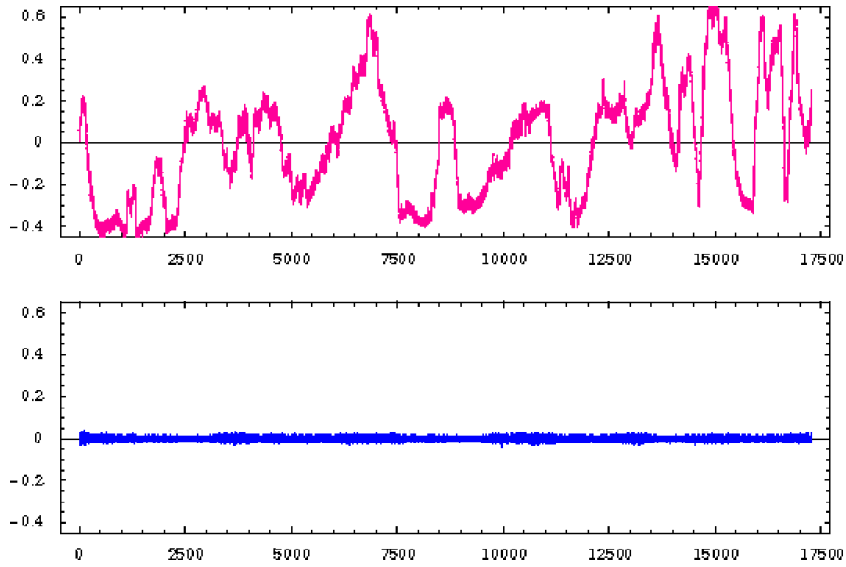

Fig. 3: Photodiode voltages over a 24 hour period with data recording every 5 s, with the detector arms orientated in a NS-EW direction and horizontal. Upper plot (red) is for detector in Mode A, i.e responding to 3-space dynamics and instrument noise, while lower plot (blue) is for Mode B in which detector only responds to instrumental noise, and demonstrates the high S/N ratio of the detector. The lower plot is dominated by higher frequency noise, as seen in the frequency spectrum in Fig. 5. A selection of the above data over a 1 hour time interval, from time steps 4900 to 5620, is shown in Fig. 4 indicating details of the 3-space wave forms.

ate in two different modes. In Mode **A** the detector is **A**ctive, and responds to both flowing 3-space and device noise. Because the two fiber coupler (FC) mating sleeves are physically adjacent a re-connection of the fibers at the two mating sleeves makes the light paths symmetrical wrt the arms, and then the detector only responds to device noise; this is the **B**ackground mode. The data stream may be mostly cheaply recorded by a PoScope USB Digital Storage Oscilloscope (DSO) that runs on a PC.

The interferometer operates by detecting the travel time difference between the two arms as given by (3). The cycle-averaged light intensity emerging from the beam joiner is given by

$$I(t) \propto \left| \mathbf{E}_1 e^{i\omega t} + \mathbf{E}_2 e^{i\omega(t+\tau+\Delta t)} \right|^2 = |\mathbf{E}|^2 \cos\left(\frac{\omega(\tau+\Delta t)}{2}\right)^2 \approx a + b\Delta t \,. \quad (4)$$

Here $\mathbf{E}_i$ are the electric field amplitudes and have the same value as the fiber splitter/joiner are 50%-50% types, and having the same direction because polarisation preserving fibers are used, ω is the light angular frequency and τ is a travel time difference caused by the light travel times not being identical, even when $\Delta t = 0$, mainly because the various splitter/joiner fibers will not be identical in length. The last expression follows because Δt is small, and so the detector operates in a linear regime, in general, unless τ has a value equal to modulo(T), where T is the light period. The main temperature effect in the detector is that τ will be temperature dependent. The photodiode detector output voltage $V(t)$ is proportional to $I(t)$, and so finally linearly related to Δt. The detector calibration constants a and b depend on k and τ, and are unknown at present, and indeed τ will be instrument dependent. The results reported herein show that the value of the calibration constant b is not given by using the effective refractive index of the optical fiber in (3), with b being much smaller than that calculation would suggest. This is in fact very fortunate as otherwise the data would be affected by the need to use the cosine form in (4), and thus would suffer from modulo effects. It is possible to determine the voltages for which (4) is in the non-linear regime by spot heating a segment of one fiber by touching with a finger, as this produces many full fringe shifts.

By having three mutually orthogonal optical-fiber interferometers it is possible to deduce the vectorial direction of $\mathbf{v}(\mathbf{r}, t)$, and so determine, in particular, if the pulses have any particular direction, and so a particular source. The simplicity of this device means that an international network of detectors may be easily set up, primarily to test for correlations in the waveforms.

5 Data analysis

Photodiode voltage readings from the detector in Mode **A** on July 11, 2007, from approximately 12:30pm local time for 24 hours, and in Mode **B** June 24 from 4pm local time for 24 hours, are shown in Fig. 3, with an arbitrary zero. The photodiode output voltages were recorded every 5 s. Most importantly the data are very different, showing that only in Mode **A** are gravitational waves detected, and with a high S/N

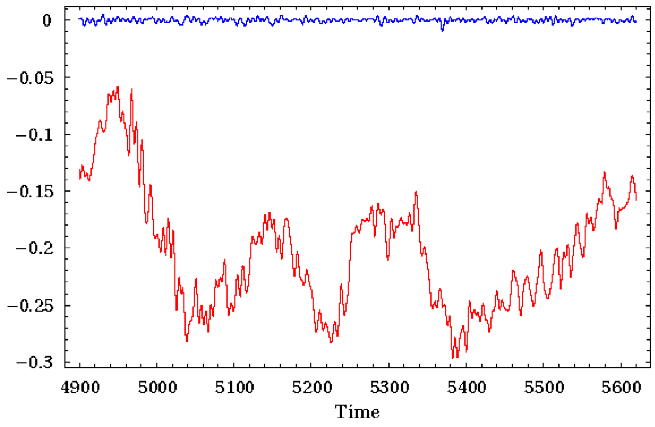

Fig. 4: Lower plot (red) shows the time series data over a 1 hour period, from time steps 4900 to 5620 in Fig. 3, showing the wave forms present in Fig. 3 in greater detail. Similar complex wave forms were seen in [10]. These plots were reconstructed from the FT after band passing the frequencies (1–3000)$\times 1.16\times 10^{-5}$Hz=(0.000116–0.034) Hz to reduce the instrument noise component, which is very small as shown in upper plot (blue).

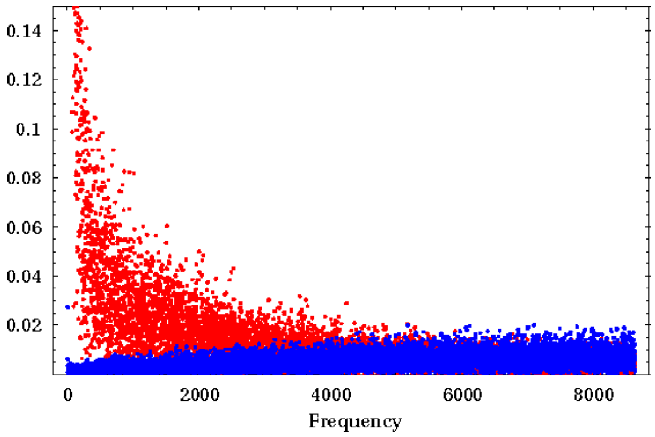

Fig. 5: Two plots of $|\widetilde{V}_s|$ from Fast Fourier Transforms of the photodiode detector voltage V_r at 5 second intervals for 24 fours. Frequency step corresponds to 1.157×10^{-5}Hz. Upper frequency spectrum (red) is for detector in Mode A, i.e responding to 3-space dynamics and instrument noise, while lower spectrum (blue) is for Mode B in which detector only responds to instrumental noise. We see that the signal in Mode A is very different from that Mode B operation, showing that the S/N ratio for the detector is very high. The instrumental noise has a mild "blue" noise spectrum, with a small increase at higher frequencies, while the 3-space turbulence has a distinctive "pink" noise spectrum.

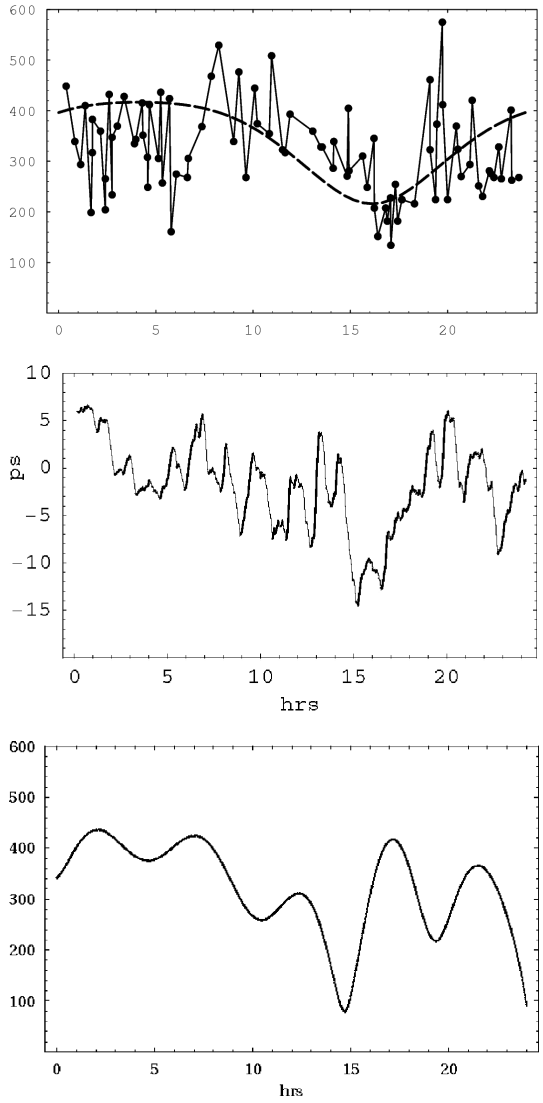

Fig. 6: *Top*: Absolute projected speeds v_P in the Miller experiment plotted against sidereal time in hours for a composite day collected over a number of days in September 1925. Maximum projected speed is 417 km/s. The data shows considerable fluctuations. The dashed curve shows the non-fluctuating variation expected over one day as the Earth rotates, causing the projection onto the plane of the interferometer of the velocity of the average direction of the 3-space flow to change. *Middle*: Data from the Cahill experiment [10] for one sidereal day on approximately August 23, 2006. We see similar variation with sidereal time, and also similar wave structure. This data has been averaged over a running 1hr time interval to more closely match the time resolution of the Miller experiment. These fluctuations are real wave phenomena of the 3-space. *Bottom*: Data from the optical-fiber experiment herein with only low frequencies included to simulate the time averaging in the other two experiments. Comparison permits an approximate calibration for the optical fiber detector, as indicated by the speed in km/s.

ratio. A 1 hour time segment of that data is shown in Fig. 4. In that plot the higher frequencies have been filtered out from both data time series, showing the exceptional S/N ratio that can be achieved.

In Fig. 5 the Fourier Transfoms of the two data time series are shown, again revealing the very different characteristics of the data from the two operating modes. The instrumental noise has a mild "blue" noise spectrum, with a small increase at higher frequencies, while the 3-space turbulence has a distinctive "pink" noise spectrum, and ranging essentially from 0 to 0.1 Hz. The FT is defined by

$$\widetilde{V}_s = \frac{1}{\sqrt{n}} \sum_{r=1}^{n} V_r e^{2\pi i(r-1)(s-1)/n} \qquad (5)$$

where $n = 17280$ corresponds to a 5 s timing interval over 24 hours.

By removing all but the FT amplitudes 1–10, and then inverse Fourier Transforming we obtain the slow changes occurring over 24 hours. The resulting data has been presented in terms of possible values for the projected speed v_P in (3), and is shown in Fig. 6 and plotted against sidereal time, after adjusting the unknown calibration constants to give a form resembling the Miller and coaxial cable experimental results so as to give some indication of the calibration of the detector. The experiment was run in an unoccupied office in which temperatures varied by some 10°C over the 24 hour periods. In future temperature control will be introduced.

6 Conclusions

As reviewed in [11, 12] gravitational waves, that is, fluctuations or turbulence in the dynamical 3-space, have been detected since the 1887 Michelson-Morley experiment, although this all went unrealised until recently. As the timing resolution improved over the century, from initially one hour to seconds now, the characteristics of the turbulence of the dynamical 3-space have become more apparent, and that at smaller timing resolutions the turbulence is seen to be very large. As shown herein this wave/pulse phenomenon is very easy to detect, and opens up a whole new window on the universe. The detector reported here took measurements every 5 s, but can be run at millisecond acquisition rates. A 3D version of the detector with three orthogonal optical-fiber interferometers will soon become operational. This will permit the determination of the directional characteristics of the 3-space pulses.

That the average 3-space flow will affect the gyroscope precessions in the GP-B satellite experiment through vorticity effects was reported in [15]. The fluctuations are also predicted to be detectable in that experiment as noted in [16]. However the much larger fluctuations detected in [10] and herein imply that these effects will be much large than reported in [16] where the time averaged waves from the DeWitte experiment [9] were used; essentially the gyro precessions will appear to have a large stochasticity.

Special thanks to Peter Morris, Thomas Goodey, Tim Eastman, Finn Stokes and Dmitri Rabounski.

Submitted on July 09, 2007
Accepted on July 16, 2007

References

1. Cahill R.T. and Kitto K. Michelson-Morley experiments revisited. *Apeiron*, 2003, v. 10(2),104–117.
2. Cahill R.T. The Michelson and Morley 1887 experiment and the discovery of absolute motion. *Progress in Physics*, 2005, v. 3, 25–29.
3. Michelson A. A. and Morley E. W. *Philos. Mag.*, 1887, S. 5, 24, No. 151, 449–463.
4. Miller D. C. *Rev. Mod. Phys.*, 1933, v. 5, 203–242.
5. Illingworth K. K. *Phys. Rev.*, 1927, v. 3, 692–696.
6. Joos G. *Ann. d. Physik*, 1930, v. 7, 385.
7. Jaseja T. S. *et al. Phys. Rev. A*, 1964, v. 133, 1221.
8. Torr D. G. and Kolen P. In: *Precision Measurements and Fundamental Constants*, Taylor, B. N. and Phillips, W. D. eds., Natl. Bur. Stand. (U.S.), Spec. Publ., 1984, v. 617, 675.
9. Cahill R. T. The Roland DeWitte 1991 experiment. *Progress in Physics*, 2006, v. 3, 60–65.
10. Cahill R. T. A new light-speed anisotropy experiment: absolute motion and gravitational waves detected. *Progress in Physics*, 2006, v. 4, 73–92.
11. Cahill R. T. Process physics: from information theory to quantum space and matter. Nova Science Pub., New York, 2005.
12. Cahill R. T. Dynamical 3-space: a review. arXiv: 0705.4146.
13. Cahill R. T. Dynamical fractal 3-space and the generalised Schrödinger equation: equivalence principle and vorticity effects. *Progress in Physics*, 2006, v. 1, 27–34.
14. Cahill R. T. Dynamical 3-space: supernovae and the Hubble expansion — the older Universe without Dark Energy. *Progress in Physics*, 2007, v. 4, 9–12.
15. Cahill R. T. Novel Gravity Probe B frame-dragging effect. *Progress in Physics*, 2005, v. 3, 30–33.
16. Cahill R. T. Novel Gravity Probe B gravitational wave detection. arXiv: physics/0407133.

On the "Size" of Einstein's Spherically Symmetric Universe

Stephen J. Crothers
Queensland, Australia
E-mail: thenarmis@yahoo.com

It is alleged by the Standard Cosmological Model that Einstein's Universe is finite but unbounded. Although this is a longstanding and widespread allegation, it is nonetheless incorrect. It is also alleged by this Model that the Universe is expanding and that it began with a Big Bang. These are also longstanding and widespread claims that are demonstrably false. The FRW models for an expanding, finite, unbounded Universe are inconsistent with General Relativity and are therefore invalid.

1 Historical basis

Non-static homogeneous models were first investigated theoretically by Friedmann in 1922. The concept of the Big Bang began with Lemaître, in 1927, who subsequently asserted that the Universe, according to General Relativity, came into existence from a "primaeval atom".

Following Friedmann, the work of Robertson and Walker resulted in the FRW line-element,

$$ds^2 = dt^2 - R^2(t)\left[\frac{dr^2}{1-kr^2} + r^2\left(d\theta^2 + \sin^2\theta\, d\varphi^2\right)\right],$$

from which is obtained the so-called "Friedmann equation",

$$\dot{R}^2 + k = \frac{8\pi G}{3}\,\rho R^2,$$

where ρ is the macroscopic proper density of the Universe and k a constant. Applying the continuity condition $T^{\mu\nu}{}_{;\mu} = 0$, to the stress tensor $T_{\mu\nu}$ of a perfect fluid

$$T_{\mu\nu} = (\rho + p)u_\mu u_\nu - p g_{\mu\nu},$$

where p is the pressure and u_μ the covariant world velocity of the fluid particles, the equation of continuity becomes

$$R\dot{\rho} + 3\dot{R}(\rho + p) = 0\,.$$

With the *ad hoc* assumption that $R(0) = 0$, the Friedmann equation is routinely written as

$$\dot{R}^2 + k = \frac{A^2}{R}\,,$$

where A is a constant. The so-called "Friedmann models" are:

(1) $k = 0$ — the flat model,

(2) $k = 1$ — the closed model,

(3) $k = -1$ — the open model,

wherein $t = 0$ is claimed to mark the beginning of the Universe and $R(0) = 0$ the cosmological singularity.

Big Bang and expansion now dominate thinking in contemporary cosmology. However, it is nonetheless easily proved that such cosmological models, insofar as they relate to the FRW line-element, with or without embellishments such as "inflation", are in fact inconsistent with the mathematical structure of the line-elements from which they are alleged, and are therefore false.

2 Spherically symmetric metric manifolds

A 3-D spherically symmetric metric manifold has, in the spherical-polar coordinates, the following form ([1, 2]),

$$ds^2 = B(R_c)dR_c^2 + R_c^2(d\theta^2 + \sin^2\theta\, d\varphi^2)\,, \qquad (1)$$

where $B(R_c)$ and $R_c = R_c(r)$ are *a priori* unknown analytic functions of the variable r of the simple line element

$$ds^2 = dr^2 + r^2(d\theta^2 + \sin^2\theta\, d\varphi^2)\,, \qquad (2)$$

$$0 \leqslant r \leqslant \infty\,.$$

Line elements (1) and (2) have precisely the same fundamental geometric form and so the geometric relations between the components of the metric tensor are exactly the same in each line element. The quantity R_c appearing in (1) is not the geodesic radial distance associated with the manifold it describes. It is in fact the *radius of curvature*, in that it determines the Gaussian curvature $G = 1/R_c^2$ (see [1, 2]). The geodesic radial distance distance, R_p, from an arbitrary point in the manifold described by (1) is an intrinsic geometric property of the line element, and is given by

$$R_p = \int \sqrt{B(R_c)}\, dR_c + C = \int \sqrt{B(R_c)}\, \frac{dR_c}{dr} dr + C\,,$$

where C is a constant of integration to be determined ([2]). Therefore, (1) can be written as

$$ds^2 = dR_p^2 + R_c^2(d\theta^2 + \sin^2\theta\, d\varphi^2)\,,$$

where

$$dR_p = \sqrt{B(R_c)}\, dR_c\,,$$

and

$$0 \leqslant R_p < \infty\,,$$

with the possibility of the line element being singular (undefined) at $R_p = 0$, since $B(R_c)$ and $R_c = R_c(r)$ are *a priori* unknown analytic functions of the variable r. In the case of (2),

$$R_c(r) \equiv r, \quad dR_p \equiv dr, \quad B(R_c(r)) \equiv 1,$$

from which it follows that $R_c \equiv R_p \equiv r$ in the case of (2). Thus $R_c \equiv R_p$ is not general, and only occurs in the special case of (2), which describes an Efcleethean* space.

The volume V of (1), and therefore of (2), is

$$\begin{aligned} V &= \int_0^{R_p} R_c^2 \, dR_p \int_0^{\pi} \sin\theta \, d\theta \int_0^{2\pi} d\varphi = \\ &= 4\pi \int_{R_c(0)}^{R_c(r)} R_c^2(r) \sqrt{B(R_c(r))} \, dR_c(r) = \\ &= 4\pi \int_0^{r} R_c^2(r) \sqrt{B(R_c(r))} \, \frac{dR_c(r)}{dr} \, dr, \end{aligned}$$

although, in the general case (1), owing to the *a priori* unknown functions $B(R_c(r))$ and $R_c(r)$, the line element (1) may be undefined at $R_p(R_c(0)) = R_p(r = 0) = 0$, which is the location of the centre of spherical symmetry of the manifold of (1) at an arbitrary point in the manifold. Also, since $R_c(r)$ is *a priori* unknown, the value of $R_c(0)$ is unknown and so it cannot be assumed that $R_c(0) = 0$. In the special case of (2), both $B(R_c(r))$ and $R_c(r)$ *are known*.

Similarly, the surface area S of (1), and hence of (2), is given by the general expression,

$$S = R_c^2(r) \int_0^{\pi} \sin\theta \, d\theta \int_0^{2\pi} d\varphi = 4\pi R_c^2(r).$$

This might not ever be zero, since, once again, $R_c(r)$ is an *a priori* unknown function and so $R_c(0)$ might not be zero. It all depends an the explicit form for $R_c(r)$, if it can be determined in a given situation, and on associated boundary conditions. References [1, 2] herein describe the mathematics in more detail.

3 The "radius" of Einstein's universe

Since a geometry is entirely determined by the *form* of its line element [3], everything must be determined from it. One cannot, as is usually done, merely foist assumptions upon it. The *intrinsic* geometry of the line element and the consequent geometrical relations between the components of the metric tensor determine all.

Consider the usual non-static cosmological line element

$$ds^2 = dt^2 - \frac{e^{g(t)}}{\left(1+\frac{k}{4}\,\bar{r}^2\right)^2}\left[d\bar{r}^2+\bar{r}^2\left(d\theta^2+\sin^2\theta\, d\varphi^2\right)\right], \quad (3)$$

wherein it is usually simply *assumed* that $0 \leqslant \bar{r} < \infty$ [3–6].

*For the geometry due to Efcleethees, usually and abominably rendered as Euclid.

However, the range on $\bar{r}$ must be determined, not assumed. It is easily proved that the foregoing usual assumption is patently false.

Once again note that in (3) the quantity $\bar{r}$ is not a radial geodesic distance. In fact, it is not even a radius of curvature on (3). It is merely a parameter for the radius of curvature and the proper radius, both of which are well-defined by the *form* of the line element (describing a spherically symmetric metric manifold). The radius of curvature, R_c, for (3), is

$$R_c = e^{\frac{1}{2}g(t)} \frac{\bar{r}}{1+\frac{k}{4}\,\bar{r}^2}. \quad (4)$$

The proper radius for (3) is given by

$$\begin{aligned} R_p &= e^{\frac{1}{2}g(t)} \int \frac{d\bar{r}}{1+\frac{k}{4}\,\bar{r}^2} = \\ &= \frac{2e^{\frac{1}{2}g(t)}}{\sqrt{k}} \left(\arctan\frac{\sqrt{k}}{2}\,\bar{r} + n\pi\right), \quad n = 0, 1, 2, \ldots \end{aligned} \quad (5)$$

Since $R_p \geqslant 0$ by definition, $R_p = 0$ is satisfied when $\bar{r} = 0 = n$. So $\bar{r} = 0$ is the lower bound on $\bar{r}$. The upper bound on $\bar{r}$ must now be ascertained from the line element and boundary conditions.

It is noted that the spatial component of (4) has a maximum of $\frac{1}{\sqrt{k}}$ for any time t, when $\bar{r} = \frac{2}{\sqrt{k}}$. Thus, as $\bar{r} \to \infty$, the spatial component of R_c runs from 0 (at $\bar{r} = 0$) to the maximum $\frac{1}{\sqrt{k}}$ (at $\bar{r} = \frac{2}{\sqrt{k}}$), then back to zero, since

$$\lim_{\bar{r}\to\infty} \frac{\bar{r}}{1+\frac{k}{4}\,\bar{r}^2} = 0. \quad (6)$$

Transform (3) by setting

$$R = R(\bar{r}) = \frac{\bar{r}}{1+\frac{k}{4}\,\bar{r}^2}, \quad (7)$$

which carries (3) into

$$ds^2 = dt^2 - e^{g(t)}\left[\frac{dR^2}{1-kR^2} + R^2\left(d\theta^2+\sin^2\theta\, d\varphi^2\right)\right]. \quad (8)$$

The quantity R appearing in (8) is *not* a radial geodesic distance. It is only a factor in a radius of curvature in that it determines the Gaussian curvature $G = \frac{1}{e^{g(t)}R^2}$. The radius of curvature of (8) is

$$R_c = e^{\frac{1}{2}g(t)} R, \quad (9)$$

and the proper radius of Einstein's universe is, by (8),

$$\begin{aligned} R_p &= e^{\frac{1}{2}g(t)} \int \frac{dR}{\sqrt{1-kR^2}} = \\ &= \frac{e^{\frac{1}{2}g(t)}}{\sqrt{k}} \left(\arcsin\sqrt{k}R + 2m\pi\right), \quad m = 0, 1, 2, \ldots \end{aligned} \quad (10)$$

Now according to (7), the minimum value of R is $R(\bar{r}=0)=0$. Also, according to (7), the maximum value

of R is $R(\bar{r}=\frac{2}{\sqrt{k}})=\frac{1}{\sqrt{k}}$. $R=\frac{1}{\sqrt{k}}$ makes (8) singular, although (3) is not singular at $\bar{r}=\frac{2}{\sqrt{k}}$. Since by (7), $\bar{r}\to\infty\Rightarrow R(\bar{r})\to 0$, then if $0\leqslant\bar{r}<\infty$ on (3) it follows that the proper radius of Einstein's universe is, according to (8),

$$R_p = e^{\frac{1}{2}g(t)}\int_0^0 \frac{dR}{\sqrt{1-kR^2}} \equiv 0\,. \tag{11}$$

Therefore, $0\leqslant\bar{r}<\infty$ on (3) is false. Furthermore, since the proper radius of Einstein's universe cannot be zero and cannot depend upon a set of coordinates (it must be an invariant), expressions (5) and (10) must agree. Similarly, the radius of curvature of Einstein's universe must be an invariant (independent of a set of coordinates), so expressions (4) and (9) must also agree, in which case $0\leqslant R<\frac{1}{\sqrt{k}}$ and $0\leqslant\bar{r}<\frac{2}{\sqrt{k}}$. Then by (5), the proper radius of Einstein's universe is

$$R_p = \lim_{\alpha\to\frac{2}{\sqrt{k}}} e^{\frac{1}{2}g(t)}\int_0^\alpha \frac{d\bar{r}}{1+\frac{k}{4}\bar{r}^2} =$$

$$= \frac{2e^{\frac{1}{2}g(t)}}{\sqrt{k}}\left[\left(\frac{\pi}{4}+n\pi\right)-m\pi\right],\quad n,m=0,1,2,\ldots$$

$$n\geqslant m\,.$$

Setting $p=n-m$ gives for the proper radius of Einstein's universe,

$$R_p = \frac{2e^{\frac{1}{2}g(t)}}{\sqrt{k}}\left(\frac{\pi}{4}+p\pi\right),\quad p=0,1,2,\ldots \tag{12}$$

Now by (10), the proper radius of Einstein's universe is

$$R_p = \lim_{\alpha\to\frac{1}{\sqrt{k}}} e^{\frac{1}{2}g(t)}\int_0^\alpha \frac{dR}{\sqrt{1-kR^2}} =$$

$$= \frac{e^{\frac{1}{2}g(t)}}{\sqrt{k}}\left[\left(\frac{\pi}{2}+2n\pi\right)-m\pi\right],\quad n,m=0,1,2,\ldots$$

$$2n\geqslant m\,.$$

Setting $q=2n-m$ gives the proper radius of Einstein's universe as,

$$R_p = \frac{e^{\frac{1}{2}g(t)}}{\sqrt{k}}\left(\frac{\pi}{2}+q\pi\right),\quad q=0,1,2,\ldots \tag{13}$$

Expressions (12) and (13) must be equal for all values of p and q. This can only occur if $g(t)$ is infinite for all values of t. Thus, the proper radius of Einstein's universe is infinite.

By (4), (7) and (9), the invariant radius of curvature of Einstein's universe is,

$$R_c\left(\frac{2}{\sqrt{k}}\right) = \frac{e^{\frac{1}{2}g(t)}}{\sqrt{k}}, \tag{14}$$

which is infinite by virtue of $g(t)=\infty\;\forall\;t$.

4 The "volume" of Einstein's universe

The volume of Einstein's universe is, according to (3),

$$V = e^{\frac{3}{2}g(t)}\int_0^{\frac{2}{\sqrt{k}}}\frac{\bar{r}^2\,d\bar{r}}{\left(1+\frac{k}{4}\bar{r}^2\right)^3}\int_0^\pi\sin\theta\,d\theta\int_0^{2\pi}d\varphi\;= \tag{15}$$

$$= \frac{4\pi e^{\frac{3}{2}g(t)}}{k^{\frac{3}{2}}}\left(\frac{\pi}{4}+p\pi\right),\quad p=0,1,2,\ldots$$

The volume of Einstein's universe is, according to (8),

$$V = e^{\frac{3}{2}g(t)}\int_0^{\frac{1}{\sqrt{k}}}\frac{R^2\,dR}{\sqrt{1-kR^2}}\int_0^\pi\sin\theta\,d\theta\int_0^{2\pi}d\varphi\;=$$

$$= e^{\frac{3}{2}g(t)}\frac{2\pi}{k^{\frac{3}{2}}}\left[\frac{\pi}{2}+(2n-m)\,\pi\right],\quad n,m=0,1,2,\ldots$$

$$2n\geqslant m\,,$$

and setting $q=2n-m$ this becomes,

$$V = \frac{2\pi e^{\frac{3}{2}g(t)}}{k^{\frac{3}{2}}}\left(\frac{\pi}{2}+q\pi\right),\quad q=0,1,2,\ldots \tag{16}$$

Since the volume of Einstein's universe must be an invariant, expressions (15) and (16) must be equal for all values of p and q. Equality can only occur if $g(t)$ is infinite for all values of the time t. Thus the volume of Einstein's universe is infinite.

In the usual treatment (8) is transformed by setting

$$R = \frac{1}{\sqrt{k}}\sin\chi, \tag{17}$$

to get

$$ds^2 = dt^2 - \frac{e^{g(t)}}{k}\left[d\chi^2+\sin^2\chi(d\theta^2+\sin^2\theta\,d\varphi^2)\right], \tag{18}$$

where it is usually asserted, without any proof (see e.g. [3, 4, 5, 6]), that

$$0\leqslant\chi\leqslant\pi\quad(\text{or } 0\leqslant\chi\leqslant 2\pi), \tag{19}$$

and whereby (18) is not singular. However, according to (7), (11), (12), and (13), χ can only take the values

$$2n\pi\leqslant\chi<\frac{\pi}{2}+2n\pi,\quad n=0,1,2,\ldots$$

so that the radius of curvature of Einstein's universe is, by (18),

$$R_c = \frac{e^{\frac{1}{2}g(t)}\sin\chi}{\sqrt{k}}$$

which must be evaluated for $\chi=\frac{\pi}{2}+2n\pi$, $n=0,1,2,\ldots$, giving

$$R_c = \frac{e^{\frac{1}{2}g(t)}}{\sqrt{k}}$$

as the radius of curvature of Einstein's universe, in concordance with (4), (7), and (9). The proper radius of Einstein's

universe is given by

$$R_p = \frac{e^{\frac{1}{2}g(t)}}{\sqrt{k}} \int_{2n\pi}^{\frac{\pi}{2}+2n\pi} d\chi = \frac{e^{\frac{1}{2}g(t)}}{\sqrt{k}} \frac{\pi}{2}, \tag{20}$$

and since the proper radius of Einstein's universe is an invariant, (20) must equal (12) and (13). Expression (20) is consistent with (12) and (13) only if $g(t)$ is infinite for all values of the time t, and so Einstein's universe is infinite.

According to (18), the volume of Einstein's universe is,

$$V = \frac{e^{\frac{3}{2}g(t)}}{k^{\frac{3}{2}}} \int_{2n\pi}^{\frac{\pi}{2}+2n\pi} \sin^2\chi \, d\chi \int_0^{\pi} \sin\theta d\theta \int_0^{2\pi} d\varphi = \\ = \frac{\pi^2 e^{\frac{3}{2}g(t)}}{k^{\frac{3}{2}}} \frac{\pi}{2}. \tag{21}$$

Since this volume must be an invariant, expression (21) must give the same value as expressions (15) and (16). This can only occur for (21) if $g(t)$ is infinite for all values of the time t, and so Einstein's universe has an infinite volume.

5 The "area" of Einstein's universe

Using (3), the invariant surface area of Einstein's universe is

$$S = R_c^2 \int_0^{\pi} \sin\theta d\theta \int_0^{2\pi} d\varphi = 4\pi R_c^2$$

which must be evaluated for $R_c(\bar{r} = \frac{2}{\sqrt{k}})$, according to (4), and so

$$S = \frac{4\pi e^{g(t)}}{k}.$$

By (8) the invariant surface area is

$$S = e^{g(t)} R^2 \int_0^{\pi} \sin\theta d\theta \int_0^{2\pi} d\varphi = 4\pi R^2 e^{g(t)},$$

which must, according to (7), be evaluated for $R(\bar{r} = \frac{2}{\sqrt{k}}) = \frac{1}{\sqrt{k}}$, to give

$$S = \frac{4\pi e^{g(t)}}{k}.$$

By (18) the invariant surface area is

$$S = \frac{e^{g(t)}}{k} \sin^2\chi \int_0^{\pi} \sin\theta d\theta \int_0^{2\pi} d\varphi = \frac{4\pi e^{g(t)}}{k} \sin^2\chi,$$

and this, according to (17), must be evaluated for $\chi = \left(\frac{\pi}{2} + 2n\pi\right)$, $n = 0, 1, 2, \ldots$, which gives

$$S = \frac{4\pi e^{g(t)}}{k}.$$

Thus the invariant surface area of Einstein's universe is infinite for all values of the time t, since $g(t)$ is infinite for all values of t.

In similar fashion the invariant great "circumference", $C = 2\pi R_c$, of Einstein's universe is infinite at any particular time, given by

$$C = \frac{2\pi e^{\frac{1}{2}g(t)}}{\sqrt{k}}.$$

6 Generalisation of the line element

Line elements (3), (8) and (18) can be generalised in the following way. In (3), replace $\bar{r}$ by $|\bar{r} - \bar{r}_0|$ to get

$$ds^2 = dt^2 - \frac{e^{g(t)}}{\left(1 + \frac{k}{4}|\bar{r} - \bar{r}_0|^2\right)^2} \times \\ \times \left[d\bar{r}^2 + |\bar{r} - \bar{r}_0|^2 (d\theta^2 + \sin^2\theta \, d\varphi^2)\right], \tag{22}$$

where $\bar{r}_0 \in \Re$ is entirely arbitrary. Line element (22) is defined on

$$0 \leqslant |\bar{r} - \bar{r}_0| < \frac{2}{\sqrt{k}} \quad \forall \quad \bar{r}_0,$$

i.e. on

$$\bar{r}_0 - \frac{2}{\sqrt{k}} < \bar{r} < \frac{2}{\sqrt{k}} + \bar{r}_0 \quad \forall \quad \bar{r}_0. \tag{23}$$

This corresponds to $0 \leqslant R_c < \frac{1}{\sqrt{k}}$ irrespective of the value of $\bar{r}_0$, and amplifies the fact that $\bar{r}$ is merely a parameter. Indeed, (4) is generalised to

$$R_c = R_c(\bar{r}) = \frac{|\bar{r} - \bar{r}_0|}{1 + \frac{k}{4}|\bar{r} - \bar{r}_0|^2},$$

where (23) applies. Note that $\bar{r}$ can approach $\bar{r}_0$ from above or below. Thus, there is nothing special about $\bar{r}_0 = 0$. If $\bar{r}_0 = 0$ and $\bar{r} \geqslant 0$, then (3) is recovered as a special case, still subject of course to the range $0 \leqslant \bar{r} < \frac{2}{\sqrt{k}}$.

Expression (7) is generalised thus,

$$|R - R_0| = \frac{|\bar{r} - \bar{r}_0|}{1 + \frac{k}{4}|\bar{r} - \bar{r}_0|^2},$$

where R_0 is an entirely arbitrary real number, and so (8) becomes

$$ds^2 = dt^2 - e^{g(t)} \times \\ \times \left[\frac{dR^2}{1 - k|R - R_0|^2} + |R - R_0|^2 (d\theta^2 + \sin^2\theta \, d\varphi^2)\right], \tag{24}$$

where

$$R_0 - \frac{1}{\sqrt{k}} < R < \frac{1}{\sqrt{k}} + R_0 \quad \forall \quad R_0. \tag{25}$$

Note that R can approach R_0 from above or below. There is nothing special about $R_0 = 0$. If $R_0 = 0$ and $R \geqslant 0$, then (8) is recovered as a special case, subject of course to the range $0 \leqslant R < \frac{1}{\sqrt{k}}$.

Similarly, (18) is generalised, according to (24), by setting

$$|R - R_0| = \frac{1}{\sqrt{k}} \sin|\chi - \chi_0|,$$

where χ_0 is an entirely arbitrary real number, and

$$2n\pi \leqslant |\chi - \chi_0| < \frac{\pi}{2} + 2n\pi, \quad n = 0, 1, 2, \ldots$$

$$\forall\, \chi_0 \in \Re.$$

Note that χ can approach χ_0 from above or below. There is nothing special about $\chi_0 = 0$. If $\chi_0 = 0$ and $\chi \geqslant 0$, then (18) is recovered as a special case, subject of course to the range $2n\pi \leqslant \chi < \frac{\pi}{2} + 2n\pi$, $n = 0, 1, 2, \ldots$

The corresponding expressions for the great circumference, the surface area, and the volume are easily obtained in like fashion.

7 Conclusions

Einstein's universe has an infinite proper radius, an infinite radius of curvature, an infinite surface area and an infinite volume at any time. Thus, in relation to the Friedmann-Robertson-Walker line-element and its variations considered herein, the concept of the Big Bang cosmology is invalid.

Submitted on July 16, 2007
Accepted on July 20, 2007

References

1. Levi-Civita T. The absolute differential calculus. Dover Publications Inc., New York, 1977.
2. Crothers S. J., Gravitation on a spherically symmetric metric manifold. *Progress in Physics*, 2005, v. 2, 68–74.
3. Tolman R. C. Relativity, thermodynamics and cosmology. Dover Publications Inc., New York, 1987.
4. Landau L., Lifshitz E. The classical theory of fields. Addison-Wesley Publishing Company, Inc., Reading, Massachusettes, 1951.
5. d'Inverno R. Introducing Einstein's relativity. Clarendon Press, Oxford, 1992.
6. Misner C. W., Thorne K. S., and Wheeler J. A. Gravitation. W. H. Freeman and Company, New York, 1973.

On the Nature of the Microwave Background at the Lagrange 2 Point. Part I

Pierre-Marie Robitaille

Dept. of Radiology, The Ohio State University, 130 Means Hall, 1654 Upham Drive, Columbus, Ohio 43210, USA
E-mail: robitaille.1@osu.edu

In this work, the nature of the microwave background is discussed. It is advanced that the 2.725 K monopole signal, first detected by Penzias and Wilson, originates from the Earth and therefore cannot be detected at the Lagrange 2 point (L2). Results obtained by the COBE, Relikt-1, and WMAP satellites are briefly reviewed. Attention is also placed on the upcoming PLANCK mission, with particular emphasis on the low frequency instrument (LFI). Since the LFI on PLANCK can operate both in absolute mode and in difference mode, this instrument should be able to unequivocally resolve any question relative to the origin of the 2.725 K monopole signal. The monopole will be discovered to originate from the Earth and not from the Cosmos. This will have implications relative to the overall performance of the PLANCK satellite, in particular, and for the future of astrophysics, in general.

1 Introduction

In 1965, a thermal signal of unknown origin, which appeared to completely engulf the Earth, irrespective of angle of observation, was first reported to exist at microwave frequencies [1]. Immediately considered of great importance, the strange finding was rapidly attributed to the universe by Dicke et al. [2] in a communication which preceded the disclosure of the actual measurements by A. A. Penzias and R. W. Wilson [1]. The observation became known as the "Cosmic Microwave Background (CMB)" nearly from the instant of discovery [1, 2]. For years, it had been predicted that such a signal must exist, if the universe evolved from a Big Bang scenario. With the advent of the Penzias and Wilson measurement [1], the long sought signature of creation seemed discovered, and cosmology entered the realm of modern science.

Since that time, the "CMB" has become a cornerstone of astrophysics [3–6]. The background and its characteristic 2.725 K monopole temperature [7, 8], the "relic of the Big Bang", is believed to span the entire known universe. While the "CMB" was initially considered weak, it is now clear that the signal was in fact quite powerful, at least when viewed from Earth orbit (8). Indeed, few experimental signals of natural origin have surpassed the microwave background in absolute signal to noise [8]. For cosmology, the "CMB" is the most important "astrophysical" finding. Experimental confirmations of its existence and characterization have consumed vast amounts of both financial and human capital. As a result, a more detailed understanding of the microwave background has emerged.

In addition to its characteristic monopole temperature at 2.725 K [8], the background has associated with it a strong (3.5 mK) dipole which is ascribed to the motion of the Earth and the Sun through the local group [9]. This powerful dipole has been observed not only on Earth, and in Earth orbit [9], but also by instruments located well beyond the Earth, like the Soviet Relikt-1 [10] and the NASA WMAP [11] satellites. Consequently, there can be little question that the dipole is real, and truly associated with motion through the local group.

Beyond the dipole, cosmology has also placed significant emphasis on the multipoles visible at microwave frequencies [12]. Accordingly, the universe has now been characterized by anisotropy maps, the most famous of which have been reported by the COBE [7] and WMAP [11] satellites. These maps reflect very slight differences in microwave power of the universe as a function of observational direction.

The recent array of scientific evidence, in support of a microwave background of cosmological origin, appears tremendous, and cosmology seems to have evolved into a precision science [13–19]. Should the 2.725 K microwave background truly belong to the universe, there can be little question that cosmology has joined the company of the established experimental disciplines. Yet, these claims remain directly linked to the validity of the assignment for the "Cosmic Microwave Background". Indeed, if the "CMB" is reassigned to a different source, astrophysics will undergo significant transformations.

2 The origin of the microwave background

Recently, the origin of the "CMB" has been brought into question, and the monopole of the microwave background has been formally reassigned to the Earth [20–29]. Such claims depend on several factors, as follows:

1. The assignment of a 2.725 K temperature to the Penzias and Wilson signal constitutes a violation of Kirchhoff's Law of Thermal Emission [30, 31]. The proper

assignment of thermal temperatures requires, according to Kirchhoff [31], equilibrium with an enclosure [30]. This is a condition which cannot be met by the universe. Therefore, the absolute magnitude of the temperature should be considered erroneous;

2. The cosmological community, in general, and the COBE [33] and WMAP [34] teams, in particular, have advanced that the Earth can be treated as a $\sim$300 K blackbody. In fact, since the Earth is 75% water covered, this assumption is not justified, based on the known behavior of sea emissions in the microwave region [26, 35]. The oceans exhibit thermal emission profiles, which depend on the Nadir angle, and are therefore not blackbody emitters at $\sim$300 K. Indeed, the oceans can produce signals very close to 0 K [26, 35]. It remains of concern that the signature of the microwave background is completely devoid of earthly interference. Not a single artifact has been reported over the entire frequency range [8] which could be attributed to an earthly signal of oceanic origin. At the same time, it is well established that water is a powerful absorber of microwave radiation. Consequently, it is reasonable to expect that the oceans cannot be microwave silent relative to this problem;
3. Powerful signals imply proximal sources. When measured from the Earth the monopole of the microwave background has a tremendous signal to noise [8]. To require that such extensive power fill the entire universe argues in favor of a nearly infinite power source well outside anything known to human science. Conversely, if the signal arises from the Earth, it would be expected to be strong when viewed from Earth [8]. The powerful nature of the microwave background in Earth orbit [8], and the lack of oceanic contaminating signal could very easily be solved, if the Penzias and Wilson signal [1] was generated by the Earth itself [20–29];
4. In the experimental setting, thermal photons, once released, report the temperature of the source which produced them in a manner which is independent of time elapsed and of subsequent source cooling. Once photons are emitted, they cannot shift their frequencies to account for changes at the source. Yet, the Big Bang scenario requires a constant and systematic shifting of photon frequencies towards lower temperatures in a manner wherein the cooling of the source is constantly monitored and reported. This is without experimental evidence in the laboratory. Experimental photons, once produced, can no longer monitor the cooling of the source. Arguments relative to photon shifting, based on an expanding universe, are theoretical and are not supported by laboratory measurements. In considering stellar red shifts, for instance, it is commonly held that the sources themselves are moving away from the observer. Thus, the photons are being shifted *as they are being produced*. In sharp contrast, a microwave background of cosmic origin requires *continuous shifting of photon frequencies long after emission*;
5. The monopole of the microwave background is characterized by a thermal profile [8]. It is a well recognized observation of physics, that a Lyman process is required to produce a group of Lyman lines. Likewise, a nuclear magnetic resonance process is required to obtain an NMR line. Similarly, a thermal process must occur to produce a thermal line. On Earth, thermal emission spectra are generated exclusively in the presence of matter in the condensed state [30]. The existence of a Planckian line in the microwave requires a process analogous to that which results in a thermal spectrum from a piece of graphite on Earth [30]. Physics has not provided a known mechanism for the creation of a photon by graphite [30]. As a result, Planck's equation, unlike all others in physics, remains detached from physical reality [30]. In this regard, it is maintained [30] that a thermal profile can only be obtained as the result of the vibration of atomic nuclei within the confines of a lattice field (or fleeting lattice field in the case of a liquid). Condensed matter, either in the solid or liquid state, is required. This condition cannot be met within the framework of Big Bang cosmology. Universality in blackbody radiation does not hold [30, 31];
6. Measurements performed by the COBE satellite reveal a systematic error relative to the measured value of the microwave background monopole temperature, derived either from the monopole or the dipole [26, 27]. These measurements can be interpreted as implying that still another field exists through which the Earth is moving [26, 27];
7. Currently, the "Cosmic Microwave Background" is thought to be continuously immersing the Earth in microwave photons from every conceivable direction in space. Under this steady state scenario, there can be no means for signal attenuation at high frequencies, as has been observed on Earth [28]. This strongly argues that the "CMB" cannot be of cosmic origin [28];
8. The "CMB" anisotropy maps reported by the WMAP satellite display instabilities which are unacceptable, given the need for reproducibility on a cosmological timescale. The results fail to meet accepted standards for image quality, based on a variety of criteria [23–25]. These findings demonstrate that the stability observed in the monopole at 2.725 K is not translated at the level of the anisotropy maps, as would be expected for a signal of cosmologic origin. This implies that the monopole arises from a stable source, while the anisotropies arise from separate unstable sources.

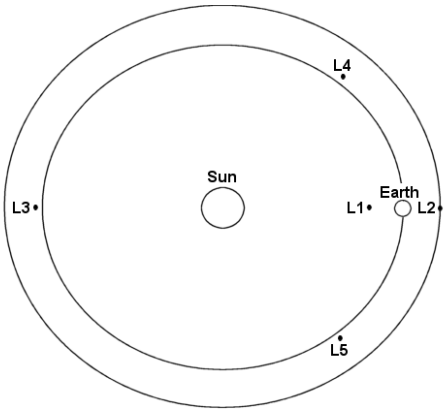

Fig. 1: Schematic representation of the Sun-Earth system depicting the position of the Lagrange 2 point, L2.

2.1 The CMB versus the EMB

Given this array of concerns relative to the assignment of the microwave background, it is clear that mankind must determine, without question, whether this signal is indeed of cosmic origin, or whether, as advanced herein and elsewhere [20–29], it is being generated by the Earth. Current satellite data make strong arguments relative to systematic errors [26, 27] and stability [25] that the monopole of the microwave background originates from the Earth. Conversely, the astrophysical community maintains that a cosmic origin remains the only valid explanation. This being said, it is perplexing that the thermal emission profile of the Earth itself, from space, has yet to be obtained. If the Earth's emission profile was obtained, over the infrared and microwave region, it would become evident that our planet is not a 300 K blackbody radiation source, as the COBE [33], WMAP [34], and PLANCK [36] teams assume. In this era of concern for global warming, it is critical to secure this data.

In the meantime, the PLANCK mission [36], planned by the European Space Agency, will provide the next opportunity to help resolve these questions. Because PLANCK [36] may well acquire the decisive evidence relative to an earthly origin for the monopole of the microwave background, it is important to understand this mission, relative to both COBE [7] and WMAP [11]. The area of greatest interest lies in the configuration of the PLANCK radiometers and the results which they should be able to deliver at the Lagrange 2 point (see Figure 1).

2.1.1 Scenario 1: a cosmic origin

The microwave background has always been viewed as a remnant of the Big Bang originating far beyond our own galaxy. The Earth, in this scenario, is being constantly bombarded by photons from every direction. The frequency distribution of these photons is represented by a 2.725 K blackbody [8]. Indeed, the "CMB" represents perhaps the most precise thermal radiation curve ever measured [8]. The Earth is traveling through the microwave background, as it continues to orbit the Sun and as the latter moves within the galaxy. This motion through the local group is associated with a strong dipole (3.346 ± 0.017 mK) in the direction $l, b = 263.85^\circ \pm 0.1^\circ$, $48.25^\circ \pm 0.04^\circ$ [11], where l and b represent galactic longitude and latitude, respectively. In addition, the "CMB" is characterized by numerous multipoles derived from the analysis of the "CMB" anisotropy maps [11]. Under this scenario, the "CMB" field experienced at ground level, in Earth orbit, or at the Lagrange 2 point (see Figure 1), should be theoretically identical, neglecting atmospheric interference. If COBE [7] and Relikt-1 [10] were launched into Earth orbit, it was largely to avoid any interference from the Earth. The WMAP [11] and PLANCK [36] satellites seek a superior monitoring position, by traveling to the Lagrange 2 point. At this position, the Earth is able to shield the satellite, at least in part, from solar radiation.

2.1.2 Scenario 2: an earthly origin

Recently [20–29], it has been advanced that the microwave background is not of cosmic origin, but rather is simply being produced by the oceans of the Earth. Since the monopole can be visualized only on Earth, or in close Earth orbit [8], it will be referred to as the Earth Microwave Background or "EMB" [28]. In this scenario, the monopole of the Earth microwave background at 2.725 K (EMBM) reports an erroneous temperature, as a result of the liquid nature of the Earth's oceans. The oceans fail to meet the requirements set forth for setting a temperature using the laws of thermal emission [30–32]. For instance, Planck has warned that objects which sustain convection can never be treated as blackbodies [37]. A thermal signature may well appear, but the temperature which is extracted from it is not necessarily real. It may be only apparent. The fundamental oscillator responsible for this signature is thought to be the weak hydrogen bond between the water molecules of the oceans. The EMB has associated with it a dipole [9]. This dipole has been extensively measured from Earth and Earth orbit, and is directly reflecting the motion of the Earth through the local group, as above. Since the Earth is producing the monopole (EMBM), while in motion through the local group, the EMB dipole or "EMBD" would be expected to exist unrelated to the presence of any other fields.

At the Lagrange 2 point, the signal generated by the oceans (EMB) will be too weak to be easily observed [34, 38]. Nonetheless, L2 will not be devoid of all microwave signals. Indeed, at this position, a microwave field must exist. This field, much like noise, will not be characterized by a single temperature. Rather, it will be a weak field, best described through the summation of many apparent temperatures, not by a single monopole. In a sense, microwave noise will be found of significant intensity, but it will be devoid of the characteristics of typical signal. For the sake of clarity, this

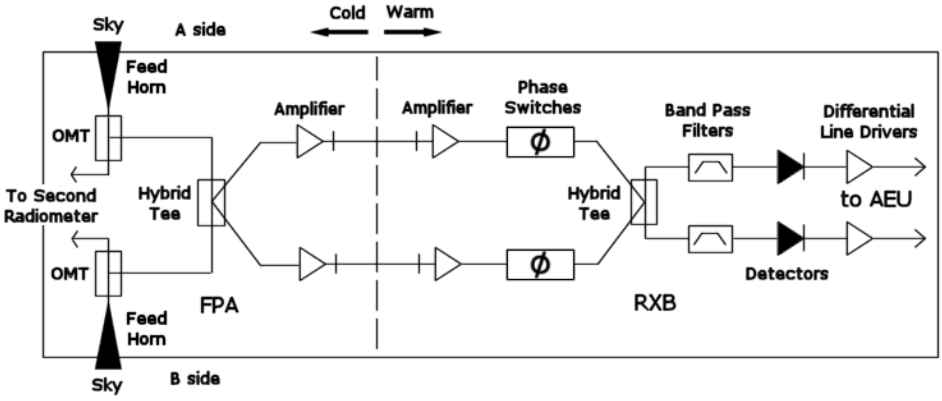

Fig. 2: Partial schematic representation of the WMAP pseudo-correlation differential radiometers [41]. Note that the signal from each horn first travels to an orthomode transducer (OMT) wherein two orthogonal outputs are produced, one for each radiometer. One output from the OMT then travels to the 180° hybrid tee before entering the phase-matched leg of the radiometer. Importantly, for the WMAP satellite, the signal from each horn is being compared directly to its paired counterpart. The satellite does not make use of internal reference loads and cannot operate in absolute mode. (Adapted from [34, 41].)

field will be referred to as the Weak Microwave Background (WMB). This weak background bathes, at least, our solar system, and perhaps much of the galaxy. However, it may or may not extend much power into intergalactic space. Interestingly, motion of the WMAP [11] or PLANCK [36] satellites through this WMB will be associated with the production of a dipole of exactly the same magnitude and direction as observed on Earth [9], since the nature of the motion through the local group has not changed at this point. As such, two dipoles can be considered. The first is associated with the EMB. It is referred to above by the acronym EMBD. The second is associated with the WMB and motion through the local group. It will be referred to henceforth as the WMBD. In actuality, even if the Earth did not produce the 2.725 K monopole, it would still sense the WMBD, as it is also traveling through the WMB. The fact, that both an EMBD and a WMBD are expected, has been used to reconcile the systematic error reported by the COBE satellite [26, 27].

In summary, under the second scenario, we now have a total of four fields to consider:

(1) the monopole of the Earth Microwave Background, the EMBM;

(2) the dipole associated directly with the Earth Microwave Background and motion through the local group, the EMBD;

(3) the Weak Microwave Background present at L2 and perhaps in much of the galaxy, the WMB, and finally

(4) the dipole associated when any object travels through the Weak Microwave Background, the WMBD.

2.1.3 The microwave anisotropies

Weak Microwave Background Anisotropies (MBA) are associated with either Scenario 1 or 2. The anisotropies form the basis of the microwave anisotropy maps now made famous by the WMAP satellite [11, 39, 40]. Under the first scenario, the MBA are tiny fluctuations in the fabric of space which represent relics of the Big Bang. However, careful analysis reveals that the anisotropy maps lack the stability required of cosmic signals [25], and are therefore devoid of cosmological significance. They represent the expected microwave variations, in the sky, associated with the fluctuating nature of microwave emissions originating from all galactic and extragalactic sources. These observations increase the probability that the second scenario is valid.

3 The WMAP versus PLANCK missions

3.1 WMAP

The WMAP satellite [11] is currently positioned at the Lagrange 2 point. WMAP operates in differential mode (see Figure 2), wherein the signal from two matched horns are constantly compared [34, 41]. In this sense, the WMAP satellite resembles the DMR instrument on COBE [33, 42]. Initially, WMAP was to rely exclusively on the magnitude of the dipole observable at L2, in order to execute the calibration of the radiometers (see Section 7.4.1 in [41]). Since the "CMB" and its 2.7 K signature are believed to be present at L2 by the WMAP team, then calibration involves the 1st derivative of the "CMB" and calculated temperature maps of the sky [41], describing the associated temperature variations based on the dipole [9]. Once WMAP reached L2, the initial approach to calibration appeared to be somewhat insufficient, and additional corrections were made for radiometer gains with the initial data release [45, 46].

WMAP is a pseudo-correlation differential spectrometer without absolute reference loads (see Figure 2). Correlation receivers are used extensively in radioastronomy, in part due to the inherent stability which they exhibit, when presented with two nearly identical signals [43, 44]. Since WMAP

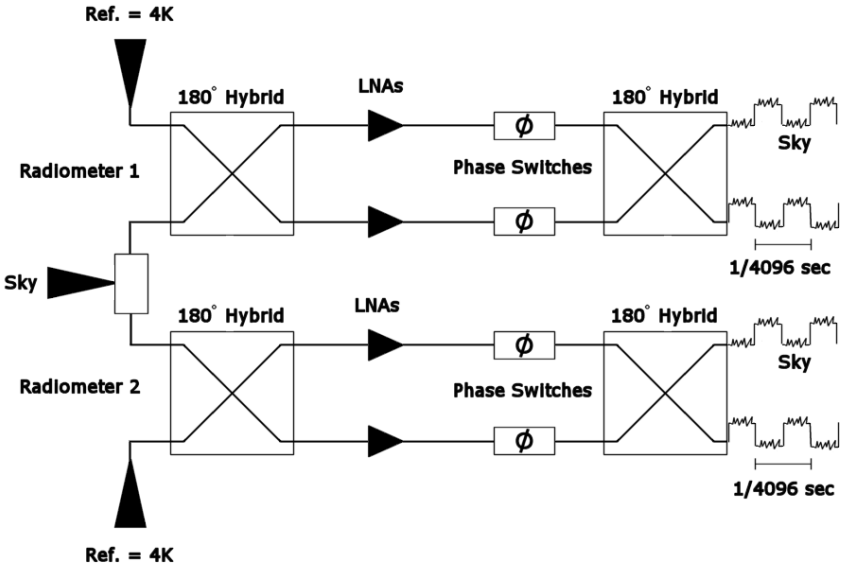

Fig. 3: Partial schematic representation of the PLANCK LFI pseudo-correlation differential radiometers [47, 48]. Prior to entering each radiometer, the signal from each sky horn travels to an orthomode transducer (OMT) where two orthogonal linearly polarized signals are produced. Each of these signals is then compared directly to a reference load maintained at 4 K. Unlike WMAP, PLANCK can operate both in absolute and differential mode. In absolute mode, PLANCK will be able to directly compare the amplitude signal observed from the sky with that produced by the reference loads. Importantly, in order to maintain a minimal knee frequency PLANCK assumes that the differences between the sky and reference signals will be small. (Adapted from [47–52].)

is devoid of reference loads, the satellite is unable to easily answer questions relative to the presence or absence of the 2.725 K "CMB" signal at the L2 point. Should only a WMB be present, WMAP could still be calibrated properly [41], because the magnitude and direction of the dipole itself ultimately governs the entire problem, independent of the underlying field. Because the dipole is being produced by motion through the local group, its magnitude and direction at L2 will be identical, irrespective of the scenario invoked above. This is true, of course, provided that the WMB exists. The WMAP team assumes the presence of a "CMB" monopole at L2 and uses its first derivative, in combination with an expected sky temperature difference map, based on the known dipole [41]. Alternatively, if only a WMB exists at L2, the dipole will still be present, and another set of theoretical constraints will also satisfy the requirements for calibration.

WMAP has been able to detect the dipole at the L2 point, but this is expected from both scenarios listed above. In any case, an objective analysis of the data products associated with this satellite reveals that, far from affirming the cosmic nature of anisotropy, WMAP refutes such conclusions [25]. The anisotropy maps derived from WMAP are much too unstable and unreliable to be fundamentally linked to signals of primordial origin [25]. WMAP has not been able to yield a definitive answer relative to the origin of the "CMB", and, to date, no signal has been measured which can be ascribed to the remnant of the Big Bang. Fortunately, it appears that the PLANCK satellite will be able to unambiguously resolve the issue.

3.2 PLANCK

Much like WMAP, the PLANCK satellite [36] is scheduled to be launched into an operational orbit at L2, the Lagrange 2 point of the Earth-Sun system. The satellite is equipped with two instruments, the low frequency instrument (LFI) and the high frequency instrument (HFI), scanning the sky at 30, 44, and 70 GHz [47–55] and 100, 143, 217, 353, 545, and 857 GHz [55–57], respectively. In contrast, the WMAP satellite scanned the 23, 33, 41, 61, and 94 GHz regions of the electromagnetic spectrum. Thus, PLANCK greatly extends the range of frequencies which will be sampled.

Still, more important differences exist between PLANCK and WMAP. The high frequency instrument on PLANCK is not differential, and frequencies from 100–857 GHz will be sampled in absolute mode, without subtraction. Moreover, while the low frequency instrument is designed to operate as a differential spectrometer, it can also function in absolute mode [47-54]. The low frequency instrument on PLANCK (see Figure 3) is also designed to function as a pseudo-correlation radiometer [47-53]. However, the signal from the sky, obtained by each horn, is being compared to a reference load maintained at 4 K (see Figure 3). These details constitute critical variations relative to the WMAP radiometer design.

Given that the LFI on PLANCK makes use of absolute reference loads, it resembles, in this important sense, the FIRAS Instrument on COBE [58]. Furthermore, since the LFI on PLANCK can operate either in absolute mode, or in difference mode [47–54], the spectrometer has a flexibility which

appears to combine the best features possible for such an instrument. In absolute mode, the LFI on PLANCK will be able to quantify completely the signal originating from the sky relative to that produced by its 4 K references. Nonetheless, the LFI was designed to operate primarily in differential mode. This has implications for the quality of its data products based on whether or not the 2.725 K monopole signal is present at L2.

3.2.1 The PLANCK LFI

The PLANCK LFI is designed as a pseudo-correlation [52] receiver (see Figure 3). For this receiver, gain instabilities in the High Electron Mobility Transistor (HEMT) amplifier, within the receiver front end, result in $1/f$ noise. The $1/f$ noise, if not properly accounted for, can produce significant stripes in the final maps [47, 48]. These stripes are also dependent on scanning strategy. The behavior of the $1/f$ noise has been carefully analyzed for the PLANCK LFI [47, 48]. Since the LFI is designed to operate primarily in differential mode, it is important to minimize the difference between the reference load temperature, T_{ref}, and the sky temperature, T_{sky}.

Currently, the PLANCK team is making the assumption that $T_{sky} = 2.725$ K, as previously reported by the COBE group [7]. As such, they have chosen to use $T_{ref} = 4$ K. Any offset between T_{sky} and T_{ref} *"can be balanced before differencing either by a variable back-end gain stage with a feedback scheme to maintain the output power as close as possible to zero, or by multiplying in software one of the two signals by a so-called gain modulation factor"* [47].

If the differences between the sky temperature and the reference temperatures are large, then the idea of using back-end gain stage feedback, to balance the two channels, should introduce substantial noise directly into the system. The situation using software and a gain modulation factor would also introduce unexpected complications.

The gain modulation factor, r, is given by the following: $r = (T_{sky} + T_n)/(T_{ref} + T_n)$ where T_n corresponds to the radiometer noise temperature. The noise temperature of the radiometer, T_n, is a fundamental property of any receiver and is determined by the overall design and quality of the instrument. T_n is critical in establishing the sensitivity of the spectrometer. For instance, the radiometer sensitivity, ΔT_{rms}, over a given integration time, is directly dependent on both T_{sky} and T_n, as follows: $\Delta T_{rms} = 2(T_{sky} + T_n)/\sqrt{\beta}$, where β is the bandwidth of the radiometer (typically taken as 20%). Note that if T_n is large, then it will be easy to achieve gain modulation factors near 1. However, the radiometer sensitivity would be severely compromised. Low T_n values are central to the performance of any receiver. Under this constraint, the gain modulation factor will be strongly affected by any differences between the T_{sky} and T_{ref}.

PLANCK has the ability to calculate the gain modulation factor, r, directly from radiometer data acquired with the spectrometer operating in absolute mode [47]. Alternatively, r can be calculated from software, using up to three approaches including, for instance, minimizing the final differenced data knee frequency, f_k. The knee frequency is the frequency at which the value of $1/f$ noise and white noise contributions are equal.

In general, it is also true that for the PLANCK LFI *"the white noise sensitivity and the knee-frequency depend on the actual temperature in the sky"* [47]. Because excessive $1/f$ noise can degrade the final images and data products [47, 48], it is important to minimize its contribution. This can be achieved *"if the post detection knee frequency f_k (i.e. the frequency at which the $1/f$ noise contribution and the ideal white noise contribution are equal) is significantly lower than the spacecraft rotation frequency ($f_{spin} \sim 0.017$ Hz)"* [48]. If the f_k is greater than, or approximately equal to f_{spin}, a degradation in the final sensitivity of the satellite will occur [47]. As this inherently depends on the real sky temperature, there are some concerns relative to the performance of the PLANCK LFI instruments.

When the knee frequencies are too high, stripes will occur in the images generated by the satellite. It is true that algorithms do exist to help remove these artifacts, provided that they are not too strong [47]. Nonetheless, when the sky temperature and the reference temperatures are not balanced, the knee frequency will rise substantially. This could diminish the quality of the data products from this satellite.

The importance of maintaining a low knee frequency for the PLANCK LFI instruments cannot be overstated. *"If the knee frequency is sufficiently low (i.e. $f_k \leqslant 0.1$ Hz), with the application of such algorithms it is possible to maintain both the increase in rms noise within few % of the white noise, and the power increase at low multipole values (i.e. $l \leqslant 200$) at a very low level (two orders of magnitude less than the CMB power). If, on the other hand, the knee frequency is high (i.e. $\gg 0.1$ Hz) then even after destriping the degradation of the final sensitivity is of several tens of % and the excess power at low multipole values is significant (up to the same order of the CMB power for $f_k \sim 10$ Hz ...) Therefore, careful attention to instrument design, analysis, and testing is essential to achieve a low $1/f$ noise knee frequency"* [48]. The PLANCK team has emphasized this further, as follows: *"It is then of great importance to decrease as much as possible the impact of $1/f$ noise before destriping and $f_k = 0.01$ Hz is an important goal for instrument studies and prototypes."*

The manner in which the knee frequency is affected by both the gain modulation factor, r, and the absolute sky temperature [48], has been described algebraically:

$$f_k(T_n) = \beta \left[\frac{A(1-r)T_n}{2(T_{sky} + T_n)} \right]^2 . \quad (1)$$

In this equation, β corresponds to the bandwidth of the receiver, typically taken at 20%, T_n is the radiometer noise

temperature, and A is a normalization factor for noise fluctuations [48]. Note that if the sky temperature, T_{sky}, is only some fraction of a Kelvin degree, this equation is moving towards:

$$f_k\left(T_n\right) = \beta\left[\frac{A\left(1-r\right)}{2}\right]^2. \qquad (2)$$

Under test conditions, the PLANCK team estimated gain modulation factors ranging from 0.936 to 0.971 for the 30, 44, and 70 GHz radiometers [47]. In flight, T_n values of 7.5, 12, and 21.5 K are expected for the 30, 44, and 70 GHz radiometers [50]. This results in r values ranging from ∼0.89–0.95, if T_{sky} is taken as 2.725 K and $T_{ref} = 4$ K. Anticipated f_k values would therefore range from ∼0.0032 Hz to ∼0.0043 Hz, well below the 16 mHz requirement. This situation will not occur under Scenario 2, wherein T_{sky} at L2 is not 2.725 K, but rather only some fraction of a Kelvin degree.

As T_{sky} will have a much lower value than foreseen, the gain modulation factor, r, will be moving away from unity. It is also clear from Eqs. 1 and 2 that the knee frequency for the LFI radiometers would rise to values substantially above those currently sought by the PLANCK team.

In the extreme case, it is simple to consider the consequence of $T_{sky} \to 0$. In this instance, gain modulation factors would drop precipitously from ∼0.89 to ∼0.65 at 30 GHz, and from ∼0.95 to ∼0.84 at 70 GHz. This would translate into substantially elevated f_k values of ∼50 mHz. Even an apparent T_{sky} value of 300 mK would result in r and f_k values in this range. Other than the direct measurement of the sky temperature by the PLANCK LFI in absolute mode, the drop in r values and the tremendous rise in f_k will constitute another indication that the 2.725 K signal does not exist at the L2 point.

Consequently, it is difficult to envision that the PLANCK team will be able to attain the desired image quality if T_{sky} is not at 2.725 K. The spectrometer is not designed to achieve maximal sensitivity in absolute mode, while in difference mode, both its r values and its f_k will be compromised. Destriping algorithms will have to be invoked in a much more central manner than anticipated.

Note that the situation with PLANCK is substantially different from WMAP. With WMAP (see Figure 2), the radiometers do not make use of an absolute reference load, but rather, the two sky horns are constantly and directly being differenced. Thus, the knee frequency for WMAP would be as predicted prior to launch. The WMAP horns are nearly perfectly balanced by the sky itself. Therefore, their performance would not be affected by the real nature of the signal at L2. This is not the case for the PLANCK satellite.

4 Conclusion

The WMAP satellite was designed as a differential spectrometer without absolute calibration. As a result, it is unable to ascertain the absolute magnitude of the microwave signals at the L2 point. The satellite has produced anisotropy maps [39, 40]. Yet, these maps lack the stability required of cosmological signals. Indeed, WMAP appears devoid of any findings relative to cosmology, as previously stated [25]. The only signal of note, and one which was not anticipated [21], is that associated with the dipole [9, 26, 27]. The dipole is important, since it can be used to quantify the motion of objects through the local group. Under the second scenario, this dipole signal implies that there is a Weak Microwave Background (WMB) at the L2 point.

In sharp contrast with WMAP, PLANCK has the advantage of being able to operate in absolute mode. In this configuration, it can directly determine whether or not there is a 2.725 K monopole signal at L2. If the signal is present, as expected by the PLANCK team, and as predicted in the first scenario, then the satellite should be able to acquire simply phenomenal maps of the sky. However, this will not occur. In the absence of a monopole, the PLANCK radiometers will be compromised when operating in difference mode, as their knee frequencies rise. This shall result in the presence of more pronounced image artifacts in the data products, which may not be easily removed through processing, potentially impacting the harvest from PLANCK. Nonetheless, PLANCK should be able to fully characterize the WMB predicted under the second scenario.

At the same time, since the 2.725 K monopole signature does not exist at the L2 point, PLANCK is poised to alter the course of human science. The satellite will help establish that there is no universality [30, 31]. The need to link Planck's equation to the physical world will become evident [30, 31]. It will be realized that the Penzias and Wilson signal did come from the Earth, and that liquids can indeed produce thermal spectra reporting incorrect temperatures. It is likely that a renewed interest will take place in condensed matter physics, particularly related to a more profound understanding of thermal emission, in general, and to the study of thermal processes in liquids, in particular. The consequences for astrophysics will be far reaching, impacting our understanding of stellar structure [59, 60], stellar evolution and cosmology. PLANCK, now, must simply lead the way.

Acknowledgements

The author thanks Dmitri Rabounski for valuable discussions. Luc Robitaille is recognized for figure preparation.

Dedication

This work is dedicated to my brother, Patrice, for his love and encouragement.

Submitted on August 06, 2007
Accepted on August 15, 2007
Published online on September 08, 2007
Revised on September 29, 2007

References

1. Penzias A.A. and Wilson R.W. A measurement of excess antenna temperature at 4080 Mc/s. *Astrophys. J.*, 1965, v. 1, 419–421.
2. Dicke R.H., Peebles P.J.E., Roll P.G., and Wilkinson D.T. Cosmic black-body radiation. *Astrophys. J.*, 1965, v. 1, 414–419.
3. Partridge R.B. 3K: The Cosmic Microwave Background Radiation. Cambridge University Press, Cambridge, 1995.
4. Lineweaver C.H., Bartlett J.G., Blanchard A., Signore M. and Silk J. The Cosmic Microwave Background. Kluwer Academic Publishers. Boston, 1997.
5. de Bernardis P., Ade P.A.R., Bock J.J., Bond J.R., Borrill J.,Boscaleri A., Coble K., Crill B.P., De Gasperis G., Farese P.C., Ferreira P.G., Ganga K., Giacometti M., Hivon E., Hristov V.V., Iacoangeli A., Jaffe A.H., Lange A.E., Martinis L., Masi1 S., Mason P.V., Mauskopf P.D., Melchiorri A., Miglio L., Montroy T., Netterfield C.B., Pascale E., Piacentini F., Pogosyan D., Prunet S., Rao S., Romeo G., Ruhl J.E., Scaramuzzi F., Sforna1 D., and Vittorio N. A flat universe from high-resolution maps of the Cosmic Microwave Background. *Nature*, 2000, v. 404, 955–959.
6. Spergel D.N., Verde L., Peiris H.V., Komatsu E., Nolta M.R., Bennett C.L., Halpern M., Hinshaw G., Jarosik N., Kogut A., Limon M., Meyer S.S., Page L., Tucker G.S., Weiland J.L., Wollack E., and Wright E.L. First year Wilkinson Microwave Anisotropy Probe (WMAP) observations: Determination of cosmological parameters. *Astrophys. J. Suppl.*, 2003, v. 148, 175–194.
7. COBE website, http://lambda.gsfc.nasa.gov/product/cobe/
8. Fixen D.J., Cheng E.S., Gales J.M., Mather J.C., Shaffer R.A., and Wright E.L. The Cosmic Microwave Background spectrum from the full COBE FIRAS data set. *Astrophys. J.*, 1996, v. 473, 576–587.
9. Lineweaver C.H. The CMB Dipole: The most recent measurement and some history. In *Microwave Background Anistropies. Proceedings of the XVIth Moriond Astrophysics Meeting*, Les Arcs, Savoie, France, March 16th-23rd, 1996, F. R. Bouchet, R. Gispert, B. Guilderdoni, and J.T.T. Van, eds., Gif-sur-Yvette: Editions Frontieres, 1997; (see also arXiv:astro-ph/9609034).
10. Klypin A.A., Strukov I.A., and Skulachev D.P. The Relikt missions: results and prospects for detection of the microwave background anisotropy. *Mon. Not. R. Astr. Soc.*, 1992, v. 258, 71–81.
11. WMAP website, http://map.gsfc.nasa.gov/
12. Spergel D.N., Bean R., Doré O., Nolta M.R., Bennett C.L., Dunkley J., Hinshaw G., Jarosik N., Komatsu E., Page L., Peiris H.V., Verde L., Halpern M., Hill R.S., Kogut A., Limon M., Meyer S.S., Odegard N., Tucker G.S., Weiland J.L., Wollack E., and Wright E.L. Wilkinson Microwave Anisotropy Probe (WMAP) three year results: implications for cosmology. *Astrophysical J. Suppl. Series*, 2007, v. 170, 377–408.
13. Burles S., Nollett K.M., and Turner M.S. Big Bang nucleosynthesis predictions for precision cosmology. *Astrophys. J.*, 2001, v. 552, L1–L5.
14. Guth A.H. Inflation and the new era of high precision cosmology. *MIT Physics Annual*, 2002, 28–39.
15. Smoot G.F. Our age of precision cosmology. *Proceedings of the 2002 International Symposium on Cosmology and Particle Astrophysics* (CosPA 02), X.G. He and K.W. Ng, Editors, World Scientific Publications, 2003, London, U.K., 314–326.
16. Seife C. Breakthrough of the year: illuminating the dark universe. *Science*, 2003, v. 302, 2038–2039.
17. NASA, new satellite data on Universe's first trillionth second. WMAP Press Release. http://map.gsfc.nasa.gov/m_or/PressRelease_03_06.html.
18. Goodman B. Big days for the Big Bang. *Princeton Alumni Weekly*, May, 2003.
19. Panek R. Out There. *New York Times Magazine*, March 11, 2007, 55–59.
20. Robitaille P.-M.L. Nuclear magnetic resonance and the age of the Universe. *American Physical Society Centennial Meeting*, Atlanta, Georgia, BC19.14, March 19–26, 1999.
21. Robitaille P-M.L. The MAP satellite: a powerful lesson in thermal physics. *Spring Meeting of the American Physical Society Northwest Section*, F4.004, May 26, 2001.
22. Robitaille P.-M.L. The collapse of the Big Bang and the gaseous sun. *New York Times*, March 17th, 2002 (accessed online from http://thermalphysics.org/pdf/times.pdf).
23. Robitaille P-M.L. WMAP: a radiological analysis. *Spring Meeting of the American Physical Society Ohio Section*, S1.00003, March 31 — April 1, 2006.
24. Robitaille P-M.L. WMAP: a radiological analysis II. *Spring Meeting of the American Physical Society Northwest Section*, G1.0005, May 19–20, 2006.
25. Robitaille P.-M.L. WMAP: a radiological analysis. *Progr. in Phys.*, 2007, v. 1, 3–18.
26. Robitaille P.-M.L. On the origins of the CMB: insight from the COBE, WMAP, and Relikt-1 Satellites. *Progr. in Phys.*, 2007, v. 1, 19–23.
27. Rabounski D. The relativistic effect of the deviation between the CMB temperatures obtained by the COBE satellite. *Progr. in Phys.*, 2007, v. 1, 24–26.
28. Robitaille P.-M.L. On the Earth Microwave Background: absorption and scattering by the atmosphere. *Progr. in Phys.*, 2007, v. 3, 3–4.
29. Robitaille P.-M.L., Rabounski D. COBE and the absolute assignment of the CMB to the Earth. *American Physical Society March Meeting*, L20.00007, March 5–9, 2007.
30. Robitaille P.-M.L. On the validity of Kirchhoff's law of thermal emission. *IEEE Trans. Plasma Science*, 2003, v. 31(6), 1263–1267.
31. Robitaille P.-M.L. An analysis of universality in blackbody radiation. *Progr. Phys.*, 2006, v. 2, 22–23.
32. Kirchhoff G. Ueber das Verhaltnis zwischen dem Emissionsvermogen und dem asbsorptionsvermogen der Körper für Waeme und Litcht. *Annalen der Physik*, 1860, v. 109, 275–301.
33. Bennett C., Kogut A., Hinshaw G., Banday A., Wright E., Gorski K., Wilkinson D., Weiss R., Smoot G., Meyer S., Mather

J., Lubin P., Loewenstein K., Lineweaver C., Keegstra P., Kaita E., Jackson P., and Cheng E. Cosmic temperature fluctuations from two years of COBE differential microwave radiometers observations. *Astrophys. J.*, 1994, v. 436, 4230–442.

34. Page L., Jackson C., Barnes C., Bennett C., Halpern M., Hinshaw G., Jarosik N., Kogut A., Limon M., Meyer S.S., Spergel D.N., Tucker G.S., Wilkinson D.T., Wollack E., and Wright E.L. The optical design and characterization of the microwave anisotropy probe. *Astrophys. J.*, 2003, v. 585, 566–586.
35. Ulaby F.T., Moore R.K., Funk A.K. Microwave remote sensing active and passive — Volume 2: Radar remote sensing and surface scattering and emission theory. London, Addison-Wesley Publishing Company, 1982, p. 880–884.
36. PLANCK website, see in http://www.rssd.esa.int
37. Planck M. The Theory of Heat Radiation. Philadelphia, PA., P. Blackinson's Son, 1914.
38. Borissova L., Rabounski D. On the nature of the Microwave Background at the Lagrange 2 point. Part II. *Prog. in Phys.*, 2007, v. 4., 84–95.
39. Bennett C.L., Halpern M., Hinshaw G., Jarosik N., Kogut A., Limon M., Meyer S.S., Page L., Spergel D.N., Tucker G.S., Wollack E., Wright E.L., Barnes C., Greason M.R., Hill R.S., Komatsu E., Nolta M.R., Odegard N., Peirs H.V., Verde L., Weiland J.L. First year Wilkinson Microwave Anisotropy Probe (WMAP) observations: preliminary maps and basic results. *Astrophys. J. Suppl. Series*, 2003, v. 148, 1–27.
40. Hinshaw G., Nolta M.R., Bennett C.L., Bean R., Doré O., Greason M.R., Halpern M., Hill R.S., Jarosik N., Kogut A., Komatsu E., Limon M., Odegard N., Meyer S.S., Page L., Peiris H.V., Spergel D.N., Tucker G.S., Verde L., Weiland J.L., Wollack E., Wright E.L. Three-year Wilkinson Microwave Anisotropy Probe (WMAP) observations: temperature analysis. *Astrophys. J. Suppl. Series*, 2007, v. 170, 288–334.
41. Jarosik N., Bennett C.L., Halpern M., Hinshaw G., Kogut A., Limon M., Meyer S.S., Page L., Pospieszalski M., Spergel D.N., Tucker G.S., Wilkinson D.T., Wollack E., Wright E.L., and Zhang Z. Design, implementation and testing of the MAP radiometers. *Astrophys. J. Suppl.*, 2003, v. 145, 413–436.
42. Kogut A., Banday A.J., Bennett C.L., Gorski K.M., Hinshaw G., Jackson P.D., Keegstra P., Lineweaver C., Smoot G.F., Tenorio L., and Wright E.L. Calibration and systematic error analysis for the COBE DMR 4 year sky maps. *Astrophys. J.*, 1996, v. 470, 653–673.
43. Egan W.F. Practical RF system design. Wiley-Interscience, Hoboken, New Jersey, 2003.
44. Rohlfs K. and Wilson T.L. Tools of radioastronomy. Springer-Verlag, Berlin, 1996.
45. Jarosik N., Barnes C., Bennett C.L., Halpern M., Hinshaw G., Kogut A., Limon M., Meyer S.S., Page L., Spergel D.N., Tucker G.S., Weiland J.L., Wollack E., Wright E.L. First-year Wilkinson Microwave Anisotropy Probe (WMAP) observations: on-orbit radiometer characterization. *Astrophys. J. Suppl. Series*, 2003, v. 148, 29–36.
46. Jarosik N., Barnes C., Greason M.R., Hill R.S., Nolta M.R., Odegard N., Weiland J.L., Bean R., Bennett C.L., Doré O., Halpern M., Hinshaw G., Kogut A., Komatsu E., Limon M., Meyer S.S., Page L., Spergel D.N., Tucker G.S., Wollack E., Wright E.L. Three-year Wilkinson Microwave Anisotropy Probe (WMAP) observations: beam profiles, data processing, radiometer characterization and systematic error limits. *Astrophys. J. Suppl. Series*, 2007, v. 170, 263–287.
47. Maino D., Burigana C., Maltoni M., Wandelt D.B., Gorski K.M., Malaspina M., Bersanelli M., Mandolesi N., Banday A.J., Hivon E.. The Planck-LFI instrument: analysis of the $1/f$ noise and implications for the scanning strategy. *Astrophys. J. Suppl. Series*, 1999, v. 140, 383–391.
48. Sieffert M., Mennella A., Burigana C., Mandolesi N. Bersanelli M., Meinhold P., and Lubin P. $1/f$ noise and other systematic effects in the PLANCK-LFI radiometers. *Astron. Astrophys.*, 2002, v. 391, 1185–1197.
49. Mennella A., Bersanelli M., Butler R.C., Maino D., Mandolesi N., Morgante G., Valenziano L., Villa F., Gaier T., Seiffert M., Levin S., Lawrence C., Meinhold P., Lubin P., Tuovinen J., Varis J., Karttaavi T., Hughes N., Jukkala P., Sjöman P., Kangaslahti P., Roddis N., Kettle D., Winder F., Blackhurst E., Davis R., Wilkinson A., Castelli C., Aja B., Artal E., de la Fuente L., Mediavilla A., Pascual J.P., Gallegos J., Martinez-Gonzalez E., de Paco P., and Pradell L. Advanced pseudo-correlation radiometers for the PLANCK-LFI instrument. arXiv: astro-ph/0307116.
50. Mennella A., Bersanelli M., Cappellini B., Maino D., Platania P., Garavaglia S., Butler R.C., Mandolesi N., Pasian F., D'Arcangelo O., Simonetto A., and Sozzi C. The low frequency instrument in the ESA PLANCK mission. arXiv: astro-ph/0310058.
51. Bersanelli M., Aja B., Artal E., Balasini M., Baldan G., Battaglia P., Bernardino T., Bhandari P., Blackhurst E., Boschini L., Bowman R., Burigana C., Butler R.C., Cappellini B., Cavaliere F., Colombo F., Cuttaia F., Davis R., Dupac X., Edgeley J., D'Arcangelo O., De La Fuente L., De Rosa A., Ferrari F., Figini L., Fogliani S., Franceschet C., Franceschi E., Jukkala P., Gaier T., Galtress A., Garavaglia S., Guzzi P., Herreros J.M., Hoyland R., Huges N., Kettle D., Kilpelä V.H., Laaninen M., Lapolla P.M., Lawrence C.R., Lawson D., Leonardi F., Leutenegger P., Levin S., Lilje P.B., Lubin P.M., Maino D., Malaspina M., Mandolesi M., Mari G., Maris M., Martinez-Gonzalez E., Mediavilla A., Meinhold P., Mennella A., Miccolis M., Morgante G., NashA., Nesti R., Pagan L., Paine C., Pascual J.P., Pasian F., Pecora M., Pezzati S., Pospieszalski M., Platania P., Prina M., Rebolo R., Roddis N., Sabatini N., Sandri M., Salmon M.J., Seiffert M., Silvestri R., Simonetto A., Smoot G.F., Sozzi C., Stringhetti L., Terenzi L., Tomasi M., Tuovinen J., Valenziano L., Varis J., Villa F.,Wade L., Wilkinson A., Winder F., and Zacchei A. PLANCK-LFI: Instrument design and ground calibration strategy. *Proc. Eur. Microwave Assoc.*, 2005, v. 1, 189–195.
52. Mennella A., Bersanelli M., Seiffert M., Kettle D., Roddis N., Wilkinson A., and Meinhold P. Offset balancing in pseudo-correlation radiometers for CMB measurements. *Astro. Astrophys.*, 2003, v. 410, 1089–1100.
53. Terenzi L., Villa F., Mennella A., Bersanelli M., Butler R.C., Cuttaia F., D'Arcangelo O., Franceschi E., Galeotta S., Maino

D., Malaspina M., Mandolesi N., Morgante G., Sandri M., Stringhetti L., Tomasi M., Valenziano L., Burigana C., Finelli F., Galaverni M., Gruppuso A., Paci F., Popa L., Procopio P., and Zuccarelli J. The PLANCK LFI RCA flight model test campaign. *New Astronomy Rev.*, 2007, v. 51, 305–309.

54. Valenziano L., Sandri M., Morgante G., Burigana C., Bersanelli M., Butler R.C., Cuttaia F., Finelli F., Franceschi E., Galaverni M., Gruppuso A., Malaspina M., Mandolesi N., Mennella A., Paci F., Popa L., Procopio P., Stringhetti L., Terenzi L., Tomasi M., Villa F., and Zuccarelli J. The low frequency instrument on-board the Planck satellite: Characteristics and performance. *New Astronomy Rev.*, 2007, v. 51, 287–297.

55. Lamarre J.M, Puget J.L., Bouchet F., Ade P.A.R., Benoit A., Bernard J.P., Bock J., De Bernardis P., Charra J., Couchot F., Delabrouille J., Efstathiou G., Giard M., Guyot G., Lange A., Maffei B., Murphy A, Pajot F., Piat M., Ristorcelli I., Santos D., Sudiwala R., Sygnet J.F., Torre J.P., Yurchenko V., and Yvon D. The PLANCK High Frequency Instrument, a third generation CMB experiment, and a full sky submillimeter survey. *New Astronomy Rev.*, 2003, v. 47, 1017–1024.

56. Piat M., Torre J.P., Bréelle E., Coulais A., Woodcraft A., Holmes W., and Sudiwala R. Modeling of PLANCK-high frequency instrument bolometers using non-linear effects in the thermometers. *Nuclear Instr. Meth. Phys. Res. A*, 2006, v. 559, 588–590.

57. Brossard J., Yurchenko V., Gleeson E, Longval Y., Maffei B., Murphy A., Ristorcelli I., and Lamarre J.M. PLANCK-HFI: Performances of an optical concept for the Cosmic Microwave Background anisotropies measurement. *Proc. 5th Intern. Conf. on Space Optics* (ICSO 2004), 30 March — 2 April 2004, Toulouse, France (ESA SP-554, June 2004).

58. Fixsen D.J., Cheng E.S., Cottingham D.A., Eplee R.E., Hewagama T., Isaacman R.B., Jensen K.A., Mather J.C., Massa D.L., Meyer S.S., Noerdlinger P.D., Read S.M., Rosen L.P., Shafer R.A., Trenholme A.R., Weiss R., Bennett C.L., Boggess N.W., Wilkinson D.T., and Wright E.L. Calibration of the COBE Firas Instrument. *Astrophys. J.*, 1994, v. 420, 457–473.

59. Robitaille P.M. The solar photosphere: evidence for condensed matter. *Prog. in Phys.*, 2006, v. 2, 17–21.

60. Robitaille P.-M. A high temperature liquid plasma model of the Sun. *Prog. in Phys.*, 2007, v. 1, 70–81.

On the Nature of the Microwave Background at the Lagrange 2 Point. Part II

Larissa Borissova and Dmitri Rabounski

E-mail: lborissova@yahoo.com; rabounski@yahoo.com

In this work the mathematical methods of General Relativity are used to answer the following questions: if a microwave background originates from the Earth, what would be its density and associated dipole measured at the altitude of a U2 aeroplane (25 km), the COBE satellite (900 km), and the 2nd Lagrange point (1.5 million km, the position of the WMAP and PLANCK satellites)? The first problem is solved via Einstein's equations for the electromagnetic field of the Earth. The second problem is solved using the geodesic equations for light-like particles (photons) which are mediators for electromagnetic radiation. We have determined that a microwave background that originates at the Earth (the Earth microwave background) decreases with altitude so that the density of the energy of such a background at the altitude of the COBE orbit (900 km) is 0.68 times less than that at the altitude of a U2 aeroplane. The density of the energy of the background at the L2 point is only $\sim 10^{-7}$ of the value detected by a U2 aeroplane or at the COBE orbit. The dipole anisotropy of the Earth microwave background, due to the rapid motion of the Earth relative to the source of another field which isn't connected to the Earth but is located in depths of the cosmos, doesn't depend on altitute from the surface of the Earth. Such a dipole will be the same irrespective of the position at which measurements are taken.

1 Problem statement: the space of the Earth and the Earth microwave background

Here we solve two theoretical problems related to the measurement of the microwave background:

(1) What is the density of the Earth microwave background which one will observe at the COBE orbit and at the L2 point?

(2) What is the anisotropy of the Earth microwave background, due to a drift of the whole space of the Earth, which one will observe in the COBE orbit and at the L2 point?

In a sense, the anisotropy we are treating is the sum of the dipole and all other multipoles.

According to General Relativity, the result of an observation depends on the velocity of the observer relative to the object he observes, and also on the properties of the local space (such as the space rotation, gravitation, deformation, curvature, etc.) where the observation is made. Therefore, we are looking for a theoretical solution of the aforementioned problems using the mathematical methods, which are specific to General Relativity.

We solve the first problem using Einstein's equations, manifest in the energy and momentum of a field of distributed matter (an electromagnetic field, for instance), depending on the distance from the field's source, and also on the properties of the space e.g. the space rotation, gravitation, etc.

We solve the second problem using the geodesic equations for light-like particles (photons, which are mediators for microwave radiation, and for any electromagnetic radiation in general). The geodesic equations give a possibility of finding a preferred direction (anisotropy) in such a field due to the presence of a linear drift of the whole reference space of the observer relative to the source of another field, which isn't connected to the observer's space, but moves with respect to it [1, 2]. In the present case, such a linear drift is due to the motion of the observer, in common with the microwave background's source, the Earth, relative to the source of another field such as the common field of a group of galaxies or that of the Universe as a whole (a weak microwave background). Then we compare our theoretical result from General Relativity to the experimental data for the microwave background, obtained in space near the Earth by the COBE satellite, located in a 900 km orbit, and also by the WMAP satellite, located at the L2 point, as far as 1.5 million km from the Earth.

In order to obtain a theoretical result expressed in quantities measurable in practice, we use the mathematical apparatus of chronometric invariants — the projections of four-dimensional quantities on the time line and spatial section of a real observer, which are the physical observable quatities in General Relativity [3, 4].

First, we introduce a space where all the mesurements are taken. Both locations, of the COBE satellite and the L2 point, are connected, by gravitation, to the gravitational field of the Earth, so both observers are connected to the space of the Earth, whose properties (e.g. rotation, gravitation, deformation, etc.) affect the observations. We therefore consider different locations of an observer in the space of the Earth.

We construct the metric for the Earth's space, which is the superposition of the metric of a non-holonomic (self-rotating) space and a gravitating space.

The space of the Earth rotates with a frequency of one revolution per day. By the theory of non-holonomic spaces

[5], a non-holonomic space (space-time) has inclinations between the times lines and the three-dimensional spatial section, cosines of which are represent by the three-dimensional linear velocity of the rotation. The metric of a non-holonomic space (space-time), which rotation is given by a linear velocity v at a given point, is described at this point by

$$ds^2 = c^2dt^2 + \frac{2v}{c}\,cdt\,(dx+dy+dz) - dx^2 - dy^2 - dz^2. \quad (1)$$

For clarity of further calculation, we change to the cylindrical coordinates r, φ, z, where

$$x = r\cos\varphi\,, \quad y = r\sin\varphi\,, \quad z = z\,, \quad (2)$$

so the metric (1) takes the form

$$\begin{aligned} ds^2 &= c^2dt^2 + \frac{2v}{c}\,(\cos\varphi+\sin\varphi)\,cdtdr + \\ &+ \frac{2vr}{c}\,(\cos\varphi-\sin\varphi)\,cdtd\varphi + \frac{2v}{c}\,cdtdz - \\ &- dr^2 - r^2d\varphi^2 - dz^2. \end{aligned} \quad (3)$$

The metric of a space, where gravitation is due to a body of a mass M, in quasi-Newtonian approximation and in the cylindrical coordinates, is

$$\begin{aligned} ds^2 = \left(1-\frac{2GM}{c^2r}\right)c^2dt^2 - \left(1+\frac{2GM}{c^2r}\right)dr^2 - \\ - r^2d\varphi^2 - dz^2, \end{aligned} \quad (4)$$

where G is the Newtonian gravitational constant. We consider a satellite which rotates in the metric (4) around the gravitating body. Both observers, located on board the COBE satellite (a 900 km orbit) and the WMAP satellite (the L2 point) respectively, are in a state of weightlessness, which is described by the weightlessness condition

$$\frac{GM}{r} = \omega^2r^2, \quad (5)$$

where r is the radius of the satellite's orbit, while ω is the angular velocity of the rotation of the observer (in common with the satellite on which he is located) around the gravitating body. So the metric (4) is

$$\begin{aligned} ds^2 = \left(1-\frac{2GM}{c^2r}-\frac{\omega^2r^2}{c^2}\right)c^2dt^2 - \frac{2\omega r^2}{c}\,cdtd\varphi - \\ - \left(1+\frac{2GM}{c^2r}\right)dr^2 - r^2d\varphi^2 - dz^2, \end{aligned} \quad (6)$$

where $\frac{GM}{r} = \omega^2r^2$. The weightless state is common to all planets and their satellites. So the Earth's space from the point of an observer located on board the COBE satellite and the WMAP satellite is in the weightless state.

We use the cylindrical coordinates, because such an observer is located on board of a satellite which orbits the Earth.

The metric of the Earth's space at the point of location of such an observer is a superposition of the metric with rotation (3) and the metric with a gravitational field (6), which is

$$\begin{aligned} ds^2 &= \left(1-\frac{2GM}{c^2r}-\frac{\omega^2r^2}{c^2}\right)c^2dt^2 + \\ &+ \frac{2v\,(\cos\varphi+\sin\varphi)}{c}\,cdtdr + \\ &+ \frac{2r\,[v\,(\cos\varphi-\sin\varphi)-\omega r]}{c}\,cdtd\varphi + \frac{2v}{c}\,cdtdz - \\ &- \left(1+\frac{2GM}{c^2r}\right)dr^2 - r^2d\varphi^2 - dz^2. \end{aligned} \quad (7)$$

Because the Earth, in common with its space, moves relative to the source of the weak microwave background, this drift should also be taken into account in the metric. This is accomplished by choosing this motion to be in the z-direction and then applying Lorentz' transformations to the z coordinate and time t

$$\tilde{t} = \frac{t+\frac{\mathrm{v}z}{c^2}}{\sqrt{1-\frac{\mathrm{v}^2}{c^2}}}\,, \qquad \tilde{z} = \frac{z+\mathrm{v}t}{\sqrt{1-\frac{\mathrm{v}^2}{c^2}}}\,, \quad (8)$$

so the resulting metric of the space of the Earth, where such a drift is taken into account, is

$$\begin{aligned} ds^2 &= \left(1-\frac{2GM}{c^2r}-\frac{\omega^2r^2}{c^2}+\frac{2v\mathrm{v}}{c^2}\right)c^2dt^2 + \\ &+ \frac{2v\,(\cos\varphi+\sin\varphi)}{c}\,cdtdr + \\ &+ \frac{2r\,[v\,(\cos\varphi-\sin\varphi)-\omega r]}{c}\,cdtd\varphi + \frac{2v}{c}\,cdt\,dz - \\ &- \left(1+\frac{2GM}{c^2r}\right)dr^2 + \frac{2v\mathrm{v}\,(\cos\varphi+\sin\varphi)}{c^2}\,dr\,dz - r^2d\varphi^2 + \\ &+ \frac{2r\mathrm{v}\,[v\,(\cos\varphi-\sin\varphi)-\omega r]}{c^2}\,d\varphi dz - \left(1-\frac{2v\mathrm{v}}{c^2}\right)dz^2, \end{aligned} \quad (9)$$

where we mean $1-\frac{\mathrm{v}^2}{c^2}\simeq 1$, because the Earth's velocity v relative to the source of the weak microwave background is small to the velocity of light c.

This is the *metric of the real physical space of the Earth*, where we process our observations.

Now we apply this metric to the reference frames of two observers, one of which is located on board the COBE satellite, in an orbit with an altitude of 900 km, while the second observer is located on board of WMAP satellite, at the L2 point, which is far as 1.5 million km from the Earth.

2 The density of the Earth microwave background at the COBE orbit and at the L2 point

Here we answer the question: what is the density of the Earth microwave background that one will observe at the COBE orbit and at the L2 point? Using the main observable characteristics of the space of the Earth, pervaded by an electromagnetic field (the microwave background, for instance), we

derive Einstein's equations for the space. Einstein's equations describe the energy and momentum of distributed matter, in this case the microwave background. So we will know precisely, through Einstein's equations, the density of the energy of the Earth microwave background which will be observed at the COBE orbit and at the L2 point.

2.1 The Earth space. Its physical properties manifest in observations of the Earth microwave background

In this particular problem we are interested in the distribution of the Earth microwave background with altitude, giving the difference in the measurement of the background at the COBE orbit and at the L2 point. We therefore neglect terms like $\frac{v\,\mathrm{v}}{c^2}$, which take into account the drift of the whole space of the Earth. The quantity $\frac{2GM}{c^2 r}$ has its maximum numerical value $\sim 10^{-9}$ at the Earth's surface, and the value substatially decreases with altitude. We therefore neglect the last terms in $g_{11} = -\left(1 + \frac{2GM}{c^2 r}\right)$, but we do not neglect the last terms in $g_{00} = 1 - \frac{2GM}{c^2 r} - \frac{\omega^2 r^2}{c^2}$, because they will be multiplied by c^2 later. In such a case the Earth space metric takes the simplified form

$$\begin{aligned} ds^2 &= \left(1 - \frac{2GM}{c^2 r} - \frac{\omega^2 r^2}{c^2}\right) c^2 dt^2 + \\ &+ \frac{2v\,(\cos\varphi + \sin\varphi)}{c}\, cdtdr + \\ &+ \frac{2r\,[v\,(\cos\varphi - \sin\varphi) - \omega r]}{c}\, cdtd\varphi + \frac{2v}{c}\, cdtdz - \\ &- dr^2 - r^2 d\varphi^2 - dz^2 . \end{aligned} \tag{10}$$

We will use this metric to determine the density of the energy of the Earth microwave background at the COBE orbit and at the L2 point. We are loooking for the main observable characteristics of the space. By the theory of physical observable quantities in General Relativity [3, 4], the observable properties of a space are determined within the fixed three-dimensional spatial section of an observer. Those are the quatities invariant within the spatial section (the so-called *chronometric invariants*): the gravitational potential w, the linear velocity of the space rotation v_i, the gravitational inertial force F_i, the angular velocity of the space rotation A_{ik}, the three-dimensional metric tensor h_{ik}, the space deformation D_{ik}, the three-dimensional Christoffel symbols Δ^i_{kn}, and the three-dimensional curvature C_{iklj}. These characteristics can be calculated through the components of the fundamental metric tensor $g_{\alpha\beta}$, which can be easily obtained from a formula for the space metric (see [3, 4] for the details).

The substantially non-zero components of the characteristics of the space of the Earth, calculated though the components $g_{\alpha\beta}$ of the metric (10), are

$$\mathrm{w} = \frac{GM}{r} + \frac{\omega^2 r^2}{2}, \tag{11}$$

$$\left.\begin{aligned} v_1 &= -v\,(\cos\varphi + \sin\varphi) \\ v_2 &= -r\,[v\,(\cos\varphi - \sin\varphi) - \omega r] \\ v_3 &= -v \end{aligned}\right\} \tag{12}$$

$$\left.\begin{aligned} F_1 &= (\cos\varphi + \sin\varphi)\, v_t + \omega^2 r - \frac{GM}{r^2} \\ F_2 &= r\,(\cos\varphi - \sin\varphi)\, v_t\,, \qquad F_3 = v_t \end{aligned}\right\} \tag{13}$$

$$\left.\begin{aligned} A_{12} &= \omega r + \frac{1}{2}\big[(\cos\varphi + \sin\varphi)\, v_\varphi - \\ &\qquad - r\,(\cos\varphi - \sin\varphi)\, v_r\big] \\ A_{23} &= -\frac{v_\varphi}{2}\,, \qquad A_{13} = -\frac{v_r}{2} \end{aligned}\right\} \tag{14}$$

$$\left.\begin{aligned} &h_{11} = h_{33} = 1\,, \quad h_{22} = r^2, \quad h^{11} = h^{33} = 1 \\ &h^{22} = \frac{1}{r^2}\,, \qquad h = r^2, \qquad \frac{\partial \ln\sqrt{h}}{\partial r} = \frac{1}{r} \\ &\Delta^1_{22} = -r\,, \qquad \Delta^2_{12} = \frac{1}{r} \end{aligned}\right\} \tag{15}$$

while all components of the tensor of the space deformation D_{ik} and the space curvature C_{iklj} are zero, in the framework of our assumptions. Here we assume the plane in cylindrical coordinates wherein the space of the Earth rotates: we assume that v doesn't depend from the z-coordinate. This assumption is due to the fact that the Earth, in common with its space, moves relative to a weak (cosmic) microwave background in the direction of its anisotropy. The quantities v_r, v_φ, and v_t denote the partial derivatives of v by the respective coordinates and time.

2.2 Einstein's equations in the Earth space. The density of the energy of distributed matter

Einstein's general covariant equations

$$R_{\alpha\beta} - \frac{1}{2}\, g_{\alpha\beta} R = -\kappa T_{\alpha\beta} + \lambda\, g_{\alpha\beta}\,, \tag{16}$$

in a reference frame of the fixed spatial section of an observer, are represented by their projections onto the observer's time line and spatial section [3, 4]. We omit the λ-term, the space deformation D_{ik}, and the space curvature, C_{iklj}, because they are zero in the framework of our problem. In such a case the projected Einstein equations, according to Zelmanov [3, 4], are

$$\left.\begin{aligned} &\frac{\partial F^i}{\partial x^i} + \frac{\partial \ln\sqrt{h}}{\partial x^i} F^i - A_{ik} A^{ik} = -\frac{\kappa}{2}\left(\rho c^2 + U\right) \\ &\frac{\partial A^{ik}}{\partial x^k} + \frac{\partial \ln\sqrt{h}}{\partial x^k} A^{ik} = -\kappa J^i \\ &2A_{ij} A^{\cdot j}_{k\cdot} + \frac{1}{2}\left(\frac{\partial F_i}{\partial x^k} + \frac{\partial F_k}{\partial x^i} - 2\Delta^m_{ik} F_m\right) = \\ &\qquad = \frac{\kappa}{2}\left(\rho c^2 h_{ik} + 2U_{ik} - U h_{ik}\right) \end{aligned}\right\} \tag{17}$$

$$
\left.\begin{aligned}
&-2\omega^2-2\omega\left(\cos\varphi+\sin\varphi\right)\frac{v_\varphi}{r}+2\omega\left(\cos\varphi-\sin\varphi\right)v_r+\left(\cos\varphi+\sin\varphi\right)v_{tr}+\left(\cos\varphi-\sin\varphi\right)\frac{v_{t\varphi}}{r}+\\
&+\left(\cos^2\varphi-\sin^2\varphi\right)\frac{v_r v_\varphi}{r}+\cos\varphi\sin\varphi\left(v_r^2-\frac{v_\varphi^2}{r^2}\right)-v_r^2-\frac{v_\varphi^2}{r^2}=-\kappa\rho c^2\\
&\frac{1}{2}\left[\left(\cos\varphi+\sin\varphi\right)\left(\frac{v_r}{r}+\frac{v_{\varphi\varphi}}{r^2}\right)+\left(\cos\varphi-\sin\varphi\right)\left(\frac{v_\varphi}{r^2}-\frac{v_{r\varphi}}{r}\right)\right]=-\kappa J^1\\
&\frac{1}{2}\left[\left(\cos\varphi+\sin\varphi\right)\left(\frac{v_\varphi}{r^3}-\frac{v_{r\varphi}}{r^2}\right)-\left(\cos\varphi-\sin\varphi\right)\frac{v_{rr}}{r}\right]=-\kappa J^2\\
&\frac{1}{2}\left(v_{rr}+\frac{v_r}{r}+\frac{v_{\varphi\varphi}}{r^2}\right)=-\kappa J^3\\
&v_r^2+\frac{v_\varphi^2}{2r^3}+3\omega^2+\frac{2GM}{r^3}+2\omega\left(\cos\varphi+\sin\varphi\right)\frac{v_\varphi}{r}-2\omega\left(\cos\varphi-\sin\varphi\right)v_r+\left(\cos\varphi+\sin\varphi\right)v_{tr}-\\
&-\left(\cos^2\varphi-\sin^2\varphi\right)\frac{v_r v_\varphi}{r}-\cos\varphi\sin\varphi\left(v_r^2-\frac{v_\varphi^2}{r^2}\right)=\kappa U_{11}\\
&\frac{r^2}{2}\left[\frac{v_r v_\varphi}{r^2}+\left(\cos\varphi+\sin\varphi\right)\frac{v_{t\varphi}}{r^2}+\left(\cos\varphi-\sin\varphi\right)\frac{v_{tr}}{r}\right]=\kappa U_{12}\\
&\frac{1}{2}\left[2\omega\frac{v_\varphi}{r}+v_{tr}+\left(\cos\varphi+\sin\varphi\right)\frac{v_\varphi^2}{r^2}-\left(\cos\varphi-\sin\varphi\right)\frac{v_r v_\varphi}{r}\right]=\kappa U_{13}\\
&2\omega^2+2\omega\left(\cos\varphi+\sin\varphi\right)\frac{v_\varphi}{r}-2\omega\left(\cos\varphi-\sin\varphi\right)v_r+\left(\cos\varphi-\sin\varphi\right)\frac{v_{t\varphi}}{r}+\frac{v_r^2}{2}+\frac{v_\varphi^2}{r^2}-\\
&-\left(\cos^2\varphi-\sin^2\varphi\right)\frac{v_r v_\varphi}{r}+\cos\varphi\sin\varphi\left(\frac{v_\varphi^2}{r^2}-v_r^2\right)=\kappa\frac{U_{22}}{r^2}\\
&\frac{r^2}{2}\left[\frac{v_{t\varphi}}{r^2}-2\omega\frac{v_r}{r}-\left(\cos\varphi+\sin\varphi\right)\frac{v_r v_\varphi}{r^2}+\left(\cos\varphi-\sin\varphi\right)\frac{v_r^2}{r}\right]=\kappa U_{23}\\
&\frac{v_r^2}{2}+\frac{v_\varphi^2}{2r^2}=\kappa U_{33}
\end{aligned}\right\}\qquad(18)
$$

where $\rho=\frac{T_{00}}{g_{00}}$, $J^i=\frac{c\,T_0^i}{\sqrt{g_{00}}}$, and $U^{ik}=c^2T^{ik}$ are the respective projections of the energy-momentum tensor $T_{\alpha\beta}$ of distributed matter on the right side of the equations: ρ is the density of the energy of the matter field, J^i is the density of the field momentum, and U^{ik} is the stress-tensor of the field.

We substitute here the formulae obtained for the space of the Earth. In this deduction we take into account the weightlessness condition $\omega^2r^2=\frac{GM}{r}$. (This is because we calculate the equations for a satellite-bound observer.) We also apply the condition $\rho c^2=U$, which is specific to any electromagnetic field; so we mean only an electromagnetic field distributed in the space. As a result, after some algebra, we obtain the projected Einstein equations for the Earth space filled with a background field of matter. The resulting Einstein equations, the system of 10 equations with partial derivatives, are given in formula (18).

(Obvious substitutions such as $\cos^2\varphi-\sin^2\varphi=\cos 2\varphi$ and $\cos\varphi\sin\varphi=\frac{1}{2}\sin 2\varphi$ can be used herein.)

We are looking for a solution of the scalar Enstein equation, the first equation of the system (18). In other words, we are looking for the density of the field's energy, ρ, which originates in the Earth, expressed through the physical properties of the space of the Earth (which decrease with distance from the Earth as well).

As seen, the quantity ρ is expressed through the distribution function of the linear velocity of the space rotation v (see the first equation of the system), which are unknown yet. A great help to us is that fact that we have only an electromagnetic field distributed in the space. This means that with use of the condition $\rho c^2=U$ we equalize ρc^2 and U taken from the Einstein equations (18) so that we get an equation containing the distribution functions of v without the properties of matter (an electromagnetic field, in our case). With such an equation, we find a specific correlation between the distribution functions.

First we calculate is the trace of the stress-tensor of distributed matter

$$U=U_{11}+\frac{U_{22}}{r^2}+U_{33}\qquad(19)$$

which comes from the 5th, 8th, and 10th equations of the

$$\left.\begin{aligned}
&(\cos\varphi-\sin\varphi)\left(\frac{v_{tr\varphi}}{r}-\frac{v_{t\varphi}}{r^2}\right)+\omega(\cos\varphi+\sin\varphi)\left(\frac{v_{r\varphi}}{r}-\frac{v_{\varphi}}{r^2}\right)-\omega(\cos\varphi-\sin\varphi)\,v_{rr}+2v_rv_{rr}+\frac{v_\varphi v_{r\varphi}}{r^2}+\\
&-\frac{v_\varphi^2}{r^3}+(\cos\varphi+\sin\varphi)\,v_{trr}-\frac{1}{2}\cos 2\varphi\left(\frac{v_\varphi v_{rr}}{r}+\frac{v_r v_{r\varphi}}{r}-\frac{v_r v_\varphi}{r^2}\right)+\frac{1}{2}\sin 2\varphi\left(\frac{v_\varphi v_{r\varphi}}{r^2}-\frac{v_\varphi^2}{r^3}-v_rv_{rr}\right)=0\\
&(\cos\varphi+\sin\varphi)\left(\frac{v_{tr\varphi}}{r^2}-\frac{v_{t\varphi}}{r^3}\right)+(\cos\varphi-\sin\varphi)\left(\frac{v_{t\varphi\varphi}}{r^3}+\frac{v_{tr}}{r^2}\right)+\omega(\cos\varphi+\sin\varphi)\left(\frac{v_r}{r^2}+\frac{v_{\varphi\varphi}}{r^3}\right)+\\
&+\omega(\cos\varphi-\sin\varphi)\left(\frac{v_\varphi}{r^3}-\frac{v_{r\varphi}}{r^2}\right)+\frac{v_\varphi v_{\varphi\varphi}}{r^4}+\frac{v_r v_{r\varphi}}{r^2}+\frac{1}{2}\cos 2\varphi\left(\frac{v_\varphi^2}{r^4}-\frac{v_r^2}{r^2}-\frac{v_r v_{\varphi\varphi}}{r^3}-\frac{v_\varphi v_{r\varphi}}{r^3}\right)+\\
&+\frac{1}{2}\sin 2\varphi\left(\frac{2v_rv_\varphi}{r^3}+\frac{v_\varphi v_{\varphi\varphi}}{r^4}-\frac{v_r v_{r\varphi}}{r^2}\right)=0
\end{aligned}\right\}\quad(24)$$

Einstein equations (18). We obtain

$$\begin{aligned}
&\kappa U=4\omega^2+4\omega(\cos\varphi+\sin\varphi)\frac{v_\varphi}{r}-\\
&-4\omega(\cos\varphi-\sin\varphi)\,v_r+2v_r^2+\frac{2v_\varphi^2}{r^2}+\\
&+\sin 2\varphi\left(\frac{v_\varphi^2}{r^2}-v_r^2\right)-\cos 2\varphi\,\frac{v_rv_\varphi}{r}+\\
&+(\cos\varphi+\sin\varphi)\,v_{tr}+(\cos\varphi-\sin\varphi)\frac{v_{t\varphi}}{r}\,.
\end{aligned}\quad(20)$$

Equalizing it to $\kappa\rho c^2$ of the first equation of the Einstein equations (18), we obtain

$$\begin{aligned}
&2\omega^2+2\omega(\cos\varphi+\sin\varphi)\frac{v_\varphi}{r}-2\omega(\cos\varphi-\sin\varphi)\,v_r+\\
&+v_r^2+\frac{v_\varphi^2}{r^2}+\frac{1}{2}\sin 2\varphi\left(\frac{v_\varphi^2}{r^2}-v_r^2\right)-\cos 2\varphi\,\frac{v_rv_\varphi}{r}+\\
&+2(\cos\varphi+\sin\varphi)\,v_{tr}+2(\cos\varphi-\sin\varphi)\frac{v_{t\varphi}}{r}=0\,.
\end{aligned}\quad(21)$$

Thus we have all physically observable components of $T_{\alpha\beta}$ expressed in only the physical observable properties of the space. Substituting the components into the conservation law for the common field of distributed matter in the space, we look for the formulae of the distribution functions of the space rotation velocity v.

The conservation law $\nabla_\sigma T^{\alpha\sigma}=0$, expressed in terms of the physical observed quantities*, is [3, 4]

$$\left.\begin{aligned}
&\frac{{}^*\partial\rho}{\partial t}+D\rho+\frac{1}{c^2}D_{ij}U^{ij}+\\
&\qquad+\left({}^*\nabla_i-\frac{1}{c^2}F_i\right)J^i-\frac{1}{c^2}F_iJ^i=0\\
&\frac{{}^*\partial J^k}{\partial t}+2\left(D_i^k+A_{i\cdot}^{\cdot k}\right)J^i+\\
&\qquad+\left({}^*\nabla_i-\frac{1}{c^2}F_i\right)U^{ik}-\rho F^k=0
\end{aligned}\right\}\quad(22)$$

*The asterisk denotes the chronometrically invariant differential operators, e.g. $\frac{{}^*\partial}{\partial t}=\frac{1}{\sqrt{g_{00}}}\frac{\partial}{\partial t}$ and $\frac{{}^*\partial}{\partial x^i}=\frac{\partial}{\partial x^i}+\frac{1}{c^2}v_i\frac{{}^*\partial}{\partial t}$; see [3, 4].

which, under the specific conditions of our problem, become

$$\left.\begin{aligned}
&\frac{\partial J^i}{\partial x^i}+\frac{\partial\ln\sqrt{h}}{\partial x^i}J^i=0\\
&\frac{\partial J^k}{\partial t}+2A_{i\cdot}^{\cdot k}J^i+\frac{\partial U^{ik}}{\partial x^i}+\Delta_{im}^kU^{im}+\\
&\qquad+\frac{\partial\ln\sqrt{h}}{\partial x^i}U^{ik}-\rho F^k=0
\end{aligned}\right\}\quad(23)$$

The first, a scalar equation of conservation, means $\nabla_i J^i=0$, i.e. the flow of the common field of distributed matter is conserved in the space of the Earth. The second, a vector equation of conservation, after substituting the components of J^i and U^{ik} from the Einstein equations (18), and also A_{ik} (14) and Δ_{kn}^i (15), give the system (24) of two non-linear differential equations with partial derivatives with respect to v (while the third equation vanishes becoming the identity "zero equals zero").

The exact solution of the system, i.e. a function which when substituted into the equations makes them identities, is

$$v=T(t)\,re^{i\varphi},\quad(25)$$

where i is the imaginary unit, while T is a function of time (its dimension is $\sec^{-1}$).

Substituting the derivatives

$$\left.\begin{aligned}
&v_r=Te^{i\varphi}\,,\qquad v_\varphi=ir\,Te^{i\varphi}\,,\quad v_t=\dot{T}re^{i\varphi}\\
&v_{t\varphi}=i\dot{T}re^{i\varphi},\quad v_{tr}=Te^{i\varphi}
\end{aligned}\right\}\quad(26)$$

into (21), we obtain, after transformations,

$$T_t(i+1)+\omega T(i-1)-\frac{iT^2}{2}+\omega^2=0\,,\quad(27)$$

where $\dot{T}_t=\frac{\partial T}{\partial t}$. We obtain, for the real part of the equation

$$\dot{T}-\omega T+\omega^2=0\,,\quad(28)$$

which is a linear differential equation of the first order

$$\dot{T}+f(t)T=g(t)\,,\quad(29)$$

whose exact solution is

$$T = e^{-F}\left(T_0 + \int_{t_0=0}^{t} g(t)\, e^{F}\, dt\right), \tag{30}$$

$$F(t) = \int f(t)\, dt\,. \tag{31}$$

Substituting $f = -\omega$, $g = -\omega^2$ and integrating the resulting expression within the limits from t to $t_0 = 0$, we obtain the solution for the real part of the function $T(t)$:

$$T(t) = e^{\omega t}\,(T_0 - \omega) + \omega\,, \tag{32}$$

where T_0 is the initial value of T.

The imaginary part of the (27) satisfies the differential equation

$$T_t + \omega T - \frac{1}{2}\,T^2 = 0\,, \tag{33}$$

which is Bernoulli's equation

$$T_t + fT^2 + gT = 0\,, \tag{34}$$

where $f = -\frac{1}{2}$ and $g = \omega$ are constant coefficients. Such a Bernoulli equation has the solution

$$\frac{1}{T} = E(t)\int \frac{f\,dt}{E(t)}\,, \qquad E(t) = e^{\int g\,dt}\,. \tag{35}$$

Integrating this expression, we obtain

$$T(t) = \frac{2\omega}{1 + Ce^{\omega t}}\,, \tag{36}$$

which is the imaginary part of T. Here C is a constant of integration. Assuming the initial value $t_0 = 0$, we obtain

$$C = \frac{2\omega}{T_0} - 1\,, \tag{37}$$

where T_0 is the initial value of T. Because, by definition $v = T\,re^{i\varphi}$ (25), T has a dimension of $\sec^{-1}$, we consider T_0 to be the initial frequency of the vibrations of the distributed matter (background).

So we obtain the final formula for the imaginary part of the solution for T:

$$T(t) = \frac{2\omega T_0}{T_0 + (2\omega - T_0)\, e^{\omega t}}\,. \tag{38}$$

We therefore write the full solution for T as a complex function, which is

$$T(t) = e^{\omega t}\,(T_0 - \omega) + \omega + i\,\frac{2\omega T_0}{(2\omega - T_0)\, e^{\omega t} + T_0}. \tag{39}$$

We see that the imaginary part of T is zero if $T_0 = 0$. Hence the imaginary part of T originates in the presence of the initial non-zero value of T.

Assuming $T_0 = 0$, we obtain: the full solution for T has only the real solution

$$T = \omega\left(1 - e^{\omega t}\right) \tag{40}$$

when $T_0 = 0$. Substituting this solution into the expression for ρc^2, i.e. the first equation of the system (18), and taking into account the geometrization condition 21 we have obtained for electromagnetic field, we obtain the real component of the density of the energy, which is

$$\rho c^2 = \frac{3\omega}{\kappa}\,(\omega - T) = \frac{3\omega^2}{\kappa}\left[1 - \left(1 - e^{\,\omega t}\right)\right]. \tag{41}$$

This is the final formula for the observable density of the energy $W = \rho c^2$ of distributed matter in the space of the Earth, where the matter is represented by an electromagnetic field which originates in the Earth, with an additional component due to the complete rotation of the Earth's space.

2.3 Calculation of the density of the Earth microwave background at the COBE orbit and at the L2 point

We simplify formula (41) according to the assumptions of our problem. The quantity $\omega = \sqrt{GM_\oplus / R^3}$, the frequency of the rotation of the Earth space for an observer existing in the weightless state, takes its maximum numerical value at the equator of the Earth's surface, where $\omega = 1.24\times10^{-3}\,\sec^{-1}$. Obviously, the numerical value of ω decreases with altitude above the surface of the Earth. Since ω is a small value, we expand $e^{\omega t}$ into the series

$$e^{\omega t} \approx 1 + \omega t + \frac{1}{2}\,\omega^2 t^2 + \ldots \tag{42}$$

where we omit the higher order terms from consideration. As a result, we obtain, for the density of the energy of distributed matter (41) in the space of the Earth (we mean an electromagnetic field originating in the Earth as above),

$$\rho c^2 = \frac{3\omega^2}{\kappa}\,, \tag{43}$$

where $\omega = \sqrt{GM_\oplus / R^3}$. (In derivation of this formula we neglected the orders of ω higher than ω^2.) It should be noted that the quantity ω is derived from the weightless condition in the space, depending on the mass of the Earth $M_\oplus$, and the distance R from the centre of the Earth.

Because microwave radiation is related to an electromagnetic field, our theoretical result (43) is applicable to a microwave background originating from the Earth.

Now, with formula (43), we calculate the ratio between the density of the energy of the Earth microwave background at the L2 point ($R_{\text{L2}} = 1.5$ million km) and at the COBE orbit ($R_{\text{COBE}} = 6{,}370 + 900 = 7{,}270$ km)

$$\frac{\rho_{\text{L2}}}{\rho_{\text{COBE}}} = \frac{R^3_{\text{COBE}}}{R^3_{\text{L2}}} \simeq 1.1\times10^{-7}. \tag{44}$$

At the altitude of a U2 aeroplane (25 km altitude, which almost coincides with the location at the Earth's surface (within the framework of the precision of our calculation), we have $R_{\text{U2}} = 6{,}370 + 25 = 6{,}395$ km. So, we obtain the ratio between the density of the Earth microwave background at the L2 point, at the COBE orbit, and that at the U2 altitude is

$$\frac{\rho_{\text{L2}}}{\rho_{\text{U2}}} = \frac{R^3_{\text{U2}}}{R^3_{\text{L2}}} \simeq 7.8\times10^{-8}, \quad \frac{\rho_{\text{COBE}}}{\rho_{\text{U2}}} = \frac{R^3_{\text{U2}}}{R^3_{\text{COBE}}} \simeq 0.68. \qquad (45)$$

We see, concerning a microwave background field which originates in the Earth (the Earth microwave background), that a measurement of the background by an absolute instrument will give almost the same result at the position of a U2 aeroplane and the COBE satellite. However, at the L2 point (as far as 1.5 million km from the Earth, the point of location of the WMAP satellite and the planned PLANCK satellite), PLANCK, with its ability to function as an absolute instrument, should sense only $\sim10^{-7}$ of the field registered either by the U2 aeroplane or by the COBE satellite.

3 The anisotropy of the Earth microwave background in the COBE orbit and at the L2 point

It is also important to understand what is the anisotropy of the Earth microwave background due to a drift of the whole space of the Earth which would one observe at the COBE orbit and at the L2 point. We solve this problem by using the equations of motion of free light-like particles (photons), which are mediators transferring electromagnetic radiation, including those in the microwave region. When treating the photons which originate in the Earth's field (the Earth microwave background, for instance), the equations of motion should manifest an anisotropy in the directions of motion of the photon due to the presence of a linear drift in the Earth's space as a whole, relative to the source of another field such as the common field of a compact group of galaxies or that of the Universe as a whole [1, 2] (a weak microwave background).

The equations of motion of free particles are the *geodesic equations*.

A light-like free particle, e.g. a free photon, moves along isotropic geodesic trajectories whose four-dimensional equations are [3, 4]

$$\frac{dK^\alpha}{d\sigma} + \Gamma^\alpha_{\mu\nu} K^\mu \frac{dx^\nu}{d\sigma} = 0\,, \qquad (46)$$

where $K^\alpha = \frac{\Omega}{c}\frac{dx^\alpha}{d\sigma}$ is the four-dimensional wave vector of the photon (the vector satisfies the condition $K_\alpha K^\alpha = 0$), while Ω is the proper cyclic frequency of the photon. The three-dimensional observable interval equals the interval of observable time $d\sigma = c\,d\tau$ along isotropic trajectories, so $ds^2 = c^2\,d\tau^2 - d\sigma^2 = 0$. In terms of the physical observable quantities, the isotropic geodesic equations are represented by their projections on the time line and spatial section of an observer [1, 2]

$$\left.\begin{aligned} &\frac{d\Omega}{d\tau} - \frac{\Omega}{c^2}\,F_i\,c^i + \frac{\Omega}{c^2}\,D_{ik}\,c^i c^k = 0\,,\\ &\frac{d}{d\tau}\left(\Omega c^i\right) + 2\Omega\left(D^i_k + A^{\cdot i}_{k\cdot}\right)c^k - \\ &\qquad - \Omega F^i + \Omega\Delta^i_{kn} c^k c^n = 0\,, \end{aligned}\right\} \qquad (47)$$

where $c^i = \frac{dx^i}{d\tau}$ is the three-dimensional vector of the observable velocity of light (the square of c^i satisfies $c_k c^k = c^2$ in the fixed spatial section of the observer). The first of the equations (the scalar equation) represents the law of energy for the particle, while the vectorial equation is the three-dimensional equation of its motion.

We apply the isotropic geodesic equations to the space metric (9), which includes a linear drift of the reference space in the z-direction with a velocity v. Because the dipole-fit velocity of the Earth, extracted from the experimentally obtained anisotropy of the microwave background, is only $\mathrm{v} = 365\pm18$ km/sec, we neglect the relativistic square in the metric (9) so that it is

$$\begin{aligned} ds^2 = &\left(1 - \frac{2GM}{c^2 r} - \frac{\omega^2 r^2}{c^2} + \frac{2v\mathrm{v}}{c^2}\right)c^2 dt^2 + \\ &+ \frac{2v\left(\cos\varphi + \sin\varphi\right)}{c}\,cdtdr + \\ &+ \frac{2r\left[v\left(\cos\varphi - \sin\varphi\right) - \omega r\right]}{c}\,cdtd\varphi + \frac{2v}{c}\,cdt\,dz - \\ &- \left(1 + \frac{2GM}{c^2 r}\right)dr^2 + \frac{2v\mathrm{v}\left(\cos\varphi + \sin\varphi\right)}{c^2}\,dr\,dz - r^2 d\varphi^2 + \\ &+ \frac{2r\mathrm{v}\left[v\left(\cos\varphi - \sin\varphi\right) - \omega r\right]}{c^2}\,d\varphi dz - \left(1 - \frac{2v\mathrm{v}}{c^2}\right)dz^2, \end{aligned} \qquad (48)$$

We use the metric with the approximation specific to an observer located on board the COBE satellite or the WMAP satellite: the observer exists in the weightless state, so $\omega^2 r^2 = \frac{GM}{r}$; the linear velocity v of the Earth's space rotation doesn't depend on the z-coordinate, the direction of the drift of the whole space. We neglect the terms $\frac{v^2}{c^2}$ and also higher order terms, but retain the term $\frac{v\mathrm{v}}{c^2}$ which takes into account the drift of the whole space of the Earth: the value of v is determined in the weightless state of the observer; it is $\simeq$7.9 km/sec close to the surface of the Earth, and hence we have, near the surface, $\frac{v^2}{c^2} \approx 7\times10^{-10}$ and $\frac{v\mathrm{v}}{c^2} \approx 3\times10^{-8}$. Both values decrease with distance (altitude) from the Earth's surface, but the term $\frac{v\mathrm{v}}{c^2}$ remains two orders higher than $\frac{v^2}{c^2}$. We also neglect $\frac{GM}{c^2 r}$ which is $\approx10^{-9}$ at the Earth's surface.

Due to the fact that the terms $\frac{v\mathrm{v}}{c^2}$ are small corrections in the metric (48), it is easy to show that the exact solution of the conservation equations $v = T(t)re^{i\varphi}$, obtained earlier in the framework of such a metric without a drift of the whole

space (10), satisfies the present metric (48) where the drift is taken into account.

Using the solution for $T(t)$ (40), and expanding $e^{\omega t}$ into series $e^{\omega t} \approx 1 + \omega t + \ldots$, we obtain

$$T = -\omega^2 t\,, \tag{49}$$

then

$$v = -\omega^2 t r e^{i\varphi}. \tag{50}$$

We assume φ to be small. We calculate the observable characteristics of the Earth space where the drift of the whole space is taken into account, i.e. the space of the metric (48). Using the components of the fundamental metric tensor $g_{\alpha\beta}$ taken from the metric (48), we obtain

$$\left.\begin{aligned} v_1 &= \omega^2 t r e^{i\varphi}\left(\cos\varphi + \sin\varphi\right)\\ v_2 &= \omega r^2\left[\omega t e^{i\varphi}\left(\cos\varphi - \sin\varphi\right) + 1\right]\\ v_3 &= \omega^2 r t e^{i\varphi} \end{aligned}\right\} \tag{51}$$

$$\left.\begin{aligned} F_1 &= -\omega^2 r e^{i\varphi}\left(\cos\varphi + \sin\varphi\right) + \omega^2 \mathrm{v} t e^{i\varphi}\\ F_2 &= -\omega^2 r^2 e^{i\varphi}\left(\cos\varphi - \sin\varphi\right) - i\omega^2 r \mathrm{v} t e^{i\varphi}\\ F_3 &= -\omega^2 r e^{i\varphi} \end{aligned}\right\} \tag{52}$$

$$\left.\begin{aligned} A_{12} &= \omega r\left[1 + \frac{\omega t}{2}\left(1 - i\right)\right]\\ A_{23} &= \frac{i\omega^2 t r e^{i\varphi}}{2}\,, \qquad A_{13} = \frac{\omega^2 t e^{i\varphi}}{2} \end{aligned}\right\} \tag{53}$$

$$\left.\begin{aligned} &h_{11} = 1\,, \quad h_{13} = \frac{\omega^2 \mathrm{v} t r\left(\cos\varphi + \sin\varphi\right) e^{i\varphi}}{c^2}\\ &h_{22} = r^2, \;\; h_{23} = \frac{\omega r^2 \mathrm{v}\left[\omega t e^{i\varphi}\left(\cos\varphi - \sin\varphi\right) + 1\right]}{c^2}\\ &h_{33} = 1 - \frac{2\omega^2 \mathrm{v} t r e^{i\varphi}}{c^2}\\ &h = r^2\left(1 + \frac{2\omega^2 \mathrm{v} t r e^{i\varphi}}{c^2}\right)\\ &h^{11} = 1\,, \quad h^{13} = -\frac{\omega^2 \mathrm{v} t r\left(\cos\varphi + \sin\varphi\right) e^{i\varphi}}{c^2}\\ &h^{22} = \frac{1}{r^2}\,, \;\; h^{23} = -\frac{\omega \mathrm{v}\left[\omega t e^{i\varphi}\left(\cos\varphi - \sin\varphi\right) + 1\right]}{c^2}\\ &h^{33} = 1 + \frac{2\omega^2 \mathrm{v} t r e^{i\varphi}}{c^2} \end{aligned}\right\} \tag{54}$$

Because the components h_{13} and h_{23} of the tensor h_{ik} depend on the time coordinate t, we obtain two non-zero components of the tensor of the space deformation D_{ik}

$$\left.\begin{aligned} D_{13} &= \frac{\omega^2 r \mathrm{v}\left(\cos\varphi + \sin\varphi\right) e^{i\varphi}}{2c^2}\\ D_{23} &= \frac{\omega^2 r^2 \mathrm{v}\left(\cos\varphi - \sin\varphi\right) e^{i\varphi}}{2c^2}\\ D_{33} &= \frac{\omega^2 r \mathrm{v} e^{i\varphi}}{c^2} \end{aligned}\right\} \tag{55}$$

the scalar $D = h^{ik} D_{ik}$ is

$$D = \frac{\omega^2 r \mathrm{v} e^{i\varphi}}{c^2}. \tag{56}$$

We now calculate the chronometric Christoffel symbols of the second kind

$$\left.\begin{aligned} &\Delta^1_{22} = -r\,, \quad \Delta^1_{23} = \frac{\omega^2 r \mathrm{v} t\left(i - 1\right)}{2c^2} - \frac{\omega r \mathrm{v}}{c^2}\\ &\Delta^1_{33} = \frac{\omega^2 \mathrm{v} t e^{i\varphi}}{c^2}\\ &\Delta^2_{12} = \frac{1}{r}\,, \quad \Delta^2_{13} = \frac{\omega^2 \mathrm{v} t\left(1 - i\right)}{2c^2 r} + \frac{\omega \mathrm{v}}{c^2 r}\\ &\Delta^2_{33} = \frac{i\omega^2 \mathrm{v} t e^{i\varphi}}{c^2 r}\\ &\Delta^3_{11} = \frac{\omega^2 \mathrm{v} t\left(\cos\varphi + \sin\varphi\right) e^{i\varphi}}{c^2}\\ &\Delta^3_{12} = \frac{\omega^2 r \mathrm{v} t\left(i + 1\right) e^{2i\varphi}}{2c^2}\,, \;\; \Delta^3_{13} = -\frac{\omega^2 \mathrm{v} t e^{i\varphi}}{c^2}\\ &\Delta^3_{22} = \frac{i\omega^2 r^2 \mathrm{v} t\left(\cos\varphi - \sin\varphi\right) e^{i\varphi}}{c^2}\\ &\Delta^3_{23} = \frac{i\omega^2 r \mathrm{v} t e^{i\varphi}}{c^2} \end{aligned}\right\} \tag{57}$$

We use the above characteristics of the Earth's space to write the isotropic geodesic equations (47) in component form. We neglect the terms proportional to $\frac{1}{c^2}$ in the equations. Besides, in the framework of our asumptions, the differential with respect to proper time τ, i.e.

$$\frac{d}{d\tau} = \frac{{}^*\partial}{\partial t} + \mathrm{v}^i \frac{{}^*\partial}{\partial x^i}\,, \tag{58}$$

can be removed with the regular partial derivative $\frac{d}{d\tau} = \frac{\partial}{\partial t}$. (The starred derivatives become the regular derivatives, and also the observable velocity of light c^i doesn't depend on the z coordinate in our case where the whole space has a drift in the z direction.)

The vectorial isotropic geodesic equations, written in component notation, are

$$\left.\begin{aligned} &\frac{dc^1}{d\tau} + 2\left(D^1_k + A^{\cdot 1}_{k\cdot}\right) c^k - F^1 + \Delta^1_{22} c^2 c^2 +\\ &\qquad + 2\Delta^1_{23} c^2 c^3 + \Delta^1_{33} c^3 c^3 = 0\\ &\frac{dc^2}{d\tau} + 2\left(D^2_k + A^{\cdot 2}_{k\cdot}\right) c^k - F^2 + 2\Delta^2_{12} c^1 c^2 +\\ &\qquad + 2\Delta^2_{13} c^1 c^3 + \Delta^2_{33} c^3 c^3 = 0\\ &\frac{dc^3}{d\tau} + 2\left(D^3_k + A^{\cdot 3}_{k\cdot}\right) c^k - F^3 + \Delta^3_{11} c^1 c^1 + 2\Delta^3_{12} c^1 c^2 +\\ &\qquad + 2\Delta^3_{13} c^1 c^3 + \Delta^3_{22} c^2 c^2 + 2\Delta^3_{23} c^2 c^3 = 0 \end{aligned}\right\} \tag{59}$$

and after substituting the observable characteristics of the space, take the form (60–62), where dot denotes differentiation with respect to time.

$$\ddot{r} - 2\omega r\left[1+\frac{\omega t\,(1-i)}{2}\right]\dot{\varphi} - \omega^2 e^{i\varphi}\left[t - \frac{\mathrm{v}r\,(\cos\varphi+\sin\varphi)}{c^2}\right]\dot{z} + \omega^2\left[r\,(\cos\varphi+\sin\varphi) - \mathrm{v}t\right]e^{i\varphi} -$$
$$- r\dot{\varphi}^2 + \frac{2\omega r\mathrm{v}}{c^2}\left[\frac{\omega t\,(i-1)}{2} - 1\right]\dot{\varphi}\dot{z} + \frac{\omega^2\mathrm{v}te^{i\varphi}}{c^2}\,\dot{z}^2 = 0\,, \tag{60}$$

$$\ddot{\varphi} + \frac{2\omega}{r}\left[1+\frac{\omega t\,(1-i)}{2}\right]\dot{r} - \frac{\omega^2 e^{i\varphi}}{r}\left[it - \frac{\mathrm{v}r\,(\cos\varphi-\sin\varphi)}{c^2}\right]\dot{z} + \frac{\omega^2}{r}\left[r\,(\cos\varphi-\sin\varphi) + i\mathrm{v}t\right]e^{i\varphi} +$$
$$+ \frac{2}{r}\,\dot{r}\dot{\varphi} - \frac{2\omega\mathrm{v}}{c^2 r}\left[\frac{\omega t\,(i-1)}{2} - 1\right]\dot{r}\dot{z} - \frac{i\omega^2\mathrm{v}t}{c^2}\,\dot{z}^2 = 0\,, \tag{61}$$

$$\ddot{z} + \omega^2 e^{i\varphi}\left[t + \frac{\mathrm{v}r\,(\cos\varphi+\sin\varphi)}{c^2}\right]\dot{r} + \omega^2 r e^{i\varphi}\left[it + \frac{\mathrm{v}r\,(\cos\varphi-\sin\varphi)}{c^2}\right]\dot{\varphi} + \frac{2\omega^2 r\,\mathrm{v}e^{i\varphi}}{c^2}\,\dot{z} +$$
$$+ \omega^2 r e^{i\varphi} + \frac{\omega^2\mathrm{v}te^{i\varphi}\,(\cos\varphi+\sin\varphi)}{c^2}\,\dot{r}^2 + \frac{\omega^2 r\mathrm{v}t\,(i+1)\,e^{2i\varphi}}{c^2}\,\dot{r}\dot{\varphi} + \frac{2\omega^2\mathrm{v}te^{i\varphi}}{c^2}\,\dot{r}\dot{z} + \tag{62}$$
$$+ \frac{i\omega^2 r^2\mathrm{v}t\,(\cos\varphi-\sin\varphi)\,e^{i\varphi}}{c^2}\,\dot{\varphi}^2 + \frac{2i\omega^2 r\mathrm{v}te^{i\varphi}}{c^2}\,\dot{\varphi}\dot{z} = 0,$$

$$\dot{r}^2 + \frac{2\omega^2 r\mathrm{v}t\,(\cos\varphi+\sin\varphi)\,e^{i\varphi}}{c^2}\,\dot{r}\dot{z} + r^2\dot{\varphi}^2 + \frac{2\omega r^2\mathrm{v}\left[\omega te^{i\varphi}\,(\cos\varphi-\sin\varphi)+1\right]}{c^2}\,\dot{\varphi}\dot{z} +$$
$$+ \left(1 - \frac{2\omega^2 r\mathrm{v}te^{i\varphi}}{c^2}\right)\dot{z}^2 = c^2. \tag{63}$$

The space-time interval ds along isotropic geogesics satisfies the condition $ds^2 = 0$. This condition, in the terms of physical observed quantities, implies constancy of the square of the three-dimensional observable velocity of light $c_i c^i = h_{ik}\,c^i c^k = c^2$ along the trajectory. This condition, for the metric (48), takes the form (63).

A system of the differential equations (60–63) describes the motion of light-like particles completely, in the given space-time of the metric (48).

Earlier in this study we considered only the real part $v = T(t)\,re^{i\varphi}$ of the solution of the conservation equations in an electromagnetic field. Because we study the motion of photons in such an electromagnetic field (in the sample of a microwave background) we only use the real solution in the system of the equations (60–63). After the function $v = T(t)\,re^{i\varphi}$ is substituted into (60–63), we have, after transformations, the formulae (64–67) (see Page 93).

We assume that a light-like signal (photon) of the Earth microwave radiation moves along the radial direction r. Because the space of the Earth at the location of a satellite (the space of the weightless state) rotates with an angular velocity ω which depends upon r, we have $\dot{\varphi} = 0$. Two satellites which measure the Earth microwave background are located at the altitudes $r_1 = 900$ km and $r_2 = 1.5$ million km respectively. Calculation of $\omega^2 = \frac{GM_\oplus}{r^3}$, where $M_\oplus = 6\times10^{27}$g is the mass of the Earth, gives the values: $\omega_1 = 10^{-3}$ sec^{-1} and $\omega_2 = 3.5\times10^{-6}$ sec^{-1}. Because both values are small, we use $\cos\varphi \simeq 1 + \omega t$ and $\sin\varphi \simeq \omega t$. Substituting these into the system of equations (64–67), and neglecting the terms of order higher than ω^2 (and also the other higher order terms), we obtain, finally,

$$\ddot{r} - \omega^2\left(t - \frac{r\mathrm{v}}{c^2}\right)\dot{z} + \omega^2\,(r - \mathrm{v}t) + \frac{\omega^2\mathrm{v}t}{c^2}\,\dot{z}^2 = 0\,, \tag{68}$$

$$\ddot{\varphi} + 2\omega\left(1 + \frac{2\omega t}{2}\right)\frac{\dot{r}}{r} + \frac{\omega^2\mathrm{v}}{c^2}\,\dot{z} + 4\omega^2 + 2\omega\frac{\dot{r}}{r} + \frac{2\omega\mathrm{v}\left(1+\frac{\omega t}{2}\right)}{c^2 r}\,\dot{r}\dot{z} = 0\,, \tag{69}$$

$$\ddot{z} + \omega^2\left(t + \frac{r\mathrm{v}}{c^2}\right)\dot{r} + \frac{2\omega^2\mathrm{v}r}{c^2}\,\dot{z} + \omega^2 r + \frac{\omega^2\mathrm{v}t}{c^2}\,\dot{r}^2 + \frac{2\omega^2\mathrm{v}t}{c^2}\,\dot{r}\dot{z} = 0\,, \tag{70}$$

$$\dot{r}^2 + \frac{2\omega^2 r\mathrm{v}t}{c^2}\,\dot{r}\dot{z} + \frac{2\omega^2 r^2\mathrm{v}}{c^2}\,\dot{z} + \left(1 - \frac{2\omega^2 r\mathrm{v}t}{c^2}\right)\dot{z}^2 = c^2. \tag{71}$$

We do choose the coordinate axes so that the z-axis is directed along the motion of the Earth, in common with its own electromagnetic field, relative to the source of another feld such as the common feld of a compact group of galaxies or that of the Universe as a whole (a weak microwave background). We also assume, for simplicity, that the orbit of the satellite, on board of which an observer is located, lies in the plane orthogonal to the z-direction. In such a case, we have $\dot{z}_0 = 0$. We obtain, assuming $\dot{z}_0 = 0$,

$$\dot{r}_0^2 = c^2, \tag{72}$$

$$\ddot{r} - \omega^2 \left[t\cos\varphi - \frac{r\mathrm{v}\left(1+\cos 2\varphi+\sin 2\varphi\right)}{c^2}\right] \dot{z} - 2\omega r \left(1+\frac{\omega t}{2}\right)\dot{\varphi} + 2\omega^2 r\left(1+\cos 2\varphi+\sin 2\varphi\right) + \\ + \omega^2 \mathrm{v}t\cos\varphi - r\dot{\varphi}^2 - \frac{2\omega r\mathrm{v}\left(\frac{\omega t}{2}+1\right)}{c^2}\dot{\varphi}\dot{z} + \frac{\omega^2 \mathrm{v}t\cos\varphi}{c^2}\dot{z}^2 = 0\,, \tag{64}$$

$$\ddot{\varphi} + 2\omega\left(1+\frac{\omega t}{2}\right)\frac{\dot{r}}{r} + \frac{\omega^2}{r}\left[t\sin\varphi + \frac{\mathrm{v}r\left(1+\cos 2\varphi-\sin 2\varphi\right)}{c^2}\right]\dot{z} + 2\omega^2\left(1+\cos 2\varphi-\sin 2\varphi\right) - \\ - \frac{\omega^2}{r}\mathrm{v}t\sin\varphi + \frac{2\dot{r}\dot{\varphi}}{r} + \frac{2\omega\mathrm{v}\left(\frac{\omega t}{2}+1\right)}{c^2 r}\dot{r}\dot{z} = 0\,, \tag{65}$$

$$\ddot{z} + \omega^2\left[t\cos\varphi + \frac{r\mathrm{v}\left(1+\cos 2\varphi+\sin 2\varphi\right)}{c^2}\right]\dot{r} - 2\omega^2 r\left[2t\sin\varphi - \frac{r\mathrm{v}\left(1+\cos 2\varphi-\sin 2\varphi\right)}{c^2}\right]\dot{\varphi} + \\ + \frac{2\omega^2 r\mathrm{v}\cos\varphi}{c^2}\dot{z} + \omega^2 r\cos\varphi + \frac{\omega^2\mathrm{v}t\left(1+\cos 2\varphi+\sin 2\varphi\right)}{2c^2}\dot{r}^2 + \frac{\omega^2\mathrm{v}t\left(\cos 2\varphi-\sin 2\varphi\right)}{c^2}\dot{r}\dot{\varphi} + \\ + \frac{2\omega^2\mathrm{v}t\cos\varphi}{c^2}\dot{r}\dot{z} + \frac{2\omega^2 r^2\mathrm{v}t\left(1-\cos 2\varphi-\sin 2\varphi\right)}{c^2}\dot{\varphi}^2 - \frac{2\omega^2 r\mathrm{v}t\sin\varphi}{c^2}\dot{\varphi}\dot{z} = 0\,, \tag{66}$$

$$\dot{r}^2 + \frac{2\omega^2 r\mathrm{v}t\left(1+\cos 2\varphi+\sin 2\varphi\right)}{c^2}\dot{r}\dot{z} + r^2\dot{\varphi}^2 + \frac{2\omega r^2\mathrm{v}\left[\frac{\omega t}{2}\left(1+\cos 2\varphi-\sin 2\varphi\right)+1\right]}{c^2}\dot{\varphi}\dot{z} + \\ + \left(1-\frac{2\omega^2 r\mathrm{v}t\cos\varphi}{c^2}\right)\dot{z}^2 = c^2. \tag{67}$$

hence we assume $\dot{r}\simeq c$. So we have $r\simeq ct$. Substituting these into the equation of motion of a photon in the z-direction (70), and taking the weightless condition into account, we obtain the equation of motion in the z direction for a photon associated with the Earth's electromagnetic field, the Earth microwave background in particular. The equation is

$$\ddot{z} + \frac{2GM_\oplus}{c^2t^2}\left(1+\frac{\mathrm{v}}{c}\right) = 0\,. \tag{73}$$

Integrating the equation with the conditions $\dot{z}_0 = 0$ and $r\simeq ct$ taken into account, we obtain

$$\dot{z} = \frac{2GM_\oplus}{cr}\left(1+\frac{\mathrm{v}}{c}\right) = \dot{z}' + \Delta z', \tag{74}$$

where the first term shows that such a photon, initially launched in the r-direction in the rotating space (gravitational field) of the Earth, is carried into the z-direction by the rotation of the space of the Earth. The second term shows carriage into the z-direction due to the motion of the Earth in this direction relative to another source such as a local group of galaxies or the whole Universe.

Denoting the first term in this formula as $\dot{z}' = \frac{2GM_\oplus}{cr}$ and the second term as $\Delta\dot{z}' = \frac{2GM_\oplus\mathrm{v}}{c^2 r}$, we obtain the relative carriage of the three-dimensional vector of the light velocity from the initial r-direction to the z-direction, due to the motion of the Earth, as

$$\frac{\Delta\dot{z}'}{\dot{z}'} = \frac{\mathrm{v}}{c}\,. \tag{75}$$

Such a relative carriage of a photon radiated from the Earth's surface, applied to the field of photons of the Earth microwave background radiated in the radial directions, reveals the anisotropy associated with the dipole component of the background.

Such a relative carriage of a photon, associated with the Earth's electromagnetic field, into the z-direction, doesn't depend on the path travelled by such a photon in the radial direction r from the Earth. This means that the anisotropy associated with the dipole component of the Earth microwave background shouldn't be dependent on altitude: it should be the same be it measured on board a U2 aeroplane (25 km), at the orbit of the COBE satellite (900 km), and at the L2 point (the WMAP satellite and PLANCK satellite, 1.5 million km from the Earth).

4 Comparing the theoretical results to experimental data. Conclusions

We have obtained, from General Relativity, two fundamental results:

- A microwave background which originates in the Earth (the EMB) decreases with altitude, such that the density of the energy of this background at the height of the COBE satellite (900 km) is just 0.68 times less that that at the height of a U2 aeroplane (25 km). The energy of the background at the L2 point (which is up to 1.5 million km from the Earth) is only $\sim 10^{-7}$ that experienced at the location either of a U2 aeroplane or of the COBE satellite;
- The anisotropy of the Earth microwave background,

due to the fast motion of the Earth relative to the source of another field, which isn't connected to the Earth but located in depths of the cosmos, does not depend on the position relative to the Earth's surface. The dipole anisotropy is therefore independent of altitude; the anisotropy will be the same be it measured at the altitude of a U2 aeroplane (25 km), the COBE satellite (900 km), or the WMAP satellite located at the L2 point (1.5 million km).

These purely theoretical conclusions, from General Relativity, cause us to consider an Earth origin of the microwave background, the monopole 2.7 K component of which was discovered in 1965 by Penzias and Wilson, in a ground-based observation [6], while the dipole 3.35 mK component was first observed in 1969 by Conklin, also via a ground-based observation [7], then studied by Henry [8], Corey [9], and also Smoot, Gorenstein, and Muller, who organized a stratosphere observation on board a U2 aeroplane [11]. (See the history of the observations in detail in Lineweaver's paper [10].)

There are many problems in the observation of the microwave background. The monopole component, at low frequencies, is easy to observe at the Earth's surface [6]. The dipole component is best observed at the altitude of a U2 aeroplane [11], at the altitude of 900 km (the COBE satellite) and also at 1.5 million km (the WMAP satellite located at the L2 point) where its anisotropy is clearly indicated [12–17]. Conversely, the monopole observed on Earth and in COBE orbit, has yet to be recorded at the L2 point: the WMAP satellite has only differential instruments on board, which are able to indicate only the anisotropy of the background, not its absolute value.

On the other hand, as shown by Robitaille [18–22], such a phenomenology of the observations has a clear explanation as an Earth microwave background which originates not in a cosmic source, but the oceans of the Earth, which produce microwave signals, in particular, with an apparent temperature of 2.7 K. Besides, as pointed out in [21, 23], the observed anisotropy of the microwave background can be explained as a relativistic effect of the motion of the observer, in common with the source of the background (the Earth), relative to the source of a noise microwave field, which has no specific temperature, and a source of which is located in depths of the cosmos (i.e. the distance from the many sources).

According to our theory, which supports the phenomenology of the Earth microwave background, proposed by Robitaille [18–22], we have four new specific terms, namely:

1. The EMB (the Earth Microwave Background);
2. The EMBM (the monopole associated with the Earth Microwave Background);
3. The EMBD (the dipole associated with the Earth Microwave Background);
4. The EMBA (the anisotropy of the Earth Microwave Background, associated with the dipole).

The PLANCK satellite (which has an absolute instrument on board), will soon be launched to the L2 point, on 31st July 2008, and should find an experimental verification of our theory.

Acknowledgement

We are very grateful to Pierre-Marie Robitaille for consultations and valuable comments. We also are thankful to Delyan Zhelyazov for a few typing mistakes found in the formulae when this issue was sent to print.

Submitted on August 29, 2007 / Accepted on September 06, 2007
First published online on September 08, 2007
Online version corrected on February 11, 2008

References

1. Borissova L. Preferred spatial directions in the Universe: a General Relativity approach. *Progress in Physics*, 2006, v. 4, 51–58.
2. Borissova L. Preferred spatial directions in the Universe. Part II. Matter distributed along orbital trajectories, and energy produced from it. *Progress in Physics*, 2006, v. 4, 59–64.
3. Zelmanov A. L. Chronometric invariants and co-moving coordinates in the general relativity theory. *Doklady Acad. Nauk USSR*, 1956, v.107 (6), 815–818.
4. Zelmanov A. L. Chronometric invariants. American Research Press, Rehoboth (NM), 2006.
5. Schouten J. A. und Struik D. J. Einführung in die neuren Methoden der Differentialgeometrie. Noordhoff, Groningen, 1938.
6. Penzias A. A. and Wilson R. W. A measurement of excess antenna temperature at 4080 Mc/s. *Astrophys. J.*, 1965, v. 1, 419–421.
7. Conklin E. K. Velocity of the Earth with respect to the Cosmic Background Radiation. *Nature*, 1969, v. 222, 971.
8. Henry P. S. Isotropy of the 3 K Background. *Nature*, 1971, v. 231, 516–518.
9. Corey B. E. and Wilkinson D. T. A measurement of the Cosmic Microwave Background Anisotropy at 19 GHz. *Bulletin of the American Astronomical Society*, 1976, v. 8, 351.
10. Lineweaver C.H. The CMB Dipole: The most recent measurement and some history. In *Microwave Background Anistropies. Proceedings of the XVIth Moriond Astrophysics Meeting*, Les Arcs, Savoie, France, March 16th-23rd, 1996, F. R. Bouchet, R. Gispert, B. Guilderdoni, and J.T.T. Van, eds., Gif-sur-Yvette: Editions Frontieres, 1997; (see also arXiv: astro-ph/9609034).
11. Smoot G. F., Gorenstein M. V. and Muller R. A. Detection of anisotropy in the Cosmic Blackbody Radiation. *Phys. Rev. Lett.*, 1977, v. 39, 898–901.
12. Boggess N.W., et al. The COBE mission: its design and perfomance two years after launch. *Astrophys. J.*, 1992, v. 397, 420–429.
13. Fixsen D.J., et al. The Cosmic Microwave Background spectrum from the full COBE FIRAS data set. *Astrophys. J.*, 1996, v. 473, 576–587.

14. Smoot G.F., et al. Preliminary results from the COBE differential microwave interferometers: large angular scale isotropy of the Cosmic Microwave Background. *Astrophys. J.*, 1991, v. 371, L1–L5.

15. Page L., et al. The optical design and characterization of the Microwave Anisotropy Probe. *Astrophys. J.*, 2003, v. 585, 566–586.

16. Bennett C.L., et al. The Microwave Anisotropy Probe mission. *Astrophys. J.*, 2003, v. 583(1), 1–23.

17. Bennett C.L., et al. First-year Wilkinson Microwave Anisotropy Probe (WMAP) observations: preliminary maps and basic results. *Astrophys. J. Suppl. Ser.*, 2003, v. 148(1), 1–27.

18. Robitaille P.-M. WMAP: a radiological analysis. *Progress in Physics*, 2007, v. 1, 3–18.

19. Robitaille P.-M. On the origins of the CMB: insight from the COBE, WMAP and Relikt-1 satellites. *Progress in Physics*, 2007, v. 1, 19–23.

20. Robitaille P.-M. On the Earth Microwave Background: absorption and scattering by the atmosphere. *Progress in Physics*, 2007, v. 3, 3–4.

21. Robitaille P.-M. and Rabounski D. COBE and the absolute assignment of the CMB to the Earth. *2007 APS March Meeting*, Denver, Colorado, Monday–Friday, March 5–9, 2007, http://meetings.aps.org/link/BAPS.2007.MAR.L20.7

22. Robitaille P.-M. On the nature of the microwave background at the Lagrange 2 Point. Part I. *Progress in Physics*, 2007, v. 4, 74–83.

23. Rabounski D. The relativistic effect of the deviation between the CMB temperatures obtained by the COBE satellite. *Progress in Physics*, 2007, v. 1, 19–21.

A New Conformal Theory of Semi-Classical Quantum General Relativity

Indranu Suhendro

Department of Physics, Karlstad University, Karlstad 651 88, Sweden
E-mail: spherical_symmetry@yahoo.com

We consider a new four-dimensional formulation of semi-classical quantum general relativity in which the classical space-time manifold, whose intrinsic geometric properties give rise to the effects of gravitation, is allowed to evolve microscopically by means of a conformal function which is assumed to depend on some quantum mechanical wave function. As a result, the theory presented here produces a unified field theory of gravitation and (microscopic) electromagnetism in a somewhat simple, effective manner. In the process, it is seen that electromagnetism is actually an emergent quantum field originating in some kind of stochastic smooth extension (evolution) of the gravitational field in the general theory of relativity.

1 Introduction

We shall show that the introduction of an external parameter, the Planck displacement vector field, that deforms ("maps") the standard general relativistic space-time $\mathbb{S}_1$ into an evolved space-time $\mathbb{S}_2$ yields a theory of general relativity whose space-time structure obeys the semi-classical quantum mechanical law of evolution. In addition, an "already quantized" electromagnetic field arises from our schematic evolution process and automatically appears as an intrinsic geometric object in the space-time $\mathbb{S}_2$. In the process of evolution, it is seen that from the point of view of the classical space-time $\mathbb{S}_1$ alone, an external deformation takes place, since, by definition, the Planck constant does not belong to its structure. In other words, relative to $\mathbb{S}_1$, the Planck constant is an external parameter. However from the global point of view of the universal (enveloping) evolution space $\mathbb{M}_4$, the Planck constant is intrinsic to itself and therefore defines the dynamical evolution of $\mathbb{S}_1$ into $\mathbb{S}_2$. In this sense, a point in $\mathbb{M}_4$ is not strictly single-valued. Rather, a point in $\mathbb{M}_4$ has a "dimension" depending on the Planck length. Therefore, it belongs to both the space-time $\mathbb{S}_1$ and the space-time $\mathbb{S}_2$.

2 Construction of a four-dimensional metric-compatible evolution manifold $\mathbb{M}_4$

We first consider the notion of a four-dimensional, universal enveloping manifold $\mathbb{M}_4$ with coordinates x^μ endowed with a *microscopic* deformation structure represented by an exterior vector field $\phi\ (\ x^\mu\ )$ which maps the enveloped space-time manifold $\mathbb{S}_1 \in \mathbb{M}_4$ at a certain initial point P_0 onto a new enveloped space-time manifold $\mathbb{S}_2 \in \mathbb{M}_4$ at a certain point P_1 through the diffeomorphism

$$x^\mu\left(P_1\right) = x^\mu\left(P_0\right) + l\,\xi^\mu,$$

where $l = \sqrt{\frac{G\hbar}{c^3}} \approx 10^{-33}$ cm is the Planck length expressed in terms of the Newtonian gravitational constant G, the Dirac-Planck constant $\hbar$, and the speed of light in vacuum c, in such a way that

$$\phi^\mu = l\,\xi^\mu$$
$$\lim_{\hbar\to 0}\phi^\mu = 0\,.$$

From its diffeomorphic structure, we therefore see that $\mathbb{M}_4$ is a kind of *strain space*. In general, the space-time $\mathbb{S}_2$ evolves from the space-time $\mathbb{S}_1$ through the non-linear mapping

$$P(\phi) : \mathbb{S}_1 \to \mathbb{S}_2\,.$$

Note that the exterior vector field ϕ can be expressed as $\phi = \phi^\mu h_\mu = \bar{\phi}^\mu g_\mu$ (the Einstein summation convention is employed throughout this work) where h_μ and g_μ are the sets of basis vectors of the space-times $\mathbb{S}_1$ and $\mathbb{S}_2$, respectively (likewise for ξ). We remark that $\mathbb{S}_1$ and $\mathbb{S}_2$ are both endowed with metricity through their immersion in $\mathbb{M}_4$, which we shall now call the *evolution manifold*. Then, the two sets of basis vectors are related by

$$g_\mu = \left(\delta^\nu_\mu + l\,\nabla_\mu\,\xi^\nu\right) h_\nu$$

or, alternatively, by

$$g_\mu = h_\mu + l\left(\bar{\nabla}_\mu\,\bar{\xi}^\nu\right) g_\nu$$

where δ^ν_μ are the components of the Kronecker delta.

At this point, we have defined the two covariant derivatives with respect to the connections ω of $\mathbb{S}_1$ and Γ of $\mathbb{S}_2$ as follows:

$$\nabla_\lambda A^{\alpha\beta\ldots}_{\mu\nu\ldots} = \partial_\lambda A^{\alpha\beta\ldots}_{\mu\nu\ldots} + \omega^\alpha_{\sigma\lambda} A^{\sigma\beta\ldots}_{\mu\nu\ldots} + \omega^\beta_{\sigma\lambda}\omega^{\alpha\sigma\ldots}_{\mu\nu\ldots} + \ldots$$
$$- \omega^\sigma_{\mu\lambda} A^{\alpha\beta\ldots}_{\sigma\nu\ldots} - \omega^\sigma_{\nu\lambda} A^{\alpha\beta\ldots}_{\mu\sigma\ldots} - \ldots$$

and

$$\bar{\nabla}_\lambda B^{\alpha\beta\ldots}_{\mu\nu\ldots} = \partial_\lambda B^{\alpha\beta\ldots}_{\mu\nu\ldots} + \Gamma^\alpha_{\sigma\lambda} B^{\sigma\beta\ldots}_{\mu\nu\ldots} + \Gamma^\beta_{\sigma\lambda} B^{\alpha\sigma}_{\mu\nu\ldots} + \ldots$$
$$- \Gamma^\sigma_{\mu\lambda} B^{\alpha\beta\ldots}_{\sigma\nu\ldots} - \Gamma^\sigma_{\nu\lambda} B^{\alpha\beta\ldots}_{\mu\sigma\ldots} - \ldots$$

for arbitrary tensor fields A and B, respectively. Here $\partial_\mu = \partial/\partial\, x^\mu$, as usual. The two covariant derivatives above are equal only in the limit $\hbar \to 0$.

Furthermore, we assume that the connections ω and Γ are generally asymmetric, and can be decomposed into their symmetric and anti-symmetric parts, respectively, as

$$\omega^{\lambda}_{\mu\nu} = \left(h^{\lambda}, \partial_{v} h_{\mu}\right) = \omega^{\lambda}_{(\mu\nu)} + \omega^{\lambda}_{[\mu\nu]}$$

and

$$\Gamma^{\lambda}_{\mu\nu} = \left(g^{\lambda}, \partial_{v} g_{\mu}\right) = \Gamma^{\lambda}_{(\mu\nu)} + \Gamma^{\lambda}_{[\mu\nu]}.$$

Here, by (a, b) we shall mean the inner product between the arbitrary vector fields a and b.

Furthermore, by direct calculation we obtain the relation

$$\partial_{\nu} g_{\mu} = \left(\omega^{\lambda}_{\mu\nu} + l\left(\nabla^{\sigma}_{\mu\xi}\right)\omega^{\lambda}_{\sigma\nu} + l\,\partial_{\nu}\left(\nabla_{\mu}\xi^{\lambda}\right)\right) h_{\lambda}\,.$$

Hence, setting

$$F^{\lambda}_{\mu\nu} = \omega^{\lambda}_{\mu\nu} + l\left(\left(\nabla_{\mu}\xi^{\sigma}\right)\omega^{\lambda}_{\sigma\nu} + \partial_{\nu}\left(\nabla_{\mu}\xi^{\lambda}\right)\right) =$$
$$= \omega^{\lambda}_{\mu\nu} + l\left(\left(\nabla_{\mu}\xi^{\sigma}\right)\omega^{\lambda}_{\sigma\nu} + \partial_{\nu}\partial^{\lambda}_{\mu\xi} + \xi^{\sigma}\partial_{\nu}\omega^{\lambda}_{\sigma\mu} + \left(\partial_{\nu}\xi^{\sigma}\right)\omega^{\lambda}_{\sigma\mu}\right)$$

we may simply write

$$\partial_{\nu} g_{\mu} = F^{\lambda}_{\mu\nu} h_{\lambda}\,.$$

Meanwhile, we also have the following inverse relation:

$$h_{\mu} = \left(\delta^{\nu}_{\mu} - l\,\bar{\nabla}_{\mu}\bar{\xi}^{\nu}\right) g_{\nu}\,.$$

Hence we obtain

$$\partial_{\nu} g_{\mu} = \left(\omega^{\lambda}_{\mu\nu} + l\left(\nabla_{\mu}\xi^{\sigma}\right)\omega^{\lambda}_{\sigma\nu} + l\,\partial_{\nu}\partial^{\lambda}_{\mu\xi} + \right.$$
$$+ l\,\xi^{\sigma}\partial_{\nu}\omega^{\lambda}_{\sigma\mu} + l\left(\partial_{\nu}\xi^{\sigma}\right)\omega^{\lambda}_{\sigma\mu} - l\,\omega^{\sigma}_{\mu\nu}\bar{\nabla}_{\sigma}\bar{\xi}^{\lambda} -$$
$$- l\left(\nabla_{\mu}\xi^{\rho}\right)\omega^{\sigma}_{\rho\nu}\bar{\nabla}_{\sigma}\bar{\xi}^{\lambda} - l\left(\partial_{v}\partial_{\mu}\xi^{\sigma}\right)\bar{\nabla}_{\sigma}\bar{\xi}^{\lambda} -$$
$$\left. - l\,\xi^{\rho}\left(\partial_{\nu}\omega^{\sigma}_{\rho\mu}\right)\bar{\nabla}_{\sigma}\bar{\xi}^{\lambda} - l\left(\partial_{\nu}\xi^{\rho}\right)\omega^{\sigma}_{\rho\mu}\bar{\nabla}_{\sigma}\bar{\xi}^{\lambda}\right) g_{\lambda}\,.$$

Using the relation $\partial_{\nu} g_{\mu} = \Gamma^{\lambda}_{\mu\nu} g_{\lambda}$ (similarly, $\partial_{\nu} h_{\mu} = \omega^{\lambda}_{\mu\nu} h_{\lambda}$), we obtain the relation between the two connections Γ and ω as follows:

$$\Gamma^{\lambda}_{\mu\nu} = \omega^{\lambda}_{\mu\nu} + l\left(\left(\nabla_{\mu}\xi^{\sigma}\right)\omega^{\lambda}_{\sigma\nu} + \partial_{\nu}\partial_{\mu}\xi^{\lambda} + \right.$$
$$+ \xi^{\sigma}\partial_{\nu}\omega^{\lambda}_{\sigma\mu}\left(\partial_{\nu}\xi^{\sigma}\right)\omega^{\lambda}_{\sigma\mu} - \omega^{\sigma}_{\mu\nu}\bar{\nabla}_{\sigma}\bar{\xi}^{\lambda} - \left(\nabla_{\mu}\xi^{\rho}\right)\omega^{\sigma}_{\rho\nu}\bar{\nabla}_{\sigma}\bar{\xi}^{\lambda} -$$
$$\left. - \left(\partial_{\nu}\partial_{\mu}\xi^{\sigma}\right)\bar{\nabla}_{\sigma}\bar{\xi}^{\lambda} - \xi^{\rho}\left(\partial_{\nu}\omega^{\sigma}_{\rho\mu}\right)\bar{\nabla}_{\sigma}\bar{\xi}^{\lambda} - \left(\partial_{\nu}\xi^{\rho}\right)\omega^{\sigma}_{\rho\mu}\bar{\nabla}_{\sigma}\bar{\xi}^{\lambda}\right)$$

which is a general non-linear relation in the components of the exterior displacement field ξ. We may now write

$$\Gamma^{\lambda}_{\mu\nu} = F^{\lambda}_{\mu\nu} + G^{\lambda}_{\mu\nu}$$

where, recalling the previous definition of $F^{\lambda}_{\mu\nu}$, it can be rewritten as

$$F^{\lambda}_{\mu\nu} = \omega^{\lambda}_{\mu\nu} + l\left(\left(\partial_{\nu}\omega^{\lambda}_{\sigma\mu} + \omega^{\rho}_{\mu\sigma}\omega^{\lambda}_{\rho\nu}\right)\xi^{\sigma} + \right.$$
$$\left. + \partial_{\nu}\partial_{\mu}\xi^{\lambda} + \left(\partial_{\mu}\xi^{\sigma}\right)\omega^{\lambda}_{\sigma\nu} + \left(\partial_{\nu}\xi^{\sigma}\right)\omega^{\lambda}_{\sigma\mu}\right)$$

and where

$$G^{\lambda}_{\mu\nu} = -l\left(\omega^{\sigma}_{\mu\nu} + l\,\left(\left(\nabla_{\mu}\xi^{\rho}\right)\omega^{\sigma}_{\rho\nu}\right.\right.$$
$$\left.\left. + \partial_{\nu}\partial_{\mu}\xi^{\sigma} + \xi^{\rho}\,\partial_{\nu}\omega^{\sigma}_{\rho\mu} + \left(\partial_{\nu}\xi^{\rho}\right)\omega^{\sigma}_{\rho\mu}\right)\right)\bar{\nabla}_{\sigma}\bar{\xi}^{\lambda}\,.$$

At this point, the intrinsic curvature tensors of the space-times $\mathbb{S}_1$ and $\mathbb{S}_2$ are respectively given by

$$K^{\sigma}{}_{\rho\mu\nu} = 2\left(h^{\sigma}, \partial_{[\mu}\partial_{\nu]} h_{\rho}\right) =$$
$$= \partial_{\mu}\omega^{\sigma}_{\rho\nu} - \partial_{\nu}\omega^{\sigma}_{\rho\mu} + \omega^{\lambda}_{\rho\nu}\omega^{\sigma}_{\lambda\mu} - \omega^{\lambda}_{\rho\mu}\omega^{\sigma}_{\lambda\nu}$$

and

$$R^{\sigma}_{\rho\mu\nu} = 2\left(g^{\sigma}, \partial_{[\mu}\partial_{\nu]} g_{\rho}\right) =$$
$$= \partial_{\mu}\Gamma^{\sigma}_{\rho\nu} - \partial_{\nu}\Gamma^{\sigma}_{\rho\mu} + \Gamma^{\lambda}_{\rho\nu}\Gamma^{\sigma}_{\lambda\mu} - \Gamma^{\lambda}_{\rho\mu}\Gamma^{\sigma}_{\lambda\nu}\,.$$

We may also define the following quantities built from the connections $\omega^{\lambda}_{\mu\nu}$ and $\Gamma^{\lambda}_{\mu\nu}$:

$$D^{\sigma}{}_{\rho\mu\nu} = \partial_{\mu}\omega^{\sigma}_{\rho\nu} + \partial_{\nu}\omega^{\sigma}_{\rho\mu} + \omega^{\lambda}_{\rho\nu}\omega^{\sigma}_{\lambda\mu} + \omega^{\lambda}_{\rho\mu}\omega^{\sigma}_{\lambda\nu}$$

and

$$E^{\sigma}{}_{\rho\mu\nu} = \partial_{\mu}\Gamma^{\sigma}_{\rho\nu} + \partial_{\nu}\Gamma^{\sigma}_{\rho\mu} + \Gamma^{\lambda}_{\rho\nu}\Gamma^{\sigma}_{\lambda\mu} + \Gamma^{\lambda}_{\rho\mu}\Gamma^{\sigma}_{\lambda\nu}$$

from which we may define two additional "curvatures" X and P by

$$X^{\sigma}{}_{\rho\mu\nu} = \left(h^{\sigma}, \partial_{\mu}\partial_{\nu} h_{\rho}\right) = \frac{1}{2}\left(K^{\sigma}{}_{\rho\mu\nu} + D^{\sigma}{}_{\rho\mu\nu}\right) =$$
$$= \partial_{\mu}\omega^{\sigma}_{\rho\nu} + \omega^{\lambda}_{\rho\nu}\omega^{\sigma}_{\lambda\mu}$$

and

$$P^{\sigma}{}_{\rho\mu\nu} = \left(g^{\sigma}, \partial_{\mu}\partial_{\nu} g_{\rho}\right) = \frac{1}{2}\left(R^{\sigma}{}_{\rho\mu\nu} + E^{\sigma}{}_{\rho\mu\nu}\right) =$$
$$= \partial_{\mu}\Gamma^{\sigma}_{\rho\nu} + \Gamma^{\lambda}_{\rho\nu}\Gamma^{\sigma}_{\lambda\mu}$$

such that $K^{\sigma}{}_{\rho\mu\nu} = 2\,X^{\sigma}{}_{\rho[\mu\nu]}$ and $R^{\sigma}{}_{\rho\mu\nu} = 2\,P^{\sigma}{}_{\rho[\mu\nu]}$.

Now, we see that

$$F^{\lambda}_{(\mu\nu)} = \omega^{\lambda}_{(\mu\nu)} + l\,\left(\frac{1}{2}\,D^{\lambda}{}_{\sigma\mu\nu}\,\xi^{\sigma} + \partial_{\nu}\partial_{\mu}\xi^{\lambda}\right) +$$
$$+ l\left(\left(\partial_{\mu}\xi^{\sigma}\right)\omega^{\lambda}_{\sigma\nu} + \left(\partial_{\nu}\xi^{\sigma}\right)\omega^{\lambda}_{\sigma\mu}\right)$$

and

$$F^{\lambda}_{[\mu\nu]} = \omega^{\lambda}_{[\mu\nu]} + \frac{1}{2}\,l\,K^{\lambda}{}_{\sigma\mu\nu}\,\xi^{\sigma}\,.$$

In addition, we also have

$$G^{\lambda}_{(\mu\nu)} = l\left(\omega^{\sigma}_{(\mu\nu)} + l\left(\frac{1}{2}\,D^{\sigma}{}_{\rho\mu\nu}\,\xi^{\rho} + \partial_{\nu}\partial_{\mu}\xi^{\sigma}\right)\right)\bar{\nabla}_{\sigma}\bar{\xi}^{\lambda} +$$
$$+ l\left(l\,\left(\left(\partial_{\mu}\xi^{\rho}\right)\omega^{\sigma}_{\rho\nu} + \left(\partial_{\nu}\xi^{\rho}\right)\omega^{\sigma}_{\rho\mu}\right)\right)\bar{\nabla}_{\sigma}\bar{\xi}^{\lambda}$$

and

$$G^{\lambda}_{[\mu\nu]} = l\left(\omega^{\sigma}_{[\mu\nu]} - \frac{1}{2}\,l\,K^{\sigma}{}_{\rho\mu\nu}\,\xi^{\rho}\right)\bar{\nabla}_{\sigma}\,\bar{\xi}^{\lambda}.$$

Now, the metric tensor g of the space-time $\mathbb{S}_1$ and the metric tensor h of the space-time $\mathbb{S}_2$ are respectively given by

$$h_{\mu\nu} = \left(h_{\mu}, h_{\nu}\right)$$

and

$$g_{\mu\nu} = \left(g_{\mu}, g_{\nu}\right)$$

where the following relations hold:

$$h_{\mu\sigma} h^{\nu\sigma} = \delta^{\nu}_{\mu}$$
$$g_{\mu\sigma} g^{\nu\sigma} = \delta^{\nu}_{\mu}$$

In general, the two conditions $h_{\mu\sigma}\, g^{\nu\sigma} \neq \delta^{\nu}_{\mu}$ and $g_{\mu\sigma}\, h^{\nu\sigma} \neq \delta^{\nu}_{\mu}$ must be fulfilled unless $l = 0$ (in the limit $\hbar \to 0$). Furthermore, we have the metricity conditions

$$\nabla_{\lambda}\, h_{\mu\nu} = 0\,,$$

and

$$\bar{\nabla}_{\lambda}\, g_{\mu\nu} = 0\,.$$

However, note that in general, $\bar{\nabla}_{\lambda}\, h_{\mu\nu} \neq 0$ and $\nabla_{\lambda} g_{\mu\nu} \neq 0$.

Hence, it is straightforward to see that in general, the metric tensor g is related to the metric tensor h by

$$g_{\mu\nu} = h_{\mu\nu} + 2\, l\, \nabla_{(\mu}\xi_{\nu)} + l^2\, \nabla_{\mu}\xi^{\lambda}\, \nabla_{\nu}\xi_{\lambda}$$

which in the linear approximation reads

$$g_{\mu\nu} = h_{\mu\nu} + 2\, l\, \nabla_{(\mu}\xi_{\nu)}\,.$$

The formal structure of our underlying geometric framework clearly implies that the same structure holds in n dimensions as well.

3 The conformal theory

We are now in the position to extract a physical theory of quantum gravity from the geometric framework in the preceding section by considering the following linear conformal mapping:

$$g_{\mu} = e^{\varphi} h_{\mu}$$

where the continuously differentiable scalar function $\varphi\,(x^{\mu})$ is the generator of the quantum displacement field in the evolution space $\mathbb{M}_4$ and therefore connects the two space-times $\mathbb{S}_1$ and $\mathbb{S}_2$.

Now, for reasons that will be apparent soon, we shall define the generator φ in terms of the canonical quantum mechanical wave function $\psi\,(x^{\mu})$ as

$$\varphi = \ln\,(1 + M\psi)^{\frac{1}{2}}$$

where

$$M = \pm\frac{1}{2}\, l\, \left(i\, \frac{m_0 c}{\hbar}\right)^2\,.$$

Here m_0 is the rest mass of the electron. Note that the sign $\pm$ signifies the signature of the space-time used.

Now, we also have the following relations:

$$g^{\mu} = e^{-\varphi} h^{\mu},$$
$$h_{\mu} = e^{-\varphi} g_{\mu},$$
$$h^{\mu} = e^{\varphi} g^{\mu},$$
$$(g_{\mu}, g^{\nu}) = (h_{\mu}, h^{\nu}) = \delta^{\nu}_{\mu},$$
$$(g_{\mu}, h^{\nu}) = e^{2\,\varphi}\delta^{\nu}_{\mu},$$
$$(h_{\mu}, g^{\nu}) = e^{-2\,\varphi}\delta^{\nu}_{\mu},$$

as well as the conformal transformation

$$g_{\mu\nu} = e^{2\varphi} h_{\mu\nu}\,.$$

Hence

$$g^{\mu\nu} = e^{-2\,\varphi}\, h^{\mu\nu}.$$

We immediately see that

$$g_{\mu\sigma}\, h^{\nu\sigma} = e^{2\varphi}\, \delta^{\nu}_{\mu}\,,$$
$$h_{\mu\sigma}\, g^{\nu\sigma} = e^{-2\varphi}\, \delta^{\nu}_{\mu}\,.$$

At this point, we see that the world-line of the space-time $\mathbb{S}_2$, $s = \int \sqrt{h_{\mu\nu}\, dx^{\mu} dx^{\nu}}$, is connected to that of the space-time $\mathbb{S}_1$, $\sigma = \int \sqrt{g_{\mu\nu}\, dx^{\mu} dx^{\nu}}$, through

$$ds = e^{2\varphi} d\sigma\,.$$

Furthermore, from the relation

$$g_{\mu} = \left(\delta^{\nu}_{\mu} + l\, \nabla_{\mu}\xi^{\nu}\right) h_{\nu} = e^{\varphi} h_{\mu}$$

we obtain the important relation

$$l\, \nabla_{\nu}\xi_{\mu} = (e^{\varphi} - 1)\, h_{\mu\nu}\,,$$

which means that

$$\Phi_{\mu\nu} = l\, \nabla_{\nu}\xi_{\mu} = \Phi_{\nu\mu}\,,$$

i.e., the quantum displacement gradient tensor field Φ is symmetric. Hence we may simply call Φ the *quantum strain tensor field*. We also see that the components of the quantum displacement field, $\phi^{\mu} = l\, \xi^{\mu}$, can now be described by the wave function ψ as

$$\phi_{\mu} = l\, \partial_{\mu}\psi$$

i.e.,

$$\psi = \psi_0 + \frac{1}{l}\int \phi_{\mu} dx^{\mu}$$

for an arbitrary initial value ψ_0 (which, most conveniently, can be chosen to be 0).

Furthermore, we note that the integrability condition $\Phi_{\mu\nu} = \Phi_{\nu\mu}$ means that the space-time $\mathbb{S}_1$ must now possess a symmetric, linear connection, i.e.,

$$\omega^{\lambda}_{\mu\nu} = \omega^{\lambda}_{\nu\mu} = \frac{1}{2}\, h^{\sigma\lambda}\, (\partial_{\nu} h_{\sigma\mu} - \partial_{\sigma} h_{\mu\nu} + \partial_{\mu} h_{\nu\sigma})\,,$$

which are just the Christoffel symbols $\left\{ {\lambda \atop \mu\nu} \right\}$ in the space-time $\mathbb{S}_1$. Hence ω is now none other than the symmetric Levi-Civita (Riemannian) connection. Using the metricity condition $\partial_{\lambda} g_{\mu\nu} = \Gamma_{\mu\nu\lambda} + \Gamma_{\nu\mu\lambda}$, i.e.,

$$\partial_{\lambda}\, g_{\mu\nu} = M h_{\mu\nu}\, \partial_{\lambda}\psi + (1 + M\,\psi)\, (\omega_{\mu\nu\lambda} + \omega_{\nu\mu\lambda})\,,$$

we obtain the mixed form

$$\omega_{\lambda\mu\nu} = \frac{1}{2}\, (1 + M\psi)^{-1}\, (\partial_{\lambda} g_{\mu\nu} - \partial_{\mu} g_{\nu\lambda} + \partial_{\nu} g_{\lambda\mu}) -$$
$$- \frac{1}{2}\, M\, (1 + M\psi)^{-1}\, (h_{\mu\nu}\partial_{\lambda}\psi - h_{\nu\lambda}\partial_{\mu}\psi + h_{\lambda\mu}\partial_{\nu}\psi)$$

i.e.,

$$\omega^{\lambda}_{\mu\nu} = \frac{1}{2}\,(1+M\psi)^{-1}\,h^{\lambda\rho}\,(\partial_\rho g_{\mu\nu} - \partial_\mu\, g_{\nu\rho} + \partial_\nu\, g_{\rho\mu}) -$$
$$-\,\frac{1}{2}\,M\,(1+M\psi)^{-1}\,\left(\delta^{\lambda}_{\mu}\partial_\nu\psi + \delta^{\lambda}_{\nu}\partial_\mu\psi - h_{\mu\nu}h^{\lambda\rho}\partial_\rho\psi\right).$$

It may be noted that we have used the customary convention in which $\Gamma_{\lambda\,\mu\nu} = g_{\lambda\rho}\,\Gamma^{\rho}_{\mu\nu}$ and $\omega_{\lambda\mu\nu} = h_{\lambda\rho}\omega^{\rho}_{\mu\nu}$.

Now we shall see why we have made the particular choice $\varphi = \ln\,(1+M\,\psi)^{\frac{1}{2}}$. In order to explicitly show that it now possess a *stochastic* part, let us rewrite the components of the metric tensor of the space-time $\mathbb{S}_2$ as

$$g_{\mu\nu} = (1+M\psi)\,h_{\mu\nu}\,.$$

Combining this relation with the linearized relation $g_{\mu\nu} = h_{\mu\nu} + 2\,l\,\nabla_{(\mu}\,\xi_{\nu)}$ and contracting the resulting relation, we obtain

$$l\,D^2\psi = 2\left(e^{2\,\varphi} - 1\right) = 2\,M\psi\,,$$

where we have defined the differential operator $D^2 = h^{\mu\nu}\nabla_\mu\nabla_\nu$ such that

$$D^2\psi = h^{\mu\nu}\left(\partial_\mu\partial_\nu\psi - \omega^{\rho}_{\mu\nu}\,\partial_\rho\psi\right).$$

Expressing M explicitly, we obtain $D^2\psi = \mp\left(\frac{m_0\,c}{\hbar}\right)^2\psi$, i.e.,

$$\left(D^2 \pm \left(\frac{m_0 c}{\hbar}\right)^2\right)\psi = 0$$

which is precisely the *Klein-Gordon equation in the presence of gravitation*.

We may note that, had we combined the relation $g_{\mu\nu} = (1+M\,\psi)\,h_{\mu\nu}$ with the fully non-linear relation

$$g_{\mu\nu} = h_{\mu\nu} + 2\,l\,\nabla_{(\mu}\xi_{\nu)} + l^2\,\nabla_\mu\xi^\lambda\nabla_\nu\xi_\lambda\,,$$

we would have obtained the following *non-linear* Klein-Gordon equation:

$$\left(D^2 \,\pm\, \left(\frac{m_0\,c}{\hbar}\right)^2\right)\psi = l^2\,h^{\rho\sigma}h^{\mu\nu}\,(\nabla_\rho\nabla_\mu\psi)\,(\nabla_\sigma\nabla_\nu\psi)\,.$$

Now, from the general relation between the connections Γ and ω given in Section 2, we obtain the following important relation:

$$\Gamma^{\lambda}_{[\mu\nu]} = -\frac{1}{2}\,l\,\left(\delta^{\lambda}_{\sigma} - l\,\bar{\nabla}_\sigma\bar{\xi}^\lambda\right)K^{\sigma}{}_{\rho\mu\nu}\,\xi^\rho,$$

which not only connects the torsion of the space-time $\mathbb{S}_2$ with the curvature of the space-time $\mathbb{S}_1$, but also describes the torsion as an intrinsic (geometric) quantum phenomenon. Note that

$$K^{\sigma}{}_{\rho\mu\nu} = \partial_\mu\left\{\begin{matrix}\sigma\\ \rho\nu\end{matrix}\right\} - \partial_\nu\left\{\begin{matrix}\sigma\\ \rho\mu\end{matrix}\right\} +$$
$$+\left\{\begin{matrix}\lambda\\ \rho\nu\end{matrix}\right\}\left\{\begin{matrix}\sigma\\ \lambda\mu\end{matrix}\right\} - \left\{\begin{matrix}\lambda\\ \rho\mu\end{matrix}\right\}\left\{\begin{matrix}\sigma\\ \lambda\nu\end{matrix}\right\}$$

are now the components of the Riemann-Christoffel curvature tensor describing the curvature of space-time in the standard general relativity theory.

Furthermore, using the relation between the two sets of basis vectors g_μ and h_μ, it is easy to see that the connection Γ is *semi-symmetric* as

$$\Gamma^{\lambda}_{\mu\nu} = \omega^{\lambda}_{\mu\nu} + \delta^{\lambda}_{\mu}\,\partial_\nu\varphi$$

or, written somewhat more explicitly,

$$\Gamma^{\lambda}_{\mu\nu} = \frac{1}{2}\,h^{\sigma\lambda}\,(\partial_\nu h_{\sigma\mu} - \partial_\sigma h_{\mu\nu} + \partial_\mu h_{\nu\sigma}) +$$
$$+\,\frac{1}{2}\,\delta^{\lambda}_{\mu}\,\partial_\nu\big(\ln(1+M\psi)\big).$$

We immediately obtain

$$\Gamma^{\lambda}_{(\mu\nu)} = \omega^{\lambda}_{\mu\nu} + \frac{1}{2}\left(\delta^{\lambda}_{\mu}\partial_\nu\varphi + \delta^{\lambda}_{\nu}\,\partial_\mu\varphi\right)$$

and

$$\Gamma^{\lambda}_{[\mu\nu]} = \frac{1}{2}\left(\delta^{\lambda}_{\mu}\partial_\nu\varphi - \delta^{\lambda}_{\nu}\partial_\mu\varphi\right).$$

Additionally, using the relation

$$\omega^{\nu}_{\nu\mu} = \omega^{\nu}_{\mu\nu} = \partial_\mu\left(\ln\sqrt{\det(h)}\right) =$$
$$= \partial_\mu\left(\ln\left(e^{-\varphi}\,\sqrt{\det(g)}\right)\right) = \partial_\mu\left(\ln\sqrt{\det(g)}\right) - \partial_\mu\varphi$$

we may now define two *semi-vectors* by the following contractions:

$$\Gamma_\mu = \Gamma^{\nu}_{\nu\mu} = \partial_\mu\left(\ln\sqrt{\det(h)}\right) + 4\,\partial_\mu\varphi$$
$$\Delta_\mu = \Gamma^{\nu}_{\mu\nu} = \partial_\mu\left(\ln\sqrt{\det(h)}\right) + \partial_\mu\varphi$$

or, written somewhat more explicitly,

$$\Gamma_\mu = \partial_\mu\left(\ln\sqrt{\det(h)} + \ln(1+M\psi)^2\right)$$
$$\Delta_\mu = \partial_\mu\left(\ln\sqrt{\det(h)} + \ln\sqrt{1+M\psi}\right).$$

We now define the *torsion vector* by

$$\tau_\mu = \Gamma^{\nu}_{[\nu\mu]} = \frac{3}{2}\,\partial_\mu\varphi\,.$$

In other words,

$$\tau_\mu = \frac{3}{4}\,\frac{M}{(1+M\psi)}\,\partial_\mu\psi\,.$$

Furthermore, it is easy to show that the curvature tensors of our two space-times $\mathbb{S}_1$ and $\mathbb{S}_2$ are now identical:

$$R^{\sigma}{}_{\rho\mu\nu} = K^{\sigma}{}_{\rho\mu\nu}$$

which is another way of saying that the conformal transformation $g_\mu = e^{\varphi}\,h_\mu$ leaves the curvature tensor of the space-time $\mathbb{S}_1$ invariant. As an immediate consequence, we obtain the ordinary expression

$$R_{\rho\sigma\mu\nu} = \frac{1}{2}\,(\partial_\mu\partial_\sigma h_{\rho\nu} + \partial_\nu\partial_\rho h_{\sigma\mu} - \partial_\nu\partial_\sigma h_{\rho\mu} - \partial_\mu\partial_\rho h_{\sigma\nu}) +$$
$$+\,h_{\alpha\beta}\left(\omega^{\alpha}_{\rho\nu}\omega^{\beta}_{\sigma\mu} - \omega^{\alpha}_{\rho\mu}\,\omega^{\beta}_{\sigma\nu}\right).$$

Hence the following cyclic symmetry in Riemannian geometry:

$$R_{\rho\sigma\mu\nu} + R_{\rho\mu\nu\sigma} + R_{\rho\nu\sigma\mu} = 0$$

is preserved in the presence of torsion. In addition, besides the obvious symmetry $R_{\rho\sigma\mu\nu} = -R_{\rho\sigma\nu\mu}$, we also have the symmetry

$$R_{\rho\sigma\mu\nu} = -R_{\sigma\rho\mu\nu}$$

which is due to the metricity condition of the space-times $\mathbb{S}_1$ and $\mathbb{S}_2$. This implies the vanishing of the so-called Homothetic curvature as

$$H_{\mu\nu} = R^{\sigma}{}_{\sigma\mu\nu} = 0\,.$$

The Weyl tensor is given in the usual manner by

$$C_{\rho\sigma\mu\nu} = R_{\rho\sigma\mu\nu} - \frac{1}{2}\left(h_{\rho\mu}R_{\sigma\nu} + h_{\sigma\nu}R_{\rho\mu} - \right.$$
$$\left. - h_{\rho\nu}R_{\sigma\mu} - h_{\sigma\mu}R_{\rho\nu}\right) - \frac{1}{6}\left(h_{\rho\nu}h_{\sigma\mu} - h_{\rho\mu}h_{\sigma\nu}\right)R\,,$$

where $R_{\mu\nu} = R^{\sigma}{}_{\mu\sigma\nu}$ are the components of the symmetric Ricci tensor and $R = R^{\mu}_{\mu}$ is the Ricci scalar.

Now, by means of the conformal relation $g_{\mu\nu} = e^{2\varphi}\,h_{\mu\nu}$ we obtain the expression

$$R_{\rho\sigma\mu\nu} = e^{-2\varphi}\Big(\partial_\mu\partial_\sigma g_{\rho\nu} + \partial_\nu\partial_\rho g_{\sigma\mu} - \partial_\nu\partial_\sigma g_{\rho\mu}\partial_\mu\partial_\rho g_{\sigma\nu} +$$
$$+ g_{\alpha\beta}\left(\Gamma^{\alpha}_{\rho\nu}\Gamma^{\beta}_{\sigma\mu} - \Gamma^{\alpha}_{\rho\mu}\Gamma^{\beta}_{\sigma\nu}\right) + \left(\partial_\mu g_{\sigma\nu} - \partial_\nu g_{\sigma\mu}\right)\partial_\rho\varphi +$$
$$+ \left(\partial_\nu g_{\rho\mu} - \partial_\mu g_{\rho\nu}\right)\partial_\sigma\varphi + \left(\partial_\rho\, g_{\sigma\nu} - \partial_\sigma g_{\rho\nu}\right)\partial_\mu\varphi +$$
$$+ \left(\partial_\sigma g_{\rho\mu} - \partial_\rho g_{\sigma\mu}\right)\partial_\nu\varphi + g_{\sigma\nu}\partial_\mu\partial_\rho\varphi + g_{\rho\mu}\partial_\nu\partial_\sigma\varphi +$$
$$- g_{\rho\nu}\partial_\mu\partial_\sigma\varphi - g_{\mu\sigma}\partial_\nu\partial_\rho\varphi + 2\left(g_{\sigma\mu}\partial_\rho\varphi\,\partial_\nu\varphi +\right.$$
$$\left. + g_{\rho\nu}\partial_\mu\varphi\,\partial_\sigma\varphi - g_{\sigma\nu}\partial_\rho\varphi\,\partial_\mu\varphi - g_{\rho\mu}\partial_\sigma\varphi\,\partial_\nu\varphi\right) +$$
$$+ g_{\alpha\beta}\left(\left(\Gamma^{\alpha}_{\rho\mu}\partial_\nu\varphi - \Gamma^{\alpha}_{\rho\nu}\partial_\mu\varphi\right)\delta^{\beta}_{\sigma} - \left(\Gamma^{\beta}_{\sigma\mu}\partial_\nu\varphi - \Gamma^{\beta}_{\sigma\nu}\partial_\mu\varphi\right)\delta^{\alpha}_{\rho}\right)\Big).$$

Note that despite the fact that the curvature tensor of the space-time $\mathbb{S}_2$ is identical to that of the space-time $\mathbb{S}_1$ and that both curvature tensors share common algebraic symmetries, the Bianchi identity in $\mathbb{S}_2$ is not the same as the ordinary Bianchi identity in the torsion-free space-time $\mathbb{S}_1$. Instead, we have the following *generalized* Bianchi identity:

$$\bar{\nabla}_\lambda R_{\rho\sigma\mu\nu} + \bar{\nabla}_\mu R_{\rho\sigma\nu\lambda} + \bar{\nabla}_\nu R_{\rho\sigma\lambda\mu} =$$
$$= 2\left(\Gamma^{\eta}_{[\mu\nu]}R_{\rho\sigma\eta\lambda} + \Gamma^{\eta}_{[\nu\lambda]}R_{\rho\sigma\eta\mu} + \Gamma^{\eta}_{[\lambda\mu]}R_{\rho\sigma\eta\nu}\right).$$

Contracting the above relation, we obtain

$$\bar{\nabla}_\mu\left(R^{\mu\nu} - \frac{1}{2}\,g^{\mu\nu}R\right) = 2\,g^{\rho\nu}\Gamma^{\sigma}_{[\lambda\rho]}\,R^{\lambda}{}_{\sigma} + \Gamma^{\lambda}_{[\rho\sigma]}R^{\rho\sigma\nu}{}_{\lambda}\,.$$

Combining the two generalized Bianchi identities above with the relation $\Gamma^{\lambda}_{[\mu\nu]} = \frac{1}{2}\left(\delta^{\lambda}_{\mu}\,\partial_\nu\varphi - \delta^{\lambda}_{\nu}\partial_\mu\varphi\right)$, as well as recalling the definition of the torsion vector, and taking into account the symmetry of the Ricci tensor, we obtain

$$\bar{\nabla}_\lambda R_{\rho\sigma\mu\nu} + \bar{\nabla}_\mu R_{\rho\sigma\nu\lambda} + \bar{\nabla}_\nu R_{\rho\sigma\lambda\mu} =$$
$$= 2\left(R_{\rho\sigma\mu\nu}\partial_\lambda\varphi + R_{\rho\sigma\nu\lambda}\partial_\mu\varphi + R_{\rho\sigma\lambda\mu}\partial_\nu\,\varphi\right)$$

and

$$\bar{\nabla}_\nu\left(R^{\mu\nu} - \frac{1}{2}\,g^{\mu\nu}R\right) = -\,2\left(R^{\mu\nu} - \frac{1}{2}\,g^{\mu\nu}R\right)\partial_\nu\varphi$$

which, upon recalling the definition of the torsion vector, may be expressed as

$$\bar{\nabla}_\nu\left(R^{\mu\nu} - \frac{1}{2}\,g^{\mu\nu}R\right) = -\,\frac{4}{3}\left(R^{\mu\nu} - \frac{1}{2}\,g^{\mu\nu}R\right)\tau_\nu\,.$$

Apart from the above generalized identities, we may also give the ordinary Bianchi identities as

$$\nabla_\lambda R_{\rho\sigma\mu\nu} + \nabla_\mu R_{\rho\sigma\nu\lambda} + \nabla_\nu R_{\rho\sigma\lambda\mu} = 0$$

and

$$\nabla_\nu\left(R^{\mu\nu} - \frac{1}{2}\,h^{\mu\nu}R\right) = 0\,.$$

4 The electromagnetic sector of the conformal theory. The fundamental equations of motion

Based on the results obtained in the preceding section, let us now take the generator φ as describing the (quantum) electromagnetic field. Then, consequently, the space-time $\mathbb{S}_1$ is understood as being *devoid* of electromagnetic interaction. As we will see, in our present theory, it is the quantum evolution of the gravitational field that gives rise to electromagnetism. In this sense, the electromagnetic field is but an *emergent* quantum phenomenon in the evolution space $\mathbb{M}_4$.

Whereas the space-time $\mathbb{S}_1$ is purely gravitational, the *evolved* space-time $\mathbb{S}_2$ does contain an electromagnetic field. In our present theory, for reasonsthat will be clear soon, we shall define the electromagnetic field $F \in \mathbb{S}_2 \in \mathbb{M}_4$ in terms of the *torsion* of the space-time $\mathbb{S}_2$ by

$$F_{\mu\nu} = 2\,\frac{m_0c^2}{\bar{e}}\,\Gamma^{\lambda}_{[\mu\nu]}u_\lambda\,,$$

where $\bar{e}$ is the (elementary) charge of the electron and

$$u_\mu = g_{\mu\nu}\,\frac{dx^\nu}{ds} = e^{2\varphi}h_{\mu\nu}\frac{dx^\nu}{ds}$$

are the covariant components of the tangent velocity vector field satisfying $u_{mu}\,u^\mu = 1$.

We have seen that the space-time $\mathbb{S}_2$ possesses a manifest quantum structure through its evolution from the purely gravitational space-time $\mathbb{S}_1$. This means that $\bar{e}$ may be defined in terms of the fundamental Planck charge $\hat{e}$ as follows:

$$\bar{e} = N\hat{e} = N\,\sqrt{4\pi\varepsilon_0\hbar c}\,,$$

where N is a positive constant and ε_0 is the permitivity of free space. Further investigation shows that $N = \sqrt{\alpha}$ where $\alpha^{-1} \approx 137$ is the conventional fine structure constant.

Let us now proceed to show that the geodesic equation of motion in the space-time $\mathbb{S}_2$ gives the (generalized) Lorentz equation of motion for the electron. The result of parallel-

transferring the velocity vector field u along the world-line (in the direction of motion of the electron) yields

$$\frac{\bar{D}\,u^\mu}{ds} = \left(\bar{\nabla}_\nu u^\mu\right) u^\nu = 0\,,$$

i.e.,

$$\frac{du^\mu}{ds} + \Gamma^\mu_{\rho\sigma} u^\rho u^\sigma = 0\,,$$

where, in general,

$$\Gamma^\lambda_{\mu\nu} = \frac{1}{2}\, g^{\sigma\lambda}\left(\partial_\nu g_{\sigma\mu} - \partial_\sigma g_{\mu\nu} + \partial_\mu g_{\nu\sigma}\right) + \Gamma^\lambda_{[\mu\nu]} - \\ - g^{\lambda\rho}\left(g_{\mu\sigma}\Gamma^\sigma_{[\rho\nu]} + g_{\nu\sigma}\,\Gamma^\sigma_{[\rho\mu]}\right).$$

Recalling our expression for the components of the torsion tensor in the preceding section, we obtain

$$\Gamma^\lambda_{\mu\nu} = \frac{1}{2}\, g^{\sigma\lambda}\,\left(\partial_\nu g_{\sigma\mu} - \partial_\sigma g_{\mu\nu} + \partial_\mu g_{\nu\sigma}\right) + \\ + g_{\mu\nu} g^{\lambda\sigma}\partial_\sigma\varphi - \delta^\lambda_\nu\,\partial_\mu\varphi$$

which is completely equivalent to the previously obtained relation

$$\Gamma^\lambda_{\mu\nu} = \omega^\lambda_{\mu\nu} + \delta^\lambda_\mu\,\partial_\nu\varphi\,.$$

Note that

$$\Delta^\lambda_{\mu\nu} = \frac{1}{2}\, g^{\sigma\lambda}\left(\partial_\nu g_{\sigma\mu} - \partial_\sigma g_{\mu\nu} + \partial_\mu g_{\nu\sigma}\right)$$

are the Christoffel symbols in the space-time $\mathbb{S}_2$. These are not to be confused with the Christoffel symbols in the space-time $\mathbb{S}_1$ given by $\omega^\lambda_{\mu\nu}$.

Furthermore, we have

$$\frac{du^\mu}{ds} + \Delta^\mu_{\rho\sigma}\, u^\rho u^\sigma = 2 g^{\mu\rho}\Gamma^\lambda_{[\rho\sigma]} u_\lambda u^\sigma.$$

Now, since we have set $F_{\mu\nu} = 2\frac{m_0\,c^2}{\bar{e}}\Gamma^\lambda_{[\mu\nu]} u_\lambda$, we obtain the equation of motion

$$m_0 c^2\,\left(\frac{du^\mu}{ds} + \Delta^\mu_{\rho\sigma} u^\rho u^\sigma\right) = \bar{e}\, F^\mu{}_\nu\, u^\nu,$$

which is none other than the Lorentz equation of motion for the electron in the presence of gravitation. Hence, it turns out that the electromagnetic field, which is non-existent in the space-time $\mathbb{S}_1$, is an *intrinsic geometric object* in the space-time $\mathbb{S}_2$. In other words, the space-time structure of $\mathbb{S}_2$ inherently contains both gravitation and electromagnetism.

Now, we see that

$$F_{\mu\nu} = \frac{m_0 c^2}{\bar{e}}\left(u_\mu\partial_\nu\varphi - u_\nu\partial_\mu\varphi\right).$$

In other words,

$$\bar{e}\, F^\mu{}_\nu\, u^\nu = m_0 c^2\left(u^\mu\frac{d\varphi}{ds} - g^{\mu\nu}\partial_\nu\varphi\right).$$

Consequently, we can rewrite the electron's equation of motion as

$$\frac{du^\mu}{ds} + \Delta^\mu_{\rho\sigma} u^\rho u^\sigma = u^\mu\frac{d\varphi}{ds} - g^{\mu\nu}\,\partial_\nu\varphi\,.$$

We may therefore define an *asymmetric fundamental tensor of the gravoelectromagnetic manifold* $\mathbb{S}_2$ by

$$\tilde{g}_{\mu\nu} = g_{\mu\nu}\,\frac{d\varphi}{ds} - \frac{\bar{e}}{m_0 c^2}\, F_{\mu\nu}$$

satisfying

$$\tilde{g}_{\mu\nu} u^\nu = \partial_\mu\varphi\,.$$

It follows immediately that

$$\left(\delta^\mu_\nu\,\frac{d\varphi}{ds} - \frac{\bar{e}}{m_0 c^2}\, F^\mu{}_\nu\right) u^\nu = g^{\mu\nu}\,\partial_\nu\varphi$$

which, when expressed in terms of the wave function ψ, gives the *Schrödinger-like* equation

$$u_\mu\,\frac{d\psi}{ds} = \frac{1}{M}\left(\partial_\mu\varphi + \frac{\bar{e}}{m_0 c^2} F_{\mu\nu} u^\nu\right)\psi\,.$$

We may now proceed to show that the electromagnetic current density given by the covariant expression

$$j^\mu = -\frac{c}{4\,\pi}\bar{\nabla}_\nu F^{\mu\nu}$$

is conserved in the present theory.

Let us first call the following expression for the covariant components of the electromagnetic field tensor in terms of the covariant components of the canonical electromagnetic four-potential A:

$$F_{\mu\nu} = \bar{\nabla}_\nu A_\mu - \bar{\nabla}_\mu A_\nu$$

such that $\bar{e}\,\bar{\nabla}_\nu A_\mu = m_0 c^2 u_\mu\partial_\nu\varphi$, i.e.,

$$m_0 c^2\,\partial_\mu\varphi = \bar{e}\, u^\nu\bar{\nabla}_\mu A_\nu$$

which directly gives the equation of motion

$$m_0 c^2\,\frac{d\varphi}{ds} = \bar{e}\, u^\mu u^\nu\bar{\nabla}_\mu A_\nu\,.$$

Hence, we obtain the following equation of state:

$$m_0 c^2\,\frac{d\psi}{ds} = 2\,\bar{e}\,\frac{(1 + M\psi)}{M}\, u^\mu u^\nu\bar{\nabla}_\mu A_\nu\,.$$

Another alternative expression for the electromagnetic field tensor is given by

$$F_{\mu\nu} = \partial_\nu A_\mu\; - \;\partial_\mu A_\nu 2\Gamma^\lambda_{[\mu\nu]} A_\lambda\; = \\ = \;\partial_\nu A_\mu - \partial_\mu A_\nu + A_\nu\,\partial_\mu\varphi - A_\mu\partial_\nu\varphi\,.$$

In the particular case in which the field-lines of the electromagnetic four-potential propagate in the direction of the electron's motion, we have

$$F_{\mu\nu} = \Lambda\,\frac{\bar{e}}{\left(1 - \frac{\beta^2}{c^2}\right)}\left(\partial_\nu u_\mu - \partial_\mu u_\nu\right)$$

where Λ is a proportionality constant and $\beta = \pm\,\bar{e}\,\sqrt{\frac{\Lambda}{m_0}}$. Then, we may define a vortical velocity field, i.e., a spin field, through the vorticity tensor which is given by

$$\omega_{\mu\nu} = \frac{1}{2}\left(\partial_\nu u_\mu - \partial_\mu u_\nu\right)$$

and hence

$$F_{\mu\nu} = 2\Lambda \, \frac{\bar{e}}{\left(1 - \frac{\beta^2}{c^2}\right)} \, \omega_{\mu\nu} \, ,$$

which describes an electrically charged spinning region in the *space-time continuum* $\mathbb{S}_2$.

Furthermore, we have the following generalized identity for the electromagnetic field tensor:

$$\bar{\nabla}_\lambda F_{\mu\nu} + \bar{\nabla}_\mu F_{\nu\lambda} + \bar{\nabla}_\nu F_{\lambda\mu} = \\ = 2 \left(\Gamma^\sigma_{[\mu\nu]} F_{\sigma\lambda} + \Gamma^\sigma_{[\nu\lambda]} F_{\sigma\mu} + \Gamma^\sigma_{[\lambda\mu]} F_{\sigma\nu} \right)$$

which, in the present theory, takes the particular form

$$\bar{\nabla}_\lambda F_{\mu\nu} + \bar{\nabla}_\mu F_{\nu\lambda} + \bar{\nabla}_\nu F_{\lambda\mu} = \\ = 2 \left(F_{\mu\nu} \partial_\lambda \varphi + F_{\nu\lambda} \partial_\mu \varphi + F_{\lambda\mu} \partial_\nu \varphi \right) .$$

Contracting, we have

$$\bar{\nabla}_\mu \, j^\mu = - \frac{c}{4\pi} \, \bar{\nabla}_\mu \left(\Gamma^\mu_{[\rho\sigma]} F^{\rho\sigma} \right) .$$

We therefore expect that the expression in the brackets indeed vanishes. For this purpose, we may set

$$j^\mu = - \frac{c}{4\pi} \, \Gamma^\mu_{[\rho\sigma]} \, F^{\rho\sigma}$$

and hence, again, using the relation

$$\Gamma^\lambda_{[\mu\nu]} = \frac{1}{2} \left(\delta^\lambda_\mu \partial_\nu \varphi - \delta^\lambda_\nu \partial_\mu \varphi \right) ,$$

we immediately see that

$$\bar{\nabla}_\mu j^\mu - \frac{c}{4\pi} \left(\partial_\nu \varphi \, \bar{\nabla}_\mu F^{\mu\nu} + F^{\mu\nu} \left(\partial_\nu \partial_\mu \varphi - \Gamma^\lambda_{[\mu\nu]} \partial_\lambda \varphi \right) \right) = \\ = - j^\mu \, \partial_\mu \varphi - \frac{c}{4\pi} \, \Gamma^\lambda_{[\mu\nu]} F^{\mu\nu} \, \partial_\lambda \varphi$$

i.e.,

$$\bar{\nabla}_\mu \, j^\mu = 0 \, .$$

At this point, we may note the following: the fact that our theory employs torsion, from which the electromagnetic field is extracted, and at the same time guarantees electromagnetic charge conservation (in the form of the above continuity equation) in a natural manner is a remarkable property.

Now, let us call the relation

$$\Gamma^\lambda_{[\mu\nu]} = - \frac{1}{2} \, l \, \left(\delta^\lambda_\sigma - l \, \bar{\nabla}_\sigma \bar{\xi}^\lambda \right) R^\sigma{}_{\rho\mu\nu} \, \xi^\rho$$

obtained in Section 3 of this work (in which $R^\sigma{}_{\rho\mu\nu} = K^\sigma{}_{\rho\mu\nu}$). This can simply be written as

$$\Gamma^\lambda_{[\mu\nu]} = - \frac{1}{2} \, l \, e^{-\varphi} R^\lambda{}_{\rho\mu\nu} \, \xi^\rho$$

i.e.,

$$\Gamma^\lambda_{[\mu\nu]} = - \frac{1}{2} \, l \, e^{-\varphi} R^\lambda{}_{\rho\mu\nu} \, g^{\rho\sigma} \partial_\sigma \psi \, .$$

Hence, we obtain the elegant result

$$F_{\mu\nu} = - \, l \, \frac{m_0 c^2}{\bar{e}} \, e^{-\varphi} R^\lambda{}_{\rho\mu\nu} \, u_\lambda \, g^{\rho\sigma} \partial_\sigma \psi$$

i.e.,

$$F_{\mu\nu} = - \frac{l}{\bar{e}} \frac{m_0 c^2}{\sqrt{1 + M\psi}} \, R^\lambda{}_{\rho\mu\nu} \, u_\lambda \, g^{\rho\sigma} \partial_\sigma \psi$$

or, in terms of the components of the (dimensionless) microscopic displacement field ξ,

$$F_{\mu\nu} = - \, l \, \frac{m_0 c^2}{\bar{e}} \, e^{-\varphi} R^\lambda{}_{\rho\mu\nu} \, u_\lambda \, g^{\rho\sigma} \xi_\sigma$$

which further reveals *how the electromagnetic field originates in the gravitational field in the space-time* $\mathbb{S}_2$ *as a quantum field*. Hence, at last, we see a complete picture of the electromagnetic field as an emergent phenomenon. This completes the long-cherished hypothesis that the electromagnetic field itself is caused by a *massive* charged particle, i.e., when $m_0 = 0$ neither gravity nor electromagnetism can exist. Finally, with this result at hand, we obtain the following equation of motion for the electron in the gravitational field:

$$\frac{du^\mu}{ds} + \Delta^\mu_{\rho\sigma} u^\rho u^\sigma = - \, l \, e^{-\varphi} R^{\rho\sigma\mu}{}_\nu \, u_\rho \, \xi_\sigma \, u^\nu$$

i.e.,

$$\frac{du^\mu}{ds} + \Delta^\mu_{\rho\sigma} u^\rho u^\sigma = - \frac{l}{\sqrt{1 + M\psi}} \, R^{\rho\sigma\mu}{}_\nu \, u_\rho \, u^\nu \, \partial_\sigma \psi \, .$$

In addition, we note that the torsion tensor is now seen to be given by

$$\tau_\mu = - \frac{1}{2} \, l \, e^{-\varphi} R_{\mu\nu} \, \xi^\nu$$

or, alternatively,

$$\tau_\mu = - \frac{1}{2} \, l \, e^{-\varphi} R_{\mu\nu} \, g^{\nu\lambda} \, \partial_\lambda \, \psi \, .$$

In other words,

$$\tau_\mu = - \frac{1}{2} \frac{l}{\sqrt{1 + M\psi}} \, R_{\mu\nu} \, g^{\nu\lambda} \, \partial_\lambda \, \psi \, .$$

Hence, the second generalized Bianchi identity finally takes the somewhat more transparent form

$$\bar{\nabla}_\nu \left(R^{\mu\nu} - \frac{1}{2} \, g^{\mu\nu} R \right) = \\ = - \frac{2}{3} \, l \, e^{-\varphi} \left(R^{\mu\nu} R_{\nu\rho} - \frac{1}{2} \, R \, R^\mu{}_\rho \right) g^{\rho\sigma} \, \partial_\sigma \, \psi$$

i.e.,

$$\bar{\nabla}_\nu \left(R^{\mu\nu} - \frac{1}{2} \, g^{\mu\nu} R \right) = \\ = - \frac{2}{3} \frac{l}{\sqrt{1 + M\psi}} \left(R^{\mu\nu} R_{\nu\rho} - \frac{1}{2} \, R \, R^\mu{}_\rho \right) g^{\rho\sigma} \, \partial_\sigma \, \psi \, .$$

5 Final remarks

The present theory, in its current form, is still in an elementary state of development. However, as we have seen, the emergence of the electromagnetic field from the quantum evolution of the gravitational field is a remarkable achievement which deserves special attention. On another occasion, we shall expect to expound the structure of the generalized Einstein's equation in the present theory with a generally non-conservative energy-momentum tensor given by

$$T_{\mu\nu} = \pm \frac{c^4}{8\pi G} \left(R_{\mu\nu} - \frac{1}{2}\, g_{\mu\nu}\, R \right)$$

which, like in the case of self-creation cosmology, seems to allow us to attribute the creation and annihilation of matter directly to the scalar generator of the quantum evolution process, and hence the wave function alone, as

$$\bar{\nabla}_\nu T^{\mu\nu} = -\frac{2}{3} \frac{l}{\sqrt{1 + M\psi}}\, T^{\mu\nu} R_{\nu\rho}\, g^{\rho\sigma}\, \partial_\sigma \psi \neq 0\,.$$

6 Acknowledgements

The author is dearly indebted to Dmitri Rabounski and Stephen J. Crothers for their continuous support and sincere assistance.

Submitted on August 23, 2007
Accepted on September 24, 2007

References

1. Thiemann T. Introduction to Modern Canonical Quantum General Relativity. arXiv: gr-qc/0110034.
2. Barber G. A. The principles of self-creation cosmology and its comparison with General Relativity. arXiv: gr-qc/0212111.
3. Brans C. H. Consistency of field equations in "self-creation" cosmologies. *Gen. Rel. Grav.*, 1987, v. 19, 949–952.

Joint Wave-Particle Properties of the Individual Photon

Bo Lehnert

Alfvén Laboratory, Royal Institute of Technology, S-10044 Stockholm, Sweden
E-mail: Bo.Lehnert@ee.kth.se

Two-slit experiments performed earlier by Tsuchiya et al. and recently by Afshar et al. demonstrate the joint wave-particle properties of the single indiviual photon, and agree with Einstein's argument against Complementarity. These results cannot be explained by conventional theory in which Maxwell's equations serve as a guiding line and basis. On the other hand a revised quantum electrodynamic theory based on a nonzero electric field divergence in the vacuum yields results which appear to be consistent with the experiments. A model of the individual photon is thus deduced from the theory, in the form of a wave packet behaving as a single entity and having simultaneous wave and particle properties.

1 Introduction

Ever since the earlier epoch of natural science, the wave-particle duality of light has appeared as something of an enigma. In Bohr's principle of Complementarity, this duality has been a cornerstone in the interpretation of quantum mechanics. Thereby the wavelike and particlelike properties are conceived to be complementary, in the sense that they are mutually exclusive, and no experiment can reveal both at once. This formulation of quantum mechanics has been successful in many applications and is widely accepted by physicists, but it is full of apparent paradoxes which made Einstein deeply uncomfortable [1].

During the latest decades additional investigations on the nature of light have been made, among which the two-slit experiments by Tsuchiya et al. [2] and Afshar et al. [3] deserve particular attention. These investigations verify that there is a joint wave-particle duality of the individual photon, thus being in agreement with Einstein's argument against Complementarity.

In this paper part of the results by Tsuchiya et al. and Afshar et al. are reviewed and compared with a revised quantum electrodynamic theory by the author. The latter theory is based on a vacuum state that is not merely an empty space but includes the electromagnetic fluctuations of the zero point energy and a corresponding nonzero electric charge density associated with a nonzero electric field divergence. A short description of the theory is presented, whereas its detailed deductions are given elsewhere [4–7].

2 The two-slit experiments

A photon-counting imaging system has earlier been elaborated by Tsuchiya et al. [2] and incorporates the ability to detect individual photons, spatial resolution, and the capability of real-time imaging and subsequent image analysis. Two parallel slits of size $50\,\mu\text{m} \times 4\,\text{mm}$ at a spacing of $250\,\mu\text{m}$ were arranged to pass light through an interference filter at a wavelength of 253.7 nm. The full size of the obtained image on the monitor screen of the experiment was 11.4 mm at the input plane. Since the purpose of the investigation was to demonstrate the interference property of a single photon itself, the spacing of individual photons was made much longer than their coherence time, so that interference between individual photons could be prevented. For this reason, neutral density filters were used to realize a very low light level, where the counting rates were of the order of 100 per second.

As the measurements started, bright very small dots appeared at random positions on the monitor screen. After 10 seconds had elapsed, a photon-counting image was seen on the screen, containing 10^3 events, but its overall shape was not yet clearly defined. After 10 minutes, however, the total accumulated counts were 6×10^4, and an interference pattern formed by the dots was clearly detected. The diameter of each dot was of the order of 6×10^{-3} of the screen size, and the fringe distance about 5×10^{-2} of it. The effect of closing one of the double slits was finally observed. Then the interference pattern did not appear, but a diffraction pattern was observed.

As concluded by Tsuchiya et al., these results cannot be explained by mutually exclusive wave and particle descriptions of the photon, but give a clear indication of the wave-particle duality of the single individual photon [2].

These important results appear not to have attracted the wide interest which they ought to deserve. However, as long as 22 years later, Afshar et al. [3] conducted a two-slit experiment based on a different methodology but with a similar outcome and conclusions. In this investigation there was a simultaneous determination of the wave and particle aspects of light in a "welcher-weg" experiment, beyond the limitations set by Bohr's principle of Complementarity. The experiment included a pair of pinholes with diameters of 40 nm and center-to-center separation of $250\,\mu$m, with light from a

diode laser of the wavelength 638 nm. These parameter values were thus not too far from those of the experiments by Tsuchiya et al. In addition, six thin wires of 127 μm diameter were placed at a distance of 0.55 m from the pinholes, and at the minima of the observed interference pattern. When this pattern was present, the disturbance to the incoming beam by the wire grid was minimal. On the other hand, when the interference pattern was absent, the wire grid obstructed the beam. Also here the investigation was conducted in the low photon flux regime, to preclude loss of which-way information due to the intrinsic indistinguishability of coherent multi-photon systems. When the flux was 3×10^4 photons per second, the average separation between successive photons was estimated to about 10 km. The experiments were performed in four ways, i.e. with both pinholes open in absence of the wire grid, with both pinholes open in presence of the wire grid, and with either pinhole open in presence of the same grid.

From the measured data the which-way information and the visibility of an interference pattern could then be determined within the same experimental setup. The which-way information thus indicates through which pinhole the particlelike photon has passed. At the same time the interference indicates that the same wavelike photon must have *sampled* both pinholes so that an interference pattern could be formed. These derived properties of the individual photon refer back to the same space-time event, i.e. to the moment when the single photon passed the plane of the pinholes.

Consequently, also these experimental results force us to agree vith Einstein's argument against Complementarity [3].

3 Shortcomings of conventional theory

In conventional quantum electrodynamics (QED), Maxwell's equations have served as a guiding line and basis when there is a vacuum state with a vanishing electric charge density and a zero electric field divergence [8]. According to Schiff [8] and Heitler [9] the Poynting vector then defines the momentum of the pure radiation field, expressed by sets of quantized plane waves. As pointed out by Feynman [10], there are nevertheless unsolved problems which lead to difficulties with Maxwell's equations that are not removed by and not directly associated with quantum mechanics. Consequently, QED will also become subject to the shortcomings of the conventional field theory.

To be more specific in connection with a theoretical model of the individual photon, we start here with the following general physical requirements to be fulfilled:

- The model should have the form of a wave or a wave packet of preserved and limited geometrical shape, propagating with undamped motion in a defined direction of three-space. This leads to an analysis in a cylindrical frame (r, φ, z) with z in the direction of propagation;
- The obtained general solutions for the field quantities should extend all over space, and no artificial boundaries would have to be introduced in the vacuum;
- The integrated total field energy should remain finite;
- The solutions should result in an angular momentum (spin) of the photon as a propagating boson particle.

Maxwell's equations in the vacuum state yield solutions for any field quantity Q having the normal mode form

$$Q = \hat{Q}(r)\exp\big[i\,(-\omega t + \bar{m}\varphi + kz)\big] \qquad (1)$$

in cylindrical geometry where ω is the frequency and k and $\bar{m}$ are the wave numbers with respect to the z and φ directions. We further introduce

$$K_0^2 = \left(\frac{\omega}{c}\right)^2 - k^2. \qquad (2)$$

When $K_0^2 > 0$ the phase velocity becomes larger and the group velocity smaller than the velocity c of light. The general solution then has field components in terms of Bessel functions $Z_{\bar{m}}(K_0\, r)$ of the first and second kind, where the r-dependence of every component is of the form $Z_{\bar{m}}/r$ or $Z_{\bar{m}+1}$ [11]. Application to a photon model then leads to the following results:

- Already the purely axisymmetric case $\bar{m} = 0$ results in a Poynting vector which yields zero spin;
- The spin also vanishes when $K_0 = 0$ and the phase and group velocities both are equal to c;
- There is no clearly defined spatial limitation of the solutions;
- With no material boundaries such as walls, the total integrated field energy becomes divergent.

Consequently, conventional theory based on Maxwell's equations in the vacuum state does not lead to a physically relevant model for the individual photon.

4 Photon physics in revised quantum electrodynamics

An extended electromagnetic theory applied to the vacuum state and aiming beyond Maxwell's equations serves as a guiding line and basis of the present theoretical approach [4–7]. In four-dimensional representation the theory has the following form

$$\left(\frac{1}{c^2}\frac{\partial^2}{\partial t^2} - \nabla^2\right) A_\mu = \mu_0 J_\mu\,, \qquad \mu = 1, 2, 3, 4\,, \qquad (3)$$

where A_μ are the electromagnetic potentials. As deduced from the requirement of Lorentz invariance, the four-current density of the right-hand member of equation (3) becomes

$$J_\mu = (\mathbf{j}, ic\bar{\rho}) = \varepsilon_0(\operatorname{div}\mathbf{E})\,(\mathbf{C}, ic)\,, \qquad \mathbf{C}^2 = c^2 \qquad (4)$$

with c as the velocity of light, $\mathbf{E}$ denoting the electric field strength, and SI units being adopted. Further $\mathbf{B} = \operatorname{curl}\mathbf{A}$ is

the magnetic field strength derived from the three-space magnetic vector potential $\mathbf{A}$. In equation (4) the velocity vector $\mathbf{C}$ has the modulus c. Maxwell's equations in the vacuum are recovered when $\operatorname{div}\mathbf{E}=0$, whereas $\operatorname{div}\mathbf{E}\neq 0$ leads to a space-charge current density (4) in the vacuum. The corresponding three-space part $\mathbf{j}=\varepsilon_0(\operatorname{div}\mathbf{E})\mathbf{C}$ appears in addition to the displacement current.

The revised basic field equations of dynamic states in a three-dimensional representation are now given by the wave equation

$$\left(\frac{\partial^2}{\partial t^2}-c^2\,\nabla^2\right)\mathbf{E}+\left(c^2\,\nabla+\mathbf{C}\,\frac{\partial}{\partial t}\right)(\operatorname{div}\mathbf{E})=0 \qquad (5)$$

for the electric field, and the equation

$$\operatorname{curl}\mathbf{E}=-\frac{\partial\mathbf{B}}{\partial t} \qquad (6)$$

of electromagnetic induction. The characteristic features of the field equations (3)–(6) are as follows:

- The theory is based on the pure radiation field in the vacuum state, including contributions from a nonzero electric charge density;
- The associated nonzero electric field divergence introduces an additional degree of freedom, leading to new solutions and new physical phenomena. This also becomes important in situations where this divergence appears to be small;
- The theory is both Lorentz and gauge invariant;
- The velocity of light is no longer a scalar c but a vector $\mathbf{C}$ with the modulus c.

To become complete, the theory has to be quantized. In absence as well as in presence of source terms, such as the right-hand member of equation (3), the quantized field equations are generally equivalent to the original field equations in which all field quantities are replaced by their expectation values, as shown by Heitler [9]. As a first step and a simplification, the general solutions of the field equations will therefore first be determined, and relevant quantum conditions will afterwards be imposed on these solutions. This is justified by the expectation values due to Heitler. The present theory may therefore not be too far from the truth, in the sense that it represents the most probable states in a first approximation to a rigorous quantum-theoretical deduction.

4.1 Application to a model of the individual photon

The theory of equations (3)–(6) is now applied to the model of an individual photon in the axisymmetric case where $\partial/\partial\varphi=0$ in a cylindrical frame (r,φ,z) with z along the direction of propagation. Screw-shaped modes where $\partial/\partial\varphi\neq 0$ end in several respects up with similar results, but become more involved and have been described elsewhere [6, 7].

The velocity vector of equation (4) is in this axisymmetric case given by

$$\mathbf{C}=c\,(0,\cos\alpha,\sin\alpha) \qquad (7)$$

where α is a constant angle, and $\cos\alpha$ and $\sin\alpha$ could in principle have either sign but are here limited to positive values for the sake of simplicity. The form (7) can be shown to imply that the electromagnetic energy has one part which propagates in the z-direction, and another part which circulates in the φ-direction around the axis of symmetry and becomes associated with the spin [6, 7]. Normal modes of the form (1) with $\bar{m}=0$ then result in general solutions for the components of $\mathbf{E}$ and $\mathbf{B}$, being given in terms of differential expressions of a generating function

$$F=G_0R(\rho)\exp\left[i\,(-\omega t+kz)\right]. \qquad (8)$$

(Here G_0 is an amplitude factor, $\rho=r/r_0$, and r_0 represents a characteristic radius of the geometrical configuration in question.) The corresponding dispersion relation becomes

$$\omega=k\,v\,,\qquad v=c\,(\sin\alpha) \qquad (9)$$

thus resulting in axial phase and group velocities, both being equal to $v<c$. Not to get into conflict with the experiments by Michelson and Morley, the condition $0<\cos\alpha\ll 1$ has to be imposed on the parameter $\cos\alpha$. As an example, $\cos\alpha\leqslant 10^{-4}$ would make the velocity v differ from c by less than the eight decimal in the value of c. As a consequence of the dispersion relation (9) with $v<c$ and of the detailed deductions, the total integrated field energy mc^2 further becomes equivalent to a total mass m and a rest mass

$$m_0=m\sqrt{1-(v/c)^2}=m\,(\cos\alpha). \qquad (10)$$

This rest mass is associated with the angular momentum which only becomes nonzero for a nonzero electric field divergence. When $\operatorname{div}\mathbf{E}$, $\cos\alpha$, and m_0 vanish, we are thus back to the conventional case of Section 3 with its spinless and physically irrelevant basis for a photon model. Even if the electric field divergence at a first glance appears to be a small quantity, it thus has a profound effect on the physics of an individual photon model.

From the obtained general solutions it has further been shown that the total integrated charge and magnetic moment vanish, whereas the total integrated mass m and angular momentum s remain nonzero.

From the solutions of the normal wave modes, a wave packet has to be formed. In accordance with experimental experience, such a packet should have a narrow line width. Its spectrum of wave numbers k should then be piled up around a main wave number k_0 and a corresponding wavelength $\lambda_0=2\pi/k_0$. The effective axial length $2z_0$ of the packet is then much larger than λ_0.

To close the system, two relevant quantum conditions have further to be imposed. The first concerns the total integrated field energy, in the sense that $mc^2=h\nu_0$ according

to Einstein and Planck, where the frequency $\nu_0 \cong c/\lambda_0$, for $\cos\alpha \ll 1$. The second condition is imposed on the total integrated angular momentum which should become equal to $s = h/2\pi$ for the photon to behave as a boson particle.

From combination with the wave packet solutions, the imposed quantum conditions result in expressions for an effective transverse diameter $2\hat{r}$ of the wave packet. In respect to the radial part R of the generating function (8), there are two alternatives which are both given by

$$2\hat{r} = \frac{\varepsilon\lambda_0}{\pi(\cos\alpha)} \tag{11}$$

and become specified as follows:

- When $\varepsilon = 1$ expression (11) stands for a part $R(\rho)$ which is convergent at the origin $\rho = 0$. This results in an effective photon diameter being only moderately small, but still becoming large as compared to atomic dimensions;
- When $\varepsilon \ll 1$ there are solutions for a part $R(\rho)$ which is divergent at $\rho = 0$. Then finite field quantities can still be obtained within a whole range of small ε, in the limit of a shrinking characteristic radius $r_0 = c_0\varepsilon$ where c_0 is a positive constant having the dimension of length. This alternative results in an an effective photon diameter which can become very small, such as to realize a state of "needle radiation" first proposed by Einstein. Then the diameter (11) can become comparable to atomic dimensions.

It is thus seen that the requirements on a photon model can be fulfilled by the present revised theory. Its wave packet solutions have joint wave-particle properties. In some respects this appears to be similar to the earlier wave-particle duality outlined by de Broglie, where there is a "pilot wave" propagating along the axis, on which wave a "particle-like" part is "surfing". However, such a subdivision is not necessary in the present case where the wave packet behaves as one single entity, having wave and particle properties at the same time.

Attention is finally called to a comparison between the definition of the momentum of the pure radiation field in terms of the Poynting vector on one hand, and that given by the expression $\mathbf{p} = -i\hbar\nabla$ in the deduction of the Schrödinger equation for a particle with mass on the other [5]. For normal modes the axial component of $\mathbf{p}$ becomes $p_z = \hbar k$ as expected. However, in the transverse direction of a photon model being spatially limited and having a finite effective diameter (11), there would arise a nonzero transverse momentum p_r as well, but this appears to be physically unacceptable for a photon model.

4.2 The present photon model and its relation to two-slit experiments

The limits of the effective photon diameter (11) can be estimated by assuming an upper limit of $2\hat{r}$ when $\varepsilon = 1$ and $\cos\alpha = 10^{-4}$, and a lower limit of $2\hat{r}$ when $\varepsilon = \cos\alpha$. Then the effective diameter would be in the range of the values $\lambda_0/\pi \leqslant 2\hat{r} \leqslant 10^4\lambda_0/\pi$, but the lower limit could even be lower when $\varepsilon < \cos\alpha$ for strongly pronounced needle radiation. From this first order estimate, and from the features of the theory, the following points should be noticed:

- The diameter of the dot-shaped marks on the monitor screen of the experiment by Tsuchiya et al. is of the order of 6×10^{-3} of the screen size, i.e. about 10^{-4} m. With the wave length $\lambda_0 = 253.7$ nm, the effective photon diameter would then be in the range of the values $7\times10^{-4} \geqslant 2\hat{r} \geqslant 7\times10^{-8}$ m. This range covers the observed size of the dots;
- The width of the parallel slits in the experiments by Tsuchiya et al. is 5×10^{-5} m and their separation distance is 25×10^{-5} m. The corresponding pinhole diameters and their center-to-center separation in the experiments by Afshar et al. are 4×10^{-5} m and 25×10^{-5} m, respectively, and the wavelength is $\lambda_0 = 638$ nm. In the latter experiments the effective diameter is estimated to be in the range $2\times10^{-7} \leqslant 2\hat{r} \leqslant 2\times10^{-3}$ m. In both experiments the estimated ranges of $2\hat{r}$ are thus seen to cover the slit widths and separation distances;
- A large variation of a small $\cos\alpha$ has only a limited effect on the phase and group velocities of equation (9). Also a considerable variation of a small ε does not influence the general deductions of the theory [4, 6, 7] even if it ends up with a substantial change of the diameter (11). This leads to the somewhat speculative question whether the state of the compound parameter $\varepsilon/\cos\alpha$ could adopt different values during the propagation of the wave packet. This could then be related to "photon oscillations" as proposed for a model with a nonzero rest mass, in analogy with neutrino oscillations [4, 7];
- As compared to the slit widths and the separation distances, the obtained ranges of $2\hat{r}$ become consistent with the statement by Afshar et al. that the same wave-like photon can *sample* both pinholes to form an interference pattern;
- Interference between cylindrical waves should take place in a similar way as between plane waves. In particular, this becomes obvious at the minima of the interference pattern where full cancellation takes place;
- Due to the requirement of a narrow line width, the wave packet length $2z_0$ by far exceeds the wave length λ_0 and the effective diameter $2\hat{r}$. Therefore the packet forms a very long and narrow wave train;
- Causality raises the question how the photon can "know" to form the interference pattern on the monitor screen already when it passes the slits. An answer may be provided by the front part of the elongated packet

which may serve as a "precursor", thereby also representing the quantum mechanical wave nature of the packet. Alternatively, there may exist a counterpart to the precursor phenomenon earlier discussed by Stratton [11] for conventional electromagnetic waves.

5 Conclusions

The two-slit experiments by Tsuchiya et al. and by Afshar et al. demonstrate the joint wave-particle properties of the individual photon, and agree with Einstein's argument against Complementarity. These experiments cannot be explained by conventional theory. The present revised theory appears on the other hand to become consistent with the experiments.

Submitted on September 17, 2007
Accepted on September 24, 2007

References

1. Merali Z. Free will — you only think you have it. *New Scientist*, 6 May 2006, p. 8–9.
2. Tsuchiya T., Inuzuka E., Kurono T., Hosoda M. Photon-counting imaging and its applications. *Advances in Electronics and Electron Physics*, 1985, v. 64A, 21–31.
3. Afshar S. S., Flores E., McDonald K. F., Knoesel E. Paradox in wave-particle duality. *Foundations of Physics*, 2007, v. 37, 295–305.
4. Lehnert B. Photon physics of revised electromagnetics. *Progress in Physics*, 2006, v. 2, 78–85.
5. Lehnert B. Momentum of the pure radiation field. *Progress in Physics*, 2007, v. 1, 27–30.
6. Lehnert B. Revised quantum electrodynamics with fundamental applications. In: Proceedings of 2007 ICTP Summer College on Plasma Physics (Edited by P. K. Shukla, L. Stenflo, and B. Eliasson), World Scientific Publishers, Singapore, 2008.
7. Lehnert B. A revised electromagnetic theory with fundamental applications. Swedish Physics Archive (Edited by D. Rabounski), The National Library of Sweden, Stockholm, 2007; and Bogoljubov Institute for Theoretical Physics (Edited by A. Zagorodny), Kiev, 2007.
8. Schiff L. I. Quantum Mechanics. McGraw-Hill Book Comp. Inc., New York, 1949, Chs. XIV, IV, and II.
9. Heitler W. The quantum theory of radiation. Third edition. Clarendon Press, Oxford, 1954, Ch. II and Appendix.
10. Feynman R. P. Lectures on physics: mainly eletromagnetism and matter. Addison-Wesley, Reading, Massachusetts, 1964.
11. Stratton J. A. Electromagnetic theory. McGraw-Hill Book Comp. Inc., New York and London, 1941, Ch. VI, Sec. 5.18.

A New Derivation of Biquaternion Schrödinger Equation and Plausible Implications

Vic Christianto* and Florentin Smarandache†

*Sciprint.org — a Free Scientific Electronic Preprint Server, http://www.sciprint.org
E-mail: admin@sciprint.org

†Department of Mathematics, University of New Mexico, Gallup, NM 87301, USA
E-mail: smarand@unm.edu

In the preceding article we argue that biquaternionic extension of Klein-Gordon equation has solution containing imaginary part, which differs appreciably from known solution of KGE. In the present article we discuss some possible interpretation of this imaginary part of the solution of biquaternionic KGE (BQKGE); thereafter we offer a new derivation of biquaternion Schrödinger equation using this method. Further observation is of course recommended in order to refute or verify this proposition.

1 Introduction

There were some attempts in literature to generalise Schrödinger equation using quaternion and biquaternion numbers. Because quaternion number use in Quantum Mechanics has often been described [1, 2, 3, 4], we only mention in this paper the use of biquaternion number. Sapogin [5] was the first to introduce biquaternion to extend Schrödinger equation, while Kravchenko [4] use biquaternion number to describe neat link between Schrödinger equation and Riccati equation.

In the present article we discuss a new derivation of biquaternion Schrödinger equation using a method used in the preceding paper. Because the previous method has been used for Klein-Gordon equation [1], now it seems natural to extend it to Schrödinger equation. This biquaternion effect may be useful in particular to explore new effects in the context of low-energy reaction (LENR) [6]. Nonetheless, further observation is of course recommended in order to refute or verify this proposition.

2 Some interpretations of preceding result of biquaternionic KGE

In our preceding paper [1], we argue that it is possible to write biquaternionic extension of Klein-Gordon equation as follows

$$\left[\left(\frac{\partial^2}{\partial t^2}-\nabla^2\right)+i\left(\frac{\partial^2}{\partial t^2}-\nabla^2\right)\right]\varphi(x,t)=-m^2\varphi(x,t). \quad (1)$$

Or this equation can be rewritten as

$$\left(\diamondsuit\bar{\diamondsuit}+m^2\right)\varphi(x,t)=0 \quad (2)$$

provided we use this definition

$$\diamondsuit=\nabla^q+i\nabla^q=\left(-i\frac{\partial}{\partial t}+e_1\frac{\partial}{\partial x}+e_2\frac{\partial}{\partial y}+e_3\frac{\partial}{\partial z}\right)+ \\ +i\left(-i\frac{\partial}{\partial T}+e_1\frac{\partial}{\partial X}+e_2\frac{\partial}{\partial Y}+e_3\frac{\partial}{\partial Z}\right) \quad (3)$$

where e_1, e_2, e_3 are *quaternion imaginary units* obeying (with ordinary quaternion symbols: $e_1=i, e_2=j, e_3=k$)

$$i^2=j^2=k^2=-1\,, \quad ij=-ji=k\,, \\ jk=-kj=i\,, \qquad ki=-ik=j\,, \quad (4)$$

and quaternion *Nabla operator* is defined as [7]

$$\nabla^q=-i\frac{\partial}{\partial t}+e_1\frac{\partial}{\partial x}+e_2\frac{\partial}{\partial y}+e_3\frac{\partial}{\partial z}\,. \quad (5)$$

Note that equation (3) and (5) included partial time-differentiation.

It is worth nothing here that equation (2) yields solution containing imaginary part, which differs appreciably from known solution of KGE:

$$y(x,t)=\left(\frac{1}{4}-\frac{i}{4}\right)m^2t^2+\text{constant}. \quad (6)$$

Some possible alternative interpretations of this *imaginary part* of the solution of biquaternionic KGE (BQKGE) are:

(a) The imaginary part implies that there is exponential term of the wave solution, which is quite similar to the Ginzburg-Landau extension of London phenomenology [8]

$$\psi(r)=|\psi(r)|\,e^{i\varphi(r)}\,, \quad (7)$$

because (6) can be rewritten (approximately) as:

$$y(x,t)=\frac{e^i}{4}m^2t^2; \quad (8)$$

(b) The aforementioned exponential term of the solution (8) can be interpreted as signature of vortices solution. Interestingly Navier-Stokes equation which implies vorticity equation can also be rewritten in terms of Yukawa equation [3];

(c) The imaginary part implies that there is spiral wave, which suggests spiralling motion of meson or other particles. Interestingly it has been argued that one can explain electron phenomena by assuming spiralling elec-

trons [9]. Alternatively this spiralling wave may already be known in the form of Bierkeland flow. For meson observation, this could be interpreted as another form of meson, which may be called "supersymmetric-meson" [1];

(d) The imaginary part of solution of BQKGE also implies that it consists of standard solution of KGE [1], and its alteration because of imaginary differential operator. That would mean the resulting wave is composed of two complementary waves;

(e) Considering some recent proposals suggesting that neutrino can have *imaginary mass* [10], the aforementioned imaginary part of solution of BQKGE can also imply that the (supersymmetric-) meson may be composed of neutrino(s). This new proposition may require new thinking both on the nature of neutrino and also supersymmetric-meson [11].

While some of these propositions remain to be seen, in deriving the preceding BQKGE we follow Dirac's phrase that "*One can generalize his physics by generalizing his mathematics*". More specifically, we focus on using a "theorem" from this principle, i.e.: "*One can generalize his mathematics by generalizing his (differential) operator*".

3 Extended biquaternion Schrödinger equation

One can expect to use the same method described above to generalize the standard Schrödinger equation [12]

$$\left[-\frac{\hbar^2}{2m}\,\Delta u + V(x)\right] u = E\,u\,, \tag{9}$$

or, in simplified form, [12, p.11]:

$$(-\Delta + w_k) f_k = 0\,, \qquad k = 0, 1, 2, 3. \tag{10}$$

In order to generalize equation (9) to biquaternion version (BQSE), we use first quaternion Nabla operator (5), and by noticing that $\Delta \equiv \nabla\nabla$, we get

$$-\frac{\hbar^2}{2m}\left(\nabla^q\bar{\nabla}^q + \frac{\partial^2}{\partial t^2}\right) u + \big(V(x) - E\big)\,u = 0\,. \tag{11}$$

Note that we shall introduce the second term in order to 'neutralize' the partial time-differentiation of $\nabla^q\bar{\nabla}^q$ operator.

To get biquaternion form of equation (11) we can use our definition in equation (3) rather than (5), so we get

$$-\frac{\hbar^2}{2m}\left(\diamondsuit\bar{\diamondsuit} + \frac{\partial^2}{\partial t^2} - i\frac{\partial^2}{\partial T^2}\right) u + \big(V(x) - E\big)\,u = 0\,. \tag{12}$$

This is an alternative version of *biquaternionic* Schrödinger equation, compared to Sapogin's [5] or Kravchenko's [4] method. We also note here that the route to *quaternionize* Schrödinger equation here is rather different from what is described by Horwitz [13, p. 6]

$$\tilde{H}\,\psi = \psi\, e_1\, E\,, \tag{13}$$

or

$$\tilde{H}\,\psi q = \psi q\,\big(q^{-1}\, e_1\, q\big)\, E\,, \tag{14}$$

where the quaternion number q, can be expressed as follows (see [13, p. 6] and [4])

$$q = q_0 + \sum_{i=1}^{3} q_i\, e_i\,. \tag{15}$$

Nonetheless, further observation is of course recommended in order to refute or verify this proposition (12).

4 Numerical solution of biquaternion Schrödinger equation

It can be shown that numerical solution (using Maxima [14]) of biquaternionic extension of Schrödinger equation yields different result compared to the standard Schrödinger equation, as follows. For clarity, all solutions were computed in 1-D only.

For standard Schrödinger equation [12], one can rewrite equation (9) as follows:

(a) For $V(x) > E$:

$$-\frac{\hbar^2}{2m}\,\Delta u + a\cdot u = 0\,; \tag{16}$$

(b) For $V(x) < E$:

$$-\frac{\hbar^2}{2m}\,\Delta u - a\cdot u = 0\,. \tag{17}$$

Numerical solution of equation (16) and (17) is given (by assuming $\hbar = 1$ and $m = 1/2$ for convenience)

(%i44) -'diff (y, x, 2) + a*y;
(%o44) $a\cdot y - \frac{d^2}{d^2x}y$

(a) For $V(x) > E$:

(%i46) ode2 (%o44, y, x);
(%o46) $y = k_1\cdot\exp(\sqrt{a\cdot x}) + k_2\cdot\exp(-\sqrt{ax})$

(b) For $V(x) < E$:

(%i45) ode2 (%o44, y, x);
(%o45) $y = k_1\cdot\sinh(\sqrt{a\cdot x}) + k_2\cdot\cosh(\sqrt{a\cdot x})$

In the meantime, numerical solution of equation (12), is given (by assuming $\hbar = 1$ and $m = 1/2$ for convenience)

(a) For $V(x) > E$:

(%i38) (%i+1)*'diff (y, x, 2) + a*y;
(%o38) $(i+1)\,\frac{d^2}{d^2x}y + a\cdot y$
(%i39) ode2 (%o38, y, x);
(%o39) $y = k_1\cdot\sin(\sqrt{\frac{a}{i+1}\cdot x}) + k_2\cdot\cos(\sqrt{\frac{a}{i+1}\cdot x})$

(b) For $V(x) < E$:

(%i40) (%i+1)*'diff (y, x, 2) - a*y;
(%o40) $(i+1)\,\frac{d^2}{d^2x}y - a\cdot y$
(%i41) ode2 (%o40, y, x);
(%o41) $y = k_1\cdot\sin(\sqrt{-\frac{a}{i+1}\cdot x}) + k_2\cdot\cos(\sqrt{-\frac{a}{i+1}\cdot x})$

Therefore, we conclude that numerical solution of biquaternionic extension of Schrödinger equation yields different result compared to the solution of standard Schrödinger equation. Nonetheless, we recommend further observation in order to refute or verify this proposition/numerical solution of biquaternion extension of spatial-differential operator of Schrödinger equation.

As side remark, it is interesting to note here that if we *introduce imaginary number* in equation (16) and equation (17), the numerical solutions will be quite different compared to solution of equation (16) and (17), as follows

$$-\frac{i\hbar^2}{2m}\,\Delta u + au = 0\,, \tag{18}$$

where $V(x) > E$, or

$$-\frac{i\hbar^2}{2m}\,\Delta u - au = 0\,, \tag{19}$$

where $V(x) < E$.

Numerical solution of equation (18) and (19) is given (by assuming $\hbar = 1$ and $m = 1/2$ for convenience)

(a) For $V(x) > E$:

(%i47) -%i*'diff (y, x, 2) + a*y;

(%o47) $a \cdot y - i\frac{d^2}{d^2x}y$

(%i48) ode2 (%o47, y, x);

(%o48) $y = k_1 \cdot \sin(\sqrt{ia \cdot x}) + k_2 \cdot \cos(\sqrt{ia \cdot x})$

(b) For $V(x) < E$:

(%i50) -%i*'diff (y, x, 2) - a*y;

(%o50) $-a \cdot y - i\frac{d^2}{d^2x}y$

(%i51) ode2 (%o50, y, x);

(%o51) $y = k_1 \cdot \sin(-\sqrt{ia \cdot x}) + k_2 \cdot \cos(-\sqrt{ia \cdot x})$

It shall be clear therefore that using different sign for differential operator yields quite different results.

Acknowledgement

Special thanks to Prof. Diego Rapoport who mentioned Sprössig's interesting paper [3]. VC would like to dedicate this article for RFF.

Submitted on September 24, 2007
Accepted on September 26, 2007

References

1. Yefremov A., Smarandache F. and Christianto V. Yang-Mills field from quaternion space geometry, and its Klein-Gordon representation. *Progress in Physics*, 2007, v. 3.
2. Yefremov A. Quaternions: algebra, geometry and physical theories. *Hypercomplex numbers in Geometry and Physics*, 2004, v. 1(1), p.105. [2a] Yefremov A. Quaternions and biquaternions: algebra, geometry, and physical theories. arXiv: math-ph/0501055.
3. Sprössig W. Quaternionic operator methods in fluid dynamics. *Proceedings of the ICCA7* held in Toulouse, 2005, edited by Pierre Angles (Oct 26, 2006 version); see also http://www.mathe.tu-freiberg.de/math/inst/amm1/Mitarbeiter/Sproessig/ws_talks.pdf
4. Kravchenko V. G., *et al*. Quaternionic factorization of Schrödinger operator. arXiv: math-ph/0305046, p. 9.
5. Sapogin V. Unitary quantum theory. *ICCF Proceedings*, listed in Infinite Energy magazine, http://www.infinite-energy.com
6. Storm E. http://www.lenr-canr.org
7. Christianto V. A new wave quantum relativistic equation from quaternionic representation of Maxwell-Dirac equation as an alternative to Barut-Dirac equation. *Electronic Journal of Theoretical Physics*, 2006, v. 3, no. 12 (http://www.ejtp.com).
8. Schrieffer J. R. and Tinkham M. Superconductivity. *Rev. Modern Phys.*, 1999, v. 71, no. 2, S313.
9. Drew H. R. A periodic structural model for the electron can calculate its intrinsic properties to an accuracy of second or third order. *Apeiron*, 2002, v. 9, no. 4.
10. Jeong E. J. Neutrinos must be tachyons. arXiv: hep-ph/9704311.
11. Sivasubramanian S., *et al.* arXiv: hep-th/0309260.
12. Straumann N. Schrödingers Entdeckung der Wellenmechanik. arXiv: quant-ph/0110097, p. 4
13. Horwitz L. Hypercomplex quantum mechanics. arXiv: quant-ph/9602001, p. 6.
14. Maxima. http://maxima.sourceforge.net. Using Lisp GNU Common Lisp (GCL).

Thirty Unsolved Problems in the Physics of Elementary Particles

Vic Christianto* and Florentin Smarandache†

*Sciprint.org — a Free Scientific Electronic Preprint Server, http://www.sciprint.org
E-mail: admin@sciprint.org

†Department of Mathematics, University of New Mexico, Gallup, NM 87301, USA
E-mail: smarand@unm.edu

Unlike what some physicists and graduate students used to think, that physics science has come to the point that the only improvement needed is merely like adding more numbers in decimal place for the masses of elementary particles or gravitational constant, there is a number of unsolved problems in this field that may require that the whole theory shall be reassessed. In the present article we discuss thirty of those unsolved problems and their likely implications. In the first section we will discuss some well-known problems in cosmology and particle physics, and then other unsolved problems will be discussed in next section.

1 Unsolved problems related to cosmology

In the present article we discuss some unsolved problems in the physics of elementary particles, and their likely implications. In the first section we will discuss some well-known problems in cosmology and particle physics, and then other unsolved problems will be discussed in next section. Some of these problems were inspired by and expanded from Ginzburg's paper [1]. The problems are:

1. The problem of the three origins. According to Marcelo Gleiser (Darthmouth College) there are three unsolved questions which are likely to play significant role in 21st-century science: the origin of the universe, the origin of life, and the origin of mind;
2. The problem of symmetry and antimatter observation. This could be one of the biggest puzzle in cosmology: If it's true according to theoretical physics (Dirac equation etc.) that there should be equal amounts of matter and antimatter in the universe, then why our observation only display vast amounts of matter and very little antimatter?
3. The problem of dark matter in cosmology model. Do we need to introduce dark matter to describe galaxy rotation curves? Or do we need a revised method in our cosmology model? Is it possible to develop a new theory of galaxy rotation which agrees with observations but without invoking dark matter? For example of such a new theory without dark matter, see Moffat and Brownstein [2, 3];
4. Cosmological constant problem. This problem represents one of the major unresolved issues in contemporary physics. It is presumed that a presently unknown symmetry operates in such a way to enable a vanishingly small constant while remaining consistent with all accepted field theoretic principles [4];
5. Antimatter hydrogen observation. Is it possible to find isolated antimatter hydrogen (antihydrogen) in astrophysics (stellar or galaxies) observation? Is there antihydrogen star in our galaxy?

Now we are going to discuss other seemingly interesting problems in the physics of elementary particles, in particular those questions which may be related to the New Energy science.

2 Unsolved problems in the physics of elementary particles

We discuss first unsolved problems in the Standard Model of elementary particles. Despite the fact that Standard Model apparently comply with most experimental data up to this day, the majority of particle physicists feel that SM is not a complete framework. E. Goldfain has listed some of the most cited reasons for this belief [5], as follows:

6. The neutrino mass problem. Some recent discovery indicates that neutrino oscillates which implies that neutrino has mass, while QM theories since Pauli predict that neutrino should have no mass [6]. Furthermore it is not yet clear that neutrino (oscillation) phenomena correspond to Dirac or Majorana neutrino [7];
7. SM does not include the contribution of gravity and gravitational corrections to both quantum field theory and renormalization group (RG) equations;
8. SM does not fix the large number of parameters that enter the theory (in particular the spectra of masses, gauge couplings, and fermion mixing angles). Some physicists have also expressed their objections that in the QCD scheme the number of quarks have increased to more than 30 particles, therefore they assert that QCD-quark model cease to be a useful model for elementary particles;

9. SM has a gauge hierarchy problem, which requires fine tuning. Another known fine-tuning problem in SM is "strong CP problem" [8, p. 18];
10. SM postulates that the origin of electroweak symmetry breaking is the Higgs mechanism. Unfortunately Higgs particle has never been found; therefore recently some physicists feel they ought to introduce more speculative theories in order to save their Higgs mechanism [9];
11. SM does not clarify the origin of its gauge group $SU(3)\times SU(2)\times U(1)$ and why quarks and lepton occur as representations of this group;
12. SM does not explain why (only) the electroweak interactions are chiral (parity-violating) [8, p. 16];
13. Charge quantization problem. SM does not explain another fundamental fact in nature, i.e. why all particles have charges which are multiples of $e/3$ [8, p. 16].

Other than the known problems with SM as described above, there are other quite fundamental problems related to the physics of elementary particles and mathematical physics in general, for instance [10]:

14. Is there dynamical explanation of quark confinement problem? This problem corresponds to the fact that quarks cannot be isolated. See also homepage by Clay Institute on this problem;
15. What is the dynamical mechanism behind Koide's mixing matrix of the lepton mass formula [11]?
16. Does neutrino mass correspond to the Koide mixing matrix [12]?
17. Does Dirac's new electron theory in 1951 reconcile the quantum mechanical view with the classical electrodynamics view of the electron [13]?
18. Is it possible to explain anomalous ultraviolet hydrogen spectrum?
19. Is there quaternion-type symmetry to describe neutrino masses?
20. Is it possible to describe neutrino oscillation dynamics with Bogoliubov-deGennes theory, in lieu of using standard Schrödinger-type wave equation [6]?
21. Solar neutrino problem — i.e. the seeming deficit of observed solar neutrinos [14]. The Sun through fusion, send us neutrinos, and the Earth through fission, antineutrinos. But observation in SuperKamiokande etc. discovers that the observed solar neutrinos are not as expected. In SuperKamiokande Lab, it is found that the number of electron neutrinos which is observed is 0.46 that which is expected [15]. One proposed explanation for the lack of electron neutrinos is that they may have oscillated into muon neutrinos;
22. Neutrino geology problem. Is it possible to observe terrestrial neutrino? The flux of terrestrial neutrino is a direct reflection of the rate of radioactive decays in the Earth and so of the associated energy production, which is presumably the main source of Earth's heat [14];
23. Is it possible to explain the origin of electroweak symmetry breaking without the Higgs mechanism or Higgs particles? For an example of such alternative theory to derive boson masses of electroweak interaction without introducing Higgs particles, see E. Goldfain [16];
24. Is it possible to write quaternionic formulation [17] of quantum Hall effect? If yes, then how?
25. Orthopositronium problem [18]. What is the dynamics behind orthopositronium observation?
26. Is it possible to conceive New Energy generation method from orthopositronium-based reaction? If yes, then how?
27. Muonium problem. Muonium is atom consisting of muon and electron, discovered by a team led by Vernon Hughes in 1960 [19]. What is the dynamics behind muonium observation?
28. Is it possible to conceive New Energy generation method from muonium-based reaction? If yes, then how?
29. Antihydrogen problem [20]. Is it possible to conceive New Energy generation method from antihydrogen-based reaction? If yes, then how?
30. Unmatter problem [21]. Would unmatter be more useful to conceiving New Energy than antimatter? If yes, then how?

It is our hope that perhaps some of these questions may be found interesting to motivate further study of elementary particles.

Acknowledgment

VC would like to dedicate this article for RFF.

Submitted on September 24, 2007
Accepted on September 26, 2007

References

1. Ginzburg V. L. What problems of physics and astrophysics seem now to be especially important and interesting (thirty years later, already on the verge of XXI century)? *Physics-Uspekhi*, 1999, v. 42(2), 353–373.
2. Moffat J. W. Scalar-Tensor-Vector gravity theory. To be published in *J. Cosmol. Astropart. Phys.*, 2006; preprint arXiv: gr-qc/0506021.
3. Moffat J. W. Spectrum of cosmic microwave fluctuations and the formation of galaxies in a modified gravity theory. arXiv: astro-ph/0602607.

4. Goldfain E. Dynamics of neutrino oscillations and the cosmological constant problem. To appear at *Far East J. Dynamical Systems*, 2007.
5. Goldfain E. Fractional dynamics in the Standard Model for particle physics. To appear at *Comm. Nonlin. Science and Numer. Simul.*, 2007; see preprint in http://www.sciencedirect.com.
6. Giunti C. Theory of neutrino oscillations. arXiv: hep-ph/0401244.
7. Singh D., *et al*. Can gravity distinguish between Dirac and Majorana neutrinos? arXiv: gr-qc/0605133.
8. Langacker P. Structure of the Standard Model. arXiv: hep-ph/0304186, p.16.
9. Djouadi A., *et al*. Higgs particles. arXiv: hep-ph/9605437.
10. Smarandache F., Christianto V., Fu Yuhua, Khrapko R., and Hutchison J. In: *Unfolding Labyrinth: Open Problems in Physics, Mathematics, Astrophysics and Other Areas of Science*, Phoenix (AZ), Hexis, 2006, p. 8–9; arxiv: math/0609238.
11. Koide Y. arXiv: hep-ph/0506247; hep-ph/0303256.
12. Krolikowski W. Towards a realistics neutrino mass formula. arXiv: hep-ph/0609187.
13. deHaas P. J. A renewed theory of electrodynamics in the framework of Dirac ether. London PIRT Conference 2004.
14. Stodolsky L. Neutrino and dark matter detection at low temperature. *Physics-Today*, August 1991, p. 3.
15. Jaffe R. L. Two state systems in QM: applications to neutrino oscillations and neutral kaons. *MIT Quantum Theory Notes, Supplementary Notes for MIT's Quantum Theory Sequence*, (August 2006), p. 26–28.
16. Goldfain E. Derivation of gauge boson masses from the dynamics of Levy flows. *Nonlin. Phenomena in Complex Systems*, 2005, v. 8, no. 4.
17. Balatsky A. V. Quaternion generalization of Laughlin state and the three dimensional fractional QHE. arXiv: cond-mat/9205006.
18. Kotov B. A., Levin B. M. and Sokolov V. I. *et al*. On the possibility of nuclear synthesis during orthopositronium formation. *Progress in Physics*, 2007, v. 3.
19. Jungmann K. Past, present and future of muonium. arXiv: nucl-ex/040401.
20. Voronin A. and Carbonell J. Antihydrogen-hydrogen annihilation at sub-kelvin temperatures. arXiv: physics/0209044.
21. Smarandache F. Matter, antimatter, and unmatter. *Infinite Energy*, 2005, v. 11, issue 62, 50–51.

LETTERS TO PROGRESS IN PHYSICS

Charles Kenneth Thornhill (1917–2007)

Jeremy Dunning-Davies

Department of Physics, University of Hull, Hull, England
E-mail: J.Dunning-Davies@hull.ac.uk

Dr. Charles Kenneth Thornhill, who died recently, was a proud, gritty Yorkshireman who, throughout his long life, genuinely remained true to himself. This led him into conflicts within the scientific community. The jury is still out on whether he was correct or not in his ideas but, be that as it may, all can learn a tremendous amount from the courage of this man in standing up for what he truly believed.

Dr. Charles Kenneth Thornhill

Dr. Charles Kenneth Thornhill was born in Sheffield on 25th November 1917. To the very end he remained fiercely proud of being a Yorkshireman. Indeed, throughout his life, he faced all problems, both personal and academic, with that gritty fortitude many associate with people from Yorkshire.

His secondary education was undertaken at the King Edward VII School in Sheffield. In 1936 he was awarded an Open (Jodrell) Scholarship for Mathematics at Queen's College, Oxford. This scholarship was worth 110 a year, a considerable amount in those days. He completed his undergraduate studies at the beginning of the Second World War and spent that war devoting his considerable mathematical talent to the aid of the war effort. During the War and in subsequent years, he worked in a variety of fields with a bias towards unsteady gasdynamics. These included external, internal, intermediate and terminal ballistics; heat transfer and erosion in gun-barrels; gasdynamics and effects of explosions; theories of damage; detonation and combustion; thermodynamics of solids and liquids under extreme conditions, etc. As a result of the war work, he was awarded the American Presidential Medal of Freedom. This was an award of which he was, quite properly, inordinately proud. The actual citation was as follows:

> *Mr. C. Kenneth Thornhill, United Kingdom, during the period of active hostilities in World War II, performed meritorious service in the field of scientific research. As a mathematician working in the field of gun erosion, he brought to the United States a comprehensive knowledge of the subject, and working in close co-operation with American scientists concerned with the study of erosion in gun barrels, he aided and stimulated the work in improving the performance of guns.*

After the war, he spent the remainder of his working life working at Fort Halstead for the Ministry of Defence.

Throughout his time at the Ministry of Defence, he had kept abreast of developments in the areas of theoretical physics that fascinated him, — those areas popularly associated with the names relativity and cosmology. One way he achieved this was through his membership of the Royal Astronomical Association. However, on his retirement in 1977 — incidentally, according to him, retirement was the job he recommended to everyone — he was able to devote his time and intellect to considering those deep problems which continue to concern so many. Also, relating to that transitional time, he commented that, up to retirement, he had worked for man but afterwards he had worked for mankind. His main interests were in the physical properties of the ether and the construction of a non-singular ethereal cosmology. Unfortunately, because of his disbelief in relativity, many refused to even listen to his views. One undoubted reason for this was his insistence on referring to the aether by that very name. It is quite likely that if he'd been willing to compromise and use words such as "vacuum" he might have had more success with publication in the better-known journals. However, some journal editors are courageous and genuinely believe in letting the scientific community at large judge the worth of peoples' work.

It is seen immediately that some of these articles make truly substantial contributions to science. Not all are incredibly long but all result from enormous thought and mathematical effort, effort in which Kenneth Thornhill's geometrical knowledge and skill are well to the fore. It is also immedi-

ately clear that here was a man who was prepared to think for himself and not allow himself to be absolutely bound by what appeared in books, whether the books in question be academic tomes or mere popular offerings.

In his life, Kenneth Thornhill was ostracised by many in the scientific establishment as some sort of "enfant terrible". In truth, many of these people really feared his intellect. That is not to say that all his thoughts were correct. The jury should still be out on many of his ideas but, to do that, the members of the jury must have read his offerings and done so with open scientific minds. Kenneth Thornhill left us all a truly enormous legacy and that is that he showed us all that it is vitally important to be true to yourself. He never pandered to the establishment rather he stuck with what he genuinely believed.

Kenneth Thornhill died peacefully on 30th June 2007 and is survived by four children, eight grandchildren and two great grandchildren. To the end he was enormously proud of all fourteen and to them must be extended our heartfelt sympathy. To the scientific community at large must be extended the hope that its members will learn the true meaning of scientific integrity from this gritty Yorkshireman. As one who was privileged to know him, albeit mainly through lengthy, enjoyable telephone conversations, I feel his scientific integrity alone will result in the words:

"Well done, thou good and faithful servant."

Submitted on August 07, 2007
Accepted on August 23, 2007

LETTERS TO PROGRESS IN PHYSICS

Max Karl Ernst Ludwig Planck: (1858 –1947)

Pierre-Marie Robitaille

Dept. of Radiology, The Ohio Sate University, 130 Means Hall, 1654 Upham Drive, Columbus, Ohio, 43221, USA
E-mail: robitaille.1@osu.edu

October 4th, 2007 marks the 60th anniversary of Planck's death. Planck was not only the father of Quantum Theory. He was also a man of profound moral and ethical values, with far reaching philosophical views. Though he lived a life of public acclaim for his discovery of the Blackbody radiation formula which bares his name, his personal life was beset with tragedy. Yet, Planck never lost his deep faith and belief in a personal God. He was admired by Einstein, not so much for his contributions to physics, but rather, for the ideals which he embodied as a person. In this work, a brief synopsis is provided on Planck, his life, and his philosophical writings. It is hoped that this will serve as an invitation to revisit the philosophical works of the man who, more than any other, helped set the course of early 20th century physics.

"Many kinds of men devote themselves to science, and not all for the sake of science herself. There are some who come into her temple because it offers them the opportunity to display their particular talents. To this class of men science is a kind of sport in the practice of which they exult, just as an athlete exults in the exercise of his muscular prowess. There is another class of men who come into the temple to make an offering of their brain pulp in the hope of securing a profitable return. These men are scientists only by the chance of some circumstance which offered itself when making a choice of career. If the attending circumstance had been different, they might have become politicians or captains of business. Should an angel of God descend and drive from the temple of science all those who belong to the categories I have mentioned, I fear the temple would be nearly emptied. But a few worshippers would still remain — some from former times and some from ours. To these latter belongs our Planck. And that is why we love him...

...(Planck's) work has given one of the most powerful of all impulses to the progress of science. His ideas will be effective as long as physical science lasts. And I hope that the example which his personal life affords will not be less effective with later generations of scientists."

Albert Einstein, 1932

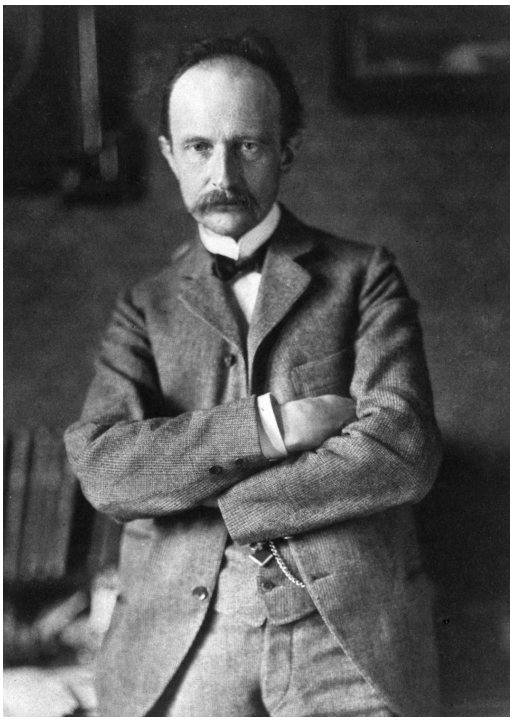

Fig. 1: Max Planck in his earlier years. AIP Emilio Segre Visual Archives, W. F. Meggers Collection. Reproduced through permission.

Biography

Max Planck, the father of quantum theory, was born on the 23rd of April 1858 in the town of Kiel, Germany [1–5]. His father had been a professor of law in the same town, while his paternal grandfather and great grandfather had been leading Lutheran theologians at the University of Göttingen. In 1867, when Planck reached the age of nine, his father received an academic appointment at the University of Munich and the Planck family relocated to this city. In Munich, he would attend the Maximillian Gymnasium and there gained his first love for Physics and Mathematics. In 1874, while still only 16, he enrolled at the University of Munich to study Physics. Beginning in 1877, he would spend one year at the University of Berlin where he was taught by Gustav Robert Kirchhoff and Hermann von Helmholtz, both of whom had been eminent physicists of the period. He was impressed with both of these men, but had little regard for the quality of their lectures. During his studies, Planck took an early interest in ther-

modynamics and immersed himself in Rudolf Clausius' work on the subject. He would receive his doctorate in physics in 1879 from the University of Munich at the age of 21. His thesis was focused on the second law of thermodynamics. In 1885, through the influence of his father, Max Planck received an appointment as an associate professor of physics at the University of Kiel. Later, he would present a paper on thermodynamics that would result in an appointment for him at the University of Berlin upon the death of Kirchoff in 1889. Kirchhoff had been the chair of theoretical physics in Berlin and Planck would become the only theoretical physicist on the faculty. He would hold this chair until his retirement in 1927, having become a full professor in 1892 [1–5].

In 1913, Planck would offer Albert Einstein a professorship in Berlin. The two of them, along with Planck's student, Professor Max von Laue, would remain close personal friends and scientific colleagues even after Einstein departed for Princeton. Rosenthal-Schneider [6] describes Planck as gentle, reserved, unpretentious, noble-minded and warm-hearted. He deeply loved mountain-climbing and music. He might well have been a concert pianist rather than a theoretical physicist, but he believed that he would do better as an average physicist than as an average pianist [1, 6].

While in Berlin, Planck would turn his attention to the emission of heat and light from solids. From these studies, his famous equation would emerge and quantum theory, through "the discovery of the elementary quantum of action", would be born [7]. Planck recognized the far reaching impact of his discovery:

"*(The essence of Quantum Physics) . . . consists in the fact that it introduces a new and universal constant, namely the elementary Quantum of Action. It was this constant which, like a new and mysterious messenger from the real world, insisted on turning up in every kind of measurement, and continued to claim a place for itself. On the other hand, it seemed so incompatible with the traditional view of the universe provided by Physics that it eventually destroyed the framework of this older view. For a time it seemed that a complete collapse of classical Physics was not beyond the bounds of possibility; gradually, however, it appeared, as had been confidently expected by all who believed in the steady advance of science, that the introduction of Quantum Theory led not to the destruction of Physics, but to a somewhat profound reconstruction, in the course of which the whole science was rendered more universal. For if the Quantum of Action is assumed to be infinitely small, Quantum Physics become merged with classical Physics. . .* " [8, p. 22–23].

Planck also believed that his equation could be applied to all objects independent of the phases of matter:

"*According to the Kirchhoff law this radiant energy is independent of the nature of the radiating substance and therefore has a universal significance*" [9, p. 18].

Planck's personal life would take a tragic turn after his discovery of the quantum in 1900 [7]. In 1909, he would lose his wife of 22 years. His oldest son, Karl, would be killed in action at Verdun in 1916. In 1917, his daughter Margerite would die in childbirth. In 1919, his second daughter Emma would suffer the same fate. In the meantime, though the First World War had just ended, Planck would win the 1918 Nobel Prize in Physics [2–5].

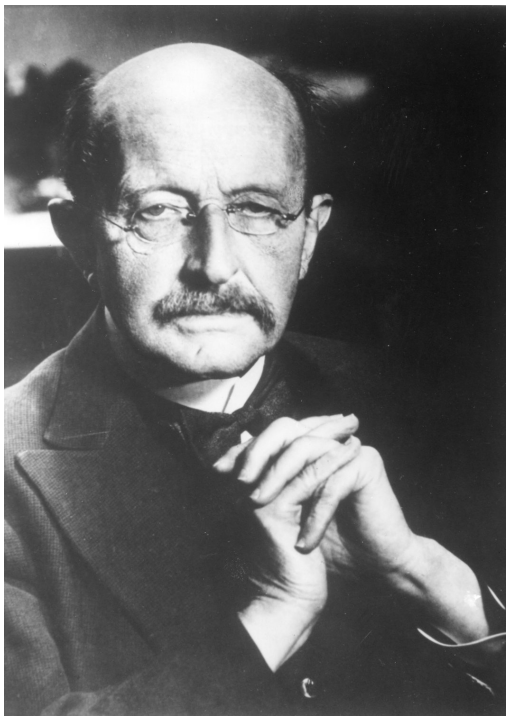

Fig. 2: Max Planck, the 1930's. AIP Emilio Segre Visual Archives. Reproduced through permission.

Unfortunately however, Planck's misfortunes continued. His home would be demolished in an ally air raid in 1944. Planck would later acknowledge gifts of food shipped from Australia by his former student Iles Rosenthal-Schneider [6]. Beginning in the early 1930's, Planck had expressed strong private and public views against the Nazi regime. Little did he realize at that time the price that he, and indeed much of the free world, would have to pay for the curse of this regime. Thus, in January 1945, his son Erwin was charged with an attempt on Hitler's life. Erwin was his only remaining child from his first marriage. Once his son was charged, Planck and von Laue tried to intervene before Heinrich Himmler, the second most powerful man in Germany [4]. But upon his arrival to Berlin, Hitler himself ordered the execution and immediate hanging of Planck's son. It is said that this execution robbed Planck of much of his will to live. Then in August 1945, the atomic bomb would be dropped on Hiroshima. Planck would express concern for the fate of mankind over these developments [6]. Eventually, Planck would be taken by the allies to Göttingen to live with his niece. He was accompanied by his second wife and their son. He would die in Göttingen on October 4, 1947 [1–5].

Philosophy of life

As Planck began to age, he devoted much of his time to philosophical works [1, 8, 9, 10]. These centered on the search for an absolute truth and on other philosophical aspects of Physics and Religion. Planck viewed science as the primary means of extracting the absolute. Planck believed that it was possible to move from the relative to the absolute. He thought that the Theory of Relativity itself promoted the absolute by quantifying in absolute terms the speed of light in a vacuum and the amount of energy within an object at rest ($E = mc^2$).

Planck saw the physical world as an objective reality and its exploration as a search for truth. Philosophers have often questioned physical reality, but men like Einstein and Planck viewed the physical world as real and the pursuit of science as forever intertwined with the search for truth [6]. These men saw the search for truth as elevating humanity. In Planck's words:

"*Science enhances the moral values of life, because it furthers a love of truth and reverence — love of truth displaying itself in the constant endeavor to arrive at more exact knowledge of the world of mind and matter around us, and reverence, because every advance in knowledge brings us face to face with the mystery of our own being*" [9, p. 122].

Thus, Planck had a deep love and respect for truthfulness. He regarded it as a central human virtue and as the most important quality of the scientist:

"*But truthfulness, this noblest of all human virtues, is authoritative even here over a well-defined domain, within which its moral commandment acquires an absolute meaning, independent of all specific viewpoints. This is probing to one's own self, before one's own conscience. Under no circumstances can there be in this domain the slightest moral compromise, the slightest moral justification for the smallest deviation. He who violates this commandment, perhaps in the endeavor to gain some momentary worldly advantage, by deliberately and knowingly shutting his eyes to the proper evaluation of the true situation, is like a spendthrift who thoughtlessly squanders away his wealth, and who must inevitably suffer, sooner or later, the grave consequences of his foolhardiness*" [1, p. 79].

He saw his quest for truth and the absolute as a never ending struggle from which he could take no rest:

"*We cannot rest and sit down lest we rust and decay. Health is maintained only through work. And as it is with all life so it is with science. We are always struggling from the relative to the absolute*" [9, p. 151].

As he continued his works in search of truth and the absolute, Planck was guided by his undying scientific faith:

"*Anyone who has taken part in the building up of science is well aware from personal experience that every endeavor in this direction is guided by an unpretentious but essential principle. This principle is faith — a faith which looks ahead*" [10, p. 121].

At the same time, Planck recognized that one could never arrive at the absolute truth. This did not deter him:

"*What will be the ultimate goal? ... research in general has a twofold aim — the effective domination of the world of senses, and the complete understanding of the real world; and that both these aims are in principle unattainable. But it would be a mistake to be discouraged on this account. Both our theoretical and practical tangible results are too great to warrant discouragement; and every day adds to them. Indeed, there is perhaps some justification for seeing in the very fact that this goal is unattainable, and the struggle unending, a blessing for the human mind in its search after knowledge. For it is in this way that its two noblest impulses — enthusiasm and reverence — are preserved and inspired anew*" [8, p. 61].

For Planck, the understanding of physical laws would occupy his entire adult life. He would write:

"*The laws of Physics have no consideration for the human senses; they depend on the facts, and not upon the obviousness of the facts*" [8, p. 73].

When he formulated his now famous Law of Thermal Radiation [7], he must have encountered tremendous opposition for what he was proposing went well beyond the senses:

"*An important scientific innovation rarely makes its way by gradually winning over and converting its opponents: it rarely happens that Saul become Paul. What does happen is that its opponents gradually die out and that the growing generation is familiarized with the idea from the beginning: another instance of the fact that the future lies with youth*" [10, p. 97].

One can but imagine the courage and scientific faith he must have held, but Planck himself summarizes well for us:

"*...in science as elsewhere fortune favors the brave*" [10, p. 112].

According to Thomas Braun "*Planck was a man of deeply religious outlook. His scientist's faith in the lawfulness of nature was inseparable from his faith in God*" [6, p. 23]. Planck believed that "*man needs science for knowledge and religion for his actions in daily life*" [6, p. 106]. For Planck: "*religion and natural science are fighting a joint battle in an incessant, never relaxing crusade against scepticism and against dogmatism, against disbelief and against superstition...*" [1, p. 186–187].

Yet, Planck made a clear distinction between science and religion stating that:

"*Religion belongs to that realm that is inviolable before the laws of causation and therefore closed to science*" [9, p. 121].

Planck seemed to marvel at the mystery of scientific discovery in a manner that most clearly conveys his religious philosophy:

"*In fact, how pitifully small, how powerless we human beings must appear to ourselves if we stop to think that the planet Earth on which we live our lives is just a minute, in-*

finitesimal mote of dust; on the other hand how peculiar it must seem that we, tiny creatures on a tiny planet, are nevertheless capable of knowing though not the essence at least the existence and the dimensions of the basic building blocks of the entire great Cosmos!" [1, p. 174].

Perhaps there is no more suitable way of closing a work on Max Planck than to recall the memorial address delivered by Professor Max von Laue at the Albani Church in Göttingen on October 7, 1947 [1, p. 7–10]. Max von Laue was a colleague of Max Planck at the University of Berlin. In 1914, he had received the Nobel Prize in Physics for his study of the diffraction of X-rays by crystals.

My Fellow Mourners:

We stand at the bier of a man who lived to be almost four-score-and-ten. Ninety years are a long life, and these particular ninety years were extraordinarily rich in experiences. Max Planck would remember, even in his old age, the sight of the Prussian and Austrian troops marching into his native town of Kiel. The birth and meteoric ascent of the German Empire occurred during his lifetime, and so did its total eclipse and ghastly disaster. These events had a most profound effect on Planck in his person, too. His eldest son, Karl, died in action at Verdun in 1916. In the Second World War, his house went up in flames during an air raid. His library, collected throughout a whole long lifetime, disappeared, no one knows where, and the most terrible blow of all fell when his second son, Erwin, lost his life in the rule of terror in January, 1945. While on a lecture tour, Max Planck, himself, was an eye-witness of the destruction of Kassel, and was buried in an air raid shelter for several hours. In the middle of May, 1945, the Americans sent a car to his estate of Rogatz on the Elbe, then a theatre of war, to take him to Göttingen. Now we are taking him to his final resting-place.

In the field of science, too, Planck's lifetime was an epoch of deep-reaching changes. The physical science of our days shows an aspect totally different from that of 1875, when Planck began to devote himself to it — and Max Planck is entitled to the lion's share in the credit for these changes. And what a wonderous story his life was! Just think — boy of seventeen, just graduated from high school, he decided to take up a science which even its most authoritative representative who he could consult, described as one of mighty meager prospects. As a student, he chose a certain branch of science, for which even its neighbor sciences had but little regard — and even within this particular branch a highly specialized field, in which literally nobody at all had any interest whatever. His first scientific papers were not read by Helmholtz, Kirchhoff and Clausius, the very men who would have found it easiest to appreciate them. Yet, he continued on his way, obeying an inner call, until he came face to face with a problem which many others had tried and failed to solve, a problem for which the very path taken by him turned out to have been the best preparation. Thus, he was able to recognize and formulate, from measurements of radiations, the law which today bears and immortalizes his name for all times. He announced it before the Berlin Physical Society on October 19, 1900. To be sure, the theoretical substantiation of it made it necessary for him to reconsider his views and to fall back on methods of the atom theory, which he had been wont to regard with certain doubts, And beyond that, he had to venture a hypothesis, the audacity of which was not clear at first, to its full extent, to anybody, not even him. But on December 14, 1900, again before the German Physical Society, he was able to present the theoretic deduction of the law of radiation. This was the birthday of quantum theory. This achievement will perpetuate his name forever.

Max von Laue, 1947

First Published Online on June 23, 2001
on http://www.thermalphysics.org
Revised March 14, 2002
Submitted on September 11, 2007
Accepted on September 17, 2007
Published online on October 04, 2007

References

1. Planck M. Scientific autobiography. Philosophical Library, New York, 1949.
2. Max Planck in: *The Nobel Foundation — Online*, http://www.nobel.se/physics/laureates/1918/index.html
3. Cannon B.D. Max Planck 1918. In: "The Nobel Prize Winners: Physics" (Frank N. Magill, Ed.), Salem Press, Pasadena, California, 1989.
4. Max Planck in: *Encyclopedia Britanica*, see *Encyclopedia Britanica Online*, http://www.britannica.com/eb/article–9108525/Max–Planck
5. Max Planck in: *Index of Biographies*, School of Mathematics and Statistics, University of St. Andrews, Scottland, U.K. http://www.groups.dcs.st-and.ac.uk/∼history/Mathematicians/Planck.html
6. Rosenthal-Schneider I. Reality and scientific thruth: discussions with Einstein, von Laue and Planck. Wayne State University Press, Detroit, 1980.
7. Planck M. Ueber das Gesetz der Energieverteilung in Normalspectrum. *Ann. Phys.*, 1901, v. 4, 553–563.
8. Planck M. The Universe in the light of modern physics. W.W. Norton & Company, Inc., New York, 1931.
9. Planck M. The new science. Meridian Books, Inc., New York, 1959.
10. Planck M. Philosophy of physics. W.W. Norton & Company Inc., New York, 1936.

Progress in Physics **is an American scientific journal on advanced studies in physics, registered with the Library of Congress (DC, USA): ISSN 1555-5534 (print version) and ISSN 1555-5615 (online version). The journal is peer reviewed and listed in the abstracting and indexing coverage of: Mathematical Reviews of the AMS (USA), DOAJ of Lund University (Sweden), Zentralblatt MATH (Germany), Scientific Commons of the University of St. Gallen (Switzerland), Open-J-Gate (India), Referential Journal of VINITI (Russia), etc.** ***Progress in Physics*** **is an open-access journal published and distributed in accordance with the Budapest Open Initiative: this means that the electronic copies of both full-size version of the journal and the individual papers published therein will always be acessed for reading, download, and copying for any user free of charge. The journal is issued quarterly (four volumes per year).**

Electronic version of this journal:
http://www.ptep-online.com

Postal address for correspondence:

Department of Mathematics and Science
University of New Mexico
200 College Road, Gallup, NM 87301, USA

Printed in the United States of America